A MATTER OF TIME

–

Towards an absolute chronology for the Middle-Upper Palaeolithic biocultural shift along the Danube fluvial corridor

Rachel J. A. Hopkins



D.Phil. Archaeological Science
Wolfson College

Trinity 2018

Dedicated to:

Paweł M. Kozłowski

for the appreciation that problems are there to be solved – they are a challenge as well as an adventure

Anne & Graham Hopkins

for supporting their daughter to become 'Indiana Jones in a lab coat'

Abstract

A MATTER OF TIME
Towards an absolute chronology for the Middle-Upper Palaeolithic biocultural shift along the Danube fluvial corridor

Rachel J. A. Hopkins, Wolfson College
D.Phil. Archaeological Science
Trinity, 2018

Recent research has shown the need for a reliable, high-resolution chronology to understand the complexity of the spatio-temporal distribution of Neanderthals and anatomically modern humans (AMH) during the transitional period between the Middle to Upper Palaeolithic. One region that has yet to benefit from the developments in dating sciences and the application of Bayesian modelling approaches is eastern Europe. This dissertation focuses on producing a more robust chronological framework for this region, especially the key area of the Danube fluvial corridor, which has been suggested as one of the conduits for early modern humans on their dispersal route into western Europe (*e.g.* Conard and Bolus, 2003). The radiocarbon data and models place the chronology for AMH dispersal on more secure footing, thereby refining our understanding of the regional variability and complexity of the Middle to Upper Palaeolithic biocultural shift.

This work is the result of four years of doctoral research within the University of Oxford's PalaeoChron ERC project, headed by Prof Tom Higham. This thesis applied recent improvements in radiocarbon dating methodologies

and analysis, such as ultrafiltration (Brock et al., 2010b), single amino acid dating (Devièse et al., 2018), and KDE modelling (Bronk Ramsey, 2017). Two strategies were pursued for sample selection. First, key sites with a deep stratigraphic record were targeted. Anthropogenically modified samples were used to initially establish site specific high resolution chronologies using Bayesian and KDE modelling. Second, type fossils, such as 'Aurignacian' osseous projectile points and human remains, were directly dated to establish spatio-temporal distributions for diagnostic finds. Furthermore, published dates from the Danube Valley and key European sites were evaluated, and – where deemed sufficiently reliable – used as comparisons and incorporated into larger regional models.

The resulting chronology is based on 606 ^{14}C measurements (440 published, 166 from this thesis), and paints a picture of complex spatio-temporal biocultural distributions. It demonstrates the validity of the Danube corridor as a conduit for AMH expansion into central Europe, and places the development as early as 50–47k cal BP based on biocultural expressions. At the same time, the results support the *Kulturpumpe* hypothesis in seeing central Europe as crucial to the development of the Early Aurignacian technocomplex, and date its initial appearance to around 43–41k cal BP. However, rather than innovation, it appears that fusion, adaptation and specialisation drive the formation of the Early Aurignacian. This is best illustrated by split-based points, which first appear further to the east where diagnostic Aurignacian lithics are absent.

Consequently, this thesis argues in favour of viewing osseous points as independent chrono-cultural markers, and stresses the importance of selecting anthropogenically modified material for dating human activity. It questions the dominant paradigm of *ex oriente lux* for explaining cultural innovations and dispersals. Instead, it proposes to further investigate the plains north of the Black Sea as a possible migration trajectory for early AMHs entering Europe. It is argued that in future, when exploring biocultural expression, it should be remembered that not all migrations move east to west, and not all developments are linear in time and space.

Acknowledgements

I am thanking my supervisor Professor Tom Higham for having given me this great opportunity to delve into the chronology of the Middle to Upper Palaeolithic along the Danube. It allowed me to work on incredible sites and material, and establish collaborations with international researchers in the fields of Prehistoric archaeology and Palaeontology. The freedom I was given to design my research, to independently pursue my investigation, and to develop my own ideas on the topic was an unforgettable experience. It is hoped that the fruits of this work will bring some of that excitement to those few who will (have to) work their way through the pages of my dissertation.

I extend my gratitude to my colleagues abroad, who have granted me access to their material for radiocarbon dating. Following the flow of the Danube, these include: Dr Walpurga Antl-Weiser, Prof Dr Maria Teschler-Nicola (Natural History Museum, Vienna, Austria), Dr Christine Neugebauer-Maresch (Institute for Oriental and European Archaeology, Vienna, Austria), Dr Bibiána Hromadová (formerly of the Slovak Academy of Science, now CNRS, Nanterre, France), Dr L'ubomíra Kamínska (Archaeological Institute, Slovak Academy of Science), Dr Matej Ruttkay (Director Archaeological Institute, Slovak Academy of Science) Dr Alena Šefčáková, Dr Anna Durisova (Natural History Museum Bratislava, Slovakia), Dr András Markó (Hungarian National Museum, Budapest), Dr Gasparik Mihaly (Hungarian National History Museum, Budapest), Dr Klára Paloás, Dr László Makádi (Geological and Geophysical Institute of Hungary, Budapest), Dr Dušan Borić (formerly of the University of Cardiff, currently at the Italian Academy for Advanced Studies in America, Columbia University, New York),

Dr Emanuela Cristiani (Università degli Studi "La Sapienza" di Roma), Dr Jean-Luc Guadelli, Dr Aleta Guadelli (CNRS, Bordeaux, France), and Dr Nikolay Sirakov (National Institute of Archaeology and Museum, Bulgarian Academy of Sciences).

Furthermore, a heartfelt thank you goes to all those researchers and excavators (named and unnamed) that came before me. Without their dedication and meticulous work none of my thesis would have been possible. It was especially Dr Philip Allsworth-Jones' book on the Szeletian (1986) that strengthened my will to find the original site publications.

Some of the fascination for radiocarbon dating in archaeology stems from spending time in the lab. Without the help of ORAU's technicians Barbara Emery, Jane Davies (may the bubble wrap be with you), Daniel Comeskey (your doughnut service shall never be forgotten), Kathryn Mears (loved your smile), Peter Ditchfield (I fixed it) and Jo Graystone (remember the medieval shoe?), my move from the theoretical to the practical application of radiocarbon dating would have been a rocky road. I also thank Dr David Chivall for being so accommodating, and letting me squeeze my work in between the commercial day-to-day business of the lab.

Good discussions were had with academic colleagues at RLAHA, including Eileen Jacob (take the world with a fiddle), Lorena Becerra Valdivia (coffee is gold), Cara Kubiak (never forget the Manchester narrow boat), Dr Richard Staff (may the smiley shirt be with you), Maciek Vencel (if in doubt, you'll find it written in cuneiform), Dr Christophe Snoeck (the only archaeologists working on dinosaurs?), Dr Rachel Wood, Prof Ruth-Ann Armitage-Fraser, and Jean-Luc Schweninger. Your tips and tricks have often helped me on the right track, and – more importantly – the coffee chats aired my head from all the constant pondering (I wish we had more). Hopefully, our discussions were insightful to at least some of you too. Special thanks are reserved for Prof Christopher Bronk Ramsey for patiently dealing with all my questions regarding the inner workings of OxCal (not to mention the extra KDE mapping functions). And, I am also indebted to Diane Baker (without

you, the lab would stop working), Elizabeth Wileman, and Hayley Sula for their administrative support.

At this point, I would like to acknowledge the work of those I have never met (and who do not know me). Their contributions to the free and open source community have made my D.Phil. work a lot easier. This thesis was written in LaTeX using TeXstudio. The maps were composed in qGIS using map data from Natural Earth[1]. All images and figures were created and amended with the help of GIMP, Inkscape, Krita, and LibreOffice. And last, but not least, version control was handled by Git and through the web-based repository manager GitLab.

This concludes my uncreative, but nonetheless sincerely felt, ode to the 'holy trinity of research', *i.e.* fieldwork, lab work, and analysis. Moving to finances: This dissertation has received funding from the European Research Council under the European Union's Seventh Framework Programme (FP7/2007-2013) / ERC grant agreement n° [324139] "PalaeoChron" awarded to Professor Tom Higham. Figures in chapter 8 that were not created by myself were sponsored by *Mission Paléolithic de Bulgarie* (French MEAE)/NAIM-BAN (Bulgaria). Furthermore, some travel expenses for outreach events, and knowledge exchange were covered by Wolfson College. Attendance of the annual meetings of the 'European Society for the study of Human Evolution' (ESHE) in 2015, 2016 and 2017 – where preliminary results from this dissertation were presented – was supported by ESHE's student travel fund. I was further excited, that my presentation of my thesis results at the 23rd International Radiocarbon Conference in Trondheim (2018) was so well received that they honoured my work with the student presentation prize.

I am also much obliged to Dr Irka Hajdas. She not only introduced me to radiocarbon dating during my undergraduate at the University of Zurich. Nearly a decade later, she enabled me to finance my last year of doctoral research, by giving me a temporary position as a radiocarbon technician at the ETH Zurich (Switzerland). Similarly, it would have been difficult

[1] https://www.naturalearthdata.com/

to complete this dissertation without the generous accommodation offer by Emeritus Professor Garry Lock and his lovely wife Jude during the last stages of writing up.

As surprising as it seems, there is a world outside of research, and I am grateful for the joy of spending time with my family and friends – especially Janamarie Truesdell, Magda Abbas, Yegor Grebnev, Maria Lidova, Stavros Dimitriadis, Maria Oddo, Liza Ross, Renate Rohner, and Petra Plüss. They kept me going through all my years at Oxford, no matter how far away I have been. I am especially grateful to my partner, Pawel Kozlowski, who has excelled at supporting me and will be forever remembered as one of those who have read my entire thesis (if I had the authority, I would grant you an M.Sc. in Archaeological Science).

Merci vell mol!



Oxford, 22 January 2019

PS: Finally, I am relieved to be able to thank all those inner demons for having lost. The thesis has been defended!

Contents

List of Figures xix

List of Tables xxxiii

I Introduction 1

1 Research objectives 3

1.1 Introduction 3

1.2 Danube corridor hypothesis 5

1.3 Research aim 6

1.4 Method choice 7

2 Thesis structure 9

II Background 11

3 The MP to UP biocultural shift 13

3.1 Archaeological evidence 15

3.1.1 Middle Palaeolithic 16

3.1.2 'Transitional' industries 17

3.1.3 Upper Palaeolithic 22

3.2 Genetic evidence 26

3.3 Environmental evidence 27

4 History of radiocarbon dating **31**

4.1 Principles of radiocarbon dating 31

4.2 Conventional vs. AMS dating 36

4.3 Challenges in ^{14}C dating the Palaeolithic 37

4.3.1 Archaeological association 37

4.3.2 Calibration 38

4.3.3 Contamination & pre-treatment methods 40

4.4 Summary 42

III Methods **45**

5 Radiocarbon dating **47**

5.1 Sample selection and sampling methods 47

5.1.1 Anthropogenically modified bone 48

5.1.2 Key-hole drilling 52

5.2 Overview of laboratory treatment 53

5.3 Sample, method and date codes at ORAU 55

5.4 Radiocarbon dating of bone 57

5.4.1 Bone diagenesis 59

5.4.2 Screening: %N and collagen preservation 60

5.4.3 Overview of bone pre-treatments 61

5.4.4 Solvent extraction 63

5.4.5 Gelatin (AG) pre-treatment protocol 64

5.4.6 Ultrafiltration (AF) pre-treatment protocol 65

5.4.7 Hydroxyproline (NRC) pre-treatment protocol 67

5.5 General quality control indicators 70

6 Analysis of $F^{14}C$ and radiocarbon dates **73**

6.1 Calibration . . . 73

6.2 Bayesian analysis . . . 76

6.3 Kernel Density Estimation (KDE) . . . 78

6.4 Software package OxCal . . . 79

6.4.1 Dates . . . 80

6.4.2 Priors . . . 81

6.4.3 Queries . . . 83

6.4.4 Outliers & inconsistent data . . . 84

6.4.5 KDE & summarising datasets . . . 87

6.4.6 Sensitivity testing . . . 88

IV Site Analysis & Chronologies **91**

7 Site selection **93**

8 Bulgaria **97**

8.1 Kozarnika . . . 100

8.1.1 Introduction . . . 100

8.1.2 Radiocarbon dating . . . 125

8.1.3 Bayesian modelling . . . 132

8.1.4 Discussion . . . 141

8.2 Manastira . . . 151

8.2.1 Introduction . . . 151

8.2.2 Radiocarbon dating . . . 154

8.2.3 Discussion . . . 156

8.3 Tabashkata . . . 157

8.3.1 Introduction . . . 157

8.3.2 Radiocarbon dating . . . 161
8.3.3 Discussion . . . 165
8.4 Temnata Dupka . . . 166
8.4.1 Introduction . . . 166
8.4.2 Radiocarbon dating . . . 200
8.4.3 Bayesian modelling . . . 209
8.4.4 Discussion . . . 228
8.5 Toplja . . . 238
8.5.1 Introduction . . . 238
8.5.2 Radiocarbon dating . . . 240
8.5.3 Discussion . . . 241

9 Serbia 243

9.1 Dubočka-Kozja . . . 246
9.1.1 Introduction . . . 246
9.1.2 Radiocarbon dating . . . 250
9.1.3 Bayesian modelling . . . 253
9.1.4 Discussion . . . 253
9.2 Tabula Traiana . . . 255
9.2.1 Introduction . . . 255
9.2.2 Radiocarbon dating . . . 264
9.2.3 Bayesian modelling . . . 267
9.2.4 Discussion . . . 268

10 Croatia 275

10.1 Bukovac . . . 278
10.1.1 Introduction . . . 278
10.1.2 Radiocarbon dating . . . 281
10.1.3 Discussion . . . 283

11 Hungary **285**

11.1 Bivak 288

11.1.1 Introduction 288

11.1.2 Radiocarbon Dating 292

11.1.3 Discussion 295

11.2 Istállóskő 297

11.2.1 Introduction 297

11.2.2 Radiocarbon Dating 317

11.2.3 Bayesian Modelling 330

11.2.4 Discussion 340

11.3 Jankovich 349

11.3.1 Introduction 349

11.3.2 Radiocarbon Dating 357

11.3.3 Bayesian Modelling 362

11.3.4 Discussion 363

11.4 Máriaremete (Remete Felső) 364

11.4.1 Introduction 365

11.4.2 Radiocarbon Dating 369

11.4.3 Discussion 371

11.5 Szeleta 373

11.5.1 Introduction 374

11.5.2 Radiocarbon Dating 380

11.5.3 Discussion 382

11.6 Peskő 384

11.6.1 Introduction 384

11.6.2 Radiocarbon Dating 393

11.6.3 Discussion 397

12 Slovakia **399**

12.1 Dzeravá Skala 402

12.1.1 Introduction 402

12.1.2 Radiocarbon dating 424

12.1.3 Bayesian modelling 440

12.1.4 Discussion 450

12.2 Šal'a 456

12.2.1 Introduction 456

12.2.2 Radiocarbon dating 458

12.2.3 Discussion 462

13 Methodological discussion & summary **463**

13.1 Radiocarbon pre-treatment 463

13.1.1 Prescreening & collagen preservation 464

13.1.2 Dating reliability 469

13.2 Modelling of radiocarbon dates 472

13.3 Summary of site discussions 473

V Regional Chronologies **475**

14 The spread of osseous points **477**

14.1 The importance of direct dating 479

14.2 The dataset 481

14.2.1 Published data 482

14.2.2 New data 491

14.3 Modelling 496

14.4 Spatio-temporal distribution 496

15 Timing the MP/UP biocultural shift **503**

15.1 Neanderthals vs. AMH 503

15.1.1 Dating record 505

15.1.2 Modelling 513

15.1.3 Spatio-temporal distribution 513

15.2 Biocultural mosaic 519

15.2.1 Published Data 520

15.2.2 New Data 532

15.2.3 Map composition 535

15.2.4 Spatio-temporal distribution 536

15.3 The spread of AMH 548

VI Conclusions **553**

16 Summary of findings **555**

17 Future work **559**

Bibliography **561**

Appendix **605**

Descriptive Catalogue **613**

A: Sites & Samples **613**

A.1 Bivak, Hungary 614

A.2 Bukovac, Croatia 616

A.3 Dubočka-Kozja, Serbia 617

A.4 Dzeravá Skala, Slovakia 622

A.5 Istállóskő, Hungary 626
A.6 Jankovich, Hungary 633
A.7 Kozarnika, Bulgaria 636
A.8 Manastira, Bulgaria 639
A.9 Mariáremete, Hungary 640
A.10 Peskő, Hungary 645
A.11 Šal'a, Slovakia 648
A.12 Szeleta, Hungary 651
A.13 Tabashkata, Bulgaria 652
A.14 Tabula Traiana, Serbia 654
A.15 Temnata Dupka, Bulgaria 660
A.16 Toplja, Bulgaria 662

B: OxCal models **665**

B.1 Code: Kozarnika 666
B.2 Code: Temnata Dupka 680
B.3 Code: Tabula Traiana 709
B.4 Code: Istállóskő 712
B.5 Code: Jankovich 722
B.6 Code: Dzeravá Skala 723
B.7 Code: Spread osseous points 744
B.8 Code: MP/UP biocultural shift 749

C: Reference sites - date lists **817**

D: Reference sites - model outputs **835**

List of Figures

1.1 Introduction: map showing location of the river Danube, which cuts through major mountain ranges and provides a corridor from the black sea to central and western Europe. 5

3.1 Background: spread of archaeological industries associated with AMHs: Uluzzian, Proto-Aurignacian, and Aurignacian (Mellars, 2011). 15

3.2 Background: NGRIP climate record for the period 55–25k cal BP with Greenland Interstadials (GIS) numbered, and approximate timings given for the CI eruption, Heinrich events (H2–H5), and the Laschamp magnetic excursion. 28

4.1 Background: effects of carbon contamination on radiocarbon dating results. 41

4.2 Background: Geißenklösterle (DE) – comparison of radiocarbon dates obtained with ion exchange gelatin preparation with those with ultrafiltration protocol Higham et al. (2012). 43

5.1 Methods: *Homo neanderthalensis* parental bone found at Šal'a (Slovakia). Photo: R. Hopkins. 48

5.2 Methods: *Equus* sp. pelvis fragment with projectile wound from Temnata, Bulgaria. Photo: R. Hopkins. 49

5.3 Methods: retoucher Kz-28 (left) with typical abrasion pattern, and faunal bone fragment Kz-19 (right) with cut marks from Kozarnika (Bulgaria). Photos: R. Hopkins. 50

5.4 Methods: left – possible shapes of bone fractures: (a) helical, (b) transverse, (c) longitudinal and transverse, (d) diagonal, (e) diagonal with step, and (f) columnar. Right – (g) Three possible angles of fractures: (A) acute, (B) obtuse, (C) right angle (after Outram, 2003). 51

5.5 Methods: osseous point from Dzeravá Skala (Slovakia), sampled for radiocarbon dating using key-hole drilling. Photo: R. Hopkins. 52

5.6 Methods: the structure of collagen. 58

5.7 Methods: bear tooth pendant Mlc-10 from Mladeč (Czech Republic), showing the tiny hole where a %N sample has been taken. Photo: R. Hopkins. . 60

6.1 Methods: comparison of IntCal04, IntCal09, and IntCal13 calibration curves for terrestrial records from the northern hemisphere. 74

6.2 Methods: boundary commands used in OxCal 4.3 to achieve different uninformative priors (Bronk Ramsey, 2009a). 81

6.3 Methods: (a) CQL input and (b) output of a simple Bayesian model using OxCal 4.3. 82

7.1 Site selection: map highlighting sites selected for radiocarbon dating, and their present country jurisdictions. 94

7.2 Site selection: map of loess distribution in Europe according to Haase et al. (2007). 96

8.1 Bulgaria: map of MP/UP sites evaluated 98

8.2 Kozarnika: location of Kozarnika cave in the valley Skomlia. In the background, the Danube plane (Guadelli et al., 1999). 101

8.3 Kozarnika: cave entrance as found in 2015 (photo: T. Higham). 102

8.4 Kozarnika: map of cave with location of excavation sector I, II, III, and IV (Ferrier et al., 2009, fig. 3). 103

8.5 Kozarnika: Pleistocene sequence with lithostratigraphy, archaeological interpretation, biostratigraphy and published chronology (Guadelli et al., 2005b, tab. 1). 104

8.6 Kozarnika: profile drawing sector II. 105

8.7 Kozarnika: profile and plana in sector III. 106

8.8 Kozarnika: lithics from (a) layer 6/7 (EUP), and (b) layer 9a (Mousterian). 108

8.9 Kozarnika: lithics from layer 6/7 (EUP). 110

8.10 Kozarnika: lithics from layer 5c. 111

8.11 Kozarnika: art from Middle and Upper Palaeolithic horizons. 113

8.12 Kozarnika: anthropomorphic figure (E10-683) found on a rib fragment from level V. 114

8.13 Kozarnika: fragment of an osseous Venus figurine found in the remains of the illicit excavation. 115

8.14 Kozarnika: human remains from sector I/II and III. 117

8.15 Kozarnika: human remains, catalogue no. K/1509, sector III. 118

8.16 Kozarnika: human remains, catalogue no. K/3322, sector III. 119

8.17 Kozarnika: map of excavation co-ordinate system in sector I/II with location of radiocarbon sampling highlighted. 120

8.18 Kozarnika: stratigraphic Model 0. 135

8.19 Kozarnika: stratigraphic Models 1 and Model 2. 136

8.20 Kozarnika: stratigraphic Model 3 and Model 4. 137

8.21 Kozarnika: stratigraphic Model 5 and Model 7. 138

8.22 Kozarnika: comparison of models KDE 0, KDE 1 and KDE 2. 140

8.23 Kozarnika: comparison of transition boundaries for stratigraphic Models 1–7: start 6/7, transition 6/7 ls/lp to 6/7 lb, and transition 6/7 to 5c. . . . 145

8.24 Kozarnika: comparison of transition boundaries for stratigraphic Models 1–7: transition 5c/5b, and 5b/5a. 146

8.25 Kozarnika: comparison of ^{14}C ages for layer A (sector III) to the chronostratigraphy of Model 3 (sector III), showing contemporaneity with layer 5c. 149

8.26 Manastira: photo of cave entrance in 2012. 152

8.27 Manastira: cave map with local coordinate system and excavation trenches from 2012, 2013, and 2015. 153

8.28 Manastira: previously dated bone fragment with signs of gnawing and digestion by hyaena, Beta-326622 > 43500 BP. 154

8.29 Manastira: human remains shortlisted for dating. 155

8.30 Tabashkata: photo of north-west cave entrance. 158

8.31 Tabashkata: map of cave with areas of excavation marked. 159

8.32 Tabashkata: left – profile drawing with layer numbers and interpretation; right – points published by Джамбазов (1963). 160

8.33 Temnata: photo of Prohodna tunnel entrance with Temnata cave entrance to the left. 167

8.34 Temnata: map showing Temnata and adjacent Prohodna. 168

8.35 Temnata: map with excavation sectors from 1920s, and from 1993–1991. . . 169

8.36 Temnata: drawings of north and south profile, sector TD-I. 171

8.37 Temnata: photos of west profile, sector TD-I. 172

8.38 Temnata: drawings of north and east profile, sector TD-V. 174

8.39 Temnata: drawings of north and west profile, sector TD-II. 176

8.40 Temnata: diagram of stratigraphy in sector TD-I and TD-V for ease of comparison. . . . 178
8.41 Temnata: MP lithics from lyaer 6. . . . 180
8.42 Temnata: MP lithics from layer 5 and 5pg. . . . 181
8.43 Temnata: engraved stone fragment, sector TD-II, layer VI. . . . 183
8.44 Temnata: lithics from layer VI (IUP), and layer 4C (EUP). . . . 184
8.45 Temnata: sagittal projection of blade refittings in layer 4, sector TD-I (Tsanova, 2006, fig. II.39). . . . 186
8.46 Temnata: EUP lithics from layer 4B, TD-I. . . . 187
8.47 Temnata: EUP lithics from layer 4A, TD-I. . . . 188
8.48 Temnata: osseous points from levels VI-VII (layer 3d), TD-V. . . . 189
8.49 Temnata: *Homo sapiens* remains from sector TD-V. . . . 190
8.50 Temnata: visualisation of previously obtained dates, calibrated, sector TD-I. 197
8.51 Temnata: visualisation of previously obtained dates, calibrated, sector TD-V. 198
8.52 Temnata: excavation sectors with local coordinate system and ^{14}C sampling highlighted. . . . 201
8.53 Temnata: distribution of faunal remains with identified anthropogenic modification according to layer attribution. . . . 204
8.54 Temnata: visualisation of dates from sectors TD-I and TD-V used in modelling. . . . 211
8.55 Temnata: stratigraphic Model 0. . . . 215
8.56 Temnata: stratigraphic Model 1 and Model 2. . . . 216
8.57 Temnata: stratigraphic Model 3. . . . 217
8.58 Temnata: stratigraphic Model 3-CI. . . . 219
8.59 Temnata: stratigraphic Model 4 and Model 5. . . . 220
8.60 Temnata: stratigraphic Model 4-CI. . . . 221
8.61 Temnata: stratigraphic Model 6. . . . 222
8.62 Temnata: stratigraphic model Simple 1. . . . 223
8.63 Temnata: stratigraphic model Simple 2. . . . 224
8.64 Temnata: comparison of KDE models 0–6. . . . 227
8.65 Temnata: comparison of modelled dates for layers 5–3d from Model 4 and Model 5. . . . 229

8.66 Temnata: KDE 3 model results with layer association and CI eruption marked. . . . 233

8.67 Temnata: bar plot shwoing distribution of anthropogenically modified bone (dated and undated) from current project, sorted according to (a) cultural layer, or (b) geological unit. . . . 235

8.68 Temnata: comparison of boundaries for the transition 5/4 calculated by the different stratigraphic models, and demonstrating a start of UP industries by 45k cal BP (marked **red**) the latest. . . . 236

8.69 Temnata: KDE 3 results with location of MP, IUP and EUP marked. . . . 237

8.70 Toplja: map shwoing cave and nearby river. . . . 239

9.1 Serbia: map of Middle and Upper Palaeolithic sites. . . . 244

9.2 Dubočka Kozja: cave location marked by arrow (photo: D. Borić). . . . 246

9.3 Dubočka Kozja: Vertical cross-section through cave length, and horizontal cross-section through cave with excavation trench and squares, and elevation (m a.s.l.) marked. . . . 247

9.4 Dubočka Kozja: profile drawings from trench 1/2013 showing quadrant location and layer identifications. . . . 248

9.5 Dubočka Kozja: drawings and photos of lithics found at the site. . . . 249

9.6 Dubočka Kozja: tooth pendant from layer 2 (left), and faunal bone fragment with cut marks from layer 4 (OxA-28687: 25370 ± 200 BP). . . . 250

9.7 Tabula Traiana: photo of cave location with Roman memorial plaque in foreground. . . . 255

9.8 Tabula Traiana: Cave entrance as seen in September 2016 with D. Borić standing next to the excavation trench 2/2008. . . . 256

9.9 Tabula Traiana: map of excavated areas and tephra sample columns (top), and vertical cave cross-section with depth of excavation trenches and pre-excavation cave floor level marked. . . . 258

9.10 Tabula Traiana: selection of lithics found at site, and photo of two dated, cut-marked faunal fragments. . . . 259

9.11 Tabula Traiana: north-west facing profile at the south-east end of trench 3/2008. . . . 260

9.12 Tabula Traiana: top – south-west facing profile at the north-est end of trenches 1/2005 and 1/2008 with location of tephra sample column 1 and tephra count/identification; bottom – photo of same south-west facing profile and its location marked with thick black line on cave plan. . . . 262

9.13 Tabula Traiana: `KDE_Model` results (code: p. 711). Dataset includes all radiocarbon measurements obtained on anthropogenically modified faunal remains. . . . 269

9.14 Tabula Traiana: Stratigraphic Model 1. 270

9.15 Tabula Traiana: modified stratigraphic models (Model 2 and Model 3) with close up of modelled transition to EUP. 271

10.1 Croatia: map of Middle and Upper Palaeolithic sites. 276

10.2 Šandalja: SBP (Karavanić, 2003, fig. 9.1). 277

10.3 Bukovac: left – photo of cave entrance; right – sketch of cave layout. 279

10.4 Bukovac: some artefacts from layer 3. 280

10.5 Bukovac: visual comparison of radiocarbon dates obtained on the antler point Pb 602. 284

11.1 Hungary: map of Middle and Upper Palaeolithic sites. 286

11.2 Bivak: photos of cave entrance and of the sediment profile. 289

11.3 Bivak: map of the cave with estimated excavation area from 1953. 290

11.4 Bivak: artefacts from the lower and upper archaeological horizon. 291

11.5 Bivak: visual comparison of the calibrated radiocarbon dates obtained from the osseous point, and the two cut-marked bone fragments. 296

11.6 Istállóskő: photo of cave entrance in 1912. 298

11.7 Istállóskő: map of excavation sectors from 1911 to 1951. 299

11.8 Istállóskő: longitudinal section of the cave highlighting the depth of excavations from 1911 to 1951. 300

11.9 Istállóskő: stratigraphic profile after Adams and Ringer (2004). 303

11.10 Istállóskő: profile drawings from Vértes' excavations with their location marked within the cave and in relation to previous excavations. 304

11.11 Istállóskő: retouched blade fragments and cores from the lower AH, Vértes excavations. 306

11.12 Istállóskő: Middle Palaeolithic tools found in the upper archaeological horizon 307

11.13 Istállóskő: retouched blade points from the upper AH with find locations for fragments refitted in no. 3. 308

11.14 Istállóskő: artefacts found by Vértes in the upper AH. 309

11.15 Istállóskő: right mandibular second molar of a ca. 9 year old child, found in 1950 (Malán, 1954, includes detailed measurements). 310

11.16 Istállóskő: visualisation of published radiocarbon dates calibrated in OxCal 4.3 using InCal13 calibration curve and grouped according to their layer attribution. 318

11.17 Istállóskő: location of Vértes' excavation trenches. 319

11.18 Istállóskő: comparison of radiocarbon dates obtained on osseous points Pb 51/13 and Pb 50/53 showing that unreliable measurements published in Davies and Hedges (2008) should not be used for further analysis, and be discarded in favour of the new new AMS ^{14}C dates. 330

11.19 Istállóskő: site stratigraphic Models 0; with charcoal GrN-1501 in lower AH (A), or in separate sterile layer (B). 332

11.20 Istállóskő: site stratigraphic Model 1 and Model 2. 334

11.21 Istállóskő: site stratigraphic Model 3 and Model 4. 335

11.22 Istállóskő: site KDE models. 337

11.23 Istállóskő: Point Model 1. 338

11.24 Istállóskő: osseous point KDE models: 339

11.25 Istállóskő: comparison of start and end boundaries for the lower AH and for the upper AH, demonstrating the huge influence the non-occupation related dating has on Bayesian modelling and the need for direct dating of osseous points in order to not overestimate their period of use. 342

11.26 Istállóskő: the bimodal distribution of osseous points observed in the model Points KDE 2 reflects an initial phase dominated by split-based points, followed by a younger phase dominated by massive-based points. 346

11.27 Jankovich: photos of cave location and view from cave. 350

11.28 Jankovich: cave map with locations of excavation trenches and local co-ordinates. 351

11.29 Jankovich: drawing of west-facing profile through cave length with 4 layer divisions 353

11.30 Jankovich: lithics from Hillebrand's excavations. 354

11.31 Jankovich: drawings of some of the osseous points found during Hillebrand's excavations 355

11.32 Jankovich: KDE model on osseous points (n=5). 362

11.33 Jankovich: comparison of calibrated radiocarbon dates on osseous points. . 364

11.34 Máriaremete: photos of location of Remete Felső cave, and of view from cave interior with profile on the left side. 365

11.35 Máriaremete: map with with cross-section and excavation squares. 366

11.36 Máriaremete: longitudinal profile (north-west-facing) from the front hall. . 366

11.37 Máriaremete: human remains. 368

11.38 Máriaremete: comparison of calibrated radiocarbon dates from human remains (OxA-33849) and anthropogenically modified fauna found in squares 2/3 and 5/6. . . . 373

11.39 Szeleta: photo of view from cave interior. . . . 374

11.40 Szeleta: map with area labels and excavation trenches showing that most of the cave has been emptied. . . . 375

11.41 Szeleta: longitudinal section through the main gallery with profile drawing (Kadić, 1916, Tafel XIV). . . . 376

11.42 Szeleta: profile drawing from the entrance and front hall of the cave (Adams and Ringer, 2004). . . . 377

11.43 Szeleta: split-based bone points published by Saád and Nemeskéri (1955). . . 378

11.44 Szeleta: calibrated radiocarbon dates grouped according to layer attribution. 383

11.45 Peskő: photos of view from inside the cave, and of excavation trenches and profiles during Kadić's excavations . . . 385

11.46 Peskő: map of the cave from top and side with excavation trenches, quadrants and cave areas marked. . . . 386

11.47 Peskő: profile drawings. . . . 387

11.48 Peskő: osseous tools, ornaments and artefacts from the upper AH. . . . 388

11.49 Peskő: lithics. . . . 389

11.50 Peskő: osseous projectile points and tools from the lower AH. . . . 390

11.51 Peskő: osseous projectile points and tools from the lower AH. . . . 391

11.52 Peskő: comparison of new and published radiocarbon dates on osseous points, demonstrating the older ages obtained after AF* compared to AG* pretreatment. . . . 398

12.1 Slovakia: map of Middle Palaeolithic to Upper Palaeolithic sites evaluated. 400

12.2 Dzeravá Skala: cave entrance (Kaminská et al., 2005b, p. 9). . . . 403

12.3 Dzeravá Skala: excavation areas from 1912/1913, 1950 and 2002/2003 with square labels and profile location. . . . 404

12.4 Dzeravá Skala: split-based point (Hillebrand, 1914, fig. 7; scale added). . . . 405

12.5 Dzeravá Skala: profile drawing from the 2013 excavation (Hillebrand, 1914). 406

12.6 Dzeravá Skala: Prošek's south-facing profile as seen by Prošek (1953) and Kaminská et al. (2005b). . . . 408

12.7 Dzeravá Skala: drawings of north and west profiles from both trench PP2, and PP1. . . . 409

12.8 Dzeravá Skala: photos of north and west profiles from both trench PP2, and PP1. 410

12.9 Dzeravá Skala: Reconciliation of the stratigraphies published by Hillebrand (1914), Prošek (1953) , and Kaminská et al. (2005b). 412

12.10 Dzeravá Skala: 'leaf point' lithics (not to scale) found by Prošek at the base of his layer 8, and by Hillebrand in the upper part of his layer 4. 413

12.11 Dzeravá Skala: lithics found by Prošek in his layer 8 and 9. 415

12.12 Dzeravá Skala: lithic and bone industry from (a) layer 5, (b) layer 9, and (c) layer 11 – discovered during the 2002/2003 excavations (after Kaminská et al., 2005b, fig. 7–8). 416

12.13 Dzeravá Skala: *Homo sapiens* tooth found during 1913 excavation in 'reddish clay'. Photograph showing occlusal, lingual, buccal and apical view (Šefčáková, 2007, fig. 5) 419

12.14 Dzeravá Skala: distribution of anthropogenically modified faunal remains from the 2002/2003 excavation season. 425

12.15 Dzeravá Skala: overview of point fragments found in 1950 listed according to typological identification by B. Hromadová. 429

12.16 Potočka zijalka: SBP (Moreau et al., 2015). 430

12.17 Dzeravá Skala: comparison of osseous point radiocarbon dates obtained on the same sample. 439

12.18 Dzeravá Skala: Stratigraphic Model 1 (left) and Model 2 (right). 443

12.19 Dzeravá Skala: Stratigraphic Model 7 (left) and Model 8 (right). 445

12.20 Dzeravá Skala: Stratigraphic Model 9 (left) and Model 10 (right). 447

12.21 Dzeravá Skala: comparison of KDE models. 449

12.22 Dzeravá Skala: comparison of boundaries calculated by Models 1–10. 452

12.23 Dzeravá Skala: distribution of anthropogenically modified faunal remains grouped according to previously proposed cultural groups based on ^{14}C ages. 453

12.24 Šal'a: Previous sampling of the frontal bone of Šal'a II for histological and DNA analysis. 458

12.25 Šal'a: previous sampling of the inside of Šal'a I (frontal bone) for unknown purpose. 460

13.1 Local summary: collagen yield after AG or AG* treatment for samples dated in this thesis. 464

13.2 Local summary: visualisation of relationship between %N results, collagen yield after AG treatment and a sample's F^{14}C value. Data points coloured according to site origin. 466

13.3 Local summary: visualisation of relationship between %N results, collagen yield after AG treatment and a sample's $F^{14}C$ value. Data points coloured according to whether or not an artefact was conserved. 467

13.4 Local summary: visualisation of relationship between original sample mass in mg, collagen yield after AG treatment and a sample's $F^{14}C$ value. Data points coloured according to whether or not an artefact was conserved. 468

13.5 Local summary: comparison of auto-duplicates and AG*/NRC protocols. . 471

14.1 Osseous points: map showing distribution of SBP finds and location of dated osseous points (published and new). 478

14.2 Osseous points: schematic illustration of why direct dating of osseous points is important to reliably establish their age (based on Istállóskő from section 11.2). 480

14.3 Osseous points: directly dated osseous and wooden points from the literature (pt. 1/2). 487

14.4 Osseous points: directly dated osseous points from the literature (pt. 2/2). 488

14.5 Osseous points: photos of osseous points directly radiocarbon dated for this dissertation (pt. 1/2). 494

14.6 Osseous points: photos of osseous points directly radiocarbon dated for this dissertation (pt. 2/2). 495

14.7 Osseous points: comparison of KDE results using direct dates on SBP (**red**, n=17, code: p 744) and on MBP (**blue**, n=32, code: p. 744), showing a bimodal distribution chronologically separating SBPs from MBPs with outlying peaks towards younger periods. 497

14.8 Osseous points: distribution of dates used for KDE model of SBP (code: p. 744). Label of dates outside the main event marked **red**, and period of the smaller events created by them highlighted in **grey**. 498

14.9 Osseous points: distribution of dates used for KDE model of MBP (code: p. 744). Label of dates outside the main event marked **red**, and period of the smaller events created by them highlighted in **grey**. 499

14.10 Osseous points: spatio-temporal distribution of SBP (**red**), MPB (**blue**) and typologically unidentified points (**green**) from 44–29.7k cal BP, in steps of 1300 years. Circle size represents probability density estimates from direct radiocarbon dates on osseous points. Code: p. 746. 501

15.1 MP/UP: map of sites with directly dated human remains. 504

15.2 MP/UP: spatio-temporal distribution of directly dated Neanderthal and AMH remains in time slices of 1000 years from 51000 cal BP to 32000 cal BP (code: p. 749). 514

15.3 MP/UP: temporal distribution of directly dated Neanderthal and AMH remains, visualised by overlaying 'KDE Neanderthals' with 'KDE AMH' for the crucial time period between 53000 – 33000 cal BP (code: p. 750 and p. 751). 516

15.4 MP/UP: KDE of directly dated late Neanderthal skeletal remains (n=12). Specimens at 45k cal BP or younger highlighted in grey. Note the absence of remains <45k cal BP in the Danube Valley (code: p. 750). 517

15.5 MP/UP: KDE of directly dated early AMH skeletal remains (n=19). Specimens older than 40k cal BP highlighted in grey. Note the absence of remains >40k cal BP in the Danube Valley (code: p. 751). 518

15.6 MP/UP: map of reference sites used for spatio-temporal comparisons. . . . 521

15.7 MP/UP: stratigraphic model for Šalitrena Pećina (code: p. 765). 524

15.8 MP/UP: stratigraphic model for Hohle Fels (code: p. 757). 526

15.9 MP/UP: comparison of priors obtained from modelling publ. data (pt. 1/3).529

15.10 MP/UP: comparison of priors obtained from modelling publ. data (pt. 2/3).530

15.11 MP/UP: comparison of priors obtained from modelling publ. data (pt. 3/3).531

15.12 MP/UP: new dates and priors obtained from modelling new data. 534

15.13 MP/UP: key for reading cultures on MAP 1 (fig. 15.14–15.16). 536

15.14 MP/UP: MAP 1 – spatio-temporal distribution of dated assemblages between 53000–47500 cal BP, visualised in time slices of 500 years (code: p. 769). 537

15.15 MP/UP: MAP 1 – spatio-temporal distribution of dated assemblages between 47000–41500 cal BP, visualised in time slices of 500 years (code: p. 769). 538

15.16 MP/UP: MAP 1 – spatio-temporal distribution of dated assemblages between 41000–35500 cal BP, visualised in time slices of 500 years (code: p. 769). 539

15.17 MP/UP: MAP 2 – spatio-temporal distribution of Neanderthal and AMH dated assemblages between 52000–41000 cal BP, visualised in time slices of 1000 years (code: p. 777). 543

15.18 MP/UP: spatio-temporal distribution of Neanderthal and AMH dated assemblages between 52000–47000 cal BP, visualised in time slices of 1000 years, demonstrating effect of alternative authorship scenario (codes: p. 785 and 794). 545

15.19 MP/UP: spatio-temporal distribution of Neanderthal and AMH dated assemblages between 52000–47000 cal BP, visualised in time slices of 1000 years, demonstrating effect of alternative authorship scenario (codes: p. 803). 546

15.20 MP/UP: MAP 3 – spread of AMH between 52000–41000 cal BP (in time slices of 1000 years). KDE mapping contour at 95%. 549

15.21 MP/UP: MAP 3 – spread of AMH between 52000–41000 cal BP (in time slices of 1000 years). KDE mapping contour set to 10. 550

16.1 Summary: attempt at visualising different larger migration and cultural influence patterns into and from Europe based on radiocarbon dating and modelling presented in this dissertation. 556

A.1 Legend for sample catalogue. 613

A.2 Catalogue Bivak: Biv-01 – Antler point with museum alterations; Biv-02 – cut-marked bone; Biv-03 – cut-marked bone. 615

A.3 Catalogue Bukovac: Buk-01 – massive based antler point. 616

A.4 Catalogue Dubočka Kozja: DK-01 – tooth pendant; DK-03 – cut-marked bone; DK-06 – cut-marked bone. 619

A.5 Catalogue Dubočka Kozja: DK-08 – cut-marked bone; DK-09 – cut-marked bone; DK-17 – cut-marked bone; DK-20 – cut-marked bone. 620

A.6 Catalogue Dubočka Kozja: DK-24 – cut-marked bone; DK-32 – cut-marked bone; DK-36 – cut-marked bone; DK-39 – cut-marked bone. 621

A.7 Catalogue Istállóskő: Istall-01 – lozangic point; Istall-02 – split-based point; Istall-04 – split-based point. 627

A.8 Catalogue Istállóskő: Istall-03 – lozangic point; Istall-05 – split-based point (?); Istall-06 – massive-based point. 628

A.9 Catalogue Istállóskő: Istall-07 – antler point; Istall-08 – split-based point; Istall-09 – cut-marked bone. 629

A.10 Istállóskő: Istall-10 – cut-marked bone; Istall-11 – cut-marked bone. 630

A.11 Catalogue Istállóskő: Istall-13 – cut-marked bone; Istall-14 – cut-marked bone. 631

A.12 Catalogue Istállóskő: Istall-16 – split-based (?) point; Istall-18 – split-based point. 632

A.13 Catalogue Jankovich: Jank-01 – antler point; Jank-02 – antler point; Jank-03 – antler point; Jank-04 – antler point. 634

A.14 Catalogue Jankovich: Jank-05 – antler point; Jank-06 – antler point. 635

A.15 Catalogue Manastira: Man-01 – *Homo sapiens*, tibia. 639

A.16 Catalogue Mariáremete: MR-01 – human vertebra; MR-02 – split bone; MR-03 – cut-marked bone. 641

A.17 Catalogue Mariáremete: MR-04 – cut-marked bone; MR-05 – cut-marked bone. . . . 642

A.18 Catalogue Mariáremete: MR-06 – cut-marked bone; MR-07 – cut-marked bone. . . . 643

A.19 Catalogue Mariáremete: MR-08 – cut-marked bone; MR-10 – cut-marked bone. . . . 644

A.20 Catalogue Peskő: Pes-01 – massive based point; Pes-02 – split-based point. 646

A.21 Catalogue Peskő: Pes-03 – antler point. . . . 647

A.22 Catalogue Šal'a: Sal-01 – Neanderthal cranial fragment. . . . 649

A.23 Catalogue Šal'a: Sal-02 – Neanderthal cranial fragment. . . . 650

A.24 Catalogue Szeleta: Szel-01 – split-based point. . . . 651

A.25 Catalogue Tabashkata: Tk-03 – massive base point. . . . 652

A.26 Catalogue Tabashkata: Tk-01 – massive base point; Tk-02 – grooved point. 653

A.27 Catalogue Tabula Traiana: Tab-01 – cut-marked bone; Tab-03 – cut-marked bone. . . . 656

A.28 Catalogue Tabula Traiana: Tab-04 – cut-marked bone; Tab-08 – cut-marked bone. . . . 657

A.29 Catalogue Tabula Traiana: Tab-11 – cut-marked bone; Tab-13 – cut-marked bone; Tab-14 – cut-marked bone. . . . 658

A.30 Catalgue Tabula Traiana: Tab-17 – cut-marked bone; Tab-34 – cut-marked bone; Tab-38 – cut-marked bone; Tab-39 – cut-marked bone. . . . 659

A.31 Catalogue Toplja: Tp-01 – detail of antler point's split base found at the base of the proximal fragment. . . . 662

A.32 Catalogue Toplja: Tp-01 – antler point with split base. . . . 663

D.33 Stratigraphic model for Bacho Kiro (code: p. 765). . . . 836

D.34 Stratigraphic model for Willendorf II (code: p. 762). . . . 837

D.35 Stratigraphic model for Geißenklösterle (code: p. 759). . . . 838

D.36 Stratigraphic model for Buran-Kaya III (code: p. 766). . . . 839

D.37 Stratigraphic model for Castelcivita (code: p. 761). . . . 840

D.38 Stratigraphic model for Cavallo (code: p. 764). . . . 840

D.39 Stratigraphic model for El Castillo (code: p. 752). . . . 841

D.40 Stratigraphic model for Fumane (code: p. 760). . . . 842

D.41 Stratigraphic model for Ksar Akil (code: p. 768). 843
D.42 Stratigraphic model for L'Arbreda (code: p. 755). 844
D.43 Stratigraphic model for Labeko Koba (code: p. 753). 845
D.44 Stratigraphic model for Riparo Mochi (code: p. 756). 846
D.45 Stratigraphic model for Isturitz (code: p. 754). 847
D.46 KDE models for Bacho Kiro (code: p. 767) and Mitoc-Malul Galben (code: p. 766). 848
D.47 KDE models for Šalitrena Pećina (code: p. 765) and the Moravian Aurignacian (code: p. 764). 849
D.48 KDE models for the Moravian Bohunician (code: p. 763) and Szeletian (code: p. 763). 850
D.49 KDE models for Willendorf II (code: p. 763) and Geißenklösterle (code: p. 760). 851
D.50 KDE models for Hohle Fels (code: p. 758) and Hohlenstein-Stadel (code: p. 760). 852
D.51 KDE models for Vogelherd (code: p. 760) and Buran-Kaya III (code: p. 767).853
D.52 KDE models for Castelcivita (code: p. 761) and Cavallo (code: p. 764). . . 854
D.53 KDE models for El Castillo (code: p. 753) and Fumane (code: p. 761). . . . 855
D.54 KDE models for Ksar Akil (code: p. 769) and L'Arbreda (code: p. 756). . . 856
D.55 KDE models for Labeko Koba (code: p. 754) and Riparo Mochi (code: p. 757). 857
D.56 KDE model for Isturitz (code: p. 755). 858

List of Tables

4.1 Background: advantages and disadvantages of AMS radiocarbon dating. . . 36

4.2 Background: the first two criteria for assessing the quality of radiocarbon dates, according to Waterbolk (1971). 39

5.1 Methods: pre-treatment protocols with code used at ORAU. 56

5.2 Methods: description of the date codes used at ORAU. 57

5.3 Methods: main pre-treatment methods for bone. ORAU lab codes given in brackets where appropriate. 62

5.4 Methods: list of standard solvent sequences used to remove contaminants from curation environment as applied at ORAU. 63

5.5 Methods: Lemon Mine background standards run with HYP samples for this thesis, and used for HPLC background correction. 70

8.1 Kozarnika: previously obtained radiocarbon dates from Gif-sur-Yvette and Laboratoire Souterrain de Modane. 122

8.2 Kozarnika: previously obtained AMS radiocarbon dates from the RESET project. 124

8.3 Kozarnika: samples for radiocarbon dating from sector III. 126

8.4 Kozarnika: samples for radiocarbon dating from sector I/II. 127

8.5 Kozarnika: new AMS radiocarbon dates on anthropogenically modified bone (ref-no. 3– 38) with archaeological context information, and pre-treatment results. 129

8.6 Kozarnika: new AMS radiocarbon dates on anthropogenically modified bone and humans (ref-no. 39–81) with archaeological context information, and pre-treatment results. 130

8.7 Kozarnika: new AMS radiocarbon dates on anthropogenically modified bone (ref-no. 82–116) with archaeological context information, and pre-treatment results. 131

8.8 Manastira: List of samples shortlisted for radiocarbon dating. 154

8.9 Manastira: new new ^{14}C date of the human radius Man-01 with AF pre-treatment results. 156

8.10 Tabashkata: new AMS radiocarbon dates on osseous points with pre-treatment results. 164

8.11 Temnata: previously published ^{14}C dates from sector TD-I with context information and pre-treatment results. 193

8.12 Temnata: previously published ^{14}C dates from sector TD-II and TD-V with context and treatment information. 194

8.13 Temnata: previously published TL dates on burnt flint, calcite and quartz. 195

8.14 Temnata: samples for radiocarbon dating from sector TD-I. 202

8.15 Temnata: samples for radiocarbon dating from sector TD-V. 203

8.16 Temnata: new AMS radiocarbon dates on anthropogenically modified faunal bone from sector TD-I, with archaeological context information, and pre-treatment results. 205

8.17 Temnata: new AMS radiocarbon dates on anthropogenically modified faunal bone from sector TD-V (pt. 1), with archaeological context information, and pre-treatment results. 206

8.18 Temnata: new AMS radiocarbon dates on anthropogenically modified faunal bone from sector TD-V (pt. 2), with archaeological context information, and pre-treatment results. 207

8.19 Toplja: Radiocarbon dating pre-treatment results for antler point. 241

9.1 Dubočka Kozja: list of anthropogenically modified faunal remains identified with original cultural interpretation. 251

9.2 Dubočka Kozja: previously obtained and new AMS radiocarbon results on anthropogenically modified faunal remains from the 2013 excavation season with archaeological context information, and pre-treatment results. 252

9.3 Tabula Traiana: previously obtained radiocarbon results faunal remains, anthropogenically modified faunal remains, and charcoals with archaeological context information, and pre-treatment results. 263

9.4 Tabula Traiana: list of anthropogenically modified faunal remains sampled for radiocarbon dating with original cultural interpretation. 265

9.5 Tabula Traiana: new AMS radiocarbon results on anthropogenically modified faunal remains with archaeological context information, and pre-treatment results. 266

10.1 Bukovac: massive-based point sampled for radiocarbon dating with context information, %N results and sample weight. 282

10.2 Bukovac: radiocarbon pre-treatment results for the osseous point. 283

10.3 Bukovac: new AMS radiocarbon results on the osseous point. 284

11.1 Bivak: radiocarbon samples – an osseous point and cut-marked bones – with context information. 293

11.2 Bivak: radiocarbon pretreatment results with treatment information, yield after pre-treatment (in mg and wt.%), and %C, stable isotopes and C:N ratio on combustion. 294

11.3 Bivak: new AMS radiocarbon dates on 1 osseous point and 2 cut-marked bone fragments. 295

11.4 Istállóskő: correlation of Pleistocene layers described by Vértes, Vörös, and Ringer. 302

11.5 Istállóskő: published radiocarbon dates obtained in the 1950s and 1960s on charcoal and bone samples from Vértes' excavations. 312

11.6 Istállóskő: published radiocarbon dates on unmodified faunal bone samples from the 2000 excavation. 314

11.7 Istállóskő: AMS radiocarbon dates from 2006/2007 on bone and charcoal samples with contexct information and pre-treatment results. 315

11.8 Istállóskő: list of samples taken for radiocarbon dating with context information and sample weight. 320

11.9 Istállóskő: anthropogenically modified faunal remains that failed radiocarbon pre-treatment. 328

11.10 Istállóskő: new AMS radiocarbon dates on anthropogenically modified faunal remains and osseous points with archaeological context information, and pre-treatment results. 329

11.11 Jankovich: pre-treatment results for the previously failed radiocarbon dating of osseous points by Davies and Hedges (2008) in 2007. Chemistry results obtained from the ORAU internal database. 357

11.12 Jankovich: osseous points sampled for radiocarbon dating, with context information, %N test results and sample weight. 358

11.13 Jankovich: radiocarbon dating pretreatment results for osseous points. . . . 360

11.14 Jankovich: new AMS radiocarbon results for osseous points. 361

11.15 Máriaremete: radiocarbon samples with context information, %N results and weight pre-treated for dating. 370

11.16 Máriaremete: radiocarbon pre-treatment results for anthropogenically modified bone and a human vertebra. 371

11.17 Máriaremete: new AMS radiocarbon results on human remains and anthropogenically modified fauna. 372

11.18 Szeleta: previously published radicoarbon dates on unmodified faunal fragments and charcoals with context and pretreatment information. 379

11.19 Szeleta: split-based points sampled for radiocarbon dating with context information, %N results and sample weight. 381

11.20 Szeleta: radiocarbon pre-treatment results for the split-based point. 381

11.21 Szeleta: new AMS radiocarbon result on split-based point. 381

11.22 Peskő: pretreatment information and results for previously published radiocarbon dates. 392

11.23 Peskő: previously published radiocarbon dates on osseous points, cut-marked bone and unmodified fauna. 392

11.24 Peskő: context information for artefacts sampled for radiocarbon dating. . . 394

11.25 Peskő: pretreatment information and results for newly radiocarbon dated osseous points. 396

11.26 Peskő: new AMS radiocarbon dates for osseous points. Calibration done in OxCal 4.3 (Bronk Ramsey, 2009a) with IntCal13 (Reimer et al., 2013). . 397

12.1 Dzeravá Skala: previously published OSL dates (Davies and Hedges, 2005). 420

12.2 Dzeravá Skala: previously failed radiocarbon dating on osseous points from the EFCHED project (Davies and Hedges, 2005, and ORAU internal database).421

12.3 Dzeravá Skala: previously published AMS ^{14}C dates (Davies and Hedges, 2005) obtained from unmodified mammal bones and one osseous point with context and treatment information. 422

12.4 Dzeravá Skala: list of anthropogenically modified ^{14}C samples with context information. 426

12.5 Dzeravá Skala: list of osseous points tested for nitrogen content, but not sampled for ^{14}C dating. 428

12.6 Dzeravá Skala: new AMS radiocarbon results on anthropogenically modified bone (Der-01 – Der-17) with archaeological context information, and pre-treatment results. 435

12.7 Dzeravá Skala: new AMS radiocarbon results on antrhopogenically modified bone (Der-18 – Der-36) with archaeological context information, and pre-treatment results. 436

12.8 Dzeravá Skala: new AMS radiocarbon results on anthropogenically modified bone (Der-38 – Der-74) with archaeological context information, and pre-treatment results. 437

12.9 Šal'a: Laboratory results from single amino acid radiocarbon pretreatment for the two Neanderthal individuals Šal'a I and Šal'a II. 461

12.10 Šal'a: New AMS radiocarbon measurements for the two Neanderthal individuals Šal'a I and Šal'a II, obtained by single amino acid dating of hydroxyproline. 461

13.1 Local summary: overview of samples that have been dates twice, either as auto-duplicates or for comparing hyrdoxyproline dating (NRC) with results obtained by AG* pre-treatment. 470

14.1 Osseous points: published direct AMS radiocarbon dates (pt. 1/2). 483

14.2 Osseous points: published direct AMS radiocarbon dates (pt. 2/2). 484

14.3 Osseous points: new direct AMS radiocarbon dates (pt. 1/2). 492

14.4 Osseous points: new direct AMS radiocarbon dates (pt. 2/2). 493

15.1 MP/UP: direct radiocarbon dates on human remains (pt. 1/2). 506

15.2 MP/UP: direct radiocarbon dates on human remains (pt. 2/2). 507

1 Appendix: results from mass-spec run no. 4951 (1 May 2017). 606

2 Appendix: results of different treatments or targets of some of the samples that were on mass-spec run no. 4951 for comparison. 607

3 Appendix: results for standards and samples dated for this dissertation from AMS wheel no. 2731, which had high AMS background. 609

4 Appendix: results from mass-spec run no. 4940 (28 March 2017). 610

C.5 Reference Sites: Dates El Castillo (Spain). 818

C.6 Reference Sites: Dates Labeko Koba (Spain). 819

C.7 Reference Sites: Dates Isturity (France). 820

C.8 Reference Sites: Dates L'Arbreda (Spain). 821

C.9 Reference Sites: Dates Hohle Fels (Germany). 822

C.10 Reference Sites: Dates Geißenklösterle (Germany). 823

C.11 Reference Sites: Dates Vogelherd and Hohlenstein-Stadel (Germany). . . . 824

C.12 Reference Sites: Dates Castelcivita and Fumane (Italy). 825

C.13 Reference Sites: Dates Willendorf II (Austria). 826

C.14 Reference Sites: Dates Moravian Bohunician(Czech Republic). 827

C.15 Reference Sites: Dates Moravian Aurignacian and Szeletian (Czech Republic). 828

C.16 Reference Sites: Dates Cavallo and Riparo Mochi (Italy). 829
C.17 Reference Sites: Dates Šalitrena Pećina (Serbia) and Bacho Kiro (Bulgaria). 830
C.18 Reference Sites: Dates Mitoc-Malul Galben (Romania). 831
C.19 Reference Sites: Dates Buran-Kaya III (Crimea). 832
C.20 Reference Sites: Dates Ksar Akil (Lebanon). 833

Part I

Introduction

Chapter 1

Research objectives

1.1 Introduction

The Middle to Upper Palaeolithic shift in Europe (*ca.* 50–35k BP) represents a crucial milestone for human evolution. It encompasses both a population shift from Neanderthals to Anatomically Modern Humans (AMHs), and a cultural shift from Middle to Upper Palaeolithic (MP/UP) industries. Our understanding of the period has been challenged by recent research conducted on western and central European sites, thereby highlighting the importance of a reliable, high-resolution chronology for accurate archaeological interpretations. It is now time to apply new developments in dating sciences to sites further to the east. Of particular importance is the Danube fluvial corridor, which has been proposed as a conduit for AMH dispersal into central and western Europe. Therefore, this dissertation aims to produce a more robust chronological framework for this region, and to test whether an initial AMH dispersal along the corridor can be substantiated.

Both the biological and cultural 'transitions' have been the focus of studies dating back to the formal beginning of archaeology and the study of human evolution (*e.g.* Dawkins, 1916; Kälin, 1946; Newton, 1898). Often, they are treated as two sides of the same coin. AMHs were seen by some

scholars as changing the cultural landscape by introducing portable and decorative art in the form of cave paintings, figurines, musical instruments and jewellery (*e.g.* Mellars, 2005). Others postulated that Neanderthals could also show 'behavioural modernity' (*e.g.* D'Errico, 2003; Langley et al., 2008; Zilhão, 2006). Over the years views shifted from a diffusionist perspective to a replacement model, and, finally, to an appreciation of the complexity of the 'transitional mosaic'.

While genetics and radiocarbon dating have demonstrated a period of overlap between Neanderthals and AMHs (*e.g.* Fu et al., 2015, 2014; Higham et al., 2014), the nature of AMH spread into Europe, and their co-existence with, and the subsequent extinction of, Neanderthal populations is still subject of debate. Any causal interpretation requires a robust chronology in order to correlate technocomplexes, skeletal remains and environmental records. The most widely used absolute dating method for this period is radiocarbon dating. Its improved pre-treatment protocols and Bayesian modelling are now increasingly applied at western, central and southern European localities (*e.g.* Benazzi et al., 2011; Higham et al., 2012, 2014; Wood et al., 2014), as well as in the Levant (*e.g.* Douka et al., 2013; Rebollo et al., 2011).

At the same time, robust dating in other territories, *e.g.* the Zagros Mountains (Becerra-Valdivia et al., 2017), remains rare. More importantly, one of the regions that has yet to benefit from the developments in dating sciences and the application of Bayesian modelling approaches is eastern Europe. This includes the key area of the Danube fluvial corridor, which has been hypothesised as one of the conduits for early modern humans into central and western Europe (see Conard and Bolus, 2003).

This dissertation aims to tackle this disparity and improve the absolute chronology for the MP/UP biocultural shift along the Danube, thereby creating the evidence base necessary to begin testing the Danube corridor hypothesis and to create an improved understanding of how AMHs and different cultural complexes may have moved along the corridor.



Figure 1.1: Introduction: map showing location of the river Danube, which cuts through major mountain ranges and provides a corridor from the black sea to central and western Europe.

1.2 Danube corridor hypothesis

To address the central question of which route AMHs used to arrive in central Europe, Conard and Bolus (2003) used the 'Aurignacian' technocomplex as a proxy. It was chosen for its close connection to symbolic behaviour and the AMH fossil record. By contrast, older technocomplexes in the area (Mousterian and *Blattspitzen*[1] assemblages) were associated with Neanderthals and the Middle Palaeolithic.

Based on this premise, they developed two competing models. In the **Danube corridor hypothesis** AMHs arrived in central Europe with the Aurignacian technocomplex after a rapid migration via the Danube Valley

[1]This is a specific southern German interpretation of the *Blattspitzen* assemblages. In other areas, these leaf-point industries are often classified as 'transitional' rather than Middle Palaeolithic and their authorship is highly debated (see chapter 3).

(see fig. 1.1). In contrast, the ***Kulturpumpe* model** saw the development of the 'Aurignacian' in central Europe, more specifically in the Swabian Jura, from where it subsequently expanded. As possible driving factors for the latter model, Conard and Bolus (2003) listed (a) competition between archaic and modern humans, (b) cultural innovation as a reaction to climatic stress during OIS3, and (c) AMH internal socio-cultural developments.

Both models were based on the observation of significantly older dates for Early Aurignacian assemblages and AMH from southern Germany, with notable sites such as Vogelherd, Hohlenstein-Stadel, Geißenklösterle and Hohle Fels (Bolus and Conard, 2006; Conard and Bolus, 2003). The very early dates for Geißenklösterle, horizon III, were subsequently supported by Higham et al. (2012). In addition, sites in Lower Austria, such as Willendorf II (cultural layer 3), may also be contemporaneous (Haesaerts and Teyssandier, 2001; Nigst et al., 2014).

Earlier dates from the Bulgarian sites of Temnata Dupka and Bacho Kiro have been used to suggest a trajectory up the Danube. However, these would only present start points, as both of these sites are located in the lower Danube. Furthermore, their lithic attribution have been criticised, and are no longer seen as diagnostic Aurignacian (Conard and Bolus, 2003). Nonetheless, the Danube corridor is still seen as the fastest and easiest route to move westwards, as seen in its frequent implicit and explicit use in arguments and on migration maps (*e.g.* Kozłowski, 2006; Mellars, 2011).

1.3 Research aim

While both expansion models fit the archaeological and chronometric evidence presented by Conard and Bolus (2003), testing these hypotheses will only become possible if a reliable chronology for the middle and lower Danube area exists. At present, even localised dating in eastern Europe is limited. In addition, the spatio-temporal distribution of industries other than the Aurignacian requires investigation.

If the *Kulturpumpe* model is correct (and the Early Aurignacian is an AMH industry), it is expected that AMHs arrived in central Europe prior to the development of the Aurignacian, thus leaving skeletal and/or cultural remains pre-dating the Early Aurignacian sites of southern Germany. The hypothesis is refuted if other regions reveal an older Early Aurignacian presence.

Testing the migration patterns within the Danube valley is more demanding. First, it requires that the Danube corridor as a conduit of AMH expansion has to be initially separated from that of an Aurignacian expansion. This avoids circularity in arguments connecting the Aurignacian to the initial AMH migration, and it allows for the visualisation of possible stages of Aurignacian development along the corridor or elsewhere Second, any interpretation is dependent on dating resolution and migration speed. In cases where the migration period is longer than the dating uncertainty, the expansion trajectory should follow the age distribution from old to young. Faster patterns of movement may lead to observed contemporaneity at locations along the Danube valley. However, the chance that an entire lack of earlier or contemporaneous evidence along the corridor is the result of a very speedy migration is remote. Some contributing factors to consider would be: (a) very small group of people, (b) very low excavation density, (c) no use of diagnostic artefacts, (d) typological misidentifications, (e) preservation issues, and (f) high dating uncertainty or low reliability.

Therefore, this dissertation sets out to improve the chronology of the Middle to Upper Palaeolithic biocultural shift along the Danube fluvial corridor, and analyse the resulting spatio-temporal patterns of skeletal remains and technocomplexes – including late MP, 'transitional' and early UP industries.

1.4 Method choice

Radiocarbon dating is the most common absolute dating method applied to the period of interest. Despite the challenges that dating at the detection

limit poses, it provides by far the highest chronological resolution. In order to increase precision and accuracy, only material with a direct connection to human activity was sampled. Additionally, pre-treatment strategies considered factors such as collagen preservation and possible contamination sources very carefully, before selecting the most adequate and up-to-date protocol. Furthermore, the research focused both on deep stratigraphies and diagnostic artefacts – especially 'Aurignacian' osseous projectile points. Subsequent data analysis incorporated extensive Bayesian modelling with outlier analysis and sensitivity testing – and the robustness of archaeological priors was independently verified using radiocarbon specific KDE modelling.

This thesis demonstrates that the combination of all these precautions as well as a critical evaluation of the published record are essential to providing a robust chronological dataset. Moreover, this unbiased but detailed approach to the archaeological record will allow the chronology to be adaptable to future insights into cultural or biological associations.

Chapter 2

Thesis structure

There are six parts to this thesis: I Introduction, II Background, III Methods, IV Site Analysis and Chronologies, V Regional Chronologies, and VI Conclusions. In part I, the research objectives (chapter 1) and the thesis structure (chapter 2) are presented.

Part II gives an overview of the background to the time period of interest and the history of the dating method applied. Chapter 3 presents the status of research into the Middle to Upper Palaeolithic (MP/UP) biocultural shift, introducing evidence from archaeology, genetics, osteology, dating and the environment. In contrast, chapter 4 offers a brief history of radiocarbon dating, reviewing crucial developments that made the method applicable to the period of interest.

Part III elaborates on the methods applied in this dissertation. Chapter 5 focuses on radiocarbon dating, sampling, screening, pre-treatment, AMS measurement, background corrections and quality control indicators. Afterwards, chapter 6 concentrates on chronometric analysis tools, such as calibration, Bayesian analysis, and KDE modelling.

Part IV is the most extensive segment of this dissertation. It briefly elaborates on the site selection process in chapter 7, before introducing each dated site in chapters 8 to 12. The sites are grouped according to their modern

country affiliation, and each of these chapters begins with a reflection on the present archaeological record of the MP/UP biocultural shift, and a discussion of the suitability of these sites for radiocarbon chronology building. The individual sections subsequently focus on each of the dated sites. First, they provide background information on location, research history, stratigraphy and previous dating. Second, the new radiocarbon dating conducted for this dissertation is presented and assessed, including specific sample selection, pre-treatment, results and quality control. Where appropriate, the composition of Bayesian and KDE models are described. The last section brings all new information together in a discussion and interpretation of the archaeological record in light of the dating and modelling work conducted as part of this project. Finally, chapter 13 provides a selective discussion and summary of some of the observations made during the site specific sample processing, analysis, and chronology building. Worth noting are the more in-depth investigations of the trends and anomalies in radiocarbon pre-treatment and dating results in subsection 13.1.

Part V uses the radiocarbon dataset created for this project in conjunction with reliable published results to investigate the spatio-temporal distribution of archaeological technocomplexes, and their possible authors, along the Danube fluvial corridor and beyond. Chapter 14 thereby focuses on the spread of osseous projectile points (most commonly seen as diagnostic of the 'Aurignacian'). Chapter 15 subsequently uses the direct dating of human remains and indirect dating of lithic technocomplexes during the MP/UP biocultural shift to visualise changes in distributions of material cultures and populations, thus testing the Danube corridor hypothesis and the *Kulturpumpe* model.

The thesis is concluded in part VI. Chapter 16 provides a summary of the findings. It highlights their impact on the Danube corridor hypothesis, the interpretation of the spread of AMH, and the role of the 'Aurignacian' osseous projectile point industries for the MP/UP biocultural shift. Chapter 17 subsequently suggests future research avenues to further improve our understanding of this crucial time period in human biocultural evolution.

Part II

Background

Chapter 3

The Middle to Upper Palaeolithic biocultural shift

The Middle to Upper Palaeolithic biocultural shift is seen as a period in human biocultural evolution with culturally and biologically homogeneous start (Neanderthal/MP) and end points (AMH/UP), which encompass a stage of great regional biocultural diversity (the 'transition'). In Europe, the discussion is often framed in the light of either an AMH expansion, or the demise of Neanderthals, and the phenomenon is alternately explained with a focus on cultural, biological or environmental arguments. Therefore, any study of this shift requires an understanding of the interconnectedness of technocultural expression and human populations, as well as knowledge of some of the environmental conditions of the period.

However, before delving into the current archaeological, genetic and environmental evidence, it is worthwhile to briefly visit some of the underlying concepts that such research follows in the first place. This includes temporal and spacial resolution of the data, and the tracking of human migrations via lithic and osseous industries.

The limiting factor for temporal resolution is the dating error, which is comprised of the error in obtained age and the error in association of dated material to event of interest (for details see 4.3.1). Radiocarbon dating is the

most frequently used method for establishing absolute chronologies. This is a direct result of ^{14}C dating both offering a diverse set of sample types that can easily be connected to the archaeological record, and providing better precision than most other available techniques. By contrast, the very high precision of Uranium-Thorium (U-Th) dating is restricted to favourable speleothem (*e.g.* Southon et al., 2012) or coral growth (*e.g.* Durand et al., 2013), which is less commonly found within the archaeological record – and not available in the key sites of the Danube fluvial corridor. Optically stimulated luminescence (OSL), Thermoluminescence (TL) and similar techniques may more frequently be connected to human activity than U-Th dated material. However, their precision is often lower than radiocarbon dating[1] and their dates less directly related to singular human activities. Therefore, these methods are frequently used to (a) independently test dating consilience, (b) date sites with poor or no organic preservations, and (c) analyse sections that date older than the reliable detection of radiocarbon.

As a consequence, the temporal resolution in the time period of interest may be simplified to the radiocarbon dating error, which, under favourable conditions, is $<$ 1000 years (prior to modelling), though often $>$ 500 years. The terms 'fast' or 'slow' developments (*e.g.* migration, or cultural change) have to be understood under these conditions. A fast, but detectable, change would still span 15-25 generations.

The emergence and spread of the Upper Palaeolithic has been framed either as a linear trajectory or a phenomenon with multiple origins (*e.g.* Bar-Yosef, 2007; Davies, 2001; Higham et al., 2012; Hublin, 2012; Mellars, 2006; Teyssandier, 2005). The illustration of migration trajectories from Mellars (2011, fig. 2) exemplifies how overview studies combine dating and cultural attributions (see fig. 3.1). Even with the inclusion of larger numbers of sites, the data points are sparsely distributed, and interpretation heavily depends on cultural categories. Areas with insufficient data are often bridged by two (untested) assumptions: (1) *ex oriente lux* (see discussion in Teyssandier,

[1] High-precision obtained from multiple analyses of different single aliquots is also significantly more labour and cost intensive than radiocarbon analysis.

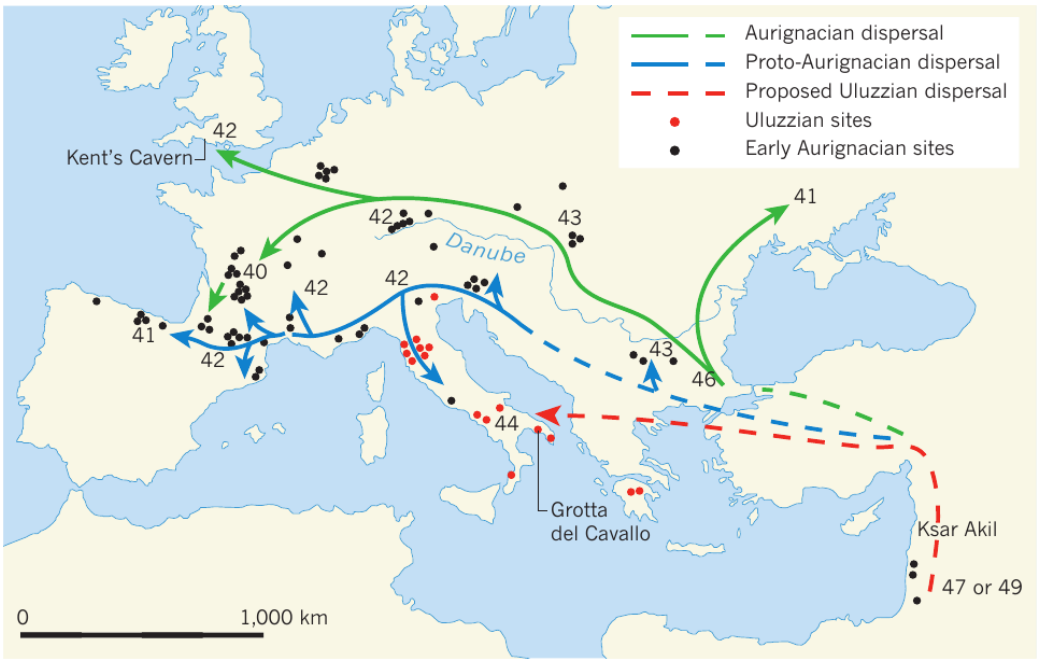


Figure 3.1: Background: spread of archaeological industries associated with AMHs (Uluzzian, Proto-Aurignacian, and Aurignacian) according to Mellars (2011, fig. 2). Numbers reflect expected time of appearance, given in years cal BP and largely based on radiocarbon dating.

2006), and (2) AMH strongly prefer to travel along rivers and coasts. However, those assumptions generally contradict each other. If AMHs do prefer open landscapes, as Henry et al. (2017) suggests, the pathway through the mountainous areas of present-day Turkey, Greece and the Balkans appears problematic. By contrast, if early AMHs preferred the mountains, the Danube corridor dispersal will require more actual data points to support it, as the use of the river valley would represent a change in behaviour.

3.1 Archaeological evidence

The archaeological technocomplexes relevant to the discussion of the Middle to Upper Palaeolithic transition are described below, and can be simplified into three main categories: Middle Palaeolithic, 'transitional', and Upper Palaeolithic. The MP assemblages are largely flake based technologies, while

the UP industries are predominantly blade and bladelet based. On the basis of associated skeletal evidence, it is assumed that this cultural division is synonymous with a division between Neanderthal and AMH populations. By contrast, the 'transitional' industries often combine characteristics from both MP and UP, and their authorship is frequently debated.

3.1.1 Middle Palaeolithic

The late Middle Palaeolithic stages in Europe are represented by Mousterian and Micoquian assemblages, allowing for some local variation and differentiation in flake technology.

The **Micoquian** was first described by Hauser (1906, 1916). Its characteristic bifacial tools have an asymmetric contour, a thicker 'back', and show frequent sharpening of the cutting edge, which led to their German classification as '*Keilmessergruppe*'[2] (Bosinski, 1967). They concentrate in central Europe, though have been in the past mistaken for bifaces belonging to the **Mousterian of Acheulian Tradition (MTA)**, which are oval and flat and cluster in western Europe (Otte, 2017; Peyrony, 1930). The naming of the MTA is unfortunate, as their bifaces have little in common with the much older, pointed, and symmetric bifaces of the Acheulean (Otte, 2017).

The **Mousterian** industry was first defined at Le Moustier (France) by Peyrony (1930), and includes Levallois blanks, side-scrapers, and notched denticulated implements (Bordes, 1961, 2000). On the basis of which characteristic flake type was dominant, the industry was subdivided into (1) Levallois, classical or **typical Mousterian**, (2) MTA (see above), and (3) discoidal or **denticulate Mousterian**. Unifacial artefacts are the norm in Mousterian assemblages – with the exception of the MTA where there is a co-occurrence of bifacial and unifacial tools (Kozłowski, 2014). According to Bayesian modelling of radiocarbon dates by Higham et al. (2014), the Mousterian in Europe ends between 41.0–39.3 cal BP (at the 95% confidence interval).

[2] Translates to 'industry with wedge shaped knives'.

3.1.2 'Transitional' industries

Several transitional technocomplexes have been described for different regions in Europe. These include the Châtelperronian in south-western France, the Uluzzian in Italy, the Lincombian-Ranisian-Jerzmanowician (LRJ) in northern Europe (found from Poland to the British Isles), the Jankovichian in Hungary, the Szeletian in Moravia and north-western Hungary, the Bohunician in Moravia, and the Bachokirian in Bulgaria. While they differ in techno-cultural expression, they all share the presence of both MP and UP features and many seem to produce characteristic 'leaf-shaped' points. The latter can lead to confusion in lithic attribution where only the description 'leaf-shaped' is used as a diagnostic feature. A more detailed analysis of technology, morphology and material can, however, distinguish between the different 'transitional' technocomplexes. In the following, some of the most striking features of the industries relevant to this dissertation are presented.

Châtelperronian

Since the description of the Châtelperronian by Breuil (1911), the nature and origin of this technocomplex found in southern France and northern Spain has been heavily debated. It is characterised by a volumetric blade reduction, curved back blades, and end-scrapers. But it is also sporadically found with bladelets, bone tools and ornaments. Ruebens et al. (2015) argue in favour of a local development from the Mousterian on the basis that both blank selection and edge modification of backed knives are conceptually similar to those found in the preceding Mousterian, whereas this concept is largely absent in other transitional industries. Roussel et al. (2016) further draw connections to the Proto-Aurignacian. However, they interpret the relationship as cultural diffusion without social intimacy, because the retouched bladelets resemble Proto-Aurignacian finds in form only – not in production.

The Châtelperronian has been found with Neanderthal skeletal remains at the Grotte du Renne and Saint Césaire (France). Therefore, Neanderthals

are presently seen as the authors of this industry dating to 45–40k cal BP (Higham et al., 2010, 2014; Hublin et al., 2012).

Uluzzian

The type site for the Uluzzian is Cavallo in southern Italy (Palma di Cesnola, 1989). It uses both unipolar and bipolar knapping to produce a flake dominated technology that shows variability in the reduction sequence (De Stefani et al., 2012; Moroni et al., 2013; Palma di Cesnola, 1989, 1993; Peresani, 2008). The type fossil is a geometric crescent-shaped backed piece named 'lunate' (originally '*semi-luna*' in Italian). Its production does not follow a fixed *chaîne opératoire*, and the resulting artefact can sometimes be of microlithic dimensions (Palma di Cesnola, 1993). In the Uluzzian, lamellar débitage is rare, and small blades and bladelets are often irregular (Gambassini, 1997; Riel-Salvatore and Negrino, 2009). Additionally, the Uluzzian encompasses a worked bone industry (d'Errico et al., 2012; Ronchitelli et al., 2009), marine shell beads, and the use of ochre and limonite pieces (Palma di Cesnola, 1989).

A tooth from the Uluzzian layers at Cavallo has revived the debate on the authorship of this particular technocomplex, as reanalysis of the specimen led Benazzi et al. (2011) to reclassify it as AMH. Zilhão et al. (2015) subsequently questioned the integrity of the find context. By contrast, the dating was not contested, and places the Uluzzian at 45–40k cal BP (Douka et al., 2014; Higham et al., 2014) – contemporaneous with the Châtelperronian.

Szeletian

The Szeletian was defined by Prošek (1953) and named after Szeleta cave in the Bükk mountains (Hungary). Its diagnostic artefact is a bi-facially flaked leaf-point, with a reduction sequence that appears to emphasise thinning, while maintaining length and width (Nerudová and Neruda, 2017). Vestiges of Levallois flaking, and Mousterian side-scrapers are common. While

some connections to the Muselievo-Samuilitsa circle in Bulgaria have been proposed, Markó (2013b) emphasises that those leaf-points were made on flint-plaquettes, and show more blade-like proportions and no ventral thinning.

However, as Markó (2013b) rightly points out, the naming is misleading. While loosely 'leaf-shaped' lithics were indeed discovered at Szeleta, the site does not show the characteristics of the Szeletian technocomplex. Instead, the terminology is now largely used for lithic assemblages found in Moravia (covering parts of the Czech Republic and Slovakia), and they date to between *ca.* 46–39k cal BP (Škrdla, 2017). It has been proposed that the Szeletian developed from the local Micoquian, and is therefore a Neanderthal derived cultural expression (Allsworth-Jones, 1986; Kaminská et al., 2011; Oliva, 1991; Svoboda, 2005; Valoch, 2000).

Jankovichian

The Jankovichian was proposed by Gábori-Csánk (1993) as a category for some of the transdanubian assemblages in Hungary, which were previously interpreted as early Szeletian. It uses Levallois technique in primary flaking, and its diagnostic artefact is a Levallois point with ventral thinning – similar to some of the lithics found in the central European MP. Furthermore, a Jankovich type point often shows a faceted butt and a large bulb. The bidirectional Levallois blade points are similar to those typically attributed to the Bohunician, while some of the tools with flake-like proportions remind of material found in the Moravian Szeletian. Those blade points with thinning on both the proximal and distal part show parallels to the Jerzmanovice type points. Additionally, Markó (2013b) sees a raw material link to the north-eastern Carpathian basin.

Only one 'largish' assemblage is known, namely from an old excavation at the eponymous site of Jankovich. However, some have suggested that the assemblage consists of material from several discrete cultural levels (*e.g.*, L. Vértes cited in Markó, 2013b). Individual diagnostic tools have been located

in the Pilis and the Gerecse mountains (north-eastern Transdanubia). No reliable radiocarbon dates are available.

Bohunician

The Bohunician is named after the suburb of Brno, where the industry was first discovered (Oliva, 1981; Valoch, 1976). The technocomplex was subsequently defined using Brno-Bohunice, Stránská skála and Ondratice I (Škrdla and Tostevin, 2005; Svoboda, 1980; Svoboda and Bar-Yosef, 2003; Valoch, 1976). It is based on an evolved Levallois technology, *i.e.* it uses a more volumetric approach compared to classical Levallois debitage. The technological focus lies on a serial production of Levallois points, which creates blades as secondary products (Škrdla, 2003b; Škrdla and Rychtaříková, 2012). Both flakes and blades were subsequently used for tool production, which included both MP and UP types – though no carinated end-scrapers or carinated burins. The bifacially retouched leaf-shaped points maintain the theme of the period. Bladelet technology is absent. Škrdla (2013, p. 4) lists the most important features as "*elongated Levallois blanks (both points and blades), precise and concave faceting of the striking platform, bidirectional (including opposed directional) dorsal scar pattern, presence of crested blades, and bidirectional cores*". Furthermore, a single marine shell was found in a Bohunician assemblage from Líšeň (Škrdla et al., 2011).

Based on radiocarbon determinations, the Bohunician dates to around 48–34k cal BP (Škrdla, 2017). It shares characteristics with industries from Boker Tachtit in the Near East (Škrdla, 2003b), Kulychivka in Western Ukraine (Demidenko and Usik, 1993; Meignen et al., 2004), and Kara Bom in Siberia (Derevianko and Rybin, 2003; Zwyns et al., 2012). In the absence of skeletal evidence for the Bohunician, an AMH origin was postulated based on the intrusive character of the technology and AMH association with analogous industries in the Near East (Hoffecker and Klein, 2009; Hublin, 2012; Nigst, 2012; Richter et al., 2009; Škrdla, 2003a,b; Svoboda and Bar-Yosef, 2003).

Bachokirian

The Bachokirian technocomplex was found in layer 11 at Bacho Kiro (Bulgaria), which remains the only known assemblage. It represents a clear break to the underlying Mousterian industry in terms of raw material procurement, technology and morphology (Kozłowski, 1979, 1982; Kozłowski, 1999). This is because it demonstrates a shift from local to imported flint, a more volumetric reduction strategy and an increasing use of blades. Links to UP industries – specifically the Aurignacian – were seen in the presence of retouched blades, stepped retouch, nosed end-scrapers (Kozłowski, 1992), and the use of a volumetric core reduction (Kozłowski, 1999). However, Teyssandier (2006) emphasises that no blade cores are known from the Bachokirian, and that the blades found indicate a bidirectional exploitation using direct hard hammer percussion – not the unidirectional concept with soft hammer typical of the Aurignacian. As a result, Teyssandier (2008) lists the Bachokirian as a possible expression of the IUP in Bulgaria.

Initial Upper Palaeolithic (IUP)

The Initial Upper Palaeolithic is characterised by a blade production that exploits both Levallois and more classical Upper Palaeolithic methods. However, unlike later UP technologies, it only applies direct hard-hammer percussion. In line with other 'transitional' industries, point production appears to be an essential feature. Skeletal evidence from Ksar Akil suggests that the IUP is associated with AMH (Douka et al., 2013).

The term IUP was initially used to describe the assemblage of level 4 at the site of Boker Tachtit, and the earliest UP levels at Ksar Akil (Marks and Ferring, 1988). It was subsequently expanded by Kuhn et al. (1999) to include Emirian assemblages from the eastern Mediterranean and Near East, which also showed mainly UP tool forms made using a combination of Levallois and prismatic core reductions. Teyssandier (2008) further includes individually described industries such as the Bachokirian (Bulgaria) and the

Bohunician (Moravia), and Tsanova (2006) proposes to also use the term for layer VI from Temnata. However, this dissertation will not go as far as Sinitsyn (2003) and Arrizabalaga et al. (2003), who applied the name to any first appearance of UP industry in a region, irrespective of the assemblages' techno-morphological character. IUP as a purely chronological marker would void any techno-cultural interpretations, as Kuhn and Zwyns (2014) discussed. For culturally undetermined assemblages with mixed MP/UP character, the description as an Early Upper Palaeolithic (EUP) industry will be used instead.

3.1.3 Upper Palaeolithic

The beginning of the Upper Palaeolithic proper is normally seen as the emergence of blade and bladelet dominated Aurignacian technocomplexes, giving the sometimes false impression that this is a homogeneous and uniform pan-European development. For this dissertation, especially the Proto-Aurignaican[3], and the Early Aurignacian[4] are of importance. They are supplemented by more localised industries, such as the Olschewian and the Kozarnikian. Gravettian appears only after the Aurignacian, but is nonetheless included here, as some of the sites in this thesis contain Gravettian levels used for modelling.

Aurignacian

The original Aurignacian categories were defined by Peyrony (1933) using western European sites, and the Proto-Aurignacian was subsequently introduced by Laplace (1966). Characteristic of both the Proto-Aurignacian and the Early Aurignacian are the use of soft hammer percussion, as well as the production of Dufour bladelets, carinated and nosed end-scrapers, and osseous projectile points. At western and central European sites, unidirectional

[3]Often also referred to as Aurignacian 0, Pre-Aurignacian I, or Archaic Aurignacian.

[4]Listed as Aurignacian I in the French nomenclature by Peyrony (1933), but also known as Classic Aurignacian or *Aurignacien ancien*.

blade production is dominant (Teyssandier, 2006). In the Aquitaine basin, the Proto-Aurignacian stratigraphically precedes the Early Aurignacian assemblages. Banks et al. (2013) interpreted the shift as a climate adaptation to the Heinrich 4 event. However, improvements in absolute dating not only suggest temporal coexistence, but also that cultural developments pre-date Heinrich 4 (Higham et al., 2012; Nigst et al., 2014).

The **Proto-Aurignacian** is rich in rectilinear Dufour bladelets (sub-type Dufour) (*e.g.* Demars and Laurent, 1989), which are longer than the Early Aurignacian types. Blades tend to be lighter, and often unretouched, while the unidirectional pyramidal bladelet cores are often on flakes. The most important sites are in the Mediterranean, with L'Arbreda and Morin in Spain; Arcy-sur-Cure, Esquicho-Grapaou, Isturitz, La laouza, Le Piage, and Mandrin in France; and Fumane and Mochi in Italy (Teyssandier, 2006). Radiocarbon dating places the beginning of the Proto-Aurignacian at L'Arbreda at ca. 42–41.5k cal BP (Wood et al., 2014), and at 42.7–41.6k cal BP at Riparo Mochi (Douka et al., 2012).

The **Early Aurignacian**'s distinct feature is the use of carinated end-scrapers for producing small, curved-profile bladelets (Bon, 2002; Sonneville-Bordes, 1960). Furthermore, the assemblages contain simple end-scrapers, and retouched blades. The production of split-based points is frequently used as a leitfossil, but others have argued that they can also be found with Proto-Aurignacian assemblages (*e.g.* Szmidt et al., 2010a). The technocomplex has a strong presence in the Aquitaine basin and the Swabian Jura, and appears as early as 42,500 cal BP at Geißenklösterle (Higham et al., 2012), and possibly as early as 43,500 cal BP at Willendorf II (Nigst et al., 2014) – therefore prior to the Heinrich 4 cold phase.

Already Hahn (1977) noticed that the clear **distinction between the Proto-Aurignacian and Early Aurignacian** is not directly applicable to central European sites. Furthermore, Hauck et al. (2018) demonstrated that the Aurignacian in the Carpathian shows significantly more variability in tool types, and greater flexibility in core reduction strategies. Investigating technological differences, some researchers suggested that a continuous

reduction sequence from blade to bladelets could be used to more reliably distinguish the Proto-Aurignacian from the Early Aurignacian (Bon, 2002; Bon and Bodu, 2002; Teyssandier, 2006, 2007). However, others found clear evidence of bladelet focused production at Proto-Aurignacian sites throughout Europe (Bataille et al., 2018; Falcucci et al., 2017; Tafelmaier, 2017). Furthermore, Falcucci et al. (2017, p. 34) found "*that no unique technological characteristics are restricted to either of the two techno-complexes*". Similarly, Tafelmaier (2017, p. 203) concluded that "[a]*lthough quantitative differences in the applied reduction concepts could be found, the main outcome is that none of the technological nor of the typological parameters reliably proved to be sufficient to differentiate the two postulated Aurignacian phases*". As a consequence, while the distinction between the Proto- and Early Aurignacian is maintained for this dissertation, it is unlikely that they represent (just) two culturally distinct groups or two chronologically discrete phases of techno-cultural development[5].

Olschewian

The Olschewian was proposed by Bayer (1929) as a term to describe the phenomenon in Hungary (and adjacent regions), of finding supposedly 'Aurignacian' osseous projectile points – especially massive-based points (MBPs) – in the absence of diagnostic Aurignacian lithics. The term has become largely obsolete in the scientific literature, but is often maintained at museums. Furthermore, this dissertation will show that the concept of an osseous projectile point industry that is independent of the immediate association with the 'Aurignacian' may significantly contribute to our understanding of the developments during the MP/UP biocultural shift.

[5]For a more detailed discussion of the nature of the Proto-/Early Aurignacian distinction see Bataille et al. (2018) and Tafelmaier (2017).

Kozarnikian

Ancient Kozarnikian is the name presently used for the archaeological level VII at Kozarnika (Bulgaria). The lithic assemblage described by Sirakov et al. (2007) is characterised by a bladelet technology that appears to typologically and technologically precede the Gravettian assemblages[6] at the site, and which is otherwise locally unknown. The bladelet tools include regular backed pieces as well as bladelets with a thin, abrupt or semi-abrupt, retouch (either bilaterally convergent or alternating). Sirakov et al. (2007) see analogies in the archaic Ahmarian from Levant, and the Proto-Aurignacian from southern Europe. The assemblage appears to occupy the relative chronostratigraphic position that the Early Aurignacian would normally hold at central and western European sites.

Gravettian

The Gravettian was first identified at the site of La Gravette in France (Lacorre, 1960). The industry is characterised by burins prevailing over endscrapers, as well as the presence of backed side blades, laterally retouched blades and microlithic tools (see typelist Demars and Laurent, 1992). Gravettian lithics are sometimes found with a variety of Venus figurines throughout Europe. The type fossils for eastern central Europe are Gravette points, microgravette point, backed bladelets, pointed retouched blades, *fléchettes*, and shouldered points (*e.g.* Lengyel et al., 2016). A seemingly uniquely eastern European (including eastern central European) manifestation of the technocomplex is the **Gravettian with bifacial leaf points** (*e.g.* Svoboda and Simán, 1989) which can be found all the way from Slovakia to the Balkans.

[6] These are often referred to as *Kozarnikien moyen* (levels IV–VI) and *Kozarnikien supérieur* (levels 0I–III), see subsection 8.1.1.

3.2 Genetic evidence

Since the first ancient mtDNA sequence obtained on a Neanderthal by Krings et al. (1997), genetics has challenged the assumed relationship between Neanderthals and AMH, and changed our understanding of the Middle to Upper Palaeolithic migration patterns. It is now clear that interbreeding occurred, at different times in different places. A 45,000 year old AMH from Ust'-Ishim in Siberia has a Neanderthal ancestor that lived around 7,000–13,000 years earlier (Fu et al., 2014), while the genome of a 37,000–42,000 year old AMH specimen from Peștera cu Oase in Romania showed evidence for a Neanderthal ancestor only four to six generations back (Fu et al., 2015).

Moreover, genetics has revealed a previously unknown type of human in Siberia, named the Denisovan. They did not contribute to the genome of modern day Eurasians, but that of Melanesians (Reich et al., 2010). It therefore appears that Denisovans did not migrate into Europe. Nonetheless, multiple interbreeding events between Denisovans, Neanderthals, and AMH are recorded in Siberia (Prüfer et al., 2014; Slon et al., 2018), thus questioning the validity of describing these groups as different human species. However, the three categories have remained useful for differentiation in research.

There appears to be low genetic diversity in archaic human populations and mating close relatives would have been common, as demonstrated by Meyer et al. (2012) for Denisovans, and by Prüfer et al. (2014) for Neanderthals. This would have had severe consequences for population dynamics and the Neanderthal population sizes AMHs would have encountered on their migrations. Prüfer et al. (2017) estimate that the low heterozygosity is indicative of populations as small as 3000 members. However, they also point out that there is less interbreeding found in the Vindija specimens.

Clues on AMH migrations can also be found in the genome. Olivieri et al. (2006) used modern DNA to demonstrate a change in genetic make-up of the AMH in the Levant at around 45–40k cal BP, tracing a return of EUP populations from the Mediterranean. In contrast, Kuhlwilm et al. (2016) found evidence in ancient DNA that supports an earlier AMH migration into

Asia. However, this AMH genetic contribution is absent in Neanderthals from Europe, and in Denisovans.

As with radiocarbon dating, genetic analysis has led to the reclassification of several fossils. For example, eight of the eleven Neanderthal remains from Riparo Mezzena turned out to not be Neanderthal at all: four were AMH, another four belonged to animals (Talamo et al., 2016).

3.3 Environmental evidence

Environmental conditions can have a significant impact on human behaviour, thus possibly influencing population dynamics, tool manufacture and migration patterns. As a result of the large spatial and temporal scale of the MP/UP biocultural shift, climate conditions have featured prominently in the debate on why and how the biological shift came about.

During the 20,000 years between 55–35k cal BP (see fig. 3.2), the Greenland ice-cores reveal eight warm periods (GIS 7–14) (Andersen et al., 2006). Additionally, two Heinrich Events (H4, H5) caused prolonged cold episodes, the Laschamp Magnetic Excursion weakened the earth's magnetic field for around one thousand years (Svensson et al., 2006), and the Campanian Ignimbrite (CI) eruption is expected to have led to adverse conditions throughout most of eastern Europe (Pyle et al., 2006).

Banks et al. (2013) argued that the UP was an adaptation to the H4 cooling event. This conclusion has been criticised by Higham et al. (2013) for poor radiocarbon modelling, by Ronchitelli et al. (2014) for the Proto-Aurignacian/Early Aurignacian dichotomy, and by Hauck et al. (2018) for the assumption that life throughout Europe would have been very similar.

Similar arguments are used when discussing the influence of the CI eruption. It is the largest recorded Quaternary explosive event, and Fedele et al. (2008) were not alone in assuming that it would have caused major changes in human biocultural expressions (*e.g.* Fitzsimmons et al., 2013; Hoffecker

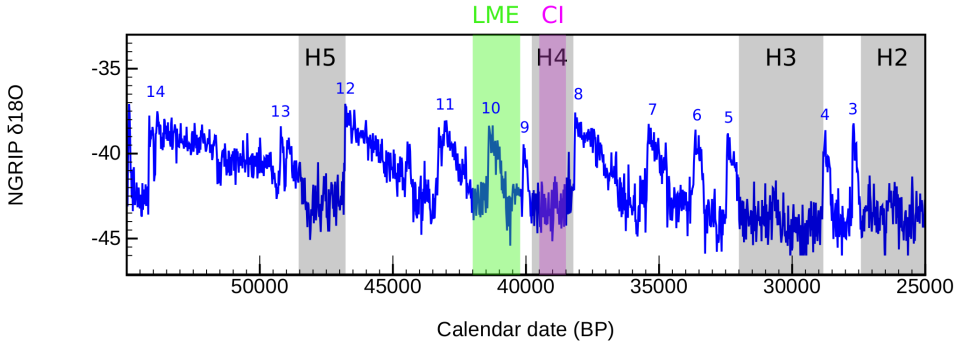


Figure 3.2: Background: NGRIP climate record (Johnsen and North Greenland Ice Core Project members, 2004) for the period 55–25k cal BP with Greenland Interstadials numbered (**blue**). Approximate timings highlighted for the CI eruption after Giaccio et al. (2017) (**magenta**), the Heinrich events H2 to H5 (**grey**), and the Laschamp magnetic excursion (**green**).

et al., 2008; Morley and Woodward, 2011). However, it can no longer be seen as the main driving factor for the development of UP industries, as it post-dates their appearance at many archaeological sites (Lowe et al., 2012) – especially at eastern European sites, where the impact of the CI would have been most severe.

In contrast, the Laschamp magnetic excursion has been referenced mainly as a cause of radiocarbon calibration issues rather than directly impacting human behaviour (Conard and Bolus, 2003; Giaccio et al., 2006). Fluctuations in ^{14}C concentration have been observed in the Tyrrhenian Basin foraminifera record (Giaccio et al., 2006), and the Bahamas speleothem record (Beck et al., 2001). However, Beck et al. (2001) list perturbations in oceanic turnover as an important contributor, and none of the other large datasets used for the development of IntCal13 (Reimer et al., 2013) reproduce the fluctuations. It therefore remains unclear to what degree the Laschamp event affected human biocultural development, or the radiocarbon chronology of the period – if at all.

As witnessed above, most research has focused on the period of around 40k cal BP, which has been described as the most unstable climatic period

of the Last Glacial period Giaccio et al. (2008). However, Feurdean et al. (2014) criticised current models for MIS 3 as too coarse for investigating regional developments. At the same time, high resolution local environmental analyses still remain too sporadic and unevenly distributed to explain pan-European migration patterns. Nonetheless, fruitful attempts at investigating local factors, such as topography, vegetation, predators, and resources (water, food, raw material), indicate that the resolution is slowly increasing (*e.g.* Nigst et al., 2014).

Environmental reconstructions are not essential to testing the Danube corridor hypothesis or the *Kulturpumpe* model. Nonetheless, when interpreting the spatio-temporal data for late Neanderthals and early AMHs, it is useful to remember some of the known conditions under which these humans had to operate.

Chapter 4

History of radiocarbon dating

4.1 Principles of radiocarbon dating

The principles of radiocarbon dating were established by Arnold and Libby (1949) and described extensively in Bowman (1990) and Aitken (1990).

The most relevant nuclear reaction to produce radiocarbon occurs in the upper atmosphere and is shown in equation 4.1. Cascade reactions from cosmic rays produce neutrons (n^0), which react with ^{14}N to generate ^{14}C and a proton (p^+).

$$n^0 + \frac{14}{7}N \rightarrow \frac{14}{6}C + p^+ \tag{4.1}$$

In the atmosphere, ^{14}C rapidly reacts with oxygen to form CO_2, which is subsequently incorporated into terrestrial plant life through photosynthesis. From there radiocarbon disseminates through the food chain. As long as new tissue is synthesised, the concentration of radiocarbon reflects concentration in the atmosphere. However, upon death, ^{14}C is no longer replenished and the decay of ^{14}C to ^{14}N through the emission of an electron (e^-) and an electron antineutrino ($\bar{v}_e$), *i.e.* beta decay, leads to an exponential decrease

of radiocarbon in the tissue.

$$\frac{14}{6}C \rightarrow \frac{14}{7}N + e^{-} + \bar{v}_e \tag{4.2}$$

The ratio of the radioactive isotope (^{14}C) to the stable isotopes of carbon (^{12}C and ^{13}C), is used to estimate the time elapsed since a tissue was disconnected from atmospheric equilibrium. This is based on the observation that radioactive decay is exponential and happens at a constant rate – unaffected by, for example, temperature or chemical reactions. The rate of decay of a particular isotope can be described by either its half life ($T_{1/2}$) or its mean life (τ). The first is related to the latter by:

$$T_{1/2} = (ln\ 2)\tau \tag{4.3}$$

where ln is the natural logarithm to the base e.

Radioactive decay is described by:

$$A = A_0 e^{-\lambda t} \tag{4.4}$$

where A is the number of atoms left after time t, A_0 the initial number of atoms at time zero, and λ the reciprocal of the mean life.

When the radiocarbon dating method was initially developed, the measured half life was 5,568 years (Anderson and Libby, 1951), which corresponded to a mean life of 8,033 years. Although we know today, that the actual half life of ^{14}C is 5,730 years (Godwin, 1962), Libby's half life is still used today to obtain a so-called conventional[1] radiocarbon age which guarantees comparability between individual dates.

[1]Conventional in this context refers to an age calculated using Libby's half life, rather than the actual half life of radiocarbon, and should not be confused with measurements obtained using traditional counting or conventional measurement methods. For AMS versus conventional measurement see section 4.2.

In simplified terms, the radiocarbon age is calculated by:

$$t = -8033\ ln\frac{A}{A_0} \tag{4.5}$$

In reality, fractionation has to be taken into account. Therefore, both the initial number as well as the number of atoms left at measurement have to be normalised:

$$t = -8033\ ln\frac{A_{SN}}{A_{ON}} \tag{4.6}$$

where A_{SN} stands for the normalised activity value of the sample, and A_{ON} the standardised dating reference.

All laboratories nowadays calibrate their ^{14}C ages directly or indirectly related to the NBS oxalic acid standard[2]. The dating reference value is defined as 95% of activity in 1950 AD normalised to $\delta^{13}C = -19‰$ with respect to PDB (Olsson, 1970):

$$A_{ON} = 0.95A_{Ox}(1 - \frac{2(19 + \delta^{13}C)}{1000}) \tag{4.7}$$

where A_{Ox} is the activity value for oxalic acid.

A_{SN} is the sample activity normalised to $-25‰$ wrt PDB, which represents the postulated mean value of terrestrial wood[3]:

$$A_{SN} = A_S(1 - \frac{2(25 + \delta^{13}C)}{1000}) \tag{4.8}$$

Both values, A_{ON} and A_{SN}, are dependent on the year the measurement was made and are not the values obtained in 1950. However, as both the

[2]This has not always been the case. Initially, laboratories used 'modern' standards like fresh wood. However, the Suess effect made such an approach untenable and the community decided to use oxalic acid and the reference year 1950 instead. Therefore, care has to be taken when dealing with dates obtained in the early years of radiocarbon dating applications (see *e.g.* Vogel and Waterbolk, 1963).

[3]The equation represents the approximation generally used (for the more precise equation see Stuiver and Polach, 1977).

sample and the oxalic acid standard are losing their radiocarbon at the same rate, their ratio will be the same as in 1950, providing an age t prior to 1950.

The resulting fractionation corrected term is called fraction ^{14}C ($F^{14}C$), often referred to as 'fraction modern carbon'. To express its error a normal distribution is used as an approximation for the Poisson distribution shown by the ^{14}C counts. From this the error in ^{14}C years (σ_t) is calculated using the following equation:

$$\sigma_t = 8033 \times \frac{\sigma_{F^{14}C}}{F^{14}C} \tag{4.9}$$

where $\sigma_{F^{14}C}$ is the error associated with a date's $F^{14}C$ value. Subsequently, if $\sigma_t > 2 \times F^{14}C$, an infinite age is ascribed.

While an error for $F^{14}C$ ($\sigma_{F^{14}C}$) is symmetric, it is important to remember, that conventional radiocarbon ages expressed in ^{14}C years are asymmetric due to the exponential relationship between ^{14}C count and conventional ^{14}C age. While some laboratories give radiocarbon ages with asymmetric errors, at ORAU, this asymmetry in the error calculation is not expressed. Consequently, all calculations involving uncalibrated radiocarbon dates must use $F^{14}C$ instead of conventional radiocarbon ages. To avoid inaccuracies, this rule is largely followed in this thesis and applies both to calculations and their representations in graphs. However, the discipline of archaeology still widely employs conventional radiocarbon ages. To foster greater understanding, it was deemed beneficial to limit the use of $F^{14}C$ in discussions in favour of conventional ages when directly comparing ages. It should be noted, though, that any statistical tests (*e.g.* χ^2 test) will still be conducted on $F^{14}C$.

So far, we illustrated how fraction modern carbon is obtained and how a radiocarbon age is derived. However, a radiocarbon age is not equivalent to a calendar age. The primary reason is that the first assumes ^{14}C concentration in the atmosphere to be constant. As the production of radiocarbon is dependent on the sun spot activity and the strength of the earth's magnetic field – both influencing the number of cosmic rays reaching the upper atmosphere – atmospheric concentration of ^{14}C actually varies over time. Additionally, the

Libby age is not an accurate description of the actual radiocarbon half life. The offset increases the error the older the measured sample. To convert a radiocarbon date (BP) into a calendar date (cal BP), calibration is required. The principles behind this process will be discussed in section 4.3.2, while a description of the specific calibration curve used is given in section 6.1.

The above calculations can provide reliable calendar dates for systems that were in dynamic equilibrium with atmospheric ^{14}C concentration. Other carbon reservoirs do, however, exist, and will contain different ^{14}C concentrations if exchange with the atmosphere is limited or slow. The resulting difference in age is called a *reservoir effect*. On the one hand, a *marine reservoir effect* is observed, for example, in samples that derive their ^{14}C concentration from deep ocean water, which cannot directly exchange carbon with the atmosphere. On the other hand, a *freshwater reservoir effect* can be caused by limestone (contains no measurable quantities of ^{14}C) dissolving in freshwater systems. In both cases the atmospheric calibration curve would yield an age older than the actual age of the sample. Approaches to resolve this problem are presented in section 15.2.1.

As shown before, the standard error for $F^{14}C$ is conventionally given at 1σ (Bowman, 1990, 49). As the error term for calibrated ages is not normal, the error range is quoted at 95% probability, unless otherwise stated.

In the past pMC ('percent modern') has been frequently used (Stuiver and Polach, 1977), which has now been largely abandoned, but can still be found in the literature. The general relationship between 'fraction modern' and 'percent modern' is given in equation 4.10:

$$F^{14}C = \frac{pMC}{100} \tag{4.10}$$

However, the use of pMC is discouraged, as the term has been used for both fractionation corrected and uncorrected values. $F^{14}C$, though, is always fractionation corrected.

Table 4.1: Background: advantages and disadvantages of AMS radiocarbon dating. For discussion see text.

Advantages	Disadvantages
Small sample size	Possible unrepresentative portion of inhomogeneous sample
More rigorous pre-treatment	Vulnerable to low levels of contamination
Sub-sampling and repeat measurements	Stability of measurement over time
Shorter measurement time	

4.2 Conventional vs. AMS dating

Initially, radiocarbon concentration in samples was measured with a beta counter, which meant that samples had to be large, radiocarbon concentration high and measurement time long enough for the measurement to provide reliable results.

In the 1980s, radiocarbon dating by accelerator mass spectrometry (AMS) became available (Dennell, 1987), with the first accelerators being installed in 1983 at the University of Arizona, USA, and at the University of Oxford, UK. By the 1990s, prices became comparable to conventional dating, causing an increase in AMS radiocarbon dates in the literature (Bayliss, 2009).

The use of AMS allowed for (a) sample sizes and (b) measurement time to be drastically reduced, as the amount of different isotopes of carbon could now be directly measured (see table 4.1). Instead of having to use 1-5 g C, a sample containing a fraction of 1 mg C could be dated (de Rooij et al., 2008). This allowed for new archaeological questions to be addressed, such as plant domestication, and dispersal of human populations (Harris et al., 1987).

However, AMS dating is not without disadvantages. Small samples are more sensitive to contamination (both from the burial environment and the laboratory) and they might be unrepresentative when dealing with inhomogeneous samples. That being said, the small size allows for more rigorous

pre-treatment. Additionally, it gives the opportunity to sub-sample a single specimen, thus enables the testing of reproducibility or homogeneity (Bronk Ramsey et al., 2004b).

4.3 Challenges in ^{14}C dating the Palaeolithic

Radiocarbon dating Palaeolithic samples poses many challenges. Dating at the detection limit of the technique, calibration, and archaeological association can all be problematic. In this section, the German site of Geißenklösterle is used as an illustrative example to highlight the historical and current issues faced by researchers. The site was chosen for its long research history and it's crucial contribution to the debate surrounding the spread of AMH along the Danube fluvial corridor.

The site is located in the Schwabian Jura of southern Germany, close to the river Danube, and provides an archaeological sequence covering Mousterian, Aurignacian and Gravettian industries (Conard and Bolus, 2003, 2008; Hahn, 1988).

Over 70 bone collagen dates have been published, but dating variability within each layer and overlap between layers was very high. Three hypothesis have been put forward to explain the discrepancy in the dataset:

1. Poor association: samples are not representative of the archaeological event of interest (Zilhão and Errico, 2003)
2. Fluctuation in atmospheric ^{14}C concentration (Conard and Bolus, 2003)
3. Contamination of sample dated (Higham et al., 2009)

4.3.1 Archaeological association

There are several published protocols that assess the reliability of radiocarbon dates (*e.g.* Pettitt et al., 2003; Spriggs and Anderson, 1993; Waterbolk, 1971).

This study will focus on Waterbolk (1971), as it specifically looks at the archaeological aspect of the quality assessment. His criteria are summarised in table 4.2.

In a first step, the *certainty of association* needs to be evaluated, *i.e.* how confident can we be that the dated material is giving us the event of interest. For example, unmodified faunal remains from a stratigraphic unit are less closely connected to the human occupation of that layer than osseous artefacts; or human remains are more securely representing a certain species' presence at a site than charcoal remains from a fireplace.

In a second step, the inbuilt sample age is assessed. If the specimen died long before it got deposited (*e.g.* use of mammoth ivory from the permafrost, or charcoal from long-lived species), there is a substantial offset between the sample date and the occupation to be dated.

At Geißenklösterle, research based on lithic refitting (Teyssandier et al., 2006) and micromorphology (Conard and Bolus, 2003) suggests little stratigraphic mixing. All radiocarbon dates were done on herbivorous faunal remains, with the large majority showing cut or percussion marks (Conard and Bolus, 2003, 2008). Therefore, it can be concluded that the radiocarbon samples have negligible inbuilt age and a high probability of association. Their selection is unlikely to be the cause of the dating variation observed.

4.3.2 Calibration

When the criticism was expressed that high variability in atmospheric radiocarbon concentration would cause the scatter in the dates form Geißenklösterle (Conard and Bolus, 2003, 2008; Zilhão and Errico, 2003), the radiocarbon community used the calibration curve IntCal04 (Reimer et al., 2004). At the time, the known age tree ring record reached back to 12,550 cal BP. Beyond that, alternative records had to be incorporated (speleothems, corals, and foraminifera in marine cores). As a consequence of reservoir effects, these records have been less reliable – to the extent that beyond 26,000 cal BP

Table 4.2: Background: the first two criteria for assessing the quality of radiocarbon dates, according to Waterbolk (1971).

Class	Certainty of Association	Sample age in relation to burial/discard
1	**Full certainty:** the sample came form the event of interest itself, e.g. a diagnostic bone point or hominid.	The age difference is so small as to be negligible (<20 years), e.g. bone, twigs or outermost tree rings.
2	**High probability:** there is a direct functional relationship between the sample and the archaeological finds, e.g. cut marked bone, shell bead, marine shell, charcoal from hearth, burnt bone, burnt sediment from hearth feature.	The time difference is several decades, e.g. charcoal from short lived wood species or objects which might have had a long period of use.
3	**Probability:** there is no functional relationship, but the quantity or size of material argues in favour of it, e.g. large herbivore bones or charcoal fragments within dense occupation level.	A time difference of several centuries, e.g. charcoal from a long lived species, objects subject to reuse, or materials which will incorporate a reservoir offset which can be estimated.
4	**Reasonable probability:** Much like 'probability', but the fragments are small and scattered, e.g. charcoal or bone fragments in a sparse occupation level, unburnt sediment, and unknown sample types.	The nature of the dated material is not precisely known, e.g. 'soil', or where materials will have a reservoir offset that is unknown, e.g. organisms feeding within freshwater system.

the datasets diverged by several millennia and no calibration curve could be constructed (van der Plicht et al., 2004).

Looking at individual records, especially the Bahamas speleothem record (Beck et al., 2001) and the radiocarbon dated foraminifera record from core CT85-5 from the Tyrrhenian Basin (Giaccio et al., 2006), an increase in radiocarbon concentration of around 6% was detected at the end of the Middle to Upper Palaeolithic transition (OIS3). The Laschamp Magnetic Excursion just before 40 ka cal BP (Giaccio et al., 2006) as well as oceanic turnover (Beck et al., 2001) were suggested as possible causes. It was concluded that calibration for the period of interest was not possible and Conard and Bolus (2003) labelled it the "Middle to Upper Palaeolithic Dating Anomaly".

Since IntCal09, a calibration curve going back to 50 ka cal BP is available and agreement beyond 26 ka cal BP has improved (Reimer et al., 2009). A further update, IntCal13 (Reimer et al., 2013), has been published and will be discussed in more detail in section 6.1. Though still showing larger variation in datasets beyond the tree ring chronology, none of the records incorporated seem to reproduce the stark fluctuations in radiocarbon concentration mentioned above. More recent work on the Bahamas speleothems (Hoffmann et al., 2010) suggests that the original work by Beck et al. (2001) contained errors caused by issues with ^{14}C blank subtraction.

Consequently, the dataset from Geißenklösterle cannot be explained by variation in atmospheric radiocarbon concentration and resulting calibration issues.

4.3.3 Contamination & pre-treatment methods

When working on the Middle to Upper Palaeolithic biocultural shift, we are approaching the limit of the radiocarbon dating technique, which is currently thought to be 8 half lives. The exponential decay causes a sample of approx. 30 ka BP to only contain a little over 2% of its original amount of ^{14}C, for a sample of 45 ka BP age a meagre 0.4% remain.

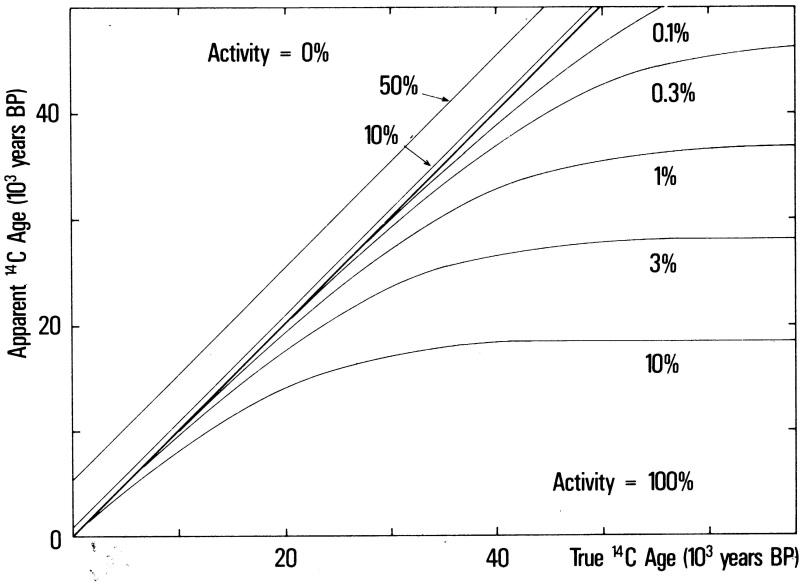


Figure 4.1: Background: effects of carbon contamination on radiocarbon dating results: Dead carbon (no measurable ^{14}C)) shows a linear shift towards older dates, modern carbon will overproportionally effect old samples and can easily lead to offsets of several thousand years.

Keeping these very low concentrations of radiocarbon in mind, we see that small amounts of contamination with young carbon (post-depositional, conservation or laboratory environment) introduces a comparatively large amount of ^{14}C, thus leading to a significant dating offset (see figure 4.1).

As an example, only 1% modern carbon added to a sample of 36 ka BP age would lead to a radiocarbon measurement of 31 ka BP. In contrast, dead carbon contamination of 1% causes the same sample to appear 80 radiocarbon years too old – which is well within one standard deviation measurement error. Furthermore, the effect of dead carbon is the same irrespective of sample age.

Laboratory derived contamination can be measured and corrected for, though they reduce dating precision (see section 5.2 for more details). Post-depositional contamination, in contrast, cannot be measured and may heavily affect dating accuracy if not entirely removed.

Comparison with other dating methods, *e.g.* luminescence, ESR, U-Series and $^{40}Ar/^{39}Ar$ of tephra layers, and improved radiocarbon pre-treatment protocols has indeed shown, that the biggest challenge in radiocarbon dating the Palaeolithic is contamination (*e.g.* Blockley et al., 2008; Chappell and Magee, 1996; Higham et al., 2009; Turney et al., 2001).

This is also demonstrable at our example site of Geißenklösterle: Higham et al. (2012) re-dated samples using an ultrafiltration pre-treatment protocol and compared the outcome with dates obtained at ORAU in the 1980s and 1990s from the same samples, but using ion exchange gelatin preparation – a protocol no longer used at the lab (see table 5.1). The more rigorous treatment with ultrafiltration gave results comparable or older than the original measurements, which was seen as evidence for insufficient contamination removal during original pre-treatment (see figure 4.2). The new dates were more consistent with the archaeology at the site as well as information obtained from other dating methods. It can be concluded, that the variance in the original radiocarbon dataset can mostly be explained through insufficient contamination removal.

Similar difference can be observed in charcoal samples when comparing standard acid base acid pre-treatments with the more rigorous ABOx-SC protocols (*e.g.* Higham et al., 2009; Wood et al., 2012).

4.4 Summary

Radiocarbon dating as a technique was invented in the middle of the 20^{th} century, and is based on the beta decay of the radioactive isotope of carbon (^{14}C). The age relates to the time of death of the organism or the formation of the tissue dated, which is when dynamic equilibrium with atmospheric carbon is no longer maintained.

Over the past nearly 70 years of application, our understanding, and thus the methodology, has seen major improvements. These include more targeted sample collection, move to AMS radiocarbon measurements, continuously

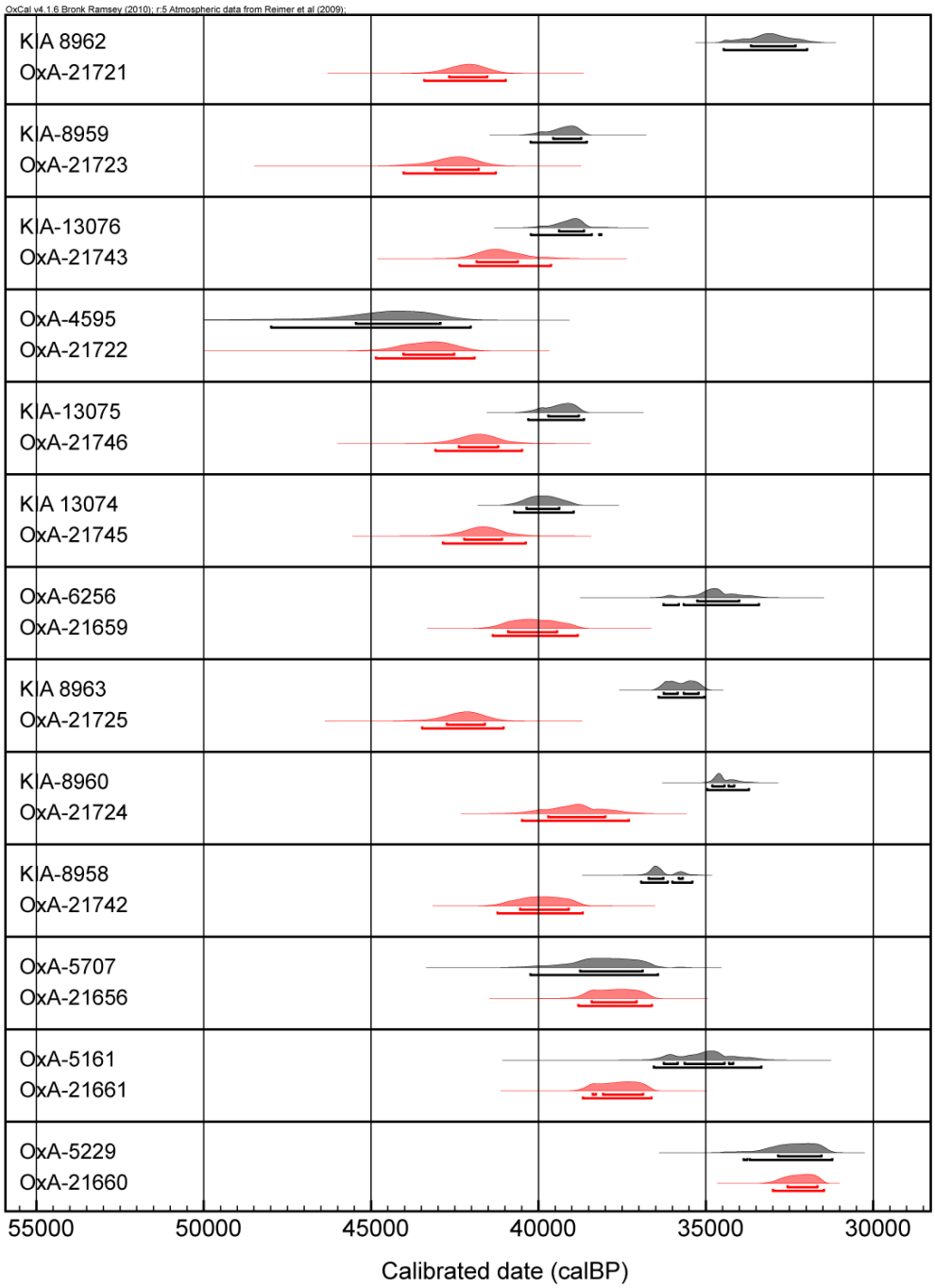


Figure 4.2: Background: Geißenklösterle (DE) – comparison of radiocarbon dates obtained with ion exchange gelatin preparation (black) with those with ultrafiltration protocol (red) (after Higham et al., 2012). Each pair between horizontal lines belongs to the same faunal sample. The dates are calibrated with IntCal09 (Reimer et al., 2009) to reflect the results of the original study.

improved and more rigorous pre-treatment strategies, and Bayesian statistics for calibration and modelling of dates.

It is these improvements that made radiocarbon dating of the Palaeolithic not only possible, but an essential tool for chronology building, inter-site comparisons and answering targeted archaeological questions. When applied rigorously, it can provide higher resolution than other radiometric and relative dating methods applied in the Palaeolithic.

Nonetheless, it is important to remember the challenges involved – sample quality, contamination removal, detection limits, and calibration. Quality control is essential at all three stages: (1) sample selection, (2) laboratory processing and (3) further statistical analysis. Consequently, when using radiocarbon data from the literature as reference, they have to fulfil the same stringent criteria to avoid noise in the chronological dataset that could cause misleading and problematic archaeological interpretations.

Part III

Methods

Chapter 5

Radiocarbon dating

This thesis is applies radiocarbon dating to establish local and regional chronologies. As discussed in section 4.3, the reliability depends heavily on sample selection, laboratory processing, calibration and statistical analysis. Therefore, the subsequent sections will examine each of these aspects in detail and describe the radiocarbon dating strategy implemented.

5.1 Sample selection and sampling methods

In order to provide the most accurate and precise date possible, the dated sample must be securely related to the event of interest and not be affected by a reservoir offset. As this thesis is primarily interested in the human occupation/presence at a site (both Neanderthal and AMH), the following sample types were collected for dating (listed from most secure to least secure):

1. Human remains (see *e.g.* fig. 5.1)
2. Artefacts of cultural significance (*e.g.* osseous points)
3. Other artefacts (*e.g.* retoucher)
4. Faunal remains showing anthropological impact (*e.g.* cut marks)



Figure 5.1: Methods: *Homo neanderthalensis* parental bone found at Šal'a (Slovakia). Photo: R. Hopkins.

Additionally, some faunal remains without any anthropological impact were selected from sterile layers. This was restricted to cases where they were necessary for Bayesian modelling, and they are not treated as representative of human activity.

Despite the fact that charcoals from fireplaces and hearth structures may come from an archaeologically secure contexts, they were not targeted for dating. This decision was partially based on association difficulties, as charcoals seemed more heavily affected by post-depositional processes such as solifluction (possibly as a result of their lower density), and are not always unequivocally linked to human activity (see also section 8.1).

5.1.1 Anthropogenically modified bone

Anthropologically modified bone encompasses a large variety of osseous remains which show varying degrees of certainty regarding their connection to human activity. Probably the most clear cut examples are finished or semi-finished artefacts such as osseous points or figurines. Although highly



Figure 5.2: Methods: *Equus* sp. pelvis fragment with projectile wound from Temnata, Bulgaria. Photo: R. Hopkins.

fragmented specimens can cause some doubt regarding their identification, in most cases, patterns of human alteration are distinctly visible.

More problematic are alterations that were not the primary focus of human activity but merely a by-product thereof. In these cases it is important to distinguish between taphonomically, anthropogenically and animal derived features. For this thesis, samples showing the following markers were selected for dating:

- projectile wounds (see fig. 5.2)
- retoucher specific markings (see fig. 5.3, left)
- cut and chop marks (see fig. 5.3, right)
- bone fractures (*e.g.* from marrow extraction)



Figure 5.3: Methods: retoucher Kz-28 (left) with typical abrasion pattern, and faunal bone fragment Kz-19 (right) with cut marks from Kozarnika (Bulgaria). Photos: R. Hopkins.

To identify cultural alterations, the bone surface was thoroughly examined with a hand lens in good light. In some cases, it was possible to further analyse the marks under a microscope.

Cut marks caused by lithic tools (see figure 5.3 right) were identified using the following criteria after Morlan (1984):

- Anatomical element that is marked
- Position on the element
- Gross morphology of the mark
- Microscopic features within the mark
- Comparison between the contour of the mark and that of the bone surface

It was assumed that cut marks and their location are connected to human activities, such as slaughtering, hunting, skinning, dismembering, defleshing or cutting up of bone material for artefact production. The marks are often straight or with minimal rotation (cutting motion), have a V-shaped profile

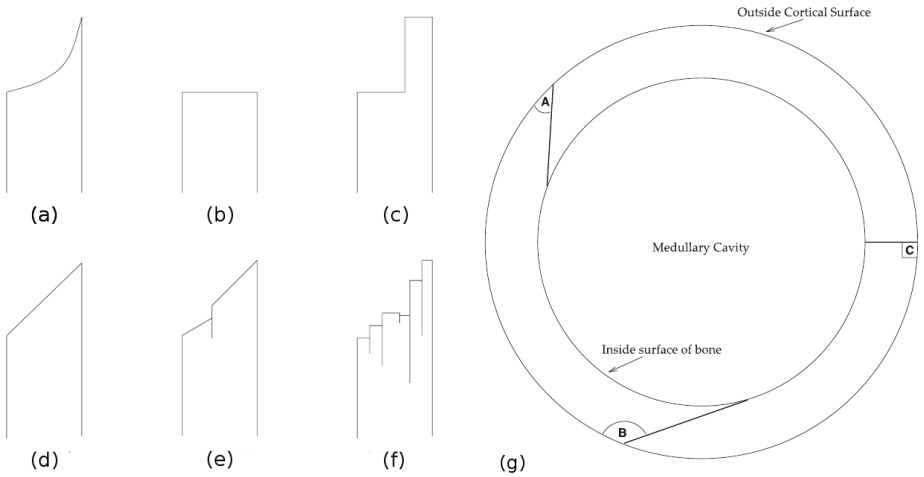


Figure 5.4: Methods: left – possible shapes of bone fractures: (a) helical, (b) transverse, (c) longitudinal and transverse, (d) diagonal, (e) diagonal with step, and (f) columnar. Right – (g) Three possible angles of fractures: (A) acute, (B) obtuse, (C) right angle (after Outram, 2003).

with one side steeper than the other, slightly irregular grooves with parallel striations and are sometimes found in (near) parallel groups (see also Greenfield, 1999).

They are distinct from marks caused by chewing, rootlet etching, vascular grooves, trowel marks and curatorial damage (for more discussion and literature see Blumenschine et al., 1996; Outram et al., 2005).

The most important criteria for identifying anthropogenically fractured faunal long bones is a fresh fracture. Fresh bone is expected to show a helical fracture (see figure 5.4), that is a curved fracture which spirals around the diaphysis. The fracture surface is smooth (visually similar to broken plastic), and the fracture in general shows acute or obtuse angles (see figure 5.4 right). The impact point for splitting the bone is often clearly distinguishable and shows radial fracture fronts. In cases where the bone was struck on a hard surface, a rebound scar should be visible opposite the impact scar. In contrast, unfresh specimens can show a larger variety of fracture types, have a rough fracture surface (similar to coarse earthenware), a higher number of right angled fractures, and are more likely to show fracture outlines that are

interrupted by micro-cracks (*e.g.* caused by water loss) present in the bone prior to fracturing.

This approach does not identify all anthropogenically fractured bones, as additional processes, such as heating prior to marrow extraction, can alter the water content of the bone and therefore cause the fracture to look like those on unfresh specimens. However, it allows for the selection of specimens with the highest probability of showing human activity at a site.

5.1.2 Key-hole drilling

All specimens were sampled with minimal damage to their distinctive features. For most faunal remains this means sampling the inside of the bone, keeping surface features and fractures intact. For artefacts, though, a key-hole drilling technique was applied in order to keep as much of the anthropogenically modified surface intact – to facilitate both future study and museum exhibition (see figure 5.5).

The sampling hole visible can be as small as 5 mm in diameter. An additional advantage of the technique is it minimises possible contamination from the conservation environment, where many artefact surfaces are treated with consolidates. However, it should be noted, that substantially more material has been extracted than immediately visible from the outside.



Figure 5.5: Methods: osseous point from Dzeravá Skala (Slovakia), sampled for radiocarbon dating using key-hole drilling. Photo: R. Hopkins.

5.2 Overview of laboratory treatment

Radiocarbon pre-treatment protocols are put in place to remove contaminants from the burial (*e.g.* humics) and excavation or curation environments (*e.g.* Paraloid B72 or PVA). There are two main approaches as described by Hedges and Law (1989):

1. Remove possible sources of contamination from the sample
2. Select a specific compound found only in the sample type dated

The first method is frequently based on applying an acid-base-acid (ABA) protocol in which carbonates, alkali soluble organics (such as humic acids) and finally dissolved CO_2 are removed to obtain the datable fraction. In the second method, a separation process such as HPLC is used to extract the specific compound believed to contain the endogenous carbon (*e.g.* hydroxyproline for bone samples). In practice, many protocols are a combination of these two approaches.

After pre-treatment, the purified sample needs to be converted into a form suitable for AMS measurement, which is graphite for this project (but could practically also be a gas sample at ORAU and other laboratories). For bone collagen samples this means that the pre-treated sample is combusted in an Elemental Analyser (EA). The generated CO_2 is purified and subsequently heated with hydrogen over an iron catalyst (Dee and Bronk Ramsey, 2000; Hedges et al., 1992). During combustion a small fraction of the carbon and nitrous oxides is sent to an isotope ratio-mass spectrometer (IR-MS) for measuring elemental and isotopic composition.

The graphite samples are pressed into stainless steel targets with a 2-mm-diameter hole using a Specac hydraulic pellet press with 0.35 ton load. This creates an even target surface that is capable of producing a good current. Finally, the targets are dated using the HVEE AMS system at ORAU as described by Bronk Ramsey et al. (2004b). Alongside the unknown samples,

anthracite background samples, oxalic acid II standards, known-age tree ring samples and marble standard are analysed.

During laboratory treatment, small amounts of carbon are often added to the sample. Contamination at the graphitisation stage is negligible, as anthracite[1] (contains no measurable ^{14}C) is graphitised in the same way as samples of unknown age and then used as an ancient (background) standard (Bronk Ramsey et al., 2004b). Consequently, all dates are corrected for AMS and graphitisation background at the same time. Routine dating precision on the AMS at ORAU is around 0.3% of 1 $F^{14}C$. Dating inaccuracy for the Palaeolithic is therefore heavily influenced by sample contamination introduced or unremoved during pre-treatment (see also section 4.3).

In order to correct for carbon added during pre-treatment and combustion, known age samples are treated alongside the unknown samples. The calculated contamination is then subtracted from the $F^{14}C$ of the unknown sample (see also section 5.4.6 and 5.4.7). While improving the accuracy of the date, this background correction will decrease the dating precision as a consequence of the variation in the actual carbon added to the treated sample.

Major contamination issues can be highlighted by 'quality control' measures, such as sample yield (amount of sample surviving pre-treatment), stable isotopes ratios, carbon concentration on combustion and ultrafilter tests (see also Brock et al., 2007, 2013; van Klinken, 1999).

In cases of known or suspected contamination through conservation materials and insufficient sample for single compound dating, a series of solvent washes are completed before starting standard chemical pre-treatment. They will be described in more detail in section 5.4.4.

[1] The anthracite samples are combusted in bulk for ORAU at the Groningen laboratory, see Bronk Ramsey et al. (2004b).

5.3 Sample, method and date codes at ORAU

Every sample and pre-treatment method used at ORAU has its own number or code. Additionally, samples are given reference numbers when collected for this dating project (whether dated or not). The following section will explain the nomenclature used at ORAU and for this project. They are followed throughout this thesis.

Each sample collected for this thesis is given a unique sample number, even if a unique identifier has already been given in the field. When selected for dating, every sample gets a P number at ORAU, every time the sample is treated, it is assigned a Q number. For example a bone sample from Kozarnika with the field sample number E7-306 is assigned the collection number Kz-10. At the radiocarbon lab it is assigned the P-number 39499 for dating. The first time it is treated, it is given a Q number of 0 (resulting in 39499.0), the second sub-sample treated would be given the Q number 1 (resulting in 39499.1).

The treatment code indicates what pre-treatment procedure was followed. For a full list of the treatment codes at ORAU see table 5.1. Considering our Kozarnika example, a subsample treated with the standard ultrafiltration protocol would be labelled 39499.0 AF. Depending on the yield, there might be enough material for several combustions. As each of those targets belong to exactly the same subsample, no new Q number is given. Instead, a target number (e.g. 01) is added, giving us 39499.0 AF 01 for the first target from the first subsample of Kz-10, treated with the ultrafiltration protocol. The pre-treatments used in this thesis are described in more details the subsequent section.

If a sample is suspected to be conserved, it is subjected to a series of solvent washes prior to routine treatment (see section 5.4.4). To differentiate between a sample with solvent wash and one without, the first is denoted by an * after the treatment code (*e.g.* AF*).

Table 5.1: Methods: pre-treatment protocols with code used at ORAU. Protocols AI, AC, RR are no longer used (grey). Protocols AI and AC are described in Hedges and Law (1989), the others (excl. NRC) in Brock et al. (2010b).

Code	Material	Generic name	Description
AF	Bone	Ultrafiltration	Acid, base, and acid washes, gelatinisation of the insoluble residue, use of Ezee-filters™ and ultrafiltration.
AG	Bone	Modified Longin	Acid, base acid washes, gelatinisation of the insoluble residue.
AI	*Bone*	*Ion Exchange*	*Acid and base washes, gelatinisation of insoluble residue. Gelatin is passed over an ion exchange resin and hydrolised. The amino acids obtained are purified with a second ion exchange resin.*
AC	*Bone*		*Acid wash, acid hydrolysis of insoluble residue and treatment of amino acids with activated charcoal and ion exchange chromatography.*
RR	*Charcoal*		*Acid wash, ultrasonication in ultrapure water, acid wash.*
ZR	Charcoal	ABA	Acid, base, acid washes
XR	Charcoal	ABOx-SC	Acid and base washes, chemical oxidation and pre-combustion.
OX	Shell		Reaction with phosphoric acid *in vacuo*.
OO	Shell		Reaction with phosphoric acid *in vacuo* after the surface of the shell is acid-etched with dilute HCl.
XB	Any	Direct combustion	No pre-treatment.
NRC	Any		Non-routine pre-treatment.

Table 5.2: Methods: description of the date codes used at ORAU.

Date Code	Description
OxA-	A date considered reliable at the time of dating.
OxA-X-	A date that may not be reliable, either because of non-routine treatment or questions during sample's pre-treatment, combustion or measurement.
OxA-V-	A date from a sample pre-treated outside of ORAU, but combusted and measured at ORAU.

These pre-treatment codes apply to ORAU only. Similar treatments can be found at other laboratories, though they are rarely identical. Consequently, when talking about samples that were dated at other laboratories, the generic names (*e.g.* ultrafiltration) are used. Where relevant, the specific methodology is explained in more detail.

If sample yield is sufficient and graphitisation successful, the resulting radiocarbon age is given an OxA number, according to the criteria listed in table 5.2.

5.4 Radiocarbon dating of bone

Bone is a composite material, made up of the mineral component biological hydroxyapatite (55-75%) and a mixture of organic molecules (25-45%). Around 90% of the latter is type I collagen (Schwarcz and Schoeninger, 1991). In general, close interactions between the insoluble collagen and mineral fraction result in better preservation of bone than that of most other organic materials (Collins et al., 2002). Unfortunately for radiocarbon dating, the large surface area of bone (around 10 m^2 g^{-1}) increases the potential for absorption of contaminants (Hedges and van Klinken, 1992).

In the vast majority of cases, pre-treatment either extracts the collagen or its amino acids. Dating the mineral matrix is generally avoided[2], as it readily

[2]Recent studies have explored the use of bio-apatite dating for arid climates and cremated bone (Snoeck et al., 2014; Zazzo, 2014; Zazzo et al., 2013). As reliable results are

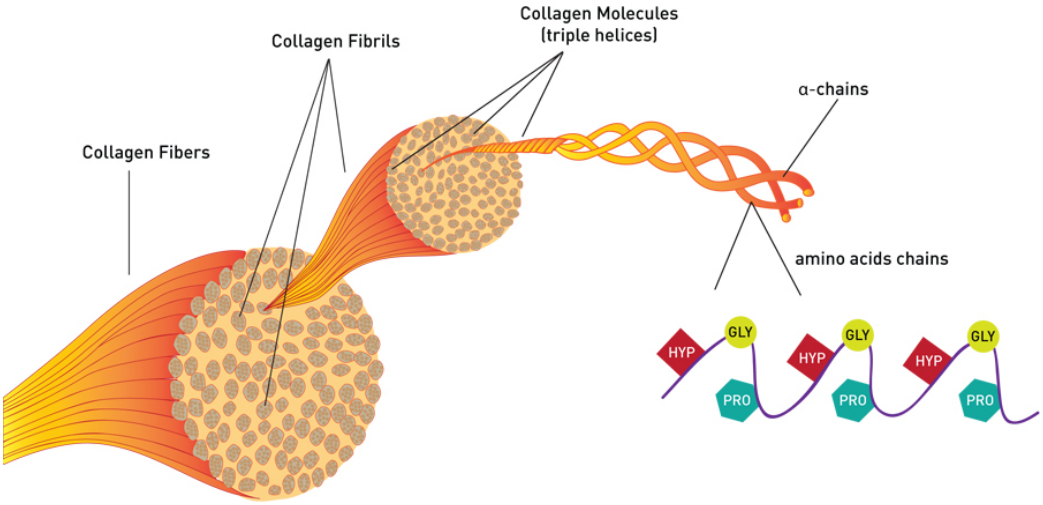


Figure 5.6: Methods: the structure of collagen (https://biology4alevel.blogspot.com/2014/08/13-globular-and-fibrous-proteins.html, 2018-07).

recrystallises and can incorporate carbonates from the ground water. These carbonates are chemically indistinguishable from the endogenous carbon of the bone apatite, thus extremely difficult to remove (Ambrose and Krigbaum, 2003; Nielsen-Marsh and Hedges, 2000).

Bone collagen is a protein (see figure 5.6). Amino acids form α-chains of distinctive and regular sequences: Gly-Pro-Y or Gly-X-Hyp, where X and Y stand for other amino acid residues. Each chain weighs around 97-102 kDa and is around 300 nm long. Due to the high glycine, proline and hydroxyproline content, the chains form left-handed plyproline II helices. These wound into triple α-helices, and are held together by hydrogen bonds. The α-helices group into microfibrils and subsequently collagen fibres, and interact with the inorganic component (Balian and Bowes, 1977; Woodhead-Galloway, 1980).

so far only obtained from the Holocene, bone apatite dating will not be further discussed in this thesis.

5.4.1 Bone diagenesis

Bone diagenesis includes both (1) a decrease in peptide length and (2) reactions of amino acids. If the bone is exposed to microorganisms, then these can cause the exposed proteins to be hydrolysed by enzymes, leaving unexposed regions unaffected (Collins et al., 2002). This enzymatic degradation is mainly relevant during the first 4,000 years of burial history. Beyond that, and in the absence of microbes, chemical deterioration in all bone areas is mainly driven by the thermal history of a bone specimen, which determines the maximum possible duration for collagen survival (for reviews see Collins et al., 2002; Hedges, 2002).

Peptide breakdown

Peptide breakdown was assumed to be caused by random chain scission through hydrolysis, as observed for gelatin and DNA degradation, and would lead to a rapid decline in peptide length (Collins et al., 1995). However, ultrafiltration seems to recover large collagen fragments from ancient bone samples, thus contradicting aforementioned model. A study by Dobberstein et al. (2009) demonstrated that a decrease in peptide length can only be observed for collagen yields below 1%. Above this threshold, α-chains are either fully intact or not present at all. However, the authors also suggest, that if the thermal history of a bone exceeds $8_{\mathrm{ka}10^{\circ}\mathrm{C}}$, possible degradation by hydrolysis and cross-linking could become more important.

Amino acid reactions

The best known amino acid reactions within the burial environment are deamination and humification. Decarboxylation (Tuross, 2002) and ester formation (Hunt, 1985) can also occur. For radiocarbon dating, humification is most relevant: Via the Maillard reaction, an amino group from our collagen protein reacts with a carbonyl group from sugar. The latter can both



Figure 5.7: Methods: bear tooth pendant Mlc-10 from Mladeč (Czech Republic), showing the tiny hole where a %N sample has been taken. Photo: R. Hopkins.

naturally be present in the bone or derive from exogenous molecules such as humics (Ames, 1992; Tuross, 2002; van Klinken and Hedges, 1995).

5.4.2 Screening: %N and collagen preservation

Collagen preservation is commonly assessed using the percent nitrogen (%N) of the whole bone powder. A study by Brock et al. (2010a) has shown that this method has a 84% probability of successfully predicting whether collagen preservation is sufficient to produce a yield of $> 1\%$ of original sample weight when using a cut-off of 0.76% N.

This value has been experimentally derived and is based on the fact that collagen contains nitrogen, consequently low to no nitrogen in a sample is indicative of poor to no collagen preservation in the bone. It is important to note, however, that a high %N value does not necessarily correspond to good preservation.

A sample of less than 5 mg is needed for analysis. This makes it an efficient way of testing bone samples to prevent costly and time consuming pre-treatment of samples with little likelihood of producing sufficient yield

for radiocarbon dating, while simultaneously selecting those with the highest likelihood of success where several samples are available. Furthermore, this method is only minimally destructive, leaving a hole of only 1mm diameter when using key-hole drilling (see figure 5.7). It therefore prevents unnecessary destruction of precious archaeological artefacts.

Other methods for assessing collagen preservation have been suggested in the past (see Brock et al., 2010a), and ZooMS (proposed by Harvey et al., 2016) has attracted some attention. Nonetheless, the success rate and simplicity of the %N approach make this method better suited for this thesis.

5.4.3 Overview of bone pre-treatments

There have been several different approaches to pre-treating bone for radiocarbon dating (see tab. 5.3), and many have seen laboratory specific variations. A breakthrough for radiocarbon dating was the Longin method (Longin, 1971), which targeted the bone collagen. Many modern protocols are derivatives of this basic principal – often with extra purifications steps. Others have directly targeted the carbon within the amino acids.

Considering the advantages and disadvantages of these treatments, a fine balance between simplicity and effectiveness had to be found. Factors to consider are (1) laboratory derived contamination, (2) contamination from the burial environment and from conservation treatment, and (3) sample yield.

The risk of the first gets amplified with increasing pre-treatment complexity. Background corrections can to some extent counteract these effects, though other forms of contamination cannot be easily corrected for – and they can have a detrimental effect on Palaeolithic dates (see section 4.3). Nonetheless, it is ill-advised to apply the most rigorous pre-treatment protocol to all samples. They often reduce sample yield significantly, and can result in unnecessary sample loss.

Table 5.3: Methods: main pre-treatment methods for bone. ORAU lab codes given in brackets where appropriate.

Method	Component extracted	Description	Advantages	Limitations	References
Longin	Gelatin	demineratlisation with acid, gelatisation at pH=3 and 90°C	time efficient	age underestimation in the Palaeolithic	Longin (1971)
Modified Longin Method (AG)	Gelatin	ABA, gelatinisation, filtration (separating gelatin from largest acid insoluble components)	time efficient	'Collagen' impure, causing age underestimation beyond 2 half-lives	Berglund et al. (1976), Protsch (1975)
Ion Exchange (AI)	Gelatin or amino acid from gelatin	A(BA), ion exchange of bulk collagen, then hydrolysed collagen	some purification of collagen	Possible carbon contamination from ion exchange column, dates underestimated	Hedges and Law (1989), Stafford et al. (1988)
Ultrafiltrtion (AF)	Gelatin	Modified Longin Method, ultrafiltration (rreoval of $<$ 30kDa component)	some purification of collagen	Possible carbon contamination ultrafilter humectant; lower collagen yield than AG; nature of contaminants removed unknown	Brown et al. (1988), Bronk Ramsey et al. (2004a), Brock et al. (2013, 2010b)
Collagenase digestion	Tripeptide (GlY-PRO-HYP)	Demineralisation, ultrafiltration, collagenase digestion, HPLC	separated product likely to be derived only from collagen	Possible carbon contamination from ion exchange column; yield ca. 10% of collagen	van Klinken et al. (1994)
Ninhydrin derivatisation	Carboxyl carbon from amino acids	Acid wash, reaction with ninhydrin. First treatment: removal of contaminating amino acids, hydrolysis; second treatment: collection of CO_2	Separated product likely to be derived only from collagen	Carboxyl carbon only 2wt% of collagen, possible contamination from CO_2	Nelson (1991), Tisnérat-Laborde et al. (2003)
Single Amino Acid (NRC)	Hydroxy-proline	Modified Longin, hydrolysis and separation of HYP through HPLC	Separated product likely to be derived only from collagen	Possible carbon contamination through lengthy pre-treatment; HYP ca. 15wt% of collagen; method under development at ORAU	Stafford et al. (1991, 1987), van Klinken and Mook (1990), Marom et al. (2012), Devièse et al. (2018)
Multi-Amino Acid (NRC)	"first 7" amino acids	Modified Longin, hydrolysis and separation of first 7 amino acids through HPLC	Separated product probably derived only from collagen	Possible carbon contamination through lengthy pre-treatment; method under development at ORAU	experimental

Therefore, three main protocols were selected for this research: hydroxyproline dating (NRC) for conservation contaminated samples with sufficient collagen yield, ultrafiltration (AF) for most regular samples, and the ORAU gelatine treatment (AG) for precious low yield artefacts. In addition, solvent washes were applied to potentially conserved samples with insufficient yield for single amino acid dating. All protocols are described in more detail in the following four sections.

5.4.4 Solvent extraction

At ORAU, the standard solvent cleaning method for unknown contaminants (see table 5.4) entails soaking the sample in acetone (40–50°C, 30–60 min.), followed by methanol and chloroform (RT, 30–60 min.), and rinsing with chloroform. Subsequently, the sample is dried in a heating block at around 40° C, before it is further pre-treated following one of the standard or experimental protocols.

Table 5.4: Methods: list of standard solvent sequences used to remove contaminants from curation environment as applied at ORAU. * Contaminants known to not be completely removable by solvent sequence (see Dee et al., 2011).

Contaminant	Solvent sequence
unknown, UHU (resin), Superglue (cyanoacrylate), OHO, Lanolin, Paraffin, Beeswax, Neatesfoot Oil, natural bitumen (pitch)	acetone, methanol, chloroform
PVA*	water, acetone, water, methanol
Shellac, varnish, PEG	water, methanol
Araldite (epoxy resin)*	sodium ethoxide (RT, 48h)
latex	chloroform, water
paper paste (methylcellulose), pearl glue (collagen-based)	water (1h)

While the same solvent wash treatment is applied to remove other known contaminants, more targeted treatments apply in cases where the contaminant can be identified as PVA, Shellac, varnish, PEG, araldite, latex, methylcellulose or collagen-based glues.

When dealing with conservation materials such as PVA, epoxy resin and Paraloid B72, solvent washes are not fully effective as shown by Dee et al. (2011). As sample contamination poses a serious issue for dating the Palaeolithic, samples conserved with polymers or resins should be avoided. While this is possible for fragmented faunal remains, precious specimens, such as human remains and archaeological artefacts, are all too often treated and alternative samples not available. Consequently, sampling of the contaminated fractions is avoided and single amino acid dating used whenever sample yield allows for it. Solvent washes are only used as a precautionary measure and in cases where identified contaminants have a high likelihood of being removed.

5.4.5 Gelatin (AG) pre-treatment protocol

The AG pre-treatment protocol at ORAU is a modified Longin method, which incorporates the basic steps of acid-base-acid washes, followed by gelatisation, and finally filtration to separate the gelatin from the largest acid insoluble components (Brock et al., 2010b).

Samples are pretreated in batches (chemlists) of around 18 crushed or powdered bone samples alongside two bone standards (of background age when processing Palaeolithic samples). The samples are initially demineralised with 0.5 M HCl at room temperature (RT). After 2h, the samples are centrifuged, decanted and the acid solution replaced with fresh 0.5 M HCl. The same procedure is followed after another 2h, after leaving them overnight, and finally after a further 2h in the morning[3].

Subsequently, the samples are centrifuged and rinsed three times with MilliQ^{TM} ultrapure water to remove residues, before 0.1 M NaOH (30 min, RT) is applied to remove humics. After another three rinses, the samples are reacidified in 0.5 M HCl solution for 15 min., followed by three rinses. The residue is gelatinised in weak acid (pH=3) at 75°C for 20 hours and

[3] 1 mL of solution is retained for each sample after the first, second, and overnight treatment to enable potential future species identification through ZooMS (Zooarchaeology by Mass-Spectrometry) analysis.

filtered using 45–90 μm high density polyethylene Ezee-filters^{TM} to remove large insoluble contaminants (Brock et al., 2013). The Ezee-filters^{TM} are cleaned by ultrasonicating in ultrapure water for 20 min., followed by passing through ultrapure water prior to use. The supernatant is subsequently frozen and freeze-dried, before being prepared for combustion (see section 5.2).

It has been demonstrated that these steps most often do not sufficiently purify the collagen sample, causing substantial offsets for contamination sensitive samples, such as those dating to the Palaeolithic. Therefore, in this study this pre-treatment protocol is only applied to samples (a) yielding insufficient collagen for the ultrafiltration (AF) or amino acid protocols, and (b) where a minimum age estimate provides important archaeological information.

5.4.6 Ultrafiltration (AF) pre-treatment protocol

The ultrafiltration protocol at ORAU initially follows the same steps as the AG treatment described above. For standard pre-treatment, the supernatant is directly ultrafiltered with a pre-cleaned 30 kDa MWCO[4] Sartorious Vivaspin 15 filter^{TM} (see Brock et al., 2010b).

For this thesis, the AG treated sample is first freeze-dried for 72h. This is done to make sure that there is enough material for dating – especially in cases of small precious samples. Whenever there is sufficient yield, a small amount of AG collagen is set aside in case later analysis of the AG sample is required. Subsequently, the remaining sample is dissolved in 10 mL of MilliQ^{TM} ultrapure water and ultrafiltered. 1mL of supernatant is collected and diluted with 2mL of MilliQ^{TM} ultrapure water to prevent the purified collagen from becoming too brittle. The sample is freeze-dried for 48h, and subsequently prepared for graphitisation (see section 5.2).

The use of ultrafilters, although having shown to improve radiocarbon dating reliability for Palaeolithic samples (see section 4.3.3), is not without

[4]MWCO = molecular weight cut off.

difficulties. First, the nature of the contaminants removed is not well understood and ultrafilters cannot remove high molecular weight contaminants, such as those sometimes found in conservation materials. If there is a suspicion that such contaminants from the curation environment might be present, alternative samples are not available (*e.g.* for human remains or artefacts) and sample yield is sufficient (*i.e.* $>$ 20 mg), single amino acid dating is preferred (see sections 5.4.7).

Second, ultrafilters can leach carbon into the sample (Brock et al., 2007; Bronk Ramsey et al., 2004a; Hüls et al., 2007). The polyethersulphone (PES) membrane in the ultrafilters used at ORAU are coated in a glycerol humectant to prevent them from drying out, which needs to be removed prior to use. A more rigorous cleaning protocol was introduced after it was noticed that low yield samples showed older than expected dates (Bronk Ramsey et al., 2004a), which is consistent with leaching of dead carbon. The improved cleaning procedure involves two washes in ultrapure water, followed by ultrasonication for 1h, and a further three washes (Brock et al., 2007; Bronk Ramsey et al., 2004a). For quality control, further precautionary steps are followed:

1. From each batch of bones treated, one ultrafilter is selected and the carbon content of 1 mL of ultrapure water used to rinse the filter before the final 2 washes is measured.

2. From each ultrafilter batch manufactured, the age of the humectant from one ultrafilter is measured by following above protocol.

3. One in every 20 submitted samples is measured in duplicate to control reproducibility.

4. Alongside every batch of bone samples, a high (approx. 500 mg starting weight) and low mass standard (approx. 200 mg starting weight) is pretreated and measured.

These measures control for (1) the amount of contamination added during ultrafiltration, (2) the age of the contaminant, (3) reproducibility of the

method and (4) variation in effect on large and small sample sizes. They have shown that the age of the humectant varies significantly and is since 2005 most often post-bomb in age Brock et al. (2013). The background correction used for ultrafiltered samples was last revised by Wood et al. (2010).

5.4.7 Hydroxyproline (NRC) pre-treatment protocol

The pre-treatment protocol for extracting hydroxyproline (HYP) for dating initially follows the same steps as describe in the gelatine (AG) protocol (see subsection 5.4.5). If the collagen yield after freeze-drying exceeds 20 mg, and the sample is suspected to have been conserved, the steps for single amino acid dating as described by Devièse et al. (2018) are followed.

Between 20–50 mg of collagen[5] is placed in a 11.5 mL screw-top glass test tube, and 6 M HCl is added via a micropipette. The volume of HCl solution is determined by sample mass, with 1 mL of 6 M HCl per 10 mg of collagen. The sample mass is always rounded up, *e.g.* 24 mg of collagen would use 3 mL of 6 M HCl. The tubes are subsequently flushed with N_2 gas for 5 min. to provide an inert atmosphere, before they are closed and placed in a heating block at 110°C for 24h. This procedure (hydrolysis) will free the amino acids by breaking the collagen's peptide bonds.

The hydrolysis solution is evaporated to dryness using a Genevac EZ-2 vacuum evaporator. Afterwards, the sample is re-dissolved in 700 µL of 0.1 M NaOH. Using an alkaline solution moderates the acidity of the sample, thus preventing degradation of the chromatographic column's stationary phase. The sample solution is filtered using a 0.2 µm PTFE syringe filter attached to a 2 mL Plastipack™ syringe, and transferred into a 1 mL HPLC total recovery vial. As retrieving as much of the sample as possible is essential, 300 µL MilliQ™ ultrapure water is added to the amino acid residue, and the solution filtered as described above.

[5] 20-30 mg is roughly needed to obtain sufficient carbon for a small graphite target (0.8 mg C), while 30-50 mg should provide enough HYP for a large graphite target (1.8 mg C).

The sample is injected into an HPLC with a Primesep A column (22 x 250 mm, particle size 5 µm; SIELC), using two phases (eluent A was MilliQ™ deionised water, and eluent B 0.3 % by volume phosphoric acid diluted with MilliQ™), and a flow rate of 18 mL/min. The column is a silica-based single mixed-mode chromatographic column (for details see Devièse et al., 2018). The main mechanism separating the amino acids is cation exchange, where the ionisable base moieties within the amino acids interact with the embedded ionic group of the column. To keep retention time consistent, the system is heated to 30°C. Furthermore, the use of carbon free eluents is central to the method, as organic solvents may could affect the radiocarbon date.

Separation of all amino acid is achieved within 290 min. However, the amino acid of interest – hydroxyproline – is collected between 15.5–17.5 min., resulting in a fraction of 36 mL. The sample is contained within MilliQ™ deionised water. To obtain just the HYP, the sample is dried in a Genevac EZ-2 Plus vacuum evaporator.

A six-point calibration curve using the HYP peak area is used to estimate the amount of HYP collected. The curve is based on the results of HYP standards of known concentrations, and resulted in the estimations that at least 5 million absorption units are needed for a large AMS target (1.8 mg C), and ca. 2.5 million units for a small AMS target (0.8 mg C) (Devièse et al., 2018, fig. 3 and tab. 4).

For combustion, the HYP is reconstituted in 25 µL of ultrapure water and pipetted onto 12 mg of Chromasorb™ in a cleaned tin capsule. The sample is subsequently combusted and graphitised, and the AMS target pressed following the same procedure as for standard collagen samples.

The HPLC system is cleaned by flushing with 0.3% phosphoric acid (eluent B) for 30 min., and then with MilliQ™ (eluent A) for 2h. In addition, dating quality is controlled by running a background standard for every 4 unknown samples – ideally one that was pre-treated along the unknowns. Re-

sults from these standards are also used for the sample specific background correction (see below).

As the pre-treatment was still in development during the period of this doctoral dissertation, the protocol, and thus the samples it was applied to, are listed as NRC ('non-routine chemistry'), and all hydroxyproline dates received a lab code starting in 'OxA-X'. However, these labels are not a quality judgement. The protocol has by now been tested on a significant number of standards and samples (*e.g.* Devièse et al., 2017), and published in Devièse et al. (2018). Nonetheless, the labels are retained for all single amino acid dated samples in this thesis.

HPLC background correction

All samples treated and dated at ORAU are corrected for carbon added during routine procedures, *i.e.* standard pre-treatment chemistry, combustion and graphitisation. As hydroxyproline dating was a non-routine protocol, all HYP samples require an additional correction for any carbon added during the chromatographic separation on the HPLC.

Modern standards (Marry Rose pig bones) run at ORAU demonstrated that dead carbon's contribution to trace carbon during HPLC analysis is negligible, and only modern carbon contamination has to be considered (Devièse et al., 2018). As a result, the following formula was applied to correct HYP radiocarbon measurements:

$$F^{14}C_{Hyp} = \frac{AMS - MF_{Mod}}{MF_{Hyp}} \tag{5.1}$$

where AMS represents the $F^{14}C$ of the sample measured; MF_{Mod} the mass fraction of modern contamination; and MF_{Hyp} the mass fraction of the sample hydroxyproline.

The mass fraction of the HYP sample was approximated using the following formula:

$$MF_{Hyp} \approx 1 - MF_{Mod} \tag{5.2}$$

Table 5.5: Methods: Lemon Mine background standards run with HYP samples for this thesis, and used for HPLC background correction. The standard 18801.166 NRC 01 failed graphitisation, and was therefore not part of the correction.

Sample	C_{Std}	AMS_{Std}	ΔAMS_{Std}
19651.165 NRC 01	1.0600	0.00116	0.00099
19651.167 NRC 01	0.9196	0.00143	0.00113
18801.166 NRC 01	0.7916	–	–

The mass fraction of modern carbon was estimated by:

$$MF_{Mod} \approx \frac{AMS_{Std} \times C_{Std}}{C_T} \tag{5.3}$$

where AMS_{Std} is the measured $F^{14}C$ of the background standards; C_{Std} the mass of carbon in the background standards as measured on the mass spectrometer; and C_T the mass of carbon of the HYP sample as measured on the isotope-ratio mass spectrometer (IR-MS). The values for the standards run with the HYP samples in this project are listed in table 5.5.

In addition to correcting the $F^{14}C$ measurement for HPLC background, the AMS error has to be adjusted. For this, the following formula was applied:

$$\sigma F^{14}C = \sqrt{\left(\frac{1}{MF_{Hyp}} \times \Delta AMS\right)^2 + \left(\frac{1}{MF_{Hyp}} \times \Delta MF_{Mod}\right)^2 + \left(\frac{MF_{Mod-AMS}}{(MF_{Hyp})^2} \times \Delta MF_{Hyp}\right)^2} \tag{5.4}$$

The error on measuring carbon content on the IR-MS was calculated based on 86 alanine standards measured in the course of this dissertation. The result of 0.0168 % is comparable to the measurement variability observed by other technicians over the past 5 years.

5.5 General quality control indicators

In addition to treatment specific quality control measures, some general quality indicators are checked to assess the reliability of each bone radiocarbon date. These include auto-duplication, running of high and low mass bone

standards, collagen yield, stable isotope measurements, carbon concentration on combustion, AMS δ^{13}C offset and AMS current.

Auto-duplication means that each sample with a P-number dividable by 20 has two separate fractions pre-treated to test for dating reproducibility. If the auto-selected sample has insufficient material for duplication, a substitute is chosen. In addition, laboratory contamination from modern carbon is assessed by running both a high mass and low mass background standard with each treated batch of 18 samples.

Collagen yields of $<$ 1 wt.% are flagged at ORAU. However, there is some discussion of how small is too small. For example, van Klinken (1999) highlighted how it is difficult to remove contaminants from samples with collagen yields of $<$ 0.5 wt.%, though also mentions that yields of 0.5–2 wt.% may sometimes be problematic. In contrast, some low yield samples give reliable radiocarbon measurements. Therefore, a yield of $<$ 1.0 wt.% that is still sufficient for a 0.8 mg C AMS target is only used to fail a sample in conjuncture with other quality control issues.

Samples at ORAU are combusted in a continuous-flow elemental analyser/mass spectrometer combination. This provides vital elemental and isotopic information that can be used for quality assessment. First, carbon concentration of the combusted sample is monitored. It has been previously noted that the average values for bone of indiscriminate quality (n=2146) combusted at ORAU is 34.8 $\pm$ 8.8 wt.%C (van Klinken, 1999), though this value has changed over the years. The dataset from this dissertation (n=191) produced an average of 41.7 $\pm$ 2.3 wt.%C, which is in line with values presently observed for samples processed at ORAU. Furthermore, this value is consistent with observations from other laboratories. For example, Kiel uses a range of 40–45 %C (Matthias Hüls, pers. comm. 11/07/2018). Higher values are seen as indicative of organic carbon added, while lower ones suggest the presence of inorganic substances.

The expected C:N ratio of bone collagen is 3.2. DeNiro (1985) argued that a C:N ratio outside the range 2.9–3.6 implies contamination. However, this

range may include samples with significant added carbon (van Klinken, 1999). Such carbon contamination could have a detrimental effect on samples dating to the Middle to Upper Palaeolithic biocultural shift. Therefore, the range is narrowed to 3.1–3.4, consistent with experience obtained at ORAU. In contrast, C:N ratios for hydroxyproline samples should be 5.0. Samples with values 4.8–5.2 are presently seen as unproblematic, though greater variability may result from small sample sizes and require further investigation.

The stable isotope measures δ^{13}C and δ^{15}N show significant inter sample variability as a result of environmental and dietary variations. Nonetheless, values substantially deviating from the norm have a high risk of contamination. For bone collagen, the ranges of -19–24 ‰ (δ^{13}C) and 2–12 ‰ (δ^{15}N) are used. Lower δ^{13}C values (*ca.* -25–28 ‰) are expected for hydroxyproline.

During AMS measurement, significant δ^{13}C offsets, variable current or a current lower/higher than the other targets on the sample wheel are flagged and assessed on a case by case basis. If they are expected to have affected dating reliability, the sample is either re-dated or failed.

Samples failing the above mentioned quality control indicators are likely less reliable as a result of contamination or collagen degradation. It is worth noting, however, that there is no guarantee that all contamination will lead to outlying quality control measures. Close to the dating limit, radiocarbon measures are very sensitive, and even small amounts of modern carbon can lead to deviations from the true age of a sample. Nonetheless, when applied in conjunction with a larger number of dates, method comparisons, archaeological priors, modelling and consilience with independent dating, it will lead to a increasingly robust dataset.

Chapter 6

Analysis of $F^{14}C$ and radiocarbon dates

As shown in chapter 4, $F^{14}C$ and radiocarbon ages cannot be directly transferred into calendar ages. Further analysis is needed to obtain archaeologically meaningful answers. This can entail a simple calibration or – in most cases – the use of Bayesian models to calculate end and start dates, phase duration and occupation frequencies.

The methodologies that are used in this thesis are described and evaluated in the following sections. As analysis is conducted within the software package OxCal 4.3 (Bronk Ramsey, 2009a), the program and the application of statistical analysis within it are presented in more detail towards the end.

6.1 Calibration

The calibration curve used for all radiocarbon measurements in this dissertation is IntCal13 (Reimer et al., 2013), an international radiocarbon calibration curve developed by the radiocarbon community for the calibration of terrestrial samples from the northern hemisphere (see fig. 6.1). It is presently

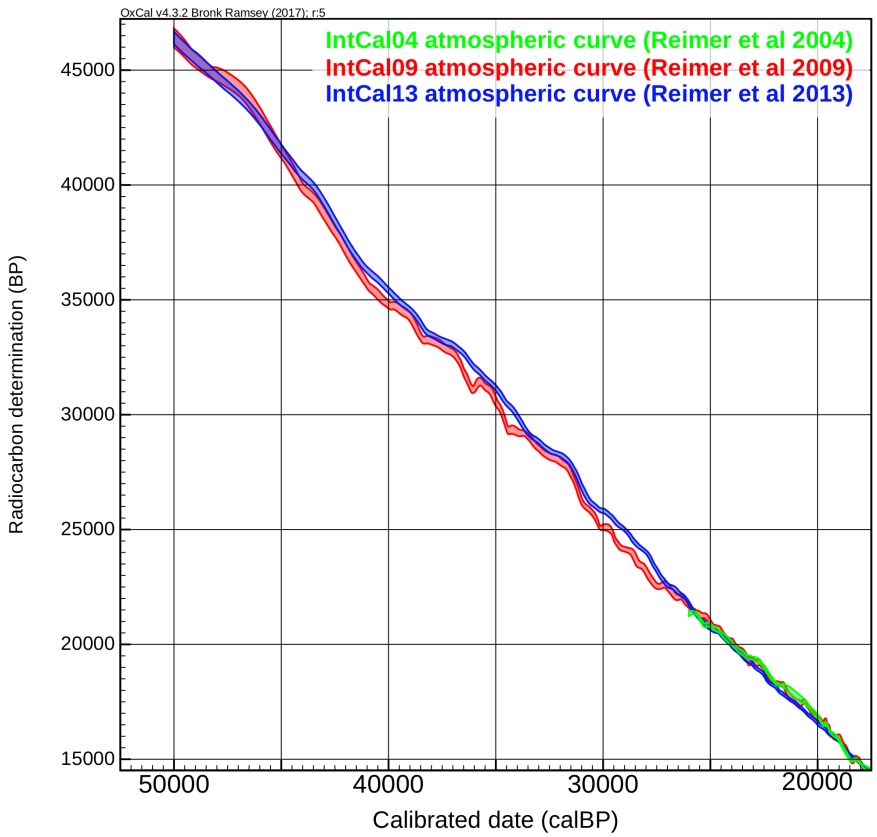


Figure 6.1: Methods: comparison of IntCal04 (**green**), IntCal09 (**red**), and IntCal13 (**blue**) calibration curves for terrestrial records from the northern hemisphere.

the most up to date curve available[1], and is after IntCal09 (Reimer et al., 2009) only the second curve that reaches as far back as 50k cal BP – a requirement for establishing more reliable chronologies for the Middle to Upper Palaeolithic biocultural shift. As the curve's underlying data and methodology can heavily influence the dating outcome, and calibration is essential to meaningful radiocarbon analysis, some of the most important features of IntCal13, as well as some of the differences to IntCal09 (and IntCal04) will be highlighted.

[1] An updated calibration curve for the terrestrial record from the Northern Hemisphere is planned to be published in 2019.

IntCal13 incorporates the dataset from IntCal09, with the addition of some newer datasets[2] (Reimer et al., 2013). For the time period of interest, they include ^{14}C measurements on terrestrial plant microfossils from the varved sediments of Lake Suigetsu (Japan), and U-series dates on speleothems from Lake Suigetsu, from the Bahamas and from Hulu Cave (Beck et al., 2001; Bronk Ramsey et al., 2012; Hoffmann et al., 2010; Kitagawa and Van Der Plicht, 1997; Kitagawa and van der Plicht, 1998, 2000; Marshall et al., 2012; Nakagawa et al., 2012; Schlolaut et al., 2012; Southon et al., 2012; Staff et al., 2010, 2013). The calibration curve is built using Bayesian modelling with Markov chain Monte Carlo sampling (specifically a Metropolis-within-Gibbs sampler), and the statistical analysis is described in more detail in Niu et al. (2013).

As a result of the spread in the underlying dataset and the methodology applied, the resulting curve is smoother than IntCal09 (see fig. 6.1). It is important to notice, that the loss of structure is affecting the radiocarbon age range between 27–32k BP, where dates calibrated with IntCal09 give older calibrated age probabilities (Bronk Ramsey et al., 2013). In addition, the time period $>$ 40k cal BP sees a flattening of the curve for IntCal13. Of special interest is also the time period around 40k cal BP, when the Laschamp magnetic excursion and the Campanian Ignimbrite (CI) volcanic eruption occurred. Here, we observe significantly more structure in local curves (*e.g.* the Suigetsu record) compared to IntCal13 and IntCal09.

Despite the limitations of the IntCal13, it presently represents the most robust curve available for the time period of interest. As the smoothing is the result of an inability to distinguish between ^{14}C patterns and noise, using IntCal09 is not a viable alternative. The introduction of more structure may not necessarily represent a more accurate radiocarbon signal.

[2]The datasets are available from http://intcal.qub.ac.uk/intcal13/.

6.2 Bayesian analysis

Throughout this thesis, Bayesian statistics are used to model radiocarbon dates and other chronological markers to obtain a chronology for the Middle to Upper Palaeolithic.

In Bayesian statistics the underlying theorem can be expressed in relation to the data obtained (x) and the unknowns or assumptions (θ). Bayes' theorem states:

$$p(\theta|x) = \frac{p(x|\theta)}{p(x)} \times p(\theta) \tag{6.1}$$

where $p(\theta)$ denotes the prior belief about a parameter; $p(x|\theta)$ the likelihood of obtaining the observation, if the parameters were known; $p(x)$ the probability of obtaining the data integrated over all possible values of the parameter; and $p(\theta|x)$ the posterior belief which incorporates the prior beliefs and data, thus the result we are interested in.

For the purpose of understanding, this can be simplified for radiocarbon dating to:

posterior information (answer)	=	standardised likelihood (radiocarbon date)	×	prior information (archaeology)

Bayesian statistics follows a radically different approach to frequentist statistics. In the latter, the sought parameter is seen as a fixed constant, i.e. the distribution of sample statistics is equal to the probability that the population statistics would fall within the stated range. In contrast, in Bayesian statistics every possible value for the unknown is explicitly given a probability before the data is obtained. The resulting posterior distribution (posterior density estimates) represents the most likely value for the unknown. The result is normally quoted at a 95% confidence interval.

Consequently, Bayesian statistics asks what random variable led to the observed data, rather than whether the observed data is likely to be a result

of an assumed variable (for a comprehensive and well written introduction see Kruschke, 2015).

Bayes' theorem and his approach to probability is not new. It was first published in the 18th century (Bayes, 1763), but it was not until the application of advanced computer technology that it found wide spread application in research and industry.

Using prior beliefs in the calculations introduces a subjective element, which becomes more important in generating the output the smaller the actual dataset. From a Bayesian perspective it is argued that such prior beliefs are present in all statistical analyses and it is, therefore, preferable to explicitly have them stated. Having them logically and coherently incorporated into the analysis allows the results to be queried and the assumptions to be tested (*e.g.* Litton and Buck, 1995). An example of this is knowing that a signal must be positive for it to be a real, physical value. In frequentist statistics, such prior knowledge must be incorporated in an *ad hoc* fashion. Accordingly, in Bayesian statistics, a heuristic cycle is run in which the "*probability sought can be continually refined by using yesterday's posterior belief as today's new priors*" (Bayliss et al., 2007). In practical terms this requires the use of modelling algorithms such as the widely used Markov Chain Monte Carlo (MCMC) simulations, where large numbers of iterations can be run and tested.

The field of radiocarbon dating and archaeology are well suited for the application of Bayesian statistical approaches: experiments can rarely be repeated, prior information is often available (*e.g.* seriation and stratigraphy), dates have non-normal error terms after calibration, and dates are expensive and at times difficult to obtain.

Originally, Bayesian statistics was introduced to the field of radiocarbon dating for calibration purposes. However, it was soon realised that it could be used to directly improve the dating methodology through increasing dating precision (*e.g.* Bronk Ramsey et al., 2010b), to test hypotheses (*e.g.* Needham et al., 1998), and to design sample selection strategies (Bayliss,

2009). Moreover, through the application of Bayesian statistics, archaeologically more meaningful questions can be addressed, including querying start and end dates or duration of a context (*e.g.* occupation, cultural expression), investigating potential mixing at a site, establishing probable minimal occupation frequency and objectively assessing dating outliers (for reviews see Bayliss, 2009; Bronk Ramsey et al., 2010a; Dee et al., 2013; Litton and Buck, 1995).

6.3 Kernel Density Estimation (KDE)

Most radiocarbon modelling in archaeology has used archaeological information as priors to inform their Bayesian models. However, it is exactly these stratigraphic assumptions that often introduce a significant bias – especially in cases where the stratigraphy is complex, excavation or its documentation poor, or significant post-depositional disturbances tainted the stratigraphic integrity. Therefore, there is meaningful information gained from determining temporal age densities within a radiocarbon dataset independent of the samples supposed stratigraphic order.

In the past, many have tried to sum radiocarbon datasets (*i.e.* superpose all the individual calibrated distributions), and struggled with separating meaningful events from the significant noise present (Armit et al., 2014; Bamforth and Grund, 2012; Buchanan et al., 2008; Contreras and Meadows, 2014; Culleton, 2008; Kerr and McCormick, 2014; Shennan, 2013; Williams, 2012). Methods correcting for noise often over-smooth the data. In addition, addressing statistical spread requires the introduction of other forms of Bayesian analysis.

This thesis uses an approach where kernel density estimation (KDE) is combined with Bayesian modelling instead. KDE is a widely used non-parametric method for analysing distributions in discrete datasets (Parzen, 1962; Rosenblatt, 1956). As such, it is a frequentist approach and does not require any formal priors. However, radiocarbon dates come as probabil-

ity distributions, and additional uncertainties are introduced via calibration. As a consequence, the KDE approach is applied to each specific MCMC state of a sampled distribution, and subsequently averaged over the different MCMC states run. This means, instead of maximising likelihood, a Metropolis-Hastings algorithm is applied. As the dates within the dataset are not fully independent, the method needs to take the KDE from other measurements into account when updating the likelihood of an individual measurement. The result is a likelihood weighted average of KDEs with slightly different bandwidths (Bronk Ramsey, 2017).

This radiocarbon specific approach to KDE modelling was developed by Bronk Ramsey (2017). It is used in this dissertation to estimate minimum occupation events, visualise distribution of occupations, test stratigraphic integrity and assumptions, and examine temporal distributions of diagnostic artefacts, such as different types of osseous points.

6.4 Software package OxCal

An important factor in the spread of Bayesian approaches to radiocarbon dating was the introduction of several programs facilitating the application of complex computational methods (see also Buck and Meson, 2015). For this dissertation, all analysis is conducted in OxCal 4.3 (Bronk Ramsey, 2009a), a software package developed and maintained by Prof C. Bronk Ramsey at the University of Oxford[3]. While it is felt that it is the most comprehensive software package, and well suited for the work presented here, it should be noted that it is by no means the only available program[4], though many others focus mainly on radiocarbon calibration.

[3]It can be accessed under `http://c14.arch.ox.ac.uk/oxcal.html`, where also an extensive user manual is available.

[4]Examples for alternative software suits are: BCal (Buck et al., 1999) from the School of Mathematics and Statistics at the University of Sheffield and accessible at `http://bcal.shef.ac.uk`; DateLab (Jones and Nicholls, 2002) from the Auckland University in New Zealand; or CALIB (Stuiver and Reimer, 1993) from the University of Washington and accessible at `http://calib.org/calib/index.html`.

OxCal is comprised of three modules: (1) project manager, (2) analysis, and (3) output. The project manager is used to input the chronological information using the Chronological Query language (CQL) in the user interface. This programming code was designed for the calibration package and described by Bronk Ramsey (1998). Throughout this thesis, CQL statements are shown in `Courier New`. The analysis module creates an output file from the CQL file (see figure 6.3). The analysis is conducted using a Metropolis-Hastings Algorithm, which is a form of Markov-Chain Monte Carlo method. Finally, the resulting data is visualised in the output module and can be viewed in either graphical or table form.

6.4.1 Dates

In OxCal, dates are either entered as `R_Date()` for radiocarbon dates or as `Date()` for non-radiocarbon dates. Between the brackets, the label, the radiocarbon age, and its the standard error (or the non-radiocarbon age range, respectively) have to be specified: *e.g.* `R_Date("14C Date 1", 34000, 250)` for a date of 34000 ± 250 BP. If a non-radiocarbon age has a uniform age range rather than a specific calendar date, a uniform distribution can be defined using `U()`. Codes for other distributions exist and can be found in the online manual.

Without any further information included in the code, OxCal will calibrate the radiocarbon dates with the newest northern hemisphere calibration curve (presently IntCal13) and visualise the other dates as is, thus placing them all on the calendar time line.

OSL and TL dates are normally reported in years before present (BP). However, unlike radiocarbon dates, "BP" does not refer to a fixed year. Instead, present refers to the year of measurement. This information is not always given in publications. For the purpose of this dissertation, the difference between 1950 and the respective present is negligibly small when compared either to the measurement error associated with these dates, or to those of the radiocarbon dates used for modelling. Therefore, OSL and

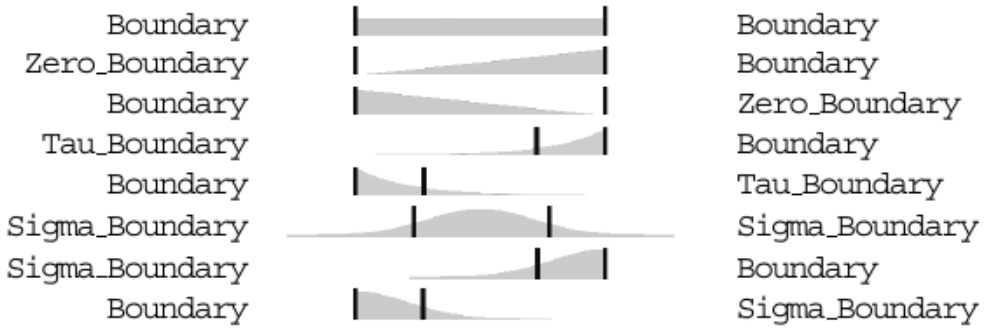


Figure 6.2: Methods: boundary commands used in OxCal 4.3 to achieve different uninformative priors (Bronk Ramsey, 2009a).

TL dates will be simplified by treating them as if they were given in years before 1950: *e.g.* an OSL age of 40000 ± 2000 years would be input as `Date("OSL",N(calBP(40000),2000))`.

6.4.2 Priors

Prior information can come in two types of beliefs: informative and uninformative. The first describes a prior belief which is based on the age relationship between samples as derived from the archaeological record (*e.g.* layer relationships) and is normally expressed in the distribution of dates into phases and sequences:

`Phase()`	➛ Group of events without internal order
`Sequence()`	➛ Group of events temporally ordered

The second refers to how dates are distributed within a phase (*e.g.* nature and speed of accumulation). The desired grouping is achieved through choosing the boundary commands accordingly (see fig. 6.2).

All events placed between two boundaries are treated as one group, including any nested phases found within. A uniform distribution of events within a phase is achieved by placing a simple `Boundary()` at either end.

(a)

```
Plot()
 {
 Outlier_Model("General",T(5),U(0,4),"t");
  Sequence("Example")
  {
   Boundary("Start 1");
   Phase("1")
   {
    R_Date("Ex-1", 33750, 850)
    {
     color="green";
     Outlier("General", 0.05);
    };
    Date("Ex-2",U(calBP(43000),calBP(70000)))
    {
     color="green";
     Outlier("General", 0.05);
    };
    R_Date("Ex-3", 38500, 1700)
    {
     color="green";
     Outlier("General", 0.05);
    };
    R_Date("Ex-4", 37650, 1450)
    {
     color="green";
     Outlier("General", 0.05);
    };
    R_Date("Ex-5", 34800, 1150)
    {
     color="green";
     Outlier("General", 0.05);
    };
   };
   Boundary("End 1");
   Interval("Interval 1 to 2");
   Boundary("Start 2");
   Phase("2")
   {
    R_Date("Ex-6", 33300, 820)
    {
     color="red";
     Outlier("General", 0.05);
    };
    R_Date("Ex-7", 32700, 300)
    {
     color="red";
     Outlier("General", 0.05);
    };
   };
   Boundary("End 2");
   Interval("Interval 2 to 3");
   Boundary("Start 3");
   Phase("3")
   {
    R_Date("Ex-8", 32200, 780)
    {
     color="red";
     Outlier("General", 0.05);
    };
    R_Date("Ex-9", 29150, 950)
    {
     color="red";
     Outlier("General", 0.05);
    };
   };
   Boundary("End 3");
  };
 };
```

(b)

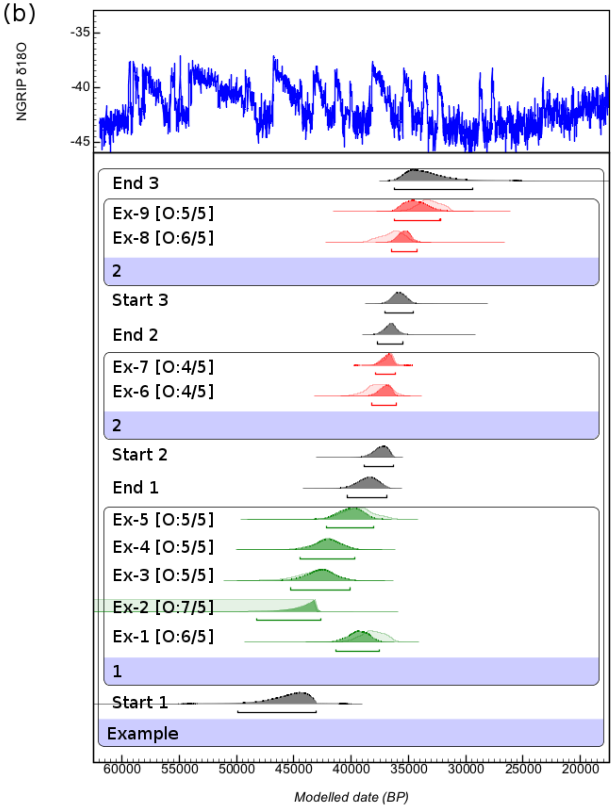


Figure 6.3: Methods: (a) CQL input and (b) output of a simple Bayesian model using OxCal 4.3.

If the event rate is steadily increasing or decreasing, a `Zero_Boundary()` is placed at the beginning or the end respectively. For an exponentially distributed group, the `Tau_Boundary()` is implemented. The `Sigma_Boundary()` allows the creation of groups where the events can spill beyond the dates of the boundary. If placed as both start and end boundaries, a normal distribution is generated, but if placed only on either start or end, the model without definitive start or end events is the consequence (Bronk Ramsey, 2009a).

The larger the scatter of radiocarbon dates within a `Phase`, the larger the age range considered for an event as a consequence of increasing number of possible date combinations. A `Phase` is therefore biased towards longer spans compared to a single radiocarbon age determination or a small group of dates (Bayliss et al., 2007). Including `Boundary` events as described above will reduce the bias, thus making them important components of any stratigraphic model (Bronk Ramsey, 2001; Buck et al., 1992). Whenever there is archaeological evidence for a hiatus or a sterile layer between two phases (*i.e.* stratigraphic layers or level), a double boundary can be introduced. In addition, in cases of a non-uniform distribution of dates, double boundaries may become necessary. Otherwise, a single boundary for separation is sufficient (see example in fig. 6.3).

6.4.3 Queries

OxCal offers several options to interrogate a model beyond simple dating of events. One of these, the `Boundary`, has already been introduced above, and allows the calculation of possible start and end dates for events or group of events. Other important functions are:

```
Boundary()    ➛ Start and end dates of events
Difference()  ➛ Difference between two inputs
Interval()    ➛ Distance between two events
```

`Span()`	➛ Distribution of events in a phase
`Order()`	➛ Probability of event order
`R_Combine()`	➛ Probability of identical event

The `Interval` command can be placed between two events to investigate, for example, over what period a palimpsest formed or how much time passed between two occupations. The function will automatically subtract one event from the other (*e.g.* one `Phase` from the one next to it). `Difference` can also be used to calculate the difference between two events, though in this case it has to be specified what is to be subtracted. In contrast, placing `Span` in a `Phase` will calculate the distribution of dates within it. If the order of events is unknown or needs to be tested, `Order` can be used to model the probability of one event (*i.e.* `Date`, `Phase` or `Boundary`) happening earlier than another.

There are two important, non-Bayesian, functions[5]: `R_Combine` (for radiocarbon dates), and `Combine` (for non-radiocarbon dates). They perform a χ^2-test to assess whether two or more (radiocarbon) dates are statistically indistinguishable. `R_Combine` takes the weighted mean of the conventional age to produce a single calibrated age, while `Combine` returns the weighted mean.

6.4.4 Outliers & inconsistent data

The quality of the archaeological answers obtained from Bayesian models depends heavily on the reliability of the data and prior information used. Archaeological and laboratory quality assurance measures can highlight samples with a high likelihood to be unreliable. Additionally, it is crucial to have a means to test the reliability of the model applied.

[5]There is strictly speaking also one for calendar dates, *i.e.* `C_Combine`, but it is redundant for this dissertation as the calendar years in BC/AD are not used.

In the past, the robustness of a model, *i.e.* its reliability and stability, was assessed through (a) an Agreement Index and (b) measuring Convergence (Bronk Ramsey, 1995). The first provides an indication of model consistency (A_{model}) and of agreement between modelled date and its prior probability distribution (A). At an index below 60% (analogous to the 0.05 significance level in a χ^2-test), the model was deemed problematic. The second measure, Convergence (C), shows the difference between similar attempts at performing the MCMC analysis, thus indicating how representative the posterior probability and how stable the model is. If convergence is less than 95%, the model is considered unstable.

If outliers are detected in the dataset, there are two different ways of dealing with them: (1) exclude them from the model, or (2) down-weight the sample, thus reducing its impact on the final outcome. In terms of analysis quality, the latter strategy is normally preferred, as it is safer to assume that we can never be certain of whether a particular measurement is an outlier. However, the approach using Agreement Index and Convergence described above falls under category one, and the only way to enhance models under such conditions is to exclude outlying data until such time as the Agreement Index and Convergence have improved. Therefore, the presently preferred method in OxCal – and applied in this thesis – is implementing an outlier model.

In an outlier model, samples are weighted according to their likelihood of being an outlier. They are further down-weighted if the model iterations identify them to be more likely an outlier. The final result averages between the model result accepting the measurement and rejecting it (for details see Bronk Ramsey, 2009a,b; Bronk Ramsey et al., 2010a).

The outlier model in OxCal is called upon using `Outlier_Model()` and requires each date to be given the attribute `Outlier()`. Normally, the general t-type outlier model is applied:

```
Outlier_Model(“General”,T(5),U(0,4),”t”);
```

The outliers are drawn from a Student's t-distribution with five degrees of freedom. The use of the Student's t-distribution accounts for extreme outliers as it is bell-shaped like a Gaussian distribution, but with larger tails. `U(0,4)` defines the scale as a uniform distribution from 10^0 to 10^4 years, thus allowing the dating offset to be anything between 1 and 10,000 years and leaving the determination to the program. The 'type' of the model is defined as "t", which means that the outliers are in the time variable (Bronk Ramsey, 2009b).

For samples that have been dated more than once and feature in the model as `R_Combine`, the individual radiocarbon measurements, `R_Date`, are treated with a different outlier model (see below), while the group as `R_Combine` follows the previously presented model.

```
Outlier_Model("SSimple",N(0,2),0,"s");
```

In this case, the outliers are taken from a normal distribution with zero as a mean and 2 as the standard deviation. There is no scaling, and the shifts are not applied to the time variable as above, but to the ^{14}C concentrations ("s") (Bronk Ramsey, 2009b).

Both models – 'General' and 'SSimple' – are also suitable for non-radiocarbon derived dates as the offset is calculated on the calendar timescale. Irrespective of the chosen model, each date (`Date`, `R_Date`) and combined date (`Combine`, `R_Combine`) is initially assigned an arbitrary 5% probability of being an outlier (see also 6.3):

```
Outlier("General",0.05);
Outlier("SSimple",0.05);
```

An appropriate `Outlier_Model` will be incorporated into all Bayesian stratigraphic models presented in this thesis. OxCal also offers other outlier options. A charcoal outlier model, which takes the old wood effect into account is quite common. However, this model will, despite the charcoal dates,

not be applied here as the error derived from the measurement uncertainty outweighs any old wood effect.

6.4.5 KDE & summarising datasets

OxCal 4.3 offers different methods to summarise datasets (see below). `Sum` simply superimposes all individual calibrated distributions, thus assuming that each date is independent. The quality is thereby heavily dependent on dating precision and accuracy, as well as random sampling – all aspects difficult to achieve in an archaeological context. Therefore, this dissertation will implement the KDE functions instead, which combine frequentist with Bayesian methods.

`Sum()`	➛	superimposes all individual calibrated distributions
`KDE_Plot()`	➛	KDE/MCMC implementation, treats all data as fully independent
`KDE_Model()`	➛	KDE/MCMC implementation, treats data as not fully independent

The difference between the two available options, the `KDE_Plot` and the `KDE_Model`, is that the former assumes each date (`Date`, `R_Date`) within the function to be fully independent, while the latter does not. As a result, `KDE_Plot` has to be used in connection with another Bayesian model (*e.g.* start and end boundaries) to prevent the resulting distribution to be over-dispersed and the underlying signal smeared – especially when dealing with larger uncertainties. `KDE_Model`, on the other hand, can be used on its own (Bronk Ramsey, 2017).

For this dissertation, the `KDE_Model` function is more appropriate, as the chosen sampling process for radiocarbon dating is not random, but focuses on anthropogenically modified bone, and thus on instances of human occupation. It is assumed that the evidence for individual occupations cluster

chronologically, though might contain some offset due to the nature of the radiocarbon dating error. At the same time, it is impossible to guarantee that each occupation instance was sampled at the same frequency, as the geological layers and archaeological levels identified are not always an adequate proxy for individual occupation instances.

For the `KDE_Model` the default parameters are chosen – a normalised *kernel*, and a uniform *factor* relative to Silverman's rule – and the events to be modelled are placed between the brackets `{...}` (see below).

```
KDE_Model("KDE", N(0,1), U(0,1)){...};
```

As a result, the model's MCMC implementation uses an equal number of random samples from each event (*e.g.* radiocarbon date) in the model within the kernel probability distribution function. A Metropolis-Hastings algorithm decides on whether to accept or reject a move. The final likelihood is the product of (a) the likelihood of the measurement, and (b) the KDE established by the other parameters (for mathematical implementation see Bronk Ramsey, 2017).

The output can be visualised in a single plot, containing the summed distribution in the background, and the MCMC derived KDE distribution in the foreground. In addition, the 1σ variability in the calculated KDE distributions is shown as a shaded band, and based on KDE snapshots that are taken at a rate of 1000 MCMC iterations.

6.4.6 Sensitivity testing

It is crucial to objectively understand how sensitive Bayesian models are to the influence of the priors used (Bayliss et al., 2007; Bronk Ramsey et al., 2010a). It is therefore advised to observe the effect of changing individual priors, for example, by implementing a different event distribution in a `Phase` or drastically increasing the outlier probability. In cases where the

influence of a prior belief is large and boundaries generated are different, archaeological assumptions can be called to argue for one model over another. The sensitivity of KDE models can easily be tested by added or subtracting events from the dataset and compare their results. In general, results based on larger datasets with good precision and accuracy tend to be more robust than those on smaller datasets or with decreased dating reliability.

Part IV

Site Analysis & Chronologies

Chapter 7

Site selection

Archaeological sites along the Danube corridor were selected for their suitability to build a more robust radiocarbon chronology of MP/UP biocultural shift, and test models of biological and cultural expansions (*e.g.* the Danube corridor hypothesis, and the *Kulturpumpe* model). The focus was on sites that contained (a) human remains, (b) a deep stratigraphy, (c) diagnostic lithic industries, or (d) osseous points. The latter were of special interest, as they are often directly datable artefacts seen as diagnostic of the 'Aurignacian' technocomplex.

The selection was not restricted to sites where the MP and UP industries were separated by a sterile layer. While such clear separation of occupation events facilitates Bayesian modelling, it also introduces the assumption that MP and UP industries – and with them Neanderthal and AMH occupations – were in all locations chronologically separated by a significant period of time. This approach was avoided due to the possibility of a fast moving AMH expansion as well as regional Neanderthal-AMH-cohabitation.

With these criteria in mind, a total of 18 sites were selected (see fig. 7.1). More information on 16 of these sites is presented in the following chapters, including more details regarding their selection process and the insights gained through radiocarbon dating and analyses. The two other localities were not sampled for radiocarbon dating as initially planned. The Mladeč

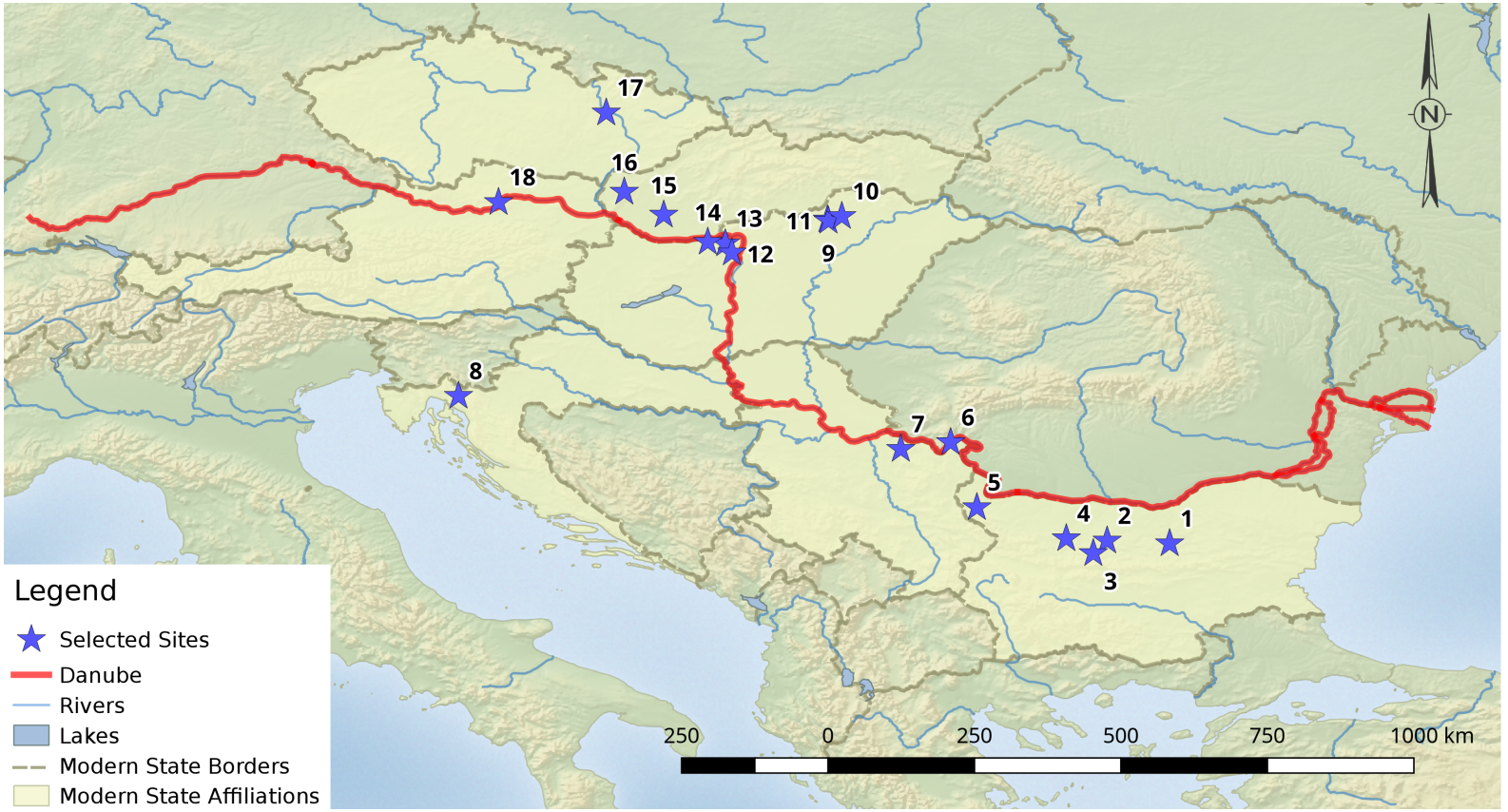


Figure 7.1: Site selection: map highlighting sites selected for radiocarbon dating, and their present country jurisdictions: (1) Manastira, (2) Tabashkata, (3) Toplja, (4) Temnata Dupka, (5) Kozarnika, (6) Tabula Traiana, (7) Dubočka Kozja, (8) Bukovac, (9) Peskő, (10) Szeleta, (11) Istállóskő, (12) Máriaremete, (13) Bivak, (14) Jankovich, (15) Šal'a, (16) Dzeravá Skala, (17) Mladeč, (18) Willendorf.

ivory point from the eponymous site and the five osseous points from Willendorf II (stored at the Natural History Museum in Vienna) gave measured nitrogen concentrations of < 0.14 %. This is well below the threshold of 0.7, and the low chance of collagen preservation does not presently warrant further damage to the artefacts.

No sites from Romania were included. While organic preservation is rare in that part of Europe, the absence of selected sites is not indicative of an absence of datable material. Instead, it reflects the difficulties accessing the archaeological remains. However, some of the sites are presently being investigated by other international teams (*e.g.* by the Collaborative Research Centre 806 'Our Way to Europe'), and it is hoped that some of their dating results will become available in the near future.

A further gap in the site distribution along the Danube fluvial corridor is observable in the Hungarian Plain and the northern parts of Serbia. This is unlikely to reflect actual occupation patterns, but is rather an artefact of archaeological research. This area is known for its thick loess deposits (see fig. 7.2), which have accumulated since the time period of interest. As a result, any layers dating to the MP to UP transition would be covered by several meters of sediment, thus making the detection of open-air sites in the region extremely difficult and rare. At the same time, the landscape offers only limited cave localities, where the impact of loess may be mitigated.

The nature of the known archaeological record leads to an involuntary focus on cave sites and an apparent neglect of open-air localities. Cave sites often offer a more stratified record. In addition, they appear to more commonly contain datable organic remains. While this situation cannot presently be improved, it is worth remembering the sample bias when interpreting the dating results.

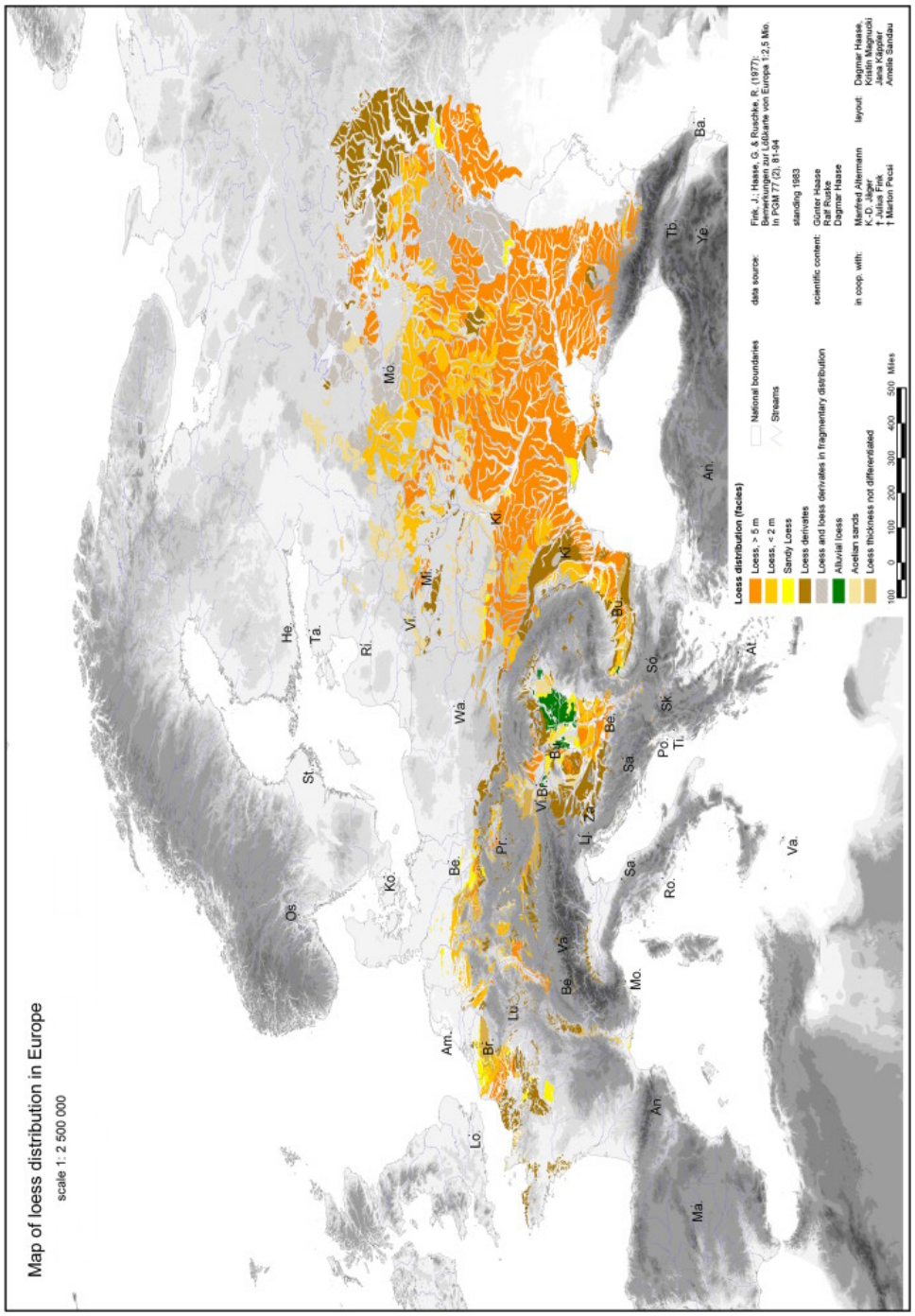


Figure 7.2: Site selection: map of loess distribution in Europe according to Haase et al. (2007).

Chapter 8

Bulgaria

Palaeolithic research has a long tradition in Bulgaria, including extensive international collaborations with researchers in Poland, France and Germany. In this chapter, the most promising Bulgarian sites in terms of stratigraphic sequences, related osseous industries, and human remains are presented (see fig. 8.1).

There are three cave sites containing a deep stratigraphy covering the Middle to Upper Palaeolithic biocultural shift with substantial archaeological material: Bacho Kiro (Бачо Киро), Temnata Dupka (Темната дупка), and Kozarnika (Козарника). All three are situated on the northern flanks of the Balkan Mountains (ca. 100 km apart, as the crow flies), and close to tributaries to the Danube.

Bacho Kiro was extensively excavated in the 1970s by a Polish-Bulgarian team led by J. Kozłowski (Kozłowski, 1982). They identified Middle Palaeolithic occupations followed by a new and distinct technocomplex termed Bachokirian, and several 'Aurignacian' and 'Gravettian' levels. The site is rich in osseous industries, including 6 spear points, two tooth pendants, and one engraved bone fragment (Гуаделu, 2011), and has yielded human remains from a *Homo neanderthalensis* as well as from a *Homo sapiens* individual. As a result, Bacho Kiro is a key site for studying the Middle to Upper Palaeolithic. Radiocarbon dating indicated an appearance of EUP

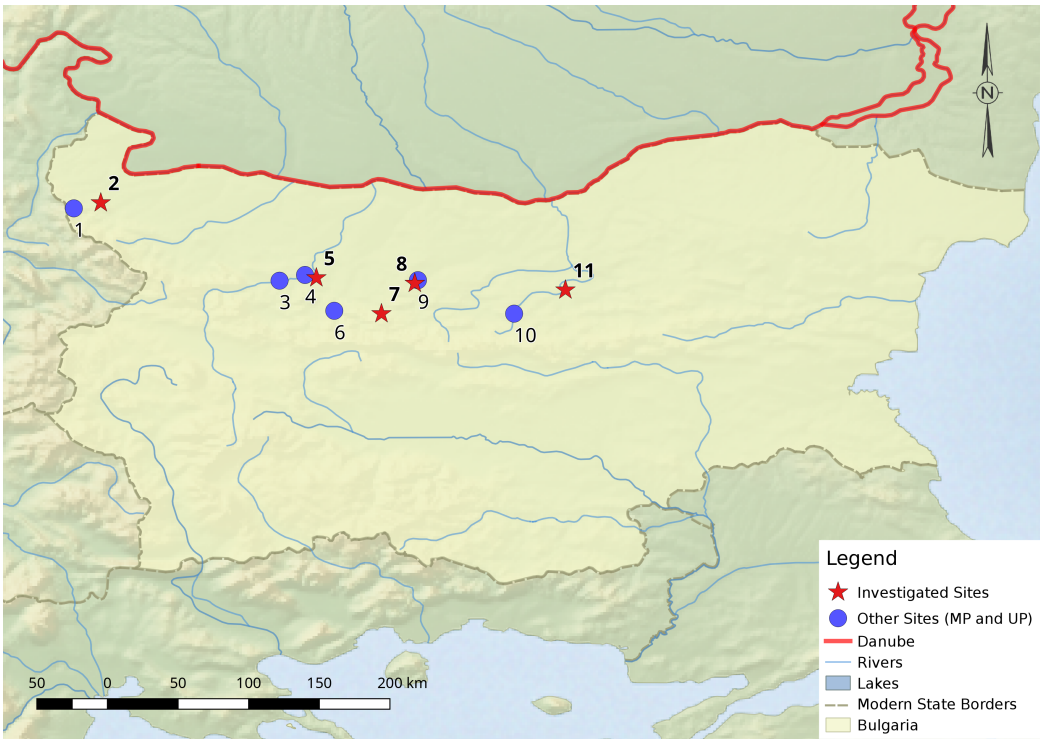


Figure 8.1: Bulgaria: map of MP/UP sites evaluated: (1) Redaka II, (2) Kozarnika, (3) Pesht, (4) Samuilitsa II, (5) Temnata Dupka, (6) Morovitsa, (7) Toplja, (8) Tabashkata Peshtera, (9) Vasil Levski Cave, (10) Bacho Kiro, (11) Manastira.

industries, which included the Bachokirian, prior to 40k cal BP (calibrated with OxCal 4.3 using IntCal13, based on dates from Hedges et al., 1994; Kozłowski, 1982), though it is expected that modern dating methods may result in even older age determinations. The site is presently being further investigated – including radiocarbon dating – by a German-Bulgarian team in collaboration with the Max Plack Institute for Evolutionary Anthropology, and the National Institute for Archaeology and Museums of the Bulgarian Academy of Sciences.

Temnata Dupka was excavated in the 1980s under the direction of N. Sirakov (Ginter et al., 2000, 2011, 1994; Kozłowski et al., 1992). The stratigraphy shows Middle Palaeolithic, 'transitional'/EUP, 'Aurignacian', 'Gravet-

tian', and 'Epigravettian' lithic industries, and initial radiocarbon dating suggested an early appearance of the UP at the site (Bluszcz et al., 1992).

A Franco-Bulgarian collaboration, led by J.-L. Guadelli and N. Sirakov, started archaeological excavations at Kozarnika in the 1990s (ongoing), and revealed an extensive stratigraphy covering the Lower, Middle and Upper Palaeolithic. Of particular interest are the late Mousterian, 'transitional' or EUP, and Kozarnikian levels, where initial radiocarbon dating suggests an early transition.

Like Bacho Kiro, both Temnata and Kozarnika yielded human remains, as well as stratified lithic and osseous industries – including osseous points. Consequently, they, too, are crucial to the understanding of the Middle to Upper Palaeolithic biocultural shift.

More recently, another, albeit smaller, site from the MP/UP was discovered: Redaka II (Fernandez and Guadelli, 2008; Guadelli et al., 2013b). Presently, the lithic and osseous assemblages remain limited. However, stratigraphy and preservation suggest potential for future analysis – especially in case of further excavations and more detailed lithic analysis.

Samuilitsa II (Самуилица II) is another site with both MP and UP material mentioned in the literature (Sirakov, 1983; Гуаделли, 2011; Джамбазов, 1959). Unfortunately, it only consists of two geological units: an upper layer (UP) and an lower layer (MP). The limited information and material available, combined with the absence of osseous points, makes the site unsuited for industry targeted or high precision dating.

Apart from the aforementioned sites with osseous points, there are also smaller Palaeolithic sites that have produced such artefacts: e.g. Morovitsa (Моровица), Pesht (Рещ), Tabashkata (Табашката), Toplja (Топля), and Vasil Levski cave (Васил Левски). In all cases, context information is limited to non-existent, leaving direct radiocarbon dating as the only means to establish chronological context.

Джамбазов (1957) published a split-based point (SBP) from the lowest layer of three upper Palaeolithic layers at Pesht. From Morovitsa, a sin-

gle SBP made of *Rangifer tarandus* is known. This species is extremely rare south of the Danube (Гуадели, 2011). Vasil Levski cave produced at least two deer antler points (Kozłowski, 1975; Джамбазов, 1963). Kozłowski (1975) interprets the fragments as Mladeč points, though Guadelli (Гуадели, 2011) rightfully comments that there is insufficient evidence to securely connect these small point tips with the large, lozangic-shaped Mladeč points. Three osseous points with round cross-sections were found at Tabashkata: one grooved point, and two massive-based points (Гуадели, 2011; Джамбазов, 1963).

Stratified human remains from the Middle to Upper Palaeolithic are rare. However, at Manastira cave (Манастира) a significant number of *Homo sapiens* skeletal fragments were discovered without any associated archaeological material. As some of them show archaic features, direct dating could test whether these individuals are early AMH.

In short, Bulgaria is rich in Palaeolithic material. From the three key stratified sites, two – Temnata and Kozarnika – were investigated for this thesis. The third, Bacho Kiro, is currently being redated by another research team and their results are expected to be published in the near future. For direct dating of osseous point industries, access was granted to Kozarnika, Tabashkata, and Toplja. Human remains were obtained from Kozarnika, and Manastira.

8.1 Kozarnika

8.1.1 Introduction

Kozarnika (43.652 N, 22.702 E) is one of the most important Palaeolithic sites in Bulgaria, having provided a stratigraphy covering the Lower, Middle and Upper Palaeolithic. It is located in the Prebalkans in the north-west of Bulgaria, some 3 km from the village Oreshets (Орешец), in the district of Belogratchik (Белоградчик), and close to the Danube planes (see fig. 8.2).



Figure 8.2: Kozarnika: location of Kozarnika cave in the valley Skomlia. In the background, the Danube plane (Guadelli et al., 1999).

The cave entrance is on the north side of the river Skomlia (Скомля) valley at an altitude of 481 m a.s.l. (Sirakov et al., 2010).

Kozarnika cave consists of one, 210 m long gallery, which can be divided into three main sections (see fig. 8.3). The front of the cave is on average 11 m wide and the vault ceiling 3.5 m above modern floor level. The boundary from this entrance section to the gallery (second section) is marked by a narrowing of the walls to approx. 5 m width and 2 m height. The gallery widens again towards the rear of the cave, reaching 18.5 m width and 5 m height at the point at which it leads to the last section, the *salle terminal* (the 'rear hall'). The rear of the cave formed as a result of a fracture in the same direction as some of the fractures visible in the gallery (Guadelli et al., 2016, 1998).

During the Middle Ages and modern period, the cave was used as a mushroom cellar and for goat herding. The latter most likely resulted in its current name Kozarnika, the 'goat herding cave'. In the past, the site has also been known as Сухи Печ, the 'dry cave' (Sirakov et al., 2010).

It was first identified as an archaeological site by R. Popov in 1931 (Попов, 1933). However, no extensive archaeological work took place until much later. In the 1960s the site was turned into a nuclear fallout shelter – the remains of the brick wall enclosing the entrance were still in place in 1994, when N. Sirakov, H. Laville and S. Ivanova returned to the site for archaeological



Figure 8.3: Kozarnika: cave entrance as found in 2015 (photo: T. Higham).

prospections (Guadelli, 1996). The only other, albeit limited, evidence of Palaeolithic occupation in the vicinity was discovered at Mirislivka (Попов, 1933), a cave directly across the valley from Kozarnika, and Magura cave (Джамбазов, 1958).

Archaeological excavations by the Franco-Bulgarian team, led by N. Sirakov and J.-L. Guadelli, started in 1996 and continue to this day. During this time, four excavation sectors were opened (see fig. 8.4), uncovering Upper (sectors I, II, and III), Middle (sectors I, II, and IV) and Lower Palaeolithic (sectors I and II) material, and leading to the discovery of over 160k lithic and faunal remains. Important finds include the human skeletal remains from both AMHs and Neanderthals (*e.g.* Tillier et al., 2017), pieces of art (*e.g.* Guadelli, 2004; Sirakov et al., 2010; Гуаделли, 2011), and the discovery of both a new lamellar lithic industry and a tephra layer from the Upper Palaeolithic (Sirakov et al., 2007; Tsanova et al., 2012).

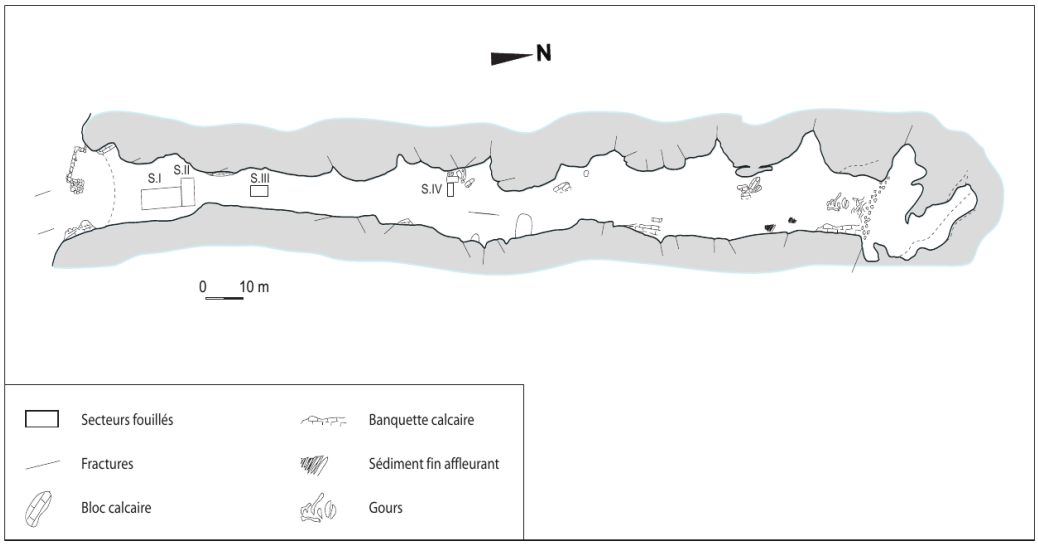


Figure 8.4: Kozarnika: map of cave with location of excavation sector I, II, III, and IV (Ferrier et al., 2009, fig. 3).

Excavation and analysis at Kozarnika over the last 20 years have been meticulous, involving a multidisciplinary approach. This, together with its deep stratigraphy and location, makes Kozarnika one of the key sites for studying the Middle to Upper Palaeolithic biocultural shift along the Danube.

Stratigraphy

During the excavation, the stratigraphy was divided into geological layers and archaeological levels. The former were labelled with Arabic numbers, the latter with Roman numerals (see fig. 8.5 and 8.6). The layers most relevant to this project are 3b to 5c (Upper Palaeolithic), layer 6/7 (in lieu of a better word 'transitional' or very early Upper Palaeolithic), and 9a (Middle Palaeolithic). What was initially identified as layer 8, later excavation showed to be den infill. Nonetheless, the original layer numbering was kept, meaning that the sequence passes from layer 7 directly to layer 9 (Sirakov et al., 2010). Both sectors I and II in the front of the cave have been extended and the stratigraphy connected. Consequently, they can be treated as one large excavation area. In contrast, sector III in the cave gallery remains isolated.

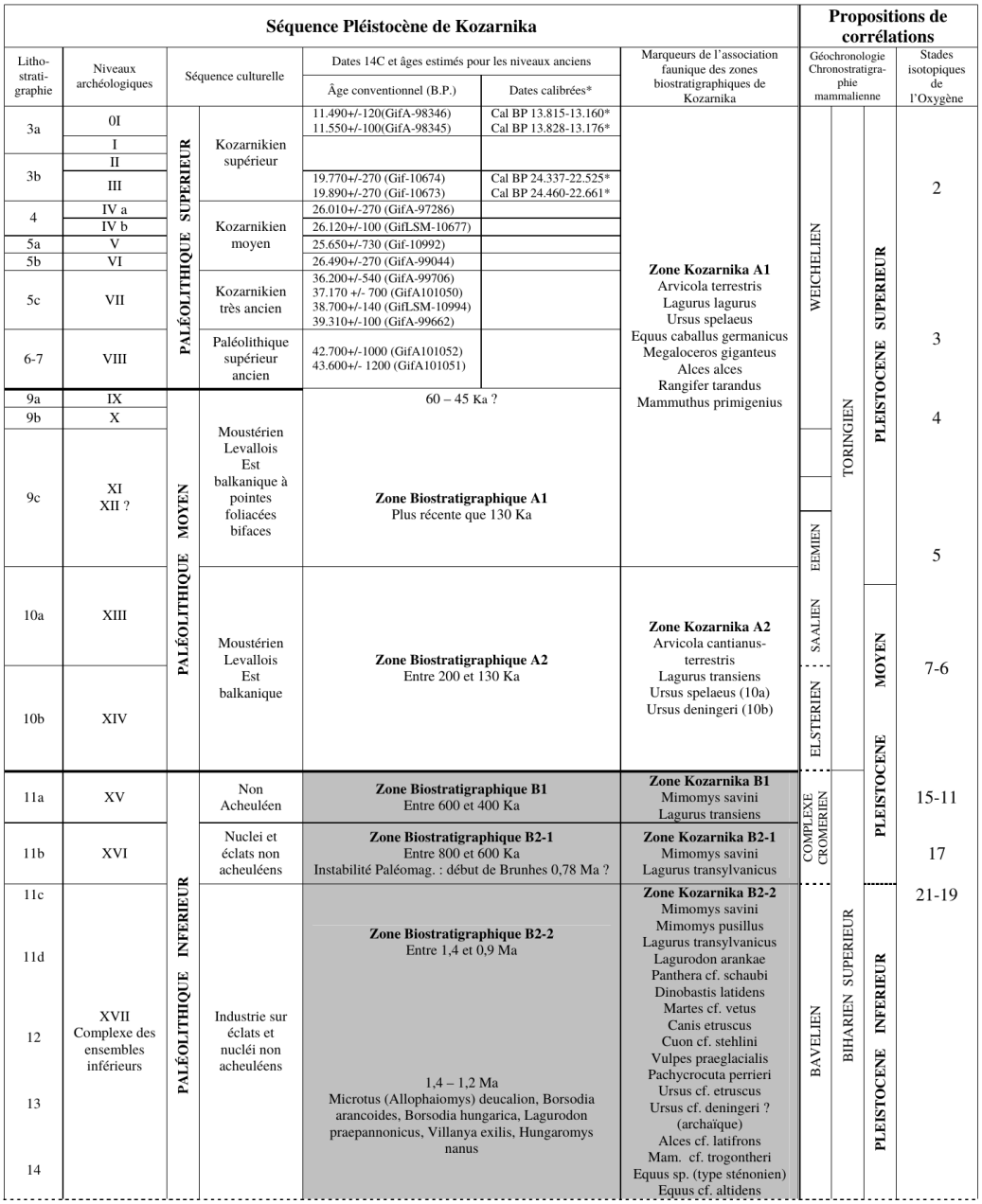


Figure 8.5: Kozarnika: Pleistocene sequence with lithostratigraphy, archaeological interpretation, biostratigraphy and published chronology (Guadelli et al., 2005b, tab. 1).



Figure 8.6: Kozarnika: North-facing profile in sector II at the limits of square D-H10/D-H11 showing layers 3 to 11b (Guadelli et al., 2000, fig. 14).

Stratigraphic units were independently labelled with Latin letters and Arabic numbers (see fig. 8.7). Here, especially layer A is of interest, as it yielded some very interesting material from the (early?) Upper Palaeolithic.

The sediment package of layers 10a–5a is around 1.2-1.5 m thick and is "*characterized by a finely powdered beige silty fraction, probably of aeolian origin*" (Sirakov et al., 2010, p. 96). The coarse fraction, calcareous gravel and heterometric pebbles, are derived from fragmentation of walls and ceiling. Their abundance decreases through the sequence, with the highest concentrations found in layer 10a. In most areas of excavation, layers 6 and 7 were too similar to be separated, resulting in the designation 6/7 for the combined unit. Sirakov et al. (2010) describes it as "*silty sediment (3-5 cm thick), light brown (layer 7) to light gray (layer 6), containing rare calcareous gravels as well as charcoal*". In some cases the layer turns into a thin charcoal horizon (Ferrier et al., 2009). From excavation season 2016 onwards, separation of layer 6/7 into three subunits – labelled 6/7 lb, 6/7 ls, and 6/7 lp – was possible for squares D7-9 and E7-9 (for area see fig. 8.17). Solifluction affected

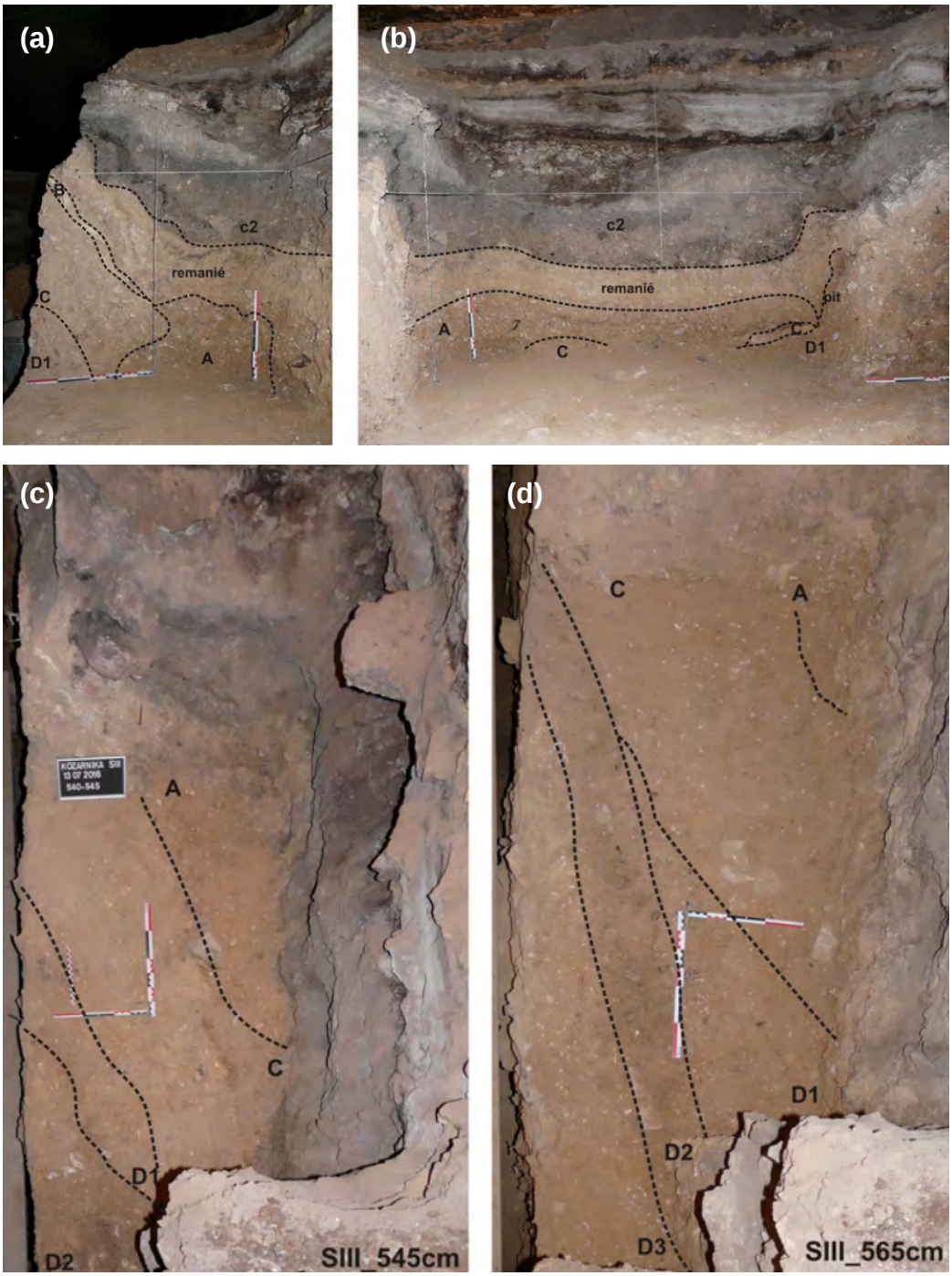


Figure 8.7: Kozarnika: sector III, south-facing (a) and west-facing (b) profiles, and plana at level 545 cm (c) and 565 cm (d) with layers c2, A, B, C, D1, D2, and D3 (Guadelli et al., 2016, fig. 47-48, photos: A. Guadelli: Mission Paléolithic de Bulgarie (French MEAE)/NAIM-BAN (Bulgaria)).

both layers 6/7 and 10a, while cryoturbation can be observed in layer 5a. Furthermore, a tephra horizon is visible in layer 5b, and associated with the CI (Y5) eruption (Lowe et al., 2012).

The sediment package of layers 4–3a is 1.14 m thick with often strongly deformed limits. It is "*composed of calcareous gravel in a light brown to whitish powdered silty matrix with a lamellar structure*" (Sirakov et al., 2010, p. 97). Sediment origin is the same as for the layers below, though their relative concentration has changed – cave wall and ceiling fractions outweigh aeolian sediment. Both the lamellar structure and evidence of cryoturbation indicate repeated frost/thaw processes post-sedimentation. The latter is strongest in layer 4, which also contains a significant number of fallen rocks (Sirakov et al., 2010, 2007).

Archaeology

At Kozarnika, the entirety of the *chaîne opératoire* is present. More than 70% of the lithics are made up of debris and intermediary steps, while around a fourth of the material has typotechnological significance. Presently, no signs of mixing of lithics between archaeological levels has been identified (Tsanova et al., 2012). Throughout the sequence the lithic record is dominated by local raw material. Silex was preferentially used, with quartz and quartzite being rare. Epigenetic processes, such as tectonic movement and repeated frost, cause the silex at the site to be fragile and cracked. The expected high number of geofacts evokes the need for extra care in identifying archaeological artefacts (Guadelli et al., 2005b).

The archaeological unit IX in layer 9a is the uppermost Middle Palaeolithic level found at Kozarnika (see fig. 8.8-b). Levallois is dominant, with centripetal or bipolar preferential debitage. The cores are small to medium sized, and often on cortical flakes or nodule fragments. Retouched forms include retouched and denticulated flakes, and scrapers. Mousterian points are rare, and some more typical leaf points (*pointes foliacées*) are present. In general, the Levallois Mousterian found in layer 9a is typical of the eastern

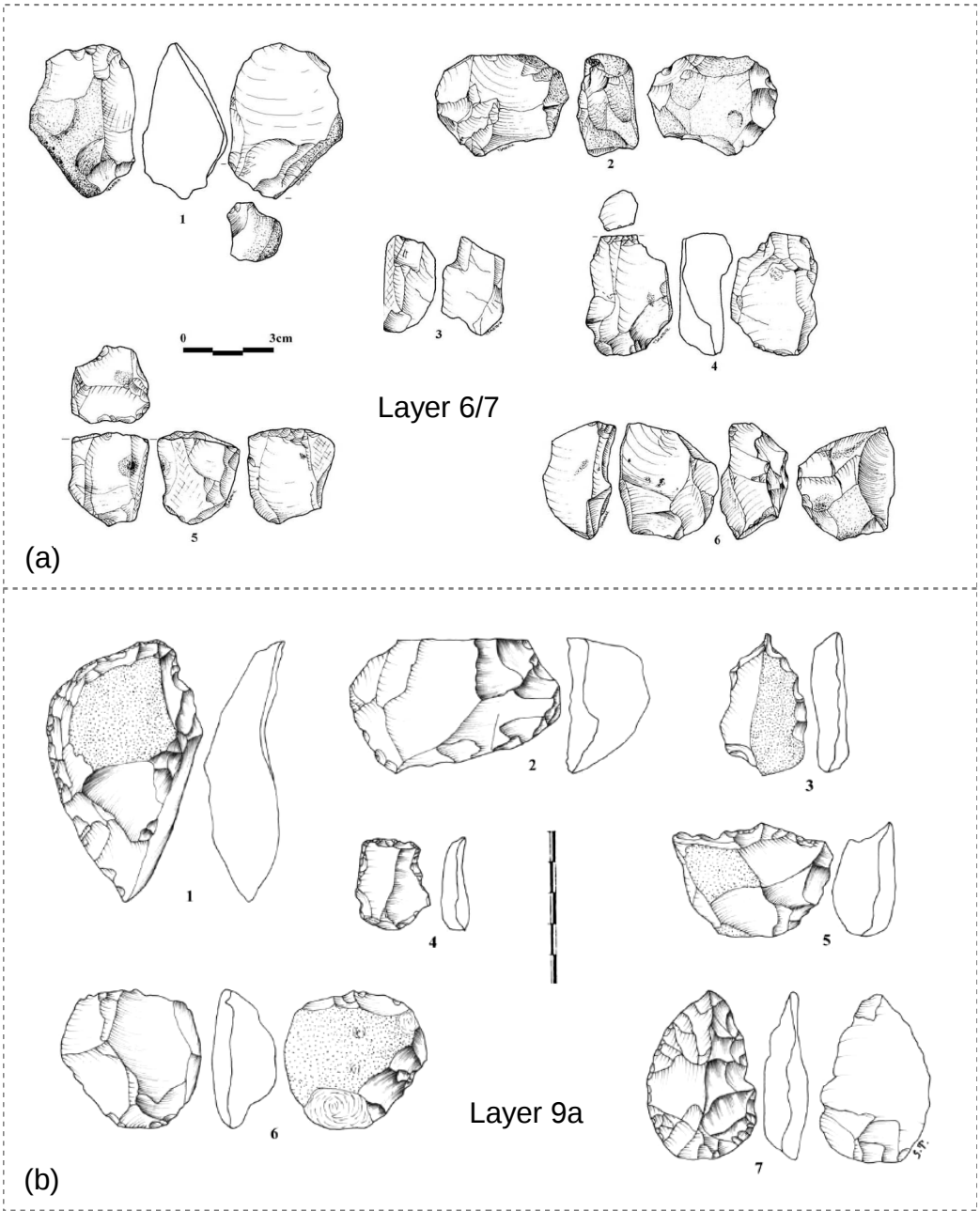


Figure 8.8: Kozarnika: lithics. (a) Layer 6/7 (EUP): 1, 4, 5, 6 – nuclei with two striking platforms for flakes and bladelets; 2 – Levallois nucleus showing the negative of a reuse on the narrow edge (similar to Gravettian debitage); 3 – bladelet nucleus with one striking platform (Guadelli et al., 2002, fig. 96). (b) Layer 9a (Mousterian): 1 – racloir convex; 2,6 – nuclei levallois; 3 – percoir; 4 – grattoir atypique; 5 – racloir transversal denticule; 7 – pointe foliacee (Guadelli et al., 2001, fig. 89).

Balkans and comparable to assemblages found at Muselievo and Samuilitsa (Guadelli et al., 2005b).

Layer 6/7 is seen to contain two distinct lithic technologies within level VIII: Levallois and lamellar. The Levallois pieces are similar to those found in the Mousterian layers below, while the blade and bladelet technologies have been interpreted as evolutionary preceding the ones found in the layers above (Guadelli et al., 2005b; Sirakov et al., 2007).

The interpretation favoured presently by the excavation team is that of interstratification, *i.e.* the alternating use of the cave in short succession between Mousterian and early Upper Palaeolithic cultures leading to a stratigraphic unit in which both lithic industries are present. While this would explain the archaeological evidence, it has to be stressed that it is based on the underlying assumption that the two different lithic technologies are synonymous with two distinct groups of people – potentially even two species of humans.

An alternate scenario could be imagined, in which the same cultural group is using two different lithic technologies (maybe before abandoning one in favour of the other). Consequently, a detailed investigation of the lithic assemblage from layer 6/7 is needed. Of interest is the study of the blade and bladelet technology, as assemblages with both Middle and Upper Palaeolithic character have been found elsewhere. In the Near East, the resulting Initial Upper Palaeolithic (IUP) technocomplex is increasingly brought up in connection with Eurasian sites, and seen as a genuine AMH cultural expression (*e.g.* Bosch et al., 2015). As their blade production is characterised by direct hard percussion, an initial comparison should be straight forward.

In 5c and subsequent layers, the lithic assemblages found are associated with different evolutionary stages of the Kozarnikian, an Upper Palaeolithic blade technology local to the Balkans. In general, the facies is characterised by a blade and bladelet production on small cores (prismatic or conical). Debitage follows unipolar direct soft percussion, less frequently bipolar.

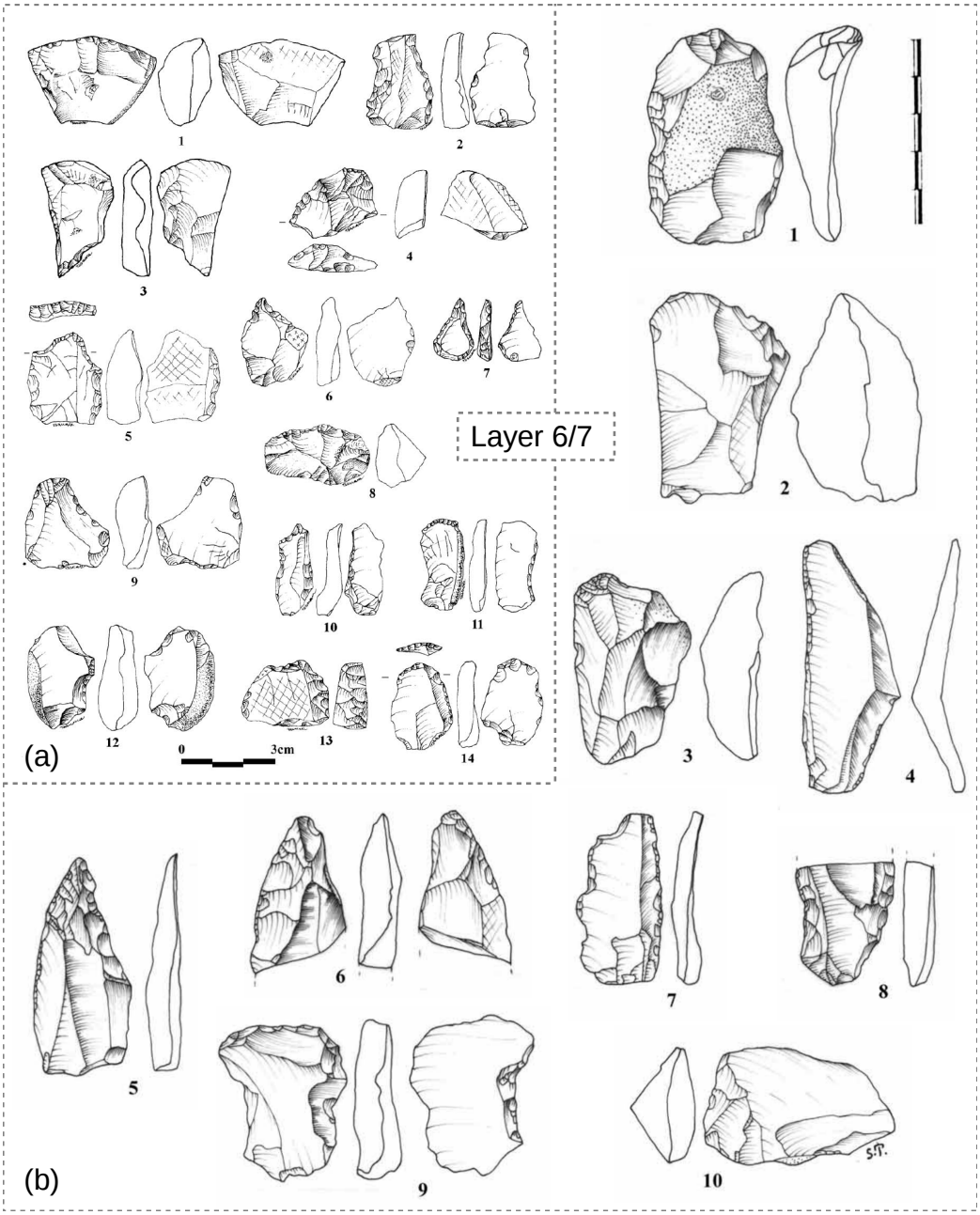


Figure 8.9: Kozarnika: lithics layer 6/7 (EUP). **(a)** 1, 8 – transversal *racloirs*; 2, 3, 12 – denticulated flakes; 4, 5, 9, 11, 13, 14 – scrapers; 6, 7, 10 – perforators (Guadelli et al., 2002, fig. 98). **(b)** 1 – scraper on a carinated flake; 2 – nucleus; 3 – atypical scraper; 4 – blade with partial marginal retouch; 5 – pointed blade or retouched Levallois point; 6 – fragment of a bifacial leaf point; 7 – blade with denticulate retouch; 8 – retouched blade reminiscent of Aurignacian style; 9 – atypical scraper on a flake; 10 – retouched flake (Guadelli et al., 2001, fig. 88).

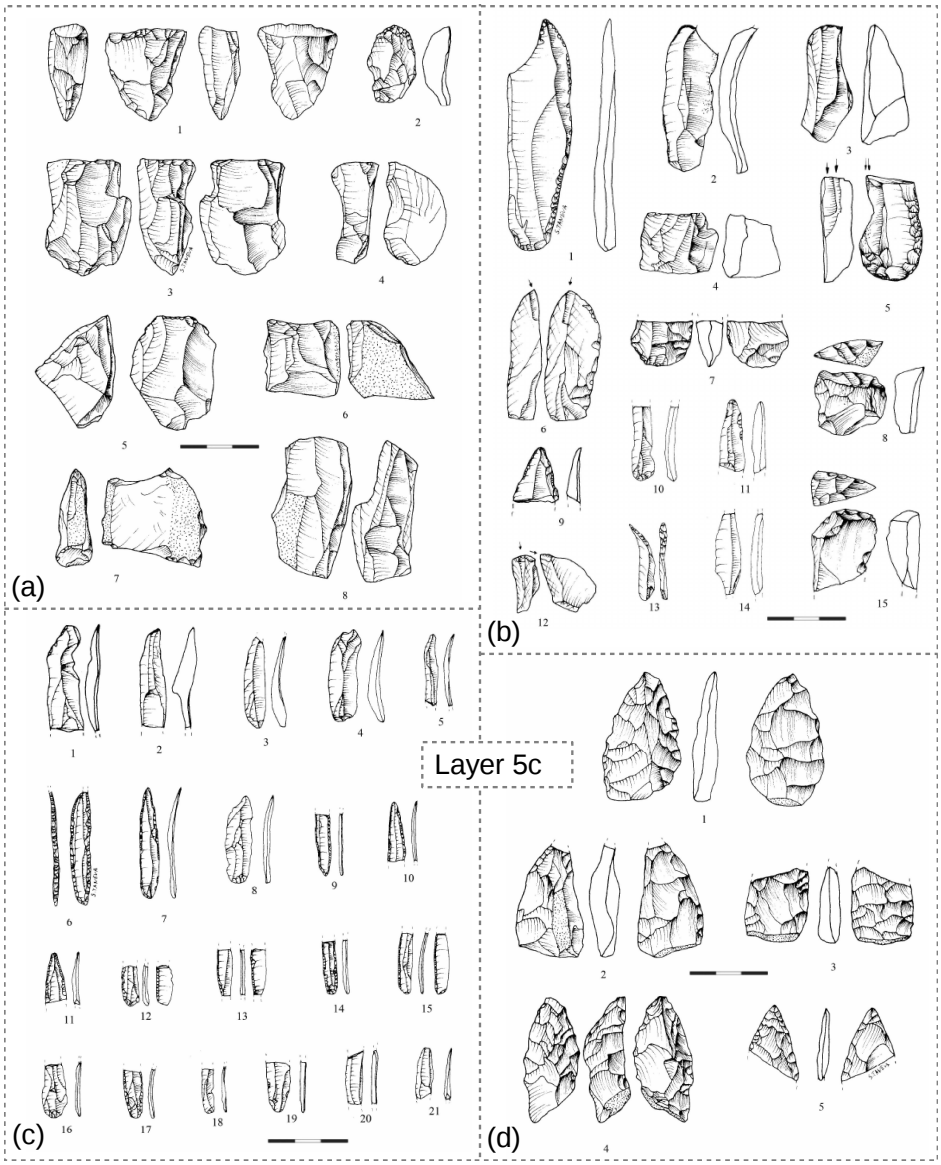


Figure 8.10: Kozarnika: lithics layer 5c. **(a)** 1, 3–8 – bladelet nuclei; 2 – scraper on a flake. **(b)** 1, 9 – pointed blades (partial, fine marginal retouch, semi-abrupt); 2 – rough blade (fine wear retouch); 3, 4 – bladelet nucleus; 6, 12 – burin on a flake or beginning of blade production on flake; 5 – burin-scraper or bladelet production on the side edge of a scraper; 8, 15 – atypical scrapers; 7 – fragment of a retouched piece (leaf point blank?); 10, 11, 14 – rough bladelet fragment from debitage; 13 – partially crested bladelet. **(c)** 1–4, 8, 16, 19 – rough bladelets; 5, 18, 20, 21 – microbladelet blanks; 6, 7 – fully backed points; 9 – bladelet fragment or backed point; 10, 11 – bladelet fragments (fine, semi-abrupt, bilateral retouch); 12, 13, 15 – bladelet fragments (alternating fine, semi-abrupt retouch). **(d)** 1, 3, 5 – tip of bifacial leaf points; 2, 4 – bifacially worked pieces, leaf point blanks (Guadelli et al., 2005a, fig. 77–80).

Level VII in layer 5c represents the oldest expression: the *Kozarnikien très ancien*[1] (Ancient Kozarnikian). It contains some backed pieces, which were usually formed by semi-abrupt retouch and become more frequent during the Middle Kozarnikian. Alternately or reversed retouched blades and bladelets are numerous and more common than in later phases. Scrapers with lateral retouch, often seen as 'Aurignacian' scrapers, are abundant, though Sirakov et al. (2007) and Guadelli et al. (2005b) emphasise that such technology is not unique to the Aurignacian. Burins are rare and there is a small series of leaf points and bifacially retouched pieces. The few larger blades in level VII are made from non-local silex. As no cores fitting these tools are present at the site, it can be concluded that they were manufactured elsewhere and retouched on site (Tsanova et al., 2012). No carinated scrapers or Aurignacian blades have been found, though Tsanova et al. (2012) makes special mention of a series of Dufour bladelets[2] identified in level VII. It can be stated, that overall the technocomplex shows some overlap with the Proto-Aurignacian and Early Aurignacian industries, and Teyssandier (2008) sees parallels to the Proto-Aurignacian found at Tincova (Romania). Nonetheless, the Ancient Kozarnikian should be seen as an individual technocomplex, until its relationship to the Proto-Aurignacian and Early Aurignacian is better understood, to avoid chronocultural schemata developed in other regions from clouding the local archaeological record.

The boundary between level VII to level VI is disturbed by cryoturbation. A chronological gap observed during previous dating is not detectable in the stratigraphic record. There are no signs of erosion, and the period of nearly 10k years was deemed too long for no sedimentation to occur. Nonetheless, from a lithic perspective levels V and VI seem to be closer connected to level VII, below, than to level IV, above. Level IV in layer 4 is characterised by backed blades and a specific type of broad and straight point (similar to the shape of a dart) of type 'Kozarnika'. In addition, IVb produced Gravettian

[1] A more detailed analysis can be found in Tsanova et al. (2012) and especially Tsanova (2006).

[2] In Sirakov et al. (2007) there was still an explicit statement that no Dufour bladelets had been found.

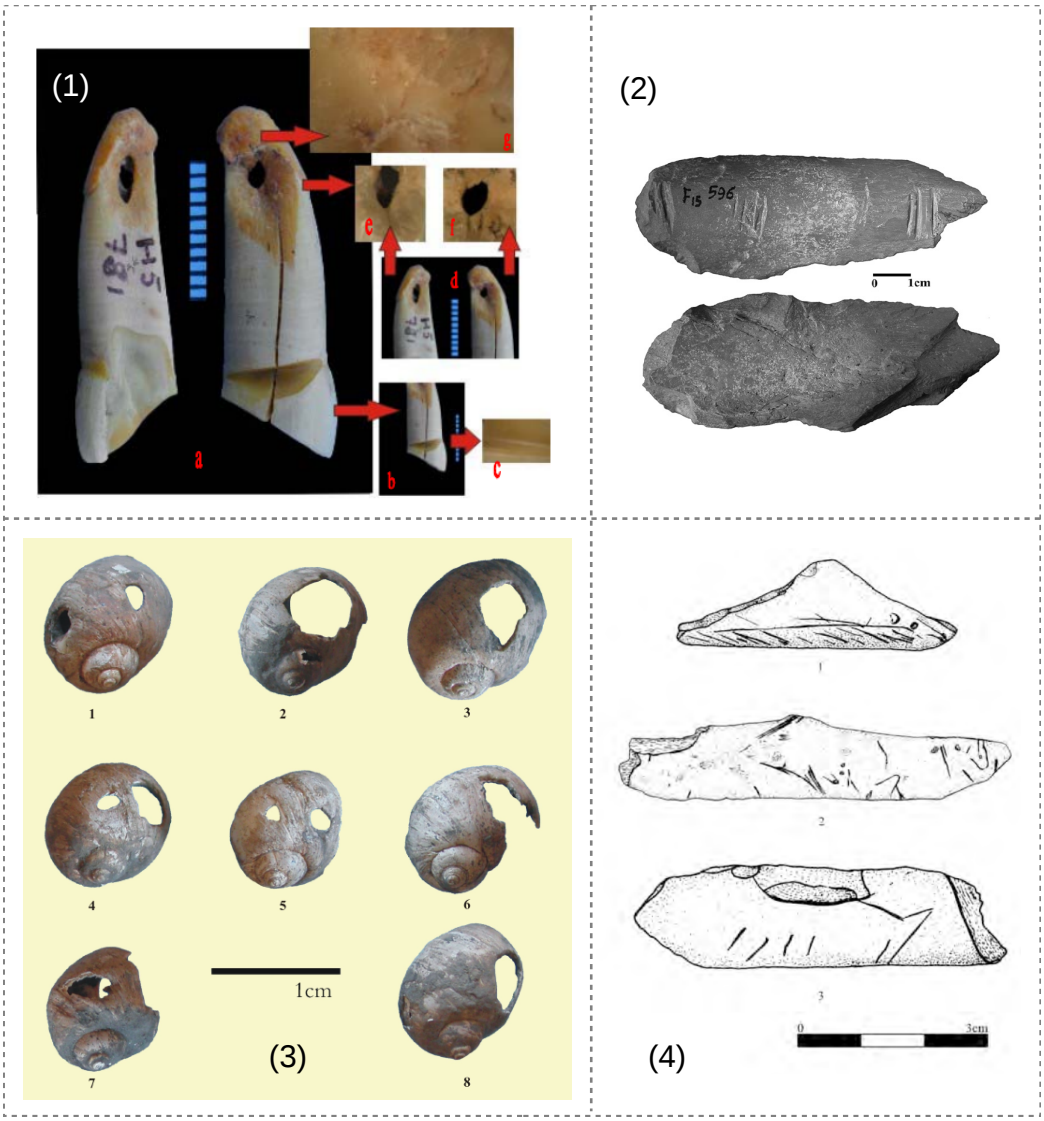


Figure 8.11: Kozarnika: Osseous artefacts. (1): pierced tooth, level VI/VII, b/c – grooves, e/f – perforation, g – traces of ochre (Guadelli et al., 2002, fig. 79). (2): engraved bone, layer 12 (Guadelli et al., 2010, fig. 14, photo: A. Guadelli: Mission Paléolithic de Bulgarie (French MEAE)/NAIM-BAN (Bulgaria)). (3): shell beads (H4-1158), level VII (Гуаделли, 2011, fig. 28).(4): 1 – fish figure, level 6/7ls; 2 – engraved bone, level 6/7ls; 3 – engraved bone, level 6/7lp (Guadelli et al., 2016, fig. 30, drawing: A. Guadelli: Mission Paléolithic de Bulgarie (French MEAE)/NAIM-BAN (Bulgaria)).



Figure 8.12: Kozarnika: anthropomorphic figure (E10-683) found on a rib fragment from level V (Guadelli et al., 2014, fig. 41, photo: A. Guadelli: Mission Paléolithic de Bulgarie (French MEAE)/NAIM-BAN (Bulgaria)).

points (Tsanova, 2003). Neither of these artefact types were found in the layers below.

The backed bladlets from the Middle and Recent Kozarnikian (*Kozarnikien moyen* and *Kozarnikien supérieur*) prompted a comparison between the Kozarnikian and the Gravettian, and the lithic assemblages were presented to external experts (Sirakov et al., 2007). While many similarities were found, it had to be noted that the dimensions observed at Kozarnika were significantly smaller, and the retouches more abrupt than observed at Gravettian sites in France.

Kozarnika is not only rich in lithics, but also in osseous artefacts. The most commonly found osseous tools are punches and retouchers from the Upper Palaeolithic sequence (Guadelli et al., 2013a; Tsanova et al., 2012). Nonetheless, there are some significant pieces of artistic expression, including portable art and ornaments. The oldest examples are two engraved bones

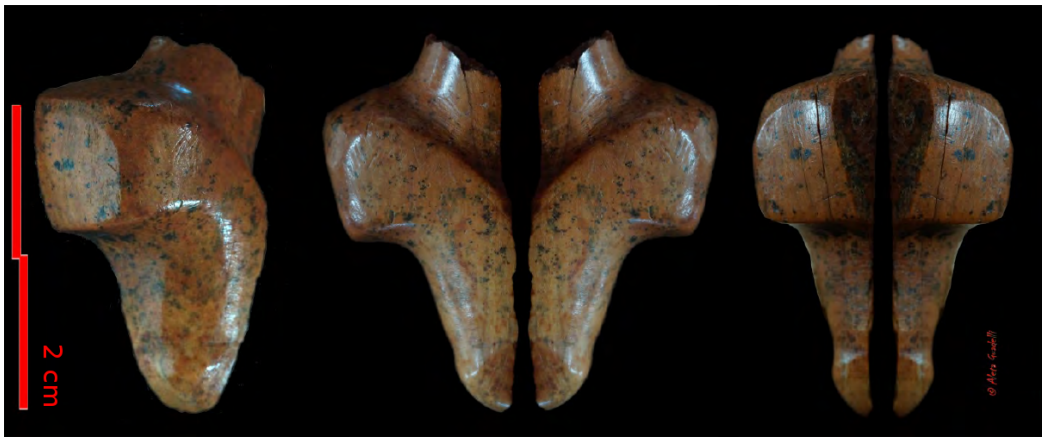


Figure 8.13: Kozarnika: fragment of an osseous Venus figurine found in the remains of the illicit excavation (Guadelli et al., 2014, fig. 40, photo: A. Guadelli: Mission Paléolithic de Bulgarie (French MEAE)/NAIM-BAN (Bulgaria)).

found in layer 12 (see fig. 8.11-2), demonstrating that such expressions do not arrive at the site with the Upper Palaeolithic, but are present as early as the Lower Palaeolithic (Sirakov et al., 2010). Fragments of portable art from levels 6/7 lp and 6/7 ls depict carved animals (see fig. 8.11-4). Starting with level VII, pierced teeth and shells appear (see fig. 8.11-1/3) – some of which show traces of ochre. Furthermore, the layer contains delicate beads of ca. 2 cm length made of thin bones (Гуаделли, 2011). Together with awls, the pendants present the diagnostic features of the osseous industry from the early Kozarnikian. Also noteworthy is an anthropomorphic figure from level V (see fig. 8.12), which shows similarities with those found at Kostenki IV.

The archaeological record in sector III is more modest. Still, an ochre rich band – layer A – caught the attention of archaeologists. Within, the fragment of a possible lozangic point was found. The only other osseous point from the site came from contact zone VII/VIII and may represent a split-based point (Гуаделли, 2011, fig. 20-1). Without a trench connecting the area to sector I/II, the precise relationship to the industries found at the front of the cave remains uncertain. Another remarkable find – a fragment of a Venus figurine (see fig. 8.13) – was made in the debris left behind by illicit excavation work, and has no secure context. Only direct dating would allow some temporal classification.

Human Remains

Human remains from the Palaeolithic are rare, and co-mingled archaeological material and a secure stratigraphic context are even scarcer. Consequently, Kozarnika offers a unique opportunity to study human remains from the Middle and Upper Palaeolithic and their relationship to the archaeological material. S. Pääbo, from the Max Planck Institute for Evolutionary Anthropology, took samples for aDNA analysis at the same time as sampling for this radiocarbon dating project was underway. Wherever possible, preliminary results from his research will be mentioned, though more detailed information is expected to feature in the forthcoming monograph on Kozarnika and in relevant journals in the near future.

Several skeletal fragments were found in sector I/II. In the Middle Palaeolithic layer 13, a cranial fragment (D13-T/1022) was discovered (see fig. 8.14-1). Further up, an upper right I1 (E15-T/651) was unearthed in layer 12 (see fig. 8.14-6). Presently, they have only been identified as *Homo* sp. In contrast, the left radius (G10-2249, G10-2248) found in layer 10b, and published in Tillier et al. (2017), clearly belonged to an infant *Homo neanderthalensis* (see fig. 8.14-3). In the initial Upper Palaeolithic layer 6/7, the first phalanx of a human hand was retrieved. Furthermore, during excavations in 2016, a lower right P3 (E9-2944) from a *Homo sapiens* was found in the layer 6/7 ls (see fig. 8.145)[3]. Another remain of a *Homo sapiens*, a third phalanx, was discovered in layer 5b (Guadelli et al., 2016, 2005b).

In sector III, the situation is more complex. Human bones initially found stemmed from illicit digging activity and have no secure archaeological context (see fig. 8.15 and 8.16). Preliminary mtDNA results indicate that the tibia K/1509, the femur K/1501, the phalanx K/1509-5, and the skull fragment F30-207 all belonged to *Homo sapiens*, while the tooth crown D2-K/3322-F18 was identified as *Homo neanderthalensis*. In addition, in 2016,

[3]Unfortunately, this particular discovery was made too late to be sampled for this dating project.



Figure 8.14: Kozarnika: human remains: 1 – *Homo* ?, cranial fragment (D13-T/1022), layer 13; 2 – *Homo* sp., upper right molar (K/3329); 3 – *Homo neanderthalensis*, left radius (G10-2248 + 2249), layer 10b; 4 – *Homo* sp., lower left I1 (G30-2110), sector III, layer A; 5 – *Homo* sp., lower right P3 (E9-2944), layer 6/7ls; 6 – upper right DI1 (E15-T/651), layer 12; 7 – *Homo* sp., fragmented right clavicle (F29-x1220), sector III, layer D (photos: J.-L. Guadelli & A. Guadelli: Mission Paléolithic de Bulgarie (French MEAE)/NAIM-BAN (Bulgaria)).

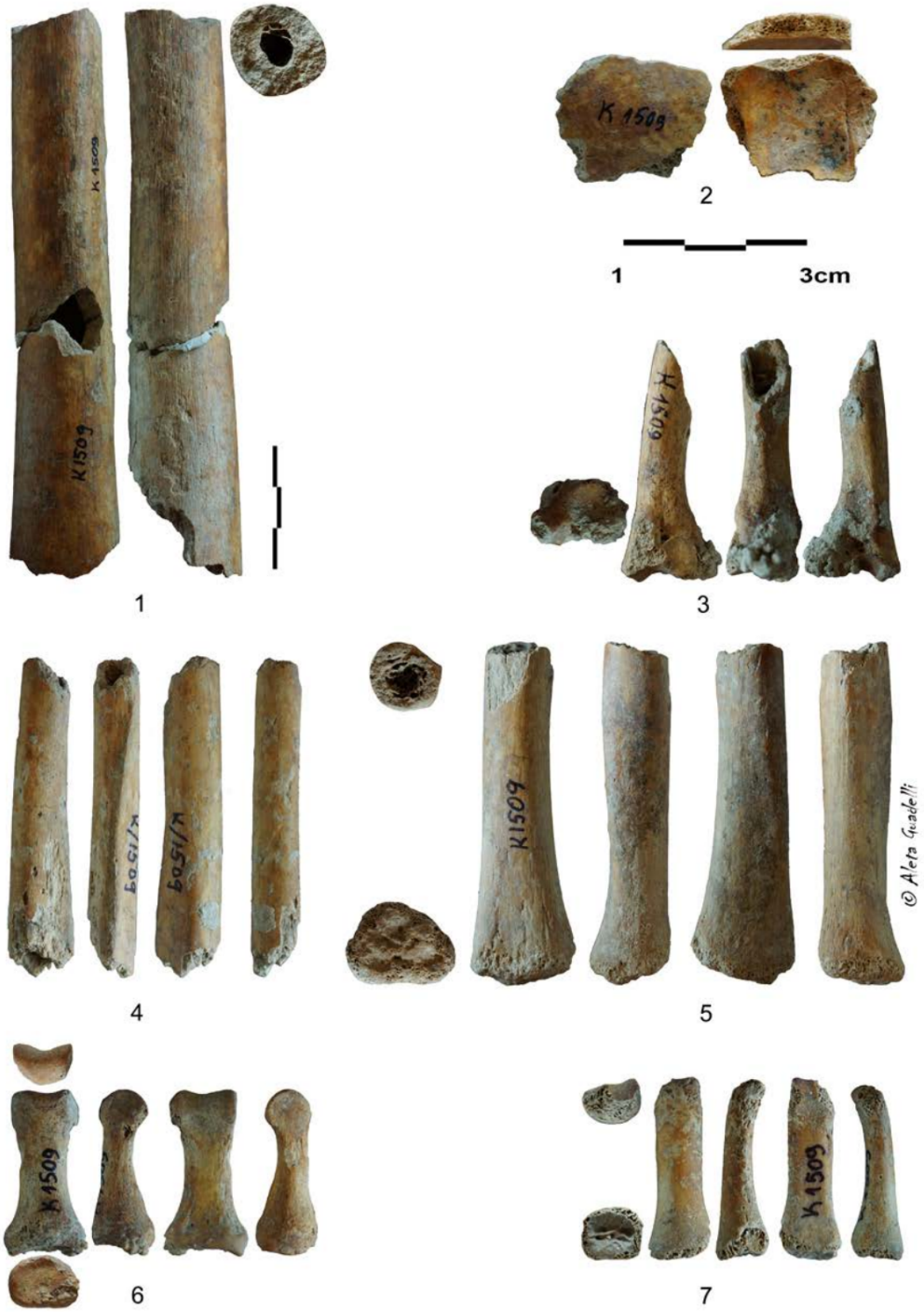


Figure 8.15: Kozarnika: human remains, catalogue no. K/1509, sector III (Guadelli et al., 2014, fig. 67, photos: A. Guadelli: Mission Paléolithic de Bulgarie (French MEAE)/NAIM-BAN (Bulgaria)).

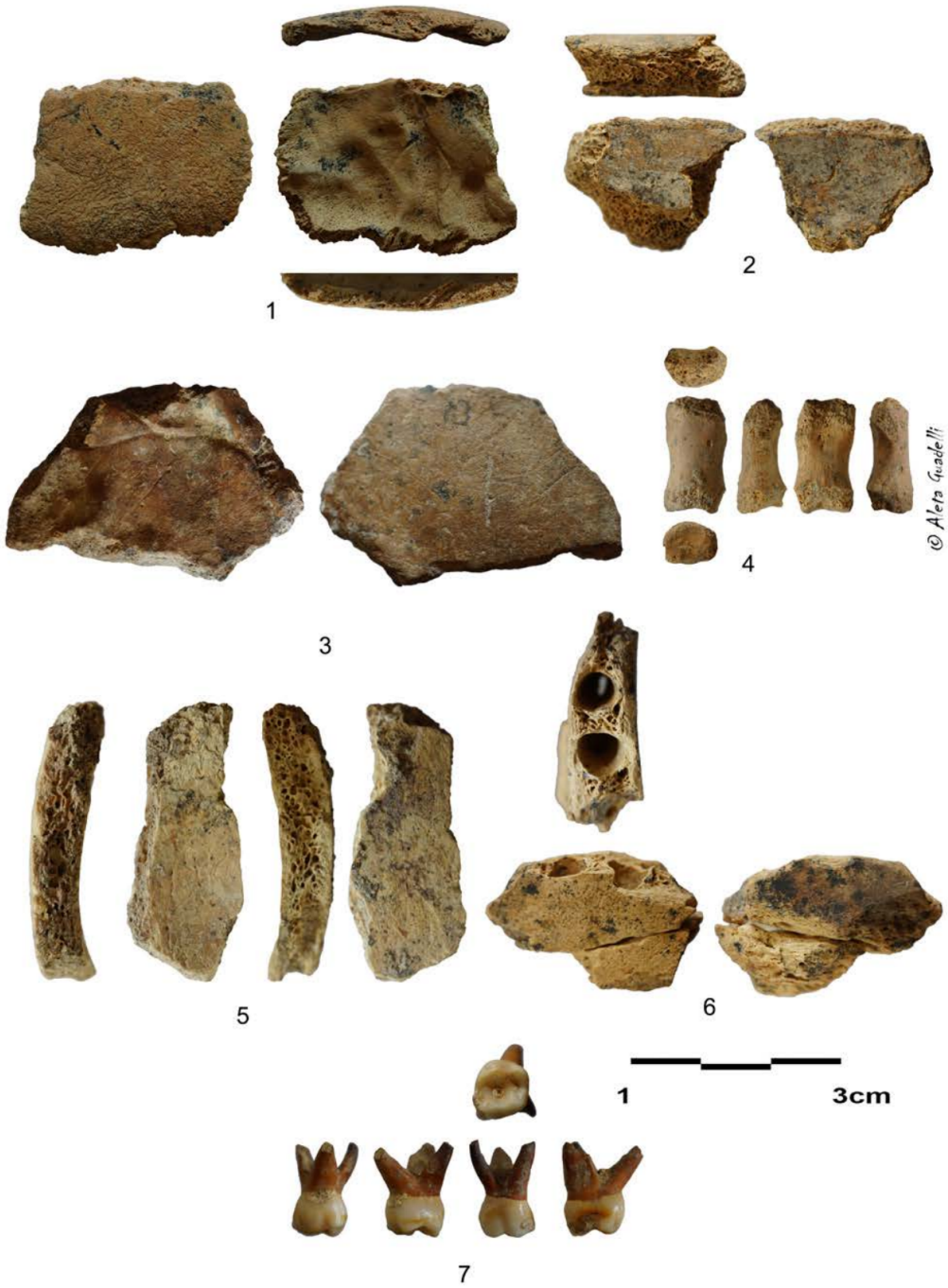


Figure 8.16: Kozarnika: human remains, catalogue no. K/3322, sector III (Guadelli et al., 2014, fig. 68, photos: A. Guadelli: Mission Paléolithic de Bulgarie (French MEAE)/NAIM-BAN (Bulgaria)).

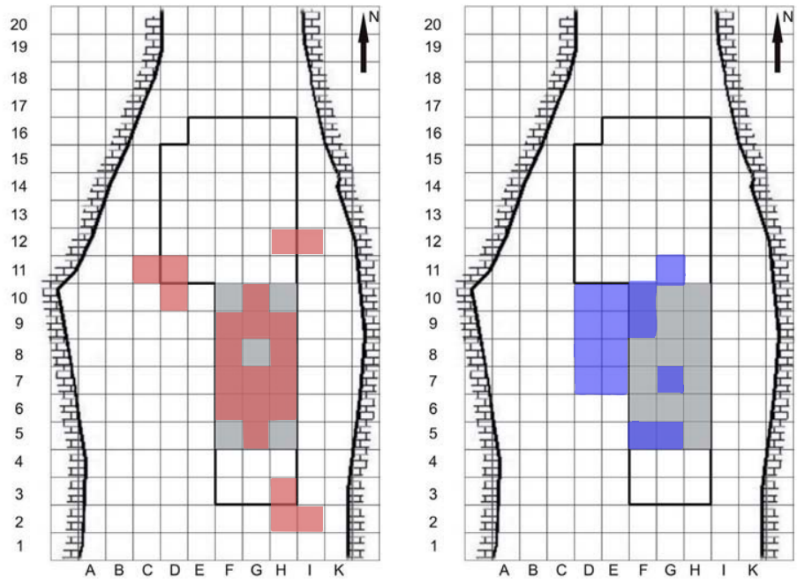


Figure 8.17: Kozarnika: map of excavation co-ordinate system in sector I/II with location of radiocarbon sampling highlighted. **red** (left) – previous dating; **blue** (right) – current project.

further human evidence was uncovered[4]: a lower left incisor I1 (G30-2110) in layer A (see fig. 8.14-4), and the fragment of a right clavicle F29-x1220 in layer D (see fig. 8.14-7). Both remain currently unclassified (Guadelli et al., 2016, section (III) Paléontologie, Archéozoologie, Taphonomie, Anthropologie).

Previous Dating

Prior to this dissertation, two separate radiocarbon dating campaigns were completed: one focusing on the age of the archaeological levels, and one in relation to the tephra analysis at the site. The locations for previous radiocarbon sampling are illustrated in figure 8.17 and compared to the squares sampled for this project.

[4]Unfortunately, these two human remains were discovered after sampling for radiocarbon dating for this project was already completed.

Just after the turn of the millennium, an initial radiocarbon dating campaign was launched (see tab. 8.1), covering all Upper Palaeolithic layers, and resulting in radiocarbon measurements from 12 charcoals, 1 charred earth sample, 2 plant remains, and 1 faunal bone fragment (Guadelli et al., 2002). The samples were all processed at the *Laboratoire des Sciences du Climate de l'environment* in Gif-sur-Yvette. The bone sample (sample no. 32) was taken from a horse femur and treated, as described in Nelson (1991), with mild acids to remove inorganic carbon and soluble organic matter, before letting the insoluble component react with ninhydrin. The reaction residue was hydrolysed to amino acids, and again reacted with ninhydrin. The carboxyl carbon was collected as CO_2 for radiocarbon measurement. The other samples were pretreated with acid-base-acid washes as described by Délibrias (1985). Eleven samples were AMS radiocarbon dated at Gif-sur-Yvette (indicated by the lab code Gif-A). The remaining five were dated using proportional gas counting (PGC) at the *Laboratoire Souterrain de Modane* in the French Alps, reducing the background level below typical levels for β-counting techniques.

The ^{14}C samples no. 1 (charred earth), 9 (plant remain), 11 (plant remain), and 32 (faunal bone), are unsuitable for the purpose of this project, as they are not securely connected to human activity at the site. In addition, sample no. 32 has an ambiguous context attribution, as it is referred to as both from layer 5c, and from level VIII (see fig. 8.5). Three further samples (no. 4, 34, 36) were collected in contact zones. Without clear level attribution, the resulting radiocarbon ages are unfit for Bayesian modelling. The remaining measurements suggest an early appearance of the Upper Palaeolithic at Kozarnika. However, the four dates of most interest to this project (covering layers 5c and 6/7) might be underestimating the true age of the samples, as the charcoal samples were only prepared using the less rigorous ABA pre-treatment.

In 2009, D. White collected charcoal and microtephra samples for the RESET (Response of Humans to Abrupt Environmental Transitions) project. The resulting 20 AMS radiocarbon measurements cover the Upper Palaeolithic layers 4 to 6/7 (see tab. 8.2, publication in preparation) and were

Table 8.1: Kozarnika: previously obtained radiocarbon dates sent to Laboratoire des Sciencess du Climate de l'environment in Gif-sur-Yvette (Guadelli et al., 2002, p. 211-215). "GifA-" dates were measured by AMS at Gif-sur-Yvette, the remaining dates by proportional gas counting (PGC) at the Laboratoire Souterrain de Modane. Geological layer given in Arabic numbers, archaeological levels in Roman numerals. ^{14}C (BP) = conventional radiocarbon age Before Present with 1σ error. Date (cal BP) = ^{14}C age calibrated using OxCal 4.3 (Bronk Ramsey, 2009a) and IntCal13 (Reimer et al., 2013). grey rows – radiocarbon ages unsuitable for modelling based on sample type and location; *italic* – ^{14}C dates >30k BP from charcoal samples treated with ABA only have to be treated with caution (for discussion see 8.1.1).

Date code	Sample no.	Matrial	Layer	Square	Depth (cm)	Treat.	^{14}C (BP)	Date (cal BP)	δ^{13}C
GifA-98345	7	charcoal	3a = 0I	H2-I2	300-310	ABA	11550 ± 100	13573 – 13177	–
GifA-98346	1	charred earth	3a = 0I	H2-I2	300-310	ABA	11490 ± 120	13551 – 13106	–
GifA-97285	9	vegetation	3a = I	G6/G5	330-334	ABA	7840 ± 70	8977 – 8453	–
Gif-10674	8	charcoal	3b = III	F6-G6	372-389	ABA	19770 ± 270	24434 – 23107	-23.61
Gif-10673	4	charcoal	3b/4 = III/IVa	H8	387-389	ABA	19890 ± 270	24605 – 23210	-22.67
GifA-97286	11	vegetation	4 = IVa	H7	391-393	ABA	26010 ± 270	30836 – 29571	–
Gif/LSM-10677	14	charcoal	4 = IVb	F7	402-405	ABA	26120 ± 100	30793 – 30029	-23.29
Gif-10992	19	charcoal	5a = V	F7	425-431	ABA	25650 ± 730	31147 – 28427	-23.42
GifA-99044	20	charcoal	5b = VI	F8	431-434	ABA	26490 ± 270	31159 – 30156	-23.98
Gif/LSM-10994	21	charcoal	5c = VII	F7	450-452	ABA	*38700 ± 1400*	*45820 – 40730*	-24.20
GifA-99706	33	charcoal	5c = VII	F8	455	ABA	*36200 ± 540*	*41837 – 39760*	–
GifA-101050	34	charcoal	5c-6/7 = VII	D10-D11	447-451	ABA	37170 ± 700	42711 – 40422	–
GifA-99662	32	faunal bone	5c = VIII	F8	457-461	ninhydrin	39310 ± 100	45106 – 41901	–
GifA-101052	36	charcoal	6/7-9 = VIII	G7	470-473	ABA	42700 ± 1000	48544 – 44375	–
GifA-101051	35	charcoal	6/7 = VIII	D11-C11	458-460	ABA	*43600 ± 1200*	*49641 – 45109*	–
GifA-101048	30	charcoal	6/7 = VIII	F8	457-461	ABA	*29310 ± 320*	*34086 – 32762*	–

obtained on single entity samples. The two main pre-treatments used were ORAU's standard ABA protocol for charcoals (labelled ZR), and ABOx (labelled XR) as described by Brock et al. (2010b). Three ^{14}C samples (no. 28, 50, and 58) were split, one fraction treated with ZR, the other with XR. A comparison of the results shows higher sample loss typical when applying the more rigorous ABOx treatment, as well as resulting higher %C on combustion. As expected with charcoal samples older than 30k BP, the XR treated fractions resulted in older radiocarbon ages – reiterating the need for caution when dealing with ABA treated charcoal samples from this time period. For subsequent work, the ZR results of sample no. 28, 50 and 58 are dismissed in favour of the more robust XR results. Furthermore, there were three results listed with experimental, non-routine chemistry (NRC) protocols, which refer to refinement experiments for ABOx treatments. OxA-X-2443-7 has a note stating that 'CuO and vacuum' were used, as was the case for OxA-X-2416-47. OxA-X-2443-8 seems to indicate that initial reaction happened under vacuum. In all cases, the charcoal samples (no. KZ-09 and 55) have an additional fraction treated with standard XR. These results are deemed more reliable.

The bulk tephra horizon observed in layer 5b could be connected to the CI (Y5) eruption at *ca.* 34k BP (Lowe et al., 2012). Further microtephra bands were found in layer 9a and 9c. Their similarities could indicate that they resulted from the same eruption, though it could not be excluded that they represent two separate events. The origin of this older tephra is presently undetermined.

To conclude, previous dating at Kozarnika has been relatively extensive (for sampled sectors see fig. 8.17), providing 17 reliable radiocarbon measures and 6 possible minimum age estimates on charcoal, as well as a securely identified CI tephra as a chronological marker in layer 5b (see tab. 8.1–8.2). The chronostratigraphy suggests few outliers, at least two human activity horizons in layer 5b (neither of which occurring during the CI Y5 eruption), and a layer 5c possibly contemporaneous to the Early Aurignacian observed at Geißenklösterle. Consequently, Kozarnika is a prime candidate for very

Table 8.2: Kozarnika: previously obtained AMS radiocarbon dates from charcoal samples, measured under the RESET project (publication in preparation). Geological layer given in Arabic numbers, archaeological level in Roman numerals. ZR = ABA pre-treatment; XR = ABOx pre-treatment (see Brock et al., 2010b); NRC = non-routine chemistry, see text for details. ^{14}C age calibrated using OxCal 4.3 (Bronk Ramsey, 2009a) and IntCal13 (Reimer et al., 2013) and rounded to 10 years. grey rows – radiocarbon ages unsuitable for modelling based on pre-treatment chemistry; *italic* – ^{14}C dates >30k BP from charcoal samples treated with ABA only have to be treated with caution (for discussion see 8.1.1).

Date code	Sample no.	Layer	Square	Depth (cm)	Treat.	Yield mg (wt.%)	%C	F^{14}C	Date BP	Date (cal BP)	δ^{13}C
OxA-25184	48	4 = IVb	F9	412-419	ZR	11.8 (42.2)	62.9	0.03315 ± 0.00078	27370 ± 190	31520 – 30990	-23.4
OxA-X-2443-7	KZ-09	4 = IVb	H12-I12	421-423	NRC	5.69 (6.1)	78.3	0.04091 ± 0.00069	25680 ± 140	30350 – 29420	-22.0
OxA-X-2443-8	KZ-09	4 = IVb	H12-I12	421-423	NRC	6.71 (7.2)	76.8	0.03926 ± 0.00066	26010 ± 140	30720 – 29780	-22.0
OxA-25355	KZ-09	4 = IVb	H12-I12	421-423	XR	3.98 (4.3)	75.8	0.04041 ± 0.00069	25770 ± 140	30470 – 29500	-21.9
OxA-24786	25	5a = V	–	–	ZR	3.95 (18.9)	63.5	0.03775 ± 0.00089	26320 ± 190	31010 – 30140	-23.7
OxA-24865	56	5b = VI	H6	441-443	XR	3.35 (4.00)	80.5	0.02923 ± 0.00064	28380 ± 170	32890 – 31660	-23.4
OxA-22914	73	5b = VI	H3	443-444	ZR	24.19 (27.9)	60.0	*0.01094 ± 0.00062*	*36250 ± 450*	*41750 – 39970*	-23.7
OxA-24059	58	5b = VI	G5	445-448	XR	4.24 (14.7)	70.5	0.01044 ± 0.00060	36650 ± 450	42020 – 40360	-23.3
OxA-22913	58	5b = VI	G5	445-448	ZR	34.75 (42.8)	65.2	0.01116 ± 0.00056	36100 ± 400	41560 – 39900	-23.5
OxA-24080	29	5c = VII	F7/G7	450-453	XR	7.51 (6.4)	77.8	0.01083 ± 0.00057	36350 ± 400	41750 – 40160	-23.2
OxA-22915	50	5c = VII	G9	449-451	ZR	22.7 (25.6)	60.8	0.01168 ± 0.00060	35750 ± 400	41300 – 39510	-23.6
OxA-24802	50	5c = VII	G9	449-451	XR	8.07 (7.4)	68.2	0.00923 ± 0.00060	37650 ± 500	42730 – 41300	-23.4
OxA-25405	51	5c = VII	F9	449-451	XR	8.83 (8.4)	89.9	0.01009 ± 0.00054	36900 ± 450	42190 – 40610	-23.0
OxA-25406	52	5c = VII	G9	451-452	XR	6.8 (6.3)	80.1	0.00926 ± 0.00057	37600 ± 500	42700 – 41250	-22.8
OxA-24058	55	5c = VII	G10	460	XR	8.85 (5.6)	79.2	0.01787 ± 0.00058	32330 ± 260	36900 – 35610	-22.4
OxA-X-2416-47	55	5c = VII	G10	460	NRC	7.79 (4.9)	83.7	0.01734 ± 0.00057	32570 ± 260	37460 – 35880	-22.7
OxA-23975	28	5c = VII	F8	445-446	XR	4.63 (19.4)	77.2	0.00879 ± 0.00054	38050 ± 500	42980 – 41600	-24.3
OxA-22916	28	5c = VII	F8	445-446	ZR	29.86 (41.3)	61.2	0.00986 ± 0.00061	37100 ± 500	42400 – 40730	-25.3
OxA-22842	66	6/7 = VIII	F6	468-470	ZR	11.06 (52.6)	61.0	*0.00599 ± 0.00058*	*41100 ± 750*	*45980 – 43280*	-23.2
OxA-24083	69	6/7 = VIII	H9	486-487	XR	3.31 (5.5)	70.9	0.00950 ± 0.00059	37400 ± 500	42590 – 41070	-24.0

early AMH occupation. However, there is substantial dating variability and uncertainty in layer 6/7, potentially caused by the use of charcoal samples towards the limit of the radiocarbon method. A thorough dating of the stratigraphy on anthropogenically modified bone will help to increase the robustness of the older part of the sequence, and provide an ideal case study for comparison. It is to be expected that the age of layer 6/7, and perhaps 5c, will be pushed further back in time with the new project.

8.1.2 Radiocarbon dating

Material & Treatment

During the summer excavation season of 2015 and 2016, a total of 109 bone fragments were sampled for radiocarbon dating: 3 potential human skeletal remains, 99 securely and 7 potentially anthropogenically modified faunal fragments. From these, 43 samples were treated for radiocarbon dating (see fig. 8.3–8.4).

The three human remains – a juvenile tibia (Kz-53), an adult femur (Kz-54), and an adult cranial fragment (Kz-55) – were found without secure archaeological context in a ditch left behind by illicit treasure hunting activity in the area that later became excavation sector III. In the same area, the fragment of a Venus figurine (Kz-57) was found. Radiocarbon dating was the only available procedure to provide temporal context and test whether these human remains and the artefact were connected to the Middle to Upper Palaeolithic biocultural shift.

During the archaeological excavation in sector III, an ochre layer (layer A) containing an osseous fragment (Kz-58) – believed to be the base of a spear point – was uncovered. Unfortunately, this sector is presently not physically connected to sectors I and II. In the absence of a distinct ochre layer in the front area of the cave (sectors I/II), linking the two independent stratigraphic sequences failed. By sampling material from within an adjacent layer A, the age of layer A could be further constrained, thus allowing at least for a

Table 8.3: Kozarnika: samples for radiocarbon dating from sector III. * – for discussion of layer attribution see section 8.1.4.

Ref-no.	Item	Excav.	Sample-no.	Sq.	Layer	x(m)	y(m)	z(m)	Weight
Kz-53	human	–	K/1509-1	–	–	–	–	–	645 mg
Kz-54	human	–	K/1509	–	–	–	–	–	474 mg
Kz-55	faunal	–	K/3322-7	–	–	–	–	–	522 mg
Kz-57	venus	2014	K/3360	–	–	–	–	–	318 mg
Kz-58	point	–	x150	F30	A?*	–	–	-5.04	279 mg
Kz-111	faunal	2016	G30-x160	G30	A2	–	–	-5.40–5.45	926 mg
Kz-112	faunal	2016	G30-x205	G30	A1	–	–	-5.45–5.50	943 mg
Kz-114	faunal	2016	F29-x1247	F29	D2	–	–	-5.50–5.55	709 mg
Kz-115	faunal	2016	F30-776	F30	C	–	–	-5.40–5.45	752 mg
Kz-116	faunal	2016	F29-x1150	F29	D2	–	–	-5.45–5.50	642, 514 mg

chronological comparison. However, no layers above were left *in situ* and no other securely anthropogenically modified faunal remains had been found. Instead, 7 samples (covering layers A, C and D) not securely connected to human activity (*i.e.* only showing possible anthropogenic cut marks) were sampled to provide some temporal understanding of sector III.

From sector I/II, 33 anthropogenically modified faunal samples were selected for radiocarbon dating (layers 3b to 6/7) with the intent of establishing a robust site chronology through Bayesian modelling. In layer 6/7, preference was given to samples collected in 2016, when three distinct subunits were identified during excavation. This provided an opportunity to increase dating precision at the lower end of the Upper Palaeolithic sequence. In general, preference was given to dating samples with full coordinates (over those with only square and depth information), and with $\%N \geq 0.5$.

As none of the sampled remains had undergone consolidation or restoration work, they were directly treated with the ORAU standard bone protocol, and ultrafiltered when gelatine preservation after AG treatment was sufficient. Kz-109 and Kz-116 were selected for auto-duplication as their P-no was a multiple of 20, as standard at ORAU.

Table 8.4: Kozarnika: samples for radiocarbon dating from sector I/II. * – for discussion of layer attribution see section 8.1.4.

Ref-no.	Item	Excav.	Sample-no.	Sq.	Layer	x(m)	y(m)	z(m)	Weight
Kz-03	faunal	2013	D7-92	D7	3b	194.55	1498.10	-3.84	894 mg
Kz-06	faunal	2013	E9-343	E9	4 (IVa)	195.33	1500.47	-3.90	577 mg
Kz-07	faunal	2014	D8-270	D8	4 (IVa)	194.94	1499.45	-3.99	360 mg
Kz-08	faunal	2013	E9-477	E9	4 (IVa)	195.53	1500.43	-3.94	575 mg
Kz-10	faunal	2013	E7-306	E7	4 (IVa)	195.02	1498.06	-3.93	610 mg
Kz-14	faunal	2014	E7-744	E7	4 (IVb)	195.59	1498.69	-4.12	888 mg
Kz-15	retoucher	2014	E10-471	E10	4 (IVb)	195.26	1501.32	-4.11	841 mg
Kz-19	faunal	2014	E9-1045	E9	4 (IVb)	195.02	1500.71	-4.11	649 mg
Kz-23	faunal	2014	D10-300	D10	4 (IVb)	194.82	1501.71	-4.10	577 mg
Kz-24	faunal	2001	F10-n469	F10	5a	196.08	1501.03	-4.23	525 mg
Kz-25	faunal	2001	F10-549	F10	5a	196.65	1501.77	-4.29	595 mg
Kz-38	faunal	1997	F8-1169	F8	5b	196.11	1499.83	-4.39	608 mg
Kz-39	faunal	1997	F8-1146	F8	5b	196.64	1499.98	-4.32	409 mg
Kz-43	faunal	2002	G5-498	G5	5c	197.82	1496.37	-4.41	626 mg
Kz-44	faunal	1999	F7-1955	F7	6/7	196.36	1498.89	-4.63	530 mg
Kz-45	faunal	2001	F10-754	F10	5b	196.24	1501.74	-4.43	555 mg
Kz-47	faunal	1997	F8-1327	F8	5c	196.63	1499.13	-4.48	605 mg
Kz-48	faunal	2002	G5-588	G5	5c (5b*)	197.93	1496.13	-4.42	494 mg
Kz-49	faunal	1997	G7-1793	G7	5c	197.78	1498.71	-4.51	601 mg
Kz-50	faunal	1999	K844	G11	5b	197.40	1560.69	-4.55	478 mg
Kz-52	faunal	2002	F5-1949	F5	6/7 (5c*)	196.38	1496.14	-4.54	615 mg
Kz-79	'venus'	2014	E10-683	E10	5a	–	–	-4.15–4.20	581 mg
Kz-80	faunal	2016	D8-1517	D8	6/7lp	–	–	-4.58–4.59	977 mg
Kz-81	faunal	2016	E8-2385	E8	6/7ls	–	–	-4.58–4.59	859 mg
Kz-82	faunal	2016	E8-2387	E8	6/7ls	–	–	-4.58–4.59	864 mg
Kz-83	faunal	2016	E7-2241	E7	6/7ls	–	–	-4.61–4.62	737 mg
Kz-85	faunal	2015	D7-887	D7	5c	–	–	-4.45–4.48	679 mg
Kz-87	faunal	2015	E9-2452	E9	5c (6/7*)	–	–	-4.50–4.53	847 mg
Kz-88	faunal	2016	D9-990	D9	5b	–	–	-4.45–4.48	766 mg
Kz-90	faunal	2015	D9-988	D9	5b	–	–	-4.43–4.45	756 mg
Kz-93	faunal	2016	E9-2712	E9	6/7lp	–	–	-4.55–4.58	815 mg
Kz-109	faunal	2016	D7-1390	D7	6/7lb	–	–	-4.61–4.62	918, 885 mg
Kz-110	faunal	2016	E7-2484	E7	6/7 lp/ls (6/7 lb*)	–	–	-4.64–4.65	919 mg

^{14}C Results

Preservation at Kozarnika was good for the age of the site with 77% of collected radiocarbon samples showing %N $>$ 0.7. Though despite initial screening, 8 of the 43 samples treated had insufficient collagen preservation for radiocarbon dating. This leaves 37 successful radiocarbon measurements from 35 bone samples (see tab. 8.5–8.6).

Unfortunately, the two samples that fully dissolved during the ABA stage of pretreatment were Kz-57 and Kz-58 – the Venus figurine and the osseous spear point from sector III. One further artefact and 4 faunal samples were also not AMS dated, as a direct result of their low gelatine yield after AG treatment: Kz-15, Kz-38, Kz-45, Kz-81, Kz-83.

Kz-54 and Kz-55 were dated despite insufficient collagen yield for ultrafiltration. They both were believed to belong to human remains and a minimum age estimate is still more informative than no date at all. As a result, Kz-54 could be excluded from the Upper Palaeolithic record. With a measurement of 2458 ± 28 BP (OxA-33473) it unmistakeably dates to the Holocene. Kz-55 resulted in an age of 48000 ± 3700 BP (OxA-33474). The question of reliability became superfluous to the project: ZooMS analysis identified the sample as *Ursus* sp., and in the absence of any identifiable anthropogenic modifications, the sample no longer has a connection to human activity.

Kz-03 was dated at AG as it was the only sample available from level III. Considering the relatively young age of 23240 ± 180 BP (OxA-35417), the sample is in all likelihood reliable. The remaining samples showed sufficient collagen yield for ultrafiltration, and were successfully dated. The autoduplicates gave statistically indistinguishable measurements and demonstrate dating reproducibility. The only remaining pre-treatment anomaly observable is a low C:N ratio of 2.9 for both Kz-88 and the second fraction of Kz-116. Both samples were combusted for graphitisation on mass-spec run no. 4151, which showed C:N ratios lower than expected for all samples as a result of calibration issues (see Appendix). The background standards on

Table 8.5: Kozarnika: new AMS radiocarbon dates on anthropogenically modified bone (ref-no 3–38) from sector I with archaeological context information, and pre-treatment results. Failed samples in grey. Ref-no. = number given to the sample for the purpose of this project. %N = nitrogen weight content before chemical pre-treatment. Treat. = Pretreatment protocols used: AG = ORAU acid-base-acid pretreatment, AF = ORAU ultrafiltration protocol (see section 5.4). Yield = sample left after chemical pre-treatment (both in mg and wt.%). %C = carbon yield on combustion. C:N = carbon to nitrogen ratio of combusted collagen sample. $F^{14}C$ = fraction modern carbon. ^{14}C (BP) = conventional radiocarbon age Before Present with 1σ error. Date (cal BP) = calibrated radiocarbon age at a 95.4% confidence interval, calculated in OxCal 4.3 (Bronk Ramsey, 2009a) using IntCal13 (Reimer et al., 2013). For Information marked with a * see discussion in section 8.1.4.

Ref-no.	Item	Sq.	Layer	Depth (cm)	%N	Treat.	Yield (mg)	Yield (wt.%)	%C	$\delta^{15}N$	$\delta^{13}C$	C:N	Lab-no	$F^{14}C$	^{14}C (BP)	Date (cal BP)
Kz-03	fauna (marked)	D7	3b = III	380-385	0.49	AG	8.88	0.99	40.4	8.4	-19.7	3.2	OxA-35417	0.05541 ± 0.00126	23240 ±180	27770 – 27200
Kz-06	fauna (marked)	E9	4 = IVa	390-393	1.71	AF	9.23	1.60	43.0	7.9	19.6	3.2	OxA-33834	0.03057 ± 0.00109	28020 ±290	32740 – 31260
Kz-07	fauna (marked)	D8	4 = IVa	395-400	1.54	AF	7.84	2.18	43.3	7.7	-19.6	3.2	OxA-34767	0.03741 ± 0.00105	26400 ±220	31070 – 30180
Kz-08	fauna (marked)	E9	4 = IVa	393-395	1.92	AF	14.43	2.51	43.0	8.5	-19.4	3.2	OxA-34768	0.03309 ± 0.00102	27380 ±250	31650 – 30920
Kz-10	fauna (marked)	E7	4 = IVa	393-395	2.03	AF	19.32	3.17	45.3	6.3	-20.7	3.3	OxA-33546	0.03330 ± 0.00109	27330 ±260	31620 – 30890
Kz-14	fauna (marked)	E7	4 = IVb	410-415	1.37	AF	30.34	3.42	42.0	4.5	-21.4	3.2	OxA-35230	0.03768 ± 0.00105	26340 ±220	31030 – 30050
Kz-15	artefact	E10	4 = IVb	410-415	0.48	AG	7.92	0.94	–	–	–	–	P-39504	–	–	–
Kz-19	fauna (marked)	E9	4 = IVb	410-415	2.91	AF	33.46	5.16	42.8	6.8	-19.8	3.2	OxA-33547	0.04030 ± 0.00110	25800 ±220	30640 – 29440
Kz-23	fauna (marked)	D10	4 = IVb	405-410	3.05	AF	25.78	4.47	43.0	5.8	-20.1	3.2	OxA-33548	0.04983 ± 0.00115	24090 ±180	28560 – 27770
Kz-24	fauna (marked)	F10	5a = V	420-425	2.20	AF	14.51	2.76	43.5	6.6	-19.3	3.2	OxA-33549	0.03346 ± 0.00111	27290 ±270	31600 – 30860
Kz-25	fauna (marked)	F10	5a = V	425-430	2.27	AF	24.84	4.17	43.3	6.2	-20.8	3.2	OxA-33550	0.03246 ± 0.00109	27540 ±270	31990 – 30970
Kz-38	fauna (marked)	F9	5b = VI	435-440	0.91	AG	4.54	0.75	–	–	–	–	P-39527	–	–	–

Table 8.6: Kozarnika: new AMS radiocarbon dates on anthropogenically modified bone and humans (ref-no. 39–81) with archaeological context information, and pre-treatment results. Samples Kz-53 to Kz-58 are from sector III, the rest from sector I/II. Failed samples in grey. For Information marked with a * see discussion in section 8.1.4.

Ref-no.	Item	Sq.	Layer	Depth (cm)	%N	Treat.	Yield (mg)	Yield (wt.%)	%C	δ^{15}N	δ^{13}C	C:N	Lab-no	F^{14}C	^{14}C (BP)	Date (cal BP)
Kz-39	fauna (marked)	F8	5b = VI	430-435	3.01	AF	35.63	8.71	42.9	2.6	-21.7	3.2	OxA-33551	0.01696 ± 0.00105	32750 ±500	38350 – 35760
Kz-43	fauna (marked)	G5	5c = VII	440-443	1.37	AF	20.25	3.24	42.9	8.2	-19.4	3.2	OxA-33552	0.01000 ± 0.00102	37000 ±800	42760 – 40080
Kz-44	fauna (marked)	F7	6/7 = VIII	460-465	0.66	AG	3.40	0.64	–	–	–	–	P-39533	–	–	–
Kz-45	fauna (marked)	F10	5b = VI	440-445	0.87	AG	6.96	1.26	40.8	8.1	-19.5	3.2	P-39534	–	–	–
Kz-47	fauna (marked)	F8	5c = VII	445-450	1.97	AF	27.77	4.59	42.9	8.9	-20.7	3.2	OxA-33835	0.00940 ± 0.00101	37500 ±900	43340 – 40320
Kz-48	fauna (marked)	G5	5b/c* = VII/VII*	443	1.68	AF	38.30	7.75	42.6	7.3	-19.6	3.2	OxA-34769	0.01054 ± 0.00098	36550 ±750	42380 – 39720
Kz-49	fauna (marked)	G7	5c = VII	450-455	1.01	AF	16.13	2.68	43.1	6.8	-19.3	3.2	OxA-33553	0.01021 ± 0.00103	36800 ±800	42620 – 39880
Kz-50	fauna (marked)	G11	5b = VI	450-455	2.18	AF	17.40	3.64	43.0	6.9	-21.9	3.1	OxA-33554	0.01513 ± 0.00108	33650 ±550	39310 – 36470
Kz-52	fauna (marked)	F5	6/7* = VIII*	453-455	1.96	AF	17.00	2.76	43.1	8.5	-19.5	3.2	OxA-33555	0.00432 ± 0.00101	43700 ±1900	> 44740
Kz-53	human	–	–	–	0.86	AF	31.90	4.95	43.3	8.3	-19.1	3.2	OxA-33472	0.73025 ± 0.00249	2525 ±27	2750 – 2490
Kz-54	human	–	–	–	0.80	AG	12.01	2.53	38.5	10.6	-18.0	3.2	OxA-33473	0.73636 ± 0.00258	2458 ±28	2710 – 2360
Kz-55	fauna*	–	–	–	0.58	AG	8.70	1.67	42.0	9.3	-23.9	3.2	OxA-33474	0.00253 ± 0.00117	48000 ±3700	> 49710
Kz-57	artefact	–	–	–	0.69	AG	0.00	0.00	–	–	–	–	P-39546	–	–	–
Kz-58	point	F30	6/7?	504	0.21	AG	0.00	0.00	–	–	–	–	P-39547	–	–	–
Kz-79	artefact	E10	5a = V	415-420	3.00	AF	15.15	2.61	42.6	6.6	-21.2	3.2	OxA-34822	0.04237 ± 0.00108	25400 ±200	30160 – 28960
Kz-80	fauna (marked)	D8	6/7lp = VIII	458-459	2.15	AF	53.15	5.44	43.1	7.9	-19.9	3.2	OxA-34823	0.00423 ± 0.00097	43900 ±1800	> 45000
Kz-81	fauna (marked)	E8	6/7ls = VIII	458-459	0.44	AG	2.43	0.28	–	–	–	–	P-42170	–	–	–

Table 8.7: Kozarnika: new AMS radiocarbon dates on anthropogenically modified bone (ref-no. 82–116) with archaeological context information, and pre-treatment results. Samples Kz-111 to Kz-116 from sector III, rest from sector I/II. Failed samples in grey. For Information marked with a * see discussion in section 8.1.4.

Ref-no.	Item	Sq.	Layer	Depth (cm)	%N	Treat.	Yield (mg)	Yield (wt.%)	%C	δ^{15}N	δ^{13}C	C:N	Lab-no	F^{14}C	^{14}C (BP)	Date (cal BP)
Kz-82	fauna (marked)	E8	6/7ls = VIII	458-459	0.90	AF	6.63	0.77	42.8	8.4	-19.9	3.2	OxA-X-2699-11	0.00481 ± 0.00100	42900 ±1700	49890 – 44120
Kz-83	fauna (marked)	E7	6/7ls = VIII	461-462	–	AG	2.02	0.27	–	–	–	–	P-42116	–	–	–
Kz-85	fauna (marked)	D7	5c = VII	445-448	0.33	AF	36.22	5.34	43.2	8.2	-20.6	3.2	OxA-34824	0.00926 ± 0.00099	37600 ±900	43440 – 40410
Kz-87	fauna (marked)	E9	5c* = VII	450-453	2.62	AF	59.29	7.00	43.8	9.2	-19.2	3.2	OxA-35234	0.00954 ± 0.00098	37400 ±800	43050 – 40440
Kz-88	fauna (marked)	D9	5b = VI	445-448	1.83	AF	25.95	3.39	40.3	9.1	-18.7	2.9*	OxA-35575	0.03130 ± 0.00104	27830 ±270	32480 – 31150
Kz-90	fauna (marked)	D9	5b = VI	443-445	2.08	AF	21.74	2.88	41.0	7.4	-20.8	3.1	OxA-35576	0.03061 ± 0.00105	28010 ±280	32710 – 31260
Kz-93	fauna (marked)	E9	6/7lp = VIII	455-458	0.91	AF	20.03	2.46	43.2	6.5	-21.4	3.2	OxA-34825	0.00427 ± 0.00098	43800 ±1800	> 44920
Kz-109	fauna (marked)	D7	6/7lb = VIII	461-462	2.51	AF	78.72	8.57	43.1	3.5	-20.9	3.2	OxA-34826	0.00702 ± 0.00098	39800 ±1100	45710 – 42090
Kz-109	fauna (marked)	D7	6/7lb = VIII	461-462	2.51	AF	71.05	8.02	43.0	3.3	-20.9	3.2	OxA-34827	0.00614 ± 0.00098	40900 ±1300	47490 – 42540
Kz-110	fauna (marked)	E7	6/7 lp,ls* = VIII	464-465	1.02	AF	20.21	2.20	43.0	8.6	-19.2	3.2	OxA-34828	0.00417 ± 0.00097	44000 ±1900	> 44990
Kz-111	fauna (cut?)	G30	A2	540-545	3.2	AF	90.94	9.82	43.5	8.0	-20.4	3.2	OxA-34829	0.01053 ± 0.00098	36600 ±750	42410 – 39780
Kz-112	fauna (cut?)	G30	A1	545-550	0.88	AF	24.18	2.56	43.2	10.3	-20.2	3.2	OxA-34830	0.00901 ± 0.00102	37800 ±900	43670 – 40630
Kz-114	fauna (cut?)	F29	D2	550-555	2.49	AF	44.78	6.31	40.5	5.0	-20.9	3.1	OxA-35577	0.00031 ± 0.00099	> 48900	–
Kz-115	fauna (cut?)	F30	C	540-545	1.12	AF	12.65	1.68	41.4	5.2	-22.7	3.1	OxA-35578	0.00246 ± 0.00100	48300 ±3300	> 49810
Kz-116	fauna (cut?)	F29	D2	545-550	2.33	AF	38.41	5.99	40.8	5.9	-21.7	3.1	OxA-35579	0.00423 ± 0.00099	43900 ±1900	> 44900
Kz-116	fauna (cut?)	F29	D2	545-550	2.33	AF	35.48	6.91	40.1	6.6	-20.1	2.9*	OxA-35580	0.00473 ± 0.00098	43000 ±1700	49930 – 44240

said run suggest that these technical issues have not affected the reliability of the radiocarbon measurement.

In conclusion, this project produced 28 radiocarbon measurements from sector I/II that are directly connected to human activity and suitable for Bayesian modelling. This includes 26 ultrafiltered anthropogenically modified faunal remains, 1 ultrafiltered anthropomorphic figurine (Kz-79), and a non-ultrafiltered anthropogenically modified faunal fragment. In addition, there are 6 dates on ultrafiltered faunal remains from sector III to provide an initial assessment of the chronological placement of layers A, C and D. From the three samples presumed to be human, two securely date to the Holocene (Kz-53 and Kz-55) and one was identified by ZooMS as belonging to a bear (Kz-55). These last three dates will no longer be relevant to answering questions about the Middle to Upper Palaeolithic biocultural shift.

8.1.3 Bayesian modelling

Kozarnika is ideal for modelling as it has both a deep stratigraphy, and well-defined archaeological horizons. In addition, it has an extensive dating record, which allows for independent investigation of the effects of sample selection on modelling results and interpretation. Eight stratigraphic and three KDE models were run (in OxCal 4.3 with IntCal13). The former were to compare age estimates for boundary transitions between different archaeological horizons, and for the archaeological material within a layer. The latter was to test the different datasets in relation to identifying timing of human activity at the cave. For all models, autoduplicates were combined using the `R_Combine` function. The actual code used can be found under Catalogue B.1.

Site Stratigraphic Models

All stratigraphic models used the outlier model `General` for assessing whether individual radiocarbon dates and combined dates were outliers within the

constraints of the model, and `SSimple` for radiocarbon dates in `R_Combine`. In both cases standard parameters for distribution, magnitude and type were implemented – `T(5),U(0,4),''t''` and `N(0,2),0,''s''`, respectively – and pior sample outlier probability set to 5%. The radiocarbon dates were sorted into phases separated by single boundaries and placed into sequence according to their archaeological level or geological layer attribution. The radiocarbon age of 34290 ± 90 BP from Giaccio et al. (2017) was placed within layer 5b (= level VI) to represent the age of the CI eruption identified by the tephra horizon. Additionally, all models were run with an empty `Date` function within each `Phase`. While this is a useful method of obtaining an exportable age probability range for a cultural layer, it requires testing to make sure the influence of additional events on the outcome of the modelling process is negligible (see section 6.4). Therefore, the same models were also run without the `Date` function for testing. Within and between all phases, the command `Interval` was used to calculate duration of phases and transitions.

Eight different stratigraphic models were run. Model 0, using previously obtained radiocarbon data, represents the *status quo* prior to this doctoral research and aids as a comparison for the new results, both in terms of changes to the dating record and the influence of using different sample strategies. Models 1–4 were all run on the newly obtained radiocarbon measurements. Contrasting Models 1/2 with Models 3/4 should allow the assessment of whether the subdivision of level IV into a and b can be supported by the dating record. Contrasting Models 1/3 with Models 2/4 explored the effect of sample Kz-48 belonging to either layer 5c or 5b. Models 5 and 6 use a combined old/new radiocarbon dataset to investigate the influence of charcoal dates on the age ranges and modelled transitions (considering charcoal samples are less securely connected to human activity and show added contamination complexity for samples older than 30k BP). And finally, Model 7 uses an OSL age estimate for the uppermost Middle Palaeolithic layer to examine the effect on the start boundary for the, possibly early Upper Palaeolithic, layer 6/7.

Model 0 (charcoal) uses previously obtained radiocarbon dates deemed suitable for modelling (see tab. 8.1 and 8.2) and the CI age proposed by Giaccio et al. (2017). The events were sorted according to their archaeological levels: VIII, VII, VI, V, IV, III, and 0I. Code listed on p. 666.

Model 1 (bone) incorporates all new radiocarbon dates on anthropogenic modified bone samples from sector I/II (see tab. 8.5 – 8.7) and the CI age proposed by Giaccio et al. (2017). The events were sorted according to geological layers with Kz-48 featuring in 5c. Layer 6/7 lp and 6/7 ls were combined as (a) the stratigraphy was unclear as to which one of the two is younger, and (b) Kz-110 could belong to either of them. Layer 4 was subdivided into level IVa and IVb. This resulted in the following phases: 6/7 ls/lp, 6/7 lb, 5c, 5b, 5a, 4(IVa), 4(IVa), 3b. Code listed on p. 667.

Model 2 (bone) incorporates the same radiocarbon dataset and `Phase` structure as Model 1, but Kz-48 is grouped under 5b. Code listed on p. 668.

Model 3 (bone) employs the same radiocarbon data set as Model 1, with Kz-48 also attributed to layer 5c. However, layer 4 is not subdived into IVa and IVb, giving the following phase structure: 6/7 ls/lp, 6/7 lb, 5c, 5b, 5a, 4, 3b. Code listed on p. 669.

Model 4 (bone) runs the same radiocarbon data set as Model 2, with Kz-48 attributed to layer 5b, and the identical phase structure as Model 3. Code listed on p. 671.

Model 5 (charcoal / bone) is based on Model 3 with the charcoal data from Model 0 added. Prior to 2015, layer 6/7 had not been subdivided. As a result, the phase structure had to be adjusted accordingly: 6/7, 5c, 5b, 5a, 4(IVa), 4(IVa), 3b. Code listed on p. 672.

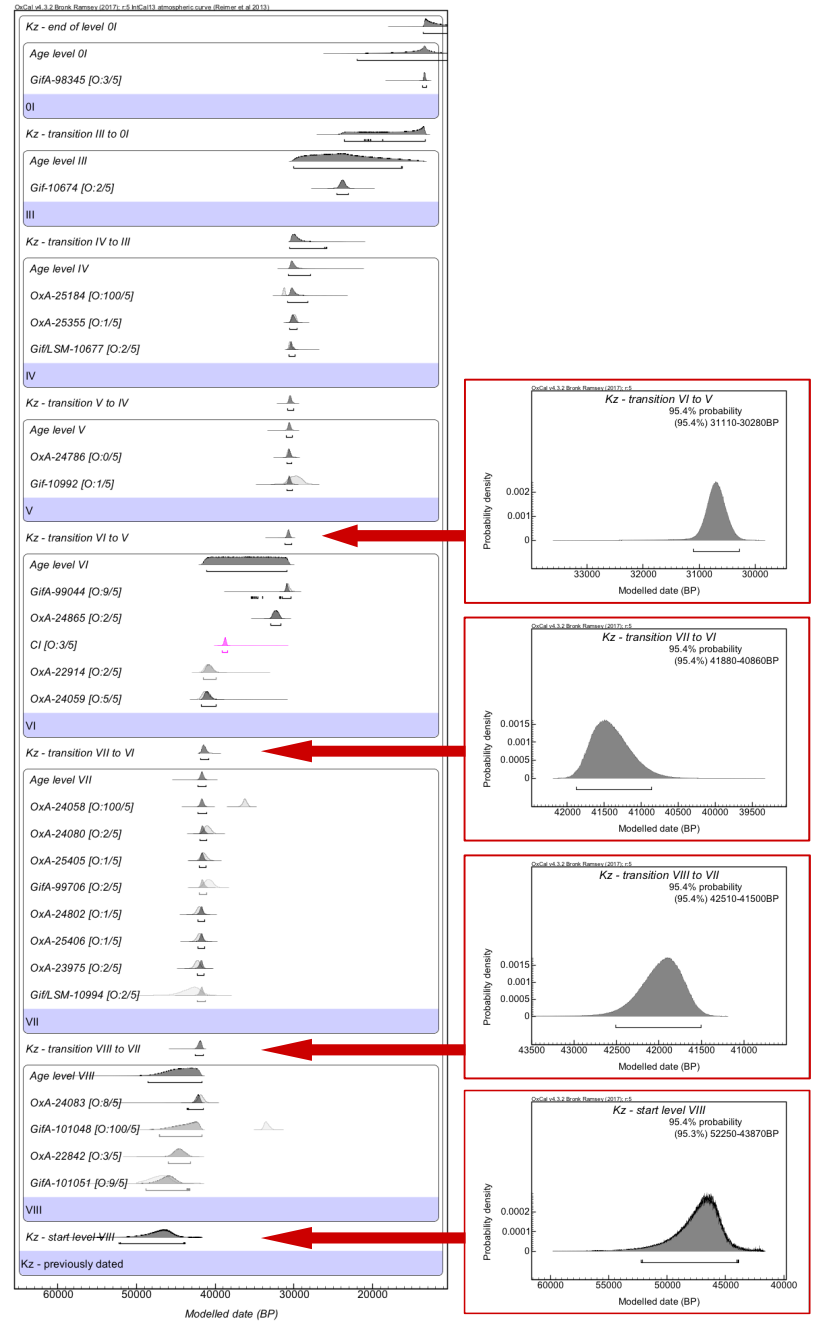


Figure 8.18: Kozarnika: stratigraphic Model O using previously obtained charcoal dates as listed in tables 8.1–8.2 and CI tephra radiocarbon age from Giaccio et al. (2017). **grey** – dates obtained with less rigorous pre-treatment protocols (code: p. 666).

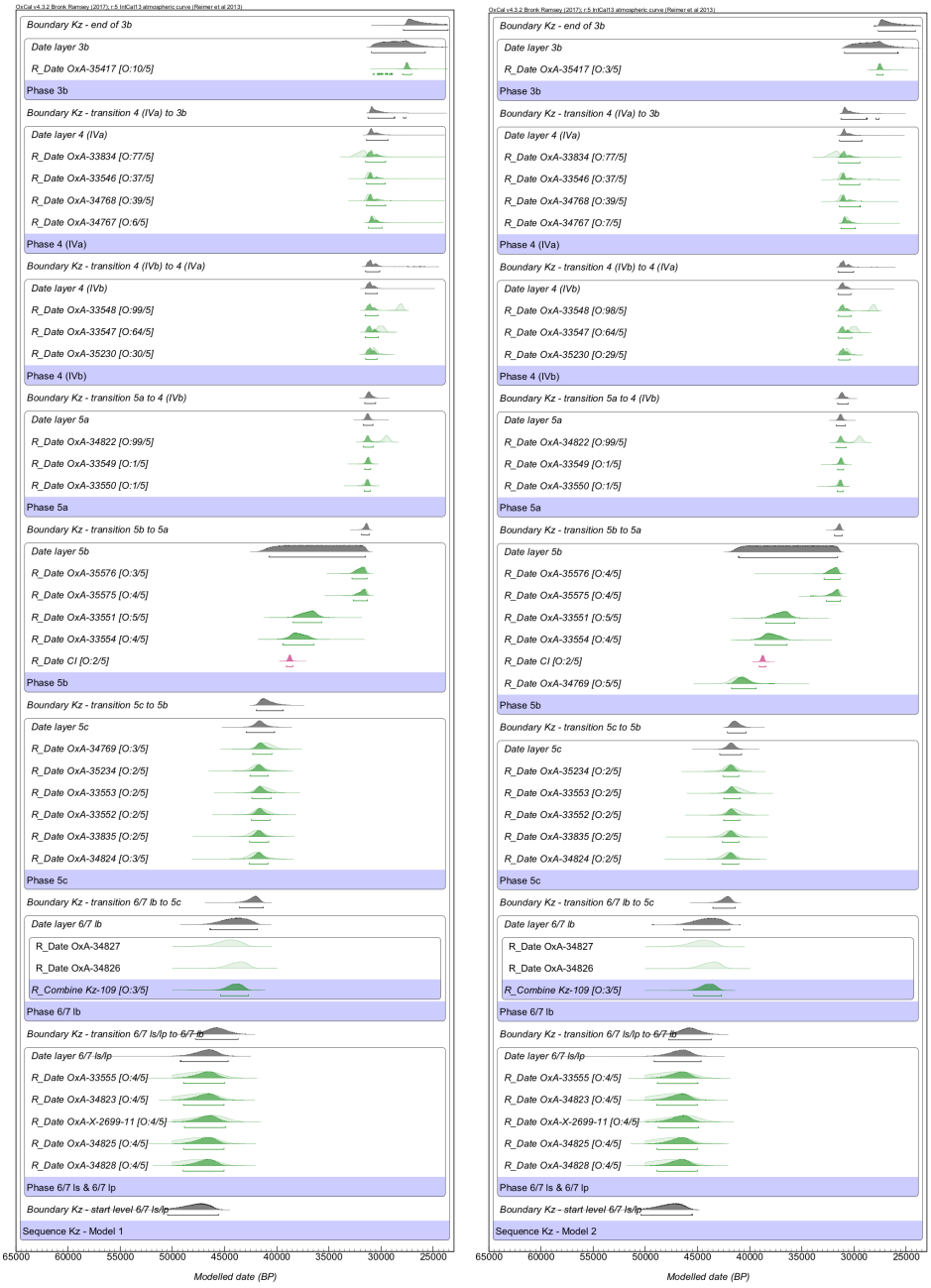


Figure 8.19: Kozarnika: stratigraphic Model 1 (left, code: p. 667) and Model 2 (right, code: p. 668). Sample Kz-48 (OxA-34769) is attributed to 5c in Model 1, and to 5b in Model 2 (see text). **green** – new ^{14}C dates on anthropogenically modified fauna (sector I/II); **magenta** – CI tephra radiocarbon age Giaccio et al. (2017); **black** – modelled ages.

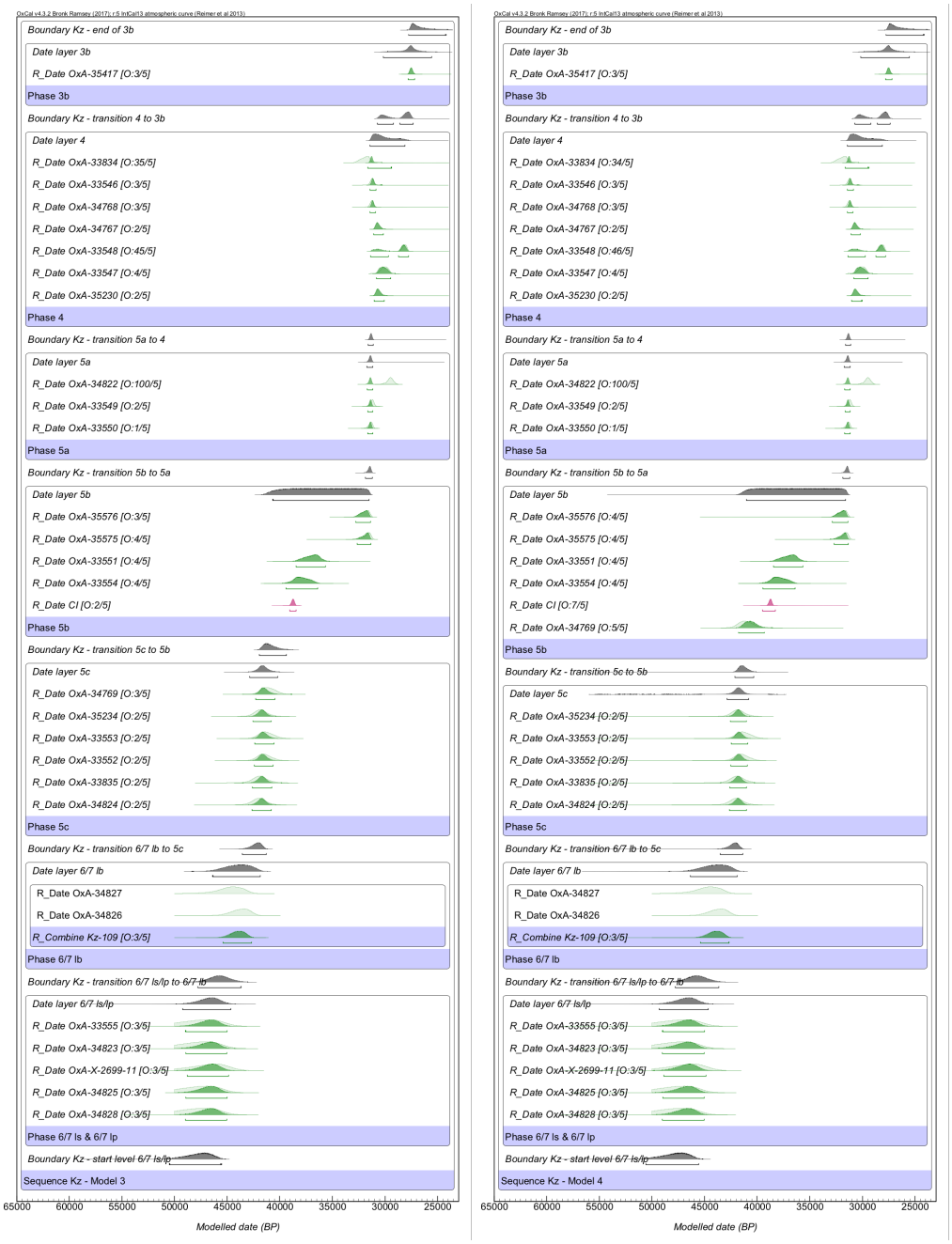


Figure 8.20: Kozarnika: stratigraphic Model 3 (left, code: p. 669) and Model 4 (right, code: p. 671). Sample Kz-48 (OxA-34769) is attributed to 5c in Model 3, and to 5b in Model 4 (see text). **green** – new ^{14}C dates on anthropogenically modified fauna (sector I/II); **magenta** – CI tephra radiocarbon age Giaccio et al. (2017); **black** – modelled ages.

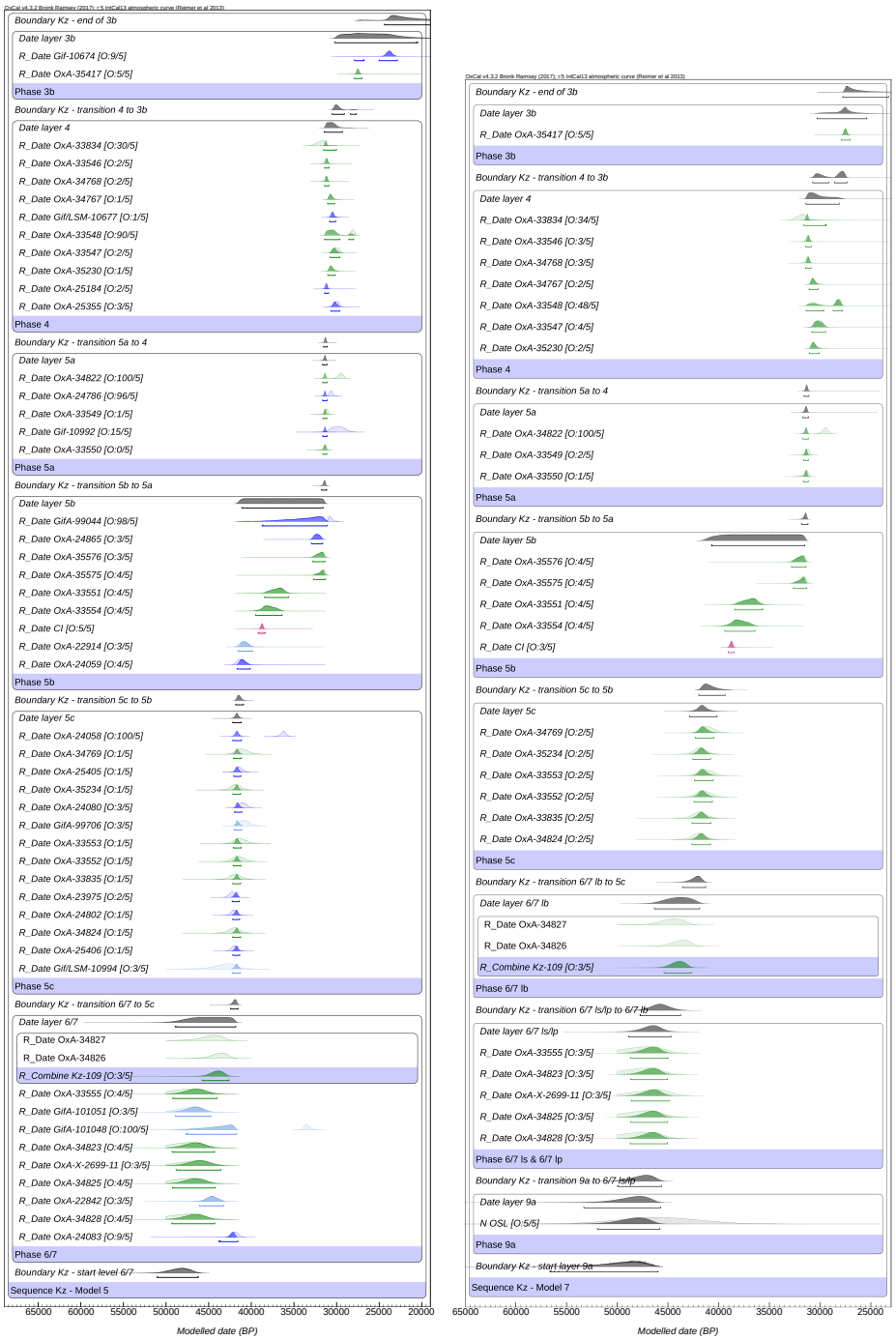


Figure 8.21: Kozarnika: Model 5 (left, code: p. 672) and Model 7 (right, code: p. 676). **green** – new ^{14}C dates on anthropogenically modified fauna (sector I/II); **blue** – previous ^{14}C dates on charcoals (sector I/II); **magenta** – CI tephra radiocarbon age Giaccio et al. (2017); **black** – modelled ages.

Model 6 (charcoal / bone) is based on Model 4 with the charcoal data from Model 0 added. Prior to 2015, layer 6/7 had not been subdivided. As a result, the phase structure had to be adjusted accordingly: 6/7, 5c, 5b, 5a, 4, 3b. Code listed on p. 674.

Model 7 (bone / OSL estimate) has the same underlying radiocarbon dataset and phase structure as Model 3. In addition, an OSL age estimate of 46000 ± 4000 for the uppermost Middle Palaeolithic layer 9a was placed in a separate phase underlying layer 6/7 ls/lp. The age is based on preliminary OSL results from work done by Maryam Heidari and G. Guérin at Bordeaux (publication forthcoming). As the age is not finalised, it is only implemented to test its possible effects on the modelled boundaries. Code listed on p. 676.

KDE Models

The OxCal function `KDE_Model` was used to summarise three different radiocarbon datasets from Kozarnika. Their purpose was threefold: (1) to independently asses the structure of human activity observed and recorded during excavation; (2) to demonstrate the effect of sampling strategy on calculating periods of human activity; and (3) to illustrate the quality of the new radiocarbon dataset based on anthropogenically modified faunal remains.

KDE 0 employs the previously obtained radiocarbon dataset on charcoal samples (see tab. 8.1 and 8.2) and used in stratigraphic Model 0 (n=23). Code listed on p. 677.

KDE 1 summarises the new radiocarbon dataset on anthropogenically modified faunal remains from sector I/II (n=27) as used in stratigraphic Models 1–4 (see tab. 8.5 – 8.7). Code listed on p. 678.

KDE 2 combines the radiocarbon record from KDE 0 and KDE 1 (n=50). Code listed on p. 678.

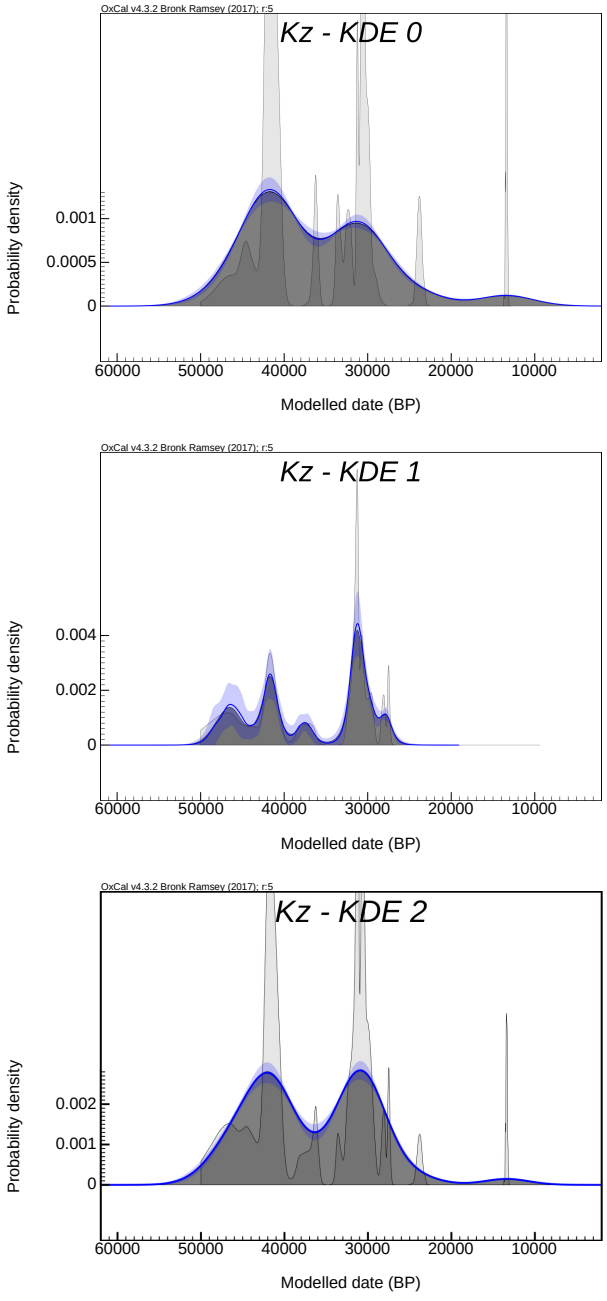


Figure 8.22: Kozarnika: comparison of KDE modelling results: KDE 0 (previously measured charcoal dates, n=23, code: p. 677); KDE 1 (new ^{14}C dates on anthropogenically modified fauna from sector I/II, n=27, code: p. 678); KDE 2 (combining data used in KDE 0 and KDE1, n=50, code: p. 678).

8.1.4 Discussion

Assessing Context Information

After running the radiocarbon measurements, some discrepancies between radiocarbon age and layer attribution prompted a thorough re-checking of the archaeological contexts of all dated samples. While the information found in excavation journals and site drawings was consistent with those found in sample bags and bone fragments for the vast majority of samples, in four cases they were not.

Kz-110 was originally labelled on site as belonging to layer 6/7 lb. Looking at the planum drawing from just above (depth: 460 cm), the location is marked as 6/7 lp, while the one from just below (depth: 465 cm) shows 6/7 ls. In addition, the sample shows patina consistent with other samples from layer 6/7 lp, but not with layer 6/7 lb. It can be concluded, that the sample actually belongs to either layer 6/7 lp or 6/7 ls. The radiocarbon age of 44000 ± BP (OxA-34828) is consistent with such an attribution.

Kz-87 was originally attributed to 5c. The find location is marked by very uneven layer limits, which leave an alternating pattern between layer 6/7 and 5c when cut horizontally. The patina differs from other artefacts from layer 5c in that sector and shows signs of heating, consistent with an origin in the 'fireplace' layer below 5c, *i.e.* at the top of layer 6/7. Consequently, the layer attribution was changed from 5c to 6/7.

Kz-48 was bagged as coming from layer 5b, however, the excavation documentation leaves attribution somewhat ambiguous. Both layers 5b and 5c were found in the vicinity of the sample, judging by plana drawings. As a result, both layer attributions were tested during Bayesian modelling.

The label on the bag for Kz-87 had the following information written on it when radiocarbon sampling was conducted: "*E9-2452, E9, 5b, 443-445 cm*". However, the excavation journal has no sample E9-2452 listed at that depth. Instead, E9-2452 is featured on the sample list for spit 450-453 cm. As the bone fragment has the number E9-2452 clearly written on it, the depth on

the bag was undoubtedly a clerical error. The location of sample E9-2452 on the planum drawing is well within layer 5c. This information is more secure than the sample list noting layer 6/7, as misspelling a layer number is significantly more likely than missing a layer in a drawing.

Human Remains

The two human remains (Kz-53 and Kz-54) from sector III evidently ended up in the Upper Palaeolithic horizon as a result of illicit treasure hunter activity, as they only date to 2525 ± 27 BP (OxA-33472) and 2458 ± 28 BP (OxA-33473), respectively. Therefore, the two samples are no longer relevant to the discussion of the early Upper Palaeolithic. The third possible human specimen sampled (Kz-55) belongs to the period of interest, as demonstrated by the radiocarbon age of 48000 ± 3700 BP (OxA-33474). Unfortunately, ZooMS analysis identifies the cranial fragment as that of a bear (*Ursus* sp.) – not a *Homo* sp. As the sample does not show any anthropogenic modifications and has no secure context, it has no direct connection to human activity at the site. As a result, it does not feature in any further analysis for this project.

Stratigraphic Model Outliers

The archaeological levels IVa and IVb cannot be satisfactorily resolved. In both stratigraphic models featuring this distinction, all radiocarbon dates were identified as outliers (see fig. 8.19), as sublevel IVa seems to provide older radiocarbon results than IVb. Consequently, a single `Phase` IV (layer 4) is to be preferred, until the existence of the two strata in layer 4 can be confirmed and better understood.

Two dates which remain clear outliers – even in a combined layer 4 – are OxA-33834 (Kz-06) and OxA-33548 (Kz-23)[5]. Nothing during pre-treatment

[5]Model 3 attributes a 35% and 45% outlier probability, Model 4 34% and 46%, Model 5 30% and 90%, Model 6 31% and 88%, and Model 7 34% and 48%.

indicated issues with the radiocarbon dating process, and the archaeological record did not suggest any ambiguous context attribution. However, layer 4 is a thin, discontinuous band with irregular layer boundaries (see fig. 8.6). Therefore, the age discrepancies could result from either intrusion, mixing of material, secondary depositioning, or misidentification of layer boundaries.

The age of the only datable figurine OxA-34822 (Kz-79) suggests that the artefact does not belong to the human occupation found in layer 5a (level V). All models give it an outlier probability of 99–100% (see fig. 8.19–8.21). The age is even younger than many dates obtained from layer 4. However, this does not appear to be the result of insufficient radiocarbon pre-treatment – which did not reveal any anomalies and the artefact had not been treated with any carbon containing conservation or consolidation products which would lead to younger dates. The only work done on the artefacts prior to dating was obtaining a silicone cast. A layer misattribution on site seems also improbable. Although the figurine was found in the top part of layer 5a, excavation documentation does not indicate that it could have been found within sedimentation fo layer 4. Consequently, it has to be concluded that the radiocarbon measurement appears reliable – placing the artefact in the later phases of the Middle Kozarnikian – and the figurine is most likely intrusive to 5a.

The ambiguous layer attribution of OxA-34769 (Kz-48) cannot be securely resolved using Bayesian modelling. Models placing OxA-34769 in layer 5c consistently give it an outlier probability of only 2% (below threshold of 5%). However, placing the specimen in layer 5b (as seen in models 1, 3, and 7) increases the outlier probability only to 5% and therefore exactly at the threshold. Model 6, which shows higher intra-layer age variability, lead to an even smaller increase, resulting in a 4% outlier probability for OxA-34769 (below threshold). Therefore, despite the date being in better accord with layer 5c, an origin in layer 5b cannot be excluded. As the effect of moving OxA-34769 on the transition boundaries is minimal (slight narrowing of the transition when placed in 5b, see fig. 8.23), the main question remains whether there was an early occupation within layer 5b or not.

Campanian Ignimbrite (CI) and layer 5b

The radiocarbon age of Giaccio et al. (2017) agrees with the chronostratigraphy and a placement within layer 5b (see fig. 8.19–8.21). The CI eruption (Y5) seems to either coincide with the occupation represented by OxA-33551 (Kz-39) and OxA-33554 (Kz-50), or to just predate it. Both scenarios would be consistent with a spread of CI tephra within level VI.

The distribution of radiocarbon dates on anthropogenically modified faunal remains identifies three possible, distinct occupations within layer 5b. The youngest, represented by OxA-35575 (Kz-88) and OxA-35576 (Kz-90), and the oldest, represented by OxA-34769 (Kz-48), do not overlap with the CI eruption. While the tephra shard count evidently peaks in layer 5b, CI tephra at low shard count was also found in the upper most part of layer 5c and the lower most part of 5a. This is evidence of some material mixing in the contact zones. Considering the radiocarbon age probability distributions of OxA-35575 and OxA-33576 overlap with the dates observed in layer 5a, and OxA-34769 with those in layer 5b, it is possible that there is also some mixing of archaeological material. While it remains possible that there were several discrete occupations within layer 5b, it seems presently more feasible to assume that layer 5b contains some material belonging to occupations otherwise recorded in levels V (layer 5a) and VII (5c). In this case, caution is advised when analysing the lithic and osseous industries found within layer 5b.

Comparison of Model Results

In general, all stratigraphic models produced boundaries that are in good agreement with each other. Nonetheless, there are some differences that require discussion (see fig. 8.23 and 8.24).

The most notable exceptions are the higher boundary precisions (transitions 6/7 to 5c, and 5c to 5a) found in Model 5 and Model 6, and the younger boundary (transition 5c to 5a) in Model 0. Model 0 is likely underestimating

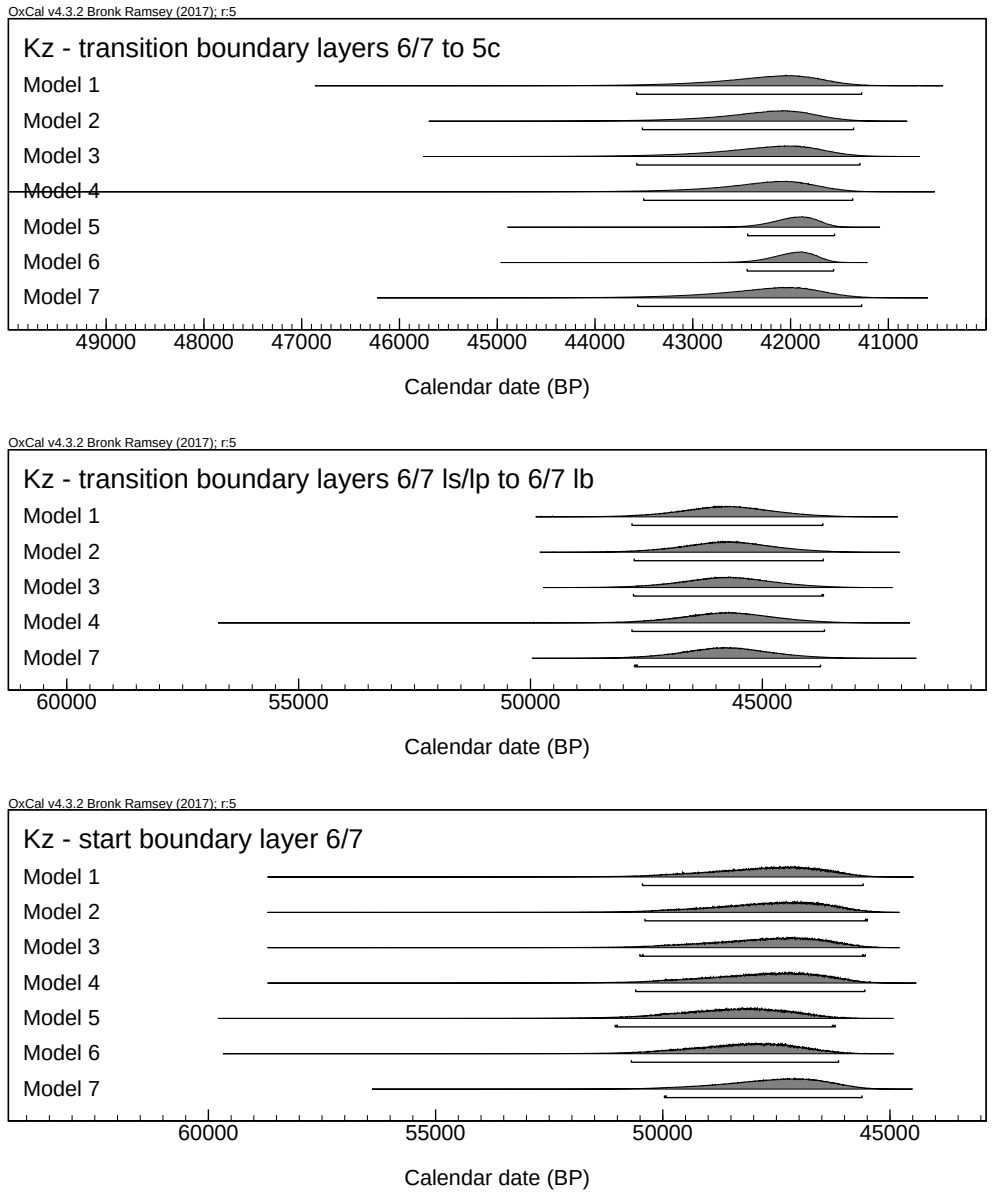


Figure 8.23: Kozarnika: comparison of transition boundaries (start layer 6/7, transition 6/7 ls/lp to 6/7 lb, and transition 6/7 to 5c) for Stratigraphic Models 1 to 7. The consistency of the boundaries demonstrates the robustness of the stratigraphic model results. The higher precision in the transition boundary 6/7 to 5c for Models 5 and 6 mainly results from the larger spread of ages in layer 6/7, caused by the charcoal dates GifA-101048, OxA-22842, and OxA-24083 – and might not be more accurate.

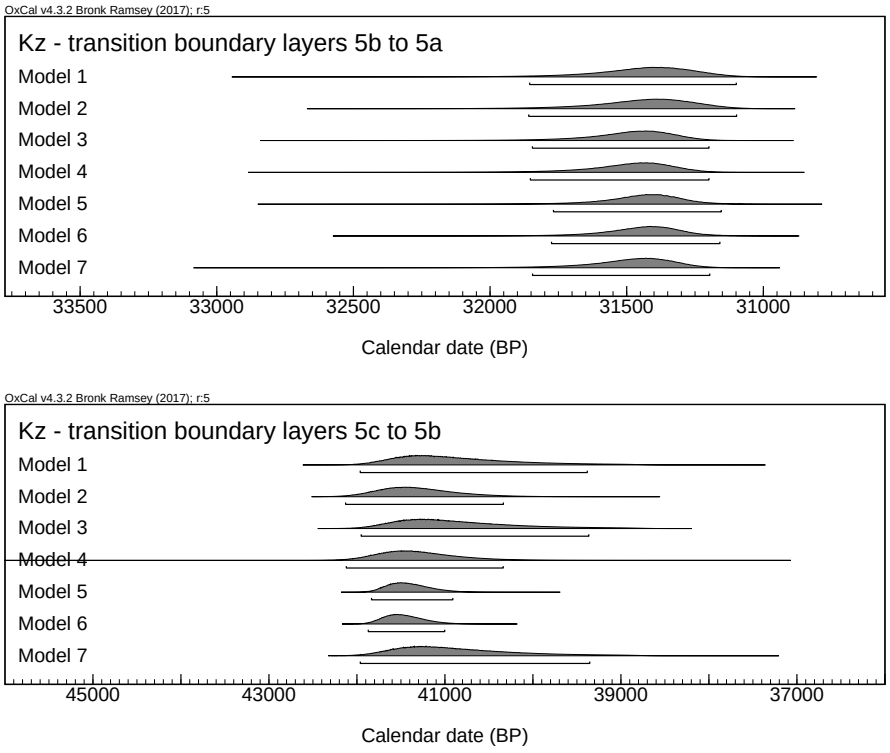


Figure 8.24: Kozarnika: comparison of transition boundaries (5c to 5b, and 5b to 5a) for Stratigraphic Models 1–7, illustrating the robustness of the model results. The higher precision produced by models 5 and 6 (boundary 5c and 5b) results from the larger spread of ages in layer 5c, and does not translate to higher accuracy.

the age of the transition, considering the limited charcoal data available for level IV (see fig. 8.18). In the case of models 5 and 6, both include the previously obtained radiocarbon record on charcoal samples, which shows less age consistent data within a layer, albeit not in direct disagreement with the chronostratigraphy of the site. Both models demonstrate how a larger age spread of radiocarbon dates within a `Phase` increases the precision of the adjacent transition `Boundary`. In contrast, more age consistent data within a `Phase`, which is also chronologically well separated from dates in adjacent units, reduces the `Boundary` precision. This is a strong reminder that a higher modelling precision might be the result of lower quality radiocarbon data – either as a result of less reliable dating or lower probability of association to

the events of interest. It does not necessarily translate into a more accurate modelling result.

There are two main scenarios to explain the higher age variation observed in charcoal samples. First, it may be caused by lower dating accuracy for charcoal samples closer to the radiocarbon detection limit. Second, it may be the result of charcoals representing a larger age range of sedimentation within a layer or level, in contrast to the more sporadic human occupation recorded by dating anthropogenically modified bones. Consequently, higher precision does not necessarily reflect (higher) accuracy.

While the charcoal data increased precision in the stratigraphic models, their effect on KDE modelling outcomes was the opposite (see fig. 8.22). Here, the charcoal data in KDE 0 obscures the anthropogenic signal at the site, producing less discrete events. In the model, there are only three main occupation events discernible, and the occupation appears to decrease over time. When using dates on anthropogenically modified bone (KDE 1), however, a minimum of five discrete human occupation events becomes apparent: (1) 50–44k cal BP, (2) 44–40k cal BP, (3) 39–36 cal BP, (4) 33–30k cal BP, and (5) 29–26 cal BP. They largely correspond to the human occupations within layers 6/7 ls/lp (level VIII), 5c (VII), middle section of 5b (VI), 5a (V) and 4 (IV), and 3b (III). These results imply an increase in occupation frequency/intensity during the Middle Kozarnikian. As the archaeological material of this period can be found in distinct geological units, it can be concluded that an increase in occupation frequency is likely to be the main contributing factor.

The model KDE 2 illustrates how important question tailored radiocarbon sampling is. Despite the large number of anthropogenically modified bone dates in the model, the charcoal samples manage to sufficiently blur discrete occupation events for the model to revert back to a near complete bimodal distribution.

The good agreement between the results of KDE 1 and the stratigraphic models is evidence for a largely intact and well identified stratigraphic se-

quence at Kozarnika. The only notable challenges are found within layer 5b. Therefore, Model 3 probably best reflects the stratigraphy at the site by being more conservative in boundary calculations – including OxA-34669 (Kz-48) in layer 5b for Model 4 may instil a false sense of accuracy by providing a higher precision boundary for the transition from layer 5c to 5b, and Stratigraphic Models 0, 1, 3, 5, and 6 have already been deemed less representative (see above).

When testing the robustness of Model 3 against the preliminary OSL data (see Model 7 in fig. 8.21), it can be shown that the start boundary of layer 6/7 remains consistent (see fig. 8.23).

Sector III

The modelled dates for each layer and their transitions in sector I/II can be compared to the radiocarbon results obtained from sector III. The unmodified faunal remains from layer C and D are significantly older than the ages from layer A, and are thus unable to further constrain the age of layer A. Therefore, the inter-sector comparison focused on layer A, represented by OxA-34829 (Kz-110) and OxA-34830 (Kz-112), and layers 6/7 until the transition to 5a, represented by Model 3 (see fig. 8.25).

While there is some overlap in the age probability distributions between layer A and layers 6/7lb and layer 5b, respectively, best agreement is found with the occupation in layer 5c. It remains to be seen whether these two units correspond to the same occupation, or to at least two distinct events (activity or cultures) using different sections of the cave in possibly short succession.

Conclusion

Radiocarbon data and modelling demonstrates a well preserved stratigraphy, and the discrete visits by humans seem to increase in frequency during the later phases of the Middle Kozarnikian. The CI tephra supports the age

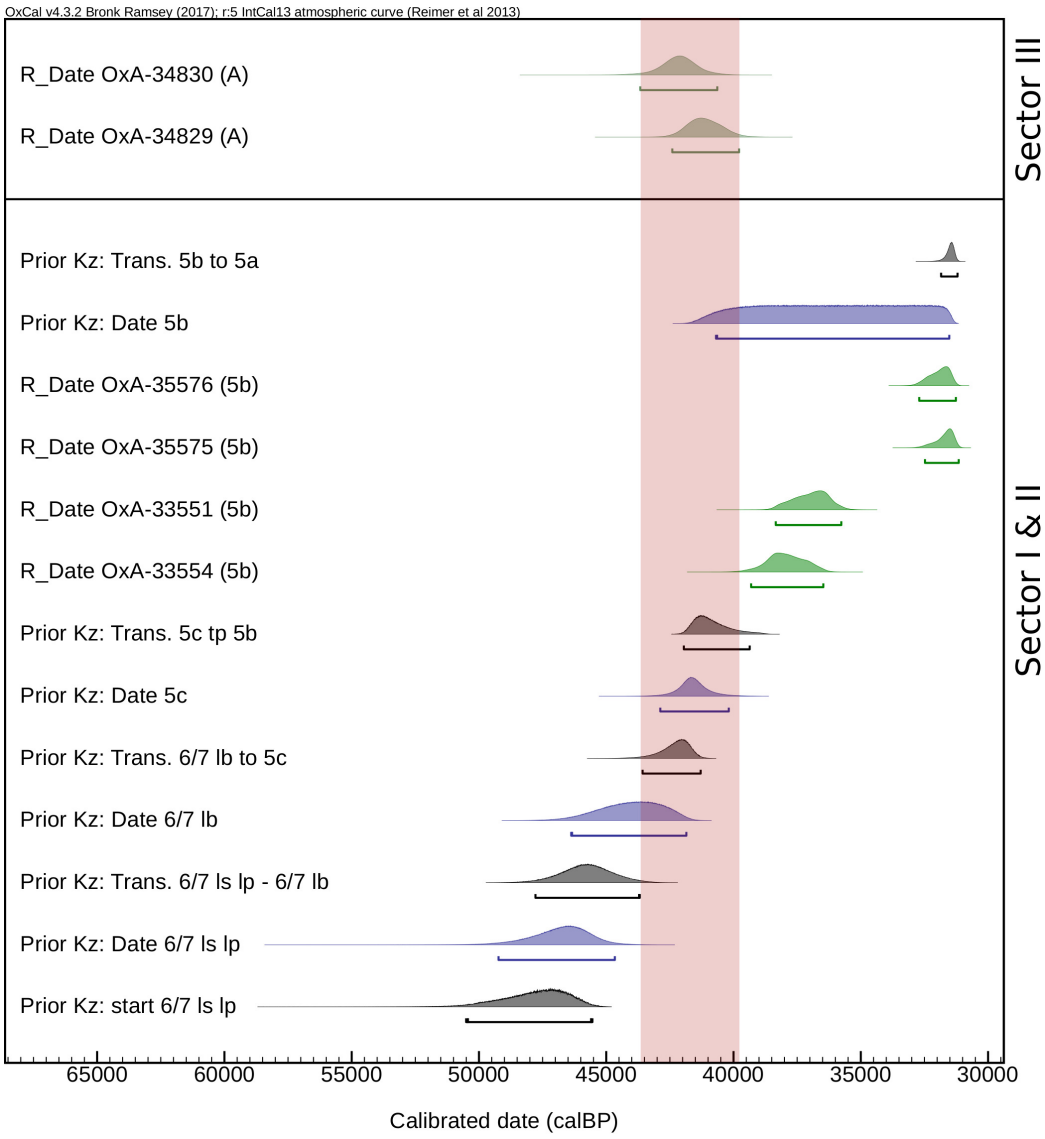


Figure 8.25: Kozarnika: comparison of radiocarbon ages (OxA-34829 and OxA-34830) for layer A (sector III) with the chronostratigraphy (sector I/II) of Model 3, demonstrating a good agreement of layer A with layer 5c. **green** – ^{14}C dates on cut-marked bone (given for layer 5b to highlight the two distinct occupations found within it); **blue** – modelled ages for layers; **black** – modelled layer boundaries; **red** – age range of layer A (at 2 SD) covering the date of layer 5c.

determinations for layer 5b, though the number of occupation events within said layer is debatable. There is evidence to suggest that some mixing of archaeological material in the contact zones to layers 5c, below, and 5a, above, might have occurred. While this debate is important to consider for the analysis of the archaeological industries found within level VI, the effect on the transition boundaries is currently negligible.

The directly dated human remains from Kozarnika are significantly younger than expected and are not connected to the MP/UP biocultural shift. As a result, only indirect connections to establish the authors of industries observed at Kozarnika were possible.

With the start of Phase 6/7 (ls/lp) at *ca.* 50-45k cal BP, the AMH presence at the cave begins, as indirectly evidenced by a *Homo sapiens* tooth found within layer 6/7 ls (see fig. 8.14-5). If the 'transitional/EUP' industry found within this horizon is solely the result of AMH visits, this boundary would also mark the end of Neanderthal occupation at Kozarnika. However, in case of accumulation of cultural material within 6/7 being the result of interstratification – short, alternating visits by both Neanderthals and AMHs –, Neanderthal presence may extend closer to 43.5–41.2k cal BP. Presently, no human skeletal evidence form Kozarnika, or the wider region, is available to support the latter scenario.

The transition at 43.5–41.2k cal BP marks the start of the earliest expression of the Kozarnikian industry at the cave (*i.e. Kozarnikien très ancien*). It shows technological and typological tendencies further observed in the overlying layers, and at the same time shares some lithic similarities with the underlying layer 6/7 (*i.e.* the leaf shaped points). Analogies are found with the archaic Ahmarian from the Levant, as well as the Proto-Aurignacian from southern Europe, albeit diagnostic elements (*e.g.* carinated scrapers, Aurignacian blades, and Dufour bladelets) are absent (Sirakov et al., 2007).

Layer A in sector III yielded an osseous point fragment. Regrettably, poor collagen preservation prevented the direct dating of the artefact. Nonetheless, the radiocarbon ages obtained from layer A are in agreement with the age

of the human occupation found in level VII. This may indicate the presence of a culture with osseous points at a similar time as the presence of split-based points (SBP) at Istállóskő, and possibly Dzeravá Skala. Whether the artefact was brought to the cave by people in transit or residing more locally requires a better understanding of how layer A stratigraphically relates to layer 5c (and thus to level VII). The former could indicate that its presence is not connected to the lithic industry found in layer 5c, thus explaining the absence of other diagnostic lithics by the brief nature of the visit. The latter scenario, on the other hand, would be consistent with the idea, that osseous points typical of the 'Aurignacian' (both SBP and lozenges shaped) can occur independently of Proto-Aurignacian or Early Aurignacian lithics – though in this particular case, the lithic assemblage would significantly outnumber any finds found at other eastern European sites with possible 'Aurignacian' osseous points. Consequently, this scenario would have to lead to the conclusion that the absence of diagnostic Proto-Aurignacian or Early Aurignacian elements is not the result of sample bias. On the contrary, it would support the hypothesis that the individual elements that define the two technocomplexes might be the result of different cultural and technological developments with diverse origins.

8.2 Manastira

8.2.1 Introduction

Manastira (43.1 N, 25.7 E) is a cave site with a large number of human remains. It is located between Veliko Tarnovo (Велико Търново) and Arbanasi (Арбанаси) on the northern flanks of the Balkan mountains. The cave opens to the west at 300 m a.s.l. (see figure 8.26) and consists of an 'entrance hall' and a gallery extending east for approx. 32 m. A denivelation of -2 m is observed between the front and the rear of the cave (Гуадели et al., 2013).



Figure 8.26: Manastira: cave entrance before archaeological excavations 2012 (photos: A. Guadelli, K. Boiadjiev: Mission Paléolithic de Bulgarie (French MEAE)/NAIM-BAN (Bulgaria)).

Manastira's archaeological potential was first discovered during prospections in 2012, which prompted a rescue excavation both in the hall and the cave gallery (see figure 8.27). Initial attempts at establishing a reliable stratigraphy proved difficult. Areas of post-depositional disturbances were frequent (caused both by treasure hunting activiy as well as animal habitation). Despite these challenges, a Pleistocene use of the cave could be established. Previous discoveries by speleologists (ca. 340 bone finds) included rhinoceros (*Coelodonta antiquitatis*) remains. Additionally, archaeological work retrieved hyaena (*Crocuta crocuta spelaea*) remains and a significant number of coprolites, as well as some megaceros (*Megaloceros* cf. *giganteus*), horse (*Equus caballus* cf. *Germanicus*) and bison (*Bison priscus*) faunal fragments (Гуадели et al., 2013).

Further excavations conducted in 2013 and 2015 (see figure 8.27) identified an *in situ* Pleistocene layer, including a 'hyaena den' and further human bones, under an often disturbed Holocene layer. This led to a special interest in the over 30 human fossil remains from Manastira – some of which were found in seemingly close connection to the hyaena occupation at the site. However, unlike many of the faunal remains found, the human fossils did not show signs of having been predated by hyaenas (Гуадели et al., 2016). I. Crèvecoeur concluded that the remains belonged to a minimum of 5 modern human individuals (3 adults, 2 adolescents, and 1 child). In the absence of lithic remains, nine bone fragments were classified based on their patina

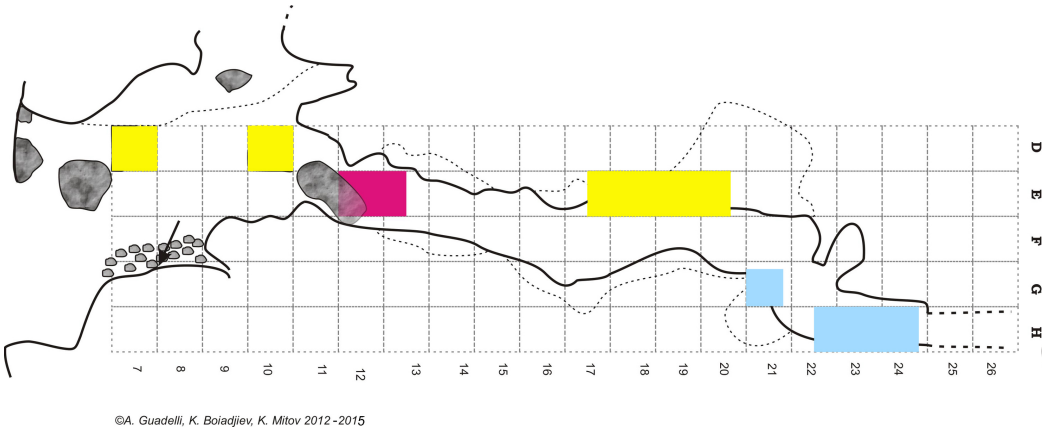


Figure 8.27: Manastira: cave map with local coordinate system and archaeological excavation trenches from 2012 (yellow), 2013 (blue) and 2015 (pink) seasons (illustration: A. Guadelli, K. Boyadzhiev, K. Mitov: Mission Paléolithic de Bulgarie (French MEAE)/NAIM-BAN (Bulgaria)).

and morphology as potentially Pleistocene in age. More importantly, some showed characteristics close to the Middle Palaeolithic fossil record discovered at Quafzeh (Israel), though a Holocene age could not be excluded (Гуаделu et al., 2013, 2014).

As a result, the fossil record found at Manastira is not only the most numerous one found within a Bulgarian cave, but also a prime candidate for rare early AMH fossil evidence in Europe.

Previous Dating

Before the start of this project, only a single sample from Manastira cave was sent for dating (see figure 8.28): A diaphyseal fragment from an *Equus caballus ssp.* radius (sample no. G23-K/19-2). Beta Analytic Inc. pretreated the sample with acid and base washes before dating the collagen to > 43500 BP (Beta-326622), citing a carbon stable isotope ratio of $\delta^{13}C = 19.1‰$ (Beta Analytic Inc. report addressed to J.-L. Guadelli, 8/7/2012). The sample showed signs of gnawing and was encrusted, which was interpreted as evidence for having been eaten and digested by a hyaena (Guadelli et al., 2012, p. 136). While it supports Pleistocene activity in the cave, it cannot be used as evidence for an early AMH fossil record: it is neither directly



Figure 8.28: Manastira: previously dated bone fragment from square G23: *Equus caballus ssp*, fragment of a radius diaphysis (G23-K/19-2), signs of gnawing and digestion by hyaena, Beta-326622 > 43500 BP. Photo: J.-L. Guadelli: Mission Paléolithic de Bulgarie (French MEAE)/NAIM-BAN (Bulgaria).

connected to the human remains found, nor to human activity in general. With cultural material absent, only direct dating of the human fossils will be able to test the hypothesis of an early AMH presence at Manastira.

8.2.2 Radiocarbon dating

Material & Treatment

Most of the human fossil remains from Manastira showed no characteristics typical of the Pleistocene. However, from the nine fragments identified as possibly Pleistocene, two were considered worthy of further analysis: Sample H24-8, a left radius, and sample K/18, a scapula fragment (see table 8.8). The latter showed a dorsal groove at the auxiliary margin, which is more commonly found within modern human specimens from the Pleistocene. The first, a radius, was rather robust and within the fossil variability of AMH dating to the Middle Palaeolithic (Гуаделu et al., 2014).

Table 8.8: Manastira: List of samples shortlisted for radiocarbon dating. Radiocarbon sample weight given in mg. grey rows – not dated.

Ref-no.	Species	Inv.-no.	Excav.	Quadrant	Weight	Comment
Man-01	*Homo sapiens*	H24-8	2013	H24	1175.44	+ DNA
Man-02	*Homo sapiens*	K/18	2012	F24	0.00	+ DNA

In collaboration with S. Pääbo and M. Hajdinjak from the Max Planck Institute in Leipzig, it was decided that those two specimens would also be

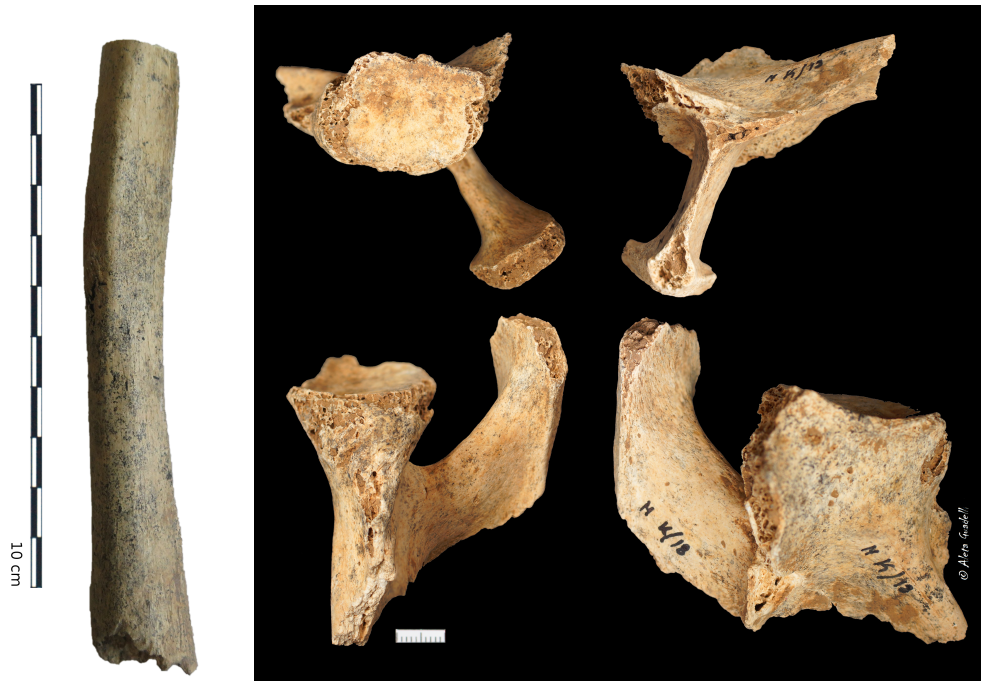


Figure 8.29: Manastira: left – Man-01, *Homo sapiens* radius (photo: R. Hopkins); right – Man-02, *Homo sapiens* cranial fragment (photo: A. Guadelli: Mission Paléolithic de Bulgarie (French MEAE)/NAIM-BAN (Bulgaria)).

prime candidates for ancient DNA analysis. Sample Man-02 (K/18) was not large enough to provide material for both radiocarbon and DNA analysis, thus priority was given to the latter.

For Man-01 (H24-8) a sample was cut from the broken end of the radius fragment, leaving any diagnostic features intact. The human remain was recently collected from excavations and had not been conserved. Consequently, no solvent wash steps were applied. Pre-treatment followed the ultrafiltration protocol as described in subsection 5.4.6.

^{14}C Results

Man-01 was successfully radiocarbon dated – though the measured age is significantly younger than expected (see table 8.9). Preservation was good (collagen yield = 4.09 wt.%). C:N ratio normal, and carbon on combustion (%C = 42.7) within the regular range observed at ORAU.

Table 8.9: Manastira: new ^{14}C date of the human radius Man-01 with AF pre-treatment results (collagen yield, carbon yield on combustion, stable isotope and C:N ratios). Age calibrated using OxCal 4.3 (Bronk Ramsey, 2009a) and IntCal13 (Reimer et al., 2013) and given at 95.4% confidence interval.

Lab-no	Yield	%C	δ^{15}N	δ^{13}C	C:N	F^{14}C	^{14}C (BP)	Date (cal BP)
OxA-33836	48.13 mg 4.09 wt.%	42.7	8.2	-20.8	3.2	0.53115 ± 0.00214	5083 ± 32	3962 – 3797

8.2.3 Discussion

Pre-treatment results indicate that the age of 5083 ± 32 BP (OxA-33836) for Man-01 is a reliable radiocarbon measurement. Consequently, it has to be concluded that the radius is – despite its robustness – not from an early AMH specimen, but securely placed within the Holocene, and there is currently no chronometric evidence to support a contemporaneity of hyaena and human activity at Manastira.

With one of the two samples showing Pleistocene characteristics safely placed within the Holocene, it is important to check in future whether preservation of Man-02 (K/18) is sufficient to allow for radiocarbon dating, despite its small sample size. Additionally, direct dating of the remaining human fossil fragments could provide insight into the temporal relationship between the at least 5 individuals found at the cave so far – especially in the light of their morphological differences.

Unfortunately, Man-01 will not help to shed light on the Middle to Upper Palaeolithic biocultural shift in Europe. However, the age of the radius falls towards the very end of the Chalcolithic in Bulgaria – a time period just preceding an archaeological hiatus of *ca.* 500-600 years before the beginning of the Bulgarian Bronze Age. With only one other directly dated fossil (Akladi Tseïri, Grave 1) of a statistically indistinguishable radiocarbon age (Boyadziev, 1995; Maniatis et al., 2016), Man-01 might provide an important puzzle piece to understanding the end of the Chalcolithic in Bulgaria.

8.3 Tabashkata

8.3.1 Introduction

Tabashkata Peshtera is located in the anticline of Lovech (Ловеч), close to the river Osam (Осъм) and *ca.* 100 m from the Vasil Levski (Васил Левски) cave, which also provided Palaeolithic material. Tabashkata has three entrances, the largest of which opens to the north and measures only 3 by 2.5 m (figure 8.31).

The site was excavated by Dzhambazow (Джамбазов) in the early 1960s. A first trench in front of one of the entrances yielded no Palaeolithic material, despite showing 7 layers. However, in a trench 8 m in front of the second entrance Dzhambazow identified five Palaeolithic layers (totalling a thickness of 160 cm) under 17 layers from younger periods (figure 8.32-left). A bit more than 20 lithic fragments were retrieved, comprising mainly of bladelets with retouches on one side, as well as three bone points (Джамбазов, 1963).

While conducting research on Palaeolithic osseous material, A. Guadelli (Гуадели, 2011) was only able to identify two of the three osseous points supposedly stored at the Historical Museum in Lovech. However, she identified two further point fragments – one of which was refitted to an already known point piece. This means, there are currently three osseous points from Tabashkata accounted for and stored in Lovech.

8.3.2 Radiocarbon dating

Samples & Treatment

The three osseous points stored at Lovech were selected for radiocarbon dating (figure 8.32). The samples were taken in February 2017 using key-hole drilling and 450 mg (Tk-01), 450 mg (Tk-02) and 320 mg (Tk-03) of bone powder was obtained. All samples were treated with initial solvent washes



Figure 8.30: Tabashkata: north-west cave entrance (photo: A. Guadelli: Mission Paléolithic de Bulgarie (French MEAE)/NAIM-BAN (Bulgaria)).

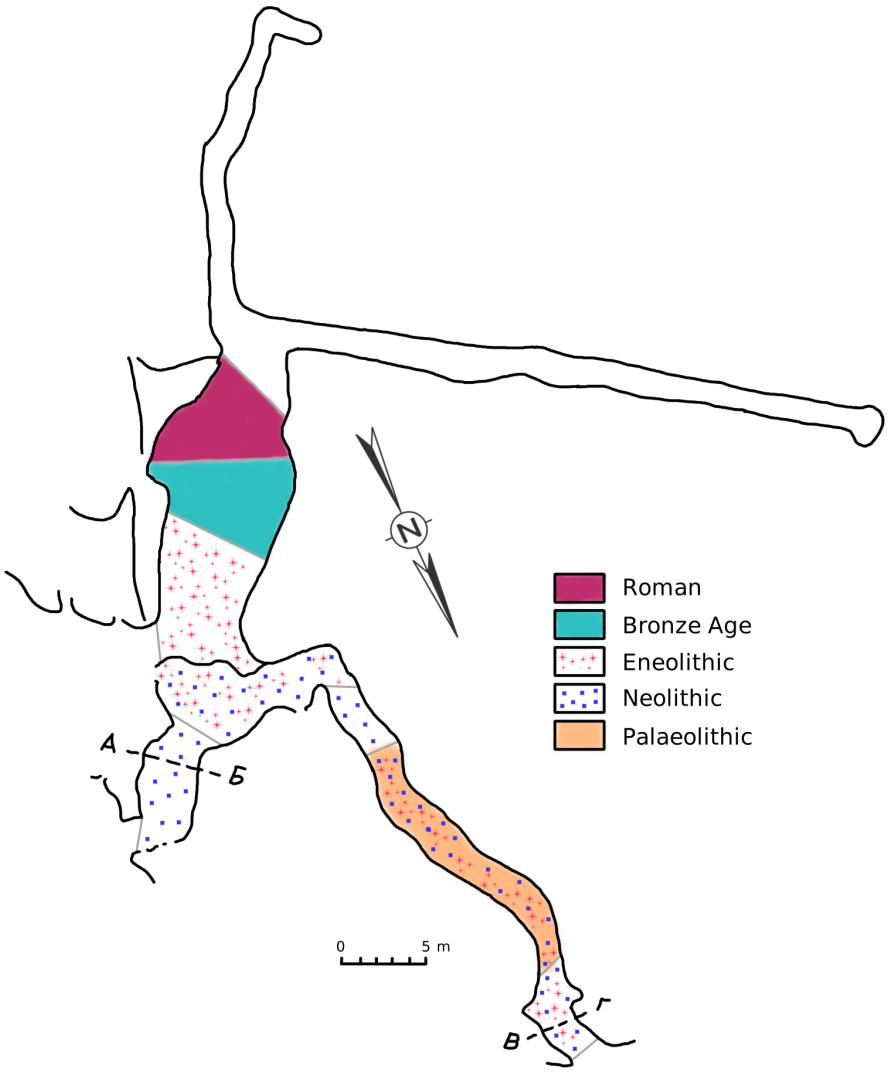


Figure 8.31: Tabashkata: map of cave and areas of excavation marked according to archaeological periods represented in record (redrawn after Джамбазов, 1963, fig. 6).

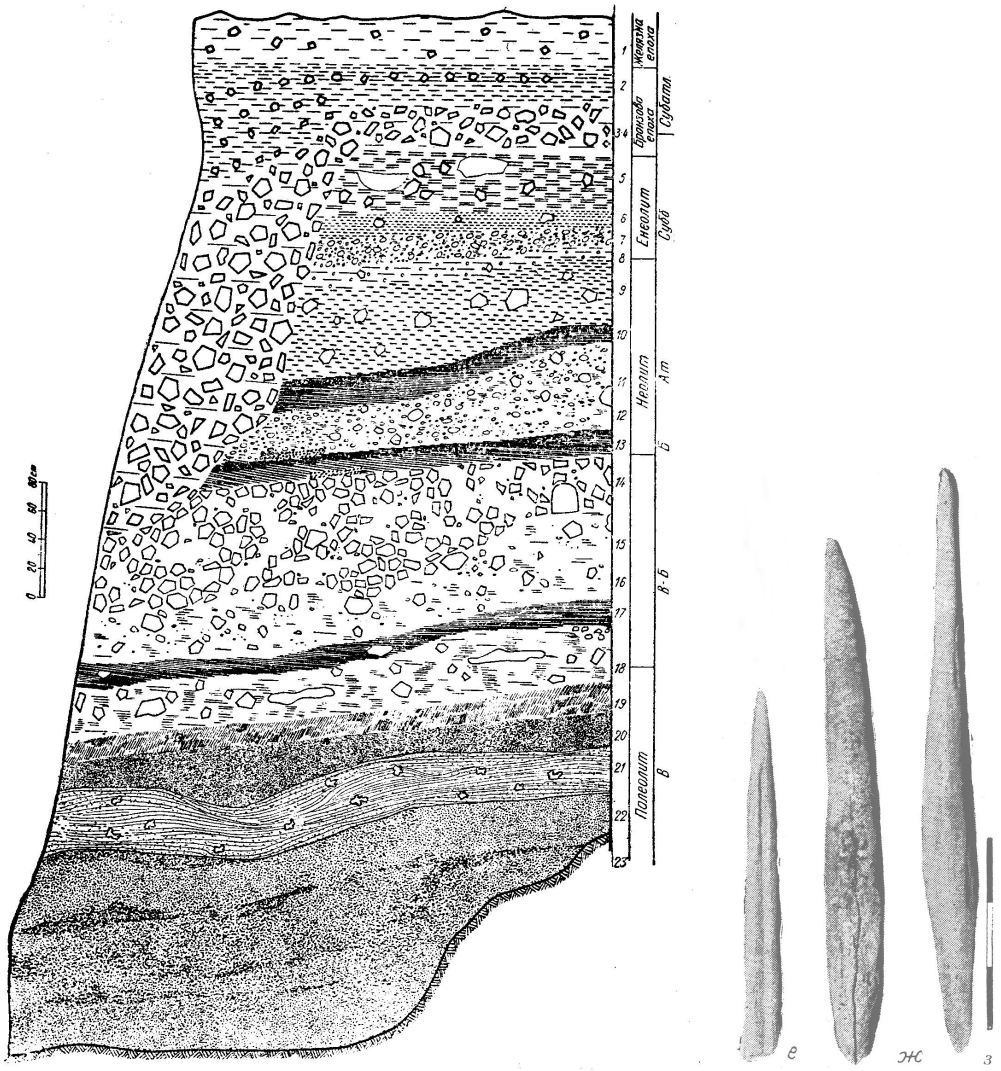


Figure 8.32: Tabashkata: left – profile drawing with layer numbers and interpretation (Джамбазов, 1963, fig. 12), layers 18–22 are labelled as Palaeolithic; right – photo of points published by Dzhambazow (Джамбазов, 1963, p. 120): the point '*е*' corresponds to ref-no. Tk-02, point '*жс*' to ref-no. Tk-03, and point '*з*' to ref-no. Tk-01.

(acetone, methanol, chloroform). This allows for extra flexibility in choosing the continuation of the pre-treatment protocol according to gelatine yield after AG: single amino acid (>20 mg), ultrafiltration (10-20 mg), dating AG (<10 mg).

Tk-01 is a massive based point made of bone. The blank was extracted by means of double grooving. There are pronounced marks from scraping in the proximal and mesial part. The distal part shows traces of scraping, which overlie traces of abrasion. While the overall shape is bi-conical, the thinness of the distal fragment is notable. The internal part still shows traces of the medullary canal. This combined with the asymmetric shape (medullary canal is at a 10° incline to the longitudinal axis) suggest that the artefact was left unfinished (Гуадели, 2011, p. 113-114).

The cross-section of the distal part is circular, the medial section elliptic and the proximal part circular (though end is damaged). The bone point is preserved on a length of 15.4 mm and cross-sectional diameters measure 9-14 mm (Гуадели, 2011, p. 113-114).

The fragmentation separating the upper 1/3 from the lower part is recent, as also evidenced by the photographs published by Dzhambazow (Джамбазов, 1963, p.120), in which that section of the point is still shown intact (figure 8.32).

There are clear traces of glue surrounding the modern breakage. Additionally, on the proximal fragment, an area of ca. 10 x 5 mm (6 cm from the proximal end) shows signs of modern refilling, possibly from cosmetic work covering an earlier sampling attempt or surface damage. On the opposite surface, the faded remains of a museum number are visible. Just below, the museum catalogue number (669) is written and underscored in black ink. The entirety of the artefact is covered in a thin film of unknown material, most likely from an attempt to consolidate the artefact surface.

To minimise visibility of the sampling location, key-hole drilling from the narrow side of the artefact was chosen, avoiding the inked area in the process.

As the internal extent of the modern material present was unknown (marked 'P' in catalogue A.13), the sampling location had to be placed further away from the widest section of the point, reducing the sample amount accessible for drilling. It was felt that closer to the proximal end would be more advantageous, as this approach also avoids further contamination originating from treated cracks in the area close to the modern fractures.

Tk-02 is probably a mesiodistal point fragment made of antler from *Cervus elaphus*. It was extracted via double grooving and subsequently shaped through scraping and abrasion. On the basis of a deep groove running axially, the point was placed within the category of grooved points from the Upper Palaeolithic. The artefact is preserved on a length of 9.4 mm, and has an elliptic mesial cross-section (9.4-10 mm in diameter) leading to a circular distal cross-section (Гуаделu, 2011, p. 113-114).

The artefact showed no signs of previous sampling. Close to the fracture, the museum inventory number (671) was written in black ink on white ground. Additionally, the number was placed in large letters written in axial orientation in the lower part of the point. The surface is shiny throughout – including where the numbers had been placed – indicating the artefact was treated with an unknown conservation substance.

The fracture at the proximal end of the fragment was used as an entry point for key-hole drilling. That way, surface as well as the most distinct features of the fracture remained intact. At the same, this approach gave access to the thickest and most robust part of the artefact.

Tk-03 has been identified as a massive base point made of antler from *Cervus elaphus*. Although the extraction method cannot be reconstructed with certainty, some isolated traces at the proximal part could be related to using double grooving. There are some traces of scraping visible parallel to the longitudinal axis, as well as abrasion at the distal part. The proximal end and large areas of the mesial part show traces of hafting, while just above

faint perpendicular marks indicated the former location of the haft binding. The lower half of the point is split from the proximal to mesial part, probably as a result of hafting. The antler point is 13.4 mm long, 14 mm wide, and 11 mm thick, with a near circular cross-section (Гуаделu, 2011, p.113-114).

The artefact shows traces of at least two earlier attempts at marking it with the museum inventory number (670): a washed looking number of formerly black ink is found slightly shifted towards the distal end from a previous number (now only partially visible). For the most recent labelling, the code was written on a white base layer and fixed with lacquer. Unlike the other two points from Tabashkata, it seems that no coating was applied to the rest of the sample surface since excavation.

The more compact, albeit smaller, region above the number labels was chosen for sampling to avoid the porous, damaged half of the antler point.

^{14}C Results

All three osseous points had sufficient collagen yield for radiocarbon dating (see table 8.10). Preservation decreased significantly with age. As a result, three different protocols had to be applied.

Tab-01 yielded a meagre 1.93 mg (0.44 wt.%) gelatine, which was only sufficient for a small AG* graphite target (0.8 mgC). As all other quality control measures were within expectations, the sample was cleared for an OxA-number. This withstanding, it is worth noting that the AG* treatment might slightly underestimate the true age of the sample.

With an absolute gelatine yield of 14.62 mg, Tab-03 could be ultrafiltered and dated to 21120 ± 130 (OxA-35534). The final collagen yield (11.10 mg, 3.6 wt.%) is indicative of good preservation. It was processed as a large graphite target (1.8 mgC) and %C on combustion, stable isotope and C:N ratio detected no issues.

Tab-02 showed great preservation, providing $>$ 20 mg of collagen after AG* treatment. As a result, Tab-02 was single amino acid dated. Hydrox-

Table 8.10: Tabashkata: New AMS radiocarbon dates on osseous points with pre-treatment results. Ref-no. = number given to the sample for the purpose of this project. Inv.-no. = Inventory number given on excavation. %N = nitrogen weight content before chemical pre-treatment. Treat. = Pretreatment protocols used: * – solvent wash, AG – gelatine, AF – ultrafiltration, NRC – single amino acid protocol (see section 5.4). Yield = sample left after chemical pre-treatment (both absolute and in wt.%). %C = carbon yield on combustion. C:N = carbon to nitrogen ratio of combusted sample. $F^{14}C$ = fraction modern carbon, ^{14}C (BP) = conventional radiocarbon age Before Present with 1σ error. Date (cal BP) = calibrated radiocarbon age at a 95.4% confidence interval, calculated in OxCal 4.3 (Bronk Ramsey, 2009a) using IntCal13 (Reimer et al., 2013).

Ref-no.	Inv. no.	Item	%N	Treat.	Yield	Yield (wt.%)	%C	$\delta^{15}N$	$\delta^{13}C$	C:N	Lab-no	$F^{14}C$	^{14}C (BP)	Date (cal BP)
Tk-01	669	massive base point	1.37	AG*	1.93 mg	0.44	39.6	7.3	-19.7	3.3	OxA-35404	0.03213 ± 0.00164	27600 ±400	32605 – 30933
Tk-02	671	grooved point	2.25	NRC	1.99 μm	0.0005	48.3	5.3	-25.2	5.1	OxA-X-2732-21	0.11816 ± 0.00155	17160 ± 110	21021 – 20411
Tk-03	670	massive base point	3.18	AF*	11.10 mg	3.60	41.8	7.3	-21.0	3.2	OxA-35534	0.07211 ± 0.00116	21120 ±130	25755 – 25163

yproline yield (1.99 mg) was sufficient for obtaining a small graphite target (0.8 mgC). The C:N ratio of 5.1 suggests good sample quality, as it lies within margin of error of the theoretical value of 5 for HYP. Carbon concentration on combustion is not very informative, because the combustion weight entered in the mass-spec file was an estimation calculated by integrating the area under the HYP peak on the HPLC chromatogram. It is susceptible to errors. The AMS results prior to HPLC correction, i.e. using standard lab and AMS background corrections, gave an $F^{14}C$ value of 0.11933 ± 0.00137 (17077 ± 92 BP). Accounting for HPLC background (see section 5.4.7), the sample dates to 17156 ± 106 BP (OxA-X-2732-21). The 'X' notation is based on the use of single amino acid dating, which at the time of treatment was a non-routine-chemistry protocol at ORAU. It does not reflect the quality of the date. All other parameters suggest it to be a reliable radiocarbon measurement.

8.3.3 Discussion

While the Tabashkata points clearly fall within the Upper Palaeolithic, they are all younger than the Aurignacian split-based or lozangic points found further up the Danube and at western European sites. The heavy based point Tk-01 is closest in time and shape to later Early Aurignacian points, albeit with a markedly narrower and longer point as well as a rounder cross-section. Tk-02 and Tk-03 show a shift towards very round cross-sections and more symmetric shape. The large temporal differences between the three points highlights that shape and shafting technique are not solely driven by raw material choice. Both Tk-02 and Tk-03 were made from antler, yet they differ typologically greatly from each other as well as from Aurignacian split-based points. Cultural preferences and differences in use may provide plausible explanations. The former component, especially, could provide incentive to investigating osseous points as a basis for an alternative cultural classification. Comparing its results to lithic industries may provide further interesting insights, and add depth to our to our picture of past societies.

The osseous points from Tabashkata demonstrate the use of the cave during at least three separate occasions, albeit not during the Early Upper Palaeolithic. Only further investigation of the lithic remains will show whether the points may be associated with the Gravettian in the region. The age and typological variability of the Tabashkata points stand as a reminder of the diversity of osseous point technology and its potential for alternative cultural classifications, independent of lithic technocomplexes.

8.4 Temnata Dupka

8.4.1 Introduction

The cave of Temnata Dupka (43.175 N, 24.074 E) is a major Palaeolithic site located in the Karlukovo Karst region, in the north-eastern Pre-Balkans of Bulgaria. The site sits on the right bank of the river Iskar - a tributary to the Danube (Ferrier and Leblanc, 1992; Sirakov, 1992). Protected access to Iskar is provided through the adjacent karstic tunnel Prohodna (see fig. 8.33–8.34). Research into the MP/UP sequence had a great influence on Bulgarian archaeology, and the study of the MP/UP biocultural shift in general.

The entrance to the cave opens to the north-east at 231 m a.s.l. at the foot of a cliff. At this point the cave ceiling is 10 m above today's floor level. The cave is composed of one main gallery of approximately 150 m length and with an average width of 12 m. It initially extends in south-west direction, before turning and continuing westwards, at which point the cave starts narrowing and debris from the ceiling increasingly blocks the area (see fig. 8.35). There are several small side galleries splitting off from the left wall, though excavation focused on the main gallery (Ferrier and Leblanc, 1992).

The present floor level shows an elevation of 6° towards the rear of the cave, while the slope just outside the entrance increases to 10°. Combined



Figure 8.33: Temnata: view of the entrance to the tunnel Prohodna with Temnata Dupka entrance to the left (Guadelli et al., 2005a, fig. 111).

with water entering the cave through fissures, this incline can lead to sediments being washed out of the gallery and explains some of the complex stratigraphy found at the site (Ferrier, 1992).

Initial research at Temnata Dupka started in 1924 with excavations led by R. Popov (Попов, 1925, 1928). He opened a total of four trenches, two towards the entrance, one close to the bend and a small one close to the left wall and the accumulation of debris from the ceiling (see fig. 8.35). While his focus was primarily with faunal remains, he also described 'Aurignacian' (now classified as Gravettian') artefacts as evidence of a Palaeolithic human presence (Попов, 1931). Based on the published stratigraphy and the archaeological and palaeontological remains, Sirakov (1992) concluded that Popov did not reach any Middle Palaeolithic deposits.

In 1983, a new Temnata research project led by N. Sirakov started with a strong focus on international and interdisciplinary collaborations. During the excavations, lasting until 1991, five sectors (see fig. 8.35) were exca-

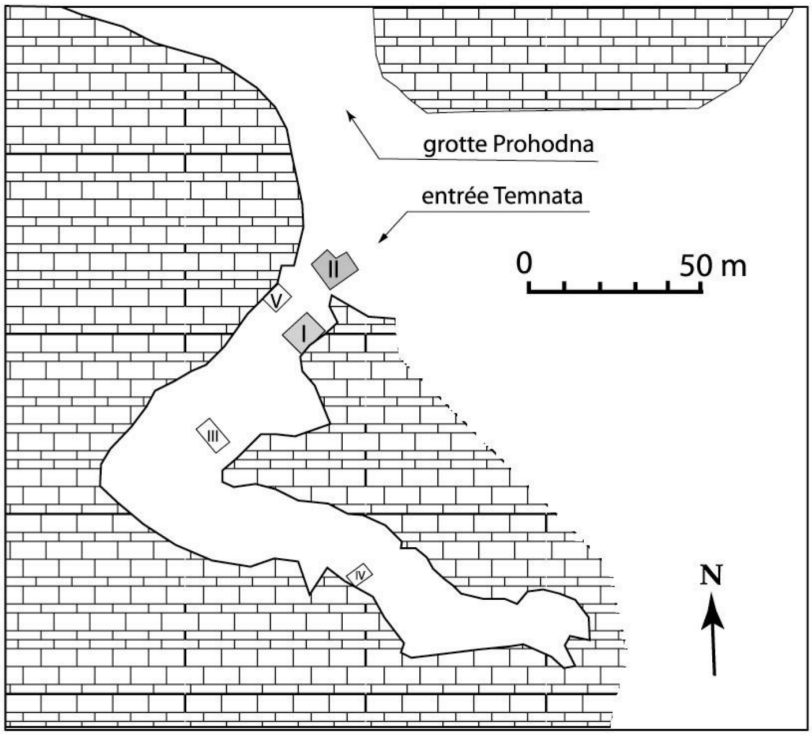


Figure 8.34: Temnata: map of cave with adjacent Prohodna karstic tunnel. Trenches from the excavations in 1983–1991 marked I–V (Tsanova, 2006, fig. II.2).

vated using spits of 5cm depth, and sediments sieved for smaller remains (*e.g.* artefacts and animal bones). Sectors TD-I and TD-V were placed at opposite sides of the antechamber and provided deep stratigraphic sequences including MP and UP material (Sirakov, 1992). Sector TD-II is located on the sloped terrace just outside the cave entrance and provided the material that led to the debate on whether and IUP industry is present at Temnata (Tsanova, 2006). The small sector TD-III (main hall) and TD-IV (entrance to a southern corridor) were used for stratigraphic comparison – both yielded no archaeology. Additionally, further trenches were located in Prohodna, though those also revealed no archaeological material (Sirakov, 1992). The vast body of results was subsequently published in four monographs, divided according to archaeological periods into Epigravettian, Gravettian, EUP/Aurignacian and MP (Ginter et al., 2000, 2011, 1994; Kozłowski et al., 1992).

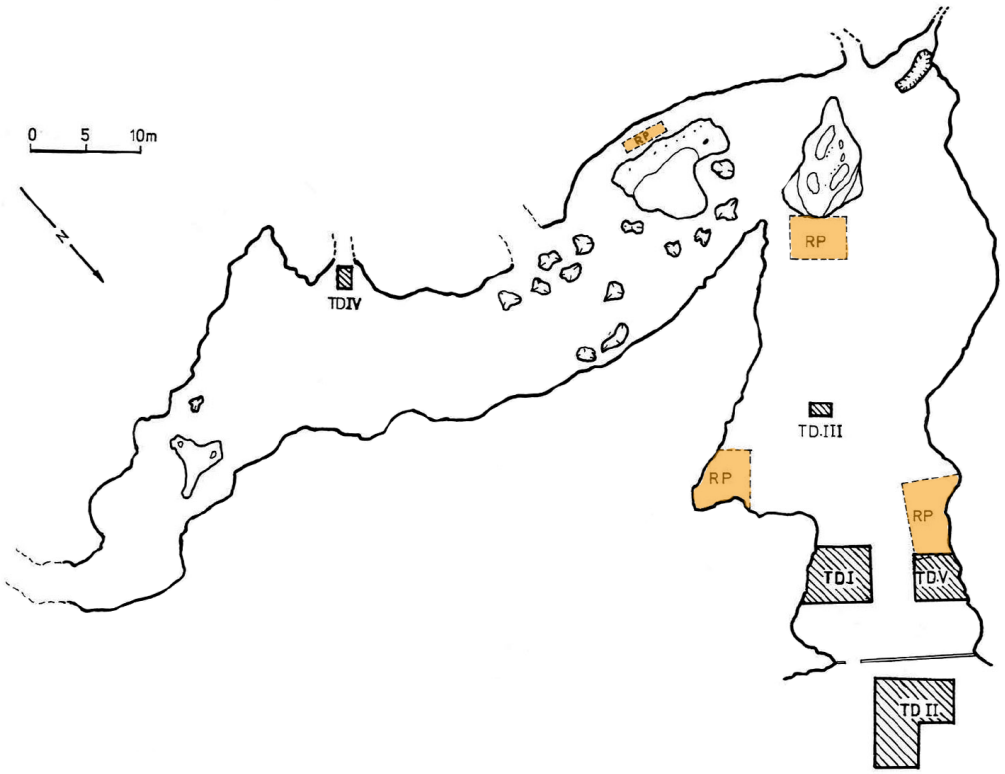


Figure 8.35: Temnata: map with excavation sectors. **orange** – location of test trenches excavated by R. Popov in the 1920s: **hatched** – sectors TD-I to TD-IV excavated between 1983 and 1991 (after Sirakov, 1992, fig. 4).

Stratigraphy

The three archaeology bearing sectors, covering the antechamber and the terrace outside the cave, show stratigraphic sequences differing from one another. In the absence of connecting trenches, analysis of sediment and layer content had to be used to connect specific stratigraphic units. As a consequence, the sector TD-I will be used as the starting point for the stratigraphic discussion, followed by a descriptions of cases in which TD-V and TD-II diverge. The description will be limited to the layers relevant for this dating project and based on Ferrier and Laville (1992).

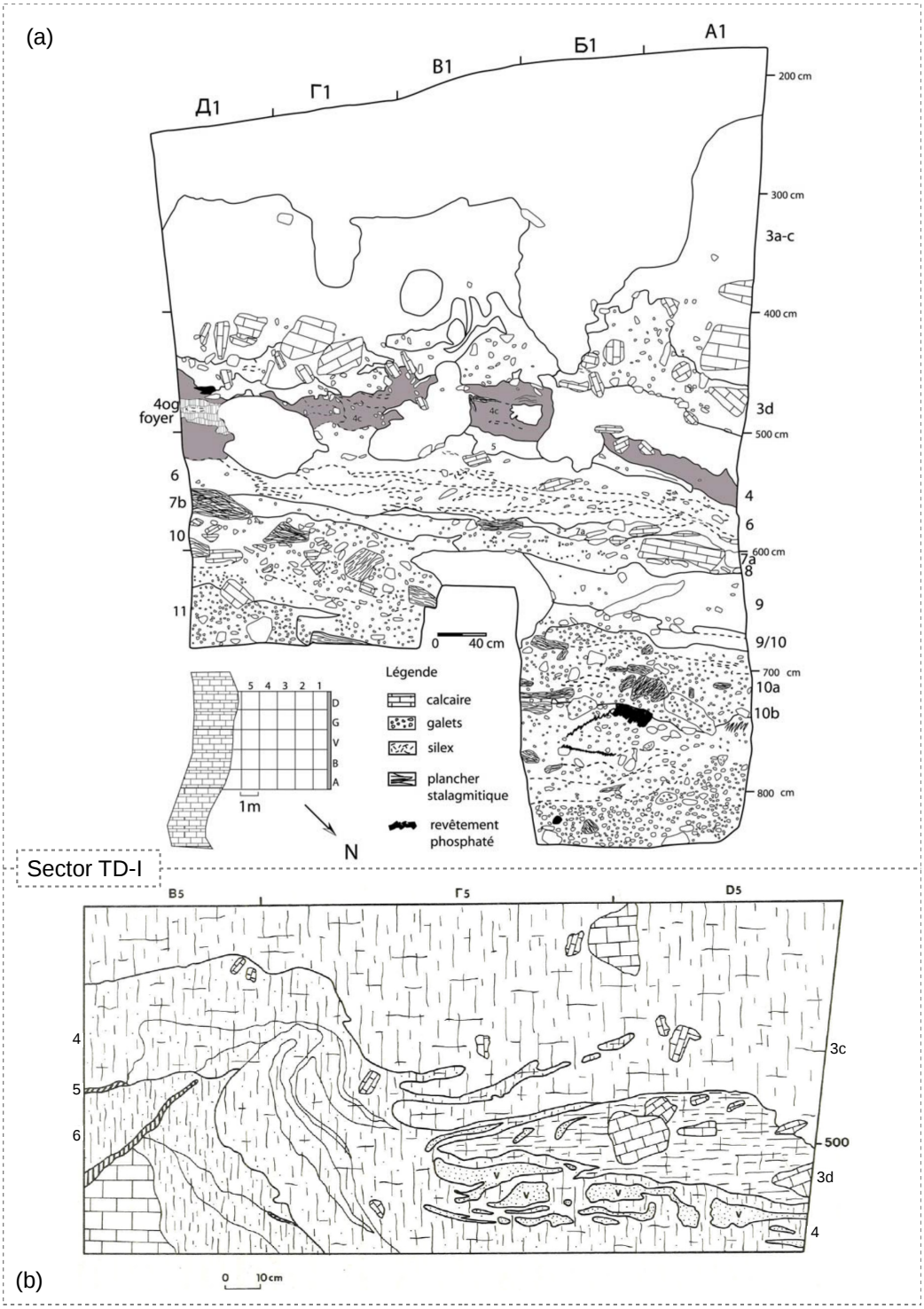


Figure 8.36: Temnata: profile drawings sector TD-I. (a) north profile with layer 4 highlighted in grey (Tsanova, 2006, fig. II.34); (b) south profile (Ferrier and Laville, 1992, fig. 3).

TD-I Sector TD-I is made up of an area of 25 m^2 which was excavated to a depth of 4.6 m – without reaching the bedrock. It was divided into 11 geological units (see fig. 8.36), of which layers 7–3a-c will be discussed in the following.

Layer 3 is a complex of stratigraphic units with similar sedimentation. Layer **3a** contains light brown, loamy clay with numerous fragments of small calcareous rocks. In contrast **3c** shows a darker colour, a higher concentration of clay and the presence of larger, heterogeneous limestone debris with diameters varying from 2–50 cm. They were easiest distinguished in the south-west of TD-I, where they were separated by **3b** – a thin lens (max. 4 cm) composed of fine, slightly silty sand with a light yellow colour. As otherwise 3a and 3c were not easily differentiated, the unit is often combined to **3a-c**.

The unit **3d** is darker in colour, and encompasses a higher concentration of clay, as well as fewer, smaller lime blocks than 3c. Layer 3d is found in most of sector TD-I, except of in the south, where 3a-c directly overlies unit 4.

A small deposit of lighter colour sediment, labelled **3e**, was observed between layer 3d and 3f and under a large rock. The unit is very localised and devoid of any archaeological material.

Layer **3f** appears more heterogeneous, containing several large limestone blocks and high concentrations of charcoal and archaeological material. The base contains lenses of greyish, more sandy sediment with volcanic material – as observed in the top part of layer 4.

The geological unit **4** comprises grey, silty clay with severely altered gravel, calcareous pebbles and some faunal fragments. The sediment appears darker towards the lower part of the layer. The upper and lower limits are irregular (see fig. 8.37-a), and there are various subunits distinguishable. In the middle section, for example, a band of white limestone sand is seen interrupting layer 4 (see fig. 8.37-b), and three charcoal concentrations asso-

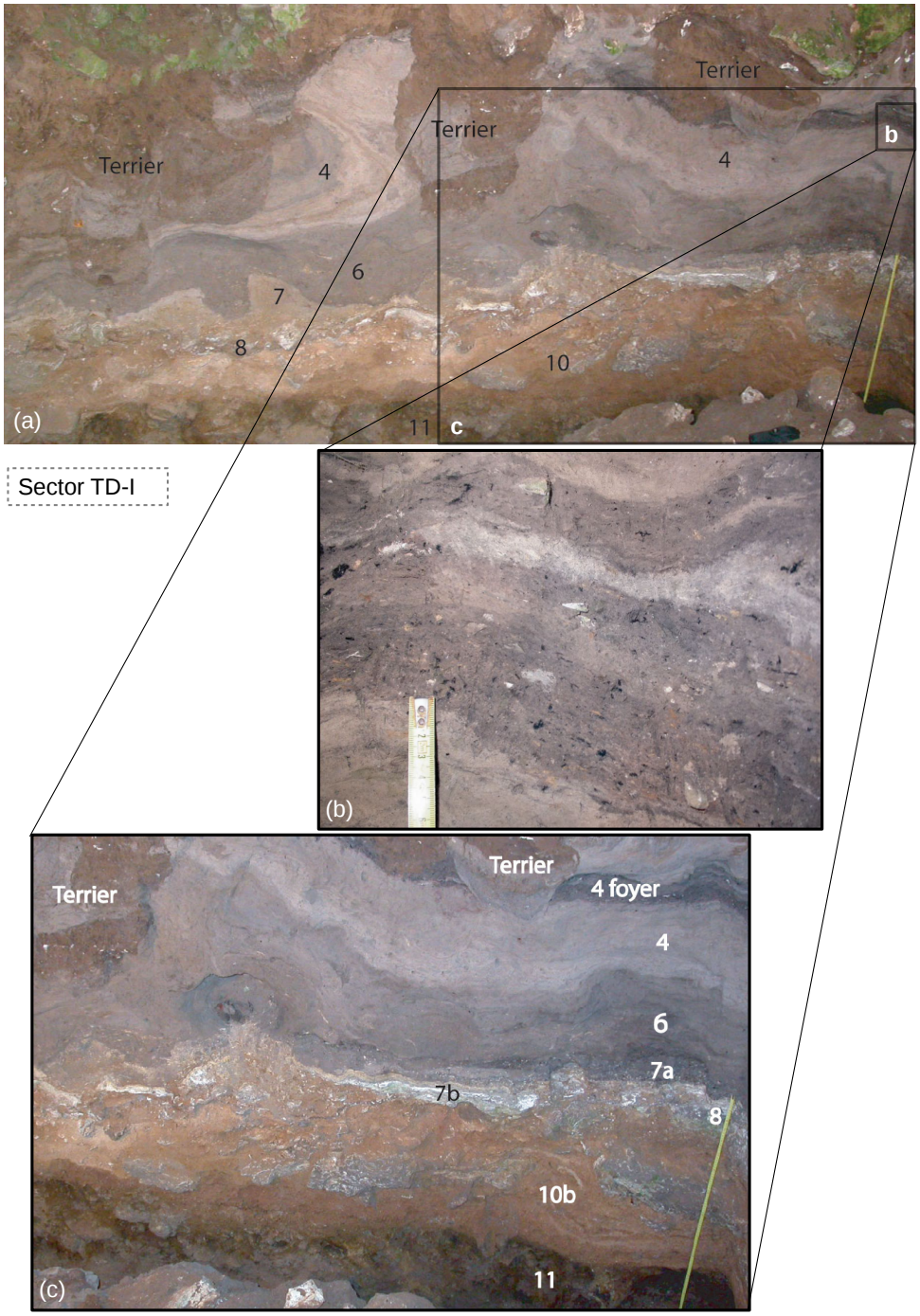


Figure 8.37: Temnata: photos of west profile in sector TD-I. (a) overview with location of magnified areas marked; (b) hearth area at the top of layer 4; (c) hearth 4og within layer 4, and deformation of layer 6 (Guadelli et al., 2005a, fig. 113, 114, 116, photos: C. Ferrier: Mission Paléolithic de Bulgarie (French MEAE)/NAIM-BAN (Bulgaria)).

ciated with high numbers of lithics were found in the northern part of sector TD-I. The latter were interpreted as washed out fireplaces.

Layer **5** appears in the southern part as an altered, discontinuous stalagmitic floor (*ca.* 5 cm thick), and in the northern and western part in the form of 15-20 cm thick, light coloured lenses.

Layer **6** is a *ca.* 50 cm thick band of grey silty-clay – very similar to layer 4 – with three subunits (see rig. 8.37). The top section (6pg) contains some limestone rocks and diffused brown sediment (similar to unit 3), and inclines towards the cave outside. Its lower limit is marked by a spread of calcareous elements. The middle section (6sn) is a 6–8 cm thick band of sandier and lighter coloured sediment, containing numerous limestone fragments and archaeological material. The lower section (6ob) has the same texture as the rest of layer 6, though is coloured black by high concentrations of charcoal. The base is enriched with calcareous fragments, most likely deriving from layer 7 underneath.

The last unit of interest is layer **7**, which is 5–20 cm thick altered limestone floor made of light brown, sandy-loamy sediment with numerous small limestone fragments. In contrast to the upper part (7a), the limestones in the lower part (7b) are covered in black deposit.

TD-V Sector TD-V is located in the north side of the antechamber, *ca.* 4 m north-west of TD-I. An area of 16 m^2 was excavated to a depth of 4.5 m. R. Popov's trench from the 1920s is visible in the south-west of the sector, protruding into the east profile. The stratigraphy shows the same main 11 divisions as observed in TD-I, though there are some significant differences in subunits that bear witness to the complex and extensive post-depositional processes at Temnata (see fig. 8.38).

Unit **3a-c** is present as a homogeneous layer of ca. 1.6 m thickness. There is no level 3b visible. The boundary with the underlying layer 3d is irregular, sometimes leaving near vertical protrusions, and lenses of 3d are occasionally found within the lower parts of 3a-c.

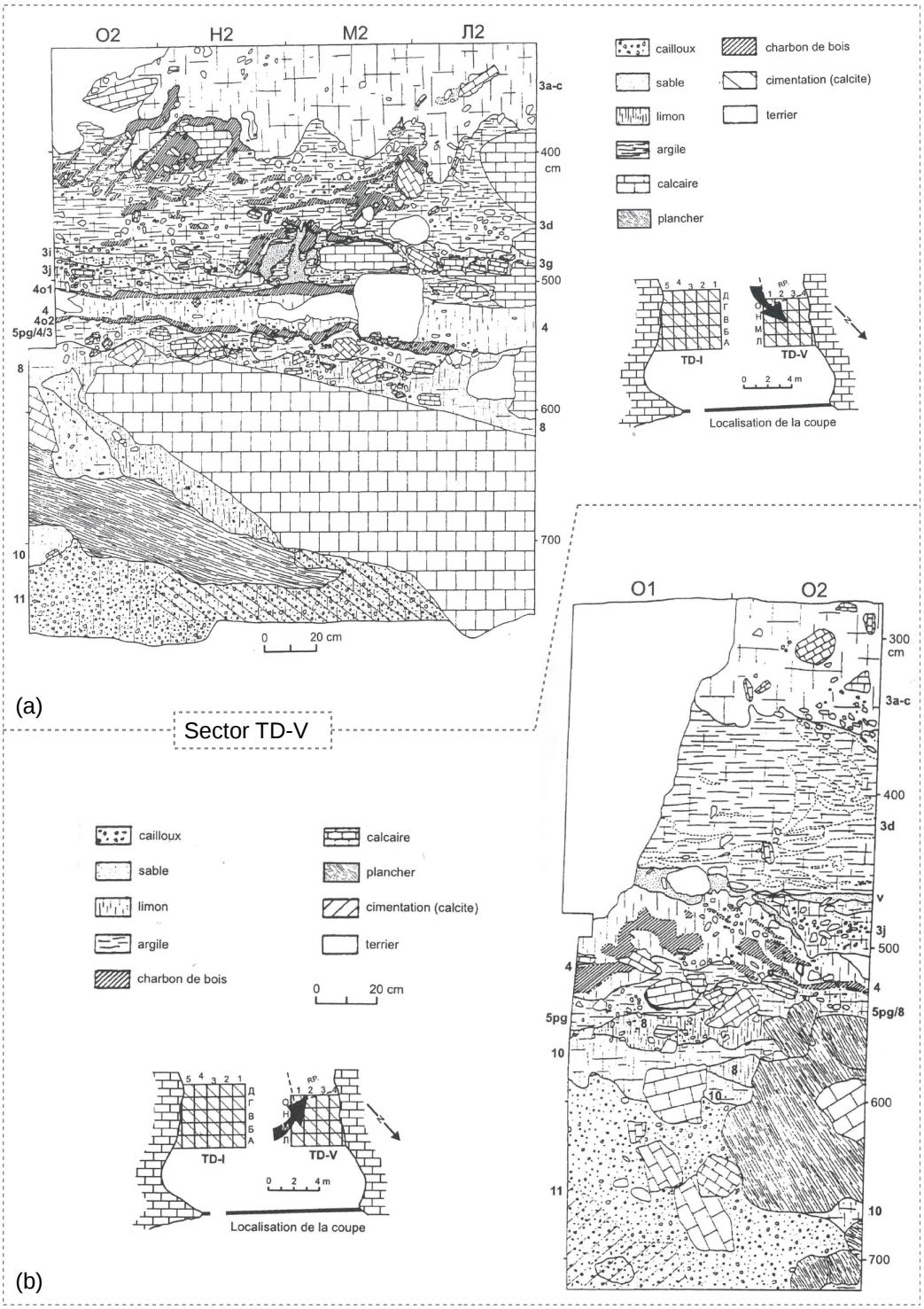


Figure 8.38: Temnata: drawings of (a) north and (b) east profile in sector TD-V (Ferrier and Laville, 2000, fig. 7–8).

Layer **3d** is thicker than in TD-I, preserved up to 1.1 m. In addition to the fine silty-clay sediment, it contains collapsed blocks in the upper part and an increasing number of scattered pebbles towards the base. Many limestone fragments are coated in a black film. The lower limit is very irregular.

Layer **3f** is not present. Instead, a complex structure of layers 3g–j underlies layer 3d in TD-V. In general, 3g overlies 3i, which in turn was found on top of 3j, which lies on layer 4. The first and last limits appear as harsh transitions, while the limit between 3i and 3j is more diffuse.

Layer **3g** shows the same colour and texture as layer 3d, though limestone granules are more numerous and volcanic material is present. Layer **3h** appears as diffuse lenses of lighter colour with locally high concentrations of volcanic material, and some scattered limestone blocks and pebbles. Unlike the other layers in the group, **3i** appears to have limited to no volcanic material, and consists of grey-yellow sandy-loam with calcareous blocks and numerous pebbles and limestone granules. Layer **3j**, in turn, is composed of yellow-beige to pale yellow silty clay with a mass of volcanic ash intruding as recorded in the north profile (see fig. 8.38-a).

As in TD-I, layer **4** shows three main subdivisions. However, the distribution appears inverted. A charcoal rich (fireplace?) structure in the top part is followed by a deposit with lighter colour and more numerous limestone fragments in the middle of layer 4. Towards the base, a second charcoal concentration (fireplace?) is found, and in some places lighter coloured lenses underlie it.

A discontinuous base of small carbonate elements with some overlying matrix, labelled **5pg**, is found under layer 4. Most likely, it represents a less developed or preserved extension of layer 5 found in TD-I.

TD-II Sector TD-II is found on the sloped terrace in front of the cave entrance. An area of 20 m^2 was excavated to a depth of 6 m. The stratigraphy differs significantly from the sequence found in sectors TD-I and TD-V. To

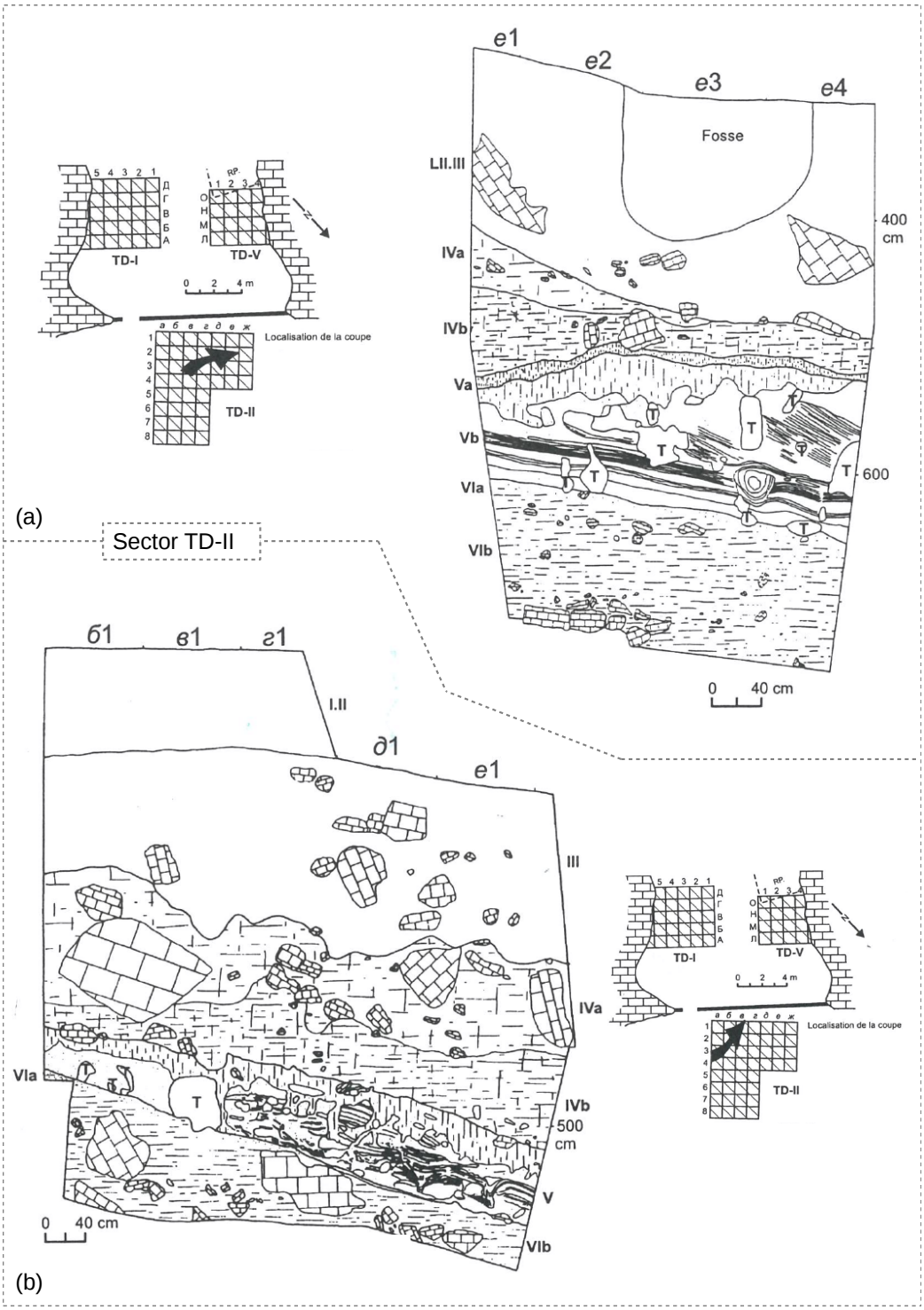


Figure 8.39: Temnata: drawing of (a) north and (b) west profile in sector TD-II (Ferrier and Laville, 2000, fig. 9–10).

avoid confusion, the layers were labelled with Roman numerals. Six main layers could be identified (see fig. 8.39).

Underlying a thick sequence of heterogeneous layers (I–III), rests the first Pleistocene unit: layer **IV**. Its original thickness remains unknown due to the erosion of the top surface. The sediment consists of silty-clayey sand of reddish to light brown colour. Several large limestone blocks are present. IVb was differentiated from IVa on the basis of increased clay concentration and a darker colour. Its lower limit is sharp and slightly undulated.

Layer **V** contains the same volcanic material found in layers 3f (TD-I), 3j and 3h (TD-V), though does not contain any archaeological material. Ferrier and Laville (1992) see the presence of fine lamination as an indication for numerous disturbances, and the enrichment in clay found in the upper part as evidence for illuviation processes. Its lower limit is again sharp, an indication for partial erosion of the underlying unit.

The geological unit **VI** was excavated to a thickness of 1.5 m. The layer is heterogeneous, and the material distribution was described as 'chaotic' by Ferrier and Laville (1992). VIa is located in the upper 10 cm. It is rich in small carbonate elements (possibly coprolite fragments) and has a yellowish-red clayey-silty sand matrix. In contrast, IVb contains an increasing number of limestone blocks.

Archaeology

According to Ginter and Kozłowski (1992), Middle Palaeolithic industries were found in layers 8–6, EUP in 4–3g, Gravettian in 3f–3c, and Epigravettian in 3a (see fig. 8.40). They further divide the EUP into three categories: (1) the IUP in layer VI in TD-II with tools from both Levallois-Mousterian and Upper Palaeolithic traditions; (2) the 'Early Aurignacian' in layer 4 in TD-I and TD-V; and (3) the Upper Palaeolithic units of 3g–j in TD-V.

For the purpose of this thesis, the discussion will focus on the lithic industries found in layers 6, 5/5pg, and 4 from TD-I and TD-II, as well as layer VI

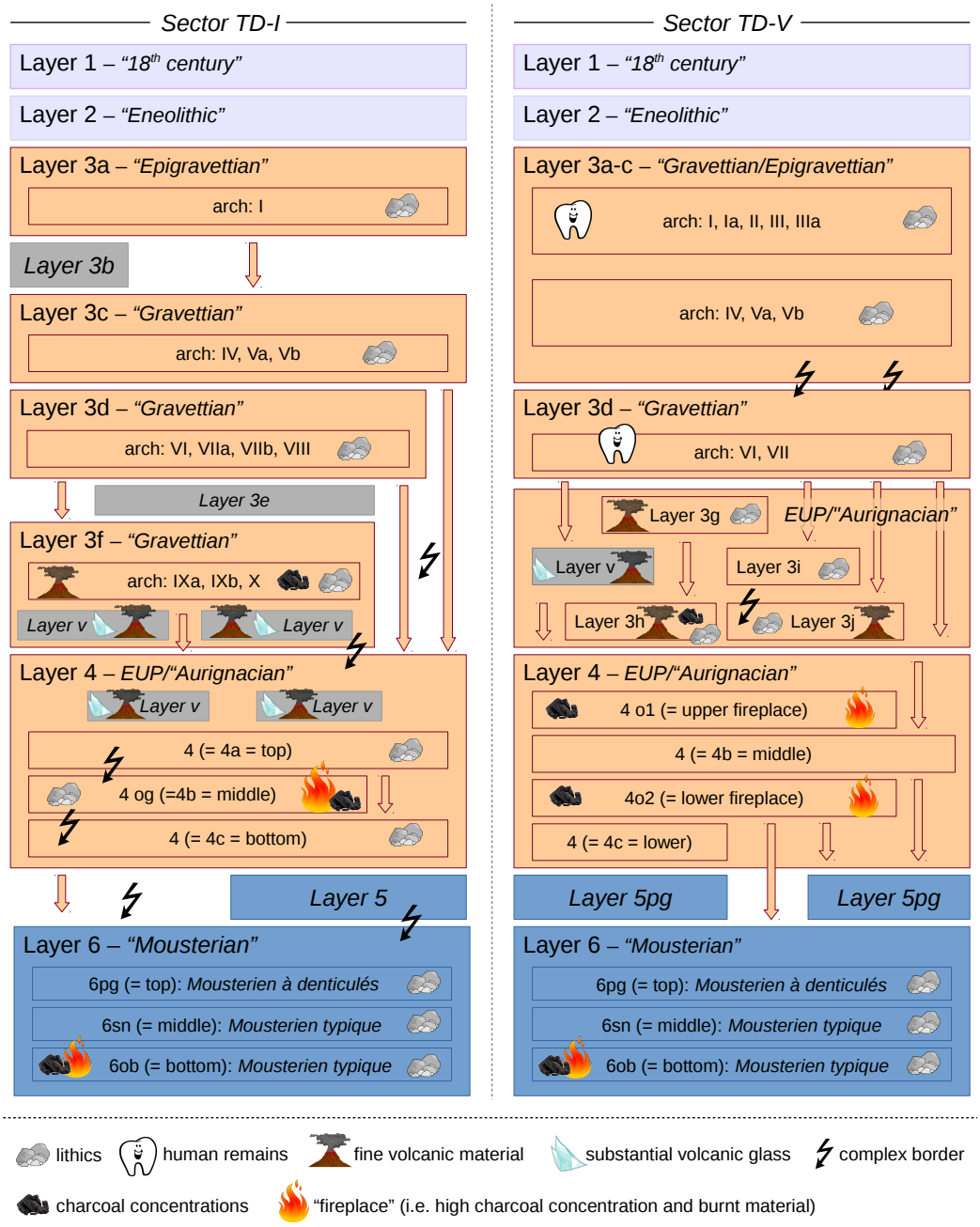


Figure 8.40: Temnata: diagram of stratigraphy sector TD-I (left) and TD-V (right) and their layer correlations, listing original cultural nomenclature from Ferrier and Laville (1992, 2000, 2011). **grey** – sterile; **lavender** – Holocene; **red** – Upper Palaeolithic; **blue** – Middle Palaeolithic. For complicated position of the tephra layer 'v', see discussion in 8.4.1.

in TD-II[6]. Throughout this sequence, local raw material heavily dominates, though minimally decreases with younger levels: e.g. 98.2% local material in MP III, 93.9% in layer VI, to 93.1% for layer 4C, and 89.3% for layer 4B.

Layer 6 contains the Middle Palaeolithic levels MP III, MP IIIa, and MP IIIb – totalling more than 7000 artefacts (see fig. 8.41). The first lithic group was found throughout layer 6 in TD-I (and in lesser quantity in TD-V), albeit not in its lighter or darker coloured subunits, or the hearth structure. The assemblage includes Levallois flakes (19), flakes from discoidal cores (43), side-scrapers (29), Mousterian points (3) and unfinished bifacial forms (4). Only two retouched blades were found. MP IIIa material originates from within the hearth structures in TD-I. It demonstrates a clear use of the Levallois technique, with initially preferential, then recurrent, and finally discoidal core reduction. Among the retouched tools were side-scrapers (14), denticulated tools (25), Levallois flakes (3), a Levallois point (1), and a Mousterian point (1). The archaeological level MP IIIb was identified in TD-I throughout layer 6 – including its lighter and darker variants – and the washed out hearth structures. The majority of cores show discoidal reduction and are very small, though some have traces of initial preferential and subsequent recurrent reduction. The retouched tools include side-scrapers (31), Levallois flakes (6), Mousterian points (5), Levallois points (2), as well as retouched flakes and blades (65). Consequently, layer 6 can be confidently attributed to the Mousterian – both *Mousterian à denticule* and *Mousterian typique* (Drobniewicz et al., 2011).

The lithic assemblage from **layer 5** in sector TD-I was labelled MP II (see fig. 8.42). It was only found in limited areas in the east and south-east of the sector at the interface to layer 6. The discoidal unilateral cores, Levallois flakes and end-scrapers place the technology within the Mousterian tradition (Drobniewicz et al., 2011).

[6]For a more detailed discussion of the Gravettian and Epigravettian lithic complexes at Temnata see Drobniewicz et al. (1992); Giourova and Schtchelinski (1994); Schtchelinski (1994); Sirakov et al. (1994).

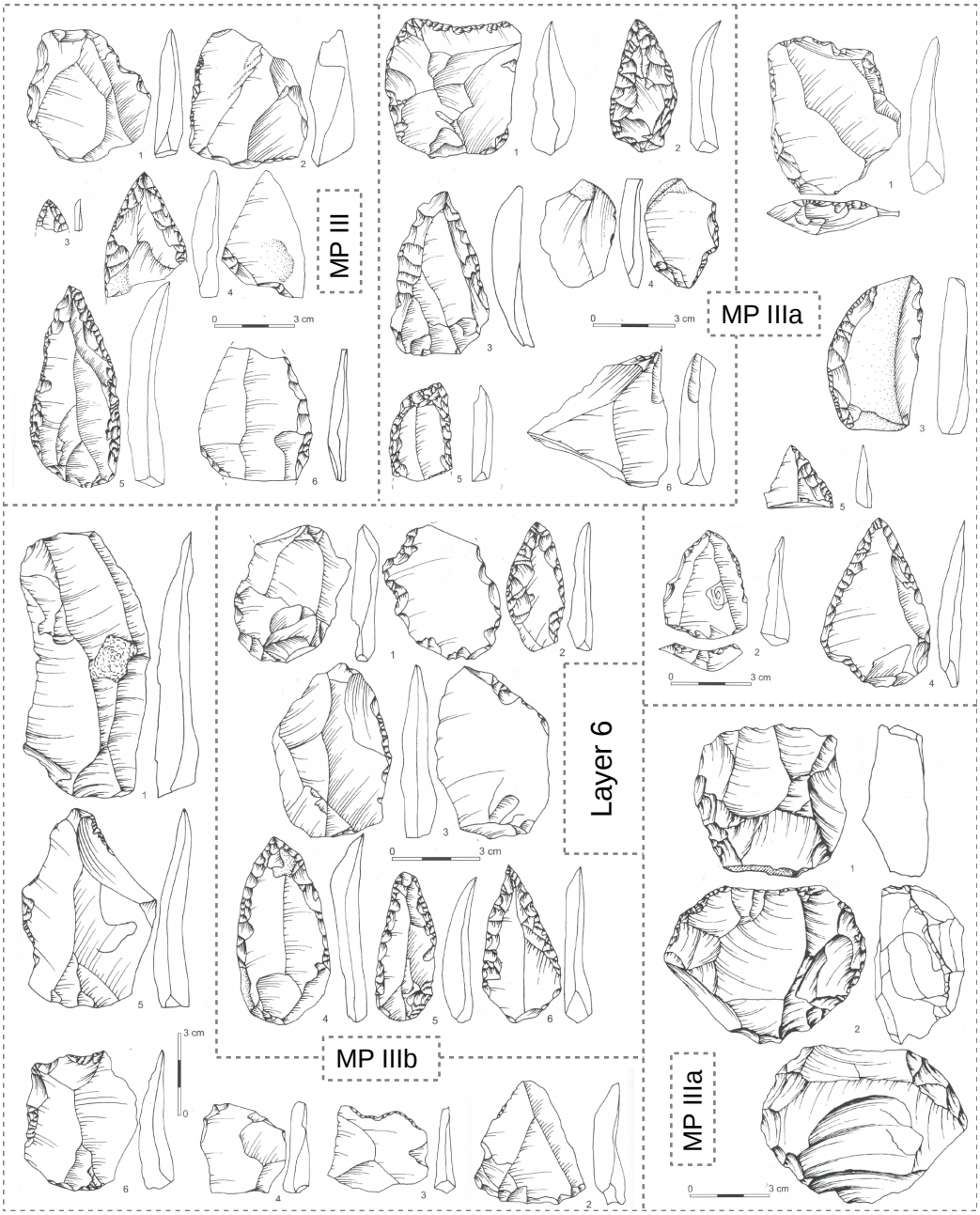


Figure 8.41: Temnata: MP lithics from layer 6, grouped according to archaeological levels. MP III: retouched tools, inlcuding Levallois flakes, Mousterian points, and a side-scraper; MP IIIa: cores (Levallois) and retouched tools, including Levallois flakes, Levallois point, Mousterian point, side-scrapers, a burin on a flake, and a notched flake; and MP IIIb: retouched tools, including Levallois points, and Mousterian points (Drobniewicz et al., 2011, pl. 42–43, 55, 59, 61, 67).

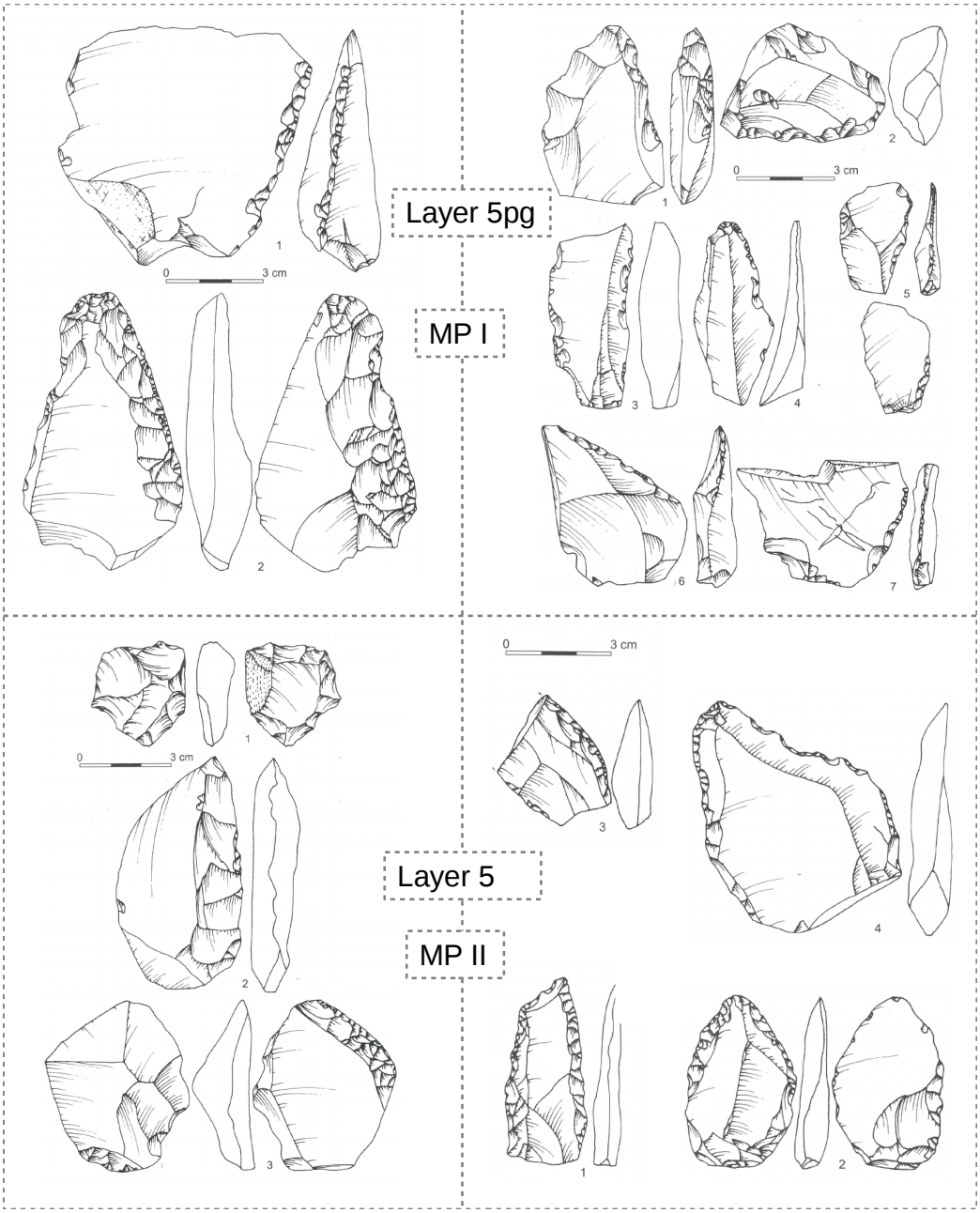
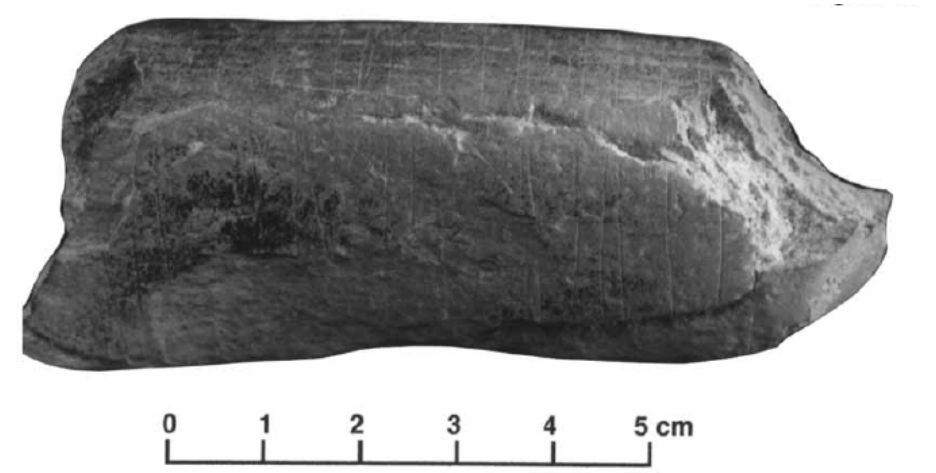


Figure 8.42: Temnata: MP lithics from layers 5 (bottom) and 5pg (top). Archaeological level MP I: retouched tools, including side-scrapers, denticulated tool, retouched flakes, and a retouched blade; MP II: core (discoidal) and retouched tools, including side-scrapers, a flake, and a blade (Drobniewicz et al., 2011, pl. 81–82, 88, 91).

Layer 5pg from TD-V – the assumed counterpart to layer 5 – is richer in lithics. Over 3300 artefacts could were retrieved. Drobniewicz et al. (2011) named the assemblage MP I (see fig. 8.42), differentiating it from MP II in layer 5. The cores bare witness to a variety of blank production methods, such as Levallois (both preferential and recurrent), discoidal, and volumetric blade production. The retouched tools include side-scrapers, denticulated tools, retouched blades and a bifacial tool (Drobniewicz et al., 2011). While the assemblage is of Mousterian character, an increase in blade production is noticeable.

Layer VI was only found in TD-II and cannot be directly connected to the sequences found in TD-I and TD-V. The layer contained a total of 2101 artefacts (see fig. 8.44). The cores evidence Levallois and discoidal reduction strategies, with blade cores demonstrating the use of the UP volumetric concept (both double and single platform). The tool assemblage contained both MP and UP types. The first is represented by Mousterian points (6), Levallois points (2), side-scrapers (mostly on Levallois flakes or blades), and denticulated tools, the latter mainly by end-scrapers, blades, and some burins (Drobniewicz et al., 2011). Lithic production in this layer applied direct hard percussion. Diagnostic Aurignacian tools or backed implements are absent. Furthermore, the layer produced evidence of artistic expression in the form of an engraved stone fragment (see fig. 8.43 and Crémades, 2000).

On the basis of a homogeneous distribution throughout the thickness of the layer, Ferrier and Laville (1992) concluded that the lithics were in secondary position. Despite this, both Drobniewicz et al. (2000b) and Tsanova (2006) concluded that the association of MP and UP technology is not the result of post-depositional processes, but a genuine association. They draw parallels to the IUP industries, like the Bohunician in the Czech Republic and the Ahmarian in the Levant. As the original deposition is thought to have come from further uphill, close to the cave entrance, a connection to the stratigraphic sequence in TD-I and TD-V was attempted. Drobniewicz et al. (2000b) suggested that layer VI may contain material from the drip stone layer 5pg (TD-V), as the character of the lithic assemblage in layer VI



Schiste gravé de Temnata Dupka (photographie M. Crémades).

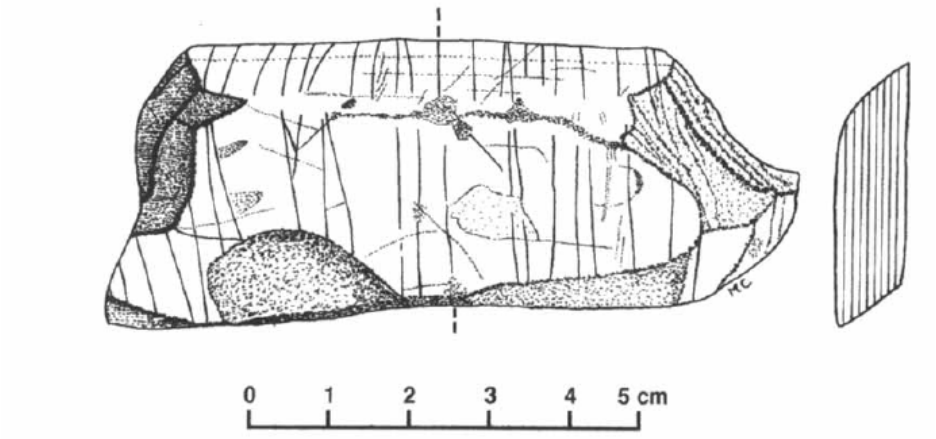


Figure 8.43: Temnata: schist fragment with engravings from sector TD-II, layer VI (Crémades, 2000, fig. 4–5).

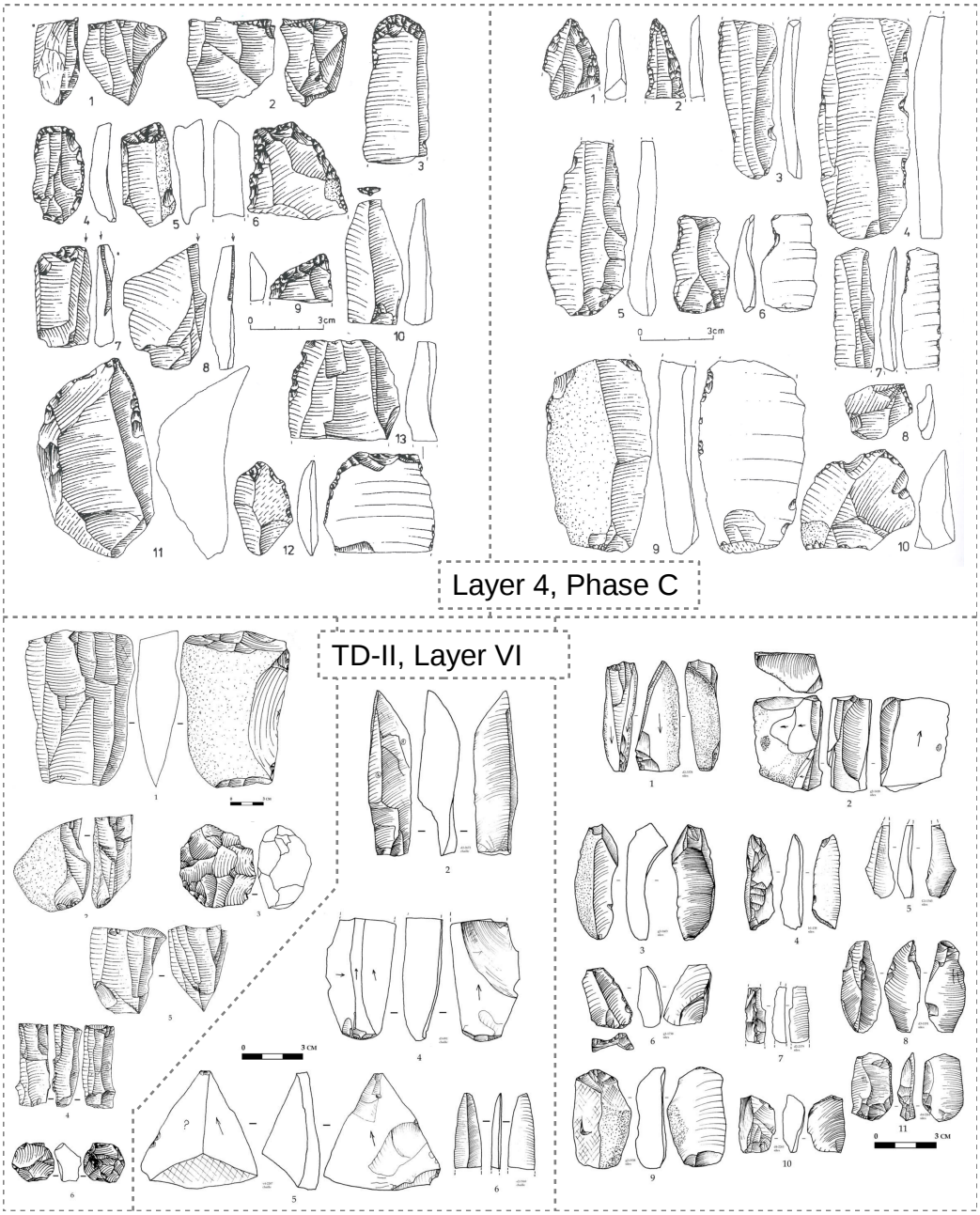


Figure 8.44: Temnata: IUP and EUP lithics. top – EUP from layer 4, phase C (TD-I): cores and tools, including endscrapers, burins, perforators, truncations, and retouched blades and flakes (Drobniewicz et al., 2000a, pl. 1–2); bottom – 'transitional' from layer VI (TD-II): nuclei (Levallois, discoidal, bipolar rotating debitage, unipolar rotating debitage), flakes, blades, and *grattoir* (Tsanova, 2006, pl.1–3).

implies an age younger than the Mousterian assemblages of layer 6, but older than the EUP material found in layer 4.

Layer 4 from sectors TD-I and TD-V shows no Levallois or discoidal core reduction, and MP tools are absent. Consequently, Drobniewicz et al. (2000a) saw layer 4 not as a continuation from layer VI described above, but as an independent complex. At the same time, layer 4 did not contain any diagnostic Aurignacian forms observed at many western European sites. While the lithics throughout the layers thickness show great similarities, three different phases could be identified, which in TD-I largely correspond to (4C) below the hearth structure, (4B) hearth complex, and (4A) above the hearth structure. The last phase is incomplete, with the top missing as a result of erosion. However, it is important to note that separation of these three phases cannot be fully achieved, as post-depositional processes have caused some overlap – as demonstrated through refittings by Tsanova (2006) and highlighted in figure 8.45.

Phase C contained slightly over 1800 artefacts (see fig. 8.44), including single and multi-platform cores, a high proportion of trimming flakes (evidence for platform rejuvenation), a significant number of blades (mostly with parallel, fewer with convergent edges) with triangular or trapezoidal cross-sections. Retouched tools are represented by retouched blades and flakes, end-scrapers, denticulated tools, burins and a single side-scraper (Drobniewicz et al., 2000a).

Phase B is connected to the hearths, which probably have been washed out from further in the cave, as sediment shows traces of liquefication. It produced over 2500 artefacts (see fig. 8.46), demonstrating blank production on site, but little tool repairing or shaping. All single platform cores were for blade production, while the double platform cores led to blades and flakes. As in previous phase, the blades show mainly parallel, some convergent, sides, and triangular cross-sections are dominant, followed by trapezoidal. The use of direct hard percussion continues. The retouched tools included retouched blades and flakes, end-scrapers, notched tools, some side-scrapers, perforators, denticulated tools and burins Drobniewicz et al. (2000a).

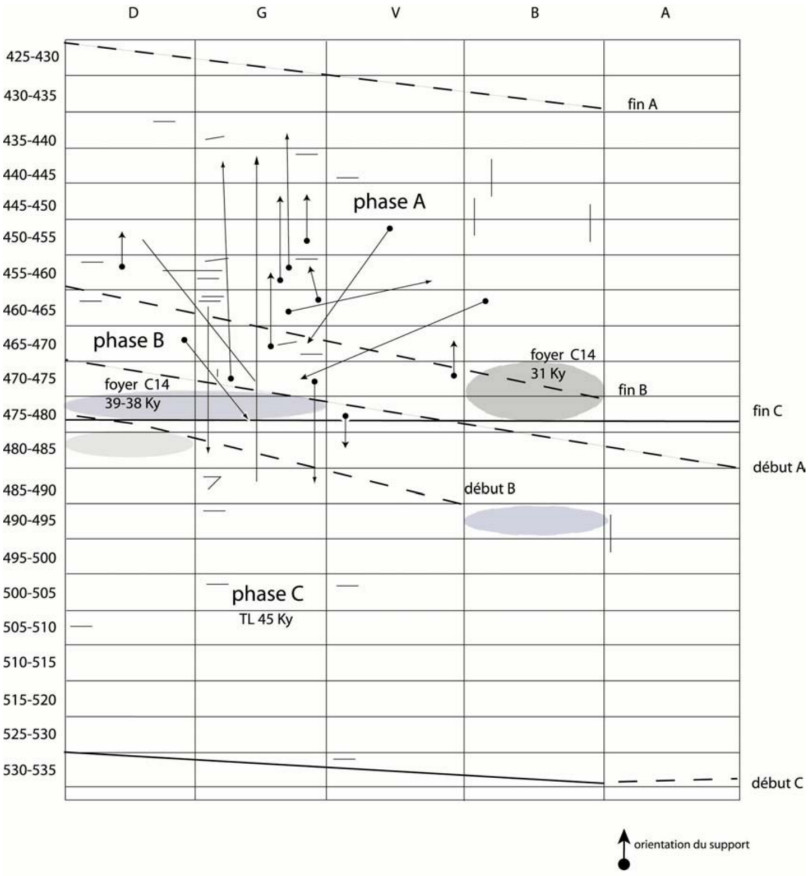


Figure 8.45: Temnata: sagittal projection of blade refittings in layer 4, sector TD-I (Tsanova, 2006, fig. II.39).

The lithic assemblage of phase A is concentrated around the hearths in Г2 and Д2 (western part of sector TD-I), and in А3, Б3 (eastern part of sector TD-I). With over 6300 artefacts, phase A has yielded the largest number of lithic artefacts of all levels contained in layer 4 (see fig. 8.47). As below, single and double platform cores and a large proportion of trimming flakes are observed. The significant number of blades are of similar size and shape as in phase C–B, and the retouched tools are represented by end-scrapers, retouched blades and flakes, several side-scrapers, notched and denticulated tools, and burins. The fireplaces are surrounded by stone slabs, which Drobniewicz et al. (2000a) see as analogous to observations in the Aurignacian layers of Abri Pataud, France.

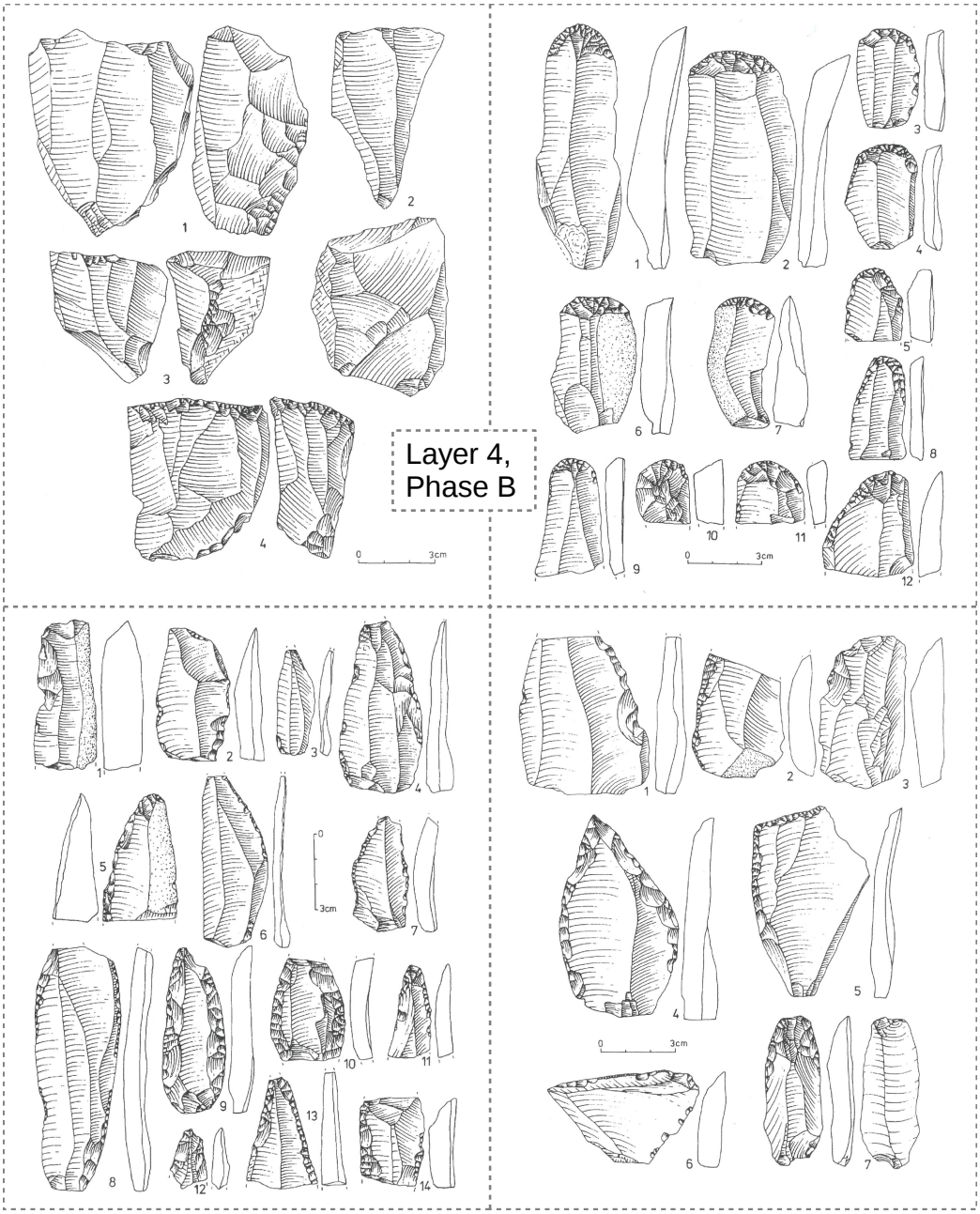


Figure 8.46: Temnata: EUP lithics from layer 4, Phase B (TD-I): cores and tools, including end-scrapers, bilaterally retouched blades, and denticulated tools, and side-scrapers (Drobniewicz et al., 2000a, pl. 4, 7, 12, 14).

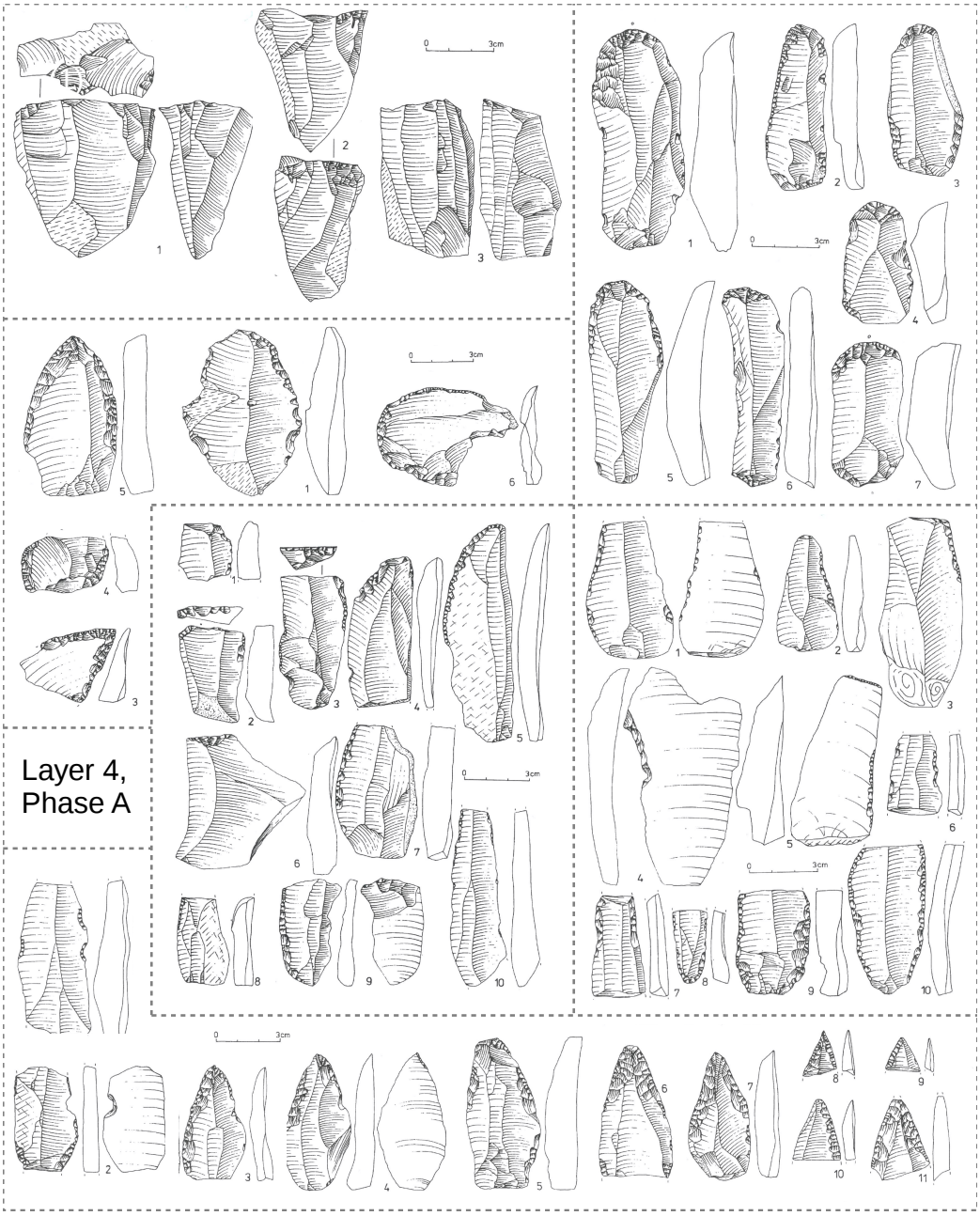


Figure 8.47: Temnata: EUP lithics from layer 4, Phase A (TD-I): cores (single-platform, and double platform) and tools, including end-scrapers, truncations, retouched blades, side-scrapers, and raclettes (Drobniewicz et al., 2000a, pl. 15, 18, 24–26, 29).

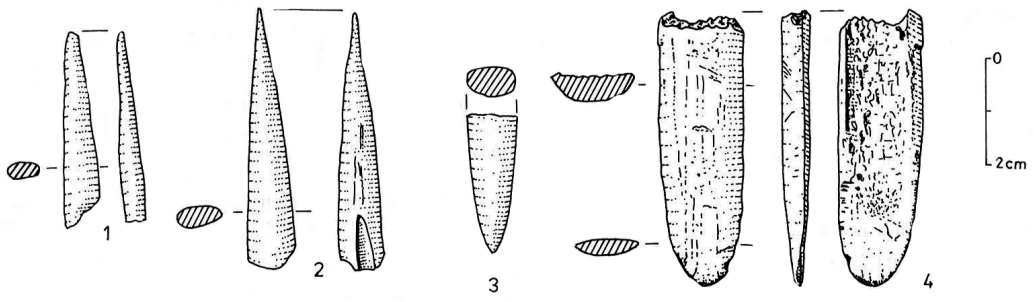


Figure 8.48: Temnata: osseous points from sector TD-V, levels VI-VII (layer 3d) (Drobniewicz et al., 1992, fig. 5).

From phase C to A, there is an increase of carenoidal and nosed end-scrapers, as well as Aurignacian retouch on end-scrapers. It is clear that layer 4 contains early Upper Palaeolithic industries, which show a significant overlap with the Early Aurignacian technocomplex. And although more diagnostic features are missing, the connection to the Aurignacian appears to be increasing over time. This is a phenomenon frequently observed in the Balkans (and more widely at Eastern European sites), leading Drobniewicz et al. (2000a) to use the term 'Balkan Aurignacian'.

In contrast, their designation of layers 3i–j as 'typical Aurignacian' is closely connected to the assumption that these layers represent the same technocomplex found at Bacho Kiro (layers 9–6a). Both leitmotifs of the Early Aurignacian and the Proto-Aurignacian mentioned by Drobniewicz et al. (2000a) – the osseous points and Dufour bladelets – were found at Bacho Kiro, and not at Temnata. Osseous tools are extremely rare at Temnata cave. The only evidence of osseous points stems from level VI-VII, i.e. layer 3d, which in turn is already well within the Gravettian technocomplex (see fig. 8.48).

Human Remains

Three human remains were found in the 'Gravettian' layers in sector TD-V (see fig. 8.49). Temnata 1 is a deciduous left mandibular lateral incisor,

which belonged to a *ca.* 5–7 year old juvenile. It was found in layer 3a, at a depth of 273-275 cm. Temnata 2 surfaced further down, in layer 3d, at a depth of 440–445 cm. It is a deciduous left mandibular central incisor, also belonging to a juvenile aged 5–7 years. The same layer, i.e. 3d, further yielded a cranial fragment from a left parietal bone belonging to an adult. It was found at a depth of 425–430 cm. None of the specimens found showed any pathologies. Morphometrics of all fragments do not contradict a *Homo sapiens* attribution, though the limited comparative dataset does not allow for more in depth analysis (Gambier, 1992).

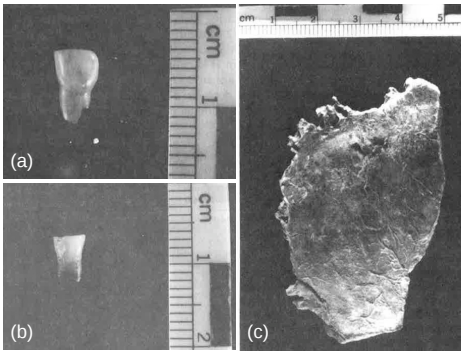


Figure 8.49: Temnata: *Homo sapiens* remains from sector TD-V. (a) left deciduous mandibular lateral incisor; (b) left deciduous mandibular central incisor; (c) cranial fragment from a left parietal bone (Gambier, 1992, fig. 1–3).

Previous Dating

Research at Temnata cave included several absolute and relative dating techniques, including radiocarbon dating, TL and ESR measurements, and tephra analysis (Bluszcz et al., 1992; Ginter et al., 1996; Paterne, 1992; Pawlikowski, 1992). In the following, the dating relevant to the archaeology found at the site is discussed, and its potential for chronological modelling is assessed.

An initial set of 29 conventional **radiocarbon** measurements was obtained on charcoals and unmodified faunal bones at the Gliwice Absolute Dating Methods (GADAM) Centre, Silesian University of Technology, and at the *Centre de Datation par le Radiocarbone*, University of Lyon (see tab.

8.11–8.12, lab codes 'Gd-' and 'Ly-'). The samples were taken from the sectors TD-I, TD-II, and TD-V, with a focus on dating the archaeological stratigraphy. They were measured using proportional gas counting, and corrected for known laboratory derived uncertainties – though they were not not fractionation corrected (Bluszcz et al., 1992).

The charcoal fragments found at Temnata were generally very small, and often heavily crushed (Lityńska-Zając, 1992). Therefore, instead of the standard ABA treatment used at the time, the charcoal samples were only treated with acid for 1h (80°C) to avoid excessive sample loss. Bluszcz et al. (1992) expected that this would not have an adverse effect on the measurement, as the limited vegetation cover would result in negligible exposure to humics. As a result, Bluszcz et al. (1992) only considered carbonate contamination – which can be dissolved in acid washes. However, recent research has shown that more rigorous treatment (*e.g.* ABOx-Sc and AOx-Sc) can improve dating precision – both with or without base wash (*e.g.* Bird et al., 1999; Sutikna et al., 2016; Wood et al., 2012).

The use of bulk samples instead of single entities for dating may also be problematic. The GADAM database describes that either isolated or scattered charcoal concentrations were submitted. Whether this refers to the actual sample treated or the general concentration in the respective layer is unclear – though the sample size required for conventional measurement, combined with the general state of the charcoals at Temnata, favour a bulk sample interpretation.

The two radiocarbon measurements (Gd-5758 and Gd-5771) on 'flowstone' from layer 7 were undertaken on encased charcoal, and pre-treated as described above. While the results are in agreement with the stratigraphy and TL ages (Bluszcz et al., 1992), they do not provide any useful constraints for modelling. The TL measurement for the same flowstone was calculated to represent an age of approx. 105 ± 35 kyr (Bluszcz et al., 1992) – far beyond the limit of radiocarbon and significantly older than layer 6.

The bone samples were pretreated using the original gelatine protocol developed by Longin (1971). Considering the age of some samples, it can be assumed that these results are minimum age estimates only. Furthermore, there is no record of the samples showing traces of human activity. As a result, they will be treated as not directly connected to the human activity at Temnata.

The very young greater than ages observed for Gd-4595 ($>$ 33100 BP) and Gd-4693 ($>$ 32200 BP) result from a higher detection threshold for conventional measurement techniques; *i.e.* no ^{14}C activity could be measured. The high 1σ errors observed for some samples directly resulted from their small sample size. In addition, Gd-4027 and Gd-4693 were so small that they had to be diluted with inactive carbon dioxide (from combustion of pit coal), in order for the samples to be large enough for the proportional gas counters used (Bluszcz et al., 1992).

To get a better temporal understanding of the 'EUP/Aurignacian', 6 'charred earth' samples were sent to ORAU for AMS dating (see tab. 8.11–8.12, lab code 'OxA-'). The samples were recovered from hearth structures within layer 4, as found both in sector TD-I and TD-V. The material contained small charcoal particles, ash and cave sediment. Prior to ABA chemical pre-treatment (*i.e.* ORAU's ZR protocol), the samples were hand-sorted to increase the concentration of carbon present (see also Hedges et al., 1989b). The samples were subsequently measured using the then operational AMS CO_2 ion source system as described by Hedges et al. (1992), and corrected for laboratory background and isotope fractionation.

Despite only charcoal being selected for dating, the dating accuracy could be influenced by the dated bulk sample containing material from several fires. In addition, insufficient sample pre-treatment may have resulted in minimum age estimates for such old samples, despite chemical pre-treatment having been more rigorous than during the earlier dating campaign. Still, the radiocarbon results seem to be in good agreement with each other and their positions within the stratigraphy.

Table 8.11: Temnata: previously published ^{14}C dates from sector TD-I (Bluszcz et al., 1992; Ginter et al., 1996) with context and treatment information. Additional information was obtained from the publicly accessible databases of the GADAM Centre, at the Silesian University of Technology (http://www.carbon14.pl/IB_Grdb/index.html), of the *Centre de Datation par le Radiocarbone*, at the *Université Claude Bernard Lyon 1* (http://carbon14.univ-lyon1.fr/banadora), and ORAU's internal database. Calibrated age calculated in OxCal 4.3 (Bronk Ramsey, 2009a) using IntCal13 (Reimer et al., 2013). grey – dates considered unsuited for modelling (see text). I = isolated charcoal distribution; S = widely scattered charcoal. ZR = ORAU's ABA treatment.

Date code	Item	Trench	Layer	Depth (cm)	Treat.	Yield (mg)	Yield (wt.%)	δ^{13}C	C:N	^{14}C (BP)	Date (cal BP)
Gd-1838	charcoal	TD-I	–	–	acid (80°C)	–	–	–	–	2670 ± 70	2960–2540
Gd-2354	bone	TD-I	4A	475–480	Longin	–	–	–	–	31900 ± 1600	40790–33440
Gd-2580	bone	TD-I	3d (base)	445–460	Longin	–	–	–	–	28900 ± 1100	35330–31030
Gd-2790	bone	TD-I	3d	435–440	Longin	–	–	–	–	21200 ± 380	26200–24500
Gd-4026	charcoal (I)	TD-I	3c	410–420	acid (80°C)	–	–	–	–	10440 ± 400	13130–11130
Gd-4027	charcoal	TD-I	3c	410–420	acid (80°C)	–	–	–	–	11200 ± 1600	18660–9480
Gd-4029	charcoal (I)	TD-I	3d	445–460	acid (80°C)	–	–	–	–	19940 ± 800	25940–22400
Gd-4030	charcoal (I)	TD-I	3d (base)	470–475	acid (80°C)	–	–	–	–	21200 ± 900	27470–23610
Gd-4231	bone	TD-I	3d	450–455	Longin	–	–	–	–	29700 ± 700	35250–32100
Gd-4232	bone	TD-I	3d	435–440	Longin	–	–	–	–	23400 ± 1600	31720–24530
Gd-4233	bone	TD-I	3f	460–465	Longin	–	–	–	–	28900 ± 1400	36680–30650
Gd-5758	flowstone	TD-I	7 (top)	–	acid (80°C) ?	–	–	–	–	> 44900	
Gd-5771	flowstone	TD-I	7 (base)	–	acid (80°C) ?	–	–	–	–	> 44000	
Ly-3439	bone	TD-I	3a	250–255	Longin	–	–	–	–	13600 ± 200	17040–15850
Ly-3440	bone	TD-I	3a	275–280	Longin	–	–	–	–	13920 ± 480	18180–15580
Ly-3441	bone	TD-I	3a	375–400	Longin	–	–	–	–	24900 ± 510	30300–27930
OxA-5169	charred earth	TD-I	4B	–	ZR	117	39.0	-24.8	–	39100 ± 1800	47760–40500
OxA-5170	charred earth	TD-I	4B	–	ZR	89.9	89.9	-24.6	–	38800 ± 1700	47080–40270
OxA-5171	charred earth	TD-I	4B	–	ZR	114	45.6	-24.8	–	38200 ± 1500	45710–40000

Table 8.12: Temnata: previously published ^{14}C dates from sector TD-II and TD-V (Bluszcz et al., 1992; Ginter et al., 1996) with context and treatment information. Additional information was obtained from the publicly accessible databases of the GADAM Centre, at the Silesian University of Technology (http://www.carbon14.pl/IB_Grdb/index.html), of the *Centre de Datation par le Radiocarbone*, at the *Université Claude Bernard Lyon 1* (http://carbon14.univ-lyon1.fr/banadora), and ORAU's internal database. Calibrated age calculated in OxCal 4.3 (Bronk Ramsey, 2009a) using IntCal13 (Reimer et al., 2013). grey – dates considered unsuited for modelling (see text). I = isolated charcoal distribution; S = widely scattered charcoal. ZR = ORAU's ABA treatment.

Date code	Item	Trench	Layer	Depth (cm)	Treat.	Yield (mg)	Yield (wt.%)	δ^{13}C	C:N	^{14}C (BP)	Date (cal BP)
Gd-4229	bone	TD-II	IV/V	–	Longin	–	–	–	–	25400 ± 1550	33750–27080
Gd-4687	bone	TD-II	VI	–	Longin	–	–	–	–	> 38700	> 42430
Gd-2488	charcoal (S)	TD-V	3a	271	acid (80°C)	–	–	–	–	540 ± 80	680–330
Gd-2578	bone	TD-V	3a	305–315	Longin	–	–	–	–	16600 ± 300	20800–19290
Gd-2581	bone	TD-V	3a	316–320	Longin	–	–	–	–	24800 ± 700	30580–27720
Gd-2785	bone	TD-V	3d (base)	405–410	Longin	–	–	–	–	21200 ± 380	26200–24500
Gd-4022	charcoal (S)	TD-V	3a	293–305	acid (80°C)	–	–	–	–	10880 ± 370	13560–11750
Gd-4025	charcoal (I)	TD-V	3a	305–310	acid (80°C)	–	–	–	–	10480 ± 280	12880–11330
Gd-4028	charcoal (S)	TD-V	3a	305–320	acid (80°C)	–	–	–	–	20100 ± 900	26400–22360
Gd-4230	bone	TD-V	3c/3d	350–360	Longin	–	–	–	–	22400 ± 900	28660–24980
Gd-4595	bone	TD-V	3g	–	Longin	–	–	–	–	> 33100	> 36780
Gd-4693	bone	TD-V	3h	–	Longin	–	–	–	–	> 32200	> 35870
Gd-6126	bone	TD-V	3d	–	Longin	–	–	–	–	24400 ± 600	29930–27470
OxA-5172	charred earth	TD-V	4b	–	ZR	71	71	-26.8	–	38300 ± 1600	46170–39910
OxA-5173	charred earth	TD-V	4b	–	ZR	69.5	69.5	-23.8	–	36900 ± 1300	43840–38960
OxA-5174	charred earth	TD-V	4a	–	ZR	36.2	36.2	-22.8	–	33000 ± 900	39540–35260

Table 8.13: Temnata: previously published TL dates (Bluszcz et al., 1992; Ferrier et al., 2011; Ginter and Kozlowski, 2011; Ginter and Kozłowski, 1992; Ginter et al., 1996). Gd-TL-411 / Gd-TL-416 and Gd-TL-272 obtained on calcite, Gd-TL-843 on quartz, and the rest on burnt flint. * – date obtained on same sample. grey rows – samples unsuitable for modelling.

Date code	trench	Sq.	Layer	Depth (cm)	Age (kyr)
Gd-TL-210	TD-I	A1	3d	435–440	22.9 ± 2.1
Gd-TL-211	TD-V	N1	3a	325-330	61.3 ± 8.6
Gd-TL-212	TD-V	N2	3a	345-350	19.6 ± 3.7
Gd-TL-213	TD-V	N1	3a	315-320	15.4 ±6.1
Gd-TL-214	TD-V	N1	3a	345-350	23.3 ± 5.1
Gd-TL-240	TD-I	B1	4	485–490	> 22
Gd-TL-241	TD-I	A1	3f	460–465	> 34
Gd-TL-254	TD-I	G1	6	500–505	67 ± 11
Gd-TL-255	TD-I	G2	4B	450–455	46 ± 8
Gd-TL-256	TD-I	G2	4C	510–515	45 ± 7
Gd-TL-409	–	–	10a	–	76 ± 26
Gd-TL-410	–	–	10b	–	31 ± 20
Gd-TL-411*	–	–	10	–	180 ± 27
Gd-TL-416*	–	–	10	–	46 ± 15
Gd-TL-843	–	–	10	–	44.2 ±1.4
Gd-TL-272	TD-I	–	7	–	105 ± 35

A series of **TL measurements** was made on burnt flint from sectors TD-I and TD-V (see tab. 8.13, numbers Gd-TL-210–256). All samples were mechanically pretreated by removing the outermost layer (*ca.* 1–2 mm), followed by crushing and grinding. The 100–150 μm fraction was selected and treated with 4% HF for 30 min. (RT), rinsed, treated with 8% HCl for 30 min. (RT), rinsed and dried. Internal dose rates were calculated using the samples' concentrations of uranium, thorium and potassium, while external dose rates were measured *in situ* (also taking a small contribution of cosmic radiation into account). Bluszcz et al. (1992) assumed ka=0.1 for efficiency of alpha radiation producing the TL signal. The glow curve was based on a heating rate of 10°C/s in a nitrogen or argon atmosphere, using

the apparatus described in Bluszcz and Pazdur (1985) and computationally automated as detailed in Bluszcz et al. (1992). A ^{90}Sr beta radiation source and a ^{60}Co gamma source were used for artificial sample irradiation, and final age calculations were done on weight normalised TL signals. Two background samples (i.e. samples annealed to erase natural TL signal) demonstrated that the triboluminescence effect from mechanical sample preparation was negligible (Bluszcz et al., 1992).

10 TL samples passed quality control assessment and resulted in reasonable TL measurements, the remaining samples could not be dated as a result of TL signal saturation, lack of plateau, or other glow curve anomalies (corresponds to a success rate of 30%). However, only seven of these dates are suitable for Bayesian modelling. Gd-TL-211 is a clear outlier in the chronostratigraphy of the site. The measurement supposedly dates sediment from lyaer 3a in TD-V, but its age appears older than any of the other measurements for UP levels (for visual comparison see fig. 8.51). On the other hand, Gd-TL-240 and Gd-TL-241 are in agreement with the chronostratigraphy, though their greater than ages will add little value, as previously published radiocarbon data for these layers are already significantly older than the threshold and provide more precise age estimates.

Bluszcz et al. (1992, p. 233) further mentions the TL dating of the speleothem (i.e. layer 7) in sector TD-I resulting in an age of 105 ± 35 kyr when using '*clean and pure calcite grains of ca. 100 μm in diameter*' (see also above), though no lab-code seems to be included in their publication. The same TL age appears in Ginter and Kozłowski (1992) with the lab code Gd-TL-272 (see tab. 8.13).

Ginter and Kozlowski (2011) and Ferrier et al. (2011) list further TL dates from layer 10 (see tab. 8.13, numbers Gd-TL-409–863). No detailed description is given, though it is mentioned that Gd-TL-411 and Gd-TL-416 were obtained on the same calcite sample, and Gd-TL-843 was measured on quartz. The age discrepancies are significant, and some dates appear in contradiction with the chronostratigraphy at the site. Until the cause of this variation is better understood, the dates are deemed unsuitable for modelling.

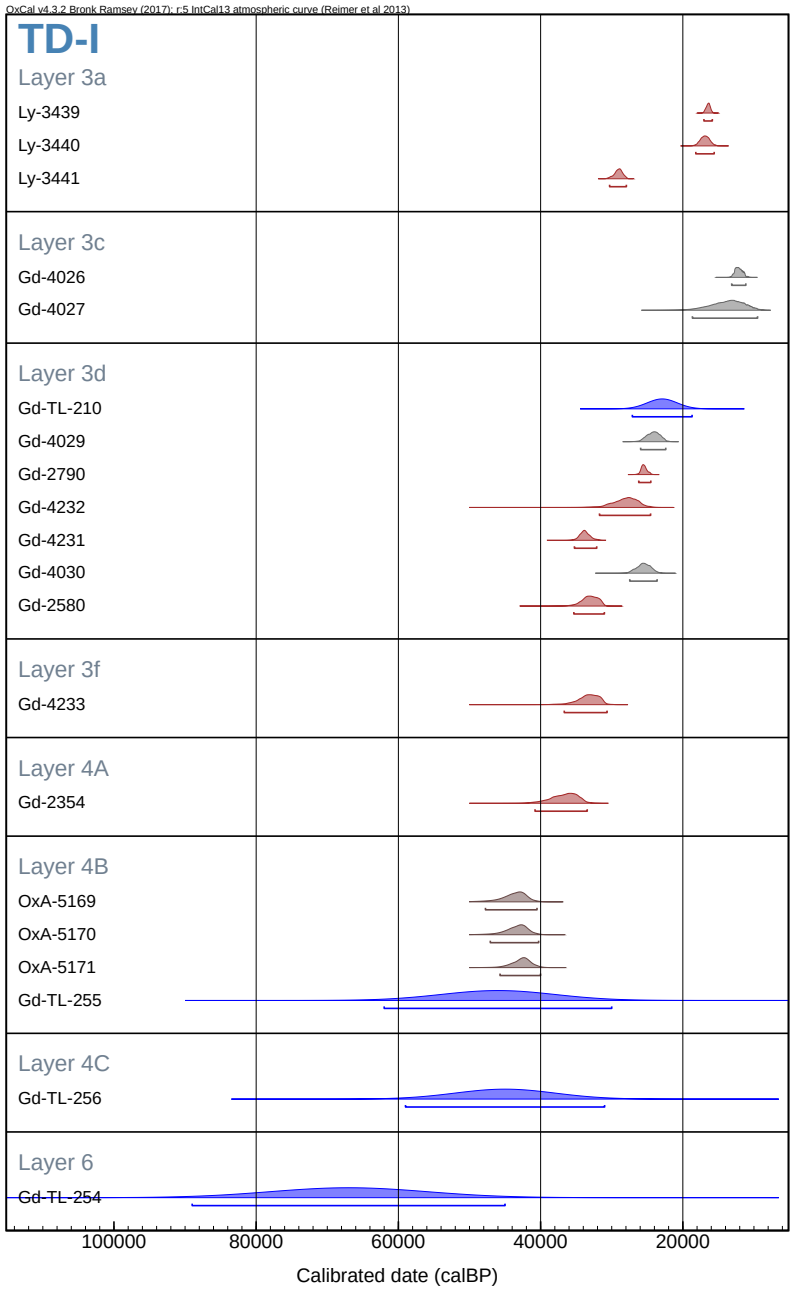


Figure 8.50: Temnata: overview of the previously obtained dates from TD-I, excluding the very young date for Gd-1838 without layer attribution and the measurements from the flowstone layer 7. **grey** – ^{14}C on charcoal; **brown** – ^{14}C on unmodified bone; **ebony** – AMS ^{14}C on charred earth (layers 4A, and 4B only); **blue** – TL on burnt flint. IntCal13 (Reimer et al., 2013) and OxCal 4.3 (Bronk Ramsey, 2009a) was used for ^{14}C calibration.

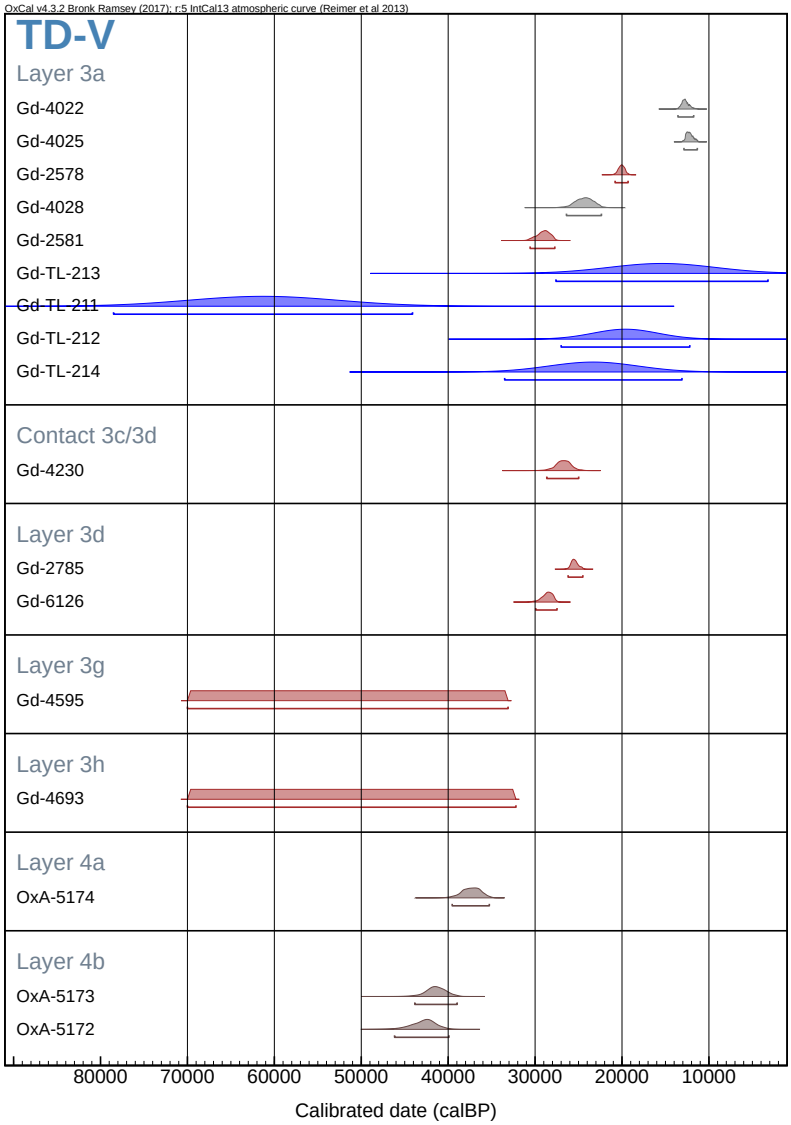


Figure 8.51: Temnata: overview of the previously obtained dates from TD-V, excluding the clearly intrusive date Gd-4229 from the top of layer 3a. **grey** – ^{14}C on charcoal; **brown** – ^{14}C on unmodified bone; **ebony** – AMS ^{14}C on charred earth (layers 4a, and 4b only); **blue** – TL on burnt flint. IntCal13 (Reimer et al., 2013) and OxCal 4.3 (Bronk Ramsey, 2009a) was used for ^{14}C calibration.

There were several **ESR measurements** made on speleothems found in sector TD-IV (Bluszcz et al., 1992). However, as they are not directly connected to the archaeology found in sectors TD-I and TD-V, they are not further discussed here.

Tephra levels were identified in sectors TD-I and TD-V (layer 'v'), and in sector TD-II (layer V). In sector TD-I, Pawlikowski (1992) describes the tephra horizon as a discontinuous layer between stratigraphic units 4 and 3f. However, in the south profile (see fig. 8.36), layer 'v' is visible mainly as a number of distorted lenses within the upper part of layer 4, with minor inclusions at the bottom of layer 3d. In sector TD-V, Pawlikowski (1992) identifies the tephra as a discontinuous layer located between layers 4 and 3d. This is clearly visible in the south profile (see fig. 8.38). However, the same profile also shows the tephra separating layers 3d from 3j, and 3j from 4. In the north profile (see fig. 8.38), a tephra accumulation is visible in square H2/M2. It is situated above the fireplace horizon 4o1 and under layer 3d, but vertically separating the layers 3g, from 3i and 3j. Sector TD-II is the only location presenting a continuous tephra horizon (50–80 cm thick), where it is placed between layers VI (IUP) and IV (equivalent to layer 3d in TD-I).

Results from microscopic and chemical analyses suggested similarities with tephra found at Crvena Stijena (Pawlikowski, 1992), where later the CI tephra was identified. However, Paterne (1992) interpreted the varying alkali ratios as the result of possible mixing of tephra originating in the Phlegrean Fields and Ischia Islands. Subsequently, Giaccio et al. (2008) securely connected the tephra found at Temnata to the CI (Y5) eruption.

In **conclusion**, there are 35 radiocarbon dates (see tab. 8.11–8.12), 16 TL measurements (see tab. 8.13), and a tephra layer connected to the CI eruption at 34290 ± 90 BP (date from Giaccio et al., 2017) at Temnata Dupka. All date measurements excluded from modelling are highlighted in grey in the respective tables.

26 radiocarbon ages can provide some chronostratigraphic information for TD-I and TD-V. This excludes dates from sector TD-II as well as samples from TD-I/TD-V that are from the contact zones, intrusive to layer 3a, or with greater than ages showing a very young minimum age. However, any model relying on these dates is likely to underestimate the age of layer accumulation – especially towards the lower end – because of dating inaccuracies related to less rigorous pre-treatment, bulk samples, and possible high measurement backgrounds. Furthermore, the bone samples used show only a *probable* connection to human activity at Temnata (i.e. no anthropogenic modifications), and the charcoal samples may have a *probable* or *highly probable* connection, though none have *full certainty*.

Of the TL dates, 7 are suitable for anchoring a stratigraphic radiocarbon model, and for providing independent dating consilience. The remaining dates had to be excluded on the basis of too little context information, high dating variability, or identification as an unquestionable outlier to the chronostratigraphy.

As with the TL dates, the CI tephra provides another independent anchoring point for the radiocarbon sequence, though its complex stratigraphic position will require testing of different model compositions. Stratigraphic modelling of new, and more accurate and precise, radiocarbon dates might even help to resolve the chronological position of the CI in relation to human activity at the cave.

8.4.2 Radiocarbon dating

The dating at Temnata cave targets the chronostratigraphy of the MP/UP transition – in particular the human activity of that period – and tries to locate the accurate placement of the CI tephra within it. As a result, anthropogenically modified fauna (largely cut marked bones) was sampled in the summers of 2015 and 2016, with a focus on the late MP and EUP layers.

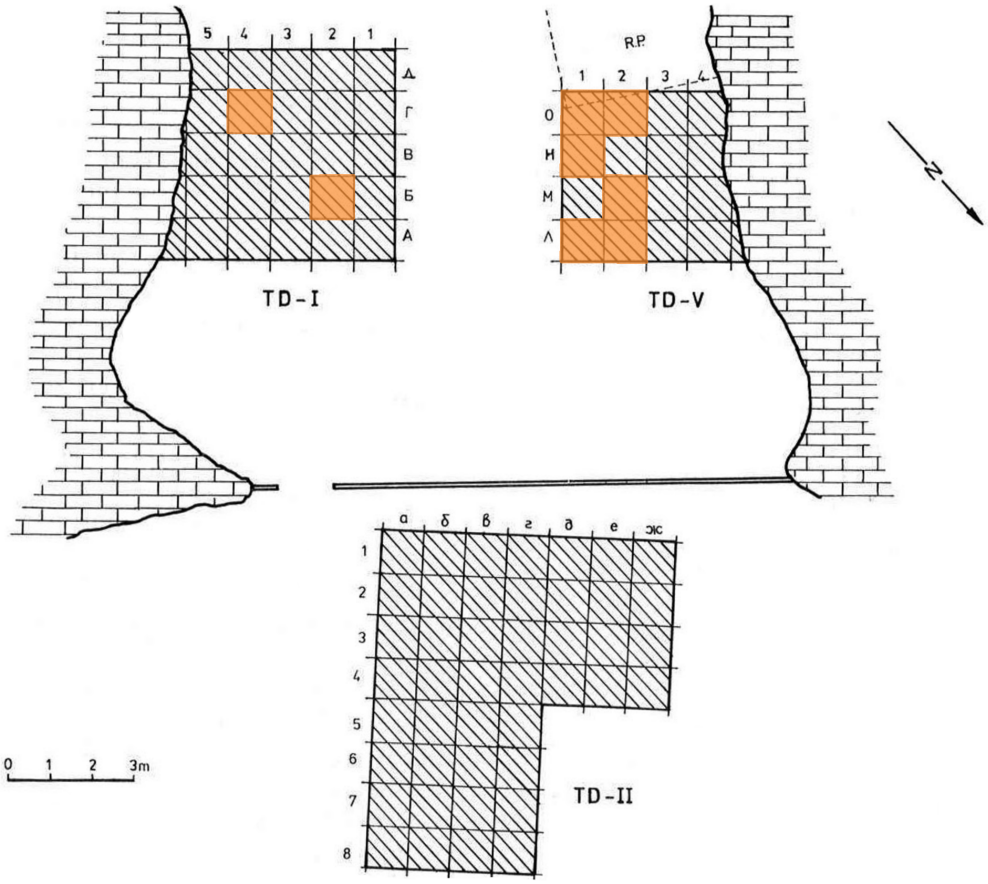


Figure 8.52: Temnata: excavation trenches with quadrant labels (Sirakov, 1992, fig. 5), and quadrants sampled for new radiocarbon dating highlighted in **orange**.

Samples & Treatment

All available faunal fragments from the 1980s/1990s excavations were checked for anthropogenic modifications. Osseous remains were numerous, though compared to the size of the site, they comprised only a small fraction of the total find material. Furthermore, the percentage of modified osseous remains was small. Consequently, all fragments from layers 6–3d, with clear cut marks, projectile impact fractures, or other likely human derived fractures, were sampled and documented (see tab. 8.14–8.15).

Table 8.14: Temnata: samples for radiocarbon dating from sector TD-I.

Ref-no.	Item	Excav.	Sample-no.	Sq.	Layer	Sampled	Treated
TD-16	faunal	–	Б2-639	Б2	4	1110 mg	1086 mg
TD-17	faunal	1985	Г4-662	Г4	4	950 mg	890 mg
TD-17	faunal	1985	Г4-662	Г4	4	950 mg	890 mg
TD-26	faunal	–	П/274-F3	–	3f	600 mg	528 mg
TD-27	faunal	–	П/274-F2	–	3f	1970 mg	937 mg
TD-30	faunal	–	Б2-591	Б2	4	6030 mg	881 mg
TD-31	faunal	–	Б2-606	Б2	4	3140 mg	651, 786 mg

The distribution of the collected specimens was not uniform. In the accessible material, no modified fauna from sector TD-II was present[7]. In contrast, both sectors TD-I and TD-V contained modified faunal bones. The samples' distribution according to quadrant is visualised in figure 8.52, while their layer distributions are seen in figure 8.53. Layer 4 (lower part), layer 5 and layer 6 are only represented in TD-V. The same holds true for layers 3dw (=3g–j), 3dg (=3g), and 3j, though in this case, the layers were only present in sector TD-V. For the same reason, layer 3f has only material from TD-I. Neither sectors provided any anthropogenically altered material from layer 3d.

With KDE modelling in mind, the two samples found in the contact zone between 4 and the section of 3 containing volcanic material were also selected for radiocarbon dating.

Most samples were drilled in Bulgaria, collecting the bone powder. However, eleven fragments were too fragile or small: TD-03, TD-04, TD-08, TD-24–27, TD-29–31. These were initially sampled with a diamond saw in Bulgaria, and subsequently surface cleaned and crushed in an iron mortar at ORAU.

All the osseous material had been flooded while stored at the Archaeological Museum in Sofia. Despite no visible traces of conservation or restoration

[7]This is something future dating projects might want to address, especially as KDE modelling has demonstrated potential for summarising and comparing datasets derived from unconnected sectors/sequences.

Table 8.15: Temnata: samples for radiocarbon dating from sector TD-V. grey – not dated.

Ref-no.	Item	Excav.	Sample-no.	Sq.	Layer	Sampled	Treated
TD-01	faunal	–	O2-2803	O2	5pg	980 mg	957 mg
TD-02	faunal	–	O1-2044	O1	5pg	620 mg	602 mg
TD-03	faunal	–	O1-1278	O1	5pg	2160 mg	846 mg
TD-04	faunal	–	O2-1339	O2	4pg	900000 mg	1087 mg
TD-05	faunal	–	Л1-1661	Л1	3jx/4	1000 mg	975 mg
TD-06	faunal	1981	H1-1168	H1	3d/4	1040 mg	1006 mg
TD-07	faunal	1989	Л2-1683	Л2	3jx	640 mg	583 mg
TD-08	faunal	1989	M2-1758	M2	3j/w	1870 mg	857, 182 mg
TD-09	faunal	1989	H1-1942	H1	3j/w	940 mg	–
TD-10	faunal	1989	Л2-1372	Л2	3dg	660 mg	629 mg
TD-14	faunal	1989	Л1-1518	Л1	3dg	1030 mg	994 mg
TD-15	faunal	1989	Л2-1469	Л2	3dg	800 mg	773 mg
TD-18	faunal	1989	H1-1201	H1	3d/w	1030 mg	937, 937 mg
TD-19	faunal	1989	H1-1253	H1	3d/w	1000 mg	974 mg
TD-20	faunal	1989	H1-1341	H1	3d/w	940 mg	886 mg
TD-21	faunal	–	O2-2775	O2	5pg	770 mg	738 mg
TD-22	faunal	–	O1-2143	O1	5pg	1630 mg	–
TD-23	faunal	–	П/1346	O2	5pg	1380 mg	–
TD-24	faunal	–	O2-2790	O2	5pg	1210 mg	908 mg
TD-25	faunal	–	Л2-1689	Л2	3j	1650 mg	903 mg
TD-28	faunal	–	M2-1859	M2	3j/3w	900 mg	755 mg
TD-29	faunal	–	Л1-2566	Л1	6lg	1700 mg	879 mg

work, it was decided to first pre-treat the samples with solvent wash steps before applying the ultrafiltration (AF) protocol with an additional freeze-drying and re-hydrolisation after AG to check for sample yield (see section 5.4).

Not all samples from layer 5pg were processed, because of their high overall number and likelihood to be near or beyond the limit of radiocarbon dating. In case of finite measurements, the remaining samples would be processed to help with KDE modelling. In contrast, TD-08 and TD-31 were ran in duplicates as part of the ORAU quality control procedures.

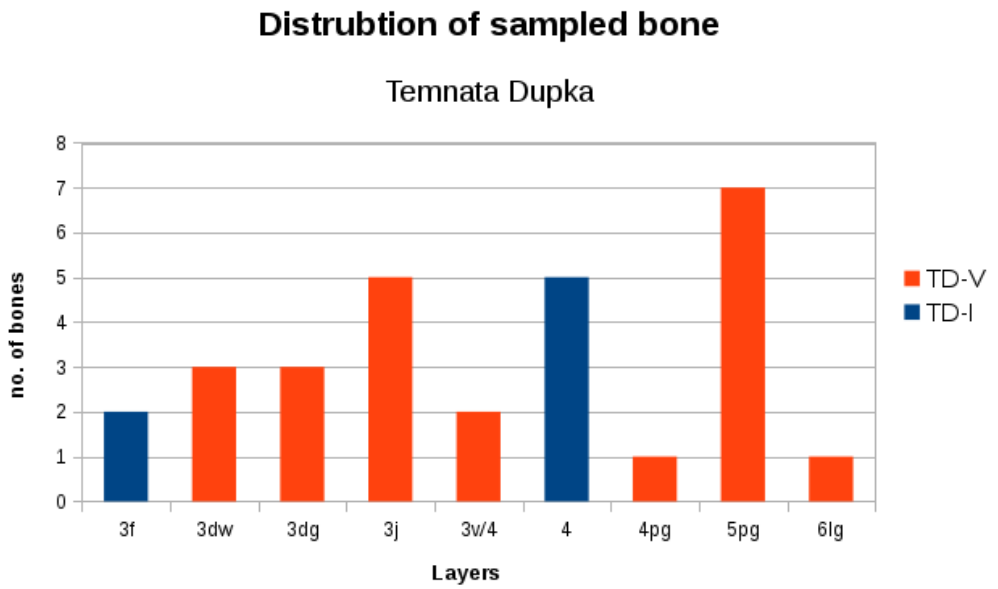


Figure 8.53: Temnata: distribution of faunal remains with identified anthropogenic modification according to layer attribution.

^{14}C Results

All but one pre-treated sample could be successfully radiocarbon dated, providing a total of 28 measurements from 24 samples for Temnata (see tab. 8.16–8.18).

TD-02 failed pre-treatment with a sample yield of only 0.49 wt.% after AG* treatment. It was decided that running a small graphite target (0.8 mgC) of a less rigorously treated sample of expected high age would be ill-advised – especially as other samples from layer 5pg were available. A second sample from layer 5pg – TD-21 – showed a low collagen yield (0.82 wt.% at AF*). However, the sample was ultrafiltered and there was sufficient collagen for a large graphite target (1.8 mgC). As a result, the sample was AMS dated, and the resulting of greater than age of $>$ 45100 BP (OxA-35236) supports this decision. The third sample yielding $<$1% collagen was TD-29 (0.54 wt.% at AF*). As with TD-21, the sample was both ultrafiltered and provided sufficient collagen for a large graphite target. Furthermore,

Table 8.16: Temnata: new AMS radiocarbon dates on anthropogenically modified faunal bone from sector TD-I, with archaeological context information, and pre-treatment results. Failed samples in grey. Ref-no. = number given to the sample for the purpose of this project. %N = nitrogen weight content before chemical pre-treatment. Treat. = Pretreatment protocols used: * = solvent wash steps, AG = ORAU acid-base-acid pretreatment, AF = ORAU ultrafiltration protocol (see section 5.4). Yield = sample left after chemical pre-treatment (both in mg and wt.%). %C = carbon yield on combustion. C:N = carbon to nitrogen ratio of combusted collagen sample. $F^{14}C$ = fraction modern carbon. ^{14}C (BP) = conventional radiocarbon age Before Present with 1σ error. Date (cal BP) = calibrated radiocarbon age at a 95.4% confidence interval, calculated in OxCal 4.3 (Bronk Ramsey, 2009a) using IntCal13 (Reimer et al., 2013).

Ref-no.	Sq.	Layer	Depth (cm)	%N	Treat.	Yield (mg)	Yield (wt.%)	%C	$\delta^{15}N$	$\delta^{13}C$	C:N	Lab-no	$F^{14}C$	^{14}C (BP)	Date (cal BP)
TD-16	Б2	4	450–452.5	2.36	AF*	38.58	3.55	43.0	7.16	-19.99	3.2	OxA-33845	0.02782 ± 0.00110	28770 ± 320	33670–31850
TD-17	Г4	4	460–465	1.29	AF*	27.92	3.14	41.9	7.89	-19.89	3.2	OxA-35231	0.03353 ± 0.00103	27270 ± 250	31540–30870
TD-26	–	3f	475–480	3.02	AF*	53.57	10.15	44.2	7.36	-19.28	3.2	OxA-35235	0.02799 ± 0.00101	28730 ± 290	33600–31860
TD-27	–	3f	475–480	1.63	AF*	58.18	6.21	43.6	7.23	-20.76	3.2	OxA-35238	0.02639 ± 0.00101	29200 ± 310	34000–32640
TD-30	Б2	4	447.5–450	0.81	AF*	23.92	2.71	40.6	5.60	-20.00	3.2	OxA-35756	0.01517 ± 0.00103	33650 ± 550	39310–36470
TD-31	Б2	4	447.5–450	1.40	AF*	31.68	4.86	42.2	6.30	-20.90	3.2	OxA-35757	0.02653 ± 0.00105	29160 ± 320	33990–32540
TD-31	Б2	4	447.5–450	1.40	AF*	34.58	4.40	41.7	6.20	-21.10	3.2	OxA-35758	0.02625 ± 0.00103	29240 ± 320	34040–32660

Table 8.17: Temnata: new AMS radiocarbon dates on anthropogenically modified faunal remains from sector TD-V (pt. 1), with archaeological context information, and pre-treatment results. Failed samples in grey. Ref-no. = number given to the sample for the purpose of this project. %N = nitrogen weight content before chemical pre-treatment. Treat. = Pretreatment protocols used: * = solvent wash protocol; AG = ORAU acid-base-acid pretreatment, AF = ORAU ultrafiltration protocol (see section 5.4). Yield = sample left after chemical pre-treatment (both in mg and wt.%). %C = carbon yield on combustion. C:N = carbon to nitrogen ratio of combusted collagen sample. $F^{14}C$ = fraction modern carbon. ^{14}C (BP) = conventional radiocarbon age Before Present with 1σ error. Date (cal BP) = calibrated radiocarbon age at a 95.4% confidence interval, calculated in OxCal 4.3 (Bronk Ramsey, 2009a) using IntCal13 (Reimer et al., 2013).

Ref-no.	Sq.	Layer	Depth (cm)	%N	Treat.	Yield (mg)	Yield (wt.%)	%C	$\delta^{15}N$	$\delta^{13}C$	C:N	Lab-no	$F^{14}C$	^{14}C (BP)	Date (cal BP)
TD-01	O2	5pg	540–545	1.16	AF*	10.37	1.08	42.7	9.18	-19.69	3.2	OxA-33874	0.00206 ± 0.00100	> 44200	(> 46850)
TD-02	O1	5pg	535–540	1.06	AG*	2.94	0.49	-	-	-	-	-	-	-	
TD-03	O1	5pg	540–545	1.13	AF*	25.62	3.03	41.0	7.70	-19.50	3.2	OxA-34401	0.00179 ± 0.00100	> 44800	(> 47530)
TD-04	O2	4pg	540–545	0.80	AF*	24.37	2.24	42.9	8.26	-20.04	3.2	OxA-33837	0.00157 ± 0.00099	> 45300	(> 48130)
TD-05	Л1	3jx/4	–	2.09	AF*	21.69	2.22	42.6	9.16	-19.85	3.2	OxA-33838	0.01026 ± 0.00102	36800 ± 800	42620–39880
TD-06	H1	3d/4	460–465	1.75	AF*	34.49	3.43	42.0	7.29	-20.74	3.2	OxA-33839	0.01486 ± 0.00104	33800 ± 550	39540–36620
TD-07	Л2	3jx	505–510	2.25	AF*	21.48	3.68	43.6	7.57	-20.58	3.2	OxA-33840	0.02722 ± 0.00107	28950 ± 310	33820–32160
TD-08	M2	3j/w	480–485	2.03	AF*	49.07	5.73	42.7	4.86	-21.32	3.2	OxA-33841	0.01489 ± 0.00102	33800 ± 550	39540–36620
TD-08	M2	3j/w	480–485	2.03	AF*	52.00	6.65	43.4	4.95	-21.31	3.2	OxA-33842	0.01522 ± 0.00103	33600 ± 550	39240–36420
TD-10	Л2	3dg	470–475	2.06	AF*	23.47	3.73	41.5	6.79	-21.53	3.1	OxA-35523	0.02227 ± 0.00104	30560 ± 370	35240–33890
TD-14	Л1	3dg	495–500	2.33	AF*	48.22	4.85	42.2	7.21	-20.78	3.2	OxA-33843	0.02124 ± 0.00115	30950 ± 450	35850–34080

Table 8.18: Temnata: new AMS radiocarbon dates on anthropogenically modified faunal remains from sector TD-V (pt. 2), with archaeological context information, and pre-treatment results. Failed samples in grey. Ref-no. = number given to the sample for the purpose of this project. %N = nitrogen weight content before chemical pre-treatment. Treat. = Pretreatment protocols used: * = solvent wash protocol, AG = ORAU acid-base-acid pretreatment, AF = ORAU ultrafiltration protocol (see section 5.4). Yield = sample left after chemical pre-treatment (both in mg and wt.%). %C = carbon yield on combustion. C:N = carbon to nitrogen ratio of combusted collagen sample. $F^{14}C$ = fraction modern carbon. ^{14}C (BP) = conventional radiocarbon age Before Present with 1σ error. Date (cal BP) = calibrated radiocarbon age at a 95.4% confidence interval, calculated in OxCal 4.3 (Bronk Ramsey, 2009a) using IntCal13 (Reimer et al., 2013).

Ref-no.	Sq.	Layer	Depth (cm)	%N	Treat.	Yield (mg)	Yield (wt.%)	%C	$\delta^{15}N$	$\delta^{13}C$	C:N	Lab-no	$F^{14}C$	^{14}C (BP)	Date (cal BP)
TD-15	JI2	3dg	480–485	3.03	AF	47.89	6.19	43.2	7.01	-20.59	3.2	OxA-33844	0.02648 ± 0.00107	29170 ± 320	33990–32550
TD-18	H1	3d/w	460–465	2.86	AF*	47.02	5.02	40.4	6.40	-19.90	2.8	OxA-X-2719-18	0.03241 ± 0.00106	27550 ± 260	31950–30990
TD-18	H1	3d/w	460–465	2.86	AF*	47.02	5.02	42.3	6.70	-20.50	3.2	OxA-35697	0.03367 ± 0.00104	27240 ± 250	31520–30860
TD-19	H1	3d/w	460–465	1.71	AF*	34.14	3.50	43.0	5.76	-20.91	3.2	OxA-33846	0.01480 ± 0.00102	33850 ± 550	39610–36680
TD-20	H1	3d/w	465–470	2.67	AF*	46.80	5.28	43.0	6.65	-20.83	3.2	OxA-33847	0.02241 ± 0.00107	30510 ± 380	35210–33850
TD-21	O2	5pg	540–545	1.83	AF*	6.02	0.82	42.7	5.01	-19.92	3.2	OxA-35236	0.00164 ± 0.00100	> 45100	(> 47900)
TD-24	O2	5pg	540–545	1.81	AF*	33.99	3.75	43.4	8.89	-19.38	3.2	OxA-35237	0.00252 ± 0.00097	48100 ± 3100	> 49800
TD-25	JI2	3j	510–515	1.17	AF*	12.85	1.42	34.5	5.20	-21.80	3.1	OxA-35550	0.01507 ± 0.00108	33700 ± 550	39390–36520
TD-28	M2	3j/3w	490–495	2.01	AF*	19.39	2.57	40.8	6.40	-20.40	2.9	OxA-35551	0.01497 ± 0.00102	33750 ± 550	39460–36570
TD-28	M2	3j/3w	490–495	2.01	AF*	19.39	2.57	42.2	5.90	-21.10	3.2	OxA-35755	0.01484 ± 0.00101	33800 ± 550	39540–36620
TD-29	JI1	6lg	595	0.78	AF*	4.71	0.54	39.2	5.70	-20.63	3.3	OxA-35239	0.00000 ± 0.00104	> 49600	(> 49590)

the specimen was the only anthropogenically modified faunal sample from layer 6, thus no replacements were available. The resulting radiocarbon age of > 49600 BP (OxA-35239) indicates that contamination was unlikely to have affected the measurement outcome.

In contrast to the poor preservation observed on the Middle Palaeolithic samples, the specimens from the Upper Palaeolithic layers showed generally very high collagen yields (1.08–10.15 wt.%).

C:N ratios for all combusted samples were within acceptable ranges. The low ratio for TD-18 (OxA-X-2719-28) and TD-28 (OxA-35551) resulted from nitrogen calibration issues on burn no. 4951 (see Appendix), and are not indicative of an unreliable radiocarbon measurement. Nonetheless, a second target from the same pretreated collagen was combusted, which gave a C:N ratio of 3.2 in both instances. All other results were statistically indistinguishable from the original measurements, supporting the dating reliability of TD-18 and TD-28.

The carbon concentrations on combustion are all within regularly observed limits. Despite TD-25 being on the lower end (34.5 %C), no other anomalies were observed, and the final measurement of 33700 ± 550 BP (OxA-35550) is consistent with dates from TD-08 (OxA-33841: 33800 ± 550 BP, OxA-33842: 33600 ± 550 BP) and TD-28 (OxA-35551: 33750 ± 550 BP, OxA-35755: 33800 ± 550 BP) – collected from the same layer 3j.

The general quality of the radiocarbon results for Temnata is further supported by the two auto-duplicates TD-08 and TD-31. Not only are their AMS measurements indistinguishable – 33800 ± 550 BP (OxA-33841) and 33600 ± 550 BP (OxA-33842) for TD-08, and 29160 ± 320 BP (OxA-35757) and 29240 ± 320 BP (OxA-35758) for TD-31 –, but also their other pretreatment results are in agreement.

It can be concluded that all 28 radiocarbon dates obtained on anthropogenically modified fauna from Temnata appear reliable and suitable for modelling – including the 'OxA-X' designated date on TD-18.

8.4.3 Bayesian modelling

Temnata is a deeply stratified site and was originally chosen with a focus on Bayesian stratigraphic analysis. However, its complex deposition history (including redepositioning, mixing, erosion and sedimentation hiatus) and limited number of anthropogenically modified remains mean that such analysis is likely to provide more information on post-depositional processes rather than occupation dynamics. Consequently, the KDE modelling, and its comparison with stratigraphic modelling results, are crucial to understanding the site. For that purpose, a total of 11 stratigraphic and 7 KDE models were run in different configurations. The actual code used can be found under Catalogue B.2.

Initially, the data identified as suitable for modelling purposes[8] was sorted according to layer attribution and calibrated in OxCal 4.3 (Bronk Ramsey, 2009a) with IntCal13 (Reimer et al., 2013). This provided a better temporal understanding of whether the CI tephra age is consistent with stratigraphic observations (see fig. 8.54).

'Greater than' ages were input using a uniform distribution with their original minimum age as the lower, and 80k cal BP as their upper age limits (see below). The upper limit was chosen to accommodate for the older TL ages, as it prevents artificially constraining them to the younger ends of their distributions. For KDE modelling purposes, where no TL dates were included, the upper limit was reduced to 70k cal BP. This improved the readability of figures without negatively affecting the modelling outputs.

```
OxA-33874  Date("OxA-3387",U(calBP(80000),calBP(44200)))
OxA-34401  Date("OxA-34401",U(calBP(80000),calBP(44800)))
OxA-33837  Date("OxA-33837",U(calBP(80000),calBP(45300)))
OxA-35236  Date("OxA-35236",U(calBP(80000),calBP(45100),))
OxA-35239  Date("OxA-35239",U(calBP(80000),calBP(49600),))
```

[8]For details on published dates see tab. 8.11–8.13, for new dates tab. 8.16–8.18.

As TD-24 (OxA-35237) shows a finite radiocarbon age that extends beyond the radiocarbon calibration curve, a workaround was implemented. The 2σ error (*i.e.* 6200 radiocarbon years) was added to the calibrated lower age limit of the 95% confidence interval (*i.e.* 49800 cal BP) to obtain an approximation of a calibrated mean value. This was subsequently input as the mean of a normal distribution, using the same 1SD error as the original date. Though this is not as reliable as a regularly calibrated radiocarbon age, it will better reflect the true age of the sample. In contrast, the regular use of R_Date would artificially limit the calibrated age range to <50 cal BP – *i.e.* the extent of the current calibration curve IntCal13.

```
OxA-35237  Date("OxA-35237",N(calBP(56000),3100))
```

The TL measurements feature as `Date` functions. Their regular results consist of a mean and 1σ error value. These are placed in the respective arguments for a normal distribution function `N`, using `calBP` to indicate the use of the calender time scale.

```
Gd-TL-210  Date("Gd-TL-210",N(calBP(22900),2100))
Gd-TL-212  Date("Gd-TL-212",N(calBP(19600),3700))
Gd-TL-213  Date("Gd-TL-213",N(calBP(15400),6100))
Gd-TL-214  Date("Gd-TL-214",N(calBP(23300),5100))
Gd-TL-254  Date("Gd-TL-254",N(calBP(67000),11000))
Gd-TL-255  Date("Gd-TL-255",N(calBP(46000),8000))
Gd-TL-256  Date("Gd-TL-256",N(calBP(45000),7000))
Gd-TL-272  Date("Gd-TL-272",N(calBP(105000),35000))
```

All duplicate samples (TD-08, TD-18, TD-28, TD-31) were included in the models as a single date using the `R_Combine` function.

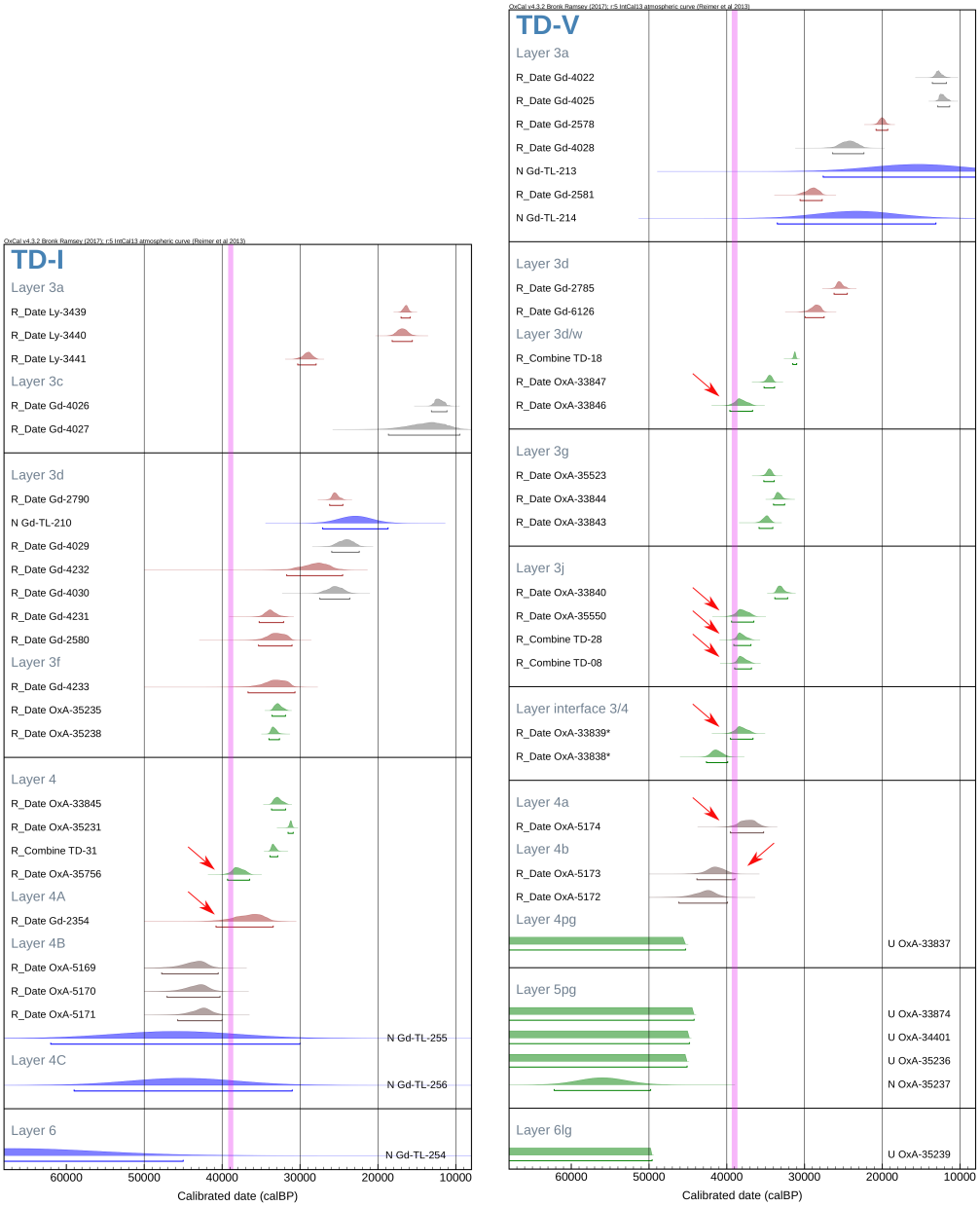


Figure 8.54: Temnata: Overview of calibrated dates from sectors TD-I (left) and TD-V (right) used in modelling. CI age range is given in **pink** and intersections with sample ages are highlighted by a red arrow (→). Ages: **grey** – ^{14}C on charcoal; **brown** – ^{14}C on unmodified bone; **ebony** – AMS ^{14}C on charred earth (layers 4A, and 4B only); **green** – new AMS ^{14}C on anthropogenically modified fauna; **blue** – TL on burnt flint. IntCal13 (Reimer et al., 2013) and OxCal 4.3 (Bronk Ramsey, 2009a) was used for ^{14}C calibration.

Site Stratigraphic Models

All stratigraphic models used the outlier model `General` for assessing whether individual and combined dates were outliers within the constraints of the model. `SSimple` was implemented to test for diverging measurements within `R_Combine`, i.e. a single sample. In both cases, the outlier probability was set to 0.05 and the standard parameters for distribution, magnitude and type were implemented. The dates were placed within phases separated by single boundaries and ordered into `Sequence` according to the published stratigraphy. Furthermore, all models were run with an empty `Date` function within each `Phase`. While this is a useful method of obtaining an exportable age probability distribution for a cultural layer, it requires testing to make sure the influence of additional events on the outcome of the modelling process is negligible. In addition, within and between all phases, the command `Interval` was used to calculate duration of phases and transition.

To account for the diverging stratigraphic sequences observed in the two dated sectors, TD-I and TD-V were run independently or semi-independently. For the latter, `Boundaries` that were expected to correspond in both trenches were set to equal. For simplification, some models group dates from both sectors into a single `Phase`, under the condition that the layers were present in both TD-I and TD-V – not only by name, but reasonably securely connectible. In cases where dates were separated by an undated layer, an empty `Phase` populated by an empty `Date` function was introduced.

Some of the samples show layer names not seen in publications: 3dg, 3dw, 3j/w, 3jx. The labels were given during excavation, and it is worth remembering that originally, no further divisions of 3d were expected to be found in sector TD-V. Therefore, 3dg corresponds to the layer later published as 3g. The 'w' or 'x' in the other three labels stands for 'volcanic material'. Considering the high concentrations of tephra found within the lower layers of unit 3 in TD-V (see discussion under Stratigraphy in section 8.4.1), 3j/w and 3jx can be simplified to 3j. 3dw appears to be either a very early denomination or from an area within TD-V where layer separation was not

possible. It denotes a section of 3d with volcanic material. It is improbable that this refers to the actual layer 3d, which did not contain any tephra. A more reasonable assumption is that 3dw refers to the tephra containing package of layers 3g–j. This interpretation would also be in agreement with the radiocarbon measurements.

As seen in figure 8.54, in TD-I the CI tephra age of 34290 ± 90 BP (see Giaccio et al., 2017) overlaps with the radiocarbon probability distributions found in 4A[9]. This is consistent with observations during excavation and seen in the south profile (see fig. 8.36). In TD-V, the CI radiocarbon age overlaps with sample ages from layer 4a, the contact zone of 3/4 and layer 3j. The overlap observed in layer 3dw is probably as a result of 3dw encompassing material from 3g–j and does not provide precise enough information. Despite this being consistent with stratigraphic observations, there remain three possible placements of the CI within the model: in layer 4a, in between layer 4 and 3j, or in layer 3j. Considering the already high number of outliers expected (as a result of post-depositional processes), placing the CI radiocarbon age in sector TD-V will not add any value to the model outcomes. It is improbable that the tephra is genuinely contemporaneous with three occupations that show different sedimentation. For further discussion on the interpretation of the CI in TD-V see section 8.4.4.

Model 0, using previously obtained radiocarbon data, represents the *status quo* prior to this doctoral research and aids as a comparison for the new results, both in terms of changes to the dating record and the influence of using different sampling strategies. Models 2 and 3 were all run on the newly obtained radiocarbon measurements. Model 3 included the TL dates to test for consilience. As the number of anthropogenically modified fauna is very limited, models 4–6 use a combined old/new dataset to investigate the influence of charcoal, unmodified fauna and TL on the age ranges and modelled transitions – while at the same time allowing for a more extensive chronostratigraphy. The first two treat the sectors TD-I and TD-V independently, to allow for the implementation of stricter stratigraphic priors. Models 3-CI and

[9]The new samples had no subunit information, though their find location suggests 4A.

4-CI investigate the effect of CI in comparison to the original models 3 and 4. And finally, the models Simple 1 and Simple 2 assume low stratigraphic integrity, and therefore combine layers into larger Phases. A comparison of the two demonstrates the the influence of unmodified fauna on the modelling outcome.

Model 0 (prev. dated) uses all previously published radiocarbon and TL measurements reasonably suitable for modelling. Separate `Sequences` were programmed for TD-I and TD-V. The first was made up of the following phases: 7, 6, 5 (empty), 4C, 4B, 4A, 3f, 3d, and 3a-c. The latter was composed of: 4b, 4a, 3v (empty), 3d, and 3a-c. 3v stands for the layer complex 3g-j. The two sectors were connected at three boundaries: transition 4C/4B from TD-I was equated with the start of 4b in TD-V, the transition 4B/4A with the transition 4b/4a, and the end boundary of 3a-c from TD-I with that of TD-V. The model represents the layer estimates based on previously available data. For modelling results see figure 8.55. Code listed on p. 680.

Model 1 (new) restricts the model data to radiocarbon dates obtained on anthropogenically modified fauna with clear layer attribution, thus excluding both TD-05 (OxA-33838) and TD-06 (OxA-33839) from the new dating project. The model implements two main stratigraphic sequences: in TD-V `Phase` 4 is followed by `Phase` 3f, in TD-V the `Sequence` is made up of 5 `Phases` (6, 5, 4, 3j, 3g). The two chronostratigraphic sequences are connected at the start and end `Boundary` for layer 4, and the end `Boundary` for layer 3f in TD-I is set to equate the end `Boundary` for layer 3g in TD-V. In addition, layer 3dw was added in a single `Phase Sequence`, equating its start `Boundary` to the transition `Boundary` 4/3j in TD-V, and its end `Boundary` to the end `Boundary` of `Phases` 3f and 3g from sector TD-I and TD-V. For modelling results see figure 8.56. Code listed on p. 681.

Model 2 (new) uses the same radiocarbon dataset on anthropogenically modified fauna as Model 1. However, the stratigraphy in sector TD-V is

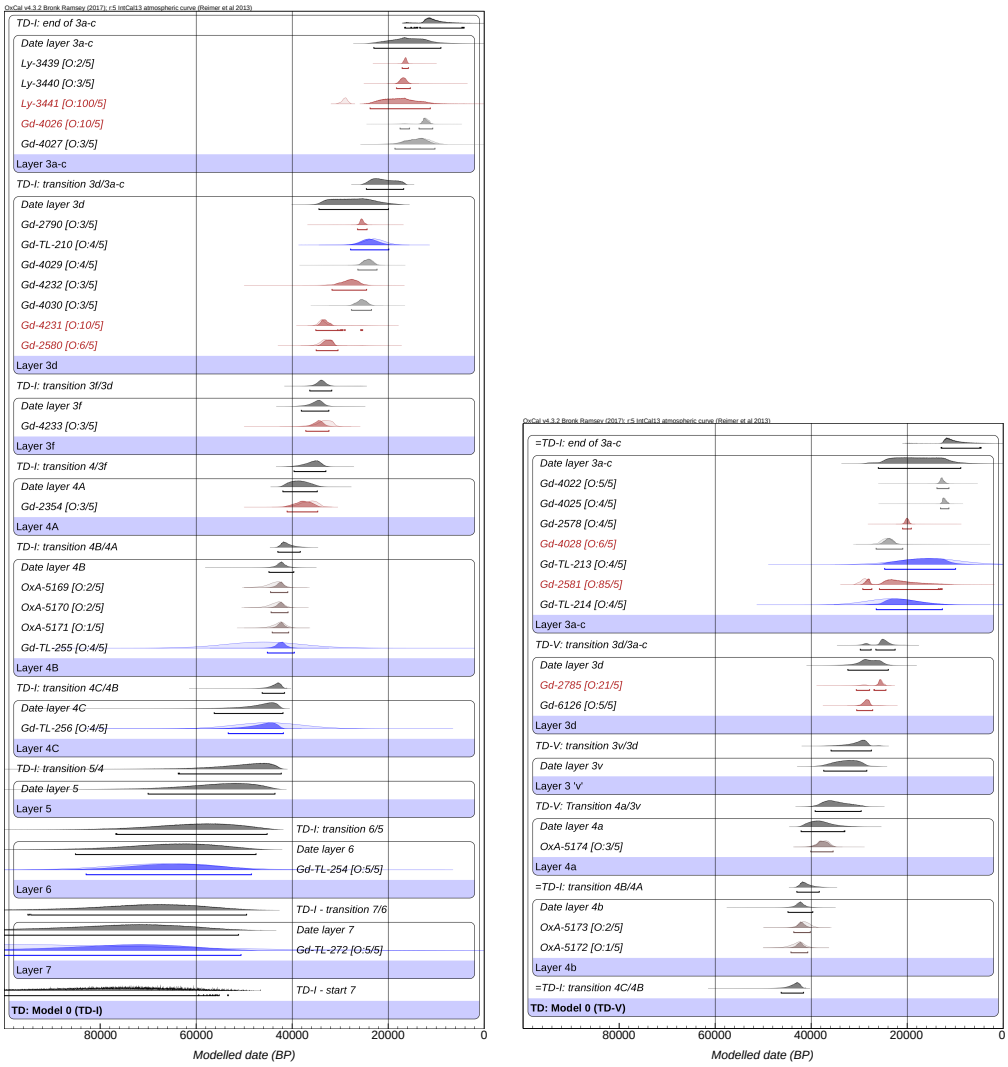


Figure 8.55: Temnata: Model 0 (code: 680), using previously published radiocarbon data. left – sector TD-I; right – sector TD-V. **grey** – ^{14}C on charcoal; **brown** – ^{14}C on unmodified bone; **ebony** – AMS ^{14}C on charred earth (layers 4A, and 4B only); **blue** – TL on burnt flint; **black** – modelled ages. Date label of outliers (> 5%) highlighted.

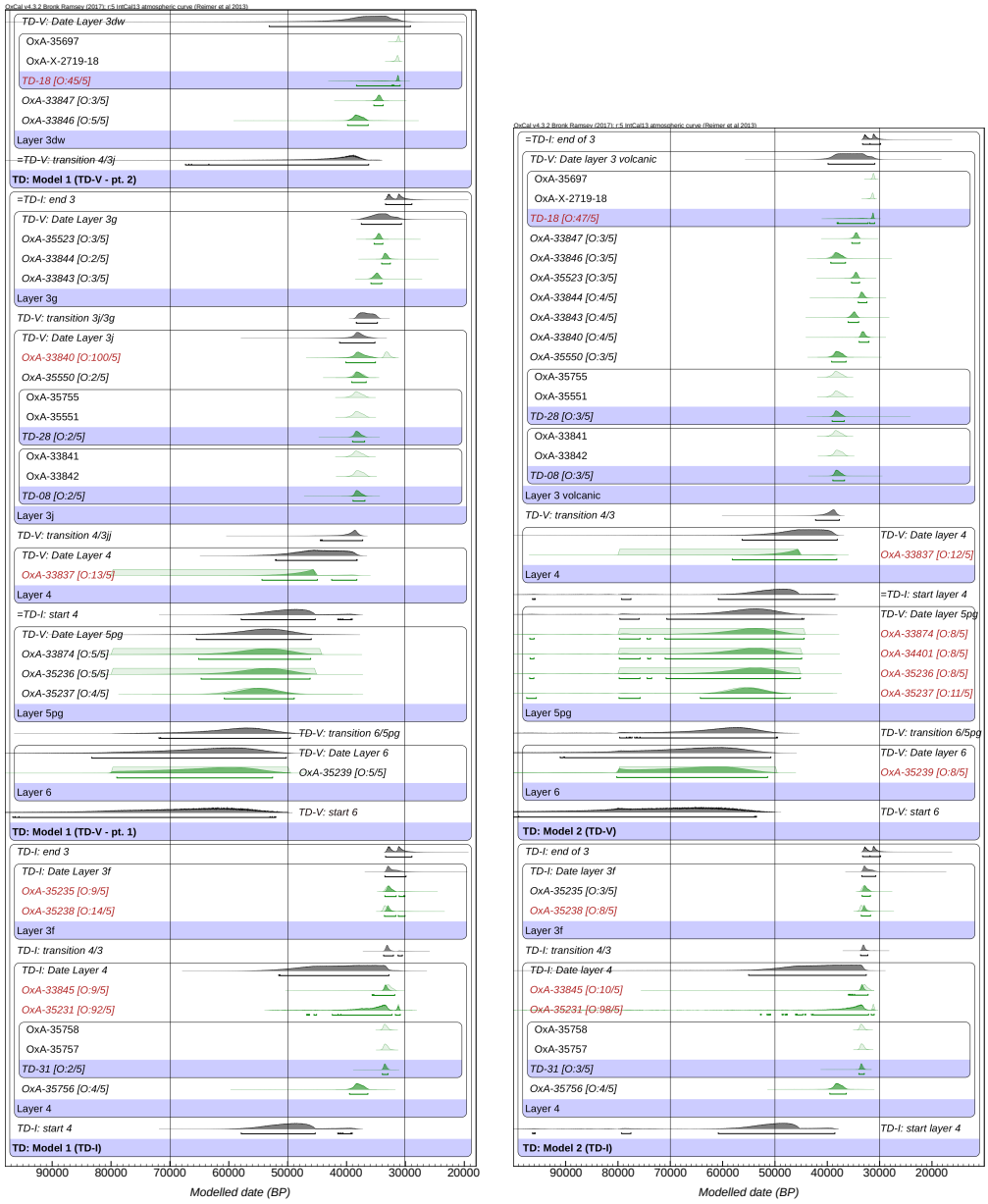


Figure 8.56: Temnata: Model 1 (left, code: p. 681) and 2 (right, code: p. 683). **green** – AMS ^{14}C on anthropogenically modified fauna; **blue** – TL on burnt flint; **black** – modelled ages. Date label of outliers ($> 5\%$) highlighted.

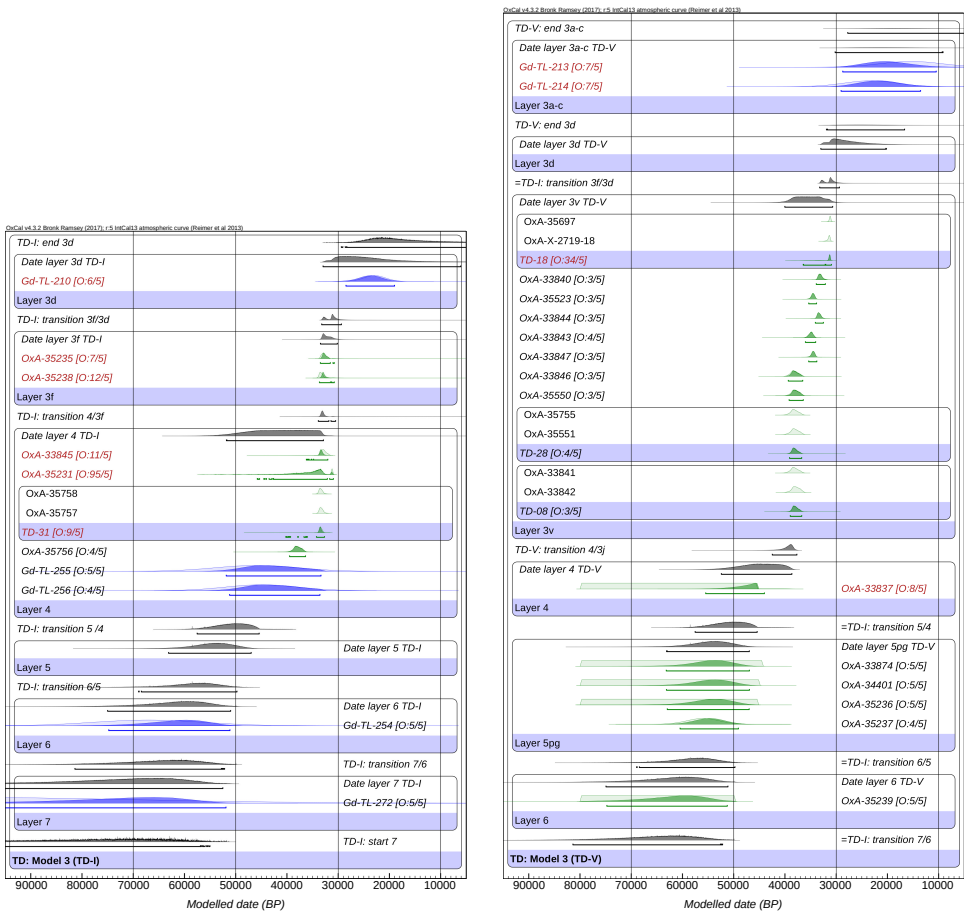


Figure 8.57: Temnata: Model 3 (code: p. 684). **green** – AMS ^{14}C on anthropogenically modified fauna; **blue** – TL on burnt flint; **black** – modelled ages. Date label of outliers ($> 5\%$) highlighted.

simplified to 4 phases. All samples coming from subunits of 3 that contained volcanic material – i.e. 3j, 3g, 3dw – were combined into `Phase` 3v. The two sectors were connected at two points. First, the start `Boundary` fo layer 4 in TD-I equates the transition `Boundary` between `Phase` 5pg and 4 in TD-V. Second, the same `Boundary` was used for the end of `Phase` 3a-c in TD-I and TD-V. The aim of simplifying the structure was to reduce the model constraints in order to avoid artificially precise results which lack in accuracy. For modelling results see figure 8.56. Code listed on p. 683.

Model 3 (new & TL) includes both the the radiocarbon data on anthropogenically modified fauna (as seen in Model 1 and 2) and the previously published TL measurements. The `Phase` structure is expanded to account for the newly included dates. For TD-I: 7, 6, 5 (empty), 4, 3f, 3d. For TD-V: 6, 5pg, 4, 3v (=3dg, 3j, and 3dw), 3d, 3a-c. The two sectors are linked at four boundaries: the transition 7/6 in TD-I equates to the start `Boundary` of 6 in TD-V, the transition 6/5 in TD-I to the transition 5pg/4 in TD-V, the transition 5/4 in TD-I to the transition 5pg/4 in TD-V, and the end `Boundary` for 3d in TD-I to the transition 3d/3a-c in TD-V. The model checks whether the radiocarbon measurements are in agreement with the TL results and investigates what influence the TL dates from the MP layers has on modelling outcome. For modelling results see figure 8.57. Code listed on p. 684.

Model 3-CI runs the same model structure as Model 3, but adds the CI age of 34290 ± 90 BP (from Giaccio et al., 2017) to layer 4 in sector TD-I. For modelling results see figure 8.58. Code listed on p. 686.

Model 4 (TD-I, all) incorporates all radiocarbon measurements (both published and new) and TL dates deemed suitable for modelling with sample origin in sector TD-I. The sequence groups the dates into the following phases: 7, 6, 5 (empty), 4C, 4B, 4A, 3f, 3d, and 3a-c. Keeping sector TD-I independent from sector TD-V in this way allows for a more detailed model. A comparison of its results with Model 5, which focuses on sector TD-V, will shed light on the chronostratigraphic differences between the two trenches. For modelling results see figure 8.59. Code listed on p. 688.

Model 4-CI is the same as Model 4, but has the CI radiocarbon age of 34290 ± 90 BP (from Giaccio et al., 2017) included in layer 4A. For modelling results see figure 8.60. Code listed on p. 690.

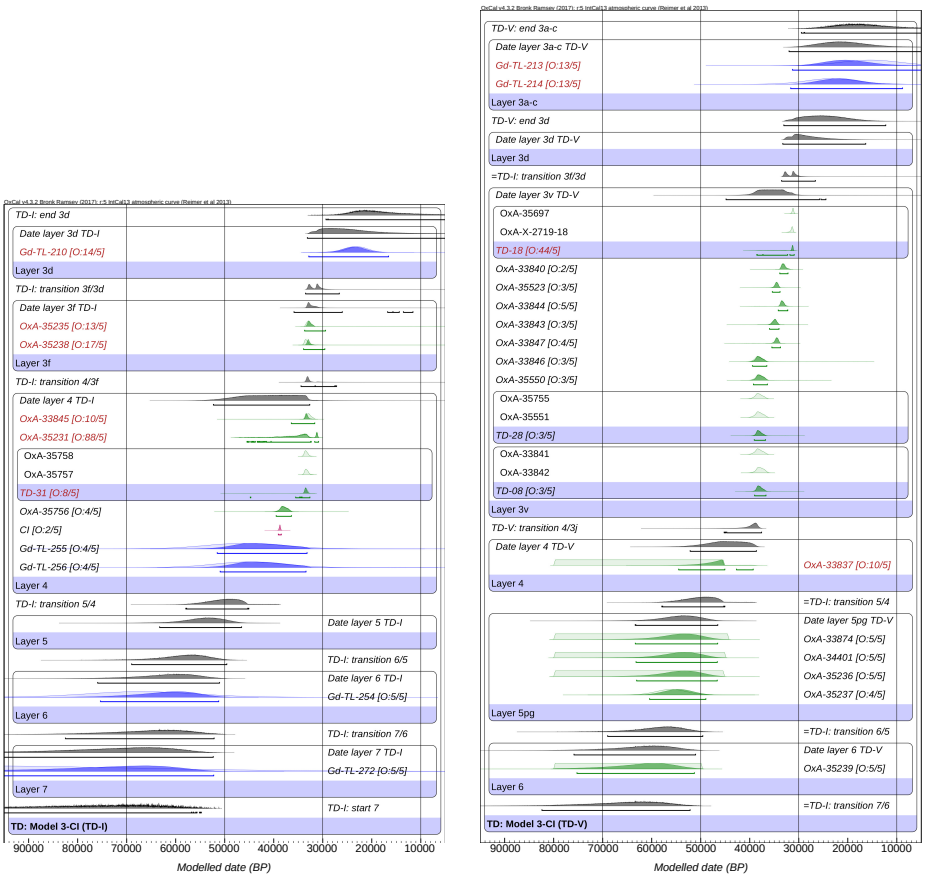


Figure 8.58: Temnata: Model 3-CI (code: p. 686). **green** – AMS ^{14}C on anthropogenically modified fauna; **blue** – TL on burnt flint; **magenta** – CI age from Giaccio et al. (2017); **black** – modelled ages. Date label of outliers (> 5%) highlighted.

Model 5 (TD-V, all) incorporates all radiocarbon measurements (both published and new) and TL dates deemed suitable for modelling with sample origin in sector TD-V. It is the counterpart to Model 4. The sequence groups the dates into the following phases: 6lp, 5pg, 4pg, 4b, 4a, 3j, 3g, 3d, 3a-c. The `Phase` 3dw is kept in a single `Phase Sequence`. Its start `Boundary` is the same as the transition 4a/3j, and its end `Boundary` as the transition 3g/3d. This way, the model accounts for the fact that 3dw contains material from throughout 3g–j. For modelling results see figure 8.59. Code listed on p. 693.

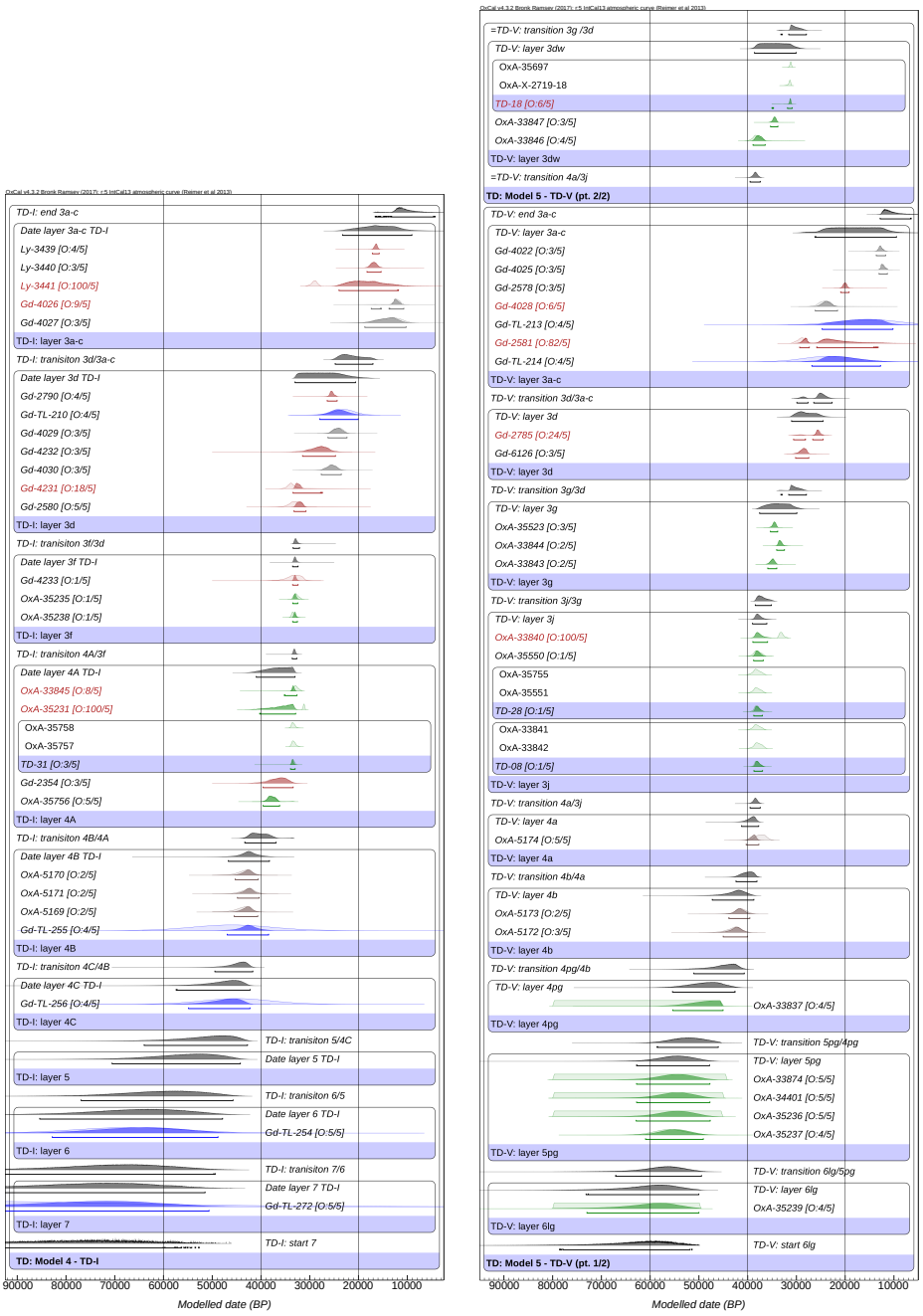


Figure 8.59: Temnata: Model 4 (left, code: p. 688) and Model 5 (right, code: p. 693) showing differences in transitions between sector TD-I (left) and TD-V (right). Dates: **grey** – ^{14}C on charcoal; **brown** – ^{14}C on unmodified bone; **ebony** – AMS ^{14}C on charred earth (layers 4A, and 4B only); **green** – AMS ^{14}C on anthropogenically modified fauna; **blue** – TL on burnt flint; **black** – modelled ages. Date label of outliers ($> 5\%$) highlighted.

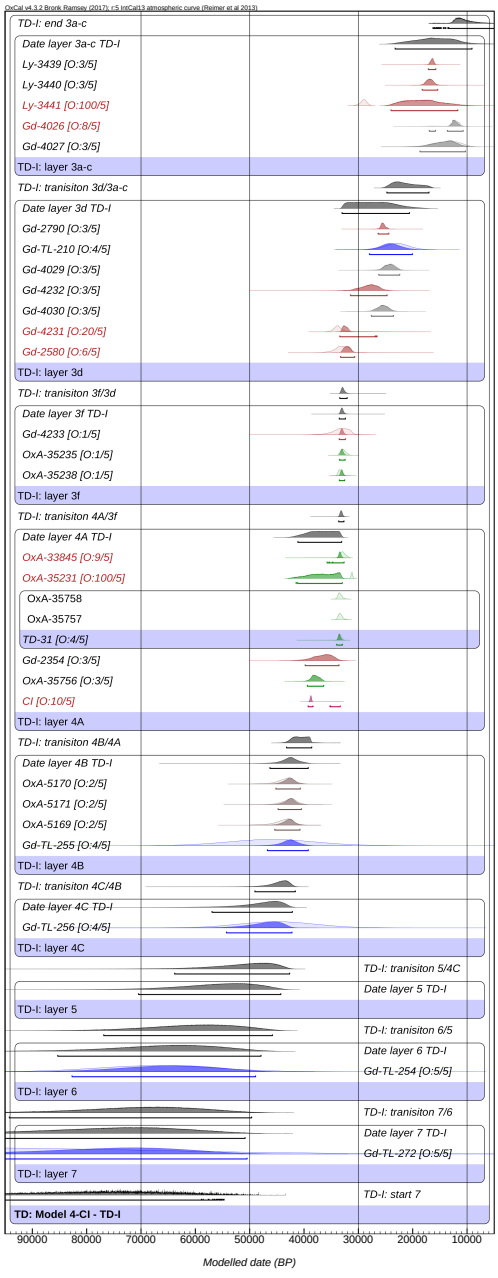


Figure 8.60: Temnata: Model 4-CI (code: p. 690). Dates: **grey** – ^{14}C on charcoal; **brown** – ^{14}C on unmodified bone; **ebony** – AMS ^{14}C on charred earth (layers 4A, and 4B only); **green** – AMS ^{14}C on anthropogenically modified fauna; **blue** – TL on burnt flint; **magenta** – CI age from Giaccio et al. (2017); **black** – modelled ages. Date label of outliers ($> 5\%$) highlighted.

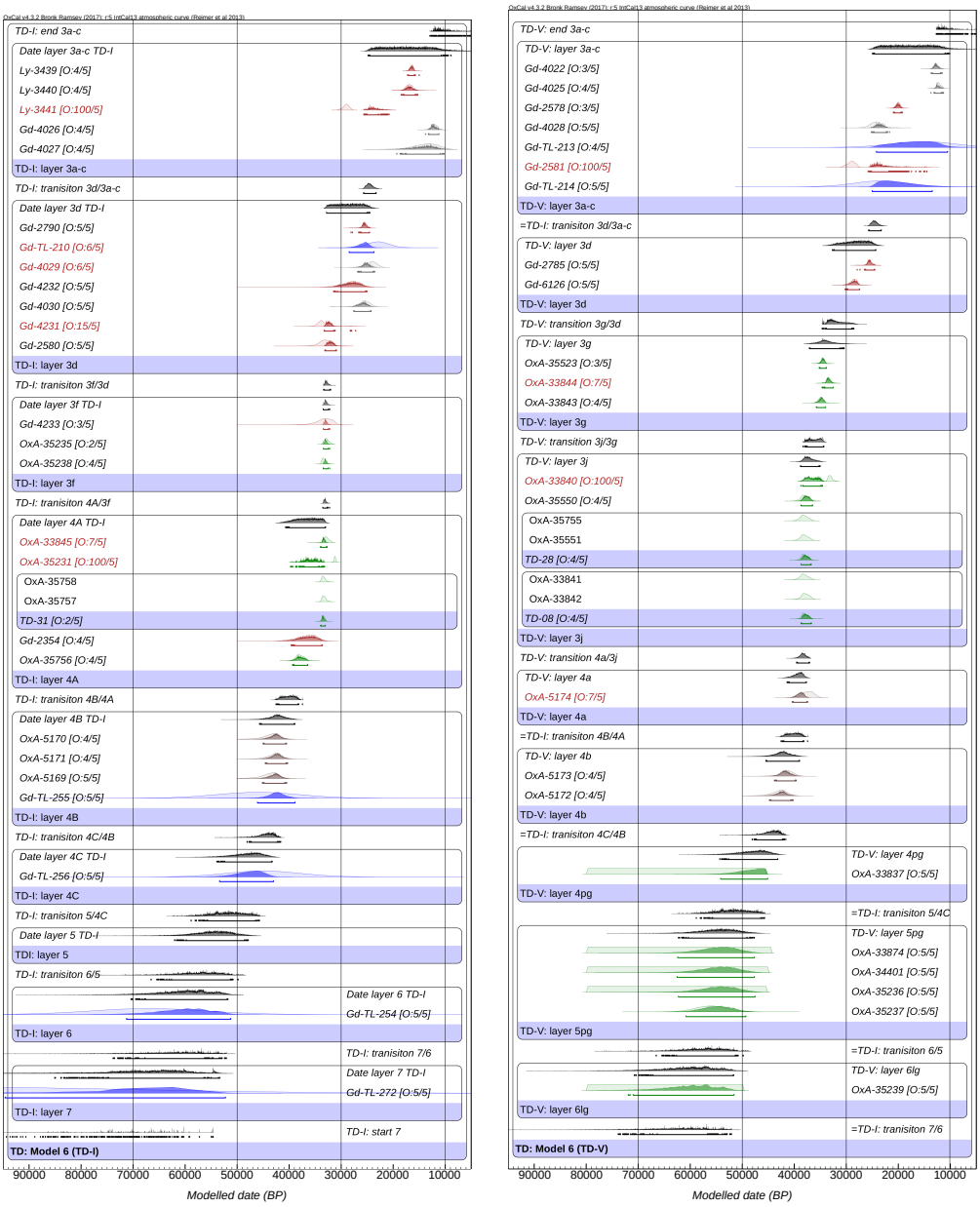


Figure 8.61: Temnata: Model 6 (code: p. 695), connecting sector TD-I and TD-V. Dates: **grey** – ^{14}C on charcoal; **brown** – ^{14}C on unmodified bone; **ebony** – AMS ^{14}C on charred earth (layers 4A, and 4B only); **green** – AMS ^{14}C on anthropogenically modified fauna; **blue** – TL on burnt flint; **black** – modelled ages. Date label of outliers (>5%) highlighted.

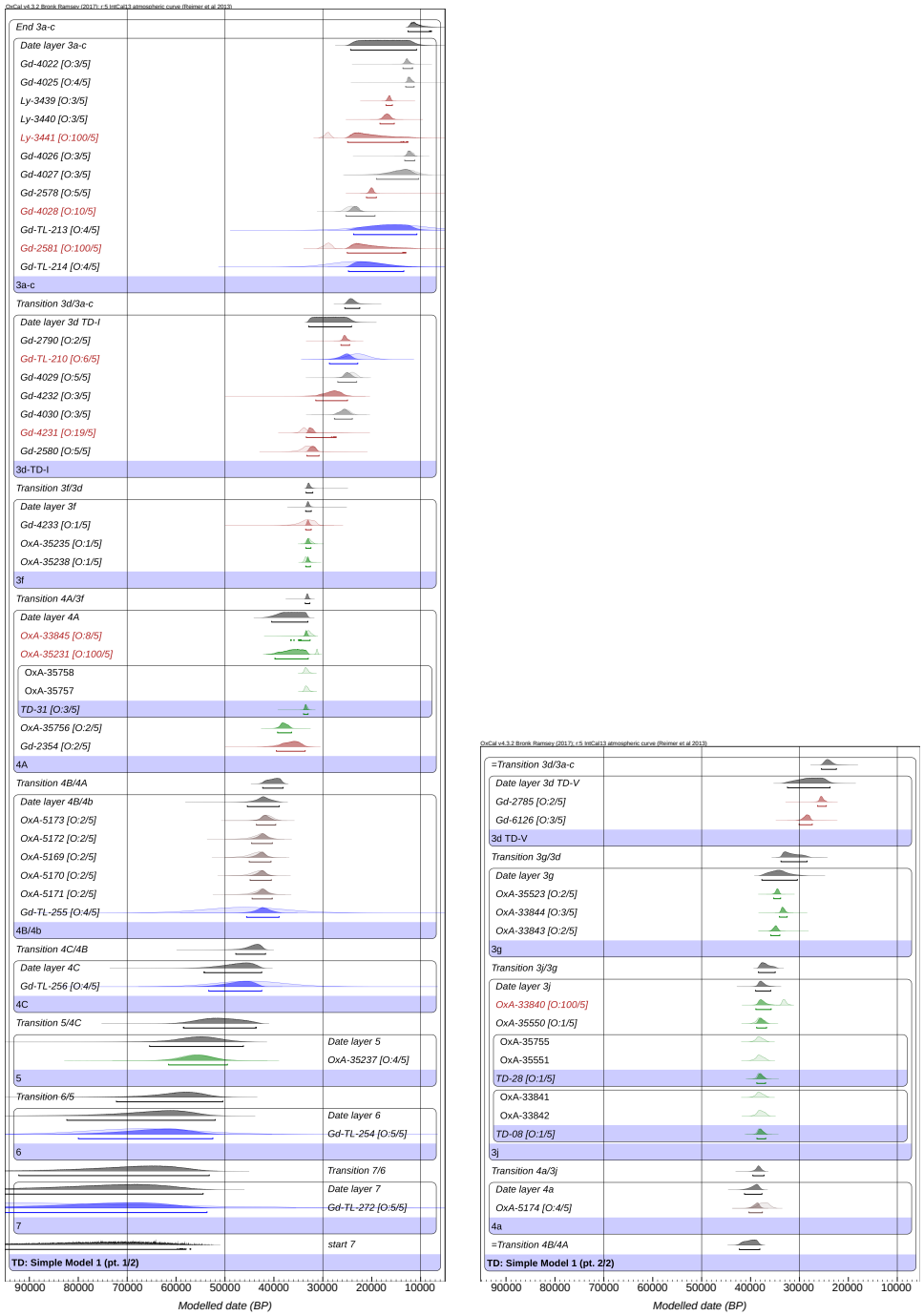


Figure 8.62: Temnata: stratigraphic model Simple 1 (code: p. 697), with combined layers and no greater than ages. Dates: **grey** – ^{14}C on charcoal; **brown** – ^{14}C on unmodified bone; **ebony** – AMS ^{14}C on charred earth (layers 4A, and 4B only); **green** – AMS ^{14}C on anthropogenically modified fauna; **blue** – TL on burnt flint; **black** – modelled ages. Date label of outliers ($> 5\%$) highlighted.

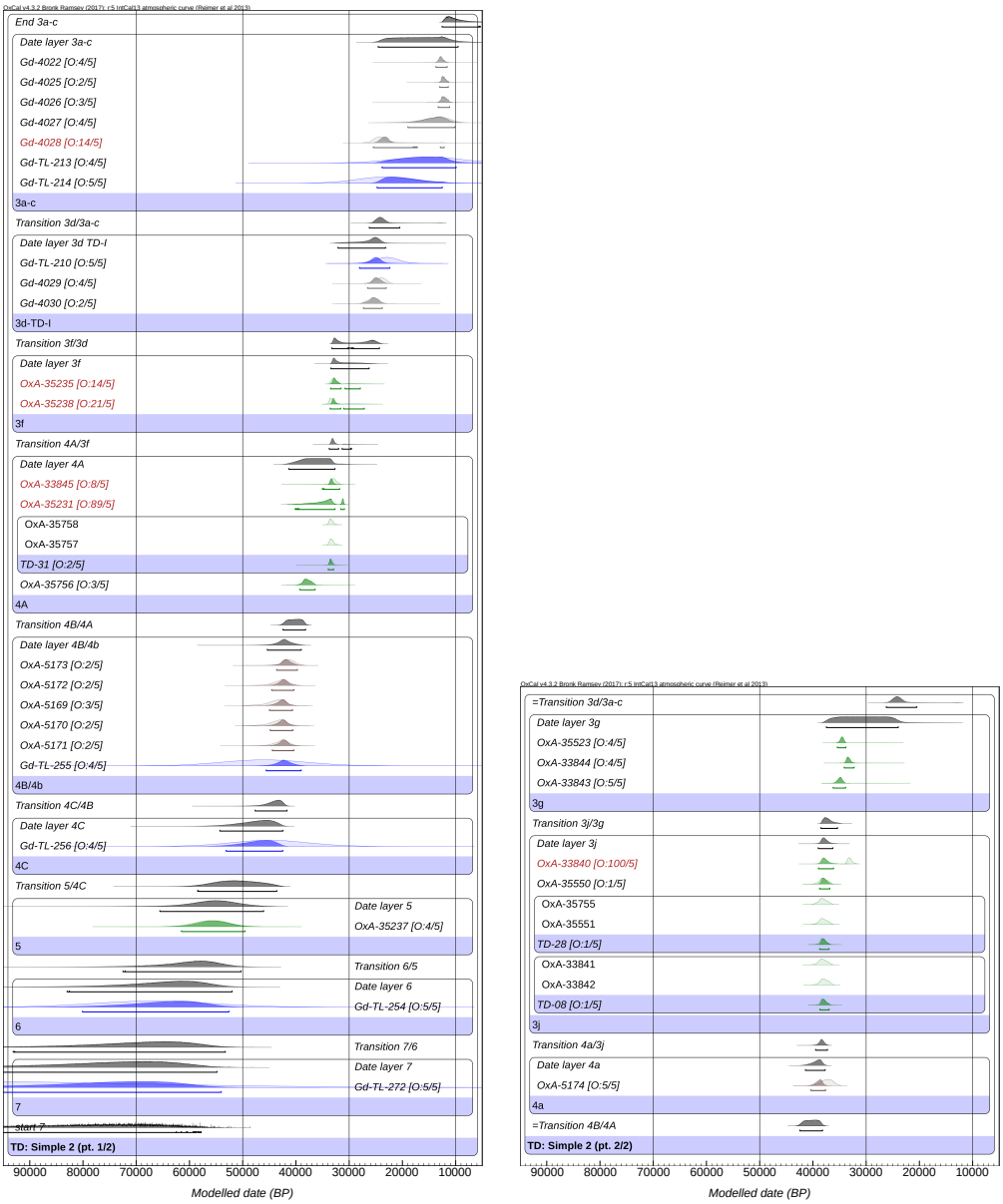


Figure 8.63: Temnata: stratigraphic model Simple 2 (code: p. 699), with combined layers, no greater than ages and no unmodified fauna. Dates: **grey** – ^{14}C on charcoal; **ebony** – AMS ^{14}C on charred earth (layers 4A, and 4B only); **green** – AMS ^{14}C on anthropogenically modified fauna; **blue** – TL on burnt flint; **black** – modelled ages. Date label of outliers ($> 5\%$) highlighted.

Model 6 uses the same dates and sequence structure as presented in models 4 and 5, without the `Phase` 3dw and its dates. The two sectors were connected at 6 boundaries: (1) the transition 7/6 from TD-I equates to the start `Boundary` of layer 6lg from TD-V, (2) the transition 6/5 from TD-I to the transition 6lg/5pg from TD-V, (3) the transition 5/4C in TD-I to the transition 5pg/4pg in TD-V, (4) the transition 4C/4B in TD-I to the transition 4pg/4b in TD-V, (5) the transition 4B/4A in TD-I to the transition 4b/4a in TD-V, and (6) the transition 3d/3a-c in TD-I to the transition 3d/3a-c in TD-V. The Phase 3dw was excluded as a third `Sequence`, because it over constrained the model, thus preventing it from running. Keeping the dates without the Phase would in turn meant giving up the important transition 3/3g. Despite these simplifications, the model has difficulties running and the results should be interpreted with caution. For modelling results see figure 8.61. Code listed on p. 695.

Simple 1 implements a simplified stratigraphy and a reduced dataset as more elaborate models seem to fail due to overly constrained conditions. It is comprised of two sequences. One holds the phases 7, 6, 5, 4C, 4B/4b, 4A, 3f, 3d (TD-I), 3a-c. The other holds the phases 4a, 3j, 3g, and 3d (TD-V) to account for the differences in layers and layer limits observed in sector TD-V. The sequences are connected at two points only, namely the transition `Boundary` 4B/4A provides the start `Boundary` for the second sequence, and the transition 3d/3a-c the end `Boundary`. The dates from transition zones, layer 3dw, and with greater than ages were excluded from the dataset. For modelling results see figure 8.62. Code listed on p. 697.

Simple 2 (no unmod. bone) runs the same model structure as Simple 1, but excludes radiocarbon dates on unmodified faunal remains from the dataset. As a result, layer 3d (TD-V) in the second sequence becomes unpopulated. For modelling results see figure 8.63. Code listed on p. 699.

KDE Models

The OxCal function `KDE_Model` was used to summarise three different radiocarbon datasets from Temnata. The purpose was to independently assess the structure of human activity observed and recorded during excavation. Especially in the light of post-depositional processes affecting the quality of the stratigraphic models, KDE analysis will be crucial to assessing different types of activity at the site, and might help to disentangle possible chronological origins for the archaeological material observed. The results are presented in figure 8.64.

KDE 0 contains the previously published radiocarbon dates on charcoals (including charred earth) and unmodified fauna that were deemed reasonably suitable for modelling (see tab. 8.11–8.12), n=26. Code listed on p. 701.

KDE 1 uses all new radiocarbon measurements, obtained on anthropogenically modified faunal remains (see tab. 8.16–8.18), n=24. It implements the uniform distribution up to 70k for greater than ages and the workaround described at the beginning of this section for OxA-35237. Code listed on p. 702.

KDE 2 reduces the dataset from KDE 0 to charcoal dates (including charred earth samples), as they have a higher likelihood of being directly connected to human activity at the cave, n=13. Code listed on p. 703.

KDE 3 combines the datasets used for KDE 1 and KDE 2 with the intent of capturing human activity related both to fire making and osseous work, n=37. It implements the uniform distribution up to 70k for greater than ages and the workaround described at the beginning of this section for OxA-35237. Code listed on p. 703.

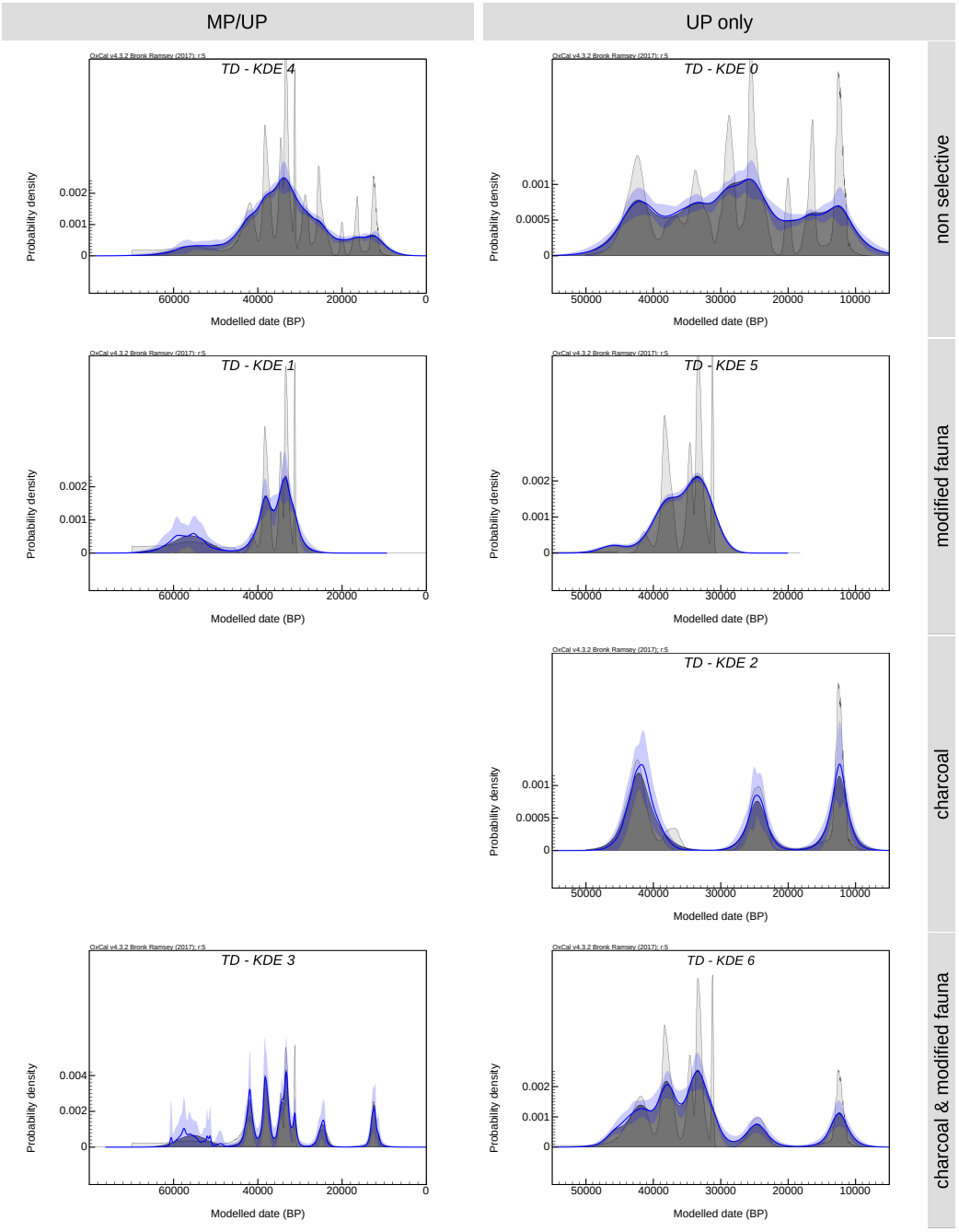


Figure 8.64: Temnata: KDE models listed according to dataset types and whether they cover the MP/UP transition (left) or only the UP (right). The right column usually excludes the dates for the MP layers 6 and 5, but otherwise shares the same data as the model to the left. The exception is KDE 4, which in addition to previously published dates (KDE 0) also includes all the new measurements. Code: p. 701.

KDE 4 runs all radiocarbon dates that were deemed reasonably suitable for modelling, i.e. combining the data used in KDE 1 and KDE 0, n=49. As with KDE 0, it shows any dated activity at the site, irrespective of human involvement. It is therefore likely to provide an insight into layer accumulation/sedimentation rather than into human presence or the age of lithics complexes. Code listed on p. 704.

KDE 5 implements the data used in KDE 1, while excluding any data from the MP layers, thus focusing on the UP only, n=19. It implements the uniform distribution up to 70k for greater than ages. Code listed on p. 706.

KDE 6 uses the same dataset as KDE 3, but excludes any data from the MP layers, thus focusing on the UP only, n=32. It implements the uniform distribution up to 70k for greater than ages. Code listed on p. 707.

8.4.4 Discussion

The original excavation documentation was not accessible. Therefore, it was not possible to consult it to see whether any of the samples had accidentally been mislabelled during excavation, cataloguing or later storage. However, the intensity and frequency of post-depositional disturbances (*e.g.* erosion, solifluction, cryoturbation, bioturbation) observed at Temnata suggest that dating outliers are to be expected and not indicative of archiving inconsistencies. As a result, the stratigraphic integrity will be assessed under the assumption that all sample context information is correct and outliers are the result of mixing, erosion and diffuse layer boundaries.

Model Outliers & Assemblage Integrity

The three stratigraphic models 0 (see fig. 8.55), 6 (see fig. 8.61) and Simple 1 (see fig. 8.62) had great difficulties to resolve all the constraints created by

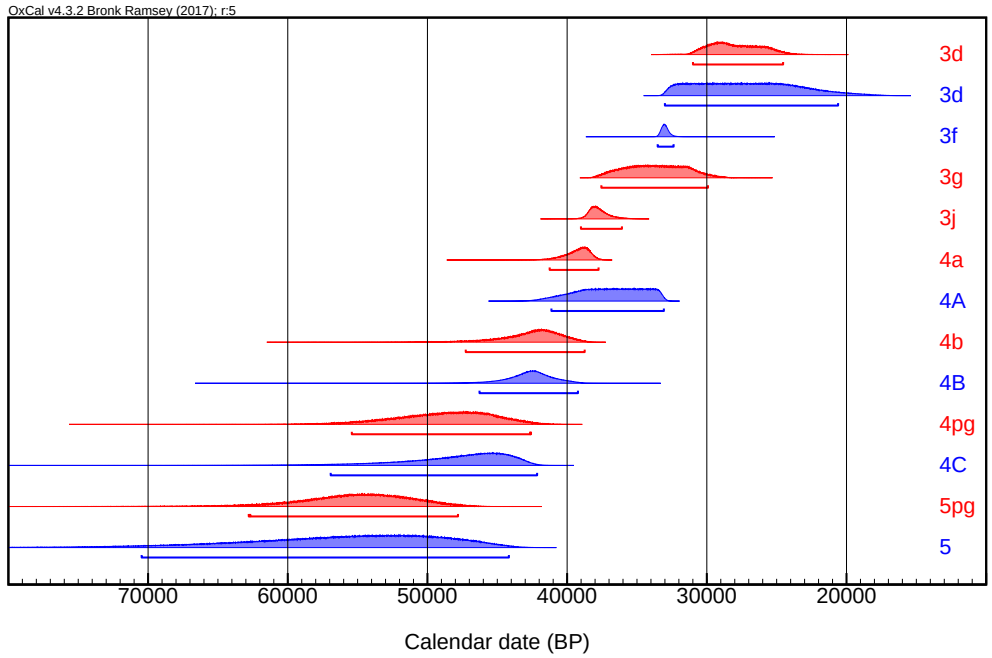


Figure 8.65: Temnata: comparison of modelled dates for layers 5 to 3d from Model 4 (**blue**), sector TD-I, and Model 5 (**red**), sector TD-V, showing the generally younger ages observed in sector TD-I.

the priors included in the models. Two main factors contributed: (1) the noise created by including dates on unmodified bone, and (2) the age discrepancy observed when comparing the stratigraphy of sectors TD-I and TD-V. The first can be demonstrated by models that exclude dates on unmodified fauna – but still connect both sectors. The stratigraphic models 1, 2 (see fig. 8.56), 3 (see fig. 8.57), and Simple 2 (see fig. 8.63) have no issues conforming to the constraints provided. Furthermore, dates on unmodified fauna are often identified as outliers by the models that include them. The second factor is illustrated by comparing the chronostratigraphy of sector TD-I with sector TD-V by means of Model 4 and 5 respectively.

The dates calculated by Model 4 and Model 5 for layers in TD-I and TD-V, respectively, show a lower precision for sector TD-I and probability distributions that extend to younger ages than observed in TD-V (see fig. 8.65). The most striking difference is observed in the date for layer 4A

compared to that for 4a. While the layers 3g–j are missing in TD-I, there are clearly samples contemporaneous with these layers observed in layer 4A, causing its Date's probability range to increase. This is likely the result of erosion caused by liquefaction, which might have led to the lighter sediment being washed out, while heavier material – such as bone – was left behind and became embedded in the soft, moist sediments of the underlying horizons.

The wide probability distribution for layer 3g is partially caused by the younger ages found in layer 3d as observed in sector TD-V, compared to those from 3d in sector TD-I. However, 3d from TD-V also includes a sample contemporaneous with layer 3f, which could mean that activity from 3f is partially also represented in 3g, but not identified as an independent layer.

When comparing the individual outliers identified by the stratigraphic models, two main categories can be distinguished: (1) greater than ages, and (2) diffuse layer boundaries.

The first case does not represent actual outliers. As a result of large uniform distributions, their modelled ages concentrate heavily on the younger side of the spectrum. Consequently, they sometimes get flagged as outliers probabilities $> 5\%$. Nonetheless, this remains within model fluctuations – rerunning the model will often reduce the likelihood just under the threshold.

The second category, however, represents post-depositional processes. As previously mentioned, dates on unmodified fauna frequently get identified as outliers, e.g. Gd-4231 and Gd-2580 from layer 3d, and Ly-3441 and Gd-2581 from 3a-c. All four show dates older than other samples from their layers, and more in line with the ages observed from just below – clearly demonstrating mixing of material at the interface. The outliers from layer 4A (OxA-33845, OxA-35231, and TD-31) demonstrate that the top of layer contains intrusive material from 3f above – maybe even from 3d or 3c, which are also sometimes found in direct contact with 4A. In layer 3j, OxA-33840 is always given a 100 % outlier probability. Its date clearly fits with 3g, and highlights the difficulty in distinguishing the layers in the complex 3g–j. And finally, TD-18 from 3dw is younger than the other two dates and fits

better with ages observed for 3d. This is not surprising, as 3dw designates the material similar in appearance to 3d, but containing volcanic material. Post-depositional processes in this area have caused visible layer boundaries to vanish.

It can, therefore, be concluded that despite post-depositional processes, the temporal sequence remains largely intact and consistent with TL measurements. As expected, TD-V appears better preserved than TD-I, and removing non-modified fauna results in a more consistent radiocarbon dataset. This can also be observed in KDE modelling, where removing data not directly connected to human activity sharpens the individual event peaks (see fig. 8.64).

Campanian Ignimbrite (CI) and the transition 3/4

As highlighted in figure 8.54, the calibrated radiocarbon age for the CI eruption overlaps with the radiocarbon probability distributions for 4A (TD-I), and 4a/3j (TD-V). Layer 3dw represents a subunit of 3 that contains volcanic material. It is in contact with layer 3d at the top and 4 at the bottom, and describes an area in which further divisions (*i.e.* 3g–j) were not possible during excavation. As a result, it is not surprising to find an overlap with the CI tephra age, though the sample in question is likely connected to the occupation represented by layer 3j.

This connection is consistent with the location of the tephra lenses found in sector TD-I, layer 4A (see south profile in figure 8.36). Minor amounts of tephra in 3f are likely resulting from mixing at the layer interface. Layer 3f significantly post-dates the CI eruption, therefore it is more probable that the inclusion of tephra occurred after erosion opened up layer 'v' to contact and mixing with the lower part of 3f.

The location of the tephra layer 'v' in TD-V (see profile in figure 8.38) also supports the dating evidence, as tephra is found most heavily in layer 4a and 3j. However, the tephra bands observed in the east profile – located

between 4 and 3j as well as above 3j – lead to the question of how the CI temporally relates to the human occupations. Three interpretations come to mind. Scenario 1 would see the eruption having occurred between the sedimentation of 4a and 3j, with the band above 3j resulting from tephra being washed out from higher up and redeposited on top of 3j. In scenario 2, the eruption would occur during sedimentation of layer 3f and other concentrations may have resulted from post-depositional processes. And finally, scenario 3 would assume that the CI tephra got deposited after 3j and some of its material seeped into cracks between layer 4 and 3j. This would explain the material dated at the top of 4a as intrusive.

The stratigraphic model 3-CI (see fig. 8.58) suggests a placement of the CI well within the `Date` calculated for layer 4A (TD-I). Model 4-CI (see fig. 8.60), on the other hand, identifies the CI as a possible outlier (10% probability) to 4A, because it expects the layer to be younger. This would contradict all three previously proposed scenarios. However, as discussed before, OxA-33845 and OxA-35231 (and possibly TD-31) seem intrusive to 4A, thus causing the models to underestimate the age of layer 4A and misinterpreting the contemporaneity of the CI tephra.

Model 5 (see fig. 8.59) – representing a more complete stratigraphic record of Temnata's occupations – provides a `Date` of 41300–37700 cal BP and for layer 4a, and 39050–36050 cal BP for layer 3j (at 95% prob.). When compared to the calibrated radiocarbon age for the CI (39050–38450 cal BP), it can be shown that the tephra layer predating the occupation in 4a is doubtful, albeit not impossible, while it post-dating the occupation in 3j becomes improbable.

More clarity is provided by the model KDE 3 (see fig. 8.66). Here, the human occupations seems to either start or immediately follow the CI eruption. Taking the erosion of the top of layer 4, as well as tephra concentrations, into account, it can be concluded that the most feasible original positions are between layer 4 and 3j, or within 3j (*i.e.* scenarios 1 or 2). It is not unreasonable to think that the use of the cave at that time was a reaction to the CI eruption and the following climatic conditions – especially in the light of

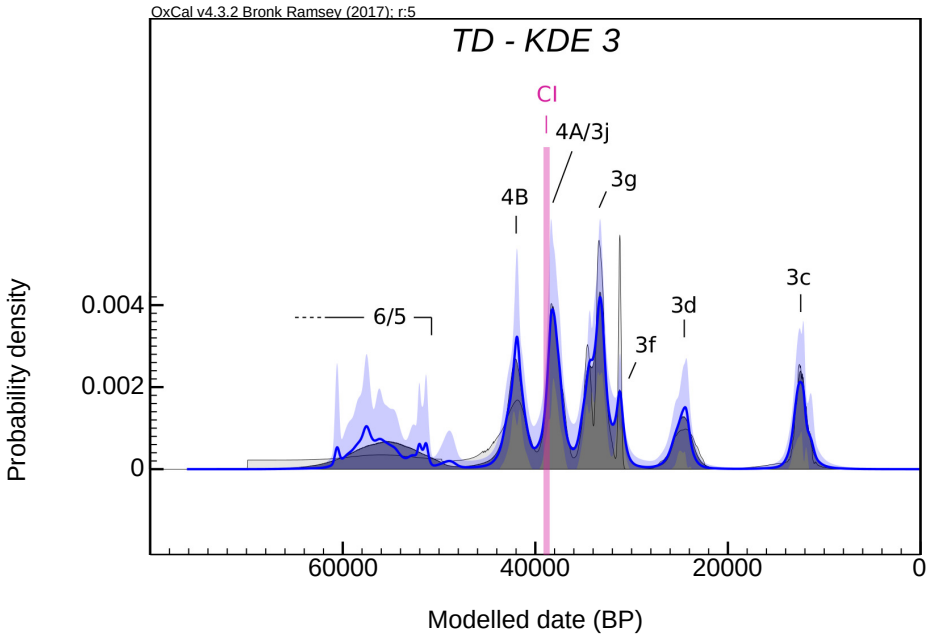


Figure 8.66: Temnata: KDE 3 model results with peaks labelled with possible corresponding stratigraphic layers. The CI tephra age (**magenta**) is superimposed to illustrate how the eruption either just predates the occupation in 3j, or is contemporaneous with it.

occupations coinciding with colder and less stable climate phases, as already observed by Marambat (1992).

Model Results & Human activity

The KDE model (see fig. 8.64) results visualise unspecific activity at the site (KDE 0 and KDE4), human activity in general (KDE 3, KDE 6), human activity leaving traces on osseous material (KDE 1, KDE 5), and those involving fire (KDE 2).

KDE 2 identifies a minimum of three distinct periods of fire making at Temnata, coinciding with the three main hearth bearing UP units: layer 4, 3d and 3a-c. They seem to further correspond to periods with more diverse lithic material, thus representing more intensive habitation. At the same time, KDE 1 and KDE 5 suggest a cave use intensive enough to leave

traces on faunal fragments throughout the 'EUP/Balkan Aurignacian', also independent of the dated fireplaces. It would be interesting to see whether the fireplaces corresponding to these habitations are located elsewhere in the cave. The absence of anthropogenically modified fauna from 3a-c in the model is a result of targeted sample selection.

When removing material not directly connected to human activity (KDE 3 and 6), a minimum of 7 activity or occupation events can be identified. They largely correspond to the dated stratigraphic units 6/5, 4B, 4A/3j, 3g, 3f, 3d and 3a-c, while the shoulder on the left slope of the 3g peak might reflect the different activity units in the package 3g-i. It is interesting to note that occupations seem discrete, with a focus on colder, less stable climates (see also Marambat, 1992). This pattern is consistent with all major Palaeolithic cave sites being situated on the northern side of the Stara Planina, where more continental climate would have causes larger temperature variations.

A shift in sedimentation is observable during the 'EUP' period (see fig. 8.67). There is a significant increase in anthropogenically modified fauna – both dated and undated – found in the geological unit 3 compared to previous layers. However, when separating the bone fragments according to the lithic interpretation of the associated layer, it can be demonstrated that most of that increase occurs during the 'EUP/Aurignacian' (*i.e.* layers 4–3g), and is largely localised to TD-V. Consequently, it can be assumed that substantial amount of archaeological evidence was washed out of the cave, affecting the western side of the antechamber more than the eastern area. But more importantly, this demonstrates cultural continuity during periods of changing environmental conditions. As already observed by (Giaccio et al., 2008), the 'EUP/Aurignacian' cultural expression arrived at Temnata prior to the CI eruption.

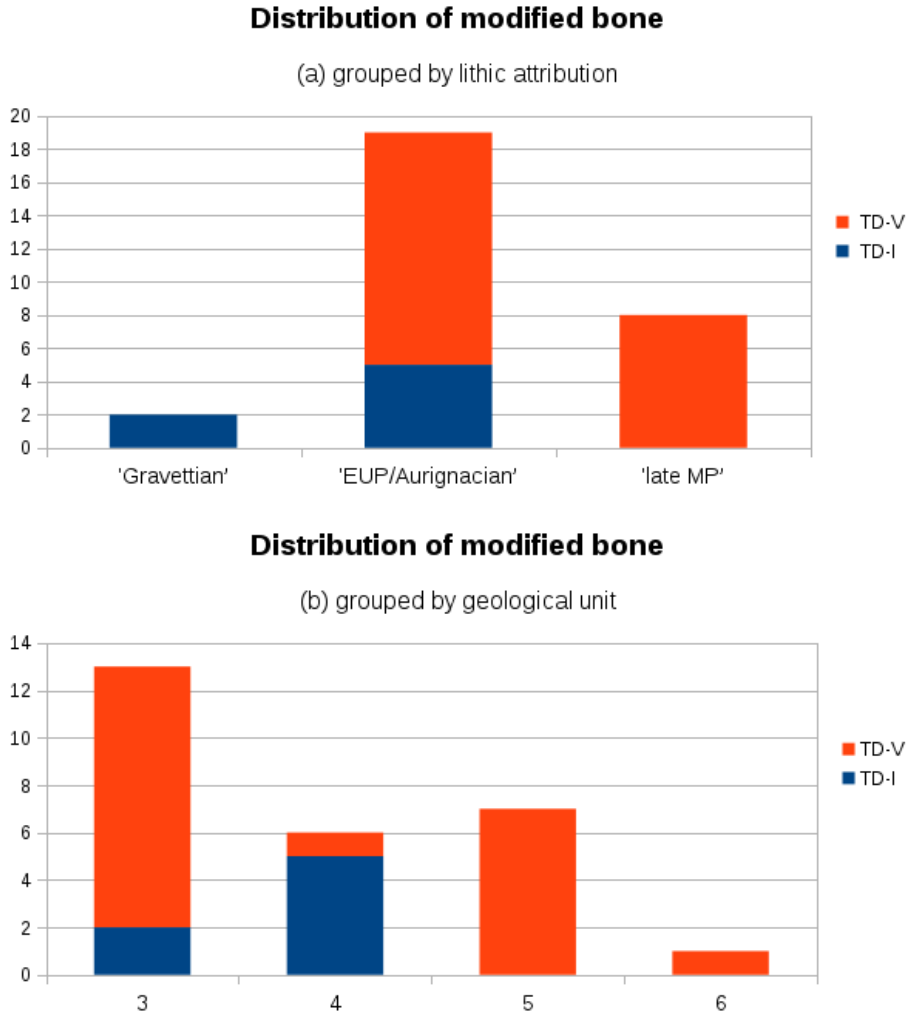


Figure 8.67: Temnata: distribution of anthropogenically modified bone (dated and undated) identified during this dating project. Original sample context information was used to group the fragments according to (a) the layers' lithic attribution, or (b) the geological unit the samples were found in. Number of faunal fragments indicated on the y-axis. 'Gravettian' = layer 3d; 'EUP/Aurignacian' = layers 3g–4; 'late MP' = layers 5–6.

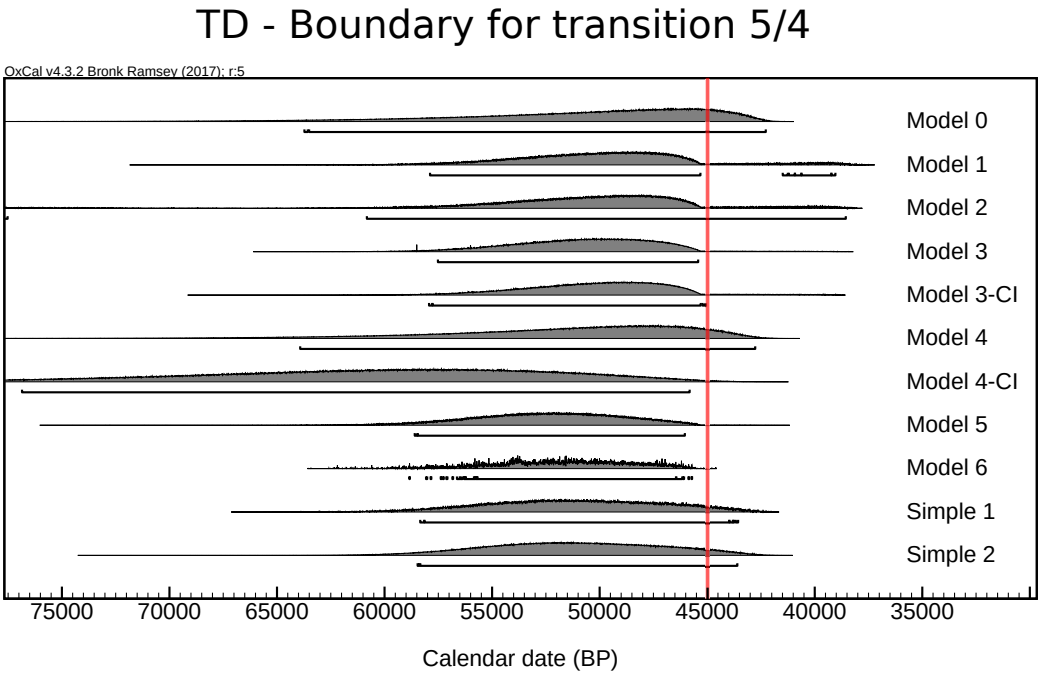


Figure 8.68: Temnata: comparison of boundaries for the transition 5/4 calculated by the different stratigraphic models, and demonstrating a start of UP industries by 45k cal BP (marked **red**) the latest.

Model Comparison & the MP/UP transition

A comparison of transition boundaries calculated by the various stratigraphic models shows generally low precision and some variability between the results obtained by different models. Nonetheless, they provide vital information for the MP/UP biocultural shift.

Of most interest to this research, is the transition between layer 5/5pg and 4, which is visualised in figure 8.68. Despite the differences observable, they all demonstrate that the transition between MP layers to UP layers at Temnata occurred before 45k cal BP. The most reliable models for sedimentation chronology are models 4 and 5 (see fig. 8.59), as they make use of all available age data and provide higher resolution by focusing on the two dated sectors independently. In contrast, the models best reflecting human activity probably are Model 3 and Model 3-CI (see fig. 8.57 and 8.58). This firmly places the start boundary for layer 4 prior to 45k cal BP.

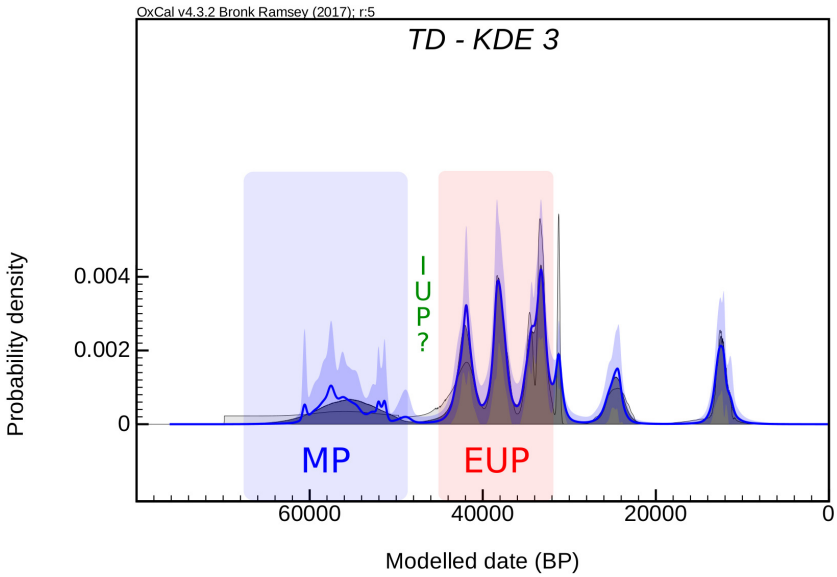


Figure 8.69: Temnata: peak attribution in KDE 3 according to samples' find locations. MP corresponds to the Middle Palaeolithic layers 6 and 5/5pg. EUP corresponds to the Early Upper Palaeolithic layers 4, 3j, and parts of 3g, which were identified as containing EUP industries possibly connected to the 'Aurignacian'. In sector TD-II, and IUP industry was found in layer VI, that might fit chronologically in the gab observed between MP and EUP.

This is consistent with results from KDE modelling, which predict an increase in activity at that time for all models (see fig. 8.64). The models KDE 1, 3, 5 and 6 further demonstrate that this is also true when focusing on human activity only.

This allows for an age estimate of layer VI from TD-II, which could not be directly dated for this project. The layer is clearly older than the CI eruption, as evidenced by the tephra containing layer superposing it. Consequently, it has to be at least contemporaneous or older than layer 4B. However, the lithics found in 4B do not suggest a continuation of the tradition observed in layer VI, nor indicate the lithics found in layer VI a contemporaneity with the material found in layer 6. This places VI in the period between the Middle and Upper Palaeolithic layers, which is currently bare of any dated human activity (see fig. 8.69), albeit an overlap with layer 5pg cannot be excluded.

Conclusion

Despite significant post-depositional processes, it can be concluded that AMHs started frequenting Temnata cave by or shortly after 45k cal BP (see fig. 8.69). They would have left behind a distinctly early Upper Palaeolithic blade industry, which shares numerous similarities with western European 'Aurignacian' complexes, albeit lacking most of the diagnostic artefacts. This is a phenomenon not uncommon at eastern European sites, including at many presented in this thesis (*e.g.* Kozarnika, layer 5c). This may indicate that Early Aurignacian or Proto-Aurignacian technocomplexes are not suited to trace the movement of the earliest AMH into Europe.

If the lithic assemblage found in layer VI, sector TD-II, is indeed genuine, it could be evidence for the IUP at Temnata. Lithic technology and stratigraphy suggest an age predating layer 4, yet post-dating layer 6, leaving a time window ranging between *ca.* 50–45k cal BP (see fig. 8.69). IUP industries are associated with AMH skeletal remains in, *e.g.*, Ksâr 'Akil in Lebanon (Bosch et al., 2015). As a result, the arrival of AMH at Temnata could be even earlier than calculated by current KDE models, and Neanderthal presence might have ended already at around 50k cal BP.

8.5 Toplja

Toplja cave is a Palaeolithic site, whose disturbed horizons have provided some remarkable osseous artefacts. From these, this project focused on re-contextualising the osseous spear point.

8.5.1 Introduction

Toplja Cave is located 6 km south-east of Goliama Jeliazna (Голяма Желязна) and on the right bank of the river Toplja (Топля). The cave has

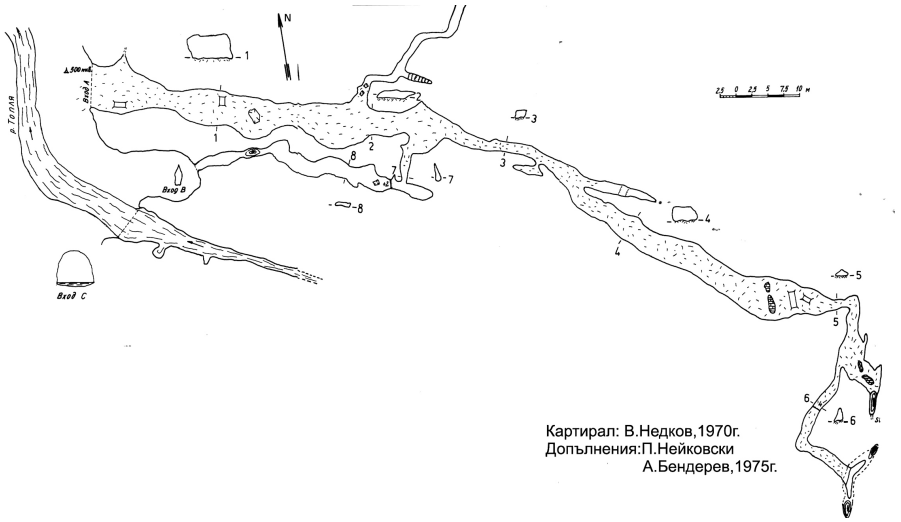


Figure 8.70: Toplja: map showing cave, including 8 cross-sections, and nearby river Toplja (drawn by V. Nedkov in 1970, with amendments by P. Neykovski and A. Benderev ifrom 1975).

two entrances (one opening to the north-west, the other to the west) and encompasses a total length of 283 m (figure 8.70).

Already at the end of the 19th century, archaeological research found material dated to the Palaeolithic and Bronze Age. In 1981, a team led by N. Sirakov (Н. Сираков) made three sondages to investigate the stratigraphy. They found that all stratigraphic units had been disturbed by 'treasure hunters', leaving the few lithic and osseous artefacts found without secure context.

One of the recovered osseous artefacts was a *pointe de sagaie* (spear point). Using the limited information available from the other remains, it could be concluded that the antler point was likely of Palaeolithic age. Direct radiocarbon dating is the only means to better understand its chrono-typological position and possible relationship to early osseous point industries. Consequently, the artefact was included within the subproject of dating Palaeolithic osseous points.

8.5.2 Radiocarbon dating

Sample & Treatment

The single osseous spear point from Toplja stored at the Historical Museum in Lovech was selected for radiocarbon dating. A substantial sample of 620 mg was drilled in February 2017 using the key-hole technique. The powder sample was subsequently treated with solvent wash steps (acetone, methanol, chloroform) to allow for extra flexibility in pretreatment protocol continuation according to gelatine yield.

Tp-01 The point was extracted from deer (*Cervus elaphus*) antler by double grooving. The surface was subsequently prepared using scraping and abrasion techniques. The point is broken into two fragments of nearly identical length. On the distal part there are strong traces of scraping and flaking. The former is most likely intentional, the latter damage. Furthermore, that fragment shows significant amount of surface distraction, probably caused by bacteria. The proximal fragment has a split base. However, on the basis of shape, size and manufacturing technique, the antler point does not fall into the category of 'split-based-points' associated with the Aurignacian. The internal part of the point shows the spongiosa preserved over the total length of the artefact and discolouration indicates that the entire point had been heat treated. The artefact is preserved over a length of 247 mm. The proximal fragment has a diameter of 15.5 mm, the distal 12.5 mm.

The proximal fragment of the precious artefact was sampled at the break using the key-hole drilling technique. This allowed for optimal access to sample material, while preserving the appearance of the artefact. The point showed signs of possible surface conservation, thus special care was given to cleaning the sample area by abrading the outer surface.

Results

The sample fully dissolved during ABA treatment, despite the promising %N result of 3.97, and could not be radiocarbon dated.

Table 8.19: Toplja: Radiocarbon dating pre-treatment results for antler point.

Ref-no.	Inv.-no.	Layer	Weight	Conserved?	%N	Treat.	Yield
Tp-01	779	Palaeolithic	620 mg	Y	3.97	AG*	0.00

8.5.3 Discussion

Unfortunately, the antler point from Toplja could not be dated due to a lack of collagen preservation. This may have been induced by heating of the artefact during or after manufacture.

In the absence of a secure archaeological context and a direct radiocarbon date, it is impossible to know how old the artefact is and whether it is at all connected to the advance of AMH in Europe. If the lithic remains and osseous tools found at the site are indeed chronologically contemporaneous, the point would clearly belong to the Upper Palaeolithic. Nonetheless, caution is advised. The limited stratigraphic integrity of the site could lead to the association of material from vastly different time periods.

Considering the round cross-section, the point might belong to the Gravettian or younger periods. It cannot be excluded, that the artefact might be connected to the cultural development of osseous points observed at nearby Tabashkata (presented in section 8.3).

Chapter 9

Serbia

The archaeological record for the Middle to Upper Palaeolithic in Serbia is sparse – despite its geographically strategic position. Proposed explanations include (a) fewer archaeological investigations, (b) less intensive occupation, (c) different nature and character of occupation or location, and (c) a loss of the settlement record. As an intensification in Palaeolithic research has resulted in the discovery of numerous new sites, it is expected that a more comprehensive occupation pattern will develop in the future. However, the presently known sites show significantly less intensive occupations than what is regularly observed in France and Spain, as well as on occasion in neighbouring Bulgaria. Therefore, factors b–c remain equally relevant. In the following, some of the sites frequently found in the literature are discussed and the site selection for this project is presented.

The only Palaeolithic human skeletal evidence from Serbia so far was found at Mala Balanica. However, U/Th dating places the bone at 113 +72/-43 ka (Roksandic et al., 2011), and thus before the critical period of the MP/UP biocultural shift.

Šalitrena Pećina was long thought to be the only known site with a stratigraphy covering the MP/UP. It contains Balkan Mousterian with side scrapers, Mousterian points, and Levallois artefacts, but also leaf-point industries. The Aurignacian material differs from material usually found in the region.

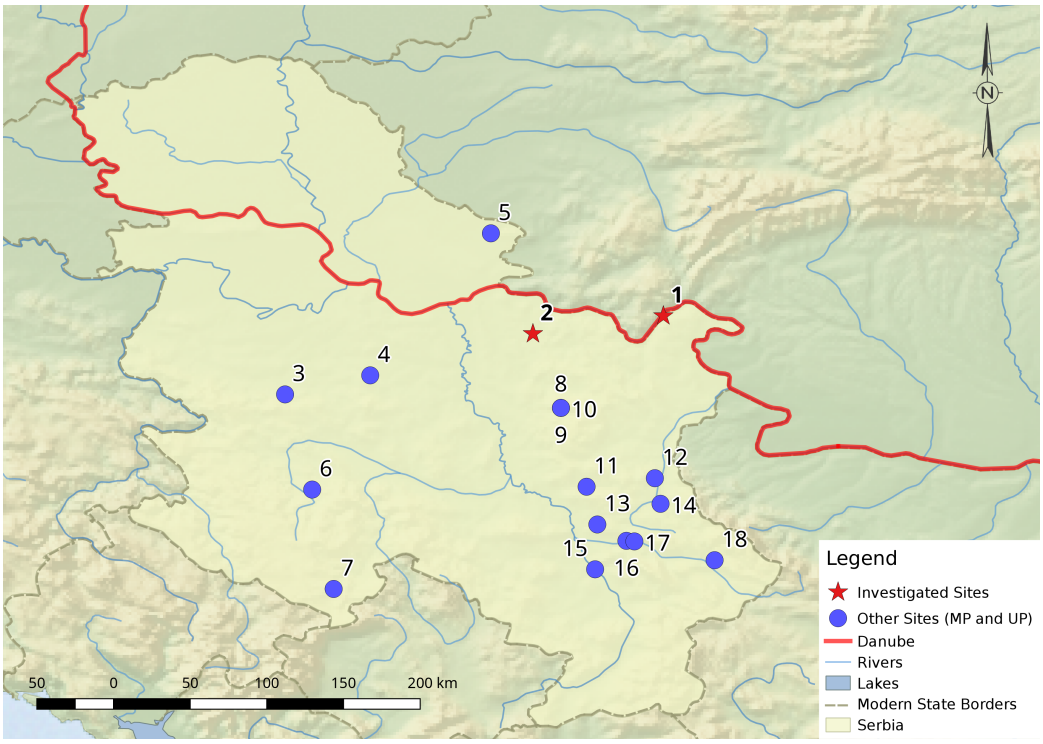


Figure 9.1: Serbia: map of evaluated Middle and Upper Palaeolithic sites: (1) Tabula Traiana, (2) Dubočka Kozja, (3) Šalitrena Pećina, (4) Risovača, (5) Crvenka-At, (6) Hadži Prodanova, (7) Smolućka, (8) Bušna cave, (9) Orlovača, (10) Bukovac, (11) Milušinačka pećina, (12) Selačka 3, (13) Meča Dupka, (14) Baranica Cave (15) Pešturina, (16) Mala & Velika Balanica, (17) Donja pećina, and (18) Kozja pećina.

Marín-Arroyo and Mihailović (2017) connected the numerous carinated endscrapers, burins, retouched and unretouched bladelets to the Early Aurignacian as seen in central Europe. In addition, osseous points were uncovered at the entrance, and typical Aurignacian long blades and endscrapers on blades were found in the cave interior. Initial dating was already ongoing when this thesis started, and its results place the Aurignacian at around 30k BP, and the Mousterian layers as young as 36/37k BP (Marín-Arroyo and Mihailović, 2017). These dates will be further discussed in chapter 15.

Another site with possible late Mousterian occupations is Pešturina. ESR dating resulted in age ranges from 102 ± 5 to 39 ± 3 ka (Blackwell et al., 2014). The site appears to be well suited for radiocarbon dating, as it re-

vealed several stratified occupations and a reasonably sized faunal assemblage. However, radiocarbon results published by Alex and Boaretto (2014) showed large variability, which is indicative of post-depositional processes affecting the sequence. Similar results were obtained for the Mousterian site of Hadži Prodanova (Alex, 2016). By contrast, all Mousterian occupations at Smolućka were beyond the limit of the radiocarbon dating technique (Alex, 2016).

Recent intensive investigations in south-eastern Serbia have recovered several traces of MP and/or UP human activity. Unfortunately, several reasons make them presently unsuitable for larger radiocarbon investigations. Velika and Mala Balanica have no EUP industries – neither IUP nor Aurignacian. Their assemblages are restricted to early Mousterian and Gravettian/Epigravettian evidence. The EUP industry at Velika pećina and Baranica is undiagnostic. Kozja pećina has very poor bone preservation, while at Donja pećina osseous remains are inexistent. At other sites, such as Meča Dupka and Milušinačka pećina, the complexity of the stratigraphy, or the limited number of artefacts prevent chrono-cultural conclusions from being drawn (see Kuhn et al., 2014).

The closest known upper Palaeolithic site to Peștera cu Oase is Crvenka-At in the Serbian Banat. The multi-occupational site regrettably contained no datable organic remains – something frequently observed for open-air localities. This lead Chu et al. (2014, 2016) to collect luminescence samples instead, and conduct minor excavations as part of the research project "Our way to Europe". The dating results are presently outstanding.

Possible Dufour bladelets (*e.g.* at Selačka 3, Orlovača) indicate that diagnostic artefacts are not entirely absent – despite the difficulties of finding EUP evidence (see *e.g.* Dogandžić et al., 2014; Kuhn et al., 2014). Future excavations might still reveal sites well suited to chronometric modelling. In the meantime, this dissertation focuses on the two ongoing excavations at Tabula Traiana and Dubočka-Kozja. Both sites contain stratified MP and possible EUP occupations, a rich faunal assemblage, and are located in the critical area of the Danube Gorge, close to where the early AMH skeletal

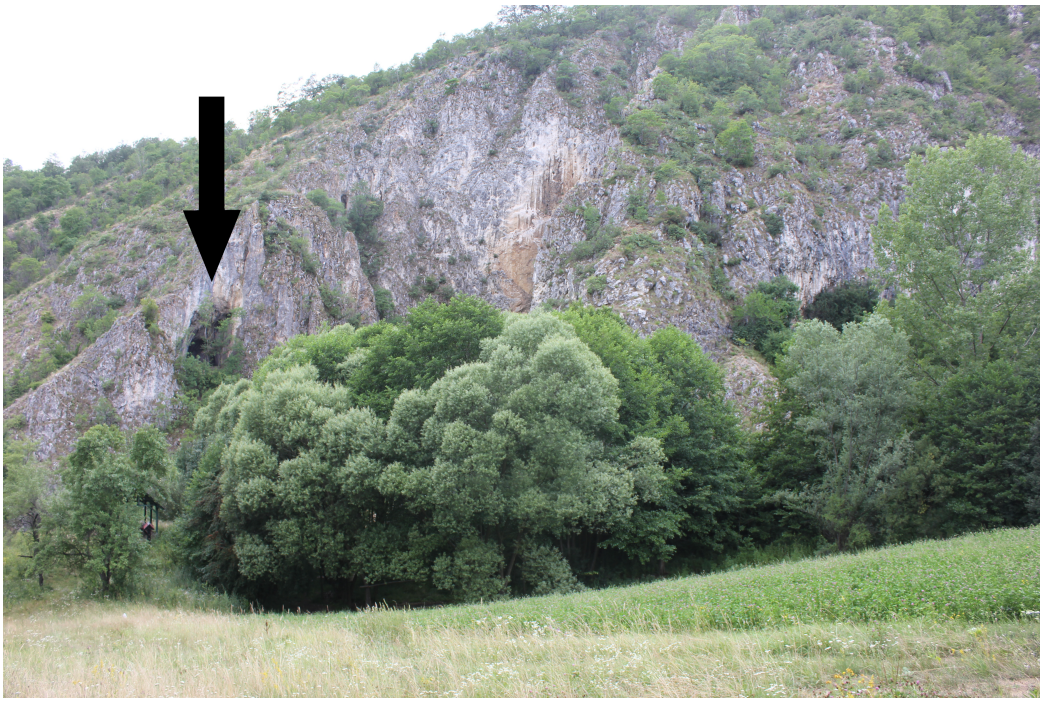


Figure 9.2: Dubočka Kozja: cave location marked by arrow (photo: D. Borić).

remains from Romania were found (*i.e.* Peștera cu Oase, Cioclovina Cave, and Muierii Cave).

9.1 Dubočka-Kozja

9.1.1 Introduction

Dubočka-Kozja Cave (44°32' 44.0" N, 21°46' 08.4" E) is a cave site located in the municipally of Dubočka in the east of Serbia, approx. 5 km from the Danube, and close to the source of the Ponor River. The cave entrance (approx. 6 m wide, 10 m high) faces east, with a single gallery extending west for approx. 15 m (see figures 9.2-9.3).

In 2013, D. Borić and his team excavated a surface of 4 m^2 (trench 1/2013) and uncovered two main Pleistocene lithographic units. Although the volume excavated was limited, the site yielded larger lithic assemblages than the

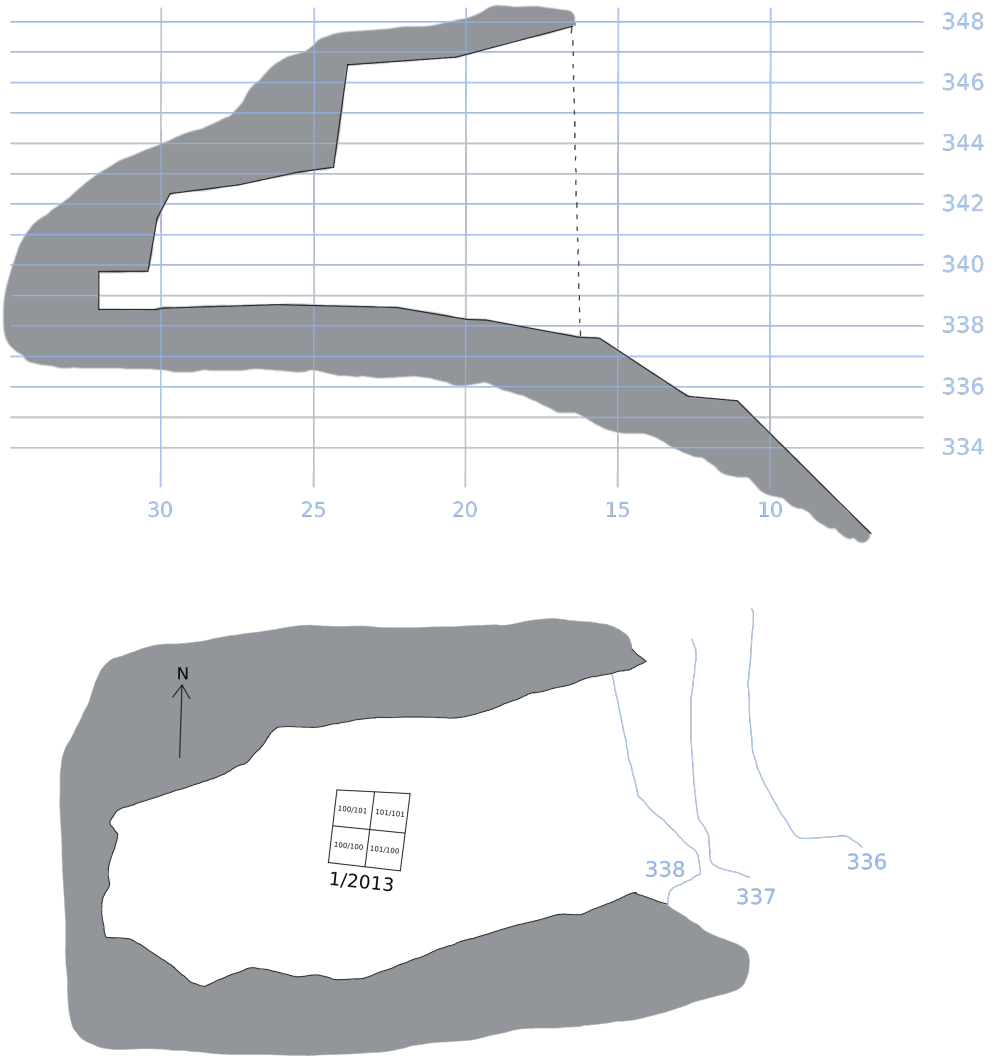


Figure 9.3: Dubočka Kozja: Top – Vertical cross-section through cave length. Vertical numbers: Altitude (m a.s.l.); Horizontal numbers: distance form Danube in m. Bottom – Horizontal cross-section through cave with excavation trench and squares, and elevation (m a.s.l.) marked (illustrations: R. Hopkins, based on plans provided by D. Borić).

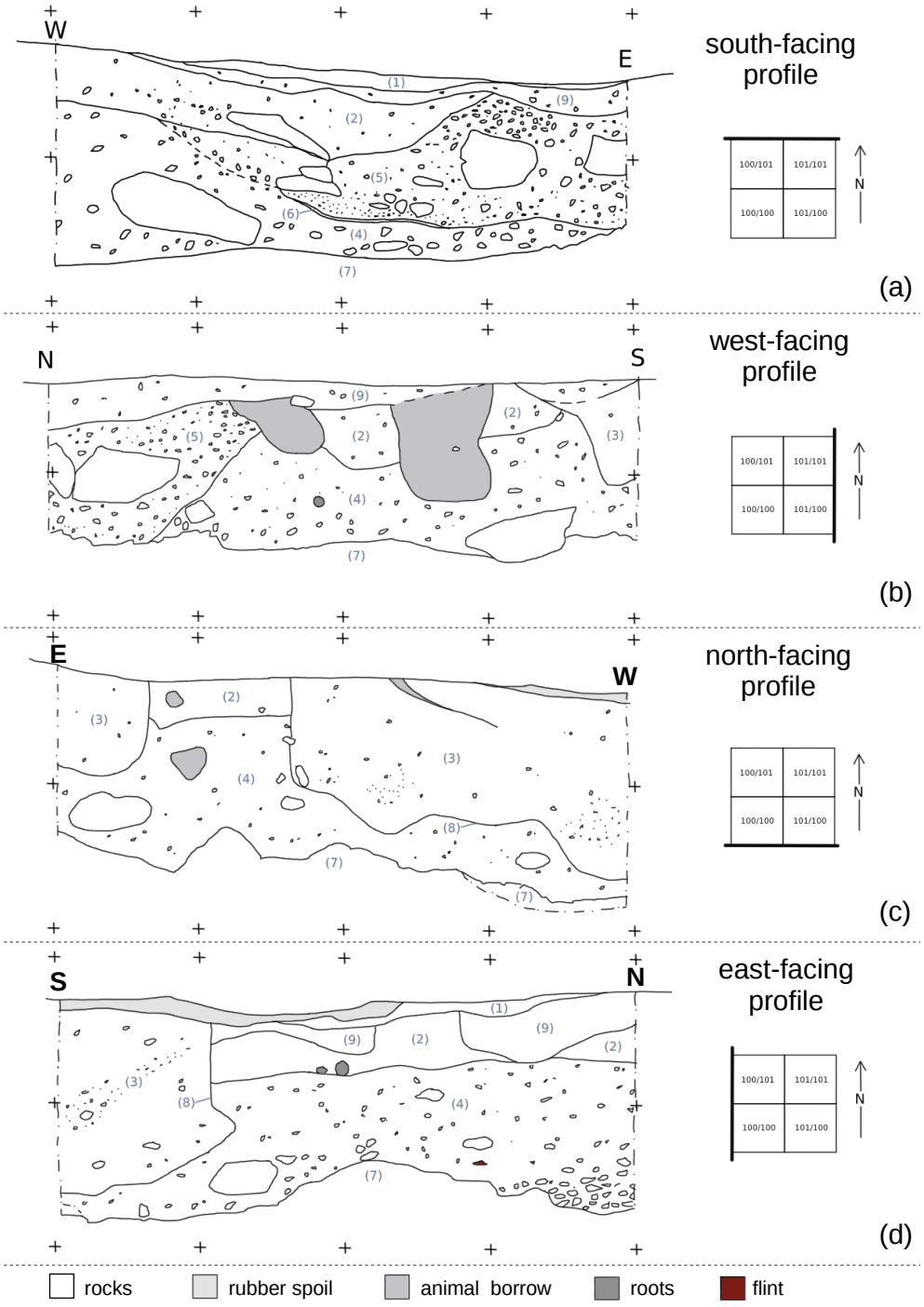


Figure 9.4: Dubočka Kozja: profile drawings from trench 1/2013 showing quadrant location and layer identifications. Crosses mark 50cm intervals (illustrations: R. Hopkins after original excavation documentation by D. Borić).



Figure 9.5: Dubočka Kozja: top – drawings of lithics found in (b, g) layer 2 (b, g), layer 3 (i), layer 4 (c–f, h, k), and layer 5 (a). bottom – photos of lithics found in layer (4) and (5) showing Levallois technology (illustrations & photos: D. Borić).

nearby site of Tabula Traiana (see section 9.2) and suggests the site was visited in the Middle Palaeolithic, Upper Palaeolithic, and again during the Neolithic.

The excavated material was separated according to geological units (given numbers in brackets) as well as spits (counting continuously from top to bottom). The geological units 1 and 9 were believed to be Holocene units (see profiles in figure 9.4). Layer 2 was attributed to the Upper Palaeolithic on the basis of flint with laminar characteristics and the absence of pottery. Unit 3 marks an "intrusional deposit due to illicit digging" (D. Borić., pers. comm. 07/12/2017), which may contain Middle and Upper Palaeolithic artefacts. Both layers 4 and 5 were tentatively seen as Middle Palaeolithic or



Figure 9.6: Dubočka Kozja: left – tooth pendant from layer 2, spit 3 (photo: R. Hopkins). Right – faunal bone fragment with cut marks from layer 4, spit 3, previously dated to 25370 ± 200 BP (OxA-28687) (illustration: R. Hopkins, photo: D. Borić, macrophoto: E. Cristiani.).

'transitional' based on the presence of Levallois technology (see figure 9.5). In addition, non-archaeology bearing units include layer 6 (a thin deposit between layers 4 and 5), layer 7 (bedrock), and layer 8 (interface between the disturbance 3 and the geological unit 4). The stratigraphy is further complicated by intruding animal borrows and roots.

Special mention should be made of a tooth pendant found in layer 2, spit 3 (see figure 9.6). Furthermore, a bone fragment showing several cut marks was discovered in layer 4, spit 3 – close to the interface with layer 2 – and gave a radiocarbon age of 25370 ± 200 BP (OxA-27861) (D. Borić., pers. comm. 07/12/2017).

9.1.2 Radiocarbon dating

Material & Treatment

In September 2016, the organic material from the 2013 excavation season was checked for anthropogenic modifications. In an initial sorting, 1 artefact and 39 samples with possible cut and chop marks were separated. From these, 6 specimens with clear, and 4 with likely anthropogenic, marks were identified

Table 9.1: Dubočka Kozja: List of anthropogenically modified faunal remains identified with original cultural interpretation. z – given as hight in m a.s.l. White rows – clear anthropogenic modifications; grey rows – marks (likely anthropogenic). * – for issues on cultural attribution see text.

Ref-no.	Inv.-no.	Layer	Arch.	x(m)	y(m)	z(m)	Weight	Conserved?
DK-01	x.9	(2), spit 3	UP*	997.58	996.64	3287.80	110 mg	N
DK-03	bag 4	(5), spit 5	MP/trans.	–	–	–	927 mg	N
DK-06	bag 93	(2), spit 2	UP*	–	–	–	768 mg	N
DK-08	bag 72	(1), spit 1	Holocene	–	–	–	778 mg	N
DK-09	bag 52	(4), spit 5	MP/trans.*	–	–	–	–	N
DK-17	bag 273	(3), spit 5	disturbed	–	–	–	799 mg	N
DK-17	bag 273	(3), spit 5	disturbed	–	–	–	835 mg	N
DK-20	bag 175	(4), spit 4	MP/trans.*	–	–	–	–	N
DK-24	bag 86	(4), spit 3	MP/trans.*	–	–	–	–	N
DK-32	bag 28	(4), spit 4	MP/trans.*	–	–	–	641 mg	N
DK-36	bag 277	(4), spit 5	MP/trans.*	–	–	–	–	N
DK-39	bag 424	(4), spit 8	MP/trans.*	–	–	–	759 mg	N

(see table 9.1). Finally, 7 samples were selected for initial dating to keep sample size small while covering as many units as possible.

The tooth pendant (DK-01) was sampled using the key-hole drilling technique and, considering the small sample size, was treated with ABA only (see section 5.4.5). In contrast, the remaining samples were crushed to powder with an iron mortar (see catalogue A.3) and treated with the ultrafiltration protocol (see section 5.4.6). Two separate fractions were taken from sample DK-17 as part of the ORAU quality control protocol[1].

^{14}C Results

Bone preservation at Dubočka Kozja seems to be generally good. Of the 40 samples initially collected, only two (DK-11 and DK-23) failed initial %N testing. All pre-treated samples were successfully dated as large graphites of 1.8 mgC (see table 9.2). Apart from the tooth pendant (DK-01), all samples were ultrafiltered and yielded collagen in the range of 1.74 wt.% to as much as

[1]Samples with a P-no dividable by 20 get dated twice to check dating reliability.

Table 9.2: Dubočka Kozja: previously obtained (grey) and new (white) AMS radiocarbon results on anthropogenically modified faunal remains from the 2013 excavation season with archaeological context information, and pre-treatment results. Ref-no. = number given to the sample for the purpose of this project. Inv.-no. = Inventory number given to the sample on excavation. Layer = layer attribution. %N = nitrogen weight content before chemical pre-treatment. Treat. = Pretreatment protocols used: AG = ORAU acid-base-acid pretreatment, AF = ORAU ultrafiltration protocol (see section 5.4 and Brock et al., 2010b). Yield = sample left after chemical pre-treatment (both in mg and wt.%). %C = carbon yield on combustion. C:N = carbon to nitrogen ratio of combusted collagen sample. $F^{14}C$ = fraction modern carbon. ^{14}C (BP) = conventional radiocarbon age Before Present with 1σ error. Date (cal BP) = calibrated radiocarbon age at a 95.4% confidence interval, calculated in OxCal 4.3 (Bronk Ramsey, 2009a) using IntCal13 (Reimer et al., 2013).

Ref-no.	Inv.-no.	Item	Trench	Sq.	Layer	Depth (cm)	%N	Treat.	Yield (mg)	Yield (wt.%)	%C	$\delta^{15}N$	$\delta^{13}C$	C:N	Lab-no	$F^{14}C$	^{14}C (BP)	Date (cal BP)
DK-01	x.9	tooth pendant	1/2013	100/99	(2), 3	388	2.78	AG	3.77	3.41	39.7	8.0	-22.2	3.1	OxA-35584	0.57424 ± 0.00208	4456 ± 29	5285 – 4968
DK-03	bag 4	fauna (marked)	1/2013	101/101/D	(5), 5	–	1.66	AF	22.29	2.41	39.2	9.2	-21.1	3.2	OxA-35585	0.00157 ± 0.00101	> 45200	> 45200
DK-06	bag 93	fauna (marked)	1/2013	101/101/A	(2), 2	–	1.05	AF	13.36	1.74	40.2	7.6	-21.6	3.1	OxA-35586	0.40263 ± 0.00182	7308 ± 36	8181 – 8026
DK-08	bag 72	fauna (marked)	1/2013	101/101	(1), 1	–	0.78	AF	51.37	6.60	41.7	7.3	-25.4	3.2	OxA-35587	0.50963 ± 0.00196	5415 ± 31	6290 –6182
DK-17	bag 273	fauna (marked)	1/2013	101/99	(3), 5	–	1.88	AF	44.46	5.56	42.0	5.6	-23.1	3.1	OxA-35588	0.0136 ± 0.00101	34500 ± 600	40581 – 37576
DK-17	bag 273	fauna (marked)	1/2013	101/99	(3), 5	–	1.88	AF	52.90	6.34	40.3	6.5	-23.1	3.1	OxA-35589	0.01424 ± 0.00102	34150 ± 600	40085 – 36922
DK-32	bag 28	fauna (marked)	1/2013	100/99	(4), 4	–	1.71	AF	23.90	3.73	41.6	8.3	-20.9	3.1	OxA-35590	0.01360 ± 0.00104	34500 ± 600	40581 – 37576
DK-39	bag 424	fauna (marked)	1/2013	100/93/A	(4), 8	–	1.24	AF	26.27	3.46	39.5	9.6	-21.1	2.8	OxA-35591	0.00000 ± 0.00099	> 50000	> 50000
–	S. no. 1/2013	fauna (marked)	1/2013	100/101/A	(4), 3	–	–	AF*	49.7	5.7	43.9	4.5	-19.1	3.3	OxA-28687	0.04251 ± 0.00106	25370 ± 200	30100 – 28922

6.6 wt%. Carbon concentration on combustion was good and stable isotope results reasonable. The low C:N ratio of 2.8 found in DK-39 resulted from tuning issues affecting burn no. 4951 and does not necessarily indicate poor dating quality[2]. DK-17 demonstrates good dating reproducibility with both radiocarbon measures being statistically indistinguishable.

9.1.3 Bayesian modelling

There are not enough samples per layer/spit unit to allow for stratigraphic modelling to improve on the dating precision. Additionally, the wide spread of ages in layer 4 and the greater than ages from layer 4 (spit 8) and layer 5 prevent anchoring the lower part of the sequence – though they do not contradict the stratigraphic sequence. As all dated material show anthropogenic modifications, a KDE model would normally provide a suitable alternative. Unfortunately, in light of the large age spread the number of dates is insufficient for generating any insightful results. Consequently, Bayesian modelling is delayed until future excavations will provide further anthropogenically modified faunal remains (or human remains) for more extensive dating.

9.1.4 Discussion

While the radiocarbon results largely support the previous assumption of Neolithic, Upper Palaeolithic and possible Middle Palaeolithic occupation at the site, they, nonetheless, demand a careful rethinking of the archaeological record at Dubočka Kozja.

Against initial expectations, layer 2 did not yield any UP radiocarbon ages, but a Mesolithic (7308 ± 36 OxA-35586) and Neolithic age (4456 ± 29 OxA-35584). Upon reinvestigating the find location of the tooth pendant (DK-01), it can be concluded that the artefact is probably intrusive to layer 2. Based on the animal burrow in layer 2, animal activity seems the

[2]For further information burn no. 4951 see Appendix.

most likely candidate for transport. Manufacturing marks on the pendant are consistent with a Neolithic attribution. Furthermore, Neolithic pottery was found above in layer 1, and some human activity in this layer was directly radiocarbon dated to 5415 ± 31 BP (OxA-35587). In contrast, there is currently no context indication that DK-06 is intrusive. The attribution of the lithic assemblage found in layer 2 to the Mesolithic is conceivable: laminar characteristics are not unique to the UP and diagnostic UP elements are missing. At the same time, the Mesolithic lithic industry in the region is not well known, making a direct comparison difficult.

The geological unit 4, previously interpreted as MP or 'transitional', clearly contains several, temporally distinct occupation horizons spanning the MP and UP. Radiocarbon ages increase with depth, consistent with missed horizon boundaries during excavation rather than mixing of material within the geological unit. In the uppermost part, a radiocarbon age of 25370 ± 200 BP implies a possible Gravettian occupation at Dubočka Kozja. Despite the Gravettian being well known in the region, no diagnostic lithics of that period were recovered at the site. DK-32 from the upper-middle section (spit 4) suggests a human presence at 34,500 ± 600 BP (OxA-35590). The same radiocarbon age was obtained from a modified bone (DK-17) in layer 3, providing evidence that the illicit excavation clearly disturbed Upper Palaeolithic (possibly 'Aurignacian') material. The identified MP character (i.e. Levallois) is supported by the greater than age obtained from the lowest part of unit 4 ($> 50,000$ BP OxA-35591).

The only anthropogenically modified sample from geological unit 5 gave an age beyond the radiocarbon time scale ($> 45,200$ BP OxA-35585), increasing the probability of a MP occupation.

Currently, there is no chronometric evidence for a late MP or 'transitional' occupation period at Dubočka Kozja. Both radiocarbon measurements in connection with Levallois material are beyond the radiocarbon limit and distinctly older than the next younger dates. This means that the temporal relationship between the geological units 4 and 5 can presently not be resolved. The stratigraphic evidence suggests, however, that 5 might be younger than

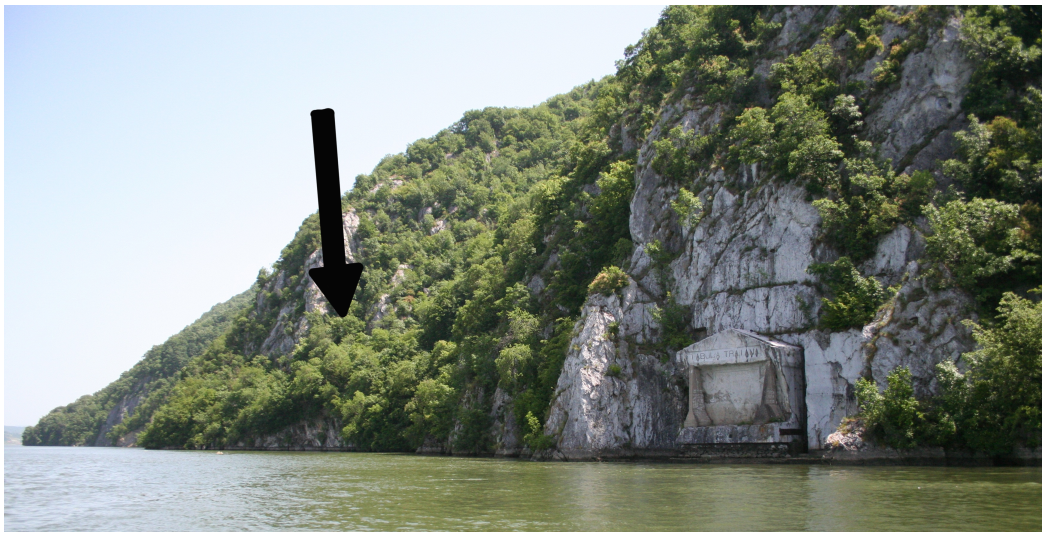


Figure 9.7: Tabula Traiana: location of cave indicated by black arrow overlooking the Danube. On the right, the Roman memorial plaque Tabula Traiana, after which the cave is named, is clearly visible (photo: D. Borić).

the lower section of unit 4 (see figure 9.4, especially profile a). In the hope of better separating the archaeological units within layer 4, the 2017 excavation season applied a finer spit division of 2 cm each (D. Borić, pers. comm. 10/01/2018).

Both DK-32 (34,500 ± 600 OxA-35590) and DK-17 (34,500 ± 600 OxA-35588 and 34,150 ± 600 OxA-35589) indicate the use of the cave site contemporaneously – on a radiocarbon time scale – to the human mandible found in nearby Peștera cu Oase (Rougier et al., 2007; Trinkaus et al., 2003).

9.2 Tabula Traiana

9.2.1 Introduction

Tabula Traiana Cave (44°39' N, 22°18' E) is a cave site in the karstic massif of the Miroč plateau (Борић and Јевтић, 2006), situated in the Danube Gorge, where the Danube cuts through the southern Carpathian Mountains.



Figure 9.8: Tabula Traiana: Cave entrance as seen in September 2016 with D. Borić standing next to the excavation trench 2/2008 (photo: R. Hopkins).

.

It was named after the Roman memorial plaque Tabula Traiana (AD 101), which is located nearby (see figure 9.7). The archaeological site is only 55 km from the crucial site of Peștera cu Oase and contains both Middle and Upper Palaeolithic archaeological remains (Borić et al., 2012).

The cave entrance measures around 4.5 m (height) by 4 m (bottom width) and is located at 90-91 m a.s.l. on the right bank of the Danube (see figures 9.7 to 9.9). A single gallery extends for 33 m in north-west direction. While the cave floor remains relatively flat during the first 15 m, it subsequently cascades upwards, resulting in a denivelation of +12 m between entrance and rear of the cave. The cave cross-section remains triangular throughout, with the exception of three chimneys. The cave walls show strong acid water corrosion, yet remain largely dry nowadays. In front of the entrance there is a small terrace (Mandić and Borić, 2015).

The site was discovered in 2004 during archaeological surveying in the region. Subsequently, archaeological excavations were conducted in the years 2004, 2005, 2008, 2009, 2013 and 2017 (see figure 9.9), uncovering two distinct Pleistocene geological horizons (further referred to as upper and lower horizon), separated by a sterile layer from the Holocene deposits. The Holocene layer contained sporadic Eneolithic, Late-Roman and Early Medieval finds (Борић and Јевтић, 2006).

The upper horizon (207)[3] is 20-63 cm thick and consists of "*greyish brown calcereous silt with fine (< 2cm), sub-rounded to sub-angular karst fragments*" (Borić et al., 2012, p. 1). The lower horizon (206)[4], found under humus on the cave terrace and beneath the upper geological horizon in the cave interior, is "*yellowish brown calcareous silt with fine rock fragments (< 2cm)*" (Borić et al., 2012, p.1).

Both horizons yielded modest lithic assemblages (see figure 9.10). Layer 207 (upper horizon) in the cave interior is attributed to the Upper Palaeolithic

[3]The excavation documentation also identifies the following layers found in other parts of the cave as being identical to layer 207: 43, 90, 100, 215 and 217.

[4]The excavation documentation also identifies the following layers found in different parts of the cave as being identical to layer 206: 209, 211, and 219.

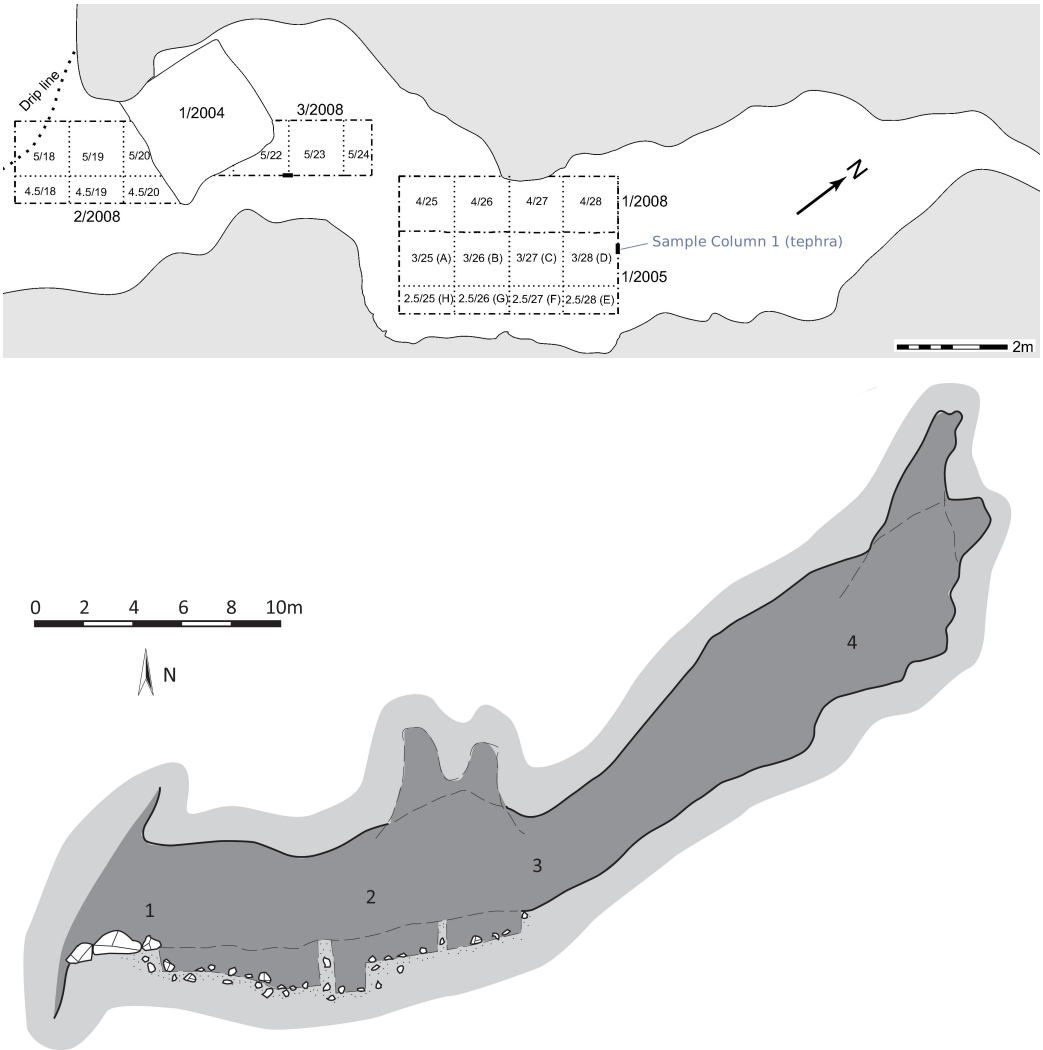


Figure 9.9: Tabula Traiana: top – map of excavated areas and tephra sample columns (after Borić et al., 2012, figure 3). In 2009, another trench was opened north-east of trench 1/2005 (D. Borić, pers. comm. 10/01/2018); bottom – vertical cross section through cave with depth of excavation trenches and pre-excavation cave floor level marked (after Mandić and Borić, 2015, p. 84).

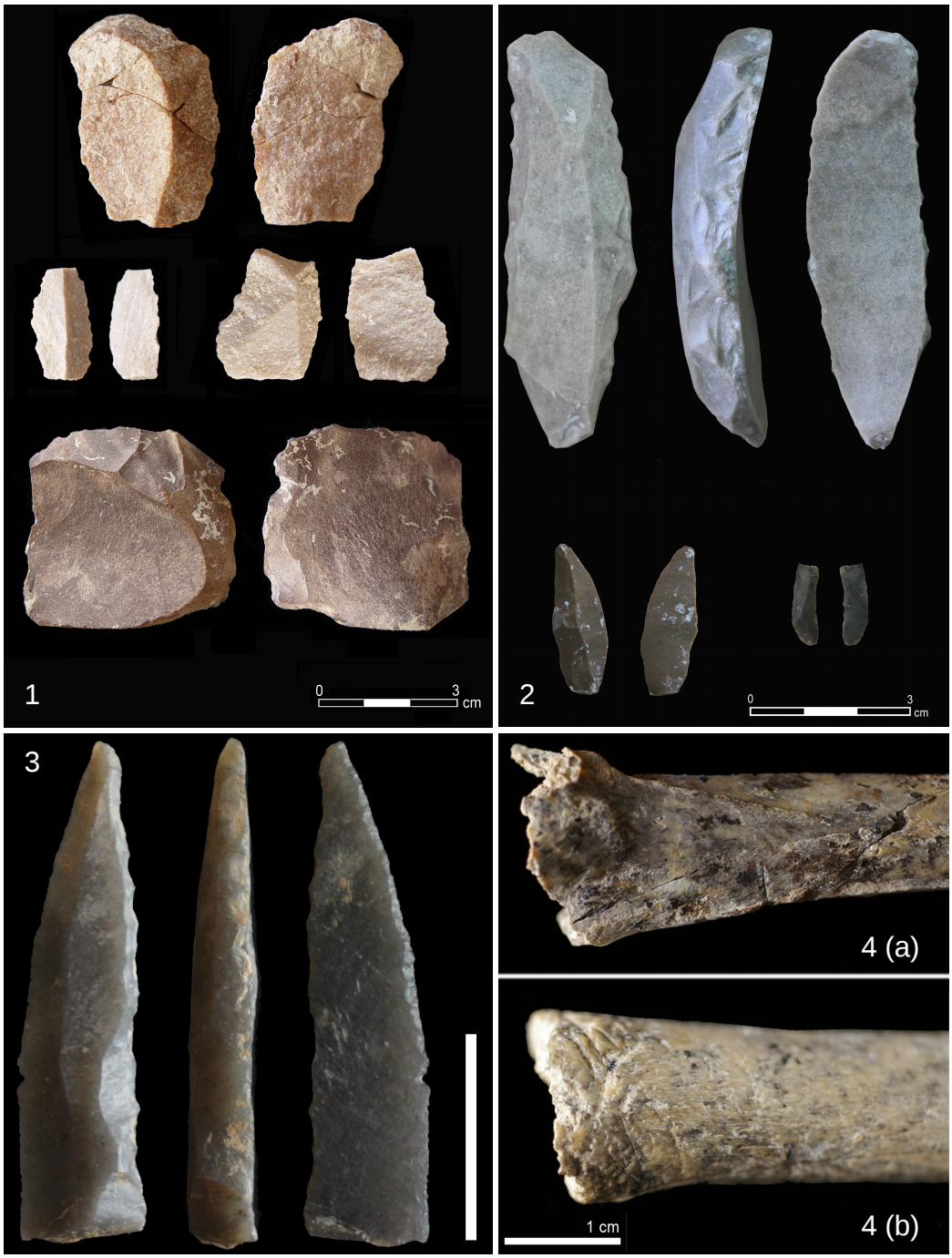


Figure 9.10: Tabula Traiana: 1 – Levallois flakes (quartzite), layer 206; 2 – large blade with bilateral continuous retouch, an unretouched bladelet, small bladelet with marginal retouch, layer 207; 3 – pointed Dufour bladelet found at cave entrance, layer 207; 4 – cut-marked faunal remains previously dated: (a) *Vulpes vulpes* femur, 34,200 ± 550 BP (OxA-23651), (b) *Capra ibex* metapodial, 33,450 ± 500 BP (OxA-24818) (photos: D. Borić).

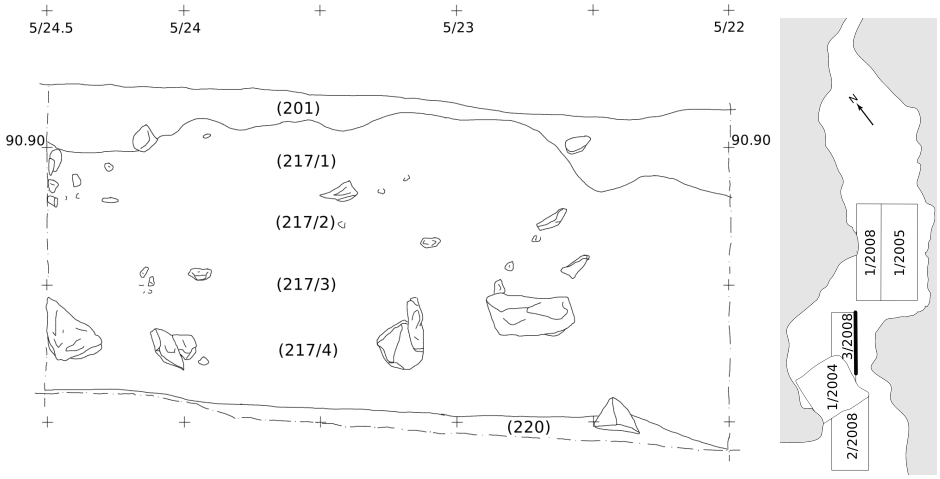


Figure 9.11: Tabula Traiana: north-west facing profile at the south-east end of trench 3/2008 with layer numbering and height marker at 90.90 m a.s.l. Location within cave marked on the right (illustration: R. Hopkins after original documentation provided by D. Borić).

on the basis of a large blade with bilateral continuous retouch, as well as some bladelets. Borić et al. (2012, p. 2) see the marginal retouch found on one of the smaller bladelets as evidence for "*extraction from prismatic rather than carinated cores within the framework of a continuous reduction sequence characteristic of the Protoaurignacian*". In line with this interpretation, a Dufour bladelet was found at the cave entrance in a layer believed to belong to the 207 unit. In contrast, unit 206 (lower horizon) at the cave entrance and on the terrace contained Levallois flakes of locally sourced quartzite and quartz, indicating a possible late Middle Palaeolithic occupation.

Both geological units show faunal remains dominated by *Capra ibex*. Several predatory species, such as cave lions, cave hyaena, cave bear, wolf, lynx, and fox remains are present. Furthermore, several species of fish could be uncovered. At present, human fossils are absent (Borić et al., 2012; Борић and Јевтић, 2006).

Previous Dating

Previous chronometric work at the site included tephra analysis and sporadic radiocarbon dating.

In 2009, as part of the RESET project[5], a column in the rear of trench 1/2005 was sampled for tephra analysis (see figures 9.9 top and 9.12). Two cryptotephra concentrations were identified in layer 207. The more recent one could be connected to the CI eruption (Y5) dated to *ca.* 40k years ago. The origin of the older deposit remains unknown (Borić et al., 2012; Lowe et al., 2012).

A total of eight radiocarbon measurements had already been obtained before the start of the radiocarbon work conducted for this dissertation (see table 9.3). Initially, a *panthera spelaea* metapodial was taken from the test trench 1/2004 and sent to the radiocarbon laboratory at the University of Arizona to test the age of the upper horizon (Борић and Јевтић, 2006). The sample was treated with 0.25 M HCl solution, rinsed with ultrapure water and filtered through 7.5 μm glass fiber, before lyophilization. No base wash was applied. Despite the light treatment and large original sample size (800 mg), collagen yield was only 0.8 wt.%. Carbon yield on combustion was a bare 13.1%, unusually low for collagen (averaging 41-43% at ORAU), leading one to question the reliability of the resulting measurement. Additionally, the stable carbon isotope measurements of -24.4 ‰ appears unusually depleted (chemistry information provided by G. Hodgins, University of Arizona, pers. comm. 22/01/2018).

Subsequently, a further 5 faunal remains and 2 charcoal samples were sent to ORAU between 2006 and 2012. All samples originated from layers believed to belong to the upper geological horizon. However, only two faunal remains showed anthropogenic cut marks: the *Vulpes vulpes* femur and the *Capra ibex* metapodial (Borić et al., 2012). In addition, the *Capra ibex*

[5]RESET stands for 'Response of Humans to Abrupt Environmental Transitions' and was a research project funded by the Natural Environment Research Council (NERC), UK.

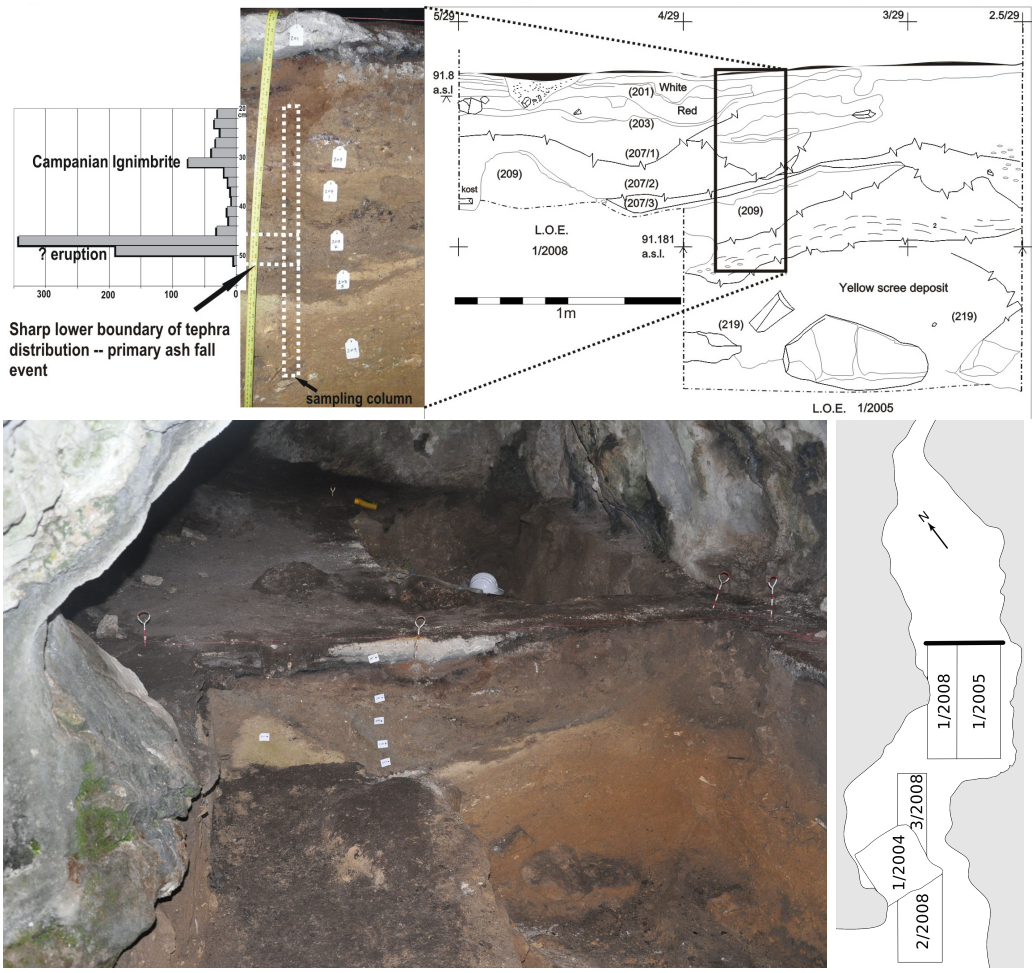


Figure 9.12: Tabula Traiana: top – south-west facing profile at the north-est end of trenches 1/2005 and 1/2008 with location of tephra sample column 1 and tephra count/identification (illustration: D. Borić); bottom – photo of same south-west facing profile (photo: D. Borić) and its location marked with thick black line on cave plan (illustration: R. Hopkins).

Table 9.3: Tabula Traiana: previously obtained radiocarbon results faunal remains, anthropogenically modified faunal remains, and charcoals with archaeological context information, and pre-treatment results. Lab-no. = radiocarbon date identification number. Sample = sample ID given on excavation. Species = Published species identification. Sq. = excavation quadrant. Layer = layer attribution. Treat. = Pretreatment protocols used: * = solvent wash, AG = ORAU acid-base-acid pretreatment, AF = ORAU ultrafiltration protocol (Brock et al., 2010b). Yield = sample left after chemical pre-treatment (both in mg and wt.%). %C = carbon yield on combustion. C:N = carbon to nitrogen ratio of combusted collagen sample. $F^{14}C$ = fraction modern carbon. ^{14}C (BP) = conventional radiocarbon age Before Present with 1σ error. Date (cal BP) = calibrated radiocarbon age at a 95.4% confidence interval, calculated in OxCal 4.3 (Bronk Ramsey, 2009a) using IntCal13 (Reimer et al., 2013). In white – results previously published in Борић and Јевтић (2006), Borić et al. (2012), and Mandić and Borić (2015); in grey – unpublished results kindly provided by (D. Borić, pers. comm. 17/11/2017).

Lab-no.	Sample	Item	Species	Trench	Sq.	Layer	Hight (m)	dated	Treat.	Yield (mg)	Yield (wt.%)	%C	$\delta^{15}N$	$\delta^{13}C$	C:N	$F^{14}C$	^{14}C (BP)	Date (cal BP)
AA-64887	–	fauna	*Panthera spelaea* (metapodial)	1/2004	1/2004	–	–	2005	acid & filter	6.4	0.8	13.1	8.5	-24.4	–	0.02057 ± 0.00308	31200 ± 1200	36774 – 31269
OxA-16419	Sample 2	fauna	*Capra ibex* (horncore)	1/2005	3/26(B)	100 (hearth)	–	2006	AF	23.46	1.8	42.0	4.8	-19.4	3.2	0.01200 ± 0.00050	35530 ±360	41036 – 39307
OxA-23651	TTC/2010 (TT 05/90/36)	fauna (marked)	*Vulpes vulpes* (femur)	1/2005	2.5/27(F)	90	–	2010	AF*	25.35	4.1	45.3	7.9	-19.0	3.2	0.01413 ± 0.00098	34200 ±550	40055 – 37120
OxA-24818	x.78/2	fauna (marked)	*Capra ibex* (metapodial)	1/2008	4/25	207	–	2011	AF	18.83	3.0	43.4	6.8	-19.8	3.1	0.01554 ± 0.00100	33450 ±500	38885 – 36390
OxA-24819	TT05/43/1	fauna	*Capra ibex* (maxilliary bone)	1/2005	3/28(D)	43	91.00	2011	AF	7.43	1.5	43.3	7.8	-18.8	3.2	0.02149 ± 0.00104	30850 ±390	35607 – 34080
OxA-26718	x.98	fauna	Capra ibex	column 1, 2009	3/30	207/1	–	2012	AF	20.1	1.5	42.9	5.0	-18.7	3.3	0.04625 ± 0.00109	24690 ±190	29206 – 28302
OxA-26719	R2(a)	charcoal	*Fraxinus*	column 1, 2009	3/31	207	–	2012	XR	7.51	3.7	81.3	–	-22.7	–	0.78780 ± 0.00252	1916 ±26	1928 – 1816
OxA-26720	R2(b)	charcoal	*Prunus*	column 1, 2009	3/30	207/2	–	2012	XR	7.12	4.0	81.0	–	-24.2	–	0.79642 ± 0.00249	1829 ±25	1858 – 1703

hornicore was found in an upper Palaeolithic fireplace (Mandić and Borić, 2015). All Oxford bone samples were pre-treated with the standard ORAU ultrafiltration protocol (AF), while the two charcoal samples were treated with ABOx-SC (XR). Additionally, OxA-23651 underwent a solvent wash treatment – usually used to remove conservation contamination.

It can be concluded that only two radiocarbon measurements fulfil the criterion of direct connection to human activity needed for this study: OxA-23651 (34200 ± 550 BP) and OxA-24818 (33450 ± 500 BP). Nonetheless, the remaining dates and tephra evidence indicate that the upper horizon includes material spanning several thousands of years, both older and younger than the CI tephra. This would be in line with the interpretation of an early Proto-Aurignacian at the site. Conversely, the two charcoal samples dated to the Roman period are unlikely to be the result of insufficient pre-treatment, but rather intrusive, and thus a reminder of the complexity of cave stratigraphies.

9.2.2 Radiocarbon dating

In this section, the new radiocarbon dating completed at Tabula Traiana is discussed. For details on the Bayesian modelling of the results see subsections 9.2.3 and 9.2.4.

Material & Treatment

In September 2016, the faunal remains from all previous excavation seasons were checked for anthropogenic modifications. In an initial sorting, 44 samples with possible cut and chop marks were separated and numbered. From these, 28 faunal fragments with anthropogenic cut and chop marks were identified. Finally, 12 samples were selected for initial radiocarbon dating (see table 9.4), covering the Holocene, the Upper Palaeolithic, and the Middle Palaeolithic.

None of the samples selected for dating were precious artefacts. Therefore, time consuming key-hole drilling was not applied. Instead, all samples

Table 9.4: Tabula Traiana: list of anthropogenically modified faunal remains sampled for radiocarbon dating with original cultural interpretation. z – given as hight in m a.s.l. Original layer attribution of samples listed, for those marked with * see discussion in text (9.2.4).

Ref-no.	Inv.-no.	Layer	Arch.	x(m)	y(m)	z(m)	Weight	Conserved?
Tab-01	x.4	210	UP	4.67	27.39	91.10	794 mg	N
Tab-03	x.58	207/3*	UP*	4.34	28.16	91.24	803 mg	N
Tab-04	x.49	207/2	UP	4.82	25.41	91.03	781 mg	N
Tab-08	x.82	207/4	UP	4.58	25.76	90.94	863 mg	N
Tab-11	x.11	217/2	UP	5.20	22.59	90.23	668 mg	N
Tab-13	x.13	215/2*	UP*	3.99	26.59	90.72	730 mg	N
Tab-13	x.13	215/2*	UP*	3.99	26.59	90.72	789 mg	N
Tab-14		200*	Holocene*	–	–	–	688 mg	N
Tab-17	TT08/211/2	211	MP	–	–	–	514 mg	N
Tab-34		220*	MP*	–	–	–	840 mg	N
Tab-38		206	MP	–	–	–	699 mg	N
Tab-39		218	MP/UP	–	–	–	683 mg	N

had a small piece cut off with a diamond saw blade (see appendix A.14). Subsequently, the surface was cleaned, before the sample was crushed with an iron steel mortar.

The resulting bone powder was chemically pre-treated with the standard ORAU gelatine (AG) and ultrafiltration (AF) protocols (for further details see section 5.4). An additional solvent wash step was deemed unnecessary, as none of the faunal samples had been conserved.

Tab-13 was selected as an auto-duplicate by ORAU's internal quality control procedures[6].

^{14}C Results

All samples had over 600 mg of bone powder available for pre-treatment and showed good to very good preservation. Gelatine yield after AG was 2-10 wt.%, allowing for ultrafiltration of all but one sample (see table 9.5). Tab-17 only had 5.20 mg at AG and was not ultrafiltered. This is unlikely to have

[6]Samples whose P-numbers are factors of 20 get dated twice to check dating reliability.

Table 9.5: Tabula Traiana: new AMS radiocarbon results on anthropogenically modified faunal remains with archaeological context information, and pre-treatment results. Ref-no. = number given to the sample for the purpose of this project. Inv.-no. = Inventory number given to the sample on excavation. Sq. = excavation quadrant. Layer = layer attribution. %N = nitrogen weight content before chemical pre-treatment. Treat. = Pretreatment protocols used: AG = ORAU acid-base-acid pretreatment, AF = ORAU ultrafiltration protocol (see section 5.4). Yield = sample left after chemical pre-treatment (both in mg and wt.%). %C = carbon yield on combustion. C:N = carbon to nitrogen ratio of combusted collagen sample. $F^{14}C$ = fraction modern carbon. ^{14}C (BP) = conventional radiocarbon age Before Present with 1σ error. Date (cal BP) = calibrated radiocarbon age at a 95.4% confidence interval, calculated in OxCal 4.3 (Bronk Ramsey, 2009a) using IntCal13 (Reimer et al., 2013). Tab-01 and Tab-14 were on burn 4951, thus low C:N ratio is not indicative of a poor collagen sample (see text). For layer attributions marked with * see discussion in text (9.2.4).

Ref-no.	Inv.-no.	Item	Trench	Sq.	Layer	Hight (m)	%N	Treat.	Yield (mg)	Yield (wt.%)	%C	$\delta^{15}N$	$\delta^{13}C$	C:N	Lab-no	$F^{14}C$	^{14}C (BP)	Date (cal BP)
Tab-01	x.4	fauna (marked)	1/2008	4/27	210	91.10	2.25	AF	55.06	6.93	38.9	2.6	-20.4	3.0	OxA-35592	0.01523 ± 0.00103	33600 ±550	39231 – 36426
Tab-03	x.58	fauna (marked)	1/2008	4/28	207/3, 209*	91.24	1.06	AF	6.08	0.76	41.0	4.0	-20.5	3.3	OxA-35762	0.00051 ± 0.00102	> 48000	> 48000
Tab-04	x.49	fauna (marked)	1/2008	4/25	207/2	91.03	2.11	AF	31.72	4.06	42.1	4.6	-19.3	3.2	OxA-35763	0.02860 ± 0.00104	28550 ±290	33402 – 31656
Tab-08	x.82	fauna (marked)	1/2008	4/25	207/4	90.94	2.42	AF	56.23	6.52	42.2	5.9	-19.4	3.2	OxA-35764	0.01062 ± 0.00099	36500 ±750	42341 – 39676
Tab-11	x.11	fauna (marked)	3/2008	5/22	217/2	90.23	1.53	AF	17.22	2.58	41.5	3.7	-19.6	3.2	OxA-35765	0.07831 ± 0.00122	20460 ±120	25066 – 24256
Tab-13	x.13	fauna (marked)	1/2008	4/26	215/2*	90.72	1.16	AF	13.59	1.86	39.5	1.6	-22.0	3.2	OxA-35766	0.00000 ± 0.00101	> 49800	> 49800
Tab-13	x.13	fauna (marked)	1/2008	4/26	215/2*	90.72	1.16	AF	15.25	1.93	38.1	1.5	-22.0	3.2	OxA-35767	0.00000 ± 0.00100	> 49900	> 49900
Tab-14	–	fauna (marked)	3/2008	5/22	200	–	1.55	AF	14.38	2.09	40.4	12.9	-17.1	2.9	OxA-35593	0.04187 ± 0.00108	25490 ±210	30291 – 29050
Tab-17	TT 08/211/2	fauna (marked)	2/2008	4.5/18	211	–	0.61	AG	5.20	1.01	41.8	5.3	-20.2	3.2	OxA-35594	0.00000 ± 0.00115	> 48800	> 48800
Tab-34	–	fauna (marked)	1/2004	–	220, 217/4*	–	1.94	AF	51.80	6.17	42.4	4.8	-19.4	3.2	OxA-35768	0.01404 ± 0.00099	34250 ±550	40132 – 37221
Tab-38	–	fauna (marked)	2008	–	206	–	2.22	AF	31.91	4.56	42.1	5.5	-19.4	3.2	OxA-35769	0.00000 ± 0.00097	> 50100	> 50100
Tab-39	–	fauna (marked)	1/2008	4/26	218	–	1.88	AF	29.13	4.26	42.6	5.1	-20.0	3.2	OxA-35770	0.00305 ± 0.00097	46500 ±2600	> 49257

affected the result as the sample gave a greater than age. As a result of additional sample loss during ultrafiltration, Tab-03 only yielded 0.76 wt% of original sample weight. Despite this being below the 1 wt.% threshold normally used as a quality control measure, the sample was AMS dated. The resulting greater than age suggests that it is a reliable date.

Most pre-treated samples show expected values for C:N ratio, %C on combustion, and stable isotope measures. Notable exceptions are Tab-01 and Tab-14 with a C:N ratio of 3.0 and 2.9, respectively. Both samples were on the mass-spectrometer run no. 4951, which showed calibration issues – nitrogen content was overestimated for all samples, leading to decreased C:N ratios. Bone standards run on the same burn show that this has not affected the reliability of the radiocarbon measurement (see Appendix). Tab-03 gave a slightly elevated C:N ratio of 3.3, albeit still within the expected value range. All samples were graphitised to large graphite targets (1.8 mgC).

9.2.3 Bayesian modelling

Two main modelling approaches were pursued: stratigraphic and KDE modelling. However, Tabula Traiana is challenging for Bayesian analysis because of three cumulative features. First, it has only two Pleistocene geological horizons, containing a large number of individual units with complex relationships. Second, four out of 13 samples gave greater than ages – three of which belong to the four samples originally attributed to the lower horizon. Third, one date, albeit finite, is beyond the age of the calibration curve.

The stratigraphic model had to be simplified to only include the two main geological units (upper and lower horizon), as well as layer 200, which was found on top of those two. A model which places the layer 218 between the lower and upper horizon would not complete. Each `Phase` is separated by a single `Boundary` because the layers are in direct contact with no sterile level in between. The ^{14}C results were added first according to their original attribution (see table 9.4), and a second run saw them rearranged according to their re-evaluated affiliation (see subsection 9.2.4). For the latter, layer

218 was placed between the lower and upper horizons as originally intended. The KDE model simply applied the OxCal command `KDE_Model` to the radiocarbon dataset.

For all models, the radiocarbon dataset was limited to dates obtained on anthropogenically modified faunal remains – including both new results from this study as well as the two previously obtained measurements (see tables 9.3 and 9.5). The stratigraphic models also include the age of the CI tephra found in layer 207 (after Giaccio et al., 2017). It was not included in the KDE model as it does not directly represent human activity at the site.

The two ages of sample Tab-13 were combined. The greater than ages were coded using their calibrated minimum ages as the younger age boundary of a uniform distribution. The upper age boundary was arbitrarily set at 60000 to keep the age distribution – and consequently the model outputs – readable. Of course, the true age of a sample could be well beyond this limit. For example, Tab-03 has an age of > 48000 BP (OxA-35762). It was entered in OxCal as: `Date("OxA-35762", U(calBP(60000), calBP(48000)))`.

9.2.4 Discussion

The modelled radiocarbon dates separate into two main age groups, one beyond radiocarbon and one within Upper Palaeolithic expectations, with a gap at around 43k cal BP (see figure 9.13). However, several possible outliers need further discussion as they skew the MP/UP transition towards older ages.

Against initial expectations, sample Tab-14 (25490 ± 210 OxA-35593) did not yield a Holocene age. Studying its find location within layer 200, it seems plausible that the sample was not found in its primary location or the layers age/origin was misinterpreted. This makes the date's use as an anchor for the younger end of the radiocarbon sequence questionable. Only further dating of material from 200 could resolve this issue, though at present no further anthropogenically modified samples are known from this horizon.

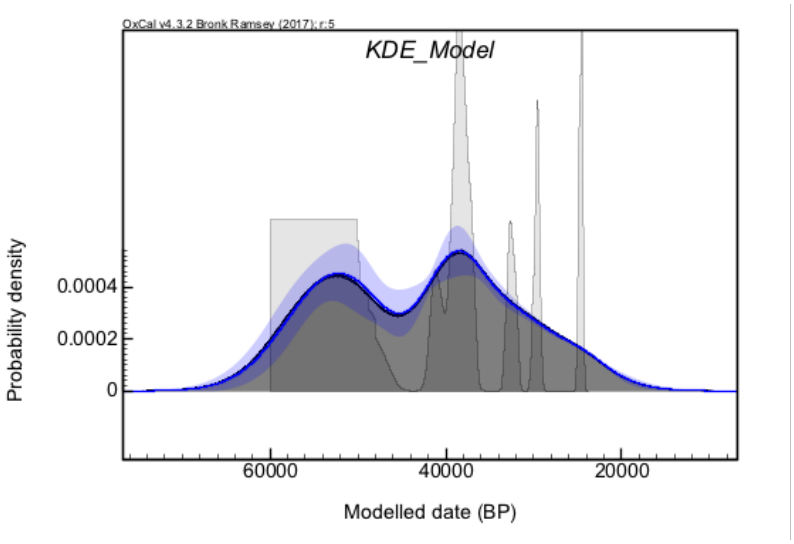


Figure 9.13: Tabula Traiana: `KDE_Model` results (code: p. 711). Dataset includes all radiocarbon measurements obtained on anthropogenically modified faunal remains.

Another striking outlier is Tab-03 (> 48000 BP OxA-35763). On first sight, it seems difficult to resolve with the age of Tab-08 (36500 ± 750 BP OxA-35764), which was found in a spit further down the sequence. However, in square 4/28 layer 207/3 is not only very thin, but directly overlies layer 209 – not 207/4 – and shows possible interlacing (see figure 9.12). Studying the find location more closely, it seems reasonable to propose that Tab-03 reflects human activity associated with layer 209, rather than 207. Consequently, the date was included in the lower horizon for the modified stratigraphic model.

The reverse situation can be observed with Tab-34 (34250 ± 550 OxA-35768). It was originally attributed to the Middle Palaeolithic layer 220, directly under the Upper Palaeolithic layer 217/4 (see figure 9.11). It appears that the sample actually belongs to the lowest part of 217/4. It was therefore moved for the modified stratigraphic model.

Tab-39 (46500 ± 2600 BP OxA-35770) had to be placed in the lower horizon for the first stratigraphic model, despite its tentative association with MP/UP material – the model would otherwise not run. However, it is the only sample from a layer with Middle Palaeolithic character that gave a

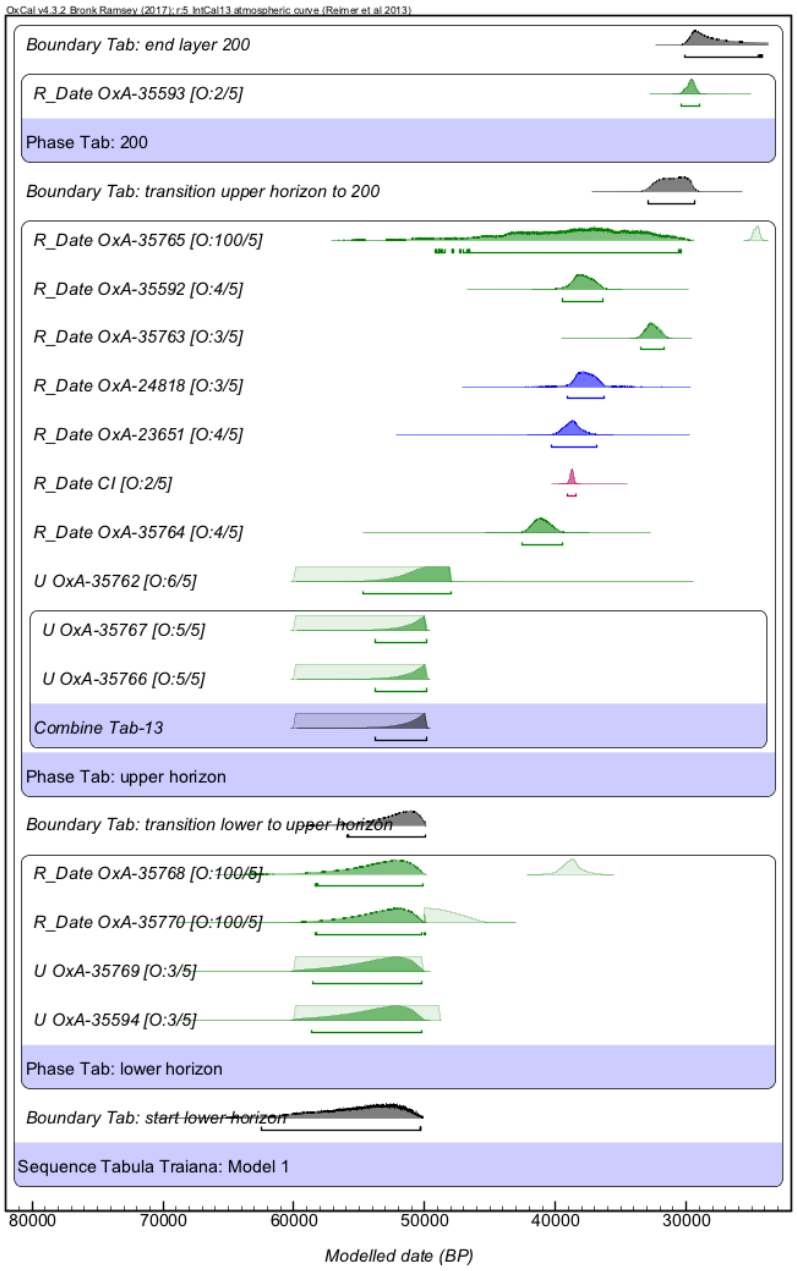


Figure 9.14: Tabula Traiana: Stratigraphic Model 1 (code: p. 709) using original geological unit attributions. green – dates obtained for this project (anthropogenically modified fauna); blue – previously obtained ^{14}C results on anthropogenically modified faunal remains; magenta – CI radiocarbon age according to Giaccio et al. (2017).

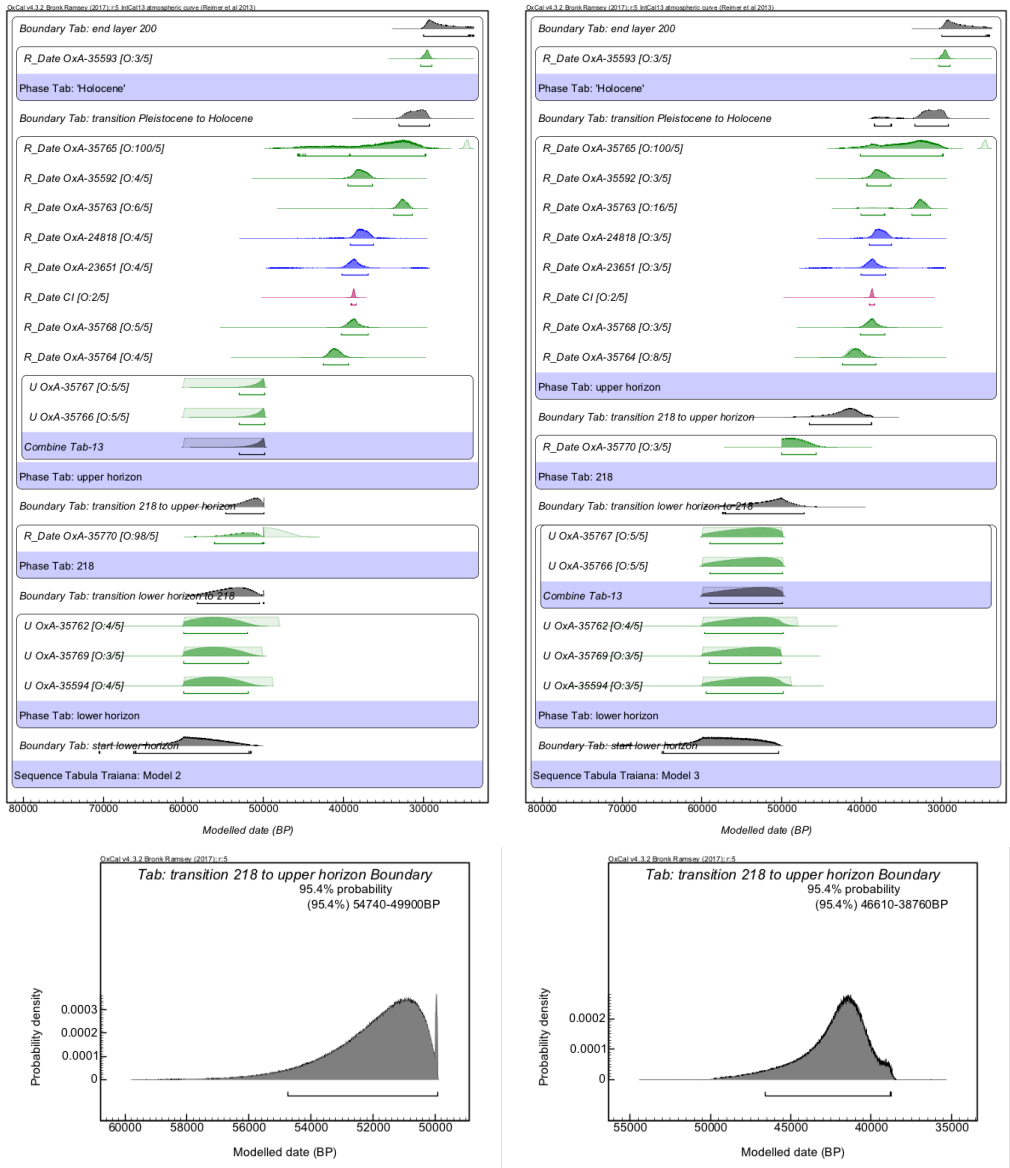


Figure 9.15: Tabula Traiana: results of modified stratigraphic models with close up of modelled transition to EUP. Compared to Model 1 Tab-03 (OxA-35762) and Tab-34 (OxA-35594) changed horizon, and Tab-34 (OxA-35770) was placed in a separate `Phase`. left – Model 2 (code: p. 709), with Tab-13 (OxA-35766) remaining in the upper horizon; right – Model 3 (code: p. 710), Tab-13 moved to the lower horizon. green – dates obtained for this project (anthropogenically modified fauna); blue – previously obtained ^{14}C results on anthropogenically modified faunal remains; magenta – CI radiocarbon age according to Giaccio et al. (2017).

finite age and might be evidence for a late MP or 'transitional' occupation at Tabula Traiana. In contrast, all dates obtained from Middle Palaeolithic layers provided greater than radiocarbon ages. Accordingly, the sample was placed in a separate phase between the extended units 206/209 and 207/217 in the modified stratigraphic model (Model 2 and 3).

From the available information it remains unclear whether Tab-13, originally attributed to 215/2, could possibly belong to unit 206/209. Therefore, the influence of sample Tab-13 (OxA-35766 and OxA-35767) on the start boundary of the upper level was tested by featuring the sample once in the upper geological horizon (Model 2) and once in the lower (Model 3).

It can be concluded that the upper horizon does not only contain evidence for early Upper Palaeolithic, but also for younger Palaeolithic occupations. However, no Gravettian lithic material has been found at the site. More importantly, the radiocarbon dating evidence supports a possible EUP occupation immediately prior, during, and after the CI eruption at 34290 ± 90 BP (see Giaccio et al., 2017). These may tentatively be associated with Proto-Aurignacian and a subsequent Early Aurignacian phase at Tabula Traiana. Though, as D'Errico and Banks (2015) cautioned, the lithic assemblage is small and diagnostic features – apart from the Dufour bladelet – are largely absent.

Depending on the stratigraphic model used, the modelled date for the transition to the early Upper Palaeolithic horizon varies significantly (see figures 9.14–9.15). The modified models are to be preferred over the original stratigraphic model, as they are more consistent with the excavation record. The shift observed between Model 2 and Model 3 is caused by Tab-13, which is left in the upper horizon for Model 2 and moved to the lower horizon for Model 3. Considering the context for Tab-13 is insecure, it seems premature to move the beginning of the Upper Palaeolithic at Tabula Traiana beyond the radiocarbon limit – something so far unobserved at other European sites. The unusual probability distribution for OxA-35770 and the boundary from the lower horizon to level 218 is a result of the finite age of Tab-39 (OxA-35770) extending beyond the range of the current radiocarbon calibration

curve. For the moment, Model 3 appears to give the most realistic estimate for a transition to the Upper Palaeolithic (46610-38760 modelled BP), albeit with a large age range. At the same time, the results from the KDE model suggest a very low occupation probability around 43k cal BP (see figure 9.13), which might reflect an occupation hiatus between the Middle and Upper Palaeolithic.

In order to better resolve the appearance of the EUP at the site, further radiocarbon dating, paired with further archaeological work, is required. Of great interest are the origin of the older cryptotephra concentration in layer 207 (as seen in figure 9.12) as well as the nature and extend of level 218. Both may help to increase precision of the transition to the Upper Palaeolithic.

Chapter 10

Croatia

Over more than a century of archaeological and anthropological research, sites on the territory of present-day Croatia have repeatedly featured in the discussion of the MP/UP biocultural shift. While many of them show the difficulties surrounding stratigraphy and layer attribution that often result from old excavations, they have also produced a significant number of human remains and some 'Aurignacian' osseous points. In the following, some of these sites are introduced and the site selection for this project is discussed (see fig. 10.1).

The most well-known site is probably Vindija cave in the Hrvatsko Zagorje Mountains. At the site, some of the *Homo neanderthalensis* remains were supposedly found in association with 'Aurignacian' points. The dating of the late Neanderthals had to be revised several times. This changed the picture from (a) a Neanderthal refuse surviving the arrival of AMH for substantial period of time to (b) late MP Neanderthals who might not be contemporaneous with the osseous point industry (*e.g.* Devièse et al., 2017; Higham et al., 2006a; Smith et al., 1999; Wolpoff et al., 1981).

The scientific dispute concerned the integrity of layer G, especially G1, and the age of the material it contained. In light of material mixing, direct radiocarbon dating seemed to offer a possible solution, though issues with conservation contamination led to the varying results mentioned before. At

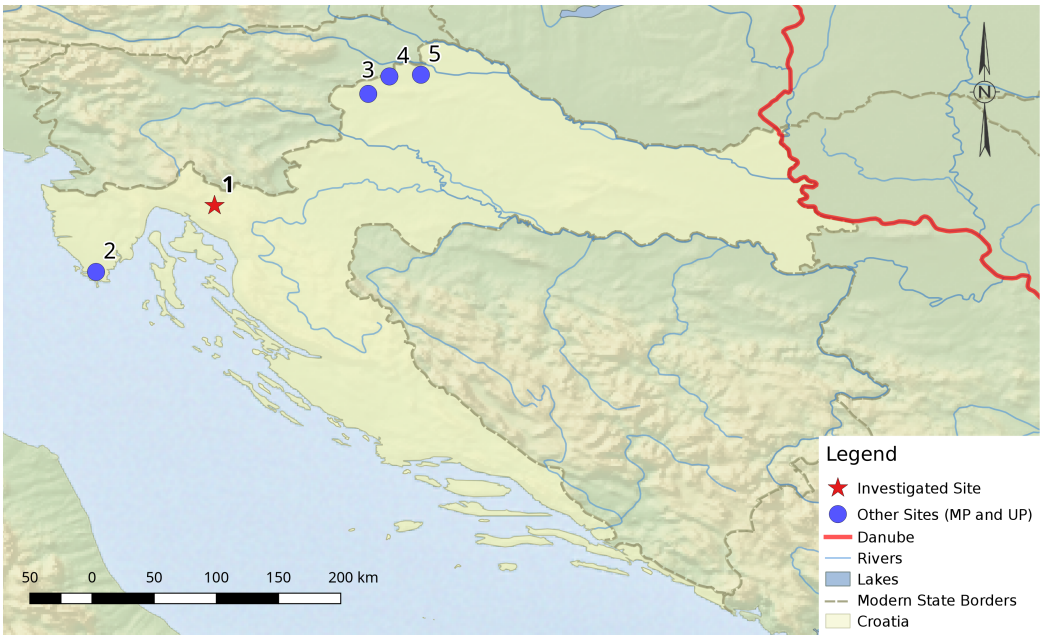


Figure 10.1: Croatia: map of Middle and Upper Palaeolithic sites: (1) Bukovac, (2) Šandalja II, (3) Krapina, (4) Velika Pećina, (5) Vindija.

the same time, the osseous point industry tested showed poor collagen preservation – despite the great DNA preservation observed in the Neanderthal remains (*e.g.* Prüfer et al., 2017). As a consequence, using anthropogenically modified faunal remains for KDE modelling of the late MP/early UP section of the stratigraphy would provide another means to assess the age and minimum number of the occupation events it contained. Regrettably, the Institute for Quaternary Palaeontology and Geology in Zagreb was only able to prepare two cut-marked bones for sampling, and access to the stored faunal material from Vindija was not granted. As this was insufficient material for KDE modelling, which requires a large number of dates to calculate reliable results, it is hoped that someone will have the opportunity to review the entire relevant faunal collection in the near future. Nonetheless, the presently published data will provide important information for the discussion of the MP/UP transition along the Danube corridor and will be more thoroughly discussed in chapter 15.

Velika Pećina is located not far from Vindija cave. The site contains both MP and UP lithic industries, as well as an osseous point industry. In addition, *Homo sapiens* remains were supposedly found in association with Proto-Aurignacian lithics, and initially indirectly dated to 33850 ± 520 BP (GrN-4979) (Malez and Vogel, 1970). However, direct dating by Smith et al. (1999) resulted in an age of 5034 ± 40 BP (OxA-8294) – even taking contamination into account, this specimen is not an early AMH. Therefore, the focus shifted onto the osseous points. Both VP-133 and VP-135 were tested for %N content, though with results of 0.23 and 0.13, respectively, neither of them seemed to have any collagen preservation.

At the cave site of Krapina, hundreds of Neanderthal bones and teeth, over 800 Mousterian lithics and several thousand faunal remains were unearthed during the excavations from 1899-1905 (Gorjanović-Kramberger, 1906; Radovčić et al., 1988; Simek and Smith, 1997). However, ESR and uranium series dating by Rink et al. (1995) places the age of the Neanderthals at around 130k, *i.e.* in the late MIS 5e, and therefore well before the MP/UP transition.

In contrast to the previous sites, Šandalja is located near the Adriatic coast. Šandalja II encompasses the Late Pleistocene and Holocene layers, which include an Aurignacian and an Epigravettian horizon, but no MP material (Karavanić, 2003). Between 1963 and 1973, Homo sapiens remains were discovered in layer B, and directly dated to 12320 ± 100 BP (GrN-4978) (Malez and Vogel, 1969). From layer H, a split-based bone point is known (see fig. 10.2). The radiocarbon date obtained from material within the horizon, 17600 ± 370 BP (Z-2422), stands in contradiction to the chronostratigraphy of the site and the older age of the overlying 'Aurignacian' level (Karavanić, 2003). Consequently, direct radiocarbon dating of the point would help in placing the artefact in a more precise and accurate chronological context.

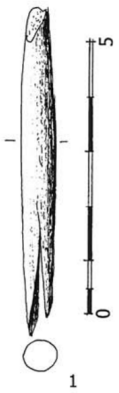


Figure 10.2: Šandalja: SBP (Karavanić, 2003, fig. 9.1).

Bukovac cave would be an archaeologically unremarkable site were it not for the discovery of an 'Aurignacian' osseous point and some punctured faunal bones that might represent remains of early musical instruments. Direct radiocarbon dating offers a unique opportunity to chronologically place this diagnostic artefact within the chronology of Upper Palaeolithic osseous points.

Croatia has a number of archaeological sites that are relevant to the study of the MP/UP biocultural transition, yet their formation processes as well as the excavation and conservation methods applied in the past pose significant challenges for modern research. As this project was unable to obtain suitable material form either Vindija or Velika Pećina, and Krapina is too old, the focus will rest on Bukovac cave. It is hoped that in the near future, an opportunity will present itself to directly date the SBP from Šandalja.

10.1 Bukovac

Bukovac is a small site in Croatia, which at the beginning of the 20th century produced an iconic antler point. With no lithic remains, direct dating of the osseous point is the only means to date the short occupation. At the same time, it provides another opportunity to expand our understanding of the 'Aurignacian' osseous point industries and their spatio-temporal distribution.

10.1.1 Introduction

Bukovac cave (45.361 N, 14.753 E) is located close to Lokve in the Gorski Kotar, only 16 km from the Adriatic coast. The cave is T-shaped, and its entrance lies at an altitude of 864 m a.s.l. facing north (see fig. 10.3). Initially, the entrance corridor extends for *ca.* 45 m in south-south-western direction, then bends to continue in south-western direction for another 9 m, before ending in a main hall continuing to either side of the corridor. The hall area is 4–6 m wide and 20-22 m long. At its south-eastern end, a small

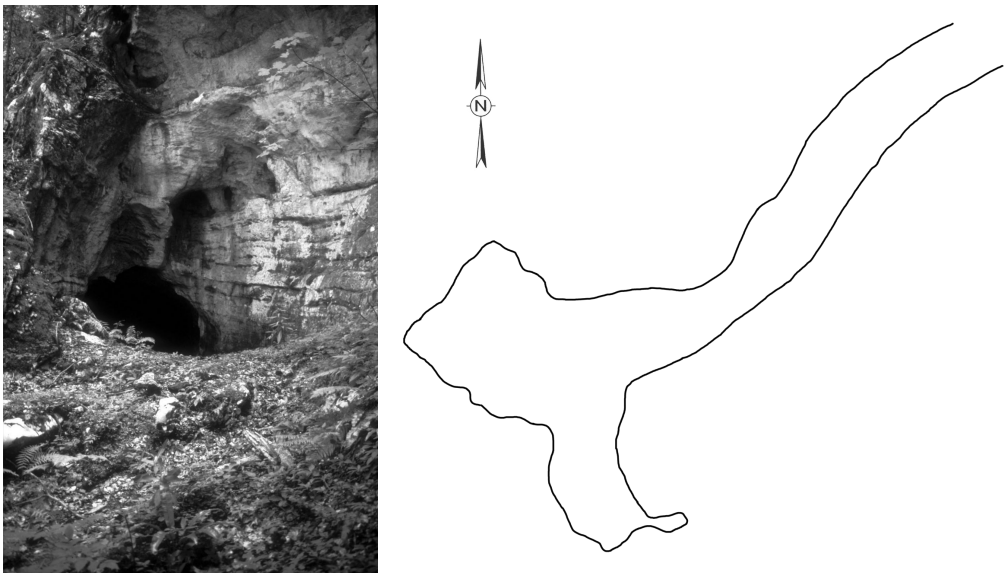


Figure 10.3: Bukovac: left – photo of cave entrance (Horusitzky, 2004, fig. 1); right – sketch of cave layout after Janković et al. (2011, p. 480).

niche with a stalagmite pillar is found. While the floor in the rear of the cave is covered with a sinter crust, there are no surface flowstones observed towards the cave entrance and the cave is presently dry (Horusitzky, 2004; Kormos, 1912).

The site was excavated in 1911 by Kormos (1912). He opened up two trenches. The first, a test trench 7 m from the cave entrance, measured 3 x 1.8 m and was excavated to a depth of 2.2 m. The second was located in the niche and extended 8 m into the main hall, and covered a total area of 28-30 m^2. The stratigraphic profile was described by Kormos (1912) as follows (from top to bottom):

1. chalky cave clay (5-10 cm)
2. sinter floor (20-30 cm)
3. brown, wet cave clay (40-50 cm)
4. reddish-brown, dry sand (90 cm)
5. yellow, loose quartz sand (60 cm)

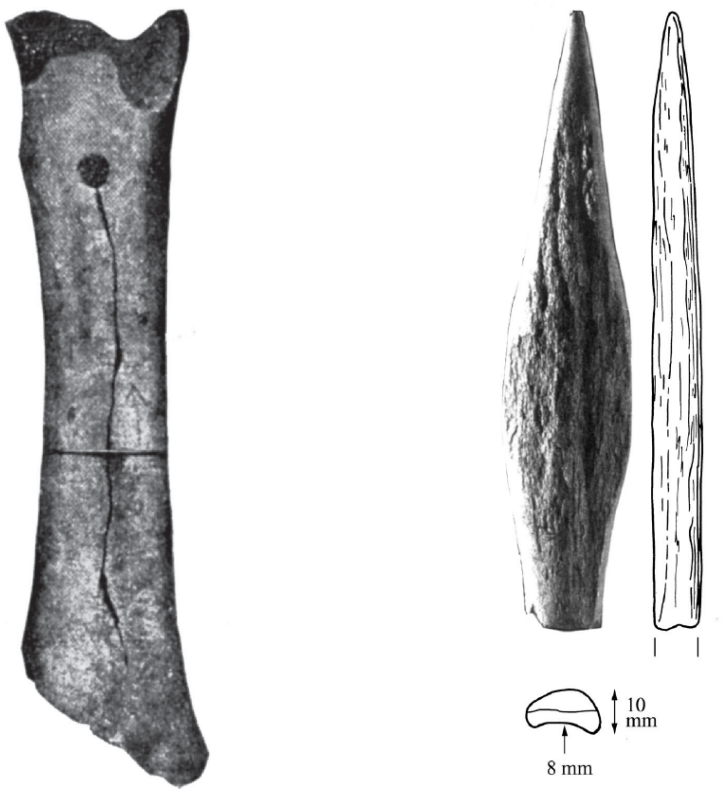


Figure 10.4: Bukovac: some artefacts from layer 3: left – femur with puncture, preserved length 157 mm (Horusitzky, 2003, fig. 2a); right – antler point, preserved length 126 mm (Horusitzky, 2004, fig. 3).

In the niche, the middle part of layer 3 showed traces of fireplaces, including charcoals from spruce wood. Additionally, the layer produced a significant number of fragmented cave bear remains – described as displaying clear chop and cut marks –, though none of the bones were calcified. Moreover, the same layer yielded the only archaeological artefacts: an antler point, a radius with a single puncture, a rib with three holes, a femur with one hole and a left femur with two punctures (see also fig. 10.4). The underlying layers appear both sterile and the only other fauna identified at the site, were five fragments from a panther (probably *Leopardus pardus L.*) (Kormos, 1912).

Subsequently, a small test excavation by (Malez, 1959) from 1956 confirmed Kormos (1912) stratigraphy, and in 2011, Janković et al. (2011) opened

another trench in the north-western end of the the main hall for further analysis. However, throughout that period no lithic remains were found.

The small assemblage has led to some speculation about the age of the human occupation. Maška saw in the punctured bone fragments a connection to artefacts from the Mousterian, though Kormos proposed an affiliation with the Magdalenian – known at the time for its osseous industry (Kormos, 1912). At the same time, he notes that such an abundance of cave bear remains would be unusual for that period. Bayer (1929) featured the antler point in his description of the Olschewa culture, which he saw as an expression of Aurignacian osseous artefacts without the presence of their diagnostic lithics. Kadić (1934), in turn, compared it to the material from Jankovich (see fig. 11.31-a). Direct radiocarbon dating will finally provide essential new insights into the question of the chronological origin of the artefact.

10.1.2 Radiocarbon dating

All but one artefact found at Bukovac are currently stored at the Hungarian National Museum in Budapest, the other appears to be missing (Horusitzky, 2004). As direct radiocarbon dating presently offers the only means to obtain further information necessary to contextualise the osseous point, the artefact Pb 602 was sampled at the museum in April 2015.

Sample & Treatment

The antler point Pb 602 was sampled using key-hole drilling from the narrow edge, ca. 4 cm from the distal point. This is an area where the surface was still largely intact, thus reducing the probability of contamination (see tab. 10.1). The powder sample was subsequently treated with consecutive solvent washes: acetone (1h, 40°), methanol (0.5h, RT), and chloroform (0.5h, RT). After treatment with ORAU's gelatine protocol (AG*), the sample was freeze-dried. Due to a yield in excess of 25 mg, the collagen sample was divided into two fractions. The first, *ca.* 2.30 mg, was combusted for

Table 10.1: Bukovac: massive-based point sampled for radiocarbon dating with context information, %N results and sample weight.

Ref-no.	Inv.-no.	Item	Excav.	Trench	Layer	%N	Weight	Cons.
Buk-01	Pb 602	MBP	1911	rear	3	3.05	361 mg	Y

graphitisation and AMS dating. The remaining fraction, *ca.* 27 mg was used for hydroxyproline dating. This allowed for a direct comparison of the ^{14}C results.

Buk-01 is a near complete massive-based antler point. The distal point appears to still be intact, while the proximal end had been damaged. The sides, as well as the point, are polished. Large areas of the dorsal and ventral surface have been eroded. Presently, the antler point has a lunate-cross section which becomes round only at the dorsal end. There is a groove/channel extending longitudinally close to the center of the artefact's dorsal side, eventually lining up with the right edge of the base. The artefact is preserved on a length of 12.6 cm, with a maximum width of 2.8 cm, and a thickness of 1 cm. The base is 1.7 cm wide.

Kormos (1912) classified the point as a Mladeč type. However, its size is substantially smaller and the base thicker and straighter. Knecht (1993b) lists Pb 602 as a split-based point[1], a classification Horusitzky (2004) supports. He argues that the general shape is consistent with the point found at Mokriška jama, which shows a split base. The use of antler for manufacture is also predominantly found with SBP (Knecht, 1993b). The small cleft observed by Horusitzky (2004) could either be the result of the base fracture that resulted in the loss of the points proximal end, or the remains of a split base. However, the split bases observed with many SBPs often reach or approximate the widest section of the point. The specimen found at Bukovac has the preserved proximal part narrowing from 2.8 cm to 1.7

[1]The classification of the material as bone probably results from a publication by Albrecht et al. (1972), as discussed by Horusitzky (2004). Everyone else analysing the material classified it as antler.

cm before showing any traces of what might have been a split base. It seems therefore more appropriate to interpret the artefact as a massive-based point.

The artefact is coated in an unknown conservation substance (possibly PVA), which left pronounced traces in the many small cavities. The museum number (Pb/602.) is written in black ink on the proximal part's dorsal surface.

^{14}C Results

Both radiocarbon measurement on Buk-01 were successful (see tab. 10.2–10.3). The mass-spectrometry results from the sample combustion show no anomalies, and both the gelatine and the hydroxyproline fraction could be graphitised to small targets (0.8 mgC). The AMS run was uneventful. The HYP measurement was subsequently corrected for HPLC background following the method described in section 5.4.7. The 'OxA-X' prefix for the hydroxyproline date was based on the use of a then non-routine chemical pretreatment and is not indicative of the quality of the measurement itself. On the contrary, despite both radiocarbon dates being reliable from a pretreatment perspective, it is the NRC date that will be more accurate. AG* treated samples of such an old age are expected to slightly underestimate the true age of the sample.

Table 10.2: Bukovac: radiocarbon pre-treatment results for the osseous point. The yield for the HYP fraction was given in mgC, which is the sample size used in the HPLC background correction (see section 5.4.7).

Ref-no.	Item	Treat.	Yield	%C	δ^{15}N	δ^{13}C	C:N
Buk-01	MBP	AG*	29.35 mg, 8.13 wt.%	39.7	4.7	-19.5	3.1
Buk-01	MBP	NRC	1.0139 mgC	40.7	5.2	-25.3	4.8

10.1.3 Discussion

It was possible to obtain two successful, direct radiocarbon measurements from the single massive-based antler point from Bukovac: one on the gela-

Table 10.3: Bukovac: new AMS radiocarbon results on the osseous point. Dates calibrated with OxCal 4.3 (Bronk Ramsey, 2009a) using IntCal13 (Reimer et al., 2013). In grey are the hydroxyproline results prior to HPLC correction (see section 5.4.7).

Ref-no.	Treat.	Lab-no	$F^{14}C$	^{14}C (BP)	Date (cal BP)
Buk-01	AG*	OxA-35953	0.02411 ± 0.00156	29950 ± 500	34990 – 33100
Buk-01	NRC	OxA-X-2732-11	0.02084 ± 0.00134	31100 ± 520	36130 – 34120
			0.02207 ± 0.00110	*30630 ± 400*	

tine (AG*), one on the hydroxyproline (NRC) fraction (see tab. 10.3). As expected, OxA-35953 (29950 ± 500 BP) is slightly younger than the hydroxyproline date OxA-X-2732-11 (31100 ± 520BP), though both dates are statistically indistinguishable (see fig. 10.5). This shows, that if AG* treatment did not remove all modern contamination from the antler powder, the quantity remaining – and thus its effect – were minimal.

For future comparison, the hydroxyproline date will be favoured over the gelatine fraction. It places the antler point at the younger tail end of the massive-based point distribution from Istállóskő. For a more detailed comparison and discussion of all directly dated osseous points see section 14.

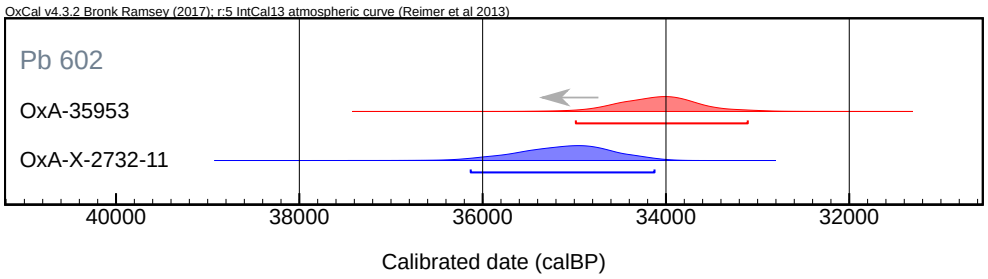


Figure 10.5: Bukovac: comparison of radiocarbon dates obtained on the antler point Pb 602. **red** – AG*; **blue** – hydroxyproline. The arrow indicates that AG* treatments are generally minimum age estimates for the period of interest.

Chapter 11

Hungary

Hungary has a long standing tradition of Palaeolithic excavations, going back to the beginning of the 20th century. Several sites have since featured in the debate on the Middle to Upper Palaeolithic biocultural shift. They cluster in two main regions: the Bükk Mountains, and the mountains of western Transdanubia (see fig. 11.1). The apparent emptiness of the Hungarian Plain is best explained by absence of evidence, rather than evidence for absence. The formation of thick loess sediments during MIS3 and MIS2 would have buried any late Middle Palaeolithic or Early Upper Palaeolithic open air sites in the region (see *e.g.* Sümegi et al., 2015), adding substantial challenges to locating human occupations.

Many of the known sites have been excavated during a period where fast paced sediment removal and less detailed find information was common. At the same time, the nature of the sites led to cultural interpretations that were often based on very few archaeological artefacts. Nonetheless, there are several sites from the period of interest that might contribute to our understanding of the biocultural shift, and would benefit from targeted radiocarbon dating. In the following, some of the main Hungarian sites will be evaluated on whether they contain the MP/UP transition, specific industries of interest, or human remains. Furthermore, the value of applying the lasted radiocarbon methods to these largely old excavations will be discussed.

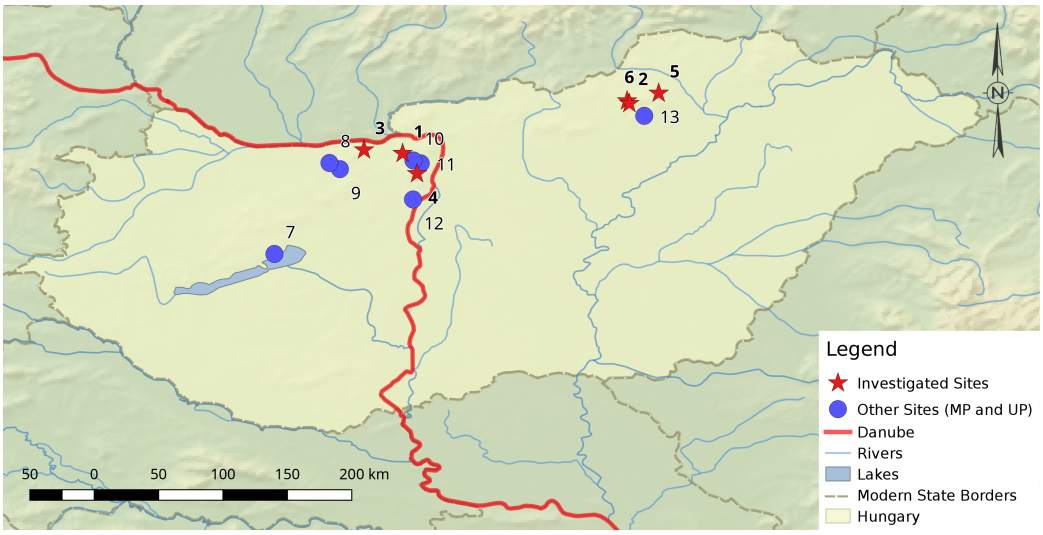


Figure 11.1: Hungary: map of Middle and Upper Palaeolithic sites: (1) Bivak, (2) Istállóskő, (3) Jankovich, (4) Máriaremete, (5) Szeleta, (6) Peskő, (7) Lovas, (8) Tata, (9) Szelim, (10) Pilisszántó, (11) Kiskevély, (12) Érd, (13) Subalyuk.

There are only three sites with human remains: Subalyuk, Máriaremete, and Istállóskő. At the first, the remains of a *Homo neanderthalensis* adult and child (*ca.* 3 years of age) were found in the Mousterian layer 11. While osseous material is available, the faunal record dates the horizon to MIS 5a–c (Svoboda, 2005) – and therefore beyond the reach of radiocarbon dating. The three adult human teeth discovered at Máriaremete were initially seen as belonging to a *Homo neanderthalensis* (Gábori-Csánk and Svoboda, 1983), though were later labelled non-diagnostic (Svoboda, 2005; Tillier et al., 2006). They were found in layer 4 in association with Jankovichian lithics (Gábori-Csánk, 1993), thus possibly within reach of the radiocarbon. And finally, Istállóskő yielded a *Homo sapiens* tooth in the upper fireplace level (Malán, 1954). While there is some reason to believe that this places the specimen within the Gravettian or later period, direct radiocarbon dating might clarify its relationship to the MP/UP shift.

What makes Istállóskő more attractive as a site are the nearly 50 'Aurignacian' osseous points – both split-based and massive-based. The only other site with such a substantial assemblage in Hungary is Jankovich cave. In addition, osseous points were discovered at Bivak, Peskő, and Szeleta.

None of the Hungarian cave or open air sites cover the full MP/UP transition, though it is worth noting that the cave sites of Jankovich, Máriaremete and Szeleta contain Jankovichian/Szeletian material. The ochre mine at Lovas has been previously placed within the Jankovichian technocomplex on the basis of a single leaf-shaped scraper (Gábori-Csánk, 1993). However, the rich osseous industry has raised questions and more recent work suggests that the site might actually belong to the Late Palaeolithic, citing artefact typology and a radiocarbon date of 11740 ± 100 BP (ETH-15199) (Dobosi, 2006). Also the interpretation of Kiskevély cave has shifted over the years. Initially, Hillebrand (1913b) classified the archaeological horizons as 'Protosolutréen' (*i.e.* 'Szeletian') and 'Magdalenien' (*i.e.* 'Gravettian') with Kiskevély blades[1]. However, the stratigraphy was problematic and the site fully excavated, yielding very limited material. In contrast, the two often cited rockshelters at Pilisszántó contained microgravette points and blunt backed blades, placing the assemblage in the 'Cave Gravettian' (Gábori, 1977) and thus the later Upper Palaeolithic.

It appears to be particularly difficult to find late Middle Palaeolithic sites in Hungary. The Middle Palaeolithic open air sites of Érd and Tata are both older than 50k cal BP. Szelim cave was fully excavated prior to WWII and only contained a small archaeological assemblage, which appears to be similar to material found at Érd and Tata (Mester, 2006).

As a result, this project focused on osseous point industries, and Szeletian/Jankovichian lithic material. The selection included Bivak, Istállóskő, Jankovich, Máriaremete, Szeleta, and Peskő. For all of these sites, access or partial access to the available material was granted, allowing for testing of stratigraphic integrity, timing of the osseous point industry and its chronological connection to the Szeletian/Jankovichian lithics.

[1] They are chipped cave bear teeth seen by Hillebrand as artefacts and later interpreted as geofacts by Jeanneret (1948). It seems like the modern debate might be leaning towards the former again.

11.1 Bivak

Bivak is a small cave site in transdanubian Hungary, relatively close to Jankovich and Máriaremete. Its archaeological assemblage is extremely small, but contained fragments of what Jánossy et al. (1957) believed to be Aurignacian split-based points. The excavation was too coarse to allow for more in-depth archaeological analysis. Therefore, direct dating of osseous points provides the only means to contextualise these important artefacts and assess their role in the spread and use of osseous point industries in the European Upper Palaeolithic.

11.1.1 Introduction

Bivak cave (N 47° 41' 58", E 18° 50' 39") is located on the western flanks of the Pilis Mountains, within the municipal limits of the village of Piliszentélek, north-east of Budapest. Its entrance opens to the west at an altitude of 515 m a.s.l. (see fig. 11.2 and 11.3), and Jánossy et al. (1957) estimated its original height to have been *ca.* 6 m. The cave has one main gallery, extending eastwards for ca. 11 m, with an average width of 4–5 m. Towards the rear of the cave, the ceiling lowers and there are two small side niches: one, nearly circular in shape, extends to the north, the other, as a narrowing triangular canal, to the south-west.

The cave was registered by K. Sebős, and an initial exploratory excavation trench was opened by K. Bertalan and J. Szenes in 1943. Ten years later, D. Janóssy and L. Vértes started intensive excavations, leaving the entire cave depleted of sediment – except for the small area in the northern niche (see fig. 11.3), which they preserved in the interest of later control analysis (Jánossy et al., 1957).

They described a package of 1–1.4 m thickness, which contained 5 geological layers underneath the Holocene humus level, with the second unit only found in some areas of the cave. Following their profile (see fig. 11.2) from

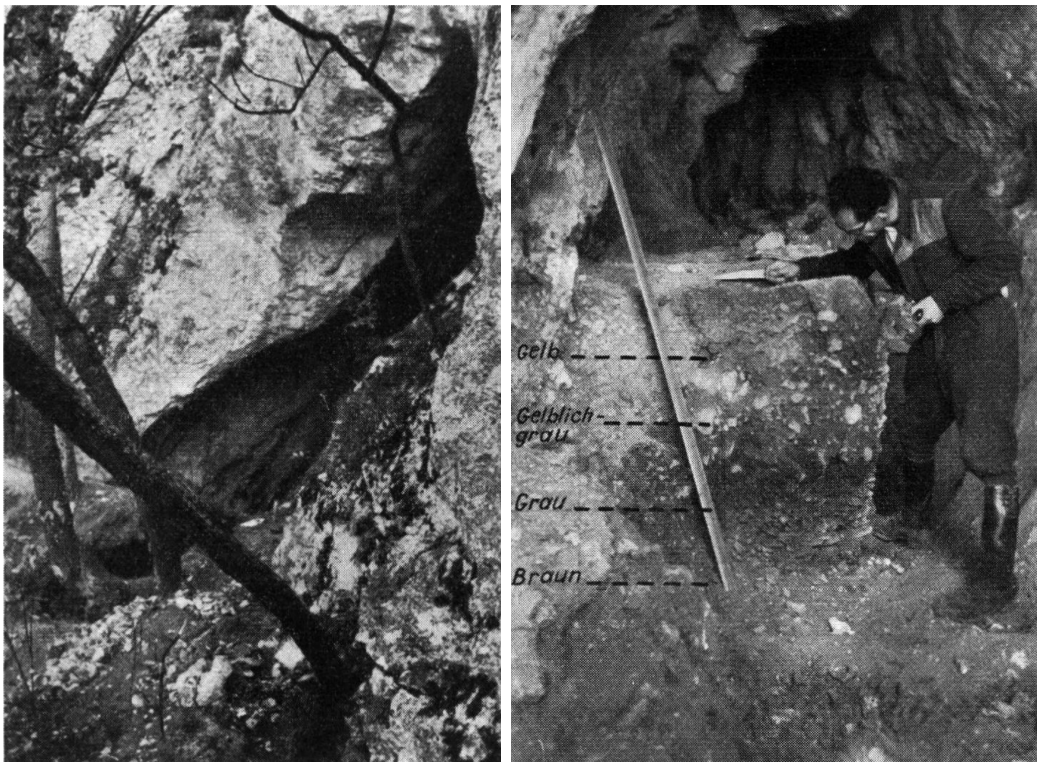


Figure 11.2: Bivak: photos of cave entrance (left) and of the sediment profile with D. Janóssy (right) (Jánossy et al., 1957, fig. 1 and 2).

top to bottom, the units were distinguished on the basis of their sediment colour as follows:

1. **yellow** layer (*ca.* 30 cm)
2. **orange** layer (constrained)
3. **yellowish-grey** layer (*ca.* 10 cm)
4. **grey** layer (*ca.* 20 cm)
5. **reddish-brown** layer (*ca.* 50 cm)

It was suggested that a sediment hiatus occurred between layers 3 and 2 to account for the localised nature of layer 2. However, it will be difficult to assess what processes were involved in creating the stratigraphy, as without

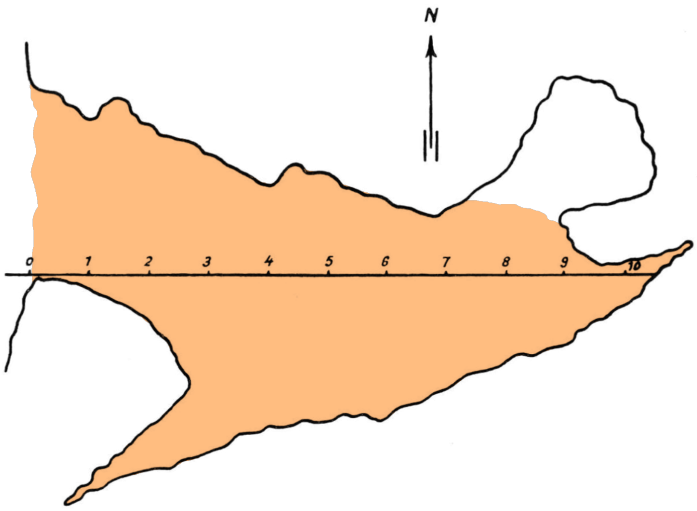


Figure 11.3: Bivak: map of the cave with estimated excavation area from 1953 highlighted in **orange** (modified from Jánossy, 1954, fig. 2).

detailed excavation records, other mechanisms (*e.g.* erosion, mixing, heating, localised activity, ...) are also possible. In regards to faunal remains, layer 3 was richest in terms of variety, and layer 4 in terms of absolute fragments retrieved.

Despite the near complete excavation, and the substantial palaeontological fauna found, the archaeological remains were scarce. Jánossy et al. (1957) believed that they had identified two archaeological horizons (a lower and an upper AH). They placed the older occupations within the grey and yellowish-grey units (*i.e.* layers 3 and 4), and the younger one within the yellowish unit (*i.e.* layer 1). This division already demonstrates that the localisation of the archaeological artefacts was crude, and it certainly combined material from more than one archaeological level.

The laurel-leaf point with 'shaft' from the lower AH (fig. 11.4-6) was linked to the Szeletian by Jánossy et al. (1957), and later placed within the context of the Jankovichian by Gábori (1977). As the same AH also yielded two fragments of osseous points (fig. 11.4-1,3), Jánossy et al. (1957) proposed a contemporaneity or cultural mixing between the 'Szeletian' and the Early

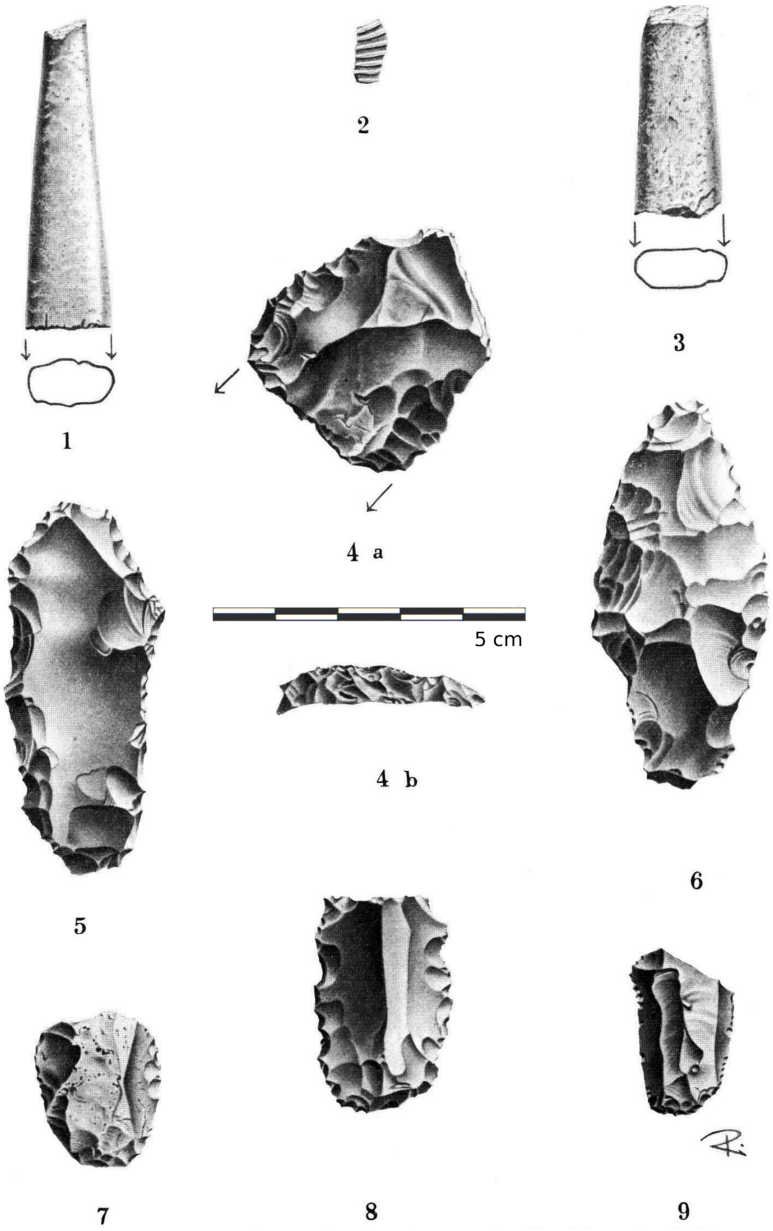


Figure 11.4: Bivak: artefacts from the lower (1, 3–6, 8) and upper (2, 7, 9) archaeological horizon. Materials used were antler (1,3), silex (4–8), shell (2), and obsidian (9). 1,3 – osseous points (SBP?); 2 – mollusc shell; 4 – scraper with trapezoidal reduction bladelet; 5 – scraper; 6 – laurel leaf-point; 7 – retouched blade fragment; 8 – fragment of a blade with *"hohem Rücken"* ('elevated back'); 9 – transverse burin (Jánossy, 1954, tab. I, scale added).

Aurignacian within Hungary. Both point fragments were published as split-based points, on the basis of their convergent form and flat-oval cross-section.

With hindsight, the loose association of a single leaf-shaped point with osseous point fragments – from within an archaeological horizon combining two geological units – is insufficient to propose any chronological interpretations and should be treated with utmost scepticism. Slightly more convincing is the proposed connection to material found at Jankovich cave, though the size of the assemblage does not allow for far-reaching comparisons.

In contrast, the upper AH did not provide any culturally diagnostic artefacts (see fig. 11.4). It was assumed that the activity would belong to the Gravettian, considering its position within the stratigraphy.

11.1.2 Radiocarbon Dating

Split-based points form a crucial role in our understanding of the Aurignacian and have featured heavily in discussions on the spread of AMH into Europe. However, the artefacts retrieved from Bivak require direct radiocarbon dating to be contextualised, as limited archaeological material and poor stratigraphic precision (possibly caused by the rough excavation methods applied) heavily limits our chronological understanding. Therefore, access to the osseous point stored at the Hungarian National Museum and the faunal remains at the Natural History Museum in Budapest was requested, leading to sampling in April and September 2015. While the focus lies on the osseous points, it was hoped that the fauna can give some insight into the archaeological levels possibly contained within the lower AH.

Sample & Treatment

All the accessible faunal material from the lower AH, *i.e.* the grey and yellowish-grey layers, was examined for anthropogenic modifications. Only two specimens with cut marks could be identified (see tab. 11.1). They were

subsequently sampled at the museum with a drill. Biv-02 was accessed from the bone interior, exposing a ca. 10x5 mm large rectangle. Regrettably, the bone was very soft, leading to minor damage of the outer surface. Biv-2 felt more robust. The sample was taken using key-hole drilling with a widened canal for more efficient sampling. The longbone was drilled from the fractured end, and sampled along the longitudinal axes. In addition, access was granted to the osseous point Pb 53/11 (see fig. 11.4-1). Key-hole drilling was applied to the damaged proximal (*i.e.* wider) end of the fragment along the longitudinal axis. Visual damage was kept to a bare minimum. In all cases, the surface was abraded prior to sampling, to minimise contamination.

Table 11.1: Bivak: radiocarbon samples – an osseous point and cut-marked bones – with context information. * lower AH corresponds to both the grey and yellowish-grey layers.

Ref-no.	Inv.-no.	Item	Excav.	Layer	%N	Weight	Cons.
Biv-01	Pb 53/111	point	1953	lower AH*	0.83	289 mg	Y
Biv-02	–	fauna	1953	grey (lower part)	1.97	491 mg	?
Biv-03	–	fauna	1953	grey	1.99	450 mg	?

The osseous point showed clear signs of conservation work. At the same time, it remained unclear whether the faunal remains were also treated or just left in storage. Consequently, all samples were first treated with solvent wash steps: acetone (1h, 40°C), methanol (0.5h, RT), and chloroform (0.5h, RT). The samples were dried over night at RT, instead of the heating block, to avoid further damage to the collagen. Subsequently, they underwent regular pretreatment following the gelatine protocol AG (see section 5.4.5). Collagen preservation was insufficient for ultrafiltration (not to mention hydroxyproline dating).

Biv-01 mesial fragment of an antler point, possibly SBP (see fig. 11.4-1, and A.2). Both proximal and distal end of the artefact are missing, and the surface is uneven and damaged. The sides are convergent and near symmetric, with a flat-oval cross-section. It was this shape that led Jánossy et al. (1957) to classify the artefact as a SBP. While it indeed matches the shape of

Table 11.2: Bivak: radiocarbon pretreatment results with treatment information, yield after pre-treatment (in mg and wt.%), and %C, stable isotopes and C:N ratio on combustion.

Ref-no.	Item	Treat.	Yield (mg)	Yield (%)	%C	δ^{15}N	δ^{13}C	C:N
Biv-01	point	AG*	1.96	0.68	38.3	2.7	-18.1	3.5
Biv-02	fauna	AG*	8.48	1.73	41.0	9.1	-23.6	3.2
Biv-03	fauna	AG*	8.96	1.99	40.3	4.2	-20.5	3.2

other SBP found in Hungary, the proximal end – where the split base would be located – is missing, and no traces of a split-base are visible. The rough surface, and the still very pronounced edges, could indicate an unfinished point. The artefact is preserved on a length of 46.8 mm, and has a maximum width of 13 mm.

The proximal part of the ventral surface shows a piece of glue, with a size of *ca.* 1x1.5 cm, and remains of a wooden pressboard attached. It marks the location the antler point used to be mounted on in the old museum exhibition. A bit further up, in the mesial part of the fragment, the museum number (Pb 51/111) is written in black ink onto the ventral surface. The entire surface, including the fractured ends, is slightly shiny – possibly a sign of conservation coating, though this could also stem from natural polishing prior or during deposition.

^{14}C Results

As a result of poor collagen preservation, the three specimens from Bivak could only be pretreated using the less rigorous AG* pretreatment protocol (as mentioned above). Despite a yield of <1%, the osseous point Biv-01 was dated. Even a minimum age estimate would be able to provide more chronological information than the published stratigraphy.

While both faunal specimens showed good combustion, stable isotopes and C:N ratio results, the point displayed depleted δ^{13}C values and an ele-

Table 11.3: Bivak: new AMS radiocarbon dates on 1 osseous point and 2 cut-marked bone fragments. Calibrated age calculated in OxCal 4.3 (Bronk Ramsey, 2009a) using IntCal13 (Reimer et al., 2013).

Ref-no.	Lab-no	$F^{14}C$	^{14}C (BP)	Date (cal BP)
Biv-01	OxA-X-2716-50	0.03060 ± 0.00189	28000 ± 500	33260 – 31090
Biv-02	OxA-35422	0.00508 ± 0.00116	42400 ± 1800	49660 – 43430
Biv-03	OxA-35423	0.00619 ± 0.00116	40800 ± 1500	48070 – 42320

vated C:N ratio (see tab. 11.2). The background bone standard (19651.166 AG* 03) from the same chemlist and identical small graphite mass-spec burn as Biv-01 (no. 4940) also gave an elevated C:N ratio (*i.e.* 3.5). During AMS measurement, it showed a high background, resulting in an age > 41800 BP – compared to typical background values ranging between > 48000 to > 50300 BP (see Appendix). Consequently, the osseous point date of 28000 ± 500 BP (OxA-X-2716-50) is certainly underestimating the true age of the sample – which is reflected in the OxA-X prefix given to the result.

The dating quality of the osseous point does not fulfil the high standards this project had hoped for. Nonetheless, judging by the background bone standard, it is improbable that the pre-treatment issues have affected the age in excess of 7000 radiocarbon years, thus minimally constraining the age window. In contrast, the dates of 42400 ± 1800 BP (OxA-35422) and 40800 ± 1500 BP (OxA-35423) for the cut-marked bone provide a good approximation, and are consistent with their relative stratigraphic position (see tab. 11.3).

11.1.3 Discussion

Dating quality at Bivak cave was not ideal as a result of poor collagen preservation, the limited material available and pre-treatment difficulties. Despite these constraints, it is apparent that the antler point is younger than the two cut-marked bone fragments dated from the grey layer. The two latter provide measurements that are statistically indistinguishable using a χ^2-test. By contrast, the date from the antler point would remain statistically younger

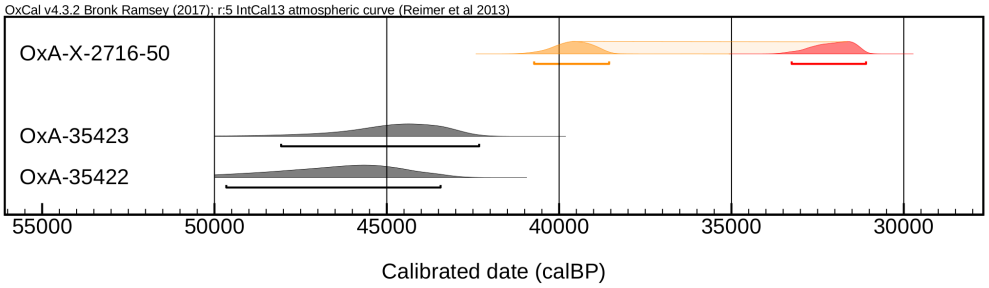


Figure 11.5: Bivak: visual comparison of the calibrated radiocarbon dates obtained from the osseous point, and the two cut-marked bone fragments. **red** – actual AMS radiocarbon age for the point Biv-01; **orange** – radiocarbon age for Biv-01 assuming the measurement underestimates the true age of the sample by 7000 ^{14}C years. Shaded background between the two dates highlights possible ages for the point within that constraint.

even when using the currently largest contamination derived offset estimated. The simplest explanation would be that the point actually belonged to layer 3, while the dated faunal remains came from layer 4. On the other hand, it may be a result of the coarse excavation techniques, which led to archaeological material from different occupations being combined. Either way, it seems unwise under these conditions to draw any direct conclusions from the supposed association of the lithics and osseous artefacts at Bivak.

The antler point date of 28000 ± 500 BP (OxA-X-2716-50) might underestimate the true age of the artefact by up to 7000 radiocarbon years (see fig. 11.5). In such a case, the artefact would be close to the group of SBP observed at Istállóskő (see below). However, in case of a smaller dating error, the artefact would group in a period dominated by massive-based points. Further (and more reliable) dating, combined with a detailed analysis of shape and style of osseous points, may improve the position of Biv-01 within the spatio-temporal context of the osseous point industry (see also chapter 14).

11.2 Istállóskő

Istállóskő has for a long time been seen as one of the most important Aurignacian sites in Hungary and its interpretation has been critical in developing models explaining the spread of AMH or the dispersal of the Aurignacian osseous projectile point industry. However, both its stratigraphic integrity and its cultural attributions have been repeatedly questioned. As a result, this dissertation aims to both evaluate the stratigraphic integrity of the site through selected radiocarbon dating, and to place the osseous projectile point industry in a proper chronological context.

11.2.1 Introduction

Istállóskő ('Stable Rock') is a cave site in the north-east of Hungary (48.072 N, 20.419 E), more precisely in the the western parts of the Bükk Mountains, close to the Bán Creek (see fig. 11.6). In close proximity lie the sites of Peskő and Szeleta, from which further osseous projectile points were sampled for dating (see sections 11.6 and 11.5).

Istállóskő cave contains one gallery, opening towards the south-west at 546 m a.s.l (see fig. 11.7– 11.8). The section expanding in north-east direction measures approximately 36 m, followed by a narrower section towards the rear, which extends eastwards for approximately 14 m. The cave has a maximum height of 10 m, and its ceiling is heavily slanted, leading to a nearly triangular cross section with the maximum height towards the western side of the cave. The side walls are, on average, around 8-9 m apart, with a maximum width of 14 m Mottl (1945); Vörös (2003).

Excavation History

Throughout the 20th century, several excavations took place (see fig. 11.7 and 11.8). The cave was divided into a front, middle and rear section. A 2x2m grid aligned SW-NE was excavated in the front and main part of the

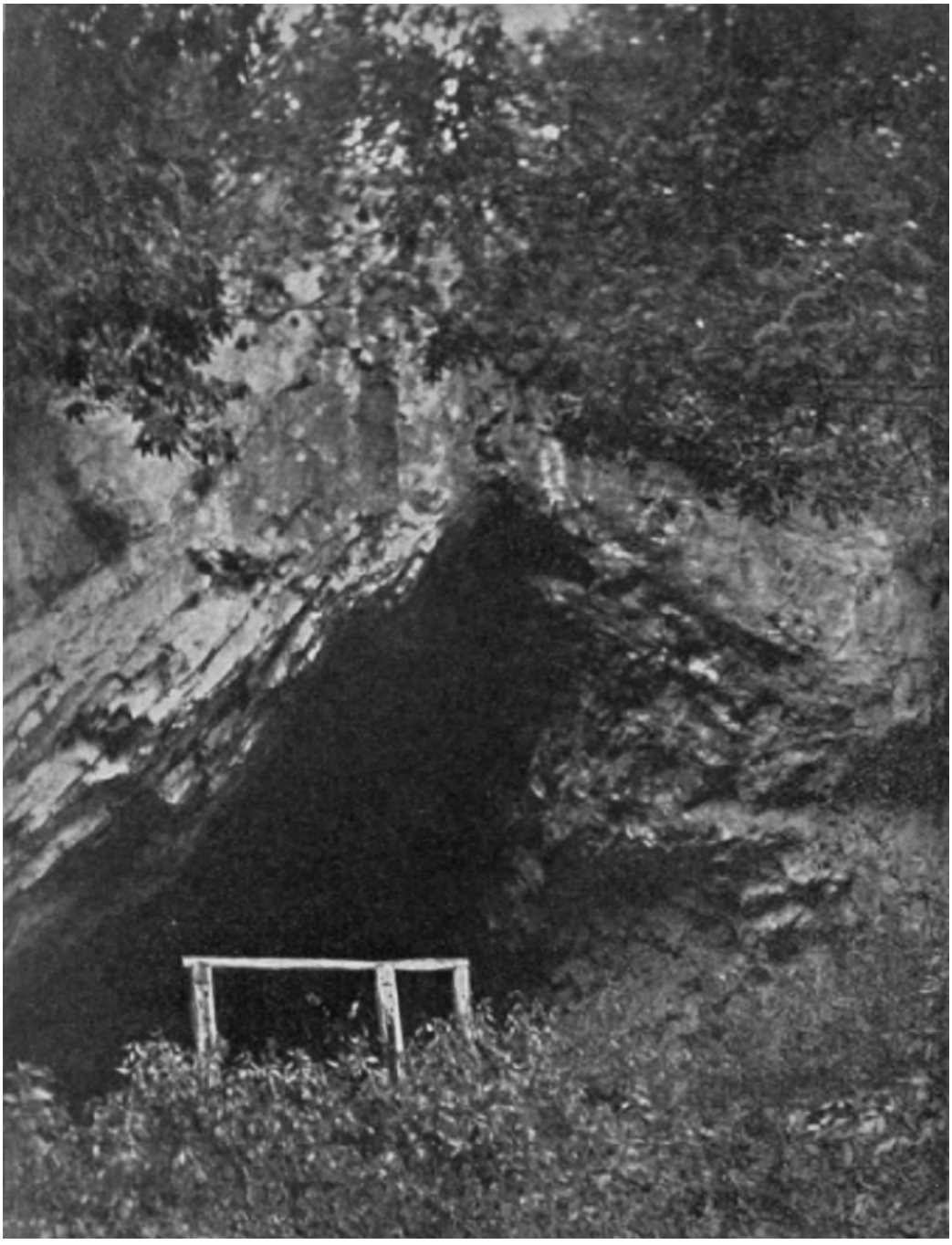


Figure 11.6: Istállóskő: photo of cave entrance in 1912 (Hillebrand, 1913c, fig. 2).

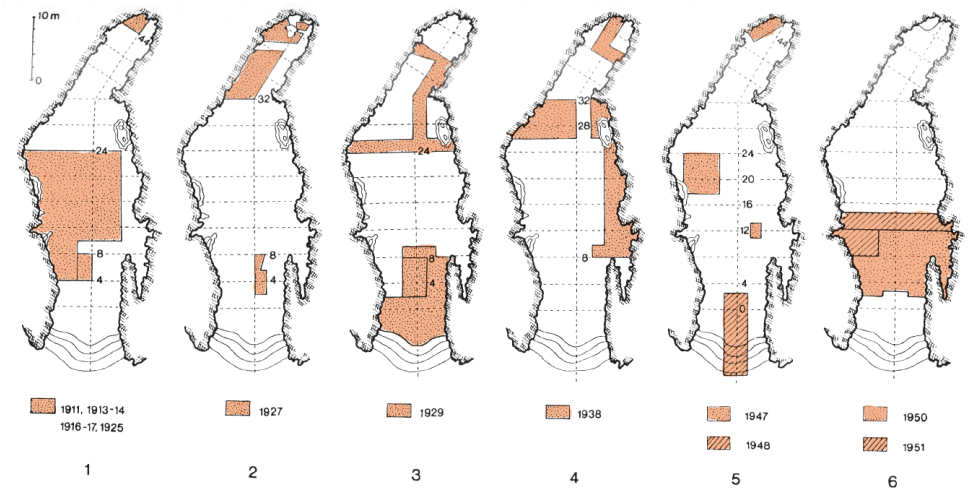


Figure 11.7: Istállóskő: excavations from 1911 to 1951, highlighting different sectors excavated by (1) Hillebrand, (2) Saád, (3) Kadić, (4) Mottl, and (5-6) Vértes (after Vörös, 2003).

cave, and another (W-E direction) was dug in the rear of the cave – in line with the cave walls (Mottl, 1945).

The cave was first surveyed by P. Roskó, then inspector of crown forests (Vörös, 2003). He handed the documentation to J. Hillebrand, who, between 1912 and 1917, excavated parts of the middle section of the cave, revealing a large hearth structure (-80cm), over 100 lithic artefacts and 4 bone tools (Hillebrand, 1913c, 1914, 1917, 1919). He further mentioned blades made of chipped bear canines of the 'Kiskevely type'[2] (Hillebrand, 1917), similar to the ones found at Dzeravá Skala. However, the artefacts were only separated by layer attribution, not by excavation season. In 1925 he extended his excavation of the culture-bearing layer and placed a test trench in the back of the cave, where he again observed the hearth structure he believed to have found in the centre of the cave (Hillebrand, 1926).

Two years later, A. Saád and G. Megay discovered the first clear Palaeolithic evidence at the site. At the rear of the cave, they document an upper

[2]J. Hillebrand named them after the Kiskevely cave in Hungary where he first encountered this artefact type (Hillebrand, 1914).

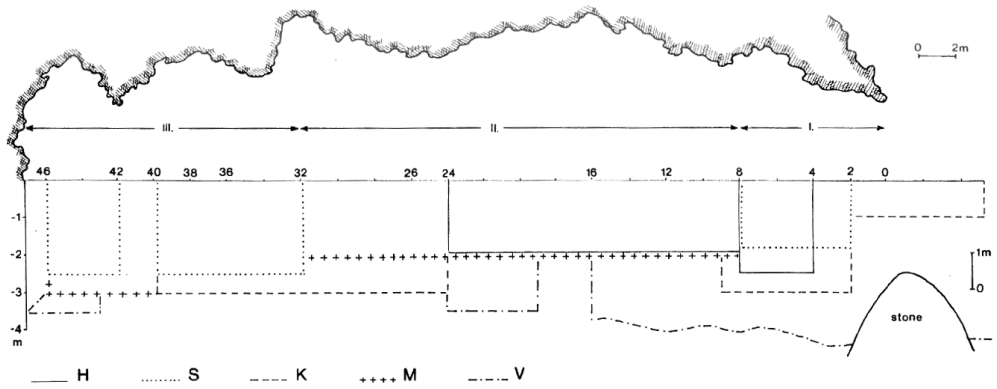


Figure 11.8: Istállóskő: longitudinal section of the cave highlighting the depth of excavations from 1911 to 1951. I – Front Section; II – Middle Section; III – Back Section. H – Hillebrand 1911-1925; S – Saád 1927; K – Kadić 1929; M – Mottl 1938; Vértes 1947-1951 (Vörös, 2003).

hearth (-200 cm) and a lower hearth (-220 cm) structure. At the cave entrance, they unearthed a prehistoric hearth containing burnt human remains. Under the artefacts identified, they – like Hillebrand before them – mention 'Kisevely tooth blades' (Saád, 1927, 1929), which were also known from Dzeravá Skala in Slovakia and other Hungarian sites.

In 1929, O. Kadić conducted extensive excavations. He removed layers in the entrance down to the bedrock and around 3 m from the middle section. Most likely, some of the Aurignacian and 'Magdalenian' artefacts reported in Kadić and Mottl (1944, pp. 40–41) from the cave entrance surfaced during these works.

During the season of 1938, M. Mottl opened up sectors in the south, and middle of the cave. While she also identified Hillebrand's hearth, it did not yield any archaeological material. In the back section, she deepened the existing trenches and found the hearth layers described by Saád and Megay (Kadić and Mottl, 1944; Mottl, 1945). Unfortunately, some of the artefact contexts remain insecure: her field reports suggest that the vast majority of the lithic artefacts belonged to a yellowish-brown layer at the rear, while some of her publications (*e.g.* Kadić and Mottl, 1944) attribute them to the hearth-levels.

Another nine years later, in 1947, L. Vértes revisited the cave and led repeated and extensive excavations at the site until 1965, exposing more than 160 square metres of cave sediment. In the first year, he discovered a hearth feature, which was surrounded by stone slabs, as well as intact skulls belonging to cave bears with Gravettian lithic artefacts at the rear of the cave (Markó, 2015). Subsequently, he opened a trial trench at the cave entrance. The main excavation seasons in 1950 and 1951 were undertaken at the front and centre of the cave, during which Vértes excavated two main culture-bearing layers (labelled f/a and f/b, later named Aurignacian I and Aurignacian II) – separated by a sterile layer. To avoid confusion with cultural attributions, the two cultural layers will from here on be referred to as the upper archaeological horizon (AH) and the lower AH. It was during these two seasons that most osseous tools, including the split-based points, were found (Vértes, 1954; Вертеш, 1951). Also worth noting are 'leaf points' discovered by Vértes in both upper and lower horizons as well as a lower dextral molar (M2) of a *Homo sapiens* in the upper AH (Malán, 1954; Thoma and Vértes, 1971). In subsequent years, Vértes opened test trenches for sedimentological studies and radiocarbon sampling.

All available faunal remains were analysed and published by Jánossy (1954), while cave bear pathologies and chronological changes in cave bear molars were investigated by Tasnádi Kubacska (1954) and Soltész (1954), respectively. Vörös (1984) subsequently examined the faunal record from the 1950/51 excavations for hunting evidence (including cave bear). In his publication, he used a new stratigraphic nomenclature in order to merge the different layer sequences from previous excavations into one schema (see overview in tab. 11.4).

In 2000, new excavations by B. Adams exposed the upper and lower AH, and samples for radiocarbon dating were taken. Between the two archaeological horizons, in the otherwise seemingly sterile layer, a leaf point was discovered (see Adams, 2001, fig. 5–6). Adams and Ringer (2004) believe it to be of the same type and material as the leaf points found at the neighbouring site of Szeleta.

Table 11.4: Istállóskő: correlation of Pleistocene layers described by Vértes (Vértes, 1954; Вертеш, 1951), Vörös (1984, 2003), and Ringer (2002) (after Markó, 2015, tab. 2).

Vértes 1951	Vértes 1955	Vörös 1986	Ringer 2002	Vörös 2003–2004
b: grainy *Magdalenian* clay (in front of the cave)	2: light yellow clay	**VI: light yellow clay ('upper microfaunal layer')**	c: cave loess with limestone debris	upper level: 'upper microfaunal layer'
c: yellow clay with stones ('*Magdalenian*')	3: yellow clay with stones	**V: yellow clay**		1: yellow loessic clay
d: greyish yellow sterile clay	4: sterile, yellow clay			
	7: yellowish brown loessy layer	**IV: yellowish brown loessy clay (large hearth)**		2: yellowish brown layer
e: cemented yellow clay (in front of the cave)				
f: warm brown stony clay [=f/a]	8: dark brown clay with stones	**III: sedimentary complex ('Upper culture-bearing layer' with 3 culture-bearing levels)**	d, e, g?: interstadial cave soils and H: hearths: Arcy-Stillfried B, Les Cottés interstadials	3: dark brown clay
g: dark brown 'lower microfaunal layer'	5: dark brown with microfauna	**II: dark brown layer**		
	11: grey debris			
	12: reddish inclusion			
[f/b]:	9: pale brown clay	**I: light brown clay ('Lower culture-bearing layer' with two culture-bearing levels)**	g?, i: interstadial cave soil(s): Hengelo interstadial and h: cave loess with limestone debris	4: light brow clay
h, i	10: in situ weathered mother rock		j, k, l: cave soil (Moershoofd) and loess	5: layers with various colours

The most recent archaeological work done at the site was conducted in 2004, from which charcoal samples (from fireplaces) and fragmented faunal remains were collected for radiocarbon dating (Davies and Hedges, 2008). Additionally, they sampled osseous projectile points held in museum collections in an attempt to shed light on the site chronostratigraphy and the appearance of osseous point industries in Europe (see section 11.2.1).

Stratigraphy and Archaeology

The cave contains up to 10 stratified layers, of which two are the archaeological horizons (the upper AH and lower AH) of interest, and one further up contained younger archaeological remains (see fig. 11.9 and 11.10). However, 13 different excavations covering approximately 520 m^2 of cave surface and exploiting 1000 m^3 of cave sediment over the past century (see fig. 11.7

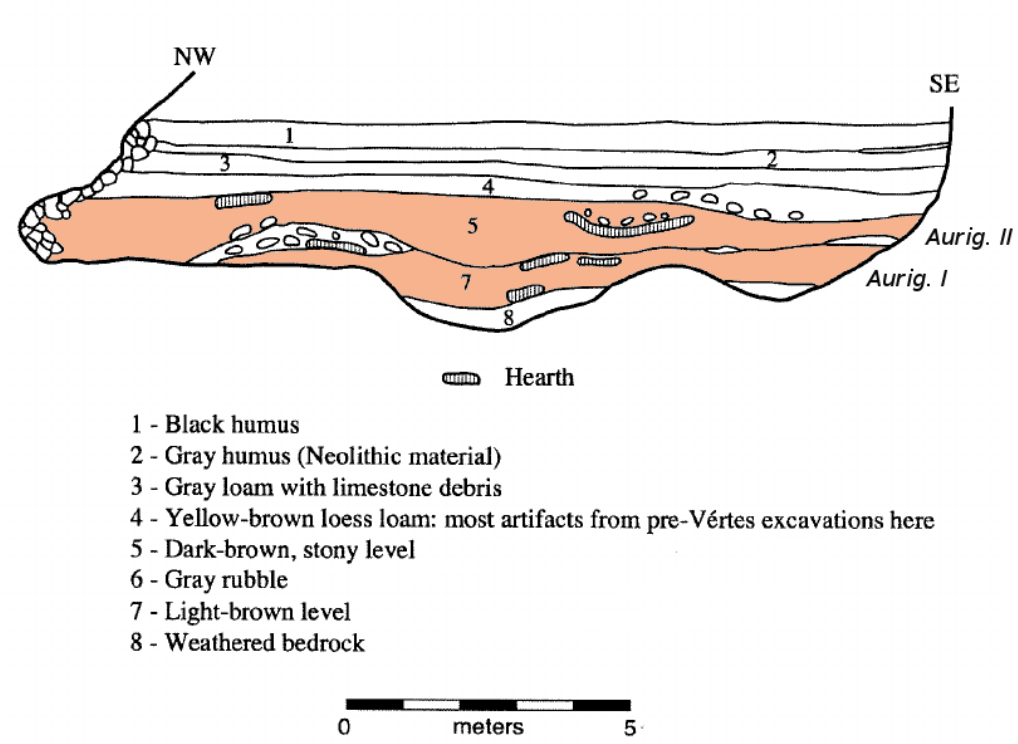


Figure 11.9: Istállóskő: stratigraphy (modified after Adams and Ringer, 2004); 'Aurig. I' (= lower AH) and 'Aurig. II' (= upper AH) highlighted.

and 11.8) do not pass without challenges, reinterpretations and adjustments. Vörös (1984, 2003) attempted to bring all the stratigraphic information together and harmonise their findings by proposing a new integrated nomenclature (see tab. 11.4).

Vörös (1984) reported around 1-1.5 m of Holocene infilling, preceded by 2.5-3.0 m of Pleistocene sedimentation. Hillebrand's excavation seems to have only reached the upper cultural horizon and found 'Magdalenian' artefacts. They were later attributed to the 'Late Middle Aurignacian', or 'Aurignacian III'. It is important to note that Hillebrand was following Peyrony's early classification system. Nowadays, these artefacts would be seen as Gravettian.

Most relevant for this project are layers f/a and f/b discovered by Vértes in his 1950-1951 excavations. They have also been referred to as the 'lower'

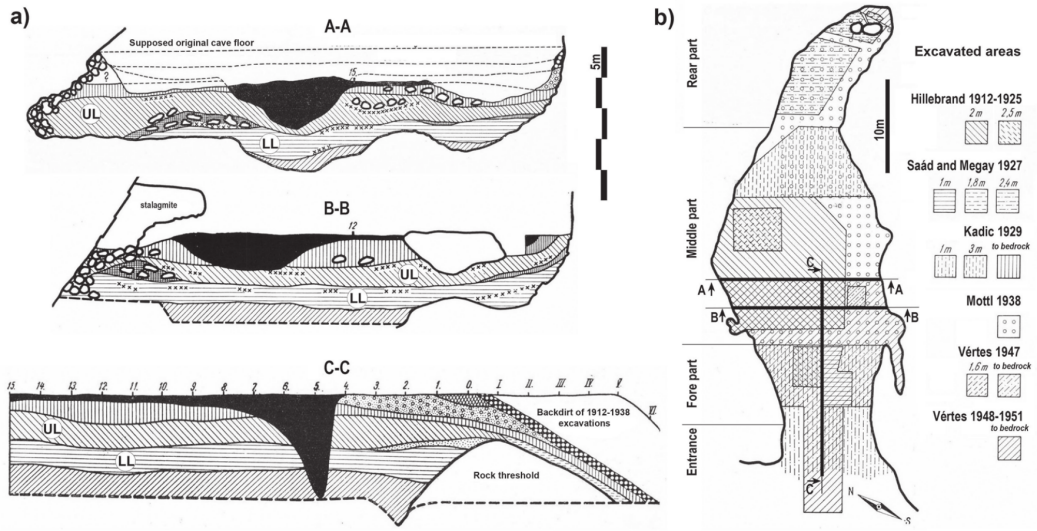


Figure 11.10: Istállóskő: (a) profile drawings from Vértes' excavations with (b) their location marked within the cave and in relation to previous excavations (Patou-Mathis et al., 2017, fig. 2). Layers: black – pit infilling; UL – upper layer; LL – lower layer.

(LL) and 'upper' layer (UL), and have been the main focus of most subsequent archaeological studies. It is from these layers that osseous projectile points, leaf shaped lithic tools, Mousterian points and supposed 'Aurignacian' industries have been reported. On the basis of the osseous projectile point industry, Vértes placed the lower layer in the 'Middle European Aurignacian I' (Early Aurignacian) and the upper layer to the 'Middle European Aurignacian II' (Evolved Aurignacian). Subsequently, the layers were repeatedly referred to as 'Aurignacian I' and 'Aurignacian II' or as lower and upper Aurignacian.

For quite some time now, researchers have questioned whether the Aurignacian osseous points (split-based points) are really associated with Aurignacian lithic industries, or whether they may even be derived from the Middle Palaeolithic 'transitional' techno-complexes[3]. Considering that a Mousterian

[3]The same question caused Moreau et al. (2015) to reanalyse and re-date material from Slovenian sites. In these cases, they concluded that no Middle Palaeolithic techno-complexes were found with the split-based points and that the lithics show clear Upper Palaeolithic character consistent with Aurignacian material, albeit not diagnostic.

point (see fig. 11.12, artefact no. 2) was found in the same place as an osseous point (upper AH), the supposed Aurignacian character of the assemblage needs to be discussed.

In general, the material from the upper AH consists of retouched blades and bladelets, 'Aurignacian' blades, side and end scrapers, a leaf shaped point, two Mousterian points and osseous projectile points. The lower AH assemblage was smaller and contained retouched blades and bladelets, end scrapers, a leaf shaped scraper, 114 osseous tools and 31 split-based points (Adams and Ringer, 2004; Markó, 2015). Adams and Ringer (2004, p.544) further mention that "*debitage and cores from both Aurignacian complexes [i.e. upper and lower AH] indicate that pyramidal blade core technology predominated*". However, Markó (2015) mentions in his reanalysis of the lithic artefacts found at Istállóskő, that typical Aurignacian II (Evolved Aurignacian) lithics, such as carenoid pieces and bladelets, are absent from the upper archaeological horizon. Furthermore, he writes:

> "[S]*even backed bladelets were unearthed in the Istállóskő cave in 1912–1951 and further two* [sic] *were left the surface of the exhibited large hearth although blunted elements are quite rare in the s. str. Aurignacian assemblages. This, together with the presence of bipolar blade cores suggests that the lithic assemblage excavated by Hillebrand and Vértes in the middle and the front section of the cave show connections with the Gravettian circle.*" (Markó, 2015, p. 30)

Other often cited artefacts, such as the supposed 'leaf point' fragment and bone flute (see fig. 11.14), were found in a complex stratigraphic context (Markó, 2015).

The key feature of the cave site is the osseous projectile points. They were divided on the basis of their typology into split-based points (SBP) and 'Mladeč/Olschewan' points. Vértes believed that the SBP belonged to the lower layer and the Early Aurignacian, while the 'Mladeč/Olschewan'

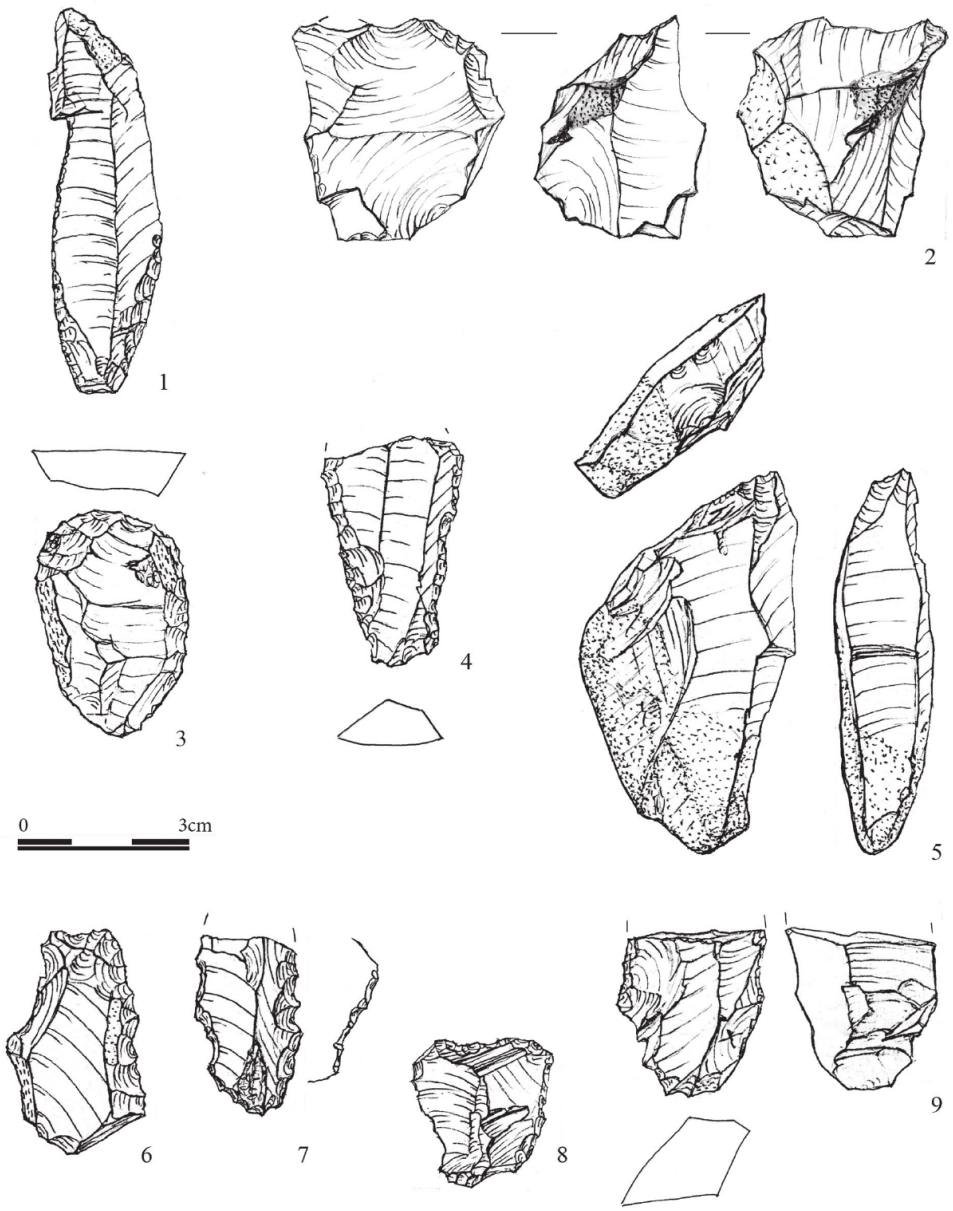


Figure 11.11: Istállóskő: retouched blade fragments and cores from the lower AH, Vértes excavations (drawing by K. Nagy, published in Markó, 2015, fig. 9).

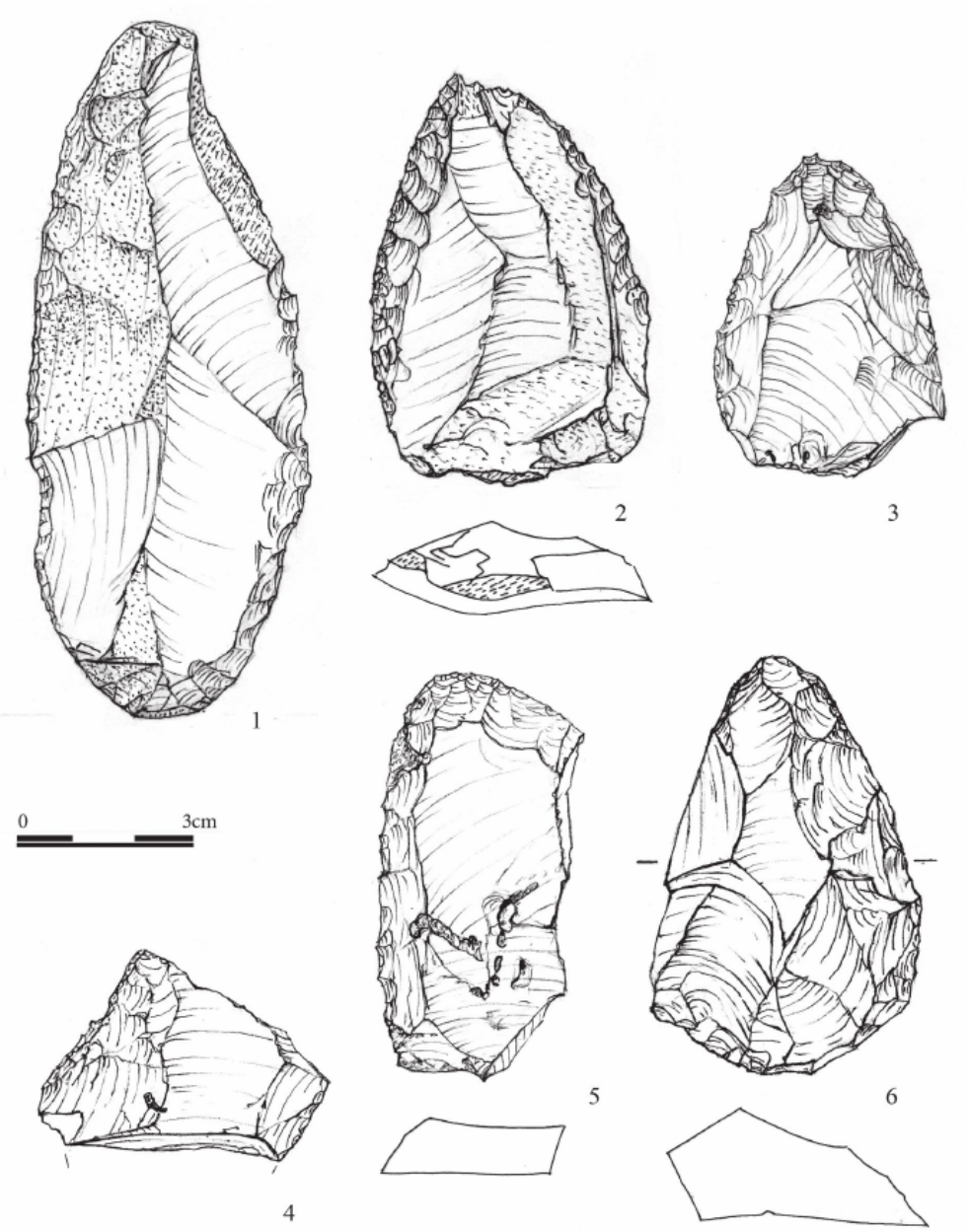


Figure 11.12: Istállóskő: Middle Palaeolithic tools found in the upper archaeological horizon (drawing by K. Nagy, published in Markó, 2015, fig. 8).

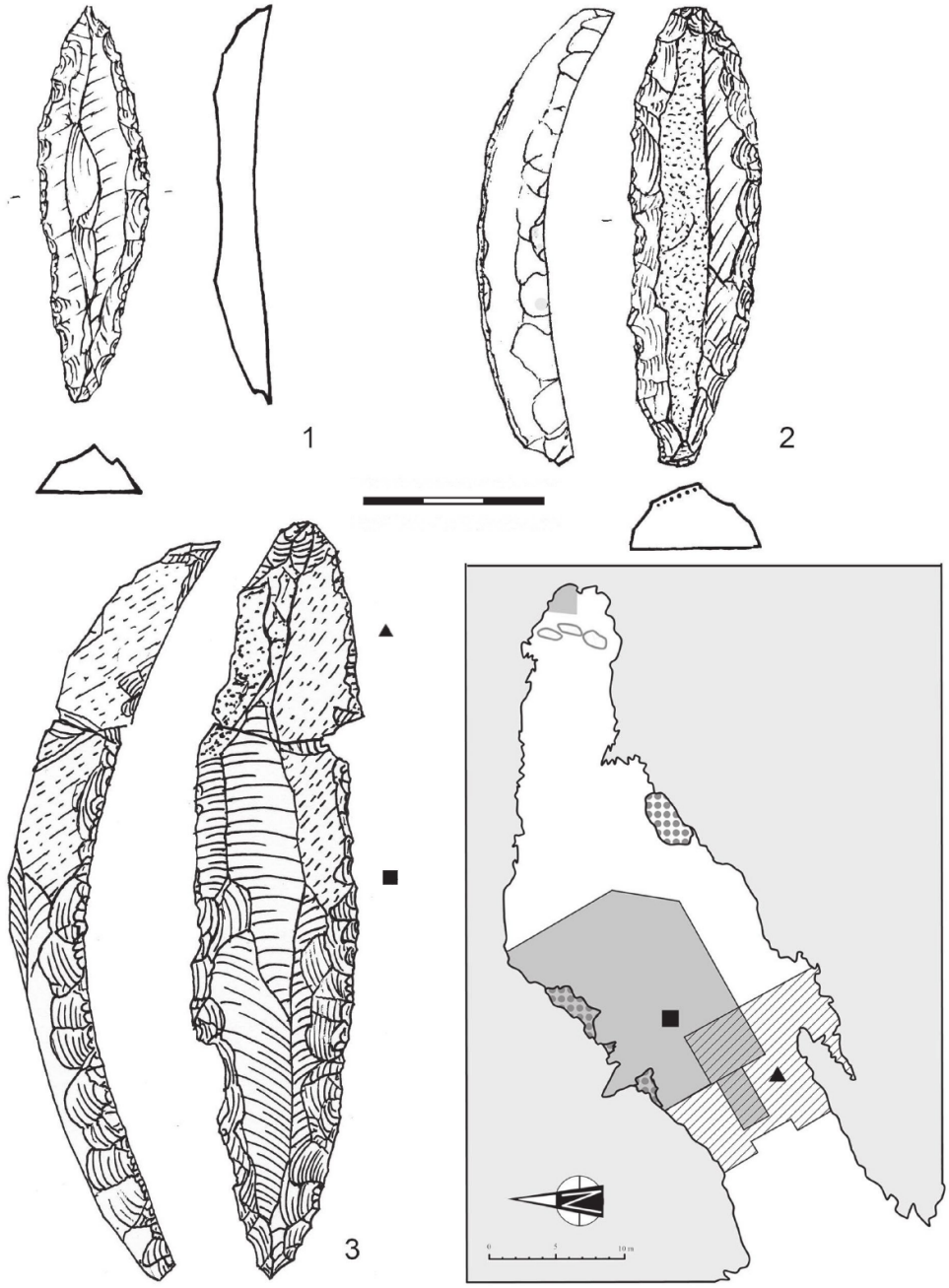


Figure 11.13: Istállóskő: retouched blade points from the upper AH with find locations for fragments refitted in no. 3 (drawing by K. Nagy, published in Markó, 2015, fig. 5).

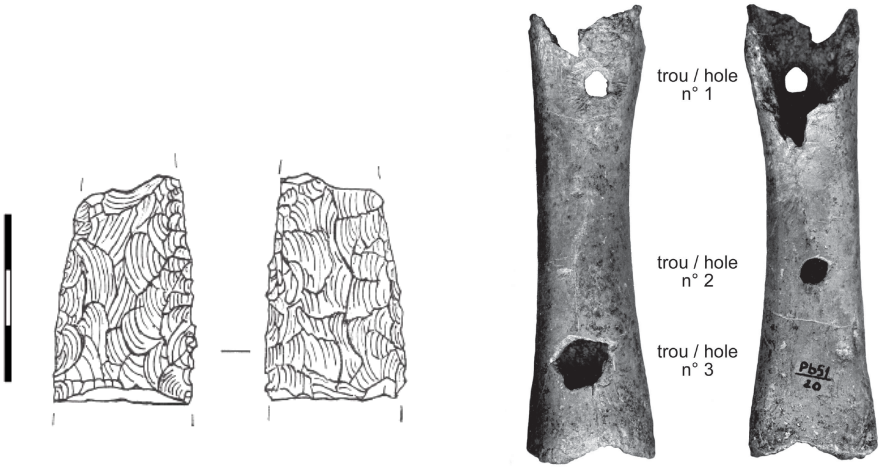


Figure 11.14: Istállóskő: artefacts found by Vértes in the upper AH: left – fragment of a 'leaf point' (drawing by K. Nagy, published in Markó, 2015, fig. 6.3); right – bone 'flute', cave bear femur, preserved on a length of 107 mm (after Horusitzky, 2003, fig. 1).

points were part of the upper layer and the Evolved Aurignacian. While the lower layer seemed to have indeed yielded only SBPs, refittings of osseous projectile point fragments (Markó, 2017) and lithics (Markó, 2015) indicate possible horizontal and vertical movement within the cave. In Markó (2017), refit group IV contains three point fragments coming from three different trenches, and refit group V and VII both contain two point fragments – each one from the upper and one from the lower AH. At the same time, another fragment (Pb.50/99) was found 7 days later in the upper AH – in the same trench and at the same depth as Pb.50/22 (refit group V) – refitted to a piece from the upper AH in trench IX (Pb.51/19) (personal communication with A. Markó, 27/08/2017).

Therefore, it must be concluded, that the Upper Palaeolithic site of Istállóskő poses several challenges; (1) inconsistencies in the documentation and excavation reports; (2) vertical and horizontal movement of artefacts, and; (3) questions surrounding the identification of the lithic industries in the lower and upper AH. However, the significant number of osseous artefacts and the presence of anthropogenically modified faunal remains (*e.g.* with cut

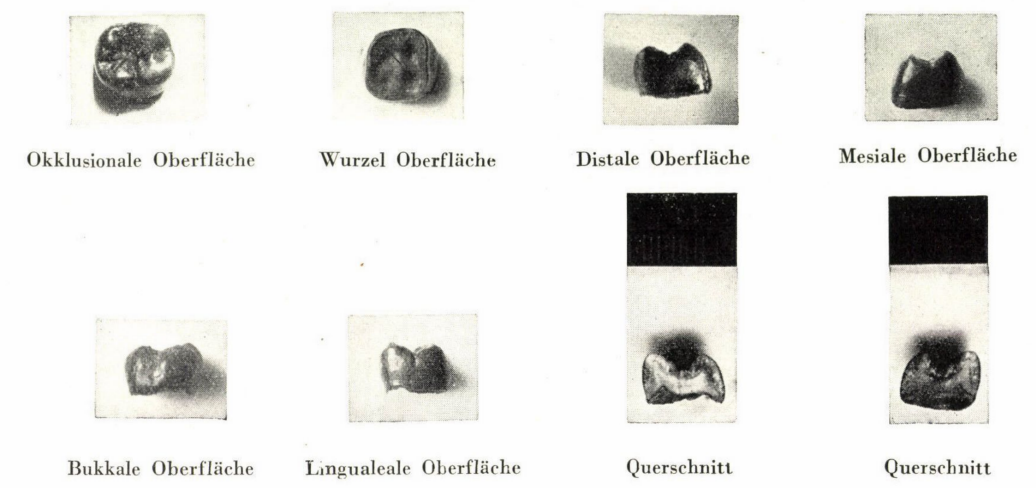


Figure 11.15: Istállóskő: right mandibular second molar of a ca. 9 year old child, found in 1950 (Malán, 1954, includes detailed measurements).

marks), make the site suitable for radiocarbon analyses. By directly dating these humanly modified objects we can establish when humans were present at the site, investigate the chronology of the culturally diagnostic SBP, and investigate the integrity of the site stratigraphy.

Human Remains

During the excavations in 1950, a *Homo sapiens* tooth was unearthed (see fig. 11.15). It was identified as a not yet erupted permanent right mandibular second molar, belonging to a *ca.* 9 year old child. According to Malán (1954, p. 145), it was found near the north-eastern wall in the *"oberen Schicht der Feuerstelle, in der 1. Höhe des II. Profils, aus der relativen 0,0–0,6 und absoluten 1,4–2,0 Tiefe"*[4]. Based on this description, most reasonable find location for the human tooth is within the yellow-brown loess loam above the upper AH, albeit an association with the upper AH cannot be excluded (see fig. 11.10). It is reasonable to believe that the specimen does not belong to an early AMH.

[4]Translation: 'the upper layer of the fireplace, at the first level of profile II, at a relative depth of 0.0–0.6 m and absolute depth of 1.4–2.0 m'.

Previous Dating

The site was radiocarbon dated as early as the 1950s. Since then, of course, radiocarbon dating has seen substantial advances – both in pretreatment and measurement. Therefore, it is vital to critically analyse the radiocarbon evidence for Istállóskő and assess its reliability.

There have been four previous radiocarbon campaigns. The first two charcoal radiocarbon dates were obtained in the late 1950s at the Groningen radiocarbon laboratory (see tab. 11.5): Gro-1501 (Vértes, 1959a; Vértes and de Vries, 1959), and Gro-1935 (de Vries, 1958). At the time, Groningen applied an acid-base-acid pretreatment protocol for charcoals (see de Vries et al., 1958). While Gro-1935 went through the full procedure, Gro-1501 was exposed to acid only to increase pre-treatment survival [5].

Prior to 1961, Groningen used a 'modern wood' standard to establish modern levels of radiocarbon and labelled their dates with the prefix 'Gro-'. When moving to the international standard of reporting all dates relative to 95% of the activity of NBS oxalic acid standard (relative ^{13}C depletion of $\delta^{13}C = 19‰$), Vogel and Waterbolk (1963) calculated that both ages are approximately 240 ± 10 radiocarbon years too young as a result of the 'Suess effect'. The sample specific recalculated results were reported as GrN-1501 (31540 ± 600 BP) and GrN-1935 (30900 ± 600 BP) (see tab. 11.5). Note that the GrN-results supersede the Gro- measurements and the latter should no longer be used for comparisons or modelling.

At the time of their publication, the charcoal date from lower AH was deemed unreliable, as it did not show the expected age difference between 'Aurignacian I' and 'Aurignacian II'. It was argued that the cotton wool, in which the charcoal was packed after collection, may have contaminated the sample. However, there is some confusion as to where the first charcoal sample was actually taken from. Vértes (1957, p. 222) writes that the date was

[5] No information was found on whether any of the samples were first treated with 12% sulphuric acid and subsequent sodium hypochlorite, a procedure listed to remove rootlets by Vogel and Waterbolk (1963).

Table 11.5: Istállóskő: published radiocarbon dates obtained in the 1950s and 1960s on charcoal and bone samples from Vértes' excavations (de Vries, 1958; Movius, 1960; Vogel and Waterbolk, 1963, 1972; Vértes, 1959a; Vértes and de Vries, 1959). All samples were dated at the Groningen radiocarbon laboratory and measured using a β-counter. * = Gro-1501 and Gro-1935 require a correction of $+240 \pm 10$ as their age was calculated using a modern wood standard (the corrected ages were calibrated). GrN samples were measured using NBS oxalic acid as standard (Vogel and Waterbolk, 1963). Therefore, GrN-1501 supersedes Gro-1501, and GrN-1935 replaces Gro-1935 (see text). Calibrated age calculated in OxCal 4.3 (Bronk Ramsey, 2009a) using IntCal13 (Reimer et al., 2013), and given at 95.4% confidence interval.

Lab-no.	Sample no.	Item	Layer	Treatment	Yield	^{14}C (BP)	^{14}C corr. (BP)	Date (cal BP)
Gro-1501	Istállóskő 1	Charcoal	Fireplace in 'grey debris' (between upper and lower layer) / top lower AH ?	Acid	–	30670 ± 500*	30910 ± 500	35916 – 34002
Gro-1935	Istállóskő 2	Charcoal	Upper AH	ABA	–	30710 ± 600*	30950 ± 600	36165 – 33920
GrN-1501	Istállóskő 1	Charcoal	Fireplace in 'grey debris' (between upper and lower layer) / top lower AH ?	Acid	–	31540 ± 600	–	36920 – 34277
GrN-1935	Istállóskő 2	Charcoal	Upper AH	ABA (alkali soluble fraction dated)	–	30900 ± 600	–	36124 – 33887
GrN-4658	Istállóskő 3	Bone collagen	Lower AH (upper part), containing split-based bone points	Acid	1.2 %C	39700 ± 900	–	45155 – 42259
GrN-4659	Istállóskő 4	Bone collagen	Lower AH (base)	Acid	0.9 %C	44300 ± 1900	–	> 45232

from charcoal *"die aus dem obersten Niveau der Aurignacian I-Schicht der Istállóskőer Höhle stammen"*[6]. This stands in contrast to two years earlier when he wrote: *"A kövek alatti tűzhelyből származik a minta. A Gro-1501-es minta a kép baloldalán, a kockázott vonalkázással jelzett réteg alján levő tűzhelyből való"*[7] (Vértes, 1954, p. 113), suggesting that the sample came from a fireplace in the 'stone layer' (= sterile layer between the lower and upper AH). Despite the inconsistency, the dates gave an indication of the old age of the Istállóskő occupations and undoubtedly furthered the archaeological interest in the site.

To have a better understanding of the age of the lower AH, two further samples were dated in the 1960s: GrN-4658 and GrN-4659 (see tab. 11.5). Both were taken from unmodified faunal remains found in the lower AH – the first from the upper part, the second from the lower part. Their bone collagen was obtained by prolonged pretreatment with dilute HCl solution and their ^{14}C measured using beta counting techniques. Unlike the initial results, both dates were reported as conventional radiocarbon ages BP. As originally expected, the results indicated that the lower layer (and thus 'Aurignacian I') was substantially older than the upper layer (*i.e.* 'Aurignacian II'). The measurements of 39700 ± 900 BP (GrN-4658) and 44300 ± 1900 BP (GrN-4659) gave raise to the idea that the Aurignacian in Eastern Europe may be older than their western counterparts, and thus contemporaneous with Mousterian industries in the region (*e.g.* Anikovich, 1992; Conard and Bolus, 2003; Hahn, 1977; Kozłowski, 1982).

From the 2000 excavation, a further 5 faunal remains and one fireplace were sampled for radiocarbon dating in order to test the old age of the site Adams and Ringer (2004). The samples were prepared in 2001 at the Illinois State Geological Survey using acid-base-acid washes (Hong Wang, pers. comm. 28/08/2017). The charcoal sample failed in pre-treatment, but

[6] Translation: *'that originates from the uppermost level of the Aurignacian I layer found at the Istállóskő cave'.*

[7] Translation: '*The sample comes from the fireplace under the stones. Gro-1501 was collected from the fireplace at the bottom of the layer, indicated by the [chequered] pattern on the left side of the figure*'.

Table 11.6: Istállóskő: published radiocarbon dates on unmodified faunal bone samples from the 2000 excavation (Adams and Ringer, 2004). All samples were pretreated at the the Illinois State Geological Survey and AMS radiocarbon dated at the Lawrence Livermore National Lab (USA). Calibrated age calculated in OxCal 4.3 (Bronk Ramsey, 2009a) using IntCal13 (Reimer et al., 2013), and given at 95.4% confidence interval.

Lab-no.	Layer	Depth	Treatment	^{14}C (BP)	Date (cal BP)
ISGS-A-0184	Lower AH	260 cm	ABA	33101 ± 512	38598 – 36127
ISGS-A-0185	Upper/Lower AH	145 cm	ABA	29035 ± 237	33775 – 32620
ISGS-A-0186	Upper AH	90-100 cm	ABA	27933 ± 224	32480 – 31250
ISGS-A-0187	Lower AH	210 cm	ABA	32701 ± 316	37875 – 35967
ISGS-A-0188	Upper AH	120 cm	ABA	31608 ± 295	36145 – 34885

the bone collagen samples were subsequently AMS dated at the Lawrence Livermore National Laboratory (see tab. 11.6).

Strikingly, four out of the five dates returned results younger than expected, placing the lower AH at around 33k BP and the upper AH at *ca.* 28-29k BP. Only ISGS-A-0188 suggested an age of 31608 ± 295 BP for the upper AH, which was more in line with previous dating. Therefore, Adams and Ringer (2004) concluded that the age of the lower layer may have been overestimated, and interpreted the previously sampled material from the lower layer as intrusive.

Consequently, another attempt at resolving the dating discrepancies was made in 2004 (Davies and Hedges, 2008). This time, the focus was on evidence of human presence at the site, resulting in the sampling of 15 bone points, 2 bone artefacts, 5 faunal remains, and 5 charcoals. Additionally, 2 cave bear remains found in the rear of the cave (without archaeological context) were sampled. Unfortunately, only 2 osseous points were (partially) successfully dated – three others resulted in an AMS measurement, but were rejected as unreliable. The dating of the faunal and charcoal remains was more successful, and resulted in 7 radiocarbon ages (see tab. 11.7).

One charcoal sample was split into two fractions (ID 3-a and ID 3-b) before submission. The sample was deemed 'delicate' by the radiocarbon

Table 11.7: Istállóskő: AMS radiocarbon dates from 2006/2007 (Davies and Hedges, 2008) on bone and charcoal samples, complemented by chemistry results from the ORAU database: pre-treatment protocol (RR = acid washes; ZR = acid-base-acid; AF = ultrafiltration; NRC = non-routine chemistry: here re-ultrafiltered), sample yield after pre-treatment (in mg and in wt.% of original sample; in parentheses yield after first ultrafiltration), stable isotope results for N and C, C:N ratio and %C upon combustion. Grey = samples failed at wheel meeting – they should not be used. The calibrated age range was obtained using IntCal13 (Reimer et al., 2013) and OxCal 4.3 (Bronk Ramsey, 2009a), and given at 95.4% confidence interval. Point HOM 53.37.8 is stored at the Herman Ottó Museum in Miskolc, Hungary; the remaining points are from the Hungarian National Museum in Budapest.

Lab-no.	Sample	Item	Excav.	Trench	Square	AH	Depth (cm)	Treat.	Yield (mg)	Yield (wt.%)	δ^{15}N	δ^{13}C	C:N	%C	F^{14}C	^{14}C (BP)	Date (cal BP)
OxA-16093	–	charcoal	2004	profile II	7 (N=260cm, E=200cm)	Upper	141	ZR	7.6	36.4	–	-23.3	–	61.5	0.02240 ± 0.00050	30510 ± 170	34815 – 34112
OxA-16094	–	charcoal	2004	profile II	7 (N=260cm; E=200cm)	Upper	141	ZR	6.7	34.0	–	-24.3	–	60.4	0.02420 ± 0.00050	29900 ± 190	34364 – 33667
OxA-16638	–	fauna	2004	profile I	N=92cm, E=200cm	Upper	167	AF	12.0	1.3	6.5	-21.5	3.1	39.2	0.02120 ± 0.00080	30970 ± 310	35574 – 34290
OxA-16639	–	fauna, cave bear	2004	profile III	rear of cave: N=0cm, E=22cm	Above upper	41	AF	8.7	1.1	1.9	-20.3	3.2	41.0	0.04180 ± 0.00110	25500 ± 210	30305 – 29060
OxA-16640	–	fauna, cave bear	2004	profile III	rear of cave: N=0cm, E=33cm	Above upper	51	AF	24.8	2.9	3.7	-20.5	3.2	40.5	0.04480 ± 0.00080	24950 ± 140	29379 – 28660
OxA-16916	ID 3-a	charcoal	2004	profile I	N=150cm; E=200cm,	Upper	160	RR	1.6	53.3	–	-25.5	–	50.1	0.02551 ± 0.00062	29470 ± 190	34034 – 33275
OxA-16917	ID 3-b	charcoal	2004	profile I	N=150cm; E=200cm,	Upper	160	RR	2.2	62.9	–	-24.6	–	58.1	0.02625 ± 0.00054	29240 ± 170	33830 – 33014
OxA-X-2170-18	HOM 53.37.8	point	1927	–	–	Lower	–	AF	4.9	1.6	7.9	-20.4	3.3	43	0.01520 ± 0.00170	33600 ± 900	40202 – 35916
OxA-X-2244-32	Pb.50/34	point	1950	I	–	Lower	160	NRC	5.8	1.8 (10.16)	6.6	-19.3	3.1	44.9	0.01300 ± 0.00040	34890 ± 250	40032 – 38794
P-20534	Pb.51/13	point	1951	VIII	–	Lower	–	NRC	3.4	1.2 (9.6)	4.9	-19.9	3.2	46.6	0.01713 ± 0.00058	32670 ± 270	37661 – 36010
P-20541	PB.50/41	point	1950	V	–	Lower	140-170	NRC	2.5	1.0 (4.7)	5.5	-18.8	3.2	46.5	0.01650 ± 0.00053	32970 ± 260	38044 – 36330
P-20543	Pb.50/53	point	1950	III	–	Lower	150-180	NRC	3.1	1.2 (5.9)	3.5	-18.8	3.2	44.6	0.61005 ± 0.021267	33970 ± 280	39156 – 37629

technicians and treated with repeated acid washes and ultrasonication steps, but without a base step (see RR protocol in Brock et al., 2010b). The results correspond well with each other, but the treatment is, of course, less rigorous than standard. Two further charcoal samples (OxA-16094 and OxA-16638) were treated with the standard ORAU charcoal protocol, using acid-base-acid washes (see ZR protocol in Brock et al., 2010b). The bone point from the Herman Ottó Museum received the standard ultrafiltration treatment used at ORAU (see AF protocol in Brock et al., 2010b). The remaining four points from which a radiocarbon measurement was obtained were all treated with a non-routine-chemistry protocol (NRC). The initial ultrafiltered collagen raised quality concerns, probably as a result of remaining humectant identified in the ultrafilter Quality Control Aliquot; this is always tested with each batch of ultrafiltered samples. All four samples were subsequently re-ultrafiltered, leading to lower collagen yields. As a consequence, three samples failed the minimum yield threshold. One passed (OxA-X-2244-32) but it should be treated with caution; it is a minimum age estimate only.

Despite the increasing size of the radiocarbon dataset (see fig. 11.16), there are regrettably few dates potentially suitable for assessing the periods of human occupations at the site or the time of osseous projectile point manufacture.

There are several arguments for rejecting the dates obtained in the 1950s as probably too unreliable, on the basis of archaeological and radiocarbon chemistry reasons[8]: (1) oxalic acid as a reference and correcting for fractionation was not yet standardised; (2) charcoal dates beyond 30,000 radiocarbon years obtained with ABA or acid only treatments often underestimate the true age of the sample (*e.g.* Higham et al., 2009; Wood et al., 2012); and (3) the clear association of the charcoal samples (and the hearths they came from) to either the upper AH or lower AH may be in doubt.

The bone collagen dates obtained in the 1960s were only decalcified, which makes it more likely that they are minimum age estimates. More importantly,

[8]Which is not the same as stating that they are clearly wrong.

both faunal samples showed no anthropogenic modifications and cannot directly be linked to human activity at the site. GrN-4659 was taken at the bottom of the lower AH and may have been wrongly attributed to the cultural horizon. With this in mind, the age of the human occupation in this lower layer cannot be pushed back to 44.3 k BP.

This leaves the dates from the more recent campaigns. ISGS-A-0185 is unhelpful as it neither has a direct connection to human activity (unmodified faunal remain), nor is its layer attribution clear. The remaining ISGS dates may shed light on the time period in which the two cultural layers accumulated, but are not indicative of events of human activity, as they too were obtained on faunal bones with no anthropogenic marks.

This leaves us with two osseous point dates for the lower AH, and possibly 3 charcoal samples from hearths in the upper AH. One of the osseous projectile points was treated using non-routine chemistry, which might underestimate the true age of the samples. The charcoal samples were pre-treated with ABA, suggesting that they too are likely to underestimate the true age of the samples. The two dates obtained from bear remains by Davies and Hedges (2008) could be used to constrain a model, but would not be indicative of human occupation.

Consequently, the best age estimate for the bone points in the lower AH is around 34k BP (*ca.* 36-40k cal BP), while the upper AH could date to around 30k BP (*ca.* 33-35k cal BP). In both cases, an older age would not be surprising from a radiocarbon dating perspective. Nonetheless, the direct evidence for human activity/occupation is not only sparse (osseous points), but insufficient to analyse either the occupation sequence of Istállóskő or securely place the osseous point industry within the European context.

11.2.2 Radiocarbon Dating

The present dating project at Istállóskő focuses on the timing of the osseous point industries as well as on the chronostratigraphy of the human presence

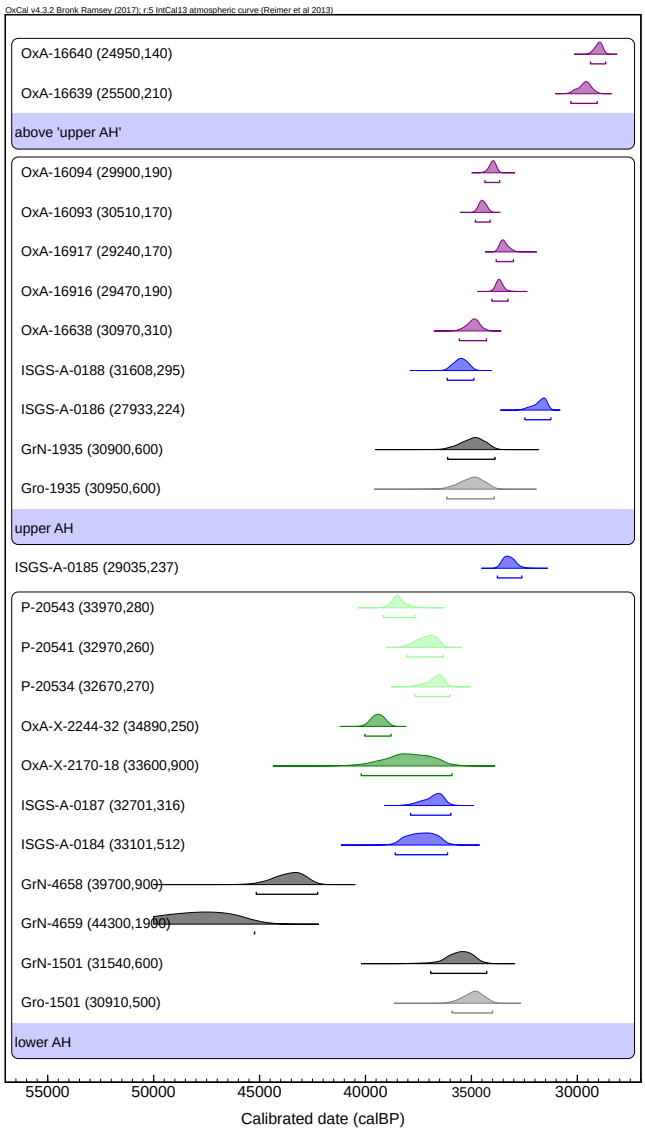


Figure 11.16: Istállóskő: published radiocarbon dates calibrated in OxCal 4.3 (Bronk Ramsey, 2009a) using InCal13 (Reimer et al., 2013) calibration curve and grouped according to their layer attribution. ISGS-A-0185 was attributed to layer 7/9 (Vértes, 1954), but also Aurignacian I/II (Adams and Ringer, 2004), thus was left in between Aurignacian I and II. **grey** = obsolete charcoal dates 1950s, **black** = charcoal and bone collagen dates 1960s ; **blue** = bone collagen dates 2001, **violet** = charcoal and bone collagen dates 2006/2007; **green** = successful dates from osseous points; **pale green** = obsolete ('failed') dates from osseous points 2006/2007 (see tab. 11.5–11.7).

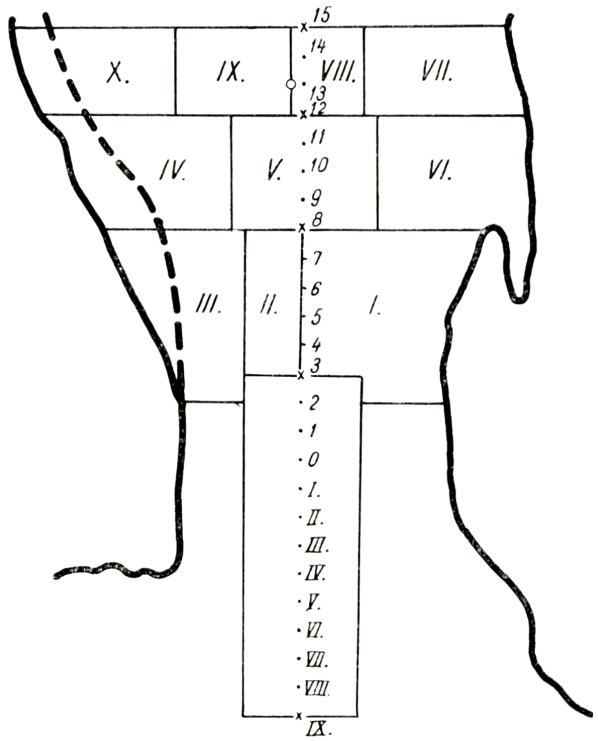


Figure 11.17: Istállóskő: location of Vértes' excavation trenches (Vértes, 1954, fig. 2).

at the cave. As a result, anthropogenically modified faunal remains (*i.e.* cut marked bones), and osseous points were sampled for %N and radiocarbon analyses between April and September 2015.

Material & Treatment

For this project, 10 bone points from the Hungarian National Museum, and 5 anthropogenically modified faunal remains from the Natural History Museum in Budapest were sampled. In both cases, the specimens cover both the lower and upper AH, and derive largely from Vértes' excavations in the 1950s (see tab. 11.8).

The faunal bone fragments showed no traces or record of conservation treatments. The osseous projectile points were surface coated (composition unknown), some contained glue at the connection point of two fragments or

Table 11.8: Istállóskő: list of samples taken for radiocarbon dating: osseous points and anthropogenically modified faunal remains with context information, sample weight and conservation status.

Ref-no.	Inv.-no.	Item	Excav.	Trench	Layer	Weight	Cons.
Istall-01	Pb 50/90 (117)	point	1950	V	Upper AH (=f/a)	297 mg	Y
Istall-02	Pb 50/159	point	1950	?	Upper AH (=f/a)	179 mg	Y
Istall-03	Pb 51/13	point	1951	VIII	Lower AH (=f/b)	296 mg	Y
Istall-04	Pb 50/53	point	1950	III	Lower AH (=f/b)	150 mg	Y
Istall-05	Pb 50/39	point	1950	I	Lower AH (=f/b)	224 mg	Y
Istall-06	Pb 50/93	point	1950	V & IV	Upper AH (=f/a)	338 mg	Y
Istall-07	Pb 51/30	point	1951	X	Lower AH (=f/b)	250 mg	Y
Istall-08	Pb 51/86	point	1951	VI	Lower AH (=f/b)	204 mg	Y
Istall-09	V.59/377	fauna	Vértés	–	felső tüzhely (=f/a)	710 mg	N
Istall-10	V.58/165	fauna	Vértés	–	alsó réteg (=f/b)	700 mg	N
Istall-11	uninventarised	fauna	Vértés	–	feslő réteg (=f/a)	500 mg	N
Istall-13	V.59/473	fauna	Vértés	–	felső tüzhely (=f/b)	710 mg	N
Istall-14	V.59/369	fauna	Vértés	–	alsó tüzhely (=f/b)	1200 mg	N
Istall-16	Pb 50/99	point	1950	III	Upper AH (=f/a)	340 mg	Y
Istall-18	167/914.22	point	1914	–	Upper? AH (=f/a)	460 mg	Y

some epoxy resins in places where the artefacts were restored for cosmetic reasons. As a result, sampling of surface material as well as areas of infilling and glue coating were altogether avoided. Nevertheless, all osseous point samples were first treated with solvent washes to remove potential contaminants from conservation/restoration materials. The powdered samples were left in acetone for 1h at 40° C, followed by 30 min. in methanol and 30 min. in chloroform at RT. After a rinse with chloroform, the samples were dried overnight in a heating block set to 30° C, before regular chemical pre-treatment was applied.

The split-based point fragment Pb.50/53 was refitted to Pb.50.13 (group III), and fragment Pb.50/99 to Pb.51/19 (group VIII) as identified by Markó (2015).

Istall-01 distal fragment of a lozangic shaped point, possibly of Mladeč type. It was found on 19 July 1950 in sector V, at a depth of 0.6–1.1 m (Dobosi, 2002). The natural structure of the antler is clearly visible on the ventral side. The dorsal side shows longitudinal striae from shaping into a

convex form. The distal point is rounded. Dobosi (2002, p. 90) describes an incision on the proximal edge, perpendicular to the axis of the point. The cross-section is flat-oval. The artefacts preserved dimensions are: 83 mm long, 23 mm wide, and 12 mm thick.

In the mesial part of the ventral side, the museum catalogue number Pb 50/90 is clearly visible in black ink. Further towards the proximal end and to the side, the remains of what appears to be an older number (117.) are seen bleeding out. In the proximal part of the ventral side, an oval area of the point has been reconstructed using epoxy resin and paint, marking the location where the previous radiocarbon sample had been taken (see Davies and Hedges, 2008). The present project used key-hole drilling from the narrow edge in the meseo-proximal part of the point fragment to keep visual damage minimal, while simultaneously avoiding the more porous areas in the distal part. Care was taken to avoid any interference from the previous sampling or any other modern reconstruction work.

Istall-02 near complete antler split-based point. It was found during the 1950s excavation, though no further information on find location was published. It is broken (step fracture) into two fragments of near equal length, which are presently held together by glue. On the dorsal and ventral side, longitudinal striae from shaping are visible. The spongiosa is still seen on the ventral side. The distal end is intact, though shows signs of wear and slight arching. The proximal end is damaged, showing one wing of the split base severely shortened, while the other is preserved over a larger area, though also missing its proximal end. Dobosi (2002, p. 99) expects the original form to have been an elongated oval. The artefact's cross-section is lenticular. The point is preserved over a length of 100 mm and has a maximum width of 13 mm.

The entire surface (excluding the split base) is marbled with a black coating (manganese?). In addition, the artefact is covered in a consolidation substance (PVA?), which also partially hides the museum number (Pb 50/159) written in black ink on proximal fragment's mesial part of the ven-

tral side. There are no signs of previous sampling. The radiocarbon sample was obtained using key-hole drilling from the narrow edge in the mesial part of the proximal fragment. This allowed for accessing maximum sample width and thickness, thus significantly reducing the risk of damage to the surface for such a narrow artefact.

Istall-03 semi-finished osseous point, possibly a rough-out of a massive-based or lozangic shaped point. It was found on 4 June 1951 in sector VIII, at a depth of *"1–0.8"* m (Dobosi, 2002, p. 100), and given the museum number Pb 51/13. The artefact is slightly bent, with a polished surface and both proximal and distal ends damaged. Dobosi (2002) writes that it was made of a rib bone. The surface is marbled with a black coating (manganese?), which seems to not cover the proximal end. The artefact is preserved on a length of 164 mm and a maximum width of 19 mm, with a oval to lenticular cross-section.

The surface appears to be coated with a conservation substance (PVA?). Reconstruction work, using epoxy resin and paint for cosmetic touch-up, is visible in the proximal part of the artefact, on the narrow side, where Davies and Hedges (2008) have previously sampled the point for radiocarbon dating (see also tab. 11.7). Fort this dissertation, the artefact was sampled from the proximal part using the key-hole drilling technique. The location was chosen, because the artefact showed an old chipped surface (probably from initial shaping), which allowed for a flat entrance point with access to the widest section of the artefact.

Istall-04 mesial fragment of a nearly complete split-based antler point. It was found on 5 June 1950 in sector III, at a depth of 1.8–2.4 m (Dobosi, 2002, p. 99). The distal end has the point missing (step fracture). The proximal end shows a split-base with one wing broken off and the other damaged and shortened, leaving only a shallow split intact. On the ventral side, spongiosa is visible. The dorsal and ventral surface show faint longitudinal striae from

shaping, and the entire surface (except the interior of the split base) is marbled with a black coating. The artefact is preserved on a length of 78 mm and a maximum width of 15 mm, and has a lenticular cross-section.

The entire surface is coated in a conservation substance (PVA?). In the proximal part, on the ventral side, the museum number Pb 50/53 is written in blank ink. Just above it, the shadow of a previous number (59.) is coming through the shiny coating, written in opposite direction to the previously mentioned number. In the mesial section, an oval area, over 20 mm long, shows reconstruction work. Epoxy resin was used to cover where Davies and Hedges (2008) had previously obtained a sample for radiocarbon dating (see tab. 11.7), and the surface was subsequently painted. For this dissertation, the artefact was sampled using key-hole drilling from the narrow edge to obtain a sample from the widest section (i.e. close to the proximal end). At the same time, this strategy avoided the museum number and the previous sampling location.

Istall-05 distal fragment of an antler point, probably a split-based point (Vértes, 1954, pl. XXXVII.5). It was found on 16 May 1950 in sector I, at a depth of 2–2.4 m (Dobosi, 2002, p. 99). The artefact has a fresh fracture *ca.* 1/3 from the distal end, which is glued together. The distal end shows minor original damage, while the proximal end has a fresh fracture. The longitudinal striations are evidence of shaping. The ventral side has some spongiosa preserved, and surface damage is visible in the mesial part of the proximal fragment. The surface of the entire distal fragment, as well as the dorsal surface of the proximal fragment are marbled with a black coating (manganese?). The artefact is slightly arched and bent, and has a oval to plano-convex cross-section. It is preserved over a length of 81 mm, with a maximum width of 14 mm.

Apart from the glue to repair the modern fracture, the artefact is coated in a conservation substance (PVA?). In the mesial port on the ventral side of the proximal fragment, the museum number Pb 50/39 is clearly written in black ink. Just below, towards the proximal end, another, washed out

number (25) is located. As a consequence of the slim form of the artefact, it was sampled using the key-hole drilling technique entering from the proximal end and sampling in longitudinal direction.

Istall-06 nearly complete point, possibly massive-based (Vértes, 1954, pl. XLI.5). The exact origin of the sample is not published (Dobosi, 2002, p. 90). The artefact is arched and slightly bent. The two fragments are glued together. The distal end shows fine abrasions. The proximal end has a wedge shaped fracture clearly visible on the dorsal side. The artefact has a rounded rectangular cross-section. The surface, especially in the mesial and distal parts, has an irregular black coating (manganese?), and shows signs of abrasion and striations. The point is preserved on a length of 143 mm, with a maximum width of 17 mm.

The museum number Pb 50/93 is written on the ventral side, and the artefact is coated in a conservation substance (PVA?). It had previously been sampled by Davies and Hedges (2008), though dating failed due to low collagen yield. For the present project, the artefact was sampled using key-hole drilling from the narrow edge of the meseo-distal part of the proximal fragment, thereby obtaining optimal access to the largest possible amount of material without interference from previous reconstruction work.

Istall-07 mesial osseous point fragment. It was found on 24 May 1951 in sector X, in layer f/b. No further depth information was given. The artefact is bent and arched. The two refitted pieces are glued together. The proximal end has an oblique cut. In contrast, the distal end is fractured and rounded. The surface shows moderate marbled, black coating. On the proximal fragment, there is surface damage on the dorsal and ventral side. Dobosi (2002, p. 88) believes the artefact to be made of polished rib. If this is correct, an attribution as a SBP as (Vértes, 1954, pl. XXXVII.1) considered would become less likely. However, it is not a chisel, as (Dobosi, 2002, p. 88) suggested. The impact fracture at the dorsal end is more typical of projectile points (Markó, 2017).

The point's surface is coated in a conservation substance, possibly PVA. Pb 51/30, the proximal fragment, had previously been sampled in the mesial part of the dorsal surface by Davies and Hedges (2008), though there was insufficient collagen for radiocarbon dating. Because of the previous sampling damage, the artefact could not be drilled at its widest section. Instead, the location for key-hole drilling was moved closer to the distal end of the proximal fragment, optimising the space between the glued fracture and previous reconstruction work.

Istall-08 near complete split-based antler point. It was found on 29 April 1951 in sector VI, layer f/b (Dobosi, 2002, p. 97). It shows several modern fractures. Not only have the pieces been glued, but the missing sections were reconstructed as a comparison with Vértes (1954, pl. XXXVII.3) demonstrates. The point is missing from the distal end, and the split wings had to be glued back. Overall, it only shows minimally convergent sides, giving them a near parallel appearance. The point's entire surface is marbled with a black coating, though appears more intense towards the dorsal end. The artefact has a flat, oval cross-section, and is preserved on a length of 100 mm, with a maximum width of 13 mm.

The artefact's surface is coated in a conservation substance, possibly PVA. The museum number Pb 51/86 is written in black ink onto the ventral surface. The previous radiocarbon sampling location from Davies and Hedges (2008) is reconstructed with epoxy resin and paint. Low collagen yield, at the time, prevented a successful radiocarbon measurement. For this project, the artefact was sampled using key-hole drilling form the narrow edge in the mesial section of the mesial fragment, equidistant from both major reconstructed fracture areas.

Istall-16 near complete antler point, possibly split-based point. The proximal fragment was found in 1950 in sector III, upper layer, at a depth of 1.5 m (Markó, 2017, tab. 1). It has a patinated fracture surface on both ends, polished margins, and a planoconvex cross-section. It is preserved on

a length of 56 mm, with a maximum width of 16 mm (Dobosi, 2002, p. 88). The medial and distal fragments were found on 5 May 1951 in sector IX, layer f/a (Dobosi, 2002, p. 90). The cross-section at the distal end is round, and plano-convex at the proximal end. The latter shows an old fracture, while the distal end is worn. The general shape is slender, and symmetric. The two fragments are preserved over a length of 94 mm, with a maximum width of 14 mm.

The medial and distal fragments were glued together at the snap fracture already prior to publication by Vértes (1954, pl. XLII.4). In contrast, the proximal fraction was initially published as a separate artefact (Vértes, 1954, pl. XLII.8), due to the refitting having only recently been discovered (Markó, 2017). All fragments show a patchy, black coating throughout the surface, except on spongy tissue.

The entire artefact shows a modern, shiny coating, possibly PVA. The museum number Pb 50/99 is clearly visible on the ventral surface of the proximal fragment, partially covering a seemingly older, washed out number. The museum number Pb 51/19, on the other hand, is written in black ink on the ventral surface of the medial fragment. None of the fragments had previously been sampled. For this project, the proximal fragment was targeted for radiocarbon sampling, as it offered the widest section of the artefact. Key-hole drilling from the narrow edge was applied, to keep surface damage to a minimum while maximising material access.

Istall-18 mesial fragment of a split-based antler point. The artefact was originally published by Gábori (1951, p. 10, pl. III.2) as a find from the Peskő cave. This information was subsequently repeated by his colleagues. However, the handwritten inventory list of the Hungarian National Museum documents that 167/914 was found prior to 1914 at Istállóskő. During that time, only the upper AH had been discovered. The correctness of the Istállóskő attribution is further supported by the fact that osseous artefacts were only discovered at Peskő from 1930 onwards (Markó, 2017).

The artefact is fractured around 2/3 towards the distal end, and mended with glue. Both the distal and proximal ends are damaged. On the latter, there are two wing stubs remaining from a split-base. The dorsal side shows several cuts and the surface is damaged in numerous places, most likely caused by post-depositional processes. Under this and the black coating, original manufacturing traces are difficult to see. The ventral surface shows spongiosa, with damage being more severe in the mesial part of the proximal fragment. Here, a former museum number (167/914.22) has become nearly intelligible, which suggests that at least some of the surface damage occurred after excavation. To consolidate the artefact, the location is filled with conservation material of unknown composition. In addition, the entire artefact is coated with what might be PVA. The artefact is preserved on a length of 115 mm, with a maximal width of 23 mm. The cross-section of the distal end is round to oval, while the proximal end is planoconvex (originally probably lenticular).

The museum number is found three times on the proximal fragment, and once on the distal fragment. On the former, it is located on the mesio-proximal part of the dorsal surface, and on the proximal and mesial part of the ventral surface. On the latter, the number features on the ventral surface. For radiocarbon sampling, the proximal fragment was unsuitable, as its heavily damaged and porous surface was drenched in an unknown conservation substance. Therefore, the distal fragment of the artefact was sampled, using the key-hole drilling technique, entering from the distal end and drilling in longitudinal direction.

^{14}C Results

Two faunal samples could not be dated (see tab. 11.9). Istall-10 gave <1 wt% yield after AG pretreatment, despite the high %N value of 3.4. Istall-14 dissolved during the first acid step. As there was sufficient remaining bone powder, a second fraction was pre-treated. Though yielding some collagen, the yield was insufficient for a reliable radiocarbon date (0.23 wt.%). The

Table 11.9: Istállóskő: anthropogenically modified faunal remains that failed radiocarbon pre-treatment. Ref-no. = number given to sample by this project. Inv.-no. = Inventory number from museum. P/Q-no. = ORAU internal sample and aliquot number. Layer = layer attribution. %N = nitrogen weight content before chemical pre-treatment. Treat. = Pretreatment protocols used: AG – gelatine (see section 5.4). Yield = sample left after chemical pre-treatment (both in mg and wt.%).

Ref-no.	Inv-no.	P/Q-no.	Layer	%N	Treat.	Yield (mg)	Yield (wt.%)
Istall-10	V.58/165	40687.0	Upper	3.42	AG	3.54	0.56
Istall-14	V.59/369	40690.0	Lower	0.04	AG	0.00	0.00
Istall-14	V.59/369	40690.1	Lower	0.04	AG	1.53	0.23

remaining three faunal samples – Istall-09, Istall-11, and Istall-13 – showed much better preservation (see tab. 11.10). All three could be ultrafiltered, showed expected %C on combustion and had acceptable C:N atomic ratios (3.2 and 3.3).

All osseous projectile points yielded radiocarbon ages. However, apart from Istall-03 and Istall-18, there was insufficient yield for ultrafiltration. Istall-06 had a collagen yield of 0.61 wt.%. Considering the importance of the artefact, the sample was still AMS dated, but given an OxA-X-number to reflect that the date is most likely a minimum age. Istall-08 yielded a little less than 1 wt% but it had an acceptable C:N ratio of 3.2. The remaining points were all above the 1% wt. collagen cut-off, yet below amount needed for ultrafiltration. The C:N ratios of all points are within range, with 6 samples (Istall-01, 02, 05, 08, 16 and 18) giving exactly 3.2, as expected of a collagen sample.

Six of the samples dated have previously been sampled by W. Davies. Two of these had low collagen yields (Pb.51/13 and Pb.51/53) and were failed (see subsection 11.2.1). The comparison to the new dates (see fig. 11.18) shows good agreement for Pb 51/13, though a statistical difference is measured for Pb 50/52 (χ^2-test: df=1, T=6.98, %5= 3.8).

Table 11.10: Istállóskő: new AMS radiocarbon dates on anthropogenically modified faunal remains and osseous points with archaeological context information, and pre-treatment results. Ref-no. = number given to the sample for the purpose of this project. Inv.-no. = Inventory number given to the sample in the museum or on excavation. Year = year of excavation. Layer = layer attribution. %N = nitrogen weight content before chemical pre-treatment. Treat. = Pretreatment protocols used: * – solvent wash; AG – gelatine; and AF – ultrafiltration (see section 5.4). Yield = sample left after chemical pre-treatment (both in mg and wt.%). %C = carbon yield on combustion. C:N = carbon to nitrogen ratio of combusted collagen sample. $F^{14}C$ = fraction modern carbon. ^{14}C (BP) = conventional radiocarbon age Before Present with 1σ error. Date (cal BP) = calibrated radiocarbon age at a 95.4% confidence interval, calculated in OxCal 4.3 (Bronk Ramsey, 2009a) using IntCal13 (Reimer et al., 2013). Osseous point previously sampled by W. Davies, but not dated: $^{\Delta}$ failed at wheel meeting; † failed during pre-treatment (Davies and Hedges, 2008).

Ref-no.	Inv.-no.	Item	Layer	Depth (m)	%N	Treat.	Yield (mg)	Yield (wt.%)	%C	$\delta^{15}N$	$\delta^{13}C$	C:N	Lab-no	$F^{14}C$	^{14}C (BP)	Date (cal BP)
Istall-01	Pb 50/90 (117)†	point	Upper	0.6-1.1	3.59	AG*	5.49	1.93	40.6	7.5	-20.3	3.2	OxA-35414	0.01551± 0.00119	33450 ± 600	39181 – 36246
Istall-02	Pb 50/159	point	Upper		3.28	AG*	1.80	1.03	41.0	5.2	-18.6	3.2	OxA-35382	0.01160± 0.00173	35800 ± 1200	42755 – 38195
Istall-03	Pb 51/13$^{\Delta}$	point	Lower	1.3	3.10	AF*	8.07	2.77	41.7	7.0	-21.6	3.1	OxA-35522	0.01677± 0.00104	32850 ± 500	38412 – 35886
Istall-04	Pb 50/53$^{\Delta}$	point	Lower	1.8-2.4	2.85	AG*	3.41	2.36	42.2	3.7	-19.1	3.3	OxA-35383	0.01109± 0.00128	36200 ± 900	42340 – 39052
Istall-05	Pb 50/39	point	Lower	2.0-2.4	2.98	AG*	6.33	2.90	40.7	4.9	-19.5	3.2	OxA-35415	0.01122± 0.00117	36100 ± 800	42127 – 39132
Istall-06	Pb 50/93†	point	Upper	1.2 & 0-0.8	2.61	AG*	2.03	0.61	41.1	4.4	-18.4	3.3	OxA-X-2716-11	0.01613± 0.00165	33200 ± 800	39486 – 35665
Istall-07	Pb 51/30†	point	Lower		3.53	AG*	2.59	1.06	42.6	8.0	-18.5	3.3	OxA-35384	0.00974± 0.00139	37200 ± 1200	43920 – 39499
Istall-08	Pb 51/86†	point	Lower		3.64	AG*	1.78	0.89	39.6	5.3	-18.5	3.2	OxA-35385	0.00921± 0.00178	37700 ± 1600	45592 – 39280
Istall-09	V.59/377	fauna	Upper		3.47	AF	8.34	1.23	42.1	7.9	-20.2	3.2	OxA-34402	0.01280± 0.00109	35000 ± 700	41272 – 38282
Istall-11	uninvent.	fauna	Upper		2.61	AF	11.20	2.31	42.5	5.9	-20.9	3.3	OxA-34403	0.04126± 0.001114	25610 ± 220	30470 – 29200
Istall-13	V.59/473	fauna	Upper		3.73	AF	48.98	7.13	42.6	5.5	-21.0	3.2	OxA-34404	0.03683± 0.00107	26520 ± 230	31115 – 30325
Istall-16	Pb 50/99	point	Upper		3.26	AG*	7.08	2.01	41.2	4.9	-19.2	3.2	OxA-35421	0.01059± 0.00116	36500 ± 900	42584 – 39380
Istall-18	167/914.22	point	Upper		3.13	AF*	7.96	1.93	43.6	7.5	-19.7	3.2	OxA-34771	0.01551± 0.00102	33450 ± 550	39025 – 36315

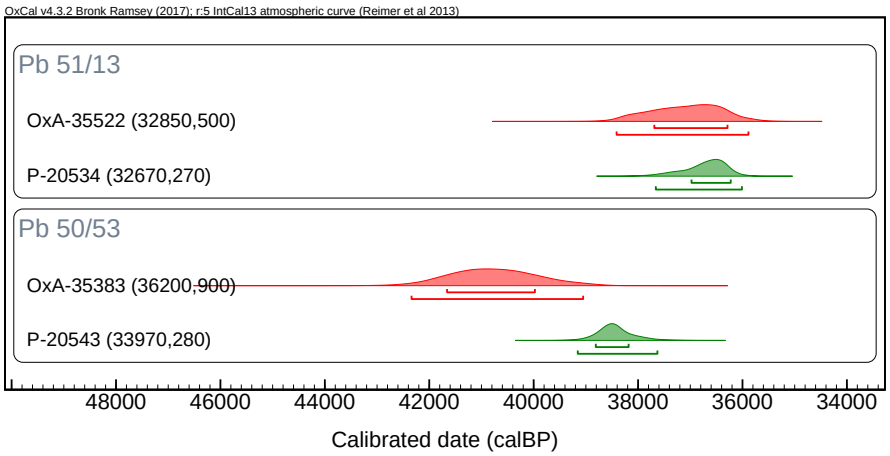


Figure 11.18: Istállóskő: comparison of radiocarbon dates obtained on osseous points Pb 51/13 and Pb 50/53 showing that unreliable measurements (*i.e.* failed at wheel meeting) published in Davies and Hedges (2008) (**green**) should not be used for further analysis, and be discarded in favour of the new new AMS ^{14}C dates (**red**).

From a chemistry perspective, it can be concluded that all new faunal dates should be reliable, but there is a chance that some of the bone point ages may slightly underestimate their true age due to low collagen yields and less intensive pre-treatment.

11.2.3 Bayesian Modelling

In this section, the Bayesian models used for Istállóskő are described. Their results and archaeological interpretations will be further discussed in section 11.2.4. The actual code used can be found under catalogue B.4.

Two major approaches to modelling were used in order to account for the complexity of the site: (1) Constraining the radiocarbon dates using the stratigraphic information as priors, and; (2) using the radiocarbon age distribution as a means of identifying periods of activity at the site irrespective of their layer attribution through a kernel density estimate (KDE) approach. Additionally, both cases were applied to the site as a whole, and to the osseous point data specifically. Priors and the dataset used may severely impact

the model results. Therefore, multiple models were run to investigate their sensitivity to different priors and radiocarbon data.

All `Sequence`/`Phase` models use the functionality of OxCal 4.3's general outlier model (with standard 0.05 probability of each sample being an outlier). In addition, the outlier model `SSimple` is used for dates within `R_Combine`, *i.e.* for OxA-16916 and OxA-16917.

All radiocarbon measurements are input as `R_Date`, with the exception of GrN-4659. As its calibrated age range extends beyond the period covered by the IntCal13 calibration curve, a workaround had to be implemented. The 2σ error (*i.e.* 3800 radiocarbon years) was added to the calibrated lower age limit at the 95% confidence interval (*i.e.* 45200 cal BP) to obtain an approximation of a calibrated mean value. This was subsequently input as the mean of a normal distribution, using the same 1σ error as the original measurement. Though this is not as reliable as a regularly calibrated radiocarbon age, it will better reflect the true age of the sample.

```
GrN-4659  Date("GrN-4659",N(calBP(49000),1900))
```

Site Stratigraphic Models

All site models include the phases 'lower AH', 'upper AH', and 'above 'upper AH". The latter is not an archaeological unit, but includes samples dated from above the archaeological horizons that can be used to constrain the model. When the model did not include any dates from the sterile layer, the two AH were separated by a double `Boundary`, despite the sterile layer between the two archaeological units not covering the entirety of the cave. When the model included a date from the sterile layer, it was placed as a separate `Phase` between the AHs and separated by a single `Boundary` on each side. Additionally, all models were run with an empty `Date` function within each `Phase`. While this is a useful method of obtaining an exportable age probability range for a cultural layer, it requires testing to make sure

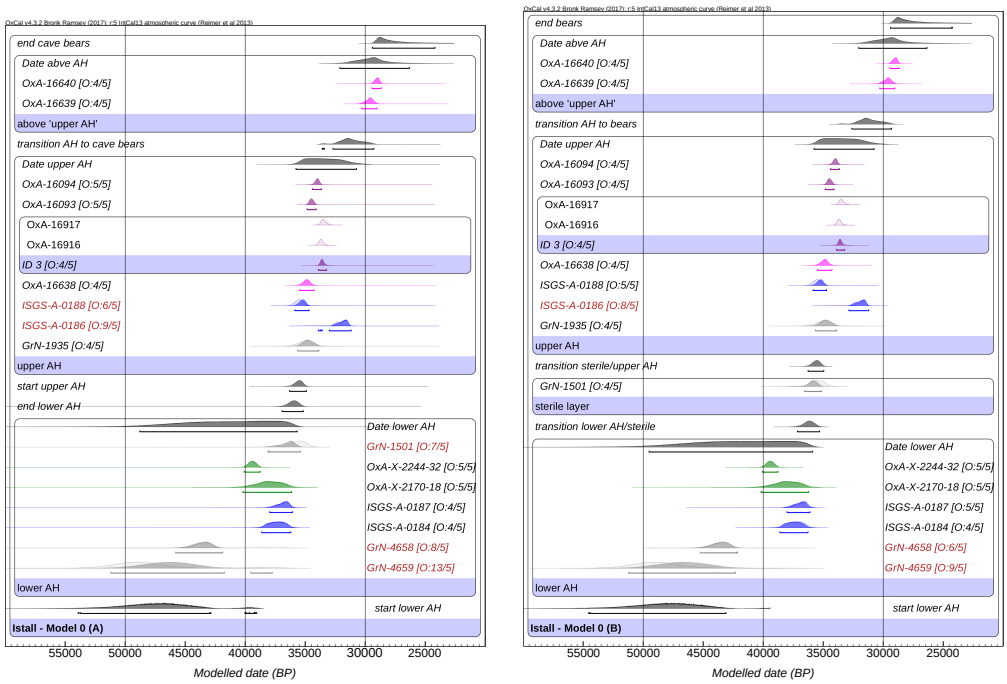


Figure 11.19: Istállóskő: site stratigraphic Models 0; with charcoal GrN-1501 in lower AH (A), or in separate sterile layer (B) (code: p. 712 and p. 712). Radiocarbon dates: **grey** – charcoal and bone (1950s/1960s); **blue** – unmodified fauna (2000); **purple** – charcoal (2006/2007) ; **magenta** – unmodified fauna (2006/2007); **green** – osseous points (2006/2007); **black** – purely modelled.

the influence of additional events on the outcome of the modelling process is negligible (see section 6.4). Therefore, the same models were also run without the `Date` function for testing. Within and between all phases, the command `Interval` was used to calculate duration of phases and transitions.

The stratigraphic Model 0 runs with previously published ^{14}C dates, to provide an assessment of the status prior to this dating project. Stratigraphic Model 1 and Model 2 focus on assessing the time period in which a layer may have accumulated material – combining both human and non-human activity. Finally, stratigraphic Model 3 and Model 4 concentrate on the timing of human activity within each layer.

Stratigraphic Model 0 includes all previously published ^{14}C dates with a clear layer attribution. This model represents the *status quo* prior to the current dating project. It is run in two versions (see fig. 11.19): (A) includes GrN-1501 in the lower AH (code: p. 712), while (B) places it within the sterile layer between the lower and upper AHs (code: p. 712).

Stratigraphic Model 1 includes all radiocarbon measurements with a clear layer attribution, irrespective of their perceived dating quality or association with human occupation. While this model is unlikely to provide conclusive information on stratigraphy or occupation, it is run to mathematically check for outliers (see fig. 11.20-left). Code listed on p. 713.

Stratigraphic Model 2 is the same as Model 1, except that the charcoal dates obtained in the 1950s were excluded. They are from a method perspective most likely to underestimate the true age of the sample. This model assumes that the bone collagen samples obtained in the 1960s do indeed belong to the lower layer and are not intrusive from below. The model results should illustrate the layer accumulation time under the constraints mentioned before (see fig. 11.20-right). Code listed on p. 715.

Stratigraphic Model 3 only includes radiocarbon measurements directly connected to human activity: Osseous points, cut-marked bones and charcoals. This model assumes that the latter ages are – despite their less rigorous treatment with ABA – reliable age estimates. This model offers insight into (1) layer accumulation history if we assume that the very old bone collagen dates belong to samples that were erroneously attributed to the lower AH; and (2) occupation events within the layers of interest (see fig. 11.21-left). Code listed on p. 716.

Stratigraphic Model 4 is the same as Model 3, except that the charcoal samples are all excluded. It assumes that their pre-treatment was insufficient

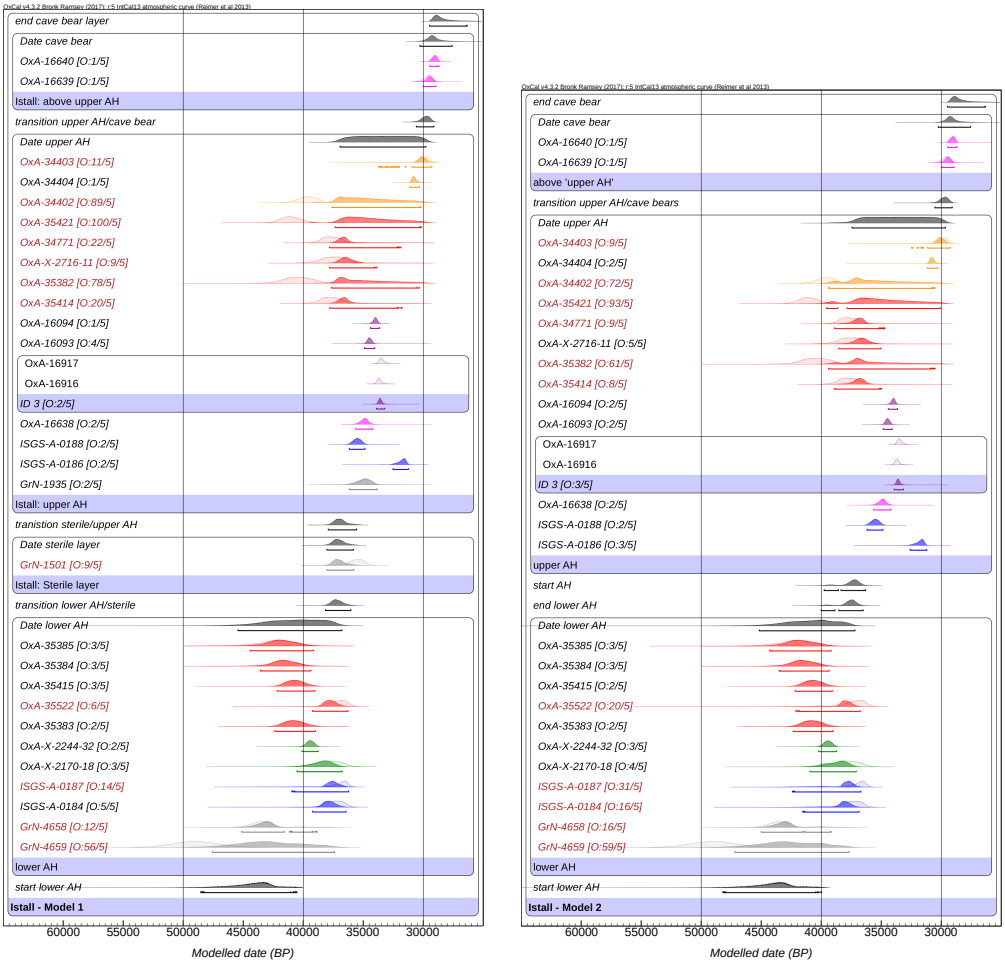


Figure 11.20: Istállóskő: site stratigraphic Model 1 (left, code: p. 713) and Model 2 (right, code: p. 715). Radiocarbon dates: **grey** – charcoal and bone (1950s/1960s); **blue** – unmodified fauna (2000); **purple** – charcoal (2006/2007) ; **magenta** – unmodified fauna (2006/2007); **green** – osseous points (2006/2007); **red** – osseous points (new); **orange** – anthropogenically modified fauna (new); **black** – purely modelled.

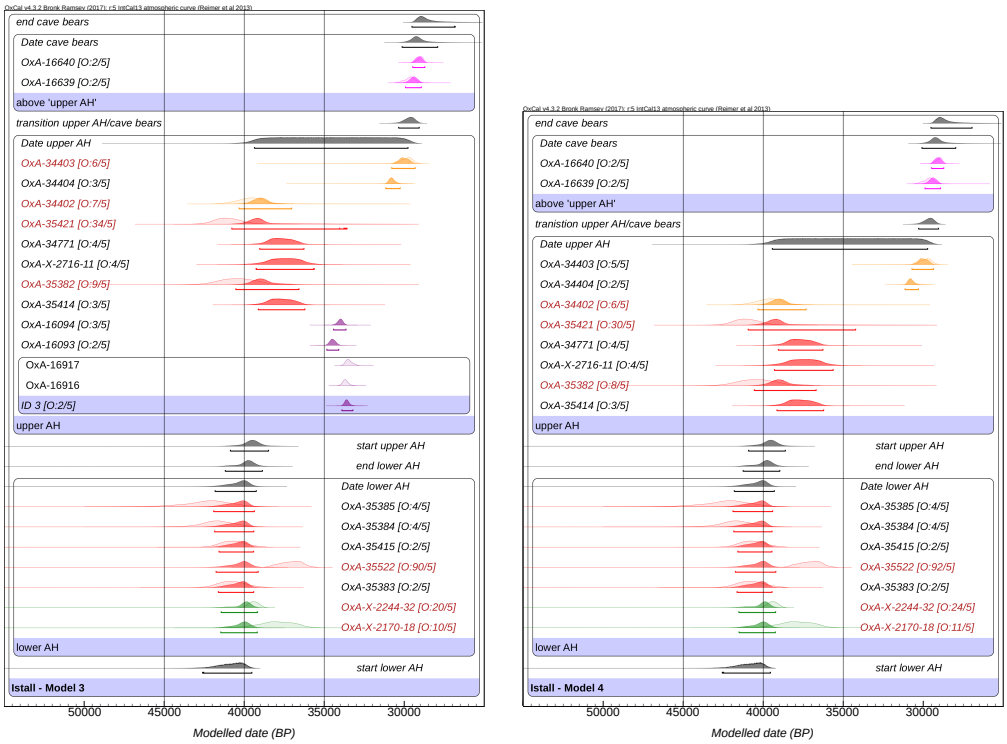


Figure 11.21: Istállóskő: site stratigraphic Model 3 (left, code: p. 716) and Model 4 (right, code: p. 717). Radiocarbon dates: **purple** – charcoal (2006/2007) ; **magenta** – unmodified fauna (2006/2007); **green** – osseous points (2006/2007); **red** – osseous points (new); **orange** – anthropogenically modified fauna (new); **black** – purely modelled.

and they represent only minimum age estimates – like many other ABA treated charcoals older than 30k BP (*e.g.* Wood et al., 2012). This model should highlight the human occupation events found within the lower and upper layers (see fig. 11.21-right). Code listed on p. 717.

Site KDE Models

All site specific KDE models use the `KDE_Model` function in OxCal 4.3 in order to identify groupings of radiocarbon dates (see fig. 11.22). They differ only in regards to the radiocarbon dataset used. The Kernel Density Estimate method is preferred over the `Sum` function, as the latter is heav-

ily influenced by the frequency with which an event has been dated (see discussion in chapter 6.2).

KDE 1 includes all available radiocarbon dates, including those with ambiguous layer attribution (n=30). It can be used to show site specific accumulation periods, but tends to hide occupation events in the noise created by samples unrelated to human activity. Code listed on p. 717.

KDE 2 is restricted to radiocarbon dates associated with human activity (osseous points, cut-marked bone, charcoals), but does not make any assumptions with regard to their reliability (n=19). Its radiocarbon dataset is identical to the Site Stratigraphic Model 3. It should highlight the periods of human activity irrespective of issues with layer identification, mixing and sample identification. Code listed on p. 718.

KDE 3 only uses the dates obtained on cut-marked faunal remains (this study) and on osseous points (this study and Davies and Hedges, 2008). The radiocarbon dataset (n=15) is identical to the one implemented in the Site Stratigraphic Model 4. This model should help highlight possible events of human activity, assuming that the charcoal dates obtained by Davies and Hedges (2008) are underestimating the age of the hearths and should therefore be excluded. Code listed on p. 719. For the effects of excluding the questionable date of OxA-X-2244-32 see the model 'Point KDE 2' (below).

Osseous Point Models

The excavation history of the site has been very complex (see section 11.2.1) and several refittings (lithics and osseous points) across both the lower AH and upper AH have been found (see section 11.2.1). It is therefore not entirely certain that the osseous points can be securely attributed to either the upper or the lower archaeological horizon. However, osseous projectile points (especially SBP) form a very specific industry, which can be independently

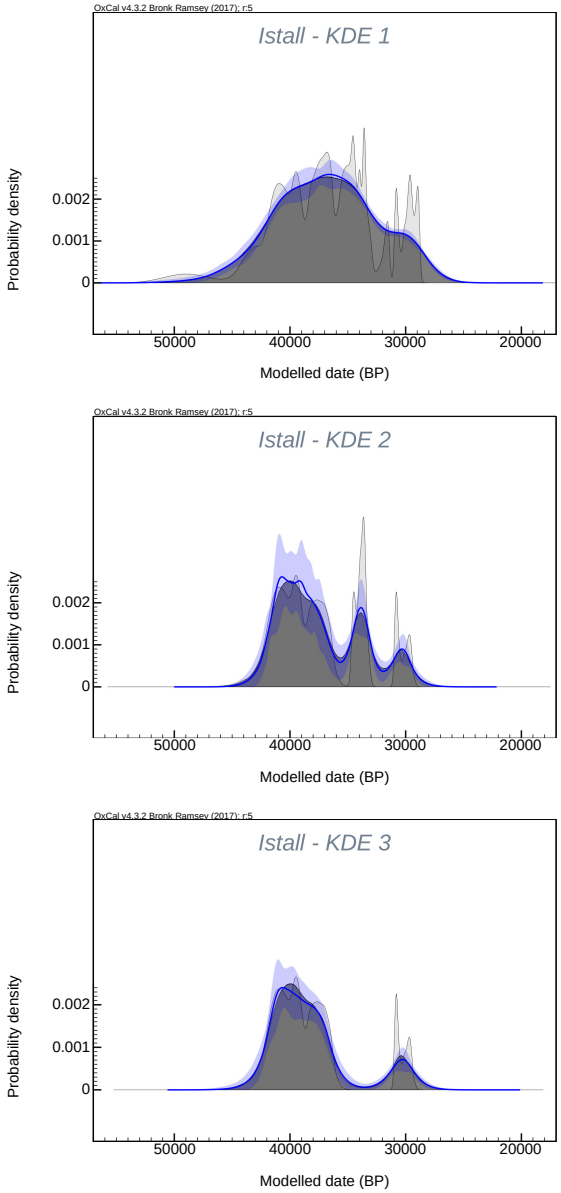


Figure 11.22: Istállóskő: site KDE models: top – KDE 1 (n=30, code: p. 717), showing general activity at the cave; middle – KDE 2 (n=19, code: p. 718), illustrating human activity (osseous points, cut-marked bone, charcoal); bottom – KDE 3 (n=15, code: p. 719), visualising human activity with traces on osseous material.

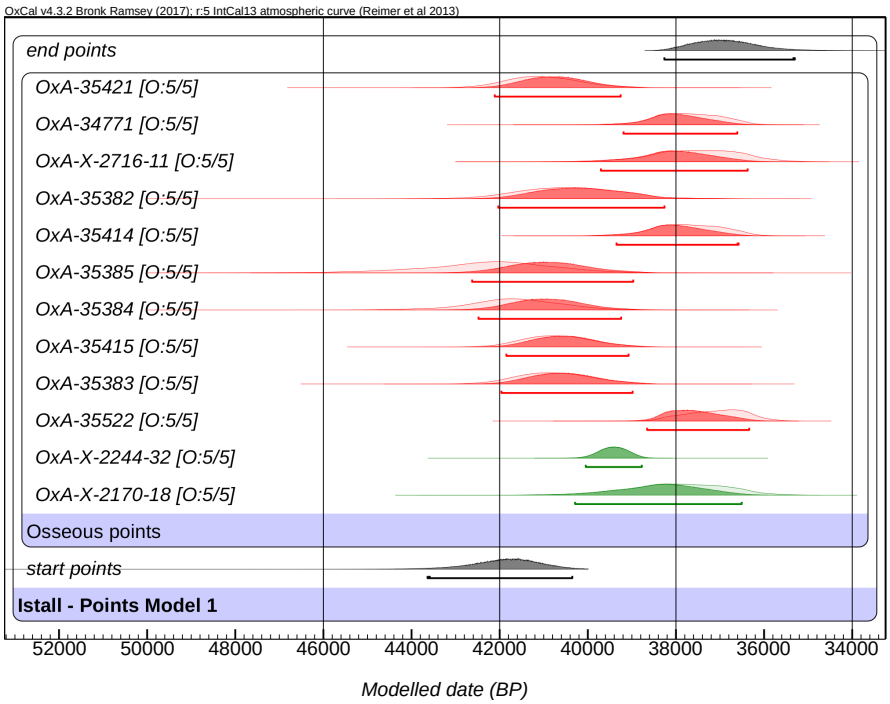


Figure 11.23: Istállóskő: Point Model 1 (code: p. 719). Radiocarbon dates: **green** – osseous points (2006/2007); **red** – osseous points (new); **black** – purely modelled.

studied, as they provide not only direct evidence for a specific human action, but are believed to be associated with a specific cultural complex.

Point Model 1 treats all bone points as belonging to a single `Phase` in order to establish a start and an end `Boundary` for their occurrence. As a result of these limited constraints, the start and end boundaries for the osseous point industry are not as restricted as one would have hoped. Nonetheless, this model can provide vital information regarding the appearance and disappearance of the industry independent of their place in the stratigraphy (see fig. 11.23). Code listed on p. 719.

Point KDE 1 shifts the focus from start and end boundaries to testing for groupings within the osseous points' dataset. While it uses the same

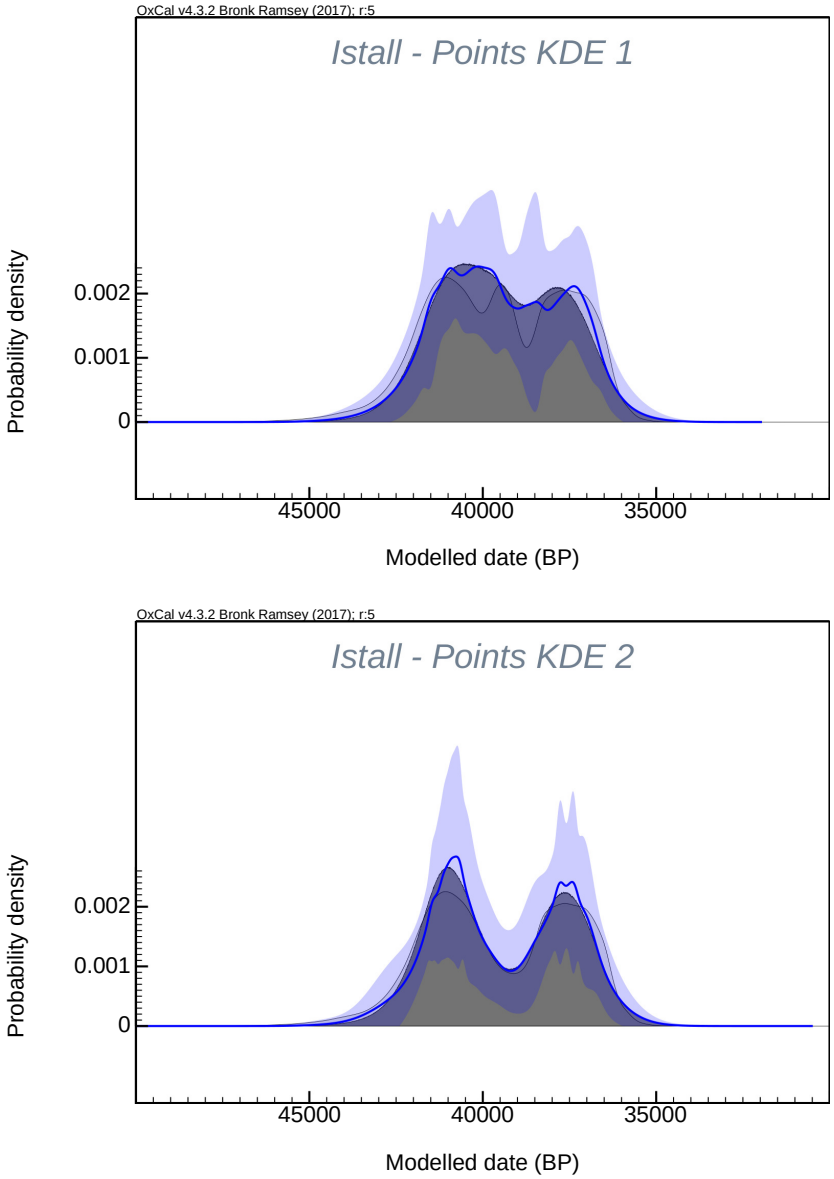


Figure 11.24: Istállóskő: osseous point KDE models: Points KDE 1 (n=12, code: p. 720), using all radiocarbon dates from osseous points as seen in Osseous Point Phase Model; and Points KDE 2 (n=11, code: p. 720), excluding OxA-X-2244-32 as its NRC treatment most likely underestimates the true age of the sample.

underlying radiocarbon dates as the previous model (n=12), it places them without further priors in a `KDE_Model` (see fig. 11.24). Code listed on p. 720.

Point KDE 2 excludes OxA-X-2244-32 from the dataset used in Point KDE 2 (leaving n=11), as there are strong concerns regarding the date's reliability (see fig. 11.24). Code listed on p. 720.

11.2.4 Discussion

As the original excavation documentation was not accessible, it was not possible to further query it to see whether any of the samples had accidentally been mislabelled during excavation, cataloguing or later in storage. Considering the fate of the SBP 167/914.22 (Istall-18) – which was before Markó (2017) erroneously attributed to the Peskő cave – it appears probable that some of the dating discrepancies are caused by archival errors. A larger source of inaccuracy, though, was introduced by the coarse excavation methods, which would combine material from finer, unidentified archaeological levels. This would have a particularly strong impact at a cave site, such as Istállóskő, where post-depositional disturbances (*e.g.* erosion, mixing) are to be expected. And finally, the old radiocarbon dataset is marked by less rigorous pre-treatment and diverse material, often not directly connected to human occupation or the periods of osseous point manufacture. The new ^{14}C dates, on the other hand, are directly connected to human activity. As far as it is possible to determine, they appear reliable and robust, despite many of them having been treated with the less rigorous AG* protocol. In the following, all these factors will be kept in mind when assessing dating outliers, stratigraphic integrity, occupation events and periods of osseous point manufacture.

Model Outliers & Stratigraphic Integrity

As expected, the charcoal date GrN-1501 is an outlier to the lower AH (see Model 0-A in fig. 11.19). Placing it in the sterile layer give ambiguous results, with acceptable dating consistency in Model 0-B, but identified as an outlier in Model 1 (see fig. 11.20). Two possible interpretations come to mind: (1) the date underestimates the true age of the sample and it actually belongs to the lower AH; and (2) the dating is reliable, the sample belongs to the sterile layer, and the outlier identification was caused by samples intrusive to the lower AH. As GrN-1501 had only been treated with acid, the former explanation is far more convincing, albeit the latter cannot be excluded.

The two bone collagen dates GrN-4658 and GrN-4649 have also been identified as statistical outliers for the lower AH by the site stratigraphic Models 0 and 1 (see fig. 11.19–11.20). While GrN-4658 is only minimally older than the oldest radiocarbon measurements obtained on osseous projectile points, none of the new radiocarbon measurements replicate the considerably older age of GrN-4659. This has significant implications for the start `Boundary` of the lower AH (see fig. 11.25). Keeping the two bone collagen samples dated in the 1960s in the model pushes the start of the lower AH back nearly 5000 years.

It has to be noted that GrN-4659 had been collected at the bottom of the lower AH. As a result, the faunal remains might have been erroneously attributed to this horizon, and its date has no relationship with the lower AH. If the samples' association to the lower AH were correct, it would in turn demonstrate the long accumulation time of the lower horizon. This is visualised in the wider probability distributions of its `Date` functions in the stratigraphic Models 0–2, compared to Models 3–4 (see fig. 11.19–11.21). Irrespective of which interpretation is accurate, all models including GrN-4658 and GrN-4659 (i.e. Models 0–2) overestimate the age of the human occupation within the lower horizon, as the samples are not securely connected to human activity.

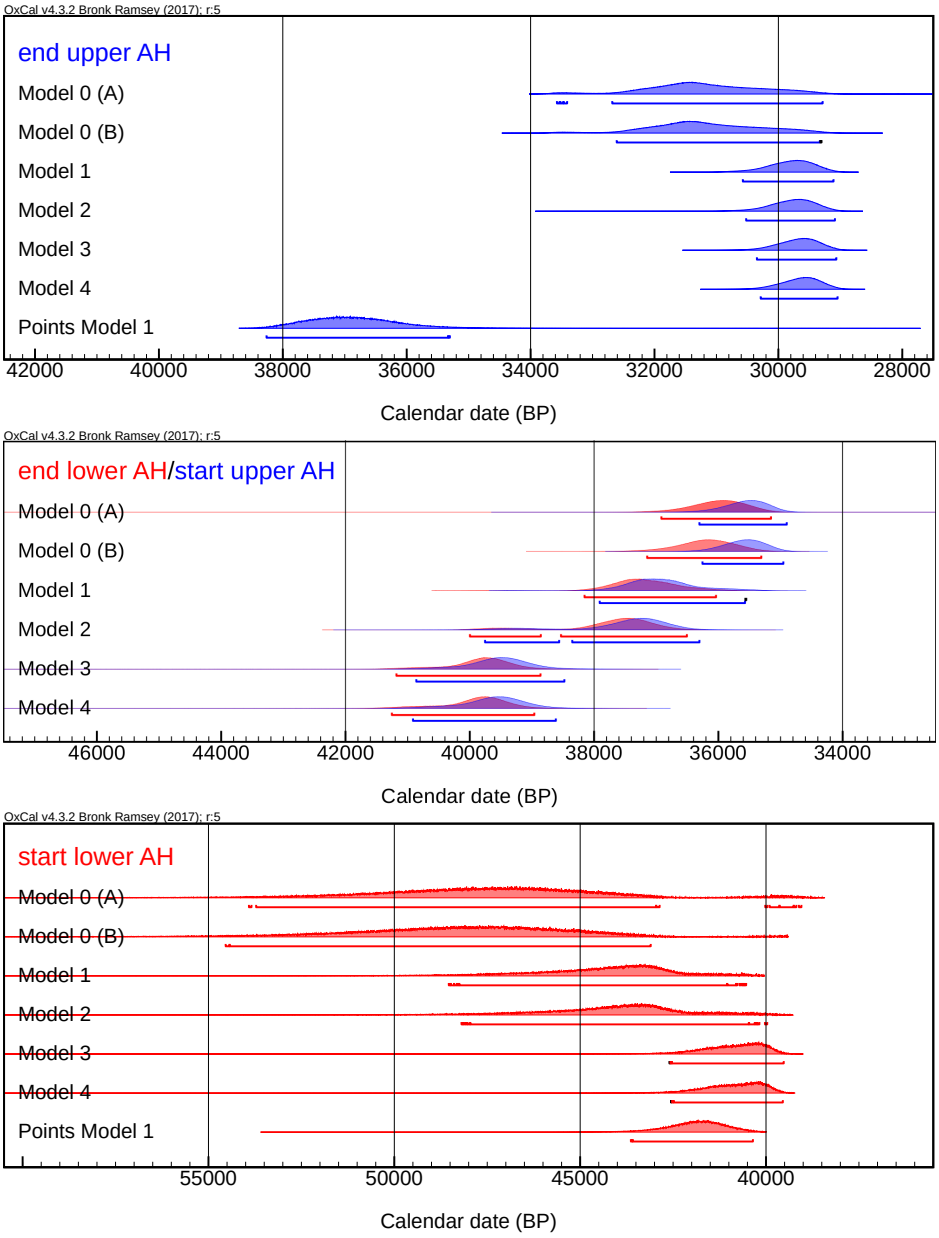


Figure 11.25: Istállóskő: comparison of start and end boundaries for the lower AH (**red**) and for the upper AH (**blue**) as calculated by the site stratigraphic models 0–4, and the point stratigraphic model Points Model 1 – demonstrating the huge influence the non-occupation related dating has on Bayesian modelling and the need for direct dating of osseous points in order to not overestimate their period of use.

Lithic and osseous point refittings have led to questions regarding the integrity of the layer divisions at Istállóskő (*e.g.* Markó, 2015, 2017). The observed vertical displacement is also evident in the stratigraphic model results. All models that include the point Istall-03 (OxA-35522), identify the date as an outlier. More importantly, its outlier probability increases when the focus is narrowed to just anthropogenically modified samples (6% in Model 1, 20% in Model 2, 90% in Model 3, and 92% in Model 4). In contrast, the points Istall-02 (OxA-35382) and Istall-16 (OxA-3542) show decreasing outlier probabilities (78% and 100% in Model 1, 61% and 72% in Model 2, 9% and 34% in Model 3, and 8% and 30% in Model 4). Both are caused by the reduction of age spread within the upper and lower horizon when shifting from general layer accumulation towards anthropogenically modified samples, and finally narrowing it down to anthropogenically modified bone. It also explains how the two previously dated bone points, OxA-X-2170-18 and OxA-X-2244-32 20, are outliers in Models 3–4 (10% and 20% in Model 3, 11% and 24%), but not in Models 0–2.

Assuming none of the dates are grossly inaccurate, it can be concluded that interference from younger samples outweighs influence from older samples. The higher dating variability in the upper AH could be the result of combining different occupation events (identified by osseous points, charcoals and cut-marked bone) within one layer, and/or the intrusion of material from layers higher up in the stratigraphic sequence (while the reverse is rare). The variability in the lower AH, in turn, stems from a partial overlap with ages observed in the upper AH. These two situations could be partially explained by post-depositional processes, such as solifluction. In these cases, the lighter sediment gets slowly washed out of the cave, while the heavier material remains behind, and is sometimes embedded in the soft, permeable sediment from the layer underneath. In other cases, the heavier material rests on the surface to be eventually covered by fresh sediment. This interpretation is further supported by the presence of the grey, sterile layer confined to areas of the cave more protected from water driven erosion (see also fig. 11.9–11.10).

A similar pattern of date distributions is seen in the stratigraphic models focusing on human activity (*i.e.* Model 3 and Model 4), which indicates that dating inaccuracy is probably not the cause of the apparent displacement. This is especially evident in the cut-marked bone dates, which were all pre-treated using ultrafiltration (AF). The higher dating consistency in these two models, compared to the stratigraphic models including material unrelated to the human occupation (Models 0–2), is in all likelihood the result of only intermittent human occupations with limited material presence. Its chronostratigraphically localised material will be less heavily affected by post-depositional processes. Moreover, the discrete nature of the cave use opens up a unique opportunity to reconstruct the original occupational sequence.

Model Results & Human Occupation

As demonstrated above, the age of the identified layers is not interchangeable with the timing of the human occupations, as a result of both sporadic human visits and post-depositional processes. In contrast to human activity focused sampling, layer targeting dating overestimates the age of the lower AH, while simultaneously underestimating the date for the transition between the lower and upper AH (see Models 0–2 in fig. 11.25).

The transitions calculated by these models are contemporaneous or older than the independently modelled end boundary for the osseous point industry at the site (see Points Model 1), thus suggesting that all points should belong to the lower AH. This stands in strong contradiction to archaeological observations. The discrepancy is resolved when focusing on dates directly connected to human activity – *i.e.* osseous points, cut-marked bones, and, optionally, charcoals. Model 3 and Model 4 calculate a date for the transition between the two archaeological horizons of *ca.* 41–38.8k cal BP, predating the end of the osseous industry. These models further demonstrate that the upper AH contains more than just the occupation associated with the osseous point industry.

This is consistent with the site specific KDE modelling results (see fig. 11.22). KDE 1[9], which investigates all activity at the site (not solely those connected to humans), presents a relatively continuous accumulation of material[10] with one wide main peak and a smaller shoulder towards the younger age range. By contrast, removing the non-human activity related material, sets apart a minimum of three occupations (seen in KDE 2). The oldest peak is associated with the osseous point industry from both the lower and upper AH. The second peak corresponds to the charcoal dates, which probably originate from the fireplace within the upper AH. The youngest peak derives from the cut-marked bones supposedly found in the upper AH. Analysis of post-depositional processes suggests that these might in actuality belong to activity from layer 4 (as described in the profile 11.9). In that case, the peak might be associated with the 'leaf point' bearing Gravettian found at Istállóskő[11]. KDE 3 demonstrates that none of the cut-marked bones or osseous points are contemporaneous with the 'fireplace peak' observed in KDE 2.

Consequently, the 'Aurignacian' point industry appears split over two layers, while sedimentation of later occupations appear difficult to distinguish from the second point based event. Such a shift in sedimentation without a clear shift in lithic industry, followed by a shift in lithic industry without a sedimentation shift was also observed at Temnata Dupka in Bulgaria (see section 8.4.4). Therefore, the nature of the first oldest occupation peak warrants further investigation.

Osseous Point Industry, Techno-Cultural Change & the CI

The osseous point industry appears to fall within the earliest and most intensive period of human occupation at the cave (see KDE 2 and 3 in fig.

[9]Trivia: the shape is reminiscent of the graph/hat/snail from *Le petit prince*.

[10]This is in relation to the radiocarbon dating resolution obtainable, and does not necessarily represent an absolute continuity throughout the time period under investigation.

[11]For the occurance of 'leaf point' with Gravettian lithics in the region see also Bárta (1988); Dobosi and Simán (2003).

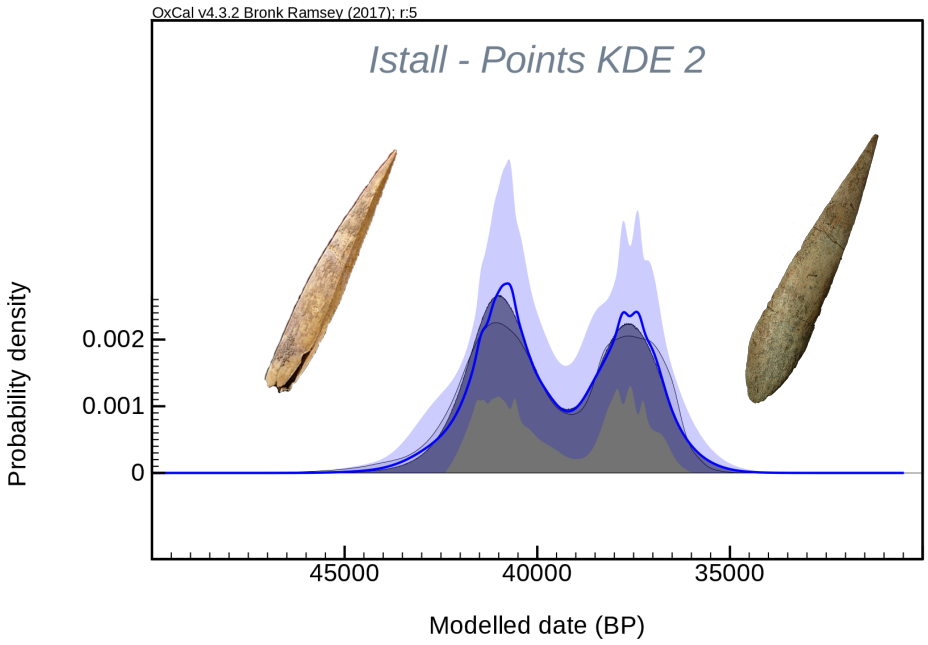


Figure 11.26: Istállóskő: the bimodal distribution of osseous points observed in the model Points KDE 2 reflects an initial phase dominated by split-based points, followed by a younger phase dominated by massive-based points.

11.22). The osseous point models Points KDE 1 and Points KDE 2 focus on this initial occupation event (see fig. 11.24). While the general site data (KDE 2 and KDE 3) presents a wide peak over the entire period, a bimodal distribution becomes visible when focusing on directly dated osseous points. The bimodality becomes more pronounced in Points KDE 2, where OxA-X-2244-32 is excluded on the basis of its questionable pretreatment.

This clearly demonstrates the importance of directly dating a significant number of osseous projectile points, rather than relying on their layer attributions. Indirect dating through layer association would have led to an overestimation of the time period in which the points had been used. More importantly, the effects of post-depositional processes would have concealed the high correlation between artefact age and typology – *i.e.* SBP vs. MBP (see fig. 11.26). The points in the older age range are split-based points with the exception of Istall-07 (OxA-35384), which was fragmented in a way which hinders a possible split-base identification. At the same time, only one

of the points (Istall-18) in the younger age group has been identified as a possible split-based point.

The transition between the lower and upper AH, as calculated by Model 3 and Model 4 (see fig. 11.25), now falls within the two peaks of the bimodal distribution in Points KDE 2 (see fig. 11.26). Moreover, the return to the cave after the initial SBP occupation coincides or post-dates the CI eruption, and mimics a pattern observed at other sites in this study. The magnitude of the CI eruption is expected to have had a significant influence on the climatic conditions in central and eastern Europe. It is therefore worth investigating whether the change in technological preferences of osseous points is an adaptation to new environmental conditions, such as climate, which do not affect lithic raw material supply. Osseous raw material use is heavily dependent on the available fauna, which in turn is susceptible to climate change. In contrast, lithics availability is more strongly correlated to geographic location.

Presently, no tephra layer has been identified at Istállóskő. However, the cave lies within the reach of the CI fallout, and with new methodologies for detecting microtephra deposits a reinvestigation of the site might be fruitful. In the light of the osseous point modelling results, the grey, sterile layer partially separating the lower from the upper AH would be an ideal place to investigate.

Conclusions

This project yielded 10 new direct radiocarbon dates on osseous points (2 AF*, 8 AG*), and 3 on anthropogenically modified bone (AF) – providing for the first time an extensive radiocarbon dataset directly connected to human activity at Istállóskő. Despite the frequent use of the gelatine protocol over ultrafiltration, the data is very consistent. It appears that the solvent wash steps eliminated any possible conservation derived contamination remaining after careful sampling.

In addition to lithics and osseous point refittings, the dating distribution and modelling results present further evidence for vertical movement caused

by post-depositional processes. It is important to note that there was some mixing between the lower and upper AH (especially in areas where the sterile layer no longer separates the two horizons), as well as some possible material intrusion from 'layer 4' into the upper AH. The UP occupation sequence can be reconstructed as follows: SBP, non-SBP (probably massive-based points), a fireplace event, and a 'Gravettian with leaf-points'. While the first originated in the lower AH, the upper AH contains at least two temporally independent occupations. As a result of post-depositional processes, a direct connection to the lithic assemblage has to be undertaken with great caution. Nonetheless, there is no directly dated evidence for a MP occupation, and no diagnostic Aurignacian lithics have been found. The latter emphasises the importance of treating the 'Aurignacian' osseous point industry (both split-based points and massive based points) as independent means of obtaining a higher resolution of variability and change in technology.

This project has demonstrated the need for dating samples directly connected to human activity – especially the direct dating of osseous points. On the one hand, indirect dating of the technocomplex by layer association overestimates the age of AMH and SBP appearance at Istállóskő as a result of sporadic, temporally distinct occupations within larger periods of sediment accumulation. On the other hand, it obscures the relationship between osseous point typology and their chronological association because of material exchange between different archaeological levels.

Therefore, the stratigraphic models Model 3, Model 4, and Points Model 1, as well as the KDE models KDE 2 and Points KDE 2 supply better approximations for the timing of human occupations and osseous industries at the site. If we associate AMH with SBPs, as most specialists do, AMH occupation started with the appearance of SBP between 43650–40350 cal BP (Points Model 1) or 42600–39500 cal BP (Model 3 and Model 4), and the earliest occupation within the upper horizon would have began 40900–38450 cal BP (Model 3) or 40950–38600 cal BP. These results are consistent with Points KDE 2, which in addition illustrates a correlation between the bimodal distribution and the typological distinction between SBP and non-

SBP (*i.e.* probably MBP). The increased use of non-SBP coincides with or post-dates the date for the CI eruption, suggesting a possible connection to environmental adaptation. Furthermore, it raises the possibility of finding tephra evidence in the remains of the grey, sterile layer separating the lower from the upper AH.

11.3 Jankovich

Jankovich cave (see fig. 11.27) is the eponymous site for the Jankovichian industry, a technocomplex believed to belong to the late stages of the Middle Palaeolithic and the beginning of the 'transitional' period. At the same time it yielded a significant number of 'Aurignacian' osseous points – some possibly associated with Jankovichian leaf-shaped lithics. Consequently, direct radiocarbon dating of this diagnostic industry is crucial to chronologically contextualise the osseous industry.

11.3.1 Introduction

Jankovich cave (N 47° 43' 26", E 18° 34' 31") is located just east of the village Bajót in the north-eastern part of Transdanubia, Hungary, at an altitude of 330 m a.s.l. and 50 m above the valley floor. It consists of a main gallery extending in south-south-west direction for *ca.* 36–40 m, though the ceiling of the front section (10–15 m) had been removed during a detonation (see fig. 11.28). In the rear section there is a tunnel leading south down to a side chamber, adding another *ca.* 10 m to the extension of the cave. This near circular hall lies 5 m lower than the main gallery. At the cave centre, a large chimney leads to the outside (see fig. 11.29). The maximum width appears to be *ca.* 14 m, with a maximum height of *ca.* 8 m, and the entrance faces northwards towards the Danube (Herrmann et al., 1957; Hillebrand, 1913a, 1915, 1917; Markó, 2013a).



Figure 11.27: Jankovich: photos of cave location (left) and view from cave (right) (Markó, 2013b, fig. 1–2).

The archaeological site first entered the literature as Öregkő cave ('Old Cliff') Hillebrand (1913a). However, after a substantial donation by B. Jankovich – the then minister of religion and education – the cave was renamed in his honour (Hillebrand, 1914; Markó, 2013b).

Excavation History

Excavations at Jankovich began in 1913, when Hillebrand opened up a test trench at what then was believed to be the rear section of the cave. He subsequently returned on a yearly basis until 1918, in which time he was able to discover various lithic artefacts – including a Mousterian point, end-scraper on a blade, and leaf-points (Hillebrand, 1913a, 1914, 1915, 1917, 1919). In 1915, a number of osseous implements and points were discovered, and in 1917 the way was freed to the archaeologically richer side chamber. Hillebrand continued excavations in 1925, when he identified three superimposed

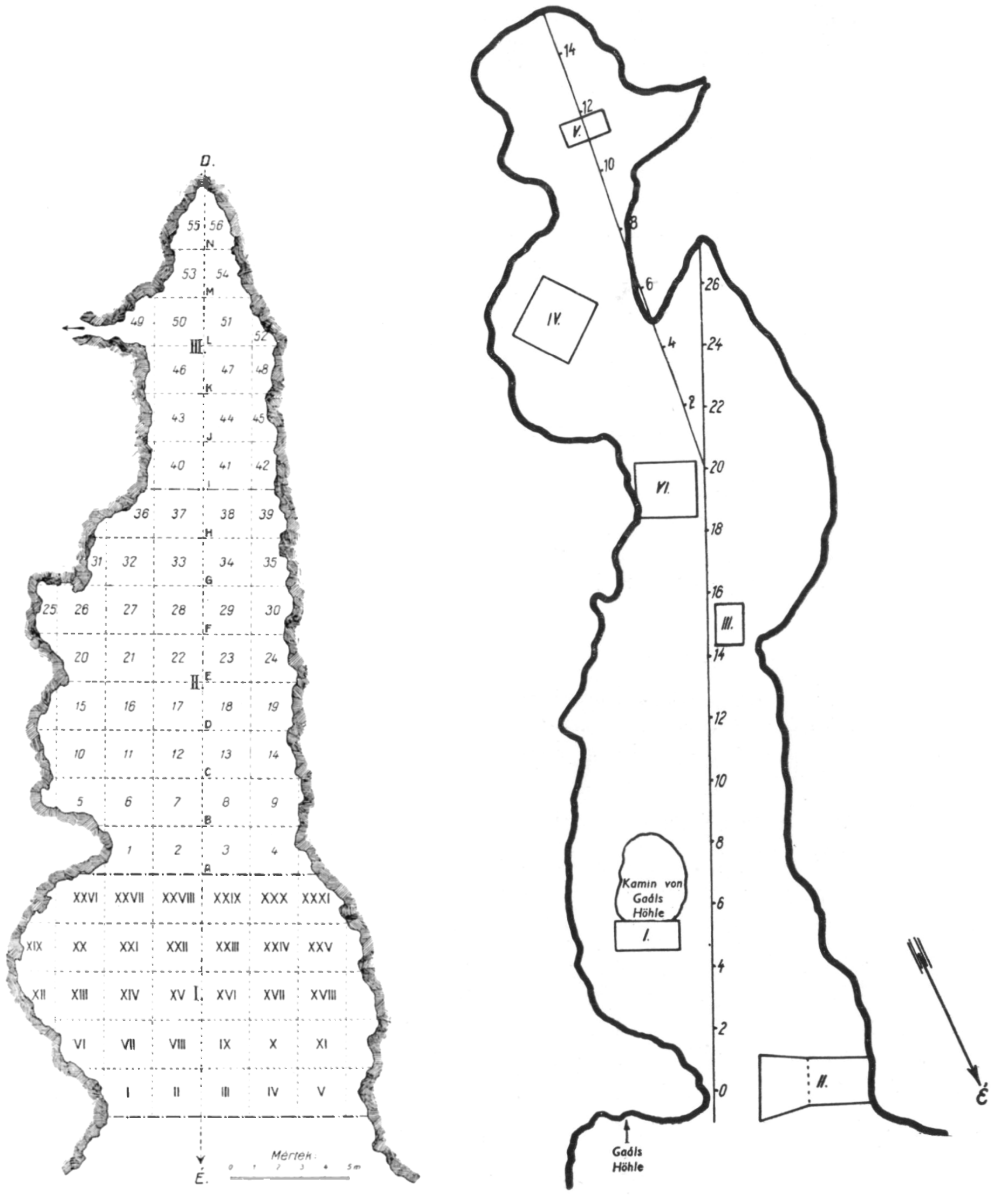


Figure 11.28: Jankovich: cave map with location of excavation trenches and local co-ordinates. left – original map before discovery of side cave, scale indicating 5 m (Hillebrand, 1917, fig. 1); right – updated excavation map after Vértes' excavation in 1956 (Herrmann et al., 1957, fig. 1). Note that the front area (marked by Roman quadrant labels) is not shown on the right map.

hearth structures with further 'wedge-shaped tools' (*i.e.* osseous points), and a concentration of leaf-shaped lithics in the side chamber (Hillebrand, 1926).

Additional excavations were conducted in 1956 under Vértes, in an attempt to test whether further divisions in the archaeology bearing layers were possible – especially in the side chamber (Herrmann et al., 1957). They placed 6 test trenches throughout the cave (see fig. 11.28), though only two locations showed layers *in situ* and their archaeological finds were few. While their excavation methodology was finer than previously, they too moved forward in rather large spits of 15-20 cm each.

Stratigraphy & Archaeology

Hillebrand (1915) described the stratigraphic sequence as follows, numbering the layers from top to bottom (see also fig. 11.29):

0. brown humus
1. **yellowing-grey** loam
2. **yellow** layer with limestone debris
3. **red** layer with limestone debris
4. **yellow** clay

The brown humus contained some Bronze Age material, while the yellow-grey layer underneath was nearly sterile. Layer 2 was substantially richer, containing both macro- and microfauna, as well as archaeological remains. Applying the terminology of the time, Hillebrand (1915) attributed the horizon to the 'Magdalenian II' (*i.e.* 'Epigravettian'). Layer 3 was only present in the rear section of the cave. Here, microfauna were few, while cave bear remains were frequent. The leaf-points in this section made him connect the horizon to the 'Solutrean' (*i.e.* 'Szeletian/Jankovichian'). The underlying yellow clay appeared empty again and it was thought that it lies upon the rock, though the bedrock was not reached during any of the excavations.

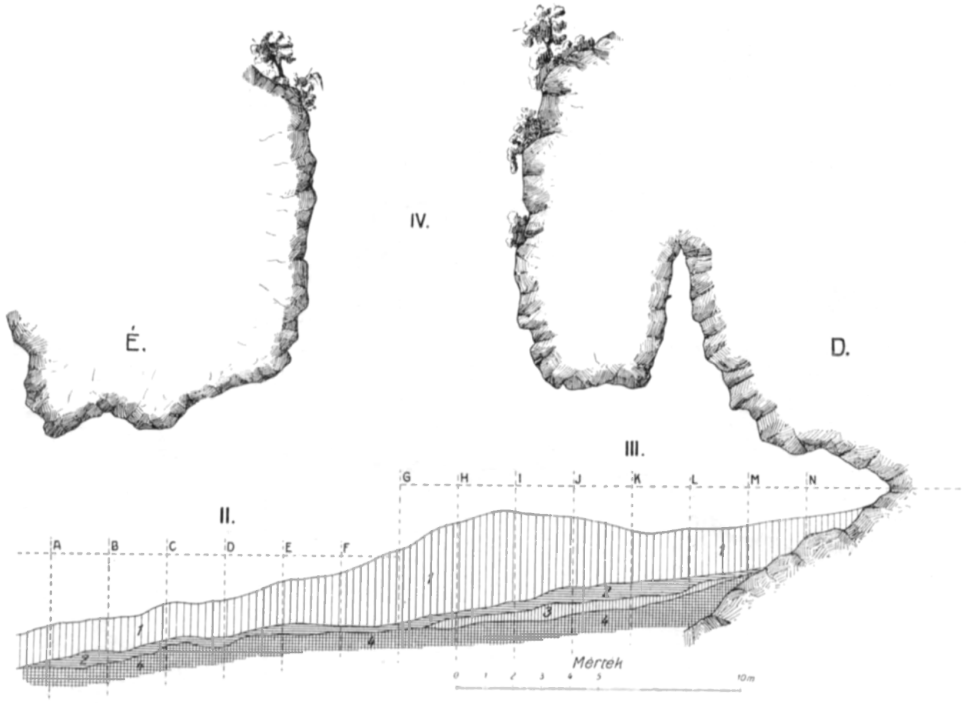


Figure 11.29: Jankovich: drawing of west-facing profile through cave length with 4 layer divisions (Hillebrand, 1917, fig. 2). Scale indicates 10 m. 1 – yellowish-grey layer; 2 – yellow layer with limestone debris; 3 – red layer with limestone debris; 4 – yellow clay.

The area richest in archaeological finds was the side chamber (see selection fig. 11.30). In 1925 Hillebrand (1926) excavated three hearth levels with typical MP lithics in the lowermost and 'Szeletian' leaf-points in the uppermost level. More importantly, both the upper and middle fireplace contained osseous points (Markó, 2013a). This indicates that there were further divisions visible, apart from the rough divisions into 5 layers described previously. This is supported by Hillebrand (1917), where he describes lighter and darker levels in sequence, with darker levels richer in archaeological material. Regrettably, the excavations did not take these subdivisions into account when labelling and archiving the find material.

The lower archaeological horizon, concentrated in the side chamber, contained high numbers of bifacial and leaf-shaped lithics, as well as antler and

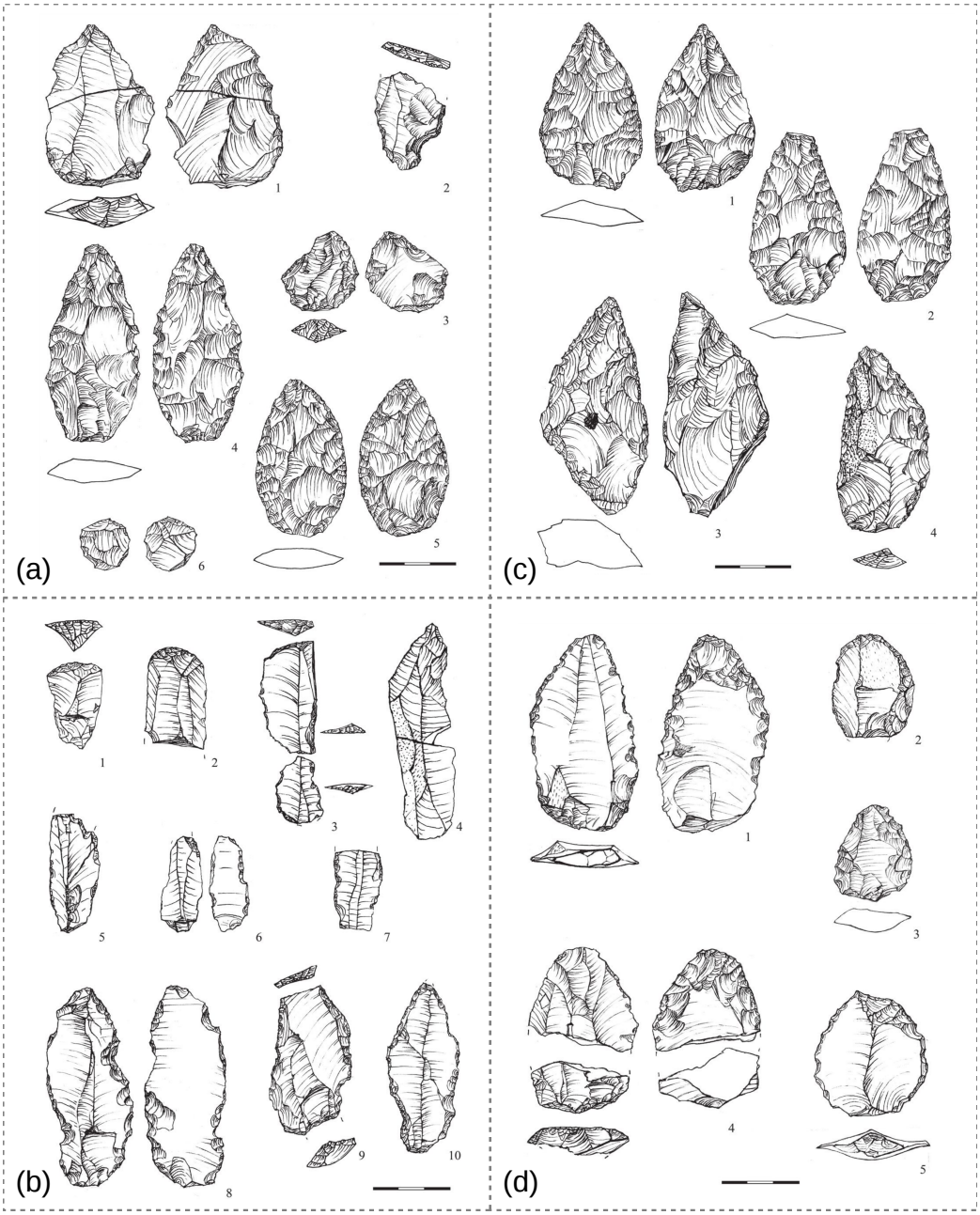


Figure 11.30: Jankovich: lithics from Hillebrand's excavations. (a) lithic tools form 1915–1917; (b) Gravettian and MP lithics found in 1915; (c) lithic tools from the upper and lower hearth layers from 1925 (d) Levallois points with ventral thinning and convergent scrapers found in 1915 (Markó, 2013b, fig. 2–4, 7).

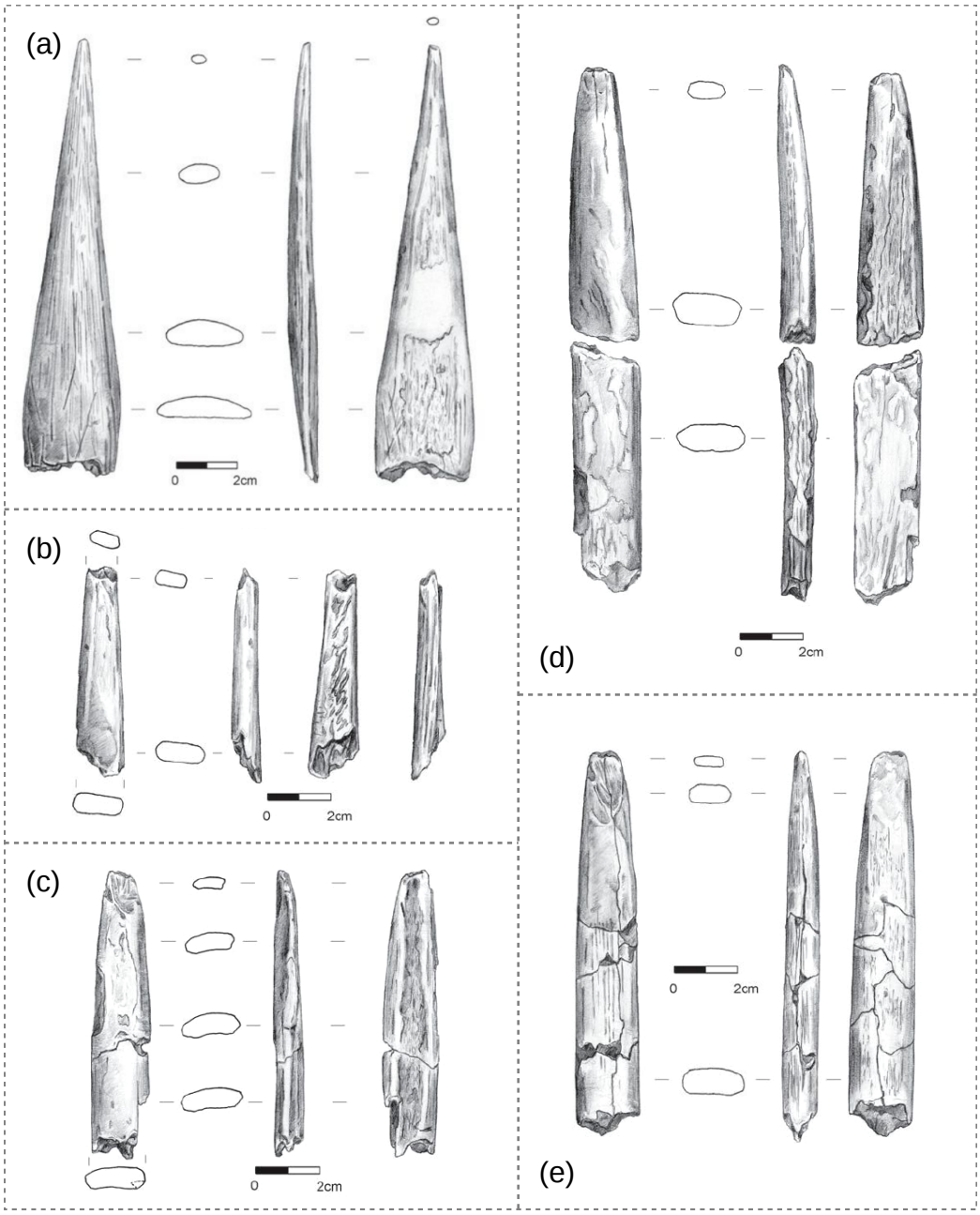


Figure 11.31: Jankovich: drawings of some of the osseous points found during Hillebrand's excavations (Markó, 2013a, fig. 2, 4–6).

ivory artefacts (see also fig. 11.31). The lithics were initially described as a Szeletian subdivision found in Transdanubia, but Gábori-Csánk (1993) used them as the basis for her definition of the Jankovichian. The use of Levallois technology in the initial stages of production led to interpretations affiliating the tools with the late MP. At the same time, the osseous points seemed to place the layer within the Early Aurignacian (Vértes, 1955) – though UP lithics were largely absent. A blunted bladelet and a carenoid scraper, listed by Vértes (1955) as Aurignacian, were instead attributed to the Gravettian by Markó (2013a), and deemed intrusive. Attempts at disentangling the situation through new excavations remained fruitless (Herrmann et al., 1957).

With such a long research history, issues surrounding material association were not limited to the stratigraphic sequence. Markó (2013b) points out, that two bifacial tools listed by (Gábori-Csánk, 1993) were actually found at Dzeravá Skala and Kiskevély cave, respectively.

Therefore, a secure relationship between leaf-shaped lithics and osseous points cannot be established – or excluded – on the basis of the reportedly shared geological layer affiliation. While neither an 'occupational' nor 'observational' contemporaneity is verifiable or refutable in the near future, direct radiocarbon dating can offer the opportunity to further contextualise the osseous point industry.

Previous dating

In 2007 Davies and Hedges (2008) sampled two osseous points from Jankovich cave: Pb 569 and Pb 570. Both samples were pre-treated with solvent wash steps to remove conservation material, followed by the standard ORAU ultrafiltration protocol (AF). Unfortunately, they showed low collagen yield and high ultrafiltration background and could not be reliably dated (see tab. 11.11).

Table 11.11: Jankovich: pre-treatment results for the previously failed radiocarbon dating of osseous points by Davies and Hedges (2008) in 2007. Chemistry results obtained from the ORAU internal database.

Ref-no.	P-no.	Weight	Treat.	Yield	Comment
Pb 569	20529	248 mg	AF*	0.6 mg, 0.2 wt.%	high UF background
Pb 570	20530	201 mg	AF*	1.8 mg, 0.9 wt.%	high UF background

11.3.2 Radiocarbon Dating

The present dating project at Jankovich focuses on the timing of the osseous point industry, which was supposedly found in association with Jankovichian lithics. As a result, osseous points stored at the Hungarian National Museum in Budapest were sampled for %N and radiocarbon dating in April 2015.

Samples & Treatment

Access was granted to 6 osseous points (see tab. 11.12). They were sampled using the key-hole drilling technique to keep surface damage to a minimum. In all cases, the surface area at the sampling location was first abraded to minimise contamination. As the points showed clear signs of consolidation work, all samples were first treated with solvent wash steps: acetone (1h, 40°C), methanol (0.5h, RT), and chloroform (0.5h, RT). The samples were dried over night at RT, instead of the heating block, to avoid further damage to the collagen.

The two previously sampled points gave very good %N results, despite the fact that their collagen preservation is poor. This led to extra care during pre-treatment. After the initial AG* protocol, all samples were freeze dried. Further treatment was dependent on gelatine yield: >20 mg led to hydroxyproline dating, >10 mg to ultrafiltration, and < 10 mg to dating the AG* sample (see section 5.4).

Jank-01 mesial fragment of an antler point with flat-oval cross-section. Both the proximal and distal ends are missing. The former shows a wedge

Table 11.12: Jankovich: osseous points sampled for radiocarbon dating, with context information, %N test results and sample weight.

Ref-no.	Inv.-no.	Item	Excav.	Trench	Layer	%N	Weight	Cons.
Jank-01	Pb 570	point	1915	side chamber	lower AH	2.81	176 mg	Y
Jank-02	Pb 569	point	1915	side chamber	lower AH	2.05	397 mg	Y
Jank-03	Pb 572	point	1915	side chamber	lower AH	3.41	382 mg	Y
Jank-04	Pb 571	point	1915	side chamber	lower AH	0.11	467 mg	Y
Jank-05	Pb 568	point	1915	side chamber	lower AH	0.83	327 mg	Y
Jank-06	Pb 567	point	1915	side chamber	lower AH	1.82	328 mg	Y

shaped fracture, the latter a step fracture. The sides are convergent. The narrow edges in the distal part show longitudinal striations. On the dorsal side there are cuts and triangular shaped surface damage. On the ventral side, the spongiosa is visible, causing an uneven and rough surface structure. The museum number (Pb/570.) is written in black ink on the dorsal side of the meseo-distal part. In the meseo part of the ventral side, the previous radiocarbon sampling location from (Davies and Hedges, 2008) is visible. The area was reconstructed using epoxy resin and cosmetically adjusted with paint. The entire surface is coated in a conservation substance, leaving yellowish-grey stains on the spongiosa structure.

Jank-02 mesial fragment of an antler point with flat-oval cross section. Both proximal and distal ends are missing. The sides are convergent, though a shift of angle is visible in the mesial part. The entire surface of the artefact shows uneven colouration, with areas of light and dark creating a marble like pattern. On the ventral surface, the spongiosa is visible, leaving a rough and uneven surface. In the mesio-proximal section of the dorsal side, the museum number (Pb/569.) is written in blank ink. In the mesial part of the ventral section the previous radiocarbon sampling location was reconstructed with epoxy resin and cosmetically adjusted with paint. The entire artefact surface is shiny from a conservation coating. To avoid interference from the previous sample location, the point had to be sampled from the narrow edge towards the distal end, allowing access to only limited material.

Jank-03 small meseo-distal fragment of a point with oval cross-section. Both proximal and distal ends are missing. The sides are strongly convergent. Longitudinal striations are visible. Several deeper cuts traverse the surface at a near 45° angle in the proximal part. The museum number (Pb/572.) is written in black ink on the mesial part of the dorsal side. The entire artefact surface is covered in a conservation coating, applied after the number. The point was sampled using key-hole drilling, entering from fracture surface of the proximal end.

Jank-04 mesial fragment of an antler point with flat-oval cross-section (see fig. 11.31-b). Both proximal and distal ends are missing. The sides are strongly convergent. There are visible longitudinal traces of shaping, despite the severe surface damage. On the ventral side, the spongiosa is visible in areas where the smothered surface was abraded. The darkened surface might indicate heat treatment, but this is difficult to distinguish from the additional spots of black coating. The museum number (Pb/571.) is written in black ink on the proximal part of the dorsal surface. The point was sampled just above the proximal fracture, to have access to the widest and thickest section of the artefact.

Jank-05 meseo-distal fragment of an antler point with lunate-cross section (see fig. 11.31-c). The proximal end is missing. The damaged distal end still shows clear longitudinal manufacturing traces (Markó, 2013a, fig. 7.3). The point is preserved in two fragments, which were glued together at the refitted fracture line. The artefact is substantially wider compared to the thickness of the other sampled points, and reminds more of the general shape of a Mladeč style point. On the dorsal surface of the proximal fragment, the museum number (Pb/568.) is written in black ink. The entire artefact is coated with a consolidation material, apparently after the two fragments had already been glued. The radiocarbon sample was taken from the damaged, narrow edge of the distal fragment with sufficient distance from the glued fracture line.

Table 11.13: Jankovich: radiocarbon dating pretreatment results for osseous points. $^{\Delta}$ collagen yield given after AG* treatment, and value in grey represents carbon yield (μg) of hydroxyproline used for HPLC background correction. grey row – failed pretreatment, not dated.

Ref-no.	Item	Treat.	Yield (mg)	Yield (wt.%)	%C	δ^{15}N	δ^{13}C	C:N
Jank-01	point	AG*	1.17	0.67	40.7	3.3	-19.0	3.6
Jank-02	point	AG*	1.62	0.41	40.4	7.3	-20.4	3.3
Jank-03	point	NRC	24.45$^{\Delta}$ *0.8746*	6.40$^{\Delta}$	42.9	6.1	-26.5	4.9
Jank-04	point	AG*	0.00	0.00	–	–	–	–
Jank-05	point	AG*	0.55	0.17	31.7	2.8	-18.2	3.9
Jank-06	point	AG*	3.63	1.11	41.1	3.4	-18.2	3.3

Jank-06 mesial fragment of an antler point with flat-oval, near lenticular cross section. One of the ends has a pronounced step fracture, which might also be the result of a broken split-base. The sides are near parallel. Some cuts are visible on the dorsal surface, and the spongiosa appears on the ventral side. The fragment is dividable into two sides, one with a shiny coating (1/3), the other with a more powdery looking surface (2/3). The museum number (Pb/567.) is written in black ink onto the mesial part of the dorsal side, seemingly on top of the shiny surface observed in the lower third. It remains to be seen whether this difference in appearance is related to hafting, conditions in the burial environment, or later conservation work. The radiocarbon sample was taken from the narrow edge of the mesial part.

^{14}C Results

Five osseous points could be AMS radiocarbon dated, while one (Jank-04) dissolved completely during the acid/base washes (see tab. 11.13–11.14). Jank-03 showed great collagen preservation, allowing the sample to be hydroxyproline dated. The remainder resulted in the expected low collagen yields and had to be dated as AG* samples. Three of them (Jank-01, Jank-

Table 11.14: Jankovich: new AMS radiocarbon results for osseous points. Dates calibrated with OxCal 4.3 (Bronk Ramsey, 2009a) using IntCal13 (Reimer et al., 2013). In grey, original radiocarbon measurement before HPLC background correction (for details see 5.4.7).

Ref-no.	Lab-no	$F^{14}C$	^{14}C (BP)	Date (cal BP)
Jank-01	OxA-X-2716-49	0.01903 ± 0.00238	31800 ± 1000	38540–34070
Jank-02	OxA-X-2716-48	0.01755 ± 0.00185	32500 ± 800	38670–34930
Jank-03	OxA-X-2732-10	0.01695 ± 0.00141	32750 ± 670	38640–35420
		0.01838 ± 0.00124	*32100 ± 550*	
Jank-05	OxA-X-2731-11	0.02051 ± 0.00589	31200 ± 2300	42570–31250
Jank-06	OxA-35386	0.02162 ± 0.00128	30800 ± 500	35810–33910

02, and Jank-05) did not pass the standard threshold of yield > 1 wt.%. They were nonetheless measured, as even minimum age estimates can provide useful insights for these precious artefacts. In general, %N results were not a good indicator of preservation status, though the success rate still divides along the 0.7% threshold.

Jank-05 did poorly during pre-treatment. It gave lower carbon concentrations on combustion and a high C:N ratio. In addition, the graphite target only contained 0.2 mgC, and was measured on an AMS run with high background (>41800 BP). Consequently, the resulting radiocarbon date shows a large error and is with great certainty severely underestimating the true age of the sample.

While the other samples produced the expected concentrations of carbon upon combustion, Jank-01 had a slightly elevated C:N ratio of 3.4. The high value for Jank-03 is well within expectations for hydroxyproline. As hydroxyproline dating was not yet a standard ORAU pre-treatment, the HPLC background correction was applied manually (for the calculation see section 5.4.7) and the date was given an 'OxA-X' classification. However, the corrected age should be treated as a reliable radiocarbon measurement and can be used for any further analysis. In contrast, both Jank-01 and Jank-02 were given 'OxA-X' numbers as a result of their low collagen yields. They should be treated as minimum age estimates.

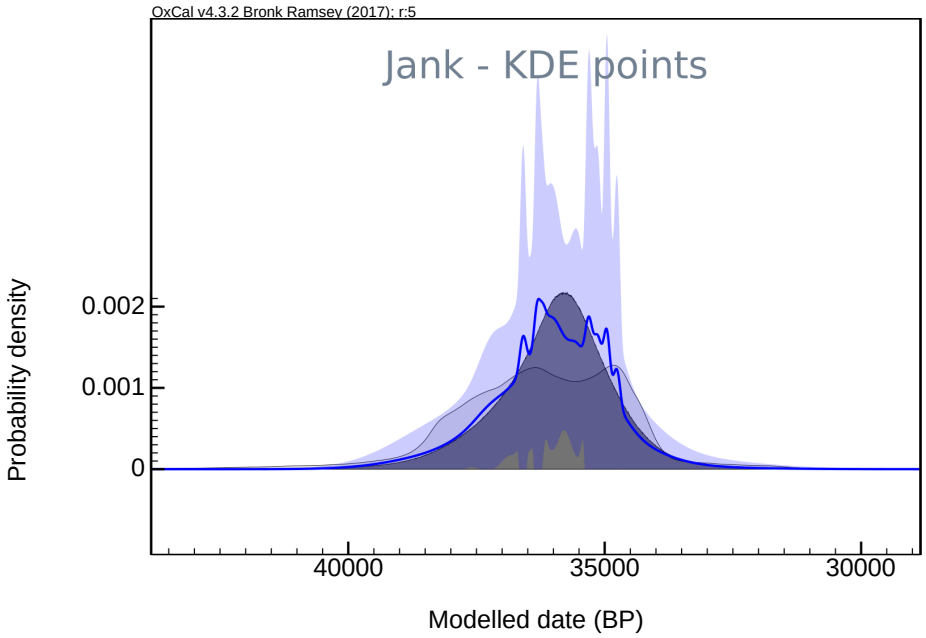


Figure 11.32: Jankovich: KDE model on osseous points (n=5, code: p. 722). It should be noted that sample size is very small and contains a high number of minimum age estimates, thus hiding any older events present in the sample set.

It can be concluded that Jank-03 provided the only reliable radiocarbon date for an osseous point from Jankovich. All other measurements are minimum age estimates only. However, it is expected that Jank-05 (OxA-X-2731-11) is the least reliable of them all, significantly underestimating the true age of the sample as a result of small collagen yield, high C:N ratio, and high AMS background.

11.3.3 Bayesian Modelling

Despite the high number of minimum age estimates, a summary of the radiocarbon dates on osseous points from Jankovich was attempted. All five dates were placed in a `KDE_Model` (code: p. 722). The result is the visualisation of a single osseous point event, assuming that the AG* dates only minimally underestimate the true age of the sample (see fig. 11.32). However, the sample size is small and highly problematic. Therefore, this event represents

the youngest possible age probability distribution for this particular set of osseous points from Jankovich cave.

11.3.4 Discussion

Thanks to the precautionary freeze-drying after AG* treatment (instead of directly proceeding to ultrafiltration), it was possible to get five osseous points radiocarbon dated (see fig. 11.33). The results place the artefacts well within the expected time frame of the 'Aurignacian'. However, OxA-X-2732-10 (Jank-03) is the only radiocarbon date that can be treated as reliable. While it corresponds well to most of the other dates, there is a reasonable probability that it represents the youngest dated point event at Jankovich. With these constraints in mind, the KDE model from Jankovich visualises the youngest possible osseous point manufacturing event given the minimum estimates obtained (see fig. 11.32).

Whether these points provide a chronologically or typologically consistent group is difficult to evaluate. The original description of having found the points at two different fireplace levels would suggest at least two independent events. Whether they separate into different categories of points as observed at Istállóskő remains unknown. While they differ in terms of convergence angle of their sides and cross-sections, the current typological definitions heavily rely on the shaping of the base. Consequently, mesial and distal fragments are hard to classify. Furthermore, the nearly rectangular cross-sections of some of the artefacts could be the hallmark of semi-finished products. If the forming of a split-base is the last step of the *chaîne operatoire* of SBP, then unfinished SBP would remain undiagnostic.

In regards to the contemporaneity of osseous point industries and the Jankovichian, the Jankovich cave will not be able to provide a definitive answer. However, if the dates obtained from Szeletian sites in Moravia are in any way indicative of the Szeletian/Jankovichian lithics observed here, an occupational association with osseous points becomes increasingly unlikely It would require an underestimation of at least 7000 years. At the same time,

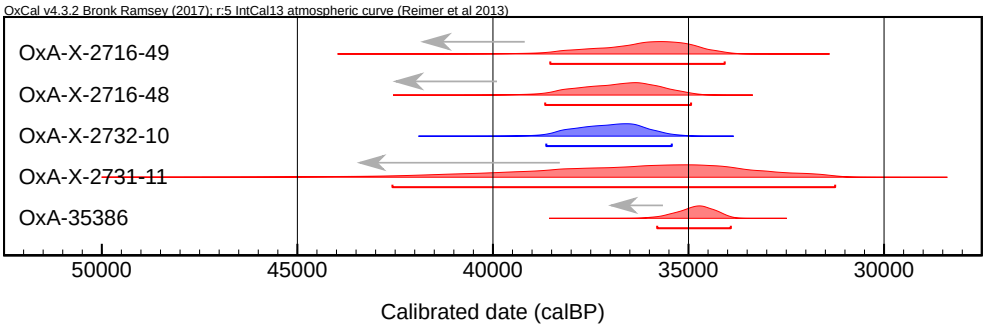


Figure 11.33: Jankovich: comparison of calibrated radiocarbon dates on osseous points. **blue** – reliable hydroxyproline date; **red** – AG* treated samples, minimum age estimates.

a secure attribution to the Aurignacian lithic technocomplex can – in the absence of diagnostic Aurignacian lithics – not be supported. A treatment of osseous industries independent of the lithics has become increasingly important (for further discussion of directly dated osseous points see chapter 14).

11.4 Máriaremete (Remete Felső)

The cave site of Máriaremete contained a single small Szeletian/Jankovichian industry in association with human remains. Both were believed to have come from the same single, brief occupation, which was excavated *in situ*. If this assumption is correct, radiocarbon dating of anthropogenically modified faunal remains from the same horizon should provide a narrow enough time window to obtain a date for the Jankovichian industry. As the lithics were deemed identical to those found at Jankovich, the age obtained at Máriaremete could then be directly compared to the osseous point industry there, which previously was seen as observationally contemporaneous (see section 11.3).

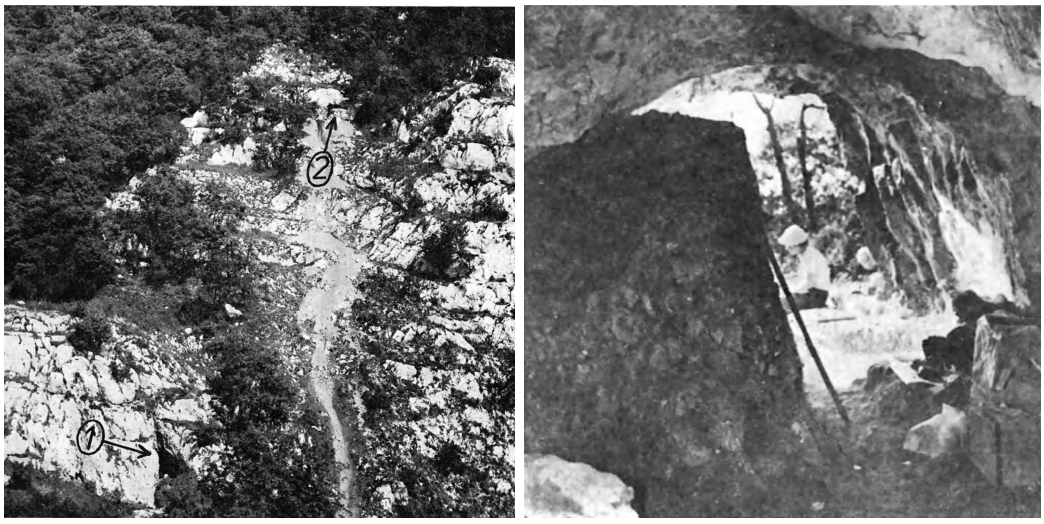


Figure 11.34: Máriaremete: left – location of Remete Felső cave (2), i.e. 'Upper Recluse', in regards to Remete cave (1); right – view from cave interior with profile on the left side (Gábori, 1977, p. 45–46).

11.4.1 Introduction

Máriaremete cave (47.559 N, 18.945 E) is located in the north-western part of the Buda Mountains and named after the small city in its vicinity (Tillier et al., 2006). The cave entrance opens toward the south-west, at an altitude of 350 m a.s.l. and 70 m above the valley floor (see fig. 11.34). Before excavations began, its entrance was only 69 cm high and 2.4 m wide, which probably prevented earlier discovery. Further down the steep cliff, the Remete cave has been known for a long time. Upon discovery of the new cave, it was originally name Remete Felső, as it was located above the known cave site, under which it can still sometimes be found today (Gábori-Csánk, 1993).

The cave consists of two main parts: a moderate gallery (the 'small hall'), followed by a narrow passage leading to the 'large hall' (see fig. 11.35). After excavations, the first hall was 6.5 m long, and 4.2 m wide, while the second hall measured 11 m in length (including the passage way) and 4.5 m in width, with a higher ceiling. To the eastern side of the large hall there is a chimney.

The cave site was excavated in 1969 and 1970 by V. Gábori-Csánk (1993). She divided the cave into two longitudinal sections with the intent to excavate

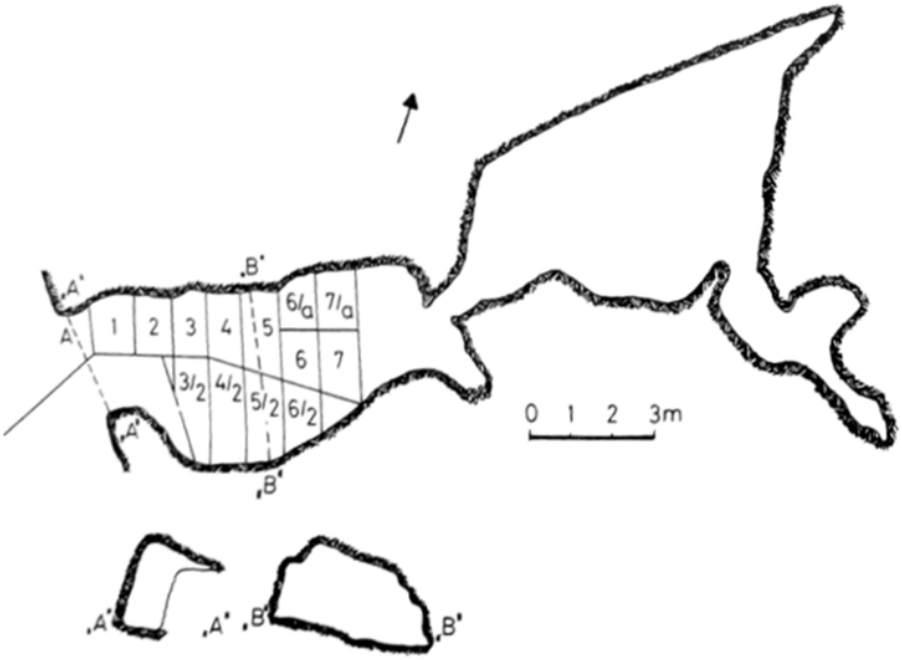


Figure 11.35: Máriaremete: map with with cross-section and excavation squares (Gábori-Csánk, 1993, fig. 12).

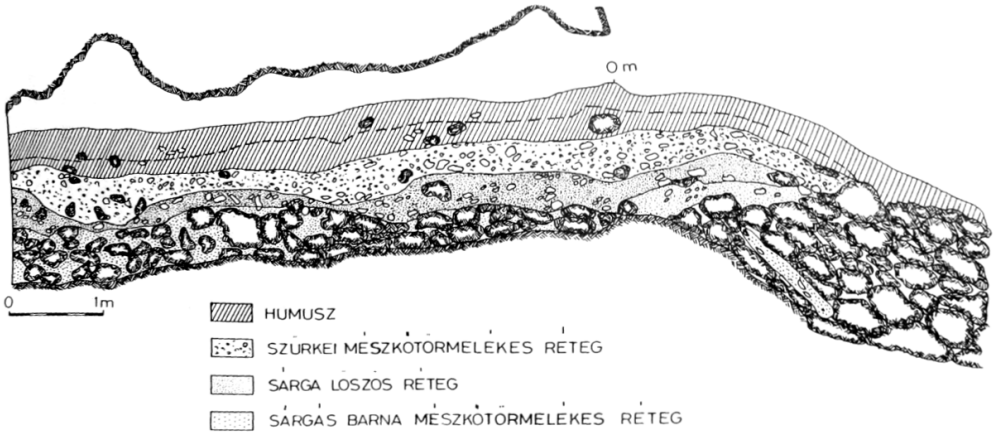


Figure 11.36: Máriaremete: longitudinal profile (north-west-facing) from the front hall (Gábori-Csánk, 1993, fig. 13). Legend reads (top to bottom): humus; grey layer with limestone debris; yellow loess layer; yellowish-brown layer with limestone debris.

one half and leaving the other for later analysis and control. In the 'small hall', she dug a trench on the north-western cave side. The trench was 3.4 m long, 1.1 m wide and 1.2 m deep (down to the bedrock) and described the following stratigraphy (see also fig. 11.36):

1. black humus (Holocene)
2. brown humus (Holocene)
3. **grey** layer with limestone debris with sharp edges (Holocene/Pleistocene)
4. **yellow** layer, loess, with limestone debris (Pleistocene)
5. **yellowish-brown** layer with collapsed limestone blocks (Pleistocene)
6. bedrock

The Pleistocene sequence started with layer 3, which contained a mixture of more recent bone fragments with faunal remains commonly observed from the Pleistocene. The presence of cryoturbation led Gábori-Csánk (1993) to place the formation during a glacial period. Layer 4, in turn, had very distinct layer limits and a homogeneous appearance, and was therefore believed to have accumulated in a brief period of time and found *in situ*. In the lower part there were sporadic concentrations of charcoal. More importantly, the top part produced some lithics and human remains, and was subsequently identified as the only Pleistocene archaeological horizon within the cave. Layer 5 was dominated by calcareous blocks, which had detached from the cave ceiling, and manganese accumulation in the lower part. Again, the sedimentation seems to represent a cold period.

The archaeological remains were scarce and concentrated in the squares 2/3 and 5/6. They totalled 9 lithic tools and 3 flakes, including a coarse biface with plano-convex section, a partial biface, a bifacial scraper, a small unfinished bifacial tool and fragments of Mousterian scrapers. Already upon excavation, Gábori-Csánk (1993) saw the assemblage as identical to that found at Jankovich cave. Whether to call them Szeletian or Jankovichian

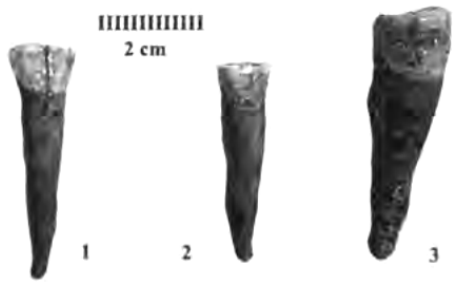


Figure 11.37: Máriaremete: human remains. Right mandibular incisors (I1, I2) and canine (C), showing substantial wear, all from an adult individual (Tillier et al., 2006, fig. 16).

subsequently depended on which cultural reference frame was used. The assemblage is briefly mentioned in Allsworth-Jones (1986). Despite the book's title 'The Szeletian', the lithics were already listed under the subcategory of the 'Jankovichian'. Gábori (1977) interpreted the composition of the assemblage – containing very few implements – as the result of a brief hunting visit.

Human Remains

The assemblage was used to postulate a Neanderthal authorship for the Jankovichian (Gábori-Csánk and Svoboda, 1983), based on the three human teeth found in squares 5/6. Gábori-Csánk (1993) saw them as directly associated with the lithics – including those from square 2/3.

The right mandibular incisors and canine were heavily worn and might have belonged to the same adult individual (see fig. 11.37). Kretzoi saw that individual as a *Homo neanderthalensis* (Gábori-Csánk, 1993). However, Tillier et al. (2006) pointed out that none of the teeth showed any metric or morphological features that would allow a distinction between Neanderthals and UP AMHs.

Consequently, only ZooMS or aDNA analysis would be able to provide a more definitive answer. In light of the few lithic remains, the robustness of

the association might also requires some further testing. Regrettably, access for dating and DNA sampling was not granted.

11.4.2 Radiocarbon Dating

According to the description and analysis provided by Gábori-Csánk (1993), the human activity found within the upper part of the yellow loess layer should belong to a single visit – or an observationally contemporaneous visit – and thus identifiable via radiocarbon dating. Further, if Gábori's (1977) interpretation of a hunting station is correct, the lithics and human remains should be associated with faunal remains showing anthropogenic modifications. As a result, the present project at Máriaremete attempted to constrain the age of the occupation by dating human activity within the same level and squares.

Samples & Treatment

In September 2015, all the faunal remains from the yellow layer in squares 2/3 and 5/6, and stored at the Geological Institute in Budapest, were searched for anthropogenic modifications. In the material a human vertebra was discovered and selected for dating. In addition, 8 modified faunal remains were sampled (see tab. 11.15). Considering the limited lithic remains, the small number of samples was expected.

From the selected material, only one (MR-02) failed the %N test. From the remaining, MR-03 showed signs of possible conservation work, and was first treated with solvents: acetone (1h, 40°C), methanol (0.5h, RT), chloroform (0.5h, RT). Afterwards, all samples with expected collagen preservation were treated with the gelatine protocol (AG), and then ultrafiltered (AF) if their yields were $>$ 10 mg (see section 5.4).

Table 11.15: Máriaremete: radiocarbon samples with context information, %N results and weight pre-treated for dating. *sárga agyag* – 'yellow clay', refers to the yellow loess, layer 4. grey row – not dated because of low %N.

Ref-no.	Inv.-no.	Item	Excav.	Sq.	Layer	Depth	%N	Weight	Cons.
MR-01	–	human	1969	6a	*sárga agyag*	100 cm	2.87	433 mg	N
MR-02	–	fauna	1969	7a	*sárga agyag*	120 cm	0.06	–	N
MR-03	–	fauna	1969	3	*sárga agyag*	80–100 cm	1.26	942 mg	?
MR-04	–	fauna	1969	3	*sárga agyag*	80–100 cm	1.80	593 mg	N
MR-05	–	fauna	1969	2–3	*sárga agyag*	120 cm	1.22	742 mg	N
MR-06	–	fauna	1969	2–3	*sárga agyag*	120 cm	2.43	623 mg	N
MR-07	–	fauna	1969	2–3	*sárga agyag*	120 cm	0.78	824 mg	N
MR-08	–	fauna	1969	6a	*sárga agyag*	100 cm	1.58	824 mg	N
MR-10	–	fauna	1969	6	*sárga agyag*	100 cm	2.33	935 mg	N

^{14}C Results

All but one sample could be radiocarbon dated (see tab. 11.16–11.17). MR-04 yielded some collagen, yet insufficient for dating. Most other samples showed good pre-treatment results, with %C on combustion and C:N ratio within expectations. The low C:N ratio for MR-07 and MR-06 was as a result of nitrogen calibration issues on burn no. 4051. The background sample results demonstrate that this has not affected the quality of the radiocarbon date (see Appendix). MR-07 had sufficient collagen yield for preparing a second target to test the dating reliability. Unfortunately, the original target failed graphitisation (mechanical error), thus a direct comparison was not possible in this case.

The only problematic date was MR-06. First, it had low collagen yield and could not be ultrafiltered like the other samples. It then showed lower %C on combustion as well as a slightly elevated C:N ratio. And finally, the small graphite target was measured on the AMS run no. 2731, which had an elevated background of >41800 BP – compared to the > 48000 BP to 50300 BP usually observed during this project. Consequently, the date of 34000 ± 1300 (OxA-X-2731-13) is significantly underestimating the true age of the sample. The dating quality is reflected in the 'OxA-X' prefix. In contrast, the 'OxA-X' attribution for MR-03 was given as a result of the low C:N

Table 11.16: Máriaremete: radiocarbon pre-treatment results for anthropogenically modified bone and a human vertebra. grey row – not dated because of low pre-treatment yield (MR-4) and mechanical error during graphitisation (MR-07.1).

Ref-no.	Item	Treat.	Yield (mg)	Yield (%)	%C	δ^{15}N	δ^{13}C	C:N
MR-01	human	AF	27.83	6.43	43.6	12.7	-19.6	3.2
MR-03	fauna	AF*	37.57	3.99	41.5	3.3	-19.8	2.9
MR-04	fauna	AG	0.82	0.14	–	–	–	–
MR-05	fauna	AF	37.16	5.00	40.9	-2.5	-20.9	3.2
MR-06	fauna	AG	1.74	0.28	31.7	4.5	-19.4	3.4
MR-07 (1)	fauna	AF	63.58	7.29	40.4	4.3	-18.1	2.9
MR-07 (2)	fauna	AF	63.58	7.29	42.8	4.0	-19.1	3.2
MR-08	fauna	AF	8.51	1.03	42.0	6.1	-20.1	3.2
MR-10	fauna	AF	83.30	8.91	41.7	3.3	-18.5	3.2

ratio observed, prior to testing showing that this has not affected the dating outcome.

To conclude, 5 out of 6 radiocarbon dates from Máriaremete seem reliable based on the radiocarbon pre-treatment results, with MR-06 providing a minimum age estimate only.

11.4.3 Discussion

The age variation observed on samples from the yellow loess layer are significant (see fig. 11.38). The human vertebra dates as young as 8145 ± 45 BP (OxA-33849), while the date on the anthropogenically modified bone MR-08 (44900 ± 2300 BP, OxA-34029) exceeds the range of the calibration curve. There are several possible explanations for such an unexpected spread: no single occupation, difficulties distinguishing layer boundaries, missed post-depositional processes, mislabelling or misplacing of artefacts, or coarse excavation methods.

According to (Gábori-Csánk, 1993), the limits of layer 4, the yellow loess, were very distinct, and while layers 3 and 5 were affected by post-depositional

Table 11.17: Máriaremete: new AMS radiocarbon results on human remains and anthropogenically modified fauna. Dates calibrated in OxCal 4.3 (Bronk Ramsey, 2009a) using IntCal 13 Reimer et al. (2013).

Ref-no.	Lab-no	$F^{14}C$	^{14}C (BP)	Date (cal BP)
MR-01	OxA-33849	0.36287 ± 0.00187	8145 ± 40	9250–9000
MR-03	OxA-X-2719-19	0.08664 ± 0.00117	19650 ± 110	24000–23360
MR-05	OxA-35660	0.09606 ± 0.00121	18820 ± 100	22950–22440
MR-06	OxA-X-2731-13	0.01460 ± 0.00245	34000 ± 1300	41540–35750
MR-07 (2)	OxA-35698	0.0103 ± 0.00099	36750 ± 750	42510–39920
MR-08	OxA-34029	0.00375 ± 0.00106	44900 ± 2300	>45290
MR-10	OxA-34030	0.00761 ± 0.00103	39200 ± 1100	45280–41700

processes, she believed layer 4 to have been *in situ*. Without visual and physical confirmation, this is difficult to verify. The profile drawings appear suspiciously 'clean' – even for layer 3, which should show signs of cryoturbation.

Without access to the original excavation documentation, the labelling of the artefacts cannot be double-checked. However, even considering the three youngest samples as intrusive or mislabelled would not leave the remaining ages as a single chronological group. Suggesting that all but one sample was misplaced seems rather far-fetched.

It appears, therefore, that layer 4 contained more than one chronologically distinguishable human occupation. Moreover, the young dates for MR-03, MR-06, and – most importantly – the human vertebra MR-01 indicate that there is sufficient variability to argue that an association of the human remains with the Jankovichian lithics is by no means secure. Even if it is assumed that the teeth belonged to an individual alive during the MP/UP transition, and MR-06 would in reality be as old as MR-08, there are still two possible occupation windows available. One of them aligns with late Neanderthal finds and Szeletian material found in Moravia. The other coincides with SBPs at Istállóskő and the Early Aurignacian at Geißenklösterle.

It is likely that the lithics found in the top part of layer 4 predate 40k cal BP. However, it remains unclear whether they do belong to a single

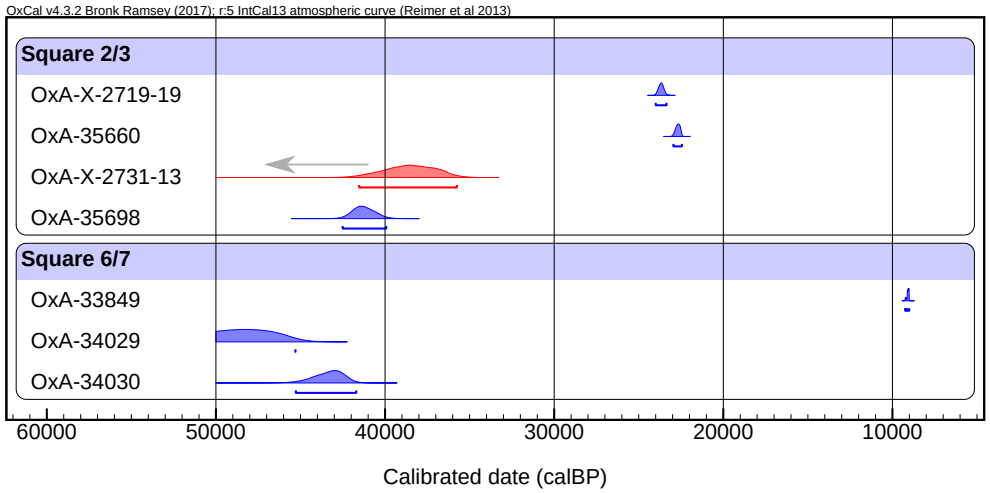


Figure 11.38: Máriaremete: comparison of calibrated radiocarbon dates from human remains (OxA-33849) and anthropogenically modified fauna found in squares 2/3 and 5/6. **red** – minimum age estimate; **blue** – reliable ^{14}C measurements.

occupation, and their actual connection to the human teeth from square 6/7 remains unknown. Only direct dating and detailed aDNA analysis could partially resolve the issue.

11.5 Szeleta

Szeleta (see fig. 11.39) is the eponymous site for the Szeletian lithic industry, though its assemblage now only has limited resemblance to the technocomplex defined by Prošek (1953) and presently found within Moravia (Markó, 2009). The site contained two main archaeological horizons, referred to as the 'Early Szeletian' and the 'Developed Szeletian'. As with Máriaremete and Jankovich, an observational contemporaneity between the Szeletian lithics and the 'Aurignacian' split-based points was postulated. Direct dating of SBP at the site enables contextualisation of this diagnostic industry irrespective of the questions regarding layer integrity.



Figure 11.39: Szeleta: view from interior (http://static.panoramio.com/photos/large/17322214.jpg, accessed 2018-06-02).

11.5.1 Introduction

Szeleta cave (N 48°06' 30", E 20°37' 54") is located within the municipality of Hámor in the Bükk Mountains. Its entrance is situated at an altitude of 347 m a.s.l., opening towards the south. In front of the cave, there is a large terrace. The cave consists of two galleries (see fig. 11.40), which extend westwards and north-westwards from the entrance hall. The main gallery is 24 m long, with an average width of 7 m and average hight of 8 m, before opening towards a rear hall of 16 m length, 12 m width, and 7 m height. At the rear of the cave, a side niche, only 0.5 m high, containing flowstones was discovered during excavations. The side gallery measures 12 m in length, 10 m width and 7 m height – narrowing towards the back (Kadić, 1916).

The main archaeological excavations were led by Kadić and Hillebrand, and took place 1906–1913 (Kadić, 1916). They discovered 7 layers. Of those,

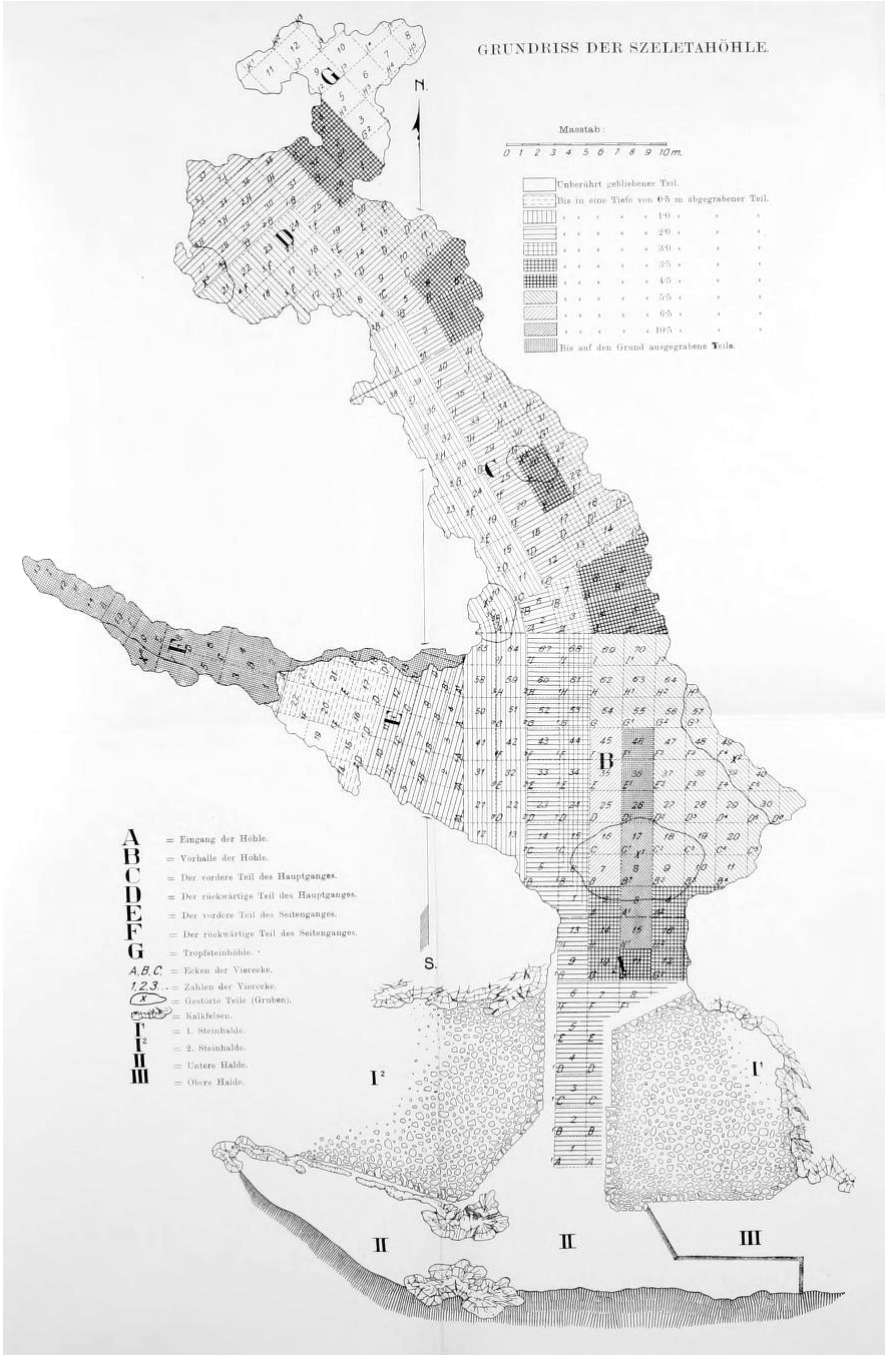


Figure 11.40: Szeleta: map with area labels and excavation trenches showing that most of the cave has been emptied during investigation (Kadić, 1916, Tafel XIII). Legend: A = cave entrance, B = front hall, C = front section of main gallery, D = rear section of main gallery, E = front section of side gallery, F = rear section of side gallery, G = flowstone cave, x = location of pits.

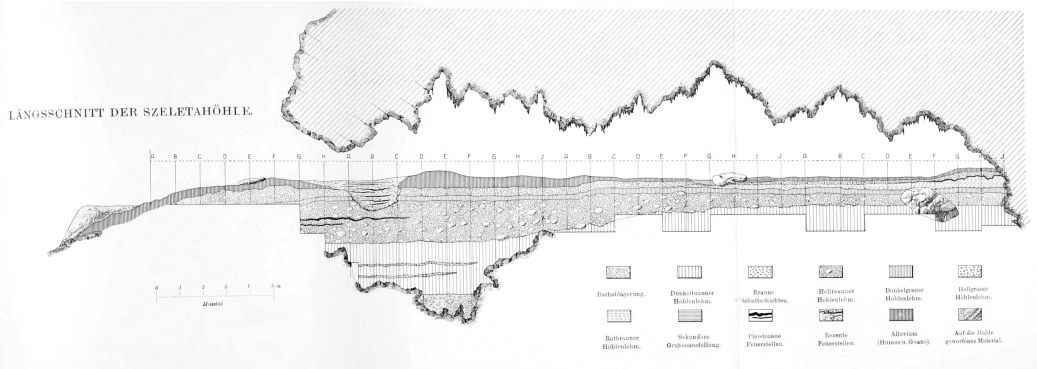


Figure 11.41: Szeleta: longitudinal section through the main gallery with profile drawing (Kadić, 1916, Tafel XIV).

numbers 2–6 were of Pleistocene origin, and the lowest (no. 1) appeared sterile (see fig. 11.42):

1. creek deposit (sterile layer)
2. **dark brown** cave loam
3. **light brown** cave loam
4. **dark grey** cave loam
5. **reddish-brown** cave loam
6. **light grey** cave loam
7. **humus** layer (Holocene)

The Palaeolithic archaeological material was concentrated in layers 3 and 6 at the entrance of the cave and the front hall. Both assemblages were dominated by leaf-points. As the artefacts from the lower level appeared to be coarsely worked and asymmetric, Kadić (1916) classified them as 'Solutréen' (now labelled 'Early Szeletian'). The ones from the upper horizon, he classified as 'Hochsolutréen' (now 'Developed Szeletian') on the basis of their symmetric, finely worked, and thin appearance. Layer 5 was only found in the rear of the main hall, but also contained very finely worked leaf points.

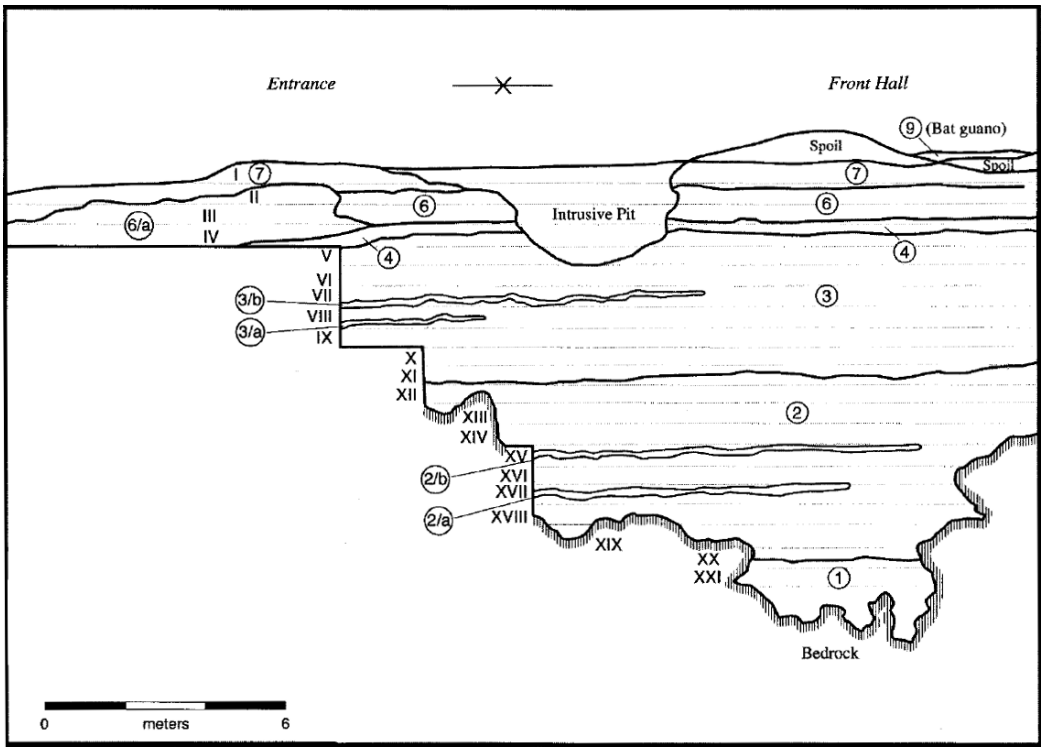


Figure 11.42: Szeleta: profile drawing from the entrance and front hall of the cave (Adams and Ringer, 2004, fig. 2). For layer description see text; 3a/3b denote charcoal horizons (*i.e.* hearths) within layer 3.

In contrast, layer 2 only held 27 non-diagnostic lithics, believed to belong to the Middle Palaeolithic (Adams and Ringer, 2004). In total, Kadić (1916) excavated 1603 artefacts.

Smaller excavations followed as a result of the significant interest the Szeletian industry attracted. Mottl (1945) excavated in 1936, and Vértes returned in the 1950s and 1960s (Vértes, 1959b, 1968), and Adams (2001) in 1999, though the archaeological material remained few. However, it was in 1928 that the first 'Aurignacian' SBP was found by Hillebrand and Parrington (University of Cambridge) (Markó, 2013a). It was subsequently published with two points found in 1947 by Saád (Saád and Nemeskéri, 1955, see also fig. 11.43), one of which was reclassified as an unmodified bone fragment, only shaped by post-depositional processes (Markó, 2013a).

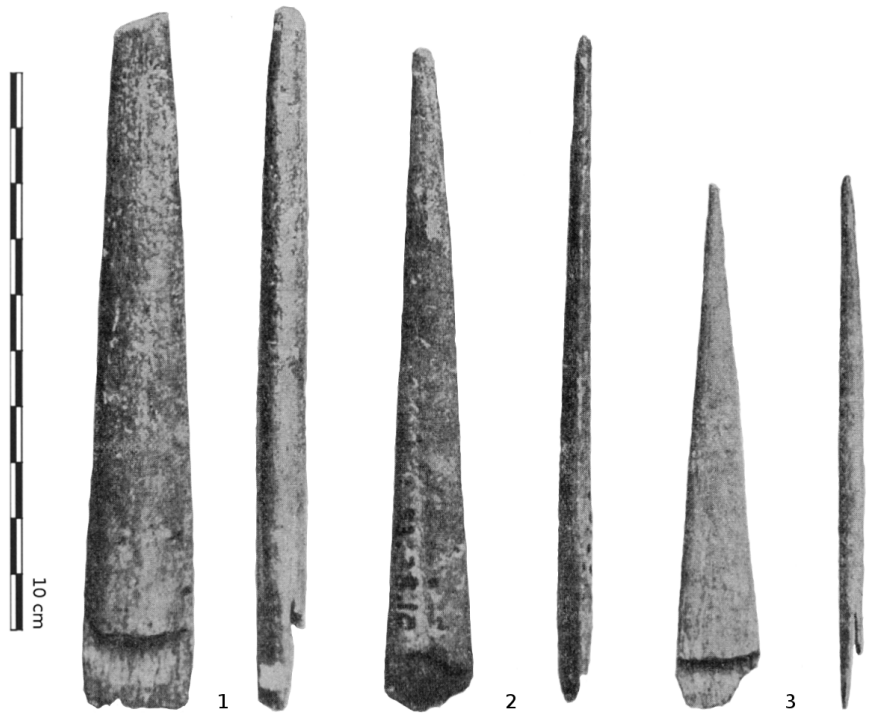


Figure 11.43: Szeleta: split-based bone points published by Saád and Nemeskéri (1955, pl. II; scale added). No. 1 – SBP, No. 2 – rolled bone fragment, No. 3 – SBP.

The artefact Pb 47/928.8 was discovered in the front section of the cave (entrance to the side gallery), at a depth corresponding to the archaeological levels IV–VII (see fig. 11.42) – which encompasses both layers 3 and 6. In Davies and Hedges (2008) the artefact is listed as belonging to layer 6/7. Either way, it was associated with leaf-shaped stone implements. No diagnostic Aurignacian lithics were found in any of the layers (Allsworth-Jones, 1986).

Previous Dating

On three separate occasions, dating of the Szeletian layers had been attempted. The results were published in Adams and Ringer (2004); Davies and Hedges (2008); Vogel and Waterbolk (1972); Vértes (1968), and are summarised in table 11.18.

Table 11.18: Szeleta: previously published radiocarbon dates on unmodified faunal fragments and charcoals with context and pretreatment information (Adams and Ringer, 2004; Davies and Hedges, 2008; Vogel and Waterbolk, 1972; Vértes, 1968). Cultures: MP – layer 2; 'Early Szeletian' – layer 3; 'Developed Szeletian' – layer 6. P-20840 showed only <0.7%N, not processed. Calibrated age calculated in OxCal 4.3 (Bronk Ramsey, 2009a) using IntCal13 (Reimer et al., 2013), and given at 95.4% confidence interval. grey rows – unsuitable for modelling.

Lab-no.	Item	Layer	Depth (m)	Treat.	Yield	^{14}C (BP)	Date (cal BP)
GX0-197	charcoal	3	–	?	–	> 41000	–
GrN-5130	bone	6	3	acid	1.1 %C	32620 ± 400	38020–35720
GrN-6058	bone	2	6	acid	1.0 %C	43000 ± 1100	49080–44550
ISGS-4460	bone	3	2.5-2.6	ABA	–	> 25200	–
ISGS-4464	bone	2/3	–	ABA	–	42960 ± 860	48400–44780
ISGS-A-0128	bone	3 (hearth)	–	ABA	–	11761 ± 62	13740–13460
ISGS-A-0129	bone	3 (hearth)	–	ABA	–	13885 ± 71	17090–16520
ISGS-A-0131	bone	6	0.8-0.9	ABA	–	22107 ± 130	26690–26000
ISGS-A-0189	charcoal	3	2.7-2.8	ABA	–	26002 ± 182	30760–29700
P-20840	bone	3/4 hearth	–	none	–	–	–
P-20841	charcoal	3/4	–	ZR	0.3mg, 1.1 wt.%	–	–
P-20523	SBP Pb.47/928.8	6/7	–	AF*	1.5mg, 0.5 wt.%	–	–

Already in the 1960s, Vértes collected samples for radiocarbon dating, resulting in 3 radiocarbon measurements (Vogel and Waterbolk, 1972; Vértes, 1968). GXO-197 was obtained on charcoal, which was found between layer 2 and layer 6 – presumably referring to layer 3. No further pretreatment or measurement information is available. GrN-5130 and GrN-6058 were both bone samples. They were treated with acid and the collagen extracted for radiocarbon dating.

In 1999, further small excavations were conducted at Szeleta cave with the intent to obtain radiocarbon samples (Adams, 2001). The samples were pretreated at the Illinois State Geological Survey using acid-base-acid washes. Two of the bone collagen samples (ISGS-4460 and ISGS-4464) were dated

using conventional methods. The other 3 bone and 1 charcoal samples were AMS dated at the Lawrence Livermore National Laboratories, USA.

Finally, in 2007, Davies and Hedges (2008) attempted to date the 'Early Szeletian' horizon as well as one of the diagnostic SBPs. Regrettably, the dating remained unsuccessful as a consequence of low collagen preservation.

None of the bone dates are directly connected to human activity at the site, as they were obtained on unmodified faunal fragments. Only the charcoal date GXO-197 may be connected to a human fire – though the limited information merely indicates that the layer might be beyond radiocarbon dating. The chronological distribution of the dataset illustrates the stratigraphic complexity, and cannot provide a secure age for any of the industries found.

11.5.2 Radiocarbon Dating

The present radiocarbon dating project at Szeleta focused on the split-based point found in 1928, to better understand the temporal distribution of SBP in the Bükk Mountains, and the wider 'transitional' and 'Aurignacian' context.

Sample & Treatment

The split-based point Pb 47/928.8 from Szeleta was sampled in April 2015 (see tab. 11.19). To avoid contamination from the previous sample location, key-hole drilling was applied to the narrow edge towards the distal end of the artefact. To remove any remaining contamination from a possible surface coating, the sample was first treated with solvent wash steps: acetone (1h, 40°), methanol (0.5h, RT), chloroform (0.5h, RT). Drying occurred over night at RT to not further damage the collagen through heating. Subsequently, the sample was treated with the less aggressive gelatine protocol (see section 5.4.5), as collagen preservation has previously been shown to be poor.

Table 11.19: Szeleta: split-based points sampled for radiocarbon dating with context information, %N results and sample weight.

Ref-no.	Inv.-no.	Item	Excav.	Trench	Sq.	Layer	Depth	%N	Weight	Cons.
Szel-01	47/928.8	SBP	1928	E	7	3/6	2–3 m	2.87	374 mg	Y

Szel-01 meseo-proximal fragment of a split-based point made from antler. The proximal end of the artefact was damaged between 1935 and 1951 (Markó, 2013a). One of the wings of the split-base has broken off, the other has a damaged proximal section. The distal end, *i.e.* the point, is missing. The surface shows transversal scraping and longitudinal and convergent shaping. The cross-section is plano-convex in the proximal and mesial part, and flat-oval in the distal part.

^{14}C Results

As expected, collagen preservation was too poor for ultrafiltration (see tab. 11.20). Nonetheless, there was sufficient AG* sample for dating (see tab. 11.21). %C on combustion, stable isotopes and C:N detect no anomalies. As a consequence, the radiocarbon date appears to be reliable, although slight underestimation of the true age of the sample cannot be excluded.

Table 11.20: Szeleta: radiocarbon pre-treatment results for the split-based point.

Ref-no.	Item	Treat.	Yield	%C	δ^{15}N	δ^{13}C	C:N
Szel-01	SBP	AG*	7.73 mg, 2.07 wt.%	42.0	3.4	-19.5	3.2

Table 11.21: Szeleta: new AMS radiocarbon result on split-based point. Date calibrated with OxCal 4.3 (Bronk Ramsey, 2009a) using IntCal13 (Reimer et al., 2013).

Ref-no.	Lab-no	F^{14}C	^{14}C (BP)	Date (cal BP)
Szel-01	OxA-35416	0.01658 ± 0.00117	32950 ± 550	38560–35890

11.5.3 Discussion

The split-based antler point from Szeleta fits well within the time frame of the 'Aurignacian' osseous point industry. Despite the AG* treatment, all quality control measures indicate that the date is reliable, though an older age cannot be excluded. The currently available radiocarbon age appears to place the point contemporaneous with MBPs from Istállóskő, and post-dating the main occurrence of SBPs there.

Comparing the radiocarbon dates currently available from Szeleta cave, some interesting preliminary observations are possible (see fig. 11.44). First, the large spread of dates causes the various stratigraphic units to overlap chronologically, and suggests that layer association remains problematic. The present dataset is unable to clarify whether this is caused by post-depositional processes (*e.g.* erosion, mixing), stratigraphic interpretations, or radiocarbon dating. It is worth noting, that all of the very young ages in layers 3 and 6 were obtained during excavations that took place nearly a century after the original work by Kadić (1916), and had to be restricted to the few not fully excavated areas of the cave. During the time separating those two investigations, the cave had been open to tourists (Adams and Ringer, 2004), and it is possible that further disturbances occurred. Furthermore, one should not underestimate the challenges involved when following previously established stratigraphies during new excavations with entirely new personnel.

Second, assuming that the three archaeological horizons are indeed self-contained activities in stratigraphic sequence, some age estimates can be proposed: *ca.* 50-45k cal BP for layer 2, *ca.* 45-40k cal BP for layer 3, and *ca.* 40-35k cal BP for layer 6. Bearing in mind that most dates are expected to underestimate the true age of the samples, this chronological grouping might move to older ages with more intensive investigation.

Third, the relationship and meaning of the leaf-shaped lithics found at Szeleta remain ambiguous. If they were indeed originally associated with layer 6, an observed contemporaneity with SBPs cannot be excluded. However, the lithics could equally well have originated in layer 5. As this unit

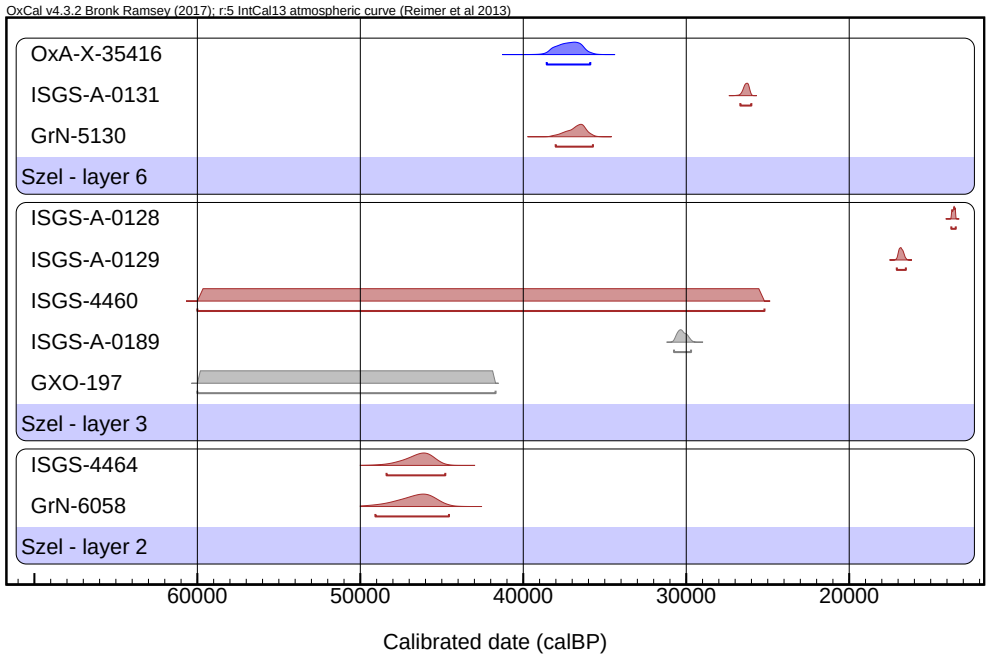


Figure 11.44: Szeleta: calibrated radiocarbon dates grouped according to layer attribution. Samples: **grey** – charcoal, **brown** – unmodified bone, **blue** – SBP. All dates likely to underestimate the true age of the samples.

was observed further into the cave, the material may have been washed down the main gallery, or remained in its original location at the front of the cave while the sediment it was associated with eroded. Alternatively, a connection to the leaf-shaped lithics found with Gravettian material at other eastern European sites may be worth investigating.

After all these years of archaeological investigation, Szeleta cave still has the potential to contribute to the discussion of the MP/UP biocultural shift. However, going forward it requires strategic dating of a significant number of anthropogenically modified faunal fragments from throughout the sequence excavated by Kadić and Hillebrand. It is assumed that a restriction to directly dating human activity may resolve some of the noise presently caused by unmodified samples.

11.6 Peskő

Peskő cave is well know for its osseous point industry, but has yielded few lithics. Previous investigations provided some of the oldest direct dates for 'Aurignacian' points – not only for the region, but for the industry as a whole. Considering the good preservation of the artefacts found at the site, it offers a unique opportunity to test the quality of the radiocarbon dating.

11.6.1 Introduction

Peskő cave[12] (N 48°02' 53", E 20°25' 25") is located within the municipal limits of the village Felsőtárkány, in the Peskő Mountains, which are part of the Bükk Mountains. The cave consists of a main corridor extending for 32 m in south-west to north-east direction (see fig. 11.46), a large side chamber (E) and two chimneys (F1 and F2). The main corridor was divided into a front (B), middle (C) and rear (D) section. The entrance faces south-west, and exits the cliff at an altitude of 745 m a.s.l. The cave has a maximum height of 10 m and a maximum width of 15 m, both dimensions narrowing towards the rear (Kadić and Mottl, 1944).

Research History

Most of the sediment at Peskő has been excavated. Work started in 1912, when J. Hillebrand (1913c) investigated two test trenches (sectors I and II in fig. 11.46). The subsequent year, Éhik (1914) opened up a larger area in parts of the front and middle sections of the cave (sector III). After WWI, Kadić returned to excavate the site in 1934, 1939 and 1940 (Kadić, 1935, 1940, 1941). Together, they removed sediment on a total surface area of 200 m^2 down to the bedrock, *i.e.* to around 2.5 m depth, while only finding 14 lithics and some large osseous tools.

[12]Not to be confused with the nearby archaeological site Peskő rockshelter.

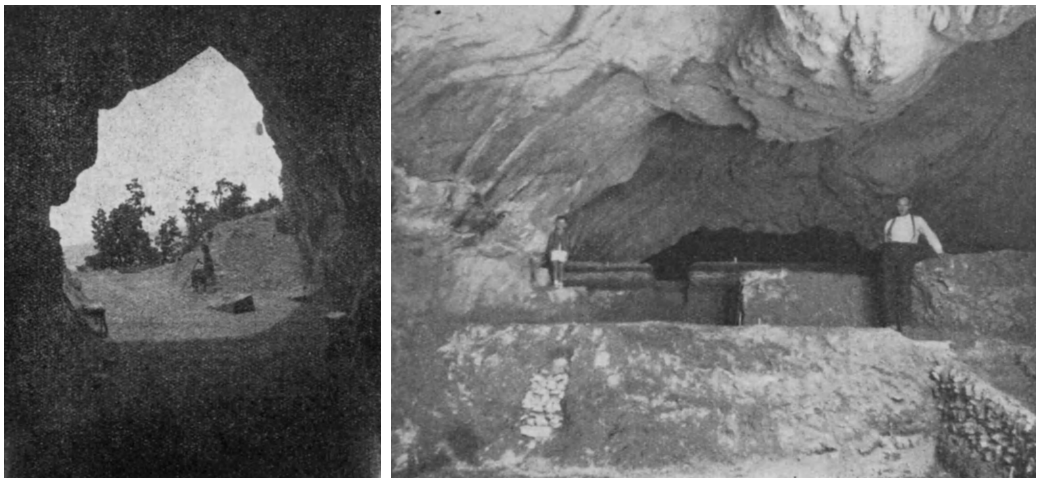


Figure 11.45: Peskő: view from inside the cave (left) and photo of excavation trenches and profiles (right) during Kadić's excavations (Kadić and Mottl, 1944, fig. 3–4).

However, what made the cave site special, was not the vast collection of archaeological artefacts from intensive Palaeolithic occupation. It was the collection of osseous spear points, published in more detail by Gábori (1951). They led the researchers to conclude that the site contained Aurignacian occupation.

In 1955, Vértes placed another test trench of ca. 2.5m^2 area at the rear of the cave, east to the coordinate number 18 (see fig. 11.46). As before, the excavation did not stop until the bedrock was reached. This time, though, 13 lithics and 2 further osseous tools were found (Vértes et al., 1956). The discrepancy in artefact numbers suggests that either previous excavations missed the place of habitation (despite their extensive nature), or their excavation methods had been too crude to properly capture it.

Stratigraphy

The most extensive description of the uncovered sediment sequence was provided by Kadić and Mottl (1944). The distinction was mainly done based on the basis of colour variation of the fine sediment. From bottom to top, the

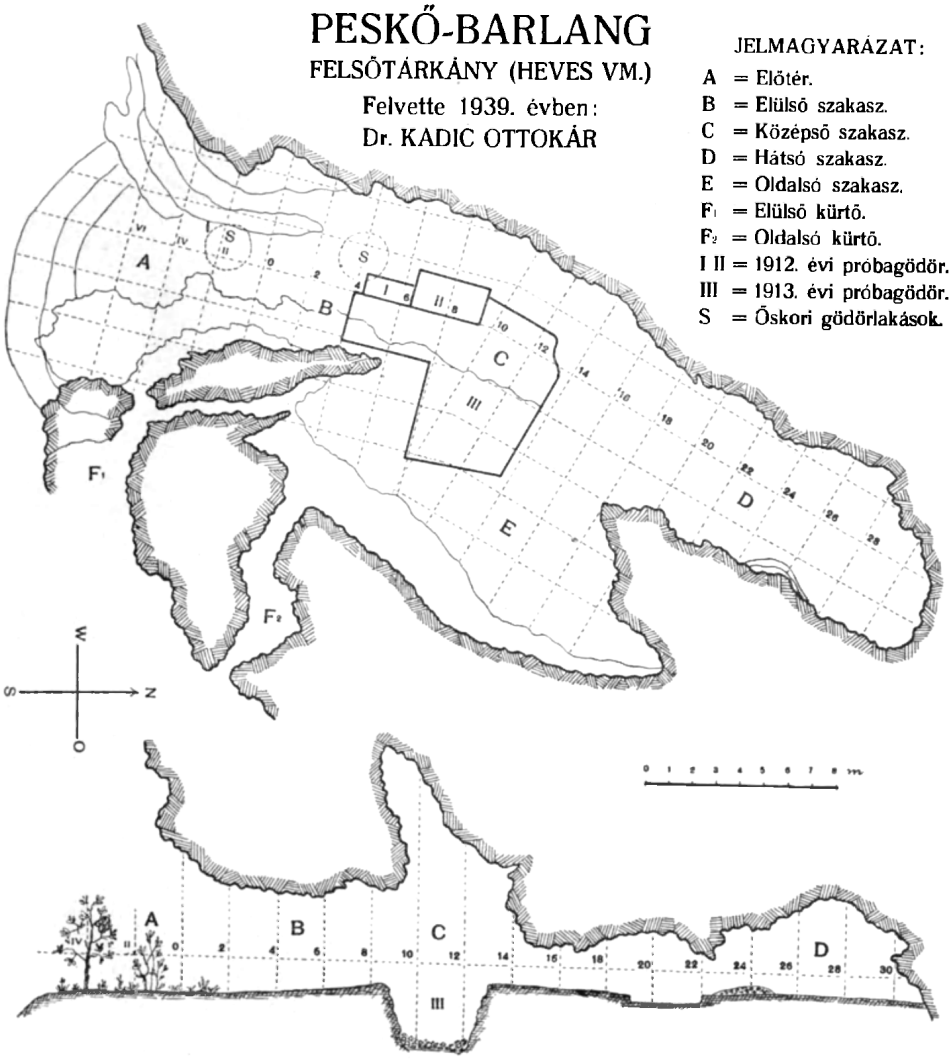


Figure 11.46: Peskő: map of the cave from top and side with excavation trenches, quadrants and cave areas marked. Scale shows 8 metres in steps of 1m. The legend reads: A = cave terrace; B = front section; C = mid section; D = rear section; E = side section; F1 = front chimney; F2 = rear chimney; I, II = trench from 1912; III = trench from 1913; S = 'prehistoric pond dwellings' (Kadić and Mottl, 1944, pl. I).

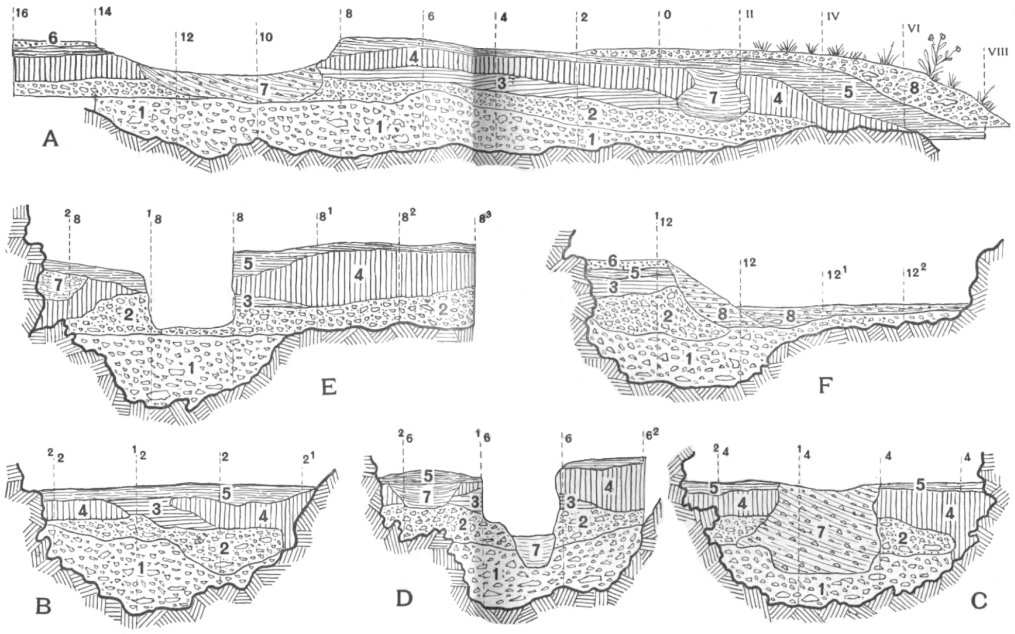


Figure 11.47: Peskő: profile drawings. The letters match the locations marked in figure 11.46 (Kadić and Mottl, 1944, pl. II).

ca. 2.5 m sequence is composed of the following layers (compare profiles in fig. 11.47):

1. **dark brown** layer with limestone debris (max. thickness 1.5 m), thin at the front and thicker at the rear of the cave
2. **greenish-grey** layer with limestone debris (avg. thickness 0.5 m), contains charcoal concentration / fireplace in the top part
3. **brick red** layer with limestone debris (avg. thickness 0.4 m), located at front and center of cave
4. **light yellow** layer with limestone debris (avg. thickness 0.5 m)
5. **humus** layer (max. thickness 1m), thickest at entrance, thinning towards the rear, penetrates to the level of lower layers on three occasions (see S in fig. 11.46)

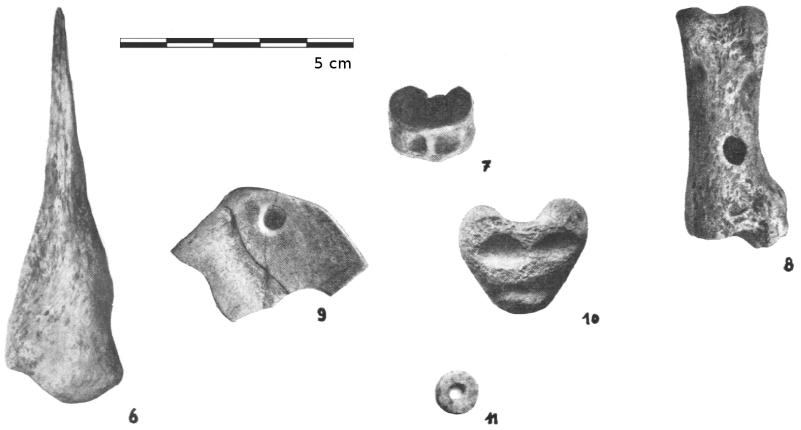


Figure 11.48: Peskő: osseous tools, ornaments, artefacts, and a possible 'idol' (no. 10) from the upper AH (Gábori, 1951, pl. VII; scale added).

Archaeology

Kadić and Mottl (1944) identified two archaeological horizons (AH). The lower AH consisted of layers 1 and 2, and the upper AH corresponded to layers 3 and 4. Based on the cultural interpretation of the 1950s, the two layers were referred to as the 'Aurignacian' and 'Magdalenian' horizons. However, this dissertation will use the more neutral terminology of lower and upper AH if no specific geological layer attribution is mentioned.

None of the layers contained any Mousterian or diagnostic 'transitional' (e.g. Szeletian leaf-points) lithics. The few retrieved lithics seem to belong to an upper Palaeolithic blade industry (see fig. 11.49). In the lower AH, some blades, scrapers and an obsidian flake were found. The osseous industry is represented by split-based points, massive-based points, polishers, awls, sticks and Kiskevély blades[13] (see fig. 11.50–11.51). The upper AH contains microbladelets and blade fragments. The osseous artefacts are awls, a modified fish bone, a punctured bone plate, and a possible 'idol' (see fig. 11.48). Both horizons included charcoal concentrations (Kadić and Mottl, 1944).

[13] made of chipped bear teeth.

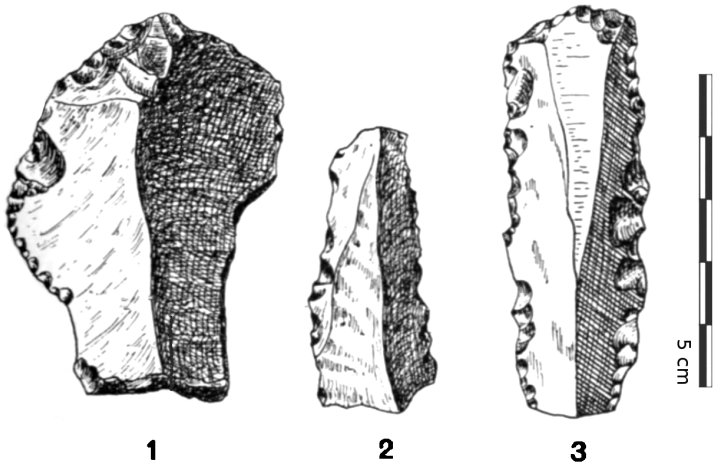


Figure 11.49: Peskő: lithics. 1 – burin/scraper; 2 – bladelet; 3 – blade with erosion polished surface (Kadić and Mottl, 1944, fig. 5; scale added).

Previous Dating

Previous attempts at dating the 'Early Aurignacian' osseous industry have resulted in 5 published radiocarbon measurements (see tab. 11.22–11.23). In the 1960s, an unmodified faunal fragment from the the '*lowest layer*' (presumably layer 1) was sent to the Centre for Isotope Research at the University of Groningen, resulting in a radiocarbon age of 35200 ± 670 BP (GrN-4950). The sample was treated with dilute acid and the extracted collagen dated using a proportional gas counter. The sample was reported as a fractionation corrected, conventional radiocarbon age (Vogel and Waterbolk, 1972).

In 2007, four artefacts were sampled for dating – two of which were listed as SBP or possible SBP, another as a lunate-sectioned point, and the last as a rib with possible decorative markings (Davies and Hedges, 2008). All samples were treated with the standard ORAU ultrafiltration protocol (AF), preceded by solvent wash steps to remove any possible museum derived contamination. Collagen preservation appeared high – especially for point artefacts – and all other pretreatment results indicated reliable measurements.

The artefact reportedly came from the '*lowest layer*' (Davies and Hedges, 2008, tab. 4), though it remains unclear whether this refers to the lower

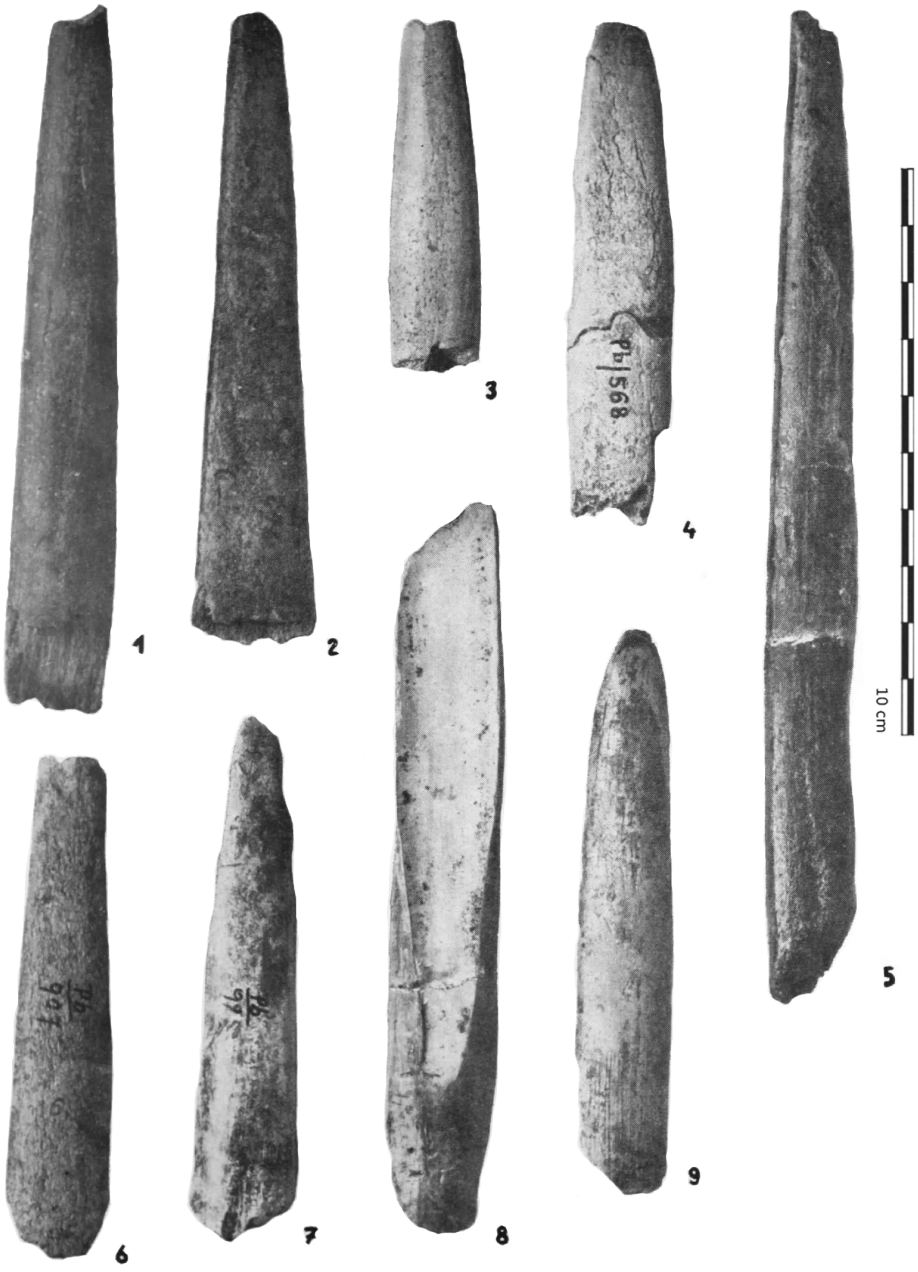


Figure 11.50: Peskő: osseous projectile points and tools from the lower AH (after Gábori, 1951, pl. III; scale added). 5,6 – dated by Davies and Hedges (2008) as SBPs (see tab. 11.22–11.23); 2 – SBP identified by Markó (2017) as belonging to Istállóskő (see section 11.2.2).

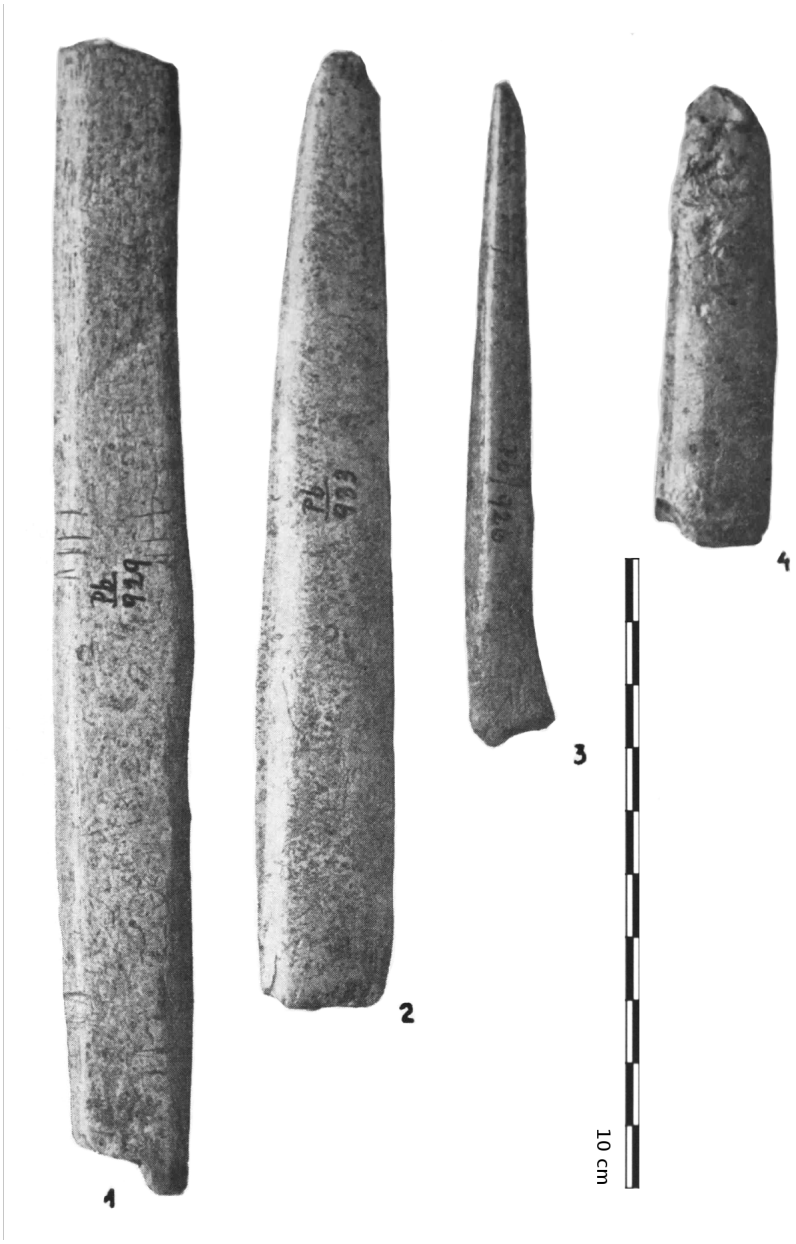


Figure 11.51: Peskő: osseous projectile points and tools from the lower AH (Gábori, 1951, pl. IV; scale added). 2,4 – dated by Davies and Hedges (2008) as lunate-sectioned bone point and as engraved rod, respectively (see tab. 11.22–11.23).

Table 11.22: Peskő: pretreatment information and results for previously published radiocarbon dates (Davies and Hedges, 2008; Vogel and Lerman, 1969; Vogel and Waterbolk, 1972). Additional information from the internal databases at ORAU. Yield given for collagen extracted, unless otherwise stated.

Lab-no	Item	Treat.	Yield (mg)	Yield (wt.%)	%C	δ^{15}N	δ^{13}C	C:N	Fig.
GrN-4950	fauna	acid	–	0.6 %C	–	–	-20.3	–	–
OxA-17964	SBP?	AF*	11.12	4.6	42.9	7.6	-19.7	3.3	11.50-5
OxA-17965	fauna (marked)	AF*	4.4	2.1	41.0	11.9	-20.9	3.2	11.51-4
OxA-17966	SBP	AF*	8.08	3.5	42.4	3.7	-18.6	3.3	11.50-6
OxA-17967	point (luna)	AF*	5.3	2.7	42.5	3.5	-19.2	3.3	11.51-2

Table 11.23: Peskő: previously published radiocarbon dates on osseous points, cut-marked bone and unmodified fauna (Davies and Hedges, 2008; Vogel and Lerman, 1969; Vogel and Waterbolk, 1972). Dates calibrated in OxCal 4.3 (Bronk Ramsey, 2009a) with IntCal13 (Reimer et al., 2013). grey row – not suitable for modelling.

Lab-no	Item	Inv.-no.	Layer	Treat.	^{14}C (BP)	Date (cal BP)
GrN-4950	fauna	–	lowest (1)	acid	35200 ± 670	41280–38510
OxA-17964	SBP?	Pb 930	lowest (1)	AF*	33500 ± 450	38840–36510
OxA-17965	fauna (marked)	Pb 929	lowest (1)	AF*	37300 ± 1600	45170–38860
OxA-17966	SBP	Pb 927	lowest (1)	AF*	36400 ± 800	42360–39470
OxA-17967	point (lunate)	Pb 933	lowest (1)	AF*	38300 ± 1500	45800–40100

0

AH, or layer 1. The museum label only lists them as 'Aurignacian'. The engraved rod was first published in (Gábori, 1951) as a fragment of an ivory rod. This material identification would cast some doubt on the radiocarbon measurement of 37300 ± 1600 BP (OxA-17965), as ivory has been shown to be used long after an animal's death. However, (Davies and Hedges, 2008) identified the material as bone from a rib. The other artefacts, listed as osseous points, will be further discussed under section 11.6.2.

All previous dates are in relatively good agreement, though indicative of several events within the lower AH. GrN-4950 is likely to underestimate the true age of the sample as a result of both the pre-treatment and measurement technique. As it is not directly connected to human activity, it will not further feature in the analysis of Peskő cave. In contrast, the direct dates on osseous points – especially 36400 ± 800 BP (OxA-17966) and 38300 ±

1500 BP (OxA-17967) – are the oldest published prior to the work on this dissertation. Considering the seemingly fantastic preservation status of the artefacts, they are well suited for re-dating in order to test the reliability of the previously obtained measurements.

11.6.2 Radiocarbon Dating

Previously dated osseous points from Peskő cave have, until now, produced the oldest radiocarbon measurements on 'Aurignacian' points. As their preservation was exemplary, they provide an opportunity to test the reliability of these dates. Only a small sample should be sufficient to replicate the dating, thus leading to minimal further damage while providing direct comparisons.

Samples & Treatment

The three previously sampled osseous points (Pb 930, Pb 927 and Pb 933) were typologically assessed and re-sampled for radiocarbon dating in September 2015 (see description below and tab. 11.24). A powder sample was collected using the key-hole drilling technique. As it was expected that the samples will not yield sufficient collagen for hydroxyproline dating, they were all treated with solvent wash steps to remove possible contamination from conservation substances (acetone 1h at 40°C, methanol 0.5h at RT, chloroform 0.5h at RT). Subsequently, they were treated with the gelatine protocol (AF) and freeze-dried. Further ultrafiltration was only applied in cases where collagen yield >10mg to guarantee datable material (see section 5.4).

Pes-01 near complete fragment of an antler point, possibly massive based point. The artefact consists of two refitted fragments, which were glued together at the fracture. They have in the meantime separated (probably as a result of glue drying out and becoming brittle), with residue visible on both contact surfaces. Both proximal and distal ends are missing. Part of the

Table 11.24: Peskő: context information for artefacts sampled for radiocarbon dating.

Ref-no.	Inv.-no.	Item	Excav.	Layer	%N	Weight	Cons.
Pes-01	Pb 930	MBP	1934	lower AH	1.66	386 mg	Y
Pes-02	Pb 927-28	SBP	1934	lower AH	1.57	121 mg	Y
Pes-03	Pb 933	point	1934	lower AH	2.86	309 mg	Y

narrow edge of the distal fragment has broken off. The entire surface shows signs of damage by post-depositional processes, and is covered in a black coating. The artefact is preserved on a length of 180 mm, with a maximal width of 16 mm, and a flat-oval, nearly rectangular, cross-section.

The museum number (Pb 930) is written in black ink on the dorsal surface at the mesial part of the proximal fragment. An older number (20.) is visible in slightly fainted black on the same side, but in the mesial part of the distal fragment. The entire artefact is heavily coated with a conservation substance (PVA?), which seemed to have darkened with age. The previous sample for radiocarbon dating was taken from the proximal part on the ventral surface of the distal fragment. The area (slightly larger than $1cm^2$) was reconstructed with epoxy resin and cosmetically covered with paint. The new ^{14}C sample was drilled from the narrow edge of the proximal fragment, to avoid contamination from epoxy, glue, and surface coating that possibly seeped into the damaged distal part of the distal fragment. To further avoid contamination from surface coating, the entrance area was abraded prior to sampling.

The antler point was published by Gábori (1951) as a SBP typical of the 'Aurignacian'. However, it does not resemble the shape of the other SBP found at Peskő and its proximal end is too severely damaged to allow for a secure identification. This is reflected by Davies and Hedges (2008, p. 41), who listed the artefact as an *"antler (split-base?) point"*. However, the lack of identifiable split-base, and its more parallel shaped sides, are reminiscent of the massive-based points found at Dzeravá Skala.

Pes-02 medial fragment of an antler point, possibly split-based point. The distal end is missing, and the proximal end damaged. The fracture at the proximal end indicates that there might be the remains of two wings still visible. The entire surface is rough and shows scratches and ablations from post-depositional processes, disguising any traces from manufacture. Furthermore, the artefact is covered in a patchy black coating. The point is preserved on a length of 90 mm, with a maximum width of 19 mm, and a planoconvex cross section.

The museum number (Pb 927) is written on the mesial part of the dorsal surface. The entire artefact is coated with a conservation substance (PVA?). The previous radiocarbon sample was taken from the meseo-distal part of the ventral side, and was subsequently reconstructed using epoxy resin and paint. To avoid contamination from this area, the new sample was taken from the narrow edge in the meseo-proximal part, accessing the wide area of the artefact through key-hole drilling.

Gábori (1951, p. 10) described the artefact as "Egy másik bőrfejtőként" (another implement for skinning or decorating skin) and suggested the possibility of it being a fragment of a osseous spear point. Davies and Hedges (2008) eventually listed it as a SBP. Considering the proximal end of the fragment, the latter interpretation appears very reasonable, despite the damage observed.

Pes-03 medial fragment of a point. Both the proximal and distal ends have broken off and are missing. The surface shows longitudinal striations from shaping, as well as scratches and surface erosion caused by post-depositional processes. The entire artefact is covered with a patchy black coating. The artefact is preserved on a length of 152 mm, with a maximum width of 24 mm. Its cross section is concave on the ventral side and convex on the dorsal side, leading to the description as "lunate-sectioned bone point" in Davies and Hedges (2008). In Gábori (1951), the artefact is listed under bone implements. It might well be that the artefact was left incomplete.

In the mesial part of the dorsal side, the museum number (Pb 933) is written in black ink. A little further down, there is a fading number 10 still visible. The entire surface of the artefact was coated with a conservation substance (PVA?). The previous radiocarbon sample was drilled from the ventral surface in the mesial section of the fragment. As before, the damage was reconstructed with epoxy resin and cosmetically adjusted with paint. To avoid this area, the new sample had to be taken from either closer to the dorsal or to the proximal end. As the pronounced lunate shape of the proximal part leaves limited manoeuvrability, the artefact was sampled from the narrow edge close to the distal end using the key-hole drilling technique.

^{14}C Results

The collagen yield was substantially lower than previously and insufficient for ultrafiltration. Nonetheless, the samples were further processes and dated (see tab. 11.25–11.26), bearing in mind that AG* treatment often leads to minimum age estimates only.

Table 11.25: Peskő: pretreatment information and results for newly radiocarbon dated osseous points.

Ref-no.	Item	Treat.	Yield (mg)	Yield (wt.%)	%C	δ^{15}N	δ^{13}C	C:N
Pes-01	MBP	AG*	6.35	1.65	41.9	7.8	-20.7	3.2
Pes-02	SBP	AG*	1.25	1.04	41.4	2.6	-19.1	3.4
Pes-03	point	AG*	7.46	2.42	40.9	3.8	-19.9	3.2

Pre-treatment results for Pes-01 and Pes-03 fall within expectations, although their δ^{13}C values were higher than previously. In contrast, Pes-02 shows an elevated C:N ratio for collagen. Its δ^{13}C value was higher and its δ^{15}N lower than previously measured. Moreover, this particular sample was on a small sample (0.8 mgC) AMS run which gave a high background (>41800 BP). As a consequence, the error is larger, and the sample most certainly underestimates the true age of the artefact. However, as it was not on

the same mass-spec combustion run (for graphitisation) as the background sample, it should be less affected than, *e.g.* Biv-01 (see Appendix).

Table 11.26: Peskő: new AMS radiocarbon dates for osseous points. Calibration done in OxCal 4.3 (Bronk Ramsey, 2009a) with IntCal13 (Reimer et al., 2013).

Ref-no.	Lab-no	$F^{14}C$	^{14}C (BP)	Date (cal BP)
Pes-01	OxA-35419	0.01925 ± 0.00118	31750 ± 500	36840–34650
Pes-02	OxA-X-2731-14	0.01588 ± 0.00233	33300 ± 1200	40660–35100
Pes-03	OxA-35420	0.01292 ± 0.00117	34950 ± 750	41370–38050

11.6.3 Discussion

The re-dating of the three osseous points from Peskő was not able to reproduce the old ages published in Davies and Hedges (2008). However, it is important to note that they do not contradict the original measurements either. The AG* treated results from ORAU are often minimum age estimates only. While the dates for Pb 930 (df=1, T=6.49, 5% = 3.8) and Pb 933 (df=1, T=4.87, 5%=3.8) fail the χ^2-test, the results for Pb 927 are statistically indistinguishable. Moreover, the new dates follow the same chronological order, indicating that their relative relationships are correct (see fig. 11.52). As a result of the expected improvement in reliability of AF* compared to AG* pretreatment, only the published results will be used for further regional analysis.

There are at least three osseous point events in the lower AH, two of which might be contemporaneous with the engraved rib dated to 45170–38860 cal BP (OxA-17965). It can further be concluded that the 'Aurignacian' osseous point industry is present at Peskő by 42360–39470 cal BP (OxA-17966) at the latest. As observed at other sites analysed for this dissertation, there might be a temporal separation between SBP and MBP – should the typological identification of the points be correct. The lunate-sectioned point predates both. However, its relationship to AMH or the other osseous point industries is currently still unknown. It might even be contemporaneous to the SBP

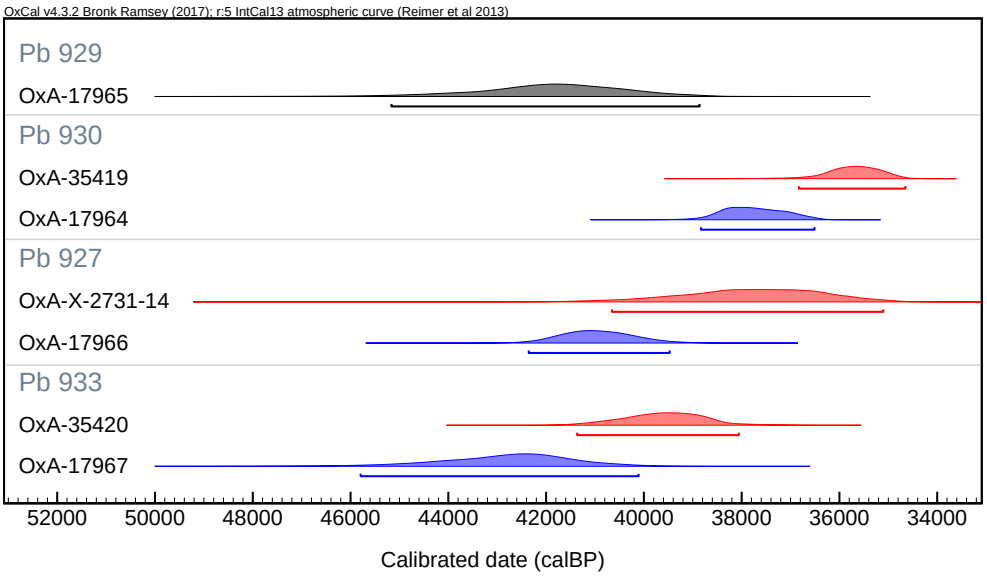


Figure 11.52: Peskő: comparison of new and published radiocarbon dates on osseous points, demonstrating the older ages obtained after AF* (**blue**) compared to AG* (**red**) pretreatment. Pb 929 (**black**) was obtained on an engraved rib fragment. It is included to show how it fits other dating from the lower AH.

found at Peskő cave. As a result, the presence of the 'Early Aurignacian' can presently not be moved further back in time to 45800–40100 cal BP (OxA-17967) by citing this artefact. For an overview discussion of all directly dated osseous points see section 14.

Chapter 12

Slovakia

Slovakia has several known Middle to Upper Palaeolithic sites (see fig. 12.1). They cluster in two regions, the west and the east of the country, with currently no substantial evidence from the centre. Neruda and Nerudová (2013, p. 3) point out that "*the area lacks stratified sites that are adequately well documented, and capture the period of transition of Middle to Upper Palaeolithic*". Nonetheless, there are several sites from the time period of interest that might contribute to our understanding of the biocultural shift. In the following, some of the main sites in Slovakia are evaluated according to whether they show both MP and UP stratigraphy, capture specific industries of interest, or contain human remains – leading to the identification of those localities most suited for this radiocarbon dating project.

Čertova pec, Dzeravá Skala and Nižný Hrabovec all have stratigraphic sequences that cover parts of the MP/UP transition. The first contains Mousterian, Szeletian and Gravettian lithic assemblages, with a sterile layer between the Mousterian and the Szeletian. Some radiocarbon dates attributed to the Szeletian indicate an age range from around 36k BP to near radiocarbon background (Kaminská, 2014; Valoch, 1996), though Neruda and Nerudová (2013) have questioned whether Bárta (1965) has adequately demonstrated a Szeletian attribution there. This, combined with the more problematic fact that the faunal material excavated was only bagged according to square meter

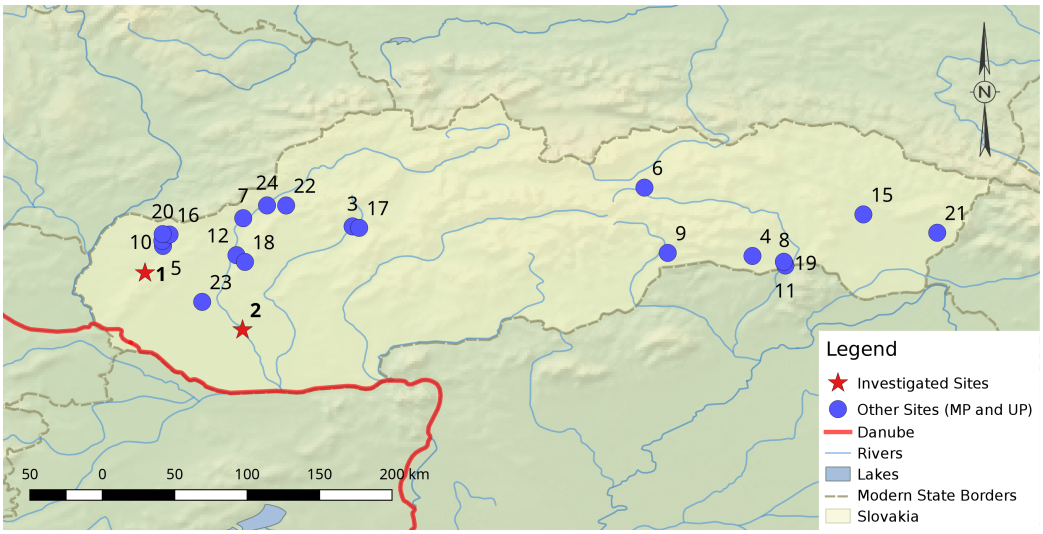


Figure 12.1: Slovakia: map of Middle Palaeolithic to Upper Palaeolithic sites evaluated: (1) Dzeravá Skala, (2) Šal'a, (3) Bojnice, (4) Čečejovce, (5) Hlboké, (6) Hôrka-Ondrej, (7) Ivanovce-Skala, (8) Kechnec, (9) Košická kotlina, (10) Kunov, (11) Milhost', (12) Moravany nad Váhom, (13) Myslava, (14) Nemsova, (15) Nižný Hrabovec, (16) Podbranč, (17) Prievidza, (18) Radošina – Čertova pec, (19) Seňa, (20) Sobotište, (21) Tibava, (22) Trenčin, (23) Vlčkovce-Vinohradky, (24) Zamarovce.

and spit (by 10 cm) – not geological layer or archaeological level – precludes the site from the project. Meanwhile, at Dzeravá skala, Middle Palaeolithic layers are possibly followed by Szeletian (or Jankovichian), Aurignacian and Gravettian. Lithic assemblages are small and largely undiagnostic, hindering a more precise identification of the MP industry and questioning the Szeletian attribution. However, the site has a large assemblage of osseous points – often referred to as Mladeč points (Kaminská et al., 2005b). The last site, Nižný Hrabovec, is currently the only Slovakian site with a Bohunician industry. They supersede layers attributed to the Middle Palaeolithic (Kaminská, 2014, pp. 103-105, pp. 120-123). Unfortunately, there is a high likelihood of secondary depositioning, which would interfere with both Bayesian analysis and age to lithic attribution.

There are several sites which cover relevant industries. From the late MP: Bojnice I and III date beyond radiocarbon (Kaminská, 2014, pp. 50, 134), Prievidza has no organic preservation (Kaminská, 2014, p. 101), Zamarovce

is a very old excavation with Micoquian lithics (possibly much older than the period of interest) (Kaminská, 2014, p. 99) and the sondages in the Myjavská pahorkatina (Sobotište 2, Sobotište 3, Podbranč, Kunov, Hlboké 1) have not provided suitable material for dating (Kaminská, 2014, p. 100-101).

From transitional industries: A large selection of Szeletian leaf points was found at Moravany nad Váhom-Dlhá. While some charcoals were found during the 1943 excavation (one dated to $33,600 \pm 300$ BP, Poz-29011), none of the excavations retrieved any datable osseous material (Kaminská et al., 2011). Ivanovce-skala was seen by both Prošek (1953) and Bárta (1966) as the most important Szeletian site. However, re-examination of the profile in 2006 identified issues with the previously published stratigraphic record (Kaminská, 2014, pp. 126-127) that require further excavation to clarify the archaeological record. Trenčianske Teplice-Pliešky, Trenčianska Turná-Hámre and Vlčkovce-Vinohradky all have to be excluded on the basis of stratigraphic inconsistencies and a lack of anthropogenically modified bone for dating (Kaminská, 2015; Kaminská et al., 2011).

From the Aurignacian: All the sites are open-air and discovered in the middle of the last century. Kechnec, especially Kechnec I, provide large lithic assemblages. However, charcoal dating only yielded ages of $27,370 \pm 210$ BP (GrA-24329) and $27,550 \pm 140$ BP (OxA-15678) and collagen preservation is too poor for dating (Kaminská, 2014, pp.155-159). At Košice-Barca I – the largest site at the Košická Kotlina complex – the 'Aurignacian' was dated to $29,680 \pm 250$ BP (GrA-16157) using charcoal. Unfortunately, none of the sites in the area show bone preservation (Kaminská, 2014, pp. 144-155). Myslava, Seňa II, Čečejovce-Vinohrady, and Čečejovce-Zvonárka have only produced surface finds, and Seňa I and Milhost', though stratified, yielded no anthropogenically modified bones or charcoals (Kaminská, 2014, p. 155, pp. 159-163).

An AMH skull was found at the Middle Palaeolithic site of Hôrka-Ondrej. While the site is likely older than 50k years, the skull turned out to be only a couple of hundred years old (Kaminská et al., 2000, p. 117). This leaves only

an AMH tooth from Dzeravá Skala and the Neanderthal cranial fragments from Šal'a (Kaminská, 2014, pp. 96-97).

As a result, dating for this project focuses on Dzeravá Skala (a reasonably stratified site with a significant osseous point collection and human remains), and the Šal'a Neanderthals. The former will provide insight on the possible arrival of AMH and the development of the Aurignacian osseous point industries in the region. The latter tests whether the two individuals could represent a late Neanderthal presence.

12.1 Dzeravá Skala

Dzeravá Skala is a key site in Slovakia for the Middle to Upper Palaeolithic. Although its lithic assemblages are relatively small, it is the only site in Slovakia that has stratified MP and UP horizons, reasonable organic preservation, and a large number of osseous spear points attributed to the Aurignacian. The complexity of the stratigraphy, combined with the limited lithic remains and the absence of most typical leitmotifs, have made a comparison of its occupational chronology difficult. Therefore, extensive radiocarbon dating of anthropogenically modified faunal remains for modelling purposes will help assess the integrity of the stratigraphy, and direct dating of the osseous points combined with techno-typological analysis may contextualise the osseous point industries.

12.1.1 Introduction

Dzeravá Skala (48.4922 N, 17.295 E) is located *ca.* 25 metres above the floor of a karst valley in the Lesser Carpathian Mountains, south-east of the village Plavecký Mikuláš in western Slovakia. The entrance is at an altitude of *ca.* 450 m a.s.l and faces east to the Morava River Plain. The cave is 18 m wide, approximately 15 m long and shows a small gallery extending around 8



Figure 12.2: Dzeravá Skala: cave entrance (Kaminská et al., 2005b, p. 9).

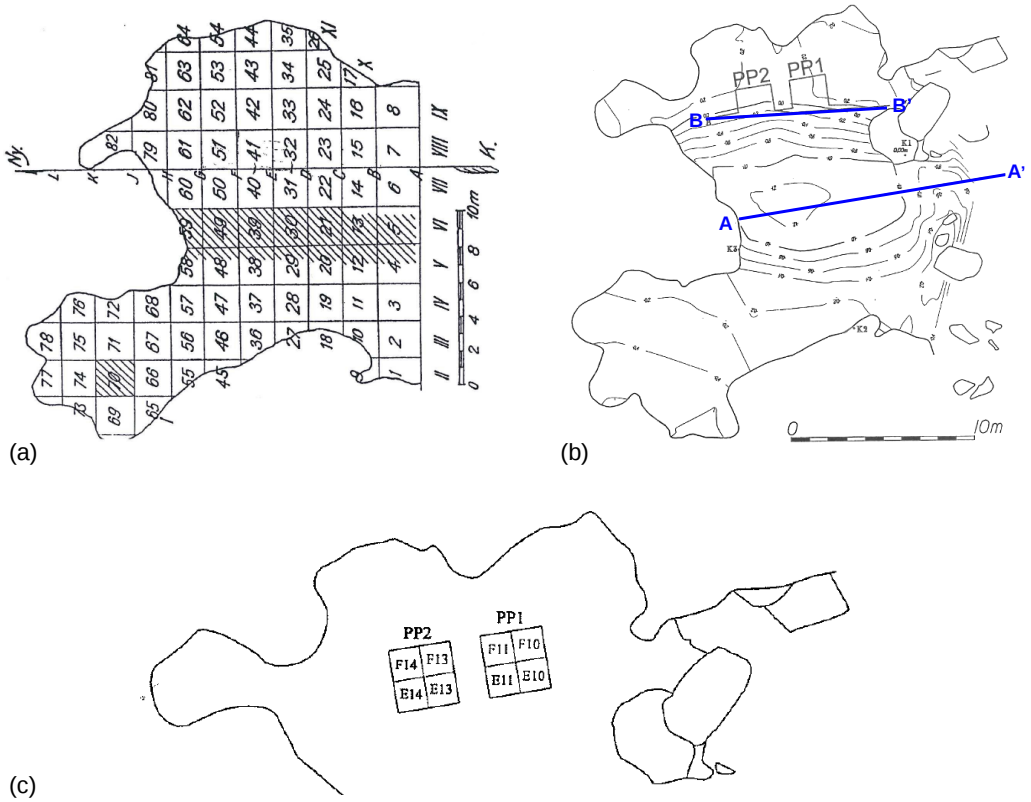


Figure 12.3: Dzeravá Skala: excavation areas. (a) – Hillebrand's excavation coordinates with trenches excavated marked with hatching; (b) – location of Prošek's excavation between his south (AA') and north (BB') profile, and Kaminská's trenches PP1 and PP2 (Kaminská et al., 2005b, p. 9); and (c) square labelling used for PP1 and PP2 (Novák, 2005, fig. 1).

m south-westwards (Allsworth-Jones, 1986; Gábori-Csánk, 1993; Hillebrand, 1913c; Kaminská et al., 2005b).

Dzeravá Skala has been translated as 'the hollow rock'[1] (Hillebrand, 1913c), but only starting with Prošek (1951) have archaeologists referred to the site by this name. Initially, the site was labelled *Pálffy barlang* ('Pálffy's cave') by Horusitzky, who first discovered the site's archaeological potential and wanted to honour its contemporary owner (Allsworth-Jones, 1986, Appendix, Site 20 Dzeravá Skala).

[1]The translation by (Kaminská et al., 2005b) as 'the Holy Rock' is misleading, as the name refers to the cavity within the rock and not any sacred ground.

Research History

The cave was first excavated by Jenö Hillebrand[2] in 1912 and 1913 (Hillebrand, 1913c, 1914). He divided the cave area into squares of 2 m length and dug a 3 m deep trench in the centre of the cave (from entrance to back), as well as a smaller test trench in sector 70 (see fig. 12.3-a). In the resulting profile he described five distinct layers: (1) black-brown topsoil, (2) soil mixed with tuff, (3) yellow soil, (4) reddish-brown soil and (5) greyish brown soil. While he attributed the first two layers to the Holocene, he interpreted layer 3 as 'Magdalenian', layer 4 as 'Protosolutrean' and layer 5 as 'Aurignacian'. In the 'lower grey clay' a split-based bone point (fig. 12.4) was found by E. Bächler. The upper part of the 'reddish clay', however, yielded an asymmetric 'leaf point' (see fig. 12.10-c) and a human tooth (see fig. 12.13). The analysis of the faunal record from 1913 were subsequently published by Éhik (1913) and Mottl (1938, 1941).

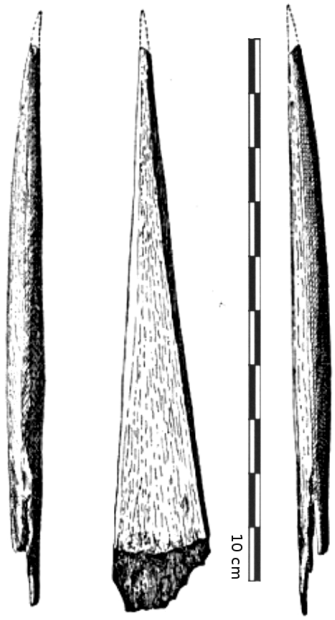


Figure 12.4: Dzeravá Skala: split-based point (Hillebrand, 1914, fig. 7; scale added).

Excavations by Horálek (1931) in 1923 and Dosedla (1950) in 1946-1949 focused on the Neolithic and Eneolithic, leaving Palaeolithic sediments untouched.

The second extensive Palaeolithic excavations were led by František Prošek (1951, 1953, 1957), but remain only partially published. Two trenches of 2 metres width were set parallel to the middle section excavated by Hillebrand (see fig. 12.3-b). Prošek originally identified 12 stratigraphic units[3] with

[2]Hillebrand published as Jenö Hillebrand when writing in Hungarian and as Eugen Hillebrand when writing in German – even if the texts are direct translations and feature in the same journal publication.

[3]He changed his original layer numbering for his 1953 publication. This dissertation will use these numbers whenever referring to any of Prošek's stratigraphic units.

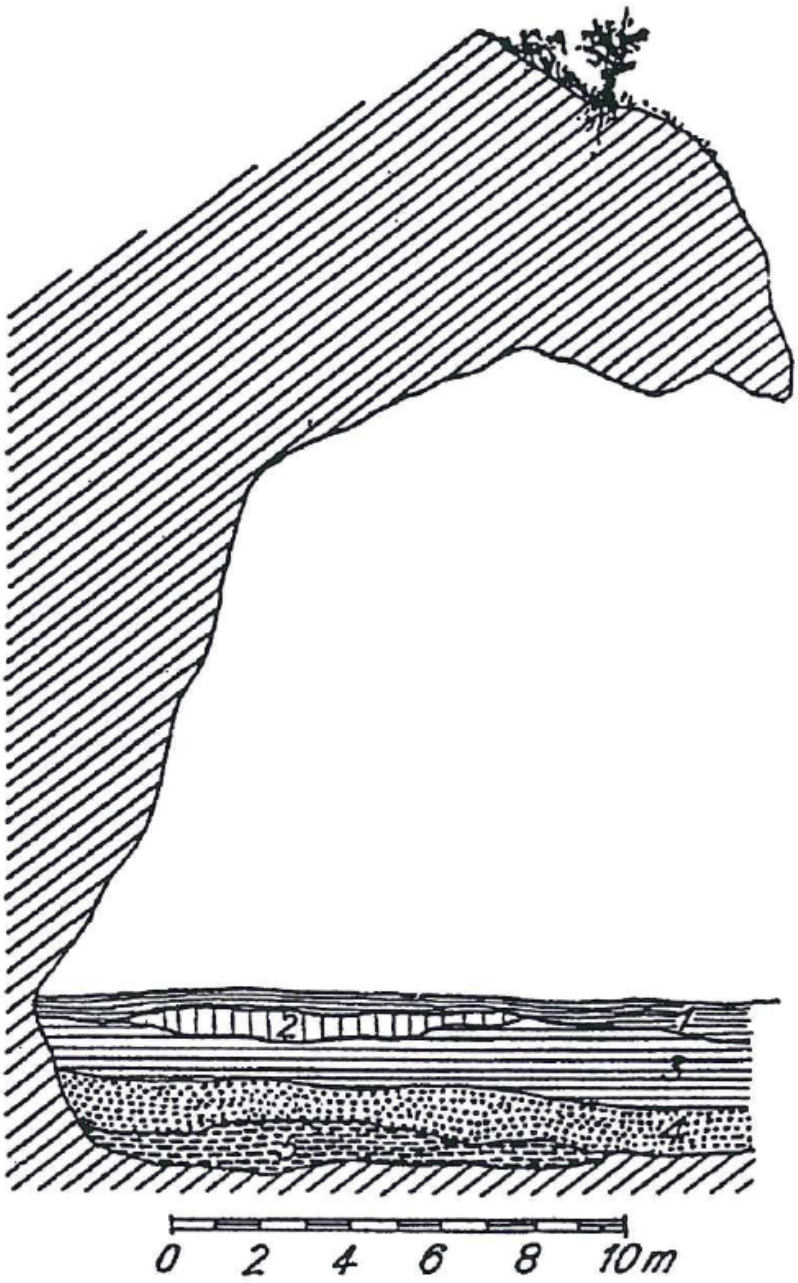


Figure 12.5: Dzeravá Skala: profile drawing from the 2013 excavation showing the 5 layers identified by Hillebrand (1914).

layers 3 to 11 attributed to the Pleistocene. In layers 1-4 modern, Medieval and Neolithic material was discovered, including a child's grave among the remains of the Lengyel Culture (Šefčáková and Thurzo, 2006). Based on two lithic blades, Prošek attributed layer 6 to the 'Magdalenien'. Below, in layer 7, he uncovered 27 stone tools, one mammoth bone point and several mammoth faunal remains, which he saw as indicative of the 'Upper Aurignacian' – nowadays referred to as the Gravettian. In layer 8, Prošek found a large cache of over 20 osseous points at various depths, but above several 'leaf points' and a 'Mousterian' point that were concentrated at the bottom of the same complex (Kaminská et al., 2005b, p. 40). An extra subdivision of layer 8 was proposed by Pelišek (1951) and is shown in figure 12.9.

In 2002 and 2003, new excavations were conducted under L'ubomíra Kaminská to better understand the stratigraphy as well as the archaeology it contained (Kaminská et al., 2005a). Prior to this third Palaeolithic campaign, the large centre area of the cave had already been excavated down to the bedrock. Therefore, new work concentrated on refreshing Prošek's north profile (BB' in fig. 12.3-b) and subsequently excavating two trenches extending northwards from the profile (see PP1 and PP2 in fig. 12.3-b–c). Material was removed in spits of 5 cm and a new system for labelling stratigraphic units was introduced. Sediments were sieved and some faunal remains used for AMS dating. Layer 2 was attributed to the Late Palaeolithic, layer 3 and 4 to the Gravettian, the inter-stratified layers 4a-5a to the Early Gravettian, layer 5 tentatively to the Aurignacian, layer 9 (containing an osseous point fragment) and its variants 9a and 9b to the Aurignacian, the upper part of layer 11 tentatively to the early Upper Palaeolithic, and the middle section of layer 11 to the Middle Palaeolithic (specifically the Micoquian, based on ^{14}C and OSL results) (Davies and Hedges, 2005; Kaminská et al., 2004).

Disentangling Stratigraphy & Archaeology

The stratigraphy at Dzeravá Skala is extremely complex, with signs of bio- and cryoturbation which make it difficult to identify layer boundaries and

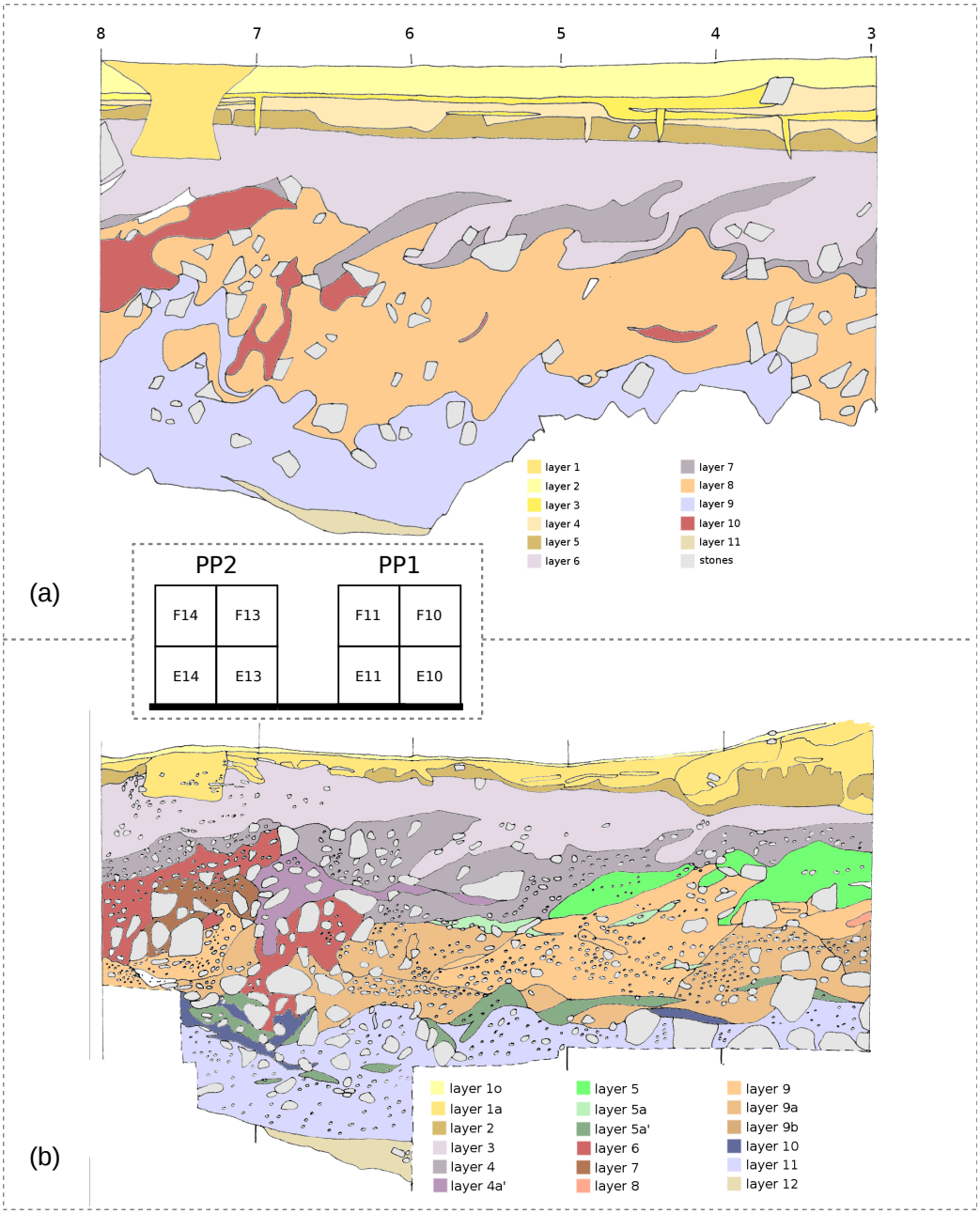


Figure 12.6: Dzeravá Skala: south-facing profile (location marked BB' in figure 12.3-b) as interpreted (a) in 1950 (after Prošek, 1953) and (b) in 2002 (after Kaminská et al., 2005b). In centre, profile location marked in relation to new excavation trenches.

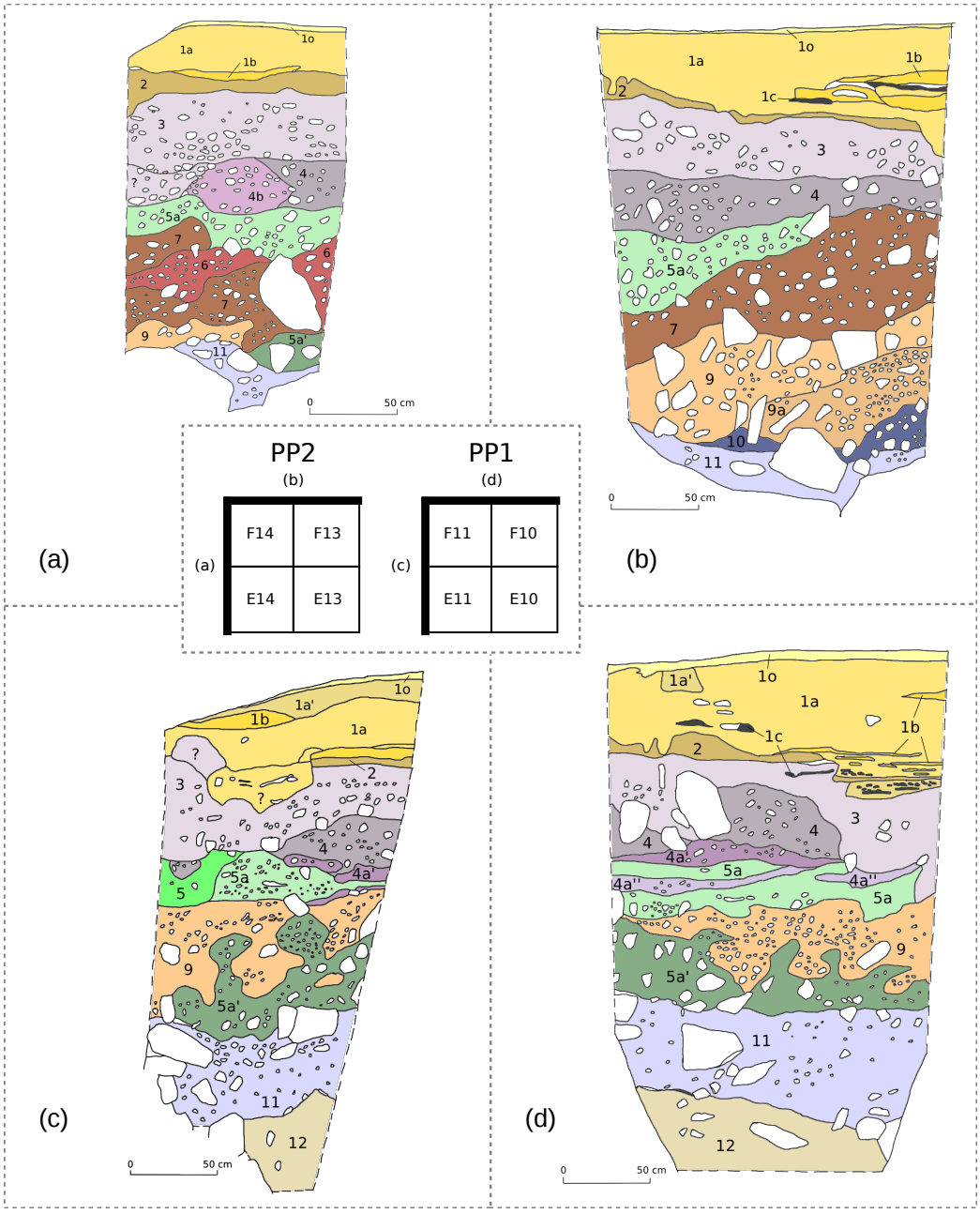


Figure 12.7: Dzeravá Skala: drawings of north (a) and west (b) profiles from trench PP2, and north (c) and west (d) profile from sector PP1 (based on Kaminská et al., 2005b). Areas marked with '?' indicate that the layer attribution from the original publication appears problematic, considering the area was clearly separated in the drawing, yet given the same layer label (see colour) as an adjacent unit.

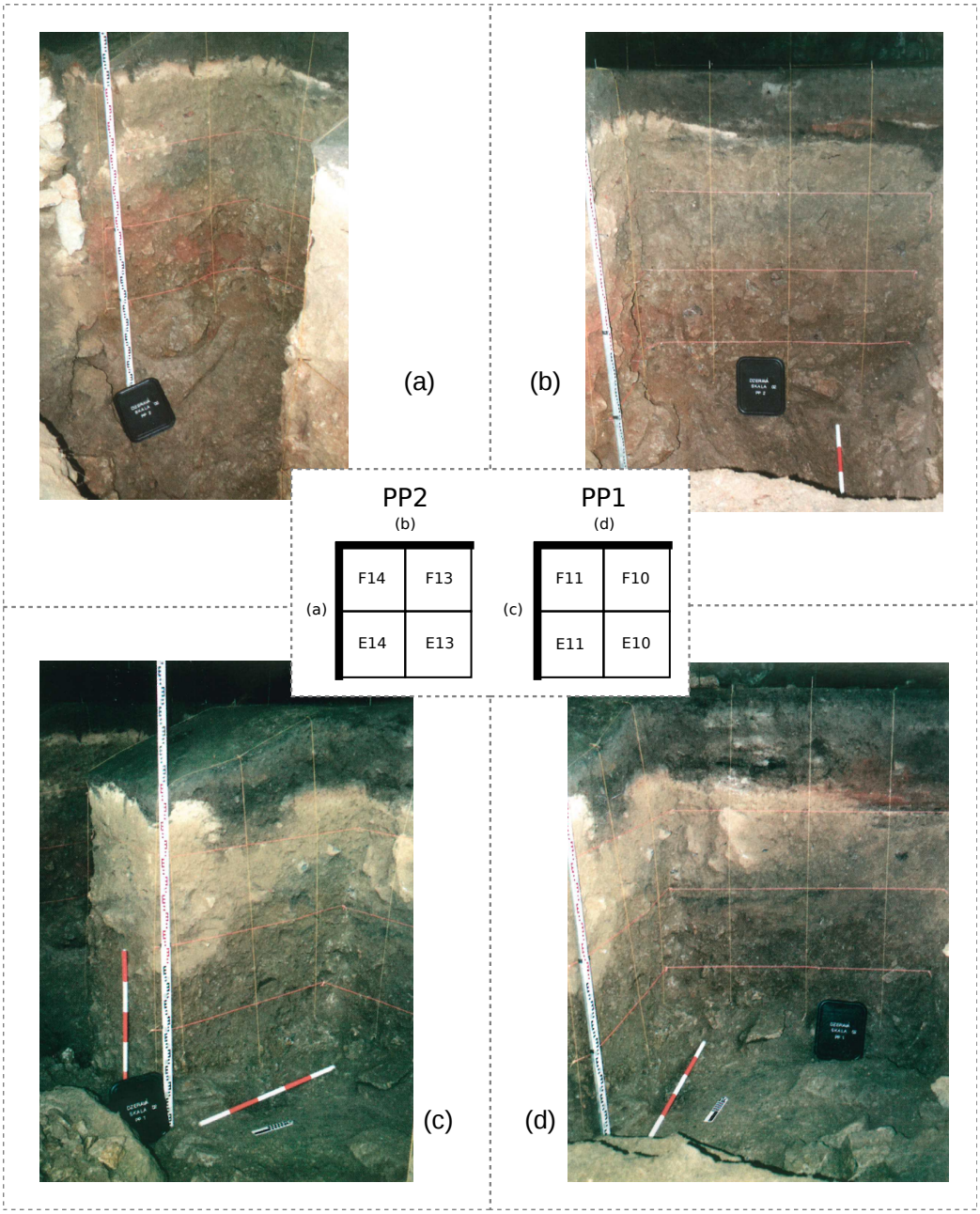


Figure 12.8: Dzeravá Skala: photos of north (a) and west (b) profile from trench PP2, and north (c) and west (d) profile from sector PP1 (based on Kaminská et al., 2005b, fig. 7–8).

possible re-depositioning of sediments and archaeological material. In addition, the three main excavations occurred over the period of nearly a century, during which excavation and analysis methods, as well as archaeological nomenclature have evolved significantly. This is illustrated by Hillebrand emptying half the cave in the same amount of time it took the most recent excavation by Kaminská to excavate 8 m^2, as well as by the different cultural names used to describe their work. However, the lithic assemblages from all excavations are rather small. As a result, it is necessary to attempt a reconciliation of the published stratigraphic records to connect the crucial osseous point finds with the lithics and to assist in archaeological interpretations (see fig. 12.9).

Hillebrand's excavation shows a simple stratigraphy of 5 consecutive layers, 2 Holocene and 3 Pleistocene (see fig. 12.5 and Hillebrand, 1914). All layers appear suspiciously horizontal for a cave site. It might be that his methods were not suited to detect finer nuances, considering the speedy and coarse excavation, though it could also be influenced by the location of his trenches. Both later excavations occurred closer to the cave walls – areas that are more prone to remodelling.

His initial stand that the Aurignacian would predate the 'Proto-solutrean' (i.e. 'Szeletian') at the site was based on a 'leaf point' (see fig. 12.10-c) found in layer 4 and a split-based point in layer 5 (Hillebrand, 1914). Gábori-Csánk's (1993) reanalysis of the lithic artefact concluded that it is neither a 'leaf point' nor Szeletian, but Jankovichian, and suggested that the osseous point was reworked. The latter appears very likely, considering the profiles of both subsequent excavations (see fig. 12.6) illustrate significant distortion of the layers corresponding to Hillebrand's layers 4 (i.e. Prošek 8, Kaminská 9) and 5 (i.e. Prošek 9, Kaminská 11). Furthermore, all later osseous point finds, including three possible SBP fragments, were discovered higher up in the sequence than Hillebrand's layer 5. From this, it can be concluded, that Hillebrand's separation of layer 4 and 5 was not consistent: the SBP actually belongs to Hillebrand's layer 4 (fig. 12.9, arrow A) – the bottom of which corresponds to Prošek's layer 8 (fig. 12.9, arrow C) – and some

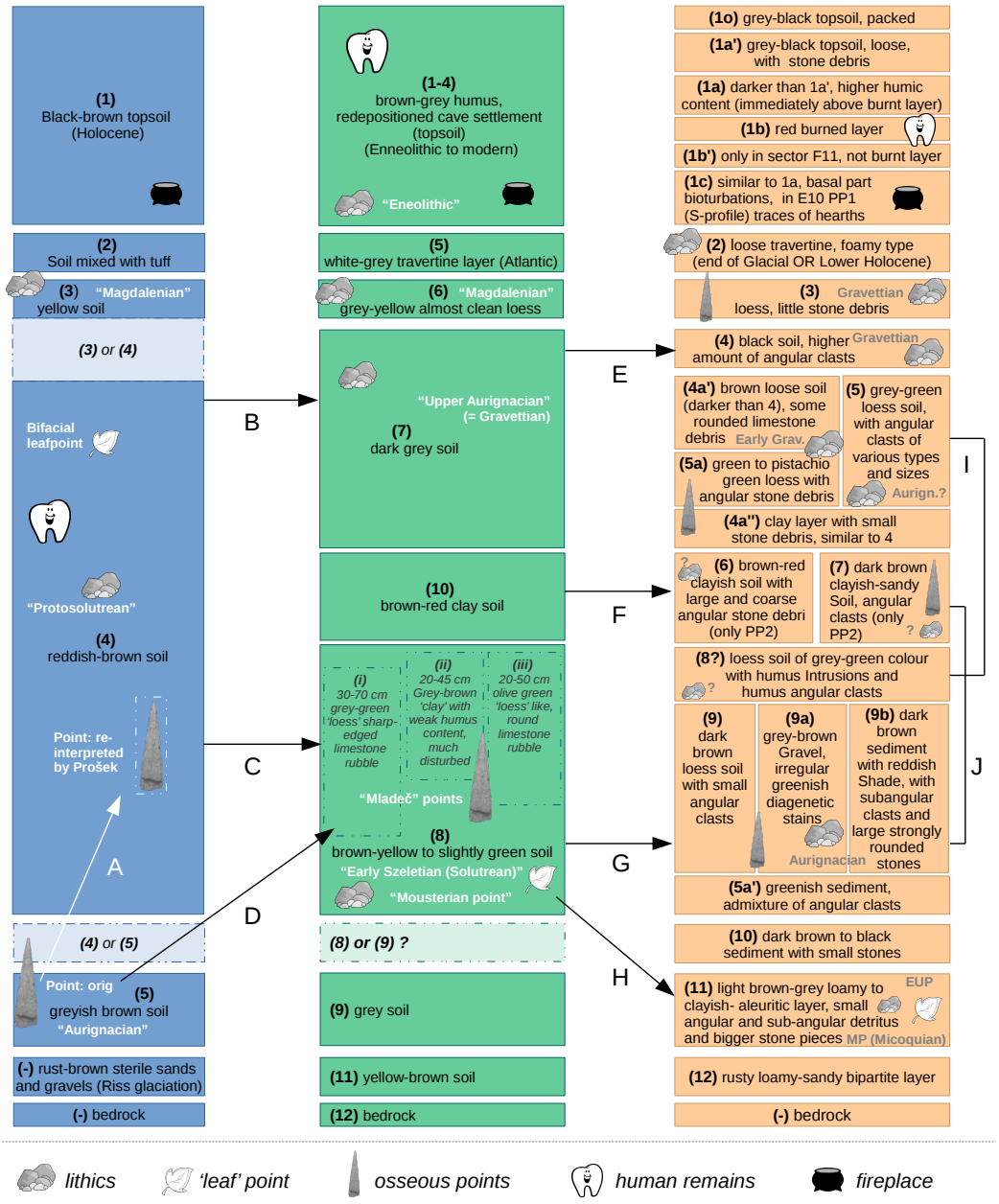


Figure 12.9: Dzeravá Skala: Reconciliation of the stratigraphies published by Hillebrand (1914) (**blue**), Prošek (1953) (**green**), and Kaminská et al. (2005b) (**red**). Same hight indicates correlated layers. The arrows (A to I) highlight additional connections discussed in the text (illustration: R. Hopkins).

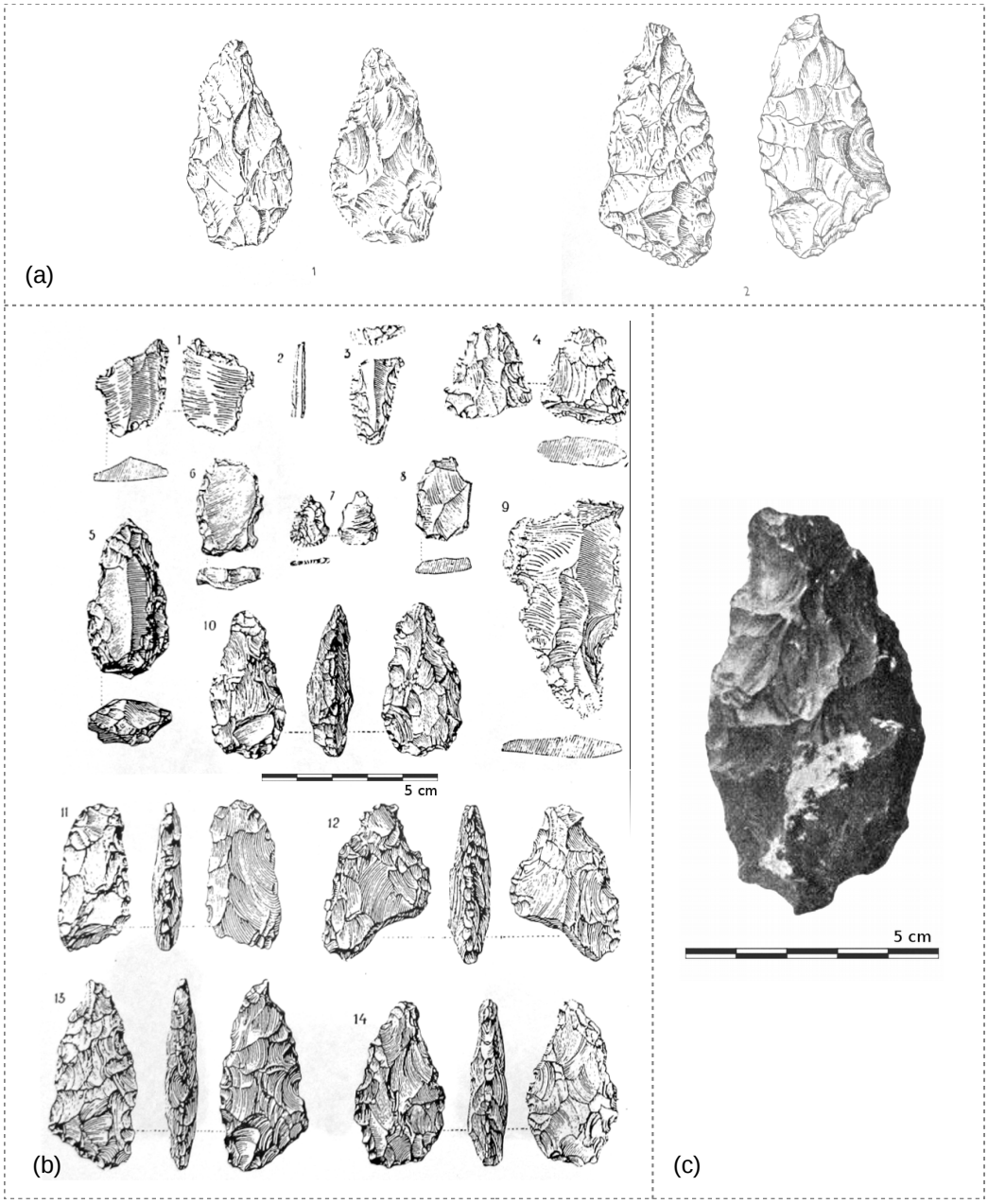


Figure 12.10: Dzeravá Skala: 'leaf point' lithics (not to scale). (a) and (b) found by Prošek at the base of his layer 8 (Gábori-Csánk, 1993, table XIV, scale added; and XV, not to scale), (c) found by Hillebrand in the upper part of his layer 4 (Hillebrand, 1914, fig. 8).

material attributed to Hillebrand's layer 5 might in reality also correspond to Prošek's layer 8 instead of layer 9 (fig. 12.9, arrow D).

This, however, leaves the issue of Hillebrand's 'leaf point' unresolved, as also a Jankovichian attribution would suggest that the artefact should predate the appearance of SBP at the site. There are two possibilities to resolve the discrepancy. First, the artefact is indeed a Jankovichian lithic and corresponds to those found at the base of Prošek's layer 8 (see fig. 12.10-a–b). In this case, Hillebrand's misattribution could have resulted from using height as an indication of chronological sequence, missing the complexity of the stratigraphic units in the area. Second, the lithic was indeed found stratigraphically above the SBP, yet is not Jankovichian in origin. At the time of excavation, the Gravettian industry was not yet defined. Prošek identified an 'Upper Aurignacian' layer above his layer 8 – the lithic industry later renamed 'Gravettian'. Bifacial points found in connection with Gravettian lithics are not uncommon at other eastern sites from Hungary to Bulgaria. Therefore, it seems plausible that the perceived unity of the Aurignacian combined with limited lithic evidence at the site led Hillebrand to miss further stratigraphic distinctions in his layer 4 (see fig. 12.9, arrow B).

Prošek proposed a sequence of 11 stratigraphic units, 4 Holocene, 1 Glacial or Holocene, 6 Pleistocene (see fig. 12.7-a and Prošek, 1953). The layers 1-4 correspond well to Hillebrand's unit 1 and Kaminská's subunits of 1, containing Eneolithic finds, human remains and several fireplaces. The underlying unit 5 did not yield any archaeological material and corresponds to Hillebrand's and Kaminská's layer 2. The youngest Pleistocene unit, layer 6, seems to correlate with Hillebrand's and Kaminská's layer 3, though Kaminská favours a Gravettian lithic attribution (Kaminská et al., 2004) and separation from the layer underneath differs in places (see fig. 12.6).

As stated previously, Prošek's layer 7 could represent the upper part of Hillebrand's layer 4. In contrast, Kaminská's profile applies finer distinctions, dividing the complex into interstratified subunits of 4 and 5 (excluding 5a'). At the same time, she proposes that layer 5 might contain Aurignacian lithics, in contrast to Gravettian lithics in layer 4. However, in light of the limited

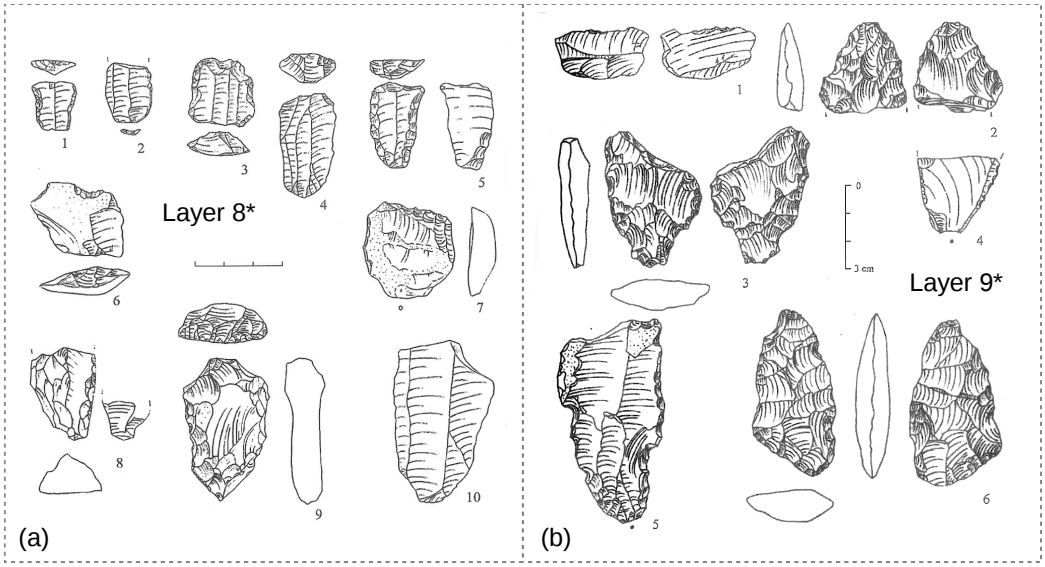


Figure 12.11: Dzeravá Skala: lithics found by Prošek, possibly in his layer 8 and layer 9, and attributed to (a) the 'Aurignacian' and (b) the 'transition' (1-4,6) and the MP (5) according to Kaminská et al. (2005b, fig. 23 and 29). Some of the artefacts are also found in fig. 12.10-b.

lithics uncovered and the lack of diagnostic artefacts, such a distinction seems premature. Based on sediment description and position in the stratigraphy (see fig. 12.6 and 12.12), it seems likely that these subunits of 4 and 5 are variants of the unit Prošek identified as layer 7 (see fig. 12.9, arrow E). This close connection is supported by an ivory point with refitted fragments found in layer 4a and 5a (see Kaminská et al., 2004, fig. 6.14).

Prošek's north profile indicates a clear connection between his layer 10 and Kaminská's layer 6 (see fig. 12.6 and 12.9, arrow F), though its stratigraphic position is ambiguous. Layer 10 is largely found in an area with severe warping of the layer interfaces. It appears both within Prošek's unit 8 as well as above it, and the location is marked by an uprising of layer 9. It is worth noting that Hillebrand's unit 4 was described as containing 'reddish-brown soil', a colour description reminiscent of Prošek's description of layer 10 as 'brown-red clay' (similarly Kaminská for layer 6) and Kaminská's 'sediment with reddish shade' for her layer 9b. No other units were characterised as 'reddish' or 'red'.

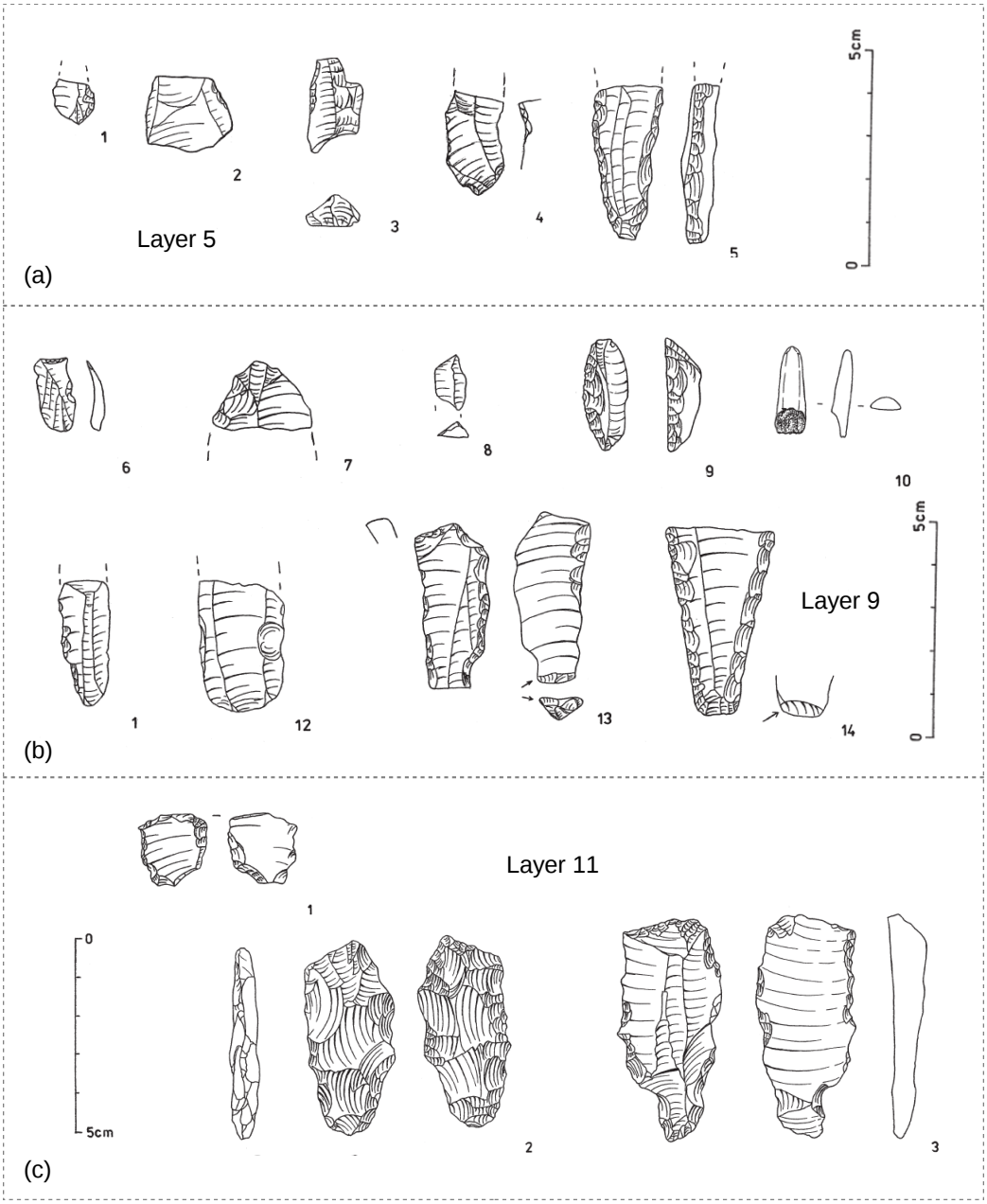


Figure 12.12: Dzeravá Skala: lithic and bone industry from (a) layer 5, (b) layer 9, and (c) layer 11 – discovered during the 2002/2003 excavations (after Kaminská et al., 2005b, fig. 7–8).

Further down the sequence, Prošek's layer 8 mostly corresponds to layer 9 in Kaminská's profile, though the limit to the layers below (Prošek 9, Kaminská 11) differ significantly. This discrepancy could be artificial and explained by the fact that the 2002/2003 excavation had to move the profile slightly northwards to clean it, leading to a slightly different layer configuration. However, if the two excavations did draw the limits differently, it may explain the distribution of archaeological material found: while the bone point and some blade fragments are inline with finds from Kaminská's layer 9, the 'Mousterian point' and the 'leaf point' assemblage (fig. 12.10-a–b) corresponds better to finds made in Kaminská's layer 11 (see fig. 12.12) and Prošek's own layer 9 (see fig. 12.11). Both Valoch (1969) and Gábori-Csánk (1993) doubted the direct stratigraphic association of the two assemblages – the osseous points and the 'leaf point' lithics – attributing the latter to the Jankovichian, and the former to the Aurignacian. In short, while the osseous point industry seems to be connectible to Kaminská's layer 9 (see fig. 12.9, arrow G), the lithics interpreted as 'Szeletian' by Prošek (1953), and 'Jankovichian' by Gábori-Csánk (1993), might be related to finds made in Kaminská's layer 11 (see fig. 12.9, arrow H).

The most recent excavation led by Kaminská introduced a significant number of additional divisions to the stratigraphy, resulting in 12 major units and several subdivisions (see fig. 12.7-b and 12.7, and Kaminská et al., 2004, 2005b). Most of the layers have been discussed in the previous paragraphs. Nonetheless, there are units which cannot be easily connected to previous excavations and need further comment, namely layers 5a', 7, 8 and 10.

Layer 7 is only found in sector PP2. In the west-profile it features both above and below layer 6, as well as above layer 9. In the north-profile, it lies between layer 5a and 9. Kaminská et al. (2005b) also identify the unit in Prošek's north-profile, where it features between layer 6 above and layer 9 below. However, in the original profile drawing by Prošek (see fig. 12.6-a), the area is occupied by both layer 11 and layer 9. It remains unclear whether it is indeed a separate horizon, or forms part of either layer 9 or 11. While Prošek's north profile may suggest that layer 7 is the result of layers 9 and

11 mixing, Kaminská's other profiles from PP2 (see fig. 12.7-a–b) make such an interpretation difficult. The sediment description of layer 7 is closest to that of layer 9 (see fig. 12.9, arrow J). Considering the complexity, issues surrounding material association are likely.

Difficulties with layer 8 stem from the fact that it is only documented as a thin lens in Prošek's cleaned profile in sector E10, and appears to be within layer 9. However, the sediment description resembles that of layer 5, which forms several angular intrusions into layer 9 in the area (see fig. 12.6-b). It can, therefore, not be excluded that layer 8 is part of layer 5 (fig. 12.9, arrow I).

It has to be noted that the labelling of layer 5a' is unfortunate. The profile drawings suggest it is not connected to other units of 5 (i.e. 5 and 5a), apart from sharing a 'greenish' colour, and lies mostly under layer 9 and above layer 11.

Layer 10 appears as repeated lenses between layer 9 and 11, sometimes underlying layer 5a'. It seems devoid of archaeological material, but its dark brown to black sediment reminds of the remains of fireplaces.

To conclude the stratigraphic and archaeological analysis: Hillebrand's original interpretation is too simplistic. Later excavations seem to have better captured the stratigraphic reality. There were several reworking and mixing episodes in the cave layers, some clearly due to cryoturbation, as suggested by Gábori-Csánk (1993). This impedes clear identification of layer limits. Furthermore, the limited number of lithics (often less than 10 per layer) without diagnostic artefacts makes archaeological culture interpretation challenging.

Nonetheless, it can be concluded that the site was visited either during the MP or the 'transitional' period, as well as the Upper Palaeolithic. As expected, the dating of the MP/UP biocultural shift at the site – while providing further insights – is unlikely to yield high precision. In contrast, the presence of split-based points suggest an early modern human occupation often connected to the 'Early Aurignacian'.



Figure 12.13: Dzeravá Skala: *Homo sapiens* tooth found during 1913 excavation in 'reddish clay'. Photograph showing occlusal, lingual, buccal and apical view (Šefčáková, 2007, fig. 5)

Despite the demanding stratigraphy, the osseous point industries can be linked to layer 9 from the 2002/2003 excavation. Consequently, it should be possible to re-contextualise the osseous points – within the stratigraphy of Dzeravá Skala as well as regional occurrence of the industry – through radiocarbon dating.

Human Remains

All three major excavation seasons discovered human remains (*i.e.* teeth) at Dzeravá Skala. Of interest to the current research is the only Pleistocene specimen, which was found by Hillebrand in 1913 in the 'reddish-clay'. It was identified as the crown of a lower right second permanent molar of a *Homo sapiens* child (see fig. 12.13). Hillebrand (1914) saw in the rather pronounced *sulcus transversalis anterior* an archaic feature, which he compared to molars found at Krapina. In his interpretation, he saw the tooth connected to the 'Proto-Solutrean' (*i.e.* Szeletian) lithics, which he believed to have found in the same layer. However, as these lithics could feasibly represent the Gravettian with leaf points, as found in eastern European sites, only direct dating (ideally paired with aDNA analysis) could help chronologically place the remains. The molar is presently stored at the Natural History Museum in Budapest, Hungary. Regrettably, requests to get access to the specimen for this project have been declined.

Table 12.1: Dzeravá Skala: previously published OSL dates (Davies and Hedges, 2005).

Date code	trench	Sq.	Layer	Depth (cm)	Age
K0085	PP1	-	9	162	35900 ± 3000
K0082	PP1	-	11 (middle)	225	57000 ± 4900

Previous dating

The 2002/2003 excavations led to the first absolute dating of the site, and resulted in 2 published OSL measurements, and a total of 19 radiocarbon ages.

In August 2003, samples for OSL dating were collected from layer 11 and 9 and analysed at the Luminescence Dating Laboratory at the Research School of Earth Sciences at the Australian National University in Canberra (Australia). 12 single quartz grain aliquots were measured per collected sample using the SAR protocol described by Murray and Wintle (2000), applying the conversion factors of Adamiec and Aitken (1998), the beta attenuation estimates from Mejdahl (1979), and the cosmic dose rate equations formulated in Prescott and Hutton (1994). For the final age, only aliquots with consistent results were used, resulting in K0085 being composed of 10 aliquots and K0082 of 8 (Nejman et al., 2005). While OSL dates the sediment, thus not necessarily the human activity at the site, these ages will be useful to anchor the lower end of the sequence as well as to check for inter-method consilience.

As part of the project 'Environmental Factors in the Chronology of Human Evolution and Dispersal' (EFCHED), funded through the Natural Environment Research Council (NERC) of the UK, seven unmodified faunal bone samples from the most recent excavation as well as five samples from a total of four osseous points were sent to ORAU for radiocarbon dating (Davies and Hedges, 2005). While three of the latter did not yield any collagen for dating (see fig. 12.2), both samples from the point 'Dz Sk 8' were successful: 31600 ± 900 BP (OxA-15334) and 31000 ± 1100 BP (OxA-15335). They

Table 12.2: Dzeravá Skala: previously failed radiocarbon dating on osseous points from the EFCHED project (Davies and Hedges, 2005, and ORAU internal database).

P-no.	Sample-no.	Trench	Size	Treat.	Yield
17280	Dz Sk 11	Prošek	460	AF*	0.00
17374	Dz Sk 9	Prošek	300	AF	0.00
17375	Dz Sk 10	Prošek	180	AF	0.00

were both treated with an ultrafiltration protocol without any solvent wash steps as described in Brock et al. (2007). However, collagen yields indicate highly varying preservation: 4.0 w.% vs. 1.70 wt.% (see fig. 12.3). As a result, the latter date had to be obtained on a small (0.8 mgC) instead of a large graphite target (1.8 mgC). Minimal variation can also be observed in the stable isotope results and the C:N ratio, though both appear to be within the acceptable range. The standard error reported is larger than usual for samples of such an age, though may be explained by the smaller target size. There were five successful bone samples (see fig. 12.3). They were treated using the same ultrafiltration protocol as the points. Sample yields varied between 0.5 to 6.10 wt.%, though the poor yield of OxA-13973 did not negatively affect the age determination. C:N ratios are slightly elevated (3.3-3.4), though remain within the expected range. Consequently, all dates are expected to be reliable measurements, albeit not directly connected to human activity.

Further unmodified faunal bone fragments were sent to the radiocarbon laboratories in Groningen (Netherlands), Waikato (New Zealand), Poznań (Poland) and Beta Analytic Inc. (USA). As a commercial facility, Beta Analytics would not provide any further details on their treatment process, apart from having obtained collagen for AMS dating. Beta-173341 (34100 ± 320 BP) seems to fit the ages reported for layer 9. Beta-173342 (36930 ± 470 BP), on the other hand, appears young for layer 11 – though it has to be noted that it is presently the only date form the upper part of said layer.

The four dates from Poznań are all marked as found 'below leafpoints'. Kaminská et al. (2004) attributed the single bifacial 'leaf point' to the middle

Table 12.3: Dzeravá Skala: previously published AMS ^{14}C dates (Davies and Hedges, 2005) obtained from unmodified mammal bones and one osseous point with context and treatment information. Additional pre-treatment information was obtained from the ORAU database, the Radiocarbon Dating Laboratory of the University of Waikato (F. Petchey, pers. comm. 23/04/2018), and the Centre for Isotope Research at the University of Groningen (M. Dee, pers. comm. 25/04/2018). Calibrated age calculated in OxCal 4.3 (Bronk Ramsey, 2009a) using IntCal13 (Reimer et al., 2013). * – Layer 8 from Prošek excavation corresponds to layer 9 from Kaminská. OxA-15534 and OxA-15535 are from the same bone point, which Davies and Hedges (2005) labelled 'Dz Sk 8'. grey – dates considered unsuited for modelling.

Date code	Item	Trench	Sq.	Layer	Depth (cm)	Treat.	Yield (mg)	Yield (wt.%)	δ^{13}C	C:N	^{14}C (BP)	Date (cal BP)
GrA-22756	fauna	PP2	F14	3	40-50	gelatine	18.50	0.45	-21.4	–	$25050 + 540/-510$	30540 – 28070
GrA-22758	fauna	PP2	F13	4	50-55	gelatine	158.7	4.57	-21.5	–	24800 ± 130	29190 – 28520
GrA-22759	fauna	PP2	F13	4b	60-65	gelatine	61.30	1.11	-20.3	3.2	31770 ± 320	36320 – 34970
OxA-13861	fauna	PP1	E10	5	105-110	AF	40.10	6.10	-21.5	3.3	24760 ± 130	29130 – 28470
Beta-173341	fauna	PP2	F13	9	180-190	–	–	–	–	–	34100 ± 320	39460 – 37760
Wk-16829	fauna	PP1	F11	9	130-135	gelatine	–	1.42	-21.7	3.2	33333 ± 820	39690 – 35770
OxA-13860	fauna	PP1	F10	5a'	145-150	AF	17.80	1.60	-18.6	3.3	35100 ± 400	40600 – 38740
Wk-14866	fauna	PP1	F11	5a'	145-150	gelatine	–	1.09	-21.5	3.3	33608 ± 569	39300 – 36410
Wk-14865	fauna	PP1	F11	9/5a'	160-165	gelatine	–	0.61	-21.1	3.2	37370 ± 2060	47330 – 38340
OxA-13973	fauna	PP1	E10	11	220-230	AF	4.30	0.50	-21.1	3.3	> 44600	> 44600
Poz-7092	fauna	PP1	F/E10	11	230-240	–	–	–	–	–	27000 ± 200	31310 – 30790
Poz-8485	fauna	PP1	F/E10	11	230-240	–	–	–	–	–	30330 ± 500	35360 – 33580
Poz-8793	fauna	PP1	F/E10	11	230-240	–	–	–	–	–	34900 ± 600	40940 – 38340
Poz-7064	fauna	PP1	F11	11	230-250	–	–	–	–	–	17400 ± 180	21540 – 20540
OxA-13859	fauna	PP1	F9	11	240-250	AF	10.80	1.60	-21.2	3.3	47000 ± 2300	> 49680
OxA-14247	fauna	PP2	E13	11	240-250	AF	11.78	2.10	-22.3	3.4	49700 ± 3000	> 49920
Beta-173342	fauna	PP2	F13	11	200-210	–	–	–	–	–	36920 ± 470	42230 – 40590
OxA-15334	point	Prošek	-	8*	-	AF	4.00	4.00	-20.3	3.1	31600 ± 900	38151 – 34052
OxA-15335	point	Prošek	-	8*	-	AF	2.80	1.70	-20.1	3.3	31000 ± 1100	38315 – 33225

part of layer 11. From that, it was concluded that the original leaf point assemblage was also found at 217-220 cm depth, thus the dates were grouped in 'above' and 'below' according to their depth. All dates are clear outliers. Considering the complexity of the layer's upper limit, it appears surprising to assume a relatively horizontal distinction within layer 11, and an issue of layer attribution cannot be excluded. Nonetheless, the large age difference is difficult to explain by misattribution alone[4]. Therefore, the Poznań dates are deemed too problematic for modelling.

The bone samples sent to Waikato were gelatinised and AMS dated. All three samples showed low collagen yield, but reasonable %C on combustion (Wk-16829: 37.6, Wk-14865: 37.8, Wk-14866: 39.3) and expected C:N ratios. The samples were taken from layers 5a', and 9, as well as from the contact zone 9/5a'. According to the profile drawings, layer 5a' clearly lies below layer 9. The radiocarbon ages, however, do not reflect this. On the contrary, the age of layer 9 and 5a' are comparable, while the sample for the contact zone 9/5a' appears much older.

As above, the Groningen dates were gelatinised and subsequently AMS dated. In line with previous results, collagen preservation varied greatly, with GrA-22756 showing a gelatine yield of only 0.45 wt.% – likely resulting in the larger radiocarbon errors reported. Nitrogen results were not recorded for GrA-22756 or GrA-22758. GrA-22759 has a C:N ratio typical of a collagen sample. Despite the limited information, all three samples appear reasonably reliable. While all samples were interpreted as indicative of the 'Gravettian' observed at the site, the date from layer 4b is with 31770 ± 320 BP (GrA-22759) significantly older than those from layer 3, 25050 +540/-510 BP (GrA-22756) and layer 4, 24800 ± 130 BP (GrA-22758).

Apart from the Poznań results, there are no indications that the radiocarbon dates represent unreliable measurements, though some stratigraphic anomalies are observable. It is important to emphasise that – with the exception of the antler point – all samples were taken from unmodified faunal

[4]A request for further pre-treatment information remained unanswered.

remains. Their connection to human activity at Dzeravá Skala relies on the integrity of their layer association alone. As the previous section demonstrated, a highly complex stratigraphy – involving mixing and redeposition of material – should caution us from taking these dates as proxies for the human occupations. The ages reflecting human activity at the cave were obtained on a single antler point. Though the two dates are in relatively good agreement with each other, they might still underestimate the true age of the artefact, as no solvent steps were included to deal with possible conservation derived contaminants. Furthermore, it has to be noted that the age is not representative of the diverse osseous points retrieved from Dzeravá Skala.

12.1.2 Radiocarbon dating

The present dating project at Dzeravá Skala focuses on the timing of the osseous point industry as well as the chronostratigraphy of the human presence at the cave. As a result a significant number of anthropogenically modified faunal remains (largely cut marked bone fragments) and osseous points were sampled in 2015 and 2016 for %N testing and radiocarbon dating.

Samples & Treatment

All faunal bone fragments from the 2002/2003 excavation, stored at the Natural History Museum in Bratislava, were checked for anthropogenically modified fragments, as the total number of bones collected was deemed manageable A total of 81 such bone fragments were identified (see fig. 12.14): 42 originated in trench PP1 and 39 in trench PP2, suggesting a relatively even distribution overall. However, there are significant differences between the layers. While both areas see an increase of human activity within layer 9, PP1 suggests a more consistent use, while PP2 favours older periods. Previous work divided layer 11 into three subunits according to depth, with material above 215 cm seen as above the 'leaf point' industry and possibly associated with the EUP, material from 215-230 cm belonging to the level

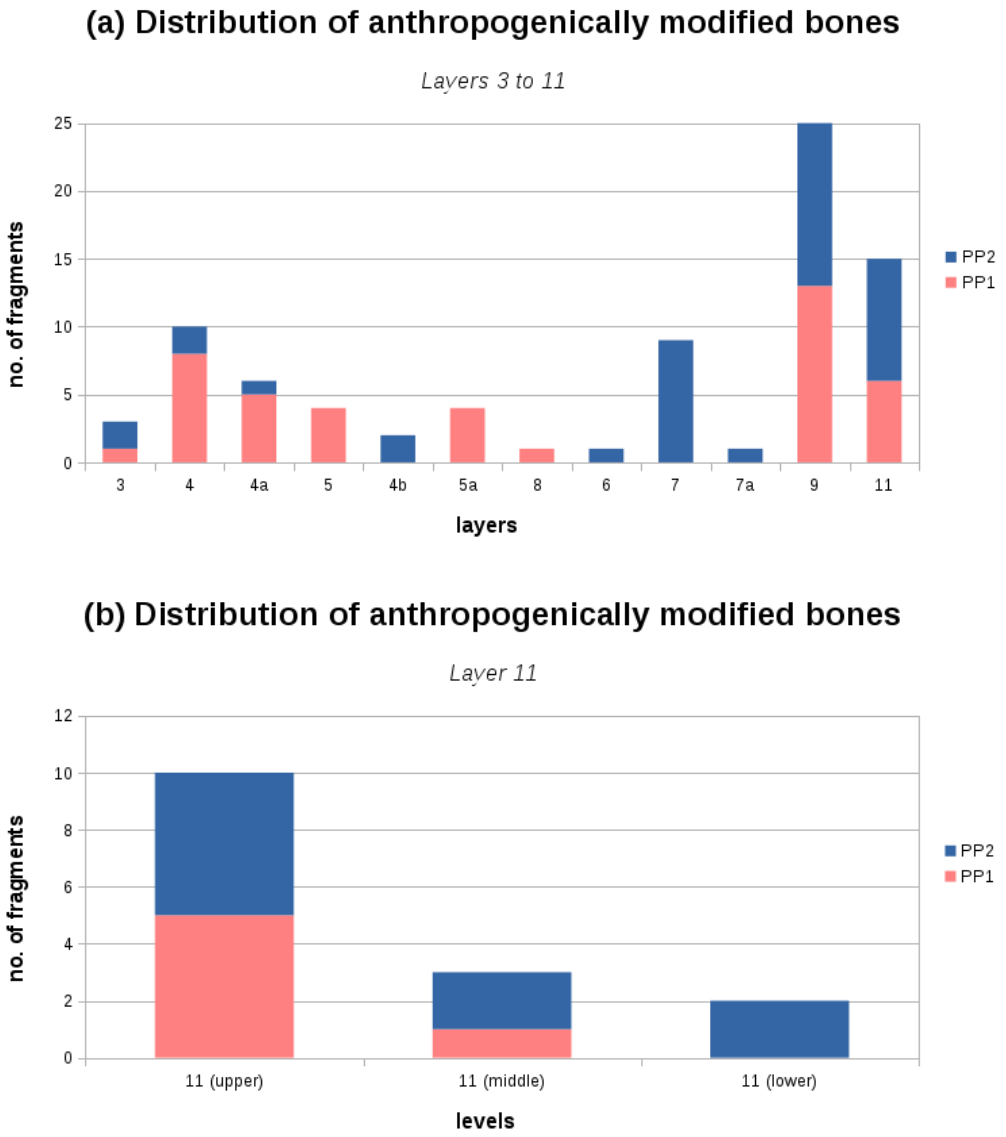


Figure 12.14: Dzeravá Skala: distribution of anthropogenically modified faunal remains from the 2002/2003 excavation season, coloured according to excavation trench (**red** – PP1; **blue** – PP2). (a) Overview of layers 3 to 11. (b) Separation within layer 11 according to depth: upper (< 215cm), middle (215–230 cm), and lower (> 230 cm).

Table 12.4: Dzeravá Skala: list of anthropogenically modified ^{14}C samples with context information. Sample weight in mg. Typological identification by B. Hromadová: SBP = split-base point; MBP = massive-base point. * – original layer numbering: Hillebrand 4/5 and Prošek 8 largely corresponds to layer 9 (see text).

Ref-no.	Item	Inv.-no.	Excav.	Trench	Sq.	Layer	Weight	%N
Der-01	SBP	Pb 579	1913	Hillebrand	–	4/5*	322	0.10
Der-03	fauna	E11/130	2002	PP1	E11	11	606, 985	0.91
Der-06	fauna	E10/93	2002	PP1	E10	9	647	2.79
Der-09	fauna	E11/97	2002	PP1	E11	9	522, 520	1.06
Der-10	fauna	E11/120	2002	PP1	E11	9	744	1.03
Der-12	fauna	F13/108	2002	PP2	F13	7	662	1.93
Der-13	fauna	PP2/412	2002	PP2	Profile	7	591	2.07
Der-14	fauna	E10/107	2002/03	PP1	E10	5	577	3.41
Der-15	fauna	E10/107	2002/03	PP1	E10	5	615	2.28
Der-17	fauna	E10/105	2002/03	PP1	E10	5	732	3.22
Der-18	fauna	E10/113	2002	PP1	E10	9	743	1.65
Der-20	fauna	E10/1058	2002	PP1	E10	9	903	3.12
Der-21	fauna	E10/85	2002/03	PP1	E10	8	707	1.98
Der-23	fauna	E10/982	2002/03	PP1	E10	4	677	2.26
Der-24	fauna	PP1/1027	2002/03	PP1	Profile	4a	655	3.00
Der-25	fauna	E11/127	2002	PP1	E11	9	808	2.78
Der-26	fauna	E11/61	2002/03	PP1	E11	4	547	2.69
Der-28	fauna	F11/143	2002	PP1	F11	11	830	1.64
Der-29	point, round	–	1950	Prošek	–	8*	401	1.80
Der-32	point	III3/160??	1950	Prošek	–	8*	334	0.84
Der-33	point (blank)	IVe/199??	1950	Prošek	–	8*	410	1.00
Der-35	point	II?/185?	1950	Prošek	–	8*	517	0.68
Der-36	MBP	IV.a/168	1950	Prošek	–	8*	392	0.68
Der-38	MBP	–	1950	Prošek	–	8*	536	3.06
Der-39	MPB	IIIc/155, IIA3/130	1950	Prošek	–	8*	640	1.13
Der-49	fauna	–	2003	PP1	F9	9	639	1.09
Der-53	fauna	–	2003	PP1	F10	11	799	1.25
Der-54	fauna	–	2003	PP1	E9	11	986	0.37
Der-55	fauna	F14/39	2002	PP2	F14	3	922	2.20
Der-56	fauna	F14/74	2002	PP2	F14	6	852	1.89
Der-57	fauna	F14/105	2002	PP2	F14	9	927	0.66
Der-58	fauna	F14/124	2002	PP2	F14	9	901	0.26
Der-59	fauna	F14/114	2002	PP2	F14	11	882	0.90
Der-66	fauna	F13/150	2002	PP2	F13	9	936	0.23
Der-71	fauna	E13/86	2002	PP2	E13	11	715	1.12
Der-72	fauna	E13/86	2002	PP2	E13	11	445	0.71
Der-73	fauna	E13/59	2002	PP2	E13	9	651	0.80
Der-74	fauna	–	2002	PP2	E13	9	793	1.01

containing 'leaf points', and material lower than 230 cm as below the 'leaf point' industry and possibly associated with the blade endscraper/perforator (see fig. 12.11-b.5) found at 240 cm depth (Davies and Hedges, 2005). The same division was initially retained for easier comparison. However, layer 11 is found higher up in PP1 than in PP2. This appears to be reflected in the data (see fig. 12.14-b). Only PP2 shows anthropogenically modified fauna at a depth lower than 230 cm. This suggests that human activity leaving traces on bone is concentrated in the upper part of the geological unit 11.

Nitrogen content of collected samples suggests reasonable collagen preservation, with only 62% of bone fragments tested passing the 0.7% threshold. Taking layer attribution and %N test results into account, 37 specimens were sampled for radiocarbon dating (see tab. 12.4). Bone fragments Der-03 to Der-28 were drilled at the museum. Samples no. Der-49 to Der-74 were cut with a diamond saw at the museum and later surface cleaned with an air abrader containing aluminium oxide powder, and crushed in an iron mortar at ORAU. Der-09 was selected for auto-duplication on the basis that its P-number was a multiple of 20 (standard ORAU quality control measure).

The faunal samples were treated with ORAU's AG protocol, then freeze-dried. Whenever possible the samples were re-hydrolysed, before continuing the AF protocol for ultrafiltration (see section 5.4). No solvent wash steps were necessary, as the fragments had not been conserved since excavation.

24 possible osseous points were tested for nitrogen concentration (see tab. 12.4 and 12.5). Der-01 was collected from the Hungarian National Museum in Budapest. It is the only point found by Hillebrand, originally attributed to his layer 5, but more likely belonging to layer 4 (would be equivalent to Kaminská's layer 9, see fig. 12.9). The Prošek points Der-29 to Der-48 are stored at the Archaeological Institute of the Slovakian Academy of Sciences in Nitra (AU SAV). They were found in Prošek's layer 8, which is likely to correspond to Kaminská's layer 9 (see fig. 12.9). The points Der-02 and Der-27, from the most recent excavation, come from layers 7 and 3, respectively, and are kept at the Natural History Museum in Bratislava.

Table 12.5: Dzeravá Skala: list of osseous points tested for nitrogen content, but not sampled for ^{14}C dating. Sample weight in mg. Typological identification by B. Hromadová: SBP = split-base point; MBP = massive-base point. * – original layer numbering: Prošek 8 largely corresponds to layer 9.

Ref-no.	Item	Inv.-no.	Excav.	Trench	Sq.	Layer	Weight	%N
Der-02	SBP/MBP	F13/145	2002	PP2	F13	7	0.16	3.51
Der-27	round point	F11/65	2002/03	PP1	F11	3	0.12	2.27
Der-30	blank	II A5/105	1950	Prošek	–	8*	0.30	2.10
Der-31	point	IVb/160?	1950	Prošek	–	8*	0.28	3.53
Der-34	point	IIA4/175	1950	Prošek	–	8*	0.55	4.00
Der-37	MBP	IV.a/168	1950	Prošek	–	8*	0.44	2.18
Der-40	point	IIIa/180	1950	Prošek	–	8*	0.43	1.49
Der-41	SBP	–	1950	Prošek	–	8*	1.90	5.35
Der-42	SBP	A1/57?	1950	Prošek	–	8*	1.41	2.88
Der-43	SBP	–	1950	Prošek	–	8*	2.69	4.40
Der-44	SBP	A2/175	1950	Prošek	–	8*	1.31	2.96
Der-45	point/awl?	43	1950	Prošek	–	8*	0.93	2.5
Der-46	point	–	1950	Prošek	–	8*	1.49	1.40
Der-47	point	–	1950	Prošek	–	8*	0.68	2.66
Der-48	SBP	–	1950	Prošek	–	8*	2.90	1.76

Finally, 8 possible osseous points were sampled for radiocarbon dating using the key-hole drilling technique (see tab. 12.4). The selection for dating was based on %N results, as well as ease of sampling. It did not focus on SBP, but on assessing the osseous assemblage as a whole. Regrettably, drilling of Der-02 and Der-27 could not be arranged, despite the promising %N results and the fact that these two points were the only ones not previously treated with PVA. The round cross-section of Der-27 is consistent with other points dated to the Gravettian and Magdalenian, and thus with the age expected for layer 3. The triangular shape and oval cross-section of Der-02, on the other hand, suggests it might chronologically belong to the Prošek points. Therefore, it will be important to date this specimen in the near future.

The chemical pre-treatment for osseous points included an initial solvent wash protocol, as the artefacts showed all the signs of conservation and restoration treatment. After AG* treatment, further procedure was determined by gelatine yield: hydroxyproline dating (i.e. NRC) for yield $>$ 20

mg, ultrafiltration (AF*) for 10–20 mg yield, and no further treatment in cases of <10 mg gelatine. In cases where yield exceeded 30 mg, enough AG* collagen was retained for a small graphite target (0.8 mgC) before further preparation to allow for a direct age comparison. Four points had previously been sampled for radiocarbon dating – labelled as Dz Sk 8, Dk Sk 9, Dk Sk 10, and Dk Sk 11 (Davies and Hedges, 2005). These might correspond to Der-31, Der-38, Der-40 and Der-41 based on traces found on the artefacts. However, no published record of which sample corresponds to which label were found.

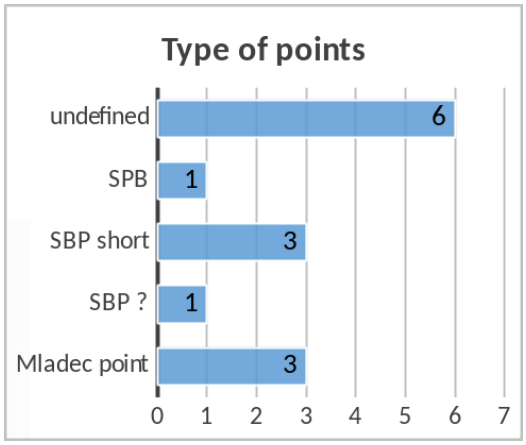


Figure 12.15: Dzeravá Skala: overview of point fragments found in 1950 listed according to typological identification by B. Hromadová. SPB = split-based point. Mladec point = massive-based points.

The original identification of the points as either 'Mladeč' or SBP type has been questioned (Horusitzky, 2008). Therefore, Bibiána Hromadová re-analysed the collection from Prošek's 1950 excavation. Permission was given to include part of her presently unpublished findings in this thesis (see also artefact description below). From the 21 osseous point fragments identified by Prošek, only 14 could be relatively securely connected to spear points (including blanks, and half-products, see tab. 12.4 and 12.5, and fig. 12.15). The nature of the others is presently difficult to determine. All artefacts were surface coated as part of their conservation treatment, most likely using PVA. Some points show further reconstructions with a combination of gypsum (for sculpting missing sections), and paint (for colouring restored areas). The ap-

plication of gypsum, glue and PVA, combined with the reconstruction style, suggests that the work had been done in the 1950s – conceivably by Prošek's team – but later treatment cannot be excluded.

Der-01 meseo-distal fragment of a split-based point (Horusitzky, 2008, p.217–218, fig. 19). The artefact is preserved on a length of 64 mm, with a maximum width of 16 mm and a maximum thickness of 9.2 mm. Both Horusitzky (2008) and Hillebrand (1914) have classified the fragment as belonging to a split-based point, despite the missing base. Horusitzky (2008) draws parallels to the single SBP found at Potočka zijalka (see fig. 12.16).



Figure 12.16: Potočka zijalka: SBP (Moreau et al., 2015).

The artefact has the museum inventory number 'Pb/579.' written on its surface with black ink, and seems coated in a shiny substance (possibly PVA). The artefact was sampled from the proximal end using key-hole drilling, with initial cleaning of the surface at the sampling location.

Der-29 10 cm long rod fragment with very regular proportions and surface shaping. Cross-section is circular. Both extremities are broken (step fractures). It is made from the compact tissue of a massive bone. There are traces of shaping on the surface: longitudinal lines and traces of scraping. A all visible traces belong to the final stages of the manufacturing process, it remains unclear how exactly this artefact had been made (B. Hromadová, pers. comm. 30/4/2018). The fragment could belong to a longer, massive spear point with circular cross-section, as it is interpreted by Kaminská et al. (2005b). The artefact was sampled from the distal end, using key-hole drilling.

Der-32 mesial or mesio-proximal antler (?) point fragment without preserved apex. Rests of the cancellous tissue is preserved on the dorsal surface. Both extremities are broken (hinge fracture). Lateral part shows traces of scraping after lateral flattening. The cross-section is elliptic, with a flatter shape of the proximal part. The fragment is preserved on a length of 95 mm, with a maximal width of 21 mm and a maximal thickness of 11 mm. Point type cannot be determined. Best description would be fusiform (B. Hromadová, pers. comm. 30/4/2018).

Remains of a museum number in black ink is partially visible on the artefact surface. Conservative surface coating was applied to the entire point fragment (possibly PVA). The artefact was sampled using key-hole drilling from the proximal end.

Der-33 point blank / raw point made from antler compact tissue with plano-convex cross-section. The object is 111 mm long, 35 mm wide and *ca.* 10 cm width. The piece is slightly torsed along its longitudinal axis. The poorly preserved surface and cancellous tissue are indicative of antler, rather than bone material. Both extremities are broken (compress damage and compressive fracture?). The compact tissue is patchily worked and flattened, though no traces of scarping are visible. General shape, size and thickness of the object suggests it belongs to an unfinished product of the point debitage, most likely a point blank (B. Hromadová, pers. comm. 30/4/2018).

The fracture is glued and reconstructed, including some cosmetic work with gypsum and paint. The object is shows a conservative surface coating (possibly PVA). On the proximal fracture, a museum number is written in black ink on a reconstructed surface. It is unclear, whether any previous sampling took place at that location. Consequently, the artefact was sampled for radiocarbon dating from the distal end, using key-hole drilling.

Der-35 mesial fragment of an antler point (Horusitzky, 2008, p. 218, fig. 20). The artefact consists of three refitted fragments, and is preserved over a

length of 132 mm, with a maximal width of 196 mm and a maximal thickness of 72 mm. Horusitzky (2008) classifies the point as having a '*pointe à base trouées*' (perforated base). However, the mesial and proximal part show severe damage of the medial surface, which could result in the half-circle shaped puncture / indention observed at the proximal end. Overall shape and fractured proximal end would also allow a classification as a split-based point.

On the distal part, the artefacts number is partially visible in black. The three fragments were refitted and glued, and the surface treated with a shiny coating (possibly PVA). However, the distal and mesial fragment detached. As a result it was possible to sample the distal fragment using key-hole drilling from its proximal end, leaving the surface – and the points critical base fracture – intact. Special care was taken to first clean the sampling surface through abrasion.

Der-36/37 near complete massive-based point (Mladeč?). The artefact consists of two glued fragments and is presently 151 mm long – though 33 mm from the mesial part are completely reconstructed with gypsum. The distal extremity is damaged (step fracture). The mesial part of the point is slightly extended, with a elliptic cross-section. Mesial and proximal parts are covered in traces of scraping, related to the shaping of the point. The dorsal surface is flattened by scrapping, with visible structures of the cancellous tissue. The proximal extremity is broken (disintegrated?), cause unknown (B. Hromadová, pers. comm. 30/4/2018).

The fragments most likely belong to a point with massive simple base. However, Horusitzky (2008, p.229) identifies the artefact as a '*pointe à base trouées*' (point with perforated base), as he identifies a 'half-hole' in the base. Considering the state of preservation and form of the fracture, it could be fruitful to compare the artefact with other faunal remains at the site, especially considering gnawing by carnivorous animals.

Der-37 has its museum number written in black ink, close to the proximal fracture. If Der-36 was ever directly labelled, the ink or the writing impres-

sion not visible. Both fragments were sampled for %N testing: Der-36 at its proximal fracture where the fragment used to be connected to the gypsum reconstruction, and Der-37 from its proximal end (see tab. 12.4 and 12.5). However, only Der-36 was selected for radiocarbon dating, applying key-hole drilling at the previous sampling location.

Der-38 near complete massive-based point (Mladeč?) made from antler. The artefact is preserved on a length of 172 mm. Both extremities are damaged. The distal part is flattened and shows signs of gnawing as a result of being chewed on by a carnivorous animal. This damage explains the unusual shape of the distal extremity and the lack of manufacturing traces. The mesial and proximal part have a elliptic cross-section, and are covered in traces of scraping, probably from shaping the object. There is a isolated series of short cuts visible on the proximal part, mostly on the lateral and frontal surface. The mesial part is massively extended with rounded divergent boards. Proximal end shows a massive simple base, which is damaged by chewing and gnawing by a carnivore. The artefact is fragmented into two major sections. Several small breakages, as well as the missing part of the point is reconstructed using gypsum (B. Hromadová, pers. comm. 30/4/2018).

The artefact was surface treated, probably using PVA, and the proximal fragment had previously been sampled for radiocarbon dating. To allow for a better comparison of dating reliability, this project also sampled the proximal fragment from its distal end. The sampling surface area was carefully cleaned to avoid contamination from glue, and PVA coating. Subsequent key-hole drilling had to carefully avoid previous sampling location. Regrettably, the very soft texture of the artefact caused a small splinter to separate from the artefacts surface. Contamination of the ^{14}C sample was avoided, though the artefact's surface was damaged.

Der-39 near complete massive-based point (Mladeč?) made from antler. The artefact is made up of three joining fragments, and preserved on a total

length of 204 mm, with a maximum width of 24 mm (mesial part) and an elliptical cross-section of the base. It is the largest MBP found at Dzeravá Skala to date. The proximal part is damaged. Nonetheless, a simple massive base is discernible, with clear longitudinal, linear traces of scraping (flattening of surface and edges). The mesial part is massive and slightly extended, with an elliptical cross-section. The distal extremity (apex), shows a recent break, and there are traces of scraping (flattering of the surface and removing of cancellous tissue) visible. Underlying these, there are longitudinal traces of re-sharpening. In the mesial part, only traces of shaping and flattening of the surface remains visible. The three fragments were glued and reconstructed using gypsum (B. Hromadová, pers. comm. 30/4/2018).

The museum number was written in black ink on the narrow side of the mesial fragment, and the artefact surface was coated in consolidation material (probably PVA). The proximal fragment was sampled, using key-hole drilling from its distal end, for radiocarbon dating. The sampling surface was thoroughly cleaned before drilling, to avoid contamination with glue from where the fractures used to be joined.

^{14}C Results

Three samples failed pre-treatment (see tab. 12.6 and 12.8): Der-01 dissolved fully during the acid-base-acid washes. Der-54, Der-58 and Der-66 – all samples selected because of their strategic position in PP2, and despite their low %N results – had AG gelatine yields significantly lower than 1 wt.%, and insufficient in absolute terms for ultrafiltration. As they did not belong to artefacts, it was deemed problematic to date them.

A single non-artefact (Der-49) yielded insufficient gelatine for ultrafiltration and had to be dated as AG. Nonetheless, the observed low C:N ratio of 2.9 is not a result of poor sample quality. The sample was combusted on mass-spec run no. 4951, which had nitrogen calibration issues. The laboratory background samples showed an identical reduction in C:N ratio, without having their radiocarbon age affected (see Appendix). The same

Table 12.6: Dzeravá Skala: new AMS radiocarbon results on anthropogenically modified bone (Der-01 – Der-17) with archaeological context information, and pre-treatment results. Failed samples in grey. Ref-no. = number given to the sample for the purpose of this project. %N = nitrogen weight content before chemical pre-treatment. Treat. = Pretreatment protocols used (see section 5.4). Yield = sample left after chemical pre-treatment (both in mg and wt.%). %C = carbon yield on combustion. C:N = carbon to nitrogen ratio of combusted collagen sample. $F^{14}C$ = fraction modern carbon. ^{14}C (BP) = conventional radiocarbon age Before Present with 1σ error. Date (cal BP) = calibrated radiocarbon age at a 95.4% confidence interval, calculated in OxCal 4.3 (Bronk Ramsey, 2009a) using IntCal13 (Reimer et al., 2013).

Ref-no.	Item	Trench	Sq.	Layer	Depth (cm)	%N	Treat.	Yield (mg)	Yield (wt.%)	%C	$\delta^{15}N$	$\delta^{13}C$	C:N	Lab-no	$F^{14}C$	^{14}C (BP)	Date (cal BP)
Der-01	point	Hillebrand	–	*4/5**		0.10	AG*	0.00	0.00	–	–	–	–	–	–	–	–
Der-03	fauna	PP1	E11	11	175-185	0.91	AF	9.05	1.49	41.3	4.4	-22.0	3.2	OxA-34012	0.01004 ± 0.00103	37000 ± 800	42755 – 40080
Der-03	faunal	PP1	E11	11	175-185	0.91	AF	38.66	3.93	42.4	4.6	-22.2	3.2	OxA-35232	0.01123 ± 0.00099	36050 ± 700	41970 – 39270
Der-06	faunal	PP1	E10	9	120-125	2.79	AF	28.42	4.39	41.8	2.9	-21.2	3.2	OxA-34013	0.04424 ± 0.00109	25050 ± 200	29570 – 28660
Der-09	faunal	PP1	E11	9	130-135	1.06	AF	10.66	2.04	41.4	2.4	-22.1	3.2	OxA-34014	0.02849 ± 0.00108	28580 ± 300	33450 – 31670
Der-09	faunal	PP1	E11	9	130-135	1.06	AF	8.80	1.69	40.9	2.3	-22.1	3.2	OxA-34015	0.02769 ± 0.00108	28810 ± 310	33685 – 31927
Der-10	faunal	PP1	E11	9	150-155	1.03	AF	14.80	1.99	41.1	3.9	-18.8	3.2	OxA-34016	0.02351 ± 0.00104	30130 ± 360	34820 – 33640
Der-12	faunal	PP2	F13	7	115-120	1.93	AF	23.18	3.50	42.4	4.4	-19.2	3.3	OxA-34017	0.01225 ± 0.00102	35350 ± 650	41350 – 38660
Der-13	faunal	PP2	Profile	7	119	2.07	AF	4.80	0.81	41.3	1.7	-21.6	3.2	OxA-34018	0.00808 ± 0.00106	38700 ± 1100	44950 – 41290
Der-14	faunal	PP1	E10	5	110	3.41	AF	33.83	5.86	41.9	2.5	-21.2	3.2	OxA-34019	0.04365 ± 0.00109	25160 ± 200	29700 – 28730
Der-15	faunal	PP1	E10	5	110	2.28	AF	50.45	8.21	42.5	3.3	-21.5	3.2	OxA-34020	0.04511 ± 0.00110	24890 ± 200	29440 – 28520
Der-17	faunal	PP1	E10	5	100-105	3.22	AF	80.58	11.01	42.6	2.3	-21.5	3.2	OxA-34021	0.04440 ± 0.00111	25020 ± 200	29540 – 28640

Table 12.7: Dzeravá Skala: new AMS radiocarbon results on anthropogenically modified bone (Der-18 – Der-36) with archaeological context information, and pre-treatment results.

Ref-no.	Item	Trench	Sq.	Layer	Depth (cm)	%N	Treat.	Yield (mg)	Yield (wt.%)	%C	δ^{15}N	δ^{13}C	C:N	Lab-no	F^{14}C	^{14}C (BP)	Date (cal BP)
Der-18	faunal	PP1	E10	9	125-130	1.65	AF	27.82	3.75	41.6	5.8	-19.5	3.2	OxA-34022	0.02546 ± 0.00106	29490 ± 340	34280 – 32900
Der-20	faunal	PP1	E10	9	125	3.12	AF	46.78	5.18	43	2.0	-21.3	3.2	OxA-35233	0.04450 ± 0.00105	25000 ± 190	29510 – 28640
Der-21	faunal	PP1	E10	8	110-115	1.98	AF	54.88	7.77	41.5	3.4	-21.4	3.2	OxA-34023	0.04575 ± 0.00113	24780 ± 200	29340 – 28390
Der-23	faunal	PP1	E10	4	82	2.26	AF	51.76	7.65	42.1	4.8	-22.0	3.2	OxA-34024	0.04608 ± 0.00112	24720 ± 200	29270 – 28320
Der-24	faunal	PP1		4a	114	3.00	AF	76.75	11.72	41.7	3.4	-21.5	3.2	OxA-34025	0.04552 ± 0.00113	24820 ± 200	29270 – 28320
Der-25	faunal	PP1	E11	9	170-175	2.78	AF	74.93	9.28	41.6	2.8	-21.9	3.2	OxA-34026	0.00678 ± 0.00102	40100 ± 1200	46270 – 42150
Der-26	faunal	PP1	E11	4	80-85	2.69	AF	48.08	8.79	41.4	3.1	-21.2	3.2	OxA-34027	0.0447 ± 0.00113	24960 ± 200	29490 – 28590
Der-28	faunal	PP1	F11	11	185-190	1.64	AF	24.68	2.97	44.6	3.2	-22.0	3.2	OxA-34028	0.00678 ± 0.00102	40100 ± 1200	46270 – 42150
Der-29	point	Prošek	–	*8**	–	1.80	AG*	33.02	8.22	40.8	3.9	-18.5	3.1	OxA-35597	0.03479 ± 0.00149	26980 ± 340	31510 – 30580
Der-29	point	Prošek	–	*8**	–	1.80	NRC	0.9491 mgC	–	33.9	3.7	-25.5	4.9	OxA-X-2732-13	0.02938 ± 0.00136	28340 ± 370	33320 – 31400
Der-32	point	Prošek	–	*8**	–	0.84	AG*	17.69	5.29	40.1	7.1	-20.2	3.1	OxA-35598	0.03151 ± 0.00146	27770 ± 370	32690 – 31050
Der-32	point	Prošek	–	*8**	–	0.84	AF*	12.43	3.72	40.9	7.3	-19.6	2.9	OxA-X-2719-20	0.02788 ± 0.00105	28760 ± 300	33640 – 31880
Der-32	point	Prošek	–	*8**	–	0.84	AF*	12.43	3.72	41.6	6.8	-20.5	3.3	OxA-35699	0.03625 ± 0.0011	26650 ± 240	31190 – 30460
Der-33	point	Prošek	–	*8**	–	1.00	AG*	1.60	0.39	39.1	7.3	-20.1	3.7	OxA-X-2716-51	0.0463 ± 0.00223	24680 ± 390	29600 – 27890
Der-35	point	Prošek	–	*8**	–	0.68	NRC	1.0175 mgC	–	34.8	3.7	-24.6	4.9	OxA-X-2732-14	0.01195 ± 0.00130	35560 ± 870	41870 – 38550
Der-36	point	Prošek	–	*8**	–	0.68	AG*	3.70	0.94	41.6	7.4	-20.5	3.4	OxA-35387	0.04374 ± 0.00142	25140 ± 260	29870 – 28620

Table 12.8: Dzeravá Skala: new AMS radiocarbon results on anthropogenically modified bone (Der-38 – Der-74) with archaeological context information, and pre-treatment results. Failed samples in grey.

Ref-no.	Item	Sq.	Layer	Depth (cm)	%N	Treat.	Yield (mg)	Yield (wt.%)	%C	δ^{15}N	δ^{13}C	C:N	Lab-no	F^{14}C	^{14}C (BP)	Date (cal BP)
Der-38	point	–	–	–	3.06	AG*	31.53	5.88	40.3	7.9	-20.3	3.1	OxA-35599	0.02237 ± 0.00145	30550 ± 500	35560 – 33750
Der-38	point	–	–	–	3.06	NRC	1.3306 mgC	–	37.4	7.2	-26.8	4.9	OxA-X-2732-15	0.01709 ± 0.00133	32690 ± 620	38500 – 35470
Der-39	point	–	–	–	1.13	AG*	25.23	3.94	39.2	8.0	-21.0	3.1	OxA-35524	0.02241 ± 0.0012	30500 ± 450	35390 – 33770
Der-39	point	–	–	–	1.13	NRC	1.5094	–	41.8	7.0	-27.8	4.9	OxA-X-2732-16	0.01692 ± 0.00138	32770 ± 660	38640 – 35470
Der-49	faunal	F9	9	200-210	1.09	AG	7.49	1.17	39.2	2.0	-21.6	2.9	OxA-35581	0.00855 ± 0.00118	38300 ± 1100	44660 – 40870
Der-53	faunal	F10	11	220-230	1.25	AF	34.44	4.31	43.9	2.1	-21.4	3.2	OxA-35240	0.00801 ± 0.00099	38800 ± 1000	44750 – 41510
Der-54	faunal	E9	11	200-210	0.37	AG	5.24	0.53	–	–	–	–	–	–	–	–
Der-55	faunal	F14	3	40-45	2.20	AF	62.20	6.74	44.0	3.1	-21.4	3.2	OxA-35241	0.04620 ± 0.00106	24700 ± 180	29190 – 28330
Der-56	faunal	F14	6	85-90	1.89	AF	46.30	5.43	44.2	3.7	-22.4	3.2	OxA-35242	0.0158 ± 0.00101	33300 ± 500	38730 – 36290
Der-57	faunal	F14	9	160-170	0.66	AF	5.54	0.60	39.1	5.3	-21.9	3.3	OxA-X-2717-18	0.01649 ± 0.00121	33000 ± 600	38700 – 35820
Der-58	faunal	F14	9	140-150	0.26	AG	0.65	0.53	–	–	–	–	–	–	–	–
Der-59	faunal	F14	11	190-200	0.90	AF	29.93	3.39	41.8	2.8	-21.4	3.2	OxA-35759	0.00570 ± 0.00100	41500 ± 1400	48410 – 42860
Der-66	faunal	F13	9	150-160	0.23	AG	2.83	0.30	–	–	–	–	–	–	–	–
Der-71	faunal	E13	11	220-230	1.12	AF	51.36	7.19	42.5	2.0	-21.2	3.2	OxA-35760	0.0024 ± 0.00098	48500 ± 3300	> 49800
Der-72	faunal	E13	11	220-230	0.71	AF	10.92	2.46	40.6	3.6	-22.0	2.6	OxA-35582	0.01052 ± 0.00102	36600 ± 800	42490 – 39680
Der-73	faunal	E13	9	170-180	0.80	AF	10.92	1.68	41.9	2.9	-21.9	3.2	OxA-35761	0.00618 ± 0.00100	40900 ± 1300	47490 – 42540
Der-74	faunal	E13	9	160-170	1.01	AF	52.03	6.56	40.5	2.7	-22.6	2.9	OxA-35583	0.00713 ± 0.00100	39700 ± 1100	45630 – 42030

effect can be observed for Der-74, and for one of the Der-32 (AF*) measurements. Assuming 2.9 to be the expected C:N ratio for burn no. 4951, the result for Der-72 would have to be seen as slightly decreased, and that for Der-32 (AG*) somewhat elevated. However, both measurements would remain within observable variation. Der-57 shows a minimally elevated C:N of 3.3 (expected value 3.2), though well within margin of error. All other pre-treatment results for anthropogenically modified fauna (excl. artefacts) suggest no quality issues. The auto-duplicate Der-03 provides statistically indistinguishable results not only for the radiocarbon measurement, but also %C on combustion, stable isotope values, and C:N ratio.

Reviewing the results obtained on osseous points (including Der-29 to Der-39), two samples appear to be problematic: Der-32 and Der-33. The latter yielded a bare 0.39 wt.% gelatine with an elevated C:N ratio on combustion of 3.7 (expected value 3.2), albeit stable isotope values comparable to the other osseous artefacts dated. Consequently, the resulting radiocarbon measurement should be treated as a minimum age estimate only.

The OxA-X attribution for OxA-X-2719-20 (Der-32) resulted from the seemingly low C:N ratio, and was given prior to further analysis of burn no. 4951 (see above). The actual issue with Der-32 is not readily visible in the pretreatment results. The C:N ratio of all three samples lie within expectations. Looking at stable isotopes, the nitrogen values of OxA-35598 agree with OxA-X-2719-20, while the carbon values of the former compare to OxA-35699. However, the two AF* treated targets resulted in two statistically distinguishable radiocarbon measurements (see fig. 12.17-a). Especially concerning is the fact that the AF* treated target OxA-35699 (26650 ± 240 BP) shows a younger radiocarbon age than the AG* target OxA-35598 (27770 ± 370 BP). To visualise the impact of this age disagreement, two `R_Combine` versions were run in OxCal 4.3. The first only included the two ages with significant age overlap (OxA-35598 and OxA-X-2719-20) and was labelled '2/3'. The second combined all three radiocarbon measurements. Der-32 (2/3) gives an age estimate of 33080 – 31580 cal BP (χ^2 test: df=1, T=4.2, 5%=3.8), Der-32 (all) of 31820 – 31140 cal BP (χ^2 test: df=2,

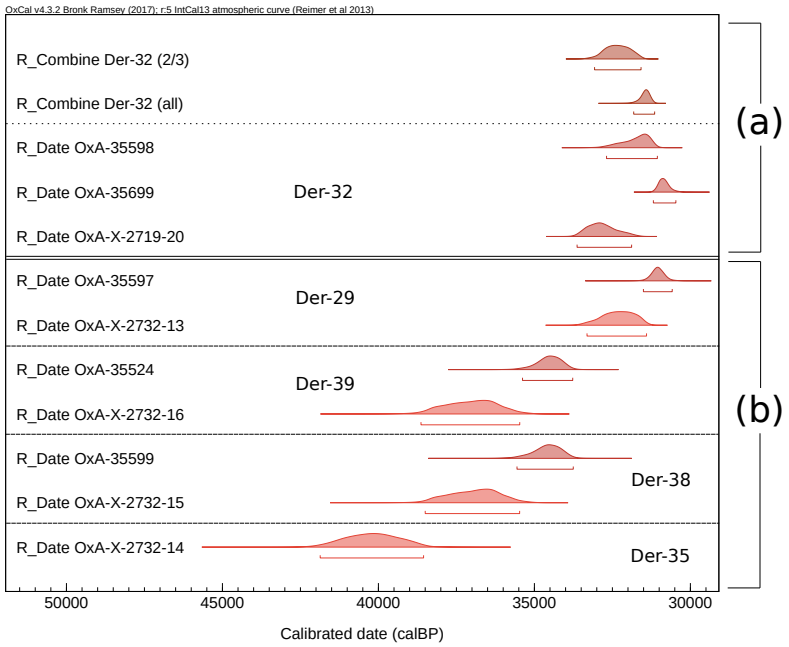


Figure 12.17: Dzeravá Skala: comparison of osseous point radiocarbon dates obtained on the same sample. (a) Der-32: AG* (OxA-35598) and AF* (OxA-35599 and OxA-X-2719-20); `R_Combine` 'Der-32 (2/3)' uses OxA-35598 and OxA-X-2719-20, 'Der-32 (all)' all three measurements. (b) Comparisons of AG* (top) and hydroxyproline (bottom) dates for Der-29, Der-38, and Der-39; Der-35 included for comparison of NRC results.

T=31.1, 5%=6.0). This work will use Der-32 (2/3) to represent the age of the artefact Der-32. This is based on two assumptions: (1) reliable dates show agreement, and (2) dates on AG* treated material are expected to be younger than those on AF* treated samples. It should, however, be noted, that this age is only an estimate and does not appear to be a reliable measurement. Presently, it remains unclear whether the true age is slightly older or younger.

The samples Der-29, Der-38 and Der-39 had very good collagen preservation. All three artefacts could both be dated as AG* and NRC (hydroxyproline). The resulting radiocarbon measurements are compared in fig. 12.17-b. As expected, the hydroxyproline ages are older than the AG* results. The increased standard error is not related to the graphite target size – each pre-

treatment led to small graphite targets (0.8 mgC). It is associated with the HPLC background correction (see subsection 5.4.7). All further work will be based on the NRC results, rather than the AG* results.

If Der-38 does indeed correspond to 'Dk Sk 8', the three ages would fall within expectations: AG* provides the youngest date (OxA-35599 30550 ± 500 BP), NRC the oldest (OxA-X-2732-15 32690 ± 620 BP), and AF in-between (OxA-15334 31600 ± 900, OxA-15335 31000 ± 1100). The single amino acid date will be preferred on the basis of chemical purity, though it is worth noting that it is not statistically distinguishable from the AF measurement.

Collagen preservation for Der-35 was also very good (28.51 mg = 5.52 wt.%), but as the yield was below 30 mg, the sample was only hydroxyproline (NRC) dated. In future, it might be worth considering reducing the threshold to 25 mg, considering the reasonable amount of carbon retrieved (1.0175 mg) and usefulness of a direct age comparison.

The only 'point' sample showing poor collagen preservation was Der-36. Its yield was just below 1 wt.% at AG*. As an artefact (massive-based point), it was still dated, though the result should be treated as a minimum age estimate only.

12.1.3 Bayesian modelling

In this section, the Bayesian models applied to Dzeravá Skala are described. Their results and archaeological interpretations will be further discussed in section 12.1.4. The actual code used can be found in catalogue B.6.

Two main modelling approaches were used to account for the complexity of the site: (1) Constraining the radiocarbon dates using stratigraphic information as priors, and (2) using the radiocarbon age distribution as a means of identifying periods of activity at the site irrespective of their layer attribution. The aim was to test the chronological integrity of the stratigra-

phy, estimate boundaries between layers, and chronologically contextualise the lithic and osseous industries.

For all osseous points that were hydroxyproline dated, the NRC results were used instead of the less reliable AG* ages, i.e. OxA-X-2732-13 for Der-29, OxA-X-2732-14 for Der-35, OxA-X-2732-15 for Der-38, and OxA-X-2732-16 for Der-39 (see section 12.1.2 and fig. 12.17). The point Der-32 is represented using `R_Combine` of only OxA-35598 and OxA-X-2719-20.

In cases of samples that were dated with the same protocol twice, `R_Combine` was used to implement the sample as a single event: Der-03 is composed of OxA-35232 and OxA-34013, Der-09 of OxA-34014 and OxA-34015, and the previously dated osseous point (Dz Sk 8) of OxA-15534 and OxA-15535. The latter, when added, is treated as an individual point, though it might be identical to Der-38.

There are some dates that extend beyond the range of the current calibration curve, despite having provided a finite radiocarbon age. If added to the model, they cause an artificial shortening of the phase by cutting off at 50k cal BP. Therefore, a workaround was implemented by adding the 2 sigma error to the calibrated younger limit at the 95.4% confidence interval, thus obtaining an estimated calibrated mean value. This is subsequently input in OxCal as the mean of a normal distribution with the original error value as the 1 sigma error (see results in box below).

There was one greater than age which was entered as a uniform distribution, using the original greater than value as the lower boundary, and 70000 cal BP as the artificial upper limit. In addition, the two OSL measurements were included using the `Date` function and a normal distribution in the calibrated age scale. For the exact code see grey box below.

```
K0082       Date("K0082 (OSL)",N(calBP(57000),4900))
K0085       Date("K0085 (OSL)",N(calBP(35900),3000))
OxA-13859   Date("OxA-13859",N(calBP(54200),2300))
OxA-13973   Date("OxA-13973",U(calBP(44600),calBP(70000)))
OxA-14247   Date("OxA-14247",N(calBP(55900),3000))
OxA-35760   Date("OxA-35760",N(calBP(56400),3300))
```

Site Stratigraphic Models

All stratigraphic models implement stratigraphic units (i.e. layers or industries) as separate `Phases` in a `Sequence`. For Models 1–10, OxCal 4.3's general outlier model was included to account for attribution uncertainties. In addition, the outlier model `SSimple` was included for dates placed in `R_Combine`. In both cases, each date was given the standard 0.05 outlier probability. The `Date` and `Interval` functions were placed within each `Phase`, and the latter also in between phases.

Several configurations of the stratigraphic model were run to investigate the effect of layer attribution issues in layers 9 and 11, as well as possible effects of the new layers 6, 7 and 8, and the introduction of samples not related to human occupation. An additional single `Phase` osseous point model was run for comparison purposes.

Model 1 uses the stratigraphic sequence as observed in the 2002/2003 excavation drawings: 11, 9, 8, 5, 4, 3. The `Phases` 6 and 7 were added in a separate `sequence`, as their relationship to layer 9 and 8 remain uncertain. The start `Boundary` of layer 7 was linked to the transition `Boundary` between layer 11 and 9, and the end `Boundary` of 6 to the transition `Boundary` between layer 8 and 5.

All new radiocarbon measurements on anthropogenically modified bones were included, and the new dates on osseous points were added to layer 9 (see fig. 12.18). Code listed on p. 723.

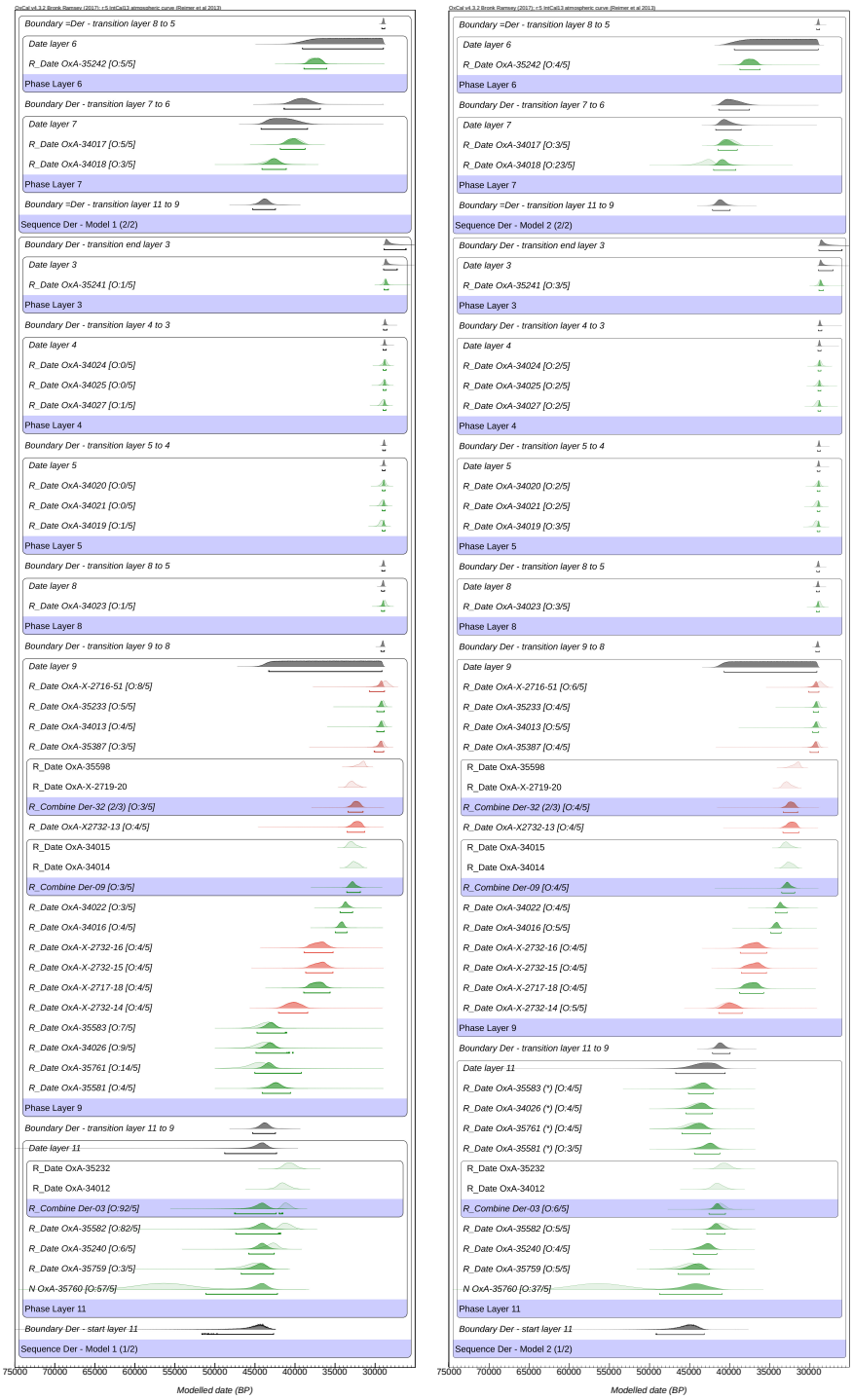


Figure 12.18: Dzeravá Skala: Stratigraphic Model 1 (left, code: p. 723) and Model 2 (right, code: p. 724). **green** – anthropogenically modified fauna; **red** – osseous points; **black** – modelled ages. Radiocarbon ages marked with (*) have been moved from layer 9 (original) to layer 11.

Model 2 applies the same sequence of phases and dates as Model 1. Considering the difficulty in identifying the limit between layer 9 and 11, this model moves the dates from the base of layer 9 (OxA-34026, OxA-35761, OxA-35583 and OxA-35581) to layer 11 in order to better quantify the effect on the boundary date between layer 11 and 9 (see fig. 12.18). The relocated dates are clearly marked with (*). Code listed on p. 724.

Model 3 adjusts the stratigraphic sequence from Model 1 by including the dates from layer 6 and 7 in `Phase` layer 9 to test what effect seeing layer 6 and 7 as part of layer 9 would have on the modelled boundaries. Sequence: 11, 9/7/6, 8, 5, 4, 3. Same radiocarbon dates on anthropogenically modified faunal bones and osseous points were included as seen in Model 1. Code listed on p. 726.

Model 4 is based on Model 3, but has OxA-34026, OxA-35761, OxA-35583 and OxA-35581 moved from layer 9 to 11 as seen in Model 2. The relocated dates re clearly marked with (*). Code listed on p. 728.

Model 5 abandons the dates attributed to layer 6 and 7, leaving a simple stratigraphical sequence: 11, 9, 8, 5, 4, 3. Otherwise, the dates and the phase attributions used are the same as in Model 1 and 3. Code listed on p. 729.

Model 6 is based on Model 5, with OxA-34026, OxA-35761, OxA-35583 and OxA-35581 moved from layer 9 to 11 as seen in Model 2. The relocated dates are clearly marked with (*). Code listed on p. 731.

Model 7 tests the influence the hypothesis of layer 8 belonging to layer 5 would have on the modelling outcome (see fig. 12.19). It uses the following simplified layer sequence: 11, 9, 5/8, 4, 3. The dates from layer 6 and 7 are excluded. Code listed on p. 732.



Figure 12.19: Dzeravá Skala: Stratigraphic Model 7 (left, code: p. 732) and Model 8 (right, code: p. 733). **green** – anthropogenically modified fauna; **red** – osseous points; **black** – modelled ages. Radiocarbon ages marked with (*) have been moved from layer 9 (original) to layer 11.

Model 8 is based on Model 7, with OxA-34026, OxA-35761, OxA-35583 and OxA-35581 moved from layer 9 to 11 as seen in Model 2 (see fig. 12.19). The relocated dates are clearly marked with (*). Code listed on p. 733.

Model 9 (OSL) implements a stratigraphy close to Model 1. Layers 11, 9, 5, 4, 3 are placed in one `sequence`. The second sequence is composed of the layers 7 and 6, with the start `boundary` of `Phase` 7 equated to the transition between `Phase` 11 and 9, and the end `boundary` of layer 6 to the transition between `Phase` 9 and 5. The floating position of layer 8 is avoided by excluding the `Date` and `Phase` from the Model.

In addition to the new radiocarbon measurements on anthropogenically modified fauna and osseous points, the previously published OSL dates K0082 and K0085 were included with the intent to examine the effect on layer 11's start `boundary` as well as general agreement between ^{14}C and OSL (see fig. 12.20). Code listed on p. 735.

Model 10 (all) focuses on testing the integrity of the stratigraphic sequence (see fig. 12.20). In addition to the radiocarbon ages obtained on anthropogenically modified faunal remains, previously obtained measurements on unmodified fauna with seemingly unambiguous layer attribution were added. This excludes Wk-14865 (labelled as coming from layer 9/5a'), as well as all the Poznan dates (unreliable measurement or layer attribution). GrA-22759 is excluded, as the relationship of layer 4b to the rest of the sequence is not secure. A more complex model could accommodate for such uncertainty, but would need a larger number of dates per layer. At the current state of dating, it would unnecessarily complicate the model without providing any additional security or precision. For the same reason, OxA-34023 and layer 8 are excluded.

To accommodate for all the dates, the `Sequence` was composed of following `Phases`: 11, 5a', 9, 5, 4, 3. Phases 6 and 7 were added in a separate phase, linking the start boundary of layer 7 to the transition between 5a'

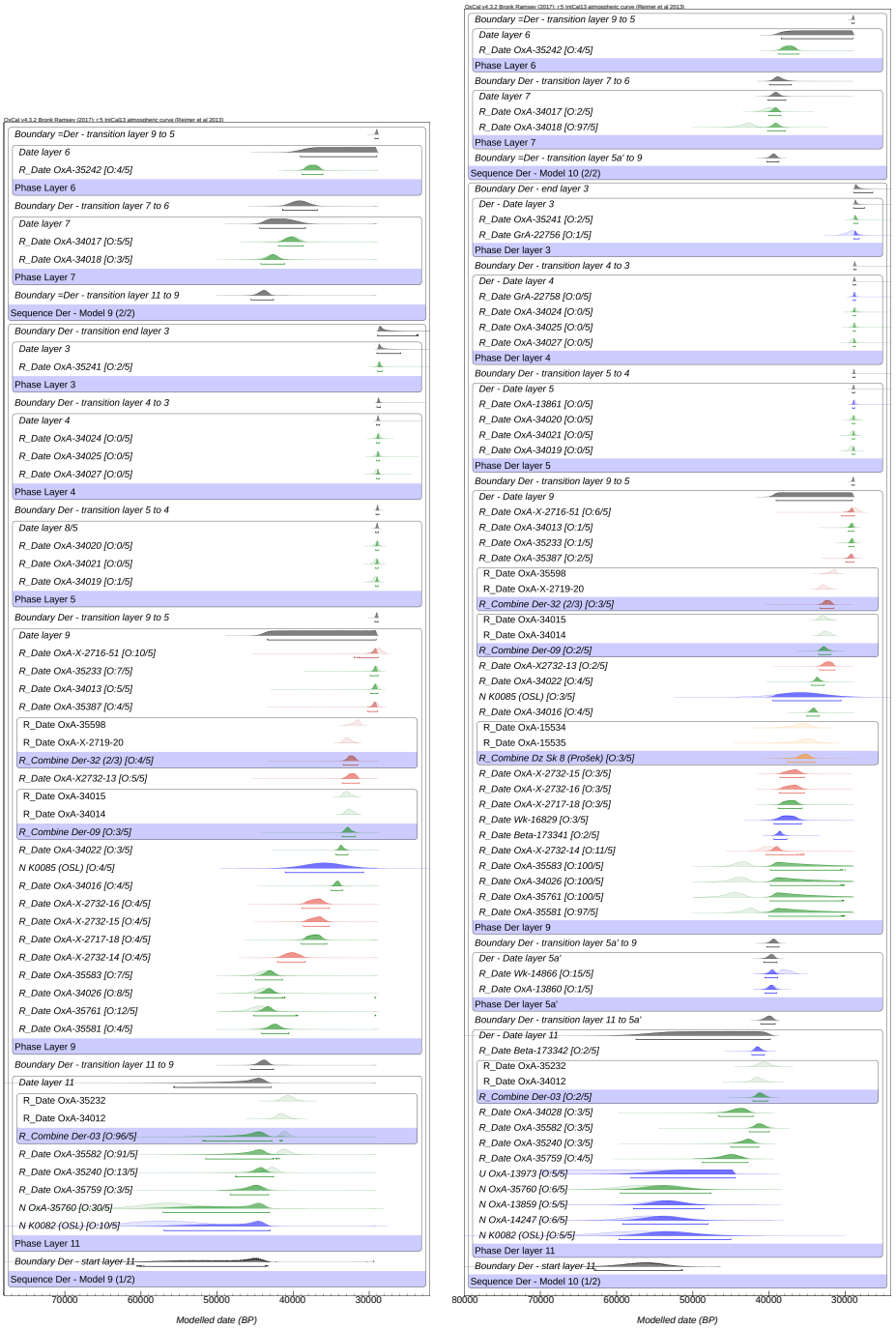


Figure 12.20: Dzeravá Skala: Stratigraphic Model 9 (left, code: p. 735) and Model 10 (right, code: p. 737). **green** – ^{14}C on anthropogenically modified fauna; **red** – new ^{14}C on osseous points; **orange** – previous ^{14}C on osseous points; **blue** – previously published age measurements, both ^{14}C dates from unmodified faunal bones and OSL ages; **black** – modelled ages.

and 9, and the end boundary of 6 with the transition between layer 9 and 5. The OSL ages K0082 and K0085 were added to Phase 11 and 9, respectively. Code listed on p. 737.

Points Model 1 attempts to obtain start and end boundaries of the occurrence of osseous points found in the 1950s, by placing the newly as well as previously obtained direct point dates in a single `Phase` between a start and end `Boundary`. Code listed on p. 739.

KDE Models

All KDE models run the `KDE_model` function, but on different radiocarbon datasets (see fig. 12.21). KDE 0 is run with previously obtained results to obtain age estimates for activity at the site. KDE 1 and KDE 2 are used to investigate temporal grouping of osseous points. KDE 3 investigates frequency of human activity at the site, which can then be compared to layer identifications and lithic industry groupings. Finally, KDE 4 runs all reliable radiocarbon measurements to visualise combined human and animal activity.

KDE 0 only uses the previously published radiocarbon dates from unmodified faunal bones (excluding the Poznan dates) to get a general idea of the activity timing at the cave (n=14). The model will not provide reliable information on occupation frequency as none of the dates are directly linked to human activity. The model contains the same workaround for ages beyond the calibration curve as the stratigraphic models and as illustrated at the beginning of the subsection (see grey box). Code listed on p. 739.

KDE 1 uses all direct dates on osseous points to test for possible temporal groupings. The results have to be treated with caution, as the number of dates included are few (n=8) and there is reason to be believe that some dates might be minimum age estimate only. Code listed on p. 740.

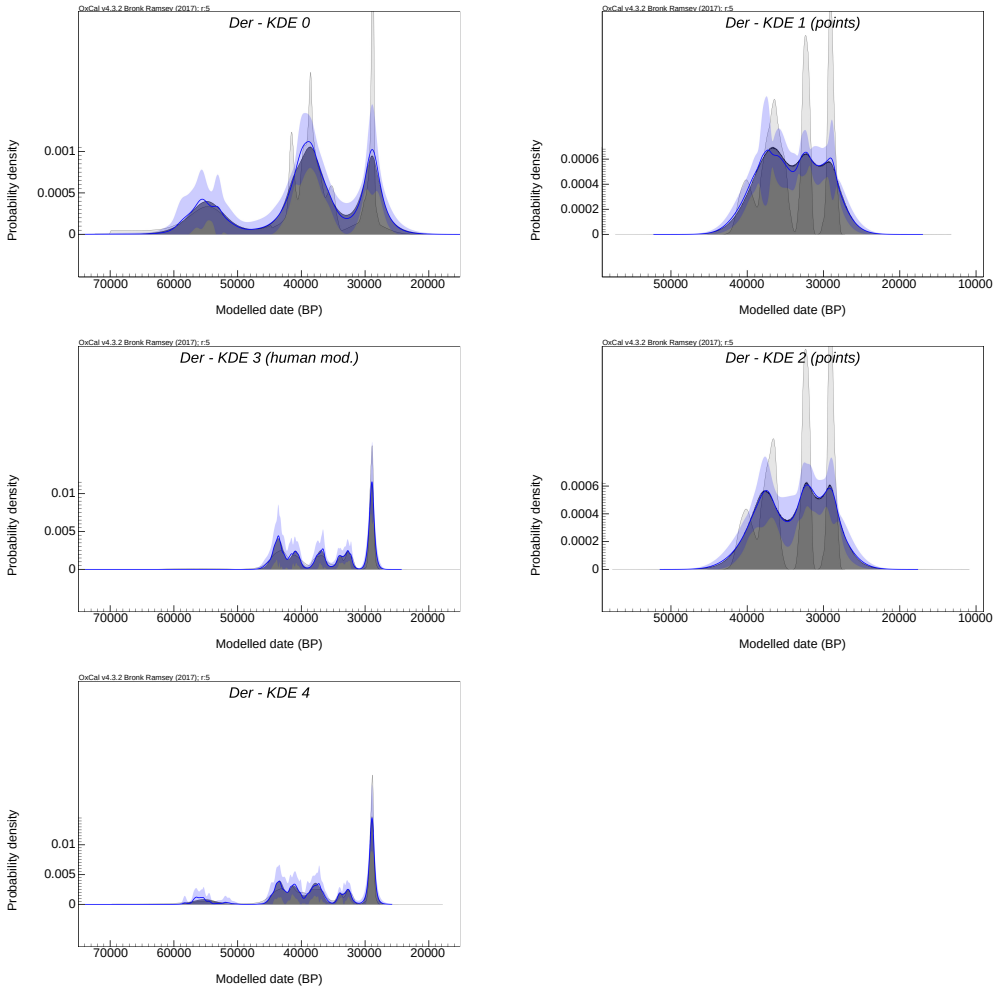


Figure 12.21: Dzeravá Skala: comparison of KDE models. KDE 0 (previously published radiocarbon dates, n=14, code: p. 739), KDE 3 (new radiocarbon dates on anthropogenically modified fauna, n=35, code: p. 740) and KDE 4 (new and old radiocarbon data, n=47, code: p. 742) investigate different activity frequencies at the site. KDE 1 (all dates on osseous points, n=8, code: p. 740) and KDE 2 (only new dates on osseous points, n=7, code: p. 740) focus on the timing of osseous point industries.

KDE 2 restricts the model to the newly measured direct radiocarbon dates on osseous points (n=7), under the assumption that 'Dk Sk 8' is better represented by the hydroxyproline date obtained on Der-38. Code listed on p. 740.

KDE 3 runs the model with both the new and published radiocarbon dates obtained on anthropogenically modified fauna (including the osseous points) (n=35). Code listed on p. 740.

KDE 4 combines the datasets from KDE 0 and KDE 3 (n=47). Code listed on p. 742.

12.1.4 Discussion

Despite generally poor collagen preservation, I was able to measure 41 radiocarbon dates on a total of 34 anthropogenically modified faunal remains from Dzeravá Skala – including 7 artefacts classified as osseous points by Prošek. For the first time, it was possible to extensively investigate the site chronology (including stratigraphic integrity and human activity) and shed light on the chronotypology of the osseous point industry. In the following, modelling results (fig. 12.18–12.21), the relationship between human activity and lithic finds, and the significance of Dzeravá Skala for the Middle to Upper Palaeolithic biocultural shift are discussed.

All models provide reproducible results when run multiple times. While the radiocarbon ages within layers 5 and above are relatively close and consistent, layers 9 and 11 show a significant spread. There are four clear outliers from the lower most section of layer 9 (OxA-34026, OxA-35761, OxA-35581, and OxA-35583), which are identified in all models that maintain their original layer attribution (Model 1, 3, 5, 7, 9, and 10). All four ages seem to be older or coincide with material from the upper part of layer 11. Evidently, the boundary between layer 11 and 9 is highly problematic. The stratigraphic

models 2, 4, 6, and 8 move the four dates from layer 9 to layer 11. As expected, this diminished the number of outliers found – only OxA-35760 from the middle section of layer 11 remains significantly older. However, previously published dates from layer 5a' (located between layer 9 and 11) are also younger than the aforementioned dates, supporting the argument that the cut-marked bones attributed to the lowest part of layer 9, are in fact associated with activity originally occurring during sedimentation of layer 11. It remains unclear whether the boundary between layers 9 and 11 was not identified correctly, or whether material exchange (i.e. mixing) between these layers occurred in parts of the cave.

Der-13 (OxA-34018) from layer 7 is an outlier in Model 2 and 10. The former resulted from moving the four layer 9 dates (OxA-34026, OxA-35761, OxA-35581, and OxA-35583) to layer 11, thus pushing the transition boundary younger than acceptable for OxA-34018. The latter is connected to the introduction of layer 5a': stratigraphically it lies under 7, but chronologically it produced younger ages. Der-13 was collected in Prošek's north profile. Kaminská et al. (2005b) identifies the location as layer 7, while Prošek (1953) places the area within layer 11. The dating supports the original interpretation.

The issues surrounding the limit between layer 11 and 9 directly affect the modelled transition boundary, thus what was previously perceived to be the start of the 'Aurignacian' at Dzeravá Skala (see fig. 12.22-b). Most models retaining the original layer attribution (Model 1, 3, 5, 7, 9), calculate the transition *ca.* 45–42k cal BP, while the adjusted models result in 42–40k cal BP (Models 2 and 4) or 42–39k cal BP (Models 6 and 8). Model 10 is the exception. Layer 5a' lies between layer 11 and 9, with a start boundary of 41–39k cal BP and an end boundary of 40–39k cal BP. Presently, the amended version, i.e. a later start for the occupation in layer 9, appears more consistent with the evidence than the original stratigraphic attribution.

None of the changes made to the stratigraphic models affect the end boundary of layer 9. This stands in contrast to the start boundary of layer 11. All models excluding OSL dates (Model 1-8) interpret Der-71 (OxA-

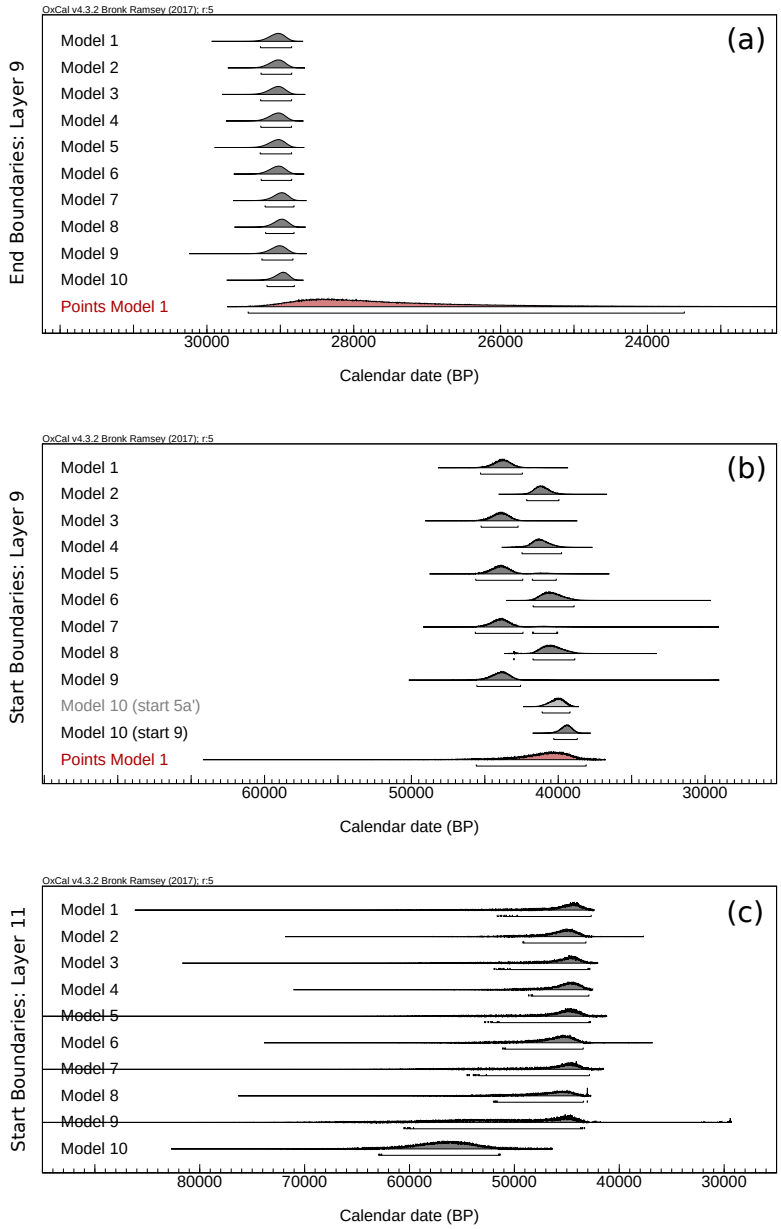


Figure 12.22: Dzeravá Skala: comparison of boundaries calculated by Models 1–10. (a) end layer 9; (b) start layer 9; (c) start layer 11. **red** – start (b) and end (a) boundary for osseous points; **grey** – start boundary of layer 5a' for general comparison. The variation observed in (b) are caused by OxA-34026, OxA-35761, OxA-35583 and OxA-35581 being moved from layer 9 to layer 11 for models with even numbers.

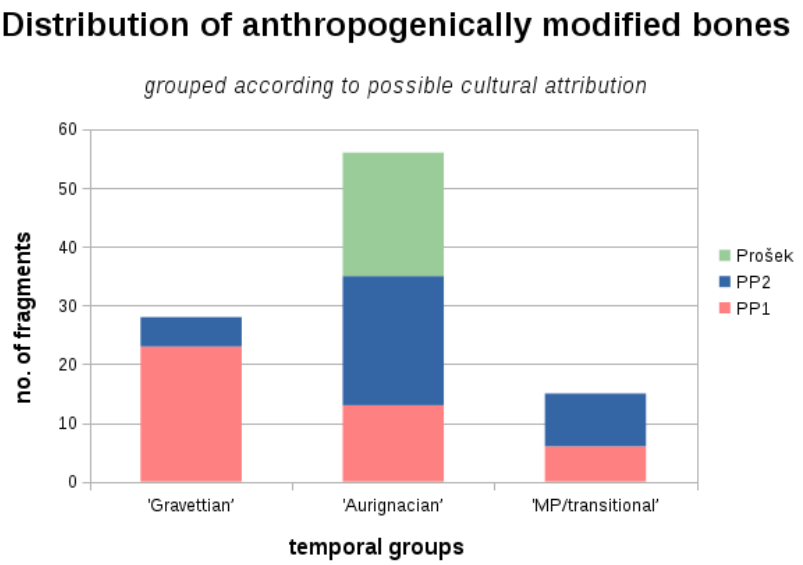


Figure 12.23: Dzeravá Skala: distribution of anthropogenically modified faunal remains grouped according to previously proposed cultural groups based on ^{14}C ages. 'Gravettian' = layers 3, 4, 4a, 5, 5a and 8; 'Aurignacian' = 6, 7 and 9; 'MP/transitional' = layer 11 (see text for discussion). **red** – trench PP1; **blue** – trench PP2; **green** – 'osseous point industry' as identified by Prošek.

35760) as a significant outlier, thus moving its age in line with the other dates from the upper part of layer 11. With the introduction of OSL ages (Model 9 and 10) and dates from unmodified faunal remains (Model 10), OxA-35760 is supported by other dating. As a result, the start boundary increases in age. It is important to be careful with the interpretation of these results. The OSL age dates sedimentation, while the non-modified faunal remains date animal activity. Both indicate that there is material > 50k cal BP to be found in layer 11. However, human activity at that time is scarce at best.

This distinction is better reflected in the KDE model results (see fig. 12.21). KDE 0 supports previous interpretations of three main occupations: 'MP / transitional', 'Aurignacian', and 'Gravettian' – with most activity during the 'Aurignacian'. The same picture can be seen in the distribution of the anthropogenically modified fauna (not all dated), when layers were grouped

according to these previously proposed categories (see fig. 12.23). However, these results reveal layer accumulation. The lithic material unearthed at Dzeravá Skala indicates only brief and infrequent visits to the cave. The actual occupation events will therefore be hidden in the noise of general activity at the site.

KDE 3 eliminates this background noise by focusing on directly dating human activity. As a consequence, the chronological picture changes drastically. There are a minimum of 6 occupation events at the cave – most of them within the time frame of the middle peak found in KDE 0 (and layer 9). The previously clear MP aged peak between 60–50k cal BP becomes insignificant (only represented by 1 date), while the youngest peak ('Gravettian') is now better defined and suggests more intense activity. Considering the sample locations, it can be hypothesised that the peak at around 44k cal BP might be connected to the 'Jankovichian' lithics. The peak at around 37k cal BP is associated with the massive-based points, the double peak between 35–31k cal BP with the osseous points showing round cross-sections and other osseous artefacts, and the peak at 29k cal BP with possible eastern 'Gravettian' expressions (layers 3, 4 and 5). The peak at 41k cal BP is represented by material in layers 9, 6 and younger 7, including an osseous spear point blank. Unfortunately, the SBP could not be dated. However, the temporal pattern of a valley at around the same time as the CI eruption, followed by a peak with MBP is reminiscent of Istállóskő (see fig. 11.24). There, the initial peak represented SBP, the second MBP. Only further dating of SBP and MBP from Dzeravá Skala will be able to test this hypothesis.

In light of these finding, it is crucial that dating of the AMH tooth from the 'reddish clay' be attempted. The sediment description heavily suggests that the layer is either related to Kaminská's layer 6 or 9b. Both cases would be connected to the earliest occupation with osseous points.

Looking at the osseous point industry in more detail, evidence suggests that their radiocarbon ages are compatible with those of layer 9. A notable exception is the point blank Der-33 (OxA-X-2716-51). It is identified as an outlier in all stratigraphic models, and has an age which is in better

agreement with those from layers above. However, the sample was only AG* treated, which could also lead to an age underestimation. At the same time, the boundary between layer 9 and above was not placed identically by Prošek (1953) and Kaminská et al. (2005b) (see fig. 12.6).

KDE models using dates obtained on Prošek's osseous 'points' show at least three temporal events, all concentrated in the Upper Palaeolithic sequence. The number of dates is insufficient to separate the two possible events on either side of 40k cal BP. However, the ages correspond well to dates obtained on cut marked faunal remains. It is therefore reasonable to assume that use of these artefacts coincided with other human activity at Dzeravá Skala, and increasing the number of directly dated point artefacts will likely show a comparable pattern as found in KDE 3, with the exception of the initial activity (peak at 44k cal BP). It appears as if that particular use of the cave site occurred independently from the use of osseous artefacts. The latest dated occurrence of osseous 'points' are from Der-33 (OxA-X-2716-51) and Der-36 (OxA-35387), a point blank and a MBP, respectively. Both were only treated with the AG* protocol, suggesting minimum ages. Der-36 is significantly younger than the other two MBP (Der-38 and Der-39) – even when comparing to the AG* results. Either there is a significant amount of undetected contamination remaining, or a younger MBP event was detected.

Removing the previously obtained date on 'Dz Sk 8' eliminates the younger shoulder of the first peak in KDE 2 (see rig. 12.21). This demonstrates the huge impact an inaccurate date would have on the modelling outcome when working with such small sample sizes. If Der-38 does indeed represent the same point sample as 'Dz Sk 8', then KDE 2 would definitively better reflect the osseous point industry. Nonetheless, further dating is advised to capture the osseous industry in its entirety.

Intensive radiocarbon dating of human activity at Dzeravá Skala largely supports the association of the osseous point industries with layer 9 from the most recent excavation in 2002/2003, and is in agreement with OSL dating at the site. The contact zone between layer 11 and 9 is problematic: it appears likely that the cut marked bones from the lowest section of unit

9 actually correspond to activity dated in the uppermost part of layer 11. There is no significant human presence during the MP, though a single dated anthropogenically modified bone might be related to the single lithic found at a depth of 240 cm (see fig. 12.10-b.9 and 12.11-b.5). It is worth noting, that this connection is circumstantial at best. The lithic interpretation has heavily relied on dating in the past: Gábori-Csánk (1993) grouped it together with the other points from layer 11 and saw it as 'Jankovichian', while Kaminská et al. (2005b) and Davies and Hedges (2005) associated it with the MP on the basis of older ^{14}C and OSL dates within the middle part of layer 11. The oldest multi-dated event (*ca.* 45–43 cal BP) stems from the upper part of layer 11, and appears better connected to the lithics interpreted as 'Jankovichian' by Gábori-Csánk (1993) as shown in figure 12.10.a–b. After this, the first occupation with osseous points (*ca.* 43–40k cal BP) follows in line with dating of SBP at the Hungarian site of Istállóskő. Unfortunately, direct dating evidence of SBP was not possible, as Der-01 failed pre-treatment. This might be resolved in future, as further SBP fragments are known from the site and show promising %N results. In general, the terminological division of 'MP/transition', 'Aurignacian' and 'Gravettian' should no longer be used. They are misleading, as they were heavily reliant on dating, rather than lithic finds. Instead, a more nuanced nomenclature – taking chronology and the osseous industry into account – might offer a less biased view. In the absence of evidence connecting the 'leaf points' from layer 11 to Neanderthals, it is possible that Dzeravá Skala mainly experienced occasional short AMH visits, which increased in frequency in younger periods.

12.2 Šal'a

12.2.1 Introduction

At Šal'a cranial fragments of two Neanderthal individuals were found (Šal'a I and Šal'a II). They were discovered near the surface in secondary deposition. It is thought that the original fossil accumulation was covered with

loess which has been eroding since the Holocene, resulting in material being transported downstream along the river Váh (Kaminská, 2014, p.75). As both individuals were found without secure context, radiocarbon dating can test whether these specimens could actually represent late Neanderthal individuals, in which case aDNA analysis might provide further fruitful insights.

Šal'a I was found in 1961. The frontal bone belongs to a young woman (20-39 years old). Based on bone preservation and indirect association with interstadial faunal remains, the cranial fragment was estimated to be 100-80k years old.

In contrast, Šal'a II displayed less archaic features. It consists of a left half of a frontal bone (found in 1995) and a left parietal bone (found in 1993). The two bones refitted along a fresh fracture line, thus establishing that they belonged to the same individual: an adult male, 40-59 years old. (Jakab, 1996, 1998, 2005).

The frontal bone of Šal'a II was split along the *sutura frontale* and there is some erosion on the frontal tuber. The parietal bone showed two flat areas, one between the parietal eminence and the sagittal suture, the other between the parietal eminence and the lambdoid suture. They could be caused by injury or taphonomic processes. As the scratches do not differ in colour, a healed wound is more likely. While the inside of the cranial fragment is intact, there is a shallow impression which could possibly stem from an epidural haematoma (Jakab, 2005).

In 1997 Prof M. Schultz cut an L-shaped sample (1.5 g) from the frontal bone for histological and DNA analysis at the Zentrum für Anatomie der Georg-August-Universität Göttingen (Jakab, 2005), but so far no results were returned (see fig. 12.24).

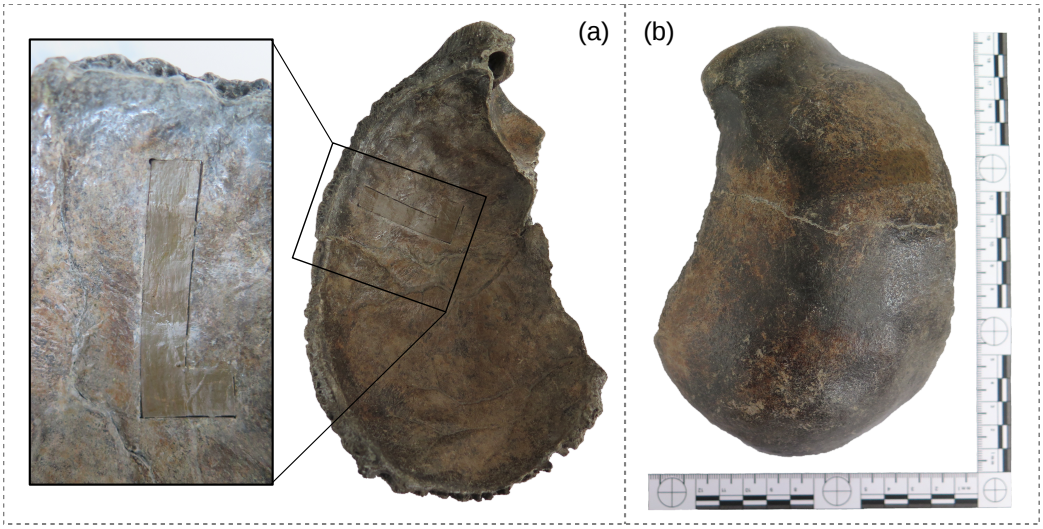


Figure 12.24: Šal'a: Previous sampling of the frontal bone of Šal'a II for histological and DNA analysis. (a) – inside of the two cranial fragments with magnification of the L-shaped sampling location from 1997 (42 x 18 mm) close to the glued fracture line. (b) – view from the outside, showing the restoration work to cover the sampling area above the refitted fracture (photos & illustrations: R. Hopkins).

12.2.2 Radiocarbon dating

Sample & Treatment

As both Neanderthal individuals were found without original context, it was decided that they should both be radiocarbon dated to assess their relevance to the MP/UP biocultural shift. As there was no information on why the large sample from 1997 did not provide any results, both specimens were initially sampled using key hole drilling to test for nitrogen concentration. At the same time, some further material was obtained and sent to S. Pääbo and M. Hajdinjak at the Max Planck Institute for Evolutionary Anthropology in Leipzip for aDNA analysis: 85 mg from Šal'a I, 70 mg from Šal'a II.

Both Neanderthal samples passed the %N test (see tab. 12.9). As a result, Šal'a II (stored at the archaeological institute in Nitra) and Šal'a I (stored at the Natural History Museum in Bratislava) could be sampled for radiocarbon dating. The order of sampling led to the unfortunate labelling of Sal-1 for

Šal'a II, and Sal-2 for Šal'a I. However, it was decided that changing the labels retrospectively would have caused more confusion than clarification.

None of the samples were treated with solvent washes. Instead, the pre-treatment protocol directly aimed at single amino acid dating: despite being a non-routine protocol, it is demonstrably more effective at removing unknown museum contaminants, and considering the age of the human remains, any modern contaminants could prove detrimental to obtaining a reliable radiocarbon measure.

Sal-1 (Šal'a II) This specimen shows significant modern conservation and restoration work (see fig. 12.24). The two bone fragments were rejoined using glue, and the previous sampling hole was filled with a resin (possibly epoxy). In addition, all modification were cosmetically treated with paint. The entire bone surface is very shiny, though no members of staff remember any general surface treatment having been applied. In general, no detailed conservation log was kept.

In order to minimise damage to the specimen, the %N sample was taken from the frontal bone in 2015, close to where the original L-shaped samples was taken. The surface around the drilling area was first removed, before applying the key-hole sampling technique, in order to avoid contamination through conservation agents. In 2016, upon returning for radiocarbon sampling, manoeuvrability in this area proved insufficient for obtaining a larger sample. As a result of the structure of the cranial fragment, sampling had to be moved to the left parietal bone and a larger sampling area of just under 1 cm^2 opened. Again, the surface was cleaned through abrasion to avoid contamination.

Sal-2 (Šal'a I) There are at least 9 small holes filled with resin (epoxy?) and repainted (see fig. 12.25). They are 2-5mm in diameter, and spread out on the side opposite the eye sockets. None of them seem to penetrate the entire bone, as they remain invisible on the outer bone surface. The entire



Figure 12.25: Šal'a: Inside of Šal'a I (frontal bone) showing 9 filled areas, where the specimen had previous been sampled for an unknown purpose (photo: R. Hopkins).

bone surface is dark, smooth and shiny. While it is possible that this is as a result of taphonomy and water erosion, it could also result from conservation treatment. No restoration logs were available.

The initial %N sample was obtained through key-hole drilling in April 2016 after removal of surface material. It was placed closer to the centre of the bone to avoid contamination from conservation fillings. Later that year, a second sample area of just under 1 cm^2 was opened to collect a sample large enough for radiocarbon dating. The location was placed close to the initial sample hole, avoiding diagnostic features and leaving the outer bone structure intact.

^{14}C Results

Despite a collagen yield after AG treatment below 20 mg, the samples were processed through the HPLC for hydroxyproline dating (see tab. 12.9). The resulting HYP yielded sufficient carbon for small graphite targets (0.5-0.8 mgC), thus demonstrating a reasonable bone preservation. Both Neanderthal

Table 12.9: Šal'a: Laboratory results from radiocarbon pretreatment for the two Neanderthal individuals. Both were single amino acid dated (see section 5.4). Ref-no. = number given to the sample for the purpose of this project. %N = nitrogen weight content before chemical pre-treatment. AG yield = gelatine yield after AG treatment (both absolute and in wt.%). mgC = amount of carbon in HYP combusted for graphitisation (value used for HPLC background correction). δ^{15}N and δ^{13}C = stable isotope measurements on combustion. %C = carbon yield on combustion. C:N = carbon to nitrogen ratio of combusted sample.

Ref-no.	Sample	%N	Weight	AG yield	mgC	%C	δ^{15}N	δ^{13}C	C:N
Sal-1	Šal'a II	1.51	494.88 mg	15.55 mg (3.14 %)	0.5400	49.1	11.7	-22.7	5.2
Sal-2	Šal'a I	2.66	367.90 mg	17.76 mg (4.83 %)	0.6395	49.2	11.5	-22.7	5.4

Table 12.10: Šal'a: New AMS radiocarbon measurements for the two Neanderthal individuals, obtained by single amino acid dating of hydroxyproline. $F^{14}C$ (AMS) = fraction modern measurement as obtained by AMS measurement. $F^{14}C$ (corr.) = fraction modern value after HPLC background correction. ^{14}C (BP) = radiocarbon age in years Before Present obtained from the corrected $F^{14}C$ value.

Ref-no.	Sample no.	Lab-no	$F^{14}C$ (AMS)	$F^{14}C$ (corr.)	^{14}C (BP)
Sal-1	Šal'a II	OxA-X-2731-15	0.00127 ± 0.00192	-0.00109 ± 0.00197	> 47100
Sal-2	Šal'a I	OxA-X-2731-16	0.00178 ± 0.00162	-0.00021 ± 0.00169	> 46200

samples show nearly identical stable isotope measurements, and expected %C on combustion. The C:N ratio is slightly elevated compared to the calculated value of 5.0, yet remains within errors observed at ORAU.

Initial $F^{14}C$ value obtained from the AMS measurement and corrected for regular laboratory and instrument background already indicate 'greater than' ages (see tab. 12.10). Nonetheless, the values were corrected for HPLC background as described in section 5.4.7. The resulting $F^{14}C$ values were translated into greater than radiocarbon ages following ORAU standard protocol, resulting in ages of >47100 BP (OxA-X-2731-15) for Sal-1 and >46200 BP (OxA-X-2731-16) for Sal-2. The OxA-X nomenclature derives from the use of non-routine chemistry, namely single amino acid dating, and is not indicative of quality issues.

12.2.3 Discussion

The human remains of two *Homo neanderthalensis* individuals found at Šal'a were hydroxyproline dated. The results securely place both specimens beyond the limit of the radiocarbon technique: Šal'a I is older than 47100 radiocarbon years, Šal'a II older than 46200. Consequently, neither of them can provide further insights into the crucial time period between 45-39k cal BP. While aDNA preservation was sufficient to identify them as Neanderthal, it was insufficient for analysing nuclear DNA (M. Hajdinjak, pers. comm. 14/03/2018).

Chapter 13

Methodological discussion & summary

This chapter will highlight some of the general observations made during the radiocarbon dating process (including pre-treatment, dating reliability and the application of radiocarbon modelling), and summarise some of the most important findings from the site specific chapters under 8 to 12.

13.1 Radiocarbon pre-treatment

Some trends and pre-treatment anomalies only become apparent when comparing samples from different sites, or analysing trends in the radiocarbon sample dataset as a whole. This is partially related to which samples were pre-treated together, but also to the fact that statistics becomes more meaningful with an increasing number of data points. Therefore, this section will first investigate trends of collagen preservation in relation to nitrogen concentration, sample age and type, and mass of material pre-treated, before assessing general dating reliability. For anomalies observed on combustion run no. 4951 and AMS measurement wheel no. 2731 see Appendix.

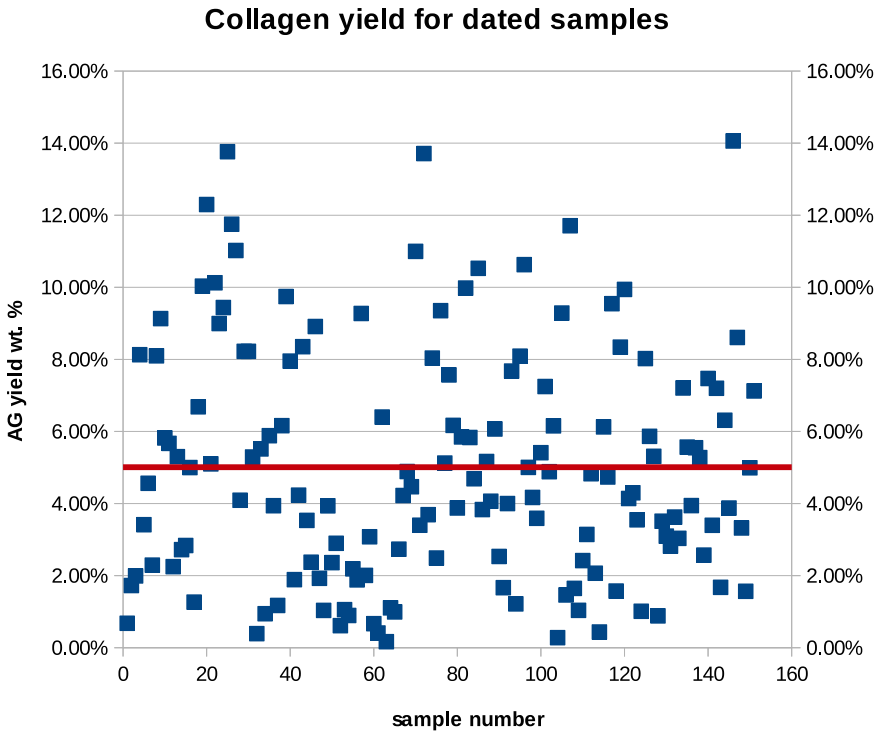


Figure 13.1: Local summary: collagen yield after AG or AG* treatment for samples dated in this thesis; mean given in **red**. The distribution shows generally well preserved bone, though with a significant number <2%.

13.1.1 Prescreening & collagen preservation

Collagen preservation and dating success was better than expected. Of all the samples analysed, 75% had measured nitrogen concentrations > 0.7%, and of those samples pre-treated for radiocarbon dating, 87% resulted in a date. Collagen yield after AG treatment ranged between 0.00–14.06 wt.% of original sample mass, with an average yield of 5.00% and a median yield of 4.56% (see fig. 13.1).

Artefacts were usually less well preserved than faunal samples. For example, osseous points showed an average and median yield of 3.27% and 2.39%, respectively. Moreover, of the 36 samples with a collagen yield <2%,

16 were osseous points. This means, 42% of points showed low preservation, compared to only 15% of faunal remains.

A comparison of nitrogen content in the collected bone powder to (a) collagen yield after AG treatment and (b) $F^{14}C$ demonstrates that sample age is not responsible for decreasing collagen preservation in this dataset (see fig. 13.2). Instead, high collagen yield correlates to high %N results, which originally formed the basis for using nitrogen concentration for bone screening (see Brock et al., 2010a). However, low yield does not necessarily mean low %N, and – as Jacob et al. (2018) have demonstrated – low %N values might not always result in insufficient collagen yield for dating.

While the relationship between nitrogen concentration and collagen yield is close to linear at sites such as Dzeravá Skala, Máriaremete, Tabula Traiana, and Kozarnika (each with different slopes), there does not appear to be any obvious relationship observable at Istállóskő, Dubočka-Kozja, Jankovich or Temnata Dupka.

Some of the most prominent outliers, *i.e.* where high %N results did not translate to high yields, can be explained by the state of the sampled artefact (see fig. 13.3). Conserved samples appear to more frequently show low preservation irrespective of their nitrogen content. This is consistent with the observation that the samples that failed pre-treatment despite their seemingly sufficient nitrogen concentrations were all artefacts (*e.g.* osseous points, Venus figurine). The use of nitrocellulose for conservation purposes would account for the increase in nitrogen, though FT-IR analysis was not sensitive enough to detect any in the powder from osseous points, and the artefact surface could not be separately tested. As the substance was not synthetically manufactured until the 1990s, it would introduce modern carbon if not fully removed. As a result, even undetected contamination will not invalidate the old age of the Istállóskő points.

It is worth noting that the samples from Temnata Dupka also show a reduced correlation (see fig. 13.3, listed as 'possibly conserved'), albeit not with yields as low as some of the conserved artefacts. The bone fragments

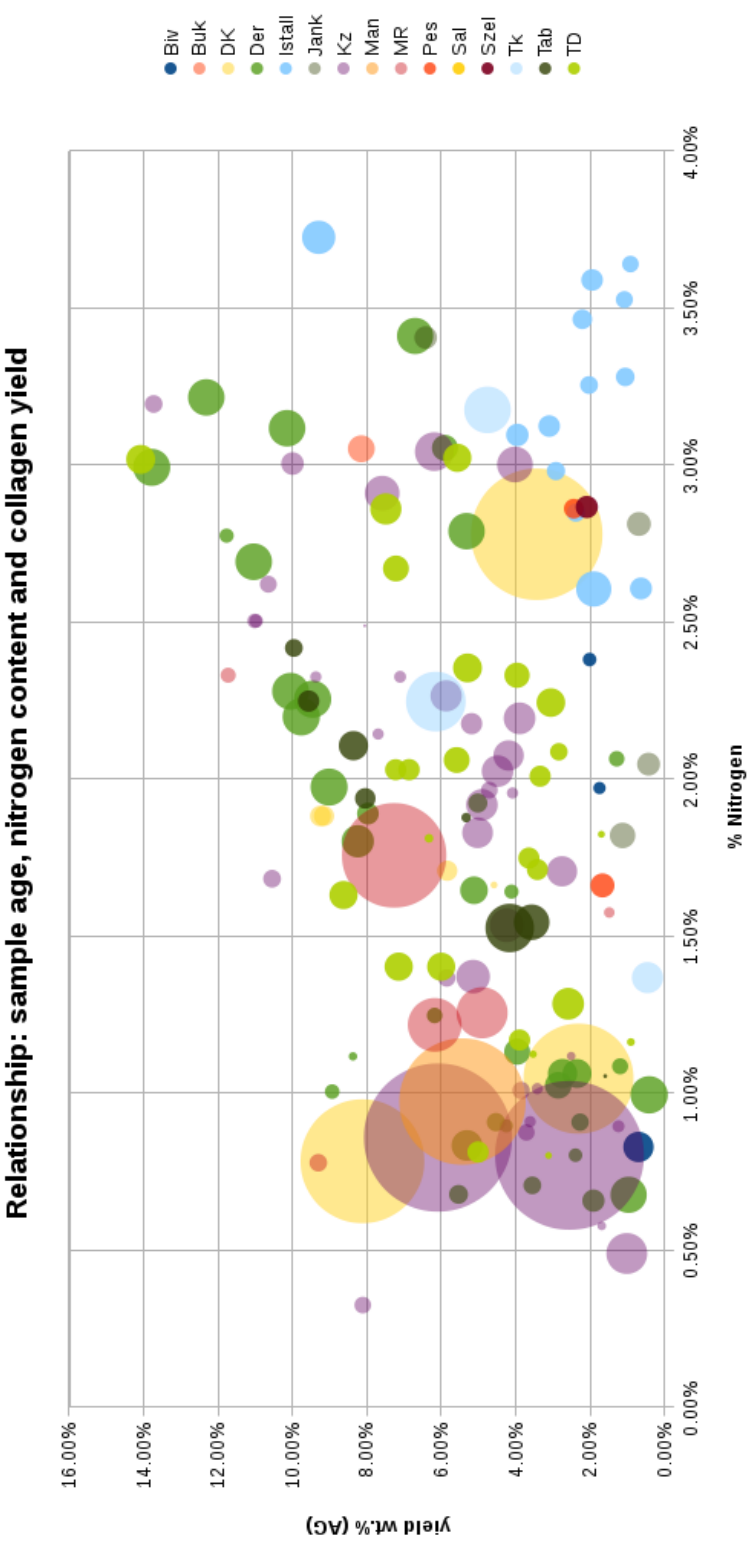


Figure 13.2: Local summary: visualisation of relationship between %N results (x-axis), collagen yield after AG treatment (y-axis) and a sample's $F^{14}C$ value (bubble). The higher the $F^{14}C$ value (*i.e.* the younger the sample) is, the larger the respective bubble size. Data points coloured according to site origin: Biv = Bivak, Buk = Bukovac, DK = Dubočka-Kozja, Der = Dzeravá Skala, Istall = Istállóskő, Jank = Jankovich, KZ = Kozarnika, Man = Manastira, Pes = Peskő, Sal = Šal'a, Szel = Szeleta, Tk = Tabashkata, Tab = Tabula Traiana, TD = Temnata Dupka.

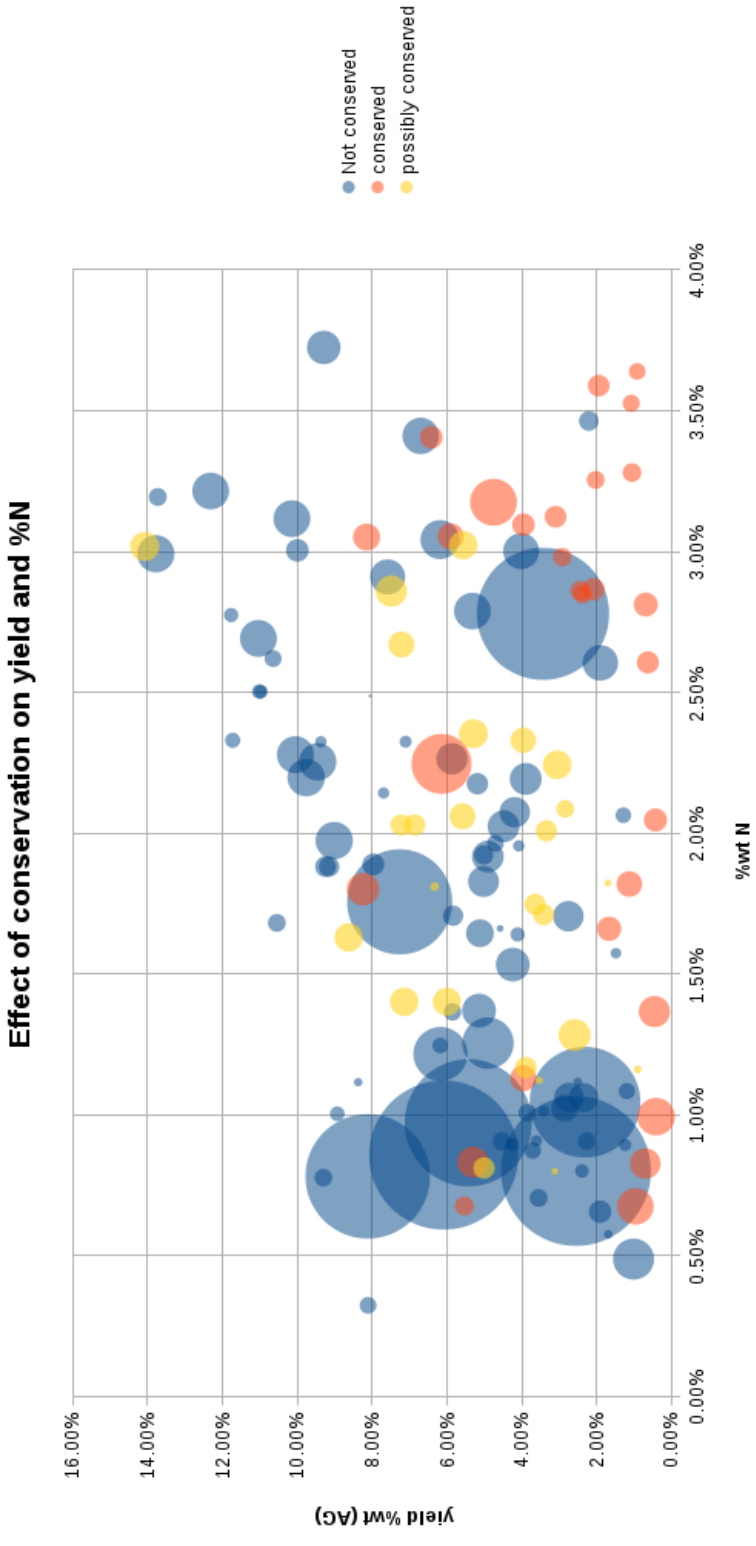


Figure 13.3: Local summary: visualisation of relationship between %N results (x-axis), collagen yield after AG treatment (y-axis) and a sample's $F^{14}C$ value (bubble). The higher the $F^{14}C$ value (*i.e.* the younger the sample) is, the larger the respective bubble size. Data points coloured according to state of artefact sampled, *i.e.* not conserved, conserved, and possibly conserved.

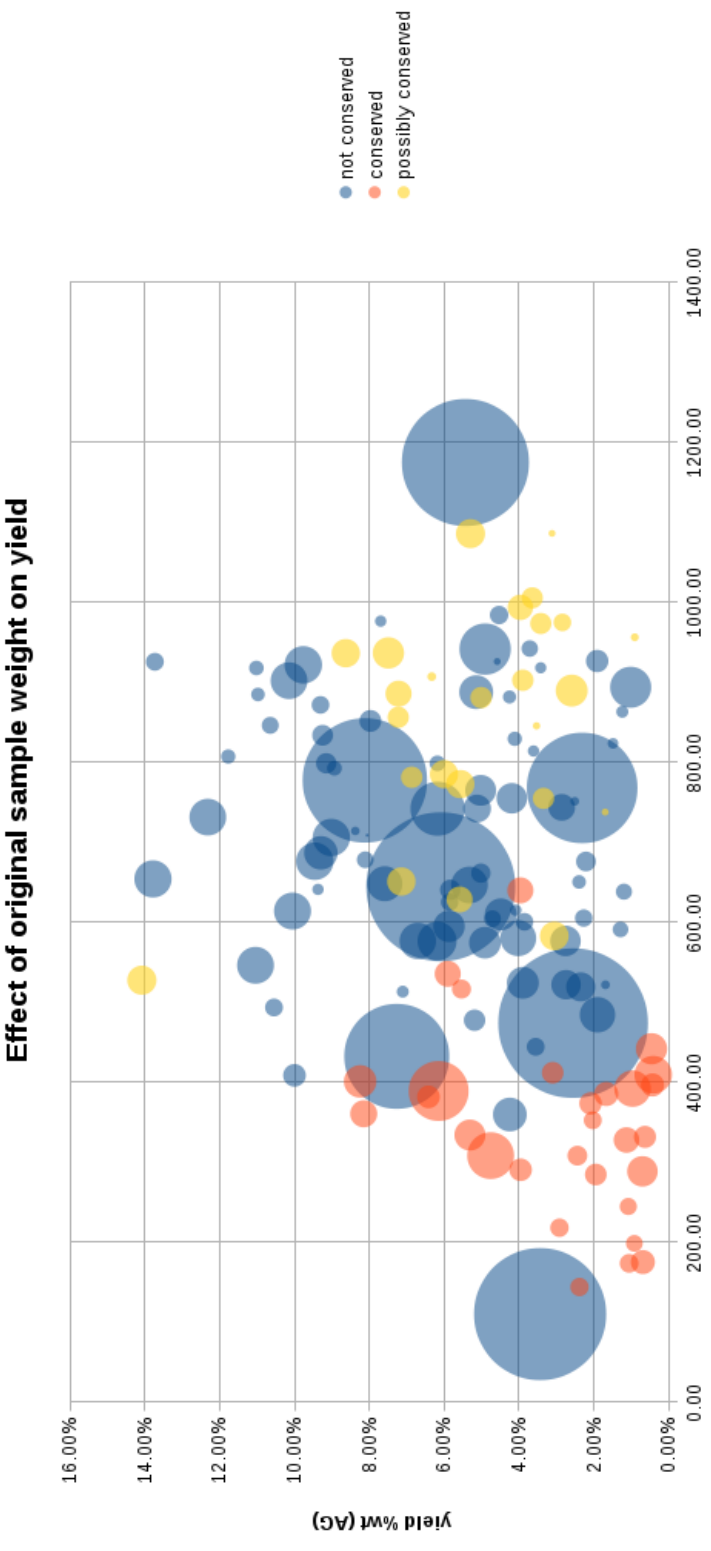


Figure 13.4: Local summary: visualisation of relationship between original sample mass in mg (x-axis), collagen yield after AG treatment (y-axis) and a sample's $F^{14}C$ value (bubble). The higher the $F^{14}C$ value (*i.e.* the younger the sample) is, the larger the respective bubble size. Data points coloured according to state of artefact sampled, *i.e.* not conserved, conserved, and possibly conserved.

had an unusual consistency (with a hard, shiny surface and a very soft interior), which was reminiscent of some conserved material. However, they have supposedly never been treated. However, many of the samples were accidentally waterlogged when the storage facility at the museum was flooded. This could have affected collagen preservation. Alternatively, the samples could have been conserved without the knowledge of collaborators in Bulgaria.

Another factor influencing collagen yield (the proxy used for assessing collagen preservation) is the original sample mass treated (see fig. 13.4). For samples of <400 mg a reduction in yield is observable. In contrast, samples >500 mg do not seem to be affected by significant sample loss during chemical pre-treatment. It is important to remember, however, that the low mass samples in the dataset are mainly represented by conserved artefacts.

In summary, all sites sampled for this dissertation showed good collagen preservation. The reduced yield observed on artefacts, especially osseous points, may be connected to both smaller sample mass and poorer collagen preservation. The latter may have been caused by prolonged exposure before burial, heat treatment, or the substantial time these objects have spent in museums since their excavation. Their high nitrogen concentration may be the result of nitrogen containing conservation materials (such as nitrocellulose), as commonly used in the early and mid 20$^{\text{th}}$ century. As a result, care is advised when interpreting nitrogen concentrations for conserved artefacts in terms of collagen preservation.

13.1.2 Dating reliability

As part of the radiocarbon quality control measures several auto-duplicates were dated, *i.e.* two fractions from the same homogenised sample were treated and dated separately from the beginning of the pre-treatment process. In addition, four samples that were selected for hydroxyproline dating had an AG* aliquot dated for direct comparison (see tab. 13.1 and fig. 13.5).

All auto-duplicates resulted in measurements that are statistically indistinguishable according to a χ^2-test. This demonstrates the reproducibility

Table 13.1: Local summary: overview of samples that have been dates twice, either as auto-duplicates or for comparing hyrdoxyproline dating (NRC) with results obtained by AG* pre-treatment.

Ref-no	Target	Lab-code	^{14}C (BP)	F^{14}C	C:N	δ^{13}C
Buk-01	38806.0 AG* 01	OxA-35953	29950 ± 500	0.02411 ± 0.00156	3.1	-19.5
Buk-01	38806.0 NRC 01	OxA-X-2732-11	31100 ± 520	0.02084 ± 0.00134	4.8	-25.3
Der-03	40314.0 AF 01	OxA-34012	37000 ± 800	0.01004 ± 0.00103	3.2	-22.0
Der-03	40314.1 AF 01	OxA-35232	36050 ± 700	0.01123 ± 0.00099	3.2	-22.2
Der-09	40320.0 AF 01	OxA-34014	28580 ± 300	0.02849 ± 0.00108	3.2	-22.1
Der-09	40320.1 AF 01	OxA-34015	28810 ± 310	0.02769 ± 0.00108	3.2	-22.1
Der-29	41370.0 AG* 01	OxA-35597	26980 ± 340	0.03479 ± 0.00149	3.1	-18.5
Der-29	41370.0 NRC 01	OxA-X-2732-13	28340 ± 370	0.02938 ± 0.00136	4.9	-25.5
Der-38	41375.0 AG* 01	OxA-35599	30550 ± 500	0.02237 ± 0.00145	3.1	-20.3
Der-38	41375.0 NRC 01	OxA-X-2732-15	32690 ± 620	0.01709 ± 0.00133	4.9	-26.8
Der-39	41376.0 AG* 01	OxA-35524	30500 ± 450	0.02241 ± 0.00120	3.1	-21.0
Der-39	41376.0 NRC 01	OxA-X-2732-16	32770 ± 660	0.01692 ± 0.00138	4.9	-27.8
DK-17	43120.0 AF 01	OxA-35588	34500 ± 600	0.01360 ± 0.00101	3.1	-23.1
DK-17	43120.1 AF 01	OxA-35589	34150 ± 600	0.01424 ± 0.00102	3.1	-23.1
Kz-109	42120.0 AF 01	OxA-34826	39800 ± 1100	0.00702 ± 0.00098	3.2	-20.9
Kz-109	42120.1 AF 01	OxA-34827	40900 ± 1300	0.00614 ± 0.00098	3.2	-20.9
Kz-116	43100.0 AF 01	OxA-35579	43900 ± 1900	0.00423 ± 0.00099	3.1	-21.7
Kz-116	43100.1 AF 01	OxA-35580	43000 ± 1700	0.00473 ± 0.00098	2.9	-20.1
Tab-13	43140.0 AF 01	OxA-35766	> 49800	0.00000 ± 0.00101	3.2	-22.0
Tab-13	43140.1 AF 01	OxA-35767	> 49900	0.00000 ± 0.00100	3.2	-22.0
TD-08	39578.0 AF* 01	OxA-33841	33800 ± 550	0.01489 ± 0.00102	3.2	-21.3
TD-08	39578.1 AF* 01	OxA-33842	33600 ± 550	0.01522 ± 0.00103	3.2	-21.3
TD-31	43080.0 AF* 01	OxA-35757	29160 ± 320	0.02653 ± 0.00105	3.2	-20.9
TD-31	43080.1 AF* 01	OxA-35758	29240 ± 320	0.02625 ± 0.00103	3.2	-21.1

and reliability of both standard pre-treatment (AG/AG* and AF/AF*) protocols used for this project.

The results obtained from hydroxyproline dating and the standard ORAU gelatine protocol with initial solvent washes (AG*) are statistically different for Der-29, Der-38 and Der-38, based on a χ^2-test, but statistically indistinguishable for Buk-01. This is consistent with initial expectations that hydroxyproline dating can more effectively eliminate exogenous carbon – especially from samples contaminated with conservation substances. At the same time, the age difference of approximately 2000 radiocarbon years is not as severe as previously observed with, for example, curated human remains

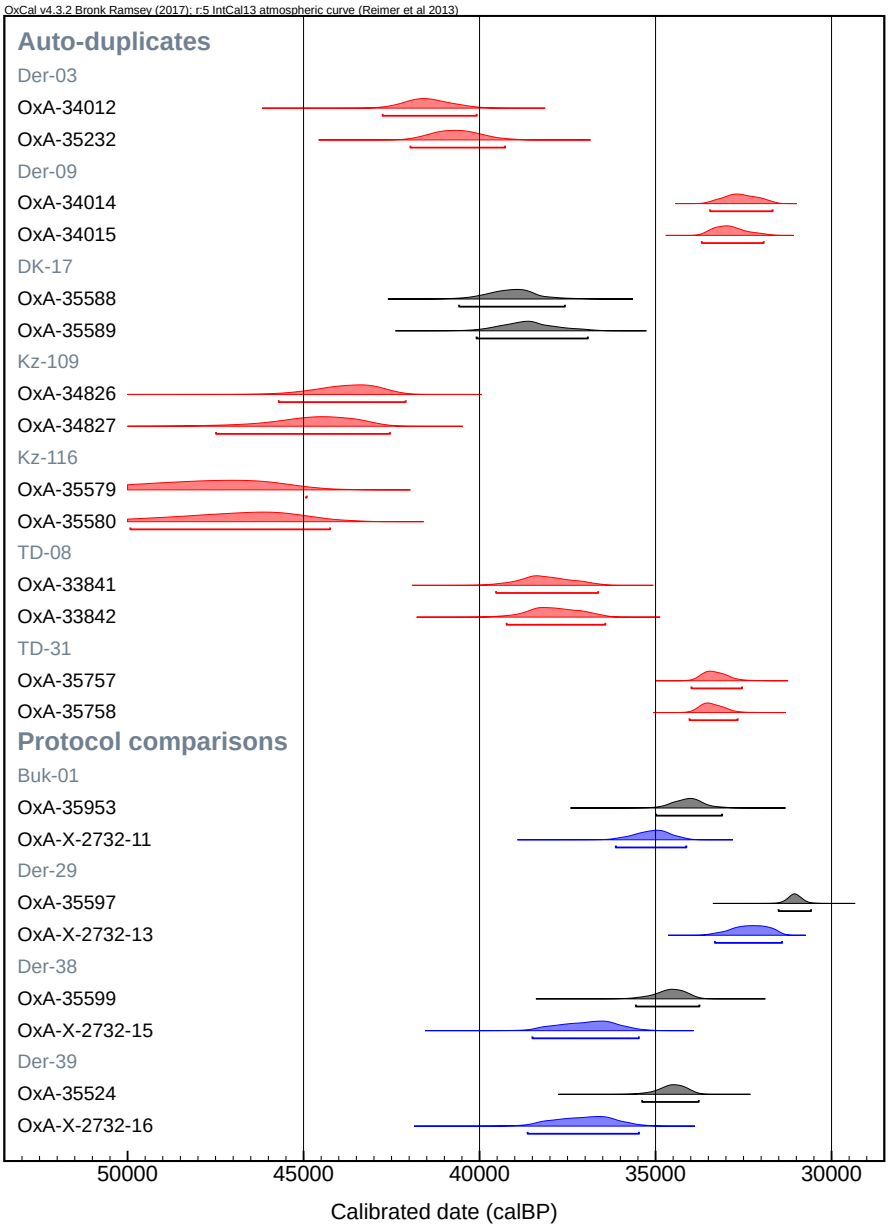


Figure 13.5: Local summary: comparison of auto-duplicates and AG*/NRC protocols. All auto-duplicates are statistically indistinguishable. Protocol comparison for Buk-01 gave statistically indistinguishable results, comparison for Der-29, Der-38, and Der-39 are statistically different. **black** – AG protocol; **red** – AF protocol; **blue** – hydroxyproline dating.

(*e.g.* Devièse et al., 2017). As a result, it can be expected that the AG* dates obtained on curated osseous points are indeed underestimating the true age of the samples. However, the offset does not appear to be as substantial as initially feared.

13.2 Modelling of radiocarbon dates

Two approaches to modelling radiocarbon dates were used for the site specific chronologies: Bayesian analysis using stratigraphic information as priors, and Kernel Density Estimates (KDE). The selection of anthropogenically modified material resulted in models that were extremely robust, even when testing for uncertainties in sample allocation and stratigraphic divisions (*e.g.* Dzeravá Skala, Kozarnika). At the same time, confidence in model outcomes could be increased by independently validating their information through KDEs.

In addition, this combined approach, in conjunction with lithic cultural identifications, allowed the temporal placement of the IUP at Temnata – despite its location outside the main stratigraphic sequence. Comparison of different KDE models provided a more nuanced understanding of sedimentation timing and the minimum number of occupation events (*e.g.* Dzeravá Skala layer 9, and Kozarnika layer 5b and its relationship to the CI), and led to an initial chronotypology of osseous points at Istállóskő.

Comparison of new and published radiocarbon data demonstrated that precise transition boundaries obtained from Bayesian modelling have to be treated with caution. They might be the result of less accurate dating or sample association, as an increased spread in dates within a `Phase` narrows the boundaries' probability distributions (*e.g.* Kozarnika, Temnata, Istállóskő).

The Mousterian in the region appears older than in western Europe, and is mostly beyond the limit of the radiocarbon dating technique. As a result, both Bayesian and KDE modelling are unable to establish a precise and

accurate transition for some of these cases (*e.g.* Tabula Traiana, Dubočka-Kozja).

Overall, the application of Bayesian and KDE modelling approaches has been essential in analysing the radiocarbon dataset. In combination with an adequate sampling strategy, these models were able to provide invaluable new insights into stratigraphic formation and integrity, as well as the timing of human occupations and cultural expressions.

13.3 Summary of site discussions

In addition to the modelling based observations listed above, some of the main findings from the site specific discussions will be highlighted here.

The analysis of human remains has once again demonstrated how important material identification and direct dating are. Thanks to ZooMS analysis it was possible to identify one of the 'human' bone fragments from Kozarnika as belonging to a bear, thus enabling it to be confidently set to one side. Furthermore, direct dating of *Homo sapiens* remains from Kozarnika and Manastira yielded younger than expected ages. Similarly, the direct dates obtained on the *Homo neanderthalensis* fragments from Šal'a place the two individuals beyond the radiocarbon dating limit, and therefore older than the MP/UP biocultural shift.

Some of the sites investigated have further known human skeletal remains. It is hoped that permission for direct dating will be granted in the near future, and that – preservation permitting – the chronology of human remains within the archaeological record can be improved.

Direct dating of osseous projectile points has increased the precision of their temporal distribution and enabled the identification of a chronotypology at Istállóskő, where SBPs largely predate MBPs. Further analysis and discussion on the spatio-temporal distribution of osseous points in general is presented in chapter 14.

The dating of the Szeletian occupation at Máriaremete revealed that the archaeological complex – previously interpreted as in situ and chronologically narrowly confined – actually contains material with a substantial temporal spread. It remains unclear whether this reflects the complex post-depositional processes that remained undetected during excavation, or whether any of the faunal material was later misattributed during the long years in storage. Either way, it is a reminder of the important insights gained by applying radiocarbon dating.

As a result of the apparently older age of the late MP in the east, many chronostratigraphies analysed for this thesis start with EUP industries (including IUP). Some of these sequences are quite elaborate (*e.g.* Kozarnika, Temnata, Dzeravá Skala), and others are simpler, but target diagnostic artefacts (*e.g.* Bukovac, Bivak, Szeleta, Peskő). They suggest an arrival of AMHs along the lower and middle Danube between 50–45k cal BP. Further analysis on the chronology of the MP/UP biocultural shift and the spread of AMHs is discussed in chapter 15.

Part V

Regional Chronologies

Chapter 14

The spread of osseous points

Aurignacian and Aurignacian-like industries have previously been key to tracking the AMH migration into Europe, and osseous points – both split-based points (SBP) and massive-based points (MBP) – featured heavily as *fossils directeurs* of that biocultural expansion (*e.g.* Conard and Bolus, 2003; Flas, 2008; Jacobi et al., 2006). However, the osseous points from the middle and lower Danube are mainly found without diagnostic Aurignacian lithics, and site specific analyses presented in this thesis illustrate that the earliest appearance of AMH may have occurred independently (see *e.g.* Temnata, Kozarnika). As a consequence, this chapter will focus on the spatio-temporal distribution of 'Aurignacian' osseous points, seen as a distinct, and directly datable cultural entity.

There are presently at least 63 sites with SBP known from throughout Europe and the Levant, and the find locations concentrate in mountainous regions (see fig. 14.1). Counting the occurrences of MBP is more difficult, as they are often defined in opposition to SBP, i.e. as non-split-based points, though they appear more numerous. From this large dataset, only specimens with direct radiocarbon dates will be considered, to avoid loss of dating precision through noise, or worse, entirely inaccurate age approximations. This reduces the dataset, which is described in more details in the following sections, to 28 different sites, and a total of 67 artefacts (see fig. 14.1).

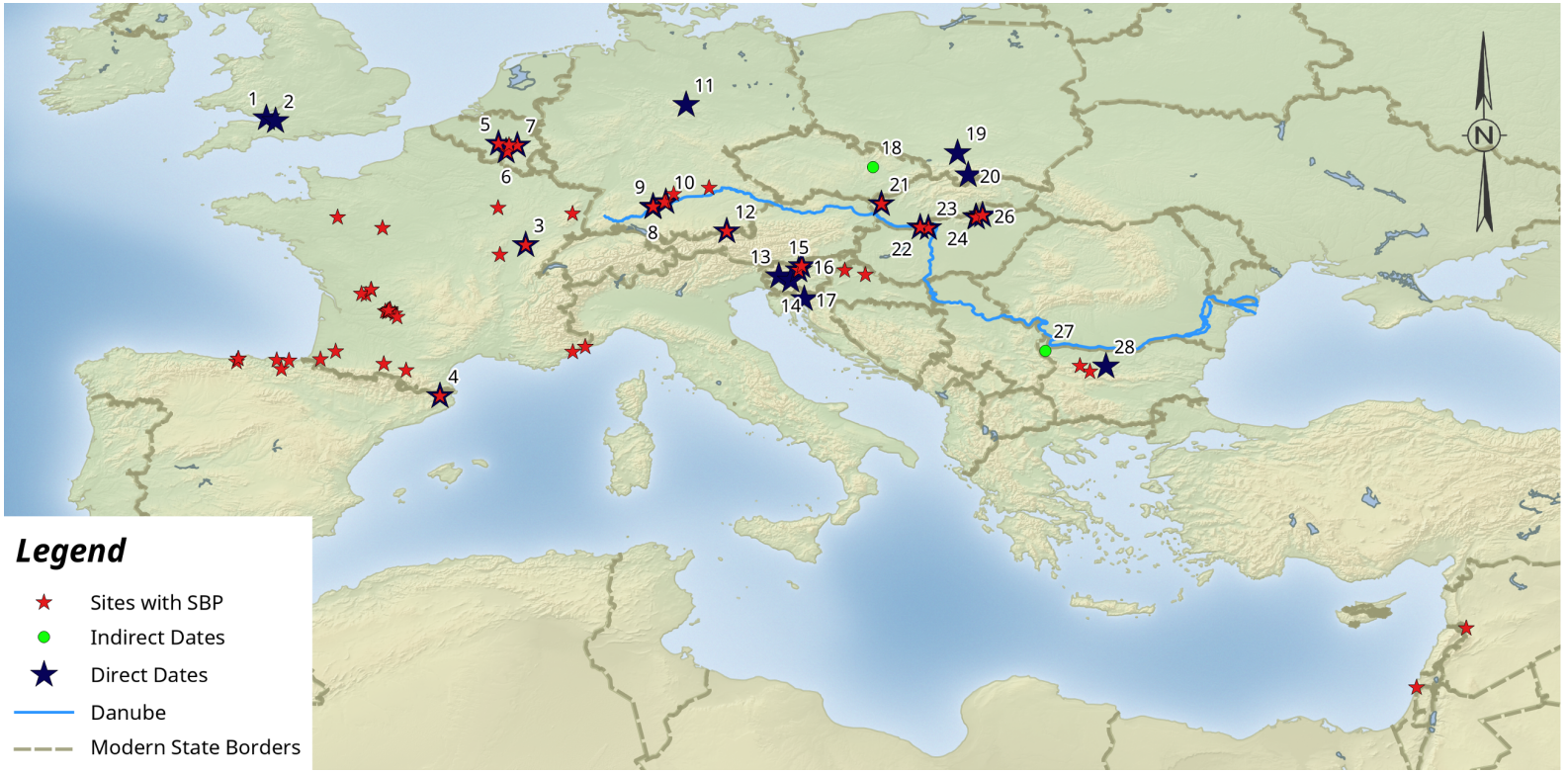


Figure 14.1: Osseous points: map showing distribution of SBP finds (after Knecht, 1993a; Tejero and Grimaldi, 2015; Wood et al., 2014) and location of dated osseous points (published and new). The latter sites are: (1) Uphill Quarry, (2) Hyaena Den, (3) Trou de la Mère Clochette, (4) L'Arbreda, (5) Spy, (6) Trou Magrite, (7) Trou al'Wesse, (8) Sirgenstein, (9) Brillenhöhle, (10) Vogelherd, (11) Hermannshöhle, (12) Tischoferhöhle, (13) Divje Babe I, (14) Ljublansko Barje, (15) Mokriška Jama, (16) Potočka Zijalka, (17) Bukovac, (18) Mladeč, (19) Mamutowa Cave, (20) Obłazowa cave, (21) Dzeravá Skala, (22) Jankovich, (23) Bivak, (24) Istállóskő, (25) Peskő, (26) Szeleta, (27) Kozarnika, (28) Tabashkata.

14.1 The importance of direct dating

Osseous artefacts, including bone and antler points, can be directly radiocarbon dated. However, material is often limited and maintaining the integrity of the sample for future, as well as other types of analyses is important. Therefore, the use of this limited resource has to be well justified. This section outlines why confining the dataset to directly dated osseous points is crucial to the investigation of their spatio-temporal distribution – irrespective of the quality of an artefact's find context – and why indirect dating via layer association and Bayesian modelling can result in imprecise and inaccurate age estimations.

The site of Istállóskő (see section section 11.2) is revisited as a case study to illustrate the effects of indirect dating on osseous point age estimations (see fig. 14.2). In its simplified form, the site contains a stratigraphy with two Palaeolithic archaeological horizons, partially separated by a sterile layer. Both layers contained osseous points (illustrated by the blue squares).

Direct dating of the antler points resulted in two temporal groups. Assuming the dating to be accurate, indirect dating, using other material from the same archaeological horizons and a stratigraphic Bayesian model, should result in start, transition, and end boundaries similar to those illustrated in dark grey. However, when the radiocarbon dataset is based on unmodified faunal remains – a strategy frequently employed in archaeological investigations – we notice that none of the boundaries (illustrated in red) line up with our expectations. Moreover, the age window for the points in the lower layer is grossly overestimated, stretching both younger and older than the age from direct dating, and thus pushing the points from the upper horizon to a time period that no longer overlaps with the directly obtained dates. It can be concluded that the noise from non-human activity at the site is detrimental to extracting the brief periods of human presence.

An alternative strategy would be to focus on dates obtained on anthropogenically modified material, *e.g.* cut marked bone. This would reduce the noise by focusing only on human activities. As a result, the calculated

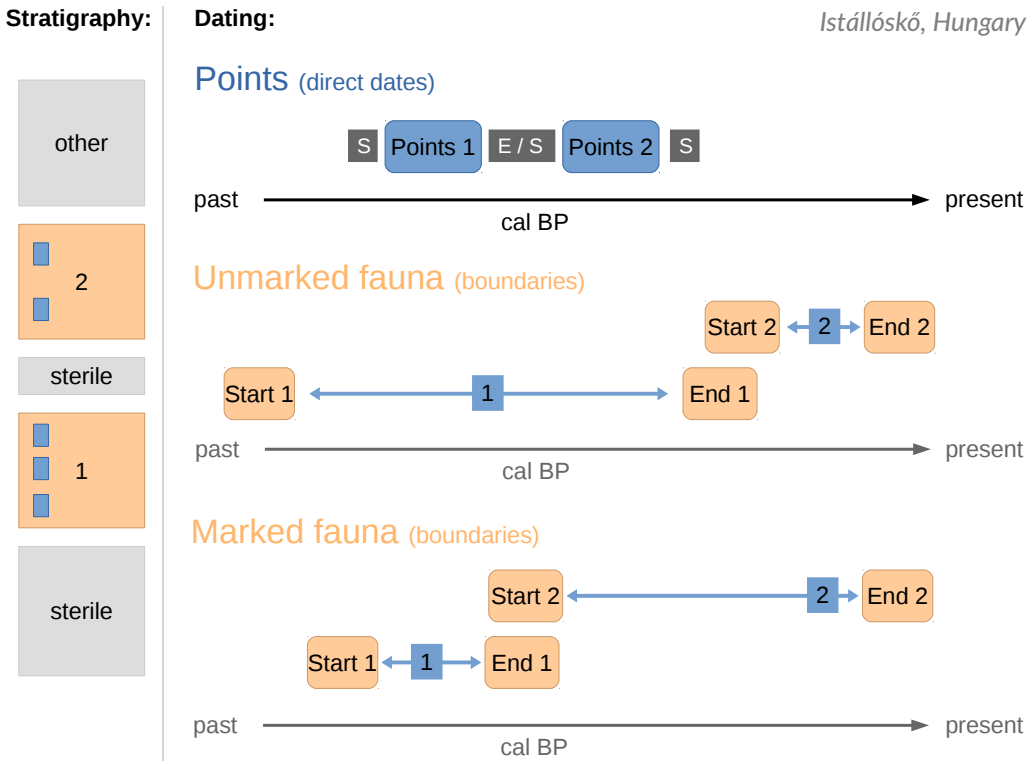


Figure 14.2: Osseous points: schematic illustration of why direct dating of osseous points is important to reliably establish their age (based on Istállóskő from section 11.2). Simplified stratigraphy shown on the left with two archaeological horizons (salmon) containing osseous points (blue), and separated by a sterile layer. On the right, the likely age range for the two osseous point industries (blue) is given, depending on whether they are directly dated (top), or indirectly dated via layer association using unmodified (centre) or anthropogenically modified bones (bottom).

boundaries are no longer in contradiction to those expected when looking at the direct dating. Nonetheless, the age window obtained for the osseous points from the upper layer extends to ages far younger than the direct dates suggest. The reduced precision is a direct result of a layer that comprises several periods of human occupations undetected during excavations, while the points are confined to human activity within the earliest period of layer formation.

It can be concluded, that osseous points offer the unique opportunity to directly date a well-defined human action (i.e. killing of an animal), which is assumed to be close enough to the actual manufacturing process to fall well within the boundaries of the radiocarbon error. Unlike ivory, there is presently no evidence for using fossil reserves for antler artefacts in the Palaeolithic. Forgoing this opportunity, by relying on indirect dating, results in additional noise introduced to the system and can lead to imprecise, and even inaccurate age estimations for these characteristic artefacts.

It is worth noting, however, that – as with other dating approaches – it is assumed that the artefact's find location is reasonably close to the original production site. Only further extensive analyses (*e.g.* via stable isotopes) might be able to test this hypothesis. However, such long distance transport would not necessarily invalidate the age of an artefact, nor the presence of a cultural expression. For it to have affected our ability to investigate the spread of a specific technology or artefact type, it needs to have occurred on a large scale, while the evidence in the area of original manufacture is largely lost. This scenario is not impossible, but deemed improbable.

14.2 The dataset

The chronometric dataset used for investigating the spread of the 'Aurignacian' osseous point industry consists of 53 direct radiocarbon dates found in the literature and 37 contributed by this research project. In the following two sections, the quality of individual measurements are assessed, and the selection used for modelling presented. The dates are categorised as (a) 'good', if pre-treatment protocol and results suggest no reliability concerns, (b) 'ok', if there is an indication that the date may slightly underestimate the true age of the sample, and (c) 'poor', if issues are detected that could cause severe dating offsets or insufficient information for assessment is available.

14.2.1 Published data

Direct dating of osseous points has slowly increased since the 1990s, though is still limited and covers only a few archaeological sites (see tab. 14.1–14.2). Unlike the points dated during this project, none of the directly dated artefacts found in publications have been physically examined for this dissertation. Therefore, typological identifications were adopted from the literature, unless documentation visibly contradicts their conclusions (see also fig. 14.3–14.4).

Re-dating of certain artefacts demonstrates differences in dating reliability, some of which are explained by pre-treatment improvements, others by singular instances of pre-treatment anomalies. As no further external constraints are used that could highlight dating inconsistencies, it is necessary to exclude dates with problematic pre-treatment protocols or results. Where necessary, further treatment information was requested from the respective radiocarbon laboratories.

The triangular shaped mesial point fragment from Uphill Quarry (England) has been dated twice at ORAU: first using the gelatine (AG) protocol, second with ultrafiltration (AF) (Jacobi and Pettitt, 2000; Jacobi et al., 2006). In both cases, the pre-treatment results flag no anomalies. However, despite the point being coated with PVA, no additional measures against conservation contamination (*e.g.* solvent wash steps) were introduced. In light of ORAU's internal comparison of AG and AF dates, the latter is seen as more reliable, and will be used to represent the age of the artefact.

At the Hyaena Den (England) an antler point was found. It shows no evidence of a split base and has a near rectangular cross-section – similar to finds from Hungary. The artefact was dated four times (Hedges et al., 1996; Jacobi et al., 2006). The first date was obtained as early as 1992, using the then standard treatment with ABA, followed by gelatinisation and purification through ion exchange (labelled internally as AI, see also Hedges and Law, 1989, Appendix I). This method has been superseded by the gelatine (AG) and ultrafiltration (AF) protocols used in later dating. All dates from

Table 14.1: Osseous points: published direct AMS radiocarbon dates on osseous points, pt. 1/2. References: [1] Jacobi and Pettitt (2000),[2] Jacobi et al. (2006), [3] Hedges et al. (1996), [4] Szmidt et al. (2010a), [5] Wood et al. (2014), [6] Flas et al. (2013), [7] Charles et al. (2003), [8] Otte et al. (1998), [9] Conard and Bolus (2003), [10] Bolus and Conard (2006), [11] Grünberg (2006), [12] Moreau et al. (2015), [13] Gaspari et al. (2011). Treatment codes: * = ORAU solvent wash; AG = ORAU gelatine; AF = ORAU ultrafiltration; AI = ORAU acid-base-acid + gelatinisation + ion exchange; ABA = acid-base-acid + gelatinisation (*i.e.* modified Longin). Comments: NS = no solvent washes applied prior to AF or AG treatment; treat. = treatment choice inadequate; yield = collagen yield after pre-treatment < 1wt.%; MIN = dates likely to underestimate true age of sample; info = insufficient treatment information. Site number refers to figure 14.1. grey rows – mark dates that will not be used in the models, see text for explanation.

No.	Country	Site.	Sample	Type	Material	Dated	Treat.	C:N	$\delta^{13}C$	Lab-no.	^{14}C (BP)	Date (cal BP)	Quality	Comment	Reference
1	England	Uphill Quarry	BRSMG Ce 16476 Up	lozenge / triangular	antler	1999	AG	3.3	-17.3	OxA-8408	28080 ± 360	32970 – 31230	ok	NS	[1], [2]
			BRSMG Ce 16476 Up	lozenge / triangular	anlter	2004	AF	3.2	-17.5	OxA-13716	31730 ± 250	36190 – 35050	good	NS	[2]
2		Hyaena Den	Wells Mus. 1484	point	antler	1992	AI	–	-20.1	OxA-3451	24600 ± 300	29340 – 27980	poor	treat., MIN	[2]
			Wells Mus. 1484	point	antler	2004	AF*	3.4	-19.2	OxA-13803	31550 ± 340	36170 – 34780	ok	C:N	[2]
			Wells Mus. 1484	point	antler	2004	AF*	3.2	-19.9	OxA-13554	33200 ± 1600	41590 – 34590	ok	yield	[3]
			Wells Mus. 1484	point	antler	2004	AG*	3.4	-19.3	OxA-13323	30240 ± 380	34940 – 33680	ok	–	[3]
3	France	Trou de la Mère Clochette	TMC 2	SBP	antler	2008	AF	3.4	-18.3	OxA-19621	33750 ± 350	38970 – 36960	good	C:N	[4]
			TMC 3	SBP	antler	2008	AF	3.3	-19.1	OxA-19622	35460 ± 250	40720 – 39440	good	–	[4]
			MCL-06	SBP	antler	2000/01	acid	–	-21.1	Beta-150312	29490 ± 190	34050 – 33300	poor	treat, info	[4]
4	Spain	L'Arbreda	B4 DB28643	lozenge	–	2009	AF*	3.2	-19.7	OxA-21783	32100 ± 450	37340 – 34980	good	–	[5]
5	Belgium	Spy	RBINS 13	SBP?	antler/bone	2006	ABA	3.1	-20.3	GrA-32619	32830 +200/–190	37620 – 36270	ok	NS	[6]
6		Trou Magrite	RBINC, Acc. No 1923	lozenge	antler	1996	AI	3.0	-19.0	OxA-6564	25080 ± 320	30030 – 28460	poor	treat., MIN	[7]
7		Trou Al'Wesse	–	Mladeč	ivory	1998	AG	2.9	-21.6	Lyon-590/OxA-7496	30750 ± 850	36910 – 33260	poor/ok	NS, MIN	[8]
8	Germany	Sirgenstein	–	MBP?	bone	–	ABA	–	–	KIA-13082	26730 +170/–160	31150 – 30670	ok	%C	[9]
			–	MBP?	bone	–	ABA	–	–	KIA-13079	27250 +180/-170	31430 – 30940	ok	%C	[9]
9		Brillenhöhle	–	MBP	antler	2003	ABA	–	–	KIA-19551	32470 +270/–260	37260 – 35730	ok	%C	[10]
			–	SBP?	antler	2003	ABA	–	–	KIA-19550	30400 +240/–230	34820 – 33960	ok	%C	[10]
10		Vogelherd	–	MBP	antler	2003	ABA	–	–	KIA-19541	31310 +240/–230	35740 – 34700	ok	%C	[10]
11		Hermannshöhle	HK 63:145	Mladeč	antler/bone	2004	AF*	3.5	-17.5	OxA-13048	29210± 210	33850 – 32900	poor	C:N	[11]
12	Austria	Tischoferhöhle	T 137	MBP?	antler	2003	ABA	–	–	KIA-19545	29500 ± 200	34070 – 33290	ok	–	[10]
			T 139	point	bone	2003	ABA	–	–	KIA-19543	32010 +510/–480	37340 – 34840	ok	–	[10]
			T 143	SBP	bone	2003	ABA	–	–	KIA-19544	31530 +210/–200	35940 – 34920	ok	–	[10]

Table 14.2: Osseous points: published direct AMS radiocarbon dates on osseous points, pt. 2/2. References: [12] Moreau et al. (2015), [14] Hofreiter and Pacher (2004), [15] Davies et al. (2015), [16] Housley (2003). Treatment codes: * = ORAU solvent wash; AG = ORAU gelatine; AF = ORAU ultrafiltration; AI = ORAU acid-base-acid + gelatinisation + ion exchange; ABA = acid-base-acid + gelatinisation (*i.e.* modified Longin). Comments: NS = no solvent washes applied prior to AF or AG treatment; treat. = treatment choice inadequate; yield = collagen yield after pre-treatment < 1wt.%; MIN = dates likely to underestimate true age of sample; UF = high UF background; AMS = variable AMS current. grey rows – mark dates that will not be used in the models as another date, deemed more reliable was included for the same specimen.

No.	Country	Site.	Sample	Type	Material	Dated	Treat.	C:N	δ^{13}C	Lab-no.	^{14}C (BP)	Date (cal BP)	Quality	Comment	Reference
13	Slovenia	Divje babe I	DB-407a	SBP	bone?	2013	AF	3.3	-19.0	OxA-28219	29760 ± 340	34570 – 33290	ok	NS	[12]
14		Ljublansko Barje	–	point	wood	2009	UW	–	-26.5	OxA-19866	38490 ± 330	43020 – 42080	good	–	[13]
15		Mokriška jama	MJ-2	flat point	antler	2013	AF	3.4	-20.7	OxA-X-2517-52	34750 ± 600	40860 – 38120	ok	NS, C:N	[12]
			MJ-1	MBP?	bone	2013	AF	3.4	-20.2	OxA-27855	32600 ± 450	38130 – 35640	ok	NS, C:N	[12]
16		Potočka zijalka	PZ-49	MBP	bone	2013	AF	3.4	-18.9	OxA-27854	30800 ± 370	35520 – 34060	ok	NS, C:N	[12]
			PZ-54	MBP?	bone	2002	ABA	–	–	VERA-2521	31080 +370/–360	35810 – 34300	ok	info	[14]
			PZ-54	MBP?	bone	2013	AF	3.4	-21.0	OxA-28038	31950 ± 450	36980 – 34840	ok	NS, C:N	[12]
			PZ-54	MBP?	bone	2013	AF	3.4	-21.0	OxA-28061	32550 ± 500	38210 – 35520	ok	NS, C:N	[12]
			PZ-59	MBP	bone	2002	ABA	–	–	VERA-2522	30140 +340/–330	34780 – 33680	ok	info	[14]
			PZ-104	point	bone	2013	AF	3.3	-20.0	OxA-27850	30380 ± 370	35040 – 33780	good	NS	[12]
			PZ-112	MBP	bone	2002	ABA	–	–	VERA-2523	31490 +350/–340	36130 – 34730	ok	info	[14]
			PZ-112	MBP	bone	2013	AF	3.4	-21.2	OxA-27849	31220 ± 400	36040 – 34420	ok	NS, C:N	[12]
			PZ-121	MBP	bone	2002	ABA	–	–	VERA-2524	29760 +330/–310	34540 – 33340	ok	info	[14]
			PZ-121	MBP	bone	2013	AF	3.4	-21.1	OxA-27852	31360 ± 400	36140 – 34560	good	NS, C:N	[12]
			PZ-126	MBP	bone	2002	ABA	–	–	VERA-2525	29740 +330/–310	34520 – 33310	ok	info	[14]
			PZ-126	MBP	bone	2013	AF	3.4	-20.4	OxA-27853	31500 ± 400	36240 – 34670	ok	NS, C:N	[12]
			PZ-128	MBP	bone	2002	ABA	–	–	VERA-2526	29560 ± 270	34220 – 33160	ok	info	[14]
			PZ-128	MBP	bone	2013	AF	3.3	-20.9	OxA-27851	30910 ± 380	35650 – 34130	good	NS	[12]
19	Poland	Mamutowa cave	14-17	Mladeč	ivory	2005	AF*	3.2	-20.8	OxA-14436	33640 ± 250	38670 – 37120	good	–	[15]
			14-67	Mladeč	ivory	2005	AF*	3.2	-20.6	OxA-14434	32280 ± 220	36690 – 35650	good	–	[15]
20		Obłazowa cave	157/88	point	antler	1992	AI	–	-17.7	OxA-3695	23420 ± 380	28430 – 26980	poor	treat.	[16]
21	Slovakia	Dzeravá Skala	Pb 580	SBP	antler	2007	AF*	3.3	-18.3	OxA-17963	35600 ± 400	41180 – 39320	good	–	[15]
			–	MBP	antler	2005	AF	3.1	-20.3	OxA-15334	31600 ± 900	38160 – 34050	ok	NS, AMS	[15]
						2005	AF	3.3	-20.1	OxA-15335	31000 ± 1100	38320 – 33220	ok	NS	[15]
24	Hungary	Istállóskő	Hermann Otto Museum, 6306; 53.37.8	point	antler	2006	AF	3.3	-20.4	OxA-X-2170-18	33600 ± 900	40210 – 35910	ok	NS	[15]
			Pb 50/34	point	antler	2007	NRC	3.1	-19.3	OxA-X-2244-32	34890 ± 250	40040 – 38790	poor	UF	[15]
25		Peskő	Pb 927	SBP	antler	2007	AF*	3.3	-18.6	OxA-17966	36400 ± 800	42360 – 39470	good	–	[15]
			Pb 930	MBP	antler	2007	AF*	3.3	-19.7	OxA-17964	33500 ± 450	38840 – 36510	good	–	[15]
			Pb 933	lunate	antler	2007	AF*	3.3	-19.2	OxA-17967	38300 ± 1500	45800 – 40100	good	–	[15]

the 2000s also used solvent washes to remove conservation contamination. OxA-13803 and OxA-13323 have a slightly elevated C:N ratio, while OxA-13554 gave a collagen yield of <1 wt.%, resulting in a larger dating error. As a result, the OxA-13803 appears to be the most reliable age estimate.

Dates of a nearly complete SBP and of two SBPs wings from the French site of Trou de la Mère Clochette were published by Szmidt et al. (2010a). Banks et al. (2013) question the identification of the wing fragments as SBPs. They argued, that the fragmentary nature of the artefacts prevents secure classification. Furthermore, the old age of TMC 3, the absence of Early Aurignacian lithics, and the possible presence of a Proto-Aurignacian assemblage contradict expectations. However, other, securely identified, SBPs have been found at the site[1], and TMC 3 is not the SBP with the oldest radiocarbon measurement. Disqualifying the artefacts *a priori* based on lithic association ignores the great variability observed throughout Europe. The wing fragments are therefore included in this study as possible SBPs

None of the Mère Clochette samples had been conserved. The wings were dated using ultrafiltration at ORAU, and appear reliable, though OxA-19621 has a slightly elevated C:N ratio. The SBP MCL-06, on the other hand, appears to have only been pre-treated using acid washes and no further pre-treatment information is available. It is, therefore, impossible to assess whether the rather young age reflects the sample age or resulted from insufficiently rigorous pre-treatment.

Wood et al. (2014) dated a lozangic shaped point from L'Arbreda (Spain), using the ORAU ultrafiltration protocol with solvent washes. Collagen yield was good, and C:N ratio a perfect 3.2.

Only three points from the Belgian collections have presently been dated. A possible SBP from Spy (Flas et al., 2013), a lozangic shaped antler point from Trou Magrite Charles et al. (2003), and a Mladeč ivory point from Trou Al'Wesse (Otte et al., 1998). Unfortunately, the second (OxA-6564)

[1]Future direct dating of those will clearly help to better understand the osseous point assemblage.

has to be excluded on the basis of insufficiently rigorous pre-treatment. The first (OxA-7496) shows acceptable pre-treatment results, though no steps to counter conservation contamination were applied. The last (OxA-7496) was only treated with ORAU's gelatine protocol (AG) and no solvent wash protocol was followed. In addition, the C:N ratio is decreased.

With the exception of Hermannshöhle, all German osseous points were dated at Kiel (Bolus and Conard, 2006; Conard and Bolus, 2003), which uses a modified Longin protocol (ABA + gelatinisation) for all their osseous samples. Huels et al. (2017) suggest that such a protocol should generally produce comparable results to ORAU's ultrafiltration, albeit testing was conducted on well preserved and non-conserved faunal remains. When the points were treated, no isotope measurements were taken. Collagen yield for all samples exceeded 1 wt.%. However, all samples gave higher than usual carbon concentration on combustion, with the exception of KIA-19550 from Brillenhöhle, which gave very low %C results[2]. Consequently, these dates may slightly underestimate the true age of the artefacts.

The Mladeč point from Hermannshöhle was dated at ORAU (Grünberg, 2006). Pre-treatment was adequate, but the high C:N ratio of 3.5 suggests the date to be unreliable, possibly underestimating the true age of the sample.

Three points from Tischoferhöhle (Austria) were also measured in Kiel, using their modified Longin method, and no isotope measurements were made. Unlike the German points, all pre-treatment results were within expectations, inducing %C on combustion.

The SBP from Divje babe I (Slovenia) was treated with ORAU's ultrafiltration protocol, though no measures against potential conservation contamination were taken (Moreau et al., 2015). Pre-treatment results indicate no anomalies. The same publication lists two dated points from Mokriška jama (Slovenia). They differ greatly in shape, with the older being very flat and

[2]This assessment already takes a *ca.* -10 wt.% offset into account. A change in reactor volume has affected the calculation which used the pressure readings to estimate carbon concentration. As a result concentrations were overestimated by 10 wt.%. The calculation was not adjusted until 2010.

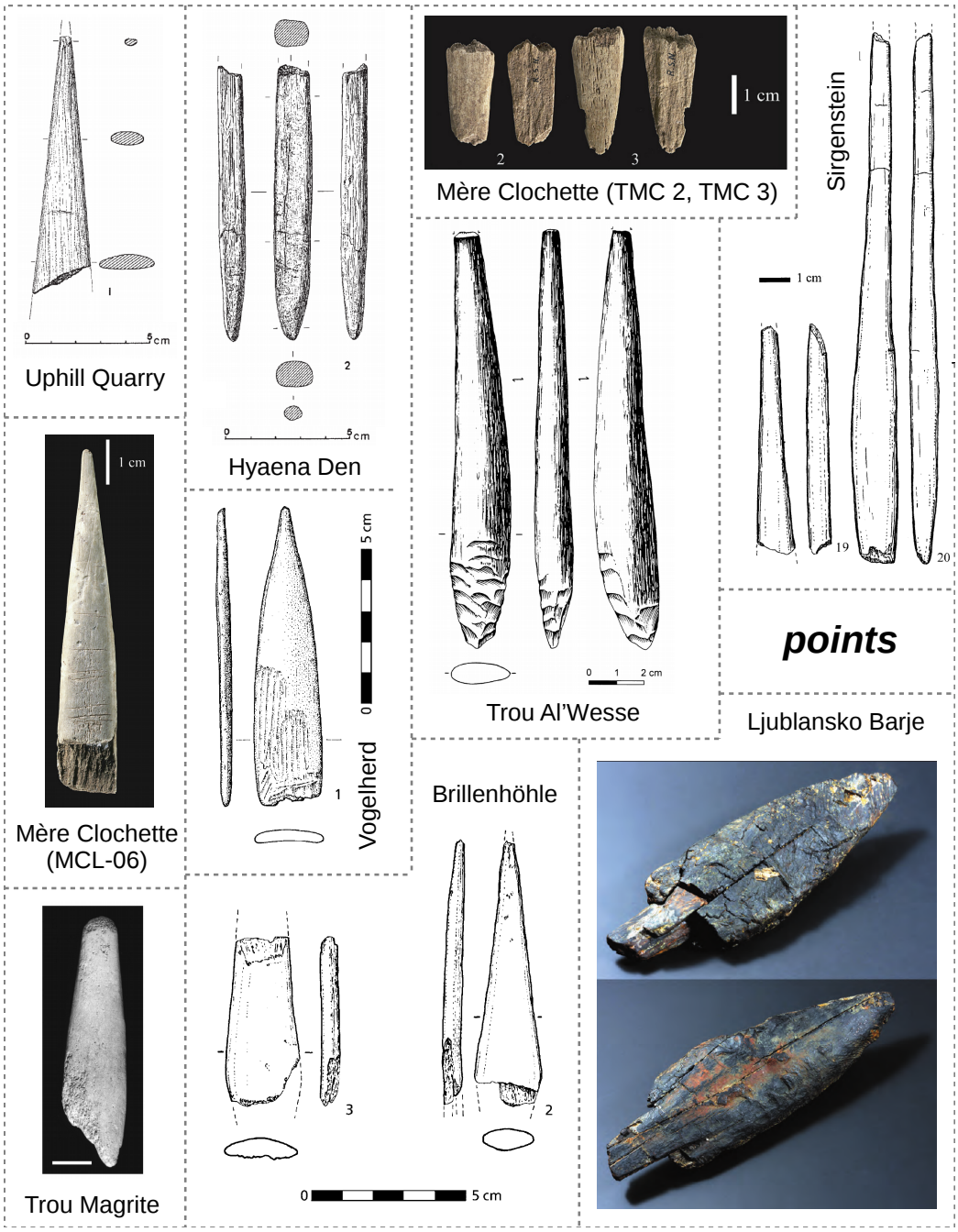


Figure 14.3: Osseous points: directly dated osseous and wooden points from the literature (pt. 1/2). While the first are believed to have been made by AMH, the authorship of the latter (Ljubljansko Barje) remains unknown. The figures were taken from Jacobi et al. (2006, fig. 8), Szmidt et al. (2010a, fig. 9, 11), Bolus and Conard (2006, fig. 3, 6), Conard and Bolus (2003, fig. 6)Otte et al. (1998, fig. 3), Charles et al. (2003, fig. 1), and Gaspari et al. (2011, fig. 15.2).

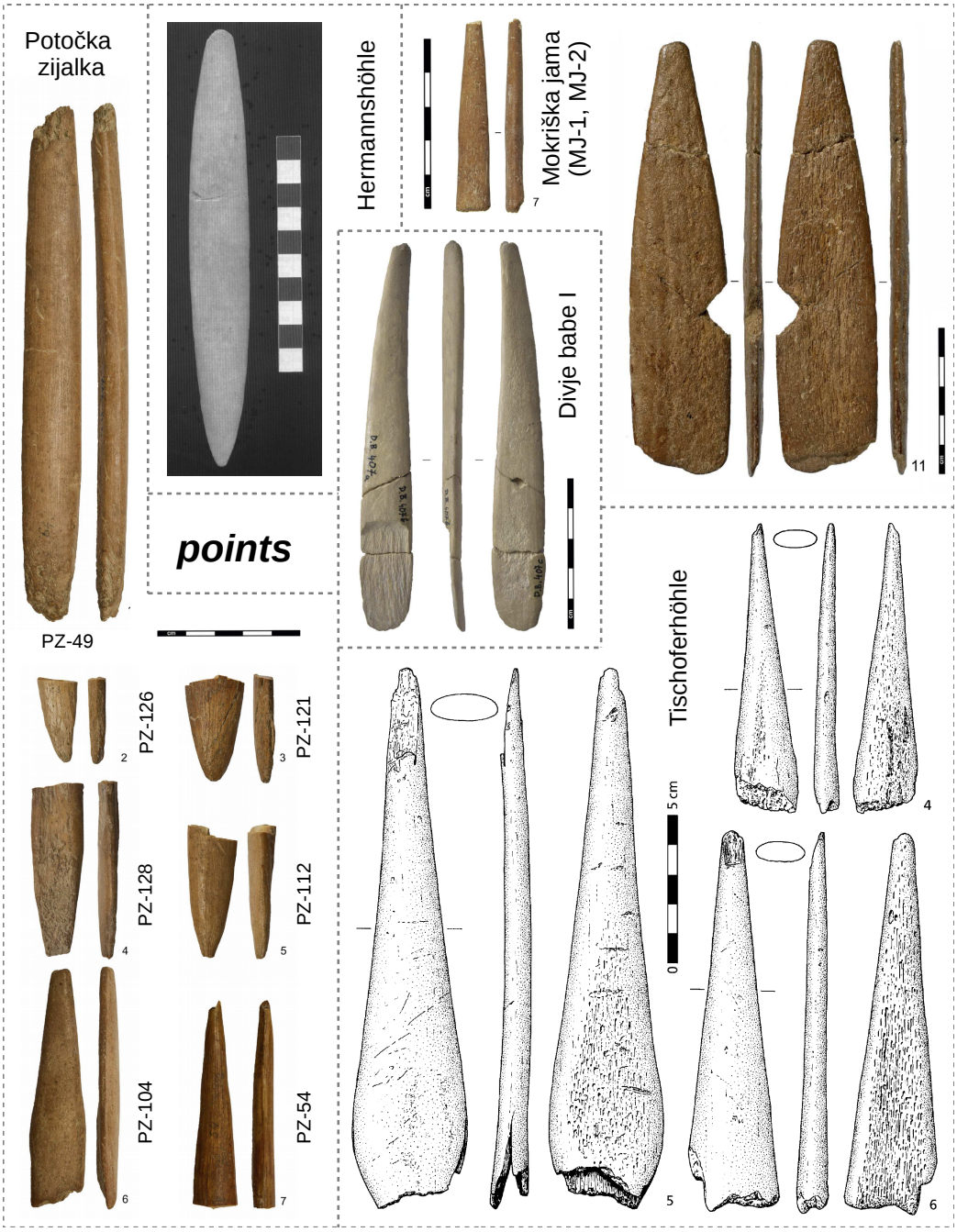


Figure 14.4: Osseous points: directly dated osseous points from the literature (pt. 2/2). The figures were taken from Moreau et al. (2015, fig. 3, 5, 6), Grünberg (2006, fig. 2), and Bolus and Conard (2006, fig. 3).

broad, and the younger looking similar to the MBPs found in Hungary. As before, the samples were ultrafiltered and no solvent steps applied. Despite both points showing slightly elevated C:N ratios, the dates should still be reliable.

There were two dating campaigns at Potočka zijalka (Slovenia) (Hofreiter and Pacher, 2004; Moreau et al., 2015). In the first instance, samples were treated in Vienna, and in the second at ORAU. While Oxford applied ultrafiltration (Brock et al., 2010b), VERA used a modified Longin protocol (Higham and Wild, 2013). Neither laboratory introduced special measures against conservation contamination. The resulting radiocarbon dates obtained by the two labs on the same artefact are statistically distinguishable (using a χ^2-test) in all but one case, with the VERA dates being younger. Moreau et al. (2015) suggest, that the sample specific background correction at ORAU is the likely origin of this difference. However, the difference could also originate in the different pre-treatment protocols used. Regrettably, no additional measurements (%C, δ^{13}C, δ^{15}N, C:N) were undertaken at VERA (E. M. Wild, pers. com. 18/07/2018), making it impossible to compare any quality control indicators and identify problematic samples. Therefore, where dates from both laboratories are available, the ORAU dates are preferred for this study.

Davies et al. (2015) dated osseous points from Mamutowa cave (Poland), Dzeravá Skala (Slovakia), Istállóskő and Peskő (Hungary). The samples from the first and the last sites, as well as the SBP from Dzeravá Skala, used solvent washes and ultrafiltration, and pre-treatment results show no anomalies. The MBP from Dzeravá Skala was dated twice, in both cases with ultrafiltration without any solvent washes. While pre-treatment results flagged no issues for OxA-15335, slight fluctuations in AMS current were detected for OxA-15334. However, the latter are expected to not have negatively affected the dating outcome. Again, no measures to counteract conservation treatment were applied for the points from Istállóskő. However, while all pre-treatment results for OxA-X-2170-18 are within expectations, the ultrafilter background

for OxA-X-2244-32 was too high, and the sample had to be re-filtered – leading to the OxA-X and NRC labels.

A single point from Obłazowa (Poland) was dated in 1992 using ABA, gelatinisation and ion exchange (Housley, 2003). Based on laboratory experience comparing AI newer pre-treatment protocols, the date is likely to severely underestimate the true age of the artefact. Additionally, the relatively low collagen yield of 2.2 mg (1.1 wt.%) suggests that any contamination issues would be exacerbated.

Despite this chapter focusing on 'Aurignacian' osseous points, a single wooden point from Ljublansko Barje (Slovenia) is worth mentioning. It is the only known example of its kind, its authorship unclear, and possibly the oldest organic projectile point found. On the basis of an initial radiocarbon date of >43970 BP (Beta-252943), and its resemblance to leaf-shaped lithic points, Gaspari et al. (2011) associate it with the Neanderthal population and the Mousterian industry in the region – though no material was found in direct association with the artefact. In contrast, a second measurement published by Gaspari et al. (2011) gave a finite age of 38490 ± 330 BP (OxA-19866) – younger than the directly dated Neanderthal remains in the region and surprisingly similar to the age of SBP from Hungary. The sample is a reminder, that non-osseous organic remains are largely missing from the archaeological record of the period, and the picture of osseous projectile point development may be more complex than the recovered evidence suggests.

Assessment of the 53 direct radiocarbon dates on 'Aurignacian' osseous points resulted in the exclusion of 17 measurements on the basis of poor reliability or the availability of more reliable dates from the same artefact. Therefore, only 35 directly dated points found in the literature fulfill the criteria needed to investigate the spread of osseous points. Of these, 8 are classified as SBP, 20 as MBP (including lozenges shaped and Mladeč points), and 7 as neither (including flat and lunate points).

14.2.2 New data

The 37 new direct dates obtained on osseous points during this dissertation are listed in tab. 14.3 and 14.4, and pre-treatment and measurement have already been discussed in detail in the respective site specific chapters (see links in tables 14.3–14.4). As a consequence, this section will only summarise reasons for exclusions.

The massive-based point Buk-01 was dated twice, and as single amino acid dating is seen as more reliable than the gelatine (AG*) protocol with solvent washes, only the NRC date will be considered. For the same reason, the single amino acid dates were selected for those samples from Dzeravá Skala that have been both dated as NRC and AG*.

Biv-01, a SBP, had to be entirely excluded on the basis of having low collagen yield, paired with both a high C:N ratio (3.5) and a high AMS background upon measurement. Jank-05 showed severe signs of reliability issues, having low yield, low %C on combustion, very high C:N (3.9) and high AMS background.

Pes-02 gave a slightly elevated C:N ratio (3.4), but more importantly, also high AMS background. The remaining Peskő samples were only dated using the gelatine and solvent wash protocols (AG*). Therefore, the published ultrafiltered results were deemed of better quality.

One of the ultrafiltered dates for Der-32 was slightly problematic. The remaining two dates were once with solvent wash and gelatine (AG*) protocols, and the other with solvent wash and ultrafiltration (AF*). Despite the fact that the issues surrounding burn 4951 should not have affected the ultrafiltered sample (see Appendix), it was felt that a combined date (AG* & AF*) would provide a more adequate representation. And, finally, Der-33 was excluded as a result of low yield in combination with a very high C:N ratio (3.7).

Table 14.3: Osseous points: new direct AMS radiocarbon dates on osseous points (pt. 1/2). Potential pre-treatment issues highlighted under 'Comment': Yield = collagen yield after pre-treatment < 1 wt.%; %C = lower than usual carbon concentration on combustion; C:N = C:N ratio outside of expectations; AMS = high AMS background. Quality assessment discussed in text, and given as good (date reliable and expected to be accurate), ok (reliable, but possibly underestimating the true age of sample), or poor (sever issues identified, date unreliable and likely inaccurate). For more details see reference links. grey rows – dates that will not be used in models (see text).

No.	Country	Site.	Ref-no.	Point	Material	Treat.	Lab-no.	^{14}C (BP)	Date (cal BP)	Quality	Comment	Reference
28	Bulgaria	Tabashkata	Tk-01	MBP	bone	AG*	OxA-35404	27600 ±400	32605 – 30933	ok	–	8.3.2
			Tk-02	grooved	antler	NRC	OxA-X-2732-21	17160 ± 110	21021 – 20411	good	–	8.3.2
			Tk-03	MBP	antler	AF*	OxA-35534	21120 ±130	25755 – 25163	ok	–	8.3.2
17	Croatia	Bukovac	Buk-01	MBP	antler	NRC	OxA-X-2732-11	31100 ± 520	36130 – 34120	good	–	10.1.2
			Buk-01	MBP	antler	AG*	OxA-35953	29950 ± 500	34990 – 33100	ok	–	10.1.2
23	Hungary	Bivak	Biv-01	SBP?	antler	AG*	OxA-X-2716-50	28000 ± 500	33260 – 31090	poor	yield, C:N, AMS	11.1.2, App.
24		Istállóskő	Istall-01	MBP (Mladeč?)	antler	AG*	OxA-35414	33450 ± 600	39181 – 36246	ok	–	11.2.2
			Istall-02	SBP	antler	AG*	OxA-35382	35800 ± 1200	42755 – 38195	ok	–	11.2.2
			Istall-03	MBP		AF*	OxA-35522	32850 ± 500	38412 – 35886	good	–	11.2.2
			Istall-04	SBP	antler	AG*	OxA-35383	36200 ± 900	42340 – 39052	ok	–	11.2.2
			Istall-05	SBP	antler	AG*	OxA-35415	36100 ± 800	42127 – 39132	ok	–	11.2.2
			Istall-06	MBP	antler?	AG*	OxA-X-2716-11	33200 ± 800	39486 – 35665	ok	yield	11.2.2
			Istall-07	SBP?	bone	AG*	OxA-35384	37200 ± 1200	43920 – 39499	ok	yield	11.2.2
			Istall-08	SBP	antler	AG*	OxA-35385	37700 ± 1600	45592 – 39280	ok	–	11.2.2
			Istall-16	SBP	antler	AG*	OxA-35421	36500 ± 900	42584 – 39380	ok	–	11.2.2
			Istall-18	SBP	antler	AF*	OxA-34771	33450 ± 550	39025 – 36315	good	–	11.2.2
22		Jankovich	Jank-01	MBP?	antler	AG*	OxA-X-2716-49	31800 ± 1000	38540 – 34070	ok	yield	11.3.2
			Jank-02	MBP?	antler	AG*	OxA-X-2716-48	32500 ± 800	38670 – 34930	ok	yield	11.3.2
			Jank-03	MBP?	antler	NRC	OxA-X-2732-10	32750 ± 670	38640 – 35420	good	–	11.3.2
			Jank-05	MBP (Mladeč?)	antler	AG*	OxA-X-2731-11	31200 ± 2300	42570 – 31250	poor	yield, %C, C:N, AMS	11.3.2, App.
			Jank-06	MBP/SBP	antler	AG*	OxA-35386	30800 ± 500	35810 – 33910	ok	–	11.3.2

Table 14.4: Osseous points: new direct AMS radiocarbon dates on osseous points (pt. 2/2). Potential pre-treatment issues highlighted under 'Comment': Yield = collagen yield after pre-treatment < 1 wt.%; %C = lower than usual carbon concentration on combustion; C:N = C:N ratio outside of expectations; burn 4951 = nitrogen calibration issues; AMS = high AMS background. Quality assessment discussed in the text, and given as good (date reliable and expected to be accurate), ok (reliable, but possibly underestimating the true age of the sample), or poor (severe issues identified, date unreliable, and likely inaccurate). For more information see reference links. grey rows – dates that will not be used in models (see text).

No.	Country	Site.	Ref-no.	Point	Material	Treat.	Lab-no.	^{14}C (BP)	Date (cal BP)	Quality	Comment	Reference
26	Hungary	Szeleta	Szel-01	SBP	antler	AG*	OxA-35416	32950 ± 550	38560 – 35890	ok	–	11.5.2
25		Peskő	Pes-01	MBP	antler	AG*	OxA-35419	31750 ± 500	36840 – 34650	ok	–	11.6.2
			Pes-02	SBP	antler	AG*	OxA-X-2731-14	33300 ± 1200	40660 – 35100	poor	C:N, AMS	11.6.2, App.
			Pes-03	point	antler	AG*	OxA-35420	34950 ± 750	41370 – 38050	ok	–	11.6.2
21	Slovakia	Dzeravá Skala	Der-29	point	antler	NRC	OxA-X-2732-13	28340 ± 370	33320 – 31400	good	–	12.1.2
			Der-29	point	antler	AG*	OxA-35597	26980 ± 340	31510 – 30580	ok	–	12.1.2
			Der-32	point	antler	AG*	OxA-35598	27770 ± 370	32690 – 31050	ok	–	12.1.2
			Der-32	point	antler	AF*	OxA-X-2719-20	28760 ± 300	33640 – 31880	ok	burn 4951	12.1.2, App.
			Der-32	point	antler	AF*	OxA-35699	26650 ± 240	31190 – 30460	poor	date issue	12.1.2
			Der-33	MBP?	antler	AG*	OxA-X-2716-51	24680 ± 390	29600 – 27890	poor	yield, C:N	12.1.2
			Der-35	SBP?	antler	NRC	OxA-X-2732-14	35560 ± 870	41870 – 38550	good	–	12.1.2
			Der-36	MBP		AG*	OxA-35387	25140 ± 260	29870 – 28620	ok	yield	12.1.2
			Der-38	MBP		AG*	OxA-35599	30550 ± 500	35560 – 33750	ok	–	12.1.2
			Der-38	MBP	antler	NRC	OxA-X-2732-15	32690 ± 620	38500 – 35470	good	–	12.1.2
			Der-39	MBP	antler	AG*	OxA-35524	30500 ± 450	35390 – 33770	ok	–	12.1.2
			Der-39	MBP	antler	NRC	OxA-X-2732-16	32770 ± 660	38640 – 35470	good	–	12.1.2



Figure 14.5: Osseous points: photos of osseous points directly radiocarbon dated for this dissertation (pt. 1/2).

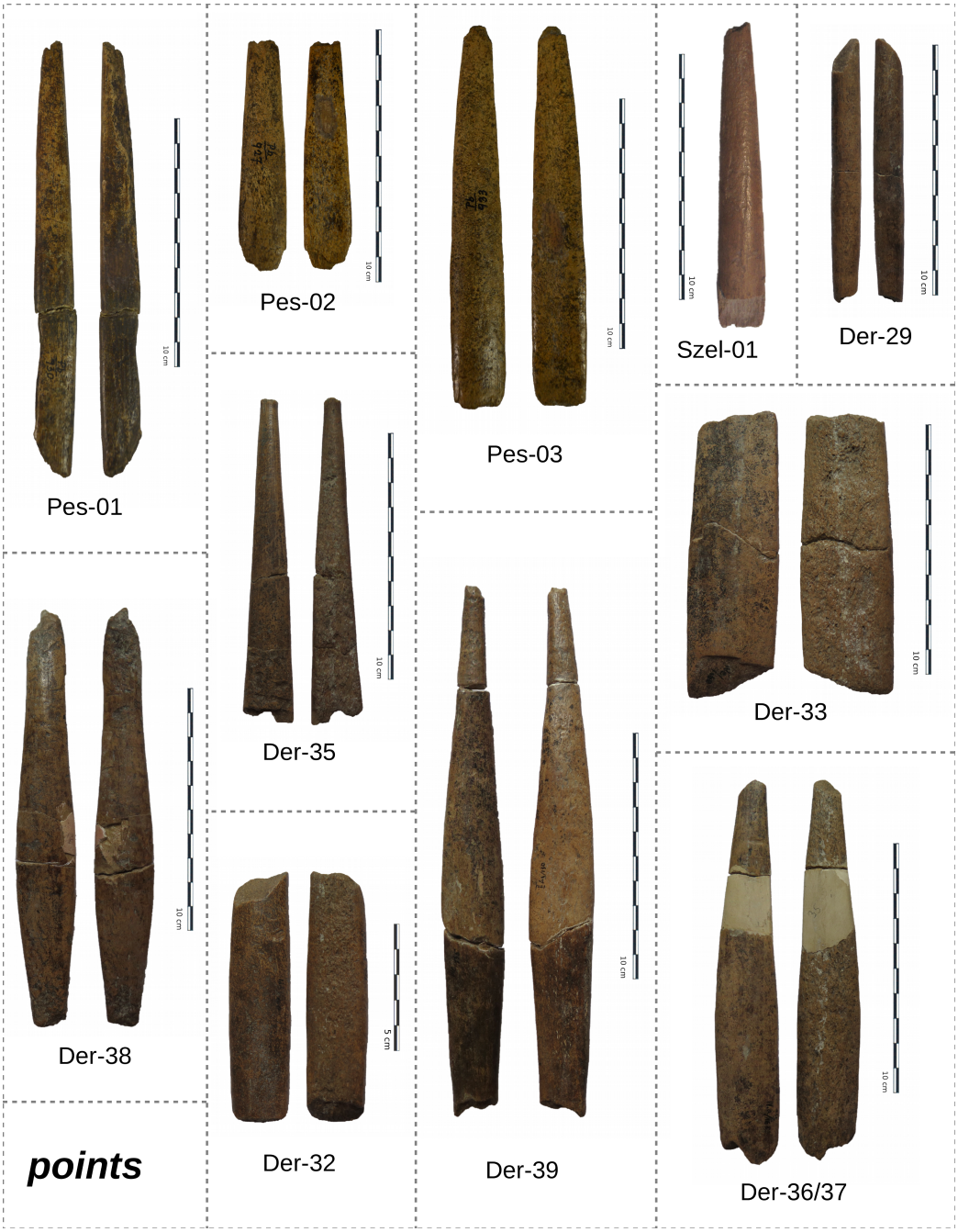


Figure 14.6: Osseous points: photos of osseous points directly radiocarbon dated for this dissertation (pt. 2/2).

In conclusion, the published dataset of directly measured osseous points (see subsection 14.2.1) could be expanded by a total of 26 new dates: 9 SBP, 12 MBP, and 5 undefined (including a grooved and a lunate point).

14.3 Modelling

To assess the temporal distribution of SBPs and MBPs, two KDE models were run in OxCal and compared. The first, used only direct dates from SBP (code: p. 744), the latter, those from MBP, lozenges shaped points and Mladeč points (code: p. 744). In both cases, the datasets were restricted according to the quality assessment discussed in the previous section (white rows in tab. 14.1–14.2 and 14.3–14.4).

In addition, the spatial component was investigated by using the individual point dates of all sufficiently reliable samples (SBP, MBP, and unclassified) and visualising their spatio-temporal occurrence with the help of OxCal's mapping function. The typology was illustrated using red for SBP, blue for MBP (including lozenges and Mladeč points), and green for the remaining or unclassified types (code: p. 746).

14.4 Spatio-temporal distribution

There is a clear temporal difference in the appearance of SBP and MBP in Europe, with the former largely predating the latter (see fig. 14.7). Both KDE models show an initial high probability event with a Gaussian distribution, followed by possible younger, smaller events. Four likely explanations would fit the pattern: (1) a new technology quickly gains popularity before slowly getting 'out of fashion'; (2) some radiocarbon dates underestimate the true age of the artefacts; (3) uncertainties in typological identifications; or (4) geographical variability.

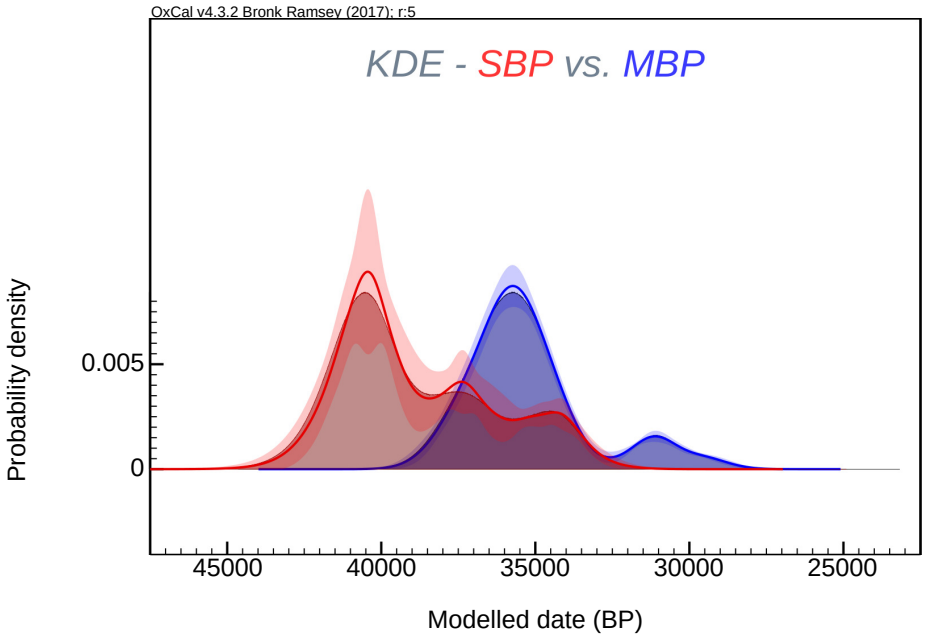


Figure 14.7: Osseous points: comparison of KDE results using direct dates on SBP (**red**, n=17, code: p 744) and on MBP (**blue**, n=32, code: p. 744), showing a bimodal distribution chronologically separating SBPs from MBPs with outlying peaks towards younger periods.

The KDE model using SBP dates shows 7 artefacts that are younger than the identified main event (see fig. 14.8). In general, both ultrafiltered and non-ultrafiltered samples are represented, but 5 artefacts were not specifically treated for conservation contamination (OxA-19621, GrA-32619, KIA-19550, KIA-19544, OxA-28219). One of the SBP wings from Trou de la Mère Clochette showed an elevated C:N of 3.4, and the point from Szeleta (OxA-35416) was treated with the AG* protocol only. For two artefacts – GrA-32619 from Spy, and for KIA-19550 from the Brillenhöhle – there is some debate over whether they might not be fragments of MBPs, though a SBP identification is presently favoured. Only a single antler point, Istall-18 (OxA-34771), appears to be both a securely identified SBP, and fully reliably dated.

The MBP KDE model identifies only 4 artefacts with dates younger than the main event (see fig. 14.9). Neither KIA-13082, nor KIA-13079 from

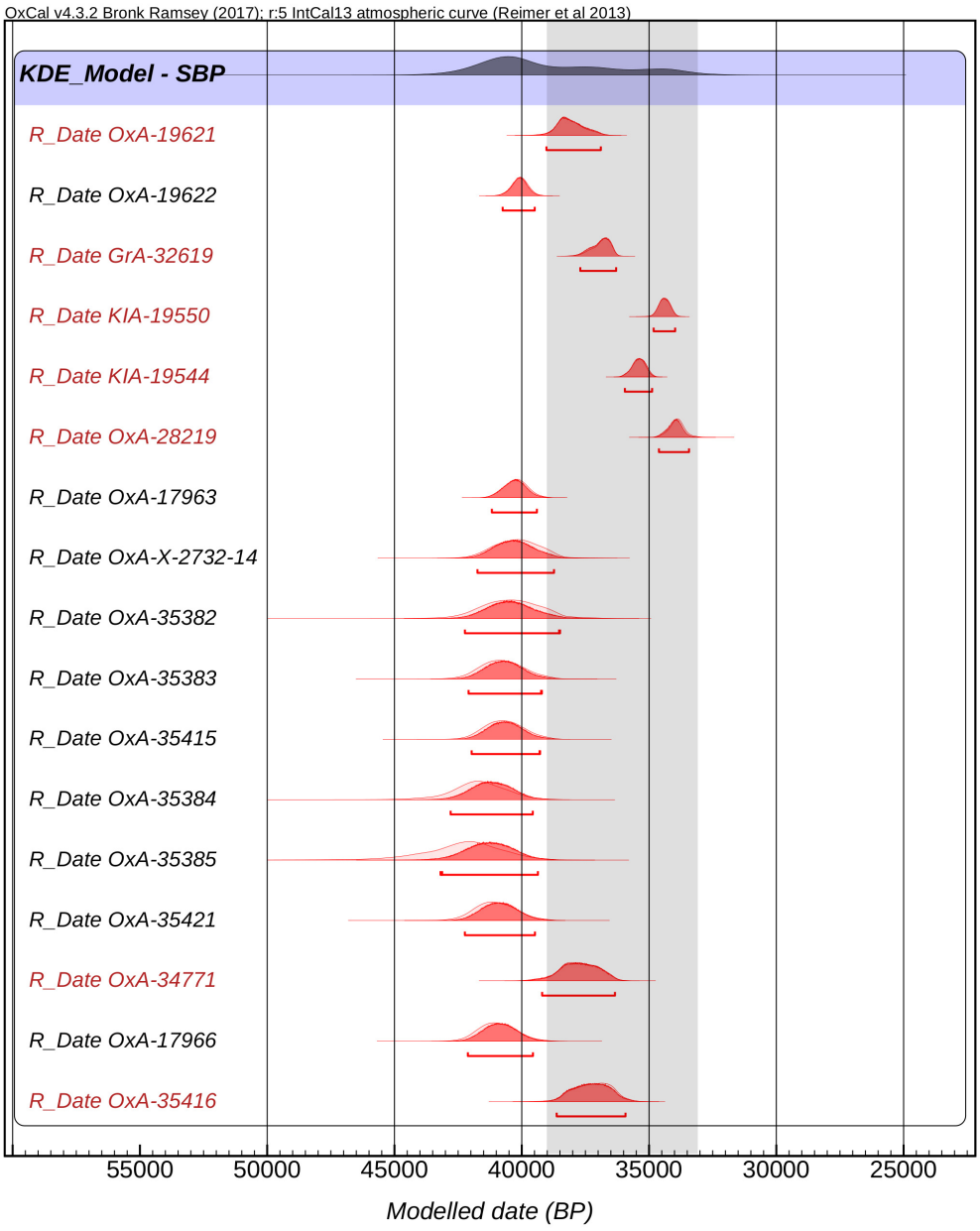


Figure 14.8: Osseous points: distribution of dates used for KDE model of SBP (code: p. 744). Label of dates outside the main event marked **red**, and period of the smaller events created by them highlighted in **grey**.

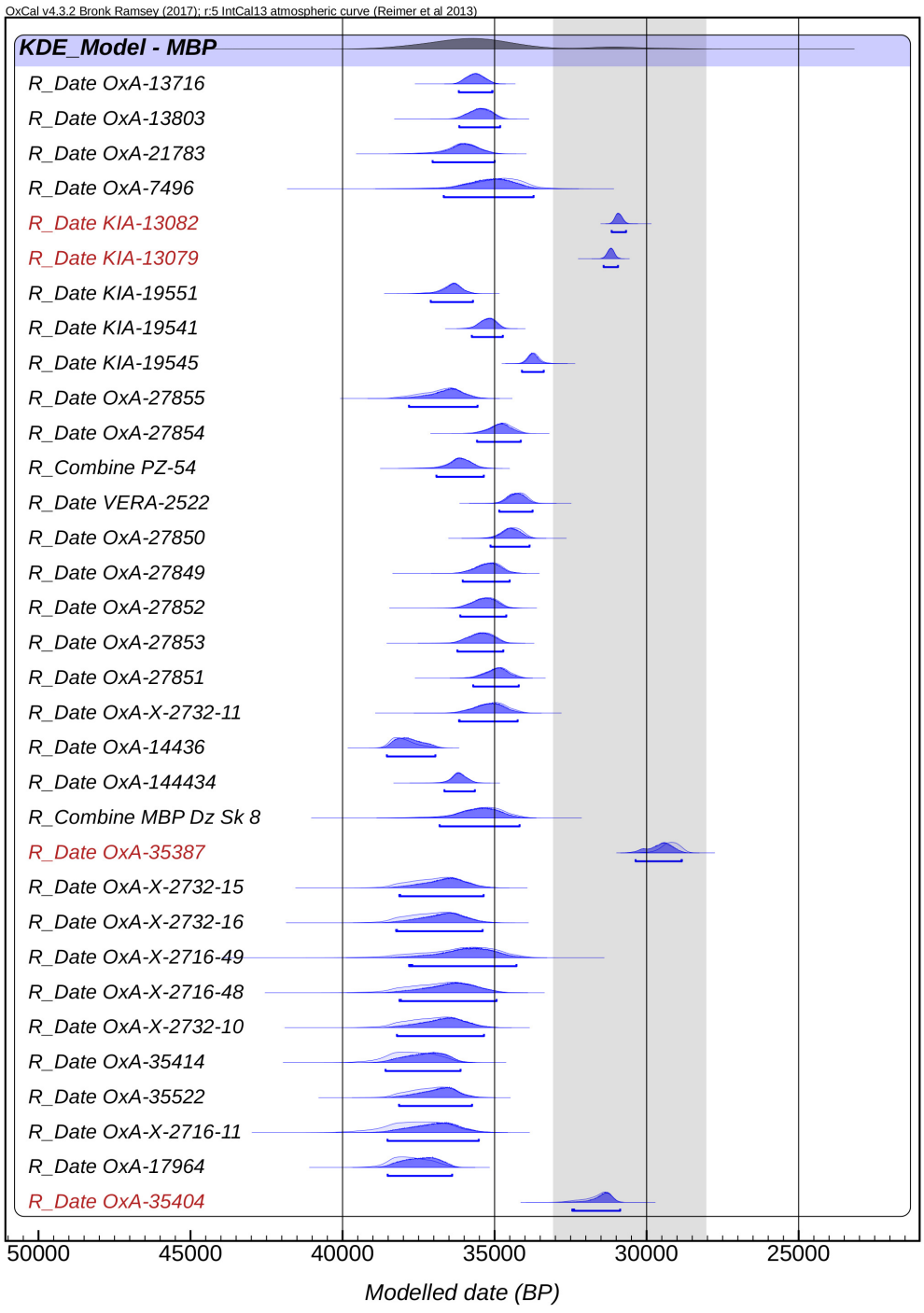


Figure 14.9: Osseous points: distribution of dates used for KDE model of MBP (code: p. 744). Label of dates outside the main event marked **red**, and period of the smaller events created by them highlighted in **grey**.

Sirgenstein had been treated for conservation contamination. On the other hand, OxA-35387 (Der-36) and OxA-35404 (Tk-01) had a yield <1 wt.%, despite only using the AG* protocol. More interestingly, both Sirgenstein points (see fig. 14.3) and Tk-01 (see fig. 14.5) show typological similarities, with a narrower body and a rounder cross-section than other MBPs. They might already represent a different stage of osseous point use.

It appears that the largest contributor to the younger events identified by both the SBP and MBP KDE models is dating reliability, followed by difficulties of securely identifying fragments of SBPs, and variability within the category MBP. At present, there is only limited evidence for the effects of a fading technology over time.

The spatio-temporal distribution of osseous points 44–29.7k cal BP is visualised in figure 14.10. It shows the use of SBPs first appearing in the Bükk mountains (Hungary), before quickly spreading westwards. Similarly, MBPs initially concentrate in the Bükk mountains and adjacent regions, before spreading westwards. The visually apparent propensity for using the latter (as seen in fig. 14.10) is a construct of sample selection. Significantly more MBPs have been dated, compared with SBPs, as the latter tend to be more fragile.

From this data, a Levantine origin of the 'Aurignacian' osseous point industry becomes increasingly less probable. Despite a lack of direct dates from that region, the scarcity of finds is consistent with a location at the geographical periphery of technological use. Therefore, 'Aurignacian' osseous points were not introduced to Europe by early AMHs migrating into the continent, but developed by them after arrival – possibly in reaction to the specific environmental conditions found in the mountainous regions of the eastern Alps and western Carpathians, and/or inspired by a locally distinct use of organic materials. Unfortunately, the antler point from Kozarnika, could not be directly dated. If indirect dating is to be trusted, the point would fall within the period of intense SBP use. However, the material – *i.e.* *Rangifer tarandus* – may have been brought from further to the north, as reindeer remains from that period are extremely rare in Bulgaria.

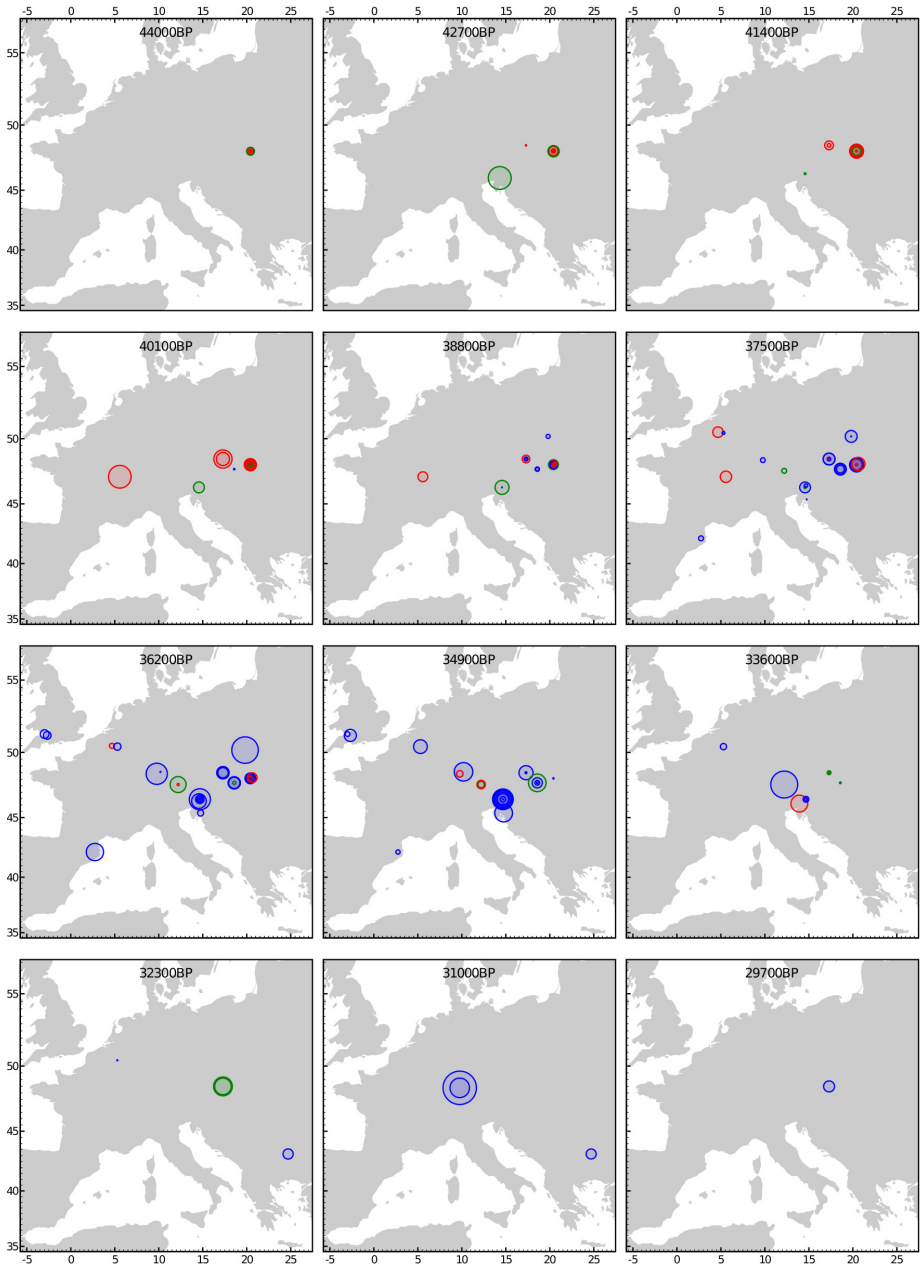


Figure 14.10: Osseous points: spatio-temporal distribution of SBP (**red**), MPB (**blue**) and typologically unidentified points (**green**) from 44–29.7k cal BP, in steps of 1300 years. Circle size represents probability density estimates from direct radiocarbon dates on osseous points. Code: p. 746.

Early SBPs may be contemporaneous with the wooden point found in Slovenia, though a slightly later development would also be compatible with the dating evidence (see second and third tiles in fig. 14.10). As Neanderthal authorship of the wooden point cannot be excluded, new finds may revive the debate around cultural exchange and transfer of knowledge. In case of an AMH authorship, wooden points may have been an attempt at transferring spear point manufacturing from lithics to organics.

The spatio-temporal analysis of 61 directly dated osseous points highlight a temporal separation of SBP and MBP, with the former predominantly in use prior to 40k cal BP, and the latter peaking after 39k cal BP. Both types appear to have been in use for a confined period of time. Outlying data appears to be largely the result of the radiocarbon dating pre-treatment process. However, more detailed typological classification[3] – ideally allowing the identification of fragmented artefacts, rather than just nearly fully intact points – is expected to further reduce the noise in the dataset.

If the Bükk mountains are indeed the origin of the 'Aurignacian' osseous point industry, as the present data suggests, then their development or use occurred independently of diagnostic Aurignacian lithics, and was not brought to the European continent by early AMH migrating into the continent. In contrast, the presence of such osseous points in Bulgaria and as far as the Levant might be the result of a eastwards migration of people or artefacts from central and eastern Europe to the Middle East.

[3] An initial large scale attempt using morphometrics was presented in the doctoral thesis by Doyon (2018), though issues of identifying fragments remain.

Chapter 15

Timing the MP/UP biocultural shift

As the name suggests, the Middle to Upper Palaeolithic biocultural shift has both a biological and a cultural component. Therefore, this chapter will first discuss the directly dated skeletal evidence for late Neanderthals and early AMHs (biology), before investigating the spatio-temporal distribution of different archaeological industries (culture) and their possible authorship (biology + culture). The third section will subsequently focus on the migration of AMHs into Europe.

15.1 Neanderthals vs. AMH

Published Neanderthal and AMH evidence from 21 different sites in Eurasia was available for the period of interest (see fig. 15.1). A dramatic broadening of the geographical scope beyond the Danube corridor is necessary to investigate the possible reasons behind their spatio-temporal pattern – as human remains from the period of interest remain scarce, and reliable direct dating is even rarer.

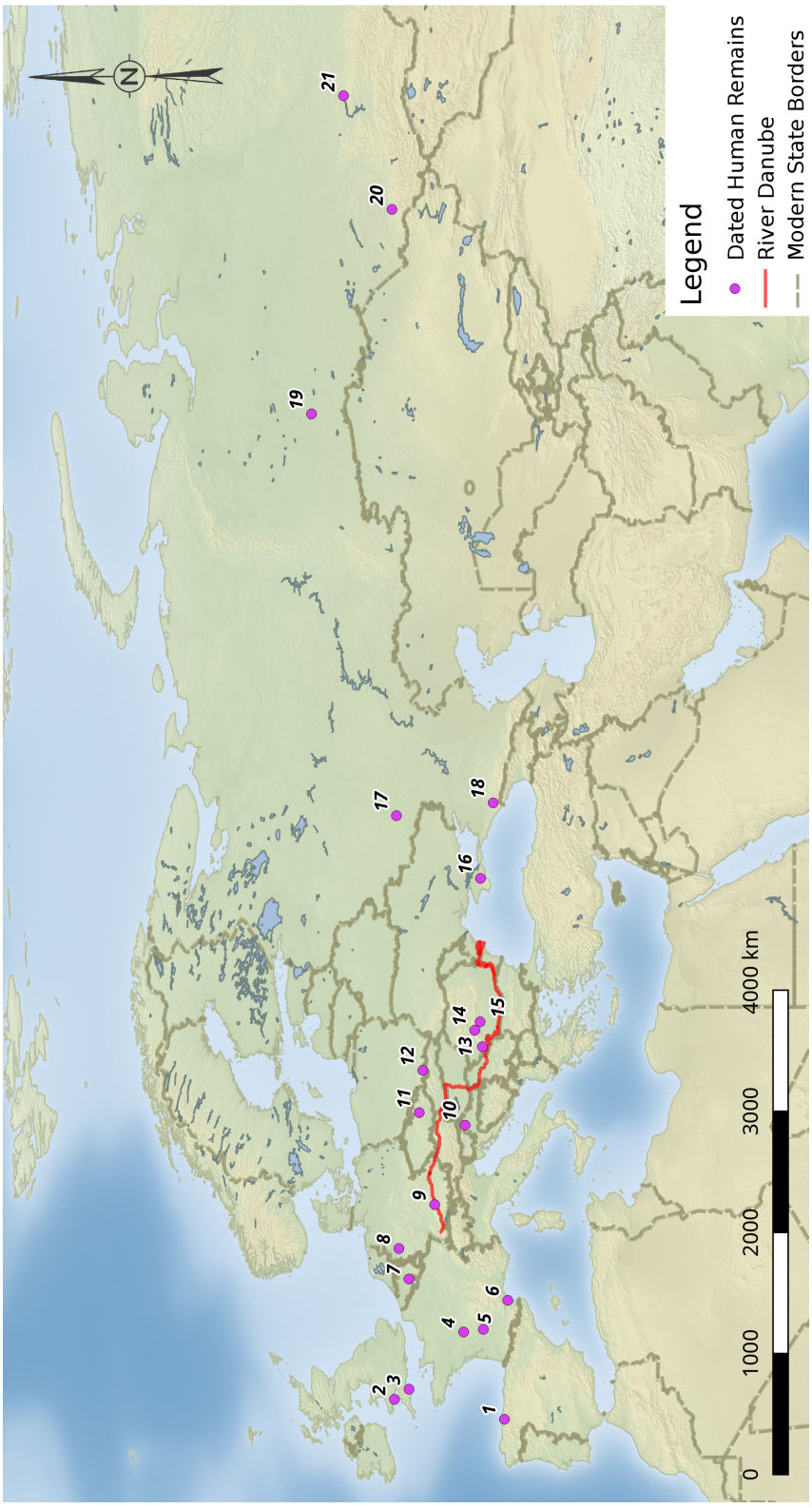


Figure 15.1: MP/UP: map of sites with directly dated human remains: (1) El Sidrón, (2) Paviland, (3) Kent's Cavern, (4) Les Rochers-de-Villeneuve, (5) Grand Abri de la Ferrassie, (6) La Crouzade, (7) Spy, (8) Kleine Feldhöfergrotte, (9) Vogelherd, (10) Vindija, (11) Mladeč, (12) Obłazowa cave, (13) Peștera cu Oase, (14) Cioclovina, (15) Peștera Muierii, (16) Buran-Kaya III, (17) Kostěnki I, (18) Mezmaiskaya, (19) Ust'-Ishim, (20) Okladnikov, (21) Pokrovka.

15.1.1 Dating record

The record was restricted to directly dated late Neanderthal and early AMH remains from around 50–30k BP (see tab. 15.1–15.2), though seemingly younger Neanderthal individuals can be found in the literature. However, the latter are excluded based on severe concerns regarding their dating reliability or species identifications. This subsection discusses the dating quality for those generally seen as reasonably reliable (*e.g.* Davies et al., 2015) and explains the selection for spatio-temporal analysis.

Neanderthals

There are directly dated late Neanderthal remains from El Sidrón (Spain), Les Rochers-de-Villeneuve, Grand Abri de la Ferrassie (France), Spy (Belgium), Kleine Feldhöfergrotte in the Neander valley (Germany), Vindija (Croatia), Mezmaiskaya and Okladnikov (Russia). Treatment and collagen preservation vary, with some dates appearing clearly more reliable than others.

The individual from El Sidrón provides an example of strong dating consistency for recent dating campaigns. All three measurements listed – performed at two different laboratories and using two different treatments – resulted in statistically indistinguishable radiocarbon ages. As a consequence, a combined age will be used to represent this Neanderthal specimen – despite detailed pre-treatment results being available for OxA-21776 only. However, it is worth noting, that larger body of Neanderthal remains from El Sidrón also illustrate the challenges of dating such an old fossil record (de Torres et al., 2010), with only more rigorous radiocarbon pre-treatment protocols (ultrafiltration, nynhydrin and carboxyl carbon dates) leading to dating consistency (Wood et al., 2013).

There are three measurements from Ferrassie 2. OxA-X-2294-14 was treated using the standard ORAU ultrafiltration protocol with additional

Table 15.1: MP/UP: direct radiocarbon dates on human remains (pt. 1/2). Treatments: AA = amino acids, HYP = single amino acid (hydroxyproline), ALA = single amino acid (alanine), UF = ultrafiltration, AF = ORAU ultrafiltration, ABA = modified Longin, S+ABA = Soxhlet + mod. Longin, AG = ORAU gelatine, * = ORAU solvent wash. Potential issues raised under 'Com.': yield = collagen yield after pre-treatment < 1 wt.%; %C = lower/higher than usual carbon concentration on combustion; C:N = C:N ratio outside of expectations; info = limited information available; treat. = other treatment seen as more adequate; MIN = minimum age estimate based on pre-treatment results; cal = date recalculated as a result of Wood et al. (2010). References: [1] de Torres et al. (2010), [2] Davies et al. (2015), [3] Jacobi and Higham (2008), [4] Hedges et al. (1989a), [5] Beauval et al. (2006), [6] Higham et al. (2014, SI), [7] Henry-Gambier and Sacchi (2008), [8] Crevecoeur et al. (2010), [9] Toussaint and Pirson (2006), [10] Semal et al. (2009), [11] Schmitz et al. (2002). Information supplemented with ORAU data. grey rows – dates not used for modelling.

no.	Country	Site	Sample	Species	Dated	Treat	yield (mg)	Yield (%)	d13C	d15N	%C	C:N	Lab-no	14C (BP)	Date (calBP)	Com.	Ref.
1	Spain	El Sidron	SID-00 00/46	Neanderthal	1998	AA	–	–	–	–	–	–	GifA-99167	48500 ± 2600	> 49890	info	[1], [2]
			SID-00 00/46	Neanderthal	1998	AA	–	–	–	–	–	–	GifA-99704	49200 ± 2500	> 49930	info	[1], [2]
			SID-00 00/46	Neanderthal	–	AF	33.8	3.3	-18.7	10.7	39.7	3.3	OxA-21776	48400 ± 3200	> 49830	–	[2]
2	UK	Paviland	O.U.M. Q.1/30	AMH	2006	AG*	23.2	3.2	-18.8	9.9	41.9	3.3	OxA-16503	28820 ± 340	33730 – 31870	treat.	[3]
			O.U.M. Q.1/30	AMH	2006	AF*	18.9	2.6	-18.2	10.3	41.9	3.2	OxA-16413	29490 ± 210	34080 – 33240	–	[3]
			Q1/29 RED LADY	AMH	2006	AF*	22.6	3.4	-18.2	10.4	42.2	3.2	OxA-16412	28870 ± 180	33590 – 32510	–	[3]
			Q1/29 RED LADY	AMH	2006	AG*	23.2	3.5	-18.6	10.1	39.2	3.3	OxA-16502	28400 ± 320	33280 – 31480	treat.	[3]
3		Kent's Cavern	KC4	AMH	1988	AC	8.7	1.7	-26.0	–	17.2	–	OxA-1621	30900 ± 900	37440 – 33400	treat.	[4]
4	France	Les Rochers-de-Villeneuve	Individual 1	Neanderthal	2005	AF	22.3	3.6	-19.0	11.6	39.4	3.2	OxA-15257	45200 ± 1100	> 46700	–	[5]
5		Ferrassie	Individual 2	Neanderthal	2008	AF*	30.74	3.0	-18.9	11.4	46.1	3.4	OxA-X-2294-14	32750 ± 450	38270 – 35850	%C, C:N	[6]
			Individual 2	Neanderthal	2010	HYP	–	–	-22.8	13.4	–	4.9	OxA-X-2395-26	35700 ± 1500	43300 – 36980	cont.	[6]
			Individual 2	Neanderthal	2010	ALA	–	–	-32.9	7.9	–	3.1	OxA-X-2403-14	32100 ± 1800	41590 – 33360	cont.	[6]
6		La Crouzade	La Crouzade 6	AMH	–	ABA?	–	–	-19.5	15.4	42.6	2.77 (3.2)	ERL-9415	30640 ± 640	36020 – 33650	info	[7]
7	Belgium	Spy	Spy 589a	Neanderthal	2008	AG	19.1	12.3	-19.5	13.9	42.3	3.4	OxA-18754	33450 ± 600	39190 – 36240	treat.	ORAU
			Spy 589a	Neanderthal	2008	AF	10.1	6.5	-19.6	14.0	42.7	3.4	OxA-17977	34700 ± 550	40660 – 38170	Cal	[8]
			Spy 589a	Neanderthal	2010	AF	10.1	6.5	-19.6	14.0	42.7	3.4	OxA-21610	33950 ± 550	39740 – 36790	treat.	[8]
			Spy 646a	Neanderthal	–	ABA	33.2	4.7	-21.8	–	–	–	GrA-32627	32970 +200/−190	37850 – 36390	info	[8]
			Spy 572a	Neanderthal	–	ABA	–	12.4	-19.8	–	41.5	3.4	GrA-21546	31810 ± 250	36250 – 35130	treat.	[9], [10]
			Spy 737a	Neanderthal	2001	AF	24.45	4.4	-18.8	11.5	40.4	3.1	OxA-10560	36250 ± 500	41820 – 39880	–	[9]
			Spy 430a	Neanderthal	–	AF	10.1	2.4	-21.6	–	43.6	3.8	OxA-17916	32550 ± 400	37930 – 35630	cal, C:N	[10]
			Spy 430a	Neanderthal	2010	AF	10.1	2.4	-21.6	11.6	43.6	3.8	OxA-21607	31950 ± 450	36980 – 34840	C:N	ORAU
			Spy 430a	Neanderthal	–	ABA	11.9	7.4	-20.1	–	46.8	3.5	GrA-32630	33940 +220/−210	38940 – 37830	C:N	10
			Spy 94a	Neanderthal	–	ABA	57.3	7.8	19.3	–	43.7	3.4	GrA-32623	35810 +260/−240	41090 – 39840	–	[10]
			Spy 92b	Neanderthal	–	ABA	15.9	9.0	-19.7	–	47.1	3.3	GrA-32626	36350 +310/−280	41600 – 40330	%C	[10]
8	Germany	Kleine Feldhöfergrotte	Individual 1	Neanderthal	2001?	acid	–	–	-19.6	–	–	–	ETH-20981	39900 ± 620	44750 – 42660	info	[11]
			Individual 1	Neanderthal	2001?	acid	–	–	-18.8	–	–	–	ETH-19661	40360 ± 760	45370 – 42810	info	[11]
			Individual 2	Neanderthal	2001?	acid	–	–	-20.0	–	–	–	ETH-19660	39240 ± 670	44350 – 42190	info	[11]

Table 15.2: MP/UP: direct radiocarbon dates on human remains (pt. 2/2). References: [12] Conard et al. (2004), [13] Grootes et al. (2004), [14] Devièse et al. (2017), [15] Wild et al. (2005), [16] Wild et al. (1998), [17] Housley (2003), [18] Trinkaus (2013), [19] Soficaru et al. (2007), [20] Soficaru and Doboş (2006), [21] Higham et al. (2007), [22] Prat et al. (2011), [23] Péan et al. (2013), [24] Richards et al. (2001), [25] Higham et al. (2006b), [26] Fu et al. (2014, SI), [27] Krause et al. (2007, SI), [28] Akimova et al. (2010). Information supplemented with ORAU db data. grey rows – dates not used for modelling.

no.	Country	Site	Sample	Species	Dated	Treat	yield (mg)	Yield (%)	d13C	d15N	%C	C:N	Lab-no	14C (BP)	Date (calBP)	Com.	Ref.
9	Germany	Vogelherd	Stetten 1	AMH	2003?	S+ABA	2.9	–	–	–	–	–	KIA-20967	4910 ± 25	5710 – 5590	info	[12], [13]
			Stetten 1	AMH	2003?	S+ABA	4.2	–	–	–	–	–	KIA-20969	4985 ± 30	5880 – 5610	info	[12], [13]
			Stetten 1	AMH	2003?	S+ABA	3.8	–	–	–	–	–	KIA-19538	4715 ± 35	5590 – 5320	info	[12], [13]
			Stetten 2	AMH	2003?	S+ABA	3.5	–	–	–	–	–	KIA-19537	3980 ± 35	4530 – 4290	info	[12], [13]
			Stetten 4	AMH	2003?	S+ABA	1.3	–	–	–	–	–	KIA-19539	4735 ± 30	5590 – 5320	info	[12], [13]
			Stetten 3	AMH	2003?	S+ABA	4.1	–	–	–	–	–	KIA-19540	4995 ± 35	5890 – 5610	info	[12], [13]
10	Croatia	Vindija	Vi-208 (SP3563)	Neanderthal	2016	HYP	35.1	5.6	-26.1	10.2	45.2	5.6	OxA-X-2689-09	42700 ± 1600	49690 – 43890	C:N	[14]
			Vi-207 (SP3562)	Neanderthal	2016	HYP	37.4	6.0	-24.4	11.5	42.2	5.6	OxA-X-2689-10	43900 ± 2000	> 44800	C:N	[14]
			Vi-33.19 (SP2756)	Neanderthal	2017	AF	62.22	11.1	-18.6	10.4	45.2	3.4	OxA-32278	45300 ± 2300	> 45580	–	[14]
			Vi-33.19 (SP2756)	Neanderthal	2017	HYP	62.22	11.1	-24.4	12.3	46.5	4.9	OxA-X-2717-11	44300 ± 1200	49950 – 45850	–	[14]
			Vi-28 (SP4162)	Neanderthal	2016	HYP	54.0	5.4	-25.5	11.7	34.3	5.0	OxA-X-2687-57	46200 ± 1500	> 46960	%C	[14]
11	Czech Rep.	Mladeč	Mladeč 8	AMH	2004?	ABA	–	–	-20.1	10.9	44.3	2.7	VERA-3075	30680 +380/−360	35380 – 33970	C:N	[15], [16]
			Mladeč 1	AMH	2004?	ABA	–	–	–	–	–	–	VERA-3073	31190 +400/−390	36010 – 34380	info	[15], [16]]
			Mladeč 2	AMH	2004?	ABA	–	–	–	–	–	–	VERA-3074	31320 +410/−390	36110 –34530	info	[15], [16]
			Mladeč 9a	AMH	2004?	ABA	–	–	–	–	–	–	VERA-3076 A	31500 +420/−400	36250 – 34650	info	[15], [16]
12	Poland	Obłazowa	Obłazowa 1	AMH	1993	AI	13.7	3.8	-18.6	–	42.4	–	OxA-4586	31000 ± 500	36010 – 34070	MIN	[17]
13	Romania	Peştera cu Oase	Mandible 1	AMH	2002	AF	1.7	0.5	-18.7	13.3	44.4	3.3	OxA-11711	34950 ± 990	41770 – 37310	yield	[18]
			Mandible 1	AMH	2002?	ABA	28.5	4.0	-19.0	–	39.6	2.6	GrA-22810	34290 +970/−870	40960 – 36530	C:N	[19]
			Cranium 2	AMH	2003	ABA	–	–	-19.5	–	–	–	GrA-24398	28890 ± 170	33590 – 32570	info, MIN	[19]
14		Cioclovina		AMH	2006	AF*	40.44	5.9	-19.6	12.7	44.4	3.4	OxA-15527	28150 ± 170	32610 – 31460	–	[19]
15		Peştera Muierii	Muierii 1	AMH	2005	UF	–	–	-20.0	–	–	–	LuA-5228	30150 ± 800	36080 – 32650	info	[20]
			Muierii 1	AMH	2006	AF	56.0	13.3	-19.3	12.3	41.5	3.4	OxA-15529	29930 ± 170	34360 – 33700	–	[20]
			Muierii 2	AMH	2005	AF	26.8	11.2	-19.1	12.4	43.7	3.4	OxA-15435	29750 ± 800	35540 – 31920	–	
			Muierii 2	AMH	2006	AF	26.8	11.2	-19.3	11.7	41.7	3.3	OxA-16252	29110 ± 190	33760 – 32840	–	[20]
16	Ukraine	Buran-Kaya III	'human bone'	AMH	2004	AF	19.9	2.8	-18.9	16.6	45.1	3.3	OxA-13302	32790 ± 280	37870 – 36120	–	[21]
				AMH	–	ABA	–	–	-19.4	–	43.2	3.3	GrA-37938	31900 +240/−220	36300 – 35260	–	[22]
				AMH	2011?	ABA	–	–	–	–	–	3.1	GrA-50457	32450 +250/−230	37060 – 35740	info	[23]
17	Russia	Kostenki I	Kostenki 1	AMH	1997	AG	20.2	3.6	-18.2	15.8	41.2	3.0	OxA-7073	32600 ± 1100	39680 – 34630	–	[24], [25]
			Kostenki 1	AMH	2005	AF	144	9.6	-18.5	14.8	38.1	3.2	OxA-15055	32070 ± 190	36380 – 35520	–	[25]
18		Mezmaiskaya	Mez 2	Neanderthal	2009	AF	108.3	14.6	-17.4	19.0	44.1	3.2	OxA-21839	39700 ± 1100	45630 – 42030	–	[6]
19		Ust'-Ishim	Ust'-Ishim 1	AMH	2011	AF	68.8	7.7	-19.2	14.2	45.8	3.2	OxA-25516	41400 ± 1300	48020 – 42860	–	[26]
			Ust'-Ishim 1	AMH	2014	AF	45.2	10	-19.2	14.2	43.4	3.3	OxA-30190	41400 ± 1400	48320 – 42790	–	[26]
20		Okladnikov	OK 1	Neanderthal	2006	AF	24.8	5.0	-18.4	15.4	40.8	3.3	OxA-15481	37800 ± 450	42750 – 41480	–	[27]
			OK 1	Neanderthal		UF	–	3.6	-19.1	12.9	44.4	3.4	KIA-27011	29990 ± 500	35030 – 33160	–	[27]
21		Pokrovka	Pokrovka	AMH	2008	AF*	34.6	6.7	-18.4	10.4	50.3	3.3	OxA-19850	27740 ± 150	31830 –31180	%C	[28]

solvent steps. The results show slightly elevated C:N ratio and %C on combustion, though still within the normally accepted range. OxA-X-2395-26 and OxA-X-2403-14 targeted single amino acids, specifically hydroxyproline and alanine (Marom et al., 2012). Higham et al. (2014, SI) suggest that bone or collagen glue may be causing the dating discrepancy[1]. In addition, OSL dating suggest that the Ferrassie 2 individual may be between 54 ± 4 ka and 43 ± 3 ka old (Frouin et al., 2017; Guérin et al., 2015). As a consequence, the radiocarbon measurements are excluded from the spatio-temporal analysis.

The exceptionally young ages for Spy have been observed in several different individuals, as well as in different pre-treatments from two laboratories (ORAU and Groningen) – though presently no hydroxyproline dating has been published [2]. In the case of Spy 589a, the originally published radiocarbon date of 34700 ± 550 BP (OxA-17977) for the ultrafiltered sample had to be recalculated (Higham et al., 2014, SI) as a result of the updated background correction (Wood et al., 2010), leading to the new date of 33950 ± 550 BP (OxA-21610). While the substantial overlap between the probability distributions for the ultrafiltered and non ultrafiltered fractions suggest only minor variability, it is important to note the slightly elevated C:N ratios. Until further dating, the scepticism expressed by Semal et al. (2012) and Higham et al. (2014, SI) towards such unusually young dates seems appropriate. The same reasoning applies to Spy 646a and Spy 572a, especially in light of less rigorous pre-treatment, elevated C:N ratio, and insufficient quality control measures.

Clearly problematic are the three dates on Spy 430a. They show anomalous C:N ratios (and elevated %C results for GrA-32630), probably caused by insufficiently removed glue (Higham et al., 2014, SI), and are excluded from further analysis. This leaves direct dates on three Neanderthal samples from Spy (737a, 94a, 93b). While these represent good candidates for late

[1]This contamination seems to have more severely affected the dating of Ferrassie 1, resulting in ages of 12910 ± 90 BP (OxA-2395-25) for AF*, 11540 ± 55 BP (OxA-2294-15) for HYP, and 12950 ± 130 (OxA-2403-18) for ALA.

[2]New radiocarbon dating of the Neanderthal individuals was conducted as part of the larger PalaeoChron project and is expected to be published in due course.

Neanderthals, it is expected that the true ages may well be slightly older. As this dissertation is not concerned with identifying the latest Neanderthal appearance, the more conservative approach calls for inclusion of these measurements.

Two individuals from the Kleine Feldhöfergrotte in the Neander Valley were dated at the ETH in Zurich (Switzerland). The treatment protocol seems to be consistent with the original Longin method (Longin, 1971), and the lack of any further quality control measurements impacts the quality assessment. Nonetheless, the dating consistency would indicate some dating reliability and supports the measurements' inclusion in the spatio-temporal analysis.

The Vindija cave in Croatia contains Neanderthal remains that have been at the centre of the discussion on Neanderthal survival in Croatia and along the Danube corridor. The age determinations for late Neanderthals at the site have seen dramatic shifts from $<$ 30k BP (Smith et al., 1999), to around 32k BP (Higham et al., 2006a), and finally age determinations of around 43–46k BP (Devièse et al., 2017). The severe contamination with conservation substances indicates that cleaning methods based on acid and base solutions (with or without ultrafiltration) led to erroneous measurements on conserved samples. Only in the case of Vi-33.19 are the AF and HYP dates statistically indistinguishable (χ^2-test), and indicate no significant contamination. However, low AMS target current led to a unsuitably imprecise measurement for the ultrafiltered fraction. For this study, only the most recent dates obtained on hydroxyproline dating will be included. Especially, OxA-X-2717-11 appears to be of very good quality. OxA-X-2689-09 and OxA-X-2689-10 gave slightly elevated C:N results, while OxA-X-2687-57 showed a decreased carbon concentration – a variability which could also have been caused by the small sample sizes.

An additional pair of Neanderthal remains from Russia were considered for this study. The specimen from Mezmaiskaya was dated in 2009 using ORAU's ultrafiltration protocol. Based on pre-treatment results, the date has to be considered reliable. By contrast, the individual from Okladnikov

was dated both at ORAU and Kiel using ultrafiltration, but resulting in significantly different dates. KIA-27011 gave an age around 8000 radiocarbon years younger than OxA-15481. Considering the high risk of modern carbon contamination, and the elevated %C and C:N results for the Kiel fraction, the Oxford measurement appears more reliable. However, unpublished hydroxyproline results suggest a greater than age for the Okladnikov individual (T. Higham, pers. comm. 31/08/2018). Therefore, both published results were excluded from spatio-temporal mapping.

AMH

Direct radiocarbon dating of early AMH is available from Paviland, Kent's Cavern (UK), La Crouzade (France), Mladeč (Czech Republic), Obłazowa (Poland), Peștera cu Oase, Cioclovina, Peștera Muierii (Romania), Buran-Kaya III (Crimea), Kostenki I, Ust'-Ishim and Pokrovka (Russia). For Paviland, the samples treated with ORAU's ultrafiltration protocol show better pre-treatment results, and will be preferred over the AG fractions in the modelling. The dating of La Crouzade is more difficult to assess. The C:N ratio was initially reported as 2.7, but referred to as 3.2 in some of the documentation (Henry-Gambier and Sacchi, 2008). While the date will feature in the modelling, it is worth bearing in mind that the date might underestimate the true age of the AMH individual.

The human remains from Mladeč were pre-treated with a modified Longin protocol. Stable isotope measurements on the collagen samples are only available for the specimen Mladeč 8, and they show elevated %C and a significantly reduced C:N ratio. The other three samples only have stable isotope results for the original bone powder used (Wild et al., 2005), which cannot inform on pre-treatment effectiveness. Nonetheless, the three dates are consistent with results obtained from tooth pendants found at the same site (R. Hopkins, unpublished). This leads to the tentative conclusion that they may indeed represent reliable measurements, and should therefore remain included in the modelling.

For Obłazowa only an AI (*i.e.* ABA + gelatinisation + ion exchange, see also Hedges and Law, 1989, Appendix I) treated sample exists. Comparisons to other dating techniques suggests that this pre-treatment protocol generally underestimates the true age of Palaeolithic samples (see also subsection 14.2.1), and at the time, no nitrogen information was collected (δ^{15}N, C:N).

The mandible found at Peștera cu Oase is of particular importance. First, it provides rare early AMH evidence from the Danube corridor. Second, DNA analysis revealed recent Neanderthal interbreeding, which probably falls within the margin of the radiocarbon error (Fu et al., 2015). Both GrA-22810 and OxA-11711 give comparable radiocarbon measurements. However, pre-treatment results are better for the fraction dated with ultrafiltration at ORAU. The low collagen yield led Trinkaus (2013) to treat it as a minimum age estimate. Only further dating would be able to provide some clarification on the matter, as all other pre-treatment results appear in favour of a reliable date. The second specimen, a cranial fragment, was only dated at Groningen. If correct, it would suggest a younger individual. However, pre-treatment results for quality control purposes are not available.

An AMH found at the nearby site of Cioclovina was dated at Oxford using ultrafiltration and solvent extraction. The pre-treatment results show slightly elevated %C and C:N ratio, albeit both within the range of accepted variability. Also the two samples from Peștera Muierii dated at ORAU show an elevation in C:N (OxA-15529, OxA-15435), and re-dating of excess collagen from Muierii 2 (OxA-16252) resulted in an age on the younger end of the former probability distribution. Nonetheless, these dates are preferred over LuA-5228, for which only very limited pre-treatment information is available.

The Buran-Kaya III samples do not appear to show any dating anomalies, though not all dates come with an equal number of pre-treatment results. The Kostenki dating is a good example of ultrafiltration not necessarily leading to older radiocarbon measurements, even though pre-treatment results appear to have improved. OxA-7073 (dated in 1997 with AG) is comparable to OxA-15055 (dated 2005 with AF).

Despite having been found very far away from the Danube corridor, the AMH from Ust'-Ishim is also crucial to understanding the nature of the Middle to Upper Palaeolithic biocultural shift. The sample's DNA indicates Neanderthal interbreeding (Fu et al., 2014), albeit less recent than the mandibula from Peștera cu Oase. The Ust'-Ishim individual was dated twice with ultrafiltration at Oxford – once in 2009 and once in 2011. Both dates are statistically indistinguishable, and place the individual as, presently, the oldest directly dated AMH.

The last Russian individual was found at Pokrovka and dated at ORAU. Pre-treatment included solvent washes and ultrafiltration. While preservation appeared good, the sample gave elevated %C results. All other measures are within expected range.

The importance of direct dating

Direct dating of human remains has long been recognised as crucial, as many important finds – such as the Peștera cu Oase mandible, and the Ust'-Ishim femoral diaphysis – derived from a non archaeological or unknown context. However, rather than increasing the number of directly dated early AMHs, efforts to radiocarbon date the specimens has reduced the number of finds: many 'archaic' skeletal remains turned out to date to the Holocene (*e.g.* Street et al., 2006). In addition, genomics and proteomics led to the reclassification of some bone fragments as non-human[3].

This effect is also evident in this dissertation. Regrettably, none of the human remains selected for dating belong to the period of the MP/UP biocultural shift (see Kozarnika 8.1, Manastira 8.2, Šal'a 12.2), and the only sample with a matching age determination had to be reclassified as an *Ursus sp.* cranial fragment after ZooMS analysis (see Kozarnika 8.1). As a consequence, the spatio-temporal distribution of Neanderthals and AMH investigated here relies solely on published data.

[3]It appears that insecure identifications often led to the misidentification of bear remains as human.

Such a development is not surprising when dealing with finds without a chronologically informative context. However, they can also occur when dealing with specimens found *in situ* in a seemingly secure Palaeolithic context. An example relevant to the Danube corridor is Vogelherd. The AMH individuals found *in situ* were believed to be securely connected to the Aurignacian occupation at the site, and used as a strong argument for connecting the Aurignacian to AMH in southern Germany and Europe (*e.g.* Conard and Bolus, 2003). However, radiocarbon dating subsequently placed the four individuals in the Holocene (see tab. 15.2 and Conard et al., 2004) – an offset that cannot derive from pre-treatment issues[4].

15.1.2 Modelling

The radiocarbon determinations selected for modelling are listed in tables 15.1 and 15.2 (white rows). Where more than one date was selected for an individual, the results are combined using the `R_Combine` or `C_Combine` function. Finite measurements with a probability distribution extending beyond the calibration curve were entered with a `Date` function. As an approximation, the new mean age was calculated by adding twice the radiocarbon error to the calibrated minimum age.

Three different outputs were run. Initially, the dates were only calibrated and mapped according to their find locations to provide a spatio-temporal overview (see fig. 15.2, code: p. 749). Second, the Neanderthal and AMH individuals were separated, running a `KDE_Model` with each group to visualise the temporal find densities (see fig. 15.3–15.5, code: p. 750 and p. 751).

15.1.3 Spatio-temporal distribution

The earliest directly dated AMH evidence comes from Ust'-Ishim (Russia) with a peak probability at around 45k cal BP (see fig. 15.2). The next

[4]This has been confirmed through HYP dating (T. Higham, pers. comm. 20/11/2018).

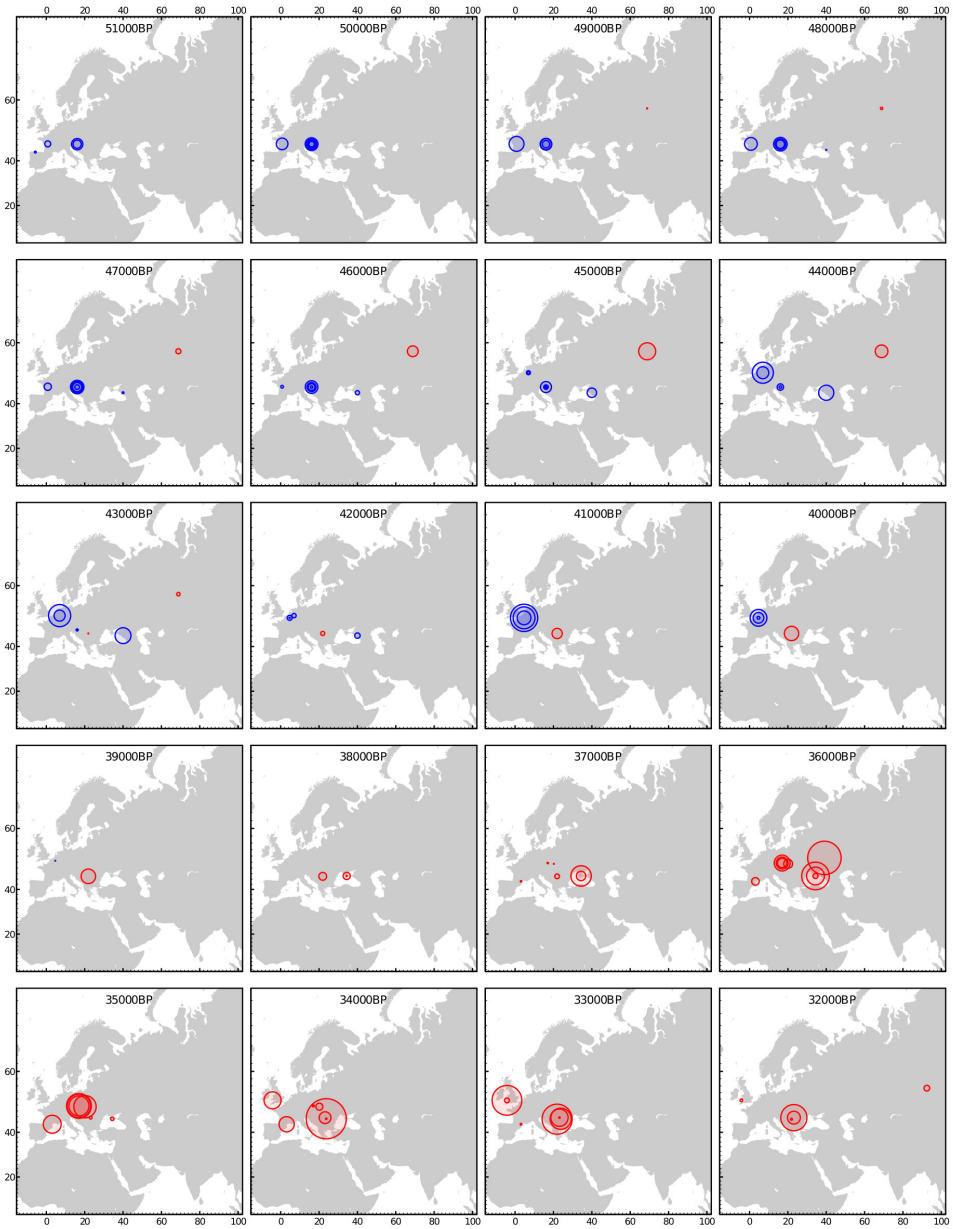


Figure 15.2: MP/UP: spatio-temporal distribution of directly dated Neanderthal (**blue**) and AMH (**red**) remains in time slices of 1000 years from 51000 cal BP to 32000 cal BP (code: p. 749). Circle size represents radiocarbon probability estimate.

younger date is already within the Danube corridor, namely from Peștera cu Oase at the Danube Gorge. The current dating resolution is unable to distinguish whether the latter occupation was contemporaneous with Neanderthals living to the east and west, or whether Neanderthal groups had already contracted to western Europe. Recent interbreeding seen in the DNA may favour the former scenario (Fu et al., 2015), and would be consistent with Prüfer et al. (2014), who suggest that Neanderthal-derived DNA in Eurasians is closely related to finds from Mezmaiskaya. Either way, the map suggests that by 40k cal BP at the latest, Neanderthals were no longer found in central and eastern Europe.

This pattern is consistent with an east-west movement of AMH, possibly even separating certain Neanderthal communities in the process, and entering central Europe via the Danube corridor. At the same time, the resolution is too coarse to distinguish between a westward contraction of Neanderthals enabling an AMH expansion, or one caused by it. There is also the possibility that these two processes were independent of each other.

Irrespective of the causality, the spatio-temporal distribution implies that AMH moved into Asia before migrating to Europe. This raises the question of whether the expansion into Europe occurred directly out of Africa (and via the Levant and Turkey) at all, or rather out of (northern) Asia (*i.e.* north-east of the Black Sea). Indirectly dated AMH remains – which are older than the Eurasian specimens, but younger than the African counterparts – do exist in the Levant (*e.g.* Trinkaus, 2005), which is commonly seen as a gateway out of Africa. At the same time, Henn et al. (2012) have shown that north African populations $<$ 40k cal BP were genetically discontinuous from previous AMH groups, thus supporting a back migration from Europe after Neanderthal interbreeding in Asia had already occurred (Garcea, 2016).

The overall temporal overlap of *ca.* 10k years between Neanderthals and AMH in Eurasia (see fig. 15.3) is likely to become narrower if some of the younger Neanderthal individuals were re-dated with more rigorous pre-treatment protocols. However, when focusing on the Danube corridor, any contemporaneity presently vanishes entirely (see fig. 15.4 and 15.5). After 45k

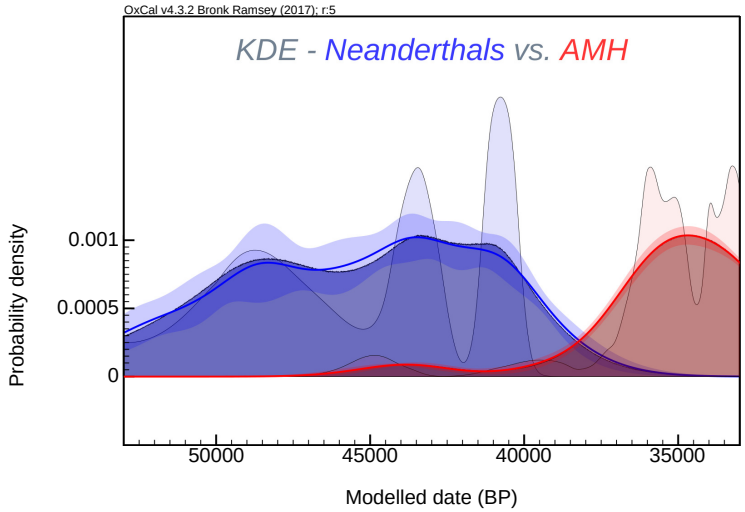


Figure 15.3: MP/UP: temporal distribution of directly dated Neanderthal (**blue**, code: p. 750) and AMH (**red**, code: p. 751) remains, visualised by overlaying 'KDE Neanderthals' (n=12) with 'KDE AMH' (n=19) for the crucial time period between 53000 – 33000 cal BP.

cal BP, Neanderthal evidence is concentrated east of the Black Sea and in western Europe. On the other hand, any AMH evidence along the Danube post-dates 43k cal BP. Without a good understanding of the range and frequency of nomadic migrations, recent interbreeding seen at Peștera cu Oase need not have taken place in the Danube corridor at all. It might as well have been the result of AMH passing Neanderthal communities further to the east – as suggested by DNA evidence (Prüfer et al., 2014).

In light of these findings, further detailed investigation of the MP/UP biocultural shift will heavily rely on inferring biological presence from cultural expressions. The more abundant, and often more stratified, archaeological evidence may provide the higher dating resolution required for addressing such complex questions. Therefore, understanding the cultural mosaic and its possible connections to certain human authors (discussed in the following two sections) is crucial. Nonetheless, it is important to remember the absence of directly dated biological evidence in the Danube corridor for the period 45–42k cal BP.

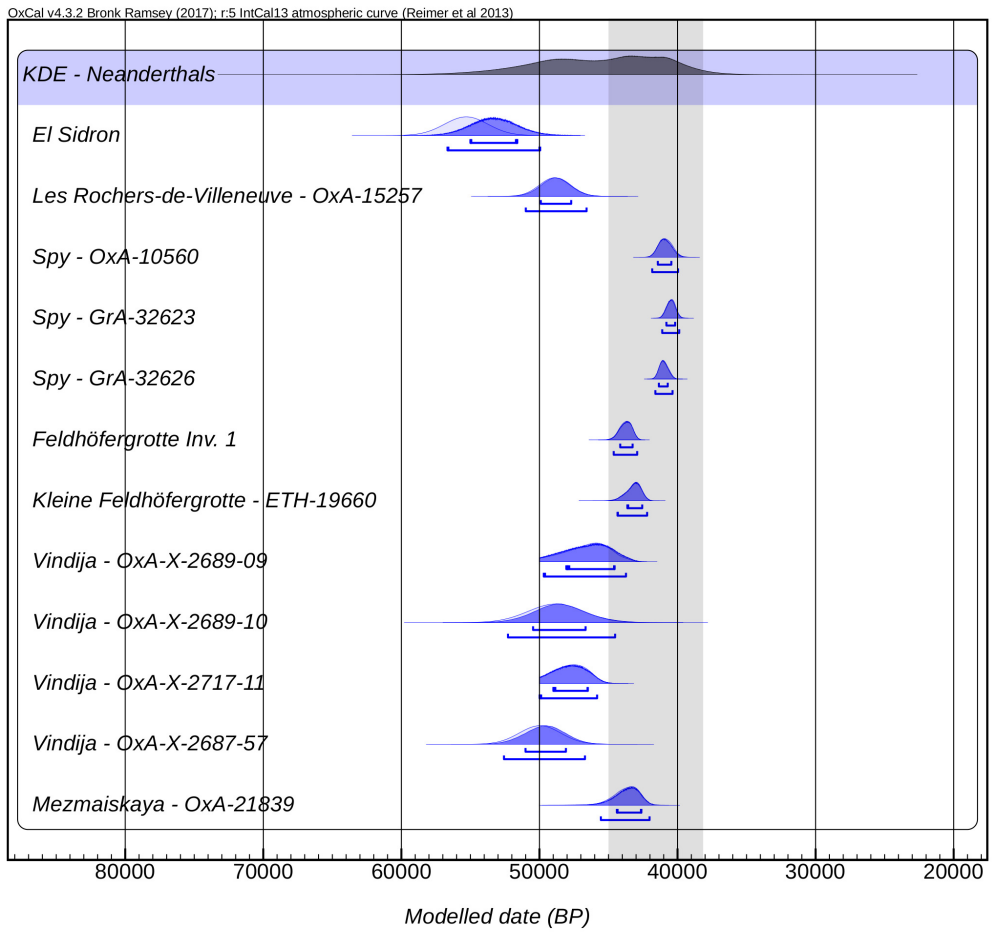


Figure 15.4: MP/UP: KDE of directly dated late Neanderthal skeletal remains (n=12). Specimens at 45k cal BP or younger highlighted in grey. Note the absence of remains <45k cal BP in the Danube Valley (code: p. 750).

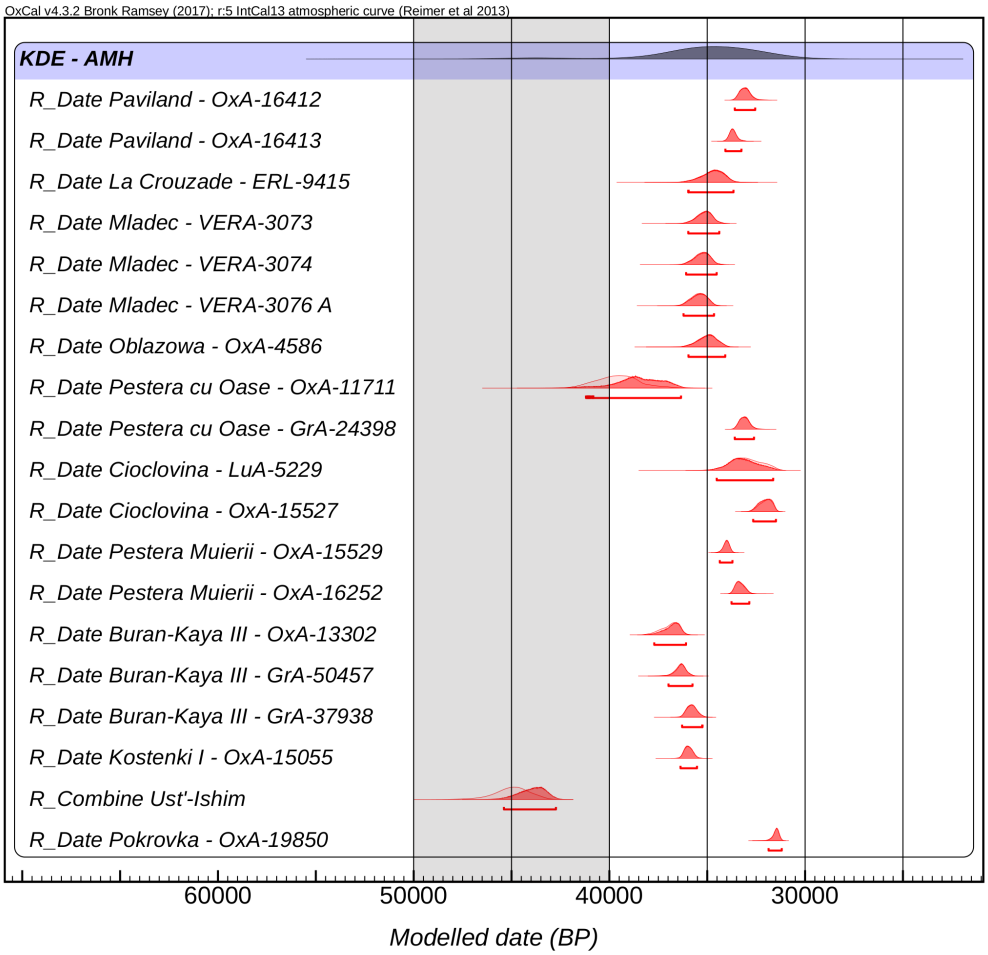


Figure 15.5: MP/UP: KDE of directly dated early AMH skeletal remains (n=19). Specimens older than 40k cal BP highlighted in grey. Note the absence of remains >40k cal BP in the Danube Valley (code: p. 751).

15.2 Biocultural mosaic

The period of the MP-UP biocultural shift has been referred to as a 'transitional mosaic' (*e.g.* Davies et al., 2015); a period when a seemingly coherent late Middle Palaeolithic structure covering Europe breaks up into a patchwork of local cultural expressions, before regaining cohesion with the manifestation of an assumed pan-European Aurignacian. As a result of the 'transitional' cultures' localised nature, isochrones between sites rely on radiometric dating and tephra analysis. Consequently, published data was used to supplement the results from the sites investigated in this dissertation, and to investigate the cultural patterning in light of the *Kulturpumpe* model, the Danube corridor hypothesis, and the spread of AMHs in general.

Any study into the reasons and nature of this transformation – and the role an influx of AMH may have had – requires an understanding of the relationships between industries, as well as between industries and their respective authors. Many of these regional technocomplexes are difficult to directly connect to a particular human species and their skeletal evidence, thus sometimes leading to conflicting conclusions (*e.g.* for the Uluzzian Benazzi et al., 2011; Zilhão et al., 2015). Therefore, other lines of reasoning, such as technological criteria, have been frequently used to distinguish between Neanderthal and AMH *modi operandi* (*e.g.* for the Bohunician Moncel and Voisin, 2006; Škrdla, 2013), or to argue in favour/against a local cultural innovation. The result of the latter distinction is then again often understood to being synonymous with establishing a Neanderthal or AMH authorship (intrusion = AMH, continuity = Neanderthal; *e.g.* for the Châtelperronian Ruebens et al., 2015).

In this context it is important to remember that all these arguments share the underlying assumption that Neanderthals and AMH did indeed occupy different niches, and produced distinguishable cultural material. At present, this is neither contradicted by the skeletal nor the archaeological record. Nevertheless, the evidence is not sufficiently abundant to *a priori* discard any alternative, co-habitation scenario for future investigations. Hu-

man skeletal finds from this period remain scarce, and separating material in the stratigraphic record that derived from brief occupations with limited temporal separation may be difficult – if not impossible.

In addition, national and regional research traditions influenced the identification, description and nomenclature of technocomplexes. As a result, some differences were historically downplayed in favour of adopting a canonical succession of 'cultures', as is seen in the frequent use of the term 'Aurignacian' for eastern European Upper Palaeolithic assemblages with only limited to no diagnostic artefacts. In contrast, other differences were emphasised in favour of maintaining national distinctions, and only intensive comparisons may eventually be able to harmonise the categories (*e.g.* Teyssandier, 2008, for expanding the IUP to the Bohunician and Bachokirian). Finally, with increasing research into the characteristics of lithic industries, categories and nomenclature may have changed, and not all regions have equally invested in updating their literature and reinvestigating their legacy material.

While it is advised to be mindful of these limitations, generalisations and extrapolations are essential to the detection of large scale patterns. Therefore, the key is transparency. In the following, the transitional mosaic is examined by adhering to the terminology from the respective literature, before proposing relationships and groupings, and using the cultural material as proxies for the presence of Neanderthals and AMH. This approach will facilitate the future revision of the spatio-temporal maps in line with new finds and research, without rendering their content meaningless.

15.2.1 Published Data

A total of 29 reference sites were selected to complement the radiocarbon data from this dissertation (see fig. 15.6). The sites were chosen as a result of their recently improved dating or their importance to the Danube corridor. The individual dates can be found in catalogue C, and were used for stratigraphic and KDE modelling to obtain age determinations for specific archaeological cultures and UP occupation timings. The model codes and

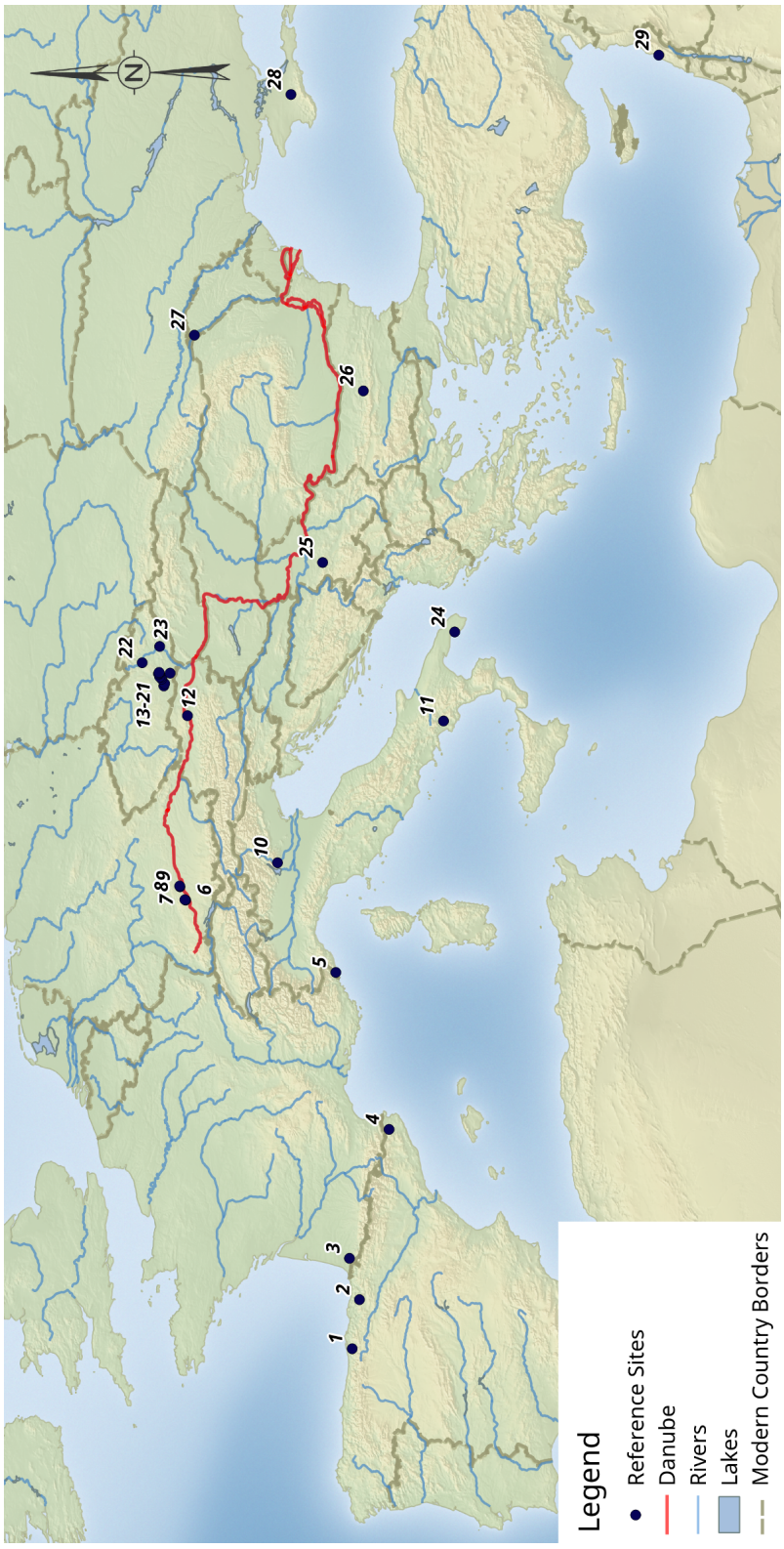


Figure 15.6: MP/UP: map of reference sites used for spatio-temporal comparisons: (1) El Castillo, (2) Labeko Koba, (3) Isturitz, (4) L'Arbreda, (5) Riparo Mochi, (6) Hohle Fels, (7) Geißenklösterle, (8) Hohlenstein-Stadel, (9) Vogelherd, (10) Fumane, (11) Castelcivita, (12) Willendorf II, (13) Moravský Krumlov IV, (14) Vedrovice V, (15) Ořechov IV, (16) Želešice III, (17) Bohunice, (18) Stránská skála, (19) Líšeň (Brno), (20) Milovice I, (21) Podolí (Brno), (22) Mladeč, (23) Napajedla III, (24) Cavallo, (25) Šalitrena Pećina, (26) Bacho Kiro, (27) Mitoc-Malu Galben, (28) Buran-Kaya III, (29) Ksar Akil.

output visualisations are provided in catalogues B.8 and D, respectively, unless otherwise included in the text. This section discusses the models and their posteriors that will be used as priors for the spatio-temporal mapping of different cultures and human occupations (see fig. 15.9–15.11).

Modelling

Whenever possible, two OxCal models were run for each site: a stratigraphic, and a KDE model. Samples that have more than one date associated with them are represented using the `R_Combine` or `Combine` functions. As seen at sites investigated for this thesis (part IV), finite radiocarbon measurements that exceed the range of the calibration curve are reproduced using the `Date` function, and the new mean was calculated by adding the standard deviation twice to the calibrated minimum age.

A stratigraphic model consists of dates grouped into phases according to archaeological levels or cultural interpretations. All models include a general `Outlier_Model` with a student T distribution and outlier type 't' (*i.e.* outlier in time). Dates within the combine functions run the outlier model `SSimple` with a Normal distribution and outlier type 's' (*i.e.* outlier in the error estimate of the date). In both cases, the prior outlier probability is set to 0.05.

In addition, each `Phase` contains the `Date` command in order to obtain an age estimate for the cultural expression it contains, and to provide the output needed for spatio-temporal mapping. The date for the layer is preferred for comparison over the use of start and end boundaries, which have been frequently used in other studies. This is done because many sites included in this thesis do not have a datable MP level constraining the start boundary for the UP. The boundary posteriors are therefore susceptible to overestimating the age of a culture's likely first appearance, while `Date` posteriors provide a more constrained estimation.

KDE modelling is restricted to dates from Upper Palaeolithic contexts – which includes the Bohunician, IUP and Bachokirian – and whenever possible

to anthropogenically modified samples. An exception is the Szeletian in Moravia, where the `KDE_Model` is used to obtain a chronological estimation for the presence of a possible Neanderthal related late MP industry. The posterior distribution is subsequently used for spatio-temporal mapping of human occupations.

All terrestrial samples are calibrated using IntCal13 (Reimer et al., 2013). Direct radiocarbon dates on marine shells are calibrated using Marine13 (Reimer et al., 2013) with the respective local ΔR found in Reimer and McCormac (2002).

Sites: the Danube corridor

Along the Danube, data were included from Bacho Kiro, Mitoc-Malu Galben, Šalitrena Pećina, Willendorf II, Hohle Fels, Hohlenstein-Stadel and Vogelherd. At Bacho Kiro, the stratigraphy was simplified to three phases: the Mousterian, Bachokirian, and the 'Aurignacian' – the latter label having been borrowed from the literature, and the Bachokirian treated as part of the IUP technocomplex in accordance with Teyssandier (2008). It is worth noting that the dating was done in the 1970s and 1980s with now largely outdated pre-treatment protocols. It is expected that the new dating project at the Max Planck Institute will eventually publish dates that are older than the currently available measurements[5]. Nonetheless, Bacho Kiro had to be included, as it reflects a crucial site along the lower Danube, and still provides minimum age estimates. The calculated `Date` ranges for the Mousterian probably underestimates the start of the probability distribution as a result of the calibration curve and no further constraints from an underlying `Phase`.

Mitoc-Malu Galben only has dated Aurignacian layers, which were as a consequence combined into a single `KDE_Model`. For Šalitrena Pećina the sparse dating was divided into a Mousterian and Aurignacian `Phase`. However, as is frequently observed in the western Balkans, there seems to be a

[5]This has been confirmed by Helen Fewlass (ESHE Meeting, 13 Sep 2018, Faro). Preliminary results place Bacho Kiro in line with Kozarnika. See discussion.

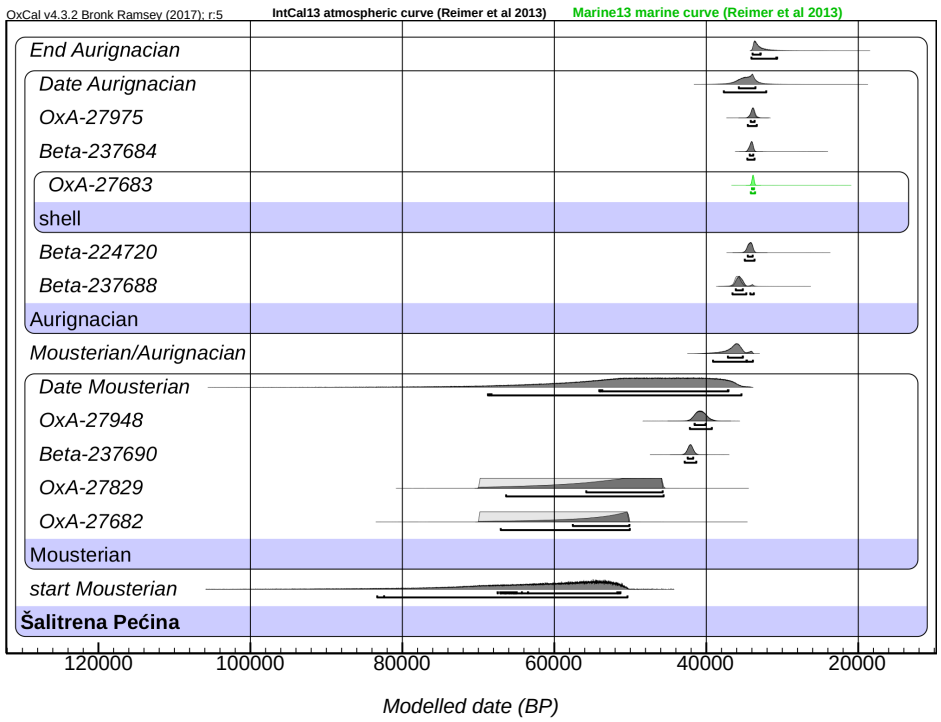


Figure 15.7: MP/UP: stratigraphic model for Šalitrena Pećina (code: p. 765).

gap in occupation between the MP and UP levels (see also Tabula Traiana and Dubočka-Kozja, chapter 9). As a result, the `Date` calculated for the Mousterian occupation is certainly covering younger ages (see fig. 15.7), and as a result was excluded from mapping. The Aurignacian is "*distinctive and differs from other Aurignacian sites in northern Bosnia, and in Romanian and Serbian Banat* [...] [and is] *more closely associated with the early Aurignacian in central and western Europe*" (Marín-Arroyo and Mihailović, 2017, p. 418).

As Willendorf II was proposed as a site with a very early onset of the Early Aurignacian, the model structure of Nigst et al. (2014) was recreated. However, the original model only used the newly obtained ABOx treated charcoals, as they generally provide more reliable age estimates. At the same time, the low number of dates provides significant flexibility in assessing the age of the only indirectly dated level AH III. For this dissertation,

a more conservative approach was chosen by including the other charcoal dates. Accordingly, the resulting `Date` for the Early Aurignacian is younger than seen in the radiocarbon model by Nigst et al. (2014) – though in line with their final assessment based on stratigraphic, palaeoenvironmental and chronological data. The result presented here is also consistent with observations at Geißenklösterle. The stratigraphic model for Geißenklösterle was taken from Higham et al. (2012, fig. 7) without any amendments, and all anthropogenically modified samples were part of the KDE model.

For Hohle Fels, a stratigraphic model was composed after the description in Conard and Bolus (2008). Despite the limited radiocarbon quality control measures available, the resulting model is consistent, albeit a large temporal spread is observable in the lower most Aurignacian, level V (see fig. 15.8).

The literature only provided eight dates for the Aurignacian at Hohlenstein-Stadel, and the stratigraphy was given in excavation spits (Conard and Bolus, 2003). This is insufficient for a meaningful stratigraphic model. At the same time, half the measurements have an insecure Aurignacian association, and were unsuitable for KDE modelling. Considering the importance of the site for the Danube corridor, a `KDE_Model` was nonetheless attempted, though the results should be treated with caution. The dating record for Vogelherd is larger, albeit still small (Conard and Bolus, 2003). As all levels were identified as Aurignacian, the dates were only run as a `KDE_Model`.

In addition to the Danubian sites described above, radiocarbon data from 11 sites in Moravia (Czech Republic) were combined to create KDE models for the Aurignacian, Bohunician, and Szeletian in the region. The sites comprised measurements from Moravský Krumlov, Vedrovice V, Ořechov IV, Želešice III, Bohunice, Stránská skála, Líšeň, Milovice I, Podolí, Mladeč, and Napajedla III, as summarised by Škrdla (2017). It remains to be seen whether the large spread of dates from Bohunician levels is the result of varying quality of radiocarbon pre-treatment, issues in industry identification, or a reflection of a prolonged cultural manifestation. Both the Szeletian and the Aurignacian appear more temporally confined (see fig. 15.10).

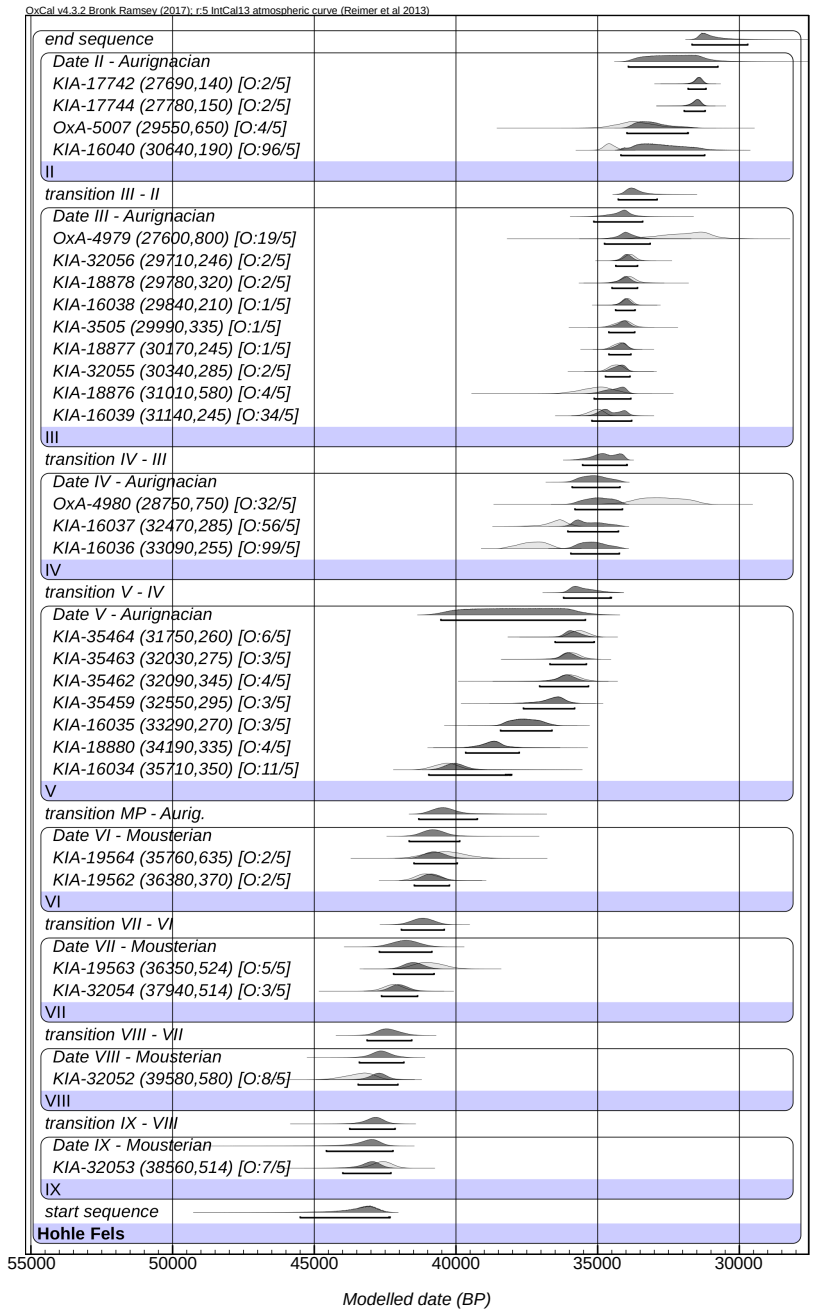


Figure 15.8: MP/UP: stratigraphic model for Hohle Fels (code: p. 757).

Sites: beyond the Danube

To test the *Kulturpumpe* model and the Danube corridor hypothesis, sites from outside the Danube fluvial corridor are required. Therefore, I also sourced the literature for dates from other sites, including Buran-Kaya III, Castelcivita, Cavallo, El Castillo, Fumane, Isturitz, Ksar Akil, L'Arbreda, Labeko Koba and Riparo Mochi. At Buran-Kaya III, the Micoquian is followed by several Aurignacian and Gravettian levels. The stratigraphic modelling followed Péan et al. (2013), including both the ninhydrin and ABA pre-treated samples. Regrettably, only one bone fragment showed anthropogenic modifications. Therefore, KDE modelling included the non-modified fauna, leading to a less direct connection to human activity at the site than those KDE models based on anthropogenically modified material.

Castelcivita is an important site as it includes Mousterian, Uluzzian, and Aurignacian assemblages. The limited dating has been mostly obtained with older pre-treatment protocols (Gambassini, 1997). The more recent date on a marine shell from Douka et al. (2014) would suggest that the overall age of the assemblages may be up to 3000 years older, and the modelling results should be treated as minimum ages for this site. In contrast, dating of the Uluzzian site of Cavallo applied the CarDS pre-treatment, and modelling was directly adopted from Douka et al. (2014). All the dates come from marine shells, providing a `KDE_Model` reflecting human activity.

For El Castillo, the stratigraphic modelling was adapted from Wood et al. (2018), and the original label of 'transitional Aurignacian' was kept for level 18C and Aurignacian for level 18B. All the dated samples were directly related to the human occupation and thus ideal for KDE modelling. Regrettably, the posterior probability distribution contains erratic fluctuations and a possibly overly constrained precision. This is probably the result of working with dates so close to the radiocarbon dating limit, where radiocarbon errors can span over a thousand years. However, a comparison of the `KDE_Model` posterior with the dates calculated for levels 18C and 18B still demonstrates consistency.

Fumane recently saw improved dating for the Uluzzian levels (Douka et al., 2014). For the younger levels (Proto-Aurignacian and Aurignacian), the stratigraphic model made use of previously obtained radiocarbon data. While the Uluzzian and Aurignacian levels are well constrained, the Proto-Aurignacian shows some substantial temporal spread. In contrast, when the same radiocarbon dataset was used for KDE modelling (charcoals and cut-marked bone), the posterior sees two temporally distinct occupations within level A2 (see fig. 15.9).

The stratigraphic model for Isturitz is based on Barshay-Szmidt et al. (2018, fig. 6), with the addition of level C5. Most dating was done on anthropogenically modified faunal remains, and was therefore suitable for KDE modelling. The posterior probability distribution shows a near complete division along the cultural divide between the Proto-Aurignacian and the Early Aurignacian.

Previous chronological work by Wood et al. (2014) on L'Arbreda and Labeko Koba resulted in robust local chronologies for the MP-UP. L'Arbreda covers the Mousterian, Proto-Aurignacian, Evolved Aurignacian and the Gravettian, while Labeko Koba contains Châtelperronian, Proto-Aurignacian and Early Aurignacian assemblages. The stratigraphic model was adopted from Wood et al. (2014, fig. 3b and 5), and KDE modelling included all anthropogenically modified remains from UP levels.

Material from Cardini's 1959 excavation was used to model the stratigraphy at Riparo Mochi after Douka et al. (2012, fig. 6). Both the `Date` posteriors for the Proto-Aurignacian and the Early Aurignacian show some temporal spread within their respective units. As all levels belonged to the UP (Proto-Aurignacian, Early Aurignacian, Gravettian), all but the samples from the sterile layer were included in the `KDE_Model`. The result shows a well defined probability distribution with three peaks, though the peaks do not align with the original layer divisions into units G, F and D.

Ksar Akil is the only non-European site included here. Often an east-west spread of AMH is interpreted as a migration from the Levant to Europe

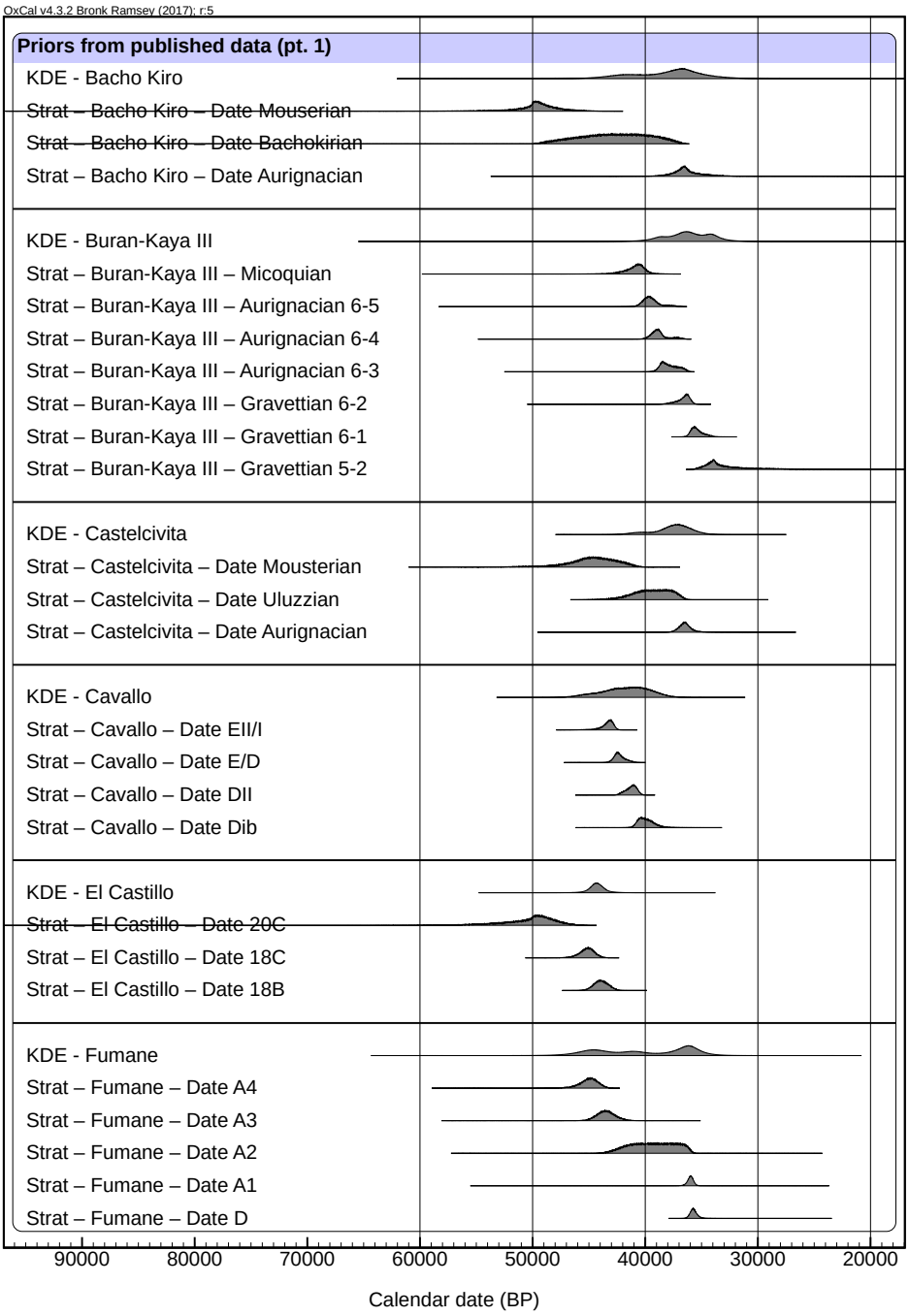


Figure 15.9: MP/UP: comparison of priors obtained from modelling published data (pt. 1/3).

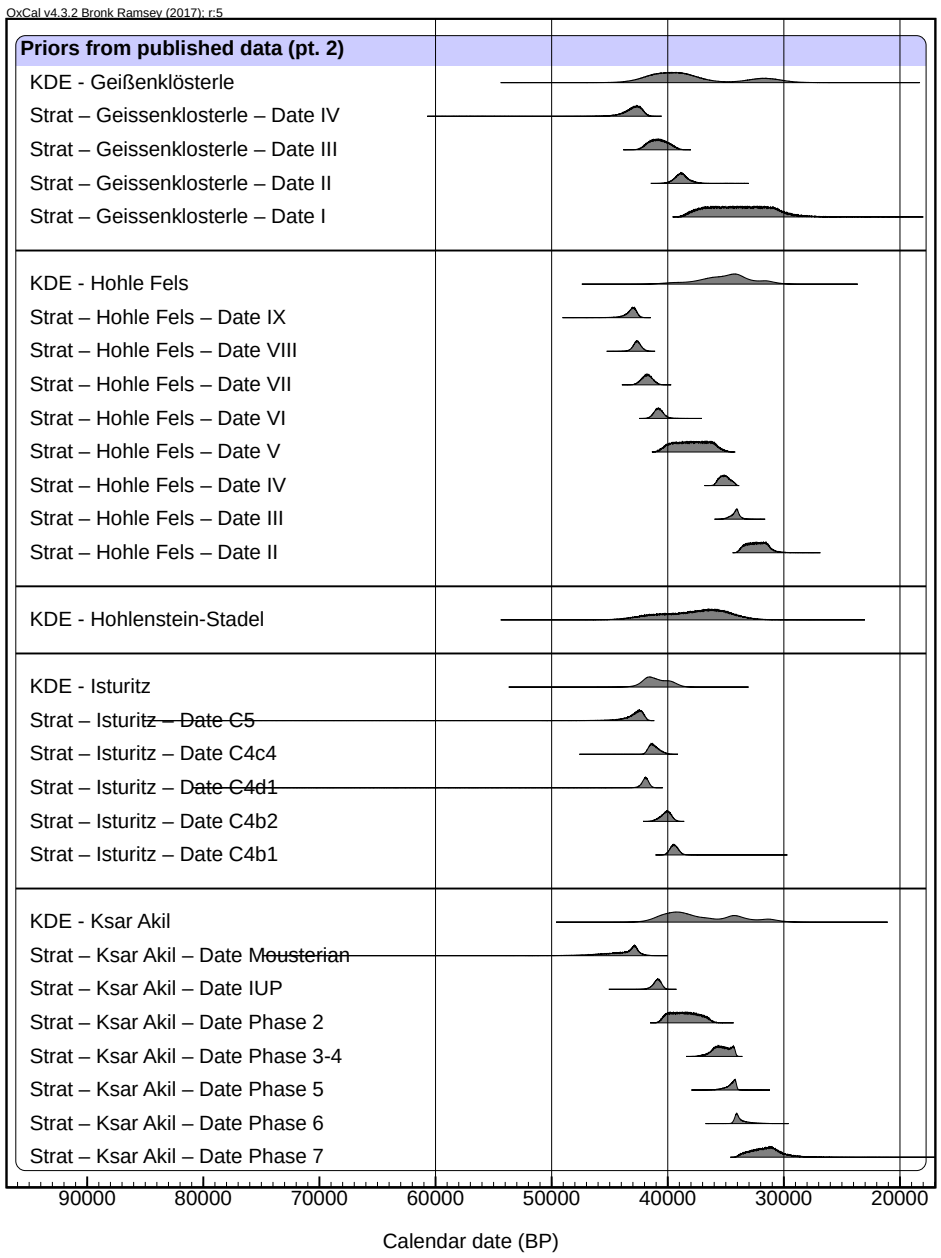


Figure 15.10: MP/UP: comparison of priors obtained from modelling published data (pt. 2/3).

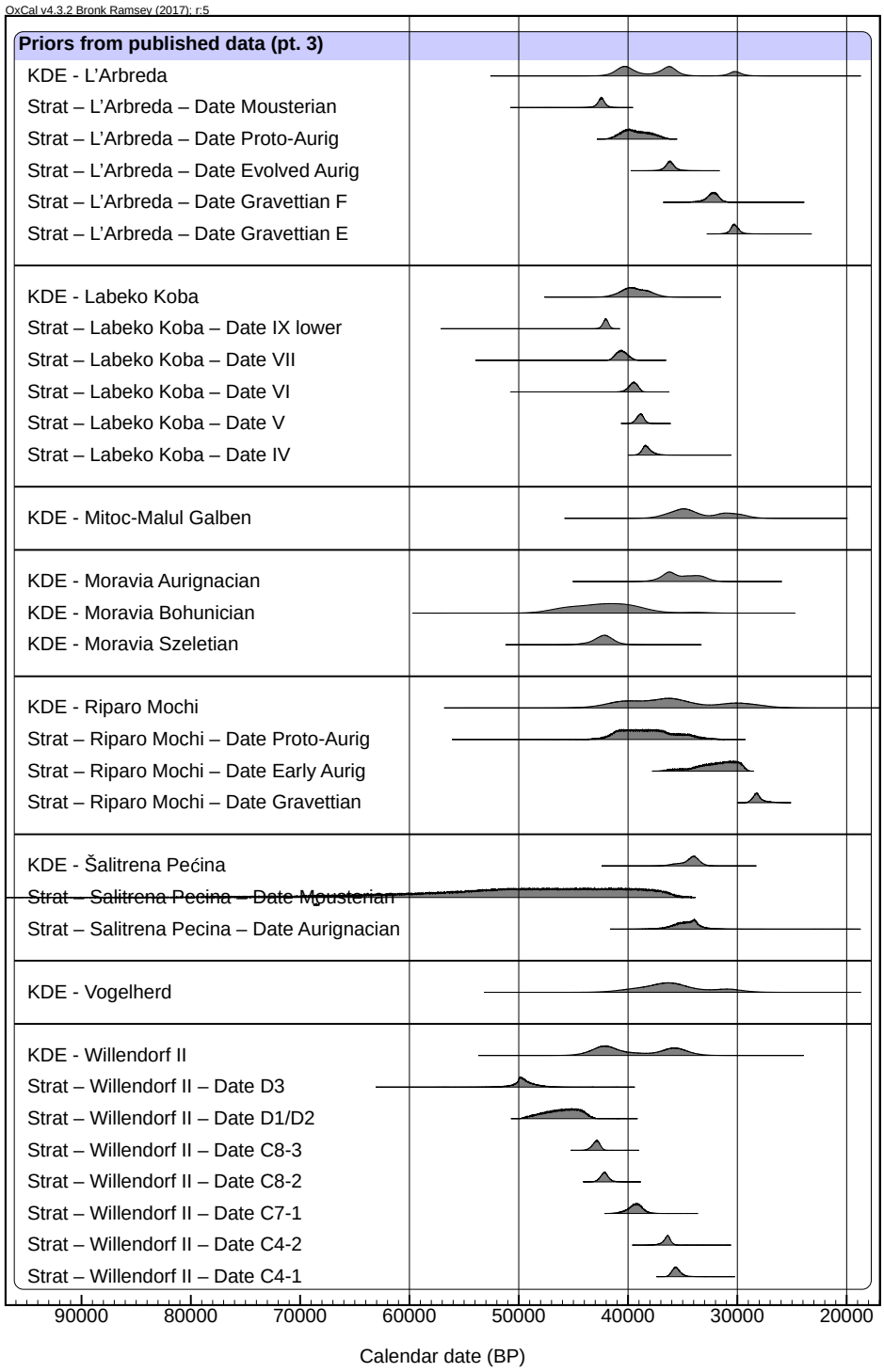


Figure 15.11: MP/UP: comparison of priors obtained from modelling published data (pt. 3/3).

(*e.g.* Müller et al., 2011), and therefore the radiocarbon chronology of Ksar Akil may shed some light on this assumption. The site will be crucial in the discussion, as it revealed an AMH partial right maxilla (Ksar Akil 2 or 'Ethelruda') in association with IUP material. In addition, the Ahmarian assemblages have featured in the debate on the origin of the Proto-Aurignacian in Europe (Teyssandier, 2008). Stratigraphic modelling for Ksar Akil was based on Model 2 from Douka et al. (2013, fig. S5), while all anthropogenically modified material from the IUP and younger levels were used for KDE modelling.

Comparing posteriors

The model outputs are shown in figures 15.9–15.11. For most sites, there is good agreement between the chronostratigraphy and the patterns observed in the KDE models. Some exceptions are Bacho Kiro, and Isturitz. At Bacho Kiro, the `KDE_Model` calculates an onset for the UP – which includes the Bachokirian – that is significantly later than the `Date` from the stratigraphic model. This is caused by the greater than radiocarbon age GrN-7545 and the poorly defined dating for the Mousterian horizon, which might in reality be beyond the reach of the radiocarbon dating method. At Isturitz, the onset of the Proto-Aurignacian is also earlier in the stratigraphic model compared to the KDE model. The lowermost Proto-Aurignacian level C5 is represented by two dates: OxA-X-2695-11 and OxA-2694-17. As the latter one has an unclear cutmark, it was not part of the KDE modelling, thus de-emphasising the earlier dates at the site. In contrast, it is interesting to note that the result of KDE modelling at Willendorf II includes the time range calculated for AH III via stratigraphic modelling – despite the fact that no samples from this horizon have been dated.

15.2.2 New Data

The modelling posteriors from the sites dated in this dissertation, and used for spatio-temporal mapping, are shown in figure 15.12. The individual as-

semblages are represented by the results of the empty `Date` function in each `Phase`. For Dzeravá Skala, they were obtained from the stratigraphic Model 10, and for Kozarnika and Temntata from their respective Model 3. The main diagnostic features at Istállóskő were the SBPs and MBPs. As a consequence, their age is represented by the model Points KDE 2, and culturally described as 'Aurignacian Point'. In addition, the individual radiocarbon dates on osseous points (unmodelled) were added for sites where no further modelling was possible: Jankovich, Bukovac, Szeleta, and Tabashkata. The direct date from Bivak was deemed too unreliable for inclusion, and the younger two points from Tabashkata date outside the period of interest and show characteristics different to the usually as 'Aurignacian' identified SBPs and MBPs.

The Upper Palaeolithic occupation timings were taken from the models KDE 3 for Dzeravá Skala, KDE 3 for Istállóskő, KDE 1 for Kozarnika, and KDE 3 for Temnata. For the latter, an additional prior of < 50000 cal BP was introduced to remove the initial occupation peak belonging to the Mousterian. None of the newly dated human remains – neither Neanderthal nor AMH – feature in the mapping as they all date outside the time window of 50–30k cal BP. Also the results from the two Serbian sites, Tabula Traiana and Dubočka-Kozja, are missing. The dating variability within the different horizons in combination with the limited lithic evidence does not presently allow a secure cultural attribution for the anthropogenically modified faunal remains.

When comparing the stratigraphic to the KDE based posteriors, some important differences are observable (see fig. 15.12). For example, at Dzeravá Skala, the KDE modelling produces a more detailed occupation pattern than seen in the reported stratigraphy, which suggests a near uniform occupation probability from 40-30k cal. A similar contrast is seen at Kozarnika, especially for layer 5b.

The largest discrepancy is found at Temnata, probably as a result of the less detailed excavation documentation and the clear erosion of certain occupation horizons. The stratigraphic model appears to overestimate the

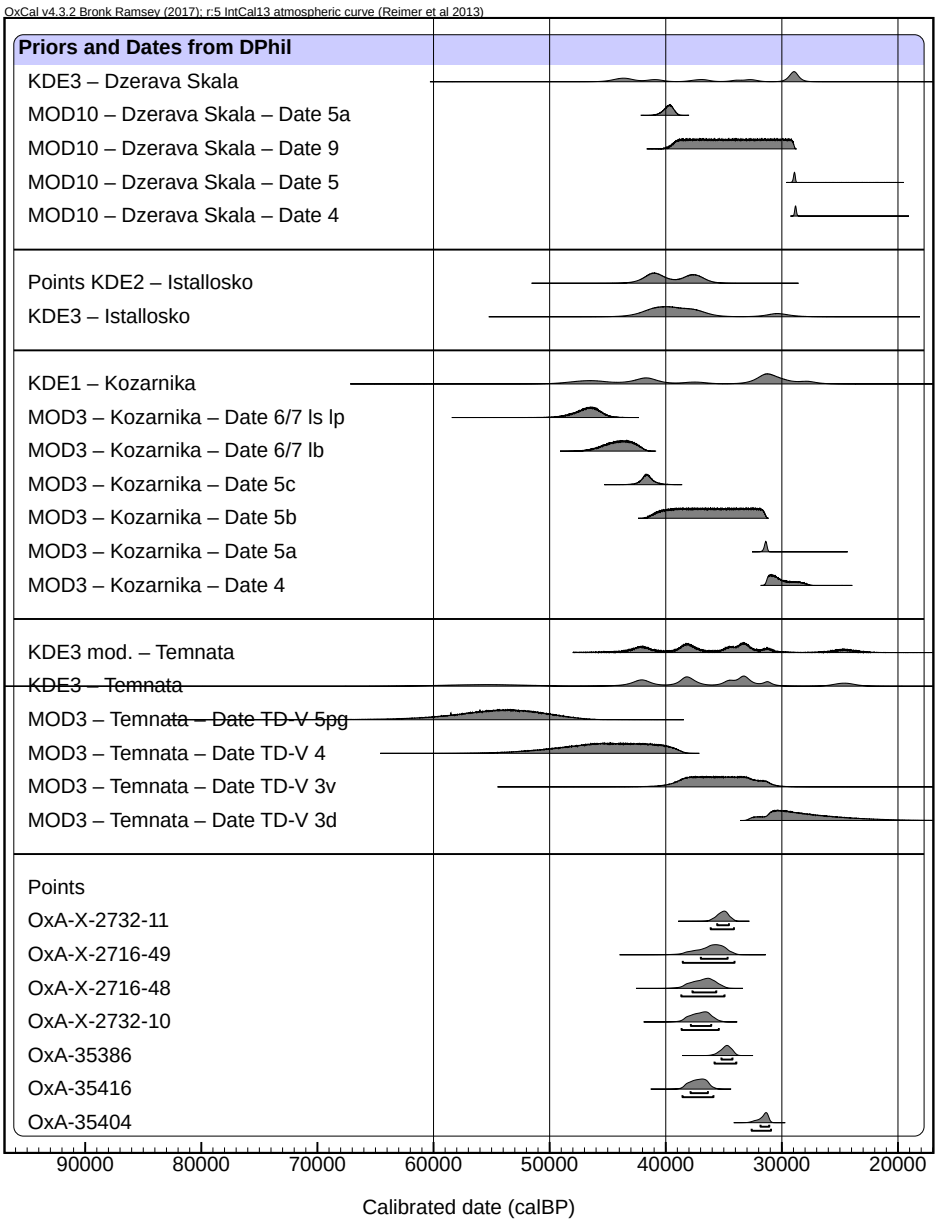


Figure 15.12: MP/UP: new dates and priors obtained from modelling new data. Directly dates osseous points from sites without any stratigraphic modelling, or with too few points for modelling, are listed at the end.

occupation periods, which has a severe effect on the estimated duration of the Mousterian from layer 5pg and the 'Aurignacian' from layer 4. In contrast, the absence of the eroded occupation between these two horizons (probably IUP, see section 8.4.4) is captured by the KDE Model, which indicates no directly dated occupation inside the cave between 50–45k cal BP. For the spatio-temporal mapping, it is therefore important to bear in mind that AMH appearance at Temnata may predate the KDE posterior for the UP shown as 'KDE3 mod. – Temnata'. The difference at Istállóskő stems from Points KDE 2 representing only the osseous industries, while KDE 3 includes later, probably Gravettian, occupation.

15.2.3 Map composition

The published and new data was combined into three spatio-temporal maps. MAP 1 represents the cultural mosaic of the 'transitional' period (see fig. 15.14–15.16), and is based on the stratigraphic model posteriors, and the KDE distributions for sites without stratigraphic modelling. The data is further complemented by radiocarbon measurements from directly dated osseous points. The code is listed on p. 769.

MAP 2 attempts to visualise the possible biological mosaic (see fig. 15.17). It includes the same data as MAP 1, but is divided by assumed authorship. Additionally, it contains the radiocarbon measurements from directly dated human remains (excluding Russian specimens) as used in section 15.1. The main code is listed on p. 777. The codes for the variations tested and shown in figures 15.18–15.19 are on p. 785, p. 794 and p. 803.

In contrast, MAP 3 solely traces the spread of AMH (see fig. 15.20–15.21). As such, it uses the KDE modelling posteriors described in the two previous subsections, and restricts the direct radiocarbon data to the Upper Palaeolithic (*i.e.* osseous points and AMHs, excluding Russia). This map will be further discussed in section 15.3. The code is listed on p. 811.

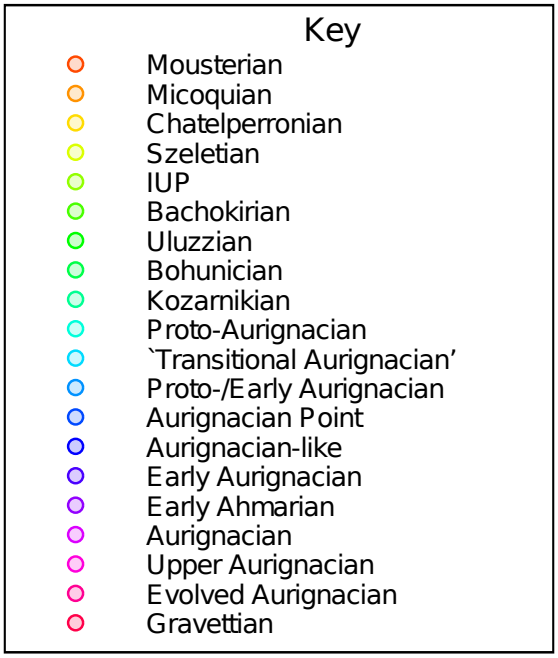


Figure 15.13: MP/UP: key for reading cultures on MAP 1 (fig. 15.14–15.16).

15.2.4 Spatio-temporal distribution

The following section investigates the cultural, and resulting biological, mosaic between 53–35k cal BP. It will first focus on the possible meaning of the cultural spatio-temporal distribution seen in MAP 1 (see fig. 15.14–15.16), before the the biological component is extrapolated by associating each cultural tradition with a specific human author as visualised in MAP 2 (see fig. 15.17). The results will inform the validity of the *Kulturpumpe* model and the Danube corridor hypothesis.

A cultural mosaic

The earliest UP technocomplex registered on the map is the 'Aurignacian-like' assemblage (●) from level 4 at Temnata (see fig. 15.14). As previously discussed (15.2.1), the early presence at the site is more likely the construct

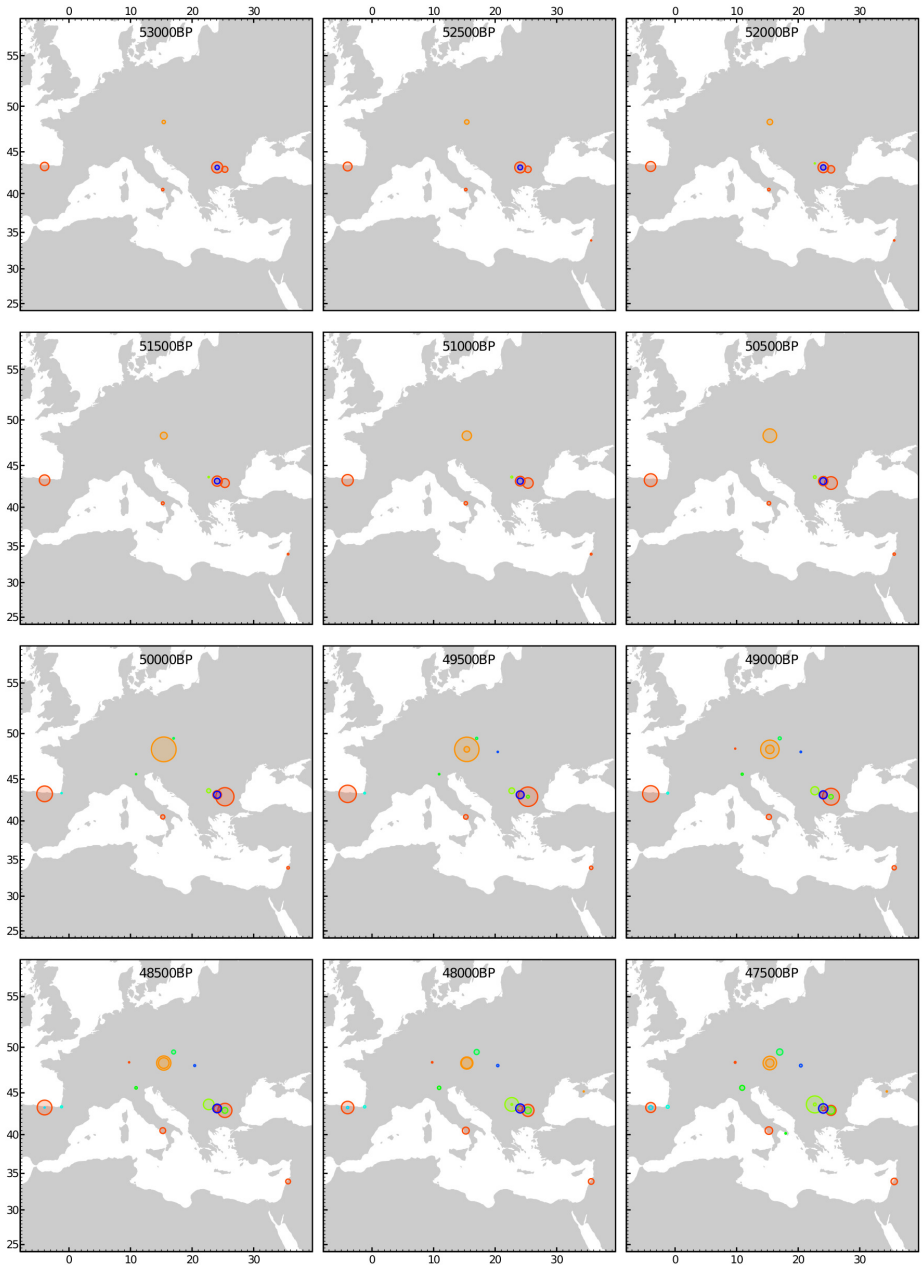


Figure 15.14: MP/UP: MAP 1 – spatio-temporal distribution of dated assemblages between 53000–47500 cal BP, visualised in time slices of 500 years (code: p. 769). The key for decoding the colours in terms of archaeological cultures can be found in figure 15.13.

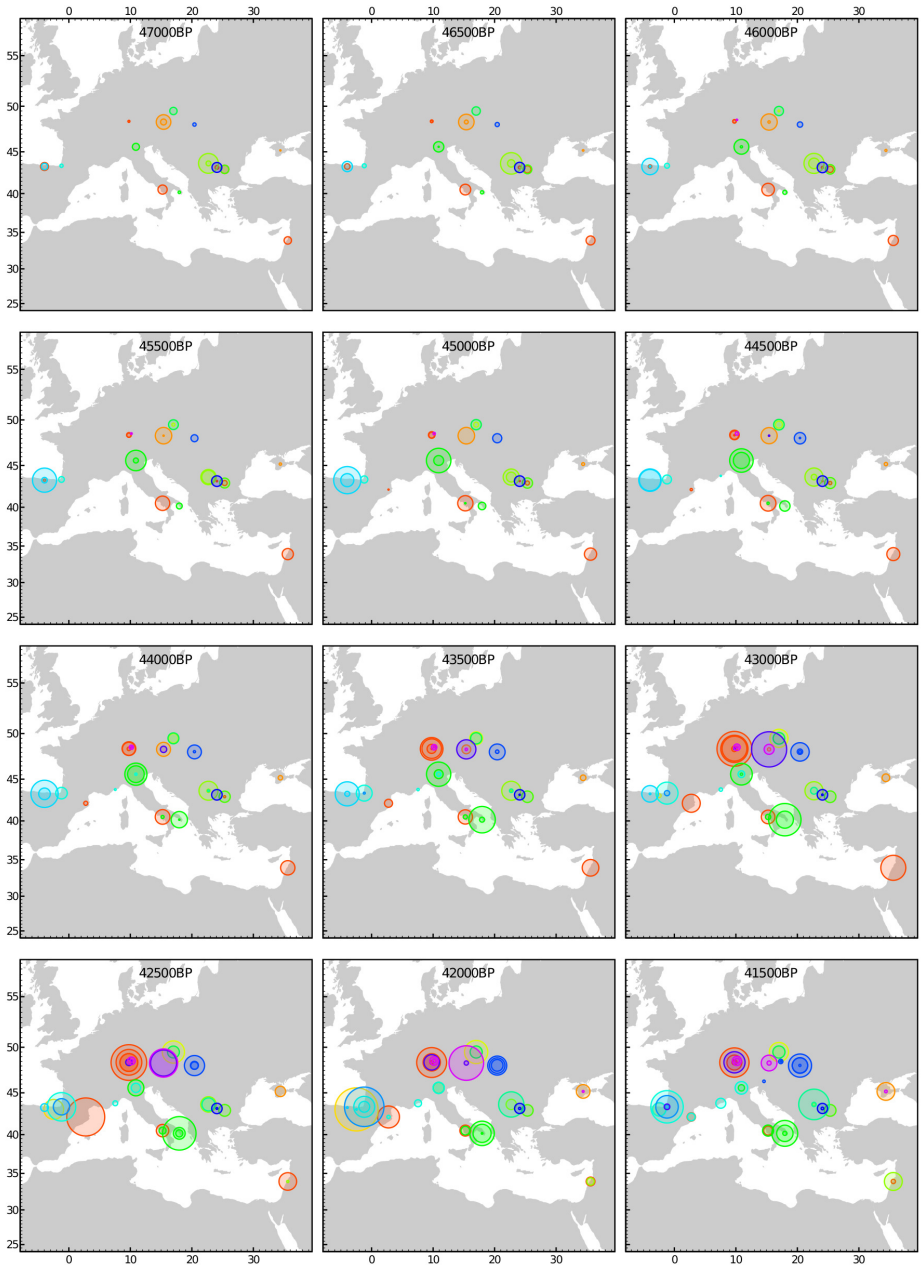


Figure 15.15: MP/UP: MAP 1 – spatio-temporal distribution of dated assemblages between 47000–41500 cal BP, visualised in time slices of 500 years (code: p. 769). The key for decoding the colours in terms of archaeological cultures can be found in figure 15.13.

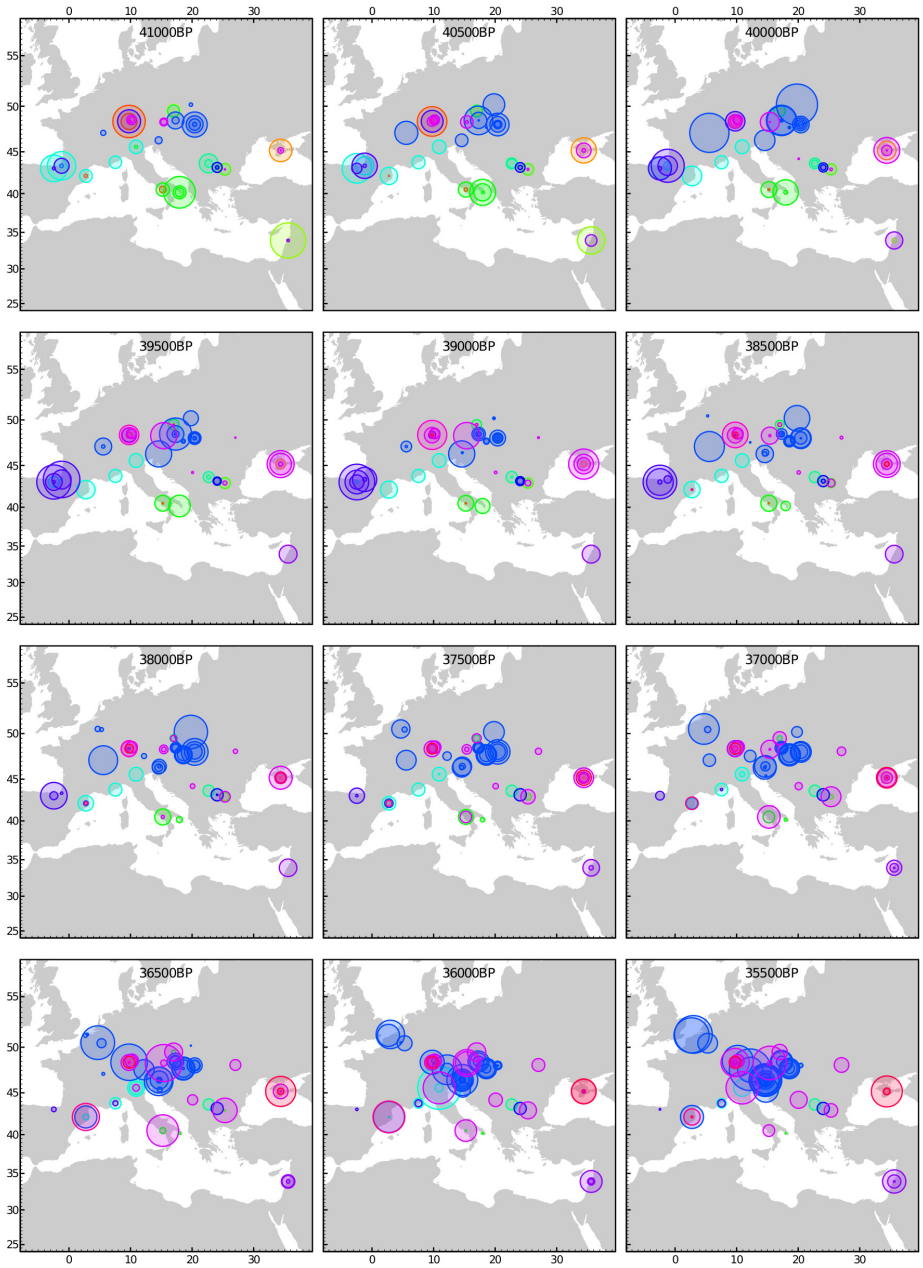


Figure 15.16: MP/UP: MAP 1 – spatio-temporal distribution of dated assemblages between 41000–35500 cal BP, visualised in time slices of 500 years (code: p. 769). The key for decoding the colours in terms of archaeological cultures can be found in figure 15.13.

of modelling than a reflection of reality. The IUP age is expected to fall between 50–45k cal BP, and pre-date the Aurignacian-like layers (see also subsection 8.4.4). As a result, Europe appears to be in the firm hands of Middle Palaeolithic assemblages (● ●) before 52k cal BP.

The first meaningful recording of an UP industry can be seen in the IUP (●) in the Balkans. The industry quickly expands to Moravia, where it manifests itself as the Bohunician (●). At the same time, the Uluzzian (●) is recorded at Fumane in northern Italy, and both appear only shortly before the Proto-Aurignacian (●) at Isturitz.

The apparently contemporaneous occupation at Dzeravá Skala is labelled Aurignacian-like (●). This is largely based on the osseous points found within the horizons, which themselves all date slightly later. It is plausible, that this early occupation is related to some of the leaf point lithics that were found at the site, or to another manifestation of the IUP along the Danube. However, the limited lithic material will make a definitive attribution challenging.

After 47k cal BP, a west to east movement of the Proto-Aurignacian (●) is visible (see fig. 15.15). The cultural influence expands along the Mediterranean coast and progressively replaces the Uluzzian (●) in northern Italy (though its presence still flourishes in the south). Though this expansion appears contemporaneous with the appearance of the Châtelperronian (●) at Labeko Koba, it is unclear whether these phenomena are related. If they are related, the Proto-Aurignacian migration may be either the result of, or allows for, an influx of Châtelperronian.

In contrast, the Szeletian (●) appears in Moravia at approximately 45k cal BP (see fig. 15.15), and fades by 40k cal BP (see fig. 15.16) – thus covering a time period of great cultural (and possibly biological) diversity in central Europe. It is contemporaneous with the Mousterian (●), Bohunician (●), Early Aurignacian (●) and Aurignacian Points (●).

As discussed in chapter 14, the earliest dated Aurignacian osseous points (●) appear in the Bükk Mountains in Hungary (see fig. 15.15). MAP 1 suggests that this development may have occurred shortly before, or con-

temporaneous with, the (Early) Aurignacian (● ●) manifestations devoid of osseous points found in the Swabian Jura (Germany). The use of the osseous points industry quickly spreads eastwards and is soon found with Aurignacian lithic assemblages (see fig. 15.16).

The contemporaneity of Proto-Aurignacian (●), Early Aurignacian (●), and Evolved Aurignacian (●) assemblages is indicative of more than just the cultural progression that was proposed by the Aquitaine model. The initial concentration of the Proto-Aurignacian in the northern Mediterranean and the Early Aurignacian further from the coast, followed by later Aurignacian manifestations (● ● ●) in most of these localities is striking. It is a strong reminder how research traditions, nomenclature and unidirectional developments may hinder our understanding of complex cultural developments. Apart from the commonly applied arguments of evolution and replacement, concepts such as innovation, fusion, disuse, and specialisation are equally important in explaining techno-cultural expressions.

The Levant is portrayed as a region that both influences and promotes techno-cultural change, and is frequently invoked as the source for European cultural developments (*e.g.* Mellars, 2011). However, the dating record for the two dominant early UP industries with an assumed connection to the Levant – the IUP (●) and the Early Aurignacian (●) – seem to both indicate otherwise. The IUP does not appear at Ksar Akil until around 42k cal BP, and the Early Ahmarian (●), which is seen as showing affinities to the Aurignacian in Europe, does not appear until 40.5k cal BP. Therefore, both are evidently post-dating equivalent developments in central Europe. This is consistent with the 'back-to-Africa' movement proposed for 45–40k cal BP (Olivieri et al., 2006).

By 40k cal BP, Europe seems to predominantly produce Upper Palaeolithic industries (see fig. 15.16), and the cultural mosaic becomes increasingly uniform. It remains to be seen whether this is a reflection of pan-European cohesion, or the result of a homogenising research tradition.

A biological mosaic

If it is assumed that each cultural expression has a specific human author, we can attempt to trace Neanderthal and AMH movements using archaeological assemblages as a proxy. In line with skeletal evidence, the Middle Palaeolithic industries (*i.e.* Mousterian and Micoquian) were attributed to Neanderthals, and the Upper Palaeolithic industries (*i.e.* IUP, Kozarnikian, Proto-Aurignacian, Transitional Aurignacian, Early Aurignacian, osseous projectile points, Early Ahmarian and younger) were assigned to AMHs. The 'transitional' industries were divided as follows. A Neanderthal origin is assumed for the Châtelperronian (after Higham et al., 2010; Hublin et al., 2012; Ruebens et al., 2015), and the Szeletian in Moravia (after Allsworth-Jones, 1986; Oliva, 1991; Svoboda, 2005; Valoch, 2000). In contrast, an AMH origin is postulated for the Bohunician (after Hoffecker, 2009; Hublin, 2012; Nigst and Haesaerts, 2012; Richter et al., 2009), Bachokirian (after Teyssandier, 2008), and the Uluzzian (Benazzi et al., 2011). The resulting spatio-temporal distribution of Neanderthal and AMH presence is supplemented with the directly dated skeletal evidence and visualised in MAP 2 (see fig. 15.17).

In the time period 52–47k cal BP, there is a clearly visible east-west migration of AMHs. They appear to be moving up the Danube corridor. If the Uluzzian is indeed representing AMH, the migration takes a trajectory both north and south of the Alps, before reaching the Atlantic. It is worth noting the Neanderthal absence in the lower Danube area at the time. This is not contradicted by the two Mousterian/Neanderthal markers seen on the map. They are from Temnata and Bacho Kiro. For modelling reasons, both sites are likely to significantly underestimate the age of late Neanderthal occupation. The remaining Neanderthal presence throughout Europe remains relatively stable during those 5000 years.

From 46–41k cal BP AMH occupation intensifies, with many new sites appearing. By the end of this period, Neanderthal settlements are concentrated to the north-west and east, separated by the AMH territories. Again,

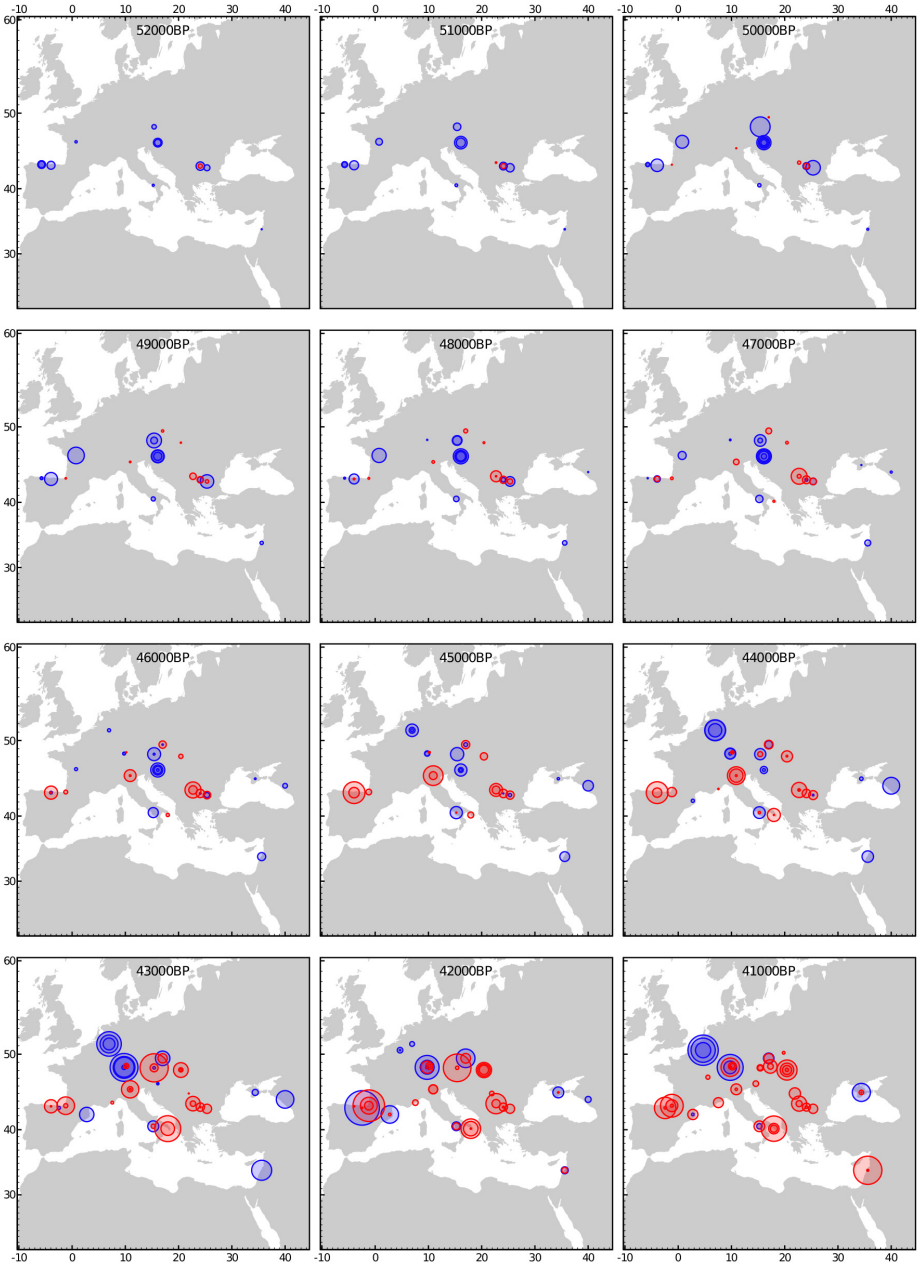


Figure 15.17: MP/UP: MAP 2 – spatio-temporal distribution of Neanderthal (**blue**) and AMH (**red**) dated assemblages between 52000–41000 cal BP, visualised in time slices of 1000 years (code: p. 777).

such a development is consistent with a migration into Europe from north of the Black Sea rather than directly from the Levant.

The biological contrarian

The available evidence seems to best support the biocultural groupings described above. Nonetheless, these proposed associations heavily rely on the assumption of single authorship, cultural classification and indirect arguments. It is therefore not surprising to find some contrarian voices. Consequently, three commonly argued scenarios and their impact on the spatio-temporal distribution of Neanderthals and AMHs are further investigated. They are ranked according to the principles of 'Occam's razor', *i.e.* discussing the most plausible alternative first, followed by interpretations that require more assumed steps to fit the current dataset,

Prior to the reanalysis of the dental remains by Benazzi et al. (2011), the Uluzzian had been interpreted as evidence for Neanderthal modernity (*e.g.* Peresani, 2008). Zilhão et al. (2015) criticised the reclassification, suggesting the two deciduous molars from Grotta del Cavallo are intrusive, and the radiocarbon age determinations of the technocomplex (*ca.* 45k cal BP) are more consistent with Neandertal fossils in the region. However, a Neanderthal origin for the Uluzzian has no effect on the AMH trajectory along the Danube (see fig. 15.18-a), though it would limit the initial expansion to areas north of the Alps.

The link between the Szeletian in Moravia and a Neanderthal authorship is based on lithic analysis suggesting a local development from the underlying Micoquian industry (Kaminská et al., 2011; Nerudová and Neruda, 2017; Valoch, 1993). While this interpretation has great local significance, as it suggests a contemporaneity between Neanderthals and AMHs in Moravia, it has little influence on the Danube corridor. An AMH authorship would maintain the time frame already provided by the Bohunician, albeit with more cultural diversity.

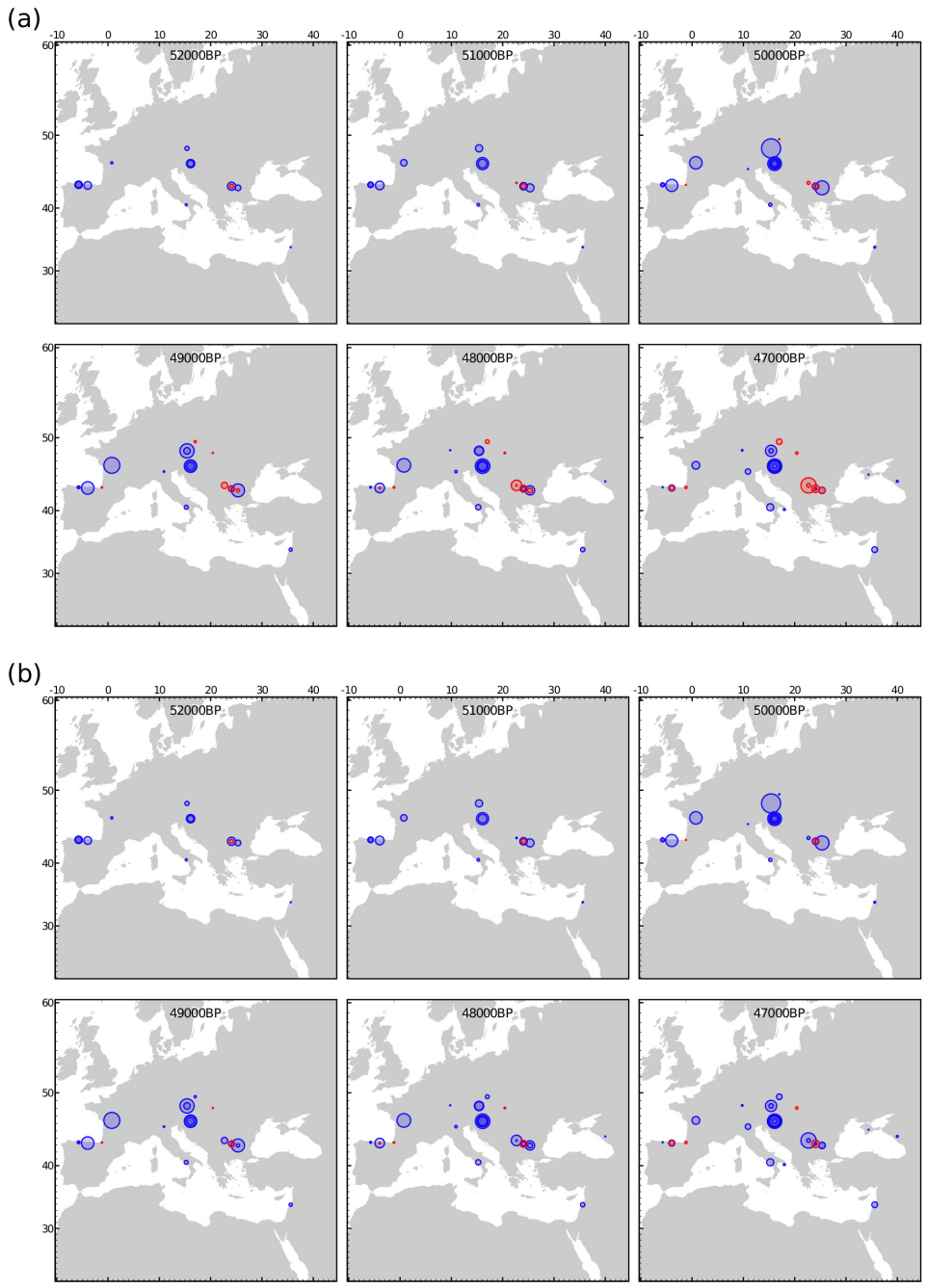


Figure 15.18: MP/UP: spatio-temporal distribution of Neanderthal (**blue**) and AMH (**red**) dated assemblages between 52000–47000 cal BP, visualised in time slices of 1000 years. In contrast to original MAP 2, following industries were changed to Neanderthal authorship: (a) Uluzzian (code: p. 785), (b) Uluzzian, Bohunician, Bachokirian, and IUP (code: p. 794).

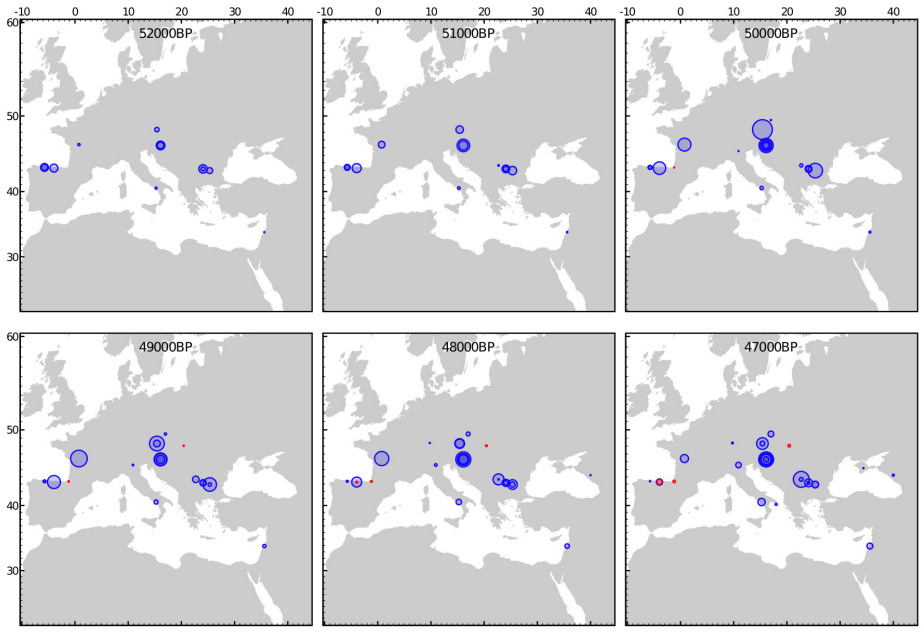


Figure 15.19: MP/UP: spatio-temporal distribution of Neanderthal (**blue**) and AMH (**red**) dated assemblages between 52000–47000 cal BP, visualised in time slices of 1000 years. In contrast to original MAP 2, following industries were changed to Neanderthal authorship: Uluzzian, Bohunician, Bachokirian, IUP, Kozarnikian level 5c, and Aurignacian-like at Temnata and Bacho Kiro (code: p. 803).

The association of the IUP with AMHs is based on skeletal evidence from the Levant, which post-dates IUP assemblages found along the Danube and in Russia. The use of Levallois technology and hard hammer percussion has been used to argue for a MP character and a possible Neanderthal origin – at least for the European assemblages. Such an interpretation would affect the Bachokirian (levels 11 and 11a) at Bacho Kiro, the IUP (level VI) at Temnata, the early UP (level 6/7) at Kozarnika, and the Bohunician in Moravia. Using those assemblages as proxy for Neanderthal presence would lead to a near synchronous appearance of AMHs in the Balkans, the middle Danube and in the Basque region (see fig. 15.18-b). The early dates for Temnata are probably overestimating the age of the Aurignacian-like level 4, as discussed previously. The use of the Danube corridor would remain a

valid interpretation. However, the dating could neither support an east-west nor a west-east direction of migration, and would suggest that the initial stages of AMH occupation are culturally disconnected. By contrast, the IUP technocomplex would have two authors, Neanderthals in Europe (including Russia) and AMHs in the Levant. This opposition requires further explanation, for example, through an assimilation process or a reduction of the IUP designation to Levantine assemblages.

If the main concerns of authorship are based on the absence of directly associated human remains and an UP assemblage character *sensu stricto* – *i.e.* no Levallois use, but clear Proto- or Early Aurignacian diagnostic tools as defined in the Aquitaine model – further assemblages would need reclassification. This would mainly affect the Aurignacian like occupations in eastern and central Europe, such as at Bacho Kiro, Temnata (levels 4 and 3v), and Kozarnika (level 5c). This radical scenario would lead to an initial appearance of AMHs at Isturitz and neighbouring regions, but would provide little evidence to explain how a new human group arrived with a lithic technocomplex distinct from material previously recorded in the area or anywhere else (see fig. 15.19). The only AMH occupation registered further east would be at Dzeravá Skala (Slovakia), where the AMH association for that period is solely based on the presence of SBPs. Despite the increasing difficulty of understanding such a dataset in light of an initial migration of AMH into central Europe, and the development of Upper Palaeolithic technology, the date for the initial AMH migration would become only minimally younger.

Conclusions

The data presented here supports an initial AMH migration to central Europe via the Danube fluvial corridor. However, in contrast to the original hypothesis, these people appear to bring with them not an Aurignacian, but an IUP tool kit.

The Early Aurignacian technocomplex, on the other hand, appears to be a central European development, though its individual components seem to not

solely be the result of local innovation, but may have resulted from fusion and specialisation. It is probable, that initial diagnostic lithics appear in Swabia after an west top east expansion of the Proto-Aurignacian along the northern Mediterranean coast, and after the development of Aurignacian like traces in eastern sites such as Kozarnika. Furthermore, the datasets indicate that projectile point use in the Aurignacian post-dates their initial development outside of a diagnostic Aurignacian sphere. The Early Aurignacian technocomplex may therefore be the result of a culturally and environmentally diverse period and region. In this light, its early manifestation in southern Germany is not surprising, considering the topographic conditions and the complex biocultural mosaic of the period (seen in MAP 1, fig. 15.15).

This composition might also help to explain the absence of fully diagnostic assemblages in the east, as only certain aspects of what was defined as Aurignacian made its way back to the south-east, and possibly the Levant. As such, the *Kulturpumpe* model seems to describe the rise of the Aurignacian better than its assumed homogeneous expansion.

15.3 The spread of AMH

In the previous section the biocultural mosaic was investigated, and therefore the dating focused on age estimation of cultural expressions. In contrast, KDE modelling of dates obtained on anthropogenic or anthropogenically modified material often allows for more detailed information on occupation fluctuations. This is partially due to the nature of the excavated record (in which shorter and temporally distinct human activities are embedded in thicker, stratigraphically distinguishable layers), and partially to the substantial temporal gap between the MP and UP presence at certain sites. As a result, the spread of AMH into Europe is further tested using dated AMH activity events from KDE modelling[6]. AMH authorship is attributed accord-

[6]For a discussion of the underlying data see section 15.2. The raw data from the reference sites can be found in catalogue C, the OxCal code for obtaining the KDE posteriors in catalogue B.8, and the visual model outputs in catalogue D.

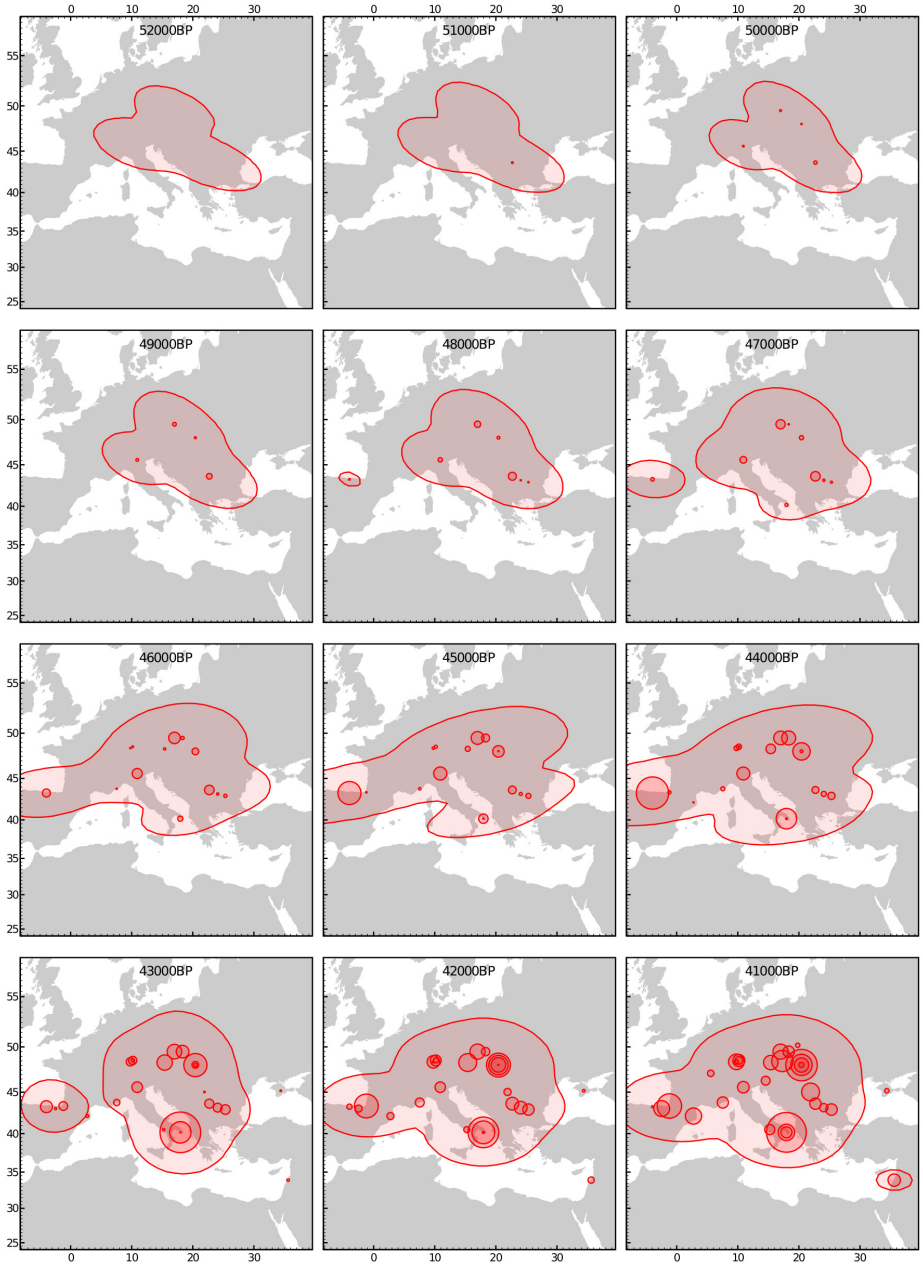


Figure 15.20: MP/UP: MAP 3 – spread of AMH between 52000–41000 cal BP (in time slices of 1000 years) based on directly dated human remains, osseous points and KDEs of UP assemblages (code: p. 811). KDE mapping contour at 95%.

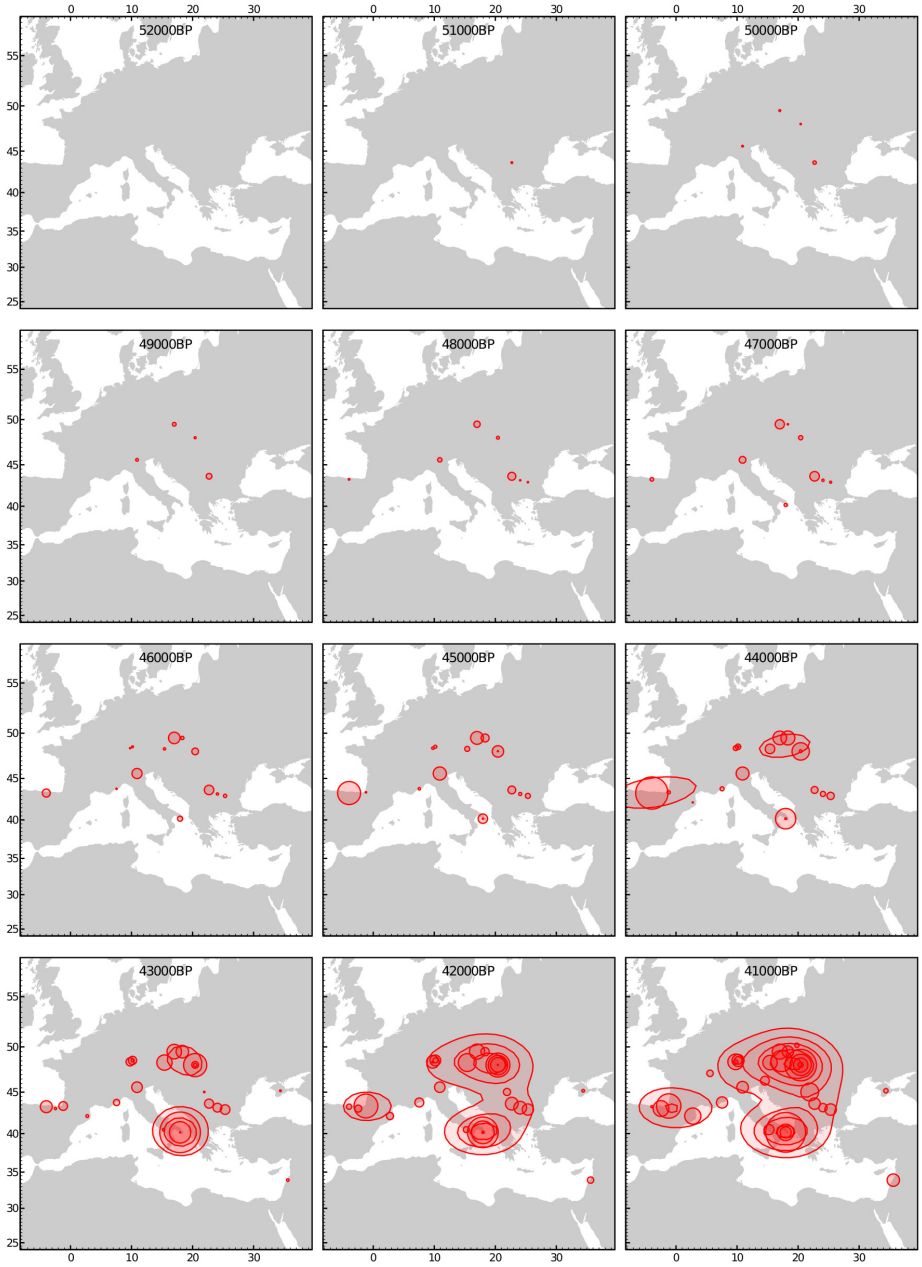


Figure 15.21: MP/UP: MAP 3 – spread of AMH between 52000–41000 cal BP (in time slices of 1000 years) based on directly dated human remains, osseous points and KDEs of UP assemblages (code: p. 811). KDE mapping contour set to 10.

ing to the criteria described in subsection 15.2.4, and the resulting MAP 3 uses KDEs to highlight spatio-temporal event concentrations. The first visualisation applies a contour outlining the 95% margin (see fig. 15.20), the second a contour setting of 10 in the OxCal options (see fig. 15.21).

As observed during the investigation of the biocultural mosaic, the earliest appearance of AMHs clearly occurs along the lower, and then middle Danube. If arguments against an AMH attribution of the Uluzzian are adhered to, the initial AMH expansion appears to solely use the Danube fluvial corridor as a conduit. However, in the current configuration, a trajectory along the northern as well as the southern confinements of the Alps is observable. Eventually, AMHs spread to the Atlantic coast, though the data resolution is insufficient to determine whether these populations would have expanded out of central Europe, or arrived from elsewhere.

Therefore, the presumed first colonisation of Europe by AMH took place between 50,000 and 45,000 cal BP – with AMH reaching central Europe by 47,000 cal BP or possibly even earlier. By 41,000 cal BP clear activity centres have been established in central Europe, the Pyrenees and southern Italy (see fig. 15.21).

Part VI

Conclusions

Chapter 16

Summary of findings

This dissertation demonstrates that AMHs likely arrived via the Danube corridor in central Europe as early as 50–47k cal BP (see chapter 15). However, they did not bring with them the Aurignacian material culture, but probably the IUP – a technocomplex which is later also found in the Levant (see fig. 16.1). Instead, the Early Aurignacian formed between 43–41k cal BP in central Europe by incorporating and adapting cultural and technological trends in its vicinity, thus amalgamating different individual material expressions. One of these are split-based points (SBPs). They first appear in the Bükk mountains (Hungary) without any diagnostic Aurignacian lithics, and later arrive in the upper Danube region (*e.g.* at Geißenklösterle), where they post-date the earliest Aurignacian lithics (see chapter 14).

Osseous points offer a unique opportunity to directly date a techno-culturally distinct human activity. As many osseous points come from coarser excavations, indirect dating may significantly overestimate the period of their occurrence, and mask temporal trends (see section 11.2 and chapter 14). Direct dating and KDE modelling revealed a temporal separation between SBPs and MBPs not only at Istállóskő, but throughout Europe.

Other technocomplexes have proven less informative for the Danube fluvial corridor. On close inspection, the Szeletian seems to vanish from the Hungarian record as a coherent techno-cultural expression (*e.g.* section 11.4),

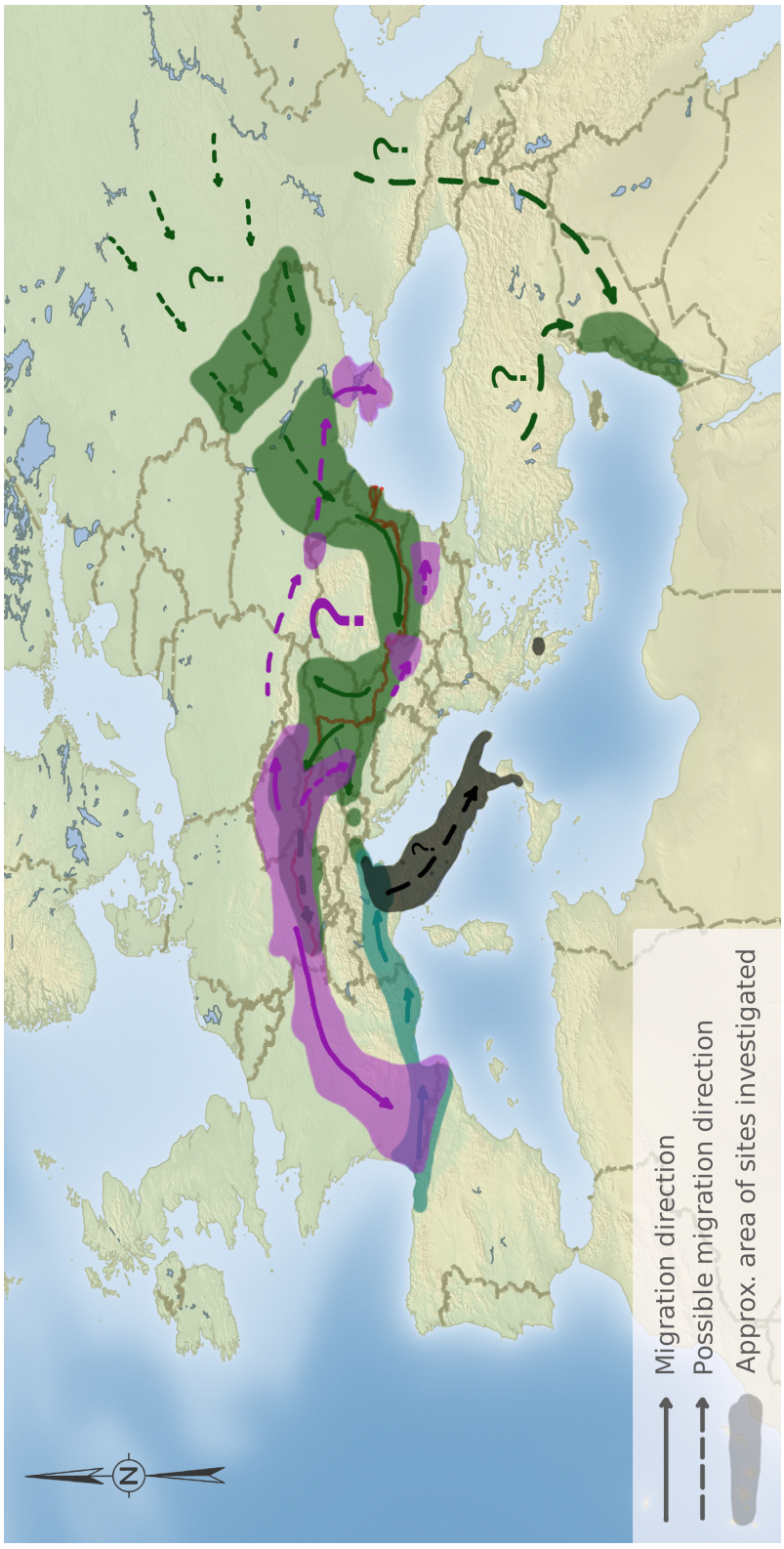


Figure 16.1: Summary: attempt at visualising different larger migration and cultural influence patterns into and from Europe based on radiocarbon dating and modelling presented in this dissertation. (1) Initial AMH migration with IUP into central Europe along the Danube corridor *ca.* 50–47k cal BP (●) with a possible fork or backflow to the Levant *ca.* 42–41k cal BP (2) Proto-Aurignacian *ca.* 49–40k cal BP (●), (3) potential Uluzzian trajectory *ca.* 50-44k cal BP (●), (4) Aurignacian expansion *ca.* 42–36k cal BP (●). For a discussion on the applicability of the Proto-/Early Aurignacian distinction see section 3.1.3, and on the rarity of Aurignacian lithics in the east see section 15.2.

and the Jankovichian has so far alluded any attempts at absolute dating. At the same time, the human remains dated for this dissertation are either older (Neanderthals) or younger (AMHs) than the period of the MP/UP biocultural shift (sections 8.1, 8.2, 12.2). While this is regrettable, it provides essential clarity in what skeletal evidence is relevant to the MP/UP debate.

The Mousterian and Micoquian assemblages in the middle/lower Danube region appear largely beyond the radiocarbon time scale (*e.g.* sections 8.1, 8.4, 9.1, 9.2). It seems that human activity was very low shortly before the arrival of AMHs. This is supported by DNA evidence suggesting low Neanderthal population numbers, and may be reflected in the increase in anthropogenically modified fauna remains found in UP compared to MP levels (*e.g.* sections 12.1, and 8.4, and chapter 15).

Throughout the dissertation, KDE modelling has proven crucial to providing independent assessment of the stratigraphic record and Bayesian modelling results. Furthermore, it enabled the age estimation for the IUP period at Temnata (see section 8.4), and could differentiate between temporally different activities within the same geological unit, or archaeological level (*e.g.* section 12.1 and 11.2). The resulting occupation timings are consistent with palaeoenvironmental analyses, which identify anthropogenic cave occupations along the Danube predominantly during colder climate periods.

This dissertation illustrates how important adequate sample selection, pretreatment, and rigorous analysis of the dating record is to disentangle spatio-temporal developments. The results support the Danube corridor hypothesis in so far as it postulated the Danube valley as a conduit for early AMH dispersal into central Europe. In contrast, the *Kulturpumpe* model better reflects the emergence of the Early Aurignacian in central Europe.

Chapter 17

Future work

This dissertation places the chronology of the MP/UP biocultural shift on more secure footing – especially in the crucial region of the Danube fluvial corridor – and sheds some light on possible early AMH migration patterns. Nonetheless, it is only an initial stepping stone in the continuing endeavour to increase our understanding of the biological and cultural changes that occurred in Europe 55,000–35,000 years ago. In the following, some opportunities for improving and expanding on these results are presented.

In terms of radiocarbon dating and chronology building, increasing the number of robust, high precision records is crucial. This requires the inclusion of more, and possibly new, archaeological sites, artefacts and human remains. Presently, the record is dominated by cave sites, which predominantly contain occupation evidence from colder periods, leading to a distinct periodicity in the dating record as seen by KDE modelling. Dating of open air sites may refine the spatio-temporal models, by providing proxies for human activities in intermittent periods. As many of these localities show an absence of radiocarbon datable material, increased use of OSL dating will become inevitable and the reduction in precision needs to be carefully addressed.

Furthermore, recent AMS developments will allow for a reduction in sample mass and a possible increase in measurement precision. This will lead

to opportunities for multiple dating of artefacts and human remains without secure context, which will substantially improve their dating reliability. As a result, directly datable, and culturally diagnostic artefacts (*e.g.* osseous points) may in future help to establish high resolution chronotypologies that are independent of lithic identification.

At the same time, radiocarbon method development needs to focus further on quality control protocols. Ideally, this includes a stronger emphasis on sample characterisation and a more precise (and sample specific) understanding of the components actually dated. As laboratory procedures are equally important as archaeological interpretations, detailed pre-treatment information should be part of any publication including (new) radiocarbon dates – irrespective of whether the study was conducted by radiocarbon specialists or the dating was commercially obtained[1].

In addition to chronological work, the identification and (re-)analysis of archaeological assemblages and human remains is essential. The result of cultural analyses (*e.g.* of lithic assemblages) will directly affect the spatio-temporal patterns and their interpretations. It is expected that the wider application of ZooMS will greatly facilitate the identification of human remains, which may identify authors of specific cultural expressions. Moreover, the uptake in aDNA studies should lead to the discovery of further links between different populations and their past interactions.

Eventually, an integrative modelling approach (incorporating data from genetics, chronology, archaeology and climate research) paired with exploratory data science should refine our understanding of past population dynamics and migration patterns, while simultaneously testing the effects of underlying assumptions. However, for such research to be effective and efficient, a well developed, standardised and maintained (!) multi-disciplinary database would be fundamental. If successful, the coming decades are promising to be exciting, thought-provoking, and possibly revolutionary times for the study of human biocultural evolution.

[1] Despite notable improvements, some articles still contain limited to no pre-treatment information – or use non-permanent links (*e.g.* Henry-Gambier and Sacchi, 2008).

Bibliography

Adamiec, G. and Aitken, M. (1998). Dose-rate conversion factors: update. *Ancient TL*, 16:37–50.

Adams, B. (2001). Recent investigations at Szeleta and Istállóskő Caves, Hungary. In *66th Annual Meeting of the Society for American Archaeology, New Oreleans, April 18-22.*

Adams, B. and Ringer, (2004). New C^{14} Dates for the Hungarian Early Upper Palaeolithic. *Current Anthropology*, 45(4):541–551.

Aitken, M. J. (1990). *Science-based Dating in Archaeology.* Longman Group UK Ltd., Harlow.

Akimova, E., Higham, T., Stasyuk, I., Buzhilova, A., Dobrovolskaya, M., and Mednikova, M. (2010). A new direct radiocarbon AMS date for an Upper Palaeolithic human bone from Siberia. *Archaeometry*, 52(6):1122–1130.

Alex, B. A. (2016). *Establishing Contexts of Encounters: Radiocarbon Dating of Archaeological Assemblages With Implications for Neanderthal-Modern Human Interactions.* unpubl. PhD, Harvard University.

Alex, B. A. and Boaretto, E. (2014). Radiocarbon chronology of Pešturina Cave. In *Palaeolithic and Mesolithic research in the Central Balkans*, pages 39–47. Serbian Archeological Society, Belgrade.

Allsworth-Jones, P. (1986). *The Szeletian and the transition from Middle to Upper Palaeolithic in Central Europe.* Clarendon Press, Oxford.

Ambrose, S. H. and Krigbaum, J. (2003). Bone chemistry and bioarchaeology. *Journal of Anthropological Archaeology*, 22(3):193–199.

Ames, J. M. (1992). The Maillard Reaction. In Hudson, B. J. F., editor, *Biochemistry of Foot Proteins*, pages 99–142. Elsevier Applied Science, London.

Andersen, K. K., Svensson, A., Johnsen, S. J., Rasmussen, S. O., Bigler, M., Röthlisberger, R., Ruth, U., Siggaard-Andersen, M.-L., Peder Steffensen, J., Dahl-Jensen, D., Vinther, B. M., and Clausen, H. B. (2006). The Greenland Ice Core Chronology 2005, 15-42 ka. Part 1: constructing the time scale. *Quaternary Science Reviews*, 25:3246–3257.

Anderson, E. and Libby, W. F. (1951). World-Wide Distribution of Natural Radiocarbon. *Physical Review*, 81(1):64–69.

Anghelinu, M. and Niţă, L. (2014). What's in a name: The Aurignacian in Romania. *Quaternary International*, 351:172–192.

Anikovich, M. (1992). Early Upper Paleolithic industries of Eastern Europe. *Journal of World Prehistory*, 6:205–245.

Armit, I., Swindles, G. T., Becker, K., Plunkett, G., and Blaauw, M. (2014). Rapid climate change did not cause population collapse at the end of the European Bronze Age. *Proceedings of the National Academy of Sciences*, 111(48):17045–17049.

Arnold, J. R. and Libby, W. F. (1949). Age Determinations by Radiocarbon Content: Checks with Samples of Known Age. *Science*, 110:678–680.

Arrizabalaga, A., Altuna, J., Areso, P., Elorza, M., García, M., Iriarte, M., Mariezkurrena, K., Mujika, J., Pemán, E., Tarriño, A., Uriz, A., Viera, L., and Straus, L. (2003). The Initial Upper Paleolithic in Northern Iberia: New Evidence from Labeko Koba. *Current Anthropology*, 44(3):413–421.

Balian, G. and Bowes, J. H. (1977). The structure and porperties of collagen. In Ward, A. G. and Courts, A., editors, *The Science and Technology of Gelatin*, pages 1–30. Academic Press, London.

Bamforth, D. B. and Grund, B. (2012). Radiocarbon calibration curves, summed probability distributions, and early Paleoindian population trends in North America. *Journal of Archaeological Science*, 39(6):1768–1774.

Banks, W. E., d'Errico, F., and Zilhão, J. (2013). Human–climate interaction during the Early Upper Paleolithic: testing the hypothesis of an adaptive shift between the Proto-Aurignacian and the Early Aurignacian. *Journal of Human Evolution*, 64(1):39–55.

Bar-Yosef, O. (2007). The dispersal of modern humans in Eurasia: a cultural interpretation. In Mellars, P., Boyle, K., Bar-Yosef, O., and Stringer, C., editors, *Rethinking the Human Revolution: New Behavioural and Biological Perspectives on the Origins and Dispersal of Modern Humans*, pages 207–217. McDonald Institute for Archaeological Research, Cambridge.

Barshay-Szmidt, C., Normand, C., Flas, D., and Soulier, M.-C. (2018). Radiocarbon dating the aurignacian sequence at isturitz (france): Implications for the timing and development of the protoaurignacian and early aurignacian in western europe. *Journal of Archaeological Science: Reports*, 17:809–838.

Bárta, J. (1965). *Slovensko v staršej a strednej dobe kamennej*. Slovenská akadémia vied, Bratislava.

Bárta, J. (1966). Szeletien-Station Ivanovce. In *Eine beachtenswerte paläolithische Fundstelle in der Westslovakei*, pages 23–27, Nitra.

Bartolomei, G., Broglio, A., Cassoli, P. F., Castelletti, L., Cattani, L., Cremaschi, M., Giacobini, G., Malerba, G., Maspero, A., Peresani, M., Sartorelli, A., and Tagliacozzo, A. (1992). La Grotte de Fumane. Un site aurignacien au pied des Alpes. *Preistoria Alpina*, 28:131–179.

Bataille, G., Tafelmaier, Y., and Weniger, G.-C. (2018). Living on the edge – A comparative approach for studying the beginning of the Aurignacian. *Quaternary International*, 474:3–29.

Bayer, J. (1929). Die Olschewa Kultur. *Eiszeit und Urgeschichte*, 6:83–100.

Bayes, T. R. (1763). An essay towards solving a problem in the doctrine of chances. *Philosophical Transactions of the Royal Society*, 53:370–418.

Bayliss, A. (2009). Rolling Out Revolution: Using Radiocarbon Dating in Archaeology. *Radiocarbon*, 51(1):123–147.

Bayliss, A., Bronk Ramsey, C., van der Plicht, J., and Whittle, A. (2007). Bradshaw and Bayes: Towards a Timetable for the Neolithic. *Cambridge Archaeological Journal*, 17(1):1–28.

Beauval, C., Lacrampe-Cuyaubère, F., Maureille, B., and Trinkaus, E. (2006). Direct radiocarbon dating and stable isotopes of the Neandertal femur from Les Rochers-de-Villeneuve (Lussac-les-Châteaux, Vienne). *Bulletins et Mémoires de la Société d'Anthropologie de Paris*, 18(1):35–42.

Becerra-Valdivia, L., Douka, K., Comeskey, D., Bazgir, B., Conard, N. J., Marean, C. W., Ollé, A., Otte, M., Tumung, L., Zeidi, M., and Higham, T. F. (2017). Chronometric investigations of the Middle to Upper Paleolithic transition in the Zagros Mountains using AMS radiocarbon dating and Bayesian age modelling. *Journal of Human Evolution*, 109:57–69.

Beck, J. W., Richards, D. A., Edwards, R. L., Silverman, B. W., Smart, P. L., Donahue, D. J., Hererra-Osterheld, S., Burr, G. S., Calsoyas, L., Jull, A. J. T., and Biddulph, D. (2001). Extremely large variations of atmospheric ^{14}C concentration during the last glacial period. *Science*, 292(5526):2453–2458.

Benazzi, S., Douka, K., Fornai, C., Bauer, C. C., Kullmer, O., Svoboda, J. A., Pap, I., Mallegni, F., Bayle, P., Coquerelle, M., Condemi, S., Ronchitelli, A., Harvati, K., and Weber, G. W. (2011). Early dispersal of modern humans in Europe and implications for Neanderthal behaviour. *Nature*, 479(7374):525–529.

Berglund, B. E., Hakansson, S., and Lagerlund, E. (1976). Radiocarbon-dated mammoth (*Mammuthus primigenius* Blumenbach) finds in South Sweden Mammoth finds in South Sweden The three dated Scanian mammoth tusks were. *Boreas*, 5:177–191.

Bietti, A., Boschian, G., Crisci, G. M., Francesco, A. M. D., Dini, M., Fontana, F., Giampietri, A., Grifoni, R., Guerreschi, A., Negrino, F., Radi, G., Tozzi, C., and Tykot, R. (2004). Inorganic Raw Materials Economy and Provenance of Chipped Industry in Some Stone Age Sites of Northern and Central Italy. *Coll. Antropol.*, page 15.

Bird, M. I., Ayliffe, L. K., Fifield, L. K., Turney, C. S. M., Cresswell, R. G., Barrows, T. T., and David, B. (1999). Radiocarbon dating of "old" charcoal using a wet oxidation, stepped-combustion procedure. *Radiocarbon*, 41(2):127–140.

Blackwell, B. A. B., Chu, S., Chaity, I., Huang, Y. E. W., Mihailović, D., Roksandić, M., Dimitrijević, V., Blickstein, J. I. B., Huang, A., and Skinner, A. R. (2014). ESR dating ungulate tooth enamel from the Mousterian layers at Pešturina, Serbia. In *Palaeolithic and Mesolithic research in the Central Balkans*, pages 21–38. Serbian Archeological Society, Belgrade.

Blockley, S. P. E., Bronk Ramsey, C., and Higham, T. F. G. (2008). The Middle to Upper Paleolithic transition: dating, stratigraphy, and isochronous markers. *Journal of Human Evolution*, 55(5):764–771.

Blumenschine, R. J., Marean, C. W., and Capaldo, S. D. (1996). Blind Tests of Inter-Analyst Correspondence and Accuracy in the Identification of Cut Marks, Percussion Marks, and Carnivore Tooth Marks on Bone Surfaces. *Journal of Archaeological Science*, 23(4):493–507.

Bluszcz, A., Hercman, H., Pazdur, A., and Pazdur, M. F. (1992). Radiometric dating. In *Temnata Cave. Excavations in Karlukovo Karst Area, Bulgaria*, volume 1.1, pages 223–239. Jagellonian University Press, Kraków.

Bluszcz, A. and Pazdur, M. F. (1985). Comparison of TL and C-14 dates of young Eolian sediments — A check of the zeroing assumption. *Nuclear Tracks and Radiation Measurements (1982)*, 10(4):703–710.

Bolus, M. and Conard, N. J. (2006). Zur Zeitstellung von Geschossspitzen aus organischen Materialien im späten Mittelpaläolithikum und Aurignacien. *Archäologisches Korrespondenzblatt*, 36:1–15.

Bon, F. (2002). *L'Aurignacien entre mer et océan. Réflexion sur l'unité des phases anciennes de l'Aurignacien dans le sud de la France.* Société préhistorique française, Paris.

Bon, F. and Bodu, P. (2002). Analyse technologique du débitage aurignacien. In Schmider, B. and Leroi-Gourhan, A., editors, *L'aurignacien de la grotte du Renne: les fouilles d'André Leroi-Gourhan à Arcy-sur-Cure (Yonne)*, pages 155–133. CNRS.

Bordes, F. (1961). Mousterian Cultures in France. *Science*, 134(3482):803–810.

Bordes, F. (2000). *Typologie du paléolithique ancien et moyen (Nouv. éd.)*. CNRS Éditions, Paris.

Borić, D., Dimitrijević, V., White, D., Lane, C., French, C. A. I., and Cristiani, E. (2012). Early modern human settling of the 'Danube corridor': the Middle to Upper Palaeolithic site of Tabula Traiana Cave in the Danube Gorges (Serbia). *Antiquity*, 86(334).

Bosch, M. D., Mannino, M. A., Prendergast, A. L., O'Connell, T. C., Demarchi, B., Taylor, S. M., Niven, L., van der Plicht, J., and Hublin, J.-J. (2015). New chronology for Ksâr 'Akil (Lebanon) supports Levantine route of modern human dispersal into Europe. *Proceedings of the National Academy of Sciences*, 112(25):7683–7688.

Bosinski, G. (1967). *Die mittelpaläolithischen Funde im westlichen Mitteleuropa*. Bohlau Verlag, Köln, Graz.

Bowman, S. (1990). *Radiocarbon dating*. British Museum Publication for the Trustees of the British Museum, London.

Boyadziev, Y. D. (1995). Chronology of Prehistoric cultures in Bulgaria. In Bailey, D. W. and Panayotov, I., editors, *Prehistoric Bulgaria*, number 22 in Monographs in World Archaeology, pages 149–191. Prehistoric Press, Madison, Wisconsin.

Breuil, H. (1911). Etudes de Morphologie Paléolothique, part 2: L'Industrie de la Grotte de Châtelperron (Allier) et d'Autre Gisements Similaires. *Revue Anthropologique*, 21(39):66–76.

Brock, F., Bronk Ramsey, C., and Higham, T. F. G. (2007). Quality assurance of ultrafiltered bone dating. *Radiocarbon*, 49(2):187 – 192.

Brock, F., Higham, T. F. G., and Bronk Ramsey, C. (2010a). Pre-screening techniques for identification of samples suitable for radiocarbon dating of poorly preserved bones. *Journal of Archaeological Science*, 37(4):855–865.

Brock, F., Higham, T. F. G., and Bronk Ramsey, C. (2013). Comments on the use of Ezee-filters™ and ultrafilters at ORAU. *Radiocarbon*, 55(1):211–212.

Brock, F., Higham, T. F. G., Ditchfield, P., and Ramsey, C. B. (2010b). Current Pretreatment Methods for AMS Radiocarbon Dating at the Oxford Radiocarbon Accelerator Unit (ORAU). *Radiocarbon*, 52(1):103–112.

Bronk Ramsey, C. (1995). Radiocarbon calibration and analysis of stratigraphy: the OxCal program. *Radiocarbon*, 37(2):425–430.

Bronk Ramsey, C. (1998). Probability and dating. *Radiocarbon*, 40(1):461–474.

Bronk Ramsey, C. (2001). Development of the radiocarbon calibration program. *Radiocarbon*, 43(2A):355–363.

Bronk Ramsey, C. (2009a). Bayesian analysis of radiocarbon dates. *Radiocarbon*, 51(1):337–360.

Bronk Ramsey, C. (2009b). Dealing with outliers and offsets in radiocarbon dating. *Radiocarbon*, 51(3):1023–1045.

Bronk Ramsey, C. (2017). Methods for summarising radiocarbon datasets. *Radiocarbon*, 59(6):1809–1833.

Bronk Ramsey, C., Dee, M., Lee, S., Nakagawa, T., and Staff, R. A. (2010a). Developments in the calibration and modeling of radiocarbon dates. *Radiocarbon*, 52(2-3):953–961.

Bronk Ramsey, C., Dee, M. W., Rowland, J. M., Higham, T. F. G., Harris, S. a., Brock, F., Quiles, A., Wild, E. M., Marcus, E. S., and Shortland, A. J. (2010b). Radiocarbon-Based Chronology for Dynastic Egypt. *Science*, 328(5985):1554–1557.

Bronk Ramsey, C., Higham, T. F. G., Bowles, A., and Hedges, R. E. M. (2004a). Improvements to the pretreatment of bone at Oxford. *Radiocarbon*, 46(1):155–163.

Bronk Ramsey, C., Higham, T. F. G., and Leach, P. (2004b). Towards high-precision AMS: progress and limitations. *Radiocarbon*, 46(1):17–24.

Bronk Ramsey, C., Scott, E. M., and Plicht, J. V. D. (2013). Calibration for Archaeological and Environmental Terrestrial Samples in the Time Range 26–50 ka cal BP. *Radiocarbon*, 55(4):1–7.

Bronk Ramsey, C., Staff, R. A., Bryant, C. L., Brock, F., Kitagawa, H., van der Plicht, J., Schlolaut, G., Marshall, M. H., Brauer, A., Lamb, H. F., Payne, R. L., Tarasov, P. E., Haraguchi, T., Gotanda, K., Yonenobu, H., Yokoyama, Y., Tada, R., and Nakagawa, T. (2012). A Complete Terrestrial Radiocarbon Record for 11.2 to 52.8 kyr B.P. *Science*, 338(6105):370–374.

Brown, T. A., Nelson, D. E., Vogel, J. S., and Southon, J. R. (1988). Improved collagen extraction by modified Longin method. *Radiocarbon*, 30(2):171–177.

Buchanan, B., Collard, M., and Edinborough, K. (2008). Paleoindian demography and the extraterrestrial impact hypothesis. *Proceedings of the National Academy of Sciences*, 105(33):11651–11654.

Buck, C. E., Christen, A. J., and James, G. N. (1999). BCal: an on-line Bayesian radiocarbon calibration tool. *Internet Archaeology*, 7.

Buck, C. E., Litton, C. D., and Smith, A. F. M. (1992). Calibration of radiocarbon results pertaining to related archaeological events. *Journal of Archaeological Science*, 19(5):497–512.

Buck, C. E. and Meson, B. (2015). On being a good Bayesian. *World Archaeology*, 47(4):567–584.

Bárta, J. (1988). Trencianske Bohuslavice, un habitat Gravettien an Slovaquie occidentale. *L'Anthropologie*, 92(4):173–182.

Chappell, J. and Magee, J. W. (1996). Beyond the radiocarbon limit in Australian archaeology and Quaternary research. *Antiquity*, 70(269):543–552.

Charles, R., Hedges, R., and Jadin, I. (2003). Aurignacian point, butchery remains and Radiocarbon Accelerator Dates from the Trou Magrite at Pont-à-Lesse (Commune of Dinant, Province of Namur, Belgium). *Anthropologica et Praehistoria*, 114:81–84.

Chirica, V. and Vornicu, D.-M. (2015). The Palaeolithic discoveries from Mitoc-Malu Galben (Romania). The Aurignacian I and I inferior layers. *Arheologia Moldovei*, 38:201–224.

Chu, W., Hauck, T. C., and Mihailović, D. (2014). Crvenka-At - Preliminary results from a lowland Aurignacian site in the Middle Danube Catchment. In *Palaeolithic and Mesolithic research in the Central Balkans*, pages 69–75. Serbian Archeological Society, Belgrade.

Chu, W., Mihailović, D., Pantović, I., Zeeden, C., Hauck, T. C., and Lehmkuhl, F. (2016). Archaeological excavations at the site of At (Vršac, Serbia). *Antiquity*.

Collins, M. J., Nielsen-Marsh, C. M., Hiller, J., Smith, C. I., Roberts, J. P., Prigodich, R. V., Wess, T. J., Csapo, J., Millard, A. R., and Turner-Walker, G. (2002). The survival of organic matter in bone: a review. *Archaeometry*, 44(3):383–394.

Collins, M. J., Riley, M. S., Child, A. M., and Turner-Walker, G. (1995). A Basic Mathematical Simulation of the Chemical Degradation of Ancient Collagen. *Journal of Archaeological Science*, 22(2):175–183.

Conard, N. J. (2003). Palaeolithic ivory sculptures from southwestern Germany and the origins of figurative art. *Nature*, 426(6968):830–832.

Conard, N. J. and Bolus, M. (2003). Radiocarbon dating the appearance of modern humans and timing of cultural innovations in Europe: new results and new challenges. *Journal of Human Evolution*, 44:331–371.

Conard, N. J. and Bolus, M. (2008). Radiocarbon dating the late Middle Paleolithic and the Aurignacian of the Swabian Jura. *Journal of Human Evolution*, 55(5):886–897.

Conard, N. J., Grootes, P. M., and Smith, F. H. (2004). Unexpectedly recent dates for human remains from Vogelherd. *Nature*, 430(6996):198–201.

Contreras, D. A. and Meadows, J. (2014). Summed radiocarbon calibrations as a population proxy: a critical evaluation using a realistic simulation approach. *Journal of Archaeological Science*, 52:591–608.

Crevecoeur, I., Bayle, P., Rougier, H., Maureille, B., Higham, T., van der Plicht, J., De Clerck, N., and Semal, P. (2010). The Spy VI child: A newly discovered Neandertal infant. *Journal of Human Evolution*, 59(6):641–656.

Crémades, M. (2000). Témoignage d'expression graphique. La pierre gravée de la couche VI, secteur TD-II. In *Temnata Cave. Excavations in Karlukovo Karst Area, Bulgaria*, volume 2.1, pages 317–332. Jagellonian University Press, Kraków.

Culleton, B. J. (2008). Crude demographic proxy reveals nothing about Paleoindian population. *Proceedings of the National Academy of Sciences*, 105(50):E111–E111.

Davies, W. (2001). A Very Model of a Modern Human Industry: New Perspectives on the Origins and Spread of the Aurignacian in Europe. *Proceedings of the Prehistoric Society*, 67:195–217.

Davies, W. and Hedges, R. E. M. (2005). Dating the Middle-to-Upper Palaeolithic Transition: A new chronometric framework. In Kaminská, L., Kozłowski, J. K., and Svoboda, J. A., editors, *Pleistocene Environments and Archaeology of the Dzerava skala Cave, Lesser Carpathians, Slovakia*, pages 59–66. Polish Academy of Arts and Sciences; Slovak Academy of Sciences, Institute of Archaeolgy; Academy of Sciences of the Czech Republic, Institute of Archaeology, Kraków.

Davies, W. and Hedges, R. E. M. (2008). Dating a type site: Fitting Szeleta Cave into its regional chronometric context. *Praehistoria*, 9-10:35–45.

Davies, W. and Nerudová, Z. (2009). Moravský Krumlov IV – its chronological place in a wider arena. In Neruda, P. and Nerudová, Z., editors, *Moravský Krumlov IV. Vícevrstvá lokalita ze středního a počátku mladého paleolitu na Moravě.*, number 29 in Anthropos, pages 84–90. Moravské zemské muzeum, Brno.

Davies, W., White, D., Lewis, M., and Stringer, C. (2015). Evaluating the transitional mosaic: frameworks of change from Neanderthals to Homo sapiens in eastern Europe. *Quaternary Science Reviews*, 118:211–242.

Dawkins, B. (1916). The Antiquity of Man. *The Edinburgh Review*, 224(457):80–98.

de Rooij, M., van der Plicht, J., and Meijer, H. A. (2008). Sample dilution for AMS ^{14}C analysis of small samples (30-150 µg C). *Radiocarbon*, 50(3):413–436.

De Stefani, M., Dini, M., Klempererova, H., Peresani, M., Ranaldo, F., Ronchitelli, A., and Ziggiotti, S. (2012). Continuity and replacement in flake production accross the Middle-Upper Palaeolithic transition: a view over the Italian Peninsula. In Pastoors, A. and Peresani, M., editors, *Flakes Not Blades: the Role of Flake Production at the Onset of the Upper Palaeolithic in Europe*, volume 5 of *Wissenschaftliche Schriften des Neanderthal Museums*, pages 135–151. Mettmann.

de Torres, T., Ortiz, J. E., Grün, R., Eggins, S., Valladas, H., Mercier, N., Tisnérat-Laborde, N., Juliá, R., Soler, V., Martínez, E., Sánchez-Moral, S., Cañaveras, J. C., Lario, J., Badal, E., Lalueza-Fox, C., Rosas, A., Santamaría, D., de la Rasilla, M., and Fortea, J. (2010). Dating of the hominid (Homo neanderthalensis) remains accumulation from El Sidrón cava (Piloña, Asturias, north Spain): an example of a multi-methodological approach to the dating of Upper Pleistocene sites. *Archaeometry*, 52(4):680–705.

de Vries, H. (1958). Radiocarbon dates for upper Eem and Würm interstadial samples. *Eiszeitalter und Gegenwart*, 9:10–17.

de Vries, H., Barendsen, G. W., and Waterbolk, H. T. (1958). Groningen radiocarbon dates II. *Science*, 127(3290):129–137.

Dee, M., Brock, F., Bowles, A., and Bronk Ramsey, C. (2011). Using a silica substrate to monitor the effectiveness of radiocarbon pretreatment. *Radiocarbon*, 53(4):705–711.

Dee, M. and Bronk Ramsey, C. (2000). Refinement of graphite target production at ORAU. *Nuclear Instruments and Methods in Physics Research Section B: Beam Interactions with Materials and Atoms*, 172:449–453.

Dee, M., Wengrow, D., Shortland, A., Stevenson, A., Brock, F., Girdland Flink, L., and Bronk Ramsey, C. (2013). An absolute chronology for early Egypt using radiocarbon dating and Bayesian statistical modelling. *Proceedings of the Royal Society A: Mathematical, Physical & Engineering Sciences*, 469(2159):20130395.

Demars, P.-Y. and Laurent, P. (1989). *Types d'outils lithiques du Paléolithique supérieur en Europe*. CNRS Éditions, Paris.

Demars, P.-Y. and Laurent, P. (1992). *Type d'outils lithiques du Palaeolithique superieur en Europe*. Presses du CNRS, Paris.

Demidenko, Y. E. and Usik, V. I. (1993). The problem of changes in Levallois technique during the technological transition from the Middle to Upper Palaeolithic. *Paléorient*, 19(2):5–15.

DeNiro, M. J. (1985). Postmortem preservation and alteration of in vivo bone collagen isotope ratios in relation to palaeodietary reconstruction. *Nature*, 317(31):806–809.

Dennell, R. W. (1987). Accelerator dating: the first years reviewed. *Antiquity*, 61:137–138.

Derevianko, A. P. and Rybin, E. P. (2003). The earliest representations of symbolic behaviour by Paleolithic humans in the Altai Mountains. *Archaeology, Ethnology and Anthropology of Eurasia*, 4(3):27–50.

D'Errico, F. (2003). The invisible frontier. A multiple species model for the origin of behavioral modernity. *Evolutionary Anthropology: Issues, News, and Reviews*, 12(4):188–202.

D'Errico, F. and Banks, W. E. (2015). Tephra studies and the reconstruction of Middle-to-Upper Paleolithic cultural trajectories. *Quaternary Science Reviews*, 118:182–193.

Devièse, T., Comeskey, D., McCullagh, J., Bronk Ramsey, C., and Higham, T. (2018). New protocol for compound-specific radiocarbon analysis of archaeological bones. *Rapid Communications in Mass Spectrometry*, 32(5):373–379.

Devièse, T., Karavanić, I., Comeskey, D., Kubiak, C., Korlević, P., Hajdinjak, M., Radović, S., Procopio, N., Buckley, M., Pääbo, S., and Higham, T. (2017). Direct dating of Neanderthal remains from the site of Vindija Cave and implications for the Middle to Upper Paleolithic transition. *Proceedings of the National Academy of Sciences*, 144(40):10606–10611.

Dobberstein, R. C., Collins, M. J., Craig, O. E., Taylor, G., Penkman, K. E. H., and Ritz-Timme, S. (2009). Archaeological collagen: Why worry about collagen diagenesis? *Archaeological and Anthropological Sciences*, 1(1):31–42.

Dobosi, V. T. (2002). Bone finds from Isállós-kő cave. *Praehistoria*, 3:79–102.

Dobosi, V. T. (2006). Lovas (Hungary) ochre mine reconsidered. *Stone Age - Mining Age - Der Anschnitt*, Beiheft 19:29–36.

Dobosi, V. T. and Simán, K. (2003). Hont–Parassa III, Orgonás, Upper Palaeolithic settlement. *Communicationes Archaeologicae Hungariae*, pages 15–29.

Dogandžić, T., McPherron, S. J., and Mihailović, D. (2014). Middle and Upper Palaeolithic in the Balkans: continuities and discontinuities of human occupations. In *Palaeolithic and Mesolithic research in the Central Balkans*, pages 83–96. Serbian Archeological Society, Belgrade.

Dosedla, J. (1950). Paleolitické stanice Dzeravá a Tmavá skala v Malých Karpatech. *Sborník Československé spoločnosti zeměpisné*, 55:39–50.

Douka, K., Bergman, C. A., Hedges, R. E. M., Wesselingh, F. P., and Higham, T. F. G. (2013). Chronology of Ksar Akil (Lebanon) and implications for the colonization of Europe by anatomically modern humans. *PloS one*, 8(9):e72931.

Douka, K., Grimaldi, S., Boschian, G., del Lucchese, A., and Higham, T. F. (2012). A new chronostratigraphic framework for the Upper Palaeolithic of Riparo Mochi (Italy). *Journal of Human Evolution*, 62(2):286–299.

Douka, K., Higham, T. F., Wood, R., Boscato, P., Gambassini, P., Karkanas, P., Peresani, M., and Ronchitelli, A. M. (2014). On the chronology of the Uluzzian. *Journal of Human Evolution*, 68:1–13.

Doyon, L. (2018). *La variabilité technologique et morphométrique des pointes de projectile aurignaciennes en matière osseuse*. unpubl. PhD, l'Université de Bordeaux et l'Université de Montréal.

Drobniewicz, B., Ginter, B., Kazior, B., and Kozłowski, J. K. (2000a). Early Upper Palaeolithic assemblages from layer 4, trench TD-I. In *Temnata Cave. Excavations in Karlukovo Karst Area, Bulgaria*, volume 2.1, pages 333–418. Jagellonian University Press, Kraków.

Drobniewicz, B., Ginter, B., Kazior, B., and Kozłowski, J. K. (2000b). 'Transitional' industry from layer VI, trench TD-II. In *Temnata Cave. Excavations in Karlukovo Karst Area, Bulgaria*, volume 2.1, pages 243–316. Jagellonian University Press, Kraków.

Drobniewicz, B., Ginter, B., Kozlowski, J. K., Sirakova, S., Sirakov, N., and Ivanova, S. (2011). Description of particular Middle Palaeolithic levels. In *Temnata Cave. Excavations in Karlukovo Karst Area, Bulgaria*, volume 3, pages 72–128. Avalon Publishing, Sofia.

Drobniewicz, B., Ginter, B., and Kozłowski, J. K. (1992). The Gravettian sequence. In *Temnata Cave. Excavations in Karlukovo Karst Area, Bulgaria*, volume 1.1, pages 295–501. Jagellonian University Press, Kraków.

Durand, N., Deschamps, P., Bard, E., Hamelin, B., Camoin, G., Thomas, A. L., Henderson, G. M., Yokoyama, Y., and Matsuzaki, H. (2013). COMPARISON OF 14C AND U-Th AGES IN CORALS FROM IODP #310 CORES OFFSHORE TAHITI. *Radiocarbon*, 55(4):2–11.

Délibrias, G. (1985). Le carbon 14. In Roth, E. and Poty, B., editors, *Méthodes de datation par les phénomènes nucléaires naturels: applications*, pages 421–458. Coll. CEA, Paris.

d'Errico, F., Borgia, V., and Ronchitelli, A. (2012). Uluzzian bone technology and its implications for the origin of behavioural modernity. *Quaternary International*, 259:59–71.

Éhik, G. (1914). A borsodmegyei Peskő-barlang pleistocaen faunája / Die Pleistozäne Fauna der Pesköhöle im Komitat Borsod. *Barlangkutatás*, 2(4):191–199, 229–232.

Éhik, J. (1913). Die Pleistozäne Fauna der Pálffyhöhle im Pozsonyer Komitat. *Barlangkutatás*, 1:87–94.

Evin, J., Marien, G., and Pachiaudi, C. (1978). Lyon natural radiocarbon measurements VII. *Radiocarbon*, 20(1):19–57.

Falcucci, A., Conard, N. J., and Peresani, M. (2017). A critical assessment of the Protoaurignacian lithic technology at Fumane Cave and its implications for the definition of the earliest Aurignacian. *PLOS ONE*, 12(12):e0189241.

Fedele, F. G., Giaccio, B., and Hajdas, I. (2008). Timescales and cultural process at 40,000 BP in the light of the Campanian Ignimbrite eruption, Western Eurasia. *Journal of Human Evolution*, 55:834–857.

Fernandez, P. and Guadelli, J.-L. (2008). Étude préliminaire des grands mammifères du repaire d'hyènes de Redaka II (Bulgarie du nord-ouest): paléontologie, paléoécologie et taphonomie. *Quaternaire*, 19(1):43–68.

Ferrier, C. (1992). Étude sédimentologique des dépôts gravettiens et épigravettiens de la grotte de Temnata. Interprétation dynamique et paléoclimatique. In *Temnata Cave. Excavations in Karlukovo Karst Area, Bulgaria*, volume 1.1, pages 65–88. Jagellonian University Press, Kraków.

Ferrier, C., Guadelli, J.-L., and Sirakov, N. (2011). Geochronology of the Middle Palaeolithic sequence – Hypothesis II. In *Temnata Cave. Excavations in Karlukovo Karst Area, Bulgaria*, volume 3, pages 140–142. Avalon Publishing, Sofia.

Ferrier, C. and Laville, H. (1992). Stratigraphie des dépôts de la grotte Temnata. In *Temnata Cave. Excavations in Karlukovo Karst Area, Bulgaria*, volume 1.1, pages 49–64. Jagellonian University Press, Kraków.

Ferrier, C. and Laville, H. (2000). Stratigraphie des dépôts aurignaciens de la grotte Temnata. In *Temnata Cave. Excavations in Karlukovo Karst Area, Bulgaria*, volume 2.1, pages 12–30. Jagellonian University Press, Kraków.

Ferrier, C. and Laville, H. (2011). Stratigraphie des dépôts du Paléolithique moyen de la grotte Temnata. In *Temnata Cave. Excavations in Karlukovo Karst Area, Bulgaria*, volume 3, pages 13–30. Avalon Publishing, Sofia.

Ferrier, C. and Leblanc, J.-C. (1992). Étude du complexe karstique Prohodna-Temnata: morphologie, genèse et évolution. In *Temnata Cave. Excavations in Karlukovo Karst Area, Bulgaria*, volume 1.1, pages 31–48. Jagellonian University Press, Kraków.

Ferrier, C., Leblanc, J.-C., Berthet, A. L., and Delfour, G. (2009). La Grotte Kozarnika (Gara Oreshets, Bulgarie): Données stratigraphic, géologiques et dédimentologieques. In *Saxa loquuntur: sbornik v čest na 65-godišninata na Nikolaj Sirakov*, pages 13–27. Avalon Publishing, Sofia.

Feurdean, A., Perşoiu, A., Tanţău, I., Stevens, T., Magyari, E., Onac, B., Marković, S., Andrič, M., Connor, S., Fărcaş, S., Gałka, M., Gaudeny, T., Hoek, W., Kolaczek, P., Kuneš, P., Lamentowicz, M., Marinova, E., Michczyńska, D., Perşoiu, I., Płóciennik, M., Słowiński, M., Stancikaite, M., Sumegi, P., Svensson, A., Tămaş, T., Timar, A., Tonkov, S., Toth, M., Veski, S., Willis, K., and Zernitskaya, V. (2014). Climate variability and associated vegetation response throughout Central and Eastern Europe (CEE) between 60 and 8 ka. *Quaternary Science Reviews*, 106:206–224.

Fitzsimmons, K. E., Hambach, U., Veres, D., and Iovita, R. (2013). The Campanian Ignimbrite Eruption: New Data on Volcanic Ash Dispersal and Its Potential Impact on Human Evolution. *PLoS ONE*, 8(6):e65839.

Flas, D. (2008). La transition du paléolithique moyen au supérieur dans la plaine septentrionale de l'europe. *Anthropologica et Praehistoria*, 119.

Flas, D., Tartar, , Bordes, J.-G., Le Brun-Ricalens, F., and Zwyns, N. (2013). New perspectives on the Aurignacian from Spy: lithic assemblage, osseous artefacts and chrono-cultural sequence. In Rougier, H. and Semal, P., editors, *Spy Cave. 125 years of multidisciplinary research at the Betche aux Rotches (Jemeppe-sur-Sambre, Province of Namur, Belgium)*, number 123/2012 in Anthropologica et Praehistoria, pages 231–255. Royal Belgian Institute of Natural Sciences, Royal Belgian Society of Anthropology and Praehistory & NEPOS Society, Brussels.

Frouin, M., Guérin, G., Lahaye, C., Mercier, N., Huot, S., Aldeias, V., Bruxelles, L., Chiotti, L., Dibble, H. L., Goldberg, P., Madelaine, S., McPherron, S. J., Sandgathe, D., Steele, T. E., and Turq, A. (2017). New luminescence dating results based on polymineral fine grains from the Middle and Upper Palaeolithic site of La Ferrassie (Dordogne, SW France). *Quaternary Geochronology*, 39:131–141.

Fu, Q., Hajdinjak, M., Moldovan, O. T., Constantin, S., Mallick, S., Skoglund, P., Patterson, N., Rohland, N., Lazaridis, I., Nickel, B., Viola, B., Prüfer, K., Meyer, M., Kelso, J., Reich, D., and Pääbo, S. (2015). An early modern human from Romania with a recent Neanderthal ancestor. *Nature*, 524:216–219.

Fu, Q., Li, H., Moorjani, P., Jay, F., Slepchenko, S. M., Bondarev, A. A., Johnson, P. L. F., Aximu-Petri, A., Prüfer, K., de Filippo, C., Meyer, M., Zwyns, N., Salazar-García, D. C., Kuzmin, Y. V., Keates, S. G., Kosintsev, P. A., Razhev, D. I., Richards, M. P., Peristov, N. V., Lachmann, M., Douka, K., Higham, T. F. G., Slatkin, M., Hublin, J.-J., Reich, D., Kelso, J., Viola, T. B., and Pääbo, S. (2014). Genome sequence of a 45,000-year-old modern human from western Siberia. *Nature*, pages 8–13.

Gábori-Csánk, V. (1993). *Le Jankovichien - Une civilisation paléolithique en Hongrie. Traduit par Zsolt Mester*. Etudes et Recherches Archéologiques de l'Université de Liège & Musée Historique de Budapest, Liège.

Gábori-Csánk, V. and Svoboda, J. A. (1983). On Hominid Evolution in South-Central Europe. *Current Anthropology*, 24(2):235–237.

Gambassini, P. (1997). *Il Paleolitico di Castelcivita, Culture e Ambiente*. Electa Napoli, Naples.

Gambier, D. (1992). Les vestiqes humains des niveaux gravettiens. In *Temnata Cave. Excavations in Karlukovo Karst Area, Bulgaria*, volume 1.1, pages 217–222. Jagellonian University Press, Kraków.

Garcea, E. A. (2016). Dispersals Out of Africa and Back to Africa: Modern origins in North Africa. *Quaternary International*, 408:79–89.

Gaspari, A., Erič, M., and Odar, B. (2011). A palaeolithic wooden point from Ljubljansko Barje, Slovenia. In *Submerged Prehistory*, pages 186–192. Oxbow Books, Oxford.

Giaccio, B., Hajdas, I., Isaia, R., Deino, A., and Nomade, S. (2017). High-precision ^{14}C and $^{40}Ar/^{39}Ar$ dating of the Campanian Ignimbrite (Y-5) reconciles the time-scales of climatic-cultural processes at 40 ka. *Scientific Reports*, 7:45940.

Giaccio, B., Hajdas, I., Peresani, M., Fedele, F. G., and Isaia, R. (2006). The Campanian Ignimbrite Tephra and its Relevance for the Timing of the Middle to Upper Palaeolithic Shift. In Conard, N. J., editor, *When Neanderthals and Modern Humans Met*, chapter 16, pages 343–375. Kerns Verlag, Tübingen.

Giaccio, B., Isaia, R., Fedele, F. G., Di Canzio, E., Hoffecker, J. F., Ronchitelli, A., Sinitsyn, A. A., Anikovich, M., Lisitsyn, S. N., and Popov, V. V. (2008). The Campanian Ignimbrite and Codola tephra layers: Two temporal/stratigraphic markers for the Early Upper Palaeolithic in southern Italy and eastern Europe. *Journal of Volcanology and Geothermal Research*, 177:208–226.

Ginter, B. and Kozlowski, J. K. (2011). Geochronology of the Middle Palaeolithic sequence – Hypothesis I. In *Temnata Cave. Excavations in Karlukovo Karst Area, Bulgaria*, volume 3, pages 139–140. Avalon Publishing, Sofia.

Ginter, B. and Kozłowski, J. K. (1992). The archaeological sequence. In *Temnata Cave. Excavations in Karlukovo Karst Area, Bulgaria*, volume 1.1, pages 289–293. Jagellonian University Press, Kraków.

Ginter, B., Kozłowski, J. K., Guadelli, J.-L., and Laville, H. (2000). *Temnata Cave. Excavations in Karlukovo Karst Area, Bulgaria*, volume 2.1. Jagellonian University Press, Kraków.

Ginter, B., Kozłowski, J. K., Guadelli, J.-L., and Sirakova, S. (2011). *Temnata Cave. Excavations in Karlukovo Karst Area, Bulgaria.*, volume 3. Avalon Publishing, Sofia.

Ginter, B., Kozłowski, J. K., and Laville, H. (1994). *Temnata Cave. Excavations in Karlukovo Karst Area, Bulgaria*, volume 1.2. Jagellonian University Press, Kraków.

Ginter, B., Kozłowski, J. K., Laville, H., Sirakov, N., and Hedges, R. E. M. (1996). The transition in the Balkans: news from Temnata Cave. In Carbonell, E. and Vaquero, M., editors, *The last Neandertals, the first Anatomically Modern Humans: a tale about the human diversity. Cultural change and human evolution: the crisis at 40 ka BP*, pages 169–200. Universitat de Rovira i Virgili, Tarragona.

Giourova, M. R. and Schtchelinski, V. E. (1994). Étude tracéologique des outillages gravettiens et épigravettiens. In *Temnata cave: excavations in Karlukovo karst area, Bulgaria*, volume 1.2. Jagellonian University Press, Kraków.

Godwin, H. (1962). Half-life of Radiocarbon. *Nature*, 195(4845):984.

Gorjanović-Kramberger, D. (1906). Der diluviale Mensch von Krapina in Kroatien. Ein Beitrag zur Paläoanthropologie. In Walkhoff, O., editor, *Studien über die Entwicklungsmechanik des Primatenskelletes*, volume II, pages 9–277. Kreidel, Wiesbaden.

Greenfield, H. J. (1999). The Origins of Metallurgy: Distinguishing Stone from Metal Cut-Marks on Bones from Archaeological Sites. *Journal of Archaeological Science*, 26:797–808.

Grootes, P. M., Nadeau, M.-J., and Rieck, A. (2004). ^{14}C-AMS at the Leibniz-Labor: radiometric dating and isotope research. *Nuclear Instruments and Methods in Physics Research Section B: Beam Interactions with Materials and Atoms*, 223-224:55–61.

Grünberg, J. M. (2006). New AMS Dates for Palaeolithic and Mesolithic Camp Sites and Single Finds in Saxony-Anhalt and Thuringia (Germany). *Proceedings of the Prehistoric Society*, 72:95–112.

Guadelli, A. (2004). Étude des incisions du plus ancien os gravé découvert dans la grotte Koyarnika (Bulgarie du Nord-Ouest). Une preuve de l'existence du symbolism au Paléolithique inférieur. *Archaeologia Bulgarica*, 3:1–7.

Guadelli, A., Fernandez, P., Guadelli, J.-L., Miteva, V., and Sirakov, N. (2013a). The Retouchers from the Gravettian Levels in Kozarnika Cave. In *The sound of bones: proceedings of the 8th meeting of the ICAZ Worked Bone Reserarch Group in Salzburg 2011*, Archaeo plus, Salzburg. Eigenverl. Univ. Salzburg, Interfakultärer Fachbereich Gerichtsmedizin.

Guadelli, A., Guadelli, J.-L., Fernandez, P., and Sirakov, N. (2013b). Preliminary GIS and intra-site spatial analysis of the faunal remains from Redaka II cave. In *Second European SCGIS Conference "Conservation of Natural and Cultural Heritage for Sustainable Development: GIS-Based Approach"*, pages 54–61.

Guadelli, J.-L. (1996). Rapport sur la mission préhistorique française en Bulgarie du Nord - La Grotte de Kozarnika. Annual report, CNRS.

Guadelli, J.-L., Sirakov, N., Anastassova, E., Berry, G., Berthet, A.-L., Courtaud, P., Delpech, F., Dimitrova, I., Djabarska, N., Ferrier, C., Fontugne, M., Guadelli, A., Iordanova, D., Iordanova, N., Ivavona, S., Kovatcheva, M., Krumov, I., Langlois, A., Leblanc, J.-C., Lenoir, M., Mallye, J.-B., Marinska, M., Miteva, V., Popov, V. V., Sirakova, S., Spassov, R., Taneva, S., Tillier, A.-M., and Tisnérat-Laborde, N. (2001). Projet de recherche conjoint: "Les plus anciennes manifestations de la presence humaine en Bulgarie du Nord". Annual report, CNRS.

Guadelli, J.-L., Sirakov, N., Anastassova, E., Berry, G., Berthet, A.-L., Delfour, G., Delpech, F., Dimitrova, I., Djabarska, N., Fernandez, P., Ferrier, C., Fontugne, M., Guadelli, A., Iordanova, D., Iordanova, N., Ivavona, S., Kovatcheva, M., Krumov, I., Leblanc, J.-C., Mallye, J.-B., Marinska, M., Miteva, V., Popov, V. V., Sirakova, S., Spassov, R., Taneva, S., and Tisnérat-Laborde, N. (2002). Projet de recherche: "Les plus anciennes manifestations de la presence humaine en Bulgarie du Nord". Annual report, CNRS.

Guadelli, J.-L., Sirakov, N., Atanassov, A., Berthet, A.-L., Delpech, F., Ferrier, C., Fontugne, M., Guadelli, A., Iordanova, D., Iordanova, N., Ivavona, S., Kovatcheva, M., Langlois, A., Leblanc, J.-C., Lucas, G., Marinska, M., Miteva, V., Popov, V. V., Sirakova, S., Spassov, R., Tisnérat-Laborde, N., and Vivent, D. (2000). Projet de recherche conjoint: "Les plus anciennes manifestations de la presence humaine en bulgarie du Nord". Annual report, CNRS.

Guadelli, J.-L., Sirakov, N., Boyadzhiev, K., Dimitrova, I., Fontugne, M., Guadelli, A., Guérin, G., Heydari, M., Hopkins, R., Jacob, E., Kovacheva, M., Krumov, I., Monesi, E., Muttoni, G., Sirakova, S., Taneva, S., Tillier, A.-M., Tisnérat-Laborde, N., Yanakieva, K., Yordanova, D., Yordanova, N., and Zahariev, N. (2016). Projet de recherche conjoint: "les plus anciennes manifestations de la presence humaine dans les balkans" - mission palaeolithique-bulgarie (MAE) - coopération scientifique et technique ABS (bulgarie/PACEA-PPP univ. bx. i). Annual report, CNRS, Bordeaux, Sofia.

Guadelli, J.-L., Sirakov, N., Boyadziev, K., Crèvecoeur, I., Dimitrova, I., Fontugne, M., Guadelli, A., Kovatcheva, M., Krumov, I., Miteva, V., Mitov, K., Sirakova, S., Taneva, S., Tisnérat-Laborde, N., Iordanova, D., and Iordanova, N. (2012). Projet de recherche conjoint: "Les plus anciennes manifestations de la presence humaine dans les Balkans". Annual report, CNRS.

Guadelli, J.-L., Sirakov, N., Christov, M., Courtaud, P., Crémades, M., Delpech, F., Ferrier, C., Fontugne, M., Gurova, M., Ivanova, S., Leblanc, J.-C., Marambat, L., Marinska, M., Popov, V., and Sirakova, S. (1998). Projet de recherche conjoint: "Les plus anciennes manifestations de la resence humaine en Bulgarie du Nord". Annual report, CNRS.

Guadelli, J.-L., Sirakov, N., Delpech, F., Ferrier, C., Fontugne, M., Guadelli, A., Iordanova, D., Iordanova, N., Ivanova, S., Kovatcheva, M., Leblanc, J.-C., Marinska, M., Miteva, V., Popov, V. V., Sirakova, S., Spassov, R., Vivent, D., and Yantcheva, G. (1999). Projet de recherche conjoint: "Les plus anciennes manifestations de la presence humaine en Bulgarie du Nord". Annual report, CNRS.

Guadelli, J.-L., Sirakov, N., Dimitrova, I., Fernandez, P., Ferrier, C., Fontugne, M., Guadelli, A., Iordanova, D., Iordanova, N., Ivanova, S., Kovatcheva, M., Kovatcheva, N., Krumov, I., Le Gall, O., Leblanc, J.-C., Marinska, M., Miteva, V., Scharf, A., Sirakova, S., Taneva, S., Tisnérat-Laborde, N., and Zlateva, R. (2005a). Projet de recherche: "Les plus anciennes manifestations de la presence humaine dans les Balkans". Annual report, CNRS.

Guadelli, J.-L., Sirakov, N., Dimitrova, I., Fernandez, P., Ferrier, C., Guadelli, A., Ivanova, S., Krumov, I., Leblanc, J.-C., Miteva, V., Popov, V. V., Sirakova, S., and Taneva, S. (2010). Projet de recherche conjoint: "Les plus anciennes manifestations de la presence humaine dans les Balkans". Annual report, CNRS.

Guadelli, J.-L., Sirakov, N., Dimitrova, I., Fontugne, M., Guadelli, A., Kent, D., Kovacheva, M., Krumov, I., Miteva, V., Monesi, E., Muttoni, G., Nikolov, P., Poucheva, P., Sirakova, S., Taneva, S., Tillier, A.-M., Tisnérat-Laborde, N., Iordanova, D., and Iordanova, N. (2014). Projet de recherche conjoint: "Les plus anciennes manifestations de la presence humaine dans les Balkans". Annual report, CNRS.

Guadelli, J.-L., Sirakov, N., Ivanova, S., Sirakova, S., Anastassova, E., Courtaud, P., Dimitrova, I., Djabarska, N., Fernandez, P., Ferrier, C., and others (2005b). Une séquence du paléolithique inférieur au paléolithique récent dans les balkans: la grotte kozarnika à orechets (nord-ouest de la bulgarie). In *Les Premiers Peuplements en Europe*, volume 1364 of *British Archaeological Reports, International Series*, page 87e103. Archaeopress.

Guérin, G., Frouin, M., Talamo, S., Aldeias, V., Bruxelles, L., Chiotti, L., Dibble, H. L., Goldberg, P., Hublin, J.-J., Jain, M., Lahaye, C., Madelaine, S., Maureille, B., McPherron, S. J., Mercier, N., Murray, A. S., Sandgathe, D., Steele, T. E., Thomsen, K. J., and Turq, A. (2015). A multi-method luminescence dating of the Palaeolithic sequence of La Ferrassie based on new excavations adjacent to the La Ferrassie 1 and 2 skeletons. *Journal of Archaeological Science*, 58:147–166.

Gábori, M. (1951). A paleolitikum csontipara Magzarországon – L'industrie de l'os du Paléolithique en Hongrie. *Archaeologia Értesitő*, 73:7–18.

Gábori, M. (1977). Archaeological Results of Investigation in Hungarian Caves. *Karszt és Barlang*, Special Issue:43–48.

Haase, D., Fink, J., Haase, G., Ruske, R., Pécsi, M., Richter, H., Altermann, M., and Jäger, K.-D. (2007). Loess in Europe — its spatial distribution based on a European Loess Map, scale 1:2,500,000. *Quaternary Science Reviews*, 26(9):1301–1312.

Haesaerts, P., Damblon, F., Nigst, P., and Hublin, J.-J. (2013). ABA and ABOx Radiocarbon Cross-Dating on Charcoal from Middle Pleniglacial Loess Deposits in Austria, Moravia, and Western Ukraine. *Radiocarbon*, 55(3–4):641–647.

Haesaerts, P. and Teyssandier, N. (2001). The early Upper Paleolithic occupations of Willendorf II (Lower Austria): a contribution to the chronostratigraphic and cultural context of the beginning of the Upper Palaeolithic in Central Europe. In Zilhão, J. and D'Errico, F., editors, *The Chronology of the Aurignacian and of the Transitional Technocomplexes Dating, Stratigraphies, Cultural Implications*, pages 133–151, Lisbon.

Hahn, J. (1977). *Aurignacian: Das ältere Jungpaläolithikum in Mittel- und Osteuropa*. Bohlau Verlag, Köln.

Hahn, J. (1988). *Die Geissenklösterle-Höhle im Achtal bei Blaubeuren*, volume 26 of *Forschungen und Berichte zur Vor- und Frühgeschichte in Baden-Württemberg*. K. Theiss.

Harris, D. R., Gove, H. E., and Damon, P. (1987). The Impact on Archaeology of Radiocarbon Dating by Accelerator Mass Spectrometry. *Philosophical Transactions of the Royal Society of London. Series A, Mathematical and Physical Sciences*, 323(1569):23–43.

Harvey, V. L., Egerton, V. M., Chamberlain, A. T., Manning, P. L., and Buckley, M. (2016). Collagen fingerprinting: A new screening technique for radiocarbon dating ancient bone. *PLOS ONE*, 11(3):e0150650.

Hauck, T. C., Lehmkuhl, F., Zeeden, C., Bösken, J., Thiemann, A., and Richter, J. (2018). The Aurignacian way of life: Contextualizing early modern human adaptation in the Carpathian Basin. *Quaternary International*, 485:150–166.

Hauser, O. (1906). *La Micoque (Dordogne), und ihre Resultate für die Kenntnis der paläolithischen Kultur*. Basel.

Hauser, O. (1916). *La Micoque: Die Kultur einer neuen Diluvialrasse*. Veit, Leipzig.

Hedges, R. E. M. (2002). Bone diagenesis: an overview of processes. *Archaeometry*, 44(3):319–328.

Hedges, R. E. M., Housley, R. A., Law, I. A., and Bronk, C. R. (1989a). Radiocarbon dates from the Oxford AMS system: Archaeometry datelist 9. *Archaeometry*, 31(2):207–234.

Hedges, R. E. M., Housley, R. A., Ramsey, C. B., and Van Klinken, G. J. (1994). Radiocarbon dates from the Oxford AMS system: Archaeometry datelist 18. *Archaeometry*, 36(2):337–374.

Hedges, R. E. M., Humm, M. J., Foreman, J., van Klinken, G. J., and Bronk Ramsey, C. (1992). Developments in Sample Combustion to Carbon Dioxide, and in the Oxford AMS Carbon Dioxide Ion Source System. *Radiocarbon*, 34(3):306–311.

Hedges, R. E. M. and Law, I. A. (1989). The radiocarbon dating of bone. *Applied Geochemistry*, 4(2):249–253.

Hedges, R. E. M., Law, I. A., Bronk, C. R., and Housley, R. A. (1989b). The Oxford Accelerator Mass Spectrometry Facility: technical developments in routine dating. *Archaeometry*, 31(2):99–113.

Hedges, R. E. M., Pettitt, P. B., Ramsey, C. B., and Klinken, G. J. V. (1996). Radiocarbon Dates from the Oxford AMS system: Archaeometry datelist 22. *Archaeometry*, 38(2):391–415.

Hedges, R. E. M. and van Klinken, G. J. (1992). A Review of Current Approaches in the Pretreatment of Bone for Radiocarbon Dating by AMS. *Radiocarbon*, 34(3):279–291.

Henn, B. M., Botigué, L. R., Gravel, S., Wang, W., Brisbin, A., Byrnes, J. K., Fadhlaoui-Zid, K., Zalloua, P. A., Moreno-Estrada, A., Bertranpetit, J., Bustamante, C. D., and Comas, D. (2012). Genomic Ancestry of North Africans Supports Back-to-Africa Migrations. *PLoS Genetics*, 8(1):e1002397.

Henry, D. O., Belmaker, M., and Bergin, S. M. (2017). The effect of terrain on Neanderthal ecology in the Levant. *Quaternary International*, 435:94–105.

Henry-Gambier, D. and Sacchi, D. (2008). La Crouzade V-VI (Aude, France): Un des plus anciens fossiles d'anatomie moderne en Europe Occidentale. *Bulletins et Mémoires de la Société d'Anthropologie de Paris*, 20(1):79–104.

Herrmann, M., Kretzoi, M., and Vértes, L. (1957). Neuere Forschung in der Jankovich-Höhle. *Folia Archaeologica*, 9:3–22.

Higham, T., Jacobi, R., Julien, M., David, F., Basell, L., Wood, R., Davies, W., and Ramsey, C. B. (2010). Chronology of the Grotte du Renne (France) and implications for the context of ornaments and human remains within the Chatelperronian. *Proceedings of the National Academy of Sciences*, 107(47):20234–20239.

Higham, T., Wood, R., Moreau, L., Conard, N., and Ramsey, C. B. (2013). Comments on "Human–climate interaction during the early Upper Paleolithic: Testing the hypothesis of an adaptive shift between the Proto-Aurignacian and the Early Aurignacian" by Banks et al. *Journal of Human Evolution*, 65(6):806–809.

Higham, T. F. G., Basell, L., Jacobi, R., Wood, R., Ramsey, C. B., and Conard, N. J. (2012). Testing models for the beginnings of the Aurignacian and the advent of figurative art and music: the radiocarbon chronology of Geißenklösterle. *Journal of Human Evolution*, 62(6):664–76.

Higham, T. F. G., Brock, F., Peresani, M., Broglio, A., Wood, R., and Douka, K. (2009). Problems with radiocarbon dating the Middle to Upper Palaeolithic transition in Italy. *Quaternary Science Reviews*, 28(13-14):1257–1267.

Higham, T. F. G., Bronk Ramsey, C., Brock, F., Baker, D., and Ditchfield, P. (2007). Radiocarbon dates from the Oxford AMS system: Archaeometry datelist 32. *Archaeometry*, 49:S1–S60.

Higham, T. F. G., Bronk Ramsey, C., Karavanić, I., Smith, F. H., and Trinkaus, E. (2006a). Revised direct radiocarbon dating of the Vindija G1 Upper Paleolithic Neandertals. *PNAS*, 103(3):553–557.

Higham, T. F. G., Douka, K., Wood, R., Ramsey, C. B., Brock, F., Basell, L., Camps, M., Arrizabalaga, A., Baena, J., Barroso-Ruíz, C., Bergman, C., Boitard, C., Boscato, P., Caparrós, M., Conard, N. J., Draily, C., Froment, A., Galván, B., Gambassini, P., Garcia-Moreno, A., Grimaldi, S., Haesaerts, P., Holt, B., Iriarte-Chiapusso, M.-J., Jelinek, A., Jordá Pardo, J. F., Maíllo-Fernández, J.-M., Marom, A., Maroto, J., Menéndez, M., Metz, L., Morin, E., Moroni, A., Negrino, F., Panagopoulou, E., Peresani, M., Pirson, S., de la Rasilla, M., Riel-Salvatore, J., Ronchitelli, A., Santamaria, D., Semal, P., Slimak, L., Soler, J., Soler, N., Villaluenga, A., Pinhasi, R., and Jacobi, R. M. (2014). The timing and spatiotemporal patterning of Neanderthal disappearance. *Nature*, 512(7514):306–309.

Higham, T. F. G., Jacobi, R. M., and Ramsey, C. B. (2006b). AMS Radiocarbon Dating of Ancient Bone Using Ultrafiltration. *Radiocarbon*, 48(2):179–195.

Higham, T. F. G. and Wild, E. M. (2013). Radiocarbon Dating of the Peştera cu Oase Faunal Remains. In Trinkaus, E., Constantin, S., and Zilhão, J., editors, *Life and death at the Peştera cu Oase: a setting for modern human emergence in Europe*, pages 70–85. Oxford University Press, New York.

Hillebrand, E. (1926). Über neuere Funde aus dem ungarländischen Paläolithikum. *Die Eiszeit*, 3:3–5.

Hillebrand, J. (1913a). A diluviális ősember nyomai a bajóti Öregkő nagy barlangjában / Die Spuren des diluvialen Urmenschen in der Bajóter Öregköhöhle. *Barlangkutatás*, 1:126–128, 147–149.

Hillebrand, J. (1913b). A Kiskevélyi barlangban 1912. évben végzett ásatások eredményei / Ergebnisse der in der Kiskevélyhöhle im Jahre 1912 vorgenommenen Grabungen. *Barlangkutatás*, 1:153–163, 187–193.

Hillebrand, J. (1913c). A pleistocaen ösember ujabb nyomai hazánkban / Neuere Spuren des diluvialen Menschen in Ungarn. *Barlangkutatás*, 1:19–25, 46–52.

Hillebrand, J. (1914). Az 1913 évi barlangkutatásaim eredményei / Ergebnisse meiner Höhlenforschunen im Jahre 1913. *Barlangkutatás*, 2:115–124, 147–153.

Hillebrand, J. (1915). A bajóti Jankovichbarlangban 1914. és 1915. években végzett kutatások eredménye (Die erforschung der Bajóter JankovichHöhle in den Jahren 1914 und 1915). *Barlangkutatás*, 3:129–141, 173–179.

Hillebrand, J. (1917). Az 1916. évi barlangkutatásom eredményéről / Über die Resultate meiner Höhlenforschungen im Jahre 1916. *Barlangkutatás*, 5:98–108, 125–130.

Hillebrand, J. (1919). Az 1917. évben végzett ásatásaim eredményei / Resultate meiner Ausgrabungen im Jahre 1917. *Barlangkutatás*, 7:6–13, 39–41.

Hoffecker, J. F. (2009). Out of Africa: modern human origins special feature: the spread of modern humans in Europe. *Proceedings of the National Academy of Sciences of the United States of America*, 106(38):16040–5.

Hoffecker, J. F., Holliday, V. T., Anikovich, M. V., Sinitsyn, A. A., Popov, V. V., Lisitsyn, S. N., Levkovskaya, G. M., Pospelova, G. A., Forman, S. L., and Giaccio, B. (2008). From the Bay of Naples to the River Don: the Campanian Ignimbrite eruption and the Middle to Upper Paleolithic transition in Eastern Europe. *Journal of Human Evolution*, 55(5):858–870.

Hoffecker, J. F. and Klein, R. G. (2009). The spread of modern humans in Europe. *PNAS*, 106(38):16040–16045.

Hoffmann, D. L., Beck, J. W., Richards, D. A., Smart, P. L., Singarayer, J. S., Ketchmark, T., and Hawkesworth, C. J. (2010). Towards radiocarbon calibration beyond 28 ka using speleothems from the Bahamas. *Earth and Planetary Science Letters*, 289:1–10.

Hofreiter, M. and Pacher, M. (2004). Using Ancient DNA to Elucidate Raw Material Origin of Bone Points from Potočka zijalka (Slovenia): Preliminary Results. *Mitteilungen der Kommission für Quartärforschung der Österreichischen Akadademie der Wissenschaften*, 13:201–210.

Horálek, F. (1931). Archeologický výzkum v jeskyni Pálffyově u Plaveckého Svatého Mikuláše. In *Sbomík vlastivedného múyea ya rok 1924-1931*, pages 12–16. Bratislava.

Horusitzky, F. Z. (2004). Les artefacts en os et bois de cerf à Bukovac, Lokve (Croatie) - Une seconde flûte possible? - Relations entre les chasseurs de Lokve et les montagnards d'Olcheva au début du Paléolithique supérieur. *Arheološki vestnik*, 55:9–37.

Horusitzky, Z. F. (2003). Les flûtes paléolithiques: Divje babe I, Istállóskő, Lokve etc. Point de vue des experts et des contestataires. Critique de l'appréciation archéologique du spécimen no 652 de Divje babe I et arguments pour la défense des spécimens Pb51/20 et Pb606 du MNM de Budapest. *Arheolški vestnik*, 54:45–66.

Horusitzky, Z. F. (2008). Reconstruction des pointes organiques aurignaciennes de la Dzeravá skala (Pálffy-barlang), Slovaquie. *L'Anthropologie*, 112(2):201–246.

Housley, R. (2003). Radiocarbon dating. In Valde-Nowak, P., Nadachowski, A., and Madeyska, T., editors, *Obłazowa Cave. Human activity, stratigraphy and palaeoenvironment*. Instytut Archeologii i Etnologii PAN, Kraków.

Housley, R., Gamble, C., Street, M., and Pettitt, P. (1997). Radiocarbon evidence for the Lateglacial Human Recolonisation of Northern Europe. *Proceedings of the Prehistoric Society*, 63:25–54.

Hublin, J.-J. (2012). The earliest modern human colonization of Europe. *Proceedings of the National Academy of Sciences*, 109(34):13471–13472.

Hublin, J.-J., Talamo, S., Julien, M., David, F., Connet, N., Bodu, P., Vandermeersch, B., and Richards, M. P. (2012). Radiocarbon dates from the Grotte du Renne and Saint-Cesaire support a Neandertal origin for the Chatelperronian. *Proceedings of the National Academy of Sciences*, 109(46):18743–18748.

Huels, M., van der Plicht, J., Brock, F., Matzerath, S., and Chivall, D. (2017). Laboratory Intercomparison of Pleistocene Bone Radiocarbon Dating Protocols. *Radiocarbon*, 59(5):1543–1552.

Hüls, C. M., Grootes, P. M., and Nadeau, M.-J. (2007). How clean is ultrafiltration cleaning of bone collagen? *Radiocarbon*, 49(2):193–200.

Hunt, S. (1985). Degradation of amino acids accompanying in vitro protein hydrolysis. In Barrett, G. C., editor, *Chemistry and biochemistry of the amino acid*, pages 376–398. Chapman and Hall, London.

Jacob, E., Querci, D., Caparros, M., Barroso Ruiz, C., Higham, T., and Devièse, T. (2018). Nitrogen content variation in archaeological bone and its implications for stable isotope analysis and radiocarbon dating. *Journal of Archaeological Science*, 93:68–73.

Jacobi, R. and Pettitt, P. (2000). An Aurignacian point from Uphill Quarry (Somerset) and the earliest settlement of Britain by *Homo sapiens sapiens*. *Antiquity*, 74(285):513–518.

Jacobi, R. M. and Higham, T. F. G. (2008). The "Red Lady" ages gracefully: new ultrafiltration AMS determinations from Paviland. *Journal of Human Evolution*, 55(5):898–907.

Jacobi, R. M., Higham, T. F. G., and Ramsey, C. B. (2006). AMS radiocarbon dating of middle and upper palaeolithic bone in the british isles: improved reliability using ultrafiltration. *Journal of Quaternary Science*, 21(5):557–573.

Jakab, J. (1996). Nový nález neandertálca na Slovensku. *Informátor Slovenskej archeologickej spoločnosti pri SAV Nitra*, 7:6.

Jakab, J. (1998). Poodhalené tajomstvo Váhu. *Slovensko*, 3:57–59.

Jakab, J. (2005). Šal'a II : documentation and description of a *Homo sapiens neanderthalensis* find from Slovakia. *Anthropologie*, 43(2-3):2005.

Janković, I., Karavanić, I., Ahern, J. C. M., and Mihelić, S. (2011). Lokalitet Pecina Bukovac. In *Hrvatski Arheološki Godišnjak / Croatian Archaeological Yearbook*, volume 8/2011, pages 480–482. Printera grupa d.o.o., Zagreb.

Jeanneret, M. (1948). La lame de Kiskevély : un produit naturel en forme d'artéfact. *Mitteilungen der Naturforschenden Gesellschaft in Bern*, 5:7–18.

Johnsen, S. J. and North Greenland Ice Core Project members (2004). North Greenland Ice Core Project Oxygen Isotope Data. online. http://www.ncdc.noaa.gov/paleo/pubs/ngrip2004/ngrip2004.html.

Jones, M. and Nicholls, G. (2002). New radiocarbon calibration software. *Radiocarbon*, 44(3):663–674.

Jánossy, D. (1954). Die Vogel- und Säugetierreste der Spätpleistozänen Schichten der Höhle von Istállóskő. *Acta Archaeologica Academiae Scientiarum Hungaricae*, 5:149–181.

Jánossy, D., Kretzoi-Varrók, S., Herrmann, M., and Vértes, L. (1957). Forschungen in der Bivakhöhle, Ungarn. *Eiszeitalter und Gegenwart*, 8:18–36.

Kadić, D. O. K. (1916). Erforschung der Szeletahöhle. *Mitteilungen aus dem Jahrbuch der Königlischen Ungarischen Geologischen Reichanstalt*, 23(4):162–301.

Kadić, O. (1934). Der Mensch der Eiszeit in Ungarn. *Jahrbuch der königlischen ungarischen geologischen Anstalt*, 30(1):1–147.

Kadić, O. (1935). A Peskő barlangban eddig végzett ásatások eredménzei. *Barlangvilág*, 5(3):49–54.

Kadić, O. (1940). A magyar barlangkutatás állása az 1939. évben / Stand der ungarischen Höhlenforschung im Jahre 1939. *Barlangvilág*, 10(1):11–16, 27–30.

Kadić, O. (1941). A magyar barlangkutatás állása az 1940. évben / Stand der ungarischen Höhlenforschung im Jahre 1940. *Barlangvilág*, 11(1):13–20, 36–38.

Kadić, O. and Mottl, M. (1944). Az északnyugati Bükk barlanjai (Die Höhlen des nordwestlichen Bükkgebirges). *Barlangkutatas*, 17:1–111.

Kaminská, L., editor (2014). *Paleolit a Mezolit*, volume 2. Archeologický Ústav Slovenskej Akadémie Vied Nitra, Nitra.

Kaminská, L. (2015). Szeletian find from Trenčianske Teplice, Slovakia. *Anthropologie*, 53(1-2):203–213.

Kaminská, L., Ford, D. C., Hajnalová, E., Hajnalová, M., Horáček, I., Kovanda, J., Ložek, V., Mlíkovský, J., and Smolíková, L. (2000). *Hôrka-Ondrej - Research of a Middle Palaeolithic Travertine Locality*. Institute of Archaeology of the National Academy of Sciences Nitra, Nitra.

Kaminská, L., Kozłowski, J. K., and Škrdla, P. (2011). New Approach to the Szeletian - chronology and cultural variability. *Eurasian Prehistory*, 8(1-2):29–49.

Kaminská, L., Kozłowski, J. K., and Svoboda, J. (2004). The 2002-2003 excavations in the Dzerava skala Cave, West Slovakia. *Anthropologie*, 42(3):321–332.

Kaminská, L., Kozłowski, J. K., and Svoboda, J. A., editors (2005a). *Pleistocene Environments and Archaeology of the Dzeravá skala Cave, Lesser Carpathians, Slovakia*. Polska Akademia Umiejętności, Kraków.

Kaminská, L., Kozłowski, J. K., and Svoboda, J. A. (2005b). Sequence of the Palaeolithic occupations. In Kaminská, L., Kozłowski, J. K., and Svoboda, J. A., editors, *Pleistocene Environments and Archaeology of the Dzerava skala Cave, Lesser Carpathians, Slovakia*, pages 7–58. Polish Academy of Arts and Sciences; Slovak Academy of Sciences, Institute of Archaeolgy; Academy of Sciences of the Czech Republic, Institute of Archaeology, Kraków.

Karavanić, I. (2003). L'industrie aurignacienne de la grotte de Šandalja II (Istrie, Croatie) dans le contexte de la région de l'Est de l'Adriatique. *L'Anthropologie*, 107(5):577–602.

Kerr, T. and McCormick, F. (2014). Statistics, sunspots and settlement: influences on sum of probability curves. *Journal of Archaeological Science*, 41:493–501.

Kitagawa, H. and Van Der Plicht, J. (1997). A 40,000-Year Varve Chronology from Lake Suigetsu, Japan: Extension of the ^{14}C Calibration Curve. *Radiocarbon*, 40(1):505–515.

Kitagawa, H. and van der Plicht, J. (1998). Atmospheric Radiocarbon Calibration to 45,000 yr B.P.: Late Glacial Fluctuations and Cosmogenic Isotope Production. *Science*, 279(5354):1187–1190.

Kitagawa, H. and van der Plicht, J. (2000). Atmospheric Radiocarbon Calibration Beyond 11,900 cal BP from Lake Suigetsu Laminated Sediments. *Radiocarbon*, 42(3):370–381.

Knecht, H. (1993a). Early Upper Paleolithic approaches to bone and antler projectile technology. *Archeological Papers of the American Anthropological Association*, 4(1):33–47.

Knecht, H. (1993b). Splits and Wedges: The Techniques and Technology of Early Aurignacian Antler Working. In *Before Lascaux: the complex record of the Early Upper Paleolithic*. CRC Press, New York: Boca Ratan.

Kormos, T. (1912). Die ersten Spuren des Urmenschen im Karst-Gebirge. *Földtani Közlöny*, 42:97–104.

Kozłowski, J. K. (1979). Le Bachokirien - La plus ancienne industrie du Paléolithique supérieur en Europe (quelques remarques à propos de la position stratigraphique et taxonomique des outillages de la couche 11 de la grotte Bacho Kiro. *Middle and Upper Palaeolithic in Balkans*, 28:77–99.

Kozłowski, J. K. (1982). *Excavation in the Bacho Kiro cave (Bulgaria). Final report.* Polish Scientific Publishers, Warsaw.

Kozłowski, J. K. (2006). Early Human Migrations: Incipient Stages of Old World Peopling. *Diogenes*, 211:9–22.

Kozłowski, J. K. (1975). Badania nad przejsciem od srodkowego do gorenego paleolitu na Balkanach (Studies on the transition from the Middle to the Upper Paleolithic in the Balkans). *Przeglad Archeologiczny*, 23:5–48.

Kozłowski, J. K. (1992). The Balkans in the Middle and Upper Palaeolithic: The Gate to Europe or a Cul-de-sac? *Proceedings of the Prehistoric Society*, 58:1–20.

Kozłowski, J. K. (1999). The evolution of the balkan aurignacian. In Davies, W. and Charles, R., editors, *Dorothy Garrod and the Progress of the Palaeolithic. Studies in the Prehistoric Archaeology of the Near East and Europe*, pages 97–117. Oxbow Books, Oxford.

Kozłowski, J. K. (2014). Middle palaeolithic variability in central europe: Mousterian vs micoquian. *Quaternary International*, 326-327:344–363.

Kozłowski, J. K., Laville, H., and Ginter, B., editors (1992). *Temnata Cave. Excavations in Karlukovo Karst Area, Bulgaria. A. Stratigraphy and Environment. B. Archaeology of Gravettian Layers*, volume 1.1. Jagellonian University Press, Kraków.

Krause, J., Orlando, L., Serre, D., Viola, B., Prüfer, K., Richards, M. P., Hublin, J.-J., Hänni, C., Derevianko, A. P., and Pääbo, S. (2007). Neanderthals in central Asia and Siberia. *Nature*, 449(7164):902–904.

Krings, M., Stone, A., Schmitz, R. W., Krainitzki, H., and Stoneking, M. (1997). Neandertal DNA sequences and the origin of modern humans. *Cell*, 90:19–30.

Kruschke, J. K. (2015). *Doing Bayesian Data Analysis*. Elservier, Oxford, 2nd edition.

Kuhlwilm, M., Gronau, I., Hubisz, M. J., de Filippo, C., Prado-Martinez, J., Kircher, M., Fu, Q., Burbano, H. A., Lalueza-Fox, C., de la Rasilla, M., Rosas, A., Rudan, P., Brajkovic, D., Kucan, , Gušic, I., Marques-Bonet, T., Andrés, A. M., Viola, B., Pääbo, S., Meyer, M., Siepel, A., and Castellano, S. (2016). Ancient gene flow from early modern humans into Eastern Neanderthals. *Nature*, 530(7591):429–433.

Kuhn, S. L., Mihailović, D., and Dimitrijević, V. (2014). The Southeast Serbia Paleolithic Project: an interim report. In *Palaeolithic and Mesolithic research in the Central Balkans*, pages 97–106. Serbian Archeological Society, Belgrade.

Kuhn, S. L., Stiner, M. C., and Güleç, E. (1999). Initial Upper Palaeolithic in south-central Turkey and its regional context: a preliminary report. *Antiquity*, 73(281):505–517.

Kuhn, S. L. and Zwyns, N. (2014). Rethinking the initial Upper Paleolithic. *Quaternary International*, 347:29–38.

Kälin, J. (1946). Zum Problem der menschlichen Stammesgeschichte. *Experientia*, II(8):272–287.

Lacorre, F. (1960). *La Gravette, Le Gravétien et le Bayaoien*. Imprimerie Barnéoud, Laval.

Langley, M. C., Clarkson, C., and Ulm, S. (2008). Behavioural Complexity in Eurasian Neanderthal Populations: a Chronological Examination of the Archaeological Evidence. *Cambridge Archaeological Journal*, 18(3):289.

Laplace, G. (1966). *Recherches sur l'origine et l'évolution des complexes leptolithiques*. De Bocard.

Lengyel, G., Mester, Z., and Szolyák, P. (2016). The Late Gravettian and Szeleta Cave, northeast Hungary. *Quaternary International*, 406:174–183.

Litton, C. D. and Buck, C. E. (1995). The Bayesian Approach To the Interpretation of Archaeological Data. *Archaeometry*, 37(1):1–24.

Lityńska-Zając, M. (1992). Charcoals from the Temnata Cave. In *Temnata Cave. Excavations in Karlukovo Karst Area, Bulgaria*, volume 1.1, pages 127–130. Jagellonian University Press, Kraków.

Longin, R. (1971). New Method of Collagen Extraction for Radiocarbon Dating. *Nature*, 230(5313):241–242.

Lowe, J., Barton, N., Blockley, S., Ramsey, C. B., Cullen, V. L., Davies, W., Gamble, C., Grant, K., Hardiman, M., Housley, R., Lane, C. S., Lee, S., Lewis, M., MacLeod, A., Menzies, M., Müller, W., Pollard, M., Price, C., Roberts, A. P., Rohling, E. J., Satow, C., Smith, V. C., Stringer, C. B., Tomlinson, E. L., White, D., Albert, P., Arienzo, I., Barker, G., Borić, D., Carandente, A., Civetta, L., Ferrier, C., Guadelli, J.-L., Karkanas, P., Koumouzelis, M., Müller, U. C., Orsi, G., Pross, J., Rosi, M., Shalamanov-Korobar, L., Sirakov, N., and Tzedakis, P. C. (2012). Volcanic ash layers illuminate the resilience of Neanderthals and early modern humans to natural hazards. *Proceedings of the National Academy of Sciences of the United States of America*, 109(34):13532–7.

Malez, M. (1959). Speleološka istraživanja krša u 1956. godini. *Ljetopis JAZU*, 63:340–354.

Malez, M. and Vogel, J. S. (1969). Rezultati određivanja apsolutne starosti pleistocenskih naslaga Šandalje II kod pule u istri. *Geološki Vjesnik*, 22:121–133.

Malez, M. and Vogel, J. S. (1970). Die Ergebnisse der Radiokarbonanalisen der quartären Schichten der Velika Pećina in Norwest-Kroatien. *Bulletin scientifique Conseil des Academies des Sciences et des Arts de la RSF de Yougoslavie*, 15(11):390–391.

Malán, M. (1954). Zahnkeim aus der zeiten Aurignacien-Schicht der Höhle von Istállóskő. *Acta Archaeologica Academiae Scientiarum Hungaricae*, 5:145–148.

Mandić, M. and Borić, D. (2015). Pećina kod trajanove table. In Ćalić, J., editor, *Caves in the Djerdap National Park*, pages 84–89. JP Nacionalni Park Đerdap, Donji Milanovac.

Maniatis, Y., Oberlin, C., and Tsirtsone, Z. (2016). Balkans 4000. In Tsirtsone, Z., editor, *The Human Face of Radiocarbon: Reassessing Chronology in prehistoric Greece and Bulgaria, 5000-3000 cal BC*, number 69 in Travaux de la Maison de l'Orient et de la Méditerranée. Maison de l'Orient et de la Méditerranée-Jean Pouilloux, Lyon.

Marambat, L. (1992). Paléoenvironnements végétaux à Temnata. La séquence gravettienne et épigravettienne. In *Temnata Cave. Excavations in Karlukovo Karst Area, Bulgaria*, volume 1.1, pages 101–126. Jagellonian University Press, Kraków.

Marks, A. E. and Ferring, C. R. (1988). The Early Upper Palaeolithic of the Levant. In *The Early Upper Palaeolithic: Evidence from Europe and the Near East*, number 437 in British Archaeological Reports International Series, pages 43–72. ArchaeoPress, Oxford.

Markó, A. (2009). Levéleszközös leletegyüttes debercsényből. *Archaeologia Értesitő*, 134:155–163.

Markó, A. (2013a). Leaf-shaped Lithic and Osseous Tools from Old Excavated Cave Sites - Demonstrating Associations. In Lang, F., editor, *The Sound of Bones - Proceedings of the 8th Meeting of the ICAZ Worked Bone Research Group in Salzburg 2011. Schriften zur Archäologie und Archäometrie der Paris Lodron-Universität Salzburg*, volume 5, Salzburg. Archaeo Plus.

Markó, A. (2013b). On the Middle Palaeolithic industry of the Jankovich cave (North-eastern Transdanubia). *Archaeologiai Értesítő*, 138:7–28.

Markó, A. (2015). Istállóskő revisited: Lithic artefacts and assemblages, sixty years after. *Acta Archaeologica Academiae Scientiarum Hungaricae*, 66:5–38.

Markó, A. (2017). Istállóskő revisited: The osseous artefacts from the lower layer. *Acta Archaeologica Academiae Scientiarum Hungaricae*, 68:193–218.

Marom, A., McCullagh, J. S. O., Higham, T. F. G., Sinitsyn, A. A., and Hedges, R. E. M. (2012). Single amino acid radiocarbon dating of Upper Paleolithic modern humans. *PNAS*, 109(18):6878–6881.

Marshall, M., Schlolaut, G., Nakagawa, T., Lamb, H., Brauer, A., Staff, R., Ramsey, C. B., Tarasov, P., Gotanda, K., Haraguchi, T., Yokoyama, Y., Yonenobu, H., and Tada, R. (2012). A novel approach to varve counting using XRF and X-radiography in combination with thin-section microscopy, applied to the Late Glacial chronology from Lake Suigetsu, Japan. *Quaternary Geochronology*, 13:70–80.

Marín-Arroyo, A. B. and Mihailović, B. (2017). The Chronometric Dating and Subsistence of Late Neanderthals and Early Anatomically Modern Humans in the Central Balkans: Insights from Šalitrena Pećina (Mionica, Serbia). *Journal of Anthropological Research*, 73(3):000–000.

Meignen, L., Geneste, J.-M., Koulakovskaia, I., and Sytnik, A. (2004). Koulichivka and its place in the Middle-Upper Paleolithic transition in Eastern Europe. In Brantingham, P. J., Kuhn, S. L., and Kerry, K. W., editors, *The Early Upper Paleolithic beyond Western Europe*, pages 30–49. University of California Press, Berkeley and Los Angeles.

Mejdahl, V. (1979). Thermoluminescence dating: beta-dose attenuation in quartz grains. *Archaeometry*, 21(1):61–72.

Mellars, P. (2005). The impossible coincidence. A single-species model for the origins of modern human behavior in Europe. *Evolutionary Anthropology: Issues, News, and Reviews*, 14(1):12–27.

Mellars, P. (2006). A new radiocarbon revolution and the dispersal of modern humans in Eurasia. *Nature*, 439(7079):931–935.

Mellars, P. (2011). Palaeoanthropology: the earliest modern humans in Europe. *Nature*, 479(7374):483–5.

Mester, Z. (2006). Mousterian Industries in Hungary - 15 Years Later. In Kulakovska, L. V., editor, *The European Middle Palaeolithic*, pages 170–179. Insitute of Archaeology of the National Academy of Sciences of Ukraine, Kiev.

Meyer, M., Kircher, M., Gansauge, M.-T., Li, H., Racimo, F., Mallick, S., Schraiber, J. G., Jay, F., Prüfer, K., de Filippo, C., Sudmant, P. H., Alkan, C., Fu, Q., Do, R., Rohland, N., Tandon, A., Siebauer, M., Green, R. E., Bryc, K., Briggs, A. W., Stenzel, U., Dabney, J., Shendure, J., Kitzman, J., Hammer, M. F., Shunkov, M. V., Derevianko, A. P., Patterson, N., Andres, A. M., Eichler, E. E., Slatkin, M., Reich, D., Kelso, J., and Pääbo, S. (2012). A High-Coverage Genome Sequence from an Archaic Denisovan Individual. *Science*, 338(6104):222–226.

Moncel, M.-H. and Voisin, J. L. (2006). Les « industries de transition » et le mode de spéciation des groupes néandertaliens en Europe entre 40 et 30 ka. *Comptes Rendus - Palevol*, 5(1-2):183–192.

Mook, W. G. (1976). Groningen Radiokarbondaten von Bohunice. In Valoch, K., editor, *Die altsteinyeitliche Fundstell in Brno-Bohunice*, number 4 in Studie Archeologického ústavu ČSAV v Brně, page 84. Academia, Prague.

Mook, W. G. (1982). Radiocarbon dating. In Kozłowski, J. K., editor, *Excavation in the Bacho Kiro Cave (Bulgaria): Final Report*, page 168. Polish Scientific Publishers, Warsaw.

Moreau, L., Odar, B., Higham, T. F. G., Horvat, A., Pirkmajer, D., and Turk, P. (2015). Reassessing the Aurignacian of Slovenia: techno-economic behaviour and direct dating of osseous projectile points. *Journal of human evolution*, 78:158–80.

Morlan, R. E. (1984). Toward the definition of criteria for the recognition of artificial bone alterations. *Quaternary Research*, 22(2):160–171.

Morley, M. W. and Woodward, J. C. (2011). The Campanian Ignimbrite (Y5) tephra at Crvena Stijena Rockshelter, Montenegro. *Quaternary Research*, 75:683–696.

Moroni, A., Boscato, P., and Ronchitelli, A. (2013). What roots for the Uluzzian? Modern behaviour in Central-Southern Italy and hypotheses on AMH dispersal routes. *Quaternary International*, 316:27–44.

Mottl, M. (1938). Faunen, Flora und Kultur des ungarischen Solutréen. *Quartär*, 1:36–54.

Mottl, M. (1941). Die Interglazial- und Interstadial-Zeiten im Lichte der Ungarischen Säugetierfauna. *Mitteilungen aus dem Jahrbuche der Königlich Ungarischen Geologischen Anstalt*, 35:1–33.

Mottl, M. (1945). Jelentés az 1936/38. évi ásatások eredményéről és az ősgerinces osztály működéséről (Bericht über die Ergebnisse der Grabungen der Jahren 1936/ 38, sowie über die Tätigkeit der Vertebraten-Abteilung der Königlichen Ungarischen Geologischen Anstalt). *A Magyar Állami Földtani Intézet évi jelentése*, 1936-38/4:1513–1552.

Movius, H. L. (1960). Radiocarbon Dates and Upper Palaeolithic Archaeology in Central and Western Europe. *Current Anthropology*, 1(5):355–391.

Müller, U. C., Pross, J., Tzedakis, P. C., Gamble, C., Kotthoff, U., Schmiedl, G., Wulf, S., and Christanis, K. (2011). The role of climate in the spread of modern humans into Europe. *Quaternary Science Reviews*, 30:273–279.

Murray, A. and Wintle, A. (2000). Luminescence dating of quartz using an improved single-aliquot regenerative-dose protocol. *Radiation Measurements*, 32(1):57–73.

Nakagawa, T., Gotanda, K., Haraguchi, T., Danhara, T., Yonenobu, H., Brauer, A., Yokoyama, Y., Tada, R., Takemura, K., Staff, R. A., Payne, R., Bronk Ramsey, C., Bryant, C., Brock, F., Schlolaut, G., Marshall, M., Tarasov, P., and Lamb, H. (2012). SG06, a fully continuous and varved sediment core from Lake Suigetsu, Japan: stratigraphy and potential for improving the radiocarbon calibration model and understanding of late Quaternary climate changes. *Quaternary Science Reviews*, 36:164–176.

Needham, S., Bronk Ramsey, C., Coombs, D., Cartwright, C., and Pettitt, P. (1998). An independent chronology for British Bronze Age metalwork : The results of the Oxford Radiocarbon Accelerator Programme. *Archaeological journal*, 154(1):55–107.

Nejman, L., Rhodes, E. J., and Grün, R. (2005). OSL dating. In Kaminská, L., Kozlowski, J. K., and Svoboda, J. A., editors, *Pleistocene Environments and Archaeology of the Dzeravá skala Cave, Lesser Carpathians, Slovakia*, pages 67–69. Polska Akademia Umiejętności, Kraków.

Nelson, D. (1991). A new method for carbon isotopic analysis of protein. *Science*, 251(4993):552–554.

Neruda, P. and Nerudová, Z. (2013). The Middle-Upper Palaeolithic transition in Moravia in the context of the Middle Danube region. *Quaternary International*, 294:3–19.

Nerudová, Z. and Neruda, P. (2017). Technology of Moravian Early Szeletian leaf point shaping: A case study of refittings from Moravský Krumlov IV open-air site (Czech Republic). *Quaternary International*, 428:91–108.

Newton, E. T. (1898). Palaeolithic man. *Proceedings of the Geologists' Association*, 15(7):246–263.

Nielsen-Marsh, C. M. and Hedges, R. E. M. (2000). Patterns of Diagenesis in Bone I: The Effects of Site Environments. *Journal of Archaeological Science*, 27(12):1151–1159.

Nigst, P. R. (2012). *The Early Upper Palaeolithic of the Middle Danube Region*. Leiden University Press, Leiden.

Nigst, P. R. and Haesaerts, P. (2012). L'Aurignacien en Basse Autriche: résultats préliminaires de l'analyse technologique de la couche culturelle 3 de Willendorf II et ses implications pour la chronologie du Paléolithique supérieur ancien en Europe centrale. *L'Anthropologie*, 116(4):575–608.

Nigst, P. R., Haesaerts, P., Damblon, F., Frank-Fellner, C., Mallol, C., Viola, B., Götzinger, M., Niven, L., Trnka, G., and Hublin, J.-J. (2014). Early modern human settlement of Europe north of the Alps occurred 43,500 years ago in a cold steppe-type environment. *Proceedings of the National Academy of Sciences of the United States of America*, 111(40):14394–9.

Niu, M., Heaton, T. J., Blackwell, P. G., and Buck, C. E. (2013). The Bayesian approach to radiocarbon calibration curve estimation: the IntCal13, Marine13, and SHCal13 methodologies. *Radiocarbon*, 55(4):1905–1922.

Novák, M. (2005). Spatial Distribution of Artifacts. In Kaminská, L., Kozłowski, J. K., and Svoboda, J. A., editors, *Pleistocene Environments and Archaeology of the Dzerava skala Cave, Lesser Carpathians, Slovakia*, pages 209–224. Polska Akademia Umiejętności, Kraków.

Oliva, M. (1981). Die Bohunicien-Station bei Podolí (Bez. Brno-Land) und ihre Stellung im beginnenden Jungpaläolithikum. *Časopis Moravského muzea, Scientiae sociales*, 66:7–45.

Oliva, M. (1991). The Szeletian in Czechoslovakia. *Antiquity*, 65(247):318–325.

Oliva, M. (2009). Geografie, stratigrafie a datování. In *Sídliště mamutích lidí v Milovicích pod Pálavou*, number 27 in Anthropos, pages 17–24. Moravské zemské muzeum, Brno.

Olivieri, A., Achilli, A., Pala, M., Battaglia, V., Fornarino, S., Al-Zahery, N., Scozzari, R., Cruciani, F., Behar, D. M., Dugoujon, J.-M., Coudray, C., Santachiara-Benerecetti, A. S., Semino, O., Bandelt, H.-J., and Torroni, A. (2006). The mtDNA Legacy of the Levantine Early Upper Palaeolithic in Africa. *Science*, 314(5806):1767–1770.

Olsson, I. U. (1970). The use of oxalic acid as a standard. In *Radiocarbon Variations and Absolute Chronology, Nobel symposium, 12th Procedings*, page 17. John Wiley & Sons, New York.

Otte, M. (2017). The Mousterian with bifacial retouch in Europe: The fundamental historical error. *Quaternary International*, 428:109–117.

Otte, M., Collin, F., Miller, R., and Engesser, K. (1998). Nouvelles datations du Trou Al'Wesse dans son contexte régional. *Notae Praehistoria*, 18:45–50.

Outram, A. K. (2003). Bone fracture and within-bone nutrients: an experimentally based method for investigating levels of marrow extraction. In *Consuming passions and patterns of consumption*, pages 51–63. McDonald Institute for Archaeological Research.

Outram, A. K., Knüsel, C. J., Knight, S., and Harding, A. F. (2005). Understanding complex fragmented assemblages of human and animal remains: a fully integrated approach. *Journal of Archaeological Science*, 32:1699–1710.

Palma di Cesnola, A. (1989). L'Uluzzien: faciès italien du leptolithique archaique. *L'Anthropologie*, 93:783–812.

Palma di Cesnola, A. (1993). *Il Paleolitico Superiore in Italia*. Garlatti e Razzai, Firenze.

Parzen, E. (1962). On estimation of a probability density function and mode. *Annals of Mathematical Statistics*, 33(3):1065–1076.

Paterne, M. (1992). Additional remarks on tephra layers from Temnata Cave. In *Temnata Cave. Excavations in Karlukovo Karst Area, Bulgaria*, volume 1.1, pages 99–100. Jagellonian University Press, Kraków.

Patou-Mathis, M., Vercoutière, C., Lengyel, G., Szolyák, P., and Mester, Z. (2017). New interpretation of the Upper Palaeolithic human occupations at Istállóskő cave (Bükk Mountains, Hungary). *Euraisan Prehistory*, 13(1):77–90.

Pawlikowski, M. (1992). Analysis of tephra layers from TD-II and TD-V excavations. In *Temnata Cave. Excavations in Karlukovo Karst Area, Bulgaria*, volume 1.1, pages 89–98. Jagellonian University Press, Kraków.

Pelišek, J. (1951). Geologicko-stratigrafické poměry kvartéru v jeskyních Malých Karpat. *Československý Kras*, 4:261–271.

Peresani, M. (2008). A New Cultural Frontier for the Last Neanderthals: The Uluzzian in Northern Italy. *Current Anthropology*, 49(4):725–731.

Pettitt, P. B., Davies, W., Gamble, C. S., and Richards, M. B. (2003). Palaeolithic radiocarbon chronology: quantifying our confidence beyond two half-lives. *Journal of Archaeological Science*, 30(12):1685–1693.

Peyrony, D. (1930). Le Moustier. Ses gisements, ses industries, ses couches géologiques. *Revue Anthropologique*, XL:48–76, 155–176.

Peyrony, D. (1933). Les industries aurignaciennes dans le bassin de la Vézère: Aurignacien et Perigordien. *Bulletin de la Société Préhistorique Française*, 30:543–549.

Prat, S., Péan, S. C., Crépin, L., Drucker, D. G., Puaud, S. J., Valladas, H., Lázničková-Galetová, M., van der Plicht, J., and Yanevich, A. (2011). The oldest anatomically modern humans from far southeast Europe: Direct dating, culture and behavior. *PLoS ONE*, 6(6):e20834.

Prescott, J. and Hutton, J. (1994). Cosmic ray contributions to dose rates for luminescence and ESR dating: Large depths and long-term time variations. *Radiation Measurements*, 23(2):497–500.

Prošek, F. (1951). Výykum Jeskyně Dzeravé Skály v Malých Karpatech. *Archeologické rozhledy*, 3:293–298.

Prošek, F. (1953). Szeletian na Slovensku. *Slovenská Archeológia*, 1:133–194.

Prošek, F. (1957). Výykum Jeskyně Dzeravé Skála v r. 1950. Referáty o pracovních výsledcích čsl. archeologů za rok 1956. In *Referáty o pracovních výsledcích čsl. archeologů ya rok 1956*, volume 1, pages 21–29.

Protsch, R. (1975). The absolute dating of Upper Pleistocene SubSaharan fossil hominids and their place in human evolution. *Journal of Human Evolution*, 4:297–322.

Prüfer, K., de Filippo, C., Grote, S., Mafessoni, F., Korlević, P., Hajdinjak, M., Vernot, B., Skov, L., Hsieh, P., Peyrégne, S., Reher, D., Hopfe, C., Nagel, S., Maricic, T., Fu, Q., Theunert, C., Rogers, R., Skoglund, P., Chintalapati, M., Dannemann, M., Nelson, B. J., Key, F. M., Rudan, P., Kućan, , Gušić, I., Golovanova, L. V., Doronichev, V. B., Patterson, N., Reich, D., Eichler, E. E., Slatkin, M., Schierup, M. H., Andrés, A. M., Kelso, J., Meyer, M., and Pääbo, S. (2017). A high-coverage Neandertal genome from Vindija Cave in Croatia. *Science*, 358(6363):655–658.

Prüfer, K., Racimo, F., Patterson, N., Jay, F., Sankararaman, S., Sawyer, S., Heinze, A., Renaud, G., Sudmant, P. H., de Filippo, C., Li, H., Mallick, S., Dannemann, M., Fu, Q., Kircher, M., Kuhlwilm, M., Lachmann, M., Meyer, M., Ongyerth, M., Siebauer, M., Theunert, C., Tandon, A., Moorjani, P., Pickrell, J., Mullikin, J. C., Vohr, S. H., Green, R. E., Hellmann, I., Johnson, P. L. F., Blanche, H., Cann, H., Kitzman, J. O., Shendure, J., Eichler, E. E., Lein, E. S., Bakken, T. E., Golovanova, L. V., Doronichev, V. B., Shunkov, M. V., Derevianko, A. P., Viola, B., Slatkin, M., Reich, D., Kelso, J., and Pääbo, S. (2014). The complete genome sequence of a Neanderthal from the Altai Mountains. *Nature*, 505(7481):43–49.

Pyle, D. M., Ricketts, G. D., Margari, V., van Andel, T. H., Sinitsyn, A. A., Praslov, N. D., and Lisitsyn, S. (2006). Wide dispersal and deposition of distal tephra during the Pleistocene 'Campanian Ignimbrite/Y5' eruption, Italy. *Quaternary Science Reviews*, 25(21):2713–2728.

Péan, S. C., Puaud, S. J., Crépin, L., Prat, S., Quiles, A., van der Plicht, J., Valladas, H., Stuart, A. J., Drucker, D. G., Patou-Mathis, M., Lanoë, F., and Yanevich, A. (2013). The Middle to Upper Paleolithic sequence of Buran-Kaya III (Crimea, Ukraine): New stratigraphic, paleoenvironmental, and chronological results. *Radiocarbon*, 55(2):1454–1469.

Radovčić, J., Smith, F. H., Trinkaus, E., and Wolpoff, M. H. (1988). *The Krapina hominids: an illustrated catalog of the skeletal collection.* Mladost and the Croatian Natural Hisotry Museum, Zagreb.

Rebollo, N., Weiner, S., Brock, F., Meignen, L., Goldberg, P., Belfer-Cohen, A., Bar-Yosef, O., and Boaretto, E. (2011). New radiocarbon dating of the transition from the Middle to the Upper Paleolithic in Kebara Cave, Israel. *Journal of Archaeological Science*, 38(9):2424–2433.

Reich, D., Green, R. E., Kircher, M., Krause, J., Patterson, N., Durand, E. Y., Viola, T. B., Briggs, A. W., Stenzel, U., Johnson, P. L. F., Maricic, T., Good, J. M., Marques-Bonet, T., Alkan, C., Fu, Q., Mallick, S., Li, H., Meyer, M., Eichler, E. E., Stoneking, M., Richards, M., Talamo, S., Shunkov, M. V., Derevianko, A. P., Hublin, J.-J., Kelso, J., Slatkin, M., and Pääbo, S. (2010). Genetic history of an archaic hominin group from Denisova Cave in Siberia. *Nature*, 468(7327):1053–1060.

Reimer, P. J., Baillie, M. G. L., Bard, E., Bayliss, A., Beck, J. W., Bertrand, C. J. H., Blackwell, P. G., Buck, C. E., Burr, G. S., Cutler, K. B., Damon, P. E., Edwards, R. L., Fairbanks, R. G., Friedrich, M., Guilderson, T. P., Hogg, A. G., Hughen, K. A., Kromer, B., McCormac, G., Manning, S. W., Bronk Ramsey, C., Reimer, R. W., Remmele, S., Southon, J. R., Stuiver, M., Talamo, S., Taylor, F. W., van der Plicht, J., and Weyhenmeyer, C. E. (2004). IntCal04 terrestrial radiocarbon age calibration, 0-26 cal kyr BP. *Radiocarbon*, 46(3):1029–1058.

Reimer, P. J., Baillie, M. G. L., Bard, E., Bayliss, A., Beck, J. W., Blackwell, P. G., Bronk Ramsey, C., Buck, C. E., Burr, G. S., Edwards, R. L., Friedrich, M., Grootes, P. M., Guilderson, T. P., Hajdas, I., Heaton, T. J., Hogg, A. G., Hughen, K. A., Kaiser, K. F., Kromer, B., McCormac, F. G., Manning, S. W., Reimer, R. W., Richards, D. A., Southon, J. R., Talamo, S., Turney, C. S. M., van der Plicht, J., and Weyhenmeyer,

C. E. (2009). IntCal09 and Marine09 radiocarbon age calibration curves, 0-50,000 years Cal BP. *Radiocarbon*, 51(4):1111–1150.

Reimer, P. J., Bard, E., Bayliss, A., Beck, J. W., Blackwell, P. G., Bronk Ramsey, C., Buck, C. E., Cheng, H., Edwards, R. L., Friedrich, M., Grootes, P. M., Guilderson, T. P., Haflidason, H., Hajdas, I., Hatté, C., Heaton, T. J., Hoffmann, D. L., Hogg, A. G., Hughen, K. A., Kaiser, K. F., Kromer, B., Manning, S. W., Niu, M., Reimer, R. W., Richards, D. A., Scott, E. M., Southon, J. R., Staff, R. A., Turney, C. S. M., van der Plicht, J., Kaiser, F. K., Kromer, B., Manning, S. W., Niu, M., Reimer, R. W., Richards, D. A., Scott, E. M., Southon, J. R., Staff, R. A., Turney, C. S. M., and Plicht, J. V. D. (2013). IntCal13 and Marine13 Radiocarbon Age Calibration Curves 0–50,000 Years cal BP. *Radiocarbon*, 55(4):1869–1887.

Reimer, P. J. and McCormac, F. G. (2002). Marine Radiocarbon Reservoir Corrections for the Mediterranean and Aegean Seas. *Radiocarbon*, 44(1):159–166.

Richards, M. P., Pettitt, P. B., Stiner, M. C., and Trinkaus, E. (2001). Stable isotope evidence for increasing dietary breadth in the European mid-Upper Paleolithic. *Proceedings of the National Academy of Sciences*, 98(11):6528–6532.

Richter, D., Tostevin, G., and Škrdla, P. (2008). Bohunician technology and thermoluminescence dating of the type locality of Brno-Bohunice (Czech Republic). *Journal of Human Evolution*, 55:871–885.

Richter, D., Tostevin, G., Škrdla, P., and Davies, W. (2009). New radiometric ages for the Early Upper Palaeolithic type locality of Brno-Bohunice (Czech Republic): comparison of OSL, IRSL, TL and ^{14}C dating results. *Journal of Archaeological Science*, 36:708–720.

Riel-Salvatore, J. and Negrino, F. (2009). Early Upper Paleolithic population dynamics and raw material procurement patterns in Italy. In Camps, M. and Szmidt, C. C., editors, *The Mediterranean Between 50-25,000 BP: Turning Points and New Directions*, pages 205–224. Oxbow Books, Oxford.

Ringer, (2002). The Chronostratigraphy and Palaeo-Human-Ecology of the Middle and Upper Palaeolithic in Northeast Hungary, between 130,000 and 10,000 BP. *Praehistoria*, 3:39–46.

Rink, W. J., Schwarcz, H. P., Smith, F. H., and Radovčić, J. (1995). ESR ages for Krapina hominids. *Nature*, 378:24.

Roksandic, M., Mihailović, D., Mercier, N., Dimitrijević, V., Morley, M. W., Rakočević, Z., Mihailović, B., Guibert, P., and Babb, J. (2011). A human mandible (BH-1) from the Pleistocene deposits of Mala Balanica cave (Sićevo Gorge, Niš, Serbia). *Journal of Human Evolution*, 61(2):186–196.

Ronchitelli, A., Benazzi, S., Boscato, P., Douka, K., and Moroni, A. (2014). Comments on "Human-climate interaction during the Early Upper Paleolithic: Testing the hypothesis of an adaptive shift between the Proto-Aurignacian and the Early Aurignacian" by Banks et al. *Journal of Human Evolution*, 73:107–111.

Ronchitelli, A., Boscato, P., and Gambassini, P. (2009). Gli ultimi neandertaliani in italia: aspetti culturali. In Facchini, F. and Belcastro, G. M., editors, *La lunga Storia di Neandertal. Biologia e Comportamento*, pages 227–257. Jaca Book, Milano.

Rosenblatt, M. (1956). Remarks on some non-parametric estimates of a density function. *Annals of Mathematical Statistics*, 27:832–837.

Rougier, H., Milota, S., Rodrigo, R., Gherase, M., Sarcina, L., Moldovan, O., Zilhão, J., Constantin, S., Franciscus, R. G., Zollikofer, C. P. E., Ponce de León, M., and Trinkaus, E. (2007). Peştera cu Oase 2 and the cranial morphology of early modern Europeans. *Proceedings of the National Academy of Sciences of the United States of America*, 104(4):1165–70.

Roussel, M., Soressi, M., and Hublin, J.-J. (2016). Châtelperronian conundrum: Blade and bladelet lithic technologies from Quinçay, France. *Journal of Human Evolution*, 95:13–32.

Ruebens, K., McPherron, S. J., and Hublin, J.-J. (2015). On the local Mousterian origin of the Châtelperronian: Integrating typo-technological, chronostratigraphic and contextual data. *Journal of Human Evolution*, 86:55–91.

Saád, A. (1927). Die Ergebnisse der Ausgrabungen in der Istállosköer Höhle im Jahre 1927. *Die Eiszeit*, 4:97–98.

Saád, A. (1929). A Bükk hegységben végzett újabb kutatások eredményei (Über die Resultate der neueren Ausgrabungen im Bükkgebirge). *Archaeologia Értesitő*, 43:238–247, 375.

Saád, and Nemeskéri, J. (1955). A Szeleta barlang 1947. évi kutatásainak eredmédnyei. *Folia Archaeologica*, 7:15–21.

Schlolaut, G., Marshall, M. H., Brauer, A., Nakagawa, T., Lamb, H. F., Staff, R. A., Bronk Ramsey, C., Bryant, C. L., Brock, F., Kossler, A., Tarasov, P. E., Yokoyama, Y., Tada, R., and Haraguchi, T. (2012). An automated method for varve interpolation and its application to the Late Glacial chronology from Lake Suigetsu, Japan. *Quaternary Geochronology*, 13:52–69.

Schmitz, R. W., Serre, D., Bonani, G., Feine, S., Hillgruber, F., Krainitzki, H., Paabo, S., and Smith, F. H. (2002). The Neandertal type site revisited: Interdisciplinary investigations of skeletal remains from the Neander Valley, Germany. *Proceedings of the National Academy of Sciences*, 99(20):13342–13347.

Schtchelinski, V. E. (1994). La fonction des outils gravettiens et épigravettiens. introduction médologique. In *Temnata Cave. Excavations in Karlukovo Karst Area, Bulgaria*, volume 1.2, pages 87–122. Jagellonian University Press, Kraków.

Schwarcz, H. P. and Schoeninger, M. J. (1991). Stable Isotope Analyses in Human Nutritional Ecology. *Yearbook of physical anthropology*, 34:283–321.

Šefčáková, A. (2007). Pleistocénne antropologické nálezy z územia Slovenska / Pleistocene anthropological finds from the territory of Slovakia. *Acta Rerum Naturalium Musei Nationalis Slovaci Bratislava*, 53(1):26–45.

Šefčáková, A. and Thurzo, M. (2006). Holocene human remains from the Dzeravá skala Cave, West Slovakia. *Journal of the National Museum, Natural History Series*, 175(1-2):31–37.

Semal, P., Hauzeur, A., Rougier, H., Crevecoeur, I., Germonpré, M., Pirson, S., Haesaerts, P., Jungels, C., Flas, D., Toussaint, M., Maureille, B., Bocherens, H., and Higham, T. (2012). Radiocarbon dating of human remains and associated archaeological material. *Anthropologica et Praehistoria*, 123(1):331–356.

Semal, P., Rougier, H., Crevecoeur, I., Jungels, C., Flas, D., Hauzeur, A., Maureille, B., Germonpré, M., Bocherens, H., Pirson, S., Cammaert, L., De Clerck, N., Hambucken, A., Higham, T., Toussaint, M., and van der Plicht, J. (2009). New data on the late Neandertals: Direct dating of the Belgian Spy fossils. *American Journal of Physical Anthropology*, 138(4):421–428.

Shennan, S. (2013). Demographic Continuities and Discontinuities in Neolithic Europe: Evidence, Methods and Implications. *Journal of Archaeological Method and Theory*, 20(2):300–311.

Simek, J. F. and Smith, F. H. (1997). Chronological changes in stone tool assemblages from Krapina (Croatia). *Journal of Human Evolution*, 32(6):561–575.

Sinitsyn, A. A. (2003). The most anicent sites of Kostenki in the context of the initial Upper Paleolithic of northern Eurasia. In Zilhão, J. and d'Errico, F., editors, *The Chronology of the Aurignacian and of the Transitional Technocomplexes. Dating, Stratigraphies, Cultural Implications*, number 33 in Trabalhos de Arqueologia, pages 89–107. Instituto Português de Arqueologia, Lisboa.

Sirakov, N. (1983). Reconstruction of the Middle Palaeolithic flint assemblages from the cave Samuilitsa II (Northern Bulgaria) and their taxonomical position seen agains the Palaeolithic of South-Eastern Europe. *Folia Quaternaria*, 55:1–110.

Sirakov, N. (1992). Introduction. In *Temnata Cave. Excavations in Karlukovo Karst Area, Bulgaria*, volume 1.1, pages 13–30. Jagellonian University Press, Kraków.

Sirakov, N., Guadelli, J.-L., Ivanova, S., Sirakova, S., Boudadi-Maligne, M., Dimitrova, I., Fernandez, P., Ferrier, C., Guadelli, A., Iordanova, D., Iordanova, N., Kovatcheva, M., Krumov, I., Leblanc, J.-C., Miteva, V., Popov, V. V., Spassov, R., Taneva, S., and Tsanova, T. (2010). An ancient continuous human presence in the Balkans and the beginnings of human settlement in western Eurasia: A Lower Pleistocene example of the Lower Palaeolithic levels in Kozarnika cave (North-western Bulgaria). *Quaternary International*, 223-224:94–106.

Sirakov, N., Sirakova, S., Ivanova, S., Gatsov, I., and Tsonev, T. (1994). The Epigravettian sequence. In *Temnata Cave. Excavations in Karlukovo Karst Area, Bulgaria*, volume 1.2, pages 169–314. Jagellonian University Press, Kraków.

Sirakov, N., Tsanova, T., Sirakova, S., Taneva, S., Krumov, I., Dimitrova, I., and Kovatcheva, N. (2007). Un nouveau faciès lamellaire du début du Paléolithique supérieur dans les Balkans. *PALEO*, 19:131–144.

Škrdla, P. (2003a). Bohunician technology: the refitting approach. In Svoboda, J. and Bar-Yosef, O., editors, *Stránská skála. Origins of the Upper Paleolithic in the Brno Basin, Moravia, Cyech Republic*, number 47 in American School of Prehistoric Research Bulletin, pages 119–151. Peabody Museum Publications, Harvard Universitz, Cambridge.

Škrdla, P. (2003b). Comparison of Boker Tachtit and Stránská skála MP/UP transitional industries. *Journal of the Israel Prehistoric Society*, 33:33–69.

Škrdla, P. (2010). Aurignacien Dolnomoravského úvalu (1. díl). *Slovácko*, 51:111–138.

Škrdla, P. (2013). The Bohunician in Moravia and adjoining regions. *Archaeology, Ethnology and Anthropology of Eurasia*, 41(3):2–13.

Škrdla, P. (2017). Middle to Upper Paleolithic transition in Moravia: New sites, new dates, new ideas. *Quaternary International*, 450:116–125.

Škrdla, P., Matějec, P., Tostevin, G., Rychtaříková, T., and Hladilová, (2011). Brno (k. ú. Líšeň, okr. Brno-město). *Přehled výzkumů*, 52(1):140–143.

Škrdla, P., Nejman, L., Rychtaříková, T., Nikolajev, P., and Lisá, L. (2014). New observations concerning the Szeletian in Moravia. *Quartär*, 61:87–101.

Škrdla, P. and Rychtaříková, T. (2012). Levallois point or blade - which blank was the target artifact of the Bohunician technology? In Pastoors, A. and Peresani, M., editors, *Flakes not Blades. The Role of Flake Production at the Onset of the Upper Palaeolithic in Europe*, Wissenschaftliche Schriften des Neanderthal Museums, pages 199–124. Neanderthal Museum, Mettmann.

Škrdla, P. and Tostevin, G. (2005). Brno-Bohunice, analýza materiálu z výzkumu v roce 2002 (Brno-Bohunice, Anlaysis of the Material from the 2002 Excavation. *Přehled výzkumů*, 4:35–61.

Slon, V., Mafessoni, F., Vernot, B., de Filippo, C., Grote, S., Viola, B., Hajdinjak, M., Peyrégne, S., Nagel, S., Brown, S., Douka, K., Higham, T., Kozlikin, M. B., Shunkov, M. V., Derevianko, A. P., Kelso, J., Meyer, M., Prüfer, K., and Pääbo, S. (2018). The genome of the offspring of a Neanderthal mother and a Denisovan father. *Nature*, 561(7721):113–116.

Smith, F. H., Trinkaus, E., Pettitt, P. B., Karavanić, I., and Paunovic, M. (1999). Direct radiocarbon dates for Vindija G(1) and Velika Pecína late Pleistocene hominid remains. *PNAS*, 96(22):12281–12286.

Snoeck, C., Lee-Thorp, J. A., and Schulting, R. J. (2014). From bone to ash: Compositional and structural changes in burned modern and archaeological bone. *Palaeogeography, Palaeoclimatology, Palaeoecology*, 416:55–68.

Soficaru, A. and Doboş, A. (2006). Early modern humans from the Peștera Muierii, Baia de Fier, Romania. *PNAS*, 103(46):17196–17201.

Soficaru, A., Petrea, C., Doboş, A., and Trinkaus, E. (2007). The Human Cranium from the Peştera Cioclovina Uscată, Romania: Context, Age, Taphonomy, Morphology, and Paleopathology. *Current Anthropology*, 48(4):611–619.

Soltész, B. (1954). Die statistische Untersuchungen der Backenzähne des Höhlenbären aus der Höhle Istállóskő. *Acta Archaeologica Academiae Scientiarum Hungaricae*, 5:187–192.

Sonneville-Bordes, D. (1960). *Le Paléolithique supérieur en Périgord*. Delmas, Bordeaux.

Southon, J., Noronha, A. L., Cheng, H., Edwards, R. L., and Wang, Y. (2012). A high-resolution record of atmospheric ^{14}C based on Hulu Cave speleothem H82. *Quaternary Science Reviews*, 33:32–41.

Spriggs, M. and Anderson, A. J. (1993). Late Colonization of East Polynesia. *Antiquity*, 67(January):200–217.

Staff, R., Bronk Ramsey, C., and Nakagawa, T. (2010). A re-analysis of the lake suigetsu terrestrial radiocarbon calibration dataset. *Nuclear Instruments and Methods in Physics Research Section B: Beam Interactions with Materials and Atoms*, 268(7):960–965.

Staff, R. A., Schlolaut, G., Ramsey, C. B., Brock, F., Bryant, C. L., Kitagawa, H., van der Plicht, J., Marshall, M. H., Brauer, A., Lamb, H. F., Payne, R. L., Tarasov, P. E., Haraguchi, T., Gotanda, K., Yonenobu, H., Yokoyama, Y., Nakagawa, T., and Suigetsu 2006 Project Members (2013). Integration of the Old and New Lake Suigetsu (Japan) Terrestrial Radiocarbon Calibration Data Sets. *Radiocarbon*, 55(4):2049–2058.

Stafford, T. W., Brendel, K., and Duhamel, R. C. (1988). Radiocarbon, ^{13}C and ^{15}N analysis of fossil bone: Removal of humates with XAD-2 resin. *Geochimica et Cosmochimica Acta*, 52(9):2257–2267.

Stafford, T. W., Hare, P. E., Currie, L., Jull, A. J. T., and Donahue, D. J. (1991). Accelerator radiocarbon dating at the molecular level. *Journal of Archaeological Science*, 18(1):35–72.

Stafford, T. W., Jull, A. J. T., Brendelt, K., Duhamelt, R. C., and Donahue, D. (1987). Study of Bone Radiocarbon Dating Accuracy At the University of Arizona NSF Accelerator Facility for Radioisotope Analysis. *Radicarbon*, 29(1):24–44.

Street, M., Terberger, T., and Orschiedt, J. (2006). A critical review of the German Paleolithic hominin record. *Journal of Human Evolution*, 51(6):551–579.

Stuiver, M. and Polach, H. A. (1977). Discussion: Reporting of ^{14}C Data. *Radiocarbon*, 19(3):355–363.

Stuiver, M. and Reimer, P. J. (1993). Extended ^{14}C Data Base and Revised Calib 3.0 ^{14}C Age Calibration Program. *Radiocarbon*, 35(1):215–230.

Sutikna, T., Tocheri, M. W., Morwood, M. J., Saptomo, E. W., Jatmiko, Awe, R. D., Wasisto, S., Westaway, K. E., Aubert, M., Li, B., Zhao, J.-x., Storey, M., Alloway, B. V., Morley, M. W., Meijer, H. J. M., van den Bergh, G. D., Grün, R., Dosseto, A., Brumm, A., Jungers, W. L., and Roberts, R. G. (2016). Revised stratigraphy and chronology for Homo floresiensis at Liang Bua in Indonesia. *Nature*, 532(7599):366–369.

Svensson, A., Andersen, K. K., Bigler, M., Clausen, H. B., Dahl-Jensen, D., Davies, S. M., Johnsen, S. J., Muscheler, R., Rasmussen, S. O., and Röthlisberger, R. (2006). The Greenland Ice Core Chronology 2005, 15–42ka. Part 2: comparison to other records. *Quaternary Science Reviews*, 25(23):3258–3267.

Svoboda, J. (1980). *Křemencová industrie y Ondratic*. Number 9 in Studie Archeologického ústavu ČSAV v Brně. Academia, Prague.

Svoboda, J. and Bar-Yosef, O., editors (2003). *Origins of the Upper Paleolithic in the Brno Basin, Moravia, Czech Republic*. Number 47 in American School of Prehistoric Research Bulletin. Peabody Museum Publications, Harvard Universitz, Cambridge.

Svoboda, J. and Simán, K. (1989). The Middle-Upper Paleolithic transition in Southeastern Central Europe (Czechoslovakia and Hungary). *Journal of World Prehistory*, 3(3):283–322.

Svoboda, J. A. (1993). The complex origin of the Upper Paleolithic in the Czech and Slovak Republics. In Knecht, H., Pike-Tay, H., and White, R., editors, *Before Lascaux: the Complex Record of the Early Upper Paleolithic*, pages 23–36. CRC Press, Boca Raton.

Svoboda, J. A. (2001). Czech Republic: Projects of the Center for Paleolithic and Paleoethnological Research (Institute of Archaeology, Academy of Sciences), Brno-Dolní Věstonice. In Noiret, P., editor, *Le Paléolithique supérieur européen. Bilan quinquennal 1996-2001*, pages 73–88. Études et Recherches Archéologiques de l'Université de Liège, Liège.

Svoboda, J. A. (2003). Chronostratigraphic background, environment, and formation of the archaeological layers. In *Stránská skála: Origins of the Upper Paleolithic in the Brno Basin*, number 47 in American School of Prehistoric Research Bulletin, pages 15–26. Peabody Museum Publications, Harvard Universitz, Cambridge.

Svoboda, J. A. (2005). The Neandertal extinction in eastern Central Europe. *Quaternary International*, 137:69–75.

Switsur, V. R. (1976). Cambridge Radiokarbondaten von Bohunice. In Valoch, K., editor, *Die altsteinyeitliche Fundstell in Brno-Bohunice*, number 4 in Studie Archeologického ústavu ČSAV v Brně, pages 85–86. Academia, Prague.

Szmidt, C. C., Brou, L., and Jaccottey, L. (2010a). Direct radiocarbon (AMS) dating of split-based points from the (Proto)Aurignacian of Trou de la Mère Clochette, Northeastern France. Implications for the characterization of the Aurignacian and the timing of technical innovations in Europe. *Journal of Archaeological Science*, 37(12):3320–3337.

Szmidt, C. C., Normand, C., Burr, G. S., Hodgins, G. W., and LaMotta, S. (2010b). AMS ^{14}C dating the Protoaurignacian/Early Aurignacian of Isturitz, France. Implications for Neanderthal–modern human interaction and the timing of technical and cultural innovations in Europe. *Journal of Archaeological Science*, 37(4):758–768.

Sümegi, P., Náfrádi, K., Molnár, D., and Sávai, S. (2015). Results of paleoecological studies in the loess region of Szeged-Öthalom (SE Hungary). *Quaternary International*, 372:66–78.

Tafelmaier, Y. (2017). *Technological variablity at the beginning of the Aurignacian in Northern Spain. Implications for the Proto- and Early Aurignacian distinction.* Number 9 in Wissenschaftliche Schriften. Neanderthal Museum.

Talamo, S., Hajdinjak, M., Mannino, M. A., Fasani, L., Welker, F., Martini, F., Romagnoli, F., Zorzin, R., Meyer, M., and Hublin, J.-J. (2016). Direct radiocarbon dating and genetic analyses on the purported Neanderthal mandible from the Monti Lessini (Italy). *Nature Publishing Group*, 6:1–9.

Tasnádi Kubacska, A. (1954). Untersuchungen an pathologisch veränderten Knochenreste verschiedener Wirbeltiere aus der Höhle von Istállóskő. *Acta Archaeologica Academiae Scientiarum Hungaricae*, 5:193–210.

Tejero, J.-M. and Grimaldi, S. (2015). Assessing bone and antler exploitation at Riparo Mochi (Balzi Rossi, Italy): implications for the characterization of the Aurignacian in South-western Europe. *Journal of Archaeological Science*, 61:59–77.

Teyssandier, N. (2005). Les débuts de l'Aurignacien en Europe. Discussion à partir des sites de Geissenklosterle, Willendorf II, Krems-Hundssteig et Bacho Kiro. *Bulletin de la Société préhistorique française*, 102(1):211–216.

Teyssandier, N. (2006). Questioning the first Aurignacian: Mono or multi cultural phenomenon during the formation of the Upper Paleolithic in central Europe and the Balkans. *Anthropologie*, 44(1):9–29.

Teyssandier, N. (2007). En route vers l'ouest? Les débuts de l'Aurignacien en Europe centrale et dans les Balkans / Auf dem Wege gen Westen? Die Anfänge des Aurignacien in Mitteleuropa und auf dem Balkan. In *Les Chemins de l'art Aurignacien en Europe / Das Aurignacien und die Anfänge der Kunst in Europa*, pages 99–113.

Teyssandier, N. (2008). Revolution or evolution: the emergence of the Upper Paleolithic in Europe. *World Archaeology*, 40(4):493–519.

Teyssandier, N., Bolus, M., and Conard, N. J. (2006). The Early Aurignacian in central Europe and its place in a European perspective. In Bar-Yosef, O. and Zilhão, J., editors, *Towards a Definition of the Aurignacian. Proceedings of the Symposium held in Lisbon, Portugal, June 25-30, 2002*, pages 241–256, Libon. Instituto Portugues de Arqueologia.

Thoma, A. and Vértes, L. (1971). Hungary. In Oakley, K. P., Campbell, B. G., and Molleson, T. I., editors, *Catalogue of Fossil Hominids, part II: Europe*, pages 223–229. British Museum, London.

Tillier, A.-M., Mester, Z., Henry-Gambier, D., Pap, I., Ringer, , and Gyenis, G. (2006). The Middle-Upper Palaeolithic Transition in Hungary: an anthropological perspective. In *En el centenario de la cueva de El Castillo: el ocaso de los Neandertales*, pages 91–106. Centro Asociado a la Universidad Nacional de Educación en Cantabria.

Tillier, A.-m., Sirakov, N., Guadelli, A., Fernandez, P., Sirakova, S., Dimitrova, I., Ferrier, C., Guérin, G., Heidari, M., Krumov, I., Leblanc, J.-C., Miteva, V., Popov, V., Taneva, S., and Guadelli, J.-L. (2017). Evidence of Neanderthals in the Balkans: The infant radius from Kozarnika Cave (Bulgaria). *Journal of Human Evolution*, 111:54–62.

Tisnérat-Laborde, N., Valladas, H., Kaltnecker, E., and Arnold, M. (2003). AMS radiocarbon dating of bones at LSCE. *Radiocarbon*, 45(3):409–419.

Toussaint, M. and Pirson, S. (2006). Neandertal Studies in Belgium: 2000–2005. *Period biol*, 108(3):373–387.

Trinkaus, E. (2005). Early Modern Humans. *Annual Review of Anthropology*, 34(1):207–230.

Trinkaus, E. (2013). Radiocarbon Dating of the Peştera cu Oase Human Remains. In *Life and death at the Peştera cu Oase: a setting for modern human emergence in Europe*, pages 229–233. Oxford University Press, New York.

Trinkaus, E., Moldovan, O., Milota, S., Bîlgăr, A., Sarcina, L., Athreya, S., Bailey, S. E., Rodrigo, R., Mircea, G., Higham, T. F. G., Ramsey, C. B., and van der Plicht, J. (2003). An early modern human from the Peştera cu Oase, Romania. *Proceedings of the National Academy of Sciences of the United States of America*, 100(20):11231–6.

Tsanova, T. (2003). Le Gravettien en Bulgarie du Nord: niveau IVb de la grotte Kozarnika. In Tsonev, T. and Kokelj, E. M., editors, *The Humanized Mineral Word : Towards social and symbolic evaluation of prehistoric technology in South Eastern Europe*, pages 33–40, Sofia.

Tsanova, T. (2006). *Les débuts du Pléolithique supérieur dans l'Est des Balkans. Réflexion à partir de l'étude taphonomique et techno-économique des ensembles lithiques des sites de Bacho Kiro (couche 11), Temnata (couches VI et 4) et Kozarnika (niveau VII).* unpubl. PhD, l'Université Bordeaux 1, Bordeaux.

Tsanova, T., Zwyns, N., Eizenberg, L., Teyssandier, N., Le Brun-Ricalens, F., and Otte, M. (2012). Le plus petit dénominateur commun: réflexion sur la variabilité des ensembles lamellaires du Paléolithique supérieur ancien d'Eurasie. Un bilan autour des exemples de Kozarnika (Est des Balkans) et Yafteh (Zagros central). *L'Anthropologie*, 116(4):469–509.

Turney, C. S. M., Bird, M. I., Fifield, L. K., Kershaw, A. P., Cresswell, R. G., Santos, G. M., di Tada, M. L., Hausladen, P. A., and Youping, Z. (2001). Development of a Robust ^{14}C Chronology for Lynch's Crater (North Queensland, Australia) Using Different Pretreatment Strategies. *Radiocarbon*, 43(1):45–54.

Tuross, N. (2002). Alterations in fossil collagen. *Archaeometry*, 44(3):427–434.

Valoch, K. (1969). Das Mittelpaläolithikum mit Blattspitzen aus der Höhle von Kulna bei Sloup in Möhren. *Casopis moravského musea v Brno*, 53.

Valoch, K. (1976). *Die altsteinzeitliche Fundstell in Brno - Bohunice.* Number 4 in Studie Archeologického ústavu ČSAV v Brně. Academia, Prague.

Valoch, K. (1993). Vedrovice V, eine Siedlung des Szeletiens in Südmähren. *Quartär*, 43/44:7–93.

Valoch, K. (1996). *Le Paléolithique en Tchéquie et on Slovaquie.* Jérôme Millon, Grenoble.

Valoch, K. (2000). More on the Question of Neanderthal Acculturation in Central Europe. *Current Anthropology*, 41(4):625–626.

Valoch, K. (2008). Brno-Bohunice, eponymous Bohunician site: new data, new ideas. In Sulgostowska, Z. and Tomaszewski, A. J., editors, *Man-Millennia-Environment. Studies in Honour of Romuald Schild*, pages 225–236. Institute of Archaeology and Ethnology, Polish Academy of Sciences, Warsaw.

van der Plicht, J., Beck, J. W., Bard, E., Baillie, M. G. L., Blackwell, P. G., Buck, C. E., Friedrich, M., Guilderson, T. P., Hughen, K. A., Kromer, B., McCormac, F. G., Bronk Ramsey, C., Reimer, P. J., Reimer, R. W., Remmele, S., Richards, D. A., Southon, J. R., Stuiver, M., and Weyhenmeyer, C. E. (2004). NotCal04 - comparison/calibration ^{14}C records 26-50 cal kyr BP. *Radiocarbon*, 46(3):1225–1238.

van Klinken, G. J. (1999). Bone collagen quality indicators for palaeodietary and radiocarbon measurements. *Journal of Archaeological Science*, 26(6):687–695.

van Klinken, G. J., Bowles, A. D., and Hedges, R. E. M. (1994). Radiocarbon dating of peptides isolated from contaminated fossil bone collagen by collagenase digestion and reversed-phase chromatography. *Geochimica et Cosmochimica Acta*, 58(11):2543–2551.

van Klinken, G. J. and Hedges, R. E. M. (1995). Experiments on Collagen-Humic Interactions: Speed of Humic Uptake, and Effects of Diverse Chemical Treatments. *Journal of Archaeological Science*, 22:263–270.

van Klinken, G. J. and Mook, W. G. (1990). Preperative high-performance liquid chromatographic seperation of individual amino acids derived from fossil bone collagen. *Radiocarbon*, 32(2):155–164.

Vogel, J. C. and Lerman, J. C. (1969). Groningen radiocarbon dates VIII. *Radiocarbon*, 11(2):351–390.

Vogel, J. S. and Waterbolk, H. T. (1963). Groningen radiocarbon dates IV. *Radiocarbon*, 5:163–202.

Vogel, J. S. and Waterbolk, H. T. (1972). Groningen radiocarbon dates X. *Radiocarbon*, 14:6–110.

Vértes, L. (1954). Neuere Ausgrabungen und paläolithische Funde in der Höhle von Istállóskő. *Acta Archaeologica Academiae Scientiarum Hungaricae*, 5:111–131.

Vértes, L. (1955). Paläolithische Kulturen der Würm I-II-Interstadials in Ungarn. *Acta Archaeologica Academiae Scientiarum Hungaricae*, 5:261–278.

Vértes, L. (1957). Az első hazai anyagon végzett rádiókarbon-vizsgálat (Ergebnis der ersten C14-Untesuchung an Ungarischem Material). *Archaeologia Értesitő*, 84(1):222.

Vértes, L. (1959a). *Untersuchungen an Höhlensedimenten: Methode und Ergebnisse*. Magyar Nemzeti Muzeum, Történeti Múzeum, Budapest.

Vértes, L. (1959b). *Untersuchungen an Höhlensedimenten*. Number II(7) in Régészeti Füzetek. Magyar Nemzeti Múzeum/Történeti Muzeum, Budapest.

Vértes, L. (1968). Szeleta-Symposium in Ungarn. 4.-11. September 1966. *Quartär*, 19:381–390.

Vértes, L. and de Vries, H. (1959). Radiokarbonbestimmung des Aurignacien II aus der Istállósköer Höhle. *Archaeologia Értesitő*, 86(2):195.

Vértes, L., Jánossy, D., Hermann, M., and Stieber, J. (1956). Ausgrabungen in der Petényi- und Peskő-Höhle. *Folia Archaeologica*, 8:3–22.

Vörös, I. (1984). Hunted mammals from the Aurignacian cave bear hunters' site in the Istállóskő cave. *Folia Archaeologica*, 35:7–31.

Vörös, I. (2003). Stratigraphy and biostratigraphy of Istállóskő cave. *Praehistoria*, 4-5:33–76.

Waterbolk, H. T. (1971). Working with radiocarbon dates. *Proceedings of the Prehistoric Society*, 37:15–33.

Wild, E., Golser, R., Hille, P., Kutschera, W., Priller, A., Puchegger, S., Rom, W., Steier, P., and Vycudilik, W. (1998). First ^{14} Results from Archaeological and Forensic Studies at the Vienna Environmental Research Accelerator. *Radiocarbon*, 40(1):273–281.

Wild, E. M., Teschler-Nicola, M., Kutschera, W., Steier, P., Trinkaus, E., and Wanek, W. (2005). Direct dating of Early Upper Palaeolithic human remains from Mladeč. *Nature*, 435(7040):332–335.

Williams, A. N. (2012). The use of summed radiocarbon probability distributions in archaeology: a review of methods. *Journal of Archaeological Science*, 39(3):578–589.

Wolpoff, M. H., Smith, F. H., Malez, M., Radovčić, J., and Rukavina, D. (1981). Upper Pleistocene Human Remains From Vindija Cave, Croatia, Yugoslavia. *American Journal of Physical Anthropology*, 54:499–545.

Wood, R., Arrizabalaga, A., Camps, M., Fallon, S., Iriarte-Chiapusso, M.-J., Jones, R., Maroto, J., de la Rasilla, M., Santamaría, D., Soler, J., Soler, N., Villaluenga, A., and Higham, T. (2014). The chronology of the earliest Upper Palaeolithic in northern Iberia: New insights from L'Arbreda, Labeko Koba and La Viña. *Journal of Human Evolution*, 69:91–109.

Wood, R., Bernaldo de Quirós, F., Maíllo-Fernández, J.-M., Tejero, J.-M., Neira, A., and Higham, T. (2018). El Castillo (Cantabria, northern Iberia) and the Transitional Aurignacian: Using radiocarbon dating to assess site taphonomy. *Quaternary International*, 474:56–70.

Wood, R. E., Bronk Ramsey, C., and Higham, T. F. G. (2010). Refining Background Corrections for Radiocarbon Dating of Bone Collagen at ORAU. *Radiocarbon*, 52(2–3):600–611.

Wood, R. E., Douka, K., Boscato, P., Haesaerts, P., Sinitsyn, A. A., and Higham, T. F. G. (2012). Testing the ABOx-SC method: Dating known-age charcoals associated with the Campanian Ignimbrite. *Quaternary Geochronology*, 9:16–26.

Wood, R. E., Higham, T. F. G., De Torres, T., TisnéRat-Laborde, N., Valladas, H., Ortiz, J. E., Lalueza-Fox, C., SáNchez-Moral, S., CañAveras, J. C., Rosas, A., SantamaríA, D., and De La Rasilla, M. (2013). A new date for the Neanderthals from El Sidrón Cave (Asturias, northern Spain). *Archaeometry*, 55(1):148–158.

Woodhead-Galloway, J. (1980). *Collagen: the anatomy of a protein*. Edward Arnold, London.

Zazzo, A. (2014). Bone and enamel carbonate diagenesis: A radiocarbon prospective. *Palaeogeography, Palaeoclimatology, Palaeoecology*, 416:168–178.

Zazzo, A., Lebon, M., Chiotti, L., Comby, C., Delqué-Količ, E., Nespoulet, R., and Reiche, I. (2013). Can we use calcined bones for ^{14}C dating the Palaeolithic? *Radiocarbon*, 55(2-3):1409–1421.

Zilhão, J. and Errico, F. D. (2003). The chronology of the Aurignacian and Transitional technocomplexes. Where do we stand? In *The Chronology of the Aurignacian and of the Transitional Technocomplexes Dating, Stratigraphies, Cultural Implications*, pages 313–349, Lisbon.

Zilhão, J. (2006). Genes, Fossils, and Culture. An Overview of the Evidence for Neandertal–Modern Human Interaction and Admixture. *Proceedings of the Prehistoric Society*, 72:1–20.

Zilhão, J., Banks, W. E., d'Errico, F., and Gioia, P. (2015). Analysis of Site Formation and Assemblage Integrity Does Not Support Attribution of the Uluzzian to Modern Humans at Grotta del Cavallo. *PLOS ONE*, 10(7):e0131181.

Zwyns, N., Rybin, E., Hublin, J.-J., and Derevianko, A. (2012). Burin-core technology and laminar reduction sequences in the initial Upper Paleolithic from Kara-Bom (Gorny-Altai, Siberia). *Quaternary International*, 259:33–47.

Борић, Д. and Јевтић, М. (2006). Истраживања археолошког локалитета Пећина изнад Трајанове табле / Archaeological Excavation at the Cave above Tabula Traiana. *Археолошки ПРЕГЛЕД / Archaeological REPORTS*, 4.

Вертеш, (1951). Новые раскопки в пещере на Ишталлошко (Novye raskopki v peschere na Istallosko). *Acta Archaeologica Academiae Scientiarum Hungaricae*, 1:15–34.

Гуадели, А. (2011). *Костни артефакти от палеолита в България (Les artefacts en matières dures animales du Paléolithique Bulgare)*. Number 6 in Дисертации (Dissertations). Bulgarian Academy of Sciences National Institute of Archaeology with Museum, Sofia.

Гуадели, А., Бояджиев, К., and Гуадели, Ж.-Л. (2016). Проучвания в пещера Манастира (Великотърновско)през 2015 г (2015 Excavations in Manastira cave, Veliko Tarnovo region). *Археологически Открития и Разкопки*, pages 50–52.

Гуадели, А., Бояджиев, К., Гуадели, Ж.-Л., Митов, К., and Кревкьор, И. (2013). Спасителни разкопки в пещера Манастира през 2012г (Fouilles de sauvetage dans la grotte Manastira 2012). *Археологически Открития и Разкопки*, pages 32–34. Text in Bulgarian with French summary.

Гуадели, А., Бояджиев, К., Гуадели, Ж.-Л., Митов, К., and Кревкьор, И. (2014). Пещера Манастира, Великотърновско (La grotte Manastira, region de Veliko Tarnovo). *Археологически Открития и Разкопки*, pages 29–31.

Джамбазов, Н. (1958). Рисунките в пещтерата Магура (the paintings at Magura Cave). *Природа и Знание, София (Nature and Knowledge, Sofia)*, 4:21–22. in Bulgarian.

Джамбазов, Н. (1963). Ловешките пещери (The Lovech Caves). *ИАИ*, XXVI:195–241.

Джамбазов, (1957). Пещерата рещ до старо село, bрачанско. *ИАИ*, XXI:1–40.

Джамбазов, (1959). Разкопки в пещерата самуилица II. *Археология*, 1-2:47–53.

Попов, . (1933). Пещерата МИРИЗЛИВКА. Приносъ къмъ дилувиалната фауна и културата на дилувиалния човькъ въ България (La grotte "Mirizlivka". Contribution à l'étude de la faune diluvienne et de la cutlure de l'homme quaternaire en Bulgarie). *Издания народния археологически музей, Софиа (Cahier du musée national d'Archéologie, Sofia)*, 26:5–69.

Попов, Р. (1925). Нови находки на предисторическия човек в България (New finds in the Prehistory of Man). *Природа*, 26:3–4.

Попов, Р. (1928). На-старите следи от каменната индустрия у нас (The oldest traces of stone industry in Bulgaria). *Природа*, 28:7.

Попов, Р. (1931). *Пещерата Темната Дупка. Ново находище от палеолита в Бълагария (Temnata Dupka cave. A new Palaeolithic deposit in Bulgaria)*. София.

Appendix

Radiocarbon Laboratory Notes

Mass-spec 'burn' no. 4951

At ORAU bone collagen samples are prepared for graphitisation by combustion and analysis via mass-spectrometry. In general, no major anomalies were observed during the combustion runs and most treated samples passed this stage without any issues. However, mass-spec 'burn' no. 4951 gave low C:N ratios for all samples, including the background standards (see tab. 1). As the individual samples came from different chemlists, *i.e.* were not pre-treated at the same time, complications were expected to result from this particular burn. In the following, it is assessed how this might have affected the reliability of the radiocarbon dates obtained on targets combusted on burn 4951.

First, it is observed that all radiocarbon measurements for background samples appear unaffected. They all produced greater than ages (see tab. 1). Therefore, a second target was combusted for some collagen samples with sufficient excess yield to allow for a direct comparison (see tab. 2). The results for Der-32, Gro-01, MR-07, TD-18 and TD-28 show that the C:N ratios on the second burn are within expectations, supporting the initial assumption that the issue is not sample specific, but resulted from the combustion. Despite some variation in stable isotope values, the second round of radiocarbon measurements are statistically indistinguishable from the original ones. MR-07 could not be directly compared, as the original sample was not dated (sample failed graphitisation), and Der-32 produced a younger age for the second target.

Kz-116 was selected for auto-duplication. Therefore, the radiocarbon age from the burn 4951 target (43100.1 AF 01) can be directly compared to the radiocarbon age obtained from a different fraction which underwent the same pre-treatment (43100.0 AF 01), but was combusted on a different burn (*i.e.*

Table 1: Appendix: results from mass-spec run no. 4951 (1 May 2017) showing issues with calibration of nitrogen content in samples and reference material, leading to low C:N ratios while leaving the $F^{14}C$ seemingly unaffected. grey rows – values not informative as either not yet calibrated (*e.g.* SETUP) or pre-entered (*e.g.* REF).

Ref-no.	Target	Type	Weight	mg C	mg N	$\delta^{13}C$	$\delta^{15}N$	%C	C:N	Lab-no	$F^{14}C$	^{14}C (BP)	AMS
ALANINE	Setup/RJAH/2015-05-2/30	SETUP	1.81	0.7730	0.2967	-27.48	-1.73	42.7	3.04	–	–	–	–
ALANINE	Setup/RJAH/2015-05-2/31	SETUP	2.15	0.8906	0.3477	-27.25	-1.94	41.4	2.99	–	–	–	–
ALANINE	Ala/RJAH/2016-05-11/70	REF	2.05	0.8282	0.3219	-27.11	-1.56	40.4	3.00	–	–	–	–
ALANINE	Ala/RJAH/2016-05-11/71	SAMPLE	2.04	0.8459	0.3304	-27.15	-1.97	41.5	2.99	–	–	–	–
UF	UF/RJAH/2017-04-12/01	UF	1	0.0056	0.0031	-32.23	0.00	0.6	0	–	–	–	–
Gro-01	42951.0 AF* 01	SAMPLE	4.89	2.0806	0.7943	-19.98	5.22	42.5	3.06	OxA-35517	0.05508 ± 0.00112	23290 ± 160	2719
Bak	18802.180 AF* 01	SAMPLE	4.9	2.0120	0.8413	-19.10	1.55	41.1	2.79	Background	0.00000 ± 0.00097	>50100	2719
TD-18	39589.0 AF* 01	SAMPLE	4.91	1.9855	0.8228	-19.91	6.40	40.4	2.82	OxA-X-2719-18	0.03241 ± 0.00106	27550 ± 260	2719
Der-49	43101.0 AG 01	SAMPLE	4.93	1.9346	0.7814	-21.57	2.03	39.2	2.89	OxA-35581	0.00855 ± 0.00118	38300 ± 1100	2721
Der-39	43127.0 AF 01	SAMPLE	4.95	1.9529	0.8012	-21.14	9.56	39.5	2.84	OxA-35591	0.00000 ± 0.00099	> 50000	2721
Bak	25774.106 AF 01	SAMPLE	4.84	1.9092	0.7735	-20.72	10.17	39.4	2.88	Background	0.00000 ± 0.00099	> 50000	2721
ALANINE	Ala/RJAH/2016-05-11/72	REF	2.22	0.8969	0.3485	-27.11	-1.56	40.4	3.00	–	–	–	–
ALANINE	Ala/RJAH/2016-05-11/73	SAMPLE	2.27	0.9237	0.3594	-27.30	-1.74	40.7	3.00	–	–	–	–
Bak	18801.180 AF 01	SAMPLE	4.95	1.9921	0.8047	-19.31	2.79	40.2	2.89	Background	0.00000 ± 0.00098	> 50100	2721
MR-07	40399.0 AF 01	SAMPLE	4.96	2.0051	0.8009	-18.14	4.31	40.4	2.92	–	–	–	–
Kz-88	43095.0 AF 01	SAMPLE	4.97	2.0005	0.8084	-18.69	9.12	40.3	2.89	OxA-35575	0.03130 *pm* 0.00104	27830 ± 270	2721
Kz-116	43100.1 AF 01	SAMPLE	4.98	1.9986	0.8079	-20.12	6.62	40.1	2.89	OxA-35580	0.00473 ± 0.00098	43000 ± 1700	2721
MR-03	40395.0 AF* 01	SAMPLE	5.01	2.0780	0.8338	-19.76	3.27	41.5	2.91	OxA-X-2719-19	0.08664 ± 0.00117	19650 ± 110	2719
TD-28	43078.0 AF* 01	SAMPLE	5.02	2.0476	0.8273	-20.37	6.40	40.8	2.89	OxA-35551	0.01497 ± 0.00102	33750 ± 550	2720
Der-32	41371.0 AF* 01	SAMPLE	5.00	2.0455	0.8095	-19.62	7.31	40.9	2.95	OxA-X-2719-20	0.02788 ± 0.00105	28760 ± 300	2719
ALANINE	Ala/RJAH/2016-05-11/74	REF	2.31	0.9332	0.3627	-27.11	-1.56	40.4	3.00	–	–	–	–
ALANINE	Ala/RJAH/2016-05-11/75	SAMPLE	2.35	0.9685	0.3769	-27.76	-2.16	41.2	3.00	–	–	–	–
Der-72	43106.0 AF 01	SAMPLE	4.65	1.8892	0.7501	-21.97	3.61	40.6	2.94	OxA-35582	0.01052 ± 0.00102	36600 ± 800	2721
Der-74	43108.0 AF 01	SAMPLE	4.83	1.9550	0.7791	-22.60	2.68	40.5	2.93	OxA-35583	0.00713 ± 0.00100	39700 ± 1100	2721
Tab-01	43131.0 AF 01	SAMPLE	4.64	1.8043	0.6970	-20.39	2.60	38.9	3.02	OxA-35592	0.01523 ± 0.00103	33600 ± 550	2721
Tab-14	43141.0 AF 01	SAMPLE	4.93	1.9930	0.7962	-17.09	12.92	40.4	2.92	OxA-35592	0.04187 ± 0.00108	25490 ± 210	2721
NBS	0.415 XB 21	SAMPLE	11.20	2.0165	0.0034	-17.22	0.00	18.0	0	Standard	1.34143 ± 0.00343	0	2723
NBS	0.415 XB 22	SAMPLE	11.98	2.1568	0.0032	-17.03	0.00	18.0	0	Standard	1.33887 ± 0.00332	0	2724
ALANINE	Ala/RJAH/2016-05-11/76	SAMPLE	2.41	0.9867	0.3759	-27.17	-1.74	40.9	3.06	–	–	–	–
ALANINE	Ala/RJAH/2016-05-11/77	REF	2.45	0.9898	0.3846	-27.11	-1.56	40.4	3.00	–	–	–	–

Table 2: Appendix: results of different treatments or targets of some of the samples that were on mass-spec run no. 4951 for comparison.

Ref-no.	**Target**	**burn**	**Weight**	**mg C**	**mg N**	δ^{13}**C**	δ^{15}**N**	**%C**	**C:N**	**Lab-no**	$\mathbf{F^{14}C}$	^{14}**C (BP)**	**AMS**
Der-32	41371.0 AF* 02	12116	4.50	1.8705	0.6643	-20.5	6.8	41.6	3.3	OxA-35699	0.03625 ± 0.0011	26650 ± 240	2725
Der-39	41376.0 AG* 01	12104	4.88	1.9141	0.7121	-21.0	8.0	39.2	3.1	OxA-35524	0.02241 ± 0.0012	30500 ± 450	2720
Der-39	41376.0 NRC 01	12119	3.61	1.5094	0.3564	-27.8	7.0	41.8	4.9	OxA-X-2732-16	0.01692 ± 0.00138	32770 ± 660	2732
Gro-01	42951.0 AF* 02	12116	4.89	2.0977	0.7330	-21.0	5.8	42.9	3.3	OxA-35700	0.05314 ± 0.00109	23580 ± 170	2725
Kz-116	43100.0 AF 01	12104	4.82	1.9688	0.7394	-21.7	5.9	40.8	3.1	OxA-35579	0.00423 ± 0.00099	43900 ± 1900	2721
MR-07	40399.0 AF 02	12116	4.95	2.1173	0.7649	-19.1	4.0	42.8	3.2	OxA-35698	0.01030 ± 0.00099	36750 *pm* 750	2725
TD-18	39589.0 AF* 02	12116	4.99	2.1120	0.7731	-20.5	6.7	42.3	3.2	OxA-35697	0.03367 ± 0.00104	27240 ± 250	2725
TD-28	43078.0 AF* 02	12116	4.81	2.0285	0.7431	-21.1	5.9	42.2	3.2	OxA-35755	0.01484 ± 0.00101	33800 ± 550	2726

no. 12104). The C:N ratio of the latter is within expectations, while the stable isotope values differ slightly, and the radiocarbon measurements are statistically indistinguishable.

For sample Der-39 only an indirect comparison is possible. This particular sample was initially treated with the AG* protocol, before the collagen yield was split into three fractions. One was directly used for dating, a second underwent ultrafiltration, and a third followed the novel hydroxyproline dating protocol. The latter two passed all stages of quality control. That the NRC fraction resulted in an older radiocarbon age than the AG* fraction fulfils expectations based on pre-treatment rigour. However, the AF* fraction combusted on burn no. 4951 resulted in a greater than age, which appears to be significantly too old.

From this it can be concluded that the sample fractions from burn 4951 should generally be reliable. In cases were measurable differences exist, the radiocarbon measurement appears to over- rather than underestimate the true age of the sample. Such a difference would require the introduction of a large amount of exogenous dead carbon. It is more realistic to suspect a fractionation issue affecting some of the samples. This interpretation would be consistent with the slightly elevated δ^{13}C values on burn 4951. Alternatively, the difference in radiocarbon age could also result from the sample specific background correction routinely applied to ultrafiltered samples.

The low C:N ratios, and lower than usual %C, result from an overestimation of nitrogen content in the measured samples. This reduces the standard C:N of 3.2 down to 2.9, as observed on the bone standards. This may have been caused by issues with the IR-MS's internal calibration for nitrogen, though other explanations (*e.g.* external introduction of nitrogen) are also possible. Either way, a leak introducing atmospheric air to the system can be excluded based on the dating results.

AMS wheel no. 2731 & 'burn' no. 4940

AMS background recorded for this project usually fluctuated between 48.0–50.3k BP. The only exception was AMS wheel no. 2731, on which the background bone sample (19651.166 AG* 03) gave a greater than age of only > 41800 BP (see tab. 3). Introduction of exogenous carbon during the chemical pre-treatment (AG*) can be excluded as the same collagen yield was used for two further combustions. Target 19651.166 AG* 01 resulted in a

Table 3: Appendix: results for standards and samples dated for this dissertation from AMS wheel no. 2731 (very small graphites). All other samples were excluded. The bone standard with high AMS background is highlighted in grey. Note that NRC measurements here are not yet HPLC background corrected and should not be used (for radiocarbon ages see section 12.2.2).

Lab-code	Target	Material	^{14}C (BP)	F^{14}C	δ^{13}C
Standard	0.411 XB	NBS oxalic acid	0	1.34131 ± 0.00146	-17.9
Standard	0.412 XB	NBS oxalic acid	0	1.33837 ± 0.00423	-17.6
Standard	0.413 XB	NBS oxalic acid	0	1.33339 ± 0.00815	-17.5
Standard	5.82 X	Groningen, CO_2	45670 ± 230	0.00340 ± 0.0001	-23.1
Standard	5.95 X	Groningen, $C0_2$	44200 ± 500	0.00409 ± 0.00024	-20.1
Standard	9032.53 UW	Tree ring, *Quercus* sp.	3833 ± 26	0.62054 ± 0.00198	-25.2
Standard	9034.118 UW	Tree ring, *Quercus* sp.	214 ± 27	0.97367 ± 0.00327	-24.6
Standard	19651.166 AG* 03	Ash Bend, Bison bone	> 41800	0.00000 ± 0.00275	-20.0
Standard	24321.68 XB	Alanine	> 49400	0.00000 ± 0.00107	-27.0
OxA-X-2731-11	38799.0 AG* 01	Jank-05	31200 ± 2300	0.02051 ± 0.00589	-18.2
OxA-X-2731-13	40398.0 AG 01	MR-06	34000 ± 1300	0.0146 ± 0.00245	-19.4
OxA-X-2731-14	40414.0 AG* 01	Pes-02	33300 ± 1200	0.01588 ± 0.00233	-19.1
OxA-X-2731-15	41377.1 NRC 01	Sal-1	*> 42400*	*0.00127 ± 0.00192*	-22.7
OxA-X-2731-16	41625.1 NRC 01	Sal-2	*> 42500*	*0.00178 ± 0.00162*	-22.7

large graphite (1.8 mg C) with a radiocarbon age of > 48900 BP, and target 19651.166 AG* 01 gave a small graphite (0.8 mg C) and an age of > 47900 BP.

The Ash Bend background bone was combusted on burn no. 4940 and it is worth noting that the C:N ratio of 3.6 was relatively high (see tab. 4). However, this is not unusual for samples of such small size (*i.e.* 0.4 mg C). The smaller the combusted samples, the larger the measurement offset in relation to the alanine standards may become. This often leads to an observed elevation in C:N ratios. As seen on other samples combusted on the same mass-spec run, those of comparable carbon content (mg) to the alanine standards show good C:N ratios, while smaller samples see an increase. The only exception is Biv-01. Despite its size of 0.65 mg C – which is in line with the reference material – its C:N is 3.5. This is indicative of a sample specific issue, and will likely affect the reliability of Biv-01's radiocarbon date.

Some complications on burn 4940 may not be excluded, as the NBS oxalic acid standard gave unusual values and had to be failed. Nonetheless, it appears improbable that this would explain the majority of AMS background observed on wheel no. 2731. Considering the young ages observed for the

Table 4: Appendix: results from mass-spec run no. 4940 (28 March 2017) showing issues with C:N ratios for most samples and reference material. grey rows – values not informative as either not yet calibrated (*e.g.* SETUP) or pre-entered (*e.g.* REF).

Ref-no.	Target	Type	Weight	mg C	mg N	δ^{13}C	δ^{15}N	%C	C:N
ALANINE	Setup/RJAH/2015-05-2/24	SETUP	1.57	0.6322	0.2865	-28.62	-3.53	40.3	2.57
ALANINE	Setup/RJAH/2015-05-2/25	SETUP	2.32	0.8743	0.3545	-27.48	-2.19	37.7	2.88
ALANINE	Ala/RJAH/2016-05-11/48	REF	1.64	0.6626	0.2575	-27.11	-1.56	40.4	3.00
ALANINE	Ala/RJAH/2016-05-11/49	SAMPLE	1.69	0.6719	0.2615	-26.88	-1.90	39.8	3.00
Istall-02	38780.0 AG* 01	SAMPLE	1.8	0.7375	0.2662	-18.65	5.18	41.0	3.23
Istall-08	38786.0 AG* 01	SAMPLE	1.78	0.7053	0.2567	-18.50	5.26	39.6	3.21
Biv-01	38804.0 AG* 01	SAMPLE	1.70	0.6519	0.2179	-18.07	2.66	38.3	3.49
Der-33	41372.0 AG* 01	SAMPLE	1.33	0.5200	0.1638	-20.07	7.30	39.1	3.70
Mlc-11	41608.0 AG* 01	SAMPLE	1.72	0.6865	0.2420	-20.39	6.28	39.9	3.31
Jank-05	38799.0 AG* 01	SAMPLE	0.55	0.1744	0.0527	-18.19	2.84	31.7	3.86
ALANINE	Ala/RJAH/2016-05-11/50	REF	1.75	0.7070	0.2747	-27.11	-1.56	40.4	3.00
ALANINE	Ala/RJAH/2016-05-11/51	SAMPLE	1.78	0.7065	0.2772	-26.99	-1.35	39.7	2.97
Jank-02	38800.0 AG* 01	SAMPLE	1.66	0.6700	0.2350	-20.37	7.28	40.4	3.33
Jank-01	38801.0 AG* 01	SAMPLE	1.17	0.4759	0.1562	-19.01	3.30	40.7	3.56
Tk-01	42829.0 AG* 01	SAMPLE	2.06	0.8160	0.2870	-19.72	7.27	39.6	3.32
Bak	19651.166 AG* 03	SAMPLE	0.88	0.4037	0.1300	-20.12	6.61	45.9	3.62
NBS	0.415 XB 16	SAMPLE	8.82	1.5452	0.0013	-16.91	0.00	17.5	0
ALANINE	Ala/RJAH/2016-05-11/52	SAMPLE	1.8	0.7295	0.2788	-27.09	-1.90	40.5	3.05
ALANINE	Ala/RJAH/2016-05-11/53	REF	1.85	0.7474	0.2904	-27.11	-1.56	40.4	3.00

Groningen standards, it is credible that they are solely the result of a high AMS background for this particular wheel.

As a result, samples pre-treated or combusted with the background bone sample 19651.166 AG* 03 should not see any adverse effect on their radiocarbon measurements. In contrast, the samples dated on AMS wheel no. 2731 will have to be interpreted with caution. This is best visible in the two Neanderthal samples (Sal-1 and Sal-2), which have both a young threshold for a greater than age. The samples Jank-05, MR-06 and Pes-02, on the other hand, show a much larger than usual dating error, and may underestimate the true age of the samples.

Descriptive Catalogue

A: Sites & Samples

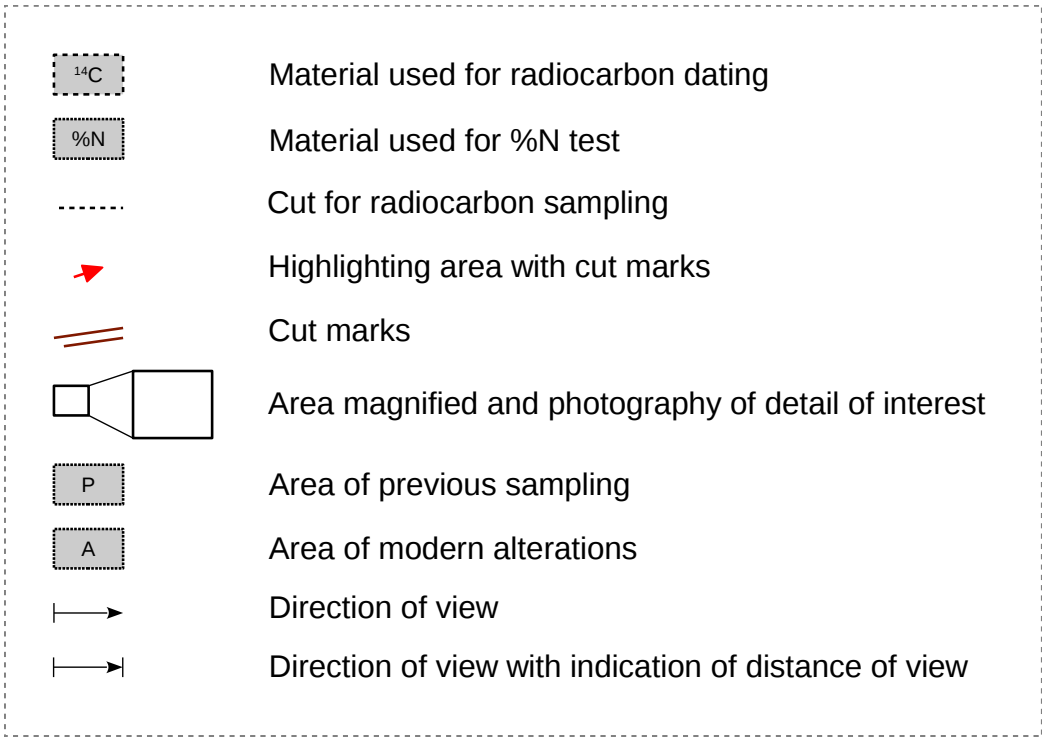


Figure A.1: Legend for sample catalogue.

A.1 Bivak, Hungary

Environment	cave
Latitude	47° 41' 58" N
Longitude	18° 50' 39" E
Altitude	536 m a.s.l.
Excavations	1943, 1953
Collaborator	András Markó, Mihaly Gasparik
PalaeoChron Code	RG/2013/PalaeoChron/23

Samples The osseous point was sampled in April 2015 at the Hungarian National Museum in Budapest, while the anthropogenically modified faunal remains were drilled in September 2015 at the Hungarian Natural History Museum in Budapest. Cons. = indication whether sample had been conserved. Weight = weight sampled in mg.

Ref-no	Sample no.	Type	Species	Level	P-no	%N	Cons.	Weight
Biv-01	Pb 53/111	SBP?	reindeer	lower AH	38804	0.83	Y	294
Biv-02	–	fauna	mammal	lower AH	40757	1.97	?	500
Biv-03	–	fauna	Megaloceros	lower AH	40758	2.38	?	490

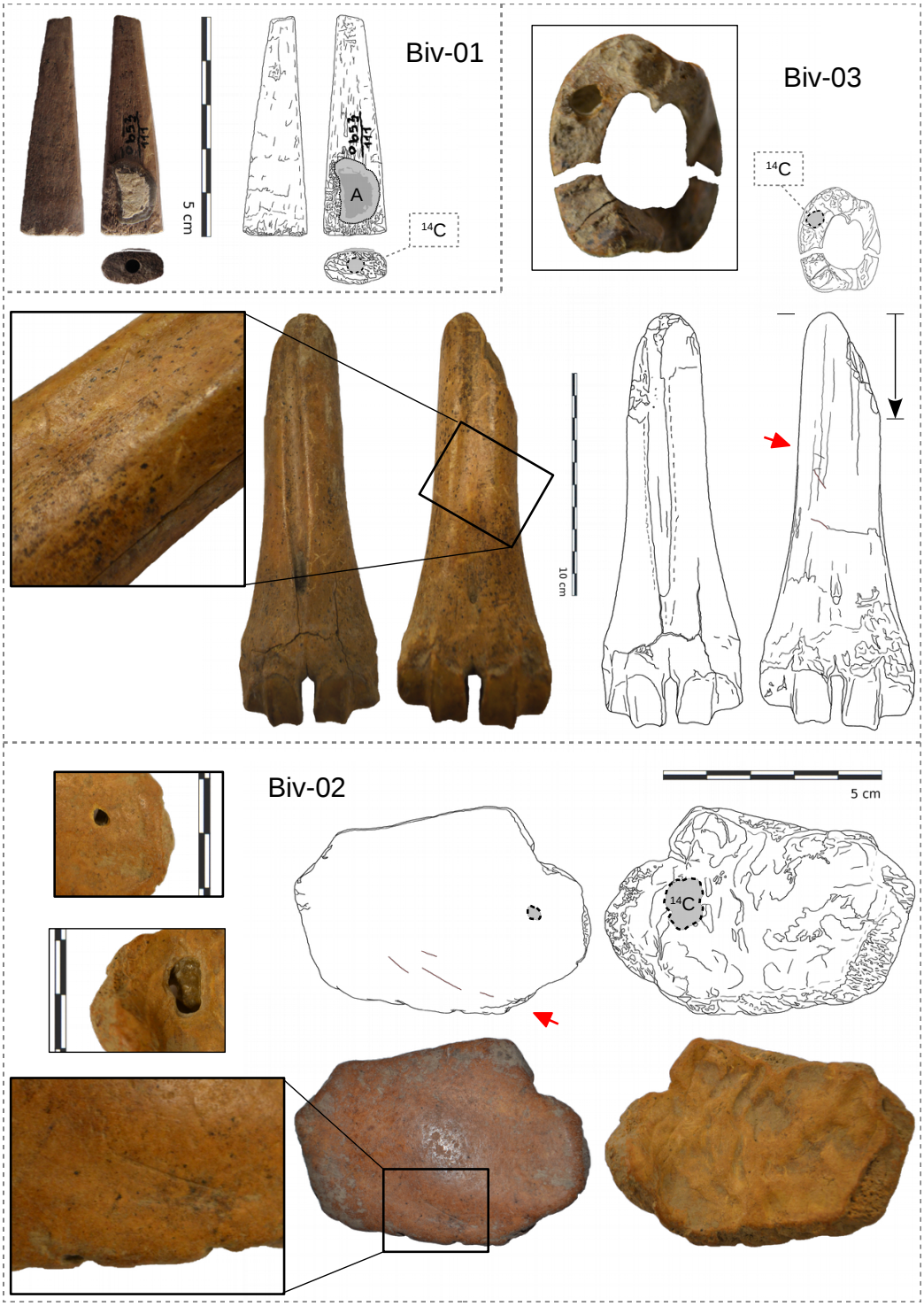


Figure A.2: Bivak: Biv-01 – Antler point with museum alterations, key-hole drilling, 28,000 ± 500 BP (OxA-X-2726-50); Biv-02 – cut-marked bone, 42,400 ± 1800 BP (OxA-35422); Biv-03 – cut-marked bone, 40,800 ± 1500 BP (OxA-35423) (illustrations & photos: R. Hopkins).

A.2 Bukovac, Croatia

Environment	cave
Latitude	45.361 N
Longitude	14.753 E
Altitude	864 m a.s.l.
Excavations	1911
Collaborator	András Markó
PalaeoChron Code	RG/2013/PalaeoChron/25

Samples The osseous point was sampled April 2015 at the Hungarian National Museum in Budapest. Cons. = indication whether sample had been conserved. Weight = weight sampled in mg.

Ref-no	Sample no.	Type	Species	Level	P-no	%N	Cons.	Weight
Buk-01	Pb 602	MBP	reindeer	3	38806	3.05	Y	361

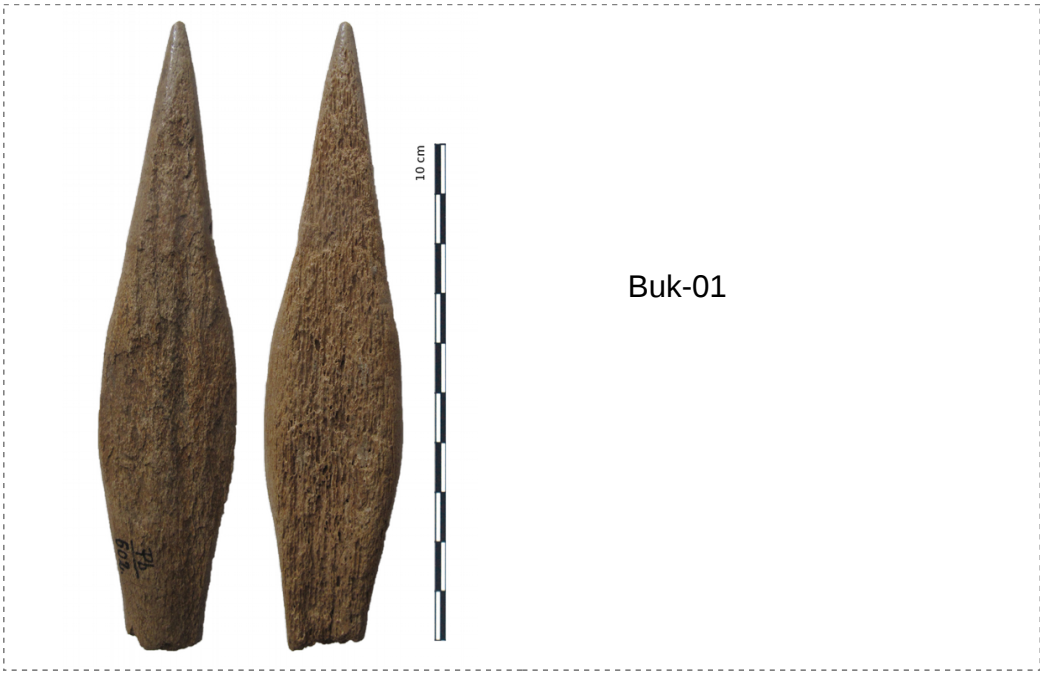


Figure A.3: Bukovac: Buk-01 – massive based antler point, key-hole drilling, 31100 ± 520 BP (OxA-X-2732-11) (illustrations & photos: R. Hopkins).

A.3 Dubočka-Kozja, Serbia

Environment	rockshelter/cave
Latitude	44° 32' 44.0" N
Longitude	21° 46' 08.4" E
Altitude	338 m a.s.l.
Excavations	2013, 2017
Collaborator	Dušan Borić & Emanuela Cristiani
PalaeoChron Code	RG/2013/PalaeoChron/88

Samples were collected from the 2013 excavation season and have not been treated with conservation substances prior to dating. In the following, all initially collected samples, their context and their %N results (if available) are listed. Undated samples are marked grey. Co-ordinates are given in metres. Mark indicates whether the marks found on the bone are anthropogenic: Y = yes, L = likely, U = unlikely. Final samples for dating were selected according to their context information and security of anthropogenic modification. For further dating details see main text, catalogue and table 9.2.

Ref-no	Trench	Quadrant	Layer	Co-ord.	Mark	P-no	%N
DK-01	1/2013	100/99	(2), spit 3	x=997.58, y=996.64, z=387.80	Y	43115	2.78
DK-02	1/2013	100/98/A	(4), spit 6		U		2.45
DK-03	1/2013	101/101/D	(5), spit 5		L	43116	1.66
DK-04	1/2013	100/99/C	(4), spit 5		U		1.74
DK-05	1/2013	100/101/A	(4), spit 3		U		0.47
DK-06	1/2013	101/101/A	(2), spit 2		L	43117	1.05
DK-07	1/2013	101/100	(?), spit 1		U		1.98
DK-08	1/2013	101/101	(1), spit 1		L	43118	0.78
DK-09	1/2013	101/100/D	(4), spit 5		Y	43119	1.76
DK-10	1/2013	100/101/B	(4), spit 4		U		2.53
DK-11	1/2013	100/101/D	(2), spit 2		U		0.23
DK-12	1/2013	100/99/C	(4), spit 6		U		1.43
DK-13	1/2013	101/100/D	(4), spit 6		U		3.48

Ref-no	Trench	Quadrant	Layer	Co-ord.	Mark	P-no	%N
DK-14	1/2013	100/98/D	(?), spit 7		U		1.65
DK-15	1/2013	100/98/D	(?), spit 7		U		2.99
DK-16	1/2013	100/98/D	(?), spit 7		U		1.53
DK-17	1/2013	101/99	(3), spit 5 (cleaning)		L	43120	1.88
DK-18	1/2013	100/101/B	(4), spit 5		U		1.95
DK-19	1/2013	101/100/C	(4), spit 4		U		1.12
DK-20	1/2013	101/99	(4), spit 4		Y	43121	1.42
DK-21	1/2013	100/101/D	(2), spit 3		U	43122	1.41
DK-22	1/2013	100/101/A	(2), spit 2		U	43123	0.59
DK-23	1/2013	101/101/A	(2), spit 2		U		0.27
DK-24	1/2013	100/101/A	(4), spit 3		Y	43124	2.00
DK-25	1/2013	100/98/A	(4), spit 6		U		1.33
DK-26	1/2013	101/99/D	(4), spit 5		U		1.49
DK-27	1/2013	100/101/A	(4), spit 5		U		-
DK-28	1/2013	100/98/B	(4), spit 5		U		1.65
DK-29	1/2013	100/98	(1), spit 1		U		-
DK-30	1/2013	100/99	(4), spit 4		U		1.88
DK-31	1/2013	100/99	(4), spit 4		U		1.72
DK-32	1/2013	100/99	(4), spit 4		Y	43125	1.71
DK-33	1/2013	100/99	(4), spit 4		U		-
DK-34	1/2013	100/99	(4), spit 4		U		2.67
DK-35	1/2013	100/98	(4), spit 6		U		1.64
DK-36	1/2013	101/98/B	(4), spit 5		Y	43126	2.14
DK-37	1/2013	100/98/C	(4), spit 8		U		1.70
DK-38	1/2013	100/93/A	(4), spit 8		U		1.04
DK-39	1/2013	100/93/A	(4), spit 8		Y	43127	1.24
DK-40	1/2013	101/98/B	(?), spit 8		U		1.38

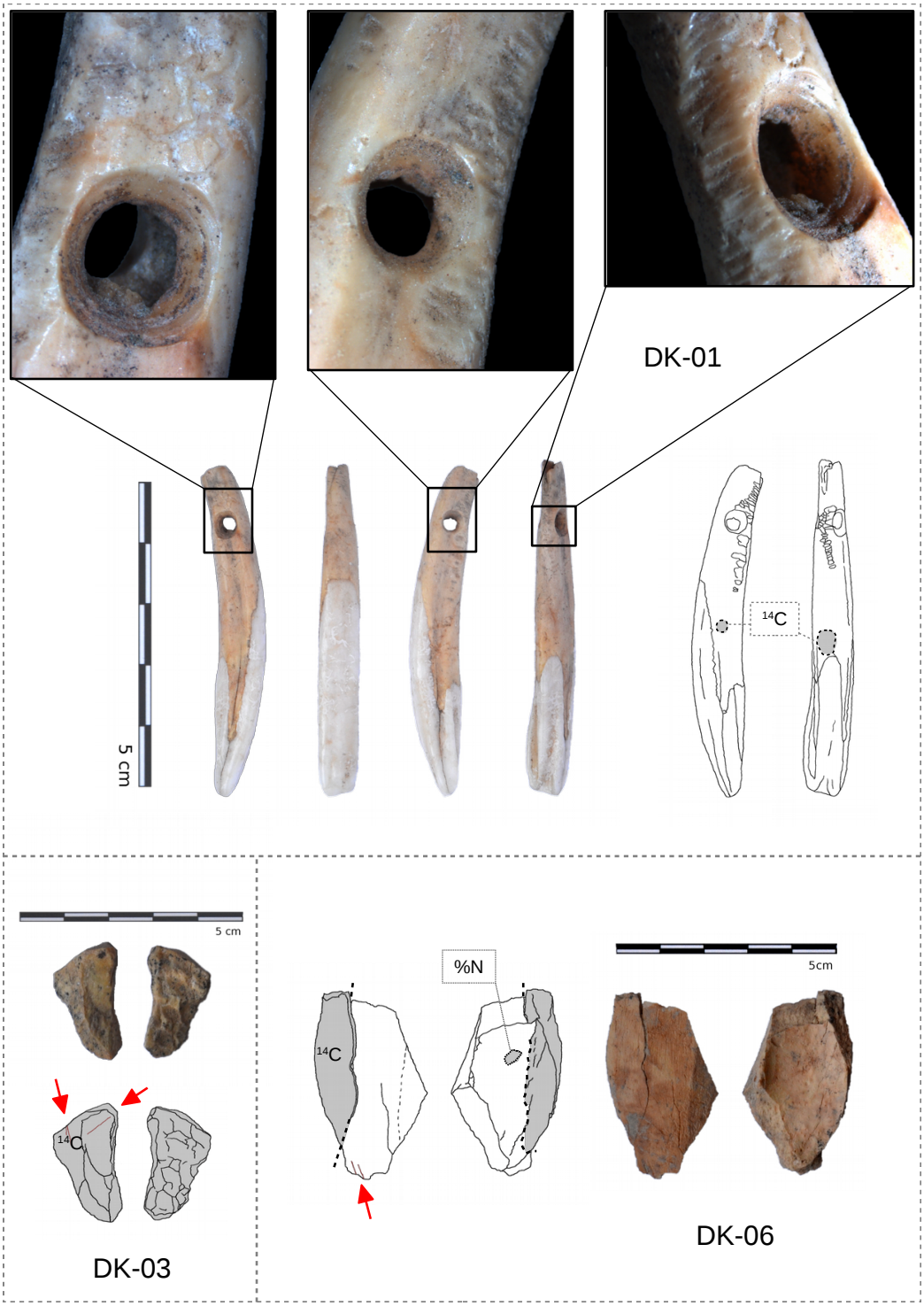


Figure A.4: Dubočka Kozja: DK-01 – tooth pendant, layer (2), spit 3, key-hole drilling, 4,456 ± 29 BP (OxA-35584); DK-03 – cut-marked bone, layer (5), spit 5, $> 45,200$ BP (OxA-35585); DK-06 – cut-marked bone, layer (2), spit 2, 7,308 ± 36 BP (OxA-35586). Illustrations & photos: R. Hopkins; macro-photography: E. Cristiani.

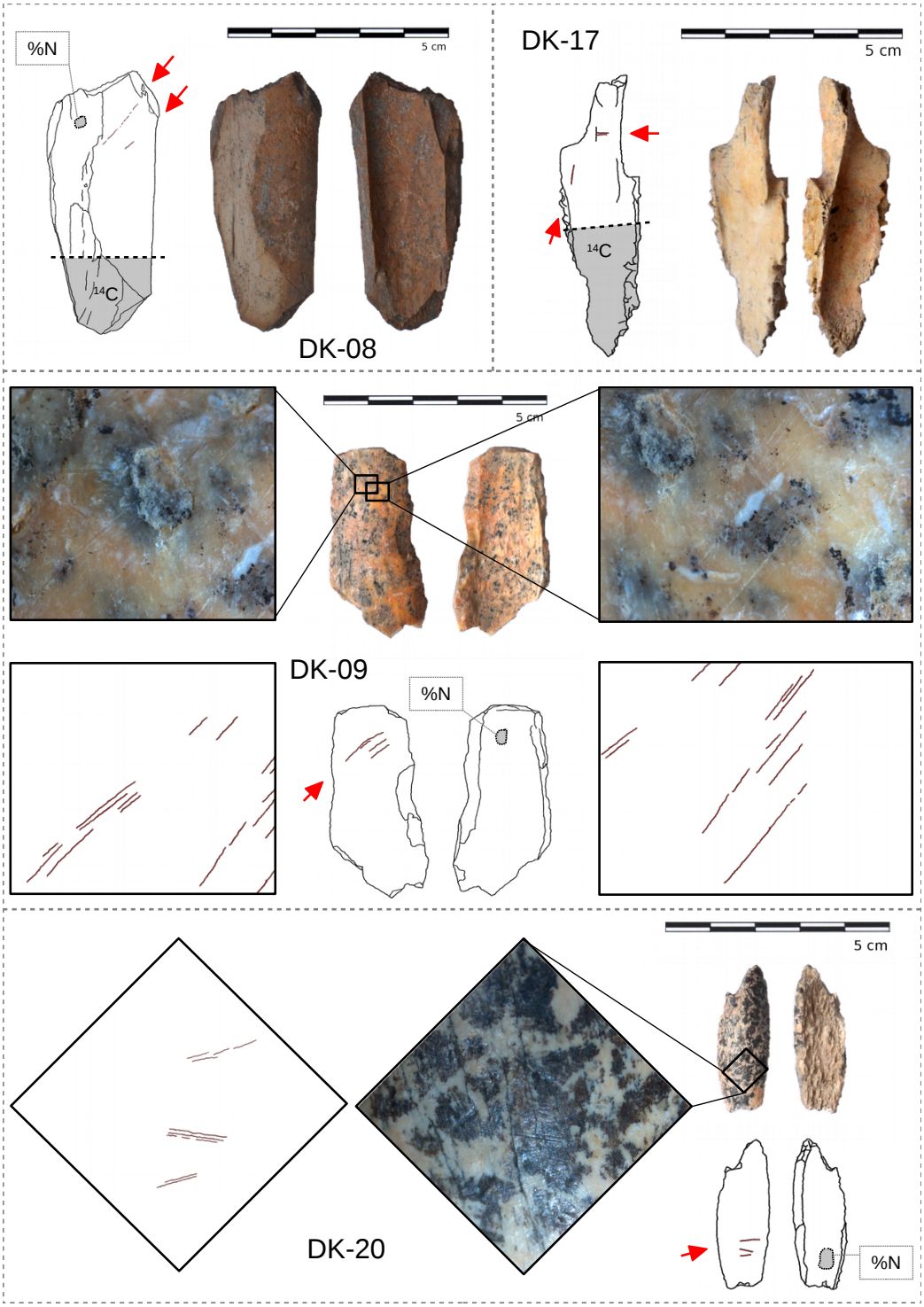


Figure A.5: Dubočka Kozja: DK-08 – cut-marked bone, layer (1), spit 1, 5,415± 31 BP (OxA-35587); DK-09 – cut-marked bone, layer (4), spit 5, undated; DK-17 – cut-marked bone, layer (3), spit 5, 34,500±600 BP (OxA-35588) & 34,150±600 BP (OxA-35589); DK-20 – cut-marked bone, layer (4), spit 4, undated. Illustrations & photos: R. Hopkins; macro-photography: E. Cristiani.

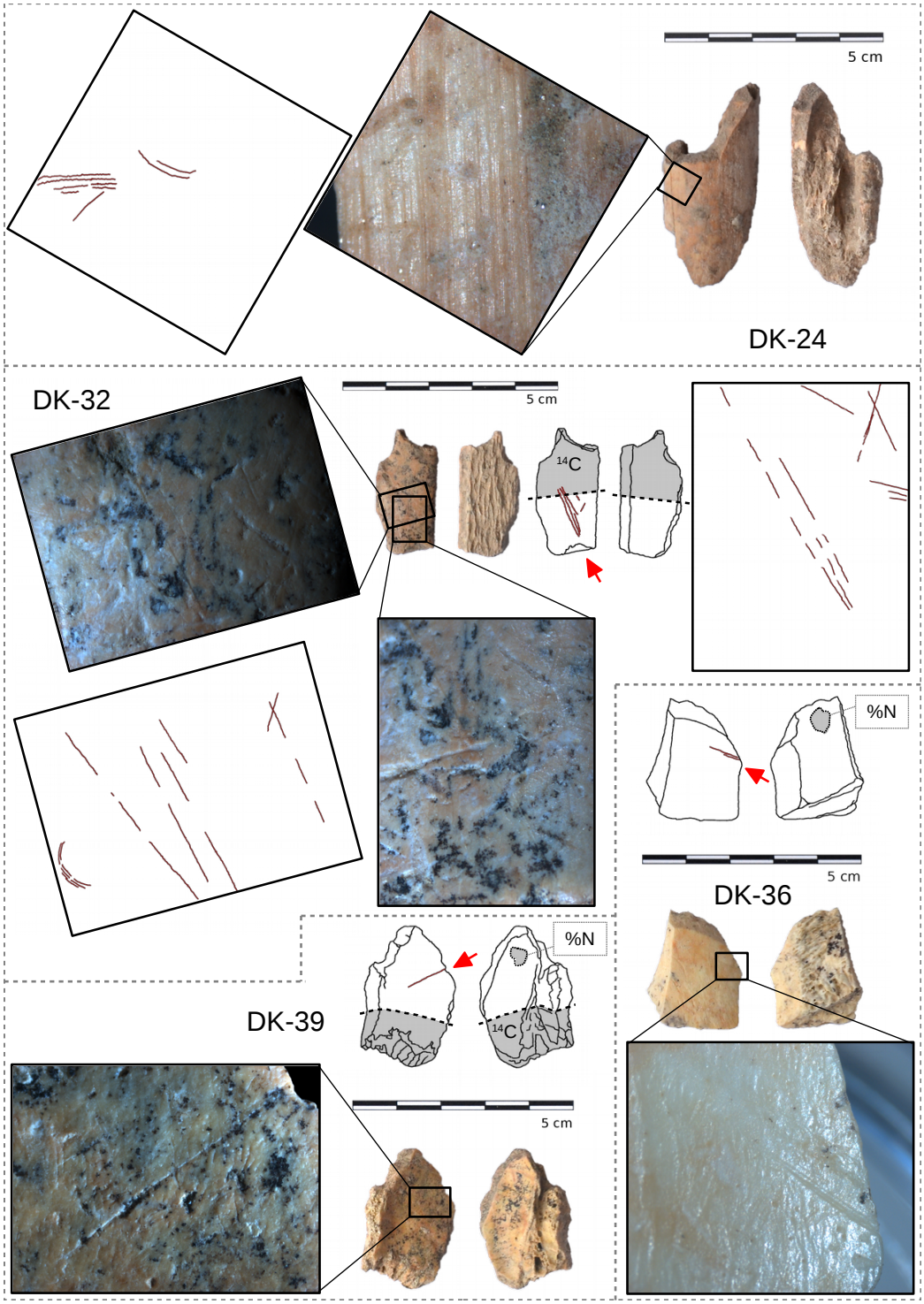


Figure A.6: Dubočka Kozja: DK-24 – cut-marked bone, layer (4), spit 3, undated; DK-32 – cut-marked bone, layer (4), spit 4, $35,500 \pm 600$ BP (OxA-35590); DK-36 – cut-marked bone, layer (4), spit 5, undated; DK-39 – cut-marked bone, layer (4), spit 8, $> 50,000$ BP (OxA-35591). Illustrations & photos: R. Hopkins; macrophotography: E. Cristiani.

A.4 Dzeravá Skala, Slovakia

Other known name	Pálffy barlang
Environment	cave
Latitude	48.497 N
Longitude	17.325 E
Altitude	450 m a.s.l.
Excavations	1912/1913, 1950, 2002/2003
Collaborators	Bibiána Hromadová, L'ubomíra Kamínska, Anna Durisova, András Markó
PalaeoChron Code	RG/2013/PalaeoChron/24

Samples The first osseous point was sampled in April 2015 at the Hungarian National Museum in Budapest. Subsequent osseous points were sampled for %N analysis in August 2015 in Nitra (SAV), and for dating in spring 2016. Anthropogenically modified faunal remains were collected in August 2015 and August 2016 at the Natural History Museum in Bratislava. For reference numbers > 48 the bone fragments were brought to Oxford and sampled at ORAU, not in Slovakia. Undated samples are marked grey.

Ref-no	Item	Inv-no.	Sq.	Layer	Depth (cm)	P-no.	%N	Weight
Der-01	point	Pb 579	4/5*	–	–	38805	0.10	
Der-02	point	F13/145	F13	7	–	–	0.16	
Der-03	fauna	E11/130	E11	11	175-185	40314	0.91	
Der-04	fauna	E10/92	E10	9	115-120	40315	2.11	
Der-05	fauna	E10/91	E10	9	115-120	40316	3.17	
Der-06	fauna	E10/93	E10	9	120-125	40317	2.79	
Der-07	fauna	E11/105	E11	9	135-140	40318	2.08	
Der-08	fauna	E11/92	E11	9	105-110	40319	1.04	
Der-09	fauna	E11/97	E11	9	130-135	40320	1.06	
Der-10	fauna	E11/120	E11	9	150-155	40321	1.03	
Der-11	fauna	E11/76	E11	9	120-125	40322	3.36	
Der-12	fauna	F13/108	F13	7	115-120	40323	1.93	
Der-13	fauna	PP2/412	Profile	7	119	40324	2.07	
Der-14	fauna	E10/107	E10	5	110	40325	3.41	
Der-15	fauna	E10/107	E10	5	110	40326	2.28	

Ref-no	Item	Inv-no.	Sq.	Layer	Depth (cm)	P-no.	%N	Weight
Der-16	fauna	E10/126	E10	5	–	40327	3.33	
Der-17	fauna	E10/105	E10	5	100-105	40328	3.22	
Der-18	fauna	E10/113	E10	9	125-130	40329	1.65	
Der-19	fauna	F10/98	F10	9	125-130	40330	3.17	
Der-20	fauna	E10/1058	E10	9	125	40331	3.12	
Der-21	fauna	E10/85	E10	8	110-115	40332	1.98	
Der-22	fauna	PP2/343	Profile	4	57	40333	0.78	
Der-23	fauna	E10/982	E10	4	82	40334	2.26	
Der-24	fauna	PP1/1027	–	4a	114	40335	3.00	
Der-25	fauna	E11/127	E11	9	170-175	40336	2.78	
Der-26	fauna	E11/61	E11	4	80-85	40337	2.69	
Der-27	point	F11/65	F11	3	65-70	–	0.12	
Der-28	fauna	F11/143	F11	11	185-190	40338	1.64	
Der-29	point	–	–	–	–	41370	1.80	
Der-29	point	–	–	–	–	41370	1.80	
Der-30	point	II A5/105	–	–	–	–	0.30	
Der-31	point	Ivb/160?	–	–	–	–	0.28	
Der-32	point	III3/160?	–	–	–	41371	0.84	
Der-33	point	Ive/199?	–	–	–	41372	1.00	
Der-34	point	IIA4/175	–	–	–	–	0.55	
Der-35	point	II?/185?	–	–	–	41373	0.68	
Der-36	point	IV.a/168	–	–	–	41374	0.68	
Der-37	point	IV.a/168	–	–	–	–	0.44	
Der-38	point	–	–	–	–	41375	3.06	
Der-39	point	IIIc/155, IIA3/130	–	–	–	41376	1.13	
Der-40	point	IIIa/180	–	–	–	–	0.43	
Der-41	point	–	–	–	–	–	1.90	
Der-42	point	A1/57?	–	–	–	–	1.41	
Der-43	point	–	–	–	–	–	2.69	
Der-44	point	A2/175	–	–	–	–	1.31	
Der-45	point	43	–	–	–	–	0.93	
Der-46	point		–	–	–	–	1.49	
Der-47	point	–	–	–	–	–	0.68	
Der-48	point	–	–	–	–	–	2.90	
Der-49	fauna	–	F9	9	200-210	43101	1.09	
Der-50	fauna	–	F9	11	230-240	–	0.25	
Der-51	fauna	–	E10	11	200-210	–	0.09	
Der-52	fauna	–	F10	11	200-210	–	2.27	
Der-53	fauna	–	F10	11	220-230	42187	1.25	

Ref-no	Item	Inv-no.	Sq.	Layer	Depth (cm)	P-no.	%N	Weight
Der-54	fauna	–	E9	11	200-210	42188	0.37	
Der-55	fauna	F14/39	F14	3	40-45	42189	2.20	
Der-56	fauna	F14/74	F14	6	85-90	42190	1.89	
Der-57	fauna	F14/105	F14	9	160-170	42191	0.66	
Der-58	fauna	F14/124	F14	9	140-150	42192	0.26	
Der-59	fauna	F14/114	F14	11	190-200	43102	0.90	
Der-60	fauna	F13/99	F13	4	85-90	43103	1.79	
Der-61	fauna	F13/75	F13	4	55-60	43104	3.08	
Der-62	fauna	F13/75	F13	4	55-60	–	0.10	
Der-63	fauna	F13/109	F13	7	120-125	–	1.76	
Der-64	fauna	F13/117	F13	7	120-130	–	1.62	
Der-65	fauna	F13/145	F13	7	130-140	–	0.50	
Der-66	fauna	F13/150	F13	9	150-160	42193	0.23	
Der-67	fauna	F13/103	F13	4b	95-100	–	0.13	
Der-68	fauna	F13/102	F13	4b	95-100	42194	0.29	
Der-69	fauna	E13/73	E13	9	150-160	–	0.22	
Der-70	fauna	E13/73	E13	9	150-160	–	0.18	
Der-71	fauna	E13/86	E13	11	220-230	43105	1.12	
Der-72	fauna	E13/86	E13	11	220-230	43106	0.71	
Der-73	fauna	E13/59	E13	9	170-180	43107	0.80	
Der-74	fauna	E13	E13	9	160-170	43108	1.01	
Der-75	fauna	E13/37	E13	4	85-90	–	0.43	
Der-76	fauna	E13/23 or E13/24	E13	3	45-50 or 50-55	–	0.84	
Der-77	fauna	E13/61	E13	7a	110-115	42195	0.45	
Der-78	fauna	E13/68	E13	11	190-200	–	0.32	
Der-79	fauna	E13/68	E13	11	190-200	–	0.34	
Der-80	fauna	F13/160	F13	11	190-200	42196	0.50	
Der-81	fauna	F13/180	F13	9	160-170	–	0.15	
Der-82	fauna	F13/128	F13	9	170-180	–	0.41	
Der-83	fauna	F13/107	F13	7	115-120	–	1.44	
Der-84	fauna	F13/144	F13	9	140-150	–	0.79	
Der-85	fauna	F13/144	F13	9	140-150	–	0.51	
Der-86	fauna	F13/144	F13	9	140-150	–	0.22	
Der-87	fauna	F14/62	F14	4a	70-75	43109	1.39	
Der-88	fauna	F14/59	F14	4	60-65	42197	1.74	
Der-89	fauna	F14/54	F14	4	55-60	–	0.08	
Der-90	fauna	F14/94	F14	7	120-130	–	0.18	
Der-91	fauna	F14/65	F14	4	75-80	–	0.16	
Der-92	fauna	F14/94	F14	7	120-130	–	0.13	

Ref-no	Item	Inv-no.	Sq.	Layer	Depth (cm)	P-no.	%N	Weight
Der-93	fauna	F10/131	F10	11	240-250	43110	2.30	
Der-94	fauna	F11/108	F11	4a	105-110	–	2.50	
Der-95	fauna	F11/105	F11	4a	95-100	–	0.62	
Der-96	fauna	F11/105	F11	4a	95-100	–	3.22	
Der-97	fauna	F11/84	F11	5a	105-110	–	2.49	
Der-98	fauna	F11/84	F11	5a	105-110	–	1.93	
Der-99	fauna	E11/64	E11	4a	85-90	–	0.34	
Der-100	fauna	E11/110	E11	5a	145-150	42198	0.93	
Der-101	fauna	E10/108	E10	5a	105-110	42199	1.46	
Der-102	fauna	E14/48	E14	11	200-210	42200	0.19	

A.5 Istállóskő, Hungary

Environment	cave
Latitude	48° 04' 18" N
Longitude	20° 25' 08" E
Altitude	546 m a.s.l.
Excavations	1912–1917, 1925, 1927, 1929, 1938, 1947–1965, 2000, 2004
Collaborators	András Markó, Mihaly Gasparik
PalaeoChron Code	RG/2013/PalaeoChron/20

Samples Osseous points with reference numbers 1–8 were drilled on 21 April 2015, and the remaining ones on 17 September 2015 at the Hungarian National Museum in Budapest. The anthropogenically modified faunal remains were sampled on 16 September 2015 at the Hungarian Natural History Museum in Budapest. Cons. = indication whether sample had been conserved. Weight = weight sampled in mg. Samples without a radiocarbon date are marked grey.

Ref-no	Sample no.	Type	Species	Level	P-no	%N	Cons.	Weight
Istall-01	Pb 50/90 (117)	point	reindeer	upper	38779	3.59	Y	297
Istall-02	Pb 50/159	point	reindeer	upper	38780	3.28	Y	179
Istall-03	Pb 51/13	point	reindeer	lower	38781	3.10	Y	296
Istall-04	Pb 50/53	point	reindeer	lower	38782	2.85	Y	150
Istall-05	Pb 50/39	point	reindeer	lower	38783	2.98	Y	224
Istall-06	Pb 50/93	point	reindeer	upper	38784	2.61	Y	338
Istall-07	Pb 51/30	point	reindeer	lower	38785	3.53	Y	250
Istall-08	Pb 51/86	point	reindeer	lower	38786	3.64	Y	204
Istall-09	V.59/377	fauna	bison	upper	40686	3.47	Y	710
Istall-10	V.58/165	fauna	ursus	lower	40687	3.42	Y	700
Istall-11	–	fauna	equus	upper	40688	2.61	Y	500
Istall-13	V.59/473	fauna	equus	upper	40689	3.73	Y	710
Istall-14	V.59/369	fauna	capra ibex	lower	40690	0.04	Y	1200
Istall-16	Pb 50/99	point	–	upper	40691	3.26	Y	340
Istall-18	167/914.22	point	–	upper?	40692	3.13	Y	460

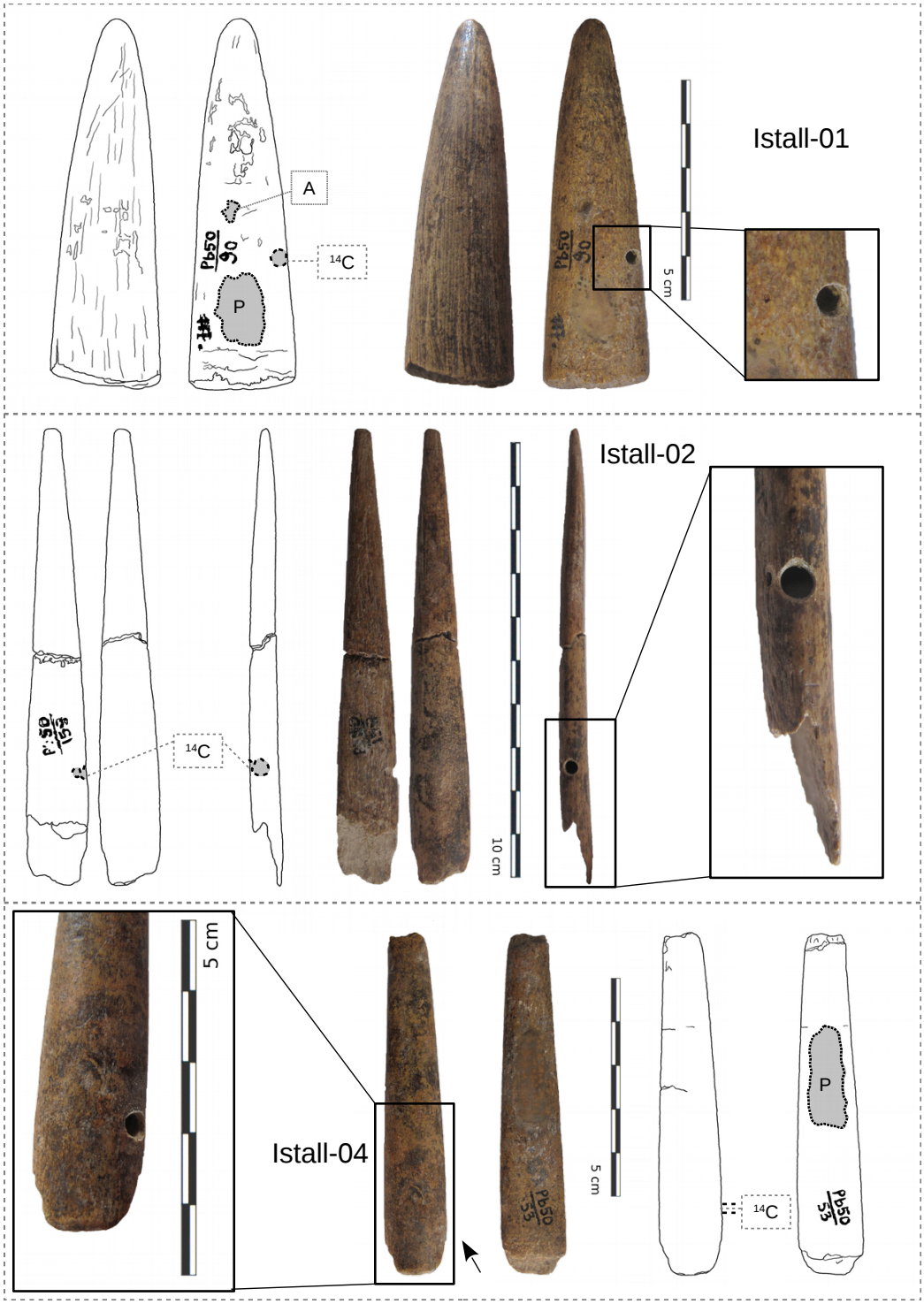


Figure A.7: Istállóskő: Istall-01 – lozangic point, key-hole drilling, 33450 ± 600 BP (OxA-35414); Istall-02 – split-based point, key-hole drilling, 35800 ± 1200 BP (OxA-35382); Istall-04 – split-based point, key-hole drilling, 36200 ± 900 BP (OxA-35383). Photos & illustrations: R. Hopkins.

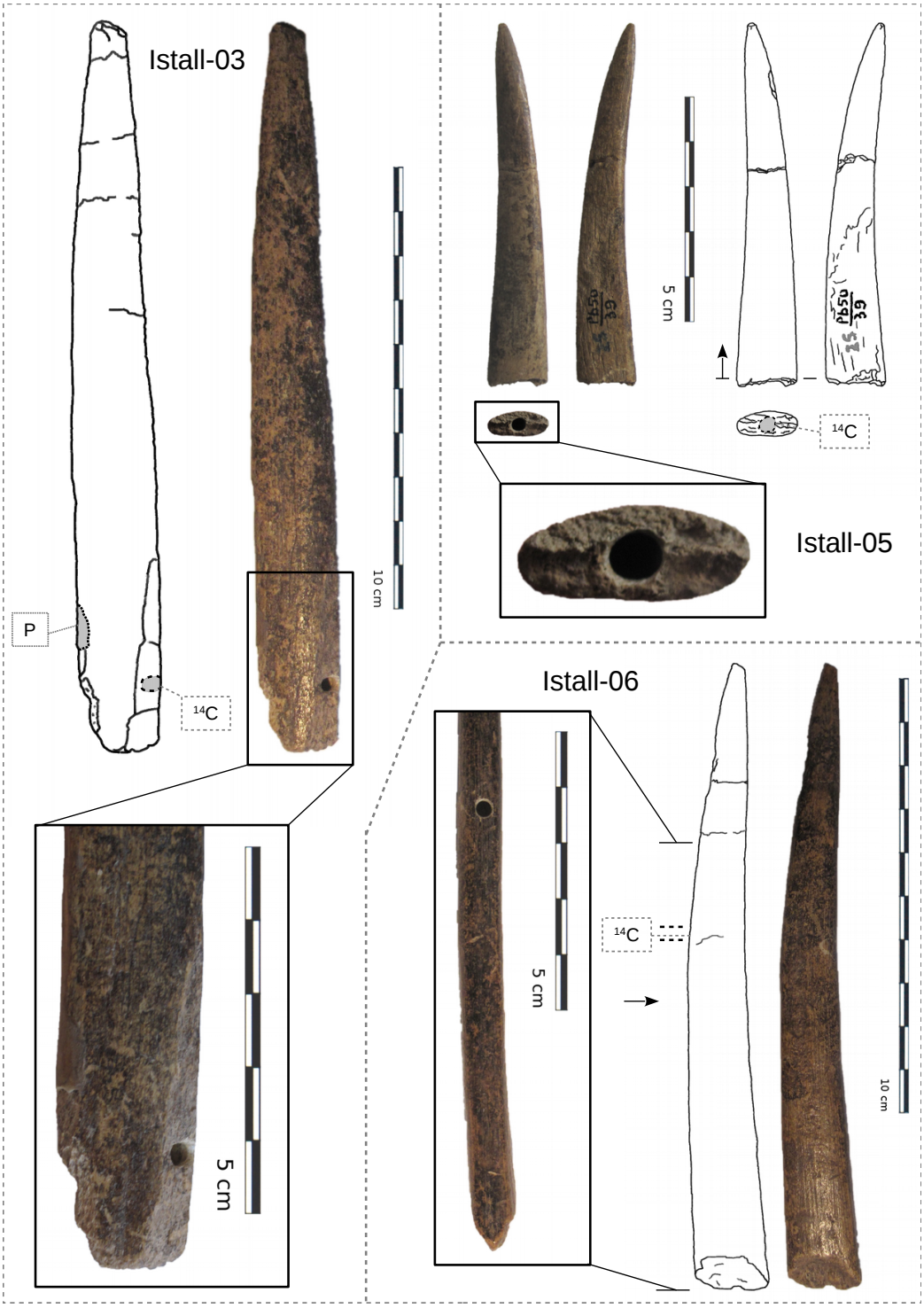


Figure A.8: Istállóskő: Istall-03 – lozangic point, key-hole drilling, 32850 ± 500 BP (OxA-35522); Istall-05 – split-based point (?), key-hole drilling, 36100 ± 800 BP (OxA-35415); Istall-06 – massive-based point, key-hole drilling, 33200 ± 800 BP (OxA-X-2716-11). Photos & illustrations: R. Hopkins.

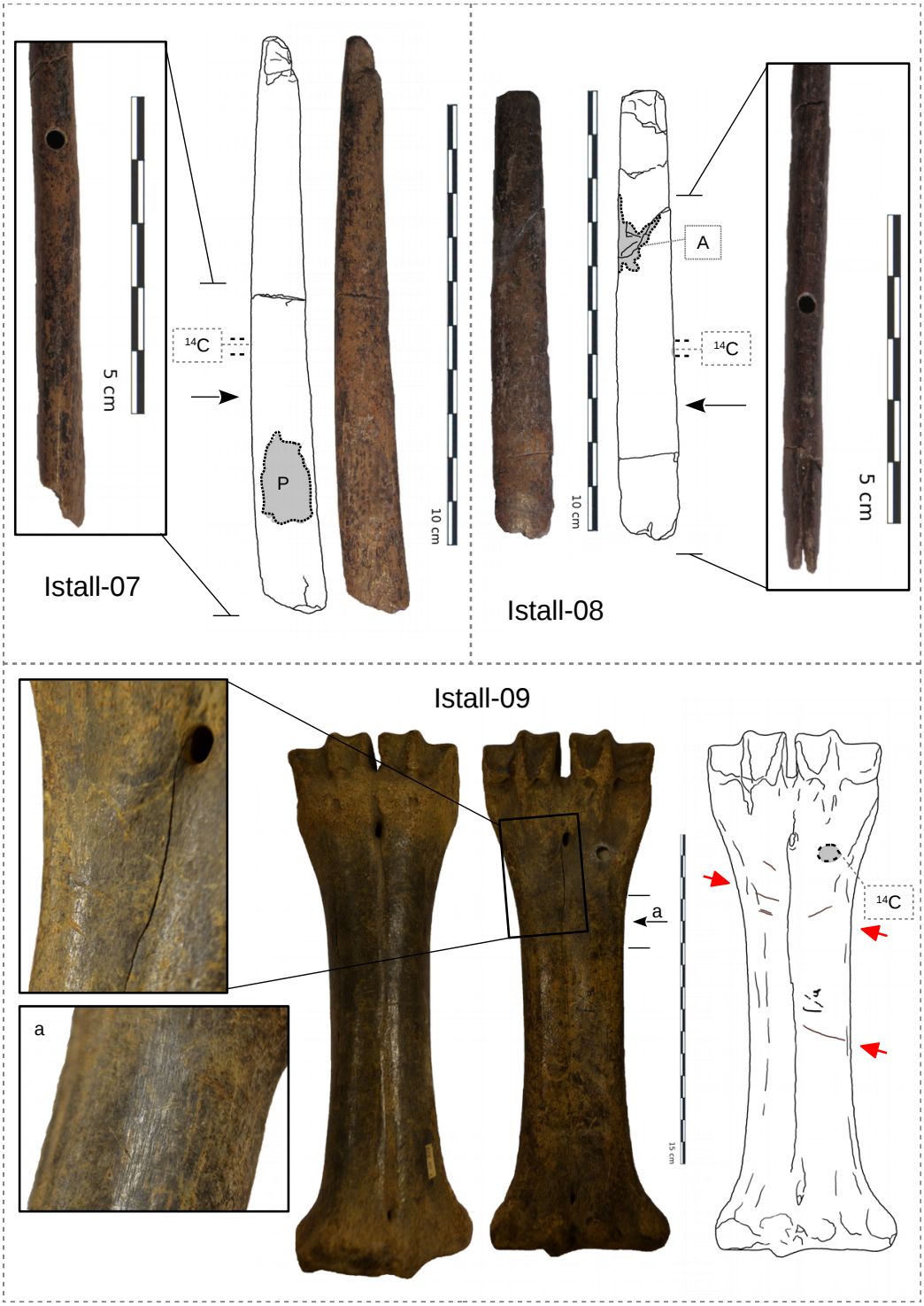


Figure A.9: Istállóskő: Istall-07 – antler point, key-hole drilling, 37200 ± 1200 BP (OxA-35384); Istall-08 – split-based point, key-hole drilling, 37700 ± 1600 BP (OxA-35385); Istall-09 – cut-marked bone, key-hole drilling, 35000 ± 700 BP (OxA-34402). Photos & illustrations: R. Hopkins.

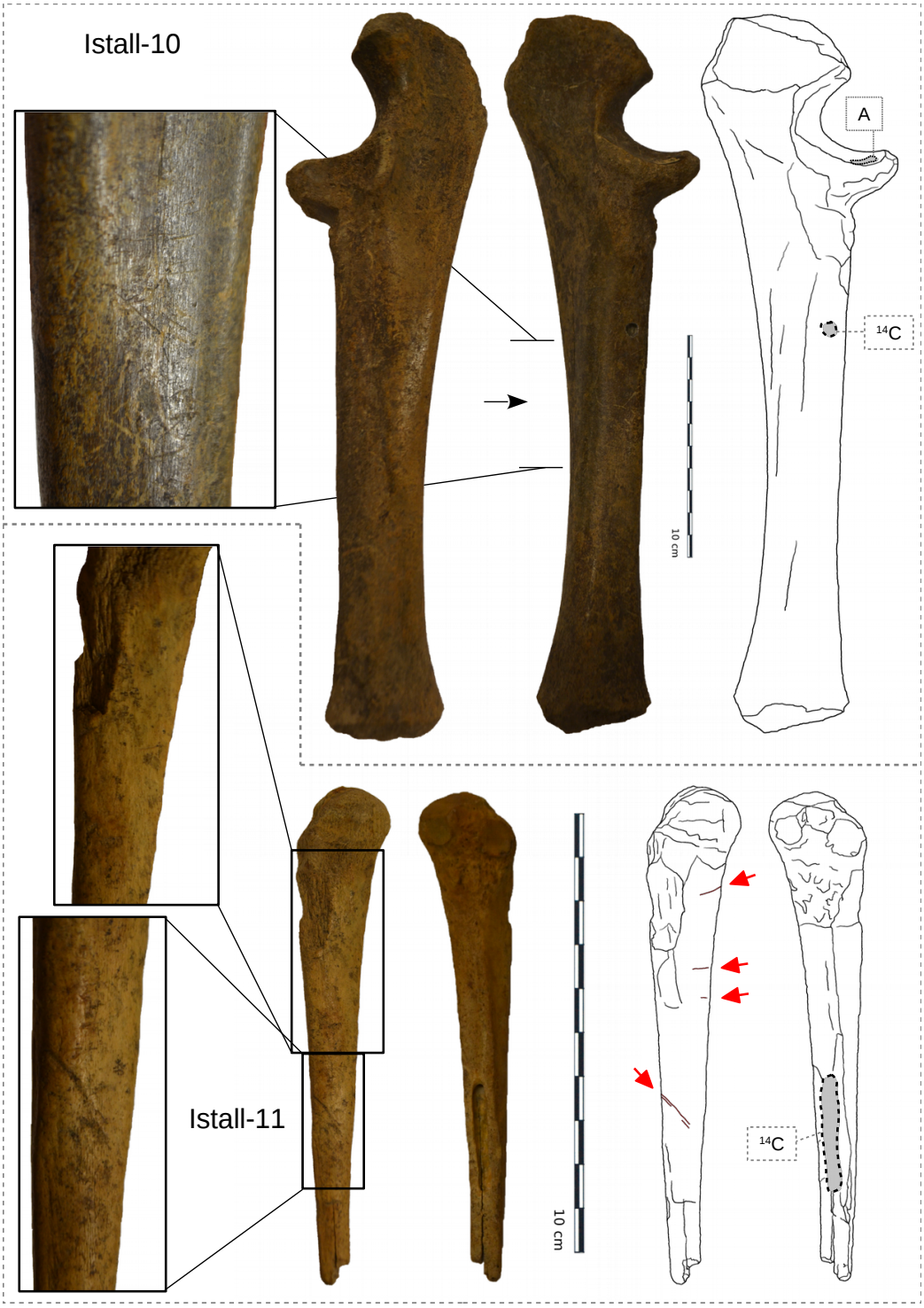


Figure A.10: Istállóskő: Istall-10 – cut-marked bone, key-hole drilling; Istall-11 – cut-marked bone, 25610 ± 220 BP (OxA-34403). Photos & illustrations: R. Hopkins.

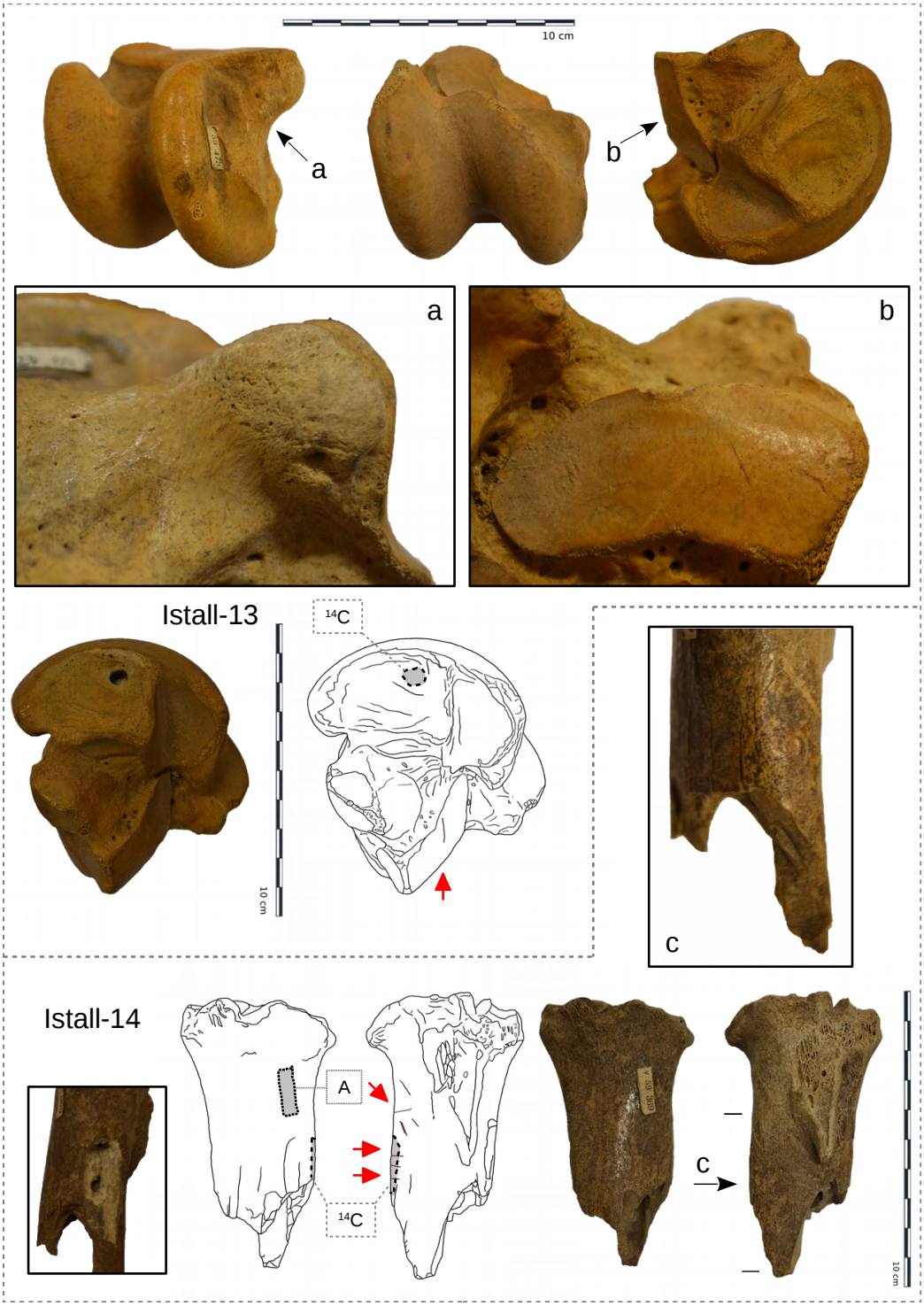


Figure A.11: Istállóskő: Istall-13 – cut-marked bone, key-hole drilling, 26520 ± 230 BP (OxA-34404); Istall-14 – cut-marked bone. Photos & illustrations: R. Hopkins.

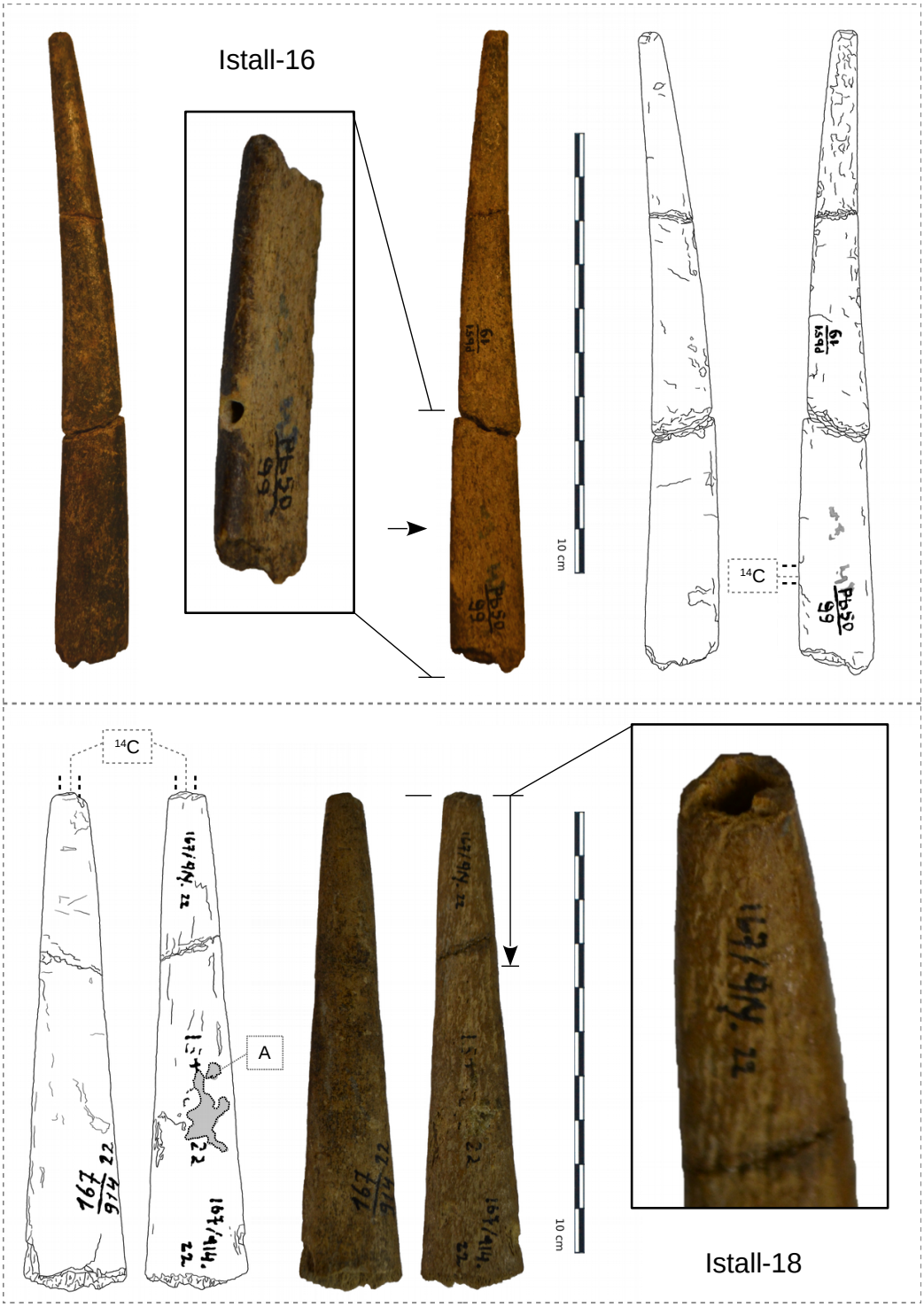


Figure A.12: Istállóskő: Istall-16 – split-based (?) point, key-hole drilling, 36500 ± 900 BP (OxA-35421); Istall-18 – split-based point, key-hole drilling, 33450 ± 550 BP (OxA-34771). Photo & illustrations: R. Hopkins.

A.6 Jankovich, Hungary

Environment	cave
Latitude	47° 43' 26" N
Longitude	18° 34' 31" E
Altitude	346 m a.s.l.
Excavations	1913–1918, 1925, 1956
Collaborators	András Markó
PalaeoChron Code	RG/2013/PalaeoChron/22

Samples All osseous points were sampled on 21 April 2015 at the Hungarian National Museum in Budapest. Weight = weight sampled in mg. Samples without a radiocarbon date are marked in grey.

Ref-no	Sample no.	Type	Species	Excavation	P-no	%N	Cons.	Weight
Jank-01	Pb 570	point	reindeer	1915	38801	2.81	Y	181
Jank-02	Pb 569	point	reindeer	1915	38800	2.05	Y	405
Jank-03	Pb 572	point	reindeer	1915	38803	3.41	Y	389
Jank-04	Pb 571	point	reindeer	1915	38802	0.11	Y	475
Jank-05	Pb 568	point	reindeer	1915	38799	0.83	Y	327
Jank-06	Pb 567	point	reindeer	1915	38798	1.82	Y	338

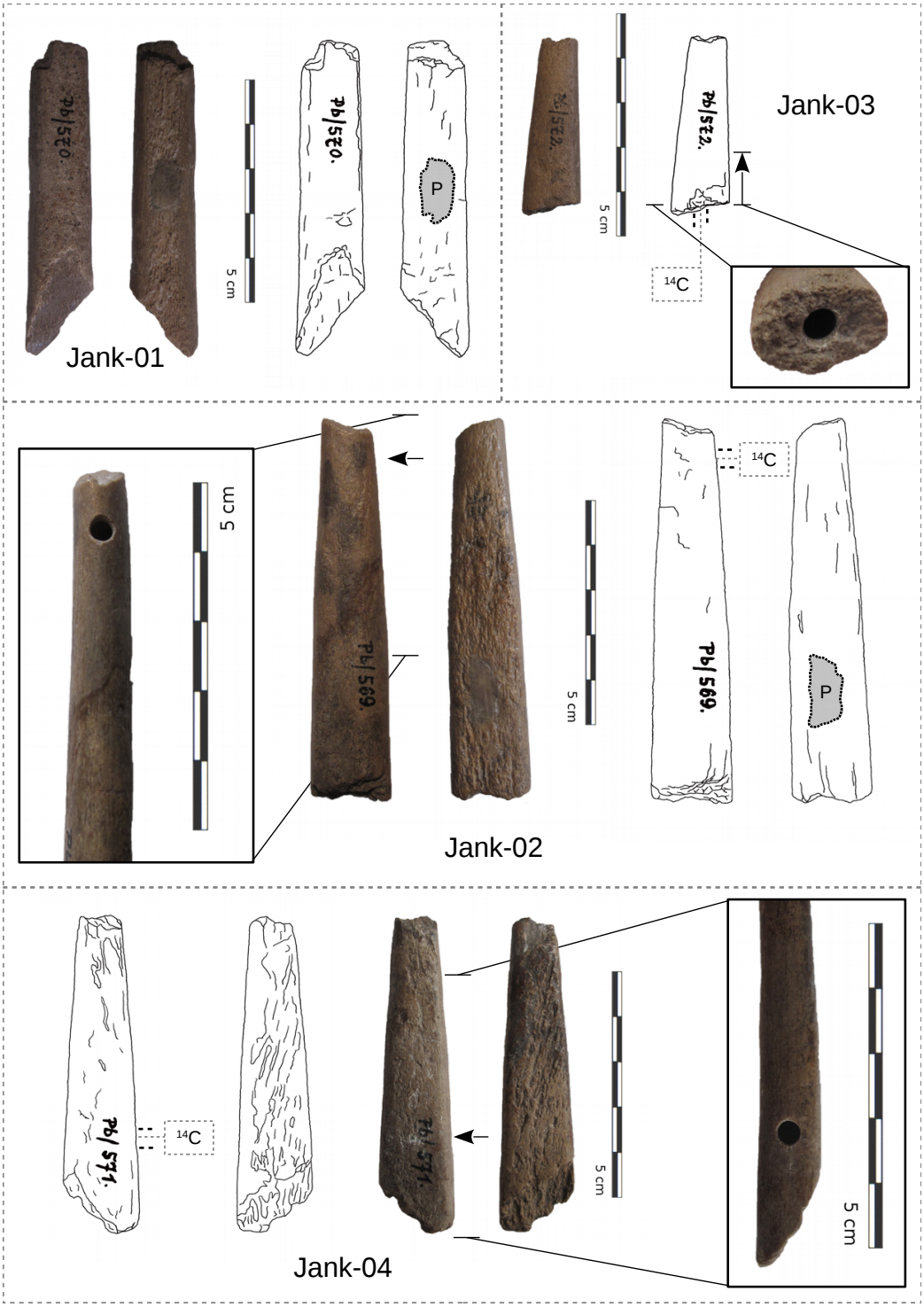


Figure A.13: Jankovich: Jank-01 – antler point, key-hole drilling, 31800 ± 1000 BP (OxA-X-2716-49); Jank-02 – antler point, key-hole drilling, 32500 ± 800 BP (OxA-X-2716-48); Jank-03 – antler point, key-hole drilling, 32750 ± 670 BP (OxA-X-2732-10); Jank-04 – antler point, key-hole drilling. Photos & illustrations: R. Hopkins.

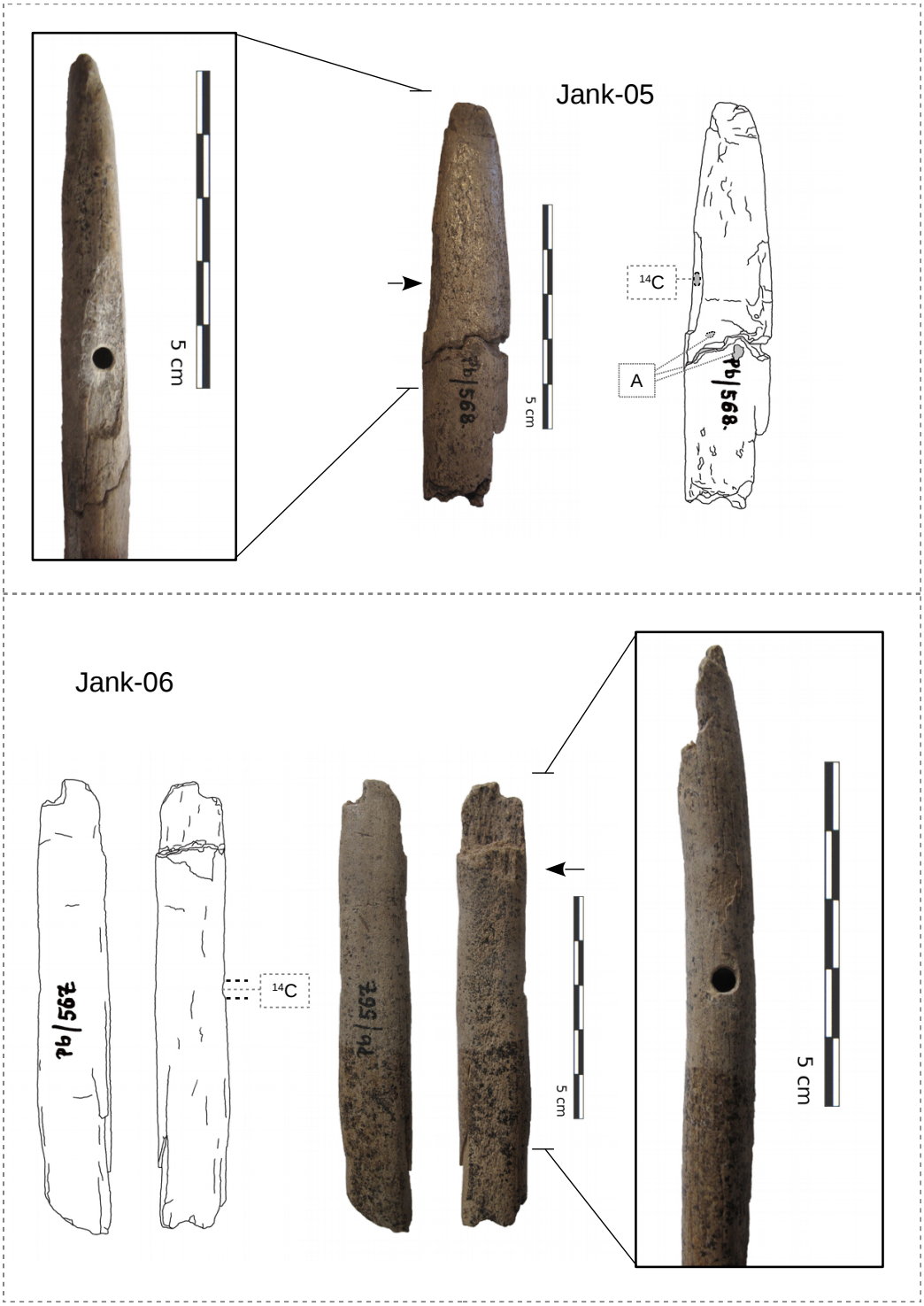


Figure A.14: Jankovich: Jank-05 – antler point, key-hole drilling, 31200 ± 2300 BP (OxA-X-2731-11); Jank-06 – antler point, key-hole drilling, 30800 ± 500 BP (OxA-35386). Photos & illustrations: R. Hopkins.

A.7 Kozarnika, Bulgaria

Original name	Козарника
Environment	cave
Latitude	43.652 N
Longitude	22.702 E
Altitude	481 m a.s.l.
Excavations	1993, 1996-present
Collaborator	Jean-Luc Guadelli, Nikolay Sirakov, Aleta Guadelli
PalaeoChron Code	RG/2013/PalaeoChron/39

Samples were collected at the site in July 2015 and 2016. Charcoal samples were initially collected, but returned in favour of anthropogenically modified bone samples. Samples in grey were not processed for dating. Sampled weight is given in mg.

Ref-no	Item	Sample-no.	Sq.	Layer	Depth (cm)	%N	Weight
Kz-02	faunal	D9-89	D9	III	370-375	0.13	
Kz-03	faunal	D7-92	D7	III	380-385	0.49	
Kz-05	faunal	D8-164	D8	III/IVa	385-390	0.14	
Kz-06	faunal	E9-343	E9	4 = IVa	390-393	1.71	
Kz-07	faunal	D8-270	D8	4 = IVa	395-400	1.54	
Kz-08	faunal	E9-477	E9	4 = IVa	393-395	1.92	
Kz-09	faunal	E9-303	E9	4 = IVa	390-393	0.63	
Kz-10	faunal	E7-306	E7	4 = IVa	393-395	2.03	
Kz-11	faunal	E7-313	E7	4 = IVa	393-395	1.40	
Kz-12	faunal	E9-1035	E9	4 = IVb	405-410	0.11	
Kz-13	faunal	E10-595	E10	4 = IVb	410-415	2.55	
Kz-14	faunal	E7-744	E7	4 = IVb	410-415	1.37	
Kz-15	artefact	E10-471	E10	4 = IVb	410-415	0.48	
Kz-16	faunal	D8-455	D8	4 = IVb	405-410	1.74	
Kz-17	faunal	E9-1105	E9	4 = IVb	410-415	2.61	
Kz-18	faunal	E7-779	E7	4 = IVb	410-415	0.31	
Kz-19	faunal	E9-1045	E9	4 = IVb	410-415	2.91	

Ref-no	Item	Sample-no.	Sq.	Layer	Depth (cm)	%N	Weight
Kz-20	faunal	D10-302	D10	4 = IVb	405-410	1.12	
Kz-21	faunal	D8-477	D8	4 = IVb	410-415	0.71	
Kz-22	faunal	E9-1078	E9	4 = IVb	410-415	1.12	
Kz-23	faunal	D10-300	D10	4 = IVb	405-410	3.05	
Kz-24	faunal	F10-n469	F10	5a = V	420-425	2.20	
Kz-25	faunal	F10-549	F10	5a = V	425-430	2.27	
Kz-26	faunal	F8-1094	F8	5a = V	425-430	0.97	
Kz-27	faunal	F10-513	F10	5a = V	425-430	2.46	
Kz-28	artefact	F10-496	F10	5a = V	425-430	0.34	
Kz-29	faunal	F8-936	F8	5a = V	420-425	1.39	
Kz-30	faunal	G10-440	G10	5a = V	425-430	0.15	
Kz-31	faunal	G10-403	G10	5a = V	420-425	0.49	
Kz-32	faunal	F10-556	F10	5a = V	425-430	1.86	
Kz-33	faunal	F10-447	F10	5a = V	420-425	1.18	
Kz-34	faunal	F9-365	F9	5a = V	425-430	2.21	
Kz-35	faunal	F8-1093	F8	5a = V	425-430	1.95	
Kz-36	faunal	G10-428	G10	5a = V	425-430	1.57	
Kz-37	faunal	F8-1012	F8	5a = V	425-430	1.36	
Kz-38	faunal	F8-1169	F8	5b = VI	435-440	0.91	
Kz-39	faunal	F8-1146	F8	5b = VI	430-435	3.01	
Kz-40	faunal	G7-1733	G7	5c = VII	450-455	0.34	
Kz-41	faunal	F6-1542	F6	6/7 = VIII	460-463	0.19	
Kz-42	faunal	F7-1414	F7	5c = VII	445-450	0.50	
Kz-43	faunal	G5-498	G5	5c = VII	440-443	1.37	
Kz-44	faunal	F7-1955	F7	6/7 = VIII	460-465	0.66	
Kz-45	faunal	F10-754	F10	5b = VI	440-445	0.87	
Kz-46	faunal	F9-1054	F9	5c = VII	465-470	0.50	
Kz-47	faunal	F8-1327	F8	5c = VII	445-450	1.97	
Kz-48	faunal	G5-588	G5	5b/5c = VI/VII	440-443	1.68	
Kz-49	faunal	G7-1793	G7	5c = VII	450-455	1.01	
Kz-50	faunal	K844	G11	under 5b	450-455	2.18	
Kz-51	faunal	G7-1359	G7	V-VI	430-435	0.71	
Kz-52	faunal	F5-1949	F5	6/7? = VIII	453-455	1.96	
Kz-53	human	K/1509-1	–	–	–	0.86	
Kz-54	human	K/1509	–	–	–	0.80	
Kz-55	faunal	K/3322-7	–	–	–	0.58	
Kz-56	human	F30-207	F30	–	–	2.22	
Kz-57	artefact	K/3360	–	–	–	0.69	

Ref-no	Item	Sample-no.	Sq.	Layer	Depth (cm)	%N	Weight
Kz-58	point	x150	F30	6/7?	504	0.21	
Kz-78	human	K/1509-5	–	–		0.81	
Kz-79	artefact	E10-683	E10	5a = V	415-420	3.00	
Kz-80	faunal	D8-1517	D8	6/7lp = VIII	458-459	2.15	
Kz-81	faunal	E8-2385	E8	6/7ls = VIII	458-459	0.44	
Kz-82	faunal	E8-2387	E8	6/7ls = VIII	458-459	0.90	
Kz-83	faunal	E7-2241	E7	6/7ls = VIII	461-462	–	
Kz-84	faunal	D7-896	D7	5c = VII	448-450	1.35	
Kz-85	faunal	D7-887	D7	5c = VII	445-448	0.33	
Kz-86	faunal	E7-1612	E7	5c = VII	445-448	5.71	
Kz-87	faunal	E9-2452	E9	5c/6/7 = VII/VIII	450-453	2.62	
Kz-88	faunal	D9-990	D9	5b = VI	445-448	1.83	
Kz-89	faunal	E8-2150	E8	6/7 = VIII	453-455	0.47	
Kz-90	faunal	D9-988	D9	5b = VI	443-445	2.08	
Kz-91	faunal	E9-2819	D9	6/7lp = VIII	458-459	1.45	
Kz-92	faunal	E9-2860	E9	6/7lp = VIII	458-459	2.64	
Kz-93	faunal	E9-2712	E9	6/7lp = VIII	455-458	0.91	
Kz-94	faunal	E9-2740	E9	6/7lp = VIII	455-458	0.82	
Kz-95	faunal	E9-2758	E9	6/7lp = VIII	455-458	1.13	
Kz-96	faunal	D8-616	D8	5a=V (upper)	415-420	1.51	
Kz-97	faunal	E8-1221	E8	5a=V (upper)	423-425	0.96	
Kz-98	faunal	E9-425	E9	5a=V (upper)	423-425	2.53	
Kz-99	faunal	E8-1286	E8	5a=V (middle)	425-430	1.65	
Kz-100	faunal	E8-1243	E8	5a=V (middle)	425-430	2.68	
Kz-101	faunal	E7-1199	E7	5a=V (middle)	425-430	2.44	
Kz-102	faunal	E9-1776	E9	5a=V (lower)	433-435	1.63	
Kz-103	faunal	E9-1797	E9	5a=V (lower)	435-438	1.50	
Kz-104	faunal	D8-802	D8	5a=V (lower)	433-435	2.08	
Kz-108	faunal	D7-1357	D7	6/7lb = VIII	460-461	3.36	
Kz-109	faunal	D7-1390	D7	6/7lb = VIII	461-462	2.51	
Kz-110	faunal	E7-2484	E7	6/7 lp/ls = VIII	464-465	1.02	
Kz-111	faunal	G30-x160	G30	A2	540-545	3.20	
Kz-112	faunal	G30-x205	G30	A1	545-550	0.88	
Kz-113	faunal	G29-x428	G29	A4	545-550	2.82	
Kz-114	faunal	F29-x1247	F29	D2	550-555	2.49	
Kz-115	faunal	F30-776	F30	C	540-545	1.12	
Kz-116	faunal	F29-x1150	F29	D2	545-550	2.33	

A.8 Manastira, Bulgaria

Original name	Манастира
Environment	cave
Latitude	43° 5’ 51” N
Longitude	25° 39’ 26” E
Altitude	300 m a.s.l.
Excavations	2012, 2013, 2015
Collaborator	Aleta Guadelli
PalaeoChron Code	RG/2013/PalaeoChron/40

Samples selected as potential early AMH (unconserved). In grey – not dated as preference was given to aDNA analysis. Man-01 identified through mtDNA as modern human (M. Hajdinjak, pers. comm. 14/03/2018).

Ref-no	Sample	Excav.	Quad.	Type	P-no	%N
Man-01	H24-8	2013	H24	*Homo sapiens*, adult, tibia	39565	0.97
Man-02	K/18	2012	F24	*Homo sapiens*, adult, scapula	39566	–

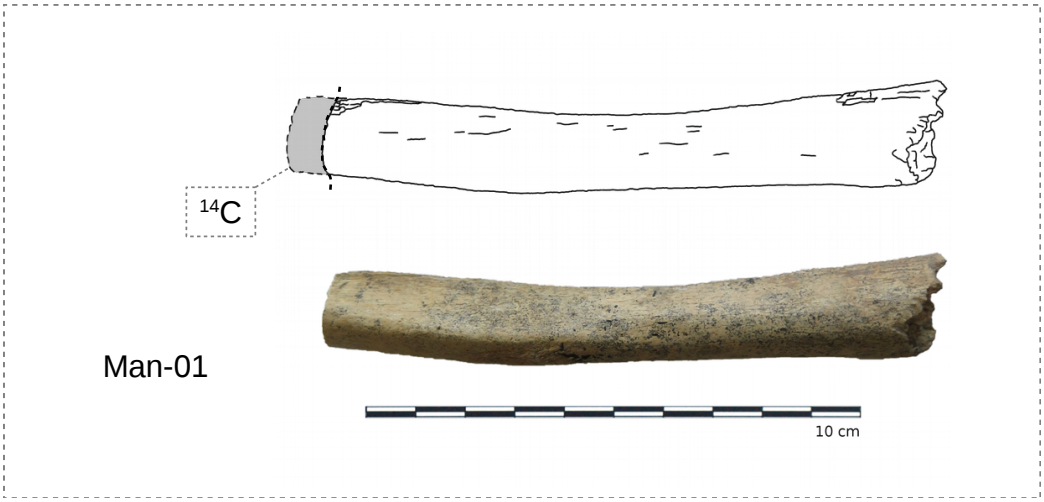


Figure A.15: Manastira: Man-01 – *Homo sapiens*, tibia, 5083 ± 32 BP (OxA-33836). Illustration & photo: R. Hopkins.

A.9 Mariáremete, Hungary

Other names	Remete Felső, Felső barlang
Environment	cave
Latitude	47.5588 N
Longitude	18.9453 E
Altitude	350 m a.s.l.
Excavations	1969–1970
Collaborator	Klára Palotás, László Makádi
PalaeoChron Code	RG/2013/PalaeoChron/51

Samples were drilled on 15 September 2015 at the Hungarian Geological Institute in Budapest. Cons. = indication whether sample had been conserved. Weight = weight sampled in mg. Depth given in cm. Samples without a radiocarbon date are marked grey.

Ref-no	Type	Sq.	Level	Depth	P-no	%N	Cons.	Weight
MR-01	human	6a	sárga agyag	100	40393	1.76	N	440
MR-02	fauna	7a	sárga agyag	120	40394	0.06	N	770
MR-03	fauna	3	sárga agyag	–	40395	1.26	N	300
MR-04	fauna	3	sárga agyag	–	40396	1.80	N	640
MR-05	fauna	2-3	sárga agyag	120	40397	1.22	N	1550
MR-06	fauna	2-3	sárga agyag	120	40398	2.43	N	640
MR-07	fauna	2-3	sárga agyag	120	40399	0.78	N	2200
MR-08	fauna	6a	sárga agyag	100	40400	1.58	N	820
MR-10	fauna	6	sárga agyag	100	40402	2.33	N	1506

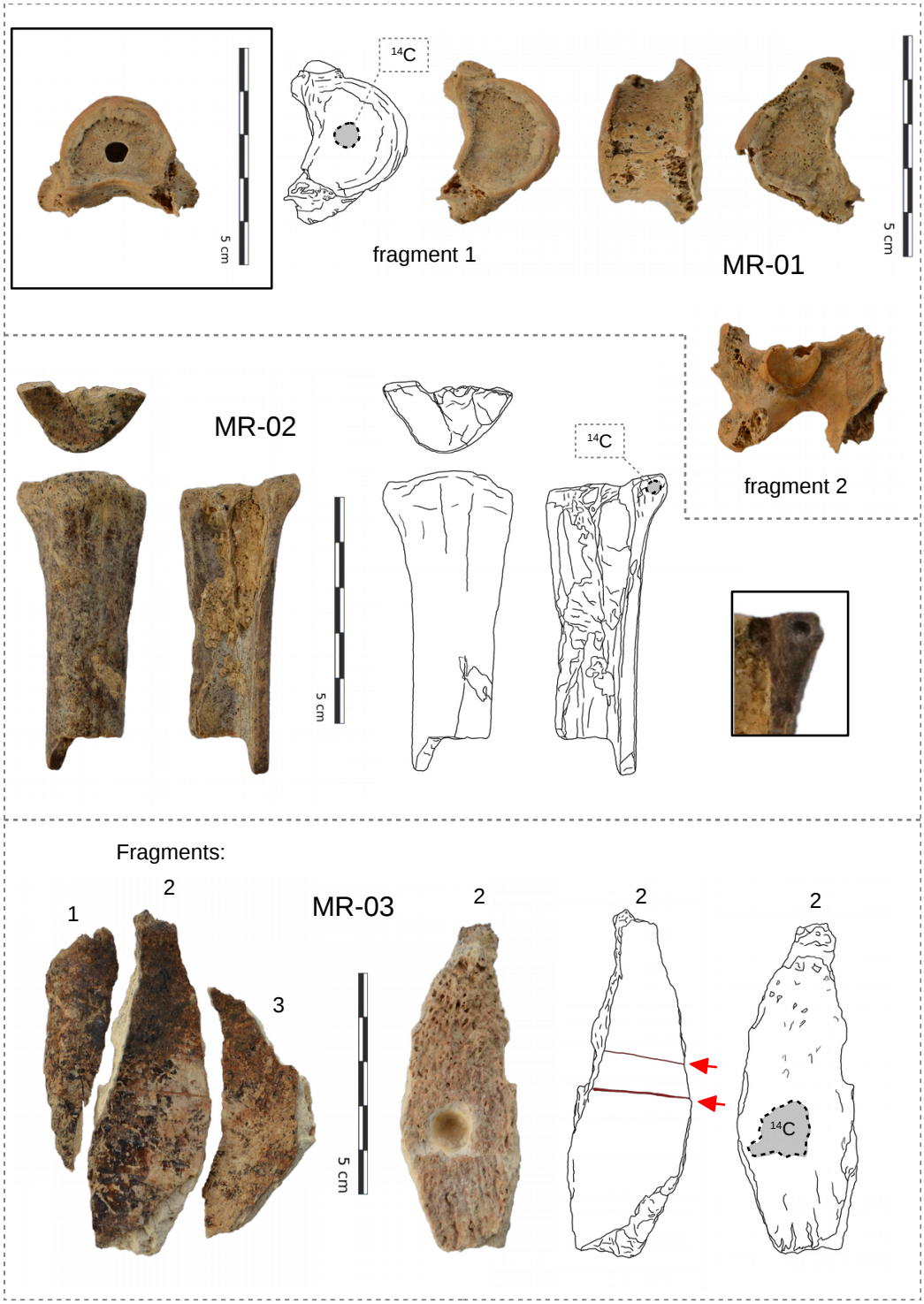


Figure A.16: Mariáremete: MR-01 – human vertebra, key-hole drilling, 8145 ± 40 BP (OxA-33849); MR-02 – split bone, key-hole drilling; MR-03 – cut-marked bone, 19650 ± 110 BP (OxA-X-2719-19). Photos & illustrations: R. Hopkins.

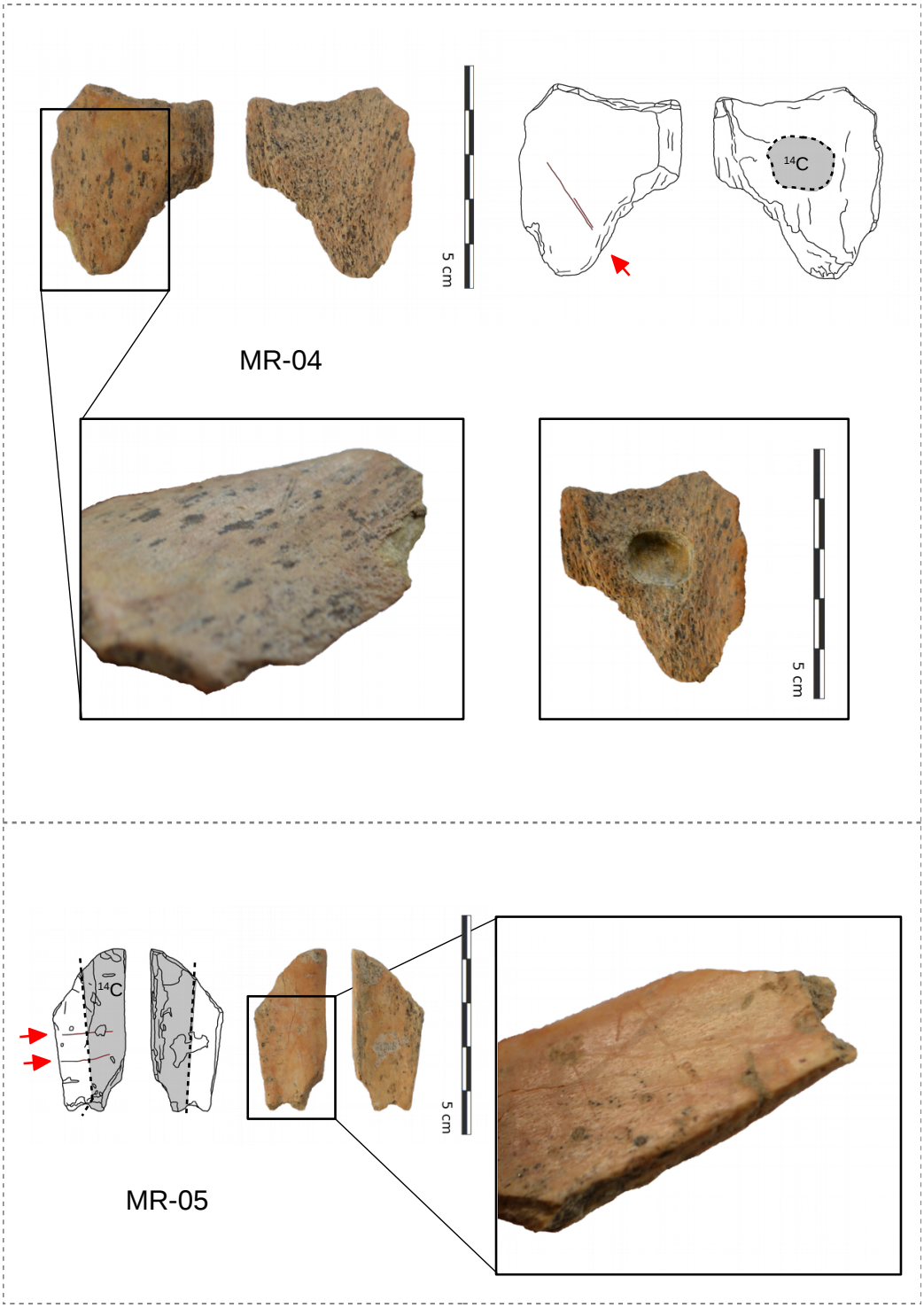


Figure A.17: Mariáremete: MR-04 – cut-marked bone; MR-05 – cut-marked bone, 18820 ± 100 BP (OxA-35660). Photos & illustrations: R. Hopkins.

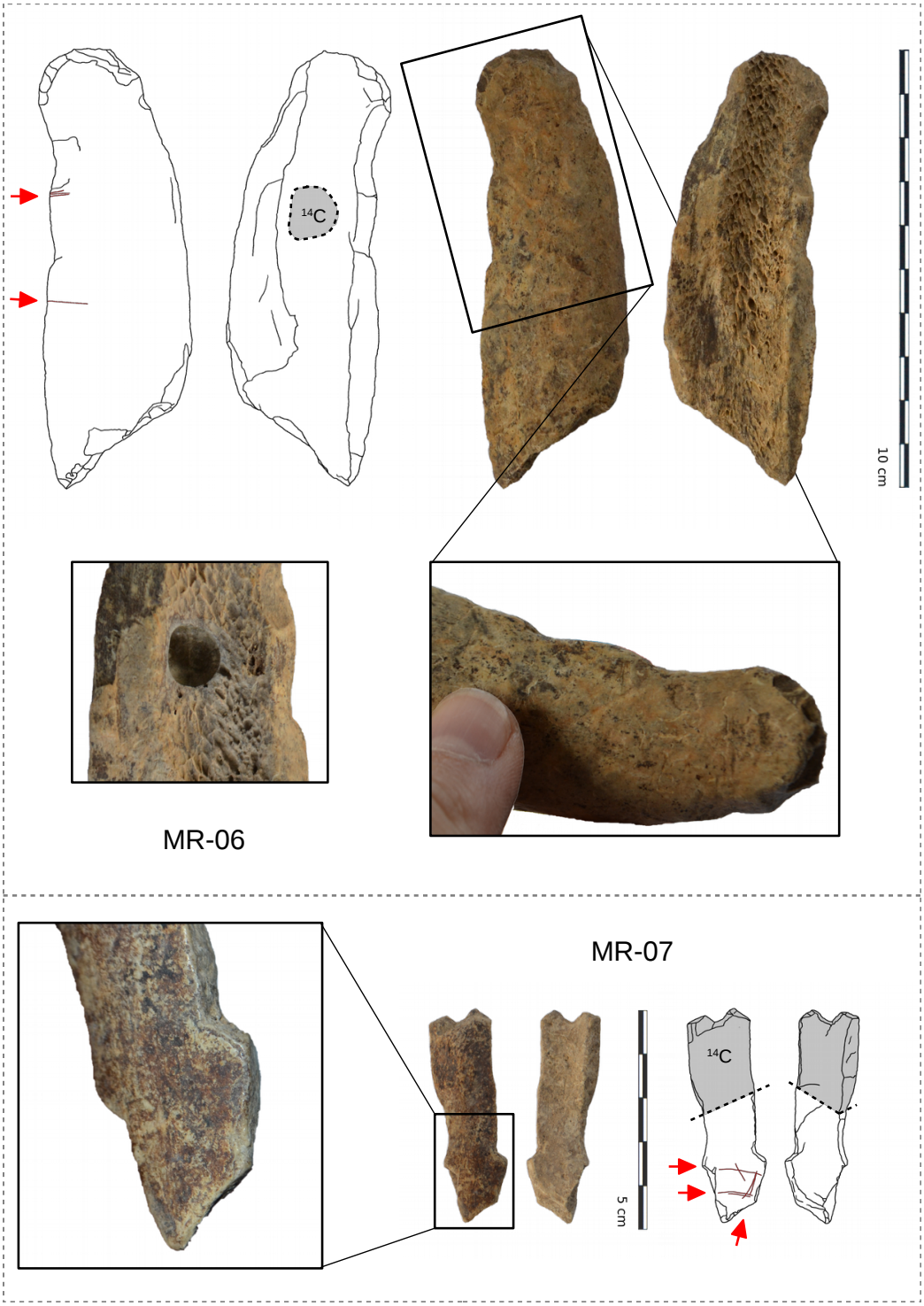


Figure A.18: Mariáremete: MR-06 – cut-marked bone, 34000 ± 1300 BP (OxA-X-2731-13); MR-07 – cut-marked bone, 36750 ± 750 BP (OxA-35698). Photos & illustrations: R. Hopkins.

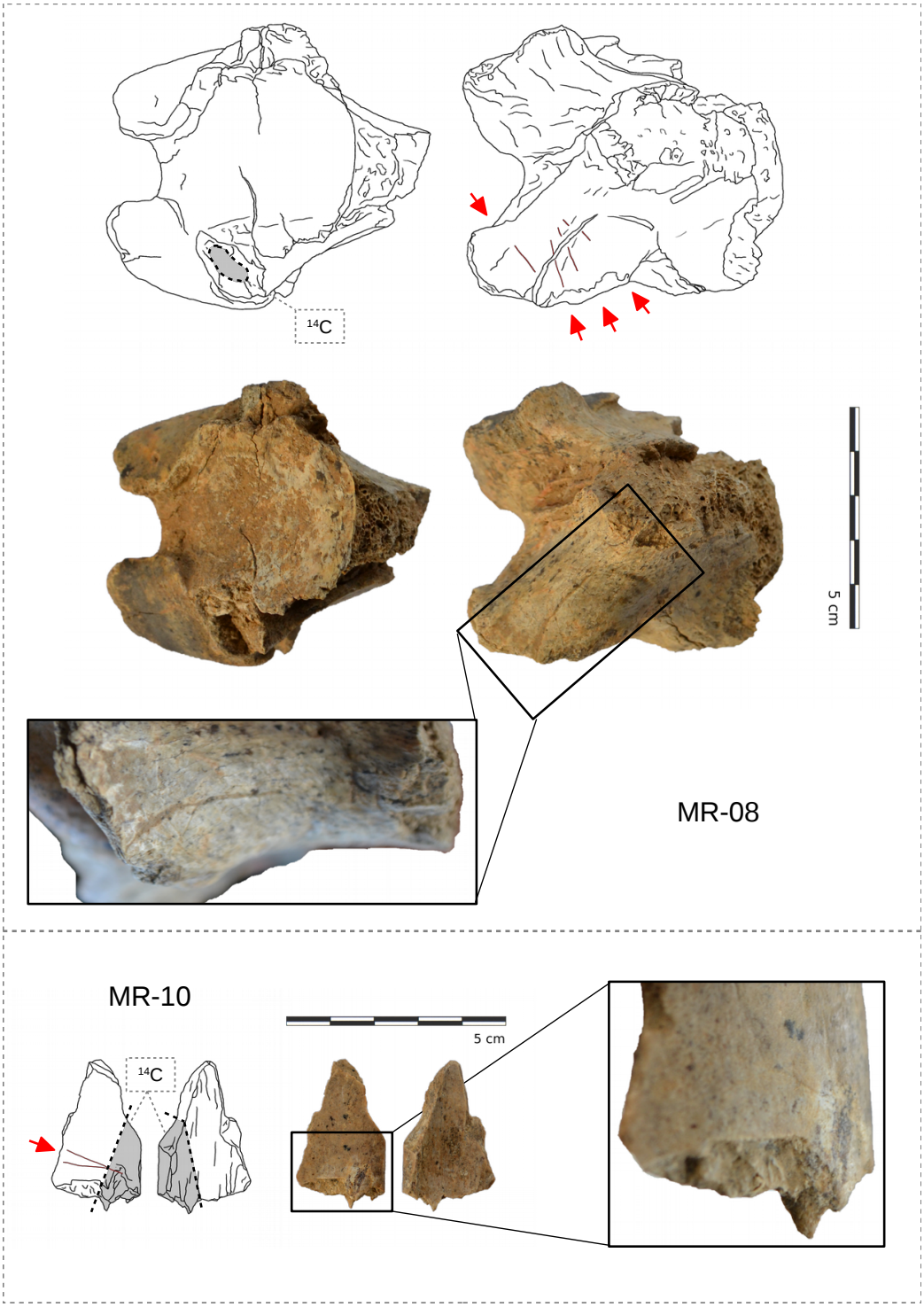


Figure A.19: Mariáremete: MR-08 – cut-marked bone, key-hole drilling, 44900 ± 2300 BP (OxA-34029); MR-10 – cut-marked bone, 39200 ± 1100 BP (OxA-34030). Photos & illustrations: R. Hopkins.

A.10 Peskő, Hungary

Environment	cave
Latitude	48° 02' 53" N
Longitude	20° 25' 25" E
Altitude	752 m a.s.l.
Excavations	1912–1913, 1934, 1939–1940, 1955
Collaborators	András Markó
PalaeoChron Code	RG/2013/PalaeoChron/52

Samples Osseous points were drilled on 17 September 2015 at the Hungarian National Museum in Budapest. The radiocarbon results given here are from this project, though previously published results are deemed more reliable (see section 11.6). Cons. = indication whether sample had been conserved. Weight = weight sampled in mg.

Ref-no	Sample no.	Type	Species	Excavation	P-no	%N	Cons.	Weight
Pes-01	Pb 930	point	reindeer	1934	40413	1.66	Y	400
Pes-02	Pb 927-28	point	Cervus sp	1934	40414	1.57	Y	110
Pes-03	Pb 933	point	reindeer	1934	40415	2.86	Y	330

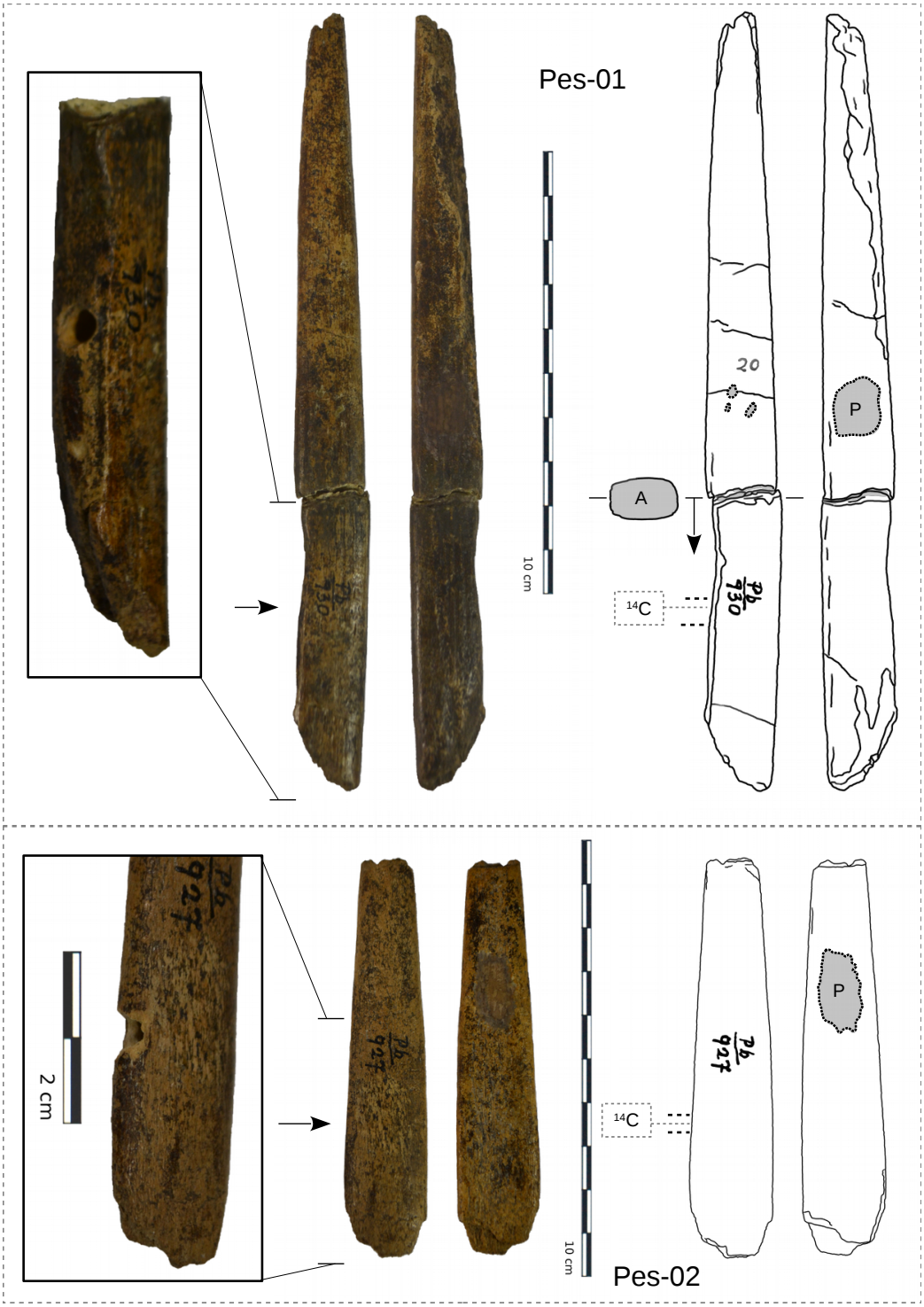


Figure A.20: Peskő: Pes-01 – massive based point, key-hole drilling, 31750 ± 500 BP (OxA-35419); Pes-02 – split-based point, key-hole drilling, 33300 ± 1200 BP (OxA-X-2731-14). Photos & illustrations: R. Hopkins.

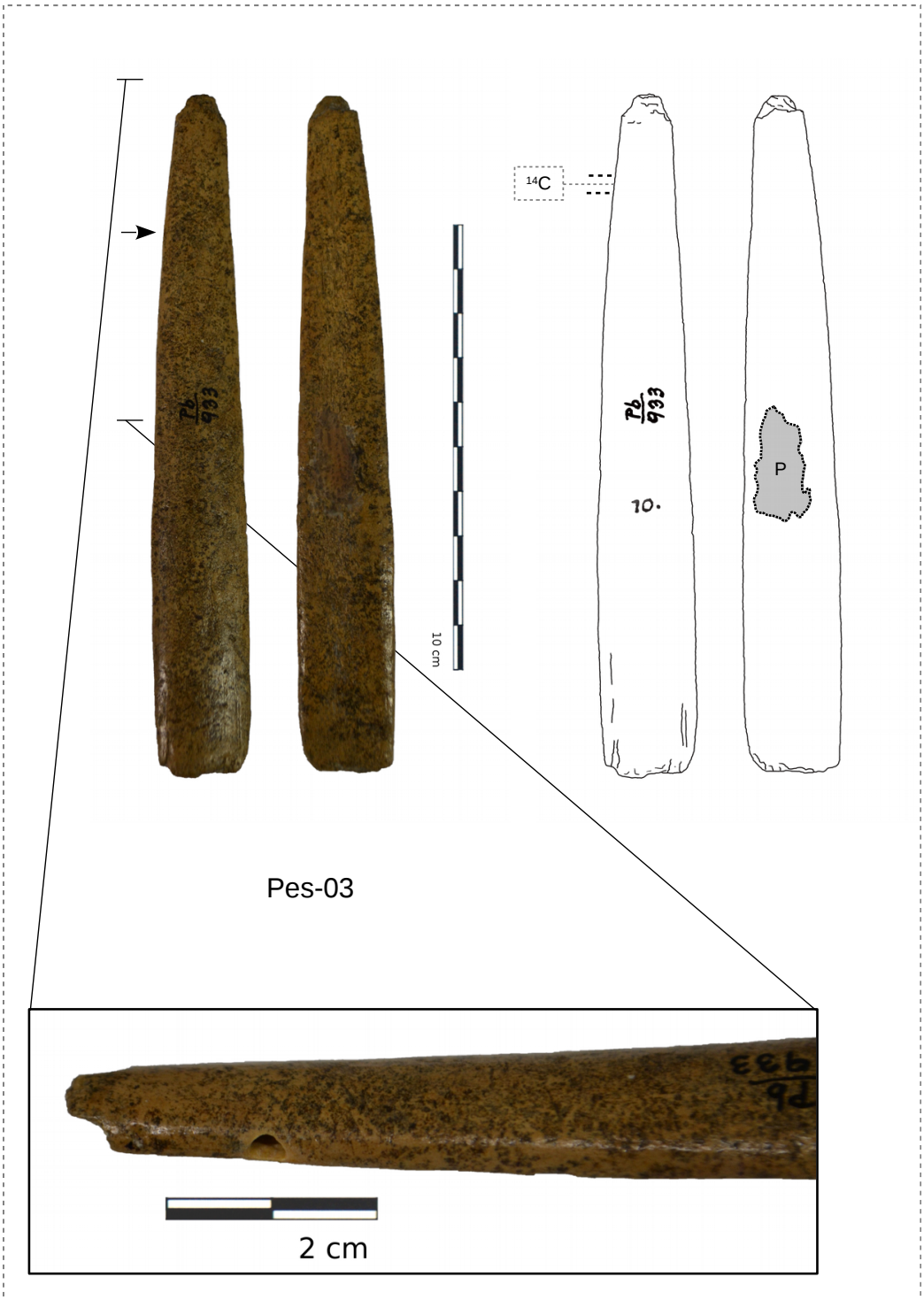


Figure A.21: Peskő: Pes-03 – antler point, key-hole drilling, 34950 ± 750 BP (OxA-35420). Photo & illustration: R. Hopkins.

A.11 Šal'a, Slovakia

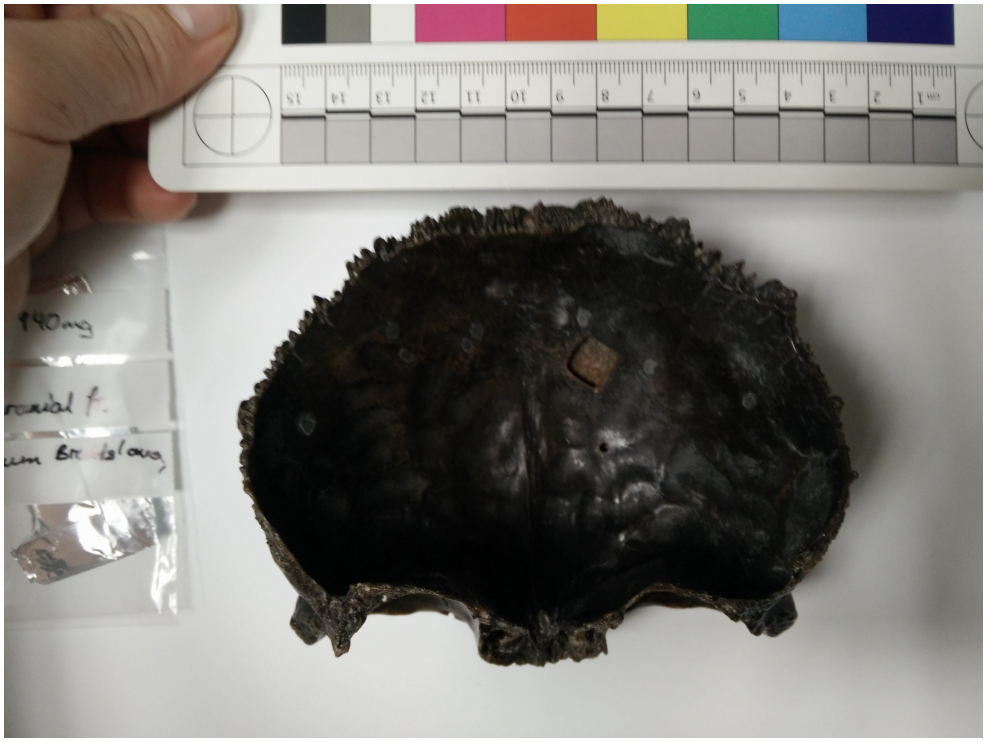
Environment	river ravine (secondary)
Latitude	48.14 N
Longitude	17.9 E
Altitude	n/a
Excavations	1961, 1993, 1995
Collaborator	Alena Šefčáková, Bibiána Hromadová
PalaeoChron Code	RG/2013/PalaeoChron/65

Samples Sal-01 was drilled on 21 August 2015 in the Archaeological Institute of the Slovakian Academy of Science in Nitra, while Sal-02 was sampled on 8 June 2016 at the Slovak National Museum in Bratislava. Cons. = indication whether sample had been conserved. Weight = weight sampled in mg.

Ref-no	Sample no.	Type	Location	Found	P-no	%N	Cons.	Weight
Sal-01	Šal'a II	human	river find	1995	41377	1.51	Y	930
Sal-02	Šal'a I	human	river find	1961	41625	2.66	Y	940



Figure A.22: Šal'a: Sal-01 – Neanderthal cranial fragment, key-hole and surface drilling, > 47100 BP (OxA-X-2731-15). Photos & illustrations: R. Hopkins.



Sal-02



Figure A.23: Šal'a: Sal-02 – Neanderthal cranial fragment, key-hole and surface drilling, > 46200 BP (OxA-X-2731-16). Photos & illustrations: R. Hopkins.

A.12 Szeleta, Hungary

Environment	cave
Latitude	48° 06' 30" N
Longitude	20° 37' 54" E
Altitude	347 m a.s.l.
Excavations	1906–1913, 1928, 1936, 1950s, 1960s, 1999
Collaborators	András Markó
PalaeoChron Code	RG/2013/PalaeoChron/21

Sample drilled on 21 April 2015 at the Hungarian National Museum in Budapest. Cons. = indication whether sample had been conserved. Weight = weight sampled in mg.

Ref-no	Sample no.	Type	Species	Level	P-no	%N	Cons.	Weight
Szel-01	47/928.8	point	reindeer	3/6	38797	2.87	Y	382

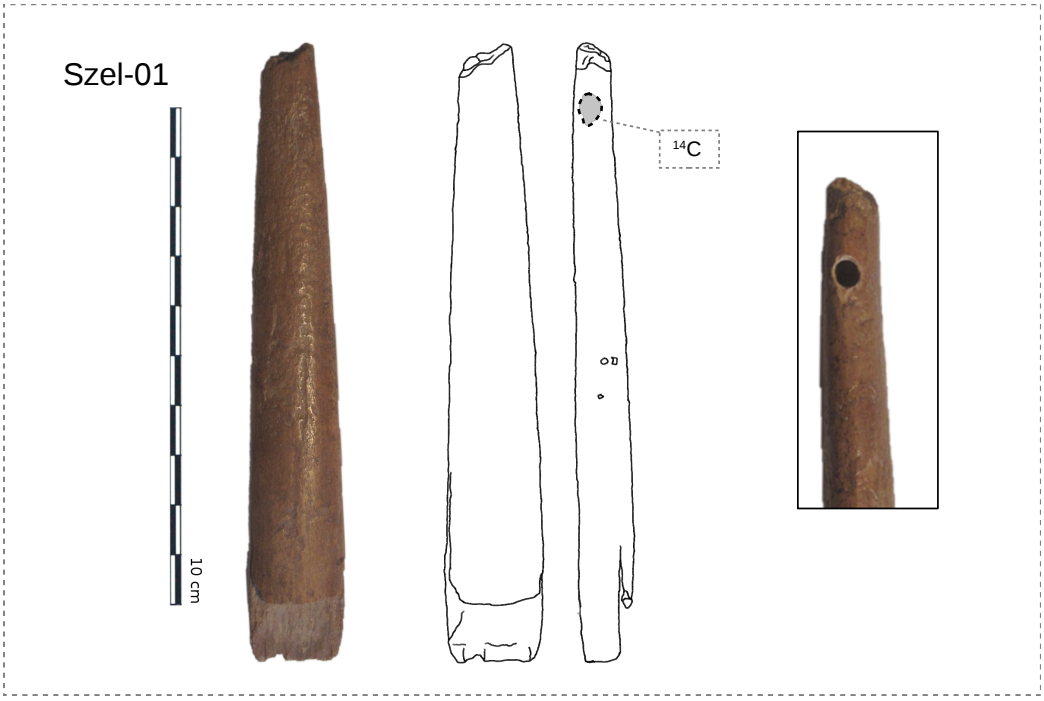


Figure A.24: Szeleta: Szel-01 – split-based point, key-hole drilling, 32950 ± 550 BP (OxA-35416). Photos & illustrations: R. Hopkins.

A.13 Tabashkata, Bulgaria

Orig. name	Табашката пещера
Environment	cave
Latitude	*ca.* 43.150 N
Longitude	*ca.* 24.710 E
Altitude	*ca.* 300 m a.s.l.
Excavations	1963
Collaborator	Aleta Guadelli
PalaeoChron Code	RG/2013/PalaeoChron/81

Samples collected in February 2017 at the Historical Museum in Lovech. Weight drilled given in mg.

Ref-no	Sample no.	Item	Conserved	P-no	%N	Weight
Tk-01	ОФ 669	massive based point	Y	42829	1.37	450
Tk-02	ОФ 671	grooved point	Y	42830	2.25	400
Tk-03	ОФ 670	massive based point	Y	42831	3.18	316

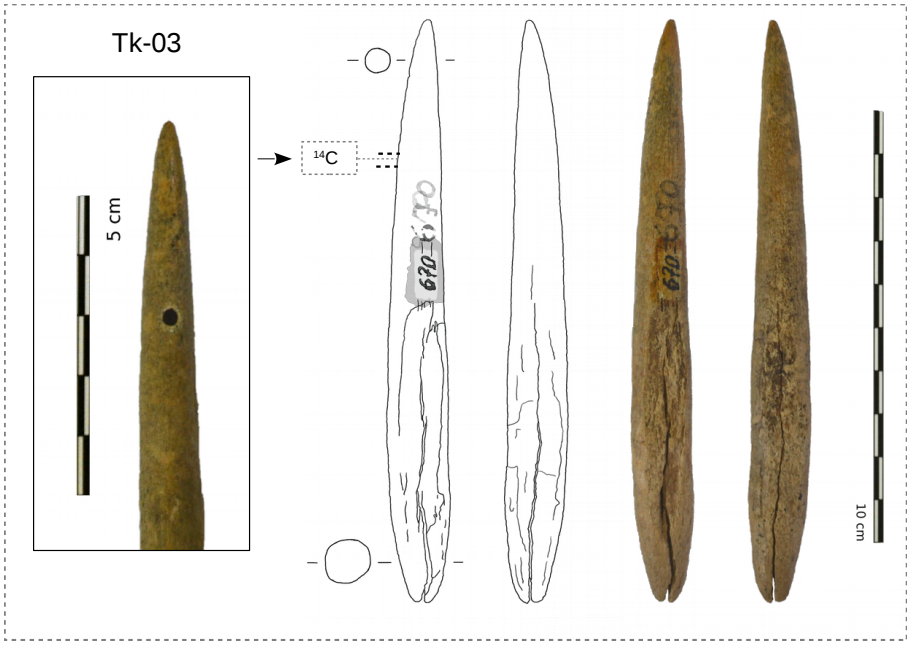


Figure A.25: Tabashkata: Tk-03 – massive base point, antler, key-hole drilling, 21120 ± 130 BP (OxA-35534). Illustration & photo: R. Hopkins.

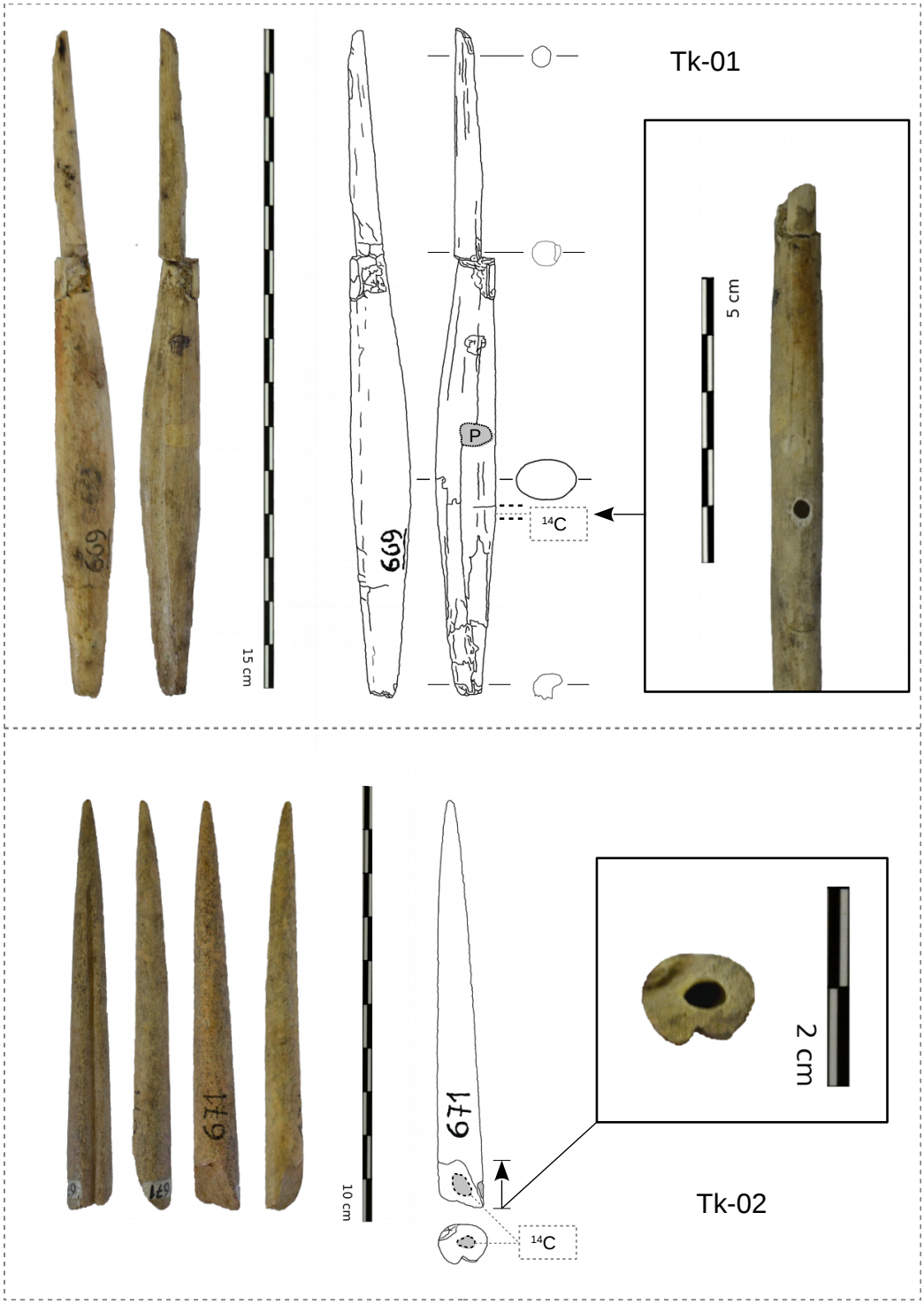


Figure A.26: Tabashkata: Tk-01 – massive base point, bone, key-hole drilling, 27600 ± 400 BP (OxA-35404); Tk-02 – grooved point, antler, 17156 ± 106 BP (OxA-X-2732-21). Illustrations & photos: R. Hopkins.

A.14 Tabula Traiana, Serbia

Environment	cave
Latitude	44° 39' N
Longitude	22° 18' E
Altitude	90-91 m a.s.l.
Excavations	2004, 2005, 2008, 2009, 2013, 2017
Collaborator	Dušan Borić & Emanuela Cristiani
PalaeoChron Code	RG/2013/PalaeoChron/87

Samples were collected from the 2004, 2005, 2008, and 2009 excavation seasons and have not been treated with conservation substances prior to dating. In the following, all initially collected samples, their context and their %N results (if available) are listed. Undated samples are marked in grey and have only bee sampled for %N testing (*ca.* 5 mg). Co-ordinates are given in metres. 'Mark' indicates whether the marks found on the bone are anthropogenic: Y = yes, M = maybe. Final samples for dating were selected according to their context information and security of anthropogenic modification. For further dating details see main text, catalogue and table 9.5.

Ref-no	Trench	Quad.	Layer	Co-ord.	Mark	P-no	%N
Tab-01	1/2008	4/27	210	x=4.67; y=27.39; z=91.10	Y	43131	2.25
Tab-02	1/2008	4/27	210	x=4.49; y=27.29; z=91.06	Y	43132	2.14
Tab-03	1/2008	4/28	207/3	x=4.34; y=28.16; z=91.24	Y	43133	1.06
Tab-04	1/2008	4/25	207/2	x=4.82; y=25.41; z=91.03	Y	43134	2.11
Tab-05	1/2008	4/27	210	x=4.78; y=27.28; z=91.01	Y	43135	2.27
Tab-06	1/2008	4/26	207/3	x=4.91; y=26.36; z=91.31	Y	43136	1.52
Tab-07	1/2008	4/27	210	x=4.70; y=27.56; z=91.13	Y	43137	1.49
Tab-08	1/2008	4/25	207/4	x=4.58; y=25.76; z=90.94	Y	43138	2.42
Tab-09	1/2009	2.5/31	207	x=2.89; y=31.16; z=91.92	Y	–	0.74
Tab-10	1/2008	4/25	216	x=4.03; y=25.18; z=90.85	Y	–	0.28
Tab-11	3/2008	5/22	217/2	x=5.20; y=22.59; z=90.23	Y	43139	1.53
Tab-12	2/2008	5/18	212	x=5.72; y=18.63; z=90.34	Y	–	2.99
Tab-13	1/2008	4/26	215/2	x=3.99; y=26.59; z=90.72	Y	43140	1.16

Ref-no	Trench	Quad.	Layer	Co-ord.	Mark	P-no	%N
Tab-14	3/2008	5/22	200	–	Y	43141	1.55
Tab-15	1/2005	2.5/27(F)	50	–	Y	–	1.92
Tab-16	1/2005	3/27(C)	72	–	Y	–	1.66
Tab-17	2/2008	4.5/18	211	–	Y	43142	0.61
Tab-18	–	–	207	–	Y	–	1.27
Tab-19	1/2005	2.5/27(F)	157	–	Y	–	1.12
Tab-20	–	–	201	–	Y	43143	1.76
Tab-21	1/2005	3/26	219/2	–	Y	43144	0.75
Tab-22	1/2008	4/25	216	–	M	–	2.36
Tab-23	2/2008	???	212	–	M	–	2.66
Tab-24	3/2008	5/24	220	–	M	–	2.57
Tab-25	3/2008	5/24	217/4	–	M	–	2.12
Tab-26	3/2008	5/23	217/3	–	Y	43145	2.20
Tab-27	3/2008	5/22	217/3	–	M	–	1.67
Tab-28	–	-TT77/1	???	–	M	–	3.33
Tab-29	–	–	206	–	M	–	1.91
Tab-30	3/2008	5/22	220	–	M	–	2.55
Tab-31	1/2008	4/27	210	–	M	–	2.12
Tab-32	1/2008	4/28	207/2	–	Y	43146	1.34
Tab-33	1/2008	4/25	207/2	–	M	–	1.29
Tab-34	1/2004	east. section	220	–	M	43147	1.94
Tab-35	3/2008	5/23	2017/3	–	Y	–	1.35
Tab-36	1/2008	4/28	207/3	–	M	–	2.66
Tab-37	1/2008	4/28	207/3	–	M	–	2.02
Tab-38	–	–	206	–	Y	43148	2.22
Tab-39	1/2008	4/26	218	–	Y	43149	1.88
Tab-40	3/2008	5/24	217/3	–	Y	43150	2.11
Tab-41	–	–	220	–	M	–	1.34
Tab-42	1/2008	4/25, 4/26	215/1	–	M	–	0.07
Tab-43	1/2008	4/25	207/4	x=4.58; y=25.59; z=90.97	Y	43151	2.08
Tab-44	1/2005	3/28(D)	ochre	–		–	1.04

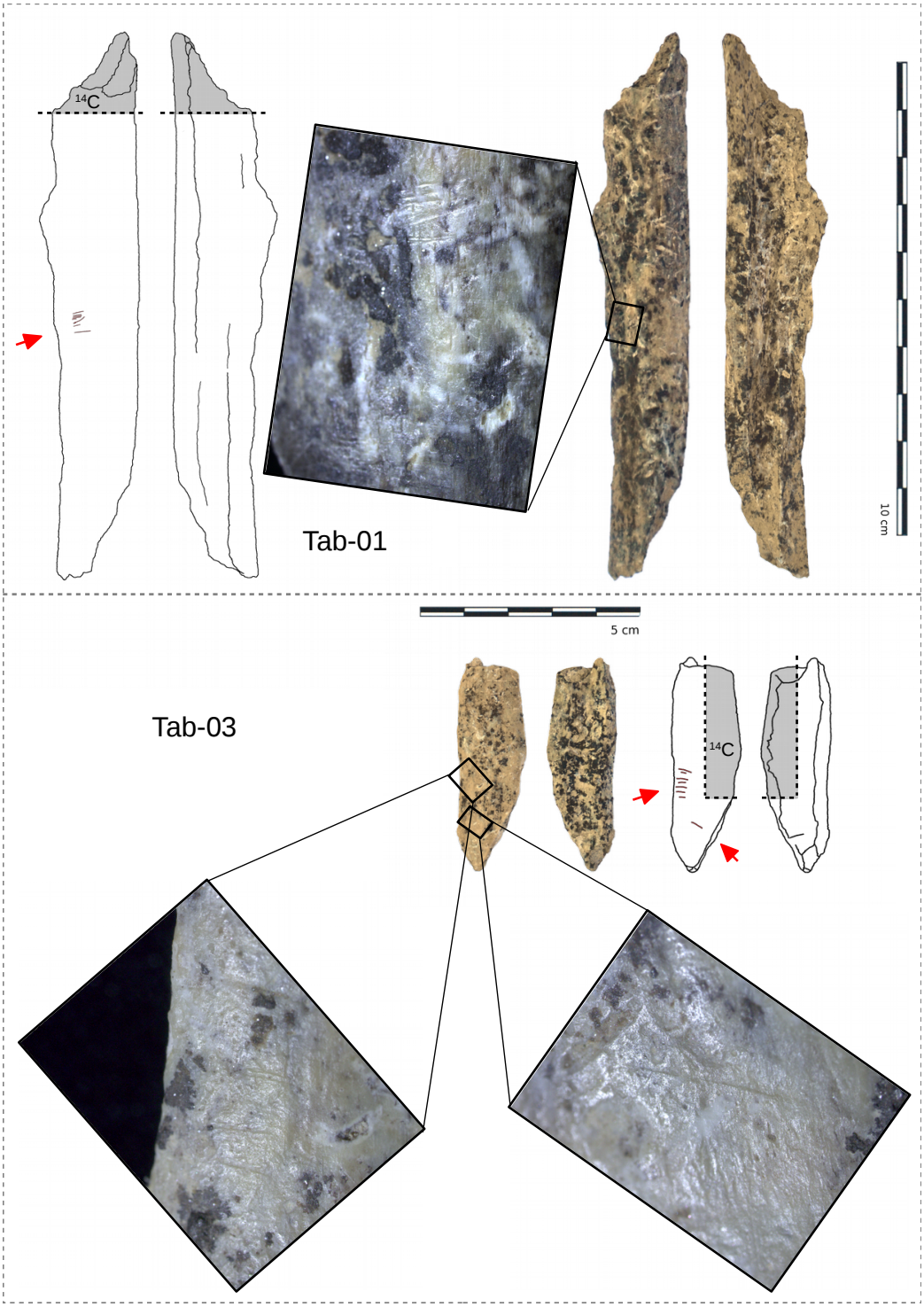


Figure A.27: Tabula Traiana: Tab-01 – cut-marked bone, layer 210, 33,600 ± 550 BP (OxA-35592); Tab-03 – cut-marked bone, layer 207/3, > 48,000 BP (OxA-35762). Illustrations & photos: R. Hopkins; macro-photography: E. Cristiani.

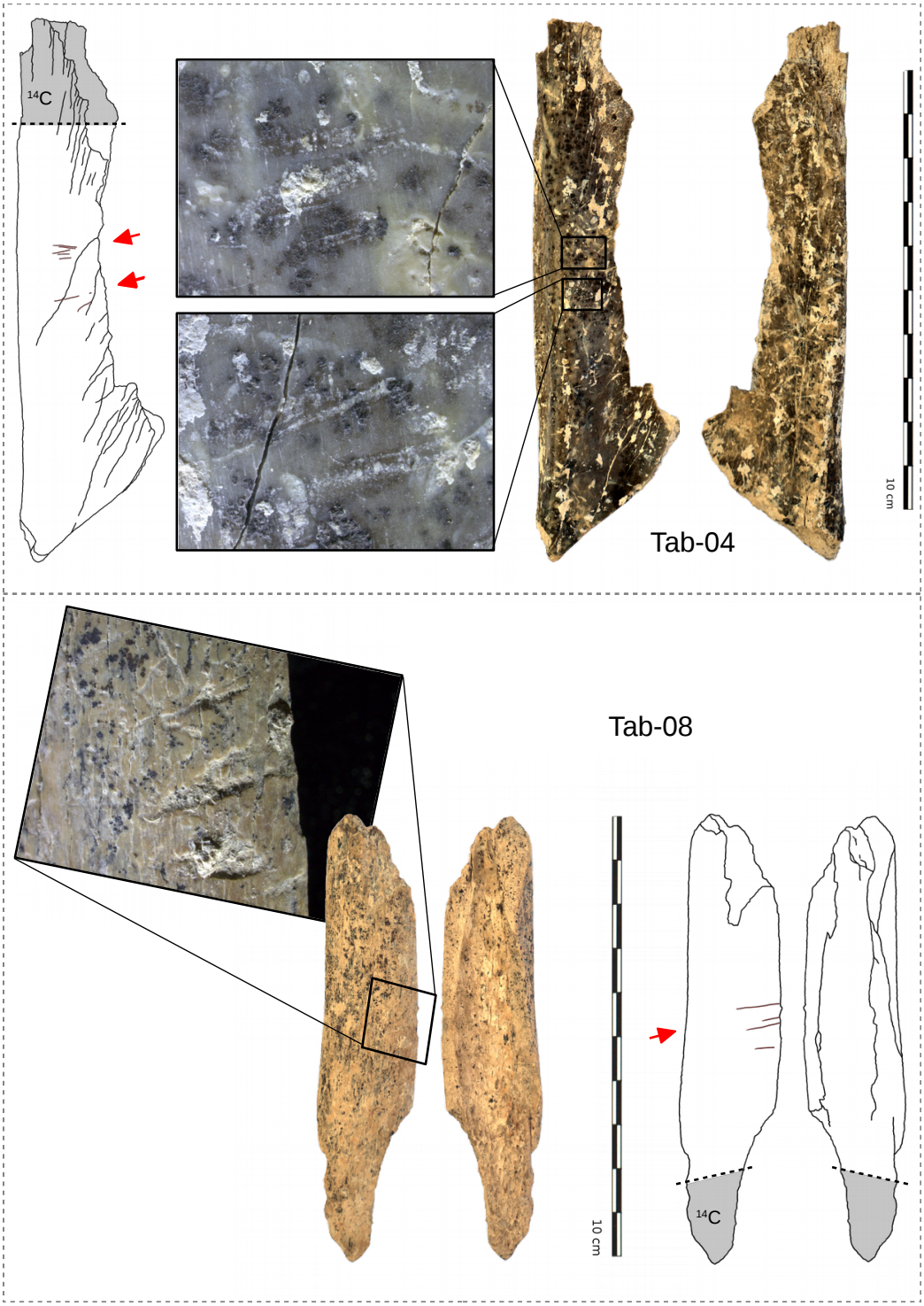


Figure A.28: Tabula Traiana: Tab-04 – cut-marked bone, layer 207/2, 28,550 ± 290 BP (OxA-35763); Tab-08 – cut-marked bone, layer 207/4, 36,500 ± 750 BP (OxA-35764). Illustrations & photos: R. Hopkins; macro-photography: E. Cristiani.

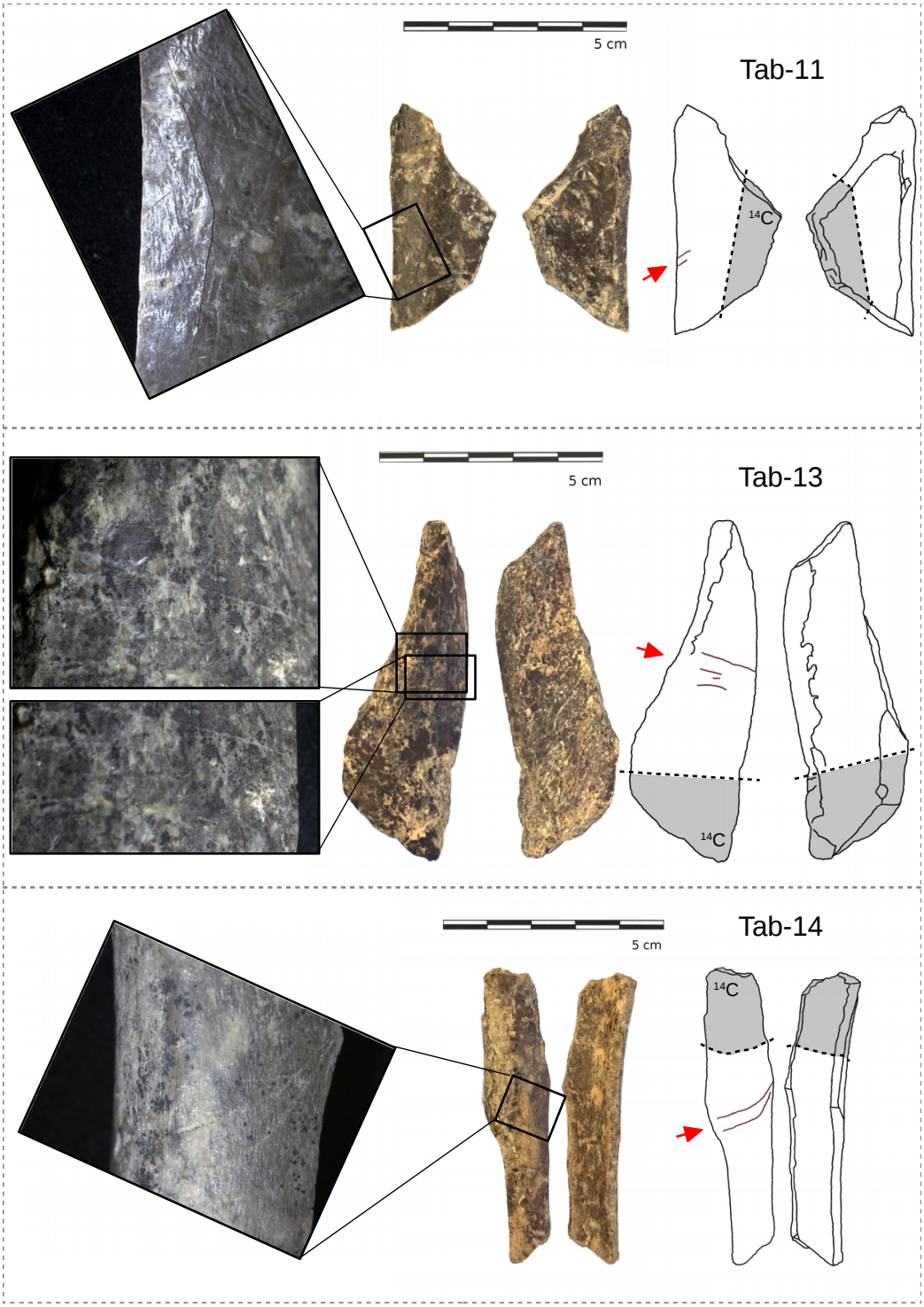


Figure A.29: Tabula Traiana: Tab-11 – cut-marked bone, layer 217/2, 20,460 ± 120 BP (OxA-35765); Tab-13 – cut-marked bone, layer 215/2, > 49,800 BP (OxA-35766) and > 49,900 BP (OxA-35767); Tab-14 – cut-marked bone, layer 200, 25,490 ± 210 BP (OxA-35593). Illustrations & photos: R. Hopkins; macrophotography: E. Cristiani.

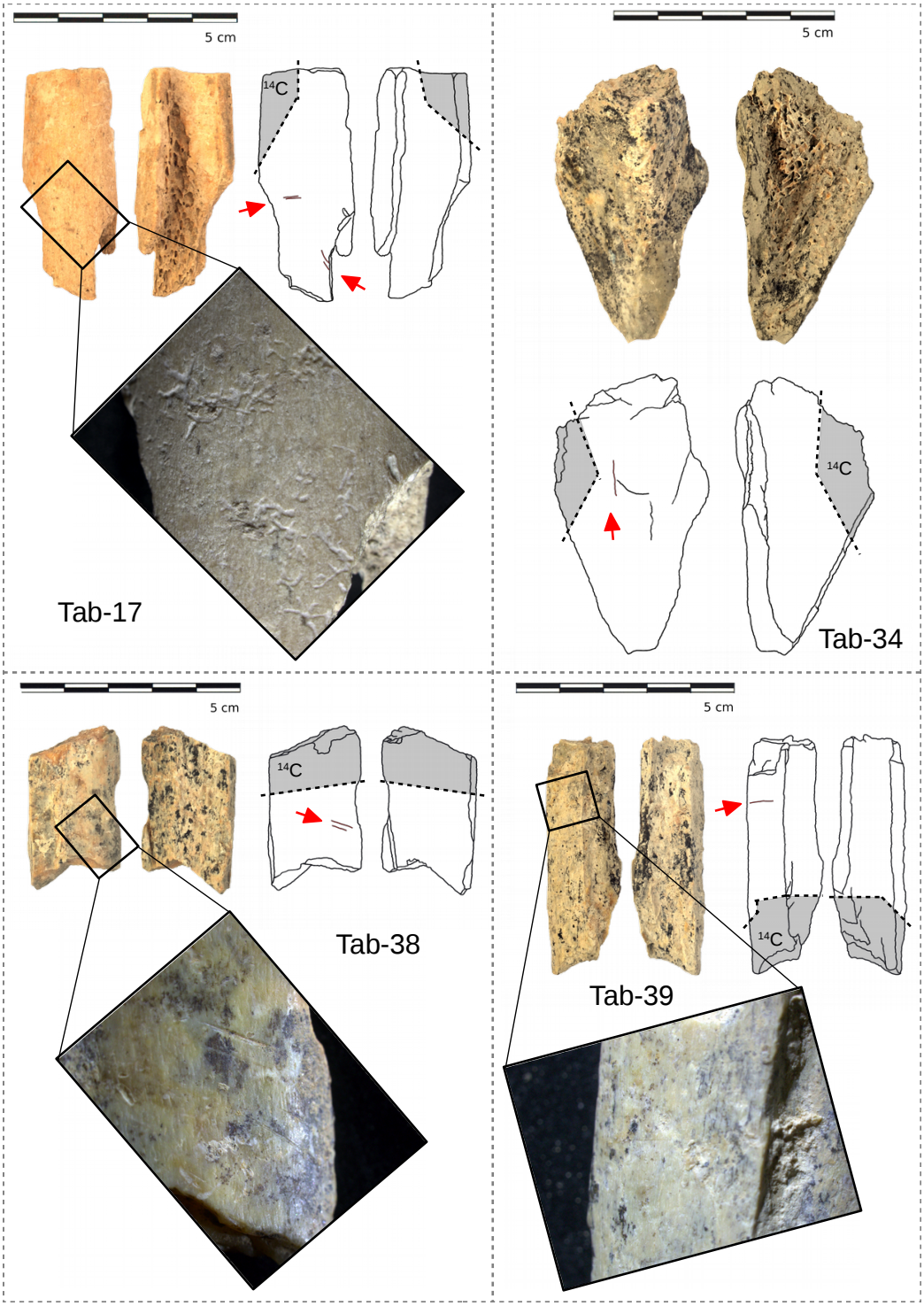


Figure A.30: Tabula Traiana: Tab-17 – cut-marked bone, layer 211, $> 48,800$ BP (OxA-35594); Tab-34 – cut-marked bone, layer 220, 34,250 ± 550 BP (OxA-35768); Tab-38 – cut-marked bone, layer 206, $> 50,100$ BP (OxA-35769); Tab-39 – cut-marked bone, layer 218, 46,500 ± 2,600 BP (OxA-35770). Illustrations & photos: R. Hopkins; macro-photography: E. Cristiani.

A.15 Temnata Dupka, Bulgaria

Orig. name	Темната дупка
Environment	cave
Latitude	43.174969 N
Longitude	24.074006 E
Altitude	231 m a.s.l.
Excavations	1929, 1983–1991
Collaborators	Nikolay Sirakov, Jean-Luc Guadelli, Aleta Guadelli
PalaeoChron Code	RG/2013/PalaeoChron/42

Samples TD-01 to TD-20 were drilled on July 2015, and TD-21 to TD-31 were sampled in July 2016, at the base camp for the Kozarnika excavation. Cons. = indication whether sample had been conserved. Weight = weight sampled in mg. Undated samples are marked in grey.

Ref-no	Sample no.	Type	Found	Trench	Sq.	Layer	P-no	%N	Cons.	Weight
TD-01	О2-2803	faunal	–	V	О2	5pg	39571	1.16	?	980
TD-02	О1-2044	faunal	–	V	О1	5pg	39572	1.06	?	620
TD-03	О1-1278	faunal	–	V	О1	5pg	39573	1.13	?	2160
TD-04	О2-1339	faunal	–	V	О2	4pg	39574	0.80	?	900000
TD-05	Л1-1661	faunal	–	V	Л1	3jx/4	39575	2.09	?	1000
TD-06	Н1-1168	faunal	1981	V	Н1	3d/4	39576	1.75	?	1040
TD-07	Л2-1683	faunal	1989	V	Л2	3jx	39577	2.25	?	640
TD-08	М2-1758	faunal	1989	V	М2	3j/w	39578	2.03	?	1870
TD-09	Н1-1942	faunal	1989	V	Н1	3j/w	–	1.85	?	940
TD-10	Л2-1372	faunal	1989	V	Л2	3dg	39581	2.06	?	660
TD-11	Л1-1129	faunal	1989	V	Л1	3dg	39582	–	?	0
TD-12	Л1-991	faunal	1989	V	Л1	3dg	39583	–	?	0
TD-13	Л2-1402	faunal	1989	V	Л2	3dg	39584	–	?	0
TD-14	Л1-1518	faunal	1989	V	Л1	3dg	39585	2.33	?	1030
TD-15	Л2-1469	faunal	1989	V	Л2	3dg	39586	3.03	?	800
TD-16	Б2-639	faunal	–	I	Б2	4	39587	2.36	?	1110
TD-17	Г4-662	faunal	1985	I	Г4	4	39588	1.29	?	950
TD-18	Н1-1201	faunal	1989	V	Н1	3d/w	39589	2.86	?	1030
TD-19	Н1-1253	faunal	1989	V	Н1	3d/w	39590	1.71	?	1000
TD-20	Н1-1341	faunal	1989	V	Н1	3d/w	39591	2.67	?	940

Ref-no	Sample no.	Type	Found	Trench	Sq.	Layer	P-no	%N	Cons.	Weight
TD-21	О2-2775	faunal	–	V	О2	5pg	42166	1.83	?	770
TD-22	О1-2143	faunal	–	V	О1	5pg	43075	1.47	N	1630
TD-23	П/1346	faunal	–	V	О2	5pg	43076	1.49	N	1380
TD-24	О2-2790	faunal	–	V	О2	5pg	42167	1.81	N	1210
TD-25	Л2-1689	faunal	–	V	Л2	3j	43077	1.17	N	1650
TD-26	П/274-F3	faunal	–	I	–	3f	42165	3.02	N	600
TD-27	П/274-F2	faunal	–	I	–	3f	42168	1.63	N	1970
TD-28	М2-1859	faunal	–	V	М2	3j/3w	43078	2.01	N	900
TD-29	Л1-2566	faunal	–	V	Л1	6lg	42169	0.78	N	1700
TD-30	Б2-591	faunal	–	I	Б2	4	43079	0.81	Y	6030
TD-31	Б2-606	faunal	–	I	Б2	4	43080	1.40	Y	3140

A.16 Toplja, Bulgaria

Orig. name	Топля
Environment	cave
Latitude	*ca.* 42.9 N
Longitude	*ca.* 24.5 E
Altitude	*ca.* 300 (?) m a.s.l.
Excavations	end 19th century, 1981
Collaborator	Aleta Guadelli
PalaeoChron Code	RG/2013/PalaeoChron/82

Samples collected in February 2017 at the Historical Museum in Lovech.

Ref-no	Sample no.	Item	Conserved	P-no	%N
Tp-01	ОФ 779	point with split base	Y	42832	3.97



Figure A.31: Toplja: Tp-01 – detail of antler point's split base found at the base of the proximal fragment. Photos: R. Hopkins.

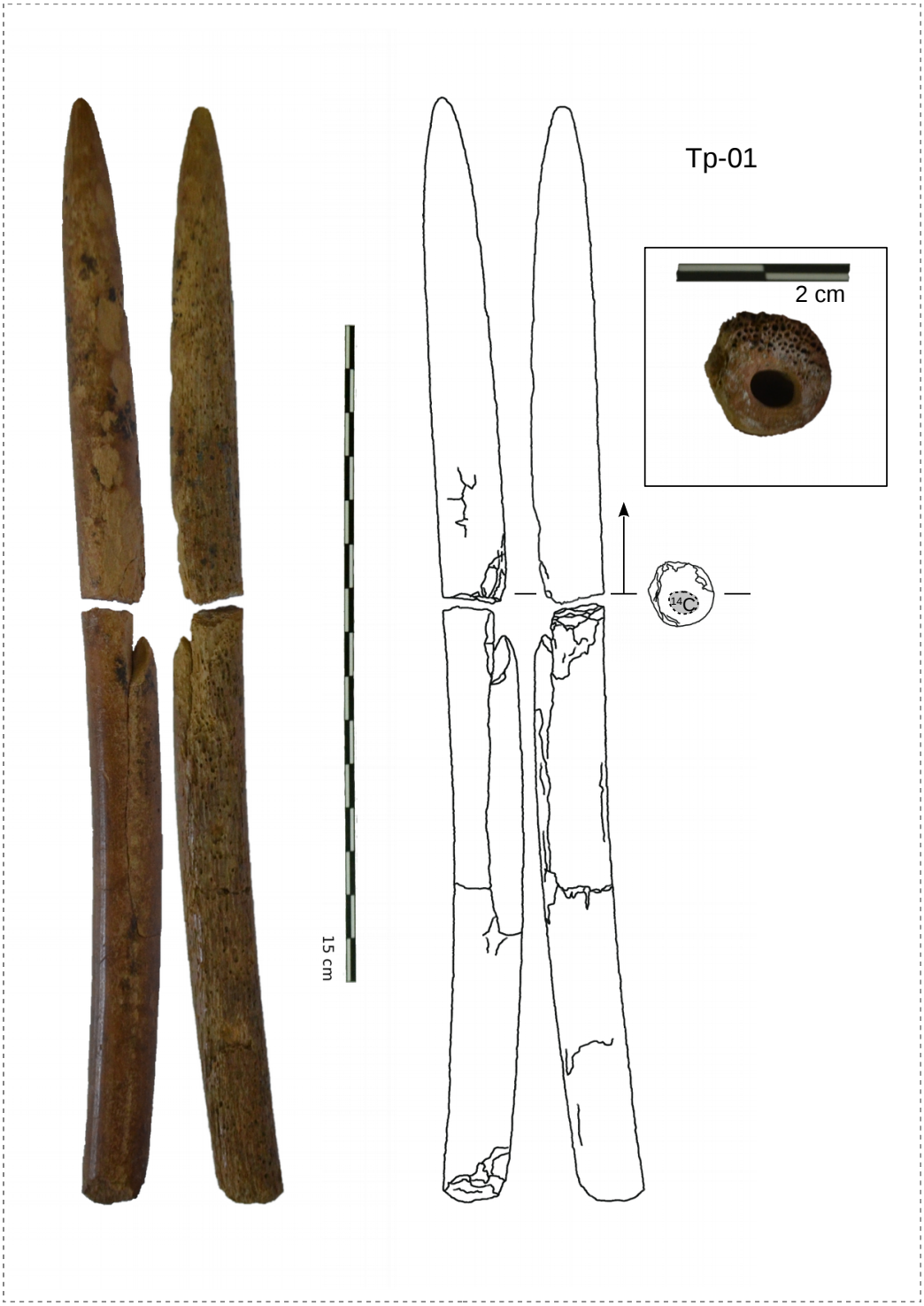


Figure A.32: Toplja: Tp-01 – antler point with split base, key-hole drilling, dating unsuccessful as a result of lacking collagen preservation. Illustrations & photos: R. Hopkins.

B: OxCal models

B.1 Code: Kozarnika

Model 0 – figure 8.18

```
 Plot("Kz - previously dated")
{
Outlier_Model("General",T(5),U(0,4),"t");
Sequence("Kz - previously dated")
{
Boundary("Kz - start level VIII");
Phase("VIII")
{
R_Date("GifA-101051", 43600, 1200)
{
Outlier("General", 0.05);
color="gray";
};
R_Date("OxA-22842", 41100, 750)
{
Outlier("General", 0.05);
color="gray";
};
R_Date("GifA-101048", 29310, 320)
{
Outlier("General", 0.05);
color="gray";
};
R_Date("OxA-24083", 37400, 500)
{
Outlier("General", 0.05);
};
Interval("Interval level VIII");
};
Boundary("Kz - transition VIII to VII");
Interval("Interval transition VIII to VII");
Phase("VII")
{
R_Date("Gif/LSM-10994", 38700, 1400)
{
Outlier("General", 0.05);
color="gray";
};
R_Date("OxA-23975", 38050, 500)
{
Outlier("General", 0.05);
};
R_Date("OxA-25406", 37600, 500)
{
Outlier("General", 0.05);
};
R_Date("OxA-24802", 37650, 500)
{
Outlier("General", 0.05);
};
R_Date("GifA-99706", 36200, 540)
{
Outlier("General", 0.05);
color="gray";
};
R_Date("OxA-25405", 36900, 450)
{
Outlier("General", 0.05);
};
R_Date("OxA-24080", 36350, 400)
{
Outlier("General", 0.05);
};
R_Date("OxA-24058", 32330, 260)
{
Outlier("General", 0.05);
};
Interval("Interval level VII");
};
Boundary("Kz - transition VII to VI");
Interval("Interval transition VII to VI");
Phase("VI")
{
R_Date("OxA-24059", 36650, 450)
{
Outlier("General", 0.05);
};
R_Date("OxA-22914", 36250, 450)
{
Outlier("General", 0.05);
color="gray";
};
R_Date("CI", 34290, 90)
{
Outlier("General", 0.05);
color="magenta";
};
R_Date("OxA-24865", 28380, 170)
{
Outlier("General", 0.05);
};
R_Date("GifA-99044", 26490, 270)
{
Outlier("General", 0.05);
};
Interval("Interval level VI");
};
Boundary("Kz - transition VI to V");
Interval("Interval transition VI to V");
Phase("V")
{
R_Date("Gif-10992", 25650, 730)
{
Outlier("General", 0.05);
};
R_Date("OxA-24786", 26320, 190)
{
Outlier("General", 0.05);
};
Interval("Interval level V");
};
Boundary("Kz - transition V to IV");
Interval("Interval transition V to IV");
Phase("IV")
{
R_Date("Gif/LSM-10677", 26120, 100)
{
Outlier("General", 0.05);
};
R_Date("OxA-25355", 25770, 140)
{
Outlier("General", 0.05);
};
R_Date("OxA-25184", 27370, 190)
{
Outlier("General", 0.05);
};
Interval("Interval level IV");
};
Boundary("Kz - transition IV to III");
Interval("Interval transition IV to III");
Phase("III")
{
R_Date("Gif-10674", 19770, 270)
{
Outlier("General", 0.05);
};
Interval("Interval level III");
};
Boundary("Kz - transition III to OI");
Interval("Interval transition III to OI");
Phase("OI")
{
R_Date("GifA-98345", 11550, 100)
{
Outlier("General", 0.05);
```

```
};
Interval("Interval level 0I");
};
```

```
Boundary("Kz - end of level 0I");
};
};
```

Model 1 – figure 8.19

```
 Plot()
{
Outlier_Model("General",T(5),U(0,4),"t");
Outlier_Model("SSimple",N(0,2),0,"s");
Sequence("Kz - Model 1")
{
Boundary("Kz - start level 6/7 ls/lp");
Phase("6/7 ls & 6/7 lp")
{
R_Date("OxA-34828", 44000, 1900)
{
Outlier("General", 0.05);
color="green";
};
R_Date("OxA-34825", 43800, 1800)
{
Outlier("General", 0.05);
color="green";
};
R_Date("OxA-X-2699-11", 42900, 1700)
{
Outlier("General", 0.05);
color="green";
};
R_Date("OxA-34823", 43900, 1800)
{
Outlier("General", 0.05);
color="green";
};
R_Date("OxA-33555", 43700, 1900)
{
Outlier("General", 0.05);
color="green";
};
Interval("Kz - Interval 6/7 ls lp");
Date("Date layer 6/7 ls/lp");
};
Boundary("Kz - transition 6/7 ls/lp to 6/7 lb");
Interval("Kz - Interval transition 6/7 ls lp to 6/7 lb");
Phase("6/7 lb")
{
R_Combine("Kz-109")
{
Outlier("General", 0.05);
color="green";
R_Date("OxA-34826", 39800, 1100)
{
Outlier("SSimple", 0.05);
color="green";
};
R_Date("OxA-34827", 40900, 1300)
{
Outlier("SSimple", 0.05);
color="green";
};
};
Interval("Kz - Interval 6/7 lb");
Date("Date layer 6/7 lb");
};
Boundary("Kz - transition 6/7 lb to 5c");
Interval("Kz - Interval transition 6/7 lb to 5c");
Phase("5c")
{
R_Date("OxA-34824", 37600, 900)
{
Outlier("General", 0.05);
color="green";
};
R_Date("OxA-33835", 37500, 900)
{
Outlier("General", 0.05);
color="green";
};
```

```
R_Date("OxA-33552", 37000, 800)
{
Outlier("General", 0.05);
color="green";
};
R_Date("OxA-33553", 36800, 800)
{
Outlier("General", 0.05);
color="green";
};
R_Date("OxA-35234", 37400, 800)
{
Outlier("General", 0.05);
color="green";
};
R_Date("OxA-34769", 36550, 750)
{
Outlier("General", 0.05);
color="green";
};
Interval("Kz - Interval 5c");
Date("Date layer 5c");
};
Boundary("Kz - transition 5c to 5b");
Interval("Kz - Interval transition 5c to 5b");
Phase("5b")
{
R_Date("CI", 34290, 90)
{
Outlier("General", 0.05);
color="#b7005c";
};
R_Date("OxA-33554", 33650, 550)
{
Outlier("General", 0.05);
color="green";
};
R_Date("OxA-33551", 32750, 500)
{
Outlier("General", 0.05);
color="green";
};
R_Date("OxA-35575", 27830, 270)
{
Outlier("General", 0.05);
color="green";
};
R_Date("OxA-35576", 28010,280)
{
Outlier("General", 0.05);
color="green";
};
Interval("Kz - Interval 5b");
Date("Date layer 5b");
};
Boundary("Kz - transition 5b to 5a");
Interval("Kz - Interval transition 5b to 5a");
Phase("5a")
{
R_Date("OxA-33550", 27540, 270)
{
Outlier("General", 0.05);
color="green";
};
R_Date("OxA-33549", 27290, 270)
{
Outlier("General", 0.05);
color="green";
};
R_Date("OxA-34822", 25400, 200)
{
Outlier("General", 0.05);
color="green";
```

```
};
Interval("Kz - Interval 5a");
Date("Date layer 5a");
};
Boundary("Kz - transition 5a to 4 (IVb)");
Phase("4 (IVb)")
{
R_Date("OxA-35230", 26340, 220)
{
Outlier("General", 0.05);
color="green";
};
R_Date("OxA-33547", 25800, 220)
{
Outlier("General", 0.05);
color="green";
};
R_Date("OxA-33548", 24090, 180)
{
Outlier("General", 0.05);
color="green";
};
Interval("Kz - Interval 4 (IVb)");
Date("Date layer 4 (IVb)");
};
Boundary("Kz - transition 4 (IVb) to 4 (IVa)");
Interval("Kz - Interval transition 5a to 4 (IVb)");
Phase("4 (IVa)")
{
R_Date("OxA-34767", 26400, 220)
{
Outlier("General", 0.05);
color="green";
};
R_Date("OxA-34768", 27380, 250)
{
Outlier("General", 0.05);
color="green";
};
R_Date("OxA-33546", 27330, 260)
{
Outlier("General", 0.05);
color="green";
};
R_Date("OxA-33834", 28020, 290)
{
Outlier("General", 0.05);
color="green";
};
Interval("Kz - Interval 4 (IVa)");
Date("Date layer 4 (IVa)");
};
Boundary("Kz - transition 4 (IVa) to 3b");
Interval("Kz - Interval transition 4 (IVa) to 3b");
Phase("3b")
{
R_Date("OxA-35417", 23240, 180)
{
Outlier("General", 0.05);
color="green";
};
Interval("Kz - Interval 3b");
Date("Date layer 3b");
};
Boundary("Kz - end of 3b");
};
};
```

Model 2 – figure 8.19

```
 Plot()
{
Outlier_Model("General",T(5),U(0,4),"t");
Outlier_Model("SSimple",N(0,2),0,"s");
Sequence("Kz - Model 2")
{
Boundary("Kz - start level 6/7 ls/lp");
Phase("6/7 ls & 6/7 lp")
{
R_Date("OxA-34828", 44000, 1900)
{
Outlier("General", 0.05);
color="green";
};
R_Date("OxA-34825", 43800, 1800)
{
Outlier("General", 0.05);
color="green";
};
R_Date("OxA-X-2699-11", 42900, 1700)
{
Outlier("General", 0.05);
color="green";
};
R_Date("OxA-34823", 43900, 1800)
{
Outlier("General", 0.05);
color="green";
};
R_Date("OxA-33555", 43700, 1900)
{
Outlier("General", 0.05);
color="green";
};
Interval("Kz - Interval 6/7 ls lp");
Date("Date layer 6/7 ls/lp");
};
Boundary("Kz - transition 6/7 ls/lp to 6/7 lb");
Interval("Kz - Interval transition 6/7 ls lp to 6/7 lb");
Phase("6/7 lb")
{
R_Combine("Kz-109")
{
Outlier("General", 0.05);
color="green";
R_Date("OxA-34826", 39800, 1100)
{
Outlier("SSimple", 0.05);
color="green";
};
R_Date("OxA-34827", 40900, 1300)
{
Outlier("SSimple", 0.05);
color="green";
};
};
Interval("Kz - Interval 6/7 lb");
Date("Date layer 6/7 lb");
};
Boundary("Kz - transition 6/7 lb to 5c");
Interval("Kz - Interval transition 6/7 lb to 5c");
Phase("5c")
{
R_Date("OxA-34824", 37600, 900)
{
Outlier("General", 0.05);
color="green";
};
R_Date("OxA-33835", 37500, 900)
{
Outlier("General", 0.05);
color="green";
};
R_Date("OxA-33552", 37000, 800)
{
Outlier("General", 0.05);
color="green";
};
R_Date("OxA-33553", 36800, 800)
{
Outlier("General", 0.05);
color="green";
};
R_Date("OxA-35234", 37400, 800)
```

```
{
Outlier("General", 0.05);
color="green";
};
Interval("Kz - Interval 5c");
Date("Date layer 5c");
};
Boundary("Kz - transition 5c to 5b");
Interval("Kz - Interval transition 5c to 5b");
Phase("5b")
{
R_Date("OxA-34769", 36550, 750)
{
Outlier("General", 0.05);
color="green";
};
R_Date("CI", 34290, 90)
{
Outlier("General", 0.05);
color="#b7005c";
};
R_Date("OxA-33554", 33650, 550)
{
Outlier("General", 0.05);
color="green";
};
R_Date("OxA-33551", 32750, 500)
{
Outlier("General", 0.05);
color="green";
};
R_Date("OxA-35575", 27830, 270)
{
Outlier("General", 0.05);
color="green";
};
R_Date("OxA-35576", 28010,280)
{
Outlier("General", 0.05);
color="green";
};
Interval("Kz - Interval 5b");
Date("Date layer 5b");
};
Boundary("Kz - transition 5b to 5a");
Interval("Kz - Interval transition 5b to 5a");
Phase("5a")
{
R_Date("OxA-33550", 27540, 270)
{
Outlier("General", 0.05);
color="green";
};
R_Date("OxA-33549", 27290, 270)
{
Outlier("General", 0.05);
color="green";
};
R_Date("OxA-34822", 25400, 200)
{
Outlier("General", 0.05);
color="green";
};
Interval("Kz - Interval 5a");
Date("Date layer 5a");
};
Boundary("Kz - transition 5a to 4 (IVb)");
Phase("4 (IVb)")
{
R_Date("OxA-35230", 26340, 220)
{
Outlier("General", 0.05);
color="green";
};
R_Date("OxA-33547", 25800, 220)
{
Outlier("General", 0.05);
color="green";
};
R_Date("OxA-33548", 24090, 180)
{
Outlier("General", 0.05);
color="green";
};
Interval("Kz - Interval 4 (IVb)");
Date("Date layer 4 (IVb)");
};
Boundary("Kz - transition 4 (IVb) to 4 (IVa)");
Interval("Kz - Interval transition 5a to 4 (IVb)");
Phase("4 (IVa)")
{
R_Date("OxA-34767", 26400, 220)
{
Outlier("General", 0.05);
color="green";
};
R_Date("OxA-34768", 27380, 250)
{
Outlier("General", 0.05);
color="green";
};
R_Date("OxA-33546", 27330, 260)
{
Outlier("General", 0.05);
color="green";
};
R_Date("OxA-33834", 28020, 290)
{
Outlier("General", 0.05);
color="green";
};
Interval("Kz - Interval 4 (IVa)");
Date("Date layer 4 (IVa)");
};
Boundary("Kz - transition 4 (IVa) to 3b");
Interval("Kz - Interval transition 4 (IVa) to 3b");
Phase("3b")
{
R_Date("OxA-35417", 23240, 180)
{
Outlier("General", 0.05);
color="green";
};
Interval("Kz - Interval 3b");
Date("Date layer 3b");
};
Boundary("Kz - end of 3b");
};
};
```

Model 3 – figure 8.20

```
 Plot()
{
Outlier_Model("General",T(5),U(0,4),"t");
Outlier_Model("SSimple",N(0,2),0,"s");
Sequence("Kz - Model 3")
{
Boundary("Kz - start level 6/7 ls/lp");
Phase("6/7 ls & 6/7 lp")
{
R_Date("OxA-34828", 44000, 1900)
{
Outlier("General", 0.05);
color="green";
};
R_Date("OxA-34825", 43800, 1800)
{
Outlier("General", 0.05);
color="green";
};
R_Date("OxA-X-2699-11", 42900, 1700)
{
Outlier("General", 0.05);
```

```
color="green";
};
R_Date("OxA-34823", 43900, 1800)
{
Outlier("General", 0.05);
color="green";
};
R_Date("OxA-33555", 43700, 1900)
{
Outlier("General", 0.05);
color="green";
};
Interval("Kz - Interval 6/7 ls lp");
Date("Date layer 6/7 ls/lp");
};
Boundary("Kz - transition 6/7 ls/lp to 6/7 lb");
Interval("Kz - Interval transition 6/7 ls lp to 6/7 lb");
Phase("6/7 lb")
{
R_Combine("Kz-109")
{
Outlier("General", 0.05);
color="green";
R_Date("OxA-34826", 39800, 1100)
{
Outlier("SSimple", 0.05);
color="green";
};
R_Date("OxA-34827", 40900, 1300)
{
Outlier("SSimple", 0.05);
color="green";
};
};
Interval("Kz - Interval 6/7 lb");
Date("Date layer 6/7 lb");
};
Boundary("Kz - transition 6/7 lb to 5c");
Interval("Kz - Interval transition 6/7 lb to 5c");
Phase("5c")
{
R_Date("OxA-34824", 37600, 900)
{
Outlier("General", 0.05);
color="green";
};
R_Date("OxA-33835", 37500, 900)
{
Outlier("General", 0.05);
color="green";
};
R_Date("OxA-33552", 37000, 800)
{
Outlier("General", 0.05);
color="green";
};
R_Date("OxA-33553", 36800, 800)
{
Outlier("General", 0.05);
color="green";
};
R_Date("OxA-35234", 37400, 800)
{
Outlier("General", 0.05);
color="green";
};
R_Date("OxA-34769", 36550, 750)
{
Outlier("General", 0.05);
color="green";
};
Interval("Kz - Interval 5c");
Date("Date layer 5c");
};
Boundary("Kz - transition 5c to 5b");
Interval("Kz - Interval transition 5c to 5b");
Phase("5b")
{
R_Date("CI", 34290, 90)
{
Outlier("General", 0.05);
color="#b7005c";
};
R_Date("OxA-33554", 33650, 550)
{
Outlier("General", 0.05);
color="green";
};
R_Date("OxA-33551", 32750, 500)
{
Outlier("General", 0.05);
color="green";
};
R_Date("OxA-35575", 27830, 270)
{
Outlier("General", 0.05);
color="green";
};
R_Date("OxA-35576", 28010,280)
{
Outlier("General", 0.05);
color="green";
};
Interval("Kz - Interval 5b");
Date("Date layer 5b");
};
Boundary("Kz - transition 5b to 5a");
Interval("Kz - Interval transition 5b to 5a");
Phase("5a")
{
R_Date("OxA-33550", 27540, 270)
{
Outlier("General", 0.05);
color="green";
};
R_Date("OxA-33549", 27290, 270)
{
Outlier("General", 0.05);
color="green";
};
R_Date("OxA-34822", 25400, 200)
{
Outlier("General", 0.05);
color="green";
};
Interval("Kz - Interval 5a");
Date("Date layer 5a");
};
Boundary("Kz - transition 5a to 4");
Interval("Kz - Interval transition 5a to 4");
Phase("4")
{
R_Date("OxA-35230", 26340, 220)
{
Outlier("General", 0.05);
color="green";
};
R_Date("OxA-33547", 25800, 220)
{
Outlier("General", 0.05);
color="green";
};
R_Date("OxA-33548", 24090, 180)
{
Outlier("General", 0.05);
color="green";
};
R_Date("OxA-34767", 26400, 220)
{
Outlier("General", 0.05);
color="green";
};
R_Date("OxA-34768", 27380, 250)
{
Outlier("General", 0.05);
color="green";
};
R_Date("OxA-33546", 27330, 260)
{
Outlier("General", 0.05);
color="green";
};
R_Date("OxA-33834", 28020, 290)
{
Outlier("General", 0.05);
color="green";
```

```
};
Interval("Kz - Interval 4");
Date("Date layer 4");
};
Boundary("Kz - transition 4 to 3b");
Interval("Kz - Interval transition 4 (IVa) to 3b");
Phase("3b")
{
R_Date("OxA-35417", 23240, 180)
{
Outlier("General", 0.05);
color="green";
};
Interval("Kz - Interval 3b");
Date("Date layer 3b");
};
Boundary("Kz - end of 3b");
};
};
```

Model 4 – figure 8.20

```
 Plot()
{
Outlier_Model("General",T(5),U(0,4),"t");
Outlier_Model("SSimple",N(0,2),0,"s");
Sequence("Kz - Model 4")
{
Boundary("Kz - start level 6/7 ls/lp");
Phase("6/7 ls & 6/7 lp")
{
R_Date("OxA-34828", 44000, 1900)
{
Outlier("General", 0.05);
color="green";
};
R_Date("OxA-34825", 43800, 1800)
{
Outlier("General", 0.05);
color="green";
};
R_Date("OxA-X-2699-11", 42900, 1700)
{
Outlier("General", 0.05);
color="green";
};
R_Date("OxA-34823", 43900, 1800)
{
Outlier("General", 0.05);
color="green";
};
R_Date("OxA-33555", 43700, 1900)
{
Outlier("General", 0.05);
color="green";
};
Interval("Kz - Interval 6/7 ls lp");
Date("Date layer 6/7 ls/lp");
};
Boundary("Kz - transition 6/7 ls/lp to 6/7 lb");
Interval("Kz - Interval transition 6/7 ls lp to 6/7 lb");
Phase("6/7 lb")
{
R_Combine("Kz-109")
{
Outlier("General", 0.05);
color="green";
R_Date("OxA-34826", 39800, 1100)
{
Outlier("SSimple", 0.05);
color="green";
};
R_Date("OxA-34827", 40900, 1300)
{
Outlier("SSimple", 0.05);
color="green";
};
};
Interval("Kz - Interval 6/7 lb");
Date("Date layer 6/7 lb");
};
Boundary("Kz - transition 6/7 lb to 5c");
Interval("Kz - Interval transition 6/7 lb to 5c");
Phase("5c")
{
R_Date("OxA-34824", 37600, 900)
{
Outlier("General", 0.05);
color="green";
};
R_Date("OxA-33835", 37500, 900)
{
Outlier("General", 0.05);
color="green";
};
R_Date("OxA-33552", 37000, 800)
{
Outlier("General", 0.05);
color="green";
};
R_Date("OxA-33553", 36800, 800)
{
Outlier("General", 0.05);
color="green";
};
R_Date("OxA-35234", 37400, 800)
{
Outlier("General", 0.05);
color="green";
};
Interval("Kz - Interval 5c");
Date("Date layer 5c");
};
Boundary("Kz - transition 5c to 5b");
Interval("Kz - Interval transition 5c to 5b");
Phase("5b")
{
R_Date("OxA-34769", 36550, 750)
{
Outlier("General", 0.05);
color="green";
};
R_Date("CI", 34290, 90)
{
Outlier("General", 0.05);
color="#b7005c";
};
R_Date("OxA-33554", 33650, 550)
{
Outlier("General", 0.05);
color="green";
};
R_Date("OxA-33551", 32750, 500)
{
Outlier("General", 0.05);
color="green";
};
R_Date("OxA-35575", 27830, 270)
{
Outlier("General", 0.05);
color="green";
};
R_Date("OxA-35576", 28010,280)
{
Outlier("General", 0.05);
color="green";
};
Interval("Kz - Interval 5b");
Date("Date layer 5b");
};
Boundary("Kz - transition 5b to 5a");
Interval("Kz - Interval transition 5b to 5a");
Phase("5a")
{
```

```
R_Date("OxA-33550", 27540, 270)
{
Outlier("General", 0.05);
color="green";
};
R_Date("OxA-33549", 27290, 270)
{
Outlier("General", 0.05);
color="green";
};
R_Date("OxA-34822", 25400, 200)
{
Outlier("General", 0.05);
color="green";
};
Interval("Kz - Interval 5a");
Date("Date layer 5a");
};
Boundary("Kz - transition 5a to 4");
Interval("Kz - Interval transition 5a to 4");
Phase("4")
{
R_Date("OxA-35230", 26340, 220)
{
Outlier("General", 0.05);
color="green";
};
R_Date("OxA-33547", 25800, 220)
{
Outlier("General", 0.05);
color="green";
};
R_Date("OxA-33548", 24090, 180)
{
Outlier("General", 0.05);
color="green";
};
R_Date("OxA-34767", 26400, 220)
{
Outlier("General", 0.05);
color="green";
};
R_Date("OxA-34768", 27380, 250)
{
Outlier("General", 0.05);
color="green";
};
R_Date("OxA-33546", 27330, 260)
{
Outlier("General", 0.05);
color="green";
};
R_Date("OxA-33834", 28020, 290)
{
Outlier("General", 0.05);
color="green";
};
Interval("Kz - Interval 4");
Date("Date layer 4");
};
Boundary("Kz - transition 4 to 3b");
Interval("Kz - Interval transition 4 (IVa) to 3b");
Phase("3b")
{
R_Date("OxA-35417", 23240, 180)
{
Outlier("General", 0.05);
color="green";
};
Interval("Kz - Interval 3b");
Date("Date layer 3b");
};
Boundary("Kz - end of 3b");
};
};
```

Model 5 – figure 8.21

```
 Plot()
{
Outlier_Model("General",T(5),U(0,4),"t");
Outlier_Model("SSimple",N(0,2),0,"s");
Sequence("Kz - Model 5")
{
Boundary("Kz - start level 6/7");
Phase("6/7")
{
R_Date("OxA-24083", 37400, 500)
{
color="blue";
Outlier("General", 0.05);
};
R_Date("OxA-34828", 44000, 1900)
{
Outlier("General", 0.05);
color="green";
};
R_Date("OxA-22842", 41100, 750)
{
Outlier("General", 0.05);
color="#5b92e5";
};
R_Date("OxA-34825", 43800, 1800)
{
Outlier("General", 0.05);
color="green";
};
R_Date("OxA-X-2699-11", 42900, 1700)
{
Outlier("General", 0.05);
color="green";
};
R_Date("OxA-34823", 43900, 1800)
{
Outlier("General", 0.05);
color="green";
};
R_Date("GifA-101048", 29310, 320)
{
Outlier("General", 0.05);
color="#5b92e5";
};
R_Date("GifA-101051", 43600, 1200)
{
Outlier("General", 0.05);
color="#5b92e5";
};
R_Date("OxA-33555", 43700, 1900)
{
Outlier("General", 0.05);
color="green";
};
R_Combine("Kz-109")
{
Outlier("General", 0.05);
color="green";
R_Date("OxA-34826", 39800, 1100)
{
Outlier("SSimple", 0.05);
color="green";
};
R_Date("OxA-34827", 40900, 1300)
{
Outlier("SSimple", 0.05);
color="green";
};
};
Interval("Kz - Interval 6/7");
Date("Date layer 6/7");
};
Boundary("Kz - transition 6/7 to 5c");
Interval("Kz - Interval transition 6/7 to 5c");
Phase("5c")
{
```

```
R_Date("Gif/LSM-10994", 38700, 1400)
{
Outlier("General", 0.05);
color="#5b92e5";
};
R_Date("OxA-25406", 37600, 500)
{
color="blue";
Outlier("General", 0.05);
};
R_Date("OxA-34824", 37600, 900)
{
Outlier("General", 0.05);
color="green";
};
R_Date("OxA-24802", 37650, 500)
{
color="blue";
Outlier("General", 0.05);
};
R_Date("OxA-23975", 38050, 500)
{
color="blue";
Outlier("General", 0.05);
};
R_Date("OxA-33835", 37500, 900)
{
Outlier("General", 0.05);
color="green";
};
R_Date("OxA-33552", 37000, 800)
{
Outlier("General", 0.05);
color="green";
};
R_Date("OxA-33553", 36800, 800)
{
Outlier("General", 0.05);
color="green";
};
R_Date("GifA-99706", 36200, 540)
{
Outlier("General", 0.05);
color="#5b92e5";
};
R_Date("OxA-24080", 36350, 400)
{
color="blue";
Outlier("General", 0.05);
};
R_Date("OxA-35234", 37400, 800)
{
Outlier("General", 0.05);
color="green";
};
R_Date("OxA-25405", 36900, 450)
{
color="blue";
Outlier("General", 0.05);
};
R_Date("OxA-34769", 36550, 750)
{
Outlier("General", 0.05);
color="green";
};
R_Date("OxA-24058", 32330, 260)
{
color="blue";
Outlier("General", 0.05);
};
Interval("Kz - Interval 5c");
Date("Date layer 5c");
};
Boundary("Kz - transition 5c to 5b");
Interval("Kz - Interval transition 5c to 5b");
Phase("5b")
{
R_Date("OxA-24059", 36650, 450)
{
color="blue";
Outlier("General", 0.05);
};
R_Date("OxA-22914", 36250, 450)
{
Outlier("General", 0.05);
color="#5b92e5";
};
R_Date("CI", 34290, 90)
{
Outlier("General", 0.05);
color="#b7005c";
};
R_Date("OxA-33554", 33650, 550)
{
Outlier("General", 0.05);
color="green";
};
R_Date("OxA-33551", 32750, 500)
{
Outlier("General", 0.05);
color="green";
};
R_Date("OxA-35575", 27830, 270)
{
Outlier("General", 0.05);
color="green";
};
R_Date("OxA-35576", 28010,280)
{
Outlier("General", 0.05);
color="green";
};
R_Date("OxA-24865", 28380, 170)
{
color="blue";
Outlier("General", 0.05);
};
R_Date("GifA-99044", 26490, 270)
{
color="blue";
Outlier("General", 0.05);
};
Interval("Kz - Interval 5b");
Date("Date layer 5b");
};
Boundary("Kz - transition 5b to 5a");
Interval("Kz - Interval transition 5b to 5a");
Phase("5a")
{
R_Date("OxA-33550", 27540, 270)
{
Outlier("General", 0.05);
color="green";
};
R_Date("Gif-10992", 25650, 730)
{
color="blue";
Outlier("General", 0.05);
};
R_Date("OxA-33549", 27290, 270)
{
Outlier("General", 0.05);
color="green";
};
R_Date("OxA-24786", 26320, 190)
{
color="blue";
Outlier("General", 0.05);
};
R_Date("OxA-34822", 25400, 200)
{
Outlier("General", 0.05);
color="green";
};
Interval("Kz - Interval 5a");
Date("Date layer 5a");
};
Boundary("Kz - transition 5a to 4");
Interval("Kz - Interval transition 5a to 4");
Phase("4")
{
R_Date("OxA-25355", 25770, 140)
{
color="blue";
Outlier("General", 0.05);
};
```

```
R_Date("OxA-25184", 27370, 190)
{
color="blue";
Outlier("General", 0.05);
};
R_Date("OxA-35230", 26340, 220)
{
Outlier("General", 0.05);
color="green";
};
R_Date("OxA-33547", 25800, 220)
{
Outlier("General", 0.05);
color="green";
};
R_Date("OxA-33548", 24090, 180)
{
Outlier("General", 0.05);
color="green";
};
R_Date("Gif/LSM-10677", 26120, 100)
{
color="blue";
Outlier("General", 0.05);
};
R_Date("OxA-34767", 26400, 220)
{
Outlier("General", 0.05);
color="green";
};
R_Date("OxA-34768", 27380, 250)
{
Outlier("General", 0.05);
color="green";
};
R_Date("OxA-33546", 27330, 260)
{
Outlier("General", 0.05);
color="green";
};
R_Date("OxA-33834", 28020, 290)
{
Outlier("General", 0.05);
color="green";
};
Interval("Kz - Interval 4");
Date("Date layer 4");
};
Boundary("Kz - transition 4 to 3b");
Interval("Kz - Interval transition 4 (IVa) to 3b");
Phase("3b")
{
R_Date("OxA-35417", 23240, 180)
{
Outlier("General", 0.05);
color="green";
};
R_Date("Gif-10674", 19770, 270)
{
color="blue";
Outlier("General", 0.05);
};
Interval("Kz - Interval 3b");
Date("Date layer 3b");
};
Boundary("Kz - end of 3b");
};
};
```

Model 6

```
 Plot()
{
Outlier_Model("General",T(5),U(0,4),"t");
Outlier_Model("SSimple",N(0,2),0,"s");
Sequence("Kz - Model 6")
{
Boundary("Kz - start level 6/7");
Phase("6/7")
{
R_Date("OxA-24083", 37400, 500)
{
color="blue";
Outlier("General", 0.05);
};
R_Date("OxA-34828", 44000, 1900)
{
Outlier("General", 0.05);
color="green";
};
R_Date("OxA-22842", 41100, 750)
{
Outlier("General", 0.05);
color="#5b92e5";
};
R_Date("OxA-34825", 43800, 1800)
{
Outlier("General", 0.05);
color="green";
};
R_Date("OxA-X-2699-11", 42900, 1700)
{
Outlier("General", 0.05);
color="green";
};
R_Date("OxA-34823", 43900, 1800)
{
Outlier("General", 0.05);
color="green";
};
R_Date("GifA-101048", 29310, 320)
{
Outlier("General", 0.05);
color="#5b92e5";
};
R_Date("GifA-101051", 43600, 1200)
{
Outlier("General", 0.05);
color="#5b92e5";
};
R_Date("OxA-33555", 43700, 1900)
{
Outlier("General", 0.05);
color="green";
};
R_Combine("Kz-109")
{
Outlier("General", 0.05);
color="green";
R_Date("OxA-34826", 39800, 1100)
{
Outlier("SSimple", 0.05);
color="green";
};
R_Date("OxA-34827", 40900, 1300)
{
Outlier("SSimple", 0.05);
color="green";
};
};
Interval("Kz - Interval 6/7");
Date("Date layer 6/7");
};
Boundary("Kz - transition 6/7 to 5c");
Interval("Kz - Interval transition 6/7 to 5c");
Phase("5c")
{
R_Date("Gif/LSM-10994", 38700, 1400)
{
Outlier("General", 0.05);
color="#5b92e5";
};
R_Date("OxA-25406", 37600, 500)
{
color="blue";
```

```
Outlier("General", 0.05);
};
R_Date("OxA-34824", 37600, 900)
{
Outlier("General", 0.05);
color="green";
};
R_Date("OxA-24802", 37650, 500)
{
color="blue";
Outlier("General", 0.05);
};
R_Date("OxA-23975", 38050, 500)
{
color="blue";
Outlier("General", 0.05);
};
R_Date("OxA-33835", 37500, 900)
{
Outlier("General", 0.05);
color="green";
};
R_Date("OxA-33552", 37000, 800)
{
Outlier("General", 0.05);
color="green";
};
R_Date("OxA-33553", 36800, 800)
{
Outlier("General", 0.05);
color="green";
};
R_Date("GifA-99706", 36200, 540)
{
Outlier("General", 0.05);
color="#5b92e5";
};
R_Date("OxA-24080", 36350, 400)
{
color="blue";
Outlier("General", 0.05);
};
R_Date("OxA-35234", 37400, 800)
{
Outlier("General", 0.05);
color="green";
};
R_Date("OxA-25405", 36900, 450)
{
color="blue";
Outlier("General", 0.05);
};
R_Date("OxA-24058", 32330, 260)
{
color="blue";
Outlier("General", 0.05);
};
Interval("Kz - Interval 5c");
Date("Date layer 5c");
};
Boundary("Kz - transition 5c to 5b");
Interval("Kz - Interval transition 5c to 5b");
Phase("5b")
{
R_Date("OxA-34769", 36550, 750)
{
Outlier("General", 0.05);
color="green";
};
R_Date("OxA-24059", 36650, 450)
{
color="blue";
Outlier("General", 0.05);
};
R_Date("OxA-22914", 36250, 450)
{
Outlier("General", 0.05);
color="#5b92e5";
};
R_Date("CI", 34290, 90)
{
Outlier("General", 0.05);
color="#b7005c";
};
R_Date("OxA-33554", 33650, 550)
{
Outlier("General", 0.05);
color="green";
};
R_Date("OxA-33551", 32750, 500)
{
Outlier("General", 0.05);
color="green";
};
R_Date("OxA-35575", 27830, 270)
{
Outlier("General", 0.05);
color="green";
};
R_Date("OxA-35576", 28010,280)
{
Outlier("General", 0.05);
color="green";
};
R_Date("OxA-24865", 28380, 170)
{
color="blue";
Outlier("General", 0.05);
};
R_Date("GifA-99044", 26490, 270)
{
color="blue";
Outlier("General", 0.05);
};
Interval("Kz - Interval 5b");
Date("Date layer 5b");
};
Boundary("Kz - transition 5b to 5a");
Interval("Kz - Interval transition 5b to 5a");
Phase("5a")
{
R_Date("OxA-33550", 27540, 270)
{
Outlier("General", 0.05);
color="green";
};
R_Date("Gif-10992", 25650, 730)
{
color="blue";
Outlier("General", 0.05);
};
R_Date("OxA-33549", 27290, 270)
{
Outlier("General", 0.05);
color="green";
};
R_Date("OxA-24786", 26320, 190)
{
color="blue";
Outlier("General", 0.05);
};
R_Date("OxA-34822", 25400, 200)
{
Outlier("General", 0.05);
color="green";
};
Interval("Kz - Interval 5a");
Date("Date layer 5a");
};
Boundary("Kz - transition 5a to 4");
Interval("Kz - Interval transition 5a to 4");
Phase("4")
{
R_Date("OxA-25355", 25770, 140)
{
color="blue";
Outlier("General", 0.05);
};
R_Date("OxA-25184", 27370, 190)
{
color="blue";
Outlier("General", 0.05);
};
R_Date("OxA-35230", 26340, 220)
{
Outlier("General", 0.05);
```

```
color="green";
};
R_Date("OxA-33547", 25800, 220)
{
Outlier("General", 0.05);
color="green";
};
R_Date("OxA-33548", 24090, 180)
{
Outlier("General", 0.05);
color="green";
};
R_Date("Gif/LSM-10677", 26120, 100)
{
color="blue";
Outlier("General", 0.05);
};
R_Date("OxA-34767", 26400, 220)
{
Outlier("General", 0.05);
color="green";
};
R_Date("OxA-34768", 27380, 250)
{
Outlier("General", 0.05);
color="green";
};
R_Date("OxA-33546", 27330, 260)
{
Outlier("General", 0.05);
color="green";
};
R_Date("OxA-33834", 28020, 290)
{
Outlier("General", 0.05);
color="green";
};
Interval("Kz - Interval 4");
Date("Date layer 4");
};
Boundary("Kz - transition 4 to 3b");
Interval("Kz - Interval transition 4 (IVa) to 3b");
Phase("3b")
{
R_Date("OxA-35417", 23240, 180)
{
Outlier("General", 0.05);
color="green";
};
R_Date("Gif-10674", 19770, 270)
{
color="blue";
Outlier("General", 0.05);
};
Interval("Kz - Interval 3b");
Date("Date layer 3b");
};
Boundary("Kz - end of 3b");
};
};
```

Model 7 – figure 8.21

```
 Plot()
{
Outlier_Model("General",T(5),U(0,4),"t");
Outlier_Model("SSimple",N(0,2),0,"s");
Sequence("Kz - Model 7")
{
Boundary("Kz - start layer 9a");
Phase("9a")
{
Date("OSL",N(calBP(46000), 4000))
{
Outlier("General", 0.05);
};
Date("Date layer 9a");
Interval("Kz - interval 9a");
};
Boundary("Kz - transition 9a to 6/7 ls/lp");
Interval("Kz - interval transition 9a to 6/7 lslp");
Phase("6/7 ls & 6/7 lp")
{
R_Date("OxA-34828", 44000, 1900)
{
Outlier("General", 0.05);
color="green";
};
R_Date("OxA-34825", 43800, 1800)
{
Outlier("General", 0.05);
color="green";
};
R_Date("OxA-X-2699-11", 42900, 1700)
{
Outlier("General", 0.05);
color="green";
};
R_Date("OxA-34823", 43900, 1800)
{
Outlier("General", 0.05);
color="green";
};
R_Date("OxA-33555", 43700, 1900)
{
Outlier("General", 0.05);
color="green";
};
Interval("Kz - Interval 6/7 ls lp");
Date("Date layer 6/7 ls/lp");
};
Boundary("Kz - transition 6/7 ls/lp to 6/7 lb");
Interval("Kz - Interval transition 6/7 ls lp to 6/7 lb");
Phase("6/7 lb")
{
R_Combine("Kz-109")
{
Outlier("General", 0.05);
color="green";
R_Date("OxA-34826", 39800, 1100)
{
Outlier("SSimple", 0.05);
color="green";
};
R_Date("OxA-34827", 40900, 1300)
{
Outlier("SSimple", 0.05);
color="green";
};
};
Interval("Kz - Interval 6/7 lb");
Date("Date layer 6/7 lb");
};
Boundary("Kz - transition 6/7 lb to 5c");
Interval("Kz - Interval transition 6/7 lb to 5c");
Phase("5c")
{
R_Date("OxA-34824", 37600, 900)
{
Outlier("General", 0.05);
color="green";
};
R_Date("OxA-33835", 37500, 900)
{
Outlier("General", 0.05);
color="green";
};
R_Date("OxA-33552", 37000, 800)
{
Outlier("General", 0.05);
color="green";
};
R_Date("OxA-33553", 36800, 800)
{
Outlier("General", 0.05);
```

```
color="green";
};
R_Date("OxA-35234", 37400, 800)
{
Outlier("General", 0.05);
color="green";
};
R_Date("OxA-34769", 36550, 750)
{
Outlier("General", 0.05);
color="green";
};
Interval("Kz - Interval 5c");
Date("Date layer 5c");
};
Boundary("Kz - transition 5c to 5b");
Interval("Kz - Interval transition 5c to 5b");
Phase("5b")
{
R_Date("CI", 34290, 90)
{
Outlier("General", 0.05);
color="#b7005c";
};
R_Date("OxA-33554", 33650, 550)
{
Outlier("General", 0.05);
color="green";
};
R_Date("OxA-33551", 32750, 500)
{
Outlier("General", 0.05);
color="green";
};
R_Date("OxA-35575", 27830, 270)
{
Outlier("General", 0.05);
color="green";
};
R_Date("OxA-35576", 28010,280)
{
Outlier("General", 0.05);
color="green";
};
Interval("Kz - Interval 5b");
Date("Date layer 5b");
};
Boundary("Kz - transition 5b to 5a");
Interval("Kz - Interval transition 5b to 5a");
Phase("5a")
{
R_Date("OxA-33550", 27540, 270)
{
Outlier("General", 0.05);
color="green";
};
R_Date("OxA-33549", 27290, 270)
{
Outlier("General", 0.05);
color="green";
};
R_Date("OxA-34822", 25400, 200)
{
Outlier("General", 0.05);
color="green";
};
Interval("Kz - Interval 5a");
Date("Date layer 5a");
};
Boundary("Kz - transition 5a to 4");
Interval("Kz - Interval transition 5a to 4");
Phase("4")
{
R_Date("OxA-35230", 26340, 220)
{
Outlier("General", 0.05);
color="green";
};
R_Date("OxA-33547", 25800, 220)
{
Outlier("General", 0.05);
color="green";
};
R_Date("OxA-33548", 24090, 180)
{
Outlier("General", 0.05);
color="green";
};
R_Date("OxA-34767", 26400, 220)
{
Outlier("General", 0.05);
color="green";
};
R_Date("OxA-34768", 27380, 250)
{
Outlier("General", 0.05);
color="green";
};
R_Date("OxA-33546", 27330, 260)
{
Outlier("General", 0.05);
color="green";
};
R_Date("OxA-33834", 28020, 290)
{
Outlier("General", 0.05);
color="green";
};
Interval("Kz - Interval 4");
Date("Date layer 4");
};
Boundary("Kz - transition 4 to 3b");
Interval("Kz - Interval transition 4 (IVa) to 3b");
Phase("3b")
{
R_Date("OxA-35417", 23240, 180)
{
Outlier("General", 0.05);
color="green";
};
Interval("Kz - Interval 3b");
Date("Date layer 3b");
};
Boundary("Kz - end of 3b");
};
};
```

KDE 0 – figure 8.22

```
 KDE_model("Kz - KDE 0")
{
R_Date("GifA-101051", 43600, 1200);
R_Date("OxA-22842", 41100, 750);
R_Date("GifA-101048", 29310, 320);
R_Date("OxA-24083", 37400, 500);
R_Date("Gif/LSM-10994", 38700, 1400);
R_Date("OxA-23975", 38050, 500);
R_Date("OxA-25406", 37600, 500);
R_Date("OxA-24802", 37650, 500);
R_Date("GifA-99706", 36200, 540);
R_Date("OxA-25405", 36900, 450);
R_Date("OxA-24080", 36350, 400);
R_Date("OxA-24058", 32330, 260);
R_Date("OxA-24059", 36650, 450);
R_Date("OxA-22914", 36250, 450);
R_Date("OxA-24865", 28380, 170);
R_Date("GifA-99044", 26490, 270);
R_Date("Gif-10992", 25650, 730);
R_Date("OxA-24786", 26320, 190);
R_Date("Gif/LSM-10677", 26120, 100);
R_Date("OxA-25355", 25770, 140);
R_Date("OxA-25184", 27370, 190);
R_Date("Gif-10674", 19770, 270);
R_Date("GifA-98345", 11550, 100);
};
```

KDE 1 – figure 8.22

```
 KDE_model("Kz - KDE 1")
{
R_Date("OxA-35417", 23240, 180)
{
};
R_Date("OxA-34767", 26400, 220);
R_Date("OxA-33546", 27330, 260);
R_Date("OxA-34768", 27380, 250);
R_Date("OxA-33834", 28020, 290);
R_Date("OxA-33548", 24090, 180);
R_Date("OxA-33547", 25800, 220);
R_Date("OxA-35230", 26340, 220);
R_Date("OxA-34822", 25400, 200);
R_Date("OxA-33549", 27290, 270);
R_Date("OxA-33550", 27540, 270);
R_Date("OxA-35575", 27830, 270);
R_Date("OxA-35576", 28010,280);
R_Date("OxA-33551", 32750, 500);
R_Date("OxA-33554", 33650, 550);
R_Date("OxA-35234", 37400, 800)
{
color="blue";
};
R_Date("OxA-34769", 36550, 750)
{
color="blue";
};
R_Date("OxA-33553", 36800, 800);
R_Date("OxA-33552", 37000, 800);
R_Date("OxA-33835", 37500, 900);
R_Date("OxA-34824", 37600, 900);
R_Combine("Kz-109")
{
R_Date("OxA-34826", 39800, 1100);
R_Date("OxA-34827", 40900, 1300);
};
R_Date("OxA-33555", 43700, 1900)
{
color="blue";
};
R_Date("OxA-34823", 43900, 1800);
R_Date("OxA-X-2699-11", 42900, 1700);
R_Date("OxA-34825", 43800, 1800);
R_Date("OxA-34828", 44000, 1900)
{
};
};
```

KDE 2 – figure 8.22

```
 KDE_model("Kz - KDE 2")
{
R_Date("GifA-101051", 43600, 1200)
{
color="gray";
};
R_Date("OxA-22842", 41100, 750)
{
color="gray";
};
R_Date("GifA-101048", 29310, 320)
{
color="gray";
};
R_Date("OxA-24083", 37400, 500)
{
};
R_Date("Gif/LSM-10994", 38700, 1400)
{
color="gray";
};
R_Date("OxA-23975", 38050, 500)
{
};
R_Date("OxA-25406", 37600, 500)
{
};
R_Date("OxA-24802", 37650, 500)
{
};
R_Date("GifA-99706", 36200, 540)
{
};
R_Date("OxA-25405", 36900, 450)
{
};
R_Date("OxA-24080", 36350, 400)
{
};
R_Date("OxA-24058", 32330, 260)
{
};
R_Date("OxA-24059", 36650, 450)
{
};
R_Date("OxA-22914", 36250, 450)
{
};
R_Date("OxA-24865", 28380, 170)
{
};
R_Date("GifA-99044", 26490, 270)
{
};
R_Date("Gif-10992", 25650, 730)
{
};
R_Date("OxA-24786", 26320, 190)
{
};
R_Date("Gif/LSM-10677", 26120, 100)
{
};
R_Date("OxA-25355", 25770, 140)
{
};
R_Date("OxA-25184", 27370, 190)
{
};
R_Date("Gif-10674", 19770, 270)
{
};
R_Date("GifA-98345", 11550, 100)
{
};
R_Date("OxA-35417", 23240, 180)
{
};
R_Date("OxA-34767", 26400, 220);
R_Date("OxA-33546", 27330, 260);
R_Date("OxA-34768", 27380, 250);
R_Date("OxA-33834", 28020, 290);
R_Date("OxA-33548", 24090, 180);
R_Date("OxA-33547", 25800, 220);
R_Date("OxA-35230", 26340, 220);
R_Date("OxA-34822", 25400, 200);
R_Date("OxA-33549", 27290, 270);
R_Date("OxA-33550", 27540, 270);
R_Date("OxA-35575", 27830, 270);
R_Date("OxA-35576", 28010,280);
R_Date("OxA-33551", 32750, 500);
R_Date("OxA-33554", 33650, 550);
R_Date("OxA-35234", 37400, 800)
{
color="blue";
};
```

```
R_Date("OxA-34769", 36550, 750)
{
color="blue";
};
R_Date("OxA-33553", 36800, 800);
R_Date("OxA-33552", 37000, 800);
R_Date("OxA-33835", 37500, 900);
R_Date("OxA-34824", 37600, 900);
R_Combine("Kz-109")
{
R_Date("OxA-34826", 39800, 1100);
R_Date("OxA-34827", 40900, 1300);
};
R_Date("OxA-33555", 43700, 1900)
{
color="blue";
};
R_Date("OxA-34823", 43900, 1800);
R_Date("OxA-X-2699-11", 42900, 1700);
R_Date("OxA-34825", 43800, 1800);
R_Date("OxA-34828", 44000, 1900)
{
};
};
```

B.2 Code: Temnata Dupka

Model 0 – figure 8.55

```
 Plot("Model 0")
{
Outlier_Model("General",T(5),U(0,4),"t");
Outlier_Model("SSimple",N(0,2),0,"s");
Sequence("TD-I")
{
Boundary("TD-I - start 7");
Phase("Layer 7")
{

Date("Gd-TL-272", N(calBP(105000),35000))
{
Outlier("General", 0.05);
color="blue";
};
Date("Date layer 7");
};
Boundary("TD-I - transition 7 to 6");
Interval("Intv transition 7/6");
Phase("Layer 6")
{
Date("Gd-TL-254", N(calBP(67000),11000))
{
Outlier("General", 0.05);
color="blue";
};
Date("Date layer 6");
};
Boundary("TD-I: transition 6 to 5");
Interval("Intv transition 6/5");
Phase("5")
{
Date("Date layer 5");
};
Boundary("TD-I: transition 5 to 4");
Interval("Intv transition 5/4");
Phase("Layer 4C")
{
Date("Gd-TL-256", N(calBP(45000),7000))
{
Outlier("General", 0.05);
color="blue";
};
Date("Date layer 4C");
};
Boundary("TD-I: transition 4C to 4B");
Interval("Intv transition 4B/4A");
Phase("Layer 4B")
{
Date("Gd-TL-255", N(calBP(46000),8000))
{
Outlier("General", 0.05);
color="blue";
};
R_Date("OxA-5171", 38200, 1500)
{
Outlier("General", 0.05);
color="#674846";
};
R_Date("OxA-5170", 38800, 1700)
{
Outlier("General", 0.05);
color="#674846";
};
R_Date("OxA-5169", 39100, 1800)
{
Outlier("General", 0.05);
color=" #674846";
};
Date("Date layer 4B");
};
Boundary("TD-I: transition 4B to 4A");
Interval("Intv transition 4B/4A");
Phase("Layer 4A")
{
R_Date("Gd-2354", 31900, 1600)
{
Outlier("General", 0.05);
color="brown";
};
Date("Date layer 4A");
};
Boundary("TD-I: transition 4 to 3f");
Interval("Intv transition 4/3f");
Phase("Layer 3f")
{
R_Date("Gd-4233", 28900, 1400)
{
Outlier("General", 0.05);
color="brown";
};
Date("Date layer 3f");
};
Boundary("TD-I: transition 3f to 3d");
Interval("Intv transition 3f/3d");
Phase("Layer 3d")
{
R_Date("Gd-2580", 28900, 1100)
{
Outlier("General", 0.05);
color="brown";
};
R_Date("Gd-4231", 29700, 700)
{
Outlier("General", 0.05);
color="brown";
};
R_Date("Gd-4030", 21200, 900)
{
Outlier("General", 0.05);
color="dimgray";
};
R_Date("Gd-4232", 23400, 1600)
{
Outlier("General", 0.05);
color="brown";
};
R_Date("Gd-4029", 19940, 800)
{
Outlier("General", 0.05);
color="dimgray";
};
Date("Gd-TL-210", N(calBP(22900),2100))
{
Outlier("General", 0.05);
color="blue";
};
R_Date("Gd-2790", 21200, 380)
{
Outlier("General", 0.05);
color="brown";
};
Date("Date layer 3d");
};
Boundary("TD-I: transition 3d to 3a-c");
Interval("Intv transition 3d/3a-c");
Phase("Layer 3a-c")
{
R_Date("Gd-4027", 11200, 1600)
{
Outlier("General", 0.05);
color="dimgray";
};
R_Date("Gd-4026", 10440, 400)
{
Outlier("General", 0.05);
color="dimgray";
};
```

```
R_Date("Ly-3441", 24900, 510)
{
Outlier("General", 0.05);
color="brown";
};
R_Date("Ly-3440", 13920, 480)
{
Outlier("General", 0.05);
color="brown";
};
R_Date("Ly-3439", 13600, 200)
{
Outlier("General", 0.05);
color="brown";
};
Date("Date layer 3a-c");
};
Boundary("TD-I: end of 3a-c");
};
Sequence("TD-V")
{
Boundary("=TD-I: transition 4C to 4B");
Phase("Layer 4b")
{
R_Date("OxA-5172", 38300, 1600)
{
Outlier("General", 0.05);
color="#674846";
};
R_Date("OxA-5173", 36900, 1300)
{
Outlier("General", 0.05);
color="#674846";
};
Date("Date layer 4b");
};
Boundary("=TD-I: transition 4B to 4A");
Interval("Intv transition 4b/4a");
Phase("Layer 4a")
{
R_Date("OxA-5174", 33000, 900)
{
Outlier("General", 0.05);
color="#674846";
};
Date("Date layer 4a");
};
Boundary("TD-V: Transition 4a to 3v");
Interval("Intv transition 4a/3v");
Phase("Layer 3 'v'")
{
Date("Date layer 3v");
};
Boundary("TD-V: transition 3v to 3d");
Interval("Intv transition 3v/3d");
Phase("Layer 3d")
{
R_Date("Gd-6126", 24400, 600)
{
Outlier("General", 0.05);
color="brown";
};
R_Date("Gd-2785", 21200, 380)
{
Outlier("General", 0.05);
color="brown";
};
Date("Date layer 3d");
};
Boundary("TD-V: transition 3d to 3a-c");
Interval("Intv transition 3d to 3a-c");
Phase("Layer 3a-c")
{
Date("Gd-TL-214", N(calBP(23300),5100))
{
Outlier("General", 0.05);
color="blue";
};
R_Date("Gd-2581", 24800, 700)
{
Outlier("General", 0.05);
color="brown";
};
Date("Gd-TL-213", N(calBP(15400),6100))
{
Outlier("General", 0.05);
color="blue";
};
R_Date("Gd-4028", 20100, 900)
{
Outlier("General", 0.05);
color="dimgray";
};
R_Date("Gd-2578", 16600, 300)
{
Outlier("General", 0.05);
color="brown";
};
R_Date("Gd-4025", 10480, 280)
{
Outlier("General", 0.05);
color="dimgray";
};
R_Date("Gd-4022", 10880, 370)
{
Outlier("General", 0.05);
color="dimgray";
};
Date("Date layer 3a-c");
};
Boundary("=TD-I: end of 3a-c");
};
};
```

Model 1 – figure 8.56

```
 Plot("TD - Model 1")
{
Outlier_Model("General",T(5),U(0,4),"t");
Outlier_Model("SSimple",N(0,2),0,"s");
Sequence("TD-I")
{
Boundary("TD-I: start 4");
Phase("Layer 4")
{
R_Date("OxA-35756", 33650, 550)
{
Outlier("General", 0.05);
color="green";
};
R_Combine("TD-31")
{
Outlier("General", 0.05);
color="green";
R_Date("OxA-35757", 29160, 320)
{
Outlier("SSimple", 0.05);
color="green";
};
R_Date("OxA-35758", 29240, 320)
{
Outlier("SSimple", 0.05);
color="green";
};
};
R_Date("OxA-35231", 27270, 250)
{
Outlier("General", 0.05);
color="green";
};
R_Date("OxA-33845", 28770, 320)
{
Outlier("General", 0.05);
color="green";
```

```
};
Date("TD-I: Date Layer 4");
Interval("TD-I: layer 4");
};
Boundary("TD-I: transition 4 to 3");
Interval("TD-I: transition 4 to 3");
Phase("Layer 3f")
{
R_Date("OxA-35238", 29200, 310)
{
Outlier("General", 0.05);
color="green";
};
R_Date("OxA-35235", 28730, 290)
{
Outlier("General", 0.05);
color="green";
};
Date("TD-I: Date Layer 3f");
Interval("TD-I: layer 3f");
};
Boundary("TD-I: end 3");
};
Sequence("TD-V")
{
Boundary("TD-V: start 6");
Phase("Layer 6")
{
Date("OxA-35239", U(calBP(80000),calBP(49600)))
{
Outlier("General", 0.05);
color="green";
};
Date("TD-V: Date Layer 6");
Interval("TD-V: layer 6");
};
Boundary("TD-V: transition 6 to 5pg");
Interval("TD-V: transition 6 to 5pg");
Phase("Layer 5pg")
{
Date("OxA-35237", N(calBP(56000),3100))
{
Outlier("General", 0.05);
color="green";
};
Date("OxA-35236", U(calBP(80000),calBP(45100)))
{
Outlier("General", 0.05);
color="green";
};
Date("OxA-33874", U(calBP(80000),calBP(44200)))
{
Outlier("General", 0.05);
color="green";
};
Date("TD-V: Date Layer 5pg");
Interval("TD-V: layer 5pg");
};
Boundary("=TD-I: start 4");
Interval("=TD-I: start 4");
Phase("Layer 4")
{
Date("OxA-33837", U(calBP(80000),calBP(45300)))
{
Outlier("General", 0.05);
color="green";
};
Date("TD-V: Date Layer 4");
Interval("TD-V: layer 4");
};
Boundary("TD-V: transition 4 to 3j");
Interval("TD-V: transition 4 to 3j");
Phase("Layer 3j")
{
R_Combine("TD-08")
{
Outlier("General", 0.05);
color="green";
R_Date("OxA-33842", 33600, 550)
{
Outlier("SSimple", 0.05);
color="green";
};
R_Date("OxA-33841", 33800, 550)
{
Outlier("SSimple", 0.05);
color="green";
};
};
R_Combine("TD-28")
{
Outlier("General", 0.05);
color="green";
R_Date("OxA-35551", 33750, 550)
{
Outlier("SSimple", 0.05);
color="green";
};
R_Date("OxA-35755", 33800, 550)
{
Outlier("SSimple", 0.05);
color="green";
};
};
R_Date("OxA-35550", 33700, 550)
{
Outlier("General", 0.05);
color="green";
};
R_Date("OxA-33840", 28950, 310)
{
Outlier("General", 0.05);
color="green";
};
Date("TD-V: Date Layer 3j");
Interval("TD-V: layer 3j");
};
Boundary("TD-V: transition 3j to 3g");
Interval("TD-V: transition 3j to 3g");
Phase("Layer 3g")
{
R_Date("OxA-33843", 30950, 450)
{
Outlier("General", 0.05);
color="green";
};
R_Date("OxA-33844", 29170, 320)
{
Outlier("General", 0.05);
color="green";
};
R_Date("OxA-35523", 30560, 370)
{
Outlier("General", 0.05);
color="green";
};
Date("TD-V: Date Layer 3g");
Interval("TD-V: layer 3g");
};
Boundary("=TD-I: end 3");
};
Sequence("TD-V")
{
Boundary("=TD-V: transition 4 to 3j");
Phase("Layer 3dw")
{
R_Date("OxA-33846", 33850, 550)
{
Outlier("General", 0.05);
color="green";
};
R_Date("OxA-33847", 30510, 380)
{
Outlier("General", 0.05);
color="green";
};
R_Combine("TD-18")
{
Outlier("General", 0.05);
color="green";
R_Date("OxA-X-2719-18", 27550, 260)
{
Outlier("SSimple", 0.05);
color="green";
};
R_Date("OxA-35697", 27240, 250)
```

```
{
Outlier("SSimple", 0.05);
color="green";
};
};
Date("TD-V: Date Layer 3dw");
Interval("TD-V: layer 3dw");
};
Boundary("=TD-I: end 3");
};
Label("TD-I");
Label("TD-V");
R_Date("OxA-33839*", 33800, 550)
{
color="green";
};
R_Date("OxA-33838*", 36800, 800)
{
color="green";
};
};
```

Model 2 – figure 8.56

```
 Plot()
{
Outlier_Model("General",T(5),U(0,4),"t");
Outlier_Model("SSimple",N(0,2),0,"s");
Sequence()
{
Boundary("TD-I: start layer 4");
Phase("Layer 4")
{
R_Date("OxA-35756", 33650, 550)
{
Outlier("General", 0.05);
color="green";
};
R_Combine("TD-31")
{
Outlier("General", 0.05);
color="green";
R_Date("OxA-35757", 29160, 320)
{
Outlier("SSimple", 0.05);
color="green";
};
R_Date("OxA-35758", 29240, 320)
{
Outlier("SSimple", 0.05);
color="green";
};
};
R_Date("OxA-35231", 27270, 250)
{
Outlier("General", 0.05);
color="green";
};
R_Date("OxA-33845", 28770, 320)
{
Outlier("General", 0.05);
color="green";
};
Date("TD-I: Date layer 4");
Interval("TD-I: Interval layer 4");
};
Boundary("TD-I: transition 4 to 3");
Interval("Interval transition 4 to 3");
Phase("Layer 3f")
{
R_Date("OxA-35238", 29200, 310)
{
Outlier("General", 0.05);
color="green";
};
R_Date("OxA-35235", 28730, 290)
{
Outlier("General", 0.05);
color="green";
};
Date("TD-I: Date layer 3f");
Interval("TD-I: Interval layer 3");
};
Boundary("TD-I: end of 3");
};
Sequence()
{
Boundary("TD-V: start 6");
Phase("Layer 6")
{
Date("OxA-35239", U(calBP(80000),calBP(49600)))
{
Outlier("General", 0.05);
color="green";
};
Date("TD-V: Date layer 6");
Interval("TD-V: Interval layer 6");
};
Boundary("TD-V: transition 6 to 5pg");
Interval("Interval transition 6 to 5");
Phase("Layer 5pg")
{
Date("OxA-35237", N(calBP(56000),3100))
{
Outlier("General", 0.05);
color="green";
};
Date("OxA-35236", U(calBP(80000),calBP(45100)))
{
Outlier("General", 0.05);
color="green";
};
Date("OxA-34401", U(calBP(80000),calBP(44800)))
{
Outlier("General", 0.05);
color="green";
};
Date("OxA-33874", U(calBP(80000),calBP(44200)))
{
Outlier("General", 0.05);
color="green";
};
Date("TD-V: Date layer 5pg");
Interval("TD-V: Interval layer 5pg");
};
Boundary("=TD-I: start layer 4");
Interval("Interval transition 5 to 4");
Phase("Layer 4")
{
Date("OxA-33837", U(calBP(80000),calBP(45300)))
{
Outlier("General", 0.05);
color="green";
};
Date("TD-V: Date layer 4");
Interval("TD-V: Interval layer 4");
};
Boundary("TD-V: transition 4 to 3");
Interval("Interval transition 4 to 3");
Phase("Layer 3 volcanic")
{
R_Combine("TD-08")
{
Outlier("General", 0.05);
color="green";
R_Date("OxA-33842", 33600, 550)
{
Outlier("SSimple", 0.05);
color="green";
};
R_Date("OxA-33841", 33800, 550)
{
Outlier("SSimple", 0.05);
color="green";
```

```
};
};
R_Combine("TD-28")
{
Outlier("General", 0.05);
color="green";
R_Date("OxA-35551", 33750, 550)
{
Outlier("SSimple", 0.05);
color="green";
};
R_Date("OxA-35755", 33800, 550)
{
Outlier("SSimple", 0.05);
color="green";
};
};
R_Date("OxA-35550", 33700, 550)
{
Outlier("General", 0.05);
color="green";
};
R_Date("OxA-33840", 28950, 310)
{
Outlier("General", 0.05);
color="green";
};
R_Date("OxA-33843", 30950, 450)
{
Outlier("General", 0.05);
color="green";
};
R_Date("OxA-33844", 29170, 320)
{
Outlier("General", 0.05);
color="green";
};
R_Date("OxA-35523", 30560, 370)
{
Outlier("General", 0.05);
color="green";
};
R_Date("OxA-33846", 33850, 550)
{
Outlier("General", 0.05);
color="green";
};
R_Date("OxA-33847", 30510, 380)
{
Outlier("General", 0.05);
color="green";
};
R_Combine("TD-18")
{
Outlier("General", 0.05);
color="green";
R_Date("OxA-X-2719-18", 27550, 260)
{
Outlier("SSimple", 0.05);
color="green";
};
R_Date("OxA-35697", 27240, 250)
{
Outlier("SSimple", 0.05);
color="green";
};
};
Date("TD-V: Date layer 3 volcanic");
Interval("TD-V: Interval layer 3 v");
};
Boundary("=TD-I: end of 3");
};
};
```

Model 3 – figure 8.57

```
 Plot()
{
Outlier_Model("General",T(5),U(0,4),"t");
Outlier_Model("SSimple",N(0,2),0,"s");
Sequence("TD-I - Model 3")
{
Boundary("TD-I: start 7");
Phase("Layer 7")
{
Date("Gd-TL-272", N(calBP(105000),35000))
{
Outlier("General", 0.05);
color="blue";
};
Date("Date layer 7 TD-I");
Interval("Intv TD-I: layer 7");
};
Boundary("TD-I: transition 7 to 6");
Interval("Intv TD-I: transition 7 to 6");
Phase("Layer 6")
{
Date("Gd-TL-254", N(calBP(67000),11000))
{
Outlier("General", 0.05);
color="blue";
};
Date("Date layer 6 TD-I");
Interval("Intv TD-I: layer 6");
};
Boundary("TD-I: transition 6 to 5");
Interval("Intv TD-I: transition 6 to 5");
Phase("Layer 5")
{
Date("Date layer 5 TD-I");
Interval("Intv TD-I: layer 5");
};
Boundary("TD-I: transition 5 to 4");
Interval("Intv TD-I: transition 5 to 4");
Phase("Layer 4")
{
Date("Gd-TL-256", N(calBP(45000),7000))
{
Outlier("General", 0.05);
color="blue";
};
Date("Gd-TL-255", N(calBP(46000),8000))
{
Outlier("General", 0.05);
color="blue";
};
R_Date("OxA-35756", 33650, 550)
{
Outlier("General", 0.05);
color="green";
};
R_Combine("TD-31")
{
Outlier("General", 0.05);
color="green";
R_Date("OxA-35757", 29160, 320)
{
Outlier("SSimple", 0.05);
color="green";
};
R_Date("OxA-35758", 29240, 320)
{
Outlier("SSimple", 0.05);
color="green";
};
};
R_Date("OxA-35231", 27270, 250)
{
Outlier("General", 0.05);
color="green";
};
R_Date("OxA-33845", 28770, 320)
{
Outlier("General", 0.05);
```

```
color="green";
};
Date("Date layer 4 TD-I");
Interval("Intv TD-I: layer 4");
};
Boundary("TD-I: transition 4 to 3f");
Interval("Intv TD-I: transition 4 to 3f");
Phase("Layer 3f")
{
R_Date("OxA-35238", 29200, 310)
{
Outlier("General", 0.05);
color="green";
};
R_Date("OxA-35235", 28730, 290)
{
Outlier("General", 0.05);
color="green";
};
Date("Date layer 3f TD-I");
Interval("Intv TD-I: layer 3f");
};
Boundary("TD-I: transition 3f to 3d");
Interval("Intv TD-I: transition 3f to 3d");
Phase("Layer 3d")
{
Date("Gd-TL-210", N(calBP(22900),2100))
{
Outlier("General", 0.05);
color="blue";
};
Date("Date layer 3d TD-I");
Interval("Intv TD-I: layer 3d");
};
Boundary("TD-I: end 3d");
};
Sequence("TD-V - Model 3")
{
Boundary("=TD-I: transition 7 to 6");
Phase("Layer 6")
{
Date("OxA-35239", U(calBP(80000),calBP(49600)))
{
Outlier("General", 0.05);
color="green";
};
Date("Date layer 6 TD-V");
Interval("TD-V: layer 6");
};
Boundary("=TD-I: transition 6 to 5");
Interval("TD-V: transition 6 to 5pg");
Phase("Layer 5pg")
{
Date("OxA-35237", N(calBP(56000),3100))
{
Outlier("General", 0.05);
color="green";
};
Date("OxA-35236", U(calBP(80000),calBP(45100)))
{
Outlier("General", 0.05);
color="green";
};
Date("OxA-34401", U(calBP(80000),calBP(44800)))
{
Outlier("General", 0.05);
color="green";
};
Date("OxA-33874", U(calBP(80000),calBP(44200)))
{
Outlier("General", 0.05);
color="green";
};
Date("Date layer 5pg TD-V");
Interval("TD-V: layer 5pg");
};
Boundary("=TD-I: transition 5 to 4");
Interval("TD-V: transition 5 pg to 4");
Phase("Layer 4")
{
Date("OxA-33837", U(calBP(80000),calBP(45300)))
{
Outlier("General", 0.05);
color="green";
};
Date("Date layer 4 TD-V");
Interval("TD-V: layer 4");
};
Boundary("TD-V: transition 4 to 3j");
Interval("TD-V: transition 4 to 3j");
Phase("Layer 3v")
{
R_Combine("TD-08")
{
Outlier("General", 0.05);
color="green";
R_Date("OxA-33842", 33600, 550)
{
Outlier("SSimple", 0.05);
color="green";
};
R_Date("OxA-33841", 33800, 550)
{
Outlier("SSimple", 0.05);
color="green";
};
};
R_Combine("TD-28")
{
Outlier("General", 0.05);
color="green";
R_Date("OxA-35551", 33750, 550)
{
Outlier("SSimple", 0.05);
color="green";
};
R_Date("OxA-35755", 33800, 550)
{
Outlier("SSimple", 0.05);
color="green";
};
};
R_Date("OxA-35550", 33700, 550)
{
Outlier("General", 0.05);
color="green";
};
R_Date("OxA-33846", 33850, 550)
{
Outlier("General", 0.05);
color="green";
};
R_Date("OxA-33847", 30510, 380)
{
Outlier("General", 0.05);
color="green";
};
R_Date("OxA-33843", 30950, 450)
{
Outlier("General", 0.05);
color="green";
};
R_Date("OxA-33844", 29170, 320)
{
Outlier("General", 0.05);
color="green";
};
R_Date("OxA-35523", 30560, 370)
{
Outlier("General", 0.05);
color="green";
};
R_Date("OxA-33840", 28950, 310)
{
Outlier("General", 0.05);
color="green";
};
R_Combine("TD-18")
{
Outlier("General", 0.05);
color="green";
R_Date("OxA-X-2719-18", 27550, 260)
{
Outlier("SSimple", 0.05);
color="green";
};
```

```
R_Date("OxA-35697", 27240, 250)
{
Outlier("SSimple", 0.05);
color="green";
};
};
Date("Date layer 3v TD-V");
Interval("TD-V: layer 3v");
};
Boundary("=TD-I: transition 3f to 3d");
Interval("TD-V: transition 3g to 3d");
Phase("Layer 3d")
{
Date("Date layer 3d TD-V");
Interval("TD-V: layer 3d");
};
Boundary("TD-V: end 3d");
Interval("TD-V: transition 3d to 3a-c");
Phase("Layer 3a-c")
{
Date("Gd-TL-214", N(calBP(23300),5100))
{
Outlier("General", 0.05);
color="blue";
};
Date("Gd-TL-213", N(calBP(15400),6100))
{
Outlier("General", 0.05);
color="blue";
};
Date("Date layer 3a-c TD-V");
Interval("TD-V: layer 3a-c");
};
Boundary("TD-V: end 3a-c");
};
};
```

Model 3-CI –figure 8.58

```
 Plot()
{
Outlier_Model("General",T(5),U(0,4),"t");
Outlier_Model("SSimple",N(0,2),0,"s");
Sequence("TD-I - Model 3")
{
Boundary("TD-I: start 7");
Phase("Layer 7")
{
Date("Gd-TL-272", N(calBP(105000),35000))
{
Outlier("General", 0.05);
color="blue";
};
Date("Date layer 7 TD-I");
Interval("Intv TD-I: layer 7");
};
Boundary("TD-I: transition 7 to 6");
Interval("Intv TD-I: transition 7 to 6");
Phase("Layer 6")
{
Date("Gd-TL-254", N(calBP(67000),11000))
{
Outlier("General", 0.05);
color="blue";
};
Date("Date layer 6 TD-I");
Interval("Intv TD-I: layer 6");
};
Boundary("TD-I: transition 6 to 5");
Interval("Intv TD-I: transition 6 to 5");
Phase("Layer 5")
{
Date("Date layer 5 TD-I");
Interval("Intv TD-I: layer 5");
};
Boundary("TD-I: transition 5 to 4");
Interval("Intv TD-I: transition 5 to 4");
Phase("Layer 4")
{
Date("Gd-TL-256", N(calBP(45000),7000))
{
Outlier("General", 0.05);
color="blue";
};
Date("Gd-TL-255", N(calBP(46000),8000))
{
Outlier("General", 0.05);
color="blue";
};
R_Date("CI", 34290, 90)
{
Outlier("General", 0.05);
color="#b7005c";
};
R_Date("OxA-35756", 33650, 550)
{
Outlier("General", 0.05);
color="green";
};
R_Combine("TD-31")
{
Outlier("General", 0.05);
color="green";
R_Date("OxA-35757", 29160, 320)
{
Outlier("SSimple", 0.05);
color="green";
};
R_Date("OxA-35758", 29240, 320)
{
Outlier("SSimple", 0.05);
color="green";
};
};
R_Date("OxA-35231", 27270, 250)
{
Outlier("General", 0.05);
color="green";
};
R_Date("OxA-33845", 28770, 320)
{
Outlier("General", 0.05);
color="green";
};
Date("Date layer 4 TD-I");
Interval("Intv TD-I: layer 4");
};
Boundary("TD-I: transition 4 to 3f");
Interval("Intv TD-I: transition 4 to 3f");
Phase("Layer 3f")
{
R_Date("OxA-35238", 29200, 310)
{
Outlier("General", 0.05);
color="green";
};
R_Date("OxA-35235", 28730, 290)
{
Outlier("General", 0.05);
color="green";
};
Date("Date layer 3f TD-I");
Interval("Intv TD-I: layer 3f");
};
Boundary("TD-I: transition 3f to 3d");
Interval("Intv TD-I: transition 3f to 3d");
Phase("Layer 3d")
{
Date("Gd-TL-210", N(calBP(22900),2100))
{
Outlier("General", 0.05);
color="blue";
};
Date("Date layer 3d TD-I");
Interval("Intv TD-I: layer 3d");
```

```
};
Boundary("TD-I: end 3d");
};
Sequence("TD-V - Model 3")
{
Boundary("=TD-I: transition 7 to 6");
Phase("Layer 6")
{
Date("OxA-35239", U(calBP(80000),calBP(49600)))
{
Outlier("General", 0.05);
color="green";
};
Date("Date layer 6 TD-V");
Interval("TD-V: layer 6");
};
Boundary("=TD-I: transition 6 to 5");
Interval("TD-V: transition 6 to 5pg");
Phase("Layer 5pg")
{
Date("OxA-35237", N(calBP(56000),3100))
{
Outlier("General", 0.05);
color="green";
};
Date("OxA-35236", U(calBP(80000),calBP(45100)))
{
Outlier("General", 0.05);
color="green";
};
Date("OxA-34401", U(calBP(80000),calBP(44800)))
{
Outlier("General", 0.05);
color="green";
};
Date("OxA-33874", U(calBP(80000),calBP(44200)))
{
Outlier("General", 0.05);
color="green";
};
Date("Date layer 5pg TD-V");
Interval("TD-V: layer 5pg");
};
Boundary("=TD-I: transition 5 to 4");
Interval("TD-V: transition 5 pg to 4");
Phase("Layer 4")
{
Date("OxA-33837", U(calBP(80000),calBP(45300)))
{
Outlier("General", 0.05);
color="green";
};
Date("Date layer 4 TD-V");
Interval("TD-V: layer 4");
};
Boundary("TD-V: transition 4 to 3j");
Interval("TD-V: transition 4 to 3j");
Phase("Layer 3v")
{
R_Combine("TD-08")
{
Outlier("General", 0.05);
color="green";
R_Date("OxA-33842", 33600, 550)
{
Outlier("SSimple", 0.05);
color="green";
};
R_Date("OxA-33841", 33800, 550)
{
Outlier("SSimple", 0.05);
color="green";
};
};
R_Combine("TD-28")
{
Outlier("General", 0.05);
color="green";
R_Date("OxA-35551", 33750, 550)
{
Outlier("SSimple", 0.05);
color="green";
};
R_Date("OxA-35755", 33800, 550)
{
Outlier("SSimple", 0.05);
color="green";
};
};
R_Date("OxA-35550", 33700, 550)
{
Outlier("General", 0.05);
color="green";
};
R_Date("OxA-33846", 33850, 550)
{
Outlier("General", 0.05);
color="green";
};
R_Date("OxA-33847", 30510, 380)
{
Outlier("General", 0.05);
color="green";
};
R_Date("OxA-33843", 30950, 450)
{
Outlier("General", 0.05);
color="green";
};
R_Date("OxA-33844", 29170, 320)
{
Outlier("General", 0.05);
color="green";
};
R_Date("OxA-35523", 30560, 370)
{
Outlier("General", 0.05);
color="green";
};
R_Date("OxA-33840", 28950, 310)
{
Outlier("General", 0.05);
color="green";
};
R_Combine("TD-18")
{
Outlier("General", 0.05);
color="green";
R_Date("OxA-X-2719-18", 27550, 260)
{
Outlier("SSimple", 0.05);
color="green";
};
R_Date("OxA-35697", 27240, 250)
{
Outlier("SSimple", 0.05);
color="green";
};
};
Date("Date layer 3v TD-V");
Interval("TD-V: layer 3v");
};
Boundary("=TD-I: transition 3f to 3d");
Interval("TD-V: transition 3g to 3d");
Phase("Layer 3d")
{
Date("Date layer 3d TD-V");
Interval("TD-V: layer 3d");
};
Boundary("TD-V: end 3d");
Interval("TD-V: transition 3d to 3a-c");
Phase("Layer 3a-c")
{
Date("Gd-TL-214", N(calBP(23300),5100))
{
Outlier("General", 0.05);
color="blue";
};
Date("Gd-TL-213", N(calBP(15400),6100))
{
Outlier("General", 0.05);
color="blue";
};
Date("Date layer 3a-c TD-V");
Interval("TD-V: layer 3a-c");
};
```

```
Boundary("TD-V: end 3a-c");
};
```

Model 4 – figure 8.59

```
 Plot()
{
Outlier_Model("General",T(5),U(0,4),"t");
Outlier_Model("SSimple",N(0,2),0,"s");
Sequence("Model 4 - pt. 1")
{
Boundary("TD-I: start 7");
Phase("TD-I: layer 7")
{
Date("Gd-TL-272", N(calBP(105000),35000))
{
Outlier("General", 0.05);
color="blue";
};
Date("Date layer 7 TD-I");
Interval("Intv TD-I: layer 7");
};
Boundary("TD-I: tranisiton 7 to 6");
Interval("Intv TD-I: transition 7 to 6");
Phase("TD-I: layer 6")
{
Date("Gd-TL-254", N(calBP(67000),11000))
{
Outlier("General", 0.05);
color="blue";
};
Date("OxA-35239", U(calBP(80000),calBP(49600)))
{
Outlier("General", 0.05);
color="green";
};
Date("Date layer 6 TD-I");
Interval("Intv TD-I: layer 6");
};
Boundary("TD-I: tranisiton 6 ro 5");
Interval("Intv TD-I: transition 6 to 5");
Phase("5")
{
Date("OxA-35237", N(calBP(56000),3100))
{
Outlier("General", 0.05);
color="green";
};
Date("OxA-35236", U(calBP(80000),calBP(45100)))
{
Outlier("General", 0.05);
color="green";
};
Date("OxA-34401", U(calBP(80000),calBP(44800)))
{
Outlier("General", 0.05);
color="green";
};
Date("OxA-33874", U(calBP(80000),calBP(44200)))
{
Outlier("General", 0.05);
color="green";
};
Date("Date layer 5 TD-I");
Interval("Intv TD-I: layer 5");
};
Boundary("TD-I: tranisiton 5 to 4C");
Interval("Intv TD-I: transition 5 to 4C");
Phase("TD-I: layer 4C")
{
Date("Gd-TL-256", N(calBP(45000),7000))
{
Outlier("General", 0.05);
color="blue";
};
Date("OxA-33837", U(calBP(80000),calBP(45300)))
{
Outlier("General", 0.05);
color="green";
};
Date("Date layer 4C TD-I");
Interval("Intv TD-I: layer 4C");
};
Boundary("TD-I: tranisiton 4C to 4B");
Interval("Intv TD-I: transition 4C to 4B");
Phase("TD-I: layer 4B")
{
Date("Gd-TL-255", N(calBP(46000),8000))
{
Outlier("General", 0.05);
color="blue";
};
R_Date("OxA-5169", 39100, 1800)
{
Outlier("General", 0.05);
color=" #674846";
};
R_Date("OxA-5171", 38200, 1500)
{
Outlier("General", 0.05);
color="#674846";
};
R_Date("OxA-5170", 38800, 1700)
{
Outlier("General", 0.05);
color="#674846";
};
R_Date("OxA-5172", 38300, 1600)
{
Outlier("General", 0.05);
color="#674846";
};
R_Date("OxA-5173", 36900, 1300)
{
Outlier("General", 0.05);
color="#674846";
};
Date("Date layer 4B TD-I");
Interval("Intv TD-I: layer 4B");
};
Boundary("TD-I: tranisiton 4B to 4A");
Interval("Intv TD-I: transition 4B to 4A");
Phase("TD-I: layer 4A")
{
R_Date("OxA-35756", 33650, 550)
{
Outlier("General", 0.05);
color="green";
};
R_Date("Gd-2354", 31900, 1600)
{
Outlier("General", 0.05);
color="brown";
};
R_Combine("TD-31")
{
Outlier("General", 0.05);
color="green";
R_Date("OxA-35757", 29160, 320)
{
Outlier("SSimple", 0.05);
color="green";
};
R_Date("OxA-35758", 29240, 320)
{
Outlier("SSimple", 0.05);
color="green";
};
};
R_Date("OxA-35231", 27270, 250)
{
Outlier("General", 0.05);
color="green";
```

```
};
R_Date("OxA-33845", 28770, 320)
{
Outlier("General", 0.05);
color="green";
};
Date("Date layer 4A TD-I");
Interval("Intv TD-I: layer 4A");
};
Boundary("TD-I: tranisiton 4A to 3f");
Interval("Intv TD-I: transition 4A to 3f");
Phase("TD-I: layer  3f")
{
R_Date("OxA-35238", 29200, 310)
{
Outlier("General", 0.05);
color="green";
};
R_Date("OxA-35235", 28730, 290)
{
Outlier("General", 0.05);
color="green";
};
R_Date("Gd-4233", 28900, 1400)
{
Outlier("General", 0.05);
color="brown";
};
Date("Date layer 3f TD-I");
Interval("Intv TD-I: layer 3f");
};
Boundary("TD-I: tranisiton 3f to 3d");
Interval("Intv TD-I: transition 3f to 3d");
Phase("TD-I: layer 3d")
{
R_Date("Gd-2580", 28900, 1100)
{
Outlier("General", 0.05);
color="brown";
};
R_Date("Gd-4231", 29700, 700)
{
Outlier("General", 0.05);
color="brown";
};
R_Date("Gd-4030", 21200, 900)
{
Outlier("General", 0.05);
color="dimgray";
};
R_Date("Gd-4232", 23400, 1600)
{
Outlier("General", 0.05);
color="brown";
};
R_Date("Gd-4029", 19940, 800)
{
Outlier("General", 0.05);
color="dimgray";
};
Date("Gd-TL-210", N(calBP(22900),2100))
{
Outlier("General", 0.05);
color="blue";
};
R_Date("Gd-2790", 21200, 380)
{
Outlier("General", 0.05);
color="brown";
};
Date("Date layer 3d TD-I");
Interval("Intv TD-I: layer 3d");
};
Boundary("TD-I: tranisiton 3d to 3a-c");
Interval("Intv TD-I: transition 3d to 3a-c");
Phase("TD-I: layer 3a-c")
{
R_Date("Gd-4027", 11200, 1600)
{
Outlier("General", 0.05);
color="dimgray";
};
R_Date("Gd-4026", 10440, 400)
{
Outlier("General", 0.05);
color="dimgray";
};
R_Date("Ly-3441", 24900, 510)
{
Outlier("General", 0.05);
color="brown";
};
R_Date("Ly-3440", 13920, 480)
{
Outlier("General", 0.05);
color="brown";
};
R_Date("Ly-3439", 13600, 200)
{
Outlier("General", 0.05);
color="brown";
};
Date("Date layer 3a-c TD-I");
Interval("Intv TD-I: layer 3a-c");
};
Boundary("TD-I: end 3a-c");
};
Sequence("Model 4 - pt. 2")
{
Boundary("=TD-I: tranisiton 4B to 4A");
Interval("Intv TD-V: transition 4b to 4a");
Phase("TD-V: layer 4a")
{
R_Date("OxA-5174", 33000, 900)
{
Outlier("General", 0.05);
color="#674846";
};
Date("TD-V: layer 4a");
Interval("Intv TD-V: layer 4a");
};
Boundary("TD-V: transition 4a to 3j");
Interval("Intv TD-V: transition 4a to 3j");
Phase("TD-V: layer 3j")
{
R_Combine("TD-08")
{
Outlier("General", 0.05);
color="green";
R_Date("OxA-33842", 33600, 550)
{
Outlier("SSimple", 0.05);
color="green";
};
R_Date("OxA-33841", 33800, 550)
{
Outlier("SSimple", 0.05);
color="green";
};
};
R_Combine("TD-28")
{
Outlier("General", 0.05);
color="green";
R_Date("OxA-35551", 33750, 550)
{
Outlier("SSimple", 0.05);
color="green";
};
R_Date("OxA-35755", 33800, 550)
{
Outlier("SSimple", 0.05);
color="green";
};
};
R_Date("OxA-35550", 33700, 550)
{
Outlier("General", 0.05);
color="green";
};
R_Date("OxA-33840", 28950, 310)
{
Outlier("General", 0.05);
color="green";
};
Date("TD-V: layer 3j");
```

```
Interval("Intv TD-V: layer 3j");
};
Boundary("TD-V: transition 3j to 3g");
Interval("Intv TD-V: transition 3j to 3g");
Phase("TD-V: layer 3g")
{
R_Date("OxA-33843", 30950, 450)
{
Outlier("General", 0.05);
color="green";
};
R_Date("OxA-33844", 29170, 320)
{
Outlier("General", 0.05);
color="green";
};
R_Date("OxA-35523", 30560, 370)
{
Outlier("General", 0.05);
color="green";
};
Date("TD-V: layer 3g");
Interval("Intv TD-V: layer 3g");
};
Boundary("TD-V: transition 3g to 3d");
Interval("Intv TD-V: transition 3g to 3d");
Phase("TD-V: layer 3d")
{
R_Date("Gd-6126", 24400, 600)
{
Outlier("General", 0.05);
color="brown";
};
R_Date("Gd-2785", 21200, 380)
{
Outlier("General", 0.05);
color="brown";
};
Date("TD-V: layer 3d");
Interval("Intv TD-V: layer 3d");
};
Boundary("=TD-I: tranisiton 3d to 3a-c");
Interval("Intv TD-V: transition 3d to 3a-c");
Phase("TD-V: layer 3a-c")
{
Date("Gd-TL-214", N(calBP(23300),5100))
{
Outlier("General", 0.05);
color="blue";
};
R_Date("Gd-2581", 24800, 700)
{
Outlier("General", 0.05);
color="brown";
};
Date("Gd-TL-213", N(calBP(15400),6100))
{
Outlier("General", 0.05);
color="blue";
};
R_Date("Gd-4028", 20100, 900)
{
Outlier("General", 0.05);
color="dimgray";
};
R_Date("Gd-2578", 16600, 300)
{
Outlier("General", 0.05);
color="brown";
};
R_Date("Gd-4025", 10480, 280)
{
Outlier("General", 0.05);
color="dimgray";
};
R_Date("Gd-4022", 10880, 370)
{
Outlier("General", 0.05);
color="dimgray";
};
Date("TD-V: layer 3a-c");
Interval("Intv TD-V: layer 3a-c");
};
Boundary("TD-V: end 3a-c");
};
Sequence("Model 4 pt. 3")
{
Boundary("=TD-V: transition 4a to 3j");
Phase("TD-V: layer 3dw")
{
R_Date("OxA-33846", 33850, 550)
{
Outlier("General", 0.05);
color="green";
};
R_Date("OxA-33847", 30510, 380)
{
Outlier("General", 0.05);
color="green";
};
R_Combine("TD-18")
{
Outlier("General", 0.05);
color="green";
R_Date("OxA-X-2719-18", 27550, 260)
{
Outlier("SSimple", 0.05);
color="green";
};
R_Date("OxA-35697", 27240, 250)
{
Outlier("SSimple", 0.05);
color="green";
};
};
Date("TD-V: layer 3dw");
Interval("Intv TD-V: layer 3dw");
};
Boundary("=TD-V: transition 3g to 3d");
};
};
```

Model 4-CI – figure 8.60

```
 Plot()
{
Outlier_Model("General",T(5),U(0,4),"t");
Outlier_Model("SSimple",N(0,2),0,"s");
Sequence("Model 4 - pt. 1")
{
Boundary("TD-I: start 7");
Phase("TD-I: layer 7")
{
Date("Gd-TL-272", N(calBP(105000),35000))
{
Outlier("General", 0.05);
color="blue";
};
Date("Date layer 7 TD-I");
Interval("Intv TD-I: layer 7");
};
Boundary("TD-I: tranisiton 7 to 6");
Interval("Intv TD-I: transition 7 to 6");
Phase("TD-I: layer 6")
{
Date("Gd-TL-254", N(calBP(67000),11000))
{
Outlier("General", 0.05);
color="blue";
};
Date("OxA-35239", U(calBP(80000),calBP(49600)))
{
Outlier("General", 0.05);
color="green";
```

```
};
Date("Date layer 6 TD-I");
Interval("Intv TD-I: layer 6");
};
Boundary("TD-I: tranisiton 6 ro 5");
Interval("Intv TD-I: transition 6 to 5");
Phase("5")
{
Date("OxA-35237", N(calBP(56000),3100))
{
Outlier("General", 0.05);
color="green";
};
Date("OxA-35236", U(calBP(80000),calBP(45100)))
{
Outlier("General", 0.05);
color="green";
};
Date("OxA-34401", U(calBP(80000),calBP(44800)))
{
Outlier("General", 0.05);
color="green";
};
Date("OxA-33874", U(calBP(80000),calBP(44200)))
{
Outlier("General", 0.05);
color="green";
};
Date("Date layer 5 TD-I");
Interval("Intv TD-I: layer 5");
};
Boundary("TD-I: tranisiton 5 to 4C");
Interval("Intv TD-I: transition 5 to 4C");
Phase("TD-I: layer 4C")
{
Date("Gd-TL-256", N(calBP(45000),7000))
{
Outlier("General", 0.05);
color="blue";
};
Date("OxA-33837", U(calBP(80000),calBP(45300)))
{
Outlier("General", 0.05);
color="green";
};
Date("Date layer 4C TD-I");
Interval("Intv TD-I: layer 4C");
};
Boundary("TD-I: tranisiton 4C to 4B");
Interval("Intv TD-I: transition 4C to 4B");
Phase("TD-I: layer 4B")
{
Date("Gd-TL-255", N(calBP(46000),8000))
{
Outlier("General", 0.05);
color="blue";
};
R_Date("OxA-5169", 39100, 1800)
{
Outlier("General", 0.05);
color=" #674846";
};
R_Date("OxA-5171", 38200, 1500)
{
Outlier("General", 0.05);
color="#674846";
};
R_Date("OxA-5170", 38800, 1700)
{
Outlier("General", 0.05);
color="#674846";
};
R_Date("OxA-5172", 38300, 1600)
{
Outlier("General", 0.05);
color="#674846";
};
R_Date("OxA-5173", 36900, 1300)
{
Outlier("General", 0.05);
color="#674846";
};
Date("Date layer 4B TD-I");
Interval("Intv TD-I: layer 4B");
};
Boundary("TD-I: tranisiton 4B to 4A");
Interval("Intv TD-I: transition 4B to 4A");
Phase("TD-I: layer 4A")
{
R_Date("CI", 34290, 90)
{
Outlier("General", 0.05);
color="#b7005c";
};
R_Date("OxA-35756", 33650, 550)
{
Outlier("General", 0.05);
color="green";
};
R_Date("Gd-2354", 31900, 1600)
{
Outlier("General", 0.05);
color="brown";
};
R_Combine("TD-31")
{
Outlier("General", 0.05);
color="green";
R_Date("OxA-35757", 29160, 320)
{
Outlier("SSimple", 0.05);
color="green";
};
R_Date("OxA-35758", 29240, 320)
{
Outlier("SSimple", 0.05);
color="green";
};
};
R_Date("OxA-35231", 27270, 250)
{
Outlier("General", 0.05);
color="green";
};
R_Date("OxA-33845", 28770, 320)
{
Outlier("General", 0.05);
color="green";
};
Date("Date layer 4A TD-I");
Interval("Intv TD-I: layer 4A");
};
Boundary("TD-I: tranisiton 4A to 3f");
Interval("Intv TD-I: transition 4A to 3f");
Phase("TD-I: layer  3f")
{
R_Date("OxA-35238", 29200, 310)
{
Outlier("General", 0.05);
color="green";
};
R_Date("OxA-35235", 28730, 290)
{
Outlier("General", 0.05);
color="green";
};
R_Date("Gd-4233", 28900, 1400)
{
Outlier("General", 0.05);
color="brown";
};
Date("Date layer 3f TD-I");
Interval("Intv TD-I: layer 3f");
};
Boundary("TD-I: tranisiton 3f to 3d");
Interval("Intv TD-I: transition 3f to 3d");
Phase("TD-I: layer 3d")
{
R_Date("Gd-2580", 28900, 1100)
{
Outlier("General", 0.05);
color="brown";
};
R_Date("Gd-4231", 29700, 700)
{
Outlier("General", 0.05);
```

```
color="brown";
};
R_Date("Gd-4030", 21200, 900)
{
Outlier("General", 0.05);
color="dimgray";
};
R_Date("Gd-4232", 23400, 1600)
{
Outlier("General", 0.05);
color="brown";
};
R_Date("Gd-4029", 19940, 800)
{
Outlier("General", 0.05);
color="dimgray";
};
Date("Gd-TL-210", N(calBP(22900),2100))
{
Outlier("General", 0.05);
color="blue";
};
R_Date("Gd-2790", 21200, 380)
{
Outlier("General", 0.05);
color="brown";
};
Date("Date layer 3d TD-I");
Interval("Intv TD-I: layer 3d");
};
Boundary("TD-I: tranisiton 3d to 3a-c");
Interval("Intv TD-I: transition 3d to 3a-c");
Phase("TD-I: layer 3a-c")
{
R_Date("Gd-4027", 11200, 1600)
{
Outlier("General", 0.05);
color="dimgray";
};
R_Date("Gd-4026", 10440, 400)
{
Outlier("General", 0.05);
color="dimgray";
};
R_Date("Ly-3441", 24900, 510)
{
Outlier("General", 0.05);
color="brown";
};
R_Date("Ly-3440", 13920, 480)
{
Outlier("General", 0.05);
color="brown";
};
R_Date("Ly-3439", 13600, 200)
{
Outlier("General", 0.05);
color="brown";
};
Date("Date layer 3a-c TD-I");
Interval("Intv TD-I: layer 3a-c");
};
Boundary("TD-I: end 3a-c");
};
Sequence("Model 4 - pt. 2")
{
Boundary("=TD-I: tranisiton 4B to 4A");
Interval("Intv TD-V: transition 4b to 4a");
Phase("TD-V: layer 4a")
{
R_Date("OxA-5174", 33000, 900)
{
Outlier("General", 0.05);
color="#674846";
};
Date("TD-V: layer 4a");
Interval("Intv TD-V: layer 4a");
};
Boundary("TD-V: transition 4a to 3j");
Interval("Intv TD-V: transition 4a to 3j");
Phase("TD-V: layer 3j")
{
R_Combine("TD-08")
{
Outlier("General", 0.05);
color="green";
R_Date("OxA-33842", 33600, 550)
{
Outlier("SSimple", 0.05);
color="green";
};
R_Date("OxA-33841", 33800, 550)
{
Outlier("SSimple", 0.05);
color="green";
};
};
R_Combine("TD-28")
{
Outlier("General", 0.05);
color="green";
R_Date("OxA-35551", 33750, 550)
{
Outlier("SSimple", 0.05);
color="green";
};
R_Date("OxA-35755", 33800, 550)
{
Outlier("SSimple", 0.05);
color="green";
};
};
R_Date("OxA-35550", 33700, 550)
{
Outlier("General", 0.05);
color="green";
};
R_Date("OxA-33840", 28950, 310)
{
Outlier("General", 0.05);
color="green";
};
Date("TD-V: layer 3j");
Interval("Intv TD-V: layer 3j");
};
Boundary("TD-V: transition 3j to 3g");
Interval("Intv TD-V: transition 3j to 3g");
Phase("TD-V: layer 3g")
{
R_Date("OxA-33843", 30950, 450)
{
Outlier("General", 0.05);
color="green";
};
R_Date("OxA-33844", 29170, 320)
{
Outlier("General", 0.05);
color="green";
};
R_Date("OxA-35523", 30560, 370)
{
Outlier("General", 0.05);
color="green";
};
Date("TD-V: layer 3g");
Interval("Intv TD-V: layer 3g");
};
Boundary("TD-V: transition 3g to 3d");
Interval("Intv TD-V: transition 3g to 3d");
Phase("TD-V: layer 3d")
{
R_Date("Gd-6126", 24400, 600)
{
Outlier("General", 0.05);
color="brown";
};
R_Date("Gd-2785", 21200, 380)
{
Outlier("General", 0.05);
color="brown";
};
Date("TD-V: layer 3d");
Interval("Intv TD-V: layer 3d");
};
Boundary("=TD-I: tranisiton 3d to 3a-c");
Interval("Intv TD-V: transition 3d to 3a-c");
```

```
Phase("TD-V: layer 3a-c")
{
Date("Gd-TL-214", N(calBP(23300),5100))
{
Outlier("General", 0.05);
color="blue";
};
R_Date("Gd-2581", 24800, 700)
{
Outlier("General", 0.05);
color="brown";
};
Date("Gd-TL-213", N(calBP(15400),6100))
{
Outlier("General", 0.05);
color="blue";
};
R_Date("Gd-4028", 20100, 900)
{
Outlier("General", 0.05);
color="dimgray";
};
R_Date("Gd-2578", 16600, 300)
{
Outlier("General", 0.05);
color="brown";
};
R_Date("Gd-4025", 10480, 280)
{
Outlier("General", 0.05);
color="dimgray";
};
R_Date("Gd-4022", 10880, 370)
{
Outlier("General", 0.05);
color="dimgray";
};
Date("TD-V: layer 3a-c");
Interval("Intv TD-V: layer 3a-c");
};
Boundary("TD-V: end 3a-c");
};
Sequence("Model 4 pt. 3")
{
Boundary("=TD-V: transition 4a to 3j");
Phase("TD-V: layer 3dw")
{
R_Date("OxA-33846", 33850, 550)
{
Outlier("General", 0.05);
color="green";
};
R_Date("OxA-33847", 30510, 380)
{
Outlier("General", 0.05);
color="green";
};
R_Combine("TD-18")
{
Outlier("General", 0.05);
color="green";
R_Date("OxA-X-2719-18", 27550, 260)
{
Outlier("SSimple", 0.05);
color="green";
};
R_Date("OxA-35697", 27240, 250)
{
Outlier("SSimple", 0.05);
color="green";
};
};
Date("TD-V: layer 3dw");
Interval("Intv TD-V: layer 3dw");
};
Boundary("=TD-V: transition 3g to 3d");
};
};
```

Model 5 – figure 8.59

```
 Plot()
{
Outlier_Model("General",T(5),U(0,4),"t");
Outlier_Model("SSimple",N(0,2),0,"s");
Sequence("TD-V")
{
Boundary("TD-V: start 6lg");
Phase("TD-V: layer 6lg")
{
Date("OxA-35239", U(calBP(80000),calBP(49600)))
{
Outlier("General", 0.05);
color="green";
};
Date("TD-V: layer 6lg");
Interval("Intv TD-V: layer 6lg");
};
Boundary("TD-V: transition 6lg to 5pg");
Interval("Intv TD-V: transition 6lg to 5pg");
Phase("TD-V: layer 5pg")
{
Date("OxA-35237", N(calBP(56000),3100))
{
Outlier("General", 0.05);
color="green";
};
Date("OxA-35236", U(calBP(80000),calBP(45100)))
{
Outlier("General", 0.05);
color="green";
};
Date("OxA-34401", U(calBP(80000),calBP(44800)))
{
Outlier("General", 0.05);
color="green";
};
Date("OxA-33874", U(calBP(80000),calBP(44200)))
{
Outlier("General", 0.05);
color="green";
};
Date("TD-V: layer 5pg");
Interval("Intv TD-V: layer 5pg");
};
Boundary("TD-V: transition 5pg to 4pg");
Interval("Intv TD-V: transition 5pg to 4pg");
Phase("TD-V: layer 4pg")
{
Date("OxA-33837", U(calBP(80000),calBP(45300)))
{
Outlier("General", 0.05);
color="green";
};
Date("TD-V: layer 4pg");
Interval("Intv TD-V: layer 4pg");
};
Boundary("TD-V: transition 4pg to 4b");
Interval("Intv TD-V: transition 4pg to 4b");
Phase("TD-V: layer 4b")
{
R_Date("OxA-5172", 38300, 1600)
{
Outlier("General", 0.05);
color="#674846";
};
R_Date("OxA-5173", 36900, 1300)
{
Outlier("General", 0.05);
color="#674846";
};
Date("TD-V: layer 4b");
Interval("Intv TD-V: layer 4b");
};
Boundary("TD-V: transition 4b to 4a");
```

```
Interval("Intv TD-V: transition 4b to 4a");
Phase("TD-V: layer 4a")
{
R_Date("OxA-5174", 33000, 900)
{
Outlier("General", 0.05);
color="#674846";
};
Date("TD-V: layer 4a");
Interval("Intv TD-V: layer 4a");
};
Boundary("TD-V: transition 4a to 3j");
Interval("Intv TD-V: transition 4a to 3j");
Phase("TD-V: layer 3j")
{
R_Combine("TD-08")
{
Outlier("General", 0.05);
color="green";
R_Date("OxA-33842", 33600, 550)
{
Outlier("SSimple", 0.05);
color="green";
};
R_Date("OxA-33841", 33800, 550)
{
Outlier("SSimple", 0.05);
color="green";
};
};
R_Combine("TD-28")
{
Outlier("General", 0.05);
color="green";
R_Date("OxA-35551", 33750, 550)
{
Outlier("SSimple", 0.05);
color="green";
};
R_Date("OxA-35755", 33800, 550)
{
Outlier("SSimple", 0.05);
color="green";
};
};
R_Date("OxA-35550", 33700, 550)
{
Outlier("General", 0.05);
color="green";
};
R_Date("OxA-33840", 28950, 310)
{
Outlier("General", 0.05);
color="green";
};
Date("TD-V: layer 3j");
Interval("Intv TD-V: layer 3j");
};
Boundary("TD-V: transition 3j to 3g");
Interval("Intv TD-V: transition 3j to 3g");
Phase("TD-V: layer 3g")
{
R_Date("OxA-33843", 30950, 450)
{
Outlier("General", 0.05);
color="green";
};
R_Date("OxA-33844", 29170, 320)
{
Outlier("General", 0.05);
color="green";
};
R_Date("OxA-35523", 30560, 370)
{
Outlier("General", 0.05);
color="green";
};
Date("TD-V: layer 3g");
Interval("Intv TD-V: layer 3g");
};
Boundary("TD-V: transition 3g to 3d");
Interval("Intv TD-V: transition 3g to 3d");
Phase("TD-V: layer 3d")
{
R_Date("Gd-6126", 24400, 600)
{
Outlier("General", 0.05);
color="brown";
};
R_Date("Gd-2785", 21200, 380)
{
Outlier("General", 0.05);
color="brown";
};
Date("TD-V: layer 3d");
Interval("Intv TD-V: layer 3d");
};
Boundary("TD-V: transition 3d to 3a-c");
Interval("Intv TD-V: transition 3d to 3a-c");
Phase("TD-V: layer 3a-c")
{
Date("Gd-TL-214", N(calBP(23300),5100))
{
Outlier("General", 0.05);
color="blue";
};
R_Date("Gd-2581", 24800, 700)
{
Outlier("General", 0.05);
color="brown";
};
Date("Gd-TL-213", N(calBP(15400),6100))
{
Outlier("General", 0.05);
color="blue";
};
R_Date("Gd-4028", 20100, 900)
{
Outlier("General", 0.05);
color="dimgray";
};
R_Date("Gd-2578", 16600, 300)
{
Outlier("General", 0.05);
color="brown";
};
R_Date("Gd-4025", 10480, 280)
{
Outlier("General", 0.05);
color="dimgray";
};
R_Date("Gd-4022", 10880, 370)
{
Outlier("General", 0.05);
color="dimgray";
};
Date("TD-V: layer 3a-c");
Interval("Intv TD-V: layer 3a-c");
};
Boundary("TD-V: end 3a-c");
};
Sequence()
{
Boundary("=TD-V: transition 4a to 3j");
Phase("TD-V: layer 3dw")
{
R_Date("OxA-33846", 33850, 550)
{
Outlier("General", 0.05);
color="green";
};
R_Date("OxA-33847", 30510, 380)
{
Outlier("General", 0.05);
color="green";
};
R_Combine("TD-18")
{
Outlier("General", 0.05);
color="green";
R_Date("OxA-X-2719-18", 27550, 260)
{
Outlier("SSimple", 0.05);
color="green";
};
R_Date("OxA-35697", 27240, 250)
```

```
{
Outlier("SSimple", 0.05);
color="green";
};
};
Date("TD-V: layer 3dw");
Interval("Intv TD-V: layer 3dw");
};
Boundary("=TD-V: transition 3g to 3d");
};
};
```

Model 6 – figure 8.61

```
 Plot()
{
Outlier_Model("General",T(5),U(0,4),"t");
Outlier_Model("SSimple",N(0,2),0,"s");
Sequence("Model 5 - TD-I")
{
Boundary("TD-I: start 7");
Phase("TD-I: layer 7")
{
Date("Gd-TL-272", N(calBP(105000),35000))
{
Outlier("General", 0.05);
color="blue";
};
Date("Date layer 7 TD-I");
Interval("Intv TD-I: layer 7");
};
Boundary("TD-I: tranisiton 7 to 6");
Interval("Intv TD-I: transition 7 to 6");
Phase("TD-I: layer 6")
{
Date("Gd-TL-254", N(calBP(67000),11000))
{
Outlier("General", 0.05);
color="blue";
};
Date("Date layer 6 TD-I");
Interval("Intv TD-I: layer 6");
};
Boundary("TD-I: tranisiton 6 ro 5");
Interval("Intv TD-I: transition 5 to 4C");
Phase("5")
{
Date("Date layer 5 TD-I");
Interval("Intv TD-I: layer 5");
};
Boundary("TD-I: tranisiton 5 to 4C");
Interval("Intv TD-I: transition 5 to 4C");
Phase("TD-I: layer 4C")
{
Date("Gd-TL-256", N(calBP(45000),7000))
{
Outlier("General", 0.05);
color="blue";
};
Date("Date layer 4C TD-I");
Interval("Intv TD-I: layer 4C");
};
Boundary("TD-I: tranisiton 4C to 4B");
Interval("Intv TD-I: transition 4C to 4B");
Phase("TD-I: layer 4B")
{
Date("Gd-TL-255", N(calBP(46000),8000))
{
Outlier("General", 0.05);
color="blue";
};
R_Date("OxA-5169", 39100, 1800)
{
Outlier("General", 0.05);
color=" #674846";
};
R_Date("OxA-5171", 38200, 1500)
{
Outlier("General", 0.05);
color="#674846";
};
R_Date("OxA-5170", 38800, 1700)
{
Outlier("General", 0.05);
color="#674846";
};
Date("Date layer 4B TD-I");
Interval("Intv TD-I: layer 4B");
};
Boundary("TD-I: tranisiton 4B to 4A");
Interval("Intv TD-I: transition 4B to 4A");
Phase("TD-I: layer 4A")
{
R_Date("OxA-35756", 33650, 550)
{
Outlier("General", 0.05);
color="green";
};
R_Date("Gd-2354", 31900, 1600)
{
Outlier("General", 0.05);
color="brown";
};
R_Combine("TD-31")
{
Outlier("General", 0.05);
color="green";
R_Date("OxA-35757", 29160, 320)
{
Outlier("SSimple", 0.05);
color="green";
};
R_Date("OxA-35758", 29240, 320)
{
Outlier("SSimple", 0.05);
color="green";
};
};
R_Date("OxA-35231", 27270, 250)
{
Outlier("General", 0.05);
color="green";
};
R_Date("OxA-33845", 28770, 320)
{
Outlier("General", 0.05);
color="green";
};
Date("Date layer 4A TD-I");
Interval("Intv TD-I: layer 4A");
};
Boundary("TD-I: tranisiton 4A to 3f");
Interval("Intv TD-I: transition 4A to 3f");
Phase("TD-I: layer  3f")
{
R_Date("OxA-35238", 29200, 310)
{
Outlier("General", 0.05);
color="green";
};
R_Date("OxA-35235", 28730, 290)
{
Outlier("General", 0.05);
color="green";
};
R_Date("Gd-4233", 28900, 1400)
{
Outlier("General", 0.05);
color="brown";
};
Date("Date layer 3f TD-I");
Interval("Intv TD-I: layer 3f");
};
Boundary("TD-I: tranisiton 3f to 3d");
```

```
Interval("Intv TD-I: transition 3f to 3d");
Phase("TD-I: layer 3d")
{
R_Date("Gd-2580", 28900, 1100)
{
Outlier("General", 0.05);
color="brown";
};
R_Date("Gd-4231", 29700, 700)
{
Outlier("General", 0.05);
color="brown";
};
R_Date("Gd-4030", 21200, 900)
{
Outlier("General", 0.05);
color="dimgray";
};
R_Date("Gd-4232", 23400, 1600)
{
Outlier("General", 0.05);
color="brown";
};
R_Date("Gd-4029", 19940, 800)
{
Outlier("General", 0.05);
color="dimgray";
};
Date("Gd-TL-210", N(calBP(22900),2100))
{
Outlier("General", 0.05);
color="blue";
};
R_Date("Gd-2790", 21200, 380)
{
Outlier("General", 0.05);
color="brown";
};
Date("Date layer 3d TD-I");
Interval("Intv TD-I: layer 3d");
};
Boundary("TD-I: tranisiton 3d to 3a-c");
Interval("Intv TD-I: transition 3d to 3a-c");
Phase("TD-I: layer 3a-c")
{
R_Date("Gd-4027", 11200, 1600)
{
Outlier("General", 0.05);
color="dimgray";
};
R_Date("Gd-4026", 10440, 400)
{
Outlier("General", 0.05);
color="dimgray";
};
R_Date("Ly-3441", 24900, 510)
{
Outlier("General", 0.05);
color="brown";
};
R_Date("Ly-3440", 13920, 480)
{
Outlier("General", 0.05);
color="brown";
};
R_Date("Ly-3439", 13600, 200)
{
Outlier("General", 0.05);
color="brown";
};
Date("Date layer 3a-c TD-I");
Interval("Intv TD-I: layer 3a-c");
};
Boundary("TD-I: end 3a-c");
};
Sequence("Model 5 - TD-V")
{
Boundary("=TD-I: tranisiton 7 to 6");
Phase("TD-V: layer 6lg")
{
Date("OxA-35239", U(calBP(80000),calBP(49600)))
{
Outlier("General", 0.05);
color="green";
};
Date("TD-V: layer 6lg");
Interval("Intv TD-V: layer 6lg");
};
Boundary("=TD-I: tranisiton 6 ro 5");
Interval("Intv TD-V: transition 6lg to 5pg");
Phase("TD-V: layer 5pg")
{
Date("OxA-35237", N(calBP(56000),3100))
{
Outlier("General", 0.05);
color="green";
};
Date("OxA-35236", U(calBP(80000),calBP(45100)))
{
Outlier("General", 0.05);
color="green";
};
Date("OxA-34401", U(calBP(80000),calBP(44800)))
{
Outlier("General", 0.05);
color="green";
};
Date("OxA-33874", U(calBP(80000),calBP(44200)))
{
Outlier("General", 0.05);
color="green";
};
Date("TD-V: layer 5pg");
Interval("Intv TD-V: layer 5pg");
};
Boundary("=TD-I: tranisiton 5 to 4C");
Interval("Intv TD-V: transition 5pg to 4pg");
Phase("TD-V: layer 4pg")
{
Date("OxA-33837", U(calBP(80000),calBP(45300)))
{
Outlier("General", 0.05);
color="green";
};
Date("TD-V: layer 4pg");
Interval("Intv TD-V: layer 4pg");
};
Boundary("=TD-I: tranisiton 4C to 4B");
Interval("Intv TD-V: transition 4pg to 4b");
Phase("TD-V: layer 4b")
{
R_Date("OxA-5172", 38300, 1600)
{
Outlier("General", 0.05);
color="#674846";
};
R_Date("OxA-5173", 36900, 1300)
{
Outlier("General", 0.05);
color="#674846";
};
Date("TD-V: layer 4b");
Interval("Intv TD-V: layer 4b");
};
Boundary("=TD-I: tranisiton 4B to 4A");
Interval("Intv TD-V: transition 4b to 4a");
Phase("TD-V: layer 4a")
{
R_Date("OxA-5174", 33000, 900)
{
Outlier("General", 0.05);
color="#674846";
};
Date("TD-V: layer 4a");
Interval("Intv TD-V: layer 4a");
};
Boundary("TD-V: transition 4a to 3j");
Interval("Intv TD-V: transition 4a to 3j");
Phase("TD-V: layer 3j")
{
R_Combine("TD-08")
{
Outlier("General", 0.05);
color="green";
R_Date("OxA-33842", 33600, 550)
{
```

```
Outlier("SSimple", 0.05);
color="green";
};
R_Date("OxA-33841", 33800, 550)
{
Outlier("SSimple", 0.05);
color="green";
};
};
R_Combine("TD-28")
{
Outlier("General", 0.05);
color="green";
R_Date("OxA-35551", 33750, 550)
{
Outlier("SSimple", 0.05);
color="green";
};
R_Date("OxA-35755", 33800, 550)
{
Outlier("SSimple", 0.05);
color="green";
};
};
R_Date("OxA-35550", 33700, 550)
{
Outlier("General", 0.05);
color="green";
};
R_Date("OxA-33840", 28950, 310)
{
Outlier("General", 0.05);
color="green";
};
Date("TD-V: layer 3j");
Interval("Intv TD-V: layer 3j");
};
Boundary("TD-V: transition 3j to 3g");
Interval("Intv TD-V: transition 3j to 3g");
Phase("TD-V: layer 3g")
{
R_Date("OxA-33843", 30950, 450)
{
Outlier("General", 0.05);
color="green";
};
R_Date("OxA-33844", 29170, 320)
{
Outlier("General", 0.05);
color="green";
};
R_Date("OxA-35523", 30560, 370)
{
Outlier("General", 0.05);
color="green";
};
Date("TD-V: layer 3g");
Interval("Intv TD-V: layer 3g");
};
Boundary("TD-V: transition 3g to 3d");
Interval("Intv TD-V: transition 3g to 3d");
Phase("TD-V: layer 3d")
{
R_Date("Gd-6126", 24400, 600)
{
Outlier("General", 0.05);
color="brown";
};
R_Date("Gd-2785", 21200, 380)
{
Outlier("General", 0.05);
color="brown";
};
Date("TD-V: layer 3d");
Interval("Intv TD-V: layer 3d");
};
Boundary("=TD-I: tranisiton 3d to 3a-c");
Interval("Intv TD-V: transition 3d to 3a-c");
Phase("TD-V: layer 3a-c")
{
Date("Gd-TL-214", N(calBP(23300),5100))
{
Outlier("General", 0.05);
color="blue";
};
R_Date("Gd-2581", 24800, 700)
{
Outlier("General", 0.05);
color="brown";
};
Date("Gd-TL-213", N(calBP(15400),6100))
{
Outlier("General", 0.05);
color="blue";
};
R_Date("Gd-4028", 20100, 900)
{
Outlier("General", 0.05);
color="dimgray";
};
R_Date("Gd-2578", 16600, 300)
{
Outlier("General", 0.05);
color="brown";
};
R_Date("Gd-4025", 10480, 280)
{
Outlier("General", 0.05);
color="dimgray";
};
R_Date("Gd-4022", 10880, 370)
{
Outlier("General", 0.05);
color="dimgray";
};
Date("TD-V: layer 3a-c");
Interval("Intv TD-V: layer 3a-c");
};
Boundary("TD-V: end 3a-c");
};
};
```

Model Simple 1 – figure 8.62

```
 Plot()
{
Outlier_Model("General",T(5),U(0,4),"t");
Outlier_Model("SSimple",N(0,2),0,"s");
Sequence("Model 9 - pt. 1")
{
Boundary("start 7");
Phase("7")
{
Date("Gd-TL-272", N(calBP(105000),35000))
{
Outlier("General", 0.05);
color="blue";
};
Date("Date layer 7");
};
Boundary("Transition 7/6");
Phase("6")
{
Date("Gd-TL-254", N(calBP(67000),11000))
{
Outlier("General", 0.05);
color="blue";
};
Date("Date layer 6");
};
Boundary("Transition 6/5");
Phase("5")
{
Date("OxA-35237", N(calBP(56000),3100))
```

```
{
Outlier("General", 0.05);
color="green";
};
Date("Date layer 5");
};
Boundary("Transition 5/4C");
Phase("4C")
{
Date("Gd-TL-256", N(calBP(45000),7000))
{
Outlier("General", 0.05);
color="blue";
};
Date("Date layer 4C");
};
Boundary("Transition 4C/4B");
Phase("4B/4b")
{
Date("Gd-TL-255", N(calBP(46000),8000))
{
Outlier("General", 0.05);
color="blue";
};
R_Date("OxA-5171", 38200, 1500)
{
Outlier("General", 0.05);
color="#674846";
};
R_Date("OxA-5170", 38800, 1700)
{
Outlier("General", 0.05);
color="#674846";
};
R_Date("OxA-5169", 39100, 1800)
{
Outlier("General", 0.05);
color=" #674846";
};
R_Date("OxA-5172", 38300, 1600)
{
Outlier("General", 0.05);
color="#674846";
};
R_Date("OxA-5173", 36900, 1300)
{
Outlier("General", 0.05);
color="#674846";
};
Date("Date layer 4B/4b");
};
Boundary("Transition 4B/4A");
Phase("4A")
{
R_Date("Gd-2354", 31900, 1600)
{
Outlier("General", 0.05);
color="brown";
};
R_Date("OxA-35756", 33650, 550)
{
Outlier("General", 0.05);
color="green";
};
R_Combine("TD-31")
{
Outlier("General", 0.05);
color="green";
R_Date("OxA-35757", 29160, 320)
{
Outlier("SSimple", 0.05);
color="green";
};
R_Date("OxA-35758", 29240, 320)
{
Outlier("SSimple", 0.05);
color="green";
};
};
R_Date("OxA-35231", 27270, 250)
{
Outlier("General", 0.05);
color="green";
};
R_Date("OxA-33845", 28770, 320)
{
Outlier("General", 0.05);
color="green";
};
Date("Date layer 4A");
};
Boundary("Transition 4A/3f");
Phase("3f")
{
R_Date("OxA-35238", 29200, 310)
{
Outlier("General", 0.05);
color="green";
};
R_Date("OxA-35235", 28730, 290)
{
Outlier("General", 0.05);
color="green";
};
R_Date("Gd-4233", 28900, 1400)
{
Outlier("General", 0.05);
color="brown";
};
Date("Date layer 3f");
};
Boundary("Transition 3f/3d");
Phase("3d-TD-I")
{
R_Date("Gd-2580", 28900, 1100)
{
Outlier("General", 0.05);
color="brown";
};
R_Date("Gd-4231", 29700, 700)
{
Outlier("General", 0.05);
color="brown";
};
R_Date("Gd-4030", 21200, 900)
{
Outlier("General", 0.05);
color="dimgray";
};
R_Date("Gd-4232", 23400, 1600)
{
Outlier("General", 0.05);
color="brown";
};
R_Date("Gd-4029", 19940, 800)
{
Outlier("General", 0.05);
color="dimgray";
};
Date("Gd-TL-210", N(calBP(22900),2100))
{
Outlier("General", 0.05);
color="blue";
};
R_Date("Gd-2790", 21200, 380)
{
Outlier("General", 0.05);
color="brown";
};
Date("Date layer 3d TD-I");
};
Boundary("Transition 3d/3a-c");
Phase("3a-c")
{
Date("Gd-TL-214", N(calBP(23300),5100))
{
Outlier("General", 0.05);
color="blue";
};
R_Date("Gd-2581", 24800, 700)
{
Outlier("General", 0.05);
color="brown";
};
Date("Gd-TL-213", N(calBP(15400),6100))
{
```

```
Outlier("General", 0.05);
color="blue";
};
R_Date("Gd-4028", 20100, 900)
{
Outlier("General", 0.05);
color="dimgray";
};
R_Date("Gd-2578", 16600, 300)
{
Outlier("General", 0.05);
color="brown";
};
R_Date("Gd-4027", 11200, 1600)
{
Outlier("General", 0.05);
color="dimgray";
};
R_Date("Gd-4026", 10440, 400)
{
Outlier("General", 0.05);
color="dimgray";
};
R_Date("Ly-3441", 24900, 510)
{
Outlier("General", 0.05);
color="brown";
};
R_Date("Ly-3440", 13920, 480)
{
Outlier("General", 0.05);
color="brown";
};
R_Date("Ly-3439", 13600, 200)
{
Outlier("General", 0.05);
color="brown";
};
R_Date("Gd-4025", 10480, 280)
{
Outlier("General", 0.05);
color="dimgray";
};
R_Date("Gd-4022", 10880, 370)
{
Outlier("General", 0.05);
color="dimgray";
};
Date("Date layer 3a-c");
};
Boundary("End 3a-c");
};
Sequence("Model 9 - pt.2")
{
Boundary("=Transition 4B/4A");
Phase("4a")
{
R_Date("OxA-5174", 33000, 900)
{
Outlier("General", 0.05);
color="#674846";
};
Date("Date layer 4a");
};
Boundary("Transition 4a/3j");
Phase("3j")
{
R_Combine("TD-08")
{
Outlier("General", 0.05);
color="green";
R_Date("OxA-33842", 33600, 550)
{
Outlier("SSimple", 0.05);
color="green";
};
R_Date("OxA-33841", 33800, 550)
{
Outlier("SSimple", 0.05);
color="green";
};
};
R_Combine("TD-28")
{
Outlier("General", 0.05);
color="green";
R_Date("OxA-35551", 33750, 550)
{
Outlier("SSimple", 0.05);
color="green";
};
R_Date("OxA-35755", 33800, 550)
{
Outlier("SSimple", 0.05);
color="green";
};
};
R_Date("OxA-35550", 33700, 550)
{
Outlier("General", 0.05);
color="green";
};
R_Date("OxA-33840", 28950, 310)
{
Outlier("General", 0.05);
color="green";
};
Date("Date layer 3j");
};
Boundary("Transition 3j/3g");
Phase("3g")
{
R_Date("OxA-33843", 30950, 450)
{
Outlier("General", 0.05);
color="green";
};
R_Date("OxA-33844", 29170, 320)
{
Outlier("General", 0.05);
color="green";
};
R_Date("OxA-35523", 30560, 370)
{
Outlier("General", 0.05);
color="green";
};
Date("Date layer 3g");
};
Boundary("Transition 3g/3d");
Phase("3d TD-V")
{
R_Date("Gd-6126", 24400, 600)
{
Outlier("General", 0.05);
color="brown";
};
R_Date("Gd-2785", 21200, 380)
{
Outlier("General", 0.05);
color="brown";
};
Date("Date layer 3d TD-V");
};
Boundary("=Transition 3d/3a-c");
};
};
```

Model Simple 2 – figure 8.63

```
 Plot()
{
Outlier_Model("General",T(5),U(0,4),"t");
Outlier_Model("SSimple",N(0,2),0,"s");
Sequence("Model 9 - pt. 1")
{
Boundary("start 7");
Phase("7")
{
Date("Gd-TL-272", N(calBP(105000),35000))
{
Outlier("General", 0.05);
color="blue";
};
Date("Date layer 7");
};
Boundary("Transition 7/6");
Phase("6")
{
Date("Gd-TL-254", N(calBP(67000),11000))
{
Outlier("General", 0.05);
color="blue";
};
Date("Date layer 6");
};
Boundary("Transition 6/5");
Phase("5")
{
Date("OxA-35237", N(calBP(56000),3100))
{
Outlier("General", 0.05);
color="green";
};
Date("Date layer 5");
};
Boundary("Transition 5/4C");
Phase("4C")
{
Date("Gd-TL-256", N(calBP(45000),7000))
{
Outlier("General", 0.05);
color="blue";
};
Date("Date layer 4C");
};
Boundary("Transition 4C/4B");
Phase("4B/4b")
{
Date("Gd-TL-255", N(calBP(46000),8000))
{
Outlier("General", 0.05);
color="blue";
};
R_Date("OxA-5171", 38200, 1500)
{
Outlier("General", 0.05);
color="#674846";
};
R_Date("OxA-5170", 38800, 1700)
{
Outlier("General", 0.05);
color="#674846";
};
R_Date("OxA-5169", 39100, 1800)
{
Outlier("General", 0.05);
color=" #674846";
};
R_Date("OxA-5172", 38300, 1600)
{
Outlier("General", 0.05);
color="#674846";
};
R_Date("OxA-5173", 36900, 1300)
{
Outlier("General", 0.05);
color="#674846";
};
Date("Date layer 4B/4b");
};
Boundary("Transition 4B/4A");
Phase("4A")
{
R_Date("OxA-35756", 33650, 550)
{
Outlier("General", 0.05);
color="green";
};
R_Combine("TD-31")
{
Outlier("General", 0.05);
color="green";
R_Date("OxA-35757", 29160, 320)
{
Outlier("SSimple", 0.05);
color="green";
};
R_Date("OxA-35758", 29240, 320)
{
Outlier("SSimple", 0.05);
color="green";
};
};
R_Date("OxA-35231", 27270, 250)
{
Outlier("General", 0.05);
color="green";
};
R_Date("OxA-33845", 28770, 320)
{
Outlier("General", 0.05);
color="green";
};
Date("Date layer 4A");
};
Boundary("Transition 4A/3f");
Phase("3f")
{
R_Date("OxA-35238", 29200, 310)
{
Outlier("General", 0.05);
color="green";
};
R_Date("OxA-35235", 28730, 290)
{
Outlier("General", 0.05);
color="green";
};
Date("Date layer 3f");
};
Boundary("Transition 3f/3d");
Phase("3d-TD-I")
{
R_Date("Gd-4030", 21200, 900)
{
Outlier("General", 0.05);
color="dimgray";
};
R_Date("Gd-4029", 19940, 800)
{
Outlier("General", 0.05);
color="dimgray";
};
Date("Gd-TL-210", N(calBP(22900),2100))
{
Outlier("General", 0.05);
color="blue";
};
Date("Date layer 3d TD-I");
};
Boundary("Transition 3d/3a-c");
Phase("3a-c")
{
Date("Gd-TL-214", N(calBP(23300),5100))
{
Outlier("General", 0.05);
color="blue";
};
Date("Gd-TL-213", N(calBP(15400),6100))
{
Outlier("General", 0.05);
color="blue";
};
R_Date("Gd-4028", 20100, 900)
{
```

```
Outlier("General", 0.05);
color="dimgray";
};
R_Date("Gd-4027", 11200, 1600)
{
Outlier("General", 0.05);
color="dimgray";
};
R_Date("Gd-4026", 10440, 400)
{
Outlier("General", 0.05);
color="dimgray";
};
R_Date("Gd-4025", 10480, 280)
{
Outlier("General", 0.05);
color="dimgray";
};
R_Date("Gd-4022", 10880, 370)
{
Outlier("General", 0.05);
color="dimgray";
};
Date("Date layer 3a-c");
};
Boundary("End 3a-c");
};
Sequence("Model 9 - pt.2")
{
Boundary("=Transition 4B/4A");
Phase("4a")
{
R_Date("OxA-5174", 33000, 900)
{
Outlier("General", 0.05);
color="#674846";
};
Date("Date layer 4a");
};
Boundary("Transition 4a/3j");
Phase("3j")
{
R_Combine("TD-08")
{
Outlier("General", 0.05);
color="green";
R_Date("OxA-33842", 33600, 550)
{
Outlier("SSimple", 0.05);
color="green";
};
R_Date("OxA-33841", 33800, 550)
{
Outlier("SSimple", 0.05);
color="green";
};
};
R_Combine("TD-28")
{
Outlier("General", 0.05);
color="green";
R_Date("OxA-35551", 33750, 550)
{
Outlier("SSimple", 0.05);
color="green";
};
R_Date("OxA-35755", 33800, 550)
{
Outlier("SSimple", 0.05);
color="green";
};
};
R_Date("OxA-35550", 33700, 550)
{
Outlier("General", 0.05);
color="green";
};
R_Date("OxA-33840", 28950, 310)
{
Outlier("General", 0.05);
color="green";
};
Date("Date layer 3j");
};
Boundary("Transition 3j/3g");
Phase("3g")
{
R_Date("OxA-33843", 30950, 450)
{
Outlier("General", 0.05);
color="green";
};
R_Date("OxA-33844", 29170, 320)
{
Outlier("General", 0.05);
color="green";
};
R_Date("OxA-35523", 30560, 370)
{
Outlier("General", 0.05);
color="green";
};
Date("Date layer 3g");
};
Boundary("=Transition 3d/3a-c");
};
};
```

KDE 0 – figure 8.64

```
 KDE_model()
{
R_Date("Ly-3439", 13600, 200)
{
color="brown";
};
R_Date("Ly-3440", 13920, 480)
{
color="brown";
};
R_Date("Ly-3441", 24900, 510)
{
color="brown";
};
R_Date("Gd-4026", 10440, 400)
{
color="dimgray";
};
R_Date("Gd-4027", 11200, 1600)
{
color="dimgray";
};
R_Date("Gd-2790", 21200, 380)
{
color="brown";
};
R_Date("Gd-4029", 19940, 800)
{
color="dimgray";
};
R_Date("Gd-4232", 23400, 1600)
{
color="brown";
};
R_Date("Gd-4030", 21200, 900)
{
color="dimgray";
};
R_Date("Gd-4231", 29700, 700)
{
color="brown";
};
R_Date("Gd-2580", 28900, 1100)
{
```

```
color="brown";
};
R_Date("Gd-4233", 28900, 1400)
{
color="brown";
};
R_Date("Gd-2354", 31900, 1600)
{
color="brown";
};
R_Date("OxA-5169", 39100, 1800)
{
color=" #674846";
};
R_Date("OxA-5170", 38800, 1700)
{
color="#674846";
};
R_Date("OxA-5171", 38200, 1500)
{
color="#674846";
};
R_Date("Gd-4022", 10880, 370)
{
color="dimgray";
};
R_Date("Gd-4025", 10480, 280)
{
color="dimgray";
};
R_Date("Gd-2578", 16600, 300)
{
color="brown";
};
R_Date("Gd-4028", 20100, 900)
{
color="dimgray";
};
R_Date("Gd-2581", 24800, 700)
{
color="brown";
};
R_Date("Gd-2785", 21200, 380)
{
color="brown";
};
R_Date("Gd-6126", 24400, 600)
{
color="brown";
};
R_Date("OxA-5174", 33000, 900)
{
color="#674846";
};
R_Date("OxA-5173", 36900, 1300)
{
color="#674846";
};
R_Date("OxA-5172", 38300, 1600)
{
color="#674846";
};
};
```

KDE 1 – figure 8.64

```
 KDE_model("TD - KDE 1")
{
R_Date("OxA-35235", 28730, 290)
{
color="green";
};
R_Date("OxA-35238", 29200, 310)
{
color="green";
};
R_Date("OxA-33845", 28770, 320)
{
color="green";
};
R_Date("OxA-35231", 27270, 250)
{
color="green";
};
R_Combine("TD-31")
{
color="green";
R_Date("OxA-35757", 29160, 320)
{
color="green";
};
R_Date("OxA-35758", 29240, 320)
{
color="green";
};
};
R_Date("OxA-35756", 33650, 550)
{
color="green";
};
R_Combine("TD-18")
{
color="green";
R_Date("OxA-X-2719-18", 27550, 260)
{
color="green";
};
R_Date("OxA-35697", 27240, 250)
{
color="green";
};
};
R_Date("OxA-33847", 30510, 380)
{
color="green";
};
R_Date("OxA-33846", 33850, 550)
{
color="green";
};
R_Date("OxA-35523", 30560, 370)
{
color="green";
};
R_Date("OxA-33844", 29170, 320)
{
color="green";
};
R_Date("OxA-33843", 30950, 450)
{
color="green";
};
R_Date("OxA-33840", 28950, 310)
{
color="green";
};
R_Date("OxA-35550", 33700, 550)
{
color="green";
};
R_Combine("TD-28")
{
color="green";
R_Date("OxA-35551", 33750, 550)
{
color="green";
};
R_Date("OxA-35755", 33800, 550)
{
color="green";
};
};
R_Combine("TD-08")
{
```

```
color="green";
R_Date("OxA-33842", 33600, 550)
{
color="green";
};
R_Date("OxA-33841", 33800, 550)
{
color="green";
};
};
R_Date("OxA-33839*", 33800, 550)
{
color="green";
};
R_Date("OxA-33838*", 36800, 800)
{
color="green";
};
Date("OxA-33837", U(calBP(70000),calBP(45300)))
{
color="green";
};
Date("OxA-33874", U(calBP(70000),calBP(44200)))
{
color="green";
};
Date("OxA-34401", U(calBP(70000),calBP(44800)))
{
color="green";
};
Date("OxA-35236", U(calBP(70000),calBP(45100)))
{
color="green";
};
Date("OxA-35237", N(calBP(56000),3100))
{
color="green";
};
Date("OxA-35239", U(calBP(70000),calBP(49600)))
{
color="green";
};
};
```

KDE 2 – figure 8.64

```
 KDE_model("TD - KDE 2")
{
R_Date("Gd-4026", 10440, 400)
{
color="dimgray";
};
R_Date("Gd-4027", 11200, 1600)
{
color="dimgray";
};
R_Date("Gd-4029", 19940, 800)
{
color="dimgray";
};
R_Date("Gd-4030", 21200, 900)
{
color="dimgray";
};
R_Date("OxA-5169", 39100, 1800)
{
color=" #674846";
};
R_Date("OxA-5170", 38800, 1700)
{
color="#674846";
};
R_Date("OxA-5171", 38200, 1500)
{
color="#674846";
};
R_Date("Gd-4022", 10880, 370)
{
color="dimgray";
};
R_Date("Gd-4025", 10480, 280)
{
color="dimgray";
};
R_Date("Gd-4028", 20100, 900)
{
color="dimgray";
};
R_Date("OxA-5174", 33000, 900)
{
color="#674846";
};
R_Date("OxA-5173", 36900, 1300)
{
color="#674846";
};
R_Date("OxA-5172", 38300, 1600)
{
color="#674846";
};
};
```

KDE 3 – figure 8.64

```
 KDE_model("TD - KDE 3")
{
R_Date("Gd-4026", 10440, 400)
{
color="dimgray";
};
R_Date("Gd-4027", 11200, 1600)
{
color="dimgray";
};
R_Date("Gd-4029", 19940, 800)
{
color="dimgray";
};
R_Date("Gd-4030", 21200, 900)
{
color="dimgray";
};
R_Date("OxA-35235", 28730, 290)
{
color="green";
};
R_Date("OxA-35238", 29200, 310)
{
color="green";
};
R_Date("OxA-33845", 28770, 320)
{
color="green";
};
R_Date("OxA-35231", 27270, 250)
{
color="green";
};
R_Combine("TD-31")
{
```

```
color="green";
R_Date("OxA-35757", 29160, 320)
{
color="green";
};
R_Date("OxA-35758", 29240, 320)
{
color="green";
};
};
R_Date("OxA-35756", 33650, 550)
{
color="green";
};
R_Date("OxA-5169", 39100, 1800)
{
color=" #674846";
};
R_Date("OxA-5170", 38800, 1700)
{
color="#674846";
};
R_Date("OxA-5171", 38200, 1500)
{
color="#674846";
};
R_Date("Gd-4022", 10880, 370)
{
color="dimgray";
};
R_Date("Gd-4025", 10480, 280)
{
color="dimgray";
};
R_Date("Gd-4028", 20100, 900)
{
color="dimgray";
};
R_Combine("TD-18")
{
color="green";
R_Date("OxA-X-2719-18", 27550, 260)
{
color="green";
};
R_Date("OxA-35697", 27240, 250)
{
color="green";
};
};
R_Date("OxA-33847", 30510, 380)
{
color="green";
};
R_Date("OxA-33846", 33850, 550)
{
color="green";
};
R_Date("OxA-35523", 30560, 370)
{
color="green";
};
R_Date("OxA-33844", 29170, 320)
{
color="green";
};
R_Date("OxA-33843", 30950, 450)
{
color="green";
};
R_Date("OxA-33840", 28950, 310)
{
color="green";
};
R_Date("OxA-35550", 33700, 550)
{
color="green";
};
R_Combine("TD-28")
{
color="green";
R_Date("OxA-35551", 33750, 550)
{
color="green";
};
R_Date("OxA-35755", 33800, 550)
{
color="green";
};
};
R_Combine("TD-08")
{
color="green";
R_Date("OxA-33842", 33600, 550)
{
color="green";
};
R_Date("OxA-33841", 33800, 550)
{
color="green";
};
};
R_Date("OxA-33839*", 33800, 550)
{
color="green";
};
R_Date("OxA-33838*", 36800, 800)
{
color="green";
};
R_Date("OxA-5174", 33000, 900)
{
color="#674846";
};
R_Date("OxA-5173", 36900, 1300)
{
color="#674846";
};
R_Date("OxA-5172", 38300, 1600)
{
color="#674846";
};
Date("OxA-33837", U(calBP(70000),calBP(45300)))
{
color="green";
};
Date("OxA-33874", U(calBP(70000),calBP(44200)))
{
color="green";
};
Date("OxA-34401", U(calBP(70000),calBP(44800)))
{
color="green";
};
Date("OxA-35236", U(calBP(70000),calBP(45100)))
{
color="green";
};
Date("OxA-35237", N(calBP(56000),3100))
{
color="green";
};
Date("OxA-35239", U(calBP(70000),calBP(49600)))
{
color="green";
};
};
```

KDE 4 – figure 8.64

```
 KDE_model("TD - KDE 4")
{
R_Date("Ly-3439", 13600, 200)
{
color="brown";
};
R_Date("Ly-3440", 13920, 480)
{
color="brown";
};
R_Date("Ly-3441", 24900, 510)
{
color="brown";
};
R_Date("Gd-4026", 10440, 400)
{
color="dimgray";
};
R_Date("Gd-4027", 11200, 1600)
{
color="dimgray";
};
R_Date("Gd-2790", 21200, 380)
{
color="brown";
};
R_Date("Gd-4029", 19940, 800)
{
color="dimgray";
};
R_Date("Gd-4232", 23400, 1600)
{
color="brown";
};
R_Date("Gd-4030", 21200, 900)
{
color="dimgray";
};
R_Date("Gd-4231", 29700, 700)
{
color="brown";
};
R_Date("Gd-2580", 28900, 1100)
{
color="brown";
};
R_Date("Gd-4233", 28900, 1400)
{
color="brown";
};
R_Date("OxA-35235", 28730, 290)
{
color="green";
};
R_Date("OxA-35238", 29200, 310)
{
color="green";
};
R_Date("OxA-33845", 28770, 320)
{
color="green";
};
R_Date("OxA-35231", 27270, 250)
{
color="green";
};
R_Combine("TD-31")
{
color="green";
R_Date("OxA-35757", 29160, 320)
{
color="green";
};
R_Date("OxA-35758", 29240, 320)
{
color="green";
};
};
R_Date("OxA-35756", 33650, 550)
{
color="green";
};
R_Date("Gd-2354", 31900, 1600)
{
color="brown";
};
R_Date("OxA-5169", 39100, 1800)
{
color=" #674846";
};
R_Date("OxA-5170", 38800, 1700)
{
color="#674846";
};
R_Date("OxA-5171", 38200, 1500)
{
color="#674846";
};
R_Date("Gd-4022", 10880, 370)
{
color="dimgray";
};
R_Date("Gd-4025", 10480, 280)
{
color="dimgray";
};
R_Date("Gd-2578", 16600, 300)
{
color="brown";
};
R_Date("Gd-4028", 20100, 900)
{
color="dimgray";
};
R_Date("Gd-2581", 24800, 700)
{
color="brown";
};
R_Date("Gd-2785", 21200, 380)
{
color="brown";
};
R_Date("Gd-6126", 24400, 600)
{
color="brown";
};
R_Combine("TD-18")
{
color="green";
R_Date("OxA-X-2719-18", 27550, 260)
{
color="green";
};
R_Date("OxA-35697", 27240, 250)
{
color="green";
};
};
R_Date("OxA-33847", 30510, 380)
{
color="green";
};
R_Date("OxA-33846", 33850, 550)
{
color="green";
};
R_Date("OxA-35523", 30560, 370)
{
color="green";
};
R_Date("OxA-33844", 29170, 320)
{
color="green";
};
R_Date("OxA-33843", 30950, 450)
{
color="green";
};
R_Date("OxA-33840", 28950, 310)
{
color="green";
};
R_Date("OxA-35550", 33700, 550)
{
color="green";
};
```

```
R_Combine("TD-28")
{
color="green";
R_Date("OxA-35551", 33750, 550)
{
color="green";
};
R_Date("OxA-35755", 33800, 550)
{
color="green";
};
};
R_Combine("TD-08")
{
color="green";
R_Date("OxA-33842", 33600, 550)
{
color="green";
};
R_Date("OxA-33841", 33800, 550)
{
color="green";
};
};
R_Date("OxA-33839*", 33800, 550)
{
color="green";
};
R_Date("OxA-33838*", 36800, 800)
{
color="green";
};
R_Date("OxA-5174", 33000, 900)
{
color="#674846";
};
R_Date("OxA-5173", 36900, 1300)
{
color="#674846";
};
R_Date("OxA-5172", 38300, 1600)
{
color="#674846";
};
Date("OxA-33874", U(calBP(70000),calBP(44200)))
{
color="green";
};
Date("OxA-34401", U(calBP(70000),calBP(44800)))
{
color="green";
};
Date("OxA-35236", U(calBP(70000),calBP(45100)))
{
color="green";
};
Date("OxA-35237", N(calBP(56000),3100))
{
color="green";
};
Date("OxA-35239", U(calBP(70000),calBP(49600)))
{
color="green";
};
};
```

KDE 5 – figure 8.64

```
 KDE_model("TD - KDE 5")
{
R_Date("OxA-35235", 28730, 290)
{
color="green";
};
R_Date("OxA-35238", 29200, 310)
{
color="green";
};
R_Date("OxA-33845", 28770, 320)
{
color="green";
};
R_Date("OxA-35231", 27270, 250)
{
color="green";
};
R_Combine("TD-31")
{
color="green";
R_Date("OxA-35757", 29160, 320)
{
color="green";
};
R_Date("OxA-35758", 29240, 320)
{
color="green";
};
};
R_Date("OxA-35756", 33650, 550)
{
color="green";
};
R_Combine("TD-18")
{
color="green";
R_Date("OxA-X-2719-18", 27550, 260)
{
color="green";
};
R_Date("OxA-35697", 27240, 250)
{
color="green";
};
};
R_Date("OxA-33847", 30510, 380)
{
color="green";
};
R_Date("OxA-33846", 33850, 550)
{
color="green";
};
R_Date("OxA-35523", 30560, 370)
{
color="green";
};
R_Date("OxA-33844", 29170, 320)
{
color="green";
};
R_Date("OxA-33843", 30950, 450)
{
color="green";
};
R_Date("OxA-33840", 28950, 310)
{
color="green";
};
R_Date("OxA-35550", 33700, 550)
{
color="green";
};
R_Combine("TD-28")
{
color="green";
R_Date("OxA-35551", 33750, 550)
{
color="green";
};
R_Date("OxA-35755", 33800, 550)
{
color="green";
};
};
```

```
R_Combine("TD-08")
{
color="green";
R_Date("OxA-33842", 33600, 550)
{
color="green";
};
R_Date("OxA-33841", 33800, 550)
{
color="green";
};
};
R_Date("OxA-33839*", 33800, 550)
{
color="green";
};
R_Date("OxA-33838*", 36800, 800)
{
color="green";
};
Date("OxA-33837", U(calBP(70000),calBP(45300)))
{
color="green";
};
};
```

KDE 6 – figure 8.64

```
 KDE_model("TD - KDE 3")
{
//charcoal, 3c, 410-420
R_Date("Gd-4026", 10440, 400)
{
color="dimgray";
};
R_Date("Gd-4027", 11200, 1600)
{
color="dimgray";
};
R_Date("Gd-4029", 19940, 800)
{
color="dimgray";
};
R_Date("Gd-4030", 21200, 900)
{
color="dimgray";
};
R_Date("OxA-35235", 28730, 290)
{
color="green";
};
R_Date("OxA-35238", 29200, 310)
{
color="green";
};
R_Date("OxA-33845", 28770, 320)
{
color="green";
};
R_Date("OxA-35231", 27270, 250)
{
color="green";
};
R_Combine("TD-31")
{
color="green";
R_Date("OxA-35757", 29160, 320)
{
color="green";
};
R_Date("OxA-35758", 29240, 320)
{
color="green";
};
};
R_Date("OxA-35756", 33650, 550)
{
color="green";
};
R_Date("OxA-5169", 39100, 1800)
{
color=" #674846";
};
R_Date("OxA-5170", 38800, 1700)
{
color="#674846";
};
R_Date("OxA-5171", 38200, 1500)
{
color="#674846";
};
R_Date("Gd-4022", 10880, 370)
{
color="dimgray";
};
R_Date("Gd-4025", 10480, 280)
{
color="dimgray";
};
R_Date("Gd-4028", 20100, 900)
{
color="dimgray";
};
R_Combine("TD-18")
{
color="green";
R_Date("OxA-X-2719-18", 27550, 260)
{
color="green";
};
R_Date("OxA-35697", 27240, 250)
{
color="green";
};
};
R_Date("OxA-33847", 30510, 380)
{
color="green";
};
R_Date("OxA-33846", 33850, 550)
{
color="green";
};
R_Date("OxA-35523", 30560, 370)
{
color="green";
};
R_Date("OxA-33844", 29170, 320)
{
color="green";
};
R_Date("OxA-33843", 30950, 450)
{
color="green";
};
R_Date("OxA-33840", 28950, 310)
{
color="green";
};
R_Date("OxA-35550", 33700, 550)
{
color="green";
};
R_Combine("TD-28")
{
color="green";
R_Date("OxA-35551", 33750, 550)
{
color="green";
};
R_Date("OxA-35755", 33800, 550)
{
color="green";
};
```

```
};
R_Combine("TD-08")
{
color="green";
R_Date("OxA-33842", 33600, 550)
{
color="green";
};
R_Date("OxA-33841", 33800, 550)
{
color="green";
};
};
R_Date("OxA-33839*", 33800, 550)
{
color="green";
};
R_Date("OxA-33838*", 36800, 800)
{
color="green";
};
R_Date("OxA-5174", 33000, 900)
{
color="#674846";
};
R_Date("OxA-5173", 36900, 1300)
{
color="#674846";
};
R_Date("OxA-5172", 38300, 1600)
{
color="#674846";
};
Date("OxA-33837", U(calBP(80000),calBP(45300)))
{
color="green";
};
};
```

B.3 Code: Tabula Traiana

Model 1 – figure 9.14

```
 Plot()
{
Outlier_Model("SSimple", N(0,2), 0, "s");
Outlier_Model("General",T(5),U(0,4),"t");
Sequence("Tabula Traiana: Model 1")
{
Boundary("Tab: start lower horizon");
Phase("Tab: lower horizon")
{
Date("OxA-35594", U(calBP(60000),calBP(48800)))
{
color="green";
Outlier("General", 0.05);
};
Date("OxA-35769", U(calBP(60000),calBP(50100)))
{
color="green";
Outlier("General", 0.05);
};
R_Date("OxA-35770", 46500, 2600)
{
color="green";
Outlier("General", 0.05);
};
R_Date("OxA-35768", 34250, 550)
{
color="green";
Outlier("General", 0.05);
};
Interval("Tab: Interval lower horizon");
Date("Tab: upper horizon");
};
Boundary("Tab: transition lower to upper horizon");
Phase("Tab: upper horizon")
{
Combine("Tab-13")
{
Outlier("General", 0.05);
Date("OxA-35766", U(calBP(60000),calBP(49800)))
{
Outlier("SSimple", 0.05);
color="green";
};
Date("OxA-35767", U(calBP(60000),calBP(49900)))
{
Outlier("SSimple", 0.05);
color="green";
};
};
Date("OxA-35762", U(calBP(60000),calBP(48000)))
{
color="green";
Outlier("General", 0.05);
};
R_Date("OxA-35764", 36500, 750)
{
color="green";
Outlier("General", 0.05);
};
//CI erruption 14C age after Giaccio et al. 2017
R_Date("CI", 34290, 90)
{
Outlier("General", 0.05);
color="#b7005c";
};
R_Date("OxA-23651", 34200, 550)
{
Outlier("General", 0.05);
color="blue";
};
R_Date("OxA-24818", 33450, 500)
{
Outlier("General", 0.05);
color="blue";
};
R_Date("OxA-35763", 28550, 290)
{
color="green";
Outlier("General", 0.05);
};
R_Date("OxA-35592", 33600, 550)
{
color="green";
Outlier("General", 0.05);
};
R_Date("OxA-35765", 20460, 120)
{
color="green";
Outlier("General", 0.05);
};
Interval("Tab: Interval upper horizon");
Date("Tab: upper horizon");
};
Boundary("Tab: transition upper horizon to 200");
Phase("Tab: 200")
{
R_Date("OxA-35593", 25490, 210)
{
color="green";
Outlier("General", 0.05);
};
Interval("Tab: Interval 200");
Date("Tab: Date 200");
};
Boundary("Tab: end layer 200");
};
};
```

Model 2 – figure 9.15

```
 Plot()
{
Outlier_Model("General",T(5),U(0,4),"t");
Outlier_Model("SSimple", N(0,2), 0, "s");
Sequence("Tabula Traiana: Model 2")
{
Boundary("Tab: start lower horizon");
Phase("Tab: lower horizon")
{
Date("OxA-35594", U(calBP(60000),calBP(48800)))
{
color="green";
Outlier("General", 0.05);
};
Date("OxA-35769", U(calBP(60000),calBP(50100)))
{
color="green";
Outlier("General", 0.05);
};
Date("OxA-35762", U(calBP(60000),calBP(48000)))
{
color="green";
Outlier("General", 0.05);
};
};
Boundary("Tab: transition lower horizon to 218");
```

```
Phase("Tab: 218")
{
R_Date("OxA-35770", 46500, 2600)
{
color="green";
Outlier("General", 0.05);
};
};
Boundary("Tab: transition 218 to upper horizon");
Phase("Tab: upper horizon")
{
Combine("Tab-13")
{
Outlier("General", 0.05);
Date("OxA-35766", U(calBP(60000),calBP(49800)))
{
Outlier("SSimple", 0.05);
color="green";
};
Date("OxA-35767", U(calBP(60000),calBP(49900)))
{
Outlier("SSimple", 0.05);
color="green";
};
};
R_Date("OxA-35764", 36500, 750)
{
color="green";
Outlier("General", 0.05);
};
R_Date("OxA-35768", 34250, 550)
{
color="green";
Outlier("General", 0.05);
};
//CI erruption 14C age after Giaccio et al. 2017
R_Date("CI", 34290, 90)
{
Outlier("General", 0.05);
color="#b7005c";
};
R_Date("OxA-23651", 34200, 550)
{
Outlier("General", 0.05);
color="blue";
};
R_Date("OxA-24818", 33450, 500)
{
Outlier("General", 0.05);
color="blue";
};
R_Date("OxA-35763", 28550, 290)
{
color="green";
Outlier("General", 0.05);
};
R_Date("OxA-35592", 33600, 550)
{
color="green";
Outlier("General", 0.05);
};
R_Date("OxA-35765", 20460, 120)
{
color="green";
Outlier("General", 0.05);
};
};
Boundary("Tab: transition Pleistocene to Holocene");
Phase("Tab: 'Holocene'")
{
R_Date("OxA-35593", 25490, 210)
{
color="green";
Outlier("General", 0.05);
};
};
Boundary("Tab: end layer 200");
};
};
```

Model 3 – figure 9.15

```
 Plot()
{
Outlier_Model("SSimple", N(0,2), 0, "s");
Outlier_Model("General",T(5),U(0,4),"t");
Sequence("Tabula Traiana: Model 3")
{
Boundary("Tab: start lower horizon");
Phase("Tab: lower horizon")
{
Date("OxA-35594", U(calBP(60000),calBP(48800)))
{
color="green";
Outlier("General", 0.05);
};
Date("OxA-35769", U(calBP(60000),calBP(50100)))
{
color="green";
Outlier("General", 0.05);
};
Date("OxA-35762", U(calBP(60000),calBP(48000)))
{
color="green";
Outlier("General", 0.05);
};
Combine("Tab-13")
{
Outlier("General", 0.05);
Date("OxA-35766", U(calBP(60000),calBP(49800)))
{
Outlier("SSimple", 0.05);
color="green";
};
Date("OxA-35767", U(calBP(60000),calBP(49900)))
{
Outlier("SSimple", 0.05);
color="green";
};
};
};
};
Boundary("Tab: transition lower horizon to 218");
Phase("Tab: 218")
{
R_Date("OxA-35770", 46500, 2600)
{
color="green";
Outlier("General", 0.05);
};
};
Boundary("Tab: transition 218 to upper horizon");
Phase("Tab: upper horizon")
{
R_Date("OxA-35764", 36500, 750)
{
color="green";
Outlier("General", 0.05);
};
R_Date("OxA-35768", 34250, 550)
{
color="green";
Outlier("General", 0.05);
};
//CI 14C date after Giaccio et al. 2017
R_Date("CI", 34290, 90)
{
Outlier("General", 0.05);
color="#b7005c";
};
R_Date("OxA-23651", 34200, 550)
{
Outlier("General", 0.05);
color="blue";
};
```

```
R_Date("OxA-24818", 33450, 500)
{
Outlier("General", 0.05);
color="blue";
};
R_Date("OxA-35763", 28550, 290)
{
color="green";
Outlier("General", 0.05);
};
R_Date("OxA-35592", 33600, 550)
{
color="green";
Outlier("General", 0.05);
};
R_Date("OxA-35765", 20460, 120)
{
color="green";
Outlier("General", 0.05);
};
};
Boundary("Tab: transition Pleistocene to Holocene");
Phase("Tab: 'Holocene'")
{
R_Date("OxA-35593", 25490, 210)
{
color="green";
Outlier("General", 0.05);
};
};
Boundary("Tab: end layer 200");
};
};
```

KDE – figure 9.13

```
 KDE_model()
{
R_Date("OxA-35593", 25490, 210);
R_Date("OxA-35592", 33600, 550);
R_Date("OxA-35763", 28550, 290);
Date("OxA-35762", U(calBP(60000),calBP(48000)));
R_Date("OxA-35764", 36500, 750);
R_Date("OxA-35765", 20460, 120);
Date("OxA-35766", U(calBP(60000),calBP(49800)));
Date("OxA-35767", U(calBP(60000),calBP(49900)));
R_Date("OxA-35770", 46500, 2600);
Date("OxA-35769", U(calBP(60000),calBP(50100)));
Date("OxA-35594", U(calBP(60000),calBP(48800)));
R_Date("OxA-35768", 34250, 550);
R_Date("OxA-23651", 34200, 550);
R_Date("OxA-24818", 33450, 500);
};
```

B.4 Code: Istállóskő

Model 0 – figure 11.19

```
 Plot("Istallosko")
{
Outlier_Model("General",T(5),U(0,4),"t");
Outlier_Model("SSimple",N(0,2),0,"s");
Sequence("Istall - Model 0")
{
Boundary("start lower AH");
Phase("lower AH")
{
Date("GrN-4659",N(calBP(49000),1900))
{
Outlier("General", 0.05);
color="gray";
};
R_Date("GrN-4658", 39700, 900)
{
Outlier("General", 0.05);
color="gray";
};
R_Date("ISGS-A-0184", 33101, 512)
{
Outlier("General", 0.05);
color="blue";
};
R_Date("ISGS-A-0187", 32701, 316)
{
Outlier("General", 0.05);
color="blue";
};
R_Date("OxA-X-2170-18", 33600, 900)
{
Outlier("General", 0.05);
color="green";
};
R_Date("OxA-X-2244-32", 34890, 250)
{
Outlier("General", 0.05);
color="green";
};
R_Date("GrN-1501", 31540, 600)
{
Outlier("General", 0.05);
color="gray";
};
Date("Date lower AH");
Interval("Intv lower AH");
};
Boundary("end lower AH");
Interval("Intv tranisiton lower/upper AH");
Boundary("start upper AH");
Phase("upper AH")
{
R_Date("GrN-1935", 30900, 600)
{
Outlier("General", 0.05);
color="gray";
};
R_Date("ISGS-A-0186", 27933, 224)
{
Outlier("General", 0.05);
color="blue";
};
R_Date("ISGS-A-0188", 31608, 295)
{
Outlier("General", 0.05);
color="blue";
};
R_Date("OxA-16638", 30970, 310)
{
Outlier("General", 0.05);
color="magenta";
};
color="purple";
R_Combine("ID 3", 0.05)
{
R_Date("OxA-16916", 29470, 190)
{
color="purple";
Outlier("SSimple", 0.05);
};
R_Date("OxA-16917", 29240, 170)
{
Outlier("SSimple", 0.05);
color="purple";
};
color="purple";
Outlier("General", 0.05);
};
R_Date("OxA-16093", 30510, 170)
{
Outlier("General", 0.05);
color="purple";
};
R_Date("OxA-16094", 29900, 190)
{
Outlier("General", 0.05);
color="purple";
};
Date("Date upper AH");
Interval("Intv upper AH");
};
Boundary("transition AH to bears");
Interval("Intv tranisiton upper AH to bears");
Phase("above 'upper AH'")
{
//(cave bear) / above Aurignacian II
R_Date("OxA-16639", 25500, 210)
{
Outlier("General", 0.05);
color="magenta";
};
//(cave bear) / above Aurignacian II
R_Date("OxA-16640", 24950, 140)
{
Outlier("General", 0.05);
color="magenta";
};
Date("Date abve AH");
Interval("Intv above AH");
};
Boundary("end bears");
};
};
```

Model 0 (B) – figure 11.19

```
 Plot("Istallosko")
{
Outlier_Model("General",T(5),U(0,4),"t");
Outlier_Model("SSimple",N(0,2),0,"s");
Sequence("Istall - Model 0")
{
Boundary("start lower AH");
Phase("lower AH")
{
Date("GrN-4659",N(calBP(49000),1900))
{
Outlier("General", 0.05);
color="gray";
};
R_Date("GrN-4658", 39700, 900)
{
Outlier("General", 0.05);
color="gray";
};
R_Date("ISGS-A-0184", 33101, 512)
{
Outlier("General", 0.05);
color="blue";
};
R_Date("ISGS-A-0187", 32701, 316)
{
Outlier("General", 0.05);
color="blue";
};
R_Date("OxA-X-2170-18", 33600, 900)
{
Outlier("General", 0.05);
color="green";
};
R_Date("OxA-X-2244-32", 34890, 250)
{
Outlier("General", 0.05);
color="green";
};
Date("Date lower AH");
Interval("Intv lower AH");
};
Boundary("transition lower AH/sterile");
Interval("Intv tranisiton lower AH/sterile");
Phase("sterile layer")
{
R_Date("GrN-1501", 31540, 600)
{
Outlier("General", 0.05);
color="gray";
};
};
Boundary("transition sterile/upper AH");
Interval("Intv tranisiton sterile/upper AH");
Phase("upper AH")
{
R_Date("GrN-1935", 30900, 600)
{
Outlier("General", 0.05);
color="gray";
};
R_Date("ISGS-A-0186", 27933, 224)
{
Outlier("General", 0.05);
color="blue";
};
R_Date("ISGS-A-0188", 31608, 295)
{
Outlier("General", 0.05);
color="blue";
};
R_Date("OxA-16638", 30970, 310)
{
Outlier("General", 0.05);
color="magenta";
};
color="purple";
R_Combine("ID 3", 0.05)
{
R_Date("OxA-16916", 29470, 190)
{
color="purple";
Outlier("SSimple", 0.05);
};
R_Date("OxA-16917", 29240, 170)
{
Outlier("SSimple", 0.05);
color="purple";
};
color="purple";
Outlier("General", 0.05);
};
R_Date("OxA-16093", 30510, 170)
{
Outlier("General", 0.05);
color="purple";
};
R_Date("OxA-16094", 29900, 190)
{
Outlier("General", 0.05);
color="purple";
};
Date("Date upper AH");
Interval("Intv upper AH");
};
Boundary("transition AH to bears");
Interval("Intv tranisiton upper AH to bears");
Phase("above 'upper AH'")
{
//(cave bear) / above Aurignacian II
R_Date("OxA-16639", 25500, 210)
{
Outlier("General", 0.05);
color="magenta";
};
//(cave bear) / above Aurignacian II
R_Date("OxA-16640", 24950, 140)
{
Outlier("General", 0.05);
color="magenta";
};
Date("Date abve AH");
Interval("Intv above AH");
};
Boundary("end bears");
};
};
```

Model 1 – figure 11.20

```
 Plot("Istallosko")
{
Outlier_Model("General",T(5),U(0,4),"t");
Outlier_Model("SSimple",N(0,2),0,"s");
Sequence("Istall - Model 1")
{
Boundary("start lower AH");
Phase("lower AH")
{
Date("GrN-4659",N(calBP(49000),1900))
{
color="grey";
Outlier("General", 0.05);
};
R_Date("GrN-4658", 39700, 900)
{
color="grey";
Outlier("General", 0.05);
};
R_Date("ISGS-A-0184", 33101, 512)
{
Outlier("General", 0.05);
color="blue";
};
```

```
R_Date("ISGS-A-0187", 32701, 316)
{
Outlier("General", 0.05);
color="blue";
};
R_Date("OxA-X-2170-18", 33600, 900)
{
Outlier("General", 0.05);
color="green";
};
R_Date("OxA-X-2244-32", 34890, 250)
{
Outlier("General", 0.05);
color="green";
};
R_Date("OxA-35383", 36200, 900)
{
Outlier("General", 0.05);
color="red";
};
R_Date("OxA-35522", 32850, 500)
{
Outlier("General", 0.05);
color="red";
};
R_Date("OxA-35415", 36100, 800)
{
Outlier("General", 0.05);
color="red";
};
R_Date("OxA-35384", 37200, 1200)
{
Outlier("General", 0.05);
color="red";
};
R_Date("OxA-35385", 37700, 1600)
{
Outlier("General", 0.05);
color="red";
};
Date("Date lower AH");
Interval("Intv lower AH");
};
Boundary("transition lower AH/sterile");
Interval("Intv transition lower AH/sterile");
Phase("Istall: Sterile layer")
{
R_Date("GrN-1501", 31540, 600)
{
color="grey";
Outlier("General", 0.05);
};
Date("Date sterile layer");
Interval("Intv sterile layer");
};
Boundary("tranistion sterile/upper AH");
Interval("Intv transition sterile/upper AH");
Phase("Istall: upper AH")
{
R_Date("GrN-1935", 30900, 600)
{
color="grey";
Outlier("General", 0.05);
};
R_Date("ISGS-A-0186", 27933, 224)
{
Outlier("General", 0.05);
color="blue";
};
R_Date("ISGS-A-0188", 31608, 295)
{
Outlier("General", 0.05);
color="blue";
};
R_Date("OxA-16638", 30970, 310)
{
Outlier("General", 0.05);
color="magenta";
};
R_Combine("ID 3")
{
Outlier("General", 0.05);
color="purple";
R_Date("OxA-16916", 29470, 190)
{
Outlier("SSimple", 0.05);
color="purple";
};
R_Date("OxA-16917", 29240, 170)
{
Outlier("SSimple", 0.05);
color="purple";
};
};
R_Date("OxA-16093", 30510, 170)
{
Outlier("General", 0.05);
color="purple";
};
R_Date("OxA-16094", 29900, 190)
{
Outlier("General", 0.05);
color="purple";
};
R_Date("OxA-35414", 33450, 600)
{
Outlier("General", 0.05);
color="red";
};
R_Date("OxA-35382", 35800, 1200)
{
Outlier("General", 0.05);
color="red";
};
R_Date("OxA-X-2716-11", 33200, 800)
{
Outlier("General", 0.05);
color="red";
};
R_Date("OxA-34771", 33450, 550)
{
Outlier("General", 0.05);
color="red";
};
R_Date("OxA-35421", 36500, 900)
{
Outlier("General", 0.05);
color="red";
};
R_Date("OxA-34402", 35000, 700)
{
Outlier("General", 0.05);
color="darkorange";
};
R_Date("OxA-34404", 26520, 230)
{
Outlier("General", 0.05);
color="darkorange";
};
R_Date("OxA-34403", 25610, 220)
{
Outlier("General", 0.05);
color="darkorange";
};
Date("Date upper AH");
Interval("Intv upper AH");
};
Boundary("transition upper AH/cave bear");
Interval("Intv transition upper AH/cave bear");
Phase("Istall: above upper AH")
{
//(cave bear) / above Aurignacian II
R_Date("OxA-16639", 25500, 210)
{
Outlier("General", 0.05);
color="magenta";
};
//(cave bear) / above Aurignacian II
R_Date("OxA-16640", 24950, 140)
{
Outlier("General", 0.05);
color="magenta";
};
Date("Date cave bear");
Interval("Intv cave bear");
};
```

```
Boundary("end cave bear layer");
};
```

Model 2 – figure 11.20

```
 Plot("Istallosko")
{
Outlier_Model("General",T(5),U(0,4),"t");
Outlier_Model("SSimple",N(0,2),0,"s");
Sequence("Istall - Model 2")
{
Boundary("start lower AH");
Phase("lower AH")
{
Date("GrN-4659",N(calBP(49000),1900))
{
color="grey";
Outlier("General", 0.05);
};
R_Date("GrN-4658", 39700, 900)
{
color="grey";
Outlier("General", 0.05);
};
R_Date("ISGS-A-0184", 33101, 512)
{
Outlier("General", 0.05);
color="blue";
};
R_Date("ISGS-A-0187", 32701, 316)
{
Outlier("General", 0.05);
color="blue";
};
R_Date("OxA-X-2170-18", 33600, 900)
{
Outlier("General", 0.05);
color="green";
};
R_Date("OxA-X-2244-32", 34890, 250)
{
Outlier("General", 0.05);
color="green";
};
R_Date("OxA-35383", 36200, 900)
{
Outlier("General", 0.05);
color="red";
};
R_Date("OxA-35522", 32850, 500)
{
Outlier("General", 0.05);
color="red";
};
R_Date("OxA-35415", 36100, 800)
{
Outlier("General", 0.05);
color="red";
};
R_Date("OxA-35384", 37200, 1200)
{
Outlier("General", 0.05);
color="red";
};
R_Date("OxA-35385", 37700, 1600)
{
Outlier("General", 0.05);
color="red";
};
Date("Date lower AH");
Interval("Intv lower AH");
};
Boundary("end lower AH");
Interval("transition lower/upper AH");
Boundary("start AH");
Phase("upper AH")
{
R_Date("ISGS-A-0186", 27933, 224)
{
Outlier("General", 0.05);
color="blue";
};
R_Date("ISGS-A-0188", 31608, 295)
{
Outlier("General", 0.05);
color="blue";
};
R_Date("OxA-16638", 30970, 310)
{
Outlier("General", 0.05);
color="magenta";
};
R_Combine("ID 3")
{
Outlier("General", 0.05);
color="purple";
R_Date("OxA-16916", 29470, 190)
{
Outlier("SSimple", 0.05);
color="purple";
};
R_Date("OxA-16917", 29240, 170)
{
Outlier("SSimple", 0.05);
color="purple";
};
};
R_Date("OxA-16093", 30510, 170)
{
Outlier("General", 0.05);
color="purple";
};
R_Date("OxA-16094", 29900, 190)
{
Outlier("General", 0.05);
color="purple";
};
R_Date("OxA-35414", 33450, 600)
{
Outlier("General", 0.05);
color="red";
};
R_Date("OxA-35382", 35800, 1200)
{
Outlier("General", 0.05);
color="red";
};
R_Date("OxA-X-2716-11", 33200, 800)
{
Outlier("General", 0.05);
color="red";
};
R_Date("OxA-34771", 33450, 550)
{
Outlier("General", 0.05);
color="red";
};
R_Date("OxA-35421", 36500, 900)
{
Outlier("General", 0.05);
color="red";
};
R_Date("OxA-34402", 35000, 700)
{
Outlier("General", 0.05);
color="darkorange";
};
R_Date("OxA-34404", 26520, 230)
{
Outlier("General", 0.05);
color="darkorange";
};
R_Date("OxA-34403", 25610, 220)
```

```
{
Outlier("General", 0.05);
color="darkorange";
};
Date("Date upper AH");
Interval("Intv upper AH");
};
Boundary("transition upper AH/cave bears");
Interval("transition upper AH/cave bear");
Phase("above 'upper AH'")
{
//(cave bear) / above Aurignacian II
R_Date("OxA-16639", 25500, 210)
{
Outlier("General", 0.05);
color="magenta";
};
//(cave bear) / above Aurignacian II
R_Date("OxA-16640", 24950, 140)
{
Outlier("General", 0.05);
color="magenta";
};
Date("Date cave bear");
Interval("Intv cave bear");
};
Boundary("end cave bear");
};
};
```

Model 3 – figure 11.21

```
 Plot("Istallosko")
{
Outlier_Model("General",T(5),U(0,4),"t");
Outlier_Model("SSimple",N(0,2),0,"s");
Sequence("Istall - Model 3")
{
Boundary("start lower AH");
Phase("lower AH")
{
R_Date("OxA-X-2170-18", 33600, 900)
{
Outlier("General", 0.05);
color="green";
};
R_Date("OxA-X-2244-32", 34890, 250)
{
Outlier("General", 0.05);
color="green";
};
R_Date("OxA-35383", 36200, 900)
{
Outlier("General", 0.05);
color="red";
};
R_Date("OxA-35522", 32850, 500)
{
Outlier("General", 0.05);
color="red";
};
R_Date("OxA-35415", 36100, 800)
{
Outlier("General", 0.05);
color="red";
};
R_Date("OxA-35384", 37200, 1200)
{
Outlier("General", 0.05);
color="red";
};
R_Date("OxA-35385", 37700, 1600)
{
Outlier("General", 0.05);
color="red";
};
Date("Date lower AH");
Interval("Intv lower AH");
};
Boundary("end lower AH");
Interval("Intv transition lower/upper AH");
Boundary("start upper AH");
Phase("upper AH")
{
R_Combine("ID 3")
{
Outlier("General", 0.05);
color="purple";
R_Date("OxA-16916", 29470, 190)
{
Outlier("SSimple", 0.05);
color="purple";
};
R_Date("OxA-16917", 29240, 170)
{
Outlier("SSimple", 0.05);
color="purple";
};
};
R_Date("OxA-16093", 30510, 170)
{
Outlier("General", 0.05);
color="purple";
};
R_Date("OxA-16094", 29900, 190)
{
Outlier("General", 0.05);
color="purple";
};
R_Date("OxA-35414", 33450, 600)
{
Outlier("General", 0.05);
color="red";
};
R_Date("OxA-35382", 35800, 1200)
{
Outlier("General", 0.05);
color="red";
};
R_Date("OxA-X-2716-11", 33200, 800)
{
Outlier("General", 0.05);
color="red";
};
R_Date("OxA-34771", 33450, 550)
{
Outlier("General", 0.05);
color="red";
};
R_Date("OxA-35421", 36500, 900)
{
Outlier("General", 0.05);
color="red";
};
R_Date("OxA-34402", 35000, 700)
{
Outlier("General", 0.05);
color="darkorange";
};
R_Date("OxA-34404", 26520, 230)
{
Outlier("General", 0.05);
color="darkorange";
};
R_Date("OxA-34403", 25610, 220)
{
Outlier("General", 0.05);
color="darkorange";
};
Date("Date upper AH");
Interval("Intv upper AH");
};
Boundary("transition upper AH/cave bears");
Interval("Intv transition upper AH/cave bears");
```

```
Phase("above 'upper AH'")
{
//(cave bear) / above Aurignacian II
R_Date("OxA-16639", 25500, 210)
{
Outlier("General", 0.05);
color="magenta";
};
//(cave bear) / above Aurignacian II
R_Date("OxA-16640", 24950, 140)
{
Outlier("General", 0.05);
color="magenta";
};
Date("Date cave bears");
Interval("Intv cave bears");
};
Boundary("end cave bears");
};
};
```

Model 4 – figure 11.21

```
 Plot("Istallosko")
{
Outlier_Model("General",T(5),U(0,4),"t");
Sequence("Istall - Model 4")
{
Boundary("start lower AH");
Phase("lower AH")
{
R_Date("OxA-X-2170-18", 33600, 900)
{
Outlier("General", 0.05);
color="green";
};
R_Date("OxA-X-2244-32", 34890, 250)
{
Outlier("General", 0.05);
color="green";
};
R_Date("OxA-35383", 36200, 900)
{
Outlier("General", 0.05);
color="red";
};
R_Date("OxA-35522", 32850, 500)
{
Outlier("General", 0.05);
color="red";
};
//Pb 50/39
R_Date("OxA-35415", 36100, 800)
{
Outlier("General", 0.05);
color="red";
};
R_Date("OxA-35384", 37200, 1200)
{
Outlier("General", 0.05);
color="red";
};
R_Date("OxA-35385", 37700, 1600)
{
Outlier("General", 0.05);
color="red";
};
Date("Date lower AH");
Interval("Intv lower AH");
};
Boundary("end lower AH");
Interval("Intv transition lower/upper AH");
Boundary("start upper AH");
Phase("upper AH")
{
R_Date("OxA-35414", 33450, 600)
{
Outlier("General", 0.05);
color="red";
};
R_Date("OxA-35382", 35800, 1200)
{
Outlier("General", 0.05);
color="red";
};
R_Date("OxA-X-2716-11", 33200, 800)
{
Outlier("General", 0.05);
color="red";
};
R_Date("OxA-34771", 33450, 550)
{
Outlier("General", 0.05);
color="red";
};
R_Date("OxA-35421", 36500, 900)
{
Outlier("General", 0.05);
color="red";
};
R_Date("OxA-34402", 35000, 700)
{
Outlier("General", 0.05);
color="darkorange";
};
R_Date("OxA-34404", 26520, 230)
{
Outlier("General", 0.05);
color="darkorange";
};
R_Date("OxA-34403", 25610, 220)
{
Outlier("General", 0.05);
color="darkorange";
};
Date("Date upper AH");
Interval("Intv upper AH");
};
Boundary("tranistion upper AH/cave bears");
Interval("Intv transition upper AH/cave bears");
Phase("above 'upper AH'")
{
//(cave bear) / above Aurignacian II
R_Date("OxA-16639", 25500, 210)
{
Outlier("General", 0.05);
color="magenta";
};
//(cave bear) / above Aurignacian II
R_Date("OxA-16640", 24950, 140)
{
Outlier("General", 0.05);
color="magenta";
};
Date("Date cave bears");
Interval("Intv cave bears");
};
Boundary("end cave bears");
};
};
```

KDE 1 – figure 11.22

```
 Kde_model("Istall - KDE 1")
{
R_Date("GrN-1501", 31540, 600)
{
color="grey";
};
Date("GrN-4659",N(calBP(49000),1900))
{
color="grey";
};
R_Date("GrN-4658", 39700, 900)
{
color="grey";
};
R_Date("ISGS-A-0184", 33101, 512)
{
color="blue";
};
R_Date("ISGS-A-0187", 32701, 316)
{
color="blue";
};
R_Date("OxA-X-2170-18", 33600, 900)
{
color="green";
};
R_Date("OxA-X-2244-32", 34890, 250)
{
color="green";
};
R_Date("OxA-35383", 36200, 900)
{
color="red";
};
R_Date("OxA-35522", 32850, 500)
{
color="red";
};
R_Date("OxA-35415", 36100, 800)
{
color="red";
};
R_Date("OxA-35384", 37200, 1200)
{
color="red";
};
R_Date("OxA-35385", 37700, 1600)
{
color="red";
};
R_Date("OxA-34402", 35000, 700)
{
color="darkorange";
};
R_Date("OxA-34404", 26520, 230)
{
color="darkorange";
};
R_Date("GrN-1935", 30900, 600)
{
color="grey";
};
R_Date("ISGS-A-0185", 29035, 237)
{
color="blue";
};
R_Date("ISGS-A-0186", 27933, 224)
{
color="blue";
};
R_Date("ISGS-A-0188", 31608, 295)
{
color="blue";
};
R_Date("OxA-16638", 30970, 310)
{
color="magenta";
};
R_Combine("ID 3")
{
R_Date("OxA-16916", 29470, 190)
{
color="purple";
};
R_Date("OxA-16917", 29240, 170)
{
color="purple";
};
};
R_Date("OxA-16093", 30510, 170)
{
color="purple";
};
R_Date("OxA-16094", 29900, 190)
{
color="purple";
};
R_Date("OxA-35414", 33450, 600)
{
color="red";
};
R_Date("OxA-35382", 35800, 1200)
{
color="red";
};
R_Date("OxA-X-2716-11", 33200, 800)
{
color="red";
};
R_Date("OxA-34403", 25610, 220)
{
color="darkorange";
};
R_Date("OxA-16639", 25500, 210)
{
color="magenta";
};
R_Date("OxA-16640", 24950, 140)
{
color="magenta";
};
R_Date("OxA-34771", 33450, 550)
{
color="red";
};
R_Date("OxA-35421", 36500, 900)
{
color="red";
};
};
```

KDE 2 – figure 11.22

```
 Kde_Model("Istall - KDE 2")
{
R_Date("OxA-X-2170-18", 33600, 900)
{
color="green";
};
R_Date("OxA-X-2244-32", 34890, 250)
{
color="green";
};
R_Date("OxA-35383", 36200, 900)
{
color="red";
};
R_Date("OxA-35522", 32850, 500)
{
color="red";
};
R_Date("OxA-35415", 36100, 800)
{
color="red";
};
```

```
R_Date("OxA-35384", 37200, 1200)
{
color="red";
};
R_Date("OxA-35385", 37700, 1600)
{
color="red";
};
R_Date("OxA-34402", 35000, 700)
{
color="darkorange";
};
R_Date("OxA-34404", 26520, 230)
{
color="darkorange";
};
R_Date("OxA-16916", 29470, 190)
{
color="purple";
};
R_Date("OxA-16917", 29240, 170)
{
color="purple";
};
R_Date("OxA-16093", 30510, 170)
{
color="purple";
};
R_Date("OxA-16094", 29900, 190)
{
color="purple";
};
R_Date("OxA-35414", 33450, 600)
{
color="red";
};
R_Date("OxA-35382", 35800, 1200)
{
color="red";
};
R_Date("OxA-X-2716-11", 33200, 800)
{
color="red";
};
R_Date("OxA-34403", 25610, 220)
{
color="darkorange";
};
R_Date("OxA-34771", 33450, 550)
{
color="red";
};
R_Date("OxA-35421", 36500, 900)
{
color="red";
};
};
```

KDE 3 – figure 11.22

```
 Kde_Model("Istall - KDE 3")
{
R_Date("OxA-X-2170-18", 33600, 900)
{
color="green";
};
R_Date("OxA-X-2244-32", 34890, 250)
{
color="green";
};
R_Date("OxA-35383", 36200, 900)
{
color="red";
};
R_Date("OxA-35522", 32850, 500)
{
color="red";
};
R_Date("OxA-35415", 36100, 800)
{
color="red";
};
R_Date("OxA-35384", 37200, 1200)
{
color="red";
};
R_Date("OxA-35385", 37700, 1600)
{
color="red";
};
R_Date("OxA-34402", 35000, 700)
{
color="darkorange";
};
R_Date("OxA-34404", 26520, 230)
{
color="darkorange";
};
R_Date("OxA-35414", 33450, 600)
{
color="red";
};
R_Date("OxA-35382", 35800, 1200)
{
color="red";
};
R_Date("OxA-X-2716-11", 33200, 800)
{
color="red";
};
R_Date("OxA-34403", 25610, 220)
{
color="darkorange";
};
R_Date("OxA-34771", 33450, 550)
{
color="red";
};
R_Date("OxA-35421", 36500, 900)
{
color="red";
};
};
```

Point Model 1 – figure 11.23

```
 Plot()
{
Outlier_Model("General",T(5),U(0,4),"t");
Sequence("Istall - Points Model 1")
{
Boundary("start points");
Phase("Osseous points")
{
R_Date("OxA-X-2170-18", 33600, 900)
{
Outlier("General", 0.05);
color="green";
};
R_Date("OxA-X-2244-32", 34890, 250)
```

```
{
Outlier("General", 0.05);
color="green";
};
R_Date("OxA-35522", 32850, 500)
{
Outlier("General", 0.05);
color="red";
};
R_Date("OxA-35383", 36200, 900)
{
Outlier("General", 0.05);
color="red";
};
R_Date("OxA-35415", 36100, 800)
{
Outlier("General", 0.05);
color="red";
};
R_Date("OxA-35384", 37200, 1200)
{
Outlier("General", 0.05);
color="red";
};
R_Date("OxA-35385", 37700, 1600)
{
Outlier("General", 0.05);
color="red";
};
R_Date("OxA-35414", 33450, 600)
{
Outlier("General", 0.05);
color="red";
};
R_Date("OxA-35382", 35800, 1200)
{
Outlier("General", 0.05);
color="red";
};
R_Date("OxA-X-2716-11", 33200, 800)
{
Outlier("General", 0.05);
color="red";
};
R_Date("OxA-34771", 33450, 550)
{
Outlier("General", 0.05);
color="red";
};
R_Date("OxA-35421", 36500, 900)
{
Outlier("General", 0.05);
color="red";
};
};
Boundary("end points");
};
};
```

Point KDE 1 – figure 11.24

```
 Kde_Model("Istall - Points KDE 1")
{
R_Date("OxA-X-2170-18", 33600, 900)
{
color="green";
};
R_Date("OxA-X-2244-32", 34890, 250)
{
color="green";
};
R_Date("OxA-35522", 32850, 500)
{
color="red";
};
R_Date("OxA-35383", 36200, 900)
{
color="red";
};
R_Date("OxA-35415", 36100, 800)
{
color="red";
};
R_Date("OxA-35384", 37200, 1200)
{
color="red";
};
R_Date("OxA-35385", 37700, 1600)
{
color="red";
};
R_Date("OxA-35414", 33450, 600)
{
color="red";
};
R_Date("OxA-35382", 35800, 1200)
{
color="red";
};
R_Date("OxA-X-2716-11", 33200, 800)
{
color="red";
};
R_Date("OxA-34771", 33450, 550)
{
color="red";
};
R_Date("OxA-35421", 36500, 900)
{
color="red";
};
};
```

Point KDE 2 – figure 11.24

```
 Kde_Model("Istall - Points KDE 2")
{
R_Date("OxA-X-2170-18", 33600, 900)
{
color="green";
};
R_Date("OxA-35522", 32850, 500)
{
color="red";
};
R_Date("OxA-35383", 36200, 900)
{
color="red";
};
R_Date("OxA-35415", 36100, 800)
{
color="red";
};
R_Date("OxA-35384", 37200, 1200)
{
color="red";
};
R_Date("OxA-35385", 37700, 1600)
{
color="red";
};
```

```
R_Date("OxA-35414", 33450, 600)
{
color="red";
};
R_Date("OxA-35382", 35800, 1200)
{
color="red";
};
R_Date("OxA-X-2716-11", 33200, 800)
{
color="red";
};
R_Date("OxA-34771", 33450, 550)
{
color="red";
};
R_Date("OxA-35421", 36500, 900)
{
color="red";
};
};
```

B.5 Code: Jankovich

KDE – figure 11.32

```
 KDE_Model()
{
R_Date("OxA-X-2716-49", 31800, 1000);
R_Date("OxA-X-2716-48", 32500, 800);
R_Date("OxA-X-2732-10", 32750, 670);
R_Date("OxA-X-2731-11", 31200, 2300);
R_Date("OxA-35386", 30800, 500);
};
```

B.6 Code: Dzeravá Skala

Model 1 - figure 12.18

```
 Plot()
{
Outlier_Model("General",T(5),U(0,4),"t");
Outlier_Model("SSimple",N(0,2),0,"s");
Sequence("Der - Model 1 (1/2)")
{
Boundary("Der - start layer 11");
Phase("Layer 11")
{
//Der-71 (AF), PP2, 11, 220-230, date: 48500, 3300,
lower limit calibrated 49800
Date("OxA-35760", N(calBP(56400), 3300))
{
Outlier("General", 0.05);
color="green";
};
R_Date("OxA-35759", 41500, 1400)
{
Outlier("General", 0.05);
color="green";
};
R_Date("OxA-35240", 38800, 1000)
{
Outlier("General", 0.05);
color="green";
};
R_Date("OxA-35582", 36600, 800)
{
Outlier("General", 0.05);
color="green";
};
R_Combine("Der-03")
{
Outlier("General", 0.05);
color="green";
R_Date("OxA-34012", 37000, 800)
{
color="green";
Outlier("SSimple", 0.05);
};
R_Date("OxA-35232", 36050, 700)
{
color="green";
Outlier("SSimple", 0.05);
};
};
Interval("Duration layer 11");
Date("Date layer 11");
};
Boundary("Der - transition layer 11 to 9");
Interval("Duration transition 11 to 9");
Phase("Layer 9")
{
R_Date("OxA-35581", 38300, 1100)
{
Outlier("General", 0.05);
color="green";
};
R_Date("OxA-35761", 40900, 1300)
{
Outlier("General", 0.05);
color="green";
};
R_Date("OxA-34026", 40100, 1200)
{
Outlier("General", 0.05);
color="green";
};
R_Date("OxA-35583", 39700, 1100)
{
Outlier("General", 0.05);
color="green";
};
R_Date("OxA-X-2732-14", 35560,870)
{
Outlier("General", 0.05);
color="#e34234";
};
R_Date("OxA-X-2717-18", 33000, 600)
{
Outlier("General", 0.05);
color="green";
};
R_Date("OxA-X-2732-15",32690, 620 )
{
Outlier("General", 0.05);
color="#e34234";
};
R_Date("OxA-X-2732-16",32770,660)
{
Outlier("General", 0.05);
color="#e34234";
};
R_Date("OxA-34016", 30130, 360)
{
Outlier("General", 0.05);
color="green";
};
R_Date("OxA-34022", 29490, 340)
{
Outlier("General", 0.05);
color="green";
};
R_Combine("Der-09")
{
Outlier("General", 0.05);
color="green";
R_Date("OxA-34014", 28580, 300)
{
Outlier("SSimple", 0.05);
color="green";
};
R_Date("OxA-34015", 28810, 310)
{
Outlier("SSimple", 0.05);
color="green";
};
};
R_Date("OxA-X2732-13", 28340, 370)
{
Outlier("General", 0.05);
color="#e34234";
};
R_Combine("Der-32 (2/3)")
{
Outlier("General", 0.05);
color="#aa381e";
R_Date("OxA-X-2719-20", 28760, 300)
{
Outlier("SSimple", 0.05);
color="#c0362c";
};
R_Date("OxA-35598", 27770, 370)
{
Outlier("SSimple", 0.05);
color="#c0362c";
};
};
R_Date("OxA-35387", 25140, 260)
{
Outlier("General", 0.05);
color="#c0362c";
};
R_Date("OxA-34013", 25050, 200)
{
Outlier("General", 0.05);
color="green";
};
```

```
R_Date("OxA-35233", 25000, 190)
{
Outlier("General", 0.05);
color="green";
};
R_Date("OxA-X-2716-51", 24680, 390)
{
Outlier("General", 0.05);
color="#c0362c";
};
Interval("Duration layer 9");
Date("Date layer 9");
};
Boundary("Der - transition layer 9 to 8");
Interval("Duration transition 9 to 8");
Phase("Layer 8")
{
R_Date("OxA-34023", 24780, 200)
{
Outlier("General", 0.05);
color="green";
};
Interval("Duration layer 8");
Date("Date layer 8");
};
Boundary("Der - transition layer 8 to 5");
Interval("Duration transition 8 to 5");
Phase("Layer 5")
{
R_Date("OxA-34019", 25160, 200)
{
Outlier("General", 0.05);
color="green";
};
R_Date("OxA-34021", 25020, 200)
{
Outlier("General", 0.05);
color="green";
};
R_Date("OxA-34020", 24890, 200)
{
Outlier("General", 0.05);
color="green";
};
Interval("Duration layer 5");
Date("Date layer 5");
};
Boundary("Der - transition layer 5 to 4");
Interval("Duration transition 5 to 4");
Phase("Layer 4")
{
R_Date("OxA-34027", 24960, 200)
{
Outlier("General", 0.05);
color="green";
};
R_Date("OxA-34025", 24820, 200)
{
Outlier("General", 0.05);
color="green";
};
R_Date("OxA-34024", 24720, 200)
{
Outlier("General", 0.05);
color="green";
};
Interval("Duration layer 4");
Date("Date layer 4");
};
Boundary("Der - transition layer 4 to 3");
Interval("Duration transition 4 to 3");
Phase("Layer 3")
{
R_Date("OxA-35241", 24700, 180)
{
Outlier("General", 0.05);
color="green";
};
Interval("Duration layer 3");
Date("Date layer 3");
};
Boundary("Der - transition end layer 3");
};
Sequence("Der - Model 1 (2/2)")
{
Boundary("=Der - transition layer 11 to 9");
Phase("Layer 7")
{
R_Date("OxA-34018", 38700, 1100)
{
Outlier("General", 0.05);
color="green";
};
R_Date("OxA-34017", 35350, 650)
{
Outlier("General", 0.05);
color="green";
};
Interval("Duration layer 7");
Date("Date layer 7");
};
Boundary("Der - transition layer 7 to 6");
Interval("Duration transition 7 to 6");
Phase("Layer 6")
{
R_Date("OxA-35242", 33300, 500)
{
Outlier("General", 0.05);
color="green";
};
Interval("Duration layer 6");
Date("Date layer 6");
};
Boundary("=Der - transition layer 8 to 5");
};
};
```

Model 2 - figure 12.18

```
 Plot()
{
Outlier_Model("General",T(5),U(0,4),"t");
Outlier_Model("SSimple",N(0,2),0,"s");
Sequence("Der - Model 2 (1/2)")
{
Boundary("Der - start layer 11");
Phase("Layer 11")
{
//Der-71 (AF), PP2, 11, 220-230, date: 48500, 3300,
lower limit calibrated 49800
Date("OxA-35760", N(calBP(56400), 3300))
{
Outlier("General", 0.05);
color="green";
};
R_Date("OxA-35759", 41500, 1400)
{
Outlier("General", 0.05);
color="green";
};
R_Date("OxA-35240", 38800, 1000)
{
Outlier("General", 0.05);
color="green";
};
R_Date("OxA-35582", 36600, 800)
{
Outlier("General", 0.05);
color="green";
};
R_Combine("Der-03")
{
Outlier("General", 0.05);
color="green";
R_Date("OxA-34012", 37000, 800)
```

```
{
color="green";
Outlier("SSimple", 0.05);
};
R_Date("OxA-35232", 36050, 700)
{
color="green";
Outlier("SSimple", 0.05);
};
};
R_Date("OxA-35581 (*)", 38300, 1100)
{
Outlier("General", 0.05);
color="green";
};
R_Date("OxA-35761 (*)", 40900, 1300)
{
Outlier("General", 0.05);
color="green";
};
R_Date("OxA-34026 (*)", 40100, 1200)
{
Outlier("General", 0.05);
color="green";
};
R_Date("OxA-35583 (*)", 39700, 1100)
{
Outlier("General", 0.05);
color="green";
};
Interval("Duration layer 11");
Date("Date layer 11");
};
Boundary("Der - transition layer 11 to 9");
Interval("Duration transition 11 to 9");
Phase("Layer 9")
{
R_Date("OxA-X-2732-14", 35560,870)
{
Outlier("General", 0.05);
color="#e34234";
};
R_Date("OxA-X-2717-18", 33000, 600)
{
Outlier("General", 0.05);
color="green";
};
R_Date("OxA-X-2732-15",32690, 620 )
{
Outlier("General", 0.05);
color="#e34234";
};
R_Date("OxA-X-2732-16",32770,660)
{
Outlier("General", 0.05);
color="#e34234";
};
R_Date("OxA-34016", 30130, 360)
{
Outlier("General", 0.05);
color="green";
};
R_Date("OxA-34022", 29490, 340)
{
Outlier("General", 0.05);
color="green";
};
R_Combine("Der-09")
{
Outlier("General", 0.05);
color="green";
R_Date("OxA-34014", 28580, 300)
{
Outlier("SSimple", 0.05);
color="green";
};
R_Date("OxA-34015", 28810, 310)
{
Outlier("SSimple", 0.05);
color="green";
};
};
R_Date("OxA-X2732-13", 28340, 370)
{
Outlier("General", 0.05);
color="#e34234";
};
R_Combine("Der-32 (2/3)")
{
Outlier("General", 0.05);
color="#aa381e";
R_Date("OxA-X-2719-20", 28760, 300)
{
Outlier("SSimple", 0.05);
color="#c0362c";
};
R_Date("OxA-35598", 27770, 370)
{
Outlier("SSimple", 0.05);
color="#c0362c";
};
};
R_Date("OxA-35387", 25140, 260)
{
Outlier("General", 0.05);
color="#c0362c";
};
R_Date("OxA-34013", 25050, 200)
{
Outlier("General", 0.05);
color="green";
};
R_Date("OxA-35233", 25000, 190)
{
Outlier("General", 0.05);
color="green";
};
R_Date("OxA-X-2716-51", 24680, 390)
{
Outlier("General", 0.05);
color="#c0362c";
};
Interval("Duration layer 9");
Date("Date layer 9");
};
Boundary("Der - transition layer 9 to 8");
Interval("Duration transition 9 to 8");
Phase("Layer 8")
{
R_Date("OxA-34023", 24780, 200)
{
Outlier("General", 0.05);
color="green";
};
Interval("Duration layer 8");
Date("Date layer 8");
};
Boundary("Der - transition layer 8 to 5");
Interval("Duration transition 8 to 5");
Phase("Layer 5")
{
R_Date("OxA-34019", 25160, 200)
{
Outlier("General", 0.05);
color="green";
};
R_Date("OxA-34021", 25020, 200)
{
Outlier("General", 0.05);
color="green";
};
R_Date("OxA-34020", 24890, 200)
{
Outlier("General", 0.05);
color="green";
};
Interval("Duration layer 5");
Date("Date layer 5");
};
Boundary("Der - transition layer 5 to 4");
Interval("Duration transition 5 to 4");
Phase("Layer 4")
{
R_Date("OxA-34027", 24960, 200)
{
Outlier("General", 0.05);
```

```
color="green";
};
R_Date("OxA-34025", 24820, 200)
{
Outlier("General", 0.05);
color="green";
};
R_Date("OxA-34024", 24720, 200)
{
Outlier("General", 0.05);
color="green";
};
Interval("Duration layer 4");
Date("Date layer 4");
};
Boundary("Der - transition layer 4 to 3");
Interval("Duration transition 4 to 3");
Phase("Layer 3")
{
R_Date("OxA-35241", 24700, 180)
{
Outlier("General", 0.05);
color="green";
};
Interval("Duration layer 3");
Date("Date layer 3");
};
Boundary("Der - transition end layer 3");
};
Sequence("Der - Model 2 (2/2)")
{
Boundary("=Der - transition layer 11 to 9");
Phase("Layer 7")
{
R_Date("OxA-34018", 38700, 1100)
{
Outlier("General", 0.05);
color="green";
};
R_Date("OxA-34017", 35350, 650)
{
Outlier("General", 0.05);
color="green";
};
Interval("Duration layer 7");
Date("Date layer 7");
};
Boundary("Der - transition layer 7 to 6");
Interval("Duration transition 7 to 6");
Phase("Layer 6")
{
R_Date("OxA-35242", 33300, 500)
{
Outlier("General", 0.05);
color="green";
};
Interval("Duration layer 6");
Date("Date layer 6");
};
Boundary("=Der - transition layer 8 to 5");
};
};
```

Model 3

```
 Plot()
{
Outlier_Model("General",T(5),U(0,4),"t");
Outlier_Model("SSimple",N(0,2),0,"s");
Sequence("Der - Model 3")
{
Boundary("Der - start layer 11");
Phase("Layer 11")
{
//Der-71 (AF), PP2, 11, 220-230, date: 48500, 3300,
lower limit calibrated 49800
Date("OxA-35760", N(calBP(56400), 3300))
{
Outlier("General", 0.05);
color="green";
};
R_Date("OxA-35759", 41500, 1400)
{
Outlier("General", 0.05);
color="green";
};
R_Date("OxA-35240", 38800, 1000)
{
Outlier("General", 0.05);
color="green";
};
R_Date("OxA-35582", 36600, 800)
{
Outlier("General", 0.05);
color="green";
};
R_Combine("Der-03")
{
Outlier("General", 0.05);
color="green";
R_Date("OxA-34012", 37000, 800)
{
color="green";
Outlier("SSimple", 0.05);
};
R_Date("OxA-35232", 36050, 700)
{
color="green";
Outlier("SSimple", 0.05);
};
};
Interval("Duration layer 11");
Date("Date layer 11");
};
Boundary("Der - transition layer 11 to 9");
Interval("Duration transition 11 to 9");
Phase("Layer 9")
{
R_Date("OxA-35581", 38300, 1100)
{
Outlier("General", 0.05);
color="green";
};
R_Date("OxA-35761", 40900, 1300)
{
Outlier("General", 0.05);
color="green";
};
R_Date("OxA-34026", 40100, 1200)
{
Outlier("General", 0.05);
color="green";
};
R_Date("OxA-35583", 39700, 1100)
{
Outlier("General", 0.05);
color="green";
};
R_Date("OxA-34018 (*)", 38700, 1100)
{
Outlier("General", 0.05);
color="green";
};
R_Date("OxA-X-2732-14", 35560,870)
{
Outlier("General", 0.05);
color="#e34234";
};
R_Date("OxA-34017 (*)", 35350, 650)
{
Outlier("General", 0.05);
color="green";
};
R_Date("OxA-35242 (*)", 33300, 500)
{
```

```
Outlier("General", 0.05);
color="green";
};
R_Date("OxA-X-2717-18", 33000, 600)
{
Outlier("General", 0.05);
color="green";
};
R_Date("OxA-X-2732-15",32690, 620 )
{
Outlier("General", 0.05);
color="#e34234";
};
R_Date("OxA-X-2732-16",32770,660)
{
Outlier("General", 0.05);
color="#e34234";
};
R_Date("OxA-34016", 30130, 360)
{
Outlier("General", 0.05);
color="green";
};
R_Date("OxA-34022", 29490, 340)
{
Outlier("General", 0.05);
color="green";
};
R_Combine("Der-09")
{
Outlier("General", 0.05);
color="green";
R_Date("OxA-34014", 28580, 300)
{
Outlier("SSimple", 0.05);
color="green";
};
R_Date("OxA-34015", 28810, 310)
{
Outlier("SSimple", 0.05);
color="green";
};
};
R_Date("OxA-X2732-13", 28340, 370)
{
Outlier("General", 0.05);
color="#e34234";
};
R_Combine("Der-32 (2/3)")
{
Outlier("General", 0.05);
color="#aa381e";
R_Date("OxA-X-2719-20", 28760, 300)
{
Outlier("SSimple", 0.05);
color="#c0362c";
};
R_Date("OxA-35598", 27770, 370)
{
Outlier("SSimple", 0.05);
color="#c0362c";
};
};
R_Date("OxA-35387", 25140, 260)
{
Outlier("General", 0.05);
color="#c0362c";
};
R_Date("OxA-34013", 25050, 200)
{
Outlier("General", 0.05);
color="green";
};
R_Date("OxA-35233", 25000, 190)
{
Outlier("General", 0.05);
color="green";
};
R_Date("OxA-X-2716-51", 24680, 390)
{
Outlier("General", 0.05);
color="#c0362c";
};
Interval("Duration layer 9");
Date("Date layer 9");
};
Boundary("Der - transition layer 9 to 8");
Interval("Duration transition 9 to 8");
Phase("Layer 8")
{
R_Date("OxA-34023", 24780, 200)
{
Outlier("General", 0.05);
color="green";
};
Interval("Duration layer 8");
Date("Date layer 8");
};
Boundary("Der - transition layer 8 to 5");
Interval("Duration transition 8 to 5");
Phase("Layer 5")
{
R_Date("OxA-34019", 25160, 200)
{
Outlier("General", 0.05);
color="green";
};
R_Date("OxA-34021", 25020, 200)
{
Outlier("General", 0.05);
color="green";
};
R_Date("OxA-34020", 24890, 200)
{
Outlier("General", 0.05);
color="green";
};
Interval("Duration layer 5");
Date("Date layer 5");
};
Boundary("Der - transition layer 5 to 4");
Interval("Duration transition 5 to 4");
Phase("Layer 4")
{
R_Date("OxA-34027", 24960, 200)
{
Outlier("General", 0.05);
color="green";
};
R_Date("OxA-34025", 24820, 200)
{
Outlier("General", 0.05);
color="green";
};
R_Date("OxA-34024", 24720, 200)
{
Outlier("General", 0.05);
color="green";
};
Interval("Duration layer 4");
Date("Date layer 4");
};
Boundary("Der - transition layer 4 to 3");
Interval("Duration transition 4 to 3");
Phase("Layer 3")
{
R_Date("OxA-35241", 24700, 180)
{
Outlier("General", 0.05);
color="green";
};
Interval("Duration layer 3");
Date("Date layer 3");
};
Boundary("Der - transition end layer 3");
};
};
```

Model 4

```
 Plot()
{
Outlier_Model("General",T(5),U(0,4),"t");
Outlier_Model("SSimple",N(0,2),0,"s");
Sequence("Der - Model 4")
{
Boundary("Der - start layer 11");
Phase("Layer 11")
{
//Der-71 (AF), PP2, 11, 220-230, date: 48500, 3300,
lower limit calibrated 49800
Date("OxA-35760", N(calBP(56400), 3300))
{
Outlier("General", 0.05);
color="green";
};
R_Date("OxA-35759", 41500, 1400)
{
Outlier("General", 0.05);
color="green";
};
R_Date("OxA-35240", 38800, 1000)
{
Outlier("General", 0.05);
color="green";
};
R_Date("OxA-35582", 36600, 800)
{
Outlier("General", 0.05);
color="green";
};
R_Combine("Der-03")
{
Outlier("General", 0.05);
color="green";
R_Date("OxA-34012", 37000, 800)
{
color="green";
Outlier("SSimple", 0.05);
};
R_Date("OxA-35232", 36050, 700)
{
color="green";
Outlier("SSimple", 0.05);
};
};
R_Date("OxA-35581 (*)", 38300, 1100)
{
Outlier("General", 0.05);
color="green";
};
R_Date("OxA-35761 (*)", 40900, 1300)
{
Outlier("General", 0.05);
color="green";
};
R_Date("OxA-34026 (*)", 40100, 1200)
{
Outlier("General", 0.05);
color="green";
};
R_Date("OxA-35583 (*)", 39700, 1100)
{
Outlier("General", 0.05);
color="green";
};
Interval("Duration layer 11");
Date("Date layer 11");
};
Boundary("Der - transition layer 11 to 9");
Interval("Duration transition 11 to 9");
Phase("Layer 9")
{
R_Date("OxA-34018 (*)", 38700, 1100)
{
Outlier("General", 0.05);
color="green";
};
R_Date("OxA-X-2732-14", 35560,870)
{
Outlier("General", 0.05);
color="#e34234";
};
R_Date("OxA-34017 (*)", 35350, 650)
{
Outlier("General", 0.05);
color="green";
};
R_Date("OxA-35242 (*)", 33300, 500)
{
Outlier("General", 0.05);
color="green";
};
R_Date("OxA-X-2717-18", 33000, 600)
{
Outlier("General", 0.05);
color="green";
};
R_Date("OxA-X-2732-15",32690, 620 )
{
Outlier("General", 0.05);
color="#e34234";
};
R_Date("OxA-X-2732-16",32770,660)
{
Outlier("General", 0.05);
color="#e34234";
};
R_Date("OxA-34016", 30130, 360)
{
Outlier("General", 0.05);
color="green";
};
R_Date("OxA-34022", 29490, 340)
{
Outlier("General", 0.05);
color="green";
};
R_Combine("Der-09")
{
Outlier("General", 0.05);
color="green";
R_Date("OxA-34014", 28580, 300)
{
Outlier("SSimple", 0.05);
color="green";
};
R_Date("OxA-34015", 28810, 310)
{
Outlier("SSimple", 0.05);
color="green";
};
};
R_Date("OxA-X2732-13", 28340, 370)
{
Outlier("General", 0.05);
color="#e34234";
};
R_Combine("Der-32 (2/3)")
{
Outlier("General", 0.05);
color="#aa381e";
R_Date("OxA-X-2719-20", 28760, 300)
{
Outlier("SSimple", 0.05);
color="#c0362c";
};
R_Date("OxA-35598", 27770, 370)
{
Outlier("SSimple", 0.05);
color="#c0362c";
};
};
R_Date("OxA-35387", 25140, 260)
{
Outlier("General", 0.05);
color="#c0362c";
};
R_Date("OxA-34013", 25050, 200)
{
```

```
Outlier("General", 0.05);
color="green";
};
R_Date("OxA-35233", 25000, 190)
{
Outlier("General", 0.05);
color="green";
};
R_Date("OxA-X-2716-51", 24680, 390)
{
Outlier("General", 0.05);
color="#c0362c";
};
Interval("Duration layer 9");
Date("Date layer 9");
};
Boundary("Der - transition layer 9 to 8");
Interval("Duration transition 9 to 8");
Phase("Layer 8")
{
R_Date("OxA-34023", 24780, 200)
{
Outlier("General", 0.05);
color="green";
};
Interval("Duration layer 8");
Date("Date layer 8");
};
Boundary("Der - transition layer 8 to 5");
Interval("Duration transition 8 to 5");
Phase("Layer 5")
{
R_Date("OxA-34019", 25160, 200)
{
Outlier("General", 0.05);
color="green";
};
R_Date("OxA-34021", 25020, 200)
{
Outlier("General", 0.05);
color="green";
};
R_Date("OxA-34020", 24890, 200)
{
Outlier("General", 0.05);
color="green";
};
Interval("Duration layer 5");
Date("Date layer 5");
};
Boundary("Der - transition layer 5 to 4");
Interval("Duration transition 5 to 4");
Phase("Layer 4")
{
R_Date("OxA-34027", 24960, 200)
{
Outlier("General", 0.05);
color="green";
};
R_Date("OxA-34025", 24820, 200)
{
Outlier("General", 0.05);
color="green";
};
R_Date("OxA-34024", 24720, 200)
{
Outlier("General", 0.05);
color="green";
};
Interval("Duration layer 4");
Date("Date layer 4");
};
Boundary("Der - transition layer 4 to 3");
Interval("Duration transition 4 to 3");
Phase("Layer 3")
{
R_Date("OxA-35241", 24700, 180)
{
Outlier("General", 0.05);
color="green";
};
Interval("Duration layer 3");
Date("Date layer 3");
};
Boundary("Der - transition end layer 3");
};
};
```

Model 5

```
 Plot()
{
Outlier_Model("General",T(5),U(0,4),"t");
Outlier_Model("SSimple",N(0,2),0,"s");
Sequence("Der - Model 5")
{
Boundary("Der - start layer 11");
Phase("Layer 11")
{
//Der-71 (AF), PP2, 11, 220-230, date: 48500, 3300,
lower limit calibrated 49800
Date("OxA-35760", N(calBP(56400), 3300))
{
Outlier("General", 0.05);
color="green";
};
R_Date("OxA-35759", 41500, 1400)
{
Outlier("General", 0.05);
color="green";
};
R_Date("OxA-35240", 38800, 1000)
{
Outlier("General", 0.05);
color="green";
};
R_Date("OxA-35582", 36600, 800)
{
Outlier("General", 0.05);
color="green";
};
R_Combine("Der-03")
{
Outlier("General", 0.05);
color="green";
R_Date("OxA-34012", 37000, 800)
{
color="green";
Outlier("SSimple", 0.05);
};
R_Date("OxA-35232", 36050, 700)
{
color="green";
Outlier("SSimple", 0.05);
};
};
Interval("Duration layer 11");
Date("Date layer 11");
};
Boundary("Der - transition layer 11 to 9");
Interval("Duration transition 11 to 9");
Phase("Layer 9")
{
R_Date("OxA-35581", 38300, 1100)
{
Outlier("General", 0.05);
color="green";
};
R_Date("OxA-35761", 40900, 1300)
{
Outlier("General", 0.05);
color="green";
};
R_Date("OxA-34026", 40100, 1200)
```

```
{
Outlier("General", 0.05);
color="green";
};
R_Date("OxA-35583", 39700, 1100)
{
Outlier("General", 0.05);
color="green";
};
R_Date("OxA-X-2732-14", 35560,870)
{
Outlier("General", 0.05);
color="#e34234";
};
R_Date("OxA-X-2717-18", 33000, 600)
{
Outlier("General", 0.05);
color="green";
};
R_Date("OxA-X-2732-15",32690, 620 )
{
Outlier("General", 0.05);
color="#e34234";
};
R_Date("OxA-X-2732-16",32770,660)
{
Outlier("General", 0.05);
color="#e34234";
};
R_Date("OxA-34016", 30130, 360)
{
Outlier("General", 0.05);
color="green";
};
R_Date("OxA-34022", 29490, 340)
{
Outlier("General", 0.05);
color="green";
};
R_Combine("Der-09")
{
Outlier("General", 0.05);
color="green";
R_Date("OxA-34014", 28580, 300)
{
Outlier("SSimple", 0.05);
color="green";
};
R_Date("OxA-34015", 28810, 310)
{
Outlier("SSimple", 0.05);
color="green";
};
};
R_Date("OxA-X2732-13", 28340, 370)
{
Outlier("General", 0.05);
color="#e34234";
};
R_Combine("Der-32 (2/3)")
{
Outlier("General", 0.05);
color="#aa381e";
R_Date("OxA-X-2719-20", 28760, 300)
{
Outlier("SSimple", 0.05);
color="#c0362c";
};
R_Date("OxA-35598", 27770, 370)
{
Outlier("SSimple", 0.05);
color="#c0362c";
};
};
R_Date("OxA-35387", 25140, 260)
{
Outlier("General", 0.05);
color="#c0362c";
};
R_Date("OxA-34013", 25050, 200)
{
Outlier("General", 0.05);
color="green";
};
R_Date("OxA-35233", 25000, 190)
{
Outlier("General", 0.05);
color="green";
};
R_Date("OxA-X-2716-51", 24680, 390)
{
Outlier("General", 0.05);
color="#c0362c";
};
Interval("Duration layer 9");
Date("Date layer 9");
};
Boundary("Der - transition layer 9 to 8");
Interval("Duration transition 9 to 8");
Phase("Layer 8")
{
R_Date("OxA-34023", 24780, 200)
{
Outlier("General", 0.05);
color="green";
};
Interval("Duration layer 8");
Date("Date layer 8");
};
Boundary("Der - transition layer 8 to 5");
Interval("Duration transition 8 to 5");
Phase("Layer 5")
{
R_Date("OxA-34019", 25160, 200)
{
Outlier("General", 0.05);
color="green";
};
R_Date("OxA-34021", 25020, 200)
{
Outlier("General", 0.05);
color="green";
};
R_Date("OxA-34020", 24890, 200)
{
Outlier("General", 0.05);
color="green";
};
Interval("Duration layer 5");
Date("Date layer 5");
};
Boundary("Der - transition layer 5 to 4");
Interval("Duration transition 5 to 4");
Phase("Layer 4")
{
R_Date("OxA-34027", 24960, 200)
{
Outlier("General", 0.05);
color="green";
};
R_Date("OxA-34025", 24820, 200)
{
Outlier("General", 0.05);
color="green";
};
R_Date("OxA-34024", 24720, 200)
{
Outlier("General", 0.05);
color="green";
};
Interval("Duration layer 4");
Date("Date layer 4");
};
Boundary("Der - transition layer 4 to 3");
Interval("Duration transition 4 to 3");
Phase("Layer 3")
{
R_Date("OxA-35241", 24700, 180)
{
Outlier("General", 0.05);
color="green";
};
Interval("Duration layer 3");
Date("Date layer 3");
};
Boundary("Der - transition end layer 3");
};
};
```

Model 6

```
 Plot()
{
Outlier_Model("General",T(5),U(0,4),"t");
Outlier_Model("SSimple",N(0,2),0,"s");
Sequence("Der - Model 6")
{
Boundary("Der - start layer 11");
Phase("Layer 11")
{
//Der-71 (AF), PP2, 11, 220-230, date: 48500, 3300,
lower limit calibrated 49800
Date("OxA-35760", N(calBP(56400), 3300))
{
Outlier("General", 0.05);
color="green";
};
R_Date("OxA-35759", 41500, 1400)
{
Outlier("General", 0.05);
color="green";
};
R_Date("OxA-35240", 38800, 1000)
{
Outlier("General", 0.05);
color="green";
};
R_Date("OxA-35582", 36600, 800)
{
Outlier("General", 0.05);
color="green";
};
R_Combine("Der-03")
{
Outlier("General", 0.05);
color="green";
R_Date("OxA-34012", 37000, 800)
{
color="green";
Outlier("SSimple", 0.05);
};
R_Date("OxA-35232", 36050, 700)
{
color="green";
Outlier("SSimple", 0.05);
};
};
R_Date("OxA-35581 (*)", 38300, 1100)
{
Outlier("General", 0.05);
color="green";
};
R_Date("OxA-35761 (*)", 40900, 1300)
{
Outlier("General", 0.05);
color="green";
};
R_Date("OxA-34026 (*)", 40100, 1200)
{
Outlier("General", 0.05);
color="green";
};
R_Date("OxA-35583 (*)", 39700, 1100)
{
Outlier("General", 0.05);
color="green";
};
Interval("Duration layer 11");
Date("Date layer 11");
};
Boundary("Der - transition layer 11 to 9");
Interval("Duration transition 11 to 9");
Phase("Layer 9")
{
R_Date("OxA-X-2732-14", 35560,870)
{
Outlier("General", 0.05);
color="#e34234";
};
R_Date("OxA-X-2717-18", 33000, 600)
{
Outlier("General", 0.05);
color="green";
};
R_Date("OxA-X-2732-15",32690, 620 )
{
Outlier("General", 0.05);
color="#e34234";
};
R_Date("OxA-X-2732-16",32770,660)
{
Outlier("General", 0.05);
color="#e34234";
};
R_Date("OxA-34016", 30130, 360)
{
Outlier("General", 0.05);
color="green";
};
R_Date("OxA-34022", 29490, 340)
{
Outlier("General", 0.05);
color="green";
};
R_Combine("Der-09")
{
Outlier("General", 0.05);
color="green";
R_Date("OxA-34014", 28580, 300)
{
Outlier("SSimple", 0.05);
color="green";
};
R_Date("OxA-34015", 28810, 310)
{
Outlier("SSimple", 0.05);
color="green";
};
};
R_Date("OxA-X2732-13", 28340, 370)
{
Outlier("General", 0.05);
color="#e34234";
};
R_Combine("Der-32 (2/3)")
{
Outlier("General", 0.05);
color="#aa381e";
R_Date("OxA-X-2719-20", 28760, 300)
{
Outlier("SSimple", 0.05);
color="#c0362c";
};
R_Date("OxA-35598", 27770, 370)
{
Outlier("SSimple", 0.05);
color="#c0362c";
};
};
R_Date("OxA-35387", 25140, 260)
{
Outlier("General", 0.05);
color="#c0362c";
};
R_Date("OxA-34013", 25050, 200)
{
Outlier("General", 0.05);
color="green";
};
R_Date("OxA-35233", 25000, 190)
{
Outlier("General", 0.05);
color="green";
};
R_Date("OxA-X-2716-51", 24680, 390)
{
Outlier("General", 0.05);
color="#c0362c";
};
Interval("Duration layer 9");
Date("Date layer 9");
```

```
};
Boundary("Der - transition layer 9 to 8");
Interval("Duration transition 9 to 8");
Phase("Layer 8")
{
R_Date("OxA-34023", 24780, 200)
{
Outlier("General", 0.05);
color="green";
};
Interval("Duration layer 8");
Date("Date layer 8");
};
Boundary("Der - transition layer 8 to 5");
Interval("Duration transition 8 to 5");
Phase("Layer 5")
{
R_Date("OxA-34019", 25160, 200)
{
Outlier("General", 0.05);
color="green";
};
R_Date("OxA-34021", 25020, 200)
{
Outlier("General", 0.05);
color="green";
};
R_Date("OxA-34020", 24890, 200)
{
Outlier("General", 0.05);
color="green";
};
Interval("Duration layer 5");
Date("Date layer 5");
};
Boundary("Der - transition layer 5 to 4");
Interval("Duration transition 5 to 4");
Phase("Layer 4")
{
R_Date("OxA-34027", 24960, 200)
{
Outlier("General", 0.05);
color="green";
};
R_Date("OxA-34025", 24820, 200)
{
Outlier("General", 0.05);
color="green";
};
R_Date("OxA-34024", 24720, 200)
{
Outlier("General", 0.05);
color="green";
};
Interval("Duration layer 4");
Date("Date layer 4");
};
Boundary("Der - transition layer 4 to 3");
Interval("Duration transition 4 to 3");
Phase("Layer 3")
{
R_Date("OxA-35241", 24700, 180)
{
Outlier("General", 0.05);
color="green";
};
Interval("Duration layer 3");
Date("Date layer 3");
};
Boundary("Der - transition end layer 3");
};
};
```

Model 7 - figure 12.19

```
 Plot()
{
Outlier_Model("General",T(5),U(0,4),"t");
Outlier_Model("SSimple",N(0,2),0,"s");
Sequence("Der - Model 7")
{
Boundary("Der - start layer 11");
Phase("Layer 11")
{
//Der-71 (AF), PP2, 11, 220-230, date: 48500, 3300,
lower limit calibrated 49800
Date("OxA-35760", N(calBP(56400), 3300))
{
Outlier("General", 0.05);
color="green";
};
R_Date("OxA-35759", 41500, 1400)
{
Outlier("General", 0.05);
color="green";
};
R_Date("OxA-35240", 38800, 1000)
{
Outlier("General", 0.05);
color="green";
};
R_Date("OxA-35582", 36600, 800)
{
Outlier("General", 0.05);
color="green";
};
R_Combine("Der-03")
{
Outlier("General", 0.05);
color="green";
R_Date("OxA-34012", 37000, 800)
{
color="green";
Outlier("SSimple", 0.05);
};
R_Date("OxA-35232", 36050, 700)
{
color="green";
Outlier("SSimple", 0.05);
};
};
Interval("Duration layer 11");
Date("Date layer 11");
};
Boundary("Der - transition layer 11 to 9");
Interval("Duration transition 11 to 9");
Phase("Layer 9")
{
R_Date("OxA-35581", 38300, 1100)
{
Outlier("General", 0.05);
color="green";
};
R_Date("OxA-35761", 40900, 1300)
{
Outlier("General", 0.05);
color="green";
};
R_Date("OxA-34026", 40100, 1200)
{
Outlier("General", 0.05);
color="green";
};
R_Date("OxA-35583", 39700, 1100)
{
Outlier("General", 0.05);
color="green";
};
R_Date("OxA-X-2732-14", 35560,870)
{
Outlier("General", 0.05);
color="#e34234";
};
R_Date("OxA-X-2717-18", 33000, 600)
{
```

```
Outlier("General", 0.05);
color="green";
};
R_Date("OxA-X-2732-15",32690, 620 )
{
Outlier("General", 0.05);
color="#e34234";
};
R_Date("OxA-X-2732-16",32770,660)
{
Outlier("General", 0.05);
color="#e34234";
};
R_Date("OxA-34016", 30130, 360)
{
Outlier("General", 0.05);
color="green";
};
R_Date("OxA-34022", 29490, 340)
{
Outlier("General", 0.05);
color="green";
};
R_Combine("Der-09")
{
Outlier("General", 0.05);
color="green";
R_Date("OxA-34014", 28580, 300)
{
Outlier("SSimple", 0.05);
color="green";
};
R_Date("OxA-34015", 28810, 310)
{
Outlier("SSimple", 0.05);
color="green";
};
};
R_Date("OxA-X2732-13", 28340, 370)
{
Outlier("General", 0.05);
color="#e34234";
};
R_Combine("Der-32 (2/3)")
{
Outlier("General", 0.05);
color="#aa381e";
R_Date("OxA-X-2719-20", 28760, 300)
{
Outlier("SSimple", 0.05);
color="#c0362c";
};
R_Date("OxA-35598", 27770, 370)
{
Outlier("SSimple", 0.05);
color="#c0362c";
};
};
R_Date("OxA-35387", 25140, 260)
{
Outlier("General", 0.05);
color="#c0362c";
};
R_Date("OxA-34013", 25050, 200)
{
Outlier("General", 0.05);
color="green";
};
R_Date("OxA-35233", 25000, 190)
{
Outlier("General", 0.05);
color="green";
};
R_Date("OxA-X-2716-51", 24680, 390)
{
Outlier("General", 0.05);
color="#c0362c";
};
Interval("Duration layer 9");
Date("Date layer 9");
};
Boundary("Der - transition layer 9 to 8/5");
Interval("Duration transition 9 to 8/5");
Phase("Layer 8/5")
{
R_Date("OxA-34019", 25160, 200)
{
Outlier("General", 0.05);
color="green";
};
R_Date("OxA-34021", 25020, 200)
{
Outlier("General", 0.05);
color="green";
};
R_Date("OxA-34020", 24890, 200)
{
Outlier("General", 0.05);
color="green";
};
R_Date("OxA-34023", 24780, 200)
{
Outlier("General", 0.05);
color="green";
};
Interval("Duration layer 8/5");
Date("Date layer 8/5");
};
Boundary("Der - transition layer 8/5 to 4");
Interval("Duration transition 8/5 to 4");
Phase("Layer 4")
{
R_Date("OxA-34027", 24960, 200)
{
Outlier("General", 0.05);
color="green";
};
R_Date("OxA-34025", 24820, 200)
{
Outlier("General", 0.05);
color="green";
};
R_Date("OxA-34024", 24720, 200)
{
Outlier("General", 0.05);
color="green";
};
Interval("Duration layer 4");
Date("Date layer 4");
};
Boundary("Der - transition layer 4 to 3");
Interval("Duration transition 4 to 3");
Phase("Layer 3")
{
R_Date("OxA-35241", 24700, 180)
{
Outlier("General", 0.05);
color="green";
};
Interval("Duration layer 3");
Date("Date layer 3");
};
Boundary("Der - transition end layer 3");
};
};
```

Model 8 - figure 12.19

```
 Plot()
{
Outlier_Model("General",T(5),U(0,4),"t");
Outlier_Model("SSimple",N(0,2),0,"s");
Sequence("Der - Model 8")
{
Boundary("Der - start layer 11");
Phase("Layer 11")
{
//Der-71 (AF), PP2, 11, 220-230, date: 48500, 3300,
lower limit calibrated 49800
Date("OxA-35760", N(calBP(56400), 3300))
{
color="green";
};
R_Date("OxA-35759", 41500, 1400)
{
Outlier("General", 0.05);
color="green";
};
R_Date("OxA-35240", 38800, 1000)
{
Outlier("General", 0.05);
color="green";
};
R_Date("OxA-35582", 36600, 800)
{
Outlier("General", 0.05);
color="green";
};
R_Combine("Der-03")
{
Outlier("General", 0.05);
color="green";
R_Date("OxA-34012", 37000, 800)
{
color="green";
Outlier("SSimple", 0.05);
};
R_Date("OxA-35232", 36050, 700)
{
color="green";
Outlier("SSimple", 0.05);
};
};
R_Date("OxA-35581 (*)", 38300, 1100)
{
Outlier("General", 0.05);
color="green";
};
R_Date("OxA-35761 (*)", 40900, 1300)
{
Outlier("General", 0.05);
color="green";
};
R_Date("OxA-34026 (*)", 40100, 1200)
{
Outlier("General", 0.05);
color="green";
};
R_Date("OxA-35583 (*)", 39700, 1100)
{
Outlier("General", 0.05);
color="green";
};
Interval("Duration layer 11");
Date("Date layer 11");
};
Boundary("Der - transition layer 11 to 9");
Interval("Duration transition 11 to 9");
Phase("Layer 9")
{
R_Date("OxA-X-2732-14", 35560,870)
{
Outlier("General", 0.05);
color="#e34234";
};
R_Date("OxA-X-2717-18", 33000, 600)
{
Outlier("General", 0.05);
color="green";
};
R_Date("OxA-X-2732-15",32690, 620 )
{
Outlier("General", 0.05);
color="#e34234";
};
R_Date("OxA-X-2732-16",32770,660)
{
Outlier("General", 0.05);
color="#e34234";
};
R_Date("OxA-34016", 30130, 360)
{
Outlier("General", 0.05);
color="green";
};
R_Date("OxA-34022", 29490, 340)
{
Outlier("General", 0.05);
color="green";
};
R_Combine("Der-09")
{
Outlier("General", 0.05);
color="green";
R_Date("OxA-34014", 28580, 300)
{
Outlier("SSimple", 0.05);
color="green";
};
R_Date("OxA-34015", 28810, 310)
{
Outlier("SSimple", 0.05);
color="green";
};
};
R_Date("OxA-X2732-13", 28340, 370)
{
Outlier("General", 0.05);
color="#e34234";
};
R_Combine("Der-32 (2/3)")
{
Outlier("General", 0.05);
color="#aa381e";
R_Date("OxA-X-2719-20", 28760, 300)
{
Outlier("SSimple", 0.05);
color="#c0362c";
};
R_Date("OxA-35598", 27770, 370)
{
Outlier("SSimple", 0.05);
color="#c0362c";
};
};
R_Date("OxA-35387", 25140, 260)
{
Outlier("General", 0.05);
color="#c0362c";
};
R_Date("OxA-34013", 25050, 200)
{
Outlier("General", 0.05);
color="green";
};
R_Date("OxA-35233", 25000, 190)
{
Outlier("General", 0.05);
color="green";
};
R_Date("OxA-X-2716-51", 24680, 390)
{
Outlier("General", 0.05);
color="#c0362c";
};
Interval("Duration layer 9");
Date("Date layer 9");
};
Boundary("Der - transition layer 9 to 8/5");
Interval("Duration transition 9 to 8/5");
Phase("Layer 8/5")
{
R_Date("OxA-34019", 25160, 200)
{
```

```
Outlier("General", 0.05);
color="green";
};
R_Date("OxA-34021", 25020, 200)
{
Outlier("General", 0.05);
color="green";
};
R_Date("OxA-34020", 24890, 200)
{
Outlier("General", 0.05);
color="green";
};
R_Date("OxA-34023", 24780, 200)
{
Outlier("General", 0.05);
color="green";
};
Interval("Duration layer 8/5");
Date("Date layer 8/5");
};
Boundary("Der - transition layer 8/5 to 4");
Interval("Duration transition 8/5 to 4");
Phase("Layer 4")
{
R_Date("OxA-34027", 24960, 200)
{
Outlier("General", 0.05);
color="green";
};
R_Date("OxA-34025", 24820, 200)
{
Outlier("General", 0.05);
color="green";
};
R_Date("OxA-34024", 24720, 200)
{
Outlier("General", 0.05);
color="green";
};
Interval("Duration layer 4");
Date("Date layer 4");
};
Boundary("Der - transition layer 4 to 3");
Interval("Duration transition 4 to 3");
Phase("Layer 3")
{
R_Date("OxA-35241", 24700, 180)
{
Outlier("General", 0.05);
color="green";
};
Interval("Duration layer 3");
Date("Date layer 3");
};
Boundary("Der - transition end layer 3");
};
};
```

Model 9 - figure 12.20

```
 Plot()
{
Outlier_Model("General",T(5),U(0,4),"t");
Outlier_Model("SSimple",N(0,2),0,"s");
Sequence("Der - Model 9 (1/2)")
{
Boundary("Der - start layer 11");
Phase("Layer 11")
{
Date("K0082 (OSL)", N(calBP(57000),4900))
{
Outlier("General", 0.05);
color="blue";
};
//Der-71 (AF), PP2, 11, 220-230, date: 48500, 3300,
lower limit calibrated 49800
Date("OxA-35760", N(calBP(56400), 3300))
{
Outlier("General", 0.05);
color="green";
};
R_Date("OxA-35759", 41500, 1400)
{
Outlier("General", 0.05);
color="green";
};
R_Date("OxA-35240", 38800, 1000)
{
Outlier("General", 0.05);
color="green";
};
R_Date("OxA-35582", 36600, 800)
{
Outlier("General", 0.05);
color="green";
};
R_Combine("Der-03")
{
Outlier("General", 0.05);
color="green";
R_Date("OxA-34012", 37000, 800)
{
color="green";
Outlier("SSimple", 0.05);
};
R_Date("OxA-35232", 36050, 700)
{
color="green";
Outlier("SSimple", 0.05);
};
};
Interval("Duration layer 11");
Date("Date layer 11");
};
Boundary("Der - transition layer 11 to 9");
Interval("Duration transition 11 to 9");
Phase("Layer 9")
{
R_Date("OxA-35581", 38300, 1100)
{
Outlier("General", 0.05);
color="green";
};
R_Date("OxA-35761", 40900, 1300)
{
Outlier("General", 0.05);
color="green";
};
R_Date("OxA-34026", 40100, 1200)
{
Outlier("General", 0.05);
color="green";
};
R_Date("OxA-35583", 39700, 1100)
{
Outlier("General", 0.05);
color="green";
};
R_Date("OxA-X-2732-14", 35560,870)
{
Outlier("General", 0.05);
color="#e34234";
};
R_Date("OxA-X-2717-18", 33000, 600)
{
Outlier("General", 0.05);
color="green";
};
R_Date("OxA-X-2732-15",32690, 620 )
{
Outlier("General", 0.05);
color="#e34234";
};
R_Date("OxA-X-2732-16",32770,660)
```

```
{
Outlier("General", 0.05);
color="#e34234";
};
R_Date("OxA-34016", 30130, 360)
{
Outlier("General", 0.05);
color="green";
};
Date("K0085 (OSL)", N(calBP(35900),2500))
{
Outlier("General", 0.05);
color="blue";
};
R_Date("OxA-34022", 29490, 340)
{
Outlier("General", 0.05);
color="green";
};
R_Combine("Der-09")
{
Outlier("General", 0.05);
color="green";
R_Date("OxA-34014", 28580, 300)
{
Outlier("SSimple", 0.05);
color="green";
};
R_Date("OxA-34015", 28810, 310)
{
Outlier("SSimple", 0.05);
color="green";
};
};
R_Date("OxA-X2732-13", 28340, 370)
{
Outlier("General", 0.05);
color="#e34234";
};
R_Combine("Der-32 (2/3)")
{
Outlier("General", 0.05);
color="#aa381e";
R_Date("OxA-X-2719-20", 28760, 300)
{
Outlier("SSimple", 0.05);
color="#c0362c";
};
R_Date("OxA-35598", 27770, 370)
{
Outlier("SSimple", 0.05);
color="#c0362c";
};
};
R_Date("OxA-35387", 25140, 260)
{
Outlier("General", 0.05);
color="#c0362c";
};
R_Date("OxA-34013", 25050, 200)
{
Outlier("General", 0.05);
color="green";
};
R_Date("OxA-35233", 25000, 190)
{
Outlier("General", 0.05);
color="green";
};
R_Date("OxA-X-2716-51", 24680, 390)
{
Outlier("General", 0.05);
color="#c0362c";
};
Interval("Duration layer 9");
Date("Date layer 9");
};
Boundary("Der - transition layer 9 to 5");
Interval("Duration transition 9 to 5");
Phase("Layer 5")
{
R_Date("OxA-34019", 25160, 200)
{
Outlier("General", 0.05);
color="green";
};
R_Date("OxA-34021", 25020, 200)
{
Outlier("General", 0.05);
color="green";
};
R_Date("OxA-34020", 24890, 200)
{
Outlier("General", 0.05);
color="green";
};
Interval("Duration layer 8/5");
Date("Date layer 8/5");
};
Boundary("Der - transition layer 5 to 4");
Interval("Duration transition 5 to 4");
Phase("Layer 4")
{
R_Date("OxA-34027", 24960, 200)
{
Outlier("General", 0.05);
color="green";
};
R_Date("OxA-34025", 24820, 200)
{
Outlier("General", 0.05);
color="green";
};
R_Date("OxA-34024", 24720, 200)
{
Outlier("General", 0.05);
color="green";
};
Interval("Duration layer 4");
Date("Date layer 4");
};
Boundary("Der - transition layer 4 to 3");
Interval("Duration transition 4 to 3");
Phase("Layer 3")
{
R_Date("OxA-35241", 24700, 180)
{
Outlier("General", 0.05);
color="green";
};
Interval("Duration layer 3");
Date("Date layer 3");
};
Boundary("Der - transition end layer 3");
};
Sequence("Der - Model 9 (2/2)")
{
Boundary("=Der - transition layer 11 to 9");
Phase("Layer 7")
{
R_Date("OxA-34018", 38700, 1100)
{
Outlier("General", 0.05);
color="green";
};
R_Date("OxA-34017", 35350, 650)
{
Outlier("General", 0.05);
color="green";
};
Interval("Duration layer 7");
Date("Date layer 7");
};
Boundary("Der - transition layer 7 to 6");
Interval("Duration transition 7 to 6");
Phase("Layer 6")
{
R_Date("OxA-35242", 33300, 500)
{
Outlier("General", 0.05);
color="green";
};
Interval("Duration layer 6");
Date("Date layer 6");
};
Boundary("=Der - transition layer 9 to 5");
};
};
```

Model 10 - figure 12.20

```
 Plot()
{
Outlier_Model("General",T(5),U(0,4),"t");
Outlier_Model("SSimple",N(0,2),0,"s");
Sequence("Der - Model 10 (1/2)")
{
Boundary("Der - start layer 11");
Phase("Der layer 11")
{
Date("K0082 (OSL)", N(calBP(57000),4900))
{
Outlier("General", 0.05);
color="blue";
};
//11, 240-250 cm, B, date: 49700, 3000,
lower limit calib 49900
Date("OxA-14247", N(calBP(55900),3000))
{
Outlier("General", 0.05);
color="blue";
};
//(11, 240-250 cm, B)  date: 7000, 2300,
lower limit calibrated 49700
Date("OxA-13859", N(calBP(54200),2300))
{
Outlier("General", 0.05);
color="blue";
};
//Der-71 (AF), PP2, 11, 220-230, date: 48500, 3300,
lower limit calibrated 49800
Date("OxA-35760", N(calBP(56400), 3300))
{
Outlier("General", 0.05);
color="green";
};
Date("OxA-13973",U(calBP(44600),calBP(70000)))
{
Outlier("General", 0.05);
color="blue";
};
R_Date("OxA-35759", 41500, 1400)
{
Outlier("General", 0.05);
color="green";
};
R_Date("OxA-35240", 38800, 1000)
{
Outlier("General", 0.05);
color="green";
};
R_Date("OxA-35582", 36600, 800)
{
Outlier("General", 0.05);
color="green";
};
R_Date("OxA-34028", 40100, 1200)
{
Outlier("General", 0.05);
color="green";
};
R_Combine("Der-03")
{
Outlier("General", 0.05);
color="green";
R_Date("OxA-34012", 37000, 800)
{
Outlier("SSimple", 0.05);
color="green";
};
R_Date("OxA-35232", 36050, 700)
{
Outlier("SSimple", 0.05);
color="green";
};
};
R_Date("Beta-173342", 36920, 470)
{
Outlier("General", 0.05);
color="blue";
};
Interval("Der - duration layer 11");
Date("Der - Date layer 11");
};
Boundary("Der - transition layer 11 to 5a'");
Interval("Der - duration transition 11 to 5a'");
Phase("Der layer 5a'")
{
R_Date("OxA-13860", 35100, 400)
{
Outlier("General", 0.05);
color="blue";
};
R_Date("Wk-14866 ", 33608, 569)
{
Outlier("General", 0.05);
color="blue";
};
Interval("Der - duration layer 5a'");
Date("Der - Date layer 5a'");
};
Boundary("Der - transition layer 5a' to 9");
Interval("Der - duration transition 5a' to 9");
Phase("Der layer 9")
{
R_Date("OxA-35581", 38300, 1100)
{
Outlier("General", 0.05);
color="green";
};
R_Date("OxA-35761", 40900, 1300)
{
Outlier("General", 0.05);
color="green";
};
R_Date("OxA-34026", 40100, 1200)
{
Outlier("General", 0.05);
color="green";
};
R_Date("OxA-35583", 39700, 1100)
{
Outlier("General", 0.05);
color="green";
};
R_Date("OxA-X-2732-14", 35560,870)
{
Outlier("General", 0.05);
color="#e34234";
};
R_Date("Beta-173341", 34100, 320)
{
Outlier("General", 0.05);
color="blue";
};
R_Date("Wk-16829", 33333, 820)
{
Outlier("General", 0.05);
color="blue";
};
R_Date("OxA-X-2717-18", 33000, 600)
{
Outlier("General", 0.05);
color="green";
};
R_Date("OxA-X-2732-16",32770,660)
{
Outlier("General", 0.05);
color="#e34234";
};
R_Date("OxA-X-2732-15",32690, 620 )
{
Outlier("General", 0.05);
color="#e34234";
};
R_Combine("Dz Sk 8 (Prošek)")
{
Outlier("General", 0.05);
color="darkorange";
R_Date("OxA-15535", 31000, 1100)
{
```

```
Outlier("SSimple", 0.05);
color="darkorange";
};
R_Date("OxA-15534", 31600, 900)
{
Outlier("SSimple", 0.05);
color="darkorange";
};
};
R_Date("OxA-34016", 30130, 360)
{
Outlier("General", 0.05);
color="green";
};
Date("K0085 (OSL)", N(calBP(35900),3000))
{
Outlier("General", 0.05);
color="blue";
};
R_Date("OxA-34022", 29490, 340)
{
Outlier("General", 0.05);
color="green";
};
R_Date("OxA-X2732-13", 28340, 370)
{
Outlier("General", 0.05);
color="#e34234";
};
R_Combine("Der-09")
{
Outlier("General", 0.05);
color="green";
R_Date("OxA-34014", 28580, 300)
{
Outlier("SSimple", 0.05);
color="green";
};
R_Date("OxA-34015", 28810, 310)
{
Outlier("SSimple", 0.05);
color="green";
};
};
R_Combine("Der-32 (2/3)")
{
Outlier("General", 0.05);
color="#aa381e";
R_Date("OxA-X-2719-20", 28760, 300)
{
Outlier("SSimple", 0.05);
color="#c0362c";
};
R_Date("OxA-34598", 27770, 370)
{
Outlier("SSimple", 0.05);
color="#c0362c";
};
};
R_Date("OxA-35387", 25140, 260)
{
Outlier("General", 0.05);
color="#c0362c";
};
R_Date("OxA-35233", 25000, 190)
{
Outlier("General", 0.05);
color="green";
};
R_Date("OxA-34013", 25050, 200)
{
Outlier("General", 0.05);
color="green";
};
R_Date("OxA-X-2716-51", 24680, 390)
{
Outlier("General", 0.05);
color="#c0362c";
};
Interval("Der - duration layer 9");
Date("Der - Date layer 9");
};
Boundary("Der - transition layer 9 to 5");
Interval("Der - duration transition 9 to 5");
Phase("Der layer 5")
{
R_Date("OxA-34019", 25160, 200)
{
Outlier("General", 0.05);
color="green";
};
R_Date("OxA-34021", 25020, 200)
{
Outlier("General", 0.05);
color="green";
};
R_Date("OxA-34020", 24890, 200)
{
Outlier("General", 0.05);
color="green";
};
R_Date("OxA-13861", 24760, 130)
{
Outlier("General", 0.05);
color="blue";
};
Interval("Der - duration layer 5");
Date("Der - Date layer 5");
};
Boundary("Der - transition layer 5 to 4");
Interval("Der - duration transition 5 to 4");
Phase("Der layer 4")
{
R_Date("OxA-34027", 24960, 200)
{
Outlier("General", 0.05);
color="green";
};
R_Date("OxA-34025", 24820, 200)
{
Outlier("General", 0.05);
color="green";
};
R_Date("OxA-34024", 24720, 200)
{
Outlier("General", 0.05);
color="green";
};
R_Date("GrA-22758", 24800, 130)
{
Outlier("General", 0.05);
color="blue";
};
Interval("Der - duration layer 4");
Date("Der - Date layer 4");
};
Boundary("Der - transition layer 4 to 3");
Interval("Der - duration transition 4 to 3");
Phase("Der layer 3")
{
R_Date("GrA-22756", 25050, 540)
{
Outlier("General", 0.05);
color="blue";
};
R_Date("OxA-35241", 24700, 180)
{
Outlier("General", 0.05);
color="green";
};
Interval("Der - duration layer 3");
Date("Der - Date layer 3");
};
Boundary("Der - end layer 3");
};
Sequence("Der - Model 10 (2/2)")
{
Boundary("=Der - transition layer 5a' to 9");
Phase("Layer 7")
{
R_Date("OxA-34018", 38700, 1100)
{
Outlier("General", 0.05);
color="green";
};
R_Date("OxA-34017", 35350, 650)
```

```
{
Outlier("General", 0.05);
color="green";
};
Interval("Duration layer 7");
Date("Date layer 7");
};
Boundary("Der - transition layer 7 to 6");
Interval("Duration transition 7 to 6");
Phase("Layer 6")
{
R_Date("OxA-35242", 33300, 500)
{
Outlier("General", 0.05);
color="green";
};
Interval("Duration layer 6");
Date("Date layer 6");
};
Boundary("=Der - transition layer 9 to 5");
};
};
```

Points Model 1

```
 Plot()
{
Sequence("Der - Points Model 1")
{
Boundary("Der - start points");
Phase("Der - points")
{
R_Date("OxA-X-2732-14", 35560,870)
{
color="#e34234";
};
R_Date("OxA-X-2732-16",32770,660)
{
color="#e34234";
};
R_Date("OxA-X-2732-15",32690, 620 )
{
color="#e34234";
};
R_Combine("Dz Sk 8 (Prošek)")
{
color="darkorange";
R_Date("OxA-15535", 31000, 1100)
{
color="darkorange";
};
R_Date("OxA-15534", 31600, 900)
{
color="darkorange";
};
};
R_Date("OxA-X2732-13", 28340, 370)
{
color="#e34234";
};
R_Combine("Der-32 (2/3)")
{
color="#aa381e";
R_Date("OxA-X-2719-20", 28760, 300)
{
color="#c0362c";
};
R_Date("OxA-35598", 27770, 370)
{
color="#c0362c";
};
};
R_Date("OxA-35387", 25140, 260)
{
color="#c0362c";
};
R_Date("OxA-X-2716-51", 24680, 390)
{
color="#c0362c";
};
Interval("Der - Interval points");
Date("Der - Date points");
};
Boundary("Der - end points");
};
};
```

KDE 0 - figure 12.21

```
 KDE_model("Der - KDE 0 v2")
{
//11, 240-250 cm, B  , date: 49700, 3000,
lower limit calib 49900
Date("OxA-14247", N(calBP(55900),3000))
{
color="blue";
};
//(11, 240-250 cm, B)  date: 7000, 2300,
lower limit calibrated 49700
Date("OxA-13859", N(calBP(54200),2300))
{
color="blue";
};
Date("OxA-13973",U(calBP(44600),calBP(70000)))
{
color="blue";
};
R_Date("Beta-173342", 36920, 470)
{
color="blue";
};
Label("Layer 5a'");
R_Date("Wk-14865 (9/5a')", 37370, 2060)
{
color="blue";
};
R_Date("OxA-13860", 35100, 400)
{
color="blue";
};
R_Date("Wk-14866 ", 33608, 569)
{
color="blue";
};
R_Date("Beta-173341", 34100, 320)
{
color="blue";
};
R_Date("Wk-16829", 33333, 820)
{
color="blue";
};
R_Combine("Dz Sk 8 (Prošek)")
{
color="darkorange";
R_Date("OxA-15535", 31000, 1100)
{
color="darkorange";
};
R_Date("OxA-15534", 31600, 900)
{
```

```
color="darkorange";
};
};
Date("K0085 (OSL)", N(calBP(29700),2500))
{
color="blue";
};
R_Date("OxA-13861", 24760, 130)
{
color="blue";
};
R_Date("GrA-22758", 24800, 130)
{
color="blue";
};
R_Date("GrA-22756", 25050, 540)
{
color="blue";
};
};
```

KDE 1 - figure 12.21

```
 KDE_model("Der - KDE 1 (points)")
{
R_Date("OxA-X-2732-14", 35560,870)
{
color="#e34234";
};
R_Date("OxA-X-2732-16",32770,660)
{
color="#e34234";
};
R_Date("OxA-X-2732-15",32690, 620 )
{
color="#e34234";
};
R_Combine("Dz Sk 8 (Prošek)")
{
color="darkorange";
R_Date("OxA-15535", 31000, 1100)
{
color="darkorange";
};
R_Date("OxA-15534", 31600, 900)
{
color="darkorange";
};
};
R_Date("OxA-X2732-13", 28340, 370)
{
color="#e34234";
};
R_Combine("Der-32 (2/3)")
{
color="#aa381e";
R_Date("OxA-X-2719-20", 28760, 300)
{
color="#c0362c";
};
R_Date("OxA-35598", 27770, 370)
{
color="#c0362c";
};
};
R_Date("OxA-35387", 25140, 260)
{
color="#c0362c";
};
R_Date("OxA-X-2716-51", 24680, 390)
{
color="#c0362c";
};
};
```

KDE 2 - figure 12.21

```
 KDE_model("Der - KDE 2 (points)")
{
R_Date("OxA-X-2732-14", 35560,870)
{
color="#e34234";
};
R_Date("OxA-X-2732-16",32770,660)
{
color="#e34234";
};
R_Date("OxA-X-2732-15",32690, 620 )
{
color="#e34234";
};
R_Date("OxA-X2732-13", 28340, 370)
{
color="#e34234";
};
R_Combine("Der-32 (2/3)")
{
color="#aa381e";
R_Date("OxA-X-2719-20", 28760, 300)
{
color="#c0362c";
};
R_Date("OxA-35598", 27770, 370)
{
color="#c0362c";
};
};
R_Date("OxA-35387", 25140, 260)
{
color="#c0362c";
};
R_Date("OxA-X-2716-51", 24680, 390)
{
color="#c0362c";
};
};
```

KDE 3 - figure 12.21

```
 KDE_model("Der - KDE 3 (human mod.)")
{
//Der-71 (AF), PP2, 11, 220-230, date: 48500, 3300,
lower limit calibrated 49800
Date("OxA-35760", N(calBP(56400), 3300))
{
color="green";
};
R_Date("OxA-35759", 41500, 1400)
{
color="green";
};
R_Date("OxA-35240", 38800, 1000)
{
color="green";
};
R_Date("OxA-35582", 36600, 800)
{
color="green";
};
R_Date("OxA-34028", 40100, 1200)
{
color="green";
};
R_Combine("Der-03")
{
color="green";
R_Date("OxA-34012", 37000, 800)
{
color="green";
};
R_Date("OxA-35232", 36050, 700)
{
color="green";
};
};
R_Date("OxA-34018", 38700, 1100)
{
color="green";
};
R_Date("OxA-34017", 35350, 650)
{
color="green";
};
R_Date("OxA-35242", 33300, 500)
{
color="green";
};
R_Date("OxA-35581", 38300, 1100)
{
color="green";
};
R_Date("OxA-35761", 40900, 1300)
{
color="green";
};
R_Date("OxA-34026", 40100, 1200)
{
color="green";
};
R_Date("OxA-35583", 39700, 1100)
{
color="green";
};
R_Date("OxA-X-2732-14", 35560,870)
{
color="#e34234";
};
R_Date("OxA-X-2717-18", 33000, 600)
{
color="green";
};
R_Date("OxA-X-2732-16",32770,660)
{
color="#e34234";
};
R_Date("OxA-X-2732-15",32690, 620 )
{
color="#e34234";
};
R_Combine("Dz Sk 8 (Prošek)")
{
color="darkorange";
R_Date("OxA-15535", 31000, 1100)
{
color="darkorange";
};
R_Date("OxA-15534", 31600, 900)
{
color="darkorange";
};
};
R_Date("OxA-34016", 30130, 360)
{
color="green";
};
R_Date("OxA-34022", 29490, 340)
{
color="green";
};
R_Date("OxA-X2732-13", 28340, 370)
{
color="#e34234";
};
R_Combine("Der-09")
{
color="green";
R_Date("OxA-34014", 28580, 300)
{
color="green";
};
R_Date("OxA-34015", 28810, 310)
{
color="green";
};
};
R_Combine("Der-32 (2/3)")
{
color="#aa381e";
R_Date("OxA-X-2719-20", 28760, 300)
{
color="#c0362c";
};
R_Date("OxA-35598", 27770, 370)
{
color="#c0362c";
};
};
R_Date("OxA-35387", 25140, 260)
{
color="#c0362c";
};
R_Date("OxA-35233", 25000, 190)
{
color="green";
};
R_Date("OxA-34013", 25050, 200)
{
color="green";
};
R_Date("OxA-X-2716-51", 24680, 390)
{
color="#c0362c";
};
R_Date("OxA-34023", 24780, 200)
{
color="green";
};
R_Date("OxA-34019", 25160, 200)
{
color="green";
};
R_Date("OxA-34021", 25020, 200)
{
color="green";
};
R_Date("OxA-34020", 24890, 200)
{
color="green";
};
R_Date("OxA-34027", 24960, 200)
{
color="green";
};
R_Date("OxA-34025", 24820, 200)
{
```

```
color="green";
};
R_Date("OxA-34024", 24720, 200)
{
color="green";
};
```

```
R_Date("OxA-35241", 24700, 180)
{
color="green";
};
};
```

KDE 4 - figure 12.21

```
 KDE_model("Der - KDE 4")
{
//11, 240-250 cm, B  , date: 49700, 3000,
lower limit calib 49900
Date("OxA-14247", N(calBP(55900),3000))
{
color="blue";
};
//(11, 240-250 cm, B)  date: 47000, 2300,
lower limit calibrated 49700
Date("OxA-13859", N(calBP(54200),2300))
{
color="blue";
};
//Der-71 (AF), PP2, 11, 220-230, date: 48500, 3300,
lower limit calibrated 49800
Date("OxA-35760", N(calBP(56400), 3300))
{
color="green";
};
Date("OxA-13973",U(calBP(44600),calBP(70000)))
{
color="blue";
};
R_Date("OxA-35759", 41500, 1400)
{
color="green";
};
R_Date("OxA-35240", 38800, 1000)
{
color="green";
};
R_Date("OxA-35582", 36600, 800)
{
color="green";
};
R_Date("OxA-34028", 40100, 1200)
{
color="green";
};
R_Combine("Der-03")
{
color="green";
R_Date("OxA-34012", 37000, 800)
{
color="green";
};
R_Date("OxA-35232", 36050, 700)
{
color="green";
};
};
R_Date("Beta-173342", 36920, 470)
{
color="blue";
};
R_Date("Wk-14865 (9/5a')", 37370, 2060)
{
color="blue";
};
R_Date("OxA-13860", 35100, 400)
{
color="blue";
};
R_Date("Wk-14866 ", 33608, 569)
{
color="blue";
};
R_Date("OxA-34018", 38700, 1100)
{
```

```
color="green";
};
R_Date("OxA-34017", 35350, 650)
{
color="green";
};
R_Date("OxA-35242", 33300, 500)
{
color="green";
};
R_Date("OxA-35581", 38300, 1100)
{
color="green";
};
R_Date("OxA-35761", 40900, 1300)
{
color="green";
};
R_Date("OxA-34026", 40100, 1200)
{
color="green";
};
R_Date("OxA-35583", 39700, 1100)
{
color="green";
};
R_Date("OxA-X-2732-14", 35560,870)
{
color="#e34234";
};
R_Date("Beta-173341", 34100, 320)
{
color="blue";
};
R_Date("Wk-16829", 33333, 820)
{
color="blue";
};
R_Date("OxA-X-2717-18", 33000, 600)
{
color="green";
};
R_Date("OxA-X-2732-16",32770,660)
{
color="#e34234";
};
R_Date("OxA-X-2732-15",32690, 620 )
{
color="#e34234";
};
R_Combine("Dz Sk 8 (Prošek)")
{
color="darkorange";
R_Date("OxA-15535", 31000, 1100)
{
color="darkorange";
};
R_Date("OxA-15534", 31600, 900)
{
color="darkorange";
};
};
R_Date("OxA-34016", 30130, 360)
{
color="green";
};
R_Date("OxA-34022", 29490, 340)
{
color="green";
};
```

```
R_Date("OxA-X2732-13", 28340, 370)
{
color="#e34234";
};
R_Combine("Der-09")
{
color="green";
R_Date("OxA-34014", 28580, 300)
{
color="green";
};
R_Date("OxA-34015", 28810, 310)
{
color="green";
};
};
R_Combine("Der-32 (2/3)")
{
color="#aa381e";
R_Date("OxA-X-2719-20", 28760, 300)
{
color="#c0362c";
};
R_Date("OxA-35598", 27770, 370)
{
color="#c0362c";
};
};
R_Date("OxA-35387", 25140, 260)
{
color="#c0362c";
};
R_Date("OxA-35233", 25000, 190)
{
color="green";
};
R_Date("OxA-34013", 25050, 200)
{
color="green";
};
R_Date("OxA-X-2716-51", 24680, 390)
{
color="#c0362c";
};
R_Date("OxA-34023", 24780, 200)
{
color="green";
};
R_Date("OxA-34019", 25160, 200)
{
color="green";
};
R_Date("OxA-34021", 25020, 200)
{
color="green";
};
R_Date("OxA-34020", 24890, 200)
{
color="green";
};
R_Date("OxA-13861", 24760, 130)
{
color="blue";
};
R_Date("OxA-34027", 24960, 200)
{
color="green";
};
R_Date("OxA-34025", 24820, 200)
{
color="green";
};
R_Date("GrA-22758", 24800, 130)
{
color="blue";
};
R_Date("OxA-34024", 24720, 200)
{
color="green";
};
R_Date("GrA-22756", 25050, 540)
{
color="blue";
};
R_Date("OxA-35241", 24700, 180)
{
color="green";
};
};
```

B.7 Code: Spread osseous points

KDE SBP points – figures 14.7 and 14.8

```
 KDE_Model("KDE - SBP points")
{
Label("Trou de la Mere Clochette, France");
R_Date("OxA-19621", 33750, 350)
{
longitude=5.571;
latitude=47.138;
color="red";
};
R_Date("OxA-19622", 35460, 250)
{
longitude=5.571;
latitude=47.138;
color="red";
};
Label("Spy, Belgium");
// originally published as 32830 +200/-190
R_Date("GrA-32619", 32830, 195)
{
longitude=4.674;
latitude=50.478;
color="red";
};
Label("Brillenhohle, Germany");
R_Date("KIA-19550", 30400, 235)
{
longitude=9.772;
latitude=48.4089;
color="red";
};
Label("Tischoferhohle, Austria");
R_Date("KIA-19544", 31530, 205)
{
longitude=12.197;
latitude=47.5924;
color="red";
};
Label("Divje babe, Slovenia");
R_Date("OxA-28219", 29760, 340)
{
longitude=13.915556;
latitude=46.112778;
color="red";
};
Label("Dzerava Skala, Slovakia");
R_Date("OxA-17963", 35600, 400)
{
longitude=17.295;
latitude=48.4922;
color="red";
};
R_Date("OxA-X-2732-14", 35560, 870)
{
longitude=17.295;
latitude=48.4922;
color="red";
};
Label("Istallosko, Hungary");
R_Date("OxA-35382", 35800, 1200)
{
longitude=20.4108;
latitude=48.0654;
color="red";
};
R_Date("OxA-35383", 36200, 900)
{
longitude=20.4108;
latitude=48.0654;
color="red";
};
R_Date("OxA-35415", 36100, 800)
{
longitude=20.4108;
latitude=48.0654;
color="red";
};
R_Date("OxA-35384", 37200, 1200)
{
longitude=20.4108;
latitude=48.0654;
color="red";
};
R_Date("OxA-35385", 37700, 1600)
{
longitude=20.4108;
latitude=48.0654;
color="red";
};
R_Date("OxA-35421", 36500, 900)
{
longitude=20.4108;
latitude=48.0654;
color="red";
};
R_Date("OxA-34771", 33450, 550)
{
longitude=20.4108;
latitude=48.0654;
color="red";
};
Label("Pesko, Hungary");
R_Date("OxA-17966", 36400, 800)
{
longitude=20.4264;
latitude=48.0468;
color="red";
};
Label("Szeleta, Hungary");
R_Date("OxA-35416", 32950, 550)
{
longitude=20.6312;
latitude=48.1186;
color="red";
};
};
```

KDE MBP points – figures 14.7 and 14.9

```
 KDE_Model("KDE - MBP")
{
Label("Uphill Quarry, England");
R_Date("OxA-13716", 31730, 250)
{
longitude=-2.9781;
latitude=51.3204;
color="blue";
};
Label("Hyaena Den, England");
R_Date("OxA-13803", 31550, 340)
{
longitude=-2.6761;
latitude=51.2263;
color="blue";
};
Label("L'Arbeda, Spain");
R_Date("OxA-21783", 32100, 450)
```

```
{
longitude=2.74401;
latitude=42.1607;
color="blue";
};
Label("Trou Al'Wesse, Belgium");
R_Date("OxA-7496", 30750, 850)
{
longitude=5.294;
latitude=50.421;
color="blue";
};
Label("Sirgenstein, Germany");
R_Date("KIA-13082", 26730, 165)
{
longitude=9.7614;
latitude=48.3842;
color="blue";
};
R_Date("KIA-13079", 27250, 175)
{
longitude=9.7614;
latitude=48.3842;
color="blue";
};
Label("Brillenhohle, Germany");
R_Date("KIA-19551", 32470, 265)
{
longitude=9.772;
latitude=48.4089;
color="blue";
};
Label("Vogelherd, Germany");
R_Date("KIA-19541", 31310, 235)
{
longitude=10.1913;
latitude=48.5603;
color="blue";
};
Label("Tischoferhohle, Austria");
R_Date("KIA-19545", 29500, 200)
{
longitude=12.197;
latitude=47.5924;
color="blue";
};
Label("Mokriška jama");
R_Date("OxA-27855", 32600, 450)
{
longitude=14.568194;
latitude=46.308806;
color="blue";
};
Label("Potocka Zijalka, Slovenia");
R_Date("OxA-27854", 30800, 370)
{
longitude=14.6691;
latitude=46.4493;
color="blue";
};
R_Combine("PZ-54")
{
longitude=14.6691;
latitude=46.4493;
color="blue";
R_Date("OxA-28038", 31950, 450)
{
color="blue";
};
R_Date("OxA-28061", 32550, 500)
{
color="blue";
};
};
R_Date("VERA-2522", 30140, 335)
{
longitude=14.6691;
latitude=46.4493;
color="blue";
};
R_Date("OxA-27850", 30380, 370)
{
longitude=14.6691;
latitude=46.4493;
color="blue";
};
R_Date("OxA-27849", 31220, 400)
{
longitude=14.6691;
latitude=46.4493;
color="blue";
};
R_Date("OxA-27852", 31360, 400)
{
longitude=14.6691;
latitude=46.4493;
color="blue";
};
R_Date("OxA-27853", 31500, 400)
{
longitude=14.6691;
latitude=46.4493;
color="blue";
};
R_Date("OxA-27851", 30910, 380)
{
longitude=14.6691;
latitude=46.4493;
color="blue";
};
Label("Bukovac, Croatia");
R_Date("OxA-X-2732-11", 31100, 520)
{
longitude=14.7527073;
latitude=45.3605642;
color="blue";
};
Label("Mamutowa, Poland");
R_Date("OxA-14436", 33640, 250)
{
longitude=19.80723;
latitude=50.16944;
color="blue";
};
R_Date("OxA-144434", 32280, 220)
{
longitude=19.80723;
latitude=50.16944;
color="blue";
};
Label("Dzerava Skala, Slovakia");
R_Combine("MBP Dz Sk")
{
longitude=17.295;
latitude=48.4922;
color="blue";
R_Date("OxA-15334", 31600, 900)
{
color="blue";
};
R_Date("OxA-15335", 31000, 1100)
{
color="blue";
};
};
R_Date("OxA-35387", 25140, 260)
{
longitude=17.295;
latitude=48.4922;
color="blue";
};
R_Date("OxA-X-2732-15", 32690, 620)
{
longitude=17.295;
latitude=48.4922;
color="blue";
};
R_Date("OxA-X-2732-16", 32770, 660)
{
longitude=17.295;
latitude=48.4922;
color="blue";
};
Label("Jankovich, Hungary");
R_Date("OxA-X-2716-49", 31800, 1000)
{
```

```
longitude=18.5753588;
latitude=47.7236726;
color="blue";
};
R_Date("OxA-X-2716-48", 32500, 800)
{
longitude=18.5753588;
latitude=47.7236726;
color="blue";
};
R_Date("OxA-X-2732-10", 32750, 670)
{
longitude=18.5753588;
latitude=47.7236726;
color="blue";
};
Label("Istallosko, Hungary");
R_Date("OxA-35414", 33450, 600)
{
longitude=20.4108;
latitude=48.0654;
color="blue";
};
R_Date("OxA-35522", 32850, 500)
{
longitude=20.4108;
latitude=48.0654;
color="blue";
};
R_Date("OxA-X-2716-11", 33200, 800)
{
longitude=20.4108;
latitude=48.0654;
color="blue";
};
Label("Pesko, Hungary");
R_Date("OxA-17964", 33500, 450)
{
longitude=20.4264;
latitude=48.0468;
color="blue";
};
Label("Tabashkata");
R_Date("OxA-35404", 27600, 400)
{
longitude=24.7;
latitude=43.14;
color="blue";
};
};
```

Map SBP and MBP – figures 14.10

```
 Plot()
{
Label("Uphill Quarry, England");
R_Date("OxA-13716", 31730, 250)
{
longitude=-2.9781;
latitude=51.3204;
color="blue";
};
Label("Hyaena Den, England");
R_Date("OxA-13803", 31550, 340)
{
longitude=-2.6761;
latitude=51.2263;
color="blue";
};
Label("Trou de la Mere Clochette, France");
R_Date("OxA-19621", 33750, 350)
{
longitude=5.571;
latitude=47.138;
color="red";
};
R_Date("OxA-19622", 35460, 250)
{
longitude=5.571;
latitude=47.138;
color="red";
};
Label("L'Arbeda, Spain");
R_Date("OxA-21783", 32100, 450)
{
longitude=2.74401;
latitude=42.1607;
color="blue";
};
Label("Spy, Belgium");
// originally published as 32830 +200/-190
R_Date("GrA-32619", 32830, 195)
{
longitude=4.674;
latitude=50.478;
color="red";
};
Label("Trou Magrite, Belgium");
Label("Trou Al'Wesse, Belgium");
R_Date("OxA-7496", 30750, 850)
{
longitude=5.294;
latitude=50.421;
color="blue";
};
Label("Sirgenstein, Germany");
R_Date("KIA-13082", 26730, 165)
{
longitude=9.7614;
latitude=48.3842;
color="blue";
};
R_Date("KIA-13079", 27250, 175)
{
longitude=9.7614;
latitude=48.3842;
color="blue";
};
Label("Brillenhohle, Germany");
R_Date("KIA-19551", 32470, 265)
{
longitude=9.772;
latitude=48.4089;
color="blue";
};
R_Date("KIA-19550", 30400, 235)
{
longitude=9.772;
latitude=48.4089;
color="red";
};
Label("Vogelherd, Germany");
R_Date("KIA-19541", 31310, 235)
{
longitude=10.1913;
latitude=48.5603;
color="blue";
};
Label("Tischoferhohle, Austria");
R_Date("KIA-19545", 29500, 200)
{
longitude=12.197;
latitude=47.5924;
color="blue";
};
R_Date("KIA-19543", 32010, 494)
{
longitude=12.197;
latitude=47.5924;
color="green";
};
R_Date("KIA-19544", 31530, 205)
{
longitude=12.197;
latitude=47.5924;
```

```
color="red";
};
Label("Divje babe, Slovenia");
R_Date("OxA-28219", 29760, 340)
{
longitude=13.915556;
latitude=46.112778;
color="red";
};
Label("Ljublansko Barje, Slovenia");
R_Date("OxA-19866", 38490, 330)
{
longitude=14.3084;
latitude=45.9717;
color="green";
};
Label("Mokriska jama, Slovenia");
R_Date("OxA-X-2517-52", 34750, 600)
{
longitude=14.568194;
latitude=46.308806;
color="green";
};
R_Date("OxA-27855", 32600, 450)
{
longitude=14.568194;
latitude=46.308806;
color="blue";
};
Label("Potocka Zijalka, Slovenia");
R_Date("OxA-27854", 30800, 370)
{
longitude=14.6691;
latitude=46.4493;
color="blue";
};
R_Combine("PZ-54")
{
longitude=14.6691;
latitude=46.4493;
color="blue";
R_Date("OxA-28038", 31950, 450)
{
color="blue";
};
R_Date("OxA-28061", 32550, 500)
{
color="blue";
};
};
R_Date("VERA-2522", 30140, 335)
{
longitude=14.6691;
latitude=46.4493;
color="blue";
};
R_Date("OxA-27850", 30380, 370)
{
longitude=14.6691;
latitude=46.4493;
color="blue";
};
R_Date("OxA-27849", 31220, 400)
{
longitude=14.6691;
latitude=46.4493;
color="blue";
};
R_Date("OxA-27852", 31360, 400)
{
longitude=14.6691;
latitude=46.4493;
color="blue";
};
R_Date("OxA-27853", 31500, 400)
{
longitude=14.6691;
latitude=46.4493;
color="blue";
};
R_Date("OxA-27851", 30910, 380)
{
longitude=14.6691;
latitude=46.4493;
color="blue";
};
Label("Bukovac, Croatia");
R_Date("OxA-X-2732-11", 31100, 520)
{
longitude=14.7527073;
latitude=45.3605642;
color="blue";
};
Label("Mamutowa, Poland");
R_Date("OxA-14436", 33640, 250)
{
longitude=19.80723;
latitude=50.16944;
color="blue";
};
R_Date("OxA-144434", 32280, 220)
{
longitude=19.80723;
latitude=50.16944;
color="blue";
};
Label("Dzerava Skala, Slovakia");
R_Date("OxA-17963", 35600, 400)
{
longitude=17.295;
latitude=48.4922;
color="red";
};
R_Combine("MBP Dz Sk 8")
{
longitude=17.295;
latitude=48.4922;
color="blue";
R_Date("OxA-15334", 31600, 900)
{
color="blue";
};
R_Date("OxA-15335", 31000, 1100)
{
color="blue";
};
};
R_Date("OxA-X-2732-13", 28340, 370)
{
longitude=17.295;
latitude=48.4922;
color="green";
};
R_Combine("Der-32")
{
longitude=17.295;
latitude=48.4922;
color="green";
R_Date("OxA-35598", 27770, 370)
{
color="green";
};
R_Date("OxA-X-2719-20", 28760, 300)
{
color="green";
};
};
R_Date("OxA-X-2732-14", 35560, 870)
{
longitude=17.295;
latitude=48.4922;
color="red";
};
R_Date("OxA-35387", 25140, 260)
{
longitude=17.295;
latitude=48.4922;
color="blue";
};
R_Date("OxA-X-2732-15", 32690, 620)
{
longitude=17.295;
latitude=48.4922;
color="blue";
};
R_Date("OxA-X-2732-16", 32770, 660)
```

```
{
longitude=17.295;
latitude=48.4922;
color="blue";
};
Label("Jankovich, Hungary");
R_Date("OxA-X-2716-49", 31800, 1000)
{
longitude=18.5753588;
latitude=47.7236726;
color="blue";
};
R_Date("OxA-X-2716-48", 32500, 800)
{
longitude=18.5753588;
latitude=47.7236726;
color="blue";
};
R_Date("OxA-X-2732-10", 32750, 670)
{
longitude=18.5753588;
latitude=47.7236726;
color="blue";
};
R_Date("OxA-35386", 30800, 500)
{
longitude=18.5753588;
latitude=47.7236726;
color="green";
};
Label("Istallosko, Hungary");
R_Date("OxA-X-2170-18", 33600, 900)
{
longitude=20.4108;
latitude=48.0654;
color="green";
};
R_Date("OxA-X-2244-32", 34890, 250)
{
longitude=20.4108;
latitude=48.0654;
color="green";
};
R_Date("OxA-35414", 33450, 600)
{
longitude=20.4108;
latitude=48.0654;
color="blue";
};
R_Date("OxA-35382", 35800, 1200)
{
longitude=20.4108;
latitude=48.0654;
color="red";
};
R_Date("OxA-35522", 32850, 500)
{
longitude=20.4108;
latitude=48.0654;
color="blue";
};
R_Date("OxA-35383", 36200, 900)
{
longitude=20.4108;
latitude=48.0654;
color="red";
};
R_Date("OxA-35415", 36100, 800)
{
longitude=20.4108;
latitude=48.0654;
color="red";
};
R_Date("OxA-X-2716-11", 33200, 800)
{
longitude=20.4108;
latitude=48.0654;
color="blue";
};
R_Date("OxA-35384", 37200, 1200)
{
longitude=20.4108;
latitude=48.0654;
color="red";
};
R_Date("OxA-35385", 37700, 1600)
{
longitude=20.4108;
latitude=48.0654;
color="red";
};
R_Date("OxA-35421", 36500, 900)
{
longitude=20.4108;
latitude=48.0654;
color="red";
};
R_Date("OxA-34771", 33450, 550)
{
longitude=20.4108;
latitude=48.0654;
color="red";
};
Label("Pesko, Hungary");
R_Date("OxA-17966", 36400, 800)
{
longitude=20.4264;
latitude=48.0468;
color="red";
};
R_Date("OxA-17964", 33500, 450)
{
longitude=20.4264;
latitude=48.0468;
color="blue";
};
R_Date("OxA-17967", 38300, 1500)
{
longitude=20.4264;
latitude=48.0468;
color="green";
};
Label("Szeleta, Hungary");
R_Date("OxA-35416", 32950, 550)
{
longitude=20.6312;
latitude=48.1186;
color="red";
};
Label("Tabashkata");
R_Date("OxA-35404", 27600, 400)
{
longitude=24.7;
latitude=43.14;
color="blue";
};
R_Date("OxA-X-2732-21", 17160, 110)
{
longitude=24.7;
latitude=43.14;
color="green";
};
R_Date("OxA-35534", 21120, 130)
{
longitude=24.7;
latitude=43.14;
color="green";
};
};
```

B.8 Code: MP/UP biocultural shift

Neanderthal vs. AMH – figure 15.2

```
 Plot()
{
C_Combine("El Sidron")
{
C_Date("El Sidron - GifA-99167",calBP(55090),2600)
{
longitude=-5.733;
latitude=43.386;
color="blue";
};
C_Date("El Sidron - GifA-99704",calBP(54930),2500)
{
color="blue";
longitude=-5.733;
latitude=43.386;
};
C_Date("El Sidron - OxA-21776",calBP(56230),3200)
{
longitude=-5.733;
latitude=43.386;
color="blue";
};
longitude=-5.733;
latitude=43.386;
color="blue";
};
R_Date("Paviland - OxA-16412",28870,180)
{
longitude=-4.2555;
latitude=51.5499;
color="red";
};
R_Date("Paviland - OxA-16413",29490,210)
{
longitude=-4.2555;
latitude=51.5499;
color="red";
};
Date("Les Rochers-de-Villeneuve - OxA-15257",
N(calBP(48900),1100))
{
longitude=0.741;
latitude=46.415;
color="blue";
};
R_Date("La Crouzade - ERL-9415",30640,640)
{
longitude=3.0905;
latitude=43.1313;
color="red";
};
R_Date("Spy - OxA-10560",36250,500)
{
longitude=4.6743;
latitude=50.4803;
color="blue";
};
R_Date("Spy - GrA-32623",35810,250)
{
longitude=4.6743;
latitude=50.4803;
color="blue";
};
R_Date("Spy - GrA-32626",36350,295)
{
longitude=4.6743;
latitude=50.4803;
color="blue";
};
R_Combine("Feldhöfergrotte Inv. 1")
{
R_Date("Kleine Feldhöfergrotte - ETH-20981",39900,620)
{
longitude=6.9363;
latitude=51.2206;
color="blue";
};
R_Date("Kleine Feldhöfergrotte - ETH-19661",40360,760)
{
longitude=6.9363;
latitude=51.2206;
color="blue";
};
longitude=6.9363;
latitude=51.2206;
color="blue";
};
R_Date("Kleine Feldhöfergrotte - ETH-19660",39240,670)
{
longitude=6.9363;
latitude=51.2206;
color="blue";
};
R_Date("Vindija - OxA-X-2689-09",42700,1600)
{
longitude=16.088;
latitude=46.305;
color="blue";
};
Date("Vindija - OxA-X-2689-10",N(calBP(48800),2000))
{
longitude=16.088;
latitude=46.305;
color="blue";
};
R_Date("Vindija - OxA-X-2717-11",44300,1200)
{
longitude=16.088;
latitude=46.305;
color="blue";
};
Date("Vindija - OxA-X-2687-57",N(calBP(49960),1500))
{
longitude=16.088;
latitude=46.305;
color="blue";
};
R_Date("Mladec - VERA-3073",31190,400)
{
longitude=17.0167;
latitude=49.707;
color="red";
};
R_Date("Mladec - VERA-3074",31320,400)
{
longitude=17.0167;
latitude=49.707;
color="red";
};
R_Date("Mladec - VERA-3076 A",31500,410)
{
longitude=17.0167;
latitude=49.707;
color="red";
};
R_Date("Oblazowa - OxA-4586",31000,500)
{
longitude=20.1563;
latitude=49.443;
color="red";
};
R_Date("Pestera cu Oase - OxA-11711",34950,990)
{
longitude=21.91;
latitude=45.0177;
color="red";
};
R_Date("Pestera cu Oase - GrA-24398",28890,170)
```

```
{
longitude=21.91;
latitude=45.0177;
color="red";
};
R_Date("Cioclovina - LuA-5229",29000,700)
{
longitude=23.1296;
latitude=45.5862;
color="red";
};
R_Date("Cioclovina - OxA-15527",28150,170)
{
longitude=23.1296;
latitude=45.5862;
color="red";
};
R_Date("Pestera Muierii - OxA-15529",29930,170)
{
longitude=23.755;
latitude=45.1895;
color="red";
};
R_Date("Pestera Muierii - OxA-16252",29110,190)
{
longitude=23.755;
latitude=45.1895;
color="red";
};
R_Date("Buran-Kaya III - OxA-13302",32790,280)
{
longitude=34.396;
latitude=45.16;
color="red";
};
R_Date("Buran-Kaya III - GrA-50457",32450,240)
{
longitude=34.396;
latitude=45.16;
color="red";
};
R_Date("Buran-Kaya III - GrA-37938",31900,230)
{
longitude=34.396;
latitude=45.16;
color="red";
};
R_Date("Kostenki I - OxA-15055",32070,190)
{
longitude=39.0488;
latitude=51.4036;
color="red";
};
R_Date("Mezmaiskaya - OxA-21839",39700,1100)
{
longitude=40.0034;
latitude=44.2217;
color="blue";
};
R_Combine("Ust'-Ishim")
{
R_Date("Ust-Ishim - OxA-25516",41400,1300)
{
longitude=68.86;
latitude=57.701;
color="red";
};
R_Date("Ust-Ishim - OxA-30190",41400,1400)
{
longitude=68.86;
latitude=57.701;
color="red";
};
longitude=68.86;
latitude=57.701;
color="red";
};
R_Date("Pokrovka - OxA-19850",27740,150)
{
longitude=92.469;
latitude=55.3295;
color="red";
};
};
```

KDE Neanderthal – figure 15.3

```
 KDE_Model("KDE - Neanderthals")
{
C_Combine("El Sidron")
{
C_Date("El Sidron - GifA-99167",calBP(55090),2600)
{
longitude=-5.733;
latitude=43.386;
color="blue";
};
C_Date("El Sidron - GifA-99704",calBP(54930),2500)
{
color="blue";
longitude=-5.733;
latitude=43.386;
};
C_Date("El Sidron - OxA-21776",calBP(56230),3200)
{
longitude=-5.733;
latitude=43.386;
color="blue";
};
longitude=-5.733;
latitude=43.386;
color="blue";
};
Date("Les Rochers-de-Villeneuve - OxA-15257",
N(calBP(48900),1100))
{
longitude=0.741;
latitude=46.415;
color="blue";
};
R_Date("Spy - OxA-10560",36250,500)
{
longitude=4.6743;
latitude=50.4803;
color="blue";
};
R_Date("Spy - GrA-32623",35810,250)
{
longitude=4.6743;
latitude=50.4803;
color="blue";
};
R_Date("Spy - GrA-32626",36350,295)
{
longitude=4.6743;
latitude=50.4803;
color="blue";
};
R_Combine("Feldhöfergrotte Inv. 1")
{
R_Date("Kleine Feldhöfergrotte - ETH-20981",39900,620)
{
longitude=6.9363;
latitude=51.2206;
color="blue";
};
R_Date("Kleine Feldhöfergrotte - ETH-19661",40360,760)
{
longitude=6.9363;
latitude=51.2206;
color="blue";
};
longitude=6.9363;
latitude=51.2206;
color="blue";
```

```
};
R_Date("Kleine Feldhöfergrotte - ETH-19660",39240,670)
{
longitude=6.9363;
latitude=51.2206;
color="blue";
};
R_Date("Vindija - OxA-X-2689-09",42700,1600)
{
longitude=16.088;
latitude=46.305;
color="blue";
};
Date("Vindija - OxA-X-2689-10",N(calBP(48800),2000))
{
longitude=16.088;
latitude=46.305;
color="blue";
};
R_Date("Vindija - OxA-X-2717-11",44300,1200)
{
longitude=16.088;
latitude=46.305;
color="blue";
};
Date("Vindija - OxA-X-2687-57",N(calBP(49960),1500))
{
longitude=16.088;
latitude=46.305;
color="blue";
};
R_Date("Mezmaiskaya - OxA-21839",39700,1100)
{
longitude=40.0034;
latitude=44.2217;
color="blue";
};
};
```

KDE AMH – figure 15.3

```
 KDE_Model("KDE - AMH")
{
R_Date("Paviland - OxA-16412",28870,180)
{
longitude=-4.2555;
latitude=51.5499;
color="red";
};
R_Date("Paviland - OxA-16413",29490,210)
{
longitude=-4.2555;
latitude=51.5499;
color="red";
};
R_Date("La Crouzade - ERL-9415",30640,640)
{
longitude=3.0905;
latitude=43.1313;
color="red";
};
R_Date("Mladec - VERA-3073",31190,400)
{
longitude=17.0167;
latitude=49.707;
color="red";
};
R_Date("Mladec - VERA-3074",31320,400)
{
longitude=17.0167;
latitude=49.707;
color="red";
};
R_Date("Mladec - VERA-3076 A",31500,410)
{
longitude=17.0167;
latitude=49.707;
color="red";
};
R_Date("Oblazowa - OxA-4586",31000,500)
{
longitude=20.1563;
latitude=49.443;
color="red";
};
R_Date("Pestera cu Oase - OxA-11711",34950,990)
{
longitude=21.91;
latitude=45.0177;
color="red";
};
R_Date("Pestera cu Oase - GrA-24398",28890,170)
{
longitude=21.91;
latitude=45.0177;
color="red";
};
R_Date("Cioclovina - LuA-5229",29000,700)
{
longitude=23.1296;
latitude=45.5862;
color="red";
};
R_Date("Cioclovina - OxA-15527",28150,170)
{
longitude=23.1296;
latitude=45.5862;
color="red";
};
R_Date("Pestera Muierii - OxA-15529",29930,170)
{
longitude=23.755;
latitude=45.1895;
color="red";
};
R_Date("Pestera Muierii - OxA-16252",29110,190)
{
longitude=23.755;
latitude=45.1895;
color="red";
};
R_Date("Buran-Kaya III - OxA-13302",32790,280)
{
longitude=34.396;
latitude=45.16;
color="red";
};
R_Date("Buran-Kaya III - GrA-50457",32450,240)
{
longitude=34.396;
latitude=45.16;
color="red";
};
R_Date("Buran-Kaya III - GrA-37938",31900,230)
{
longitude=34.396;
latitude=45.16;
color="red";
};
R_Date("Kostenki I - OxA-15055",32070,190)
{
longitude=39.0488;
latitude=51.4036;
color="red";
};
R_Combine("Ust'-Ishim")
{
R_Date("Ust-Ishim - OxA-25516",41400,1300)
{
longitude=68.86;
latitude=57.701;
color="red";
};
R_Date("Ust-Ishim - OxA-30190",41400,1400)
{
```

```
longitude=68.86;
latitude=57.701;
color="red";
};
longitude=68.86;
latitude=57.701;
color="red";
};
```

```
R_Date("Pokrovka - OxA-19850",27740,150)
{
longitude=92.469;
latitude=55.3295;
color="red";
};
};
```

El Castillo (Stratigraphy) – figure D.39

```
 Plot()
{
Outlier_Model("General",T(5),U(0,4),"t");
Sequence("El Castillo - after Wood et al. 2018")
{
Boundary("Start 20C");
Phase("20C")
{
Date("OxA-22204",N(calBP(56640),3400))
{
Outlier(0.05);
};
Date("OxA-22205",N(calBP(57270),3700))
{
Outlier(0.05);
};
R_Date("GifA-89144", 39300, 1900)
{
color="red";
Outlier(0.05);
};
Date("GifA-92506",N(calBP(49360),2900))
{
color="red";
Outlier(0.05);
};
Interval("20C length");
Date("Date Mousterian");
};
Boundary("20C/19");
Phase("19")
{
Date("OxA-21974",N(calBP(49680),2100))
{
Outlier(0.05);
};
Interval("19 length");
Date("Date sterile 1");
};
Boundary("19/18C");
Phase("18C")
{
R_Date("OxA-22403", 42700, 1600)
{
Outlier(0.05);
};
R_Date("OxA-22202", 43100, 1700)
{
Outlier(0.05);
};
R_Date("OxA-22203", 42000, 1500)
{
Outlier(0.05);
};
R_Date("GifA-89147", 39500, 2000)
{
color="red";
Outlier(0.05);
};
R_Date("OxA-2478", 39800, 1400)
{
color="red";
Outlier(0.05);
};
R_Date("AA-2405", 40000, 2100)
{
color="red";
Outlier(0.05);
};
R_Date("OxA-2476", 40700, 1500)
{
color="red";
Outlier(0.05);
};
R_Date("OxA-2477", 41100, 1700)
{
color="red";
Outlier(0.05);
};
Date("Date Transitional Aurignacian 18C");
};
Boundary("18C/18B");
Phase("18B")
{
Date("OxA-21973",N(calBP(50740),2400))
{
Outlier(0.05);
};
Date("OxA-21972",N(calBP(50500),2300))
{
Outlier(0.05);
};
R_Date("AA-2406", 38500, 1800)
{
color="red";
Outlier(0.05);
};
R_Date("OxA-2473", 37100, 2200)
{
color="red";
Outlier(0.05);
};
R_Date("AA-2407", 37700, 1800)
{
color="red";
Outlier(0.05);
};
R_Date("OxA-2474", 38500, 1300)
{
color="red";
Outlier(0.05);
};
R_Date("OxA-2475", 40700, 1600)
{
color="red";
Outlier(0.05);
};
Interval("18 length");
Date("Date Transitional Aurignacian 18B");
};
Boundary("18B/17-16");
Phase("17-16")
{
R_Date("OxA-22200", 38600, 1000)
{
Outlier(0.05);
};
R_Date("OxA-22201", 39100, 1000)
{
Outlier(0.05);
};
R_Date("GifA95539", 34300, 1000)
{
color="red";
Outlier(0.05);
};
```

```
Interval("17-16 length");
Date("Date sterile 2");
};
Boundary("End 17-16");
};
};
```

El Castillo (KDE) – figure D.53

```
 Plot()
{
KDE_Model("KDE - El Castillo",N(0,1), U(0,1),)
{
R_Date("OxA-22202",43100,1700);
R_Date("OxA-22403",42700,1600);
R_Date("OxA-22203",42000,1500);
R_Date("OxA-2477",41100,1700);
R_Date("OxA-2476",40700,1500);
R_Date("OxA-2475",40700,1600);
R_Date("AA-2405",40000,2100);
R_Date("OxA-2478",39800,1400);
R_Date("GifA-89147",39500,2000);
R_Date("AA-2406",38500,1800);
R_Date("OxA-2474",38500,1300);
R_Date("AA-2407",37700,1800);
R_Date("OxA-2473",37100,2200);
};
};
```

Labeka Koba (Stratigraphy) – figure D.43

```
 Plot()
{
Outlier_Model("General",T(5),U(0,4),"t");
Outlier_Model("SSimple",N(0,2),0,"s");
Sequence("Labeko Koba")
{
Boundary("Start IX");
Phase("Level IX lower - Pre-Chatelperronian")
{
R_Date("OxA-22564",37900,900)
{
Outlier("General", 0.05);
};
Date("Date IX lower (pre)");
};
Boundary("below/Chatelperronian points");
Phase("Level IX lower - Chatelperronian")
{
R_Date("OxA-22562",38100,900)
{
Outlier("General", 0.05);
};
R_Date("OxA-22561",38000,900)
{
Outlier("General", 0.05);
};
R_Date("OxA-22563",37800,900)
{
Outlier("General", 0.05);
};
R_Date("OxA-22560",37400,800)
{
Outlier("General", 0.05);
};
Date("Date Chatelperronian");
};
Boundary("IX lower/IX upper");
Phase("Level IX upper - n/a")
{
R_Date("OxA-23199",38400,900)
{
Outlier("General", 0.05);
};
R_Date("OxA-21777",37700,900)
{
Outlier("General", 0.05);
};
R_Combine("LAB-22")
{
Outlier("General", 0.05);
R_Date("OxA-22559",36000,700)
{
Outlier("SSimple", 0.05);
};
R_Date("OxA-22653",36850,800)
{
Outlier("SSimple", 0.05);
};
};
R_Date("OxA-21792",36550,750)
{
Outlier("General", 0.05);
};
Date("Date IX upper");
};
Boundary("IX upper/VII");
Phase("Level VII - Proto-Aurignacian")
{
R_Date("OxA-21766",36850,800)
{
Outlier("General", 0.05);
};
R_Date("OxA-X-2314-43",36500,750)
{
Outlier("General", 0.05);
};
R_Combine("LAB-6")
{
Outlier("General", 0.05);
R_Date("OxA-21793",35400,650)
{
Outlier("SSimple", 0.05);
};
R_Date("OxA-21840",35250,650)
{
Outlier("SSimple", 0.05);
};
};
Date("Date Proto-Aurignacian");
};
Boundary("VII/VI");
Phase("Level VI - Early Aurignacian")
{
R_Date("OxA-21778",35100,600)
{
Outlier("General", 0.05);
};
R_Combine("LAB-19")
{
Outlier("General", 0.05);
R_Date("OxA-21794",34750,600)
{
Outlier("SSimple", 0.05);
};
R_Date("OxA-21841",32150,450)
{
Outlier("SSimple", 0.05);
};
};
Date("Date Early Aurignacian - VI");
```

```
};
Boundary("VI/V");
Phase("Level V - Early Aurignacian")
{
R_Date("OxA-21767",34750,600)
{
Outlier("General", 0.05);
};
R_Date("OxA-21779",34650,600)
{
Outlier("General", 0.05);
};
Date("Date Early Aurignacian - V");
};
Boundary("V/IV");
Phase("Level IV - Early Aurignacian")
{
R_Date("OxA-21768",33600,500)
{
Outlier("General", 0.05);
};
R_Date("OxA-21780",33550,550)
{
Outlier("General", 0.05);
};
Date("Date Early Aurignacian - IV");
};
Boundary("End IV");
};
};
```

Labeka Koba (KDE) – figure D.55

```
 Plot()
{
KDE_Model("KDE - Labeko Koba",N(0,1), U(0,1),)
{
R_Date("OxA-21766",36850,800);
R_Date("OxA-X-2314-43",36500,750);
R_Date("OxA-21840",35250,650);
R_Combine("LAB-6")
{
R_Date("OxA-21793",35400,650);
R_Date("OxA-21840",35250,650);
};
R_Date("OxA-21778",35100,600);
R_Combine("LAB-19")
{
R_Date("OxA-21794",34750,600);
R_Date("OxA-21841",32150,450);
};
R_Date("OxA-21767",34750,600);
R_Date("OxA-21779",34650,600);
R_Date("OxA-21780",33550,550);
R_Date("OxA-21768",33600,500);
};
};
```

Isturitz (Stratigraphy) – figure D.45

```
 Plot()
{
Outlier_Model("General",T(5),U(0,4),"t");
Outlier_Model("SSimple",N(0,2),0,"s");
Sequence("Isturitz")
{
Boundary("Start C5");
Phase("C 5")
{
Date("OxA-X-2695-11",N(calBP(48650),2400))
{
Outlier("General", 0.05);
};
R_Date("OxA-X-2694-17",38900,1000)
{
Outlier("General", 0.05);
};
Date("Date Proto-Aurignacian C5");
};
Boundary("C5/C4d1");
Phase("C 4d1")
{
R_Date("AA-69187",40000,2800)
{
Outlier("General", 0.05);
};
R_Date("OxA-23435",37500,900)
{
Outlier("General", 0.05);
};
R_Date("OxA-23436",37400,900)
{
Outlier("General", 0.05);
};
R_Combine("Sample 365")
{
Outlier("General", 0.05);
R_Date("OxA-23432",37000,800)
{
Outlier("SSimple", 0.05);
};
R_Date("OxA-23433",37000,800)
{
Outlier("SSimple", 0.05);
};
};
R_Date("OxA-23434",37000,800)
{
Outlier("General", 0.05);
};
Date("Date Proto-Aurignacian C4d1");
};
Boundary("C4d1/C4c4");
Phase("C 4c4")
{
Date("AA-69184",N(calBP(47820),3600))
{
Outlier("General", 0.05);
};
R_Date("AA-69183",37580,780)
{
Outlier("General", 0.05);
};
R_Date("AA-69180",37300,1800)
{
Outlier("General", 0.05);
};
R_Date("AA-69179",37000,1600)
{
Outlier("General", 0.05);
};
R_Date("AA-69185",36990,720)
{
Outlier("General", 0.05);
};
R_Date("AA-69181",36800,860)
{
Outlier("General", 0.05);
};
Date("Date Proto-/Early Aurignacian C4c4");
};
Boundary("C4c4/C4b2");
```

```
Phase("C 4b2")
{
R_Date("OxA-X-2698-50",35150,650)
{
Outlier("General", 0.05);
};
R_Date("OxA-34636",35050,650)
{
Outlier("General", 0.05);
};
R_Date("OxA-34773",34950,600)
{
Outlier("General", 0.05);
};
R_Date("OxA-34637",34850,600)
{
Outlier("General", 0.05);
};
Date("Date Early Aurignacian C4b2");
};
Boundary("C4b2/C4b1");
Phase("C 4b1")
{
R_Date("OxA-34635",35250,650)
{
Outlier("General", 0.05);
};
R_Date("OxA-34633",35250,650)
{
Outlier("General", 0.05);
};
R_Date("OxA-34772",34950,600)
{
Outlier("General", 0.05);
};
R_Date("OxA-34634",34700,600)
{
Outlier("General", 0.05);
};
Date("Date Early Aurignacian C4b1");
};
Boundary("End C4b1");
};
};
```

Isturitz (KDE) – figure D.56

```
 Plot()
{
KDE_Model("KDE - Isturitz",N(0,1), U(0,1),)
{
R_Date("AA-69179",37000,1600);
R_Date("AA-69180",37300,1800);
R_Date("AA-69181",36800,860);
R_Date("AA-69183",37580,780);
Date("AA-69184",N(calBP(47820),3600));
R_Date("AA-69185",36990,720);
R_Date("OxA-34634",34700,600);
R_Date("OxA-34772",34950,600);
R_Date("OxA-34633",35250,650);
R_Date("OxA-34635",35250,650);
R_Date("OxA-34773",34950,600);
R_Date("OxA-34636",35050,650);
R_Date("OxA-X-2698-50",35150,650);
R_Date("OxA-23432",37000,800);
R_Date("OxA-23433",37000,800);
R_Date("OxA-23434",37000,800);
R_Date("OxA-23436",37400,900);
R_Date("OxA-23435",37500,900);
R_Date("AA-69187",40000,2800);
Date("OxA-X-2695-11",N(calBP(48650),2400));
};
};
```

L'Arbreda (Stratigraphy) – figure D.42

```
 Plot()
{
Outlier_Model("General",T(5),U(0,4),"t");
Outlier_Model("SSimple",N(0,2),0,"s");
Sequence("L'Arbreda")
{
Boundary("Start I");
Phase("Level I - Mousterian")
{
R_Date("OxA-21704",39200,1000)
{
Outlier("General", 0.05);
};
R_Date("OxA-21702",39200,1000)
{
Outlier("General", 0.05);
};
R_Date("OxA-19994",38350,400)
{
Outlier("General", 0.05);
};
R_Date("OxA-21662",37300,800)
{
Outlier("General", 0.05);
};
R_Combine("ABD 15")
{
Outlier("General", 0.05);
R_Date("OxA-21703",32300,450)
{
Outlier("SSimple", 0.05);
};
R_Date("OxA-21663",32100,450)
{
Outlier("SSimple", 0.05);
};
};
Date("Date Mousterian");
};
Boundary("End I");
Boundary("start H");
Phase("Level H - Proto-Aurignacian")
{
R_Date("OxA-21784",36000,700)
{
Outlier("General", 0.05);
};
R_Date("OxA-21664",35900,650)
{
Outlier("General", 0.05);
};
R_Date("OxA-21665",35850,700)
{
Outlier("General", 0.05);
};
R_Combine("ABD 12")
{
Outlier("General", 0.05);
R_Date("SANU-29017",34800,760)
{
Outlier("SSimple", 0.05);
};
R_Date("SANU-29019",35900,860)
{
Outlier("SSimple", 0.05);
};
```

```
};
R_Date("OxA-21674",33800,550)
{
Outlier("General", 0.05);
};
R_Date("SANU-29016",35700,830)
{
Outlier("General", 0.05);
};
R_Date("SANU-29018",32100,540)
{
Outlier("General", 0.05);
};
R_Date("SANU-29014",31900,530)
{
Outlier("General", 0.05);
};
Date("Date Proto-Aurignacian");
};
Boundary("End H");
Boundary("Start G");
Phase("Level G - Evolved Aurignacian")
{
R_Date("OxA-21666",32750,450)
{
Outlier("General", 0.05);
};
R_Date("OxA-21667",32250,450)
{
Outlier("General", 0.05);
};
R_Date("OxA-21783",32100,450)
{
Outlier("General", 0.05);
};
Date("Date Evolved Aurignacian");
};
Boundary("End G");
Boundary("Start F");
Phase("Level F - Gravettian")
{
R_Date("OxA-21782",28280,290)
{
Outlier("General", 0.05);
};
R_Date("OxA-21781",28260,280)
{
Outlier("General", 0.05);
};
Date("Date Gravettian - F");
};
Boundary("End F");
Boundary("Start E");
Phase("Level E - Gravettian")
{
R_Date("OxA-21668",26100,210)
{
Outlier("General", 0.05);
};
R_Date("OxA-21669",25780,210)
{
Outlier("General", 0.05);
};
Date("Date Gravettian - E");
};
Boundary("End E");
};
};
```

L'Arbreda (KDE) – figure D.54

```
 Plot()
{
KDE_Model("KDE - L'Arbreda",N(0,1), U(0,1),)
{
R_Date("OxA-21669",25780,210);
R_Date("OxA-21668",26100,210);
R_Date("OxA-21667",32250,450);
R_Date("OxA-21783",32100,450);
R_Date("OxA-21666",32750,450);
R_Date("SANU-29018",32100,540);
R_Date("SANU-29017",34800,760);
R_Date("SANU-29019",35900,860);
R_Date("SANU-29016",35700,830);
R_Date("SANU-29014",31900,530);
R_Date("OxA-21674",33800,550);
R_Date("OxA-21665",35850,700);
R_Date("OxA-21784",36000,700);
R_Date("OxA-21664",35900,650);
};
};
```

Riparo Mochi (Stratigraphy) – figure D.44

```
 Plot()
{
Outlier_Model("General",T(5),U(0,4),"t");
Sequence("Riparo Mochi")
{
Boundary("start Proto-Aurignacian");
Phase("Unit G - Proto-Aurignacian")
{
Phase("charcoals")
{
Curve("IntCal13","IntCal13.14c");
R_Date("Rome-2",37400,1300)
{
Outlier("General", 0.05);
};
R_Date("OxA-19569",36350,260)
{
Outlier("General", 0.05);
};
R_Date("OxA-3591",35700,850)
{
Outlier("General", 0.05);
};
R_Date("OxA-3592",34870,800)
{
Outlier("General", 0.05);
};
R_Date("OxA-3590",34680,760)
{
Outlier("General", 0.05);
};
R_Date("OxA-3589",33400,750)
{
Outlier("General", 0.05);
};
R_Date("OxA-3588",32280,580)
{
Outlier("General", 0.05);
};
};
Phase("shells")
{
Curve("Marine13","Marine13.14c");
Delta_R("LocalMarine",40,15);
R_Date("OxA-19290",36750,260)
{
Outlier("General", 0.05);
};
```

```
R_Date("OxA-20630",33180,230)
{
Outlier("General", 0.05);
};
R_Date("OxA-20360",31960,150)
{
Outlier("General", 0.05);
};
R_Date("OxA-19802",30770,150)
{
Outlier("General", 0.05);
};
};
Date("Date Proto-Aurignacian");
};
Boundary("Proto-Aurignacian/Early Aurignacian");
Phase("Unit F - Early Aurignacian")
{
Phase("charcoal")
{
Curve("IntCal13","IntCal13.14c");
R_Date("Rome-1",27230,570)
{
Outlier("General", 0.05);
};
};
Phase("shells")
{
Curve("Marine13","Marine13.14c");
Delta_R("LocalMarine",40,15);
R_Date("OxA-20629",32910,220)
{
Outlier("General", 0.05);
};
R_Date("OxA-19614",32370,160)
{
Outlier("General", 0.05);
};
R_Date("OxA-19728",26410,110)
{
Outlier("General", 0.05);
};
R_Date("OxA-19857",26030,110)
{
Outlier("General", 0.05);
};
};
Date("Date Early Aurignacian");
};
Boundary("end Early Aurignacian");
Phase("Unit E - none")
{
Phase("shell")
{
Curve("Marine13","Marine13.14c");
Delta_R("LocalMarine",40,15);
R_Date("OxA-19801",25490,110)
{
Outlier("General", 0.05);
};
};
Date("Date sterile");
};
Boundary("start Gravettian");
Phase("Unit D - Gravettian")
{
Phase("shell")
{
Curve("Marine13","Marine13.14c");
Delta_R("LocalMarine",40,15);
R_Date("OxA-19800",24600,100)
{
Outlier("General", 0.05);
};
};
Date("Date Gravettian");
};
Boundary("end Gravettian unit D");
};
};
```

Riparo Mochi (KDE) – figure D.55

```
 Plot()
{
KDE_Model("KDE - Riparo Mochi",N(0,1), U(0,1),)
{
Phase("shells")
{
Curve("Marine13","Marine13.14c");
Delta_R("LocalMarine",040,15);
R_Date("OxA-19800",24600,100);
R_Date("OxA-19857",26030,110);
R_Date("OxA-19728",26410,110);
R_Date("OxA-20629",32910,220);
R_Date("OxA-19614",32370,160);
R_Date("OxA-20360",31960,150);
R_Date("OxA-19802",30770,150);
R_Date("OxA-20630",33180,230);
R_Date("OxA-19290",36750,260);
};
Phase("charcoals")
{
Curve("IntCal13","IntCal13.14c");
R_Date("Rome-1",27230,570);
R_Date("OxA-3588",32280,580);
R_Date("OxA-3589",33400,750);
R_Date("OxA-3590",34680,760);
R_Date("OxA-3591",35700,850);
R_Date("OxA-3592",34870,800);
R_Date("Rome-2",37400,1300);
};
};
};
```

Hohle Fels (Stratigraphy) – figure 15.8

```
 Plot()
{
Outlier_Model("General",T(5),U(0,4),"t");
Sequence("Hohle Fels")
{
Boundary("start sequence");
Phase("IX")
{
R_Date("KIA-32053",38560,514)
{
Outlier("General", 0.05);
};
Date("Date IX - Mousterian");
};
Boundary("transition IX - VIII");
Phase("VIII")
{
R_Date("KIA-32052",39580,580)
{
Outlier("General", 0.05);
};
Date("Date VIII - Mousterian");
};
Boundary("transition VIII - VII");
```

```
Phase("VII")
{
R_Date("KIA-32054",37940,514)
{
Outlier("General", 0.05);
};
R_Date("KIA-19563",36350,524)
{
Outlier("General", 0.05);
};
Date("Date VII - Mousterian");
};
Boundary("transition VII - VI");
Phase("VI")
{
R_Date("KIA-19562",36380,370)
{
Outlier("General", 0.05);
};
R_Date("KIA-19564",35760,635)
{
Outlier("General", 0.05);
};
Date("Date VI - Mousterian");
};
Boundary("transition MP - Aurig.");
Phase("V")
{
R_Date("KIA-16034",35710,350)
{
Outlier("General", 0.05);
};
R_Date("KIA-18880",34190,335)
{
Outlier("General", 0.05);
};
R_Date("KIA-16035",33290,270)
{
Outlier("General", 0.05);
};
R_Date("KIA-35459",32550,295)
{
Outlier("General", 0.05);
};
R_Date("KIA-35462",32090,345)
{
Outlier("General", 0.05);
};
R_Date("KIA-35463",32030,275)
{
Outlier("General", 0.05);
};
R_Date("KIA-35464",31750,260)
{
Outlier("General", 0.05);
};
Date("Date V - Aurignacian");
};
Boundary("transition V - IV");
Phase("IV")
{
R_Date("KIA-16036",33090,255)
{
Outlier("General", 0.05);
};
R_Date("KIA-16037",32470,285)
{
Outlier("General", 0.05);
};
R_Date("OxA-4980",28750,750)
{
Outlier("General", 0.05);
};
Date("Date IV - Aurignacian");
};
Boundary("transition IV - III");
Phase("III")
{
R_Date("KIA-16039",31140,245)
{
Outlier("General", 0.05);
};
R_Date("KIA-18876",31010,580)
{
Outlier("General", 0.05);
};
R_Date("KIA-32055",30340,285)
{
Outlier("General", 0.05);
};
R_Date("KIA-18877",30170,245)
{
Outlier("General", 0.05);
};
R_Date("KIA-3505",29990,335)
{
Outlier("General", 0.05);
};
R_Date("KIA-16038",29840,210)
{
Outlier("General", 0.05);
};
R_Date("KIA-18878",29780,320)
{
Outlier("General", 0.05);
};
R_Date("KIA-32056",29710,246)
{
Outlier("General", 0.05);
};
R_Date("OxA-4979",27600,800)
{
Outlier("General", 0.05);
};
Date("Date III - Aurignacian");
};
Boundary("transition III - II");
Phase("II")
{
R_Date("KIA-16040",30640,190)
{
Outlier("General", 0.05);
};
R_Date("OxA-5007",29550,650)
{
Outlier("General", 0.05);
};
R_Date("KIA-17744",27780,150)
{
Outlier("General", 0.05);
};
R_Date("KIA-17742",27690,140)
{
Outlier("General", 0.05);
};
Date("Date II - Aurignacian");
};
Boundary("end sequence");
};
};
```

Hohle Fels (KDE) – figure D.50

```
 KDE_Model("KDE - Hohle Fels",N(0,1), U(0,1),)
{
R_Date("OxA-5007",29550,650);
R_Date("KIA-17742",27690,140);
R_Date("KIA-17744",27780,150);
R_Date("KIA-16040",30640,190);
R_Date("OxA-4979",27600,800);
R_Date("KIA-32056",29710,246);
R_Date("KIA-32055",30340,285);
R_Date("KIA-16038",29840,210);
R_Date("KIA-18877",30170,245);
R_Date("KIA-18876",31010,580);
```

```
R_Date("KIA-16039",31140,245);
R_Date("KIA-18878",29780,320);
R_Date("KIA-3505",29990,335);
R_Date("OxA-4980",28750,750);
R_Date("KIA-16037",32470,285);
R_Date("KIA-16036",33090,255);
R_Date("KIA-35464",31750,260);
R_Date("KIA-35463",32030,275);
R_Date("KIA-35462",32090,345);
R_Date("KIA-35459",32550,295);
R_Date("KIA-16035",33290,270);
R_Date("KIA-18880",34190,335);
R_Date("KIA-16034",35710,350);
};
```

Geißenklösterle (Stratigraphy) – figure D.35

```
 Plot()
{
Outlier_Model("General",T(5),U(0,4),"t");
Sequence("Geissenklosterle")
{
Boundary("Transition V/IV");
Phase("IV")
{
R_Date("OxA-21720", 35500, 650)
{
Outlier(0.05);
};
Age("ESR mean", N( 42700, 1300))
{
color="red";
Outlier(0.05);
};
Date("Date MP - IV");
};
Boundary("Transition IV/Sterile");
Phase("Sterile")
{
R_Date("OxA-21657", 39400, 1100)
{
Outlier(0.05);
};
R_Date("OxA-21658", 38300, 900)
{
Outlier(0.05);
};
Date("Date sterile");
};
Boundary("Transition Sterile/IIIc");
Phase("III")
{
R_Date("OxA-21723", 37800, 900)
{
Outlier(1.00);
};
R_Date("OxA-21659**", 35050, 600)
{
Outlier(0.05);
};
R_Date("OxA-21721**", 37300, 800)
{
Outlier(0.05);
};
R_Date("OxA-21743**", 36100, 700)
{
Outlier(0.05);
};
R_Date("OxA-21722", 38900, 1000)
{
Outlier(1.00);
};
R_Date("OxA-21745", 36650, 750)
{
Outlier(1.00);
};
R_Date("OxA-21746**", 36850, 800)
{
Outlier(0.05);
};
R_Date("OxA-21725", 37400, 800)
{
Outlier(1.00);
};
R_Date("OxA-21744", 36850, 750)
{
Outlier(1.00);
};
R_Date("OxA-21726**", 34200, 550)
{
Outlier(0.05);
};
Age("TL mean", N( 40200, 1500))
{
color="red";
Outlier(0.05);
};
Interval("Interval AHIII");
Date("Date Early Aurignacian -  III");
};
Boundary("Transition III/II");
Phase("II")
{
R_Date("OxA-21742", 34800, 600)
{
Outlier(1.00);
};
R_Date("OxA-21727**", 34100, 550)
{
Outlier(0.05);
};
R_Date("OxA-21724**", 33950, 550)
{
Outlier(0.05);
};
R_Date("OxA-21737", 35700, 650)
{
Outlier(1.00);
};
R_Date("OxA-21738**", 34900, 600)
{
Outlier(0.05);
};
R_Date("OxA-21656", 33000, 500)
{
Outlier(1.00);
};
Interval("Interval AHII");
Date("Date Aurignacian - II");
};
Boundary("End Aurignacian");
Phase("Gravettian")
{
R_Date("OxA-21661", 32900, 450)
{
Outlier(0.05);
};
R_Date("OxA-21739", 28600, 290)
{
Outlier(0.05);
};
R_Date("OxA-21660", 27960, 290)
{
Outlier(0.05);
};
R_Date("OxA-21740", 26420, 230)
{
Outlier(0.05);
};
Date("Date Gravettian - I");
};
Boundary("End");
Axis(-52923.5, -26574.5);
};
};
```

Geißenklösterle (KDE) – figure D.49

```
 Plot()
{
KDE_Model("KDE - Geissenklosterle",N(0,1), U(0,1),)
{
R_Date("OxA-21660",27960,290);
R_Date("OxA-21661",32900,450);
R_Date("OxA-21740",26420,230);
R_Date("OxA-21739",28600,290);
R_Date("OxA-21738",34900,600);
R_Date("OxA-21727",34100,550);
R_Date("OxA-21724",33950,550);
R_Date("OxA-21726",34200,550);
R_Date("OxA-21659",35050,600);
R_Date("OxA-21745",36650,750);
R_Date("OxA-21746",36850,800);
R_Date("OxA-21743",36100,700);
R_Date("OxA-21721",37300,800);
};
};
```

Hohlenstein-Stadel (KDE) – figure D.50

```
 Plot()
{
KDE_Model("KDE - Hohlenstein-Stadel",N(0,1), U(0,1),)
{
R_Date("KIA-8951",31440,250);
R_Date("KIA-13077",32270,265);
R_Date("KIA-8949",33920,305);
R_Date("KIA-8950",36910,474);
R_Date("KIA-8948",41710,549);
R_Date("KIA-8947",42410,644);
R_Date("KIA-8946",39970,474);
R_Date("KIA-8945",40220,529);
};
};
```

Vogelherd (KDE) – figure D.51

```
 Plot()
{
KDE_Model("KDE - Vogelherd",N(0,1), U(0,1),)
{
R_Date("PL0001337A",35810,710);
R_Date("PL0001342A",34100,1100);
R_Date("KIA-8970",33080,255);
R_Date("KIA-8969",32500,255);
R_Date("PL0001339A",32180,960);
R_Date("PL0001338A",32400,1700);
R_Date("KIA-8968",31790,240);
R_Date("GrN-6661",30650,560);
R_Date("GrN-6662",27630,830);
R_Date("KIA-8957",26160,150);
};
};
```

Fumane (Stratigraphy) – figure D.40

```
 Plot()
{
Outlier_Model("General",T(5),U(0,4),"t");
Sequence("Ref - Fumane")
{
Boundary("start Uluzzian");
Phase("A4")
{
R_Date("OxA-21733",41000,1300)
{
Outlier("General", 0.05);
};
R_Date("OxA-21734",42000,1400)
{
Outlier("General", 0.05);
};
R_Date("OxA-21735",42000,1700)
{
Outlier("General", 0.05);
};
Date("Date A4 - Uluzzian");
};
Boundary("transition A4 - A3");
Phase("A3")
{
R_Date("OxA-21736",39100,1000)
{
Outlier("General", 0.05);
};
R_Date("OxA-X-2295-52",41300,1300)
{
Outlier("General", 0.05);
};
Date("Date A3 - Uluzzian");
};
Boundary("transition A3 - A2");
Phase("A2")
{
R_Date("UtC-2047",32100,500)
{
Outlier("General", 0.05);
};
R_Date("UtC-2044",31600,400)
{
Outlier("General", 0.05);
};
R_Date("UtC-2051",32800,400)
{
Outlier("General", 0.05);
};
R_Date("UtC-1774",40000,4000)
{
Outlier("General", 0.05);
};
R_Date("UtC-2048",36500,600)
{
Outlier("General", 0.05);
};
R_Date("UtC-2688",36800,1200)
{
Outlier("General", 0.05);
};
R_Date("UtC-2689",35400,1100)
{
```

```
Outlier("General", 0.05);
};
R_Date("UtC-2690",34200,900)
{
Outlier("General", 0.05);
};
Date("Date A2 - Proto-Aurignacian");
};
Boundary("transition A2 - A1");
Phase("A1")
{
R_Date("UtC-2049",31900,500)
{
Outlier("General", 0.05);
};
Date("Date A1 - Proto-Aurignacian");
};
Boundary("transition A - D");
Phase("D")
{
R_Date("UtC-1775",31700,1200)
{
Outlier("General", 0.05);
};
R_Date("UtC-2045",32300,400)
{
Outlier("General", 0.05);
};
R_Date("UtC-2046",32300,500)
{
Outlier("General", 0.05);
};
Date("Date D - Aurignacian");
};
Boundary("end Aurignacian");
};
};
```

Fumane (KDE) – see figure D.53

```
 Plot (){
KDE_Model("KDE - Fumane",N(0,1), U(0,1),)
{
R_Date("UtC-1775",31700,1200);
R_Date("UtC-2045",32300,400);
R_Date("UtC-2046",32300,500);
R_Date("UtC-2049",31900,500);
R_Date("UtC-2047",32100,500);
R_Date("UtC-2044",31600,400);
R_Date("UtC-2051",32800,400);
Date("UtC-1774",N(calBP(48030),4000));
R_Date("UtC-2048",36500,600);
R_Date("UtC-2688",36800,1200);
R_Date("UtC-2689",35400,1100);
R_Date("UtC-2690",34200,900);
R_Date("OxA-21736",39100,1000);
R_Date("OxA-X-2295-52",41300,1300);
R_Date("OxA-21733",41000,1300);
R_Date("OxA-21734",42000,1400);
R_Date("OxA-21735",42000,1700);
};
};
```

Castelcivitas (Stratigraphy)– figure D.37

```
 Plot()
{
Outlier_Model("General",T(5),U(0,4),"t");
Sequence("Castelcivita")
{
Boundary("start Mousterian");
Phase("Mousterian")
{
R_Date("GrN-13984",42700,900)
{
Outlier("General", 0.05);
};
R_Date("GrN-13982",39100,1300)
{
Outlier("General", 0.05);
};
Date("Mousterian");
};
Boundary("transition Mousterian - Uluzzian");
Phase("Uluzzian")
{
R_Date("F-71",32470,650)
{
Outlier("General", 0.05);
};
R_Date("GrN-13985",33330,430)
{
Outlier("General", 0.05);
};
R_Date("F-107",33220,780)
{
Outlier("General", 0.05);
};
R_Date("OxA-22622",36120,360)
{
Outlier("General", 0.05);
};
Date("Uluzzian");
};
Boundary("transition Uluzzian - Aurignacian");
Phase("Dufour Aurignacian")
{
R_Date("F-105",31950,650)
{
Outlier("General", 0.05);
};
R_Date("F-72",32930,720)
{
Outlier("General", 0.05);
};
R_Date("Beta-58184/CAMS-4622",32930,490)
{
Outlier("General", 0.05);
};
Date("Aurignacian");
};
Boundary("end Aurignacian");
};
};
```

Castelcivitas (KDE) – figure D.52

```
 Plot()
{
KDE_Model("KDE - Castelcivita",N(0,1), U(0,1),)
{
R_Date("F-105",31950,650);
R_Date("F-72",32930,720);
R_Date("Beta-58184/CAMS-4622",32930,490);
R_Date("F-71",32470,650);
R_Date("GrN-13985",33330,430);
R_Date("F-107",33220,780);
R_Date("OxA-22622",36120,360);
};
};
```

Willendorf II (Stratigraphy) – see figure D.34

```
 Plot()
{
Outlier_Model("General",T(5),U(0,4),"t");
Outlier_Model("SSimple",N(0,2),0,"s");
Sequence("Willendorf II")
{
Boundary("Start D3");
Phase("D3 - Micoquian")
{
R_Date("OxA-17401",48500,800)
{
Outlier("General", 0.05);
};
Date("Date Micoquian D3");
};
Boundary("D3/D1-D2");
Phase("D1-D2 - Micoquian")
{
Date("OxA-25837",N(calBP(48822),1100))
{
Outlier("General", 0.05);
};
R_Date("OxA-25838",43400,900)
{
Outlier("General", 0.05);
};
R_Date("OxA-17399",41280,380)
{
Outlier("General", 0.05);
};
R_Date("OxA-17400",41800,400)
{
Outlier("General", 0.05);
};
R_Date("OxA-17398",39980,350)
{
Outlier("General", 0.05);
};
R_Combine("A-2541")
{
Outlier("General", 0.05);
R_Date("GrA-52417",40870,438)
{
Outlier("SSimple", 0.05);
};
R_Date("OxA-25836",43200,900)
{
Outlier("SSimple", 0.05);
};
};
Date("Date Micoquian D1-D2");
};
Boundary("end D1-D2");
Boundary("start C8-3");
Phase("C8-3 - Early Aurignacian")
{
Date("Date Early Aurignaican C8-3");
};
Boundary("C8-3/C8-2");
Phase("C8-2 - Aurignacian")
{
R_Combine("A-1915")
{
Outlier("General", 0.05);
R_Date("OxA-23520",39000,500)
{
Outlier("SSimple", 0.05);
};
R_Date("GrA-45012",38790,374)
{
Outlier("SSimple", 0.05);
};
};
R_Date("GrA-896",37930,750)
{
Outlier("General", 0.05);
};
R_Date("GrA-35411",37320,369)
{
Outlier("General", 0.05);
};
R_Date("OxA-17397",37980,300)
{
Outlier("General", 0.05);
};
R_Combine("A-1935")
{
Outlier("General", 0.05);
R_Date("GrA-44894",37420,285)
{
Outlier("SSimple", 0.05);
};
R_Date("GrA-35409",37910,409)
{
Outlier("SSimple", 0.05);
};
R_Date("OxA-22295",36500,450)
{
Outlier("SSimple", 0.05);
};
};
Date("Date Aurignaican C8-2");
};
Boundary("end C8-2");
Boundary("start C7-1");
Phase("C7-1 - Aurignacian")
{
R_Date("GraA-38250",34570,368)
{
Outlier("General", 0.05);
};
Date("Date Aurignaican C7-1");
};
Boundary("C7-1/C6");
Phase("C6")
{
Date("Date C6");
};
Boundary("C6/C5");
Phase("C5")
{
Date("Date C5");
};
Boundary("C5/C4");
Phase("C4-2")
{
R_Combine("A-2421")
{
Outlier("General", 0.05);
R_Date("GrA-45804",32360,200)
{
Outlier("SSimple", 0.05);
};
R_Date("GrA-45011",32790,205)
{
Outlier("SSimple", 0.05);
};
R_Date("OxA-22294",31750,260)
```

```
{
Outlier("SSimple", 0.05);
};
R_Date("OxA-23562",33850,800)
{
Outlier("SSimple", 0.05);
};
};
Date("Date C4-2");
};
Boundary("C4-2/C4-1");
Phase("C4-1")
{
R_Date("GrA-35403",31250,220)
{
Outlier("General", 0.05);
};
R_Date("GrA-35404",31770,240)
{
Outlier("General", 0.05);
};
R_Combine("A-1912")
{
Outlier("General", 0.05);
R_Date("GrA-35406",31170,220)
{
Outlier("SSimple", 0.05);
};
R_Date("OxA-17396",32230,190)
{
Outlier("SSimple", 0.05);
};
};
Date("Date C4-1");
};
Boundary("End C4-1");
};
};
```

Willendorf II (KDE) – see figure D.49

```
 Plot()
{
KDE_Model("KDE - Willendorf II",N(0,1), U(0,1),)
{
R_Date("GrA-35403",31250,220);
R_Date("GrA-35404",31770,240);
R_Combine("A-1912")
{
R_Date("GrA-35406",31170,220);
R_Date("OxA-17396",32230,190);
};
R_Combine("A-1921")
{
R_Date("GrA-45804",32360,200);
R_Date("GrA-45011",32790,205);
R_Date("OxA-22294",31750,260);
R_Date("OxA-23562",33850,800);
};
R_Date("GraA-38250",34570,368);
R_Date("GrA-896",37930,750);
R_Date("GrA-35411",37320,369);
R_Date("OxA-17397",37980,300);
R_Combine("A-1935")
{
R_Date("GrA-44894",37420,285);
R_Date("GrA-35409",37910,409);
R_Date("OxA-22295",36500,450);
};
R_Combine("A-1915")
{
R_Date("GrA-45012",38790,374);
R_Date("OxA-23520",39000,500);
};
};
};
```

Moravian Bohunician (KDE) – see figure D.48

```
 Plot()
{
KDE_Model("KDE - Bohunician Moravia",N(0,1), U(0,1),)
{
R_Date("GrN-12297",38200,1100);
R_Date("GrN-12298",38500,1400);
R_Date("AA-32059",37900,1100);
R_Date("AA-32060",37270,990);
R_Date("AA-32061",35080,830);
R_Date("GrN-11504",34530,830);
R_Date("GrN-11808",35320,320);
R_Date("AA-41475",34440,720);
R_Date("AA-41476",36570,940);
R_Date("AA-41477",34530,770);
R_Date("AA-41478",36350,990);
R_Date("AA-41480",34680,820);
R_Date("AA-32058",38300,1100);
Date("GrN-12606",N(calBP(48350),3100));
R_Date("GrN-6165",42900,1700);
R_Date("OxA-14843",42100,450);
R_Date("OxA-14844",43250,550);
R_Date("OxA-14845",41250,450);
R_Date("GrN-16920",36000,1100);
R_Date("OxA-14846",43600,550);
R_Date("OxA-14847",42750,550);
R_Date("OxA-14848",41350,450);
R_Date("Q-1044",40173,1200);
R_Date("GrN-6802",41400,1400);
R_Date("OxA-18320",29490,240);
R_Date("OxA-18298",36050,260);
R_Date("OxA-18299",38690,320);
R_Date("OxA-18300",38770,330);
R_Date("OxA-18301",40050,360);
R_Date("OxA-18302",34770,240);
R_Date("OxA-18303",38200,330);
R_Date("OxA-18343",36540,310);
R_Date("ANU-12024",32740,530);
R_Date("ANU-27214",35025,730);
R_Date("WK-17757",40000,2000);
};
};
```

Moravian Szeletian (KDE) – see figure D.48

```
 Plot()
{
KDE_Model("KDE - Szeletian Moravia",N(0,1), U(0,1),)
{
R_Date("GrN-12375",39500,1100);
R_Date("GrN-12374",37650,550);
R_Date("GrN-15514",37600,800);
R_Date("GrN-15513",35150,650);
R_Date("OxA-18297",36820,250);
R_Date("OxA-18294",37550,280);
R_Date("OxA-18295",37980,290);
R_Date("OxA-18296",38350,310);
R_Date("OxA-27342",41300,700);
R_Combine("A-2006")
{
R_Date("GrA-44892",40190,390);
R_Date("GrA-35395",40670,550);
R_Date("OxA-17753",37540,300);
R_Date("OxA-17735",37640,300);
R_Date("GrA-44961",39810,550);
R_Date("OxA-22292",38600,550);
R_Date("OxA-22293",39100,650);
R_Date("OxA-23518",41500,700);
};
};
};
```

Moravian Aurignacian (KDE) – see figure D.47

```
 Plot()
{
KDE_Model("KDE - Aurignacian Moravia")
{
R_Date("GrN-12605",30980,360);
R_Date("GrN-14829",32350,900);
R_Date("GrN-16918",32600,1700);
R_Date("AA-41479",33030,620);
R_Date("AA-41472",29020,440);
R_Date("GrN-14826",29200,450);
R_Date("GrN-22107",28780,230);
R_Date("GrN-22108",32030,370);
R_Date("GrA-32566",29820,180);
R_Date("GrA-32568",30620,190);
R_Date("GrA-28280",32330,900);
R_Date("OxA-18304",32230,190);
R_Date("OxA-18305",32540,200);
};
};
```

Cavallo (Stratigraphy) – see figure D.38

```
 Plot()
{
Curve("Marine13","Marine13.14c");
Outlier_Model("General",T(5),U(0,4),"t");
Outlier_Model("SSimple",N(0,2),0,"s");
Sequence("Cavallo")
{
Boundary("start Uluzzian");
Phase("Evolved Uluzzian / EII-I")
{
R_Date("OxA-19242",39990,340)
{
Outlier("General", 0.05);
};
Date("Date EII-I");
};
Boundary("EII-I/E-D");
Phase("E-D")
{
R_Combine("Cvl-5 (OxA-19256/X-2280-16)")
{
Outlier("General", 0.05);
R_Date("OxA-19256",39060,310)
{
Outlier("SSimple", 0.05);
};
R_Date("OxA-X-2280-16",38300,400)
{
Outlier("SSimple", 0.05);
};
};
Date("Date E-D");
};
Boundary("E-D/DII");
Phase("Final Uluzzian / DII")
{
R_Date("OxA-19257",42360,400)
{
Outlier("General", 0.05);
};
R_Date("OxA-19258",36000,400)
{
Outlier("General", 0.05);
};
Date("Date DII");
};
Boundary("DII/DIb");
Phase("Final Uluzzian / DIb")
{
R_Date("OxA-20631",36780,310)
{
Outlier("General", 0.05);
};
R_Date("OxA-19255",36260,250)
{
Outlier("General", 0.05);
};
R_Date("OxA-19254",35080,230)
{
Outlier("General", 0.05);
};
Date("Date DIb");
};
Boundary("end Uluzzian");
};
};
```

Cavallo (KDE)– see figure D.52

```
 Plot()
{
Curve("Marine13","Marine13.14c");
KDE_Model("KDE - Cavallo",N(0,1), U(0,1),)
{
R_Date("OxA-19254",35080,230);
R_Date("OxA-19255",36260,250);
R_Date("OxA-20631",36780,310);
R_Date("OxA-19257",42360,400);
R_Date("OxA-19258",36000,400);
R_Date("OxA-19256",39060,310);
R_Date("OxA-X-2280-16",38300,400);
R_Date("OxA-19242",39990,340);
};
};
```

Šalitrena Pećina (Stratigraphy) – see figure 15.7

```
 Plot()
{
Outlier_Model("General",T(5),U(0,4),"t");
Curve("IntCal13","IntCal13.14c");
Sequence("Salitrena Pecina")
{
Boundary("start Mousterian");
Phase("Mousterian")
{
Date("OxA-27682",U(calBP(50200),calBP(70000)))
{
Outlier("General", 0.05);
};
Date("OxA-27829",U(calBP(45700),calBP(70000)))
{
Outlier("General", 0.05);
};
R_Date("Beta-237690",37760,520)
{
Outlier("General", 0.05);
};
R_Date("OxA-27948",36150,750)
{
Outlier("General", 0.05);
};
Date("Date Mousterian");
};
Boundary("Mousterian/Aurignacian");
Phase("Aurignacian")
{
R_Date("Beta-237688",31980,360)
{
Outlier("General", 0.05);
};
R_Date("Beta-224720",30190,400)
{
Outlier("General", 0.05);
};
Phase("shell")
{
Curve("Marine13","Marine13.14c");
Delta_R("LocalMarine",58,15);
R_Date("OxA-27683",30150,150)
{
Outlier("General", 0.05);
};
};
R_Date("Beta-237684",29980,280)
{
Outlier("General", 0.05);
};
R_Date("OxA-27975",29700,340)
{
Outlier("General", 0.05);
};
Date("Date Aurignacian");
};
Boundary("End Aurignacian");
};
};
```

Šalitrena Pećina (KDE) – see figure D.47

```
 Plot()
{
KDE_Model("KDE - Salitrena Pecina", N(0,1), U(0,1),)
{
Curve("IntCal13","IntCal13.14c");
R_Date("Beta-237688",31980,360);
R_Date("Beta-224720",30190,400);
R_Date("OxA-27975",29700,340);
Phase("shell")
{
Curve("Marine13","Marine13.14c");
Delta_R("LocalMarine",58,15);
R_Date("OxA-27683",30150,150);
};
R_Date("Beta-237684",29980,280);
};
};
```

Bacho Kiro (Stratigraphy) – see figure D.33

```
 Plot()
{
Outlier_Model("General",T(5),U(0,4),"t");
Sequence("Bacho Kiro")
{
Boundary("start Mousterian");
Phase("Mousterian")
{
Date("GrN-7570",U(calBP(47500),calBP(70000)))
{
Outlier("General", 0.05);
};
R_Date("OxA-11421",51500,2400)
{
Outlier("General", 0.05);
};
Date("Date Mousterian");
};
Boundary("Mousterian/Bachokirian");
Phase("Bachokirian")
{
Date("GrN-7545",U(calBP(43000),calBP(70000)))
{
Outlier("General", 0.05);
};
R_Date("OxA-3213",38500,1700)
```

```
{
Outlier("General", 0.05);
};
R_Date("OxA-3183",37650,1450)
{
Outlier("General", 0.05);
};
R_Date("OxA-3212",34800,1150)
{
Outlier("General", 0.05);
};
Date("Date Bachokirian");
};
Boundary("Bachokirian/Aurignacian");
Phase("Aurignacian")
{
R_Date("GrN-7569",32700,300)
{
Outlier("General", 0.05);
};
R_Date("GrN-7560",32700,300)
{
Outlier("General", 0.05);
};
R_Date("OxA-3181",32200,780)
{
Outlier("General", 0.05);
};
R_Date("OxA-3182",33300,820)
{
Outlier("General", 0.05);
};
R_Date("Ly-1102",29150,950)
{
Outlier("General", 0.05);
};
Date("Date Aurignacian");
};
Boundary("end Aurignacian");
};
};
```

Bacho Kiro (KDE) – see figure D.46

```
 Plot()
{
KDE_("KDE - Bacho Kiro", N(0,1), U(0,1),)
{
R_Date("OxA-3181",32200,780);
R_Date("OxA-3183",37650,1450);
R_Date("OxA-3212",34800,1150);
R_Date("OxA-3213",38500,1700);
R_Date("Ly-1102",29150,950);
R_Date("GrN-7569",32700,300);
R_Date("OxA-3182",33300,820);
R_Date("GrN-7560",32700,300);
};
};
```

Mitoc-Malul Galben (KDE) – see figure D.46

```
 Plot()
{
KDE_Model("KDE - Mitoc-Malul Galben", N(0,1), U(0,1),)
{
R_Date("GrN-11190",27410,430);
R_Date("GrN-12637",31850,800);
R_Combine("comb. 8B (GrA-27261/27268)")
{
R_Date("GrA-27261",27700,180);
R_Date("GrA-27268",27750,160);
};
R_Date("GrN-15451",26530,400);
R_Date("GrN-15454",29410,310);
R_Date("GrA-1355",25380,120);
R_Date("OxA-1646",31100,900);
R_Date("GrA-1648",31000,330);
R_Date("GrN-15456",25930,450);
R_Date("GrN-20443",30240,454);
R_Date("GrN-20770",31160,549);
R_Date("GrN-20442",30920,390);
R_Date("GrN-20444",31160,529);
R_Date("GrA-1357",32730,220);
};
};
```

Buran-Kaya (Stratigraphy) – figure D.36

```
 Plot()
{
Outlier_Model("General",T(5),U(0,4),"t");
Outlier_Model("SSimple",N(0,2),0,"s");
Sequence("Buran-Kaya III")
{
Boundary("Start Micoquian");
Phase("Layer B - Micoquian")
{
R_Date("OxA-25879",37700,900)
{
Outlier("General", 0.05);
};
R_Combine("Combine B")
{
Outlier("General", 0.05);
R_Date("GifA-11218/SacA-25135",36500,1200)
{
Outlier("SSimple", 0.05);
};
R_Date("GrA-47319",35590,280)
{
Outlier("SSimple", 0.05);
};
};
Date("Date Micoquian");
};
Boundary("B/6-5 - Start Aurignacian");
Phase("Layer 6-5 - Aurignacian")
{
R_Combine("Combine 6-5")
{
Outlier("General", 0.05);
R_Date("GrA-47318",32800,220)
{
Outlier("SSimple", 0.05);
};
R_Date("GifA-11217/SacA-25134",35900,1100)
{
Outlier("SSimple", 0.05);
```

```
};
};
Date("Date Aurig 6-5");
};
Boundary("6-5/6-4");
Phase("Layer 6-4 - Aurignacian")
{
R_Combine("Combine 6-4")
{
Outlier("General", 0.05);
R_Date("GrA-48399",31250,2115)
{
Outlier("SSimple", 0.05);
};
R_Date("GifA-11220/SacA-25134",35900,1100)
{
Outlier("SSimple", 0.05);
};
};
R_Date("GifA-11221/SaxA-25138",32740,780)
{
Outlier("General", 0.05);
};
Date("Date Aurig 6-4");
};
Boundary("6-4/6-3");
Phase("Layer 6-3 - Aurignacian")
{
R_Combine("Combine Horse")
{
Outlier("General", 0.05);
R_Date("GrA-40485",34050,250)
{
Outlier("SSimple", 0.05);
};
R_Date("GifA-80181/SacA-12260",34910,950)
{
Outlier("SSimple", 0.05);
};
};
Date("Date Aurig 6-3");
};
Boundary("6-3/6-2 - end Aurignacian");
Phase("Layer 6-2 - Gravettian")
{
R_Date("GrA-50457",32450,240)
{
Outlier("General", 0.05);
};
R_Date("GrA-50460",29440,185)
{
Outlier("General", 0.05);
};
Date("Date Gravettian 6-2");
};
Boundary("6-2/6-1");
Phase("Layer 6-1 - Gravettian")
{
R_Date("GrA-37938",31900,230)
{
Outlier("General", 0.05);
};
R_Date("GifA-10021/SacA-19018",31320,820)
{
Outlier("General", 0.05);
};
R_Date("GifA-11216/SacA-25133",31530,670)
{
Outlier("General", 0.05);
};
R_Combine("Combine 6-1")
{
Outlier("General", 0.05);
R_Date("GrA-53942",29640,165)
{
Outlier("SSimple", 0.05);
};
R_Date("OxA-25669",32200,450)
{
Outlier("SSimple", 0.05);
};
};
Date("Date Gravettian 6-1");
};
Boundary("6-1/5-2");
Phase("Layer 5-2 - Gravettian")
{
R_Combine("Combine 5-2")
{
Outlier("General", 0.05);
R_Date("GrA-47316",30100,175)
{
Outlier("SSimple", 0.05);
};
R_Date("GifA-11222/SacA-25139",33790,880)
{
Outlier("SSimple", 0.05);
};
};
Date("Date Gravettian 5-2");
};
Boundary("end Gravettian");
Boundary("start Swiderian");
Phase("Layer 4 - Swiderian")
{
R_Date("OxA-25670",10040,45)
{
Outlier("General", 0.05);
};
R_Combine("Combine 4")
{
Outlier("General", 0.05);
R_Date("GrA-50461",10010,60)
{
Outlier("SSimple", 0.05);
};
R_Date("GifA-11219/SacA-25139",10050,70)
{
Outlier("SSimple", 0.05);
};
};
Date("Date Swiderian");
};
Boundary("End 4");
};
};
```

Buran-Kaya (KDE) – see figure D.51

```
 Plot()
{
KDE_Model("KDE - Buran-Kaya III", N(0,1), U(0,1),)
{
R_Date("OxA-13302",32790,280);
R_Date("GrA-50457",32450,240);
R_Date("GrA-37938",31900,230);
R_Date("OxA-25670",10040,45);
R_Date("GifA-10021/SacA-19018",31320,820);
R_Date("GifA-11216/SacA-25133",31530,670);
R_Date("GrA-50460",29440,185);
R_Date("GifA-11221/SaxA-25138",32740,780);
R_Combine("Combine 4")
{
R_Date("GrA-50461",10010,60);
R_Date("GifA-11219/SacA-25139",10050,70);
};
R_Combine("Combine 5-2")
{
R_Date("GrA-47316",30100,175);
R_Date("GifA-11222/SacA-25139",33790,880);
};
R_Combine("Combine 6-1")
{
R_Date("GrA-53942",29640,165);
R_Date("OxA-25669",32200,450);
```

```
};
R_Combine("Combine 6-4")
{
R_Date("GrA-48399",31250,2115);
R_Date("GifA-11220/SacA-25134",35900,1100);
};
R_Combine("Combine 6-5")
{
R_Date("GrA-47318",32800,220);
R_Date("GifA-11217/SacA-25134",35900,1100);
};
R_Combine("Combine Horse")
{
R_Date("GrA-40485",34050,250);
R_Date("GifA-80181/SacA-12260",34910,950);
};
};
};
```

Ksar Akil (Stratigraphy) – see figure D.41

```
 Plot()
{
Outlier_Model("General",T(5),U(0,4),"t");
Outlier_Model("SSimple",N(0,2),0,"s");
Curve("Marine13","Marine13.14c");
Delta_R("LocalMarine",53,43);
Sequence("Ksar Akil")
{
Boundary("Start Mousterian");
Phase("Mousterian (Ewing XXXII-XXVII)")
{
Phase("terrestrial")
{
Curve("IntCal13","IntCal13.14c");
Date("G-88177 ",N(calBP(51000),4000))
{
Outlier("General", 0.05);
};
Date("G-88174",N(calBP(47000),9000))
{
Outlier("General", 0.05);
};
R_Date("GrN-2579",43750,1500)
{
Outlier("General", 0.05);
};
};
R_Date("OxA-25656",39530,330)
{
Outlier("General", 0.05);
};
R_Date("OxA-20491",39310,330)
{
Outlier("General", 0.05);
};
Date("Date Mousterian");
};
Boundary("Mousterian/S.C. 3");
Boundary("S.C. 3/KA 1");
Phase("IUP (Ewing XXIII-XXI)")
{
R_Combine("KA 51 (OxA-20489/20490)")
{
Outlier("General", 0.05);
R_Date("OxA-20490",37430,320)
{
Outlier("SSimple", 0.05);
};
R_Date("OxA-20489",36790,270)
{
Outlier("SSimple", 0.05);
};
};
R_Date("OxA-20025",36390,210)
{
Outlier("General", 0.05);
};
R_Date("OxA-20880",34940,200)
{
Outlier("General", 0.05);
};
R_Date("OxA-22667",34320,190)
{
Outlier("General", 0.05);
};
R_Date("OxA-25655",30890,160)
{
Outlier("General", 0.05);
};
Date("Date IUP");
};
Boundary("KA 1/KA 2");
Phase("Early Ahmarian (Ewing XX-XV)")
{
Phase("Levels XX-XIX")
{
R_Date("OxA-22664",35510,240)
{
Outlier("General", 0.05);
};
R_Date("OxA-20879",35010,240)
{
Outlier("General", 0.05);
};
R_Date("OxA-X-2361-14",32960,160)
{
Outlier("General", 0.05);
};
};
Phase("Levels XVIII-XV")
{
R_Date("OxA-20877",36270,240)
{
Outlier("General", 0.05);
};
R_Date("OxA-22665",36040,240)
{
Outlier("General", 0.05);
};
R_Date("OxA-20486",35780,240)
{
Outlier("General", 0.05);
};
R_Date("OxA-22269",35390,250)
{
Outlier("General", 0.05);
};
R_Date("OxA-20876",35020,240)
{
Outlier("General", 0.05);
};
R_Date("OxA-25653",34830,240)
{
Outlier("General", 0.05);
};
R_Date("OxA-20488",34230,210)
{
Outlier("General", 0.05);
};
R_Date("OxA-25652",33300,230)
{
Outlier("General", 0.05);
};
R_Date("OxA-20487",33930,220)
{
Outlier("General", 0.05);
};
R_Date("OxA-X-2338-8",33760,210)
{
Outlier("General", 0.05);
};
R_Date("OxA-X-2342-57",28130,110)
{
Outlier("General", 0.05);
```

```
};
};
Date("Date Early Ahmarian");
};
Boundary("KA 2/S.C. 2");
Boundary("S.C. 2/KA 3");
Phase("Phases 3-4 (Ewing XII-IX/Tixier12)")
{
R_Date("OxA-20024",35520,200)
{
Outlier("General", 0.05);
};
R_Date("OxA-25585",34550,250)
{
Outlier("General", 0.05);
};
Phase("terrestrial")
{
Curve("IntCal13","IntCal13.14c");
R_Date("MC-1192",32000,1500)
{
Outlier("General", 0.05);
};
};
R_Date("OxA-20023",30360,140)
{
Outlier("General", 0.05);
};
Date("Date Phases 3-4");
};
Boundary("KA 3-4/ KA 5");
Phase("Phase 5 (Ewing VIII-VII/Tixier 10h-11c)")
{
Phase("terrestrial")
{
Curve("IntCal13","IntCal13.14c");
R_Date("OxA-1805",32400,1100)
{
Outlier("General", 0.05);
};
R_Date("OxA-1804",31200,1300)
{
Outlier("General", 0.05);
};
};
R_Date("OxA-20875",30640,160)
{
Outlier("General", 0.05);
};
R_Date("GrN-2195",28840,380)
{
Outlier("General", 0.05);
};
Date("Date Phases 5");
};
Boundary("KA 5/KA 6");
Phase("Phase 6 (Ewing IV/Tixier 10a-8ac)")
{
Curve("IntCal13","IntCal13.14c");
R_Date("OxA-1803",30250,850)
{
Outlier("General", 0.05);
};
R_Date("OxA-19194",30250,170)
{
Outlier("General", 0.05);
};
R_Date("OxA-1798",29300,800)
{
Outlier("General", 0.05);
};
Date("Date Phases 6");
};
Boundary("KA 6/KA 7");
Phase("Phase 7 (Ewing V/Tixier 8a-7)")
{
Curve("IntCal13","IntCal13.14c");
R_Date("OxA-1797",26900,600)
{
Outlier("General", 0.05);
};
R_Date("MC-1191",26500,900)
{
Outlier("General", 0.05);
};
Date("Date Phases 7");
};
Boundary("End KA 7");
};
};
```

Ksar Akil (KDE) – see figure D.54

```
 Plot()
{
KDE_Model("KDE - Ksar Akil",N(0,1),U(0,1),)
{
Curve("IntCal13","IntCal13.14c");
R_Date("OxA-19194",30250,170);
R_Date("OxA-20875",30640,160);
R_Date("OxA-25585",34550,250);
R_Date("OxA-20024",35520,200);
R_Date("OxA-20876",35020,240);
R_Date("OxA-22665",36040,240);
R_Date("OxA-1797",26900,600);
R_Date("OxA-1798",29300,800);
R_Date("OxA-1803",30250,850);
R_Date("OxA-1804",31200,1300);
R_Date("OxA-1805",32400,1100);
R_Date("MC-1191",26500,900);
R_Date("MC-1192",32000,1500);
R_Date("GrN-2195",28840,380);
Phase("shells")
{
Curve("Marine13","Marine13.14c");
Delta_R("LocalMarine",53,43);
R_Date("OxA-20023",30360,140);
R_Date("OxA-X-2342-57",28130,110);
R_Date("OxA-20877",36270,240);
R_Date("OxA-22269",35390,250);
R_Date("OxA-20487",33930,220);
R_Date("OxA-25652",33300,230);
R_Date("OxA-20486",35780,240);
R_Date("OxA-X-2338-8",33760,210);
R_Date("OxA-25653",34830,240);
R_Date("OxA-20488",34230,210);
R_Date("OxA-22664",35510,240);
R_Date("OxA-X-2361-14",32960,160);
R_Date("OxA-20879",35010,240);
R_Date("OxA-20025",36390,210);
R_Date("OxA-25655",30890,160);
R_Date("OxA-20880",34940,200);
R_Date("OxA-22667",34320,190);
R_Combine("KA 51 (OxA-20489/20490)")
{
R_Date("OxA-20489",36790,270);
R_Date("OxA-20490",37430,320);
};
};
};
};
```

Spatio-temporal distribution: map 1 – see figures 15.14–15.16

```
 Plot()
{
Date(Prior("Strat - Bacho Kiro - Date Mouserian",
"Priors_Strat/BachoKiro_Date_Mousterian.prior",))
{
latitude=42.947378;
longitude=25.331867;
site="Bacho Kiro";
culture="Mousterian";
author="Neanderthal";
};
Date(Prior("Strat - Willendorf II - Date D3",
"Priors_Strat/Willendorf_Date_Micoquian_D3.prior",))
{
latitude=48.323;
longitude=15.399;
site="Willendorf II";
culture="Micoquian";
author="Neanderthal";
};
Date(Prior("Strat - Labeko Koba - Date IX lower",
"Priors_Strat/LabekoKoba_Date_Chatelperronian.prior",))
{
latitude=43.066;
longitude=-2.458;
site="Labeko Koba";
culture="Chatelperronian";
author="Neanderthal";
};
Date(Prior("KDE - Moravia Szeletian",
"Priors_KDE/KDE_Szeletian_Moravia.prior",))
{
latitude=49.5;
longitude=17;
site="Moravia Szeletian";
culture="Szeletian";
author="Neanderthal";
};
Date(Prior("Strat - Ksar Akil - Date IUP",
"Priors_Strat/KsarAkil_Date_IUP.prior",))
{
latitude=33.916667;
longitude=35.6;
site="Ksar Akil";
culture="IUP";
author="AMH";
};
Date(Prior("Strat - Bacho Kiro - Date Bachokirian",
"Priors_Strat/BachoKiro_Date_Bachokirian.prior",))
{
latitude=42.947378;
longitude=25.331867;
site="Bacho Kiro";
culture="Bachokirian";
author="AMH";
};
Date(Prior("Strat - Castelcivita - Date Uluzzian",
"Priors_Strat/Castelcivitas_Uluzzian.prior",))
{
latitude=40.495;
longitude=15.237;
site="Castelcivita";
culture="Uluzzian";
author="AMH";
};
Date(Prior("KDE - Moravia Bohunician",
"Priors_KDE/KDE_Bohunician_Moravia.prior",))
{
latitude=49.5;
longitude=17;
site="Moravia Bohunician";
culture="Bohunician";
author="AMH";
};
Date(Prior("MOD3 - Kozarnika - Date 5c",
"Priors_Strat_DPhil/Kz_MOD3_Date_5c.prior",))
{
latitude=43.651722;
longitude=22.702472;
site="Kozarnika";
culture="Kozarnikian";
author="AMH";
};
Date(Prior("Strat - Fumane - Date A2",
"Priors_Strat/Fumane_Date_A2_Proto_Aurignacian.prior",))
{
latitude=45.57;
longitude=10.902;
site="Fumane";
culture="Proto-Aurignacian";
author="AMH";
};
Date(Prior("Strat - El Castillo - Date 18C",
"Priors_Strat/ElCastillo_Date_Transitional_Aurignacian_18C.prior",))
{
latitude=43.2875;
longitude=-3.9598;
site="El Castillo";
culture="‘Transitional Aurignacian’";
author="AMH";
};
Date(Prior("Strat - Isturitz - Date C4d1",
"Priors_Strat/Isturitz_Date_Proto_Aurignacian_C4d1.prior",))
{
latitude=43.371;
longitude=-1.196;
site="Isturitz";
culture="Proto-/Early Aurignacian";
author="AMH";
};
R_Date("OxA-X-2732-11",31100,520)
{
latitude=45.3605642;
longitude=14.7527073;
site="Bukovac";
culture="Aurignacian Point";
author="AMH";
};
Date(Prior("MOD3 - Temnata - Date TD-V 4",
"Priors_Strat_DPhil/TD_Date_4_TD_V.prior",))
{
latitude=43.174969;
longitude=24.074006;
site="Temnata";
culture="Aurignacian-like";
author="AMH";
};
Date(Prior("Strat - Geissenklosterle - Date III",
"Priors_Strat/Geissenklosterle_EarlyAurig.prior",))
{
latitude=48.401;
longitude=9.772;
site="Geißenklösterle";
culture="Early Aurignacian";
author="AMH";
};
Date(Prior("Strat - Ksar Akil - Date Phase 2",
"Priors_Strat/KsarAkil_Date_Early_Ahmarian.prior",))
{
latitude=33.916667;
longitude=35.6;
site="Ksar Akil";
culture="Early Ahmarian";
author="AMH";
};
Date(Prior("Strat - Bacho Kiro - Date Aurignacian",
"Priors_Strat/BachoKiro_Date_Aurignacian.prior",))
{
latitude=42.947378;
longitude=25.331867;
site="Bacho Kiro";
culture="Aurignacian";
author="AMH";
};
Date(Prior("Strat - Geissenklosterle - Date II",
"Priors_Strat/Geissenklosterle_UpperAurig.prior",))
{
latitude=48.401;
longitude=9.772;
site="Geißenklösterle";
culture="Upper Aurignacian";
author="AMH";
};
Date(Prior("Strat - L’Arbreda - Date Evolved Aurig",
"Priors_Strat/LArbreda_Date_Evolved_Aurignacian.prior",))
{
```

```
latitude=42.161;
longitude=2.747;
site="L'Arbreda";
culture="Evolved Aurignacian";
author="AMH";
};
Date(Prior("Strat - Buran-Kaya III - Gravettian 6-2",
"Priors_Strat/BuranKayaIII_Date_Gravettian_6_2.prior",))
{
latitude=45.16;
longitude=34.396;
site="Buran-Kaya III";
culture="Gravettian";
author="AMH";
};
Date(Prior("Strat - Buran-Kaya III - Micoquian",
"Priors_Strat/BuranKayaIII_Date_Micoquian.prior",))
{
latitude=45.16;
longitude=34.396;
site="Buran-Kaya III";
culture="Micoquian";
author="Neanderthal";
};
Date(Prior("Strat - Buran-Kaya III - Aurignacian 6-5",
"Priors_Strat/BuranKayaIII_Date_Aurig_6_5.prior",))
{
latitude=45.16;
longitude=34.396;
site="Buran-Kaya III";
culture="Aurignacian";
author="AMH";
};
Date(Prior("Strat - Buran-Kaya III - Aurignacian 6-4",
"Priors_Strat/BuranKayaIII_Date_Aurig_6_4.prior",))
{
latitude=45.16;
longitude=34.396;
site="Buran-Kaya III";
culture="Aurignacian";
author="AMH";
};
Date(Prior("Strat - Buran-Kaya III - Aurignacian 6-3",
"Priors_Strat/BuranKayaIII_Date_Aurig_6_3.prior",))
{
latitude=45.16;
longitude=34.396;
site="Buran-Kaya III";
culture="Aurignacian";
author="AMH";
};
Date(Prior("Strat - Buran-Kaya III - Gravettian 6-1",
"Priors_Strat/BuranKayaIII_Date_Gravettian_6_1.prior",))
{
latitude=45.16;
longitude=34.396;
site="Buran-Kaya III";
culture="Gravettian";
author="AMH";
};
Date(Prior("Strat - Buran-Kaya III - Gravettian 5-2",
"Priors_Strat/BuranKayaIII_Date_Gravettian_5_2.prior",))
{
latitude=45.16;
longitude=34.396;
site="Buran-Kaya III";
culture="Gravettian";
author="AMH";
};
Date(Prior("Strat - Castelcivita - Date Mousterian",
"Priors_Strat/Castelcivita_Mousterian.prior",))
{
latitude=40.495;
longitude=15.237;
site="Castelcivita";
culture="Mousterian";
author="Neanderthal";
};
Date(Prior("Strat - Castelcivita - Date Aurignacian",
"Priors_Strat/Castelcivita_Aurignacian.prior",))
{
latitude=40.495;
longitude=15.237;
site="Castelcivita";
culture="Aurignacian";
author="AMH";
};
Date(Prior("Strat - Cavallo - Date EII/I",
"Priors_Strat/CAVALLO_Date_EII_I_Uluzzian.prior",))
{
latitude=40.154;
longitude=17.96;
site="Cavallo";
culture="Uluzzian";
author="AMH";
};
Date(Prior("Strat - Cavallo - Date E/D",
"Priors_Strat/CAVALLO_Date_E_D_Uluzzian.prior",))
{
latitude=40.154;
longitude=17.96;
site="Cavallo";
culture="Uluzzian";
author="AMH";
};
Date(Prior("Strat - Cavallo - Date DII",
"Priors_Strat/CAVALLO_Date_DII_Uluzzian.prior",))
{
latitude=40.154;
longitude=17.96;
site="Cavallo";
culture="Uluzzian";
author="AMH";
};
Date(Prior("Strat - Cavallo - Date Dib",
"Priors_Strat/CAVALLO_Date_DIb_Uluzzian.prior",))
{
latitude=40.154;
longitude=17.96;
site="Cavallo";
culture="Uluzzian";
author="AMH";
};
Date(Prior("Strat - El Castillo - Date 20C",
"Priors_Strat/ElCastillo_Date_Mousterian.prior",))
{
latitude=43.2875;
longitude=-3.9598;
site="El Castillo";
culture="Mousterian";
author="Neanderthal";
};
Date(Prior("Strat - El Castillo - Date 18B",
"Priors_Strat/ElCastillo_Date_Transitional_Aurignacian_18B.prior",))
{
latitude=43.2875;
longitude=-3.9598;
site="El Castillo";
culture="'Transitional Aurignacian'";
author="AMH";
};
Date(Prior("Strat - Fumane - Date A4",
"Priors_Strat/Fumane_Date_A4_Uluzzian.prior",))
{
latitude=45.57;
longitude=10.902;
site="Fumane";
culture="Uluzzian";
author="AMH";
};
Date(Prior("Strat - Fumane - Date A3",
"Priors_Strat/Fumane_Date_A3_Uluzzian.prior",))
{
latitude=45.57;
longitude=10.902;
site="Fumane";
culture="Uluzzian";
author="AMH";
};
Date(Prior("Strat - Fumane - Date A1",
"Priors_Strat/Fumane_Date_A1_Proto_Aurignacian.prior",))
{
latitude=45.57;
longitude=10.902;
site="Fumane";
culture="Proto-Aurignacian";
```

```
author="AMH";
};
Date(Prior("Strat - Fumane - Date D",
"Priors_Strat/Fumane_Date_D_Aurignacian.prior",))
{
latitude=45.57;
longitude=10.902;
site="Fumane";
culture="Aurignacian";
author="AMH";
};
Date(Prior("Strat - Geissenklosterle - Date IV",
"Priors_Strat/Geissenklosterle_Mousterian.prior",))
{
latitude=48.401;
longitude=9.772;
site="Geißenklösterle";
culture="Mousterian";
author="Neanderthal";
};
Date(Prior("Strat - Geissenklosterle - Date I",
"Priors_Strat/Geissenklosterle_Gravettian.prior",))
{
latitude=48.401;
longitude=9.772;
site="Geißenklösterle";
culture="Gravettian";
author="AMH";
};
Date(Prior("Strat - Hohle Fels - Date IX",
"Priors_Strat/HohleFels_Date_IX_Mousterian.prior",))
{
latitude=48.378;
longitude=9.758;
site="Hohle Fels";
culture="Mousterian";
author="Neanderthal";
};
Date(Prior("Strat - Hohle Fels - Date VIII",
"Priors_Strat/HohleFels_Date_VIII_Mousterian.prior",))
{
latitude=48.378;
longitude=9.758;
site="Hohle Fels";
culture="Mousterian";
author="Neanderthal";
};
Date(Prior("Strat - Hohle Fels - Date VII",
"Priors_Strat/HohleFels_Date_VII_Mousterian.prior",))
{
latitude=48.378;
longitude=9.758;
site="Hohle Fels";
culture="Mousterian";
author="Neanderthal";
};
Date(Prior("Strat - Hohle Fels - Date VI",
"Priors_Strat/HohleFels_Date_VI_Mousterian.prior",))
{
latitude=48.378;
longitude=9.758;
site="Hohle Fels";
culture="Mousterian";
author="Neanderthal";
};
Date(Prior("Strat - Hohle Fels - Date V",
"Priors_Strat/HohleFels_Date_V_Aurignacian.prior",))
{
latitude=48.378;
longitude=9.758;
site="Hohle Fels";
culture="Aurignacian";
author="AMH";
};
Date(Prior("Strat - Hohle Fels - Date IV",
"Priors_Strat/HohleFels_Date_IV_Aurignacian.prior",))
{
latitude=48.378;
longitude=9.758;
site="Hohle Fels";
culture="Aurignacian";
author="AMH";
};
Date(Prior("Strat - Hohle Fels - Date III",
"Priors_Strat/HohleFels_Date_III_Aurignacian.prior",))
{
latitude=48.378;
longitude=9.758;
site="Hohle Fels";
culture="Aurignacian";
author="AMH";
};
Date(Prior("Strat - Hohle Fels - Date II",
"Priors_Strat/HohleFels_Date_II_Aurignacian.prior",))
{
latitude=48.378;
longitude=9.758;
site="Hohle Fels";
culture="Aurignacian";
author="AMH";
};
Date(Prior("KDE - Hohlenstein-Stadel",
"Priors_KDE/KDE_Hohlenstein_Stadel_short_.prior",))
{
latitude=48.551;
longitude=10.168;
site="Hohlenstein-Stadel";
culture="Aurignacian";
author="AMH";
};
Date(Prior("Strat - Isturitz - Date C5",
"Priors_Strat/Isturitz_Date_Proto_Aurignacian_C5.prior",))
{
latitude=43.371;
longitude=-1.196;
site="Isturitz";
culture="Proto-Aurignacian";
author="AMH";
};
Date(Prior("Strat - Isturitz - Date C4c4",
"Priors_Strat/Isturitz_ProtoEarly_Aurignacian_C4c4.prior",))
{
latitude=43.371;
longitude=-1.196;
site="Isturitz";
culture="Proto-Aurignacian";
author="AMH";
};
Date(Prior("Strat - Isturitz - Date C4b2",
"Priors_Strat/Isturitz_Date_Early_Aurignacian_C4b2.prior",))
{
latitude=43.371;
longitude=-1.196;
site="Isturitz";
culture="Early Aurignacian";
author="AMH";
};
Date(Prior("Strat - Isturitz - Date C4b1",
"Priors_Strat/Isturitz_Date_Early_Aurignacian_C4b1.prior",))
{
latitude=43.371;
longitude=-1.196;
site="Isturitz";
culture="Early Aurignacian";
author="AMH";
};
Date(Prior("Strat - Ksar Akil - Date Mousterian",
"Priors_Strat/KsarAkil_Date_Mousterian.prior",))
{
latitude=33.916667;
longitude=35.6;
site="Ksar Akil";
culture="Mousterian";
author="Neanderthal";
};
Date(Prior("Strat - Ksar Akil - Date Phase 3-4",
"Priors_Strat/KsarAkil_Date_Phases_3_4.prior",))
{
latitude=33.916667;
longitude=35.6;
site="Ksar Akil";
culture="Early Ahmarian";
author="AMH";
};
Date(Prior("Strat - Ksar Akil - Date Phase 5",
"Priors_Strat/KsarAkil_Date_Phases_5.prior",))
```

```
{
latitude=33.916667;
longitude=35.6;
site="Ksar Akil";
culture="Early Ahmarian";
author="AMH";
};
Date(Prior("Strat - Ksar Akil - Date Phase 6",
"Priors_Strat/KsarAkil_Date_Phases_6.prior",))
{
latitude=33.916667;
longitude=35.6;
site="Ksar Akil";
culture="Early Ahmarian";
author="AMH";
};
Date(Prior("Strat - Ksar Akil - Date Phase 7",
"Priors_Strat/KsarAkil_Date_Phases_7.prior",))
{
latitude=33.916667;
longitude=35.6;
site="Ksar Akil";
culture="Early Ahmarian";
author="AMH";
};
Date(Prior("Strat - L'Arbreda - Date Mousterian",
"Priors_Strat/LArbreda_Date_Mousterian.prior",))
{
latitude=42.161;
longitude=2.747;
site="L'Arbreda";
culture="Mousterian";
author="Neanderthal";
};
Date(Prior("Strat - L'Arbreda - Date Proto-Aurig",
"Priors_Strat/LArbreda_Date_Proto_Aurignacian.prior",))
{
latitude=42.161;
longitude=2.747;
site="L'Arbreda";
culture="Proto-Aurignacian";
author="AMH";
};
Date(Prior("Strat - L'Arbreda - Date Gravettian F",
"Priors_Strat/LArbreda_Date_Gravettian_F.prior",))
{
latitude=42.161;
longitude=2.747;
site="L'Arbreda";
culture="Gravettian";
author="AMH";
};
Date(Prior("Strat - L'Arbreda - Date Gravettian E",
"Priors_Strat/LArbreda_Date_Gravettian_E.prior",))
{
latitude=42.161;
longitude=2.747;
site="L'Arbreda";
culture="Gravettian";
author="AMH";
};
Date(Prior("Strat - Labeko Koba - Date VII",
"Priors_Strat/LabekoKoba_Date_Proto_Aurignacian.prior",))
{
latitude=43.066;
longitude=-2.458;
site="Labeko Koba";
culture="Proto-Aurignacian";
author="AMH";
};
Date(Prior("Strat - Labeko Koba - Date VI",
"Priors_Strat/LabekoKoba_Date_Early_Aurignacian_VI.prior",))
{
latitude=43.066;
longitude=-2.458;
site="Labeko Koba";
culture="Early Aurignacian";
author="AMH";
};
Date(Prior("Strat - Labeko Koba - Date V",
"Priors_Strat/LabekoKoba_Date_Early_Aurignacian_V.prior",))
{
latitude=43.066;
longitude=-2.458;
site="Labeko Koba";
culture="Early Aurignacian";
author="AMH";
};
Date(Prior("Strat - Labeko Koba - Date IV",
"Priors_Strat/LabekoKoba_Date_Early_Aurignacian_IV.prior",))
{
latitude=43.066;
longitude=-2.458;
site="Labeko Koba";
culture="Early Aurignacian";
author="AMH";
};
Date(Prior("KDE - Mitoc-Malul Galben",
"Priors_KDE/KDE_Mitoc_Malul_Galben.prior",))
{
latitude=48.111;
longitude=27.036;
site="Mitoc-Malul Galben";
culture="Aurignacian";
author="AMH";
};
Date(Prior("KDE - Moravia Aurignacian",
"Priors_KDE/KDE_Aurignacian_Moravia.prior",))
{
latitude=49.5;
longitude=17;
site="Moravia Aurignacian";
culture="Aurignacian";
author="AMH";
};
Date(Prior("Strat - Riparo Mochi - Date Proto-Aurig",
"Priors_Strat/RiparoMochi_Date_Proto_Aurignacian.prior",))
{
latitude=43.7894;
longitude=7.5475;
site="Riparo Mochi";
culture="Proto-Aurignacian";
author="AMH";
};
Date(Prior("Strat - Riparo Mochi - Date Early Aurig",
"Priors_Strat/RiparoMochi_Date_Early_Aurignacian.prior",))
{
latitude=43.7894;
longitude=7.5475;
site="Riparo Mochi";
culture="Early Aurignacian";
author="AMH";
};
Date(Prior("Strat - Riparo Mochi - Date Gravettian",
"Priors_Strat/RiparoMochi_Date_Gravettian.prior",))
{
latitude=43.7894;
longitude=7.5475;
site="Riparo Mochi";
culture="Gravettian";
author="AMH";
};
Date(Prior("Strat - Salitrena Pecina - Date Aurignacian",
"Priors_Strat/SalitrenaPecina_Date_Aurignacian.prior",))
{
latitude=44.1905;
longitude=20.0835;
site="Šalitrena Pećina";
culture="Aurignacian";
author="AMH";
};
Date(Prior("KDE - Vogelherd",
"Priors_KDE/KDE_Vogelherd.prior",))
{
latitude=48.5606;
longitude=10.1913;
site="Vogelherd";
culture="Aurignacian";
author="AMH";
};
Date(Prior("Strat - Willendorf II - Date D1/D2",
"Priors_Strat/Willendorf_Date_Micoquian_D1_D2.prior",))
{
latitude=48.323;
longitude=15.399;
site="Willendorf II";
```

```
culture="Micoquian";
author="Neanderthal";
};
Date(Prior("Strat - Willendorf II - Date C8-3",
"Priors_Strat/Willendorf_Date_Early_Aurignaican_C8_3.prior",))
{
latitude=48.323;
longitude=15.399;
site="Willendorf II";
culture="Early Aurignacian";
author="AMH";
};
Date(Prior("Strat - Willendorf II - Date C8-2",
"Priors_Strat/Willendorf_Date_Aurignaican_C8_2.prior",))
{
latitude=48.323;
longitude=15.399;
site="Willendorf II";
culture="Aurignacian";
author="AMH";
};
Date(Prior("Strat - Willendorf II - Date C7-1",
"Priors_Strat/Willendorf_Date_Aurignaican_C7_1.prior",))
{
latitude=48.323;
longitude=15.399;
site="Willendorf II";
culture="Aurignacian";
author="AMH";
};
Date(Prior("Strat - Willendorf II - Date C4-2",
"Priors_Strat/Willendorf_Date_C4_2.prior",))
{
latitude=48.323;
longitude=15.399;
site="Willendorf II";
culture="Aurignacian";
author="AMH";
};
Date(Prior("Strat - Willendorf II - Date C4-1",
"Priors_Strat/Willendorf_Date_C4_1.prior",))
{
latitude=48.323;
longitude=15.399;
site="Willendorf II";
culture="Aurignacian";
author="AMH";
};
Date(Prior("MOD10 - Dzerava Skala - Date 5a",
"Priors_Strat_DPhil/Der_MOD10_Date_5a_.prior",))
{
latitude=48.496987;
longitude=17.324692;
site="Dzerava Skala";
culture="Aurignacian Point";
author="AMH";
};
Date(Prior("MOD10 - Dzerava Skala - Date 9",
"Priors_Strat_DPhil/Der_MOD10_Date_9.prior",))
{
latitude=48.496987;
longitude=17.324692;
site="Dzerava Skala";
culture="Aurignacian Point";
author="AMH";
};
Date(Prior("MOD10 - Dzerava Skala - Date 5",
"Priors_Strat_DPhil/Der_MOD10_Date_5.prior",))
{
latitude=48.496987;
longitude=17.324692;
site="Dzerava Skala";
culture="Gravettian";
author="AMH";
};
Date(Prior("MOD10 - Dzerava Skala - Date 4",
"Priors_Strat_DPhil/Der_MOD10_Date_4.prior",))
{
latitude=48.496987;
longitude=17.324692;
site="Dzerava Skala";
culture="Gravettian";
author="AMH";
};
Date(Prior("Points KDE2 - Istallosko",
"Priors_KDE_DPhil/Istall_Points_KDE_2.prior",))
{
latitude=48.071667;
longitude=20.418889;
site="Istallosko";
culture="Aurignacian Point";
author="AMH";
};
R_Date("OxA-X-2716-49",31800,1000)
{
latitude=47.723889;
longitude=18.575278;
site="Jankovich";
culture="Aurignacian Point";
author="AMH";
};
R_Date("OxA-X-2716-48",32500,800)
{
latitude=47.723889;
longitude=18.575278;
site="Jankovich";
culture="Aurignacian Point";
author="AMH";
};
R_Date("OxA-X-2732-10",32750,670)
{
latitude=47.723889;
longitude=18.575278;
site="Jankovich";
culture="Aurignacian Point";
author="AMH";
};
R_Date("OxA-35386",30800,500)
{
latitude=47.723889;
longitude=18.575278;
site="Jankovich";
culture="Aurignacian Point";
author="AMH";
};
Date(Prior("MOD3 - Kozarnika - Date 6/7 ls lp",
"Priors_Strat_DPhil/Kz_MOD3_Date_6_7_ls_lp.prior",))
{
latitude=43.651722;
longitude=22.702472;
site="Kozarnika";
culture="IUP";
author="AMH";
};
Date(Prior("MOD3 - Kozarnika - Date 6/7 lb",
"Priors_Strat_DPhil/Kz_MOD3_Date_6_7_lb.prior",))
{
latitude=43.651722;
longitude=22.702472;
site="Kozarnika";
culture="IUP";
author="AMH";
};
Date(Prior("MOD3 - Kozarnika - Date 5b",
"Priors_Strat_DPhil/Kz_MOD3_Date_5b.prior",))
{
latitude=43.651722;
longitude=22.702472;
site="Kozarnika";
culture="Kozarnikian";
author="AMH";
};
Date(Prior("MOD3 - Kozarnika - Date 5a",
"Priors_Strat_DPhil/Kz_MOD3_Date_5a.prior",))
{
latitude=43.651722;
longitude=22.702472;
site="Kozarnika";
culture="Kozarnikian";
author="AMH";
};
Date(Prior("MOD3 - Kozarnika - Date 4",
"Priors_Strat_DPhil/Kz_MOD3_Date_4.prior",))
{
latitude=43.651722;
longitude=22.702472;
```

```
site="Kozarnika";
culture="Kozarnikian";
author="AMH";
};
R_Date("OxA-35404",27600,400)
{
latitude=43.15;
longitude=24.71;
site="Tabashkata";
culture="Aurignacian Point";
author="AMH";
};
Date(Prior("MOD3 - Temnata - Date TD-V 5pg",
"Priors_Strat_DPhil/TD_Date_5pg_TD_V.prior",))
{
latitude=43.174969;
longitude=24.074006;
site="Temnata";
culture="Mousterian";
author="Neanderthal";
};
Date(Prior("MOD3 - Temnata - Date TD-V 3v",
"Priors_Strat_DPhil/TD_Date_3v_TD_V.prior",))
{
latitude=43.174969;
longitude=24.074006;
site="Temnata";
culture="Aurignacian-like";
author="AMH";
};
Date(Prior("MOD3 - Temnata - Date TD-V 3d",
"Priors_Strat_DPhil/TD_Date_3d_TD_V.prior",))
{
latitude=43.174969;
longitude=24.074006;
site="Temnata";
culture="Gravettian";
author="AMH";
};
R_Date("OxA-17967",38300,1500)
{
latitude=48.0468;
longitude=20.4264;
site="Pesko";
culture="Aurignacian Point";
author="AMH";
};
R_Date("OxA-17964",33500,450)
{
latitude=48.0468;
longitude=20.4264;
site="Pesko";
culture="Aurignacian Point";
author="AMH";
};
R_Date("OxA-17966",36400,800)
{
latitude=48.0468;
longitude=20.4264;
site="Pesko";
culture="Aurignacian Point";
author="AMH";
};
R_Date("OxA-19621",33750,350)
{
latitude=47.138;
longitude=5.571;
site="Trou de la Mere Clochette";
culture="Aurignacian Point";
author="AMH";
};
R_Date("OxA-19622",35460,250)
{
latitude=47.138;
longitude=5.571;
site="Trou de la Mere Clochette";
culture="Aurignacian Point";
author="AMH";
};
R_Date("OxA-14436",33640,250)
{
latitude=50.16944;
longitude=19.80723;
site="Mamutowa cave";
culture="Aurignacian Point";
author="AMH";
};
R_Date("OxA-14434",35460,220)
{
latitude=50.16944;
longitude=19.80723;
site="Mamutowa cave";
culture="Aurignacian Point";
author="AMH";
};
R_Date("OxA-17963",35600,400)
{
latitude=48.4922;
longitude=17.295;
site="Dzerava skala";
culture="Aurignacian Point";
author="AMH";
};
R_Date("OxA-X-2170-18",33600,900)
{
latitude=48.0654;
longitude=20.4108;
site="Istallosko";
culture="Aurignacian Point";
author="AMH";
};
R_Date("OxA-21783",32100,450)
{
latitude=42.1607;
longitude=2.74401;
site="Arbreda";
culture="Aurignacian Point";
author="AMH";
};
R_Date("OxA-13716",31730,250)
{
latitude=51.3204;
longitude= 2.9781;
site="Uphill Quarry cave 8 ";
culture="Aurignacian Point";
author="AMH";
};
R_Date("OxA-13803",31550,340)
{
latitude=51.2263;
longitude=2.6761;
site="Hyaena Den cave ";
culture="Aurignacian Point";
author="AMH";
};
R_Date("GrA-32619",32830,195)
{
latitude=50.4781;
longitude=4.679;
site="Grotte de la Betche-aux-Rotches, Spy";
culture="Aurignacian Point";
author="AMH";
};
R_Date("OxA-7496",30750,850)
{
latitude=50.421;
longitude=5.294;
site="Trou al'Wesse";
culture="Aurignacian Point";
author="AMH";
};
R_Date("KIA-19541",31310,235)
{
latitude=48.5603;
longitude=10.1913;
site="Vogelherd cave";
culture="Aurignacian Point";
author="AMH";
};
R_Date("KIA-19551",32470,265)
{
latitude=48.4089;
longitude=9.772;
site="Brillenhohle";
culture="Aurignacian Point";
author="AMH";
```

```
};
R_Date("KIA-19550[a]",30400,235)
{
latitude=48.4089;
longitude=9.772;
site="Brillenhohle";
culture="Aurignacian Point";
author="AMH";
};
R_Date("KIA-13082",26730,165)
{
latitude=48.3842;
longitude=9.7614;
site="Sirgenstein cave";
culture="Aurignacian Point";
author="AMH";
};
R_Date("KIA-13079",27250,175)
{
latitude=48.3842;
longitude=9.7614;
site="Sirgenstein cave";
culture="Aurignacian Point";
author="AMH";
};
R_Date("KIA-19543[a]",32010,494)
{
latitude=47.5924;
longitude=12.197;
site="Tischoferhohle";
culture="Aurignacian Point";
author="AMH";
};
R_Date("KIA-19544[a]",31530,205)
{
latitude=47.5924;
longitude=12.197;
site="Tischoferhohle";
culture="Aurignacian Point";
author="AMH";
};
R_Date("KIA-19545",29500,200)
{
latitude=47.5924;
longitude=12.197;
site="Tischoferhohle";
culture="Aurignacian Point";
author="AMH";
};
R_Date("VERA-2522",30140,335)
{
latitude=46.4493;
longitude=14.6691;
site="Potocka zijalka";
culture="Aurignacian Point";
author="AMH";
};
R_Date("OxA-27854",30800,370)
{
latitude=46.4493;
longitude=14.6691;
site="Potocka zijalka";
culture="Aurignacian Point";
author="AMH";
};
R_Date("OxA-28038",31950,450)
{
latitude=46.4493;
longitude=14.6691;
site="Potocka zijalka";
culture="Aurignacian Point";
author="AMH";
};
R_Date("OxA-28061",32550,550)
{
latitude=46.4493;
longitude=14.6691;
site="Potocka zijalka";
culture="Aurignacian Point";
author="AMH";
};
R_Date("OxA-27850",30380,370)
{
latitude=46.4493;
longitude=14.6691;
site="Potocka zijalka";
culture="Aurignacian Point";
author="AMH";
};
R_Date("OxA-27849",31220,400)
{
latitude=46.4493;
longitude=14.6691;
site="Potocka zijalka";
culture="Aurignacian Point";
author="AMH";
};
R_Date("OxA-27852",31360,400)
{
latitude=46.4493;
longitude=14.6691;
site="Potocka zijalka";
culture="Aurignacian Point";
author="AMH";
};
R_Date("OxA-27853",31500,400)
{
latitude=46.4493;
longitude=14.6691;
site="Potocka zijalka";
culture="Aurignacian Point";
author="AMH";
};
R_Date("OxA-27851",30910,380)
{
latitude=46.4493;
longitude=14.6691;
site="Potocka zijalka";
culture="Aurignacian Point";
author="AMH";
};
R_Date("OxA-15334",31600,900)
{
latitude=48.4922;
longitude=17.295;
site="Dzerava skala";
culture="Aurignacian Point";
author="AMH";
};
R_Date("OxA-15335",31000,1000)
{
latitude=48.4922;
longitude=17.295;
site="Dzerava skala";
culture="Aurignacian Point";
author="AMH";
};
R_Date("OxA-28219",29760,340)
{
latitude=46.112778;
longitude=13.915556;
site="Divije babe I";
culture="Aurignacian Point";
author="AMH";
};
R_Date("OxA-X-2517-52",34750,600)
{
latitude=46.308806;
longitude=14.568194;
site="Morkiska jama";
culture="Aurignacian Point";
author="AMH";
};
R_Date("OxA-27855",32600,450)
{
latitude=46.308806;
longitude=14.568194;
site="Morkiska jama";
culture="Aurignacian Point";
author="AMH";
};
};
```

Spatio-temporal distribution: map 2 – see figure 15.17

```
 Plot()
{
Date(Prior("Strat - Bacho Kiro - Date Mouserian",
"Priors_Strat/BachoKiro_Date_Mousterian.prior",))
{
latitude=42.947378;
longitude=25.331867;
site="Bacho Kiro";
culture="Mousterian";
author="Neanderthal";
};
Date(Prior("Strat - Willendorf II - Date D3",
"Priors_Strat/Willendorf_Date_Micoquian_D3.prior",))
{
latitude=48.323;
longitude=15.399;
site="Willendorf II";
culture="Micoquian";
author="Neanderthal";
};
Date(Prior("Strat - Labeko Koba - Date IX lower",
"Priors_Strat/LabekoKoba_Date_Chatelperronian.prior",))
{
latitude=43.066;
longitude=-2.458;
site="Labeko Koba";
culture="Chatelperronian";
author="Neanderthal";
};
Date(Prior("KDE - Moravia Szeletian",
"Priors_KDE/KDE_Szeletian_Moravia.prior",))
{
latitude=49.5;
longitude=17;
site="Moravia Szeletian";
culture="Szeletian";
author="Neanderthal";
};
Date(Prior("Strat - Ksar Akil - Date IUP",
"Priors_Strat/KsarAkil_Date_IUP.prior",))
{
latitude=33.916667;
longitude=35.6;
site="Ksar Akil";
culture="IUP";
author="AMH";
};
Date(Prior("Strat - Bacho Kiro - Date Bachokirian",
"Priors_Strat/BachoKiro_Date_Bachokirian.prior",))
{
latitude=42.947378;
longitude=25.331867;
site="Bacho Kiro";
culture="Bachokirian";
author="AMH";
};
Date(Prior("Strat - Castelcivita - Date Uluzzian",
"Priors_Strat/Castelcivitas_Uluzzian.prior",))
{
latitude=40.495;
longitude=15.237;
site="Castelcivita";
culture="Uluzzian";
author="AMH";
};
Date(Prior("KDE - Moravia Bohunician",
"Priors_KDE/KDE_Bohunician_Moravia.prior",))
{
latitude=49.5;
longitude=17;
site="Moravia Bohunician";
culture="Bohunician";
author="AMH";
};
Date(Prior("MOD3 - Kozarnika - Date 5c",
"Priors_Strat_DPhil/Kz_MOD3_Date_5c.prior",))
{
latitude=43.651722;
longitude=22.702472;
site="Kozarnika";
culture="Kozarnikian";
author="AMH";
};
Date(Prior("Strat - Fumane - Date A2",
"Priors_Strat/Fumane_Date_A2_Proto_Aurignacian.prior",))
{
latitude=45.57;
longitude=10.902;
site="Fumane";
culture="Proto-Aurignacian";
author="AMH";
};
Date(Prior("Strat - El Castillo - Date 18C",
"Priors_Strat/ElCastillo_Date_Transitional_Aurignacian_18C.prior",))
{
latitude=43.2875;
longitude=-3.9598;
site="El Castillo";
culture="'Transitional Aurignacian'";
author="AMH";
};
Date(Prior("Strat - Isturitz - Date C4d1",
"Priors_Strat/Isturitz_Date_Proto_Aurignacian_C4d1.prior",))
{
latitude=43.371;
longitude=-1.196;
site="Isturitz";
culture="Proto-/Early Aurignacian";
author="AMH";
};
R_Date("OxA-X-2732-11",31100,520)
{
latitude=45.3605642;
longitude=14.7527073;
site="Bukovac";
culture="Aurignacian Point";
author="AMH";
};
Date(Prior("MOD3 - Temnata - Date TD-V 4",
"Priors_Strat_DPhil/TD_Date_4_TD_V.prior",))
{
latitude=43.174969;
longitude=24.074006;
site="Temnata";
culture="Aurignacian-like";
author="AMH";
};
Date(Prior("Strat - Geissenklosterle - Date III",
"Priors_Strat/Geissenklosterle_EarlyAurig.prior",))
{
latitude=48.401;
longitude=9.772;
site="Geißenklösterle";
culture="Early Aurignacian";
author="AMH";
};
Date(Prior("Strat - Ksar Akil - Date Phase 2",
"Priors_Strat/KsarAkil_Date_Early_Ahmarian.prior",))
{
latitude=33.916667;
longitude=35.6;
site="Ksar Akil";
culture="Early Ahmarian";
author="AMH";
};
Date(Prior("Strat - Bacho Kiro - Date Aurignacian",
"Priors_Strat/BachoKiro_Date_Aurignacian.prior",))
{
latitude=42.947378;
longitude=25.331867;
site="Bacho Kiro";
culture="Aurignacian";
author="AMH";
};
Date(Prior("Strat - Geissenklosterle - Date II",
"Priors_Strat/Geissenklosterle_UpperAurig.prior",))
{
latitude=48.401;
longitude=9.772;
site="Geißenklösterle";
```

```
culture="Upper Aurignacian";
author="AMH";
};
Date(Prior("Strat - L'Arbreda - Date Evolved Aurig",
"Priors_Strat/LArbreda_Date_Evolved_Aurignacian.prior",))
{
latitude=42.161;
longitude=2.747;
site="L'Arbreda";
culture="Evolved Aurignacian";
author="AMH";
};
Date(Prior("Strat - Buran-Kaya III - Gravettian 6-2",
"Priors_Strat/BuranKayaIII_Date_Gravettian_6_2.prior",))
{
latitude=45.16;
longitude=34.396;
site="Buran-Kaya III";
culture="Gravettian";
author="AMH";
};
Date(Prior("Strat - Buran-Kaya III - Micoquian",
"Priors_Strat/BuranKayaIII_Date_Micoquian.prior",))
{
latitude=45.16;
longitude=34.396;
site="Buran-Kaya III";
culture="Micoquian";
author="Neanderthal";
};
Date(Prior("Strat - Buran-Kaya III - Aurignacian 6-5",
"Priors_Strat/BuranKayaIII_Date_Aurig_6_5.prior",))
{
latitude=45.16;
longitude=34.396;
site="Buran-Kaya III";
culture="Aurignacian";
author="AMH";
};
Date(Prior("Strat - Buran-Kaya III - Aurignacian 6-4",
"Priors_Strat/BuranKayaIII_Date_Aurig_6_4.prior",))
{
latitude=45.16;
longitude=34.396;
site="Buran-Kaya III";
culture="Aurignacian";
author="AMH";
};
Date(Prior("Strat - Buran-Kaya III - Aurignacian 6-3",
"Priors_Strat/BuranKayaIII_Date_Aurig_6_3.prior",))
{
latitude=45.16;
longitude=34.396;
site="Buran-Kaya III";
culture="Aurignacian";
author="AMH";
};
Date(Prior("Strat - Buran-Kaya III - Gravettian 6-1",
"Priors_Strat/BuranKayaIII_Date_Gravettian_6_1.prior",))
{
latitude=45.16;
longitude=34.396;
site="Buran-Kaya III";
culture="Gravettian";
author="AMH";
};
Date(Prior("Strat - Buran-Kaya III - Gravettian 5-2",
"Priors_Strat/BuranKayaIII_Date_Gravettian_5_2.prior",))
{
latitude=45.16;
longitude=34.396;
site="Buran-Kaya III";
culture="Gravettian";
author="AMH";
};
Date(Prior("Strat - Castelcivita - Date Mousterian",
"Priors_Strat/Castelcivita_Mousterian.prior",))
{
latitude=40.495;
longitude=15.237;
site="Castelcivita";
culture="Mousterian";
author="Neanderthal";
};
Date(Prior("Strat - Castelcivita - Date Aurignacian",
"Priors_Strat/Castelcivita_Aurignacian.prior",))
{
latitude=40.495;
longitude=15.237;
site="Castelcivita";
culture="Aurignacian";
author="AMH";
};
Date(Prior("Strat - Cavallo - Date EII/I",
"Priors_Strat/CAVALLO_Date_EII_I_Uluzzian.prior",))
{
latitude=40.154;
longitude=17.96;
site="Cavallo";
culture="Uluzzian";
author="AMH";
};
Date(Prior("Strat - Cavallo - Date E/D",
"Priors_Strat/CAVALLO_Date_E_D_Uluzzian.prior",))
{
latitude=40.154;
longitude=17.96;
site="Cavallo";
culture="Uluzzian";
author="AMH";
};
Date(Prior("Strat - Cavallo - Date DII",
"Priors_Strat/CAVALLO_Date_DII_Uluzzian.prior",))
{
latitude=40.154;
longitude=17.96;
site="Cavallo";
culture="Uluzzian";
author="AMH";
};
Date(Prior("Strat - Cavallo - Date Dib",
"Priors_Strat/CAVALLO_Date_DIb_Uluzzian.prior",))
{
latitude=40.154;
longitude=17.96;
site="Cavallo";
culture="Uluzzian";
author="AMH";
};
Date(Prior("Strat - El Castillo - Date 20C",
"Priors_Strat/ElCastillo_Date_Mousterian.prior",))
{
latitude=43.2875;
longitude=-3.9598;
site="El Castillo";
culture="Mousterian";
author="Neanderthal";
};
Date(Prior("Strat - El Castillo - Date 18B",
"Priors_Strat/ElCastillo_Date_Transitional_Aurignacian_18B.prior",))
{
latitude=43.2875;
longitude=-3.9598;
site="El Castillo";
culture="'Transitional Aurignacian'";
author="AMH";
};
Date(Prior("Strat - Fumane - Date A4",
"Priors_Strat/Fumane_Date_A4_Uluzzian.prior",))
{
latitude=45.57;
longitude=10.902;
site="Fumane";
culture="Uluzzian";
author="AMH";
};
Date(Prior("Strat - Fumane - Date A3",
"Priors_Strat/Fumane_Date_A3_Uluzzian.prior",))
{
latitude=45.57;
longitude=10.902;
site="Fumane";
culture="Uluzzian";
author="AMH";
};
Date(Prior("Strat - Fumane - Date A1",
```

```
"Priors_Strat/Fumane_Date_A1_Proto_Aurignacian.prior",))
{
latitude=45.57;
longitude=10.902;
site="Fumane";
culture="Proto-Aurignacian";
author="AMH";
};
Date(Prior("Strat - Fumane - Date D",
"Priors_Strat/Fumane_Date_D_Aurignacian.prior",))
{
latitude=45.57;
longitude=10.902;
site="Fumane";
culture="Aurignacian";
author="AMH";
};
Date(Prior("Strat - Geissenklosterle - Date IV",
"Priors_Strat/Geissenklosterle_Mousterian.prior",))
{
latitude=48.401;
longitude=9.772;
site="Geißenklösterle";
culture="Mousterian";
author="Neanderthal";
};
Date(Prior("Strat - Geissenklosterle - Date I",
"Priors_Strat/Geissenklosterle_Gravettian.prior",))
{
latitude=48.401;
longitude=9.772;
site="Geißenklösterle";
culture="Gravettian";
author="AMH";
};
Date(Prior("Strat - Hohle Fels - Date IX",
"Priors_Strat/HohleFels_Date_IX_Mousterian.prior",))
{
latitude=48.378;
longitude=9.758;
site="Hohle Fels";
culture="Mousterian";
author="Neanderthal";
};
Date(Prior("Strat - Hohle Fels - Date VIII",
"Priors_Strat/HohleFels_Date_VIII_Mousterian.prior",))
{
latitude=48.378;
longitude=9.758;
site="Hohle Fels";
culture="Mousterian";
author="Neanderthal";
};
Date(Prior("Strat - Hohle Fels - Date VII",
"Priors_Strat/HohleFels_Date_VII_Mousterian.prior",))
{
latitude=48.378;
longitude=9.758;
site="Hohle Fels";
culture="Mousterian";
author="Neanderthal";
};
Date(Prior("Strat - Hohle Fels - Date VI",
"Priors_Strat/HohleFels_Date_VI_Mousterian.prior",))
{
latitude=48.378;
longitude=9.758;
site="Hohle Fels";
culture="Mousterian";
author="Neanderthal";
};
Date(Prior("Strat - Hohle Fels - Date V",
"Priors_Strat/HohleFels_Date_V_Aurignacian.prior",))
{
latitude=48.378;
longitude=9.758;
site="Hohle Fels";
culture="Aurignacian";
author="AMH";
};
Date(Prior("Strat - Hohle Fels - Date IV",
"Priors_Strat/HohleFels_Date_IV_Aurignacian.prior",))
{
latitude=48.378;
longitude=9.758;
site="Hohle Fels";
culture="Aurignacian";
author="AMH";
};
Date(Prior("Strat - Hohle Fels - Date III",
"Priors_Strat/HohleFels_Date_III_Aurignacian.prior",))
{
latitude=48.378;
longitude=9.758;
site="Hohle Fels";
culture="Aurignacian";
author="AMH";
};
Date(Prior("Strat - Hohle Fels - Date II",
"Priors_Strat/HohleFels_Date_II_Aurignacian.prior",))
{
latitude=48.378;
longitude=9.758;
site="Hohle Fels";
culture="Aurignacian";
author="AMH";
};
Date(Prior("KDE - Hohlenstein-Stadel",
"Priors_KDE/KDE_Hohlenstein_Stadel_short_.prior",))
{
latitude=48.551;
longitude=10.168;
site="Hohlenstein-Stadel";
culture="Aurignacian";
author="AMH";
};
Date(Prior("Strat - Isturitz - Date C5",
"Priors_Strat/Isturitz_Date_Proto_Aurignacian_C5.prior",))
{
latitude=43.371;
longitude=-1.196;
site="Isturitz";
culture="Proto-Aurignacian";
author="AMH";
};
Date(Prior("Strat - Isturitz - Date C4c4",
"Priors_Strat/Isturitz_ProtoEarly_Aurignacian_C4c4.prior",))
{
latitude=43.371;
longitude=-1.196;
site="Isturitz";
culture="Proto-Aurignacian";
author="AMH";
};
Date(Prior("Strat - Isturitz - Date C4b2",
"Priors_Strat/Isturitz_Date_Early_Aurignacian_C4b2.prior",))
{
latitude=43.371;
longitude=-1.196;
site="Isturitz";
culture="Early Aurignacian";
author="AMH";
};
Date(Prior("Strat - Isturitz - Date C4b1",
"Priors_Strat/Isturitz_Date_Early_Aurignacian_C4b1.prior",))
{
latitude=43.371;
longitude=-1.196;
site="Isturitz";
culture="Early Aurignacian";
author="AMH";
};
Date(Prior("Strat - Ksar Akil - Date Mousterian",
"Priors_Strat/KsarAkil_Date_Mousterian.prior",))
{
latitude=33.916667;
longitude=35.6;
site="Ksar Akil";
culture="Mousterian";
author="Neanderthal";
};
Date(Prior("Strat - Ksar Akil - Date Phase 3-4",
"Priors_Strat/KsarAkil_Date_Phases_3_4.prior",))
{
latitude=33.916667;
longitude=35.6;
```

```
site="Ksar Akil";
culture="Early Ahmarian";
author="AMH";
};
Date(Prior("Strat - Ksar Akil - Date Phase 5",
"Priors_Strat/KsarAkil_Date_Phases_5.prior",))
{
latitude=33.916667;
longitude=35.6;
site="Ksar Akil";
culture="Early Ahmarian";
author="AMH";
};
Date(Prior("Strat - Ksar Akil - Date Phase 6",
"Priors_Strat/KsarAkil_Date_Phases_6.prior",))
{
latitude=33.916667;
longitude=35.6;
site="Ksar Akil";
culture="Early Ahmarian";
author="AMH";
};
Date(Prior("Strat - Ksar Akil - Date Phase 7",
"Priors_Strat/KsarAkil_Date_Phases_7.prior",))
{
latitude=33.916667;
longitude=35.6;
site="Ksar Akil";
culture="Early Ahmarian";
author="AMH";
};
Date(Prior("Strat - L'Arbreda - Date Mousterian",
"Priors_Strat/LArbreda_Date_Mousterian.prior",))
{
latitude=42.161;
longitude=2.747;
site="L'Arbreda";
culture="Mousterian";
author="Neanderthal";
};
Date(Prior("Strat - L'Arbreda - Date Proto-Aurig",
"Priors_Strat/LArbreda_Date_Proto_Aurignacian.prior",))
{
latitude=42.161;
longitude=2.747;
site="L'Arbreda";
culture="Proto-Aurignacian";
author="AMH";
};
Date(Prior("Strat - L'Arbreda - Date Gravettian F",
"Priors_Strat/LArbreda_Date_Gravettian_F.prior",))
{
latitude=42.161;
longitude=2.747;
site="L'Arbreda";
culture="Gravettian";
author="AMH";
};
Date(Prior("Strat - L'Arbreda - Date Gravettian E",
"Priors_Strat/LArbreda_Date_Gravettian_E.prior",))
{
latitude=42.161;
longitude=2.747;
site="L'Arbreda";
culture="Gravettian";
author="AMH";
};
Date(Prior("Strat - Labeko Koba - Date VII",
"Priors_Strat/LabekoKoba_Date_Proto_Aurignacian.prior",))
{
latitude=43.066;
longitude=-2.458;
site="Labeko Koba";
culture="Proto-Aurignacian";
author="AMH";
};
Date(Prior("Strat - Labeko Koba - Date VI",
"Priors_Strat/LabekoKoba_Date_Early_Aurignacian_VI.prior",))
{
latitude=43.066;
longitude=-2.458;
site="Labeko Koba";
culture="Early Aurignacian";
author="AMH";
};
Date(Prior("Strat - Labeko Koba - Date V",
"Priors_Strat/LabekoKoba_Date_Early_Aurignacian_V.prior",))
{
latitude=43.066;
longitude=-2.458;
site="Labeko Koba";
culture="Early Aurignacian";
author="AMH";
};
Date(Prior("Strat - Labeko Koba - Date IV",
"Priors_Strat/LabekoKoba_Date_Early_Aurignacian_IV.prior",))
{
latitude=43.066;
longitude=-2.458;
site="Labeko Koba";
culture="Early Aurignacian";
author="AMH";
};
Date(Prior("KDE - Mitoc-Malul Galben",
"Priors_KDE/KDE_Mitoc_Malul_Galben.prior",))
{
latitude=48.111;
longitude=27.036;
site="Mitoc-Malul Galben";
culture="Aurignacian";
author="AMH";
};
Date(Prior("KDE - Moravia Aurignacian",
"Priors_KDE/KDE_Aurignacian_Moravia.prior",))
{
latitude=49.5;
longitude=17;
site="Moravia Aurignacian";
culture="Aurignacian";
author="AMH";
};
Date(Prior("Strat - Riparo Mochi - Date Proto-Aurig",
"Priors_Strat/RiparoMochi_Date_Proto_Aurignacian.prior",))
{
latitude=43.7894;
longitude=7.5475;
site="Riparo Mochi";
culture="Proto-Aurignacian";
author="AMH";
};
Date(Prior("Strat - Riparo Mochi - Date Early Aurig",
"Priors_Strat/RiparoMochi_Date_Early_Aurignacian.prior",))
{
latitude=43.7894;
longitude=7.5475;
site="Riparo Mochi";
culture="Early Aurignacian";
author="AMH";
};
Date(Prior("Strat - Riparo Mochi - Date Gravettian",
"Priors_Strat/RiparoMochi_Date_Gravettian.prior",))
{
latitude=43.7894;
longitude=7.5475;
site="Riparo Mochi";
culture="Gravettian";
author="AMH";
};
Date(Prior("Strat - Salitrena Pecina - Date Aurignacian",
"Priors_Strat/SalitrenaPecina_Date_Aurignacian.prior",))
{
latitude=44.1905;
longitude=20.0835;
site="Šalitrena Pećina";
culture="Aurignacian";
author="AMH";
};
Date(Prior("KDE - Vogelherd",
"Priors_KDE/KDE_Vogelherd.prior",))
{
latitude=48.5606;
longitude=10.1913;
site="Vogelherd";
culture="Aurignacian";
author="AMH";
};
```

```
Date(Prior("Strat - Willendorf II - Date D1/D2",
"Priors_Strat/Willendorf_Date_Micoquian_D1_D2.prior",))
{
latitude=48.323;
longitude=15.399;
site="Willendorf II";
culture="Micoquian";
author="Neanderthal";
};
Date(Prior("Strat - Willendorf II - Date C8-3",
"Priors_Strat/Willendorf_Date_Early_Aurignaican_C8_3.prior",))
{
latitude=48.323;
longitude=15.399;
site="Willendorf II";
culture="Early Aurignacian";
author="AMH";
};
Date(Prior("Strat - Willendorf II - Date C8-2",
"Priors_Strat/Willendorf_Date_Aurignaican_C8_2.prior",))
{
latitude=48.323;
longitude=15.399;
site="Willendorf II";
culture="Aurignacian";
author="AMH";
};
Date(Prior("Strat - Willendorf II - Date C7-1",
"Priors_Strat/Willendorf_Date_Aurignaican_C7_1.prior",))
{
latitude=48.323;
longitude=15.399;
site="Willendorf II";
culture="Aurignacian";
author="AMH";
};
Date(Prior("Strat - Willendorf II - Date C4-2",
"Priors_Strat/Willendorf_Date_C4_2.prior",))
{
latitude=48.323;
longitude=15.399;
site="Willendorf II";
culture="Aurignacian";
author="AMH";
};
Date(Prior("Strat - Willendorf II - Date C4-1",
"Priors_Strat/Willendorf_Date_C4_1.prior",))
{
latitude=48.323;
longitude=15.399;
site="Willendorf II";
culture="Aurignacian";
author="AMH";
};
Date(Prior("MOD10 - Dzerava Skala - Date 5a",
"Priors_Strat_DPhil/Der_MOD10_Date_5a_.prior",))
{
latitude=48.496987;
longitude=17.324692;
site="Dzerava Skala";
culture="Aurignacian Point";
author="AMH";
};
Date(Prior("MOD10 - Dzerava Skala - Date 9",
"Priors_Strat_DPhil/Der_MOD10_Date_9.prior",))
{
latitude=48.496987;
longitude=17.324692;
site="Dzerava Skala";
culture="Aurignacian Point";
author="AMH";
};
Date(Prior("MOD10 - Dzerava Skala - Date 5",
"Priors_Strat_DPhil/Der_MOD10_Date_5.prior",))
{
latitude=48.496987;
longitude=17.324692;
site="Dzerava Skala";
culture="Gravettian";
author="AMH";
};
Date(Prior("MOD10 - Dzerava Skala - Date 4",
"Priors_Strat_DPhil/Der_MOD10_Date_4.prior",))
{
latitude=48.496987;
longitude=17.324692;
site="Dzerava Skala";
culture="Gravettian";
author="AMH";
};
Date(Prior("Points KDE2 - Istallosko",
"Priors_KDE_DPhil/Istall_Points_KDE_2.prior",))
{
latitude=48.071667;
longitude=20.418889;
site="Istallosko";
culture="Aurignacian Point";
author="AMH";
};
R_Date("OxA-X-2716-49",31800,1000)
{
latitude=47.723889;
longitude=18.575278;
site="Jankovich";
culture="Aurignacian Point";
author="AMH";
};
R_Date("OxA-X-2716-48",32500,800)
{
latitude=47.723889;
longitude=18.575278;
site="Jankovich";
culture="Aurignacian Point";
author="AMH";
};
R_Date("OxA-X-2732-10",32750,670)
{
latitude=47.723889;
longitude=18.575278;
site="Jankovich";
culture="Aurignacian Point";
author="AMH";
};
R_Date("OxA-35386",30800,500)
{
latitude=47.723889;
longitude=18.575278;
site="Jankovich";
culture="Aurignacian Point";
author="AMH";
};
Date(Prior("MOD3 - Kozarnika - Date 6/7 ls lp",
"Priors_Strat_DPhil/Kz_MOD3_Date_6_7_ls_lp.prior",))
{
latitude=43.651722;
longitude=22.702472;
site="Kozarnika";
culture="IUP";
author="AMH";
};
Date(Prior("MOD3 - Kozarnika - Date 6/7 lb",
"Priors_Strat_DPhil/Kz_MOD3_Date_6_7_lb.prior",))
{
latitude=43.651722;
longitude=22.702472;
site="Kozarnika";
culture="IUP";
author="AMH";
};
Date(Prior("MOD3 - Kozarnika - Date 5b",
"Priors_Strat_DPhil/Kz_MOD3_Date_5b.prior",))
{
latitude=43.651722;
longitude=22.702472;
site="Kozarnika";
culture="Kozarnikian";
author="AMH";
};
Date(Prior("MOD3 - Kozarnika - Date 5a",
"Priors_Strat_DPhil/Kz_MOD3_Date_5a.prior",))
{
latitude=43.651722;
longitude=22.702472;
site="Kozarnika";
culture="Kozarnikian";
author="AMH";
```

```
};
Date(Prior("MOD3 - Kozarnika - Date 4",
"Priors_Strat_DPhil/Kz_MOD3_Date_4.prior",))
{
latitude=43.651722;
longitude=22.702472;
site="Kozarnika";
culture="Kozarnikian";
author="AMH";
};
R_Date("OxA-35404",27600,400)
{
latitude=43.15;
longitude=24.71;
site="Tabashkata";
culture="Aurignacian Point";
author="AMH";
};
Date(Prior("MOD3 - Temnata - Date TD-V 5pg",
"Priors_Strat_DPhil/TD_Date_5pg_TD_V.prior",))
{
latitude=43.174969;
longitude=24.074006;
site="Temnata";
culture="Mousterian";
author="Neanderthal";
};
Date(Prior("MOD3 - Temnata - Date TD-V 3v",
"Priors_Strat_DPhil/TD_Date_3v_TD_V.prior",))
{
latitude=43.174969;
longitude=24.074006;
site="Temnata";
culture="Aurignacian-like";
author="AMH";
};
Date(Prior("MOD3 - Temnata - Date TD-V 3d",
"Priors_Strat_DPhil/TD_Date_3d_TD_V.prior",))
{
latitude=43.174969;
longitude=24.074006;
site="Temnata";
culture="Gravettian";
author="AMH";
};
R_Date("OxA-17967",38300,1500)
{
latitude=48.0468;
longitude=20.4264;
site="Pesko";
culture="Aurignacian Point";
author="AMH";
};
R_Date("OxA-17964",33500,450)
{
latitude=48.0468;
longitude=20.4264;
site="Pesko";
culture="Aurignacian Point";
author="AMH";
};
R_Date("OxA-17966",36400,800)
{
latitude=48.0468;
longitude=20.4264;
site="Pesko";
culture="Aurignacian Point";
author="AMH";
};
R_Date("OxA-19621",33750,350)
{
latitude=47.138;
longitude=5.571;
site="Trou de la Mere Clochette";
culture="Aurignacian Point";
author="AMH";
};
R_Date("OxA-19622",35460,250)
{
latitude=47.138;
longitude=5.571;
site="Trou de la Mere Clochette";
culture="Aurignacian Point";
author="AMH";
};
R_Date("OxA-14436",33640,250)
{
latitude=50.16944;
longitude=19.80723;
site="Mamutowa cave";
culture="Aurignacian Point";
author="AMH";
};
R_Date("OxA-14434",35460,220)
{
latitude=50.16944;
longitude=19.80723;
site="Mamutowa cave";
culture="Aurignacian Point";
author="AMH";
};
R_Date("OxA-17963",35600,400)
{
latitude=48.4922;
longitude=17.295;
site="Dzerava skala";
culture="Aurignacian Point";
author="AMH";
};
R_Date("OxA-X-2170-18",33600,900)
{
latitude=48.0654;
longitude=20.4108;
site="Istallosko";
culture="Aurignacian Point";
author="AMH";
};
R_Date("OxA-21783",32100,450)
{
latitude=42.1607;
longitude=2.74401;
site="Arbreda";
culture="Aurignacian Point";
author="AMH";
};
R_Date("OxA-13716",31730,250)
{
latitude=51.3204;
longitude= 2.9781;
site="Uphill Quarry cave 8 ";
culture="Aurignacian Point";
author="AMH";
};
R_Date("OxA-13803",31550,340)
{
latitude=51.2263;
longitude=2.6761;
site="Hyaena Den cave ";
culture="Aurignacian Point";
author="AMH";
};
R_Date("GrA-32619",32830,195)
{
latitude=50.4781;
longitude=4.679;
site="Grotte de la Betche-aux-Rotches, Spy";
culture="Aurignacian Point";
author="AMH";
};
R_Date("OxA-7496",30750,850)
{
latitude=50.421;
longitude=5.294;
site="Trou al'Wesse";
culture="Aurignacian Point";
author="AMH";
};
R_Date("KIA-19541",31310,235)
{
latitude=48.5603;
longitude=10.1913;
site="Vogelherd cave";
culture="Aurignacian Point";
author="AMH";
};
R_Date("KIA-19551",32470,265)
```

```
{
latitude=48.4089;
longitude=9.772;
site="Brillenhohle";
culture="Aurignacian Point";
author="AMH";
};
R_Date("KIA-19550[a]",30400,235)
{
latitude=48.4089;
longitude=9.772;
site="Brillenhohle";
culture="Aurignacian Point";
author="AMH";
};
R_Date("KIA-13082",26730,165)
{
latitude=48.3842;
longitude=9.7614;
site="Sirgenstein cave";
culture="Aurignacian Point";
author="AMH";
};
R_Date("KIA-13079",27250,175)
{
latitude=48.3842;
longitude=9.7614;
site="Sirgenstein cave";
culture="Aurignacian Point";
author="AMH";
};
R_Date("KIA-19543[a]",32010,494)
{
latitude=47.5924;
longitude=12.197;
site="Tischoferhohle";
culture="Aurignacian Point";
author="AMH";
};
R_Date("KIA-19544[a]",31530,205)
{
latitude=47.5924;
longitude=12.197;
site="Tischoferhohle";
culture="Aurignacian Point";
author="AMH";
};
R_Date("KIA-19545",29500,200)
{
latitude=47.5924;
longitude=12.197;
site="Tischoferhohle";
culture="Aurignacian Point";
author="AMH";
};
R_Date("VERA-2522",30140,335)
{
latitude=46.4493;
longitude=14.6691;
site="Potocka zijalka";
culture="Aurignacian Point";
author="AMH";
};
R_Date("OxA-27854",30800,370)
{
latitude=46.4493;
longitude=14.6691;
site="Potocka zijalka";
culture="Aurignacian Point";
author="AMH";
};
R_Date("OxA-28038",31950,450)
{
latitude=46.4493;
longitude=14.6691;
site="Potocka zijalka";
culture="Aurignacian Point";
author="AMH";
};
R_Date("OxA-28061",32550,550)
{
latitude=46.4493;
longitude=14.6691;
site="Potocka zijalka";
culture="Aurignacian Point";
author="AMH";
};
R_Date("OxA-27850",30380,370)
{
latitude=46.4493;
longitude=14.6691;
site="Potocka zijalka";
culture="Aurignacian Point";
author="AMH";
};
R_Date("OxA-27849",31220,400)
{
latitude=46.4493;
longitude=14.6691;
site="Potocka zijalka";
culture="Aurignacian Point";
author="AMH";
};
R_Date("OxA-27852",31360,400)
{
latitude=46.4493;
longitude=14.6691;
site="Potocka zijalka";
culture="Aurignacian Point";
author="AMH";
};
R_Date("OxA-27853",31500,400)
{
latitude=46.4493;
longitude=14.6691;
site="Potocka zijalka";
culture="Aurignacian Point";
author="AMH";
};
R_Date("OxA-27851",30910,380)
{
latitude=46.4493;
longitude=14.6691;
site="Potocka zijalka";
culture="Aurignacian Point";
author="AMH";
};
R_Date("OxA-15334",31600,900)
{
latitude=48.4922;
longitude=17.295;
site="Dzerava skala";
culture="Aurignacian Point";
author="AMH";
};
R_Date("OxA-15335",31000,1000)
{
latitude=48.4922;
longitude=17.295;
site="Dzerava skala";
culture="Aurignacian Point";
author="AMH";
};
R_Date("OxA-28219",29760,340)
{
latitude=46.112778;
longitude=13.915556;
site="Divije babe I";
culture="Aurignacian Point";
author="AMH";
};
R_Date("OxA-X-2517-52",34750,600)
{
latitude=46.308806;
longitude=14.568194;
site="Morkiska jama";
culture="Aurignacian Point";
author="AMH";
};
R_Date("OxA-27855",32600,450)
{
latitude=46.308806;
longitude=14.568194;
site="Morkiska jama";
culture="Aurignacian Point";
author="AMH";
```

```
};
Label("Humans");
R_Date("OxA-21839",39700,1100)
{
longitude=40.0034;
latitude=44.2217;
culture="MP";
author="Neanderthal";
species="Neanderthal";
site="Mezmaiskaya";
};
Date("OxA-15257",N(calBP(48900),1100))
{
longitude=0.741;
latitude=46.415;
culture="Mousterian";
author="Neanderthal";
species="Neanderthal";
site="Les Rochers-de-Villeneuve";
};
R_Date("ETH-20981",39900,620)
{
longitude=6.9363;
latitude=51.2206;
culture="MP";
author="Neanderthal";
species="Neanderthal";
site="Kleine Feldhöfergrotte";
};
R_Date("ETH-19660",39240,670)
{
longitude=6.9363;
latitude=51.2206;
culture="MP";
author="Neanderthal";
species="Neanderthal";
site="Kleine Feldhöfergrotte";
};
R_Date("GrA-32626",36350,295)
{
longitude=4.6743;
latitude=50.4803;
culture="LRJ or Mousterian";
author="Neanderthal";
species="Neanderthal";
site="Spy";
};
R_Date("GrA-32623",35810,250)
{
longitude=4.6743;
latitude=50.4803;
culture="LRJ or Mousterian";
author="Neanderthal";
species="Neanderthal";
site="Spy";
};
R_Date("ETH-19661",40360,760)
{
longitude=6.9363;
latitude=51.2206;
culture="MP";
author="Neanderthal";
species="Neanderthal";
site="Kleine Feldhöfergrotte";
};
R_Date("OxA-10560",36250,500)
{
longitude=4.6743;
latitude=50.4803;
culture="unknown";
author="Neanderthal";
species="Neanderthal";
site="Spy";
};
Date("GifA-99167",N(calBP(55090),2600))
{
longitude=-5.733;
latitude=43.386;
culture="Mousterian";
author="Neanderthal";
species="Neanderthal";
site="El Sidron";
};
Date("GifA-99704",N(calBP(54930),2500))
{
longitude=-5.733;
latitude=43.386;
culture="Mousterian";
author="Neanderthal";
species="Neanderthal";
site="El Sidron";
};
Date("OxA-21776",N(calBP(56230),3200))
{
longitude=-5.733;
latitude=43.386;
culture="Mousterian";
author="Neanderthal";
species="Neanderthal";
site="El Sidron";
};
R_Date("OxA-X-2689-09",42700,1600)
{
longitude=16.088;
latitude=46.305;
culture="MP";
author="Neanderthal";
species="Neanderthal";
site="Vindija";
};
Date("OxA-X-2689-10",N(calBP(48800),2000))
{
longitude=16.088;
latitude=46.305;
culture="MP";
author="Neanderthal";
species="Neanderthal";
site="Vindija";
};
R_Date("OxA-X-2717-11",44300,1200)
{
longitude=16.088;
latitude=46.305;
culture="MP";
author="Neanderthal";
species="Neanderthal";
site="Vindija";
};
Date("OxA-X-2687-57",N(calBP(49960),1500))
{
longitude=16.088;
latitude=46.305;
culture="MP";
author="Neanderthal";
species="Neanderthal";
site="Vindija";
};
R_Date("GrA-50457",32450,240)
{
longitude=34.396;
latitude=45.16;
culture="Gravettian";
author="AMH";
species="AMH";
site="Buran-Kaya III";
};
R_Date("GrA-24398",28890,170)
{
longitude=21.91;
latitude=45.0177;
culture="unknown";
author="AMH";
species="AMH";
site="Pestera cu Oase";
};
R_Date("OxA-4586",31000,500)
{
longitude=20.1563;
latitude=49.443;
culture="Aurignacian";
author="AMH";
species="AMH";
site="Oblazowa";
};
R_Date("VERA-3074",31320,400)
{
```

```
longitude=17.0167;
latitude=49.707;
culture="Aurignacian";
author="AMH";
species="AMH";
site="Mladec";
};
R_Date("OxA-11711",34950,990)
{
longitude=21.91;
latitude=45.0177;
culture="unknown";
author="AMH";
species="AMH";
site="Pestera cu Oase";
};
R_Date("GrA-37938",31900,230)
{
longitude=34.396;
latitude=45.16;
culture="Gravettian";
author="AMH";
species="AMH";
site="Buran-Kaya III";
};
R_Date("VERA-3073",31190,400)
{
longitude=17.0167;
latitude=49.707;
culture="Aurignacian";
author="AMH";
species="AMH";
site="Mladec";
};
R_Date("VERA-3076 A",31500,410)
{
longitude=17.0167;
latitude=49.707;
culture="Aurignacian";
author="AMH";
species="AMH";
site="Mladec";
};
R_Date("OxA-16412",28870,180)
{
longitude=-4.2555;
latitude=51.5499;
culture="Gravettian";
author="AMH";
species="";
site="Paviland";
};
R_Date("OxA-16413",29490,210)
{
longitude=-4.2555;
latitude=51.5499;
culture="Gravettian";
author="AMH";
species="";
site="Paviland";
};
R_Date("ERL-9415",30640,640)
{
longitude=3.0905;
latitude=43.1313;
culture="Aurignacian";
author="AMH";
species="AMH";
site="La Crouzade";
};
R_Date("OxA-15527",28150,170)
{
longitude=23.1296;
latitude=45.5862;
culture="Aurignacian?";
author="AMH";
species="AMH";
site="Cioclovina";
};
R_Date("OxA-15529",29930,170)
{
longitude=23.755;
latitude=45.1895;
culture="Uluzzian";
author="AMH";
species="AMH";
site="Pestera Muierii";
};
R_Date("OxA-16252",29110,190)
{
longitude=23.755;
latitude=45.1895;
culture="Uluzzian";
author="AMH";
species="AMH";
site="Pestera Muierii";
};
R_Date("OxA-13302",32790,280)
{
longitude=34.396;
latitude=45.16;
culture="Gravettian";
author="AMH";
species="AMH";
site="Buran-Kaya III";
};
};
```

Spatio-temporal distribution: map 2 modified – see figure 15.18-a

```
 Plot()
{
Date(Prior("Strat - Bacho Kiro - Date Mouserian",
"Priors_Strat/BachoKiro_Date_Mousterian.prior",))
{
latitude=42.947378;
longitude=25.331867;
site="Bacho Kiro";
culture="Mousterian";
author="Neanderthal";
};
Date(Prior("Strat - Willendorf II - Date D3",
"Priors_Strat/Willendorf_Date_Micoquian_D3.prior",))
{
latitude=48.323;
longitude=15.399;
site="Willendorf II";
culture="Micoquian";
author="Neanderthal";
};
Date(Prior("Strat - Labeko Koba - Date IX lower",
"Priors_Strat/LabekoKoba_Date_Chatelperronian.prior",))
{
latitude=43.066;
longitude=-2.458;
site="Labeko Koba";
culture="Chatelperronian";
author="Neanderthal";
};
Date(Prior("KDE - Moravia Szeletian",
"Priors_KDE/KDE_Szeletian_Moravia.prior",))
{
latitude=49.5;
longitude=17;
site="Moravia Szeletian";
culture="Szeletian";
author="Neanderthal";
};
```

```
Date(Prior("Strat - Ksar Akil - Date IUP",
"Priors_Strat/KsarAkil_Date_IUP.prior",))
{
latitude=33.916667;
longitude=35.6;
site="Ksar Akil";
culture="IUP";
author="AMH";
};
Date(Prior("Strat - Bacho Kiro - Date Bachokirian",
"Priors_Strat/BachoKiro_Date_Bachokirian.prior",))
{
latitude=42.947378;
longitude=25.331867;
site="Bacho Kiro";
culture="Bachokirian";
author="AMH";
};
Date(Prior("Strat - Castelcivita - Date Uluzzian",
"Priors_Strat/Castelcivitas_Uluzzian.prior",))
{
latitude=40.495;
longitude=15.237;
site="Castelcivita";
culture="Uluzzian";
author="Neanderthal";
};
Date(Prior("KDE - Moravia Bohunician",
"Priors_KDE/KDE_Bohunician_Moravia.prior",))
{
latitude=49.5;
longitude=17;
site="Moravia Bohunician";
culture="Bohunician";
author="AMH";
};
Date(Prior("MOD3 - Kozarnika - Date 5c",
"Priors_Strat_DPhil/Kz_MOD3_Date_5c.prior",))
{
latitude=43.651722;
longitude=22.702472;
site="Kozarnika";
culture="Kozarnikian";
author="AMH";
};
Date(Prior("Strat - Fumane - Date A2",
"Priors_Strat/Fumane_Date_A2_Proto_Aurignacian.prior",))
{
latitude=45.57;
longitude=10.902;
site="Fumane";
culture="Proto-Aurignacian";
author="AMH";
};
Date(Prior("Strat - El Castillo - Date 18C",
"Priors_Strat/ElCastillo_Date_Transitional_
Aurignacian_18C.prior",))
{
latitude=43.2875;
longitude=-3.9598;
site="El Castillo";
culture="‘Transitional Aurignacian’";
author="AMH";
};
Date(Prior("Strat - Isturitz - Date C4d1",
"Priors_Strat/Isturitz_Date_Proto_Aurignacian_C4d1.prior",))
{
latitude=43.371;
longitude=-1.196;
site="Isturitz";
culture="Proto-/Early Aurignacian";
author="AMH";
};
R_Date("OxA-X-2732-11",31100,520)
{
latitude=45.3605642;
longitude=14.7527073;
site="Bukovac";
culture="Aurignacian Point";
author="AMH";
};
Date(Prior("MOD3 - Temnata - Date TD-V 4",
"Priors_Strat_DPhil/TD_Date_4_TD_V.prior",))
{
latitude=43.174969;
longitude=24.074006;
site="Temnata";
culture="Aurignacian-like";
author="AMH";
};
Date(Prior("Strat - Geissenklosterle - Date III",
"Priors_Strat/Geissenklosterle_EarlyAurig.prior",))
{
latitude=48.401;
longitude=9.772;
site="Geißenklösterle";
culture="Early Aurignacian";
author="AMH";
};
Date(Prior("Strat - Ksar Akil - Date Phase 2",
"Priors_Strat/KsarAkil_Date_Early_Ahmarian.prior",))
{
latitude=33.916667;
longitude=35.6;
site="Ksar Akil";
culture="Early Ahmarian";
author="AMH";
};
Date(Prior("Strat - Bacho Kiro - Date Aurignacian",
"Priors_Strat/BachoKiro_Date_Aurignacian.prior",))
{
latitude=42.947378;
longitude=25.331867;
site="Bacho Kiro";
culture="Aurignacian";
author="AMH";
};
Date(Prior("Strat - Geissenklosterle - Date II",
"Priors_Strat/Geissenklosterle_UpperAurig.prior",))
{
latitude=48.401;
longitude=9.772;
site="Geißenklösterle";
culture="Upper Aurignacian";
author="AMH";
};
Date(Prior("Strat - L’Arbreda - Date Evolved Aurig",
"Priors_Strat/LArbreda_Date_Evolved_Aurignacian.prior",))
{
latitude=42.161;
longitude=2.747;
site="L’Arbreda";
culture="Evolved Aurignacian";
author="AMH";
};
Date(Prior("Strat - Buran-Kaya III - Gravettian 6-2",
"Priors_Strat/BuranKayaIII_Date_Gravettian_6_2.prior",))
{
latitude=45.16;
longitude=34.396;
site="Buran-Kaya III";
culture="Gravettian";
author="AMH";
};
Date(Prior("Strat - Buran-Kaya III - Micoquian",
"Priors_Strat/BuranKayaIII_Date_Micoquian.prior",))
{
latitude=45.16;
longitude=34.396;
site="Buran-Kaya III";
culture="Micoquian";
author="Neanderthal";
};
Date(Prior("Strat - Buran-Kaya III - Aurignacian 6-5",
"Priors_Strat/BuranKayaIII_Date_Aurig_6_5.prior",))
{
latitude=45.16;
longitude=34.396;
site="Buran-Kaya III";
culture="Aurignacian";
author="AMH";
};
Date(Prior("Strat - Buran-Kaya III - Aurignacian 6-4",
"Priors_Strat/BuranKayaIII_Date_Aurig_6_4.prior",))
{
latitude=45.16;
```

```
longitude=34.396;
site="Buran-Kaya III";
culture="Aurignacian";
author="AMH";
};
Date(Prior("Strat - Buran-Kaya III - Aurignacian 6-3",
"Priors_Strat/BuranKayaIII_Date_Aurig_6_3.prior",))
{
latitude=45.16;
longitude=34.396;
site="Buran-Kaya III";
culture="Aurignacian";
author="AMH";
};
Date(Prior("Strat - Buran-Kaya III - Gravettian 6-1",
"Priors_Strat/BuranKayaIII_Date_Gravettian_6_1.prior",))
{
latitude=45.16;
longitude=34.396;
site="Buran-Kaya III";
culture="Gravettian";
author="AMH";
};
Date(Prior("Strat - Buran-Kaya III - Gravettian 5-2",
"Priors_Strat/BuranKayaIII_Date_Gravettian_5_2.prior",))
{
latitude=45.16;
longitude=34.396;
site="Buran-Kaya III";
culture="Gravettian";
author="AMH";
};
Date(Prior("Strat - Castelcivita - Date Mousterian",
"Priors_Strat/Castelcivita_Mousterian.prior",))
{
latitude=40.495;
longitude=15.237;
site="Castelcivita";
culture="Mousterian";
author="Neanderthal";
};
Date(Prior("Strat - Castelcivita - Date Aurignacian",
"Priors_Strat/Castelcivita_Aurignacian.prior",))
{
latitude=40.495;
longitude=15.237;
site="Castelcivita";
culture="Aurignacian";
author="AMH";
};
Date(Prior("Strat - Cavallo - Date EII/I",
"Priors_Strat/CAVALLO_Date_EII_I_Uluzzian.prior",))
{
latitude=40.154;
longitude=17.96;
site="Cavallo";
culture="Uluzzian";
author="Neanderthal";
};
Date(Prior("Strat - Cavallo - Date E/D",
"Priors_Strat/CAVALLO_Date_E_D_Uluzzian.prior",))
{
latitude=40.154;
longitude=17.96;
site="Cavallo";
culture="Uluzzian";
author="Neanderthal";
};
Date(Prior("Strat - Cavallo - Date DII",
"Priors_Strat/CAVALLO_Date_DII_Uluzzian.prior",))
{
latitude=40.154;
longitude=17.96;
site="Cavallo";
culture="Uluzzian";
author="Neanderthal";
};
Date(Prior("Strat - Cavallo - Date Dib",
"Priors_Strat/CAVALLO_Date_DIb_Uluzzian.prior",))
{
latitude=40.154;
longitude=17.96;
site="Cavallo";
culture="Uluzzian";
author="Neanderthal";
};
Date(Prior("Strat - El Castillo - Date 20C",
"Priors_Strat/ElCastillo_Date_Mousterian.prior",))
{
latitude=43.2875;
longitude=-3.9598;
site="El Castillo";
culture="Mousterian";
author="Neanderthal";
};
Date(Prior("Strat - El Castillo - Date 18B",
"Priors_Strat/ElCastillo_Date_Transitional_Aurignacian_18B.prior",))
{
latitude=43.2875;
longitude=-3.9598;
site="El Castillo";
culture="‘Transitional Aurignacian’";
author="AMH";
};
Date(Prior("Strat - Fumane - Date A4",
"Priors_Strat/Fumane_Date_A4_Uluzzian.prior",))
{
latitude=45.57;
longitude=10.902;
site="Fumane";
culture="Uluzzian";
author="Neanderthal";
};
Date(Prior("Strat - Fumane - Date A3",
"Priors_Strat/Fumane_Date_A3_Uluzzian.prior",))
{
latitude=45.57;
longitude=10.902;
site="Fumane";
culture="Uluzzian";
author="Neanderthal";
};
Date(Prior("Strat - Fumane - Date A1",
"Priors_Strat/Fumane_Date_A1_Proto_Aurignacian.prior",))
{
latitude=45.57;
longitude=10.902;
site="Fumane";
culture="Proto-Aurignacian";
author="AMH";
};
Date(Prior("Strat - Fumane - Date D",
"Priors_Strat/Fumane_Date_D_Aurignacian.prior",))
{
latitude=45.57;
longitude=10.902;
site="Fumane";
culture="Aurignacian";
author="AMH";
};
Date(Prior("Strat - Geissenklosterle - Date IV",
"Priors_Strat/Geissenklosterle_Mousterian.prior",))
{
latitude=48.401;
longitude=9.772;
site="Geißenklösterle";
culture="Mousterian";
author="Neanderthal";
};
Date(Prior("Strat - Geissenklosterle - Date I",
"Priors_Strat/Geissenklosterle_Gravettian.prior",))
{
latitude=48.401;
longitude=9.772;
site="Geißenklösterle";
culture="Gravettian";
author="AMH";
};
Date(Prior("Strat - Hohle Fels - Date IX",
"Priors_Strat/HohleFels_Date_IX_Mousterian.prior",))
{
latitude=48.378;
longitude=9.758;
site="Hohle Fels";
culture="Mousterian";
author="Neanderthal";
```

```
};
Date(Prior("Strat - Hohle Fels - Date VIII",
"Priors_Strat/HohleFels_Date_VIII_Mousterian.prior",))
{
latitude=48.378;
longitude=9.758;
site="Hohle Fels";
culture="Mousterian";
author="Neanderthal";
};
Date(Prior("Strat - Hohle Fels - Date VII",
"Priors_Strat/HohleFels_Date_VII_Mousterian.prior",))
{
latitude=48.378;
longitude=9.758;
site="Hohle Fels";
culture="Mousterian";
author="Neanderthal";
};
Date(Prior("Strat - Hohle Fels - Date VI",
"Priors_Strat/HohleFels_Date_VI_Mousterian.prior",))
{
latitude=48.378;
longitude=9.758;
site="Hohle Fels";
culture="Mousterian";
author="Neanderthal";
};
Date(Prior("Strat - Hohle Fels - Date V",
"Priors_Strat/HohleFels_Date_V_Aurignacian.prior",))
{
latitude=48.378;
longitude=9.758;
site="Hohle Fels";
culture="Aurignacian";
author="AMH";
};
Date(Prior("Strat - Hohle Fels - Date IV",
"Priors_Strat/HohleFels_Date_IV_Aurignacian.prior",))
{
latitude=48.378;
longitude=9.758;
site="Hohle Fels";
culture="Aurignacian";
author="AMH";
};
Date(Prior("Strat - Hohle Fels - Date III",
"Priors_Strat/HohleFels_Date_III_Aurignacian.prior",))
{
latitude=48.378;
longitude=9.758;
site="Hohle Fels";
culture="Aurignacian";
author="AMH";
};
Date(Prior("Strat - Hohle Fels - Date II",
"Priors_Strat/HohleFels_Date_II_Aurignacian.prior",))
{
latitude=48.378;
longitude=9.758;
site="Hohle Fels";
culture="Aurignacian";
author="AMH";
};
Date(Prior("KDE - Hohlenstein-Stadel",
"Priors_KDE/KDE_Hohlenstein_Stadel_short_.prior",))
{
latitude=48.551;
longitude=10.168;
site="Hohlenstein-Stadel";
culture="Aurignacian";
author="AMH";
};
Date(Prior("Strat - Isturitz - Date C5",
"Priors_Strat/Isturitz_Date_Proto_Aurignacian_C5.prior",))
{
latitude=43.371;
longitude=-1.196;
site="Isturitz";
culture="Proto-Aurignacian";
author="AMH";
};
Date(Prior("Strat - Isturitz - Date C4c4",
"Priors_Strat/Isturitz_ProtoEarly_Aurignacian_C4c4.prior",))
{
latitude=43.371;
longitude=-1.196;
site="Isturitz";
culture="Proto-Aurignacian";
author="AMH";
};
Date(Prior("Strat - Isturitz - Date C4b2",
"Priors_Strat/Isturitz_Date_Early_Aurignacian_C4b2.prior",))
{
latitude=43.371;
longitude=-1.196;
site="Isturitz";
culture="Early Aurignacian";
author="AMH";
};
Date(Prior("Strat - Isturitz - Date C4b1",
"Priors_Strat/Isturitz_Date_Early_Aurignacian_C4b1.prior",))
{
latitude=43.371;
longitude=-1.196;
site="Isturitz";
culture="Early Aurignacian";
author="AMH";
};
Date(Prior("Strat - Ksar Akil - Date Mousterian",
"Priors_Strat/KsarAkil_Date_Mousterian.prior",))
{
latitude=33.916667;
longitude=35.6;
site="Ksar Akil";
culture="Mousterian";
author="Neanderthal";
};
Date(Prior("Strat - Ksar Akil - Date Phase 3-4",
"Priors_Strat/KsarAkil_Date_Phases_3_4.prior",))
{
latitude=33.916667;
longitude=35.6;
site="Ksar Akil";
culture="Early Ahmarian";
author="AMH";
};
Date(Prior("Strat - Ksar Akil - Date Phase 5",
"Priors_Strat/KsarAkil_Date_Phases_5.prior",))
{
latitude=33.916667;
longitude=35.6;
site="Ksar Akil";
culture="Early Ahmarian";
author="AMH";
};
Date(Prior("Strat - Ksar Akil - Date Phase 6",
"Priors_Strat/KsarAkil_Date_Phases_6.prior",))
{
latitude=33.916667;
longitude=35.6;
site="Ksar Akil";
culture="Early Ahmarian";
author="AMH";
};
Date(Prior("Strat - Ksar Akil - Date Phase 7",
"Priors_Strat/KsarAkil_Date_Phases_7.prior",))
{
latitude=33.916667;
longitude=35.6;
site="Ksar Akil";
culture="Early Ahmarian";
author="AMH";
};
Date(Prior("Strat - L'Arbreda - Date Mousterian",
"Priors_Strat/LArbreda_Date_Mousterian.prior",))
{
latitude=42.161;
longitude=2.747;
site="L'Arbreda";
culture="Mousterian";
author="Neanderthal";
};
Date(Prior("Strat - L'Arbreda - Date Proto-Aurig",
"Priors_Strat/LArbreda_Date_Proto_Aurignacian.prior",))
{
```

```
latitude=42.161;
longitude=2.747;
site="L'Arbreda";
culture="Proto-Aurignacian";
author="AMH";
};
Date(Prior("Strat - L'Arbreda - Date Gravettian F",
"Priors_Strat/LArbreda_Date_Gravettian_F.prior",))
{
latitude=42.161;
longitude=2.747;
site="L'Arbreda";
culture="Gravettian";
author="AMH";
};
Date(Prior("Strat - L'Arbreda - Date Gravettian E",
"Priors_Strat/LArbreda_Date_Gravettian_E.prior",))
{
latitude=42.161;
longitude=2.747;
site="L'Arbreda";
culture="Gravettian";
author="AMH";
};
Date(Prior("Strat - Labeko Koba - Date VII",
"Priors_Strat/LabekoKoba_Date_Proto_Aurignacian.prior",))
{
latitude=43.066;
longitude=-2.458;
site="Labeko Koba";
culture="Proto-Aurignacian";
author="AMH";
};
Date(Prior("Strat - Labeko Koba - Date VI",
"Priors_Strat/LabekoKoba_Date_Early_Aurignacian_VI.prior",))
{
latitude=43.066;
longitude=-2.458;
site="Labeko Koba";
culture="Early Aurignacian";
author="AMH";
};
Date(Prior("Strat - Labeko Koba - Date V",
"Priors_Strat/LabekoKoba_Date_Early_Aurignacian_V.prior",))
{
latitude=43.066;
longitude=-2.458;
site="Labeko Koba";
culture="Early Aurignacian";
author="AMH";
};
Date(Prior("Strat - Labeko Koba - Date IV",
"Priors_Strat/LabekoKoba_Date_Early_Aurignacian_IV.prior",))
{
latitude=43.066;
longitude=-2.458;
site="Labeko Koba";
culture="Early Aurignacian";
author="AMH";
};
Date(Prior("KDE - Mitoc-Malul Galben",
"Priors_KDE/KDE_Mitoc_Malul_Galben.prior",))
{
latitude=48.111;
longitude=27.036;
site="Mitoc-Malul Galben";
culture="Aurignacian";
author="AMH";
};
Date(Prior("KDE - Moravia Aurignacian",
"Priors_KDE/KDE_Aurignacian_Moravia.prior",))
{
latitude=49.5;
longitude=17;
site="Moravia Aurignacian";
culture="Aurignacian";
author="AMH";
};
Date(Prior("Strat - Riparo Mochi - Date Proto-Aurig",
"Priors_Strat/RiparoMochi_Date_Proto_Aurignacian.prior",))
{
latitude=43.7894;
longitude=7.5475;
site="Riparo Mochi";
culture="Proto-Aurignacian";
author="AMH";
};
Date(Prior("Strat - Riparo Mochi - Date Early Aurig",
"Priors_Strat/RiparoMochi_Date_Early_Aurignacian.prior",))
{
latitude=43.7894;
longitude=7.5475;
site="Riparo Mochi";
culture="Early Aurignacian";
author="AMH";
};
Date(Prior("Strat - Riparo Mochi - Date Gravettian",
"Priors_Strat/RiparoMochi_Date_Gravettian.prior",))
{
latitude=43.7894;
longitude=7.5475;
site="Riparo Mochi";
culture="Gravettian";
author="AMH";
};
Date(Prior("Strat - Salitrena Pecina - Date Aurignacian",
"Priors_Strat/SalitrenaPecina_Date_Aurignacian.prior",))
{
latitude=44.1905;
longitude=20.0835;
site="Šalitrena Pećina";
culture="Aurignacian";
author="AMH";
};
Date(Prior("KDE - Vogelherd",
"Priors_KDE/KDE_Vogelherd.prior",))
{
latitude=48.5606;
longitude=10.1913;
site="Vogelherd";
culture="Aurignacian";
author="AMH";
};
Date(Prior("Strat - Willendorf II - Date D1/D2",
"Priors_Strat/Willendorf_Date_Micoquian_D1_D2.prior",))
{
latitude=48.323;
longitude=15.399;
site="Willendorf II";
culture="Micoquian";
author="Neanderthal";
};
Date(Prior("Strat - Willendorf II - Date C8-3",
"Priors_Strat/Willendorf_Date_Early_Aurignaican_C8_3.prior",))
{
latitude=48.323;
longitude=15.399;
site="Willendorf II";
culture="Early Aurignacian";
author="AMH";
};
Date(Prior("Strat - Willendorf II - Date C8-2",
"Priors_Strat/Willendorf_Date_Aurignaican_C8_2.prior",))
{
latitude=48.323;
longitude=15.399;
site="Willendorf II";
culture="Aurignacian";
author="AMH";
};
Date(Prior("Strat - Willendorf II - Date C7-1",
"Priors_Strat/Willendorf_Date_Aurignaican_C7_1.prior",))
{
latitude=48.323;
longitude=15.399;
site="Willendorf II";
culture="Aurignacian";
author="AMH";
};
Date(Prior("Strat - Willendorf II - Date C4-2",
"Priors_Strat/Willendorf_Date_C4_2.prior",))
{
latitude=48.323;
longitude=15.399;
site="Willendorf II";
culture="Aurignacian";
```

```
author="AMH";
};
Date(Prior("Strat - Willendorf II - Date C4-1",
"Priors_Strat/Willendorf_Date_C4_1.prior",))
{
latitude=48.323;
longitude=15.399;
site="Willendorf II";
culture="Aurignacian";
author="AMH";
};
Date(Prior("MOD10 - Dzerava Skala - Date 5a",
"Priors_Strat_DPhil/Der_MOD10_Date_5a_.prior",))
{
latitude=48.496987;
longitude=17.324692;
site="Dzerava Skala";
culture="Aurignacian Point";
author="AMH";
};
Date(Prior("MOD10 - Dzerava Skala - Date 9",
"Priors_Strat_DPhil/Der_MOD10_Date_9.prior",))
{
latitude=48.496987;
longitude=17.324692;
site="Dzerava Skala";
culture="Aurignacian Point";
author="AMH";
};
Date(Prior("MOD10 - Dzerava Skala - Date 5",
"Priors_Strat_DPhil/Der_MOD10_Date_5.prior",))
{
latitude=48.496987;
longitude=17.324692;
site="Dzerava Skala";
culture="Gravettian";
author="AMH";
};
Date(Prior("MOD10 - Dzerava Skala - Date 4",
"Priors_Strat_DPhil/Der_MOD10_Date_4.prior",))
{
latitude=48.496987;
longitude=17.324692;
site="Dzerava Skala";
culture="Gravettian";
author="AMH";
};
Date(Prior("Points KDE2 - Istallosko",
"Priors_KDE_DPhil/Istall_Points_KDE_2.prior",))
{
latitude=48.071667;
longitude=20.418889;
site="Istallosko";
culture="Aurignacian Point";
author="AMH";
};
R_Date("OxA-X-2716-49",31800,1000)
{
latitude=47.723889;
longitude=18.575278;
site="Jankovich";
culture="Aurignacian Point";
author="AMH";
};
R_Date("OxA-X-2716-48",32500,800)
{
latitude=47.723889;
longitude=18.575278;
site="Jankovich";
culture="Aurignacian Point";
author="AMH";
};
R_Date("OxA-X-2732-10",32750,670)
{
latitude=47.723889;
longitude=18.575278;
site="Jankovich";
culture="Aurignacian Point";
author="AMH";
};
R_Date("OxA-35386",30800,500)
{
latitude=47.723889;
longitude=18.575278;
site="Jankovich";
culture="Aurignacian Point";
author="AMH";
};
Date(Prior("MOD3 - Kozarnika - Date 6/7 ls lp",
"Priors_Strat_DPhil/Kz_MOD3_Date_6_7_ls_lp.prior",))
{
latitude=43.651722;
longitude=22.702472;
site="Kozarnika";
culture="IUP";
author="AMH";
};
Date(Prior("MOD3 - Kozarnika - Date 6/7 lb",
"Priors_Strat_DPhil/Kz_MOD3_Date_6_7_lb.prior",))
{
latitude=43.651722;
longitude=22.702472;
site="Kozarnika";
culture="IUP";
author="AMH";
};
Date(Prior("MOD3 - Kozarnika - Date 5b",
"Priors_Strat_DPhil/Kz_MOD3_Date_5b.prior",))
{
latitude=43.651722;
longitude=22.702472;
site="Kozarnika";
culture="Kozarnikian";
author="AMH";
};
Date(Prior("MOD3 - Kozarnika - Date 5a",
"Priors_Strat_DPhil/Kz_MOD3_Date_5a.prior",))
{
latitude=43.651722;
longitude=22.702472;
site="Kozarnika";
culture="Kozarnikian";
author="AMH";
};
Date(Prior("MOD3 - Kozarnika - Date 4",
"Priors_Strat_DPhil/Kz_MOD3_Date_4.prior",))
{
latitude=43.651722;
longitude=22.702472;
site="Kozarnika";
culture="Kozarnikian";
author="AMH";
};
R_Date("OxA-35404",27600,400)
{
latitude=43.15;
longitude=24.71;
site="Tabashkata";
culture="Aurignacian Point";
author="AMH";
};
Date(Prior("MOD3 - Temnata - Date TD-V 5pg",
"Priors_Strat_DPhil/TD_Date_5pg_TD_V.prior",))
{
latitude=43.174969;
longitude=24.074006;
site="Temnata";
culture="Mousterian";
author="Neanderthal";
};
Date(Prior("MOD3 - Temnata - Date TD-V 3v",
"Priors_Strat_DPhil/TD_Date_3v_TD_V.prior",))
{
latitude=43.174969;
longitude=24.074006;
site="Temnata";
culture="Aurignacian-like";
author="AMH";
};
Date(Prior("MOD3 - Temnata - Date TD-V 3d",
"Priors_Strat_DPhil/TD_Date_3d_TD_V.prior",))
{
latitude=43.174969;
longitude=24.074006;
site="Temnata";
culture="Gravettian";
```

```
author="AMH";
};
R_Date("OxA-17967",38300,1500)
{
latitude=48.0468;
longitude=20.4264;
site="Pesko";
culture="Aurignacian Point";
author="AMH";
};
R_Date("OxA-17964",33500,450)
{
latitude=48.0468;
longitude=20.4264;
site="Pesko";
culture="Aurignacian Point";
author="AMH";
};
R_Date("OxA-17966",36400,800)
{
latitude=48.0468;
longitude=20.4264;
site="Pesko";
culture="Aurignacian Point";
author="AMH";
};
R_Date("OxA-19621",33750,350)
{
latitude=47.138;
longitude=5.571;
site="Trou de la Mere Clochette";
culture="Aurignacian Point";
author="AMH";
};
R_Date("OxA-19622",35460,250)
{
latitude=47.138;
longitude=5.571;
site="Trou de la Mere Clochette";
culture="Aurignacian Point";
author="AMH";
};
R_Date("OxA-14436",33640,250)
{
latitude=50.16944;
longitude=19.80723;
site="Mamutowa cave";
culture="Aurignacian Point";
author="AMH";
};
R_Date("OxA-14434",35460,220)
{
latitude=50.16944;
longitude=19.80723;
site="Mamutowa cave";
culture="Aurignacian Point";
author="AMH";
};
R_Date("OxA-17963",35600,400)
{
latitude=48.4922;
longitude=17.295;
site="Dzerava skala";
culture="Aurignacian Point";
author="AMH";
};
R_Date("OxA-X-2170-18",33600,900)
{
latitude=48.0654;
longitude=20.4108;
site="Istallosko";
culture="Aurignacian Point";
author="AMH";
};
R_Date("OxA-21783",32100,450)
{
latitude=42.1607;
longitude=2.74401;
site="Arbreda";
culture="Aurignacian Point";
author="AMH";
};
R_Date("OxA-13716",31730,250)
{
latitude=51.3204;
longitude= 2.9781;
site="Uphill Quarry cave 8 ";
culture="Aurignacian Point";
author="AMH";
};
R_Date("OxA-13803",31550,340)
{
latitude=51.2263;
longitude=2.6761;
site="Hyaena Den cave ";
culture="Aurignacian Point";
author="AMH";
};
R_Date("GrA-32619",32830,195)
{
latitude=50.4781;
longitude=4.679;
site="Grotte de la Betche-aux-Rotches, Spy";
culture="Aurignacian Point";
author="AMH";
};
R_Date("OxA-7496",30750,850)
{
latitude=50.421;
longitude=5.294;
site="Trou al'Wesse";
culture="Aurignacian Point";
author="AMH";
};
R_Date("KIA-19541",31310,235)
{
latitude=48.5603;
longitude=10.1913;
site="Vogelherd cave";
culture="Aurignacian Point";
author="AMH";
};
R_Date("KIA-19551",32470,265)
{
latitude=48.4089;
longitude=9.772;
site="Brillenhohle";
culture="Aurignacian Point";
author="AMH";
};
R_Date("KIA-19550[a]",30400,235)
{
latitude=48.4089;
longitude=9.772;
site="Brillenhohle";
culture="Aurignacian Point";
author="AMH";
};
R_Date("KIA-13082",26730,165)
{
latitude=48.3842;
longitude=9.7614;
site="Sirgenstein cave";
culture="Aurignacian Point";
author="AMH";
};
R_Date("KIA-13079",27250,175)
{
latitude=48.3842;
longitude=9.7614;
site="Sirgenstein cave";
culture="Aurignacian Point";
author="AMH";
};
R_Date("KIA-19543[a]",32010,494)
{
latitude=47.5924;
longitude=12.197;
site="Tischoferhohle";
culture="Aurignacian Point";
author="AMH";
};
R_Date("KIA-19544[a]",31530,205)
{
latitude=47.5924;
longitude=12.197;
```

```
site="Tischoferhohle";
culture="Aurignacian Point";
author="AMH";
};
R_Date("KIA-19545",29500,200)
{
latitude=47.5924;
longitude=12.197;
site="Tischoferhohle";
culture="Aurignacian Point";
author="AMH";
};
R_Date("VERA-2522",30140,335)
{
latitude=46.4493;
longitude=14.6691;
site="Potocka zijalka";
culture="Aurignacian Point";
author="AMH";
};
R_Date("OxA-27854",30800,370)
{
latitude=46.4493;
longitude=14.6691;
site="Potocka zijalka";
culture="Aurignacian Point";
author="AMH";
};
R_Date("OxA-28038",31950,450)
{
latitude=46.4493;
longitude=14.6691;
site="Potocka zijalka";
culture="Aurignacian Point";
author="AMH";
};
R_Date("OxA-28061",32550,550)
{
latitude=46.4493;
longitude=14.6691;
site="Potocka zijalka";
culture="Aurignacian Point";
author="AMH";
};
R_Date("OxA-27850",30380,370)
{
latitude=46.4493;
longitude=14.6691;
site="Potocka zijalka";
culture="Aurignacian Point";
author="AMH";
};
R_Date("OxA-27849",31220,400)
{
latitude=46.4493;
longitude=14.6691;
site="Potocka zijalka";
culture="Aurignacian Point";
author="AMH";
};
R_Date("OxA-27852",31360,400)
{
latitude=46.4493;
longitude=14.6691;
site="Potocka zijalka";
culture="Aurignacian Point";
author="AMH";
};
R_Date("OxA-27853",31500,400)
{
latitude=46.4493;
longitude=14.6691;
site="Potocka zijalka";
culture="Aurignacian Point";
author="AMH";
};
R_Date("OxA-27851",30910,380)
{
latitude=46.4493;
longitude=14.6691;
site="Potocka zijalka";
culture="Aurignacian Point";
author="AMH";
};
R_Date("OxA-15334",31600,900)
{
latitude=48.4922;
longitude=17.295;
site="Dzerava skala";
culture="Aurignacian Point";
author="AMH";
};
R_Date("OxA-15335",31000,1000)
{
latitude=48.4922;
longitude=17.295;
site="Dzerava skala";
culture="Aurignacian Point";
author="AMH";
};
R_Date("OxA-28219",29760,340)
{
latitude=46.112778;
longitude=13.915556;
site="Divije babe I";
culture="Aurignacian Point";
author="AMH";
};
R_Date("OxA-X-2517-52",34750,600)
{
latitude=46.308806;
longitude=14.568194;
site="Morkiska jama";
culture="Aurignacian Point";
author="AMH";
};
R_Date("OxA-27855",32600,450)
{
latitude=46.308806;
longitude=14.568194;
site="Morkiska jama";
culture="Aurignacian Point";
author="AMH";
};
Label("Humans");
R_Date("OxA-21839",39700,1100)
{
longitude=40.0034;
latitude=44.2217;
culture="MP";
author="Neanderthal";
species="Neanderthal";
site="Mezmaiskaya";
};
Date("OxA-15257",N(calBP(48900),1100))
{
longitude=0.741;
latitude=46.415;
culture="Mousterian";
author="Neanderthal";
species="Neanderthal";
site="Les Rochers-de-Villeneuve";
};
R_Date("ETH-20981",39900,620)
{
longitude=6.9363;
latitude=51.2206;
culture="MP";
author="Neanderthal";
species="Neanderthal";
site="Kleine Feldhöfergrotte";
};
R_Date("ETH-19660",39240,670)
{
longitude=6.9363;
latitude=51.2206;
culture="MP";
author="Neanderthal";
species="Neanderthal";
site="Kleine Feldhöfergrotte";
};
R_Date("GrA-32626",36350,295)
{
longitude=4.6743;
latitude=50.4803;
culture="LRJ or Mousterian";
```

```
author="Neanderthal";
species="Neanderthal";
site="Spy";
};
R_Date("GrA-32623",35810,250)
{
longitude=4.6743;
latitude=50.4803;
culture="LRJ or Mousterian";
author="Neanderthal";
species="Neanderthal";
site="Spy";
};
R_Date("ETH-19661",40360,760)
{
longitude=6.9363;
latitude=51.2206;
culture="MP";
author="Neanderthal";
species="Neanderthal";
site="Kleine Feldhöfergrotte";
};
R_Date("OxA-10560",36250,500)
{
longitude=4.6743;
latitude=50.4803;
culture="unknown";
author="Neanderthal";
species="Neanderthal";
site="Spy";
};
Date("GifA-99167",N(calBP(55090),2600))
{
longitude=-5.733;
latitude=43.386;
culture="Mousterian";
author="Neanderthal";
species="Neanderthal";
site="El Sidron";
};
Date("GifA-99704",N(calBP(54930),2500))
{
longitude=-5.733;
latitude=43.386;
culture="Mousterian";
author="Neanderthal";
species="Neanderthal";
site="El Sidron";
};
Date("OxA-21776",N(calBP(56230),3200))
{
longitude=-5.733;
latitude=43.386;
culture="Mousterian";
author="Neanderthal";
species="Neanderthal";
site="El Sidron";
};
R_Date("OxA-X-2689-09",42700,1600)
{
longitude=16.088;
latitude=46.305;
culture="MP";
author="Neanderthal";
species="Neanderthal";
site="Vindija";
};
Date("OxA-X-2689-10",N(calBP(48800),2000))
{
longitude=16.088;
latitude=46.305;
culture="MP";
author="Neanderthal";
species="Neanderthal";
site="Vindija";
};
R_Date("OxA-X-2717-11",44300,1200)
{
longitude=16.088;
latitude=46.305;
culture="MP";
author="Neanderthal";
species="Neanderthal";
site="Vindija";
};
Date("OxA-X-2687-57",N(calBP(49960),1500))
{
longitude=16.088;
latitude=46.305;
culture="MP";
author="Neanderthal";
species="Neanderthal";
site="Vindija";
};
R_Date("GrA-50457",32450,240)
{
longitude=34.396;
latitude=45.16;
culture="Gravettian";
author="AMH";
species="AMH";
site="Buran-Kaya III";
};
R_Date("GrA-24398",28890,170)
{
longitude=21.91;
latitude=45.0177;
culture="unknown";
author="AMH";
species="AMH";
site="Pestera cu Oase";
};
R_Date("OxA-4586",31000,500)
{
longitude=20.1563;
latitude=49.443;
culture="Aurignacian";
author="AMH";
species="AMH";
site="Oblazowa";
};
R_Date("VERA-3074",31320,400)
{
longitude=17.0167;
latitude=49.707;
culture="Aurignacian";
author="AMH";
species="AMH";
site="Mladec";
};
R_Date("OxA-11711",34950,990)
{
longitude=21.91;
latitude=45.0177;
culture="unknown";
author="AMH";
species="AMH";
site="Pestera cu Oase";
};
R_Date("GrA-37938",31900,230)
{
longitude=34.396;
latitude=45.16;
culture="Gravettian";
author="AMH";
species="AMH";
site="Buran-Kaya III";
};
R_Date("VERA-3073",31190,400)
{
longitude=17.0167;
latitude=49.707;
culture="Aurignacian";
author="AMH";
species="AMH";
site="Mladec";
};
R_Date("VERA-3076 A",31500,410)
{
longitude=17.0167;
latitude=49.707;
culture="Aurignacian";
author="AMH";
species="AMH";
site="Mladec";
};
```

```
R_Date("OxA-16412",28870,180)
{
longitude=-4.2555;
latitude=51.5499;
culture="Gravettian";
author="AMH";
species="";
site="Paviland";
};
R_Date("OxA-16413",29490,210)
{
longitude=-4.2555;
latitude=51.5499;
culture="Gravettian";
author="AMH";
species="";
site="Paviland";
};
R_Date("ERL-9415",30640,640)
{
longitude=3.0905;
latitude=43.1313;
culture="Aurignacian";
author="AMH";
species="AMH";
site="La Crouzade";
};
R_Date("OxA-15527",28150,170)
{
longitude=23.1296;
latitude=45.5862;
culture="Aurignacian?";
author="AMH";
species="AMH";
site="Cioclovina";
};
R_Date("OxA-15529",29930,170)
{
longitude=23.755;
latitude=45.1895;
culture="Uluzzian";
author="AMH";
species="AMH";
site="Pestera Muierii";
};
R_Date("OxA-16252",29110,190)
{
longitude=23.755;
latitude=45.1895;
culture="Uluzzian";
author="AMH";
species="AMH";
site="Pestera Muierii";
};
R_Date("OxA-13302",32790,280)
{
longitude=34.396;
latitude=45.16;
culture="Gravettian";
author="AMH";
species="AMH";
site="Buran-Kaya III";
};
};
```

Spatio-temporal distribution: map 2 modified – see figure 15.18-b

```
 Plot()
{
Date(Prior("Strat - Bacho Kiro - Date Mouserian",
"Priors_Strat/BachoKiro_Date_Mousterian.prior",))
{
latitude=42.947378;
longitude=25.331867;
site="Bacho Kiro";
culture="Mousterian";
author="Neanderthal";
};
Date(Prior("Strat - Willendorf II - Date D3",
"Priors_Strat/Willendorf_Date_Micoquian_D3.prior",))
{
latitude=48.323;
longitude=15.399;
site="Willendorf II";
culture="Micoquian";
author="Neanderthal";
};
Date(Prior("Strat - Labeko Koba - Date IX lower",
"Priors_Strat/LabekoKoba_Date_Chatelperronian.prior",))
{
latitude=43.066;
longitude=-2.458;
site="Labeko Koba";
culture="Chatelperronian";
author="Neanderthal";
};
Date(Prior("KDE - Moravia Szeletian",
"Priors_KDE/KDE_Szeletian_Moravia.prior",))
{
latitude=49.5;
longitude=17;
site="Moravia Szeletian";
culture="Szeletian";
author="Neanderthal";
};
Date(Prior("Strat - Ksar Akil - Date IUP",
"Priors_Strat/KsarAkil_Date_IUP.prior",))
{
latitude=33.916667;
longitude=35.6;
site="Ksar Akil";
culture="IUP";
author="Neanderthal";
};
Date(Prior("Strat - Bacho Kiro - Date Bachokirian",
"Priors_Strat/BachoKiro_Date_Bachokirian.prior",))
{
latitude=42.947378;
longitude=25.331867;
site="Bacho Kiro";
culture="Bachokirian";
author="Neanderthal";
};
Date(Prior("Strat - Castelcivita - Date Uluzzian",
"Priors_Strat/Castelcivitas_Uluzzian.prior",))
{
latitude=40.495;
longitude=15.237;
site="Castelcivita";
culture="Uluzzian";
author="Neanderthal";
};
Date(Prior("KDE - Moravia Bohunician",
"Priors_KDE/KDE_Bohunician_Moravia.prior",))
{
latitude=49.5;
longitude=17;
site="Moravia Bohunician";
culture="Bohunician";
author="Neanderthal";
};
Date(Prior("MOD3 - Kozarnika - Date 5c",
"Priors_Strat_DPhil/Kz_MOD3_Date_5c.prior",))
{
latitude=43.651722;
longitude=22.702472;
site="Kozarnika";
culture="Kozarnikian";
author="AMH";
```

```
};
Date(Prior("Strat - Fumane - Date A2",
"Priors_Strat/Fumane_Date_A2_Proto_Aurignacian.prior",))
{
latitude=45.57;
longitude=10.902;
site="Fumane";
culture="Proto-Aurignacian";
author="AMH";
};
Date(Prior("Strat - El Castillo - Date 18C",
"Priors_Strat/ElCastillo_Date_Transitional_
Aurignacian_18C.prior",))
{
latitude=43.2875;
longitude=-3.9598;
site="El Castillo";
culture="‘Transitional Aurignacian’";
author="AMH";
};
Date(Prior("Strat - Isturitz - Date C4d1",
"Priors_Strat/Isturitz_Date_Proto_Aurignacian_C4d1.prior",))
{
latitude=43.371;
longitude=-1.196;
site="Isturitz";
culture="Proto-/Early Aurignacian";
author="AMH";
};
R_Date("OxA-X-2732-11",31100,520)
{
latitude=45.3605642;
longitude=14.7527073;
site="Bukovac";
culture="Aurignacian Point";
author="AMH";
};
Date(Prior("MOD3 - Temnata - Date TD-V 4",
"Priors_Strat_DPhil/TD_Date_4_TD_V.prior",))
{
latitude=43.174969;
longitude=24.074006;
site="Temnata";
culture="Aurignacian-like";
author="AMH";
};
Date(Prior("Strat - Geissenklosterle - Date III",
"Priors_Strat/Geissenklosterle_EarlyAurig.prior",))
{
latitude=48.401;
longitude=9.772;
site="Geißenklösterle";
culture="Early Aurignacian";
author="AMH";
};
Date(Prior("Strat - Ksar Akil - Date Phase 2",
"Priors_Strat/KsarAkil_Date_Early_Ahmarian.prior",))
{
latitude=33.916667;
longitude=35.6;
site="Ksar Akil";
culture="Early Ahmarian";
author="AMH";
};
Date(Prior("Strat - Bacho Kiro - Date Aurignacian",
"Priors_Strat/BachoKiro_Date_Aurignacian.prior",))
{
latitude=42.947378;
longitude=25.331867;
site="Bacho Kiro";
culture="Aurignacian";
author="AMH";
};
Date(Prior("Strat - Geissenklosterle - Date II",
"Priors_Strat/Geissenklosterle_UpperAurig.prior",))
{
latitude=48.401;
longitude=9.772;
site="Geißenklösterle";
culture="Upper Aurignacian";
author="AMH";
};
Date(Prior("Strat - L’Arbreda - Date Evolved Aurig",
"Priors_Strat/LArbreda_Date_Evolved_Aurignacian.prior",))
{
latitude=42.161;
longitude=2.747;
site="L’Arbreda";
culture="Evolved Aurignacian";
author="AMH";
};
Date(Prior("Strat - Buran-Kaya III - Gravettian 6-2",
"Priors_Strat/BuranKayaIII_Date_Gravettian_6_2.prior",))
{
latitude=45.16;
longitude=34.396;
site="Buran-Kaya III";
culture="Gravettian";
author="AMH";
};
Date(Prior("Strat - Buran-Kaya III - Micoquian",
"Priors_Strat/BuranKayaIII_Date_Micoquian.prior",))
{
latitude=45.16;
longitude=34.396;
site="Buran-Kaya III";
culture="Micoquian";
author="Neanderthal";
};
Date(Prior("Strat - Buran-Kaya III - Aurignacian 6-5",
"Priors_Strat/BuranKayaIII_Date_Aurig_6_5.prior",))
{
latitude=45.16;
longitude=34.396;
site="Buran-Kaya III";
culture="Aurignacian";
author="AMH";
};
Date(Prior("Strat - Buran-Kaya III - Aurignacian 6-4",
"Priors_Strat/BuranKayaIII_Date_Aurig_6_4.prior",))
{
latitude=45.16;
longitude=34.396;
site="Buran-Kaya III";
culture="Aurignacian";
author="AMH";
};
Date(Prior("Strat - Buran-Kaya III - Aurignacian 6-3",
"Priors_Strat/BuranKayaIII_Date_Aurig_6_3.prior",))
{
latitude=45.16;
longitude=34.396;
site="Buran-Kaya III";
culture="Aurignacian";
author="AMH";
};
Date(Prior("Strat - Buran-Kaya III - Gravettian 6-1",
"Priors_Strat/BuranKayaIII_Date_Gravettian_6_1.prior",))
{
latitude=45.16;
longitude=34.396;
site="Buran-Kaya III";
culture="Gravettian";
author="AMH";
};
Date(Prior("Strat - Buran-Kaya III - Gravettian 5-2",
"Priors_Strat/BuranKayaIII_Date_Gravettian_5_2.prior",))
{
latitude=45.16;
longitude=34.396;
site="Buran-Kaya III";
culture="Gravettian";
author="AMH";
};
Date(Prior("Strat - Castelcivita - Date Mousterian",
"Priors_Strat/Castelcivita_Mousterian.prior",))
{
latitude=40.495;
longitude=15.237;
site="Castelcivita";
culture="Mousterian";
author="Neanderthal";
};
Date(Prior("Strat - Castelcivita - Date Aurignacian",
"Priors_Strat/Castelcivita_Aurignacian.prior",))
{
```

```
latitude=40.495;
longitude=15.237;
site="Castelcivita";
culture="Aurignacian";
author="AMH";
};
Date(Prior("Strat - Cavallo - Date EII/I",
"Priors_Strat/CAVALLO_Date_EII_I_Uluzzian.prior",))
{
latitude=40.154;
longitude=17.96;
site="Cavallo";
culture="Uluzzian";
author="Neanderthal";
};
Date(Prior("Strat - Cavallo - Date E/D",
"Priors_Strat/CAVALLO_Date_E_D_Uluzzian.prior",))
{
latitude=40.154;
longitude=17.96;
site="Cavallo";
culture="Uluzzian";
author="Neanderthal";
};
Date(Prior("Strat - Cavallo - Date DII",
"Priors_Strat/CAVALLO_Date_DII_Uluzzian.prior",))
{
latitude=40.154;
longitude=17.96;
site="Cavallo";
culture="Uluzzian";
author="Neanderthal";
};
Date(Prior("Strat - Cavallo - Date Dib",
"Priors_Strat/CAVALLO_Date_DIb_Uluzzian.prior",))
{
latitude=40.154;
longitude=17.96;
site="Cavallo";
culture="Uluzzian";
author="Neanderthal";
};
Date(Prior("Strat - El Castillo - Date 20C",
"Priors_Strat/ElCastillo_Date_Mousterian.prior",))
{
latitude=43.2875;
longitude=-3.9598;
site="El Castillo";
culture="Mousterian";
author="Neanderthal";
};
Date(Prior("Strat - El Castillo - Date 18B",
"Priors_Strat/ElCastillo_Date_Transitional_
Aurignacian_18B.prior",))
{
latitude=43.2875;
longitude=-3.9598;
site="El Castillo";
culture="‘Transitional Aurignacian’";
author="AMH";
};
Date(Prior("Strat - Fumane - Date A4",
"Priors_Strat/Fumane_Date_A4_Uluzzian.prior",))
{
latitude=45.57;
longitude=10.902;
site="Fumane";
culture="Uluzzian";
author="Neanderthal";
};
Date(Prior("Strat - Fumane - Date A3",
"Priors_Strat/Fumane_Date_A3_Uluzzian.prior",))
{
latitude=45.57;
longitude=10.902;
site="Fumane";
culture="Uluzzian";
author="Neanderthal";
};
Date(Prior("Strat - Fumane - Date A1",
"Priors_Strat/Fumane_Date_A1_Proto_Aurignacian.prior",))
{
latitude=45.57;
longitude=10.902;
site="Fumane";
culture="Proto-Aurignacian";
author="AMH";
};
Date(Prior("Strat - Fumane - Date D",
"Priors_Strat/Fumane_Date_D_Aurignacian.prior",))
{
latitude=45.57;
longitude=10.902;
site="Fumane";
culture="Aurignacian";
author="AMH";
};
Date(Prior("Strat - Geissenklosterle - Date IV",
"Priors_Strat/Geissenklosterle_Mousterian.prior",))
{
latitude=48.401;
longitude=9.772;
site="Geißenklösterle";
culture="Mousterian";
author="Neanderthal";
};
Date(Prior("Strat - Geissenklosterle - Date I",
"Priors_Strat/Geissenklosterle_Gravettian.prior",))
{
latitude=48.401;
longitude=9.772;
site="Geißenklösterle";
culture="Gravettian";
author="AMH";
};
Date(Prior("Strat - Hohle Fels - Date IX",
"Priors_Strat/HohleFels_Date_IX_Mousterian.prior",))
{
latitude=48.378;
longitude=9.758;
site="Hohle Fels";
culture="Mousterian";
author="Neanderthal";
};
Date(Prior("Strat - Hohle Fels - Date VIII",
"Priors_Strat/HohleFels_Date_VIII_Mousterian.prior",))
{
latitude=48.378;
longitude=9.758;
site="Hohle Fels";
culture="Mousterian";
author="Neanderthal";
};
Date(Prior("Strat - Hohle Fels - Date VII",
"Priors_Strat/HohleFels_Date_VII_Mousterian.prior",))
{
latitude=48.378;
longitude=9.758;
site="Hohle Fels";
culture="Mousterian";
author="Neanderthal";
};
Date(Prior("Strat - Hohle Fels - Date VI",
"Priors_Strat/HohleFels_Date_VI_Mousterian.prior",))
{
latitude=48.378;
longitude=9.758;
site="Hohle Fels";
culture="Mousterian";
author="Neanderthal";
};
Date(Prior("Strat - Hohle Fels - Date V",
"Priors_Strat/HohleFels_Date_V_Aurignacian.prior",))
{
latitude=48.378;
longitude=9.758;
site="Hohle Fels";
culture="Aurignacian";
author="AMH";
};
Date(Prior("Strat - Hohle Fels - Date IV",
"Priors_Strat/HohleFels_Date_IV_Aurignacian.prior",))
{
latitude=48.378;
longitude=9.758;
site="Hohle Fels";
```

```
culture="Aurignacian";
author="AMH";
};
Date(Prior("Strat - Hohle Fels - Date III",
"Priors_Strat/HohleFels_Date_III_Aurignacian.prior",))
{
latitude=48.378;
longitude=9.758;
site="Hohle Fels";
culture="Aurignacian";
author="AMH";
};
Date(Prior("Strat - Hohle Fels - Date II",
"Priors_Strat/HohleFels_Date_II_Aurignacian.prior",))
{
latitude=48.378;
longitude=9.758;
site="Hohle Fels";
culture="Aurignacian";
author="AMH";
};
Date(Prior("KDE - Hohlenstein-Stadel",
"Priors_KDE/KDE_Hohlenstein_Stadel_short_.prior",))
{
latitude=48.551;
longitude=10.168;
site="Hohlenstein-Stadel";
culture="Aurignacian";
author="AMH";
};
Date(Prior("Strat - Isturitz - Date C5",
"Priors_Strat/Isturitz_Date_Proto_Aurignacian_C5.prior",))
{
latitude=43.371;
longitude=-1.196;
site="Isturitz";
culture="Proto-Aurignacian";
author="AMH";
};
Date(Prior("Strat - Isturitz - Date C4c4",
"Priors_Strat/Isturitz_ProtoEarly_Aurignacian_C4c4.prior",))
{
latitude=43.371;
longitude=-1.196;
site="Isturitz";
culture="Proto-Aurignacian";
author="AMH";
};
Date(Prior("Strat - Isturitz - Date C4b2",
"Priors_Strat/Isturitz_Date_Early_Aurignacian_C4b2.prior",))
{
latitude=43.371;
longitude=-1.196;
site="Isturitz";
culture="Early Aurignacian";
author="AMH";
};
Date(Prior("Strat - Isturitz - Date C4b1",
"Priors_Strat/Isturitz_Date_Early_Aurignacian_C4b1.prior",))
{
latitude=43.371;
longitude=-1.196;
site="Isturitz";
culture="Early Aurignacian";
author="AMH";
};
Date(Prior("Strat - Ksar Akil - Date Mousterian",
"Priors_Strat/KsarAkil_Date_Mousterian.prior",))
{
latitude=33.916667;
longitude=35.6;
site="Ksar Akil";
culture="Mousterian";
author="Neanderthal";
};
Date(Prior("Strat - Ksar Akil - Date Phase 3-4",
"Priors_Strat/KsarAkil_Date_Phases_3_4.prior",))
{
latitude=33.916667;
longitude=35.6;
site="Ksar Akil";
culture="Early Ahmarian";
author="AMH";
};
Date(Prior("Strat - Ksar Akil - Date Phase 5",
"Priors_Strat/KsarAkil_Date_Phases_5.prior",))
{
latitude=33.916667;
longitude=35.6;
site="Ksar Akil";
culture="Early Ahmarian";
author="AMH";
};
Date(Prior("Strat - Ksar Akil - Date Phase 6",
"Priors_Strat/KsarAkil_Date_Phases_6.prior",))
{
latitude=33.916667;
longitude=35.6;
site="Ksar Akil";
culture="Early Ahmarian";
author="AMH";
};
Date(Prior("Strat - Ksar Akil - Date Phase 7",
"Priors_Strat/KsarAkil_Date_Phases_7.prior",))
{
latitude=33.916667;
longitude=35.6;
site="Ksar Akil";
culture="Early Ahmarian";
author="AMH";
};
Date(Prior("Strat - L'Arbreda - Date Mousterian",
"Priors_Strat/LArbreda_Date_Mousterian.prior",))
{
latitude=42.161;
longitude=2.747;
site="L'Arbreda";
culture="Mousterian";
author="Neanderthal";
};
Date(Prior("Strat - L'Arbreda - Date Proto-Aurig",
"Priors_Strat/LArbreda_Date_Proto_Aurignacian.prior",))
{
latitude=42.161;
longitude=2.747;
site="L'Arbreda";
culture="Proto-Aurignacian";
author="AMH";
};
Date(Prior("Strat - L'Arbreda - Date Gravettian F",
"Priors_Strat/LArbreda_Date_Gravettian_F.prior",))
{
latitude=42.161;
longitude=2.747;
site="L'Arbreda";
culture="Gravettian";
author="AMH";
};
Date(Prior("Strat - L'Arbreda - Date Gravettian E",
"Priors_Strat/LArbreda_Date_Gravettian_E.prior",))
{
latitude=42.161;
longitude=2.747;
site="L'Arbreda";
culture="Gravettian";
author="AMH";
};
Date(Prior("Strat - Labeko Koba - Date VII",
"Priors_Strat/LabekoKoba_Date_Proto_Aurignacian.prior",))
{
latitude=43.066;
longitude=-2.458;
site="Labeko Koba";
culture="Proto-Aurignacian";
author="AMH";
};
Date(Prior("Strat - Labeko Koba - Date VI",
"Priors_Strat/LabekoKoba_Date_Early_Aurignacian_VI.prior",))
{
latitude=43.066;
longitude=-2.458;
site="Labeko Koba";
culture="Early Aurignacian";
author="AMH";
};
Date(Prior("Strat - Labeko Koba - Date V",
```

```
"Priors_Strat/LabekoKoba_Date_Early_Aurignacian_V.prior",))
{
latitude=43.066;
longitude=-2.458;
site="Labeko Koba";
culture="Early Aurignacian";
author="AMH";
};
Date(Prior("Strat - Labeko Koba - Date IV",
"Priors_Strat/LabekoKoba_Date_Early_Aurignacian_IV.prior",))
{
latitude=43.066;
longitude=-2.458;
site="Labeko Koba";
culture="Early Aurignacian";
author="AMH";
};
Date(Prior("KDE - Mitoc-Malul Galben",
"Priors_KDE/KDE_Mitoc_Malul_Galben.prior",))
{
latitude=48.111;
longitude=27.036;
site="Mitoc-Malul Galben";
culture="Aurignacian";
author="AMH";
};
Date(Prior("KDE - Moravia Aurignacian",
"Priors_KDE/KDE_Aurignacian_Moravia.prior",))
{
latitude=49.5;
longitude=17;
site="Moravia Aurignacian";
culture="Aurignacian";
author="AMH";
};
Date(Prior("Strat - Riparo Mochi - Date Proto-Aurig",
"Priors_Strat/RiparoMochi_Date_Proto_Aurignacian.prior",))
{
latitude=43.7894;
longitude=7.5475;
site="Riparo Mochi";
culture="Proto-Aurignacian";
author="AMH";
};
Date(Prior("Strat - Riparo Mochi - Date Early Aurig",
"Priors_Strat/RiparoMochi_Date_Early_Aurignacian.prior",))
{
latitude=43.7894;
longitude=7.5475;
site="Riparo Mochi";
culture="Early Aurignacian";
author="AMH";
};
Date(Prior("Strat - Riparo Mochi - Date Gravettian",
"Priors_Strat/RiparoMochi_Date_Gravettian.prior",))
{
latitude=43.7894;
longitude=7.5475;
site="Riparo Mochi";
culture="Gravettian";
author="AMH";
};
Date(Prior("Strat - Salitrena Pecina - Date Aurignacian",
"Priors_Strat/SalitrenaPecina_Date_Aurignacian.prior",))
{
latitude=44.1905;
longitude=20.0835;
site="Šalitrena Pećina";
culture="Aurignacian";
author="AMH";
};
Date(Prior("KDE - Vogelherd",
"Priors_KDE/KDE_Vogelherd.prior",))
{
latitude=48.5606;
longitude=10.1913;
site="Vogelherd";
culture="Aurignacian";
author="AMH";
};
Date(Prior("Strat - Willendorf II - Date D1/D2",
"Priors_Strat/Willendorf_Date_Micoquian_D1_D2.prior",))
{
latitude=48.323;
longitude=15.399;
site="Willendorf II";
culture="Micoquian";
author="Neanderthal";
};
Date(Prior("Strat - Willendorf II - Date C8-3",
"Priors_Strat/Willendorf_Date_Early_Aurignaican_C8_3.prior",))
{
latitude=48.323;
longitude=15.399;
site="Willendorf II";
culture="Early Aurignacian";
author="AMH";
};
Date(Prior("Strat - Willendorf II - Date C8-2",
"Priors_Strat/Willendorf_Date_Aurignaican_C8_2.prior",))
{
latitude=48.323;
longitude=15.399;
site="Willendorf II";
culture="Aurignacian";
author="AMH";
};
Date(Prior("Strat - Willendorf II - Date C7-1",
"Priors_Strat/Willendorf_Date_Aurignaican_C7_1.prior",))
{
latitude=48.323;
longitude=15.399;
site="Willendorf II";
culture="Aurignacian";
author="AMH";
};
Date(Prior("Strat - Willendorf II - Date C4-2",
"Priors_Strat/Willendorf_Date_C4_2.prior",))
{
latitude=48.323;
longitude=15.399;
site="Willendorf II";
culture="Aurignacian";
author="AMH";
};
Date(Prior("Strat - Willendorf II - Date C4-1",
"Priors_Strat/Willendorf_Date_C4_1.prior",))
{
latitude=48.323;
longitude=15.399;
site="Willendorf II";
culture="Aurignacian";
author="AMH";
};
Date(Prior("MOD10 - Dzerava Skala - Date 5a",
"Priors_Strat_DPhil/Der_MOD10_Date_5a_.prior",))
{
latitude=48.496987;
longitude=17.324692;
site="Dzerava Skala";
culture="Aurignacian Point";
author="AMH";
};
Date(Prior("MOD10 - Dzerava Skala - Date 9",
"Priors_Strat_DPhil/Der_MOD10_Date_9.prior",))
{
latitude=48.496987;
longitude=17.324692;
site="Dzerava Skala";
culture="Aurignacian Point";
author="AMH";
};
Date(Prior("MOD10 - Dzerava Skala - Date 5",
"Priors_Strat_DPhil/Der_MOD10_Date_5.prior",))
{
latitude=48.496987;
longitude=17.324692;
site="Dzerava Skala";
culture="Gravettian";
author="AMH";
};
Date(Prior("MOD10 - Dzerava Skala - Date 4",
"Priors_Strat_DPhil/Der_MOD10_Date_4.prior",))
{
latitude=48.496987;
longitude=17.324692;
```

```
site="Dzerava Skala";
culture="Gravettian";
author="AMH";
};
Date(Prior("Points KDE2 - Istallosko",
"Priors_KDE_DPhil/Istall_Points_KDE_2.prior",))
{
latitude=48.071667;
longitude=20.418889;
site="Istallosko";
culture="Aurignacian Point";
author="AMH";
};
R_Date("OxA-X-2716-49",31800,1000)
{
latitude=47.723889;
longitude=18.575278;
site="Jankovich";
culture="Aurignacian Point";
author="AMH";
};
R_Date("OxA-X-2716-48",32500,800)
{
latitude=47.723889;
longitude=18.575278;
site="Jankovich";
culture="Aurignacian Point";
author="AMH";
};
R_Date("OxA-X-2732-10",32750,670)
{
latitude=47.723889;
longitude=18.575278;
site="Jankovich";
culture="Aurignacian Point";
author="AMH";
};
R_Date("OxA-35386",30800,500)
{
latitude=47.723889;
longitude=18.575278;
site="Jankovich";
culture="Aurignacian Point";
author="AMH";
};
Date(Prior("MOD3 - Kozarnika - Date 6/7 ls lp",
"Priors_Strat_DPhil/Kz_MOD3_Date_6_7_ls_lp.prior",))
{
latitude=43.651722;
longitude=22.702472;
site="Kozarnika";
culture="IUP";
author="Neanderthal";
};
Date(Prior("MOD3 - Kozarnika - Date 6/7 lb",
"Priors_Strat_DPhil/Kz_MOD3_Date_6_7_lb.prior",))
{
latitude=43.651722;
longitude=22.702472;
site="Kozarnika";
culture="IUP";
author="Neanderthal";
};
Date(Prior("MOD3 - Kozarnika - Date 5b",
"Priors_Strat_DPhil/Kz_MOD3_Date_5b.prior",))
{
latitude=43.651722;
longitude=22.702472;
site="Kozarnika";
culture="Kozarnikian";
author="AMH";
};
Date(Prior("MOD3 - Kozarnika - Date 5a",
"Priors_Strat_DPhil/Kz_MOD3_Date_5a.prior",))
{
latitude=43.651722;
longitude=22.702472;
site="Kozarnika";
culture="Kozarnikian";
author="AMH";
};
Date(Prior("MOD3 - Kozarnika - Date 4",
"Priors_Strat_DPhil/Kz_MOD3_Date_4.prior",))
{
latitude=43.651722;
longitude=22.702472;
site="Kozarnika";
culture="Kozarnikian";
author="AMH";
};
R_Date("OxA-35404",27600,400)
{
latitude=43.15;
longitude=24.71;
site="Tabashkata";
culture="Aurignacian Point";
author="AMH";
};
Date(Prior("MOD3 - Temnata - Date TD-V 5pg",
"Priors_Strat_DPhil/TD_Date_5pg_TD_V.prior",))
{
latitude=43.174969;
longitude=24.074006;
site="Temnata";
culture="Mousterian";
author="Neanderthal";
};
Date(Prior("MOD3 - Temnata - Date TD-V 3v",
"Priors_Strat_DPhil/TD_Date_3v_TD_V.prior",))
{
latitude=43.174969;
longitude=24.074006;
site="Temnata";
culture="Aurignacian-like";
author="AMH";
};
Date(Prior("MOD3 - Temnata - Date TD-V 3d",
"Priors_Strat_DPhil/TD_Date_3d_TD_V.prior",))
{
latitude=43.174969;
longitude=24.074006;
site="Temnata";
culture="Gravettian";
author="AMH";
};
R_Date("OxA-17967",38300,1500)
{
latitude=48.0468;
longitude=20.4264;
site="Pesko";
culture="Aurignacian Point";
author="AMH";
};
R_Date("OxA-17964",33500,450)
{
latitude=48.0468;
longitude=20.4264;
site="Pesko";
culture="Aurignacian Point";
author="AMH";
};
R_Date("OxA-17966",36400,800)
{
latitude=48.0468;
longitude=20.4264;
site="Pesko";
culture="Aurignacian Point";
author="AMH";
};
R_Date("OxA-19621",33750,350)
{
latitude=47.138;
longitude=5.571;
site="Trou de la Mere Clochette";
culture="Aurignacian Point";
author="AMH";
};
R_Date("OxA-19622",35460,250)
{
latitude=47.138;
longitude=5.571;
site="Trou de la Mere Clochette";
culture="Aurignacian Point";
author="AMH";
};
R_Date("OxA-14436",33640,250)
```

```
{
latitude=50.16944;
longitude=19.80723;
site="Mamutowa cave";
culture="Aurignacian Point";
author="AMH";
};
R_Date("OxA-14434",35460,220)
{
latitude=50.16944;
longitude=19.80723;
site="Mamutowa cave";
culture="Aurignacian Point";
author="AMH";
};
R_Date("OxA-17963",35600,400)
{
latitude=48.4922;
longitude=17.295;
site="Dzerava skala";
culture="Aurignacian Point";
author="AMH";
};
R_Date("OxA-X-2170-18",33600,900)
{
latitude=48.0654;
longitude=20.4108;
site="Istallosko";
culture="Aurignacian Point";
author="AMH";
};
R_Date("OxA-21783",32100,450)
{
latitude=42.1607;
longitude=2.74401;
site="Arbreda";
culture="Aurignacian Point";
author="AMH";
};
R_Date("OxA-13716",31730,250)
{
latitude=51.3204;
longitude= 2.9781;
site="Uphill Quarry cave 8 ";
culture="Aurignacian Point";
author="AMH";
};
R_Date("OxA-13803",31550,340)
{
latitude=51.2263;
longitude=2.6761;
site="Hyaena Den cave ";
culture="Aurignacian Point";
author="AMH";
};
R_Date("GrA-32619",32830,195)
{
latitude=50.4781;
longitude=4.679;
site="Grotte de la Betche-aux-Rotches, Spy";
culture="Aurignacian Point";
author="AMH";
};
R_Date("OxA-7496",30750,850)
{
latitude=50.421;
longitude=5.294;
site="Trou al'Wesse";
culture="Aurignacian Point";
author="AMH";
};
R_Date("KIA-19541",31310,235)
{
latitude=48.5603;
longitude=10.1913;
site="Vogelherd cave";
culture="Aurignacian Point";
author="AMH";
};
R_Date("KIA-19551",32470,265)
{
latitude=48.4089;
longitude=9.772;
site="Brillenhohle";
culture="Aurignacian Point";
author="AMH";
};
R_Date("KIA-19550[a]",30400,235)
{
latitude=48.4089;
longitude=9.772;
site="Brillenhohle";
culture="Aurignacian Point";
author="AMH";
};
R_Date("KIA-13082",26730,165)
{
latitude=48.3842;
longitude=9.7614;
site="Sirgenstein cave";
culture="Aurignacian Point";
author="AMH";
};
R_Date("KIA-13079",27250,175)
{
latitude=48.3842;
longitude=9.7614;
site="Sirgenstein cave";
culture="Aurignacian Point";
author="AMH";
};
R_Date("KIA-19543[a]",32010,494)
{
latitude=47.5924;
longitude=12.197;
site="Tischoferhohle";
culture="Aurignacian Point";
author="AMH";
};
R_Date("KIA-19544[a]",31530,205)
{
latitude=47.5924;
longitude=12.197;
site="Tischoferhohle";
culture="Aurignacian Point";
author="AMH";
};
R_Date("KIA-19545",29500,200)
{
latitude=47.5924;
longitude=12.197;
site="Tischoferhohle";
culture="Aurignacian Point";
author="AMH";
};
R_Date("VERA-2522",30140,335)
{
latitude=46.4493;
longitude=14.6691;
site="Potocka zijalka";
culture="Aurignacian Point";
author="AMH";
};
R_Date("OxA-27854",30800,370)
{
latitude=46.4493;
longitude=14.6691;
site="Potocka zijalka";
culture="Aurignacian Point";
author="AMH";
};
R_Date("OxA-28038",31950,450)
{
latitude=46.4493;
longitude=14.6691;
site="Potocka zijalka";
culture="Aurignacian Point";
author="AMH";
};
R_Date("OxA-28061",32550,550)
{
latitude=46.4493;
longitude=14.6691;
site="Potocka zijalka";
culture="Aurignacian Point";
author="AMH";
```

```
};
R_Date("OxA-27850",30380,370)
{
latitude=46.4493;
longitude=14.6691;
site="Potocka zijalka";
culture="Aurignacian Point";
author="AMH";
};
R_Date("OxA-27849",31220,400)
{
latitude=46.4493;
longitude=14.6691;
site="Potocka zijalka";
culture="Aurignacian Point";
author="AMH";
};
R_Date("OxA-27852",31360,400)
{
latitude=46.4493;
longitude=14.6691;
site="Potocka zijalka";
culture="Aurignacian Point";
author="AMH";
};
R_Date("OxA-27853",31500,400)
{
latitude=46.4493;
longitude=14.6691;
site="Potocka zijalka";
culture="Aurignacian Point";
author="AMH";
};
R_Date("OxA-27851",30910,380)
{
latitude=46.4493;
longitude=14.6691;
site="Potocka zijalka";
culture="Aurignacian Point";
author="AMH";
};
R_Date("OxA-15334",31600,900)
{
latitude=48.4922;
longitude=17.295;
site="Dzerava skala";
culture="Aurignacian Point";
author="AMH";
};
R_Date("OxA-15335",31000,1000)
{
latitude=48.4922;
longitude=17.295;
site="Dzerava skala";
culture="Aurignacian Point";
author="AMH";
};
R_Date("OxA-28219",29760,340)
{
latitude=46.112778;
longitude=13.915556;
site="Divije babe I";
culture="Aurignacian Point";
author="AMH";
};
R_Date("OxA-X-2517-52",34750,600)
{
latitude=46.308806;
longitude=14.568194;
site="Morkiska jama";
culture="Aurignacian Point";
author="AMH";
};
R_Date("OxA-27855",32600,450)
{
latitude=46.308806;
longitude=14.568194;
site="Morkiska jama";
culture="Aurignacian Point";
author="AMH";
};
Label("Humans");
R_Date("OxA-21839",39700,1100)
{
longitude=40.0034;
latitude=44.2217;
culture="MP";
author="Neanderthal";
species="Neanderthal";
site="Mezmaiskaya";
};
Date("OxA-15257",N(calBP(48900),1100))
{
longitude=0.741;
latitude=46.415;
culture="Mousterian";
author="Neanderthal";
species="Neanderthal";
site="Les Rochers-de-Villeneuve";
};
R_Date("ETH-20981",39900,620)
{
longitude=6.9363;
latitude=51.2206;
culture="MP";
author="Neanderthal";
species="Neanderthal";
site="Kleine Feldhöfergrotte";
};
R_Date("ETH-19660",39240,670)
{
longitude=6.9363;
latitude=51.2206;
culture="MP";
author="Neanderthal";
species="Neanderthal";
site="Kleine Feldhöfergrotte";
};
R_Date("GrA-32626",36350,295)
{
longitude=4.6743;
latitude=50.4803;
culture="LRJ or Mousterian";
author="Neanderthal";
species="Neanderthal";
site="Spy";
};
R_Date("GrA-32623",35810,250)
{
longitude=4.6743;
latitude=50.4803;
culture="LRJ or Mousterian";
author="Neanderthal";
species="Neanderthal";
site="Spy";
};
R_Date("ETH-19661",40360,760)
{
longitude=6.9363;
latitude=51.2206;
culture="MP";
author="Neanderthal";
species="Neanderthal";
site="Kleine Feldhöfergrotte";
};
R_Date("OxA-10560",36250,500)
{
longitude=4.6743;
latitude=50.4803;
culture="unknown";
author="Neanderthal";
species="Neanderthal";
site="Spy";
};
Date("GifA-99167",N(calBP(55090),2600))
{
longitude=-5.733;
latitude=43.386;
culture="Mousterian";
author="Neanderthal";
species="Neanderthal";
site="El Sidron";
};
Date("GifA-99704",N(calBP(54930),2500))
{
longitude=-5.733;
```

```
latitude=43.386;
culture="Mousterian";
author="Neanderthal";
species="Neanderthal";
site="El Sidron";
};
Date("OxA-21776",N(calBP(56230),3200))
{
longitude=-5.733;
latitude=43.386;
culture="Mousterian";
author="Neanderthal";
species="Neanderthal";
site="El Sidron";
};
R_Date("OxA-X-2689-09",42700,1600)
{
longitude=16.088;
latitude=46.305;
culture="MP";
author="Neanderthal";
species="Neanderthal";
site="Vindija";
};
Date("OxA-X-2689-10",N(calBP(48800),2000))
{
longitude=16.088;
latitude=46.305;
culture="MP";
author="Neanderthal";
species="Neanderthal";
site="Vindija";
};
R_Date("OxA-X-2717-11",44300,1200)
{
longitude=16.088;
latitude=46.305;
culture="MP";
author="Neanderthal";
species="Neanderthal";
site="Vindija";
};
Date("OxA-X-2687-57",N(calBP(49960),1500))
{
longitude=16.088;
latitude=46.305;
culture="MP";
author="Neanderthal";
species="Neanderthal";
site="Vindija";
};
R_Date("GrA-50457",32450,240)
{
longitude=34.396;
latitude=45.16;
culture="Gravettian";
author="AMH";
species="AMH";
site="Buran-Kaya III";
};
R_Date("GrA-24398",28890,170)
{
longitude=21.91;
latitude=45.0177;
culture="unknown";
author="AMH";
species="AMH";
site="Pestera cu Oase";
};
R_Date("OxA-4586",31000,500)
{
longitude=20.1563;
latitude=49.443;
culture="Aurignacian";
author="AMH";
species="AMH";
site="Oblazowa";
};
R_Date("VERA-3074",31320,400)
{
longitude=17.0167;
latitude=49.707;
culture="Aurignacian";
author="AMH";
species="AMH";
site="Mladec";
};
R_Date("OxA-11711",34950,990)
{
longitude=21.91;
latitude=45.0177;
culture="unknown";
author="AMH";
species="AMH";
site="Pestera cu Oase";
};
R_Date("GrA-37938",31900,230)
{
longitude=34.396;
latitude=45.16;
culture="Gravettian";
author="AMH";
species="AMH";
site="Buran-Kaya III";
};
R_Date("VERA-3073",31190,400)
{
longitude=17.0167;
latitude=49.707;
culture="Aurignacian";
author="AMH";
species="AMH";
site="Mladec";
};
R_Date("VERA-3076 A",31500,410)
{
longitude=17.0167;
latitude=49.707;
culture="Aurignacian";
author="AMH";
species="AMH";
site="Mladec";
};
R_Date("OxA-16412",28870,180)
{
longitude=-4.2555;
latitude=51.5499;
culture="Gravettian";
author="AMH";
species="";
site="Paviland";
};
R_Date("OxA-16413",29490,210)
{
longitude=-4.2555;
latitude=51.5499;
culture="Gravettian";
author="AMH";
species="";
site="Paviland";
};
R_Date("ERL-9415",30640,640)
{
longitude=3.0905;
latitude=43.1313;
culture="Aurignacian";
author="AMH";
species="AMH";
site="La Crouzade";
};
R_Date("OxA-15527",28150,170)
{
longitude=23.1296;
latitude=45.5862;
culture="Aurignacian?";
author="AMH";
species="AMH";
site="Cioclovina";
};
R_Date("OxA-15529",29930,170)
{
longitude=23.755;
latitude=45.1895;
culture="Uluzzian";
author="AMH";
species="AMH";
```

```
site="Pestera Muierii";
};
R_Date("OxA-16252",29110,190)
{
longitude=23.755;
latitude=45.1895;
culture="Uluzzian";
author="AMH";
species="AMH";
site="Pestera Muierii";
};
```

```
R_Date("OxA-13302",32790,280)
{
longitude=34.396;
latitude=45.16;
culture="Gravettian";
author="AMH";
species="AMH";
site="Buran-Kaya III";
};
};
```

Spatio-temporal distribution: map 2 modified – see figure 15.19

```
 Plot()
{
Date(Prior("Strat - Bacho Kiro - Date Mouserian",
"Priors_Strat/BachoKiro_Date_Mousterian.prior",))
{
latitude=42.947378;
longitude=25.331867;
site="Bacho Kiro";
culture="Mousterian";
author="Neanderthal";
};
Date(Prior("Strat - Willendorf II - Date D3",
"Priors_Strat/Willendorf_Date_Micoquian_D3.prior",))
{
latitude=48.323;
longitude=15.399;
site="Willendorf II";
culture="Micoquian";
author="Neanderthal";
};
Date(Prior("Strat - Labeko Koba - Date IX lower",
"Priors_Strat/LabekoKoba_Date_Chatelperronian.prior",))
{
latitude=43.066;
longitude=-2.458;
site="Labeko Koba";
culture="Chatelperronian";
author="Neanderthal";
};
Date(Prior("KDE - Moravia Szeletian",
"Priors_KDE/KDE_Szeletian_Moravia.prior",))
{
latitude=49.5;
longitude=17;
site="Moravia Szeletian";
culture="Szeletian";
author="Neanderthal";
};
Date(Prior("Strat - Ksar Akil - Date IUP",
"Priors_Strat/KsarAkil_Date_IUP.prior",))
{
latitude=33.916667;
longitude=35.6;
site="Ksar Akil";
culture="IUP";
author="Neanderthal";
};
Date(Prior("Strat - Bacho Kiro - Date Bachokirian",
"Priors_Strat/BachoKiro_Date_Bachokirian.prior",))
{
latitude=42.947378;
longitude=25.331867;
site="Bacho Kiro";
culture="Bachokirian";
author="Neanderthal";
};
Date(Prior("Strat - Castelcivita - Date Uluzzian",
"Priors_Strat/Castelcivitas_Uluzzian.prior",))
{
latitude=40.495;
longitude=15.237;
site="Castelcivita";
culture="Uluzzian";
author="Neanderthal";
};
Date(Prior("KDE - Moravia Bohunician",
"Priors_KDE/KDE_Bohunician_Moravia.prior",))
{
latitude=49.5;
longitude=17;
site="Moravia Bohunician";
culture="Bohunician";
author="Neanderthal";
};
Date(Prior("MOD3 - Kozarnika - Date 5c",
"Priors_Strat_DPhil/Kz_MOD3_Date_5c.prior",))
{
latitude=43.651722;
longitude=22.702472;
site="Kozarnika";
culture="Kozarnikian";
author="Neanderthal";
};
Date(Prior("Strat - Fumane - Date A2",
"Priors_Strat/Fumane_Date_A2_Proto_Aurignacian.prior",))
{
latitude=45.57;
longitude=10.902;
site="Fumane";
culture="Proto-Aurignacian";
author="AMH";
};
Date(Prior("Strat - El Castillo - Date 18C",
"Priors_Strat/ElCastillo_Date_Transitional_Aurignacian_18C.prior",))
{
latitude=43.2875;
longitude=-3.9598;
site="El Castillo";
culture="'Transitional Aurignacian'";
author="AMH";
};
Date(Prior("Strat - Isturitz - Date C4d1",
"Priors_Strat/Isturitz_Date_Proto_Aurignacian_C4d1.prior",))
{
latitude=43.371;
longitude=-1.196;
site="Isturitz";
culture="Proto-/Early Aurignacian";
author="AMH";
};
R_Date("OxA-X-2732-11",31100,520)
{
latitude=45.3605642;
longitude=14.7527073;
site="Bukovac";
culture="Aurignacian Point";
author="AMH";
};
Date(Prior("MOD3 - Temnata - Date TD-V 4",
"Priors_Strat_DPhil/TD_Date_4_TD_V.prior",))
{
latitude=43.174969;
longitude=24.074006;
site="Temnata";
```

```
culture="Aurignacian-like";
author="Neanderthal";
};
Date(Prior("Strat - Geissenklosterle - Date III",
"Priors_Strat/Geissenklosterle_EarlyAurig.prior",))
{
latitude=48.401;
longitude=9.772;
site="Geißenklösterle";
culture="Early Aurignacian";
author="AMH";
};
Date(Prior("Strat - Ksar Akil - Date Phase 2",
"Priors_Strat/KsarAkil_Date_Early_Ahmarian.prior",))
{
latitude=33.916667;
longitude=35.6;
site="Ksar Akil";
culture="Early Ahmarian";
author="AMH";
};
Date(Prior("Strat - Bacho Kiro - Date Aurignacian",
"Priors_Strat/BachoKiro_Date_Aurignacian.prior",))
{
latitude=42.947378;
longitude=25.331867;
site="Bacho Kiro";
culture="Aurignacian";
author="Neanderthal";
};
Date(Prior("Strat - Geissenklosterle - Date II",
"Priors_Strat/Geissenklosterle_UpperAurig.prior",))
{
latitude=48.401;
longitude=9.772;
site="Geißenklösterle";
culture="Upper Aurignacian";
author="AMH";
};
Date(Prior("Strat - L'Arbreda - Date Evolved Aurig",
"Priors_Strat/LArbreda_Date_Evolved_Aurignacian.prior",))
{
latitude=42.161;
longitude=2.747;
site="L'Arbreda";
culture="Evolved Aurignacian";
author="AMH";
};
Date(Prior("Strat - Buran-Kaya III - Gravettian 6-2",
"Priors_Strat/BuranKayaIII_Date_Gravettian_6_2.prior",))
{
latitude=45.16;
longitude=34.396;
site="Buran-Kaya III";
culture="Gravettian";
author="AMH";
};
Date(Prior("Strat - Buran-Kaya III - Micoquian",
"Priors_Strat/BuranKayaIII_Date_Micoquian.prior",))
{
latitude=45.16;
longitude=34.396;
site="Buran-Kaya III";
culture="Micoquian";
author="Neanderthal";
};
Date(Prior("Strat - Buran-Kaya III - Aurignacian 6-5",
"Priors_Strat/BuranKayaIII_Date_Aurig_6_5.prior",))
{
latitude=45.16;
longitude=34.396;
site="Buran-Kaya III";
culture="Aurignacian";
author="AMH";
};
Date(Prior("Strat - Buran-Kaya III - Aurignacian 6-4",
"Priors_Strat/BuranKayaIII_Date_Aurig_6_4.prior",))
{
latitude=45.16;
longitude=34.396;
site="Buran-Kaya III";
culture="Aurignacian";
author="AMH";
};
Date(Prior("Strat - Buran-Kaya III - Aurignacian 6-3",
"Priors_Strat/BuranKayaIII_Date_Aurig_6_3.prior",))
{
latitude=45.16;
longitude=34.396;
site="Buran-Kaya III";
culture="Aurignacian";
author="AMH";
};
Date(Prior("Strat - Buran-Kaya III - Gravettian 6-1",
"Priors_Strat/BuranKayaIII_Date_Gravettian_6_1.prior",))
{
latitude=45.16;
longitude=34.396;
site="Buran-Kaya III";
culture="Gravettian";
author="AMH";
};
Date(Prior("Strat - Buran-Kaya III - Gravettian 5-2",
"Priors_Strat/BuranKayaIII_Date_Gravettian_5_2.prior",))
{
latitude=45.16;
longitude=34.396;
site="Buran-Kaya III";
culture="Gravettian";
author="AMH";
};
Date(Prior("Strat - Castelcivita - Date Mousterian",
"Priors_Strat/Castelcivita_Mousterian.prior",))
{
latitude=40.495;
longitude=15.237;
site="Castelcivita";
culture="Mousterian";
author="Neanderthal";
};
Date(Prior("Strat - Castelcivita - Date Aurignacian",
"Priors_Strat/Castelcivita_Aurignacian.prior",))
{
latitude=40.495;
longitude=15.237;
site="Castelcivita";
culture="Aurignacian";
author="AMH";
};
Date(Prior("Strat - Cavallo - Date EII/I",
"Priors_Strat/CAVALLO_Date_EII_I_Uluzzian.prior",))
{
latitude=40.154;
longitude=17.96;
site="Cavallo";
culture="Uluzzian";
author="Neanderthal";
};
Date(Prior("Strat - Cavallo - Date E/D",
"Priors_Strat/CAVALLO_Date_E_D_Uluzzian.prior",))
{
latitude=40.154;
longitude=17.96;
site="Cavallo";
culture="Uluzzian";
author="Neanderthal";
};
Date(Prior("Strat - Cavallo - Date DII",
"Priors_Strat/CAVALLO_Date_DII_Uluzzian.prior",))
{
latitude=40.154;
longitude=17.96;
site="Cavallo";
culture="Uluzzian";
author="Neanderthal";
};
Date(Prior("Strat - Cavallo - Date Dib",
"Priors_Strat/CAVALLO_Date_DIb_Uluzzian.prior",))
{
latitude=40.154;
longitude=17.96;
site="Cavallo";
culture="Uluzzian";
author="Neanderthal";
};
Date(Prior("Strat - El Castillo - Date 20C",
```

```
"Priors_Strat/ElCastillo_Date_Mousterian.prior",))
{
latitude=43.2875;
longitude=-3.9598;
site="El Castillo";
culture="Mousterian";
author="Neanderthal";
};
Date(Prior("Strat - El Castillo - Date 18B",
"Priors_Strat/ElCastillo_Date_Transitional_
Aurignacian_18B.prior",))
{
latitude=43.2875;
longitude=-3.9598;
site="El Castillo";
culture="‘Transitional Aurignacian’";
author="AMH";
};
Date(Prior("Strat - Fumane - Date A4",
"Priors_Strat/Fumane_Date_A4_Uluzzian.prior",))
{
latitude=45.57;
longitude=10.902;
site="Fumane";
culture="Uluzzian";
author="Neanderthal";
};
Date(Prior("Strat - Fumane - Date A3",
"Priors_Strat/Fumane_Date_A3_Uluzzian.prior",))
{
latitude=45.57;
longitude=10.902;
site="Fumane";
culture="Uluzzian";
author="Neanderthal";
};
Date(Prior("Strat - Fumane - Date A1",
"Priors_Strat/Fumane_Date_A1_Proto_Aurignacian.prior",))
{
latitude=45.57;
longitude=10.902;
site="Fumane";
culture="Proto-Aurignacian";
author="AMH";
};
Date(Prior("Strat - Fumane - Date D",
"Priors_Strat/Fumane_Date_D_Aurignacian.prior",))
{
latitude=45.57;
longitude=10.902;
site="Fumane";
culture="Aurignacian";
author="AMH";
};
Date(Prior("Strat - Geissenklosterle - Date IV",
"Priors_Strat/Geissenklosterle_Mousterian.prior",))
{
latitude=48.401;
longitude=9.772;
site="Geißenklösterle";
culture="Mousterian";
author="Neanderthal";
};
Date(Prior("Strat - Geissenklosterle - Date I",
"Priors_Strat/Geissenklosterle_Gravettian.prior",))
{
latitude=48.401;
longitude=9.772;
site="Geißenklösterle";
culture="Gravettian";
author="AMH";
};
Date(Prior("Strat - Hohle Fels - Date IX",
"Priors_Strat/HohleFels_Date_IX_Mousterian.prior",))
{
latitude=48.378;
longitude=9.758;
site="Hohle Fels";
culture="Mousterian";
author="Neanderthal";
};
Date(Prior("Strat - Hohle Fels - Date VIII",
"Priors_Strat/HohleFels_Date_VIII_Mousterian.prior",))
{
latitude=48.378;
longitude=9.758;
site="Hohle Fels";
culture="Mousterian";
author="Neanderthal";
};
Date(Prior("Strat - Hohle Fels - Date VII",
"Priors_Strat/HohleFels_Date_VII_Mousterian.prior",))
{
latitude=48.378;
longitude=9.758;
site="Hohle Fels";
culture="Mousterian";
author="Neanderthal";
};
Date(Prior("Strat - Hohle Fels - Date VI",
"Priors_Strat/HohleFels_Date_VI_Mousterian.prior",))
{
latitude=48.378;
longitude=9.758;
site="Hohle Fels";
culture="Mousterian";
author="Neanderthal";
};
Date(Prior("Strat - Hohle Fels - Date V",
"Priors_Strat/HohleFels_Date_V_Aurignacian.prior",))
{
latitude=48.378;
longitude=9.758;
site="Hohle Fels";
culture="Aurignacian";
author="AMH";
};
Date(Prior("Strat - Hohle Fels - Date IV",
"Priors_Strat/HohleFels_Date_IV_Aurignacian.prior",))
{
latitude=48.378;
longitude=9.758;
site="Hohle Fels";
culture="Aurignacian";
author="AMH";
};
Date(Prior("Strat - Hohle Fels - Date III",
"Priors_Strat/HohleFels_Date_III_Aurignacian.prior",))
{
latitude=48.378;
longitude=9.758;
site="Hohle Fels";
culture="Aurignacian";
author="AMH";
};
Date(Prior("Strat - Hohle Fels - Date II",
"Priors_Strat/HohleFels_Date_II_Aurignacian.prior",))
{
latitude=48.378;
longitude=9.758;
site="Hohle Fels";
culture="Aurignacian";
author="AMH";
};
Date(Prior("KDE - Hohlenstein-Stadel",
"Priors_KDE/KDE_Hohlenstein_Stadel_short_.prior",))
{
latitude=48.551;
longitude=10.168;
site="Hohlenstein-Stadel";
culture="Aurignacian";
author="AMH";
};
Date(Prior("Strat - Isturitz - Date C5",
"Priors_Strat/Isturitz_Date_Proto_Aurignacian_C5.prior",))
{
latitude=43.371;
longitude=-1.196;
site="Isturitz";
culture="Proto-Aurignacian";
author="AMH";
};
Date(Prior("Strat - Isturitz - Date C4c4",
"Priors_Strat/Isturitz_ProtoEarly_Aurignacian_C4c4.prior",))
{
latitude=43.371;
```

```
longitude=-1.196;
site="Isturitz";
culture="Proto-Aurignacian";
author="AMH";
};
Date(Prior("Strat - Isturitz - Date C4b2",
"Priors_Strat/Isturitz_Date_Early_Aurignacian_C4b2.prior",))
{
latitude=43.371;
longitude=-1.196;
site="Isturitz";
culture="Early Aurignacian";
author="AMH";
};
Date(Prior("Strat - Isturitz - Date C4b1",
"Priors_Strat/Isturitz_Date_Early_Aurignacian_C4b1.prior",))
{
latitude=43.371;
longitude=-1.196;
site="Isturitz";
culture="Early Aurignacian";
author="AMH";
};
Date(Prior("Strat - Ksar Akil - Date Mousterian",
"Priors_Strat/KsarAkil_Date_Mousterian.prior",))
{
latitude=33.916667;
longitude=35.6;
site="Ksar Akil";
culture="Mousterian";
author="Neanderthal";
};
Date(Prior("Strat - Ksar Akil - Date Phase 3-4",
"Priors_Strat/KsarAkil_Date_Phases_3_4.prior",))
{
latitude=33.916667;
longitude=35.6;
site="Ksar Akil";
culture="Early Ahmarian";
author="AMH";
};
Date(Prior("Strat - Ksar Akil - Date Phase 5",
"Priors_Strat/KsarAkil_Date_Phases_5.prior",))
{
latitude=33.916667;
longitude=35.6;
site="Ksar Akil";
culture="Early Ahmarian";
author="AMH";
};
Date(Prior("Strat - Ksar Akil - Date Phase 6",
"Priors_Strat/KsarAkil_Date_Phases_6.prior",))
{
latitude=33.916667;
longitude=35.6;
site="Ksar Akil";
culture="Early Ahmarian";
author="AMH";
};
Date(Prior("Strat - Ksar Akil - Date Phase 7",
"Priors_Strat/KsarAkil_Date_Phases_7.prior",))
{
latitude=33.916667;
longitude=35.6;
site="Ksar Akil";
culture="Early Ahmarian";
author="AMH";
};
Date(Prior("Strat - L'Arbreda - Date Mousterian",
"Priors_Strat/LArbreda_Date_Mousterian.prior",))
{
latitude=42.161;
longitude=2.747;
site="L'Arbreda";
culture="Mousterian";
author="Neanderthal";
};
Date(Prior("Strat - L'Arbreda - Date Proto-Aurig",
"Priors_Strat/LArbreda_Date_Proto_Aurignacian.prior",))
{
latitude=42.161;
longitude=2.747;
site="L'Arbreda";
culture="Proto-Aurignacian";
author="AMH";
};
Date(Prior("Strat - L'Arbreda - Date Gravettian F",
"Priors_Strat/LArbreda_Date_Gravettian_F.prior",))
{
latitude=42.161;
longitude=2.747;
site="L'Arbreda";
culture="Gravettian";
author="AMH";
};
Date(Prior("Strat - L'Arbreda - Date Gravettian E",
"Priors_Strat/LArbreda_Date_Gravettian_E.prior",))
{
latitude=42.161;
longitude=2.747;
site="L'Arbreda";
culture="Gravettian";
author="AMH";
};
Date(Prior("Strat - Labeko Koba - Date VII",
"Priors_Strat/LabekoKoba_Date_Proto_Aurignacian.prior",))
{
latitude=43.066;
longitude=-2.458;
site="Labeko Koba";
culture="Proto-Aurignacian";
author="AMH";
};
Date(Prior("Strat - Labeko Koba - Date VI",
"Priors_Strat/LabekoKoba_Date_Early_Aurignacian_VI.prior",))
{
latitude=43.066;
longitude=-2.458;
site="Labeko Koba";
culture="Early Aurignacian";
author="AMH";
};
Date(Prior("Strat - Labeko Koba - Date V",
"Priors_Strat/LabekoKoba_Date_Early_Aurignacian_V.prior",))
{
latitude=43.066;
longitude=-2.458;
site="Labeko Koba";
culture="Early Aurignacian";
author="AMH";
};
Date(Prior("Strat - Labeko Koba - Date IV",
"Priors_Strat/LabekoKoba_Date_Early_Aurignacian_IV.prior",))
{
latitude=43.066;
longitude=-2.458;
site="Labeko Koba";
culture="Early Aurignacian";
author="AMH";
};
Date(Prior("KDE - Mitoc-Malul Galben",
"Priors_KDE/KDE_Mitoc_Malul_Galben.prior",))
{
latitude=48.111;
longitude=27.036;
site="Mitoc-Malul Galben";
culture="Aurignacian";
author="AMH";
};
Date(Prior("KDE - Moravia Aurignacian",
"Priors_KDE/KDE_Aurignacian_Moravia.prior",))
{
latitude=49.5;
longitude=17;
site="Moravia Aurignacian";
culture="Aurignacian";
author="AMH";
};
Date(Prior("Strat - Riparo Mochi - Date Proto-Aurig",
"Priors_Strat/RiparoMochi_Date_Proto_Aurignacian.prior",))
{
latitude=43.7894;
longitude=7.5475;
site="Riparo Mochi";
culture="Proto-Aurignacian";
author="AMH";
```

```
};
Date(Prior("Strat - Riparo Mochi - Date Early Aurig",
"Priors_Strat/RiparoMochi_Date_Early_Aurignacian.prior",))
{
latitude=43.7894;
longitude=7.5475;
site="Riparo Mochi";
culture="Early Aurignacian";
author="AMH";
};
Date(Prior("Strat - Riparo Mochi - Date Gravettian",
"Priors_Strat/RiparoMochi_Date_Gravettian.prior",))
{
latitude=43.7894;
longitude=7.5475;
site="Riparo Mochi";
culture="Gravettian";
author="AMH";
};
Date(Prior("Strat - Salitrena Pecina - Date Aurignacian",
"Priors_Strat/SalitrenaPecina_Date_Aurignacian.prior",))
{
latitude=44.1905;
longitude=20.0835;
site="Šalitrena Pećina";
culture="Aurignacian";
author="AMH";
};
Date(Prior("KDE - Vogelherd",
"Priors_KDE/KDE_Vogelherd.prior",))
{
latitude=48.5606;
longitude=10.1913;
site="Vogelherd";
culture="Aurignacian";
author="AMH";
};
Date(Prior("Strat - Willendorf II - Date D1/D2",
"Priors_Strat/Willendorf_Date_Micoquian_D1_D2.prior",))
{
latitude=48.323;
longitude=15.399;
site="Willendorf II";
culture="Micoquian";
author="Neanderthal";
};
Date(Prior("Strat - Willendorf II - Date C8-3",
"Priors_Strat/Willendorf_Date_Early_Aurignaican_C8_3.prior",))
{
latitude=48.323;
longitude=15.399;
site="Willendorf II";
culture="Early Aurignacian";
author="AMH";
};
Date(Prior("Strat - Willendorf II - Date C8-2",
"Priors_Strat/Willendorf_Date_Aurignaican_C8_2.prior",))
{
latitude=48.323;
longitude=15.399;
site="Willendorf II";
culture="Aurignacian";
author="AMH";
};
Date(Prior("Strat - Willendorf II - Date C7-1",
"Priors_Strat/Willendorf_Date_Aurignaican_C7_1.prior",))
{
latitude=48.323;
longitude=15.399;
site="Willendorf II";
culture="Aurignacian";
author="AMH";
};
Date(Prior("Strat - Willendorf II - Date C4-2",
"Priors_Strat/Willendorf_Date_C4_2.prior",))
{
latitude=48.323;
longitude=15.399;
site="Willendorf II";
culture="Aurignacian";
author="AMH";
};
Date(Prior("Strat - Willendorf II - Date C4-1",
"Priors_Strat/Willendorf_Date_C4_1.prior",))
{
latitude=48.323;
longitude=15.399;
site="Willendorf II";
culture="Aurignacian";
author="AMH";
};
Date(Prior("MOD10 - Dzerava Skala - Date 5a",
"Priors_Strat_DPhil/Der_MOD10_Date_5a_.prior",))
{
latitude=48.496987;
longitude=17.324692;
site="Dzerava Skala";
culture="Aurignacian Point";
author="AMH";
};
Date(Prior("MOD10 - Dzerava Skala - Date 9",
"Priors_Strat_DPhil/Der_MOD10_Date_9.prior",))
{
latitude=48.496987;
longitude=17.324692;
site="Dzerava Skala";
culture="Aurignacian Point";
author="AMH";
};
Date(Prior("MOD10 - Dzerava Skala - Date 5",
"Priors_Strat_DPhil/Der_MOD10_Date_5.prior",))
{
latitude=48.496987;
longitude=17.324692;
site="Dzerava Skala";
culture="Gravettian";
author="AMH";
};
Date(Prior("MOD10 - Dzerava Skala - Date 4",
"Priors_Strat_DPhil/Der_MOD10_Date_4.prior",))
{
latitude=48.496987;
longitude=17.324692;
site="Dzerava Skala";
culture="Gravettian";
author="AMH";
};
Date(Prior("Points KDE2 - Istallosko",
"Priors_KDE_DPhil/Istall_Points_KDE_2.prior",))
{
latitude=48.071667;
longitude=20.418889;
site="Istallosko";
culture="Aurignacian Point";
author="AMH";
};
R_Date("OxA-X-2716-49",31800,1000)
{
latitude=47.723889;
longitude=18.575278;
site="Jankovich";
culture="Aurignacian Point";
author="AMH";
};
R_Date("OxA-X-2716-48",32500,800)
{
latitude=47.723889;
longitude=18.575278;
site="Jankovich";
culture="Aurignacian Point";
author="AMH";
};
R_Date("OxA-X-2732-10",32750,670)
{
latitude=47.723889;
longitude=18.575278;
site="Jankovich";
culture="Aurignacian Point";
author="AMH";
};
R_Date("OxA-35386",30800,500)
{
latitude=47.723889;
longitude=18.575278;
site="Jankovich";
culture="Aurignacian Point";
```

```
author="AMH";
};
Date(Prior("MOD3 - Kozarnika - Date 6/7 ls lp",
"Priors_Strat_DPhil/Kz_MOD3_Date_6_7_ls_lp.prior",))
{
latitude=43.651722;
longitude=22.702472;
site="Kozarnika";
culture="IUP";
author="Neanderthal";
};
Date(Prior("MOD3 - Kozarnika - Date 6/7 lb",
"Priors_Strat_DPhil/Kz_MOD3_Date_6_7_lb.prior",))
{
latitude=43.651722;
longitude=22.702472;
site="Kozarnika";
culture="IUP";
author="Neanderthal";
};
Date(Prior("MOD3 - Kozarnika - Date 5b",
"Priors_Strat_DPhil/Kz_MOD3_Date_5b.prior",))
{
latitude=43.651722;
longitude=22.702472;
site="Kozarnika";
culture="Kozarnikian";
author="AMH";
};
Date(Prior("MOD3 - Kozarnika - Date 5a",
"Priors_Strat_DPhil/Kz_MOD3_Date_5a.prior",))
{
latitude=43.651722;
longitude=22.702472;
site="Kozarnika";
culture="Kozarnikian";
author="AMH";
};
Date(Prior("MOD3 - Kozarnika - Date 4",
"Priors_Strat_DPhil/Kz_MOD3_Date_4.prior",))
{
latitude=43.651722;
longitude=22.702472;
site="Kozarnika";
culture="Kozarnikian";
author="AMH";
};
R_Date("OxA-35404",27600,400)
{
latitude=43.15;
longitude=24.71;
site="Tabashkata";
culture="Aurignacian Point";
author="AMH";
};
Date(Prior("MOD3 - Temnata - Date TD-V 5pg",
"Priors_Strat_DPhil/TD_Date_5pg_TD_V.prior",))
{
latitude=43.174969;
longitude=24.074006;
site="Temnata";
culture="Mousterian";
author="Neanderthal";
};
Date(Prior("MOD3 - Temnata - Date TD-V 3v",
"Priors_Strat_DPhil/TD_Date_3v_TD_V.prior",))
{
latitude=43.174969;
longitude=24.074006;
site="Temnata";
culture="Aurignacian-like";
author="Neanderthal";
};
Date(Prior("MOD3 - Temnata - Date TD-V 3d",
"Priors_Strat_DPhil/TD_Date_3d_TD_V.prior",))
{
latitude=43.174969;
longitude=24.074006;
site="Temnata";
culture="Gravettian";
author="AMH";
};
R_Date("OxA-17967",38300,1500)
{
latitude=48.0468;
longitude=20.4264;
site="Pesko";
culture="Aurignacian Point";
author="AMH";
};
R_Date("OxA-17964",33500,450)
{
latitude=48.0468;
longitude=20.4264;
site="Pesko";
culture="Aurignacian Point";
author="AMH";
};
R_Date("OxA-17966",36400,800)
{
latitude=48.0468;
longitude=20.4264;
site="Pesko";
culture="Aurignacian Point";
author="AMH";
};
R_Date("OxA-19621",33750,350)
{
latitude=47.138;
longitude=5.571;
site="Trou de la Mere Clochette";
culture="Aurignacian Point";
author="AMH";
};
R_Date("OxA-19622",35460,250)
{
latitude=47.138;
longitude=5.571;
site="Trou de la Mere Clochette";
culture="Aurignacian Point";
author="AMH";
};
R_Date("OxA-14436",33640,250)
{
latitude=50.16944;
longitude=19.80723;
site="Mamutowa cave";
culture="Aurignacian Point";
author="AMH";
};
R_Date("OxA-14434",35460,220)
{
latitude=50.16944;
longitude=19.80723;
site="Mamutowa cave";
culture="Aurignacian Point";
author="AMH";
};
R_Date("OxA-17963",35600,400)
{
latitude=48.4922;
longitude=17.295;
site="Dzerava skala";
culture="Aurignacian Point";
author="AMH";
};
R_Date("OxA-X-2170-18",33600,900)
{
latitude=48.0654;
longitude=20.4108;
site="Istallosko";
culture="Aurignacian Point";
author="AMH";
};
R_Date("OxA-21783",32100,450)
{
latitude=42.1607;
longitude=2.74401;
site="Arbreda";
culture="Aurignacian Point";
author="AMH";
};
R_Date("OxA-13716",31730,250)
{
latitude=51.3204;
longitude= 2.9781;
```

```
site="Uphill Quarry cave 8 ";
culture="Aurignacian Point";
author="AMH";
};
R_Date("OxA-13803",31550,340)
{
latitude=51.2263;
longitude=2.6761;
site="Hyaena Den cave ";
culture="Aurignacian Point";
author="AMH";
};
R_Date("GrA-32619",32830,195)
{
latitude=50.4781;
longitude=4.679;
site="Grotte de la Betche-aux-Rotches, Spy";
culture="Aurignacian Point";
author="AMH";
};
R_Date("OxA-7496",30750,850)
{
latitude=50.421;
longitude=5.294;
site="Trou al'Wesse";
culture="Aurignacian Point";
author="AMH";
};
R_Date("KIA-19541",31310,235)
{
latitude=48.5603;
longitude=10.1913;
site="Vogelherd cave";
culture="Aurignacian Point";
author="AMH";
};
R_Date("KIA-19551",32470,265)
{
latitude=48.4089;
longitude=9.772;
site="Brillenhohle";
culture="Aurignacian Point";
author="AMH";
};
R_Date("KIA-19550[a]",30400,235)
{
latitude=48.4089;
longitude=9.772;
site="Brillenhohle";
culture="Aurignacian Point";
author="AMH";
};
R_Date("KIA-13082",26730,165)
{
latitude=48.3842;
longitude=9.7614;
site="Sirgenstein cave";
culture="Aurignacian Point";
author="AMH";
};
R_Date("KIA-13079",27250,175)
{
latitude=48.3842;
longitude=9.7614;
site="Sirgenstein cave";
culture="Aurignacian Point";
author="AMH";
};
R_Date("KIA-19543[a]",32010,494)
{
latitude=47.5924;
longitude=12.197;
site="Tischoferhohle";
culture="Aurignacian Point";
author="AMH";
};
R_Date("KIA-19544[a]",31530,205)
{
latitude=47.5924;
longitude=12.197;
site="Tischoferhohle";
culture="Aurignacian Point";
author="AMH";
};
R_Date("KIA-19545",29500,200)
{
latitude=47.5924;
longitude=12.197;
site="Tischoferhohle";
culture="Aurignacian Point";
author="AMH";
};
R_Date("VERA-2522",30140,335)
{
latitude=46.4493;
longitude=14.6691;
site="Potocka zijalka";
culture="Aurignacian Point";
author="AMH";
};
R_Date("OxA-27854",30800,370)
{
latitude=46.4493;
longitude=14.6691;
site="Potocka zijalka";
culture="Aurignacian Point";
author="AMH";
};
R_Date("OxA-28038",31950,450)
{
latitude=46.4493;
longitude=14.6691;
site="Potocka zijalka";
culture="Aurignacian Point";
author="AMH";
};
R_Date("OxA-28061",32550,550)
{
latitude=46.4493;
longitude=14.6691;
site="Potocka zijalka";
culture="Aurignacian Point";
author="AMH";
};
R_Date("OxA-27850",30380,370)
{
latitude=46.4493;
longitude=14.6691;
site="Potocka zijalka";
culture="Aurignacian Point";
author="AMH";
};
R_Date("OxA-27849",31220,400)
{
latitude=46.4493;
longitude=14.6691;
site="Potocka zijalka";
culture="Aurignacian Point";
author="AMH";
};
R_Date("OxA-27852",31360,400)
{
latitude=46.4493;
longitude=14.6691;
site="Potocka zijalka";
culture="Aurignacian Point";
author="AMH";
};
R_Date("OxA-27853",31500,400)
{
latitude=46.4493;
longitude=14.6691;
site="Potocka zijalka";
culture="Aurignacian Point";
author="AMH";
};
R_Date("OxA-27851",30910,380)
{
latitude=46.4493;
longitude=14.6691;
site="Potocka zijalka";
culture="Aurignacian Point";
author="AMH";
};
R_Date("OxA-15334",31600,900)
{
```

```
latitude=48.4922;
longitude=17.295;
site="Dzerava skala";
culture="Aurignacian Point";
author="AMH";
};
R_Date("OxA-15335",31000,1000)
{
latitude=48.4922;
longitude=17.295;
site="Dzerava skala";
culture="Aurignacian Point";
author="AMH";
};
R_Date("OxA-28219",29760,340)
{
latitude=46.112778;
longitude=13.915556;
site="Divije babe I";
culture="Aurignacian Point";
author="AMH";
};
R_Date("OxA-X-2517-52",34750,600)
{
latitude=46.308806;
longitude=14.568194;
site="Morkiska jama";
culture="Aurignacian Point";
author="AMH";
};
R_Date("OxA-27855",32600,450)
{
latitude=46.308806;
longitude=14.568194;
site="Morkiska jama";
culture="Aurignacian Point";
author="AMH";
};
Label("Humans");
R_Date("OxA-21839",39700,1100)
{
longitude=40.0034;
latitude=44.2217;
culture="MP";
author="Neanderthal";
species="Neanderthal";
site="Mezmaiskaya";
};
Date("OxA-15257",N(calBP(48900),1100))
{
longitude=0.741;
latitude=46.415;
culture="Mousterian";
author="Neanderthal";
species="Neanderthal";
site="Les Rochers-de-Villeneuve";
};
R_Date("ETH-20981",39900,620)
{
longitude=6.9363;
latitude=51.2206;
culture="MP";
author="Neanderthal";
species="Neanderthal";
site="Kleine Feldhöfergrotte";
};
R_Date("ETH-19660",39240,670)
{
longitude=6.9363;
latitude=51.2206;
culture="MP";
author="Neanderthal";
species="Neanderthal";
site="Kleine Feldhöfergrotte";
};
R_Date("GrA-32626",36350,295)
{
longitude=4.6743;
latitude=50.4803;
culture="LRJ or Mousterian";
author="Neanderthal";
species="Neanderthal";
site="Spy";
};
R_Date("GrA-32623",35810,250)
{
longitude=4.6743;
latitude=50.4803;
culture="LRJ or Mousterian";
author="Neanderthal";
species="Neanderthal";
site="Spy";
};
R_Date("ETH-19661",40360,760)
{
longitude=6.9363;
latitude=51.2206;
culture="MP";
author="Neanderthal";
species="Neanderthal";
site="Kleine Feldhöfergrotte";
};
R_Date("OxA-10560",36250,500)
{
longitude=4.6743;
latitude=50.4803;
culture="unknown";
author="Neanderthal";
species="Neanderthal";
site="Spy";
};
Date("GifA-99167",N(calBP(55090),2600))
{
longitude=-5.733;
latitude=43.386;
culture="Mousterian";
author="Neanderthal";
species="Neanderthal";
site="El Sidron";
};
Date("GifA-99704",N(calBP(54930),2500))
{
longitude=-5.733;
latitude=43.386;
culture="Mousterian";
author="Neanderthal";
species="Neanderthal";
site="El Sidron";
};
Date("OxA-21776",N(calBP(56230),3200))
{
longitude=-5.733;
latitude=43.386;
culture="Mousterian";
author="Neanderthal";
species="Neanderthal";
site="El Sidron";
};
R_Date("OxA-X-2689-09",42700,1600)
{
longitude=16.088;
latitude=46.305;
culture="MP";
author="Neanderthal";
species="Neanderthal";
site="Vindija";
};
Date("OxA-X-2689-10",N(calBP(48800),2000))
{
longitude=16.088;
latitude=46.305;
culture="MP";
author="Neanderthal";
species="Neanderthal";
site="Vindija";
};
R_Date("OxA-X-2717-11",44300,1200)
{
longitude=16.088;
latitude=46.305;
culture="MP";
author="Neanderthal";
species="Neanderthal";
site="Vindija";
};
Date("OxA-X-2687-57",N(calBP(49960),1500))
```

```
{
longitude=16.088;
latitude=46.305;
culture="MP";
author="Neanderthal";
species="Neanderthal";
site="Vindija";
};
R_Date("GrA-50457",32450,240)
{
longitude=34.396;
latitude=45.16;
culture="Gravettian";
author="AMH";
species="AMH";
site="Buran-Kaya III";
};
R_Date("GrA-24398",28890,170)
{
longitude=21.91;
latitude=45.0177;
culture="unknown";
author="AMH";
species="AMH";
site="Pestera cu Oase";
};
R_Date("OxA-4586",31000,500)
{
longitude=20.1563;
latitude=49.443;
culture="Aurignacian";
author="AMH";
species="AMH";
site="Oblazowa";
};
R_Date("VERA-3074",31320,400)
{
longitude=17.0167;
latitude=49.707;
culture="Aurignacian";
author="AMH";
species="AMH";
site="Mladec";
};
R_Date("OxA-11711",34950,990)
{
longitude=21.91;
latitude=45.0177;
culture="unknown";
author="AMH";
species="AMH";
site="Pestera cu Oase";
};
R_Date("GrA-37938",31900,230)
{
longitude=34.396;
latitude=45.16;
culture="Gravettian";
author="AMH";
species="AMH";
site="Buran-Kaya III";
};
R_Date("VERA-3073",31190,400)
{
longitude=17.0167;
latitude=49.707;
culture="Aurignacian";
author="AMH";
species="AMH";
site="Mladec";
};
R_Date("VERA-3076 A",31500,410)
{
longitude=17.0167;
latitude=49.707;
culture="Aurignacian";
author="AMH";
species="AMH";
site="Mladec";
};
R_Date("OxA-16412",28870,180)
{
longitude=-4.2555;
latitude=51.5499;
culture="Gravettian";
author="AMH";
species="AMH";
site="Paviland";
};
R_Date("OxA-16413",29490,210)
{
longitude=-4.2555;
latitude=51.5499;
culture="Gravettian";
author="AMH";
species="AMH";
site="Paviland";
};
R_Date("ERL-9415",30640,640)
{
longitude=3.0905;
latitude=43.1313;
culture="Aurignacian";
author="AMH";
species="AMH";
site="La Crouzade";
};
R_Date("OxA-15527",28150,170)
{
longitude=23.1296;
latitude=45.5862;
culture="Aurignacian?";
author="AMH";
species="AMH";
site="Cioclovina";
};
R_Date("OxA-15529",29930,170)
{
longitude=23.755;
latitude=45.1895;
culture="Uluzzian";
author="AMH";
species="AMH";
site="Pestera Muierii";
};
R_Date("OxA-16252",29110,190)
{
longitude=23.755;
latitude=45.1895;
culture="Uluzzian";
author="AMH";
species="AMH";
site="Pestera Muierii";
};
R_Date("OxA-13302",32790,280)
{
longitude=34.396;
latitude=45.16;
culture="Gravettian";
author="AMH";
species="AMH";
site="Buran-Kaya III";
};
};
```

Spatio-temporal distribution: map 3 – see figures 15.20 and 15.21

```
 Plot()
{
Date(Prior("KDE - Bacho Kiro",
"Priors_KDE/KDE_Bacho_Kiro.prior",))
{
latitude=42.947378;
longitude=25.331867;
site="Bacho Kiro";
culture="Bachokirian/UP";
author="AMH";
};
Date(Prior("KDE - Buran-Kaya III",
"Priors_KDE/KDE_Buran_Kaya_III.prior",))
{
latitude=45.16;
longitude=34.396;
site="Buran-Kaya III";
culture="UP";
author="AMH";
};
Date(Prior("KDE - Castelcivita",
"Priors_KDE/KDE_Castelcivita.prior",))
{
latitude=40.495;
longitude=15.237;
site="Castelcivita";
culture="Uluzzian/UP";
author="AMH";
};
Date(Prior("Strat - Cavallo - Date EII/I",
"Priors_Strat/CAVALLO_Date_EII_I_Uluzzian.prior",))
{
latitude=40.154;
longitude=17.96;
site="Cavallo";
culture="Uluzzian";
author="AMH";
};
Date(Prior("Strat - Cavallo - Date E/D",
"Priors_Strat/CAVALLO_Date_E_D_Uluzzian.prior",))
{
latitude=40.154;
longitude=17.96;
site="Cavallo";
culture="Uluzzian";
author="AMH";
};
Date(Prior("Strat - Cavallo - Date DII",
"Priors_Strat/CAVALLO_Date_DII_Uluzzian.prior",))
{
latitude=40.154;
longitude=17.96;
site="Cavallo";
culture="Uluzzian";
author="AMH";
};
Date(Prior("Strat - Cavallo - Date Dib",
"Priors_Strat/CAVALLO_Date_DIb_Uluzzian.prior",))
{
latitude=40.154;
longitude=17.96;
site="Cavallo";
culture="Uluzzian";
author="AMH";
};
Date(Prior("KDE - El Castillo",
"Priors_KDE/KDE_El_Castillo.prior",))
{
latitude=43.2875;
longitude=-3.9598;
site="El Castillo";
culture="‘Transitional Aurignacian’";
author="AMH";
};
Date(Prior("KDE - Fumane",
"Priors_KDE/KDE_Fumane.prior",))
{
latitude=45.57;
longitude=10.902;
site="Fumane";
culture="Uluzzian/UP";
author="AMH";
};
Date(Prior("KDE - Geißenklösterle",
"Priors_KDE/KDE_Geissenklosterle.prior",))
{
latitude=48.401;
longitude=9.772;
site="Geißenklösterle";
culture="UP";
author="AMH";
};
Date(Prior("KDE - Hohle Fels",
"Priors_KDE/KDE_Hohle_Fels.prior",))
{
latitude=48.378;
longitude=9.758;
site="Hohle Fels";
culture="UP";
author="AMH";
};
Date(Prior("KDE - Hohlenstein-Stadel",
"Priors_KDE/KDE_Hohlenstein_Stadel_short_.prior",))
{
latitude=48.551;
longitude=10.168;
site="Hohlenstein-Stadel";
culture="Aurignacian";
author="AMH";
};
Date(Prior("KDE - Isturitz",
"Priors_KDE/KDE_Isturitz.prior",))
{
latitude=43.371;
longitude=-1.196;
site="Isturitz";
culture="UP";
author="AMH";
};
Date(Prior("KDE - Ksar Akil",
"Priors_KDE/KDE_Ksar_Akil.prior",))
{
latitude=33.916667;
longitude=35.6;
site="Ksar Akil";
culture="UP";
author="AMH";
};
Date(Prior("KDE - L’Arbreda",
"Priors_KDE/KDE_LArbreda.prior",))
{
latitude=42.161;
longitude=2.747;
site="L’Arbreda";
culture="UP";
author="AMH";
};
Date(Prior("KDE - Labeko Koba",
"Priors_KDE/KDE_Labeko_Koba.prior",))
{
latitude=43.066;
longitude=-2.458;
site="Labeko Koba";
culture="UP";
author="AMH";
};
Date(Prior("KDE - Mitoc-Malul Galben",
"Priors_KDE/KDE_Mitoc_Malul_Galben.prior",))
{
latitude=48.111;
longitude=27.036;
site="Mitoc-Malul Galben";
culture="Aurignacian";
author="AMH";
};
Date(Prior("KDE - Moravia Aurignacian",
"Priors_KDE/KDE_Aurignacian_Moravia.prior",))
{
latitude=49.5;
longitude=17;
site="Moravia Aurignacian";
culture="Aurignacian";
author="AMH";
};
Date(Prior("KDE - Moravia Bohunician",
"Priors_KDE/KDE_Bohunician_Moravia.prior",))
```

```
{
latitude=49.5;
longitude=17;
site="Moravia Bohunician";
culture="Bohunician";
author="AMH";
};
Date(Prior("KDE - Riparo Mochi",
"Priors_KDE/KDE_Riparo_Mochi.prior",))
{
latitude=43.7894;
longitude=7.5475;
site="Riparo Mochi";
culture="UP";
author="AMH";
};
Date(Prior("KDE - Šalitrena Pećina",
"Priors_KDE/KDE_Salitrena_Pecina.prior",))
{
latitude=44.1905;
longitude=20.0835;
site="Šalitrena Pećina";
culture="Aurignacian";
author="AMH";
};
Date(Prior("Strat - Salitrena Pecina - Date Aurignacian",
"Priors_Strat/SalitrenaPecina_Date_Aurignacian.prior",))
{
latitude=44.1905;
longitude=20.0835;
site="Šalitrena Pećina";
culture="Aurignacian";
author="AMH";
};
Date(Prior("KDE - Vogelherd",
"Priors_KDE/KDE_Vogelherd.prior",))
{
latitude=48.5606;
longitude=10.1913;
site="Vogelherd";
culture="Aurignacian";
author="AMH";
};
Date(Prior("KDE - Willendorf II",
"Priors_KDE/KDE_Willendorf_II.prior",))
{
latitude=48.323;
longitude=15.399;
site="Willendorf II";
culture="Aurignacian";
author="AMH";
};
R_Date("OxA-X-2732-11",31100,520)
{
latitude=45.3605642;
longitude=14.7527073;
site="Bukovac";
culture="Aurignacian Point";
author="AMH";
};
Date(Prior("KDE3 - Dzerava Skala",
"Priors_KDE_DPhil/Der_KDE_3.prior",))
{
latitude=49.496987;
longitude=18.324692;
site="Dzerava Skala";
culture="UP";
author="AMH";
};
Date(Prior("Points KDE2 - Istallosko",
"Priors_KDE_DPhil/Istall_Points_KDE_2.prior",))
{
latitude=48.071667;
longitude=20.418889;
site="Istallosko";
culture="Aurignacian Point";
author="AMH";
};
R_Date("OxA-X-2716-49",31800,1000)
{
latitude=47.723889;
longitude=18.575278;
site="Jankovich";
culture="Aurignacian Point";
author="AMH";
};
R_Date("OxA-X-2716-48",32500,800)
{
latitude=47.723889;
longitude=18.575278;
site="Jankovich";
culture="Aurignacian Point";
author="AMH";
};
R_Date("OxA-X-2732-10",32750,670)
{
latitude=47.723889;
longitude=18.575278;
site="Jankovich";
culture="Aurignacian Point";
author="AMH";
};
R_Date("OxA-35386",30800,500)
{
latitude=47.723889;
longitude=18.575278;
site="Jankovich";
culture="Aurignacian Point";
author="AMH";
};
Date(Prior("KDE - Kozarnika",
"Priors_KDE_DPhil/Kz_KDE_1.prior",))
{
latitude=43.651722;
longitude=22.702472;
site="Kozarnika";
culture="UP";
author="AMH";
};
R_Date("OxA-35416",32950,550)
{
latitude=48.108333;
longitude=20.631667;
site="Szeleta";
culture="Aurignacian Point";
author="AMH";
};
R_Date("OxA-35404",27600,400)
{
latitude=43.15;
longitude=24.71;
site="Tabashkata";
culture="Aurignacian Point";
author="AMH";
};
Date(Prior("KDE3 - Temnata",
"Priors_KDE_DPhil/KDE3_mod_Temnata.prior",))
{
latitude=43.174969;
longitude=24.074006;
site="Temnata";
culture="UP";
author="AMH";
};
R_Date("OxA-17967",38300,1500)
{
latitude=48.0468;
longitude=20.4264;
site="Pesko";
culture="Aurignacian Point";
author="AMH";
};
R_Date("OxA-17964",33500,450)
{
latitude=48.0468;
longitude=20.4264;
site="Pesko";
culture="Aurignacian Point";
author="AMH";
};
R_Date("OxA-17966",36400,800)
{
latitude=48.0468;
longitude=20.4264;
site="Pesko";
culture="Aurignacian Point";
```

```
author="AMH";
};
R_Date("OxA-19621",33750,350)
{
latitude=47.138;
longitude=5.571;
site="Trou de la Mere Clochette";
culture="Aurignacian Point";
author="AMH";
};
R_Date("OxA-19622",35460,250)
{
latitude=47.138;
longitude=5.571;
site="Trou de la Mere Clochette";
culture="Aurignacian Point";
author="AMH";
};
R_Date("OxA-14436",33640,250)
{
latitude=50.16944;
longitude=19.80723;
site="Mamutowa cave";
culture="Aurignacian Point";
author="AMH";
};
R_Date("OxA-14434",35460,220)
{
latitude=50.16944;
longitude=19.80723;
site="Mamutowa cave";
culture="Aurignacian Point";
author="AMH";
};
R_Date("OxA-17963",35600,400)
{
latitude=48.4922;
longitude=17.295;
site="Dzerava skala";
culture="Aurignacian Point";
author="AMH";
};
R_Date("OxA-X-2170-18",33600,900)
{
latitude=48.0654;
longitude=20.4108;
site="Istallosko";
culture="Aurignacian Point";
author="AMH";
};
R_Date("OxA-21783",32100,450)
{
latitude=42.1607;
longitude=2.74401;
site="Arbreda";
culture="Aurignacian Point";
author="AMH";
};
R_Date("OxA-13716",31730,250)
{
latitude=51.3204;
longitude= 2.9781;
site="Uphill Quarry cave 8 ";
culture="Aurignacian Point";
author="AMH";
};
R_Date("OxA-13803",31550,340)
{
latitude=51.2263;
longitude=2.6761;
site="Hyaena Den cave ";
culture="Aurignacian Point";
author="AMH";
};
R_Date("GrA-32619",32830,195)
{
latitude=50.4781;
longitude=4.679;
site="Grotte de la Betche-aux-Rotches, Spy";
culture="Aurignacian Point";
author="AMH";
};
R_Date("OxA-7496",30750,850)
{
latitude=50.421;
longitude=5.294;
site="Trou al'Wesse";
culture="Aurignacian Point";
author="AMH";
};
R_Date("KIA-19541",31310,235)
{
latitude=48.5603;
longitude=10.1913;
site="Vogelherd cave";
culture="Aurignacian Point";
author="AMH";
};
R_Date("KIA-19551",32470,265)
{
latitude=48.4089;
longitude=9.772;
site="Brillenhohle";
culture="Aurignacian Point";
author="AMH";
};
R_Date("KIA-19550[a]",30400,235)
{
latitude=48.4089;
longitude=9.772;
site="Brillenhohle";
culture="Aurignacian Point";
author="AMH";
};
R_Date("KIA-13082",26730,165)
{
latitude=48.3842;
longitude=9.7614;
site="Sirgenstein cave";
culture="Aurignacian Point";
author="AMH";
};
R_Date("KIA-13079",27250,175)
{
latitude=48.3842;
longitude=9.7614;
site="Sirgenstein cave";
culture="Aurignacian Point";
author="AMH";
};
R_Date("KIA-19543[a]",32010,494)
{
latitude=47.5924;
longitude=12.197;
site="Tischoferhohle";
culture="Aurignacian Point";
author="AMH";
};
R_Date("KIA-19544[a]",31530,205)
{
latitude=47.5924;
longitude=12.197;
site="Tischoferhohle";
culture="Aurignacian Point";
author="AMH";
};
R_Date("KIA-19545",29500,200)
{
latitude=47.5924;
longitude=12.197;
site="Tischoferhohle";
culture="Aurignacian Point";
author="AMH";
};
R_Date("VERA-2522",30140,335)
{
latitude=46.4493;
longitude=14.6691;
site="Potocka zijalka";
culture="Aurignacian Point";
author="AMH";
};
R_Date("OxA-27854",30800,370)
{
latitude=46.4493;
longitude=14.6691;
```

```
site="Potocka zijalka";
culture="Aurignacian Point";
author="AMH";
};
R_Date("OxA-28038",31950,450)
{
latitude=46.4493;
longitude=14.6691;
site="Potocka zijalka";
culture="Aurignacian Point";
author="AMH";
};
R_Date("OxA-28061",32550,550)
{
latitude=46.4493;
longitude=14.6691;
site="Potocka zijalka";
culture="Aurignacian Point";
author="AMH";
};
R_Date("OxA-27850",30380,370)
{
latitude=46.4493;
longitude=14.6691;
site="Potocka zijalka";
culture="Aurignacian Point";
author="AMH";
};
R_Date("OxA-27849",31220,400)
{
latitude=46.4493;
longitude=14.6691;
site="Potocka zijalka";
culture="Aurignacian Point";
author="AMH";
};
R_Date("OxA-27852",31360,400)
{
latitude=46.4493;
longitude=14.6691;
site="Potocka zijalka";
culture="Aurignacian Point";
author="AMH";
};
R_Date("OxA-27853",31500,400)
{
latitude=46.4493;
longitude=14.6691;
site="Potocka zijalka";
culture="Aurignacian Point";
author="AMH";
};
R_Date("OxA-27851",30910,380)
{
latitude=46.4493;
longitude=14.6691;
site="Potocka zijalka";
culture="Aurignacian Point";
author="AMH";
};
R_Date("OxA-15334",31600,900)
{
latitude=48.4922;
longitude=17.295;
site="Dzerava skala";
culture="Aurignacian Point";
author="AMH";
};
R_Date("OxA-15335",31000,1000)
{
latitude=48.4922;
longitude=17.295;
site="Dzerava skala";
culture="Aurignacian Point";
author="AMH";
};
R_Date("OxA-28219",29760,340)
{
latitude=46.112778;
longitude=13.915556;
site="Divije babe I";
culture="Aurignacian Point";
author="AMH";
};
R_Date("OxA-X-2517-52",34750,600)
{
latitude=46.308806;
longitude=14.568194;
site="Morkiska jama";
culture="Aurignacian Point";
author="AMH";
};
R_Date("OxA-27855",32600,450)
{
latitude=46.308806;
longitude=14.568194;
site="Morkiska jama";
culture="Aurignacian Point";
author="AMH";
};
Label("Homo sapiens");
R_Date("GrA-50457",32450,240)
{
longitude=34.396;
latitude=45.16;
culture="Gravettian";
author="AMH";
species="AMH";
site="Buran-Kaya III";
};
R_Date("GrA-24398",28890,170)
{
longitude=21.91;
latitude=45.0177;
culture="unknown";
author="AMH";
species="AMH";
site="Pestera cu Oase";
};
R_Date("VERA-3074",31320,400)
{
longitude=17.0167;
latitude=49.707;
culture="Aurignacian";
author="AMH";
species="AMH";
site="Mladec";
};
R_Date("OxA-11711",34950,990)
{
longitude=21.91;
latitude=45.0177;
culture="unknown";
author="AMH";
species="AMH";
site="Pestera cu Oase";
};
R_Date("GrA-37938",31900,230)
{
longitude=34.396;
latitude=45.16;
culture="Gravettian";
author="AMH";
species="AMH";
site="Buran-Kaya III";
};
R_Date("VERA-3073",31190,400)
{
longitude=17.0167;
latitude=49.707;
culture="Aurignacian";
author="AMH";
species="AMH";
site="Mladec";
};
R_Date("VERA-3076 A",31500,410)
{
longitude=17.0167;
latitude=49.707;
culture="Aurignacian";
author="AMH";
species="AMH";
site="Mladec";
};
R_Date("OxA-16412",28870,180)
{
```

```
longitude=-4.2555;
latitude=51.5499;
culture="Gravettian";
author="AMH";
species="";
site="Paviland";
};
R_Date("OxA-16413",29490,210)
{
longitude=-4.2555;
latitude=51.5499;
culture="Gravettian";
author="AMH";
species="";
site="Paviland";
};
R_Date("ERL-9415",30640,640)
{
longitude=3.0905;
latitude=43.1313;
culture="Aurignacian";
author="AMH";
species="AMH";
site="La Crouzade";
};
R_Date("OxA-15527",28150,170)
{
longitude=23.1296;
latitude=45.5862;
culture="Aurignacian?";
author="AMH";
species="AMH";
site="Cioclovina";
};
R_Date("OxA-15529",29930,170)
{
longitude=23.755;
latitude=45.1895;
culture="Uluzzian";
author="AMH";
species="AMH";
site="Pestera Muierii";
};
R_Date("OxA-16252",29110,190)
{
longitude=23.755;
latitude=45.1895;
culture="Uluzzian";
author="AMH";
species="AMH";
site="Pestera Muierii";
};
R_Date("OxA-13302",32790,280)
{
longitude=34.396;
latitude=45.16;
culture="Gravettian";
author="AMH";
species="AMH";
site="Buran-Kaya III";
};
};
```

C: Reference sites - date lists

Table C.5: Reference Sites: published radiocarbon dates from El Castillo (Spain) used for modelling. Dates calibrated in OxCal 4.3 (Bronk Ramsey, 2009a) using IntCal13 (Reimer et al., 2013). Date part of model: 'S' = stratigraphic, 'K' = KDE.

Material	Type	Sample	Context	Culture	Author	Treat.	Yield (mg)	Yield (%)	$\delta^{13}C$	$\delta^{15}N$	%C	C:N	Lab-no.	^{14}C (BP)	σ	Date (calBP)	Ref.	S	K
bone	cutmark	CS15	Phase 18C	'Transitional Aurignacian'	AMH	AF*	21.3	2.7	-21.7	4.9	43.6	3.2	OxA-22403	42700	1600	49690 – 43890	Wood et al. (2018)	Y	Y
bone	cutmark	CS17	Phase 18C	'Transitional Aurignacian'	AMH	AF*	25.6	2.5	-20.5	–	41.8	3.0	OxA-22202	43100	1700	49950 – 44350	Wood et al. (2018)	Y	Y
bone	cutmark	CS19	Phase 18C	'Transitional Aurignacian'	AMH	AF*	14.9	1.8	-20.3	–	41.4	3.0	OxA-22203	42000	1500	49060 – 43180	Wood et al. (2018)	Y	Y
bone	cutmark	CS25	Phase 19	none	none	AF	14.5	3.4	-20.0	5.1	41.4	3.2	OxA-21974	44900	2100	>45480	Wood et al. (2018)	Y	N
bone	cutmark	CS27	Phase 20C	Mousterian	Neand.	AF*	12.7	1.3	-20.3	–	41.9	3.1	OxA-22204	48700	3400	>49840	Wood et al. (2018)	Y	N
bone	cutmark	CS31	Phase 20C	Mousterian	Neand.	AF	19.5	1.9	-20.8	–	40.3	3.1	OxA-22205	49400	3700	>49870	Wood et al. (2018)	Y	N
bone	cutmark	CS5	Phase 18B	'Transitional Aurignacian'	AMH	AF	12.9	2.7	-20.8	6.1	44.3	3.2	OxA-21972	45800	2300	>45900	Wood et al. (2018)	Y	N
bone	cutmark	CS6	Phase 18B	'Transitional Aurignacian'	AMH	AF*	11.2	2.4	-19.4	3.1	43.8	3.2	OxA-21973	46000	2400	>45940	Wood et al. (2018)	Y	N
bone	no mod	CS2	Phase 17 – 16	none	none	AF	33.7	3.3	-22.0	–	41.4	2.9	OxA-22200	38600	1000	44610 – 41340	Wood et al. (2018)	Y	N
bone	no mod	CS3	Phase 17 – 16	none	none	AF	17.1	1.7	-20.1	–	42.1	3.0	OxA-22201	39100	1000	44960 – 41750	Wood et al. (2018)	Y	N
charcoal	charcoal	–	Phase 17 – 16	none	none	–	–	–	–	–	–	–	GifA-95539	34300	1000	41140 – 36440	Wood et al. (2018)	Y	N
charcoal	charcoal	–	Phase 18B	'Transitional Aurignacian'	AMH	ZR	25.0	60.4	-26.4	–	63.3	-	OxA-2473	37100	2200	47680 – 37700	Wood et al. (2018)	Y	Y
charcoal	charcoal	–	Phase 18B	'Transitional Aurignacian'	AMH	ZR	29.2	60.2	-26.5	–	63.3	–	OxA-2474	38500	1300	45350 – 40710	Wood et al. (2018)	Y	Y
charcoal	charcoal	–	Phase 18B	'Transitional Aurignacian'	AMH	ZR	93.0	48.9	-25.1	–	23.1	–	OxA-2475	40700	1600	48290 – 42180	Wood et al. (2018)	Y	Y
charcoal	charcoal	–	Phase 18B	'Transitional Aurignacian'	AMH	–	–	–	–	–	–	–	AA-2406	38500	1800	47210 – 39810	Wood et al. (2018)	Y	Y
charcoal	charcoal	–	Phase 18B	'Transitional Aurignacian'	AMH	–	–	–	–	–	–	–	AA-2407	37700	1800	46320 – 38880	Wood et al. (2018)	Y	Y
charcoal	charcoal	–	Phase 18C	'Transitional Aurignacian'	AMH	ZR	58.3	56.1	-26.7	–	60.0	–	OxA-2478	39800	1400	46760 – 41720	Wood et al. (2018)	Y	Y
charcoal	charcoal	–	Phase 18C	'Transitional Aurignacian'	AMH	ZR	93.4	61.0	-25.6	–	50.0	–	OxA-2477	41100	1700	48830 – 42420	Wood et al. (2018)	Y	Y
charcoal	charcoal	–	Phase 18C	'Transitional Aurignacian'	AMH	ZR	131.0	60.6	-26.4	–	56.7	–	OxA-2476	40700	1500	47980 – 42250	Wood et al. (2018)	Y	Y
charcoal	charcoal	–	Phase 18C	'Transitional Aurignacian'	AMH	–	–	–	–	–	–	–	AA-2405	40000	2100	49120 – 41370	Wood et al. (2018)	Y	Y
charcoal	charcoal	–	Phase 18C	'Transitional Aurignacian'	AMH	–	–	–	–	–	–	–	GifA-89147	39500	2000	48690 – 40840	Wood et al. (2018)	Y	Y
charcoal	charcoal	–	Phase 20C	Mousterian	Neand.	–	–	–	–	–	–	–	GifA-89144	39300	1900	48270 – 40660	Wood et al. (2018)	Y	N
charcoal	charcoal	–	Phase 20C	Mousterian	Neand.	–	–	–	–	–	–	–	GifA-92506	43300	2900	>43560	Wood et al. (2018)	Y	N

Table C.6: Reference Sites: published radiocarbon dates from Labeko Koba (Spain) used for modelling. Dates calibrated in OxCal 4.3 (Bronk Ramsey, 2009a) using IntCal13 (Reimer et al., 2013). Date part of model: 'S' = stratigraphic, 'K' = KDE.

Material	Type	Sample	Context	Culture	Author	Treat.	Yield (mg)	Yield (%)	$\delta^{13}C$	$\delta^{15}N$	%C	C:N	Lab-no.	^{14}C (BP)	σ	Date (calBP)	Ref.	S	K
bone	artefact	LAB-10	Level V	Early Aurig.	AMH	AF	11.7	1.8	-20.5	2.8	41.2	3.2	OxA-21767	34750	600	40860 – 38120	Wood et al. (2014)	Y	Y
bone	artefact	LAB-12	Level V	Early Aurig.	AMH	AF	21.8	3.2	-19.2	5.3	43.9	3.2	OxA-21779	34650	600	40750 – 37890	Wood et al. (2014)	Y	Y
bone	artefact	LAB-14	Level IV	Early Aurig.	AMH	AF	10.9	1.1	-19.4	6.6	43.4	3.3	OxA-21780	33550	550	39160 – 36380	Wood et al. (2014)	Y	Y
bone	artefact	LAB-17	LevelIV	Early Aurig.	AMH	AF	9.9	1.5	-19.1	5.3	43.1	3.4	OxA-21768	33600	500	39100 – 36490	Wood et al. (2014)	Y	Y
bone	artefact	LAB-20	Level VI	Early Aurig.	AMH	AF	23.9	2.6	-19.4	4.5	45.2	3.3	OxA-21778	35100	600	41060 – 38510	Wood et al. (2014)	Y	Y
bone	artefact	LAB-4	Level VII	Proto-Aurig.	AMH	AF	12.6	2.0	-21.2	4.2	43.6	3.3	OxA-21766	36850	800	42650 – 39930	Wood et al. (2014)	Y	Y
bone	artefact	LAB-5	Level VII	Proto-Aurig.	AMH	AF	8.2	1.3	-19.5	4.4	43.4	3.3	OxA-X-2314-43	36500	750	42350 – 39670	Wood et al. (2014)	Y	Y
bone	artefact?	LAB-19	Level VI	Early Aurig.	AMH	AF	15.4	1.8	-20.7	6.6	42.9	3.3	OxA-21794	34750	600	40860 – 38120	Wood et al. (2014)	Y	Y
bone	artefact?	LAB-19	Level VI	Early Aurig.	AMH	AF	–	–	–	–	–	–	OxA-21841	32150	450	37440 – 35040	Wood et al. (2014)	Y	Y
bone	cutmark	LAB-6	Level VII	Proto-Aurig.	AMH	AF	29.6	2.8	-19.2	5.2	43.6	3.3	OxA-21793	35400	650	41390 – 38700	Wood et al. (2014)	Y	Y
bone	chipped	LAB-6	Level VII	Proto-Aurig.	AMH	AF*	–	–	–	–	–	–	OxA-21840	35250	650	41280 – 38580	Wood et al. (2014)	Y	Y
bone	cutmark	LAB-22	Level IX upper	none	none	AF	11.2	1.5	-20.6	6.4	40.1	3.2	OxA-22559	36000	700	41930 – 39210	Wood et al. (2014)	Y	N
bone	cutmark	LAB-22	Level IX upper	none	none	AF	11.4	1.6	-20.3	6.9	44.7	3.2	OxA-22653	36850	800	42650 – 39930	Wood et al. (2014)	Y	N
bone	cutmark	LAB-23	Level IX lower	Chatelper.	Neand.	AF	8.5	1.0	-20.6	3.8	42.0	3.2	OxA-22560	37400	800	43050 – 40440	Wood et al. (2014)	Y	N
bone	cutmark	LAB-24	Level IX lower	Chatelper.	Neand.	AF	12.5	1.3	-20.3	4.1	41.0	3.2	OxA-22561	38000	900	43890 – 40880	Wood et al. (2014)	Y	N
bone	cutmark	LAB-26	Level IX lower	Chatelper.	Neand.	AF	11.2	1.3	-20.1	3.0	42.6	3.1	OxA-22562	38100	900	43990 – 41000	Wood et al. (2014)	Y	N
bone	cutmark	LAB-27	Level IX lower	Chatelper.	Neand.	AF	17.7	2.6	-20.2	3.7	42.3	3.1	OxA-22563	37800	900	43670 – 40630	Wood et al. (2014)	Y	N
bone	cutmark, percussion	LAB-2	Level IX upper	none	none	AF*	13.6	2.2	-19.5	5.1	43.3	3.4	OxA-21792	36550	750	42380 – 39720	Wood et al. (2014)	Y	N
bone	no mod	LAB-28	Level IX lower	Pre-Chatelper.	Neand.	AF*	9.0	0.9	-19.9	3.4	40.9	3.1	OxA-22564	37900	900	43790 – 40760	Wood et al. (2014)	Y	N
bone	no mod	LAB-3	Level IX upper	none	none	AF	16.6	1.3	-19.4	7.4	41.2	3.4	OxA-23199	38400	900	44230 – 41310	Wood et al. (2014)	Y	N
bone	percussion	LAB-1	Level IX upper	none	none	AF*	17.8	2.6	-19.1	5.6	38.2	3.2	OxA-21777	37700	900	43550 – 40520	Wood et al. (2014)	Y	N

Table C.7: Reference Sites: published radiocarbon dates from Isturitz (France) used for modelling. Dates calibrated in OxCal 4.3 (Bronk Ramsey, 2009a) using IntCal13 (Reimer et al., 2013). Date part of model: 'S' = stratigraphic, 'K' = KDE.

Material	Type	Sample	Context	Culture	Author	Treat.	Yield (mg)	Yield (%)	$\delta^{13}C$	$\delta^{15}N$	%C	C:N	Lab-no.	^{14}C (BP)	σ	Date (calBP)	Ref.	S	K
bone	cutmark	3	C 5	Proto-Aurig.	AMH	AF	6.0	0.6	-20.5	6.5	32.9	3.4	OxA-X-2695-11	43200	2400	>43850	Barshay-Szmidt et al. (2018)	Y	Y
bone	cutmark	8	C 4d1j	Proto-Aurig.	AMH	AF	7.9	1.4	-20.9	4.5	42.0	3.1	OxA-23436	37400	900	43260 – 40240	Barshay-Szmidt et al. (2018)	Y	Y
bone	cutmark	64	C 4b1	Early Aurig.	AMH	AF	11.2	1.8	-20.4	9.3	44.9	3.2	OxA-34633	35250	650	41280 – 38580	Barshay-Szmidt et al. (2018)	Y	Y
bone	cutmark	286	C 4d1c	Proto-Aurig.	AMH	ABA	27.2	5.0	-20.9	5.6	20.5	3.3	AA-69187	40000	2800	49980 – 41180	Barshay-Szmidt et al. (2018)	Y	Y
bone	cutmark	296	C 4b1	Early Aurig.	AMH	AF	25.0	3.6	-21.2	7.4	40.3	3.2	OxA-34634	34700	600	40810 – 38010	Barshay-Szmidt et al. (2018)	Y	Y
bone	cutmark	365	C 4d1j	Proto-Aurig.	AMH	AF	9.4	1.9	-20.9	4.8	41.9	3.2	OxA-23432	37000	800	42760 – 40080	Barshay-Szmidt et al. (2018)	Y	Y
bone	cutmark	365	C 4d1j	Proto-Aurig.	AMH	AF	24.4	4.1	-20.8	5.1	42.7	3.1	OxA-23433	37000	800	42760 – 40080	Barshay-Szmidt et al. (2018)	Y	Y
bone	cutmark	523	C 4b1	Early Aurig.	AMH	AF	15.3	2.8	-20.3	8.0	43.4	3.2	OxA-34635	35250	650	41280 – 38580	Barshay-Szmidt et al. (2018)	Y	Y
bone	cutmark	637	C 4c4	Proto-/Early Aurig.	AMH	ABA	44.6	8.8	-20.5	6.7	31.4	3.3	AA-69183	37580	780	43170 – 40660	Szmidt et al. (2010b)	Y	Y
bone	cutmark	1003	C 4c4	Proto-/Early Aurig.	AMH	ABA	37.4	7.0	-21.5	7.1	31.2	3.4	AA-69184	40200	3600	>40620	Szmidt et al. (2010b)	Y	Y
bone	cutmark	1074	C 4c4	Proto-/Early Aurig.	AMH	ABA	70.7	13.3	-21.0	7.1	39.0	3.3	AA-69179	37000	1600	44920 – 38610	Szmidt et al. (2010b)	Y	Y
bone	cutmark, impact	330	C 4b2	Early Aurig.	AMH	AF	19.6	3.8	-21.0	8.6	43.3	3.2	OxA-34636	35050	650	41150 – 38410	Barshay-Szmidt et al. (2018)	Y	Y
bone	cutmark, impact	397	C 4d1j	Proto-Aurig.	AMH	AF	8.8	1.4	-21.0	4.0	42.9	3.2	OxA-23434	37000	800	42760 – 40080	Barshay-Szmidt et al. (2018)	Y	Y
bone	cutmark, impact	676	C 4b2	Early Aurig.	AMH	AF	30.0	3.8	-21.1	7.4	43.4	3.2	OxA-34773	34950	600	40960 – 38380	Barshay-Szmidt et al. (2018)	Y	Y
bone	cutmark, impact	939	C 4b2	Early Aurig.	AMH	AF	5.3	0.8	-21.1	9.4	41.0	3.2	OxA-X-2698-50	35150	650	41210 – 38490	Barshay-Szmidt et al. (2018)	Y	Y
bone	cutmark, percussion	327	C 4c4	Proto-/Early Aurig.	AMH	ABA	48.8	9.4	-24.3	7.8	29.8	3.3	AA-69185	36990	720	42620 – 40210	Szmidt et al. (2010b)	Y	Y
bone	cutmark, percussion	725	C 4c4	Proto-/Early Aurig.	AMH	ABA	41.2	7.8	-20.5	7.8	42.1	3.3	AA-69180	37300	1800	45970 – 38550	Szmidt et al. (2010b)	Y	Y
bone	cutmark, percussion	736	C 4c4	Proto-/Early Aurig.	AMH	ABA	38.3	7.3	-21.0	7.1	34.7	3.3	AA-69181	36800	860	42720 – 39770	Szmidt et al. (2010b)	Y	Y
bone	cutmark?	9	C 5	Proto-Aurig.	AMH	AF	5.2	0.5	-20.0	6.0	41.5	3.2	OxA-X-2694-17	38900	1000	44820 – 41590	Barshay-Szmidt et al. (2018)	Y	N
bone	impact marks	275	C 4d1j	Proto-Aurig.	AMH	AF	9.1	1.6	-20.8	5.1	42.3	3.2	OxA-23435	37500	900	43340 – 40320	Barshay-Szmidt et al. (2018)	Y	Y
bone	impact marks	602	C 4b1	Early Aurig.	AMH	AF	16.4	2.5	-21.2	7.6	43.8	3.1	OxA-34772	34950	600	40960 – 38380	Barshay-Szmidt et al. (2018)	Y	Y
bone	no mod	677	C 4b2	Early Aurig.	AMH	AF	19.1	3.8	-20.1	9.3	43.3	3.2	OxA-34637	34850	600	40920 – 38280	Barshay-Szmidt et al. (2018)	Y	N

Table C.8: Reference Sites: published radiocarbon dates from l'Arbreda (Spain) used for modelling. Dates calibrated in OxCal 4.3 (Bronk Ramsey, 2009a) using IntCal13 (Reimer et al., 2013). Date part of model: 'S' = stratigraphic, 'K' = KDE.

Material	Type	Sample	Context	Culture	Author	Treat.	Yield (mg)	Yield (%)	$\delta^{13}C$	$\delta^{15}N$	%C	C:N	Lab-no.	^{14}C (BP)	σ	Date (calBP)	Ref.	S	K
bone	artefact	ABD 22	Level H	Proto-Aurig.	AMH	AF*	10.7	3.2	-19.7	9.3	43.7	3.2	OxA-21674	33800	550	39540 – 36620	Wood et al. (2014)	Y	Y
bone	artefact	ABD 7	Level H	Proto-Aurig.	AMH	AF*	11.5	3.7	-18.3	6.1	43.1	3.2	OxA-21784	36000	700	41930 – 39210	Wood et al. (2014)	Y	Y
bone	cutmark	ABD 18	Level H	Proto-Aurig.	AMH	AF*	40.9	6.4	-20.7	6.0	44.8	3.2	OxA-21664	35900	650	41790 – 39190	Wood et al. (2014)	Y	Y
bone	cutmark	ABD 20	Level H	Proto-Aurig.	AMH	AF*	15.2	3.0	-18.8	10.3	42.9	3.2	OxA-21665	35850	700	41820 – 39040	Wood et al. (2014)	Y	Y
bone	cutmark	ABD 25	Level G	Evolved Aurig.	AMH	AF	54.0	7.7	-20.4	4.3	43.4	3.3	OxA-21666	32750	450	38270 – 35850	Wood et al. (2014)	Y	Y
bone	cutmark	ABD 27	Level G	Evolved Aurig.	AMH	AF	23.6	3.4	-20.8	4.6	46.9	3.3	OxA-21667	32250	450	37630 – 35150	Wood et al. (2014)	Y	Y
bone	cutmark	ABD 31	Level E	Gravettian	AMH	AF	35.4	5.7	-20.0	7.7	45.5	3.3	OxA-21669	25780	210	30610 – 29440	Wood et al. (2014)	Y	Y
bone	cutmark, percussion	ABD 11	Level H	Proto-Aurig.	AMH	AF*	7.0	1.5	-19.4	8.3	42.1	3.2	SANU-29017	34800	760	41270 – 37710	Wood et al. (2014)	Y	Y
bone	cutmark, percussion	ABD 11	Level H	Proto-Aurig.	AMH	AF*	8.7	1.8	-19.4	8.6	44.1	3.2	SANU-29019	35900	860	42060 – 38840	Wood et al. (2014)	Y	Y
bone	cutmark, percussion	ABD 30	Level E	Gravettian	AMH	AF*	34.3	4.1	-20.6	4.9	45.6	3.3	OxA-21668	26100	210	30850 – 29750	Wood et al. (2014)	Y	Y
bone	fracture	ABD 12	Level H	Proto-Aurig.	AMH	AF*	4.5	1.5	-19.0	9.7	38.4	3.2	SANU-29018	32100	540	37690 – 34880	Wood et al. (2014)	Y	Y
bone	fracture	ABD 13	Level I	Mousterian	Neanderthal	AF*	35.6	4.3	-20.0	4.4	42.4	3.2	OxA-21662	37300	800	42970 – 40350	Wood et al. (2014)	Y	N
bone	fracture	ABD 14	Level I	Mousterian	Neanderthal	AF*	16.9	2.6	-19.5	5.8	46.1	3.3	OxA-21702	39200	1000	45030 – 41820	Wood et al. (2014)	Y	N
bone	fracture	ABD 15	Level I	Mousterian	Neanderthal	AF*	15.7	4.4	-19.4	3.1	45.6	3.2	OxA-21663	32100	450	37340 – 34980	Wood et al. (2014)	Y	N
bone	fracture	ABD 15	Level I	Mousterian	Neanderthal	AF*	27.7	3.6	-19.6	4.7	47.1	3.3	OxA-21703	32300	450	37710 – 35210	Wood et al. (2014)	Y	N
bone	fracture	ABD 17	Level I	Mousterian	Neanderthal	AF*	11.6	2.6	-19.4	6.2	47.0	3.3	OxA-21704	39200	1000	45030 – 41820	Wood et al. (2014)	Y	N
bone	no mod	ABD 2	Level F	Gravettian	AMH	AF	22.3	2.9	-20.5	7.8	46.1	3.2	OxA-21781	28260	280	32980 – 31420	Wood et al. (2014)	Y	N
bone	no mod	ABD 5	Level F	Gravettian	AMH	AF	28.9	3.3	-19.2	5.1	45.2	3.3	OxA-21782	28280	290	33030 – 31420	Wood et al. (2014)	Y	N
bone	percussion	ABD 10	Level H	Proto-Aurig.	AMH	AF*	8.7	1.5	-19.8	9.0	34.5	3.2	SANU-29016	35700	830	41880 – 38710	Wood et al. (2014)	Y	Y
bone	percussion	ABD 9	Level H	Proto-Aurig.	AMH	AF*	9.7	2.5	-19.7	5.7	45.3	3.2	SANU-29014	31900	530	37290 – 34710	Wood et al. (2014)	Y	Y
bone	point (lozangic)	ABD 6	Level G	Evolved Aurig.	AMH	AF*	12.2	6.1	-19.7	3.2	44.5	3.2	OxA-21783	32100	450	37340 – 34980	Wood et al. (2014)	Y	Y
charcoal	charcoal	ARB 5	Level I	Mousterian	Neanderthal	XR	9.2	4.8	-24.5	–	39.7	–	OxA-19994	38350	400	43020 – 41920	Wood et al. (2014)	Y	N

Table C.9: Reference Sites: published radiocarbon dates from Hohle Fels (Germany) used for modelling. Dates calibrated in OxCal 4.3 (Bronk Ramsey, 2009a) using IntCal13 (Reimer et al., 2013). Date part of model: 'S' = stratigraphic, 'K' = KDE.

Material	Type	Sample	Context	Culture	Author	Treat.	Yield (mg)	Yield (%)	$\delta^{13}C$	$\delta^{15}N$	%C	C:N	Lab-no.	^{14}C (BP)	σ	Date (calBP)	Ref.	S	K
bone	artefact	–	IIc	Gravettian	AMH	AI	33.2	6.6	-18.5	–	42.7	–	OxA-5007	29550	650	34930 – 32020	Housley et al. (1997)	Y	Y
bone	retoucher	–	IV	Aurignacian	AMH	–	–	15.5	–	–	–	–	KIA-16036	33090	+260/-250	38190 – 36460	Conard and Bolus (2003)	Y	Y
bone	retoucher	–	Va	Aurignacian	AMH	–	–	9.2	–	–	–	–	KIA-35464	31750	260	36220 – 35050	Conard and Bolus (2008)	Y	Y
bone	retoucher	–	Va	Aurignacian	AMH	–	–	10.3	–	–	–	–	KIA-35459	32550	+300/-290	37550 – 35790	Conard and Bolus (2008)	Y	Y
bone	cutmark?	–	VII	MP	Neand.	–	–	6.8	–	–	–	–	KIA-32054	37940	+530/-500	42930 – 41500	Conard and Bolus (2008)	Y	N
bone	cutmark?	–	VIII	MP	Neand.	–	–	2.9	–	–	–	–	KIA-32052	39580	+600/-560	44430 – 42500	Conard and Bolus (2008)	Y	N
bone	cutmarks	–	IIIa	Aurignacian	AMH	–	–	6.6	–	–	–	–	KIA-32055	30340	+290/-280	34840 – 33870	Conard and Bolus (2008)	Y	Y
bone	cutmarks	–	Va	Aurignacian	AMH	–	–	9.5	–	–	–	–	KIA-35462	32090	+350/-340	36810 – 35170	Conard and Bolus (2008)	Y	Y
bone	cutmarks	–	Va	Aurignacian	AMH	–	–	14.2	–	–	–	–	KIA-35463	32030	+280/-270	36500 – 35280	Conard and Bolus (2008)	Y	Y
bone	cutmarks?	–	VI	MP	Neand.	–	–	17.7	–	–	–	–	KIA-19562	36380	+380/-360	41720 – 40230	Conard and Bolus (2008)	Y	N
bone	impact	–	IIIa	Aurignacian	AMH	–	–	15.7	–	–	–	–	KIA-16039	31140	+250/-240	35600 – 34580	Conard and Bolus (2003)	Y	Y
bone	impact	–	IIIa	Aurignacian	AMH	–	–	8.0	–	–	–	–	KIA-32056	29710	'210/-200	34320 – 33430	Conard and Bolus (2008)	Y	Y
bone	impact	–	IIIb	Aurignacian	AMH	–	–	–	–	–	–	–	KIA-3505	29990	+340/-330	34690 – 33570	Conard and Bolus (2008)	Y	Y
bone	impact	–	IX	MP	Neand.	–	–	4.7	–	–	–	–	KIA-32053	38560	+530/-500	43370 – 41910	Conard and Bolus (2008)	Y	N
bone	impact	–	Va	Aurignacian	AMH	–	–	17.8	–	–	–	–	KIA-16035	33290	270	38390 – 36670	Conard (2003)	Y	Y
bone	impact	–	VII	MP	Neand.	–	–	12.8	–	–	–	–	KIA-19563	36350	+540/-510	41920 – 39940	Conard and Bolus (2008)	Y	N
bone	Impact, cutmarks	–	IIcf	Gravettian	AMH	–	–	20.1	–	–	–	–	KIA-17742	27690	140	31730 – 31160	Conard and Bolus (2003)	Y	Y
bone	Impact, cutmarks	–	IIe	Aurignacian/ Gravettian	AMH	–	–	15.9	–	–	–	–	KIA-16040	30640	190	34950 – 34170	Conard and Bolus (2003)	Y	Y
bone	Impact, cutmarks	–	IIIa	Aurignacian	AMH	–	–	14.4	–	–	–	–	KIA-16038	29840	210	34350 – 33600	Conard and Bolus (2003)	Y	Y
bone	Impact, cutmarks	–	IV	Aurignacian	AMH	–	–	14.4	–	–	–	–	KIA-16037	32470	+290/-280	37360 – 35710	Conard and Bolus (2008)	Y	Y
bone	Impact, cutmarks	–	Va	Aurignacian	AMH	–	–	18.6	–	–	–	–	KIA-16034	35710	+360/-340	41180 – 39550	Conard (2003)	Y	Y
bone	Impact, cutmarks	–	VI	MP	Neand.	–	–	16.0	–	–	–	–	KIA-19564	35760	+660/-610	41660 – 39050	Conard and Bolus (2008)	Y	N
bone	point	–	IIcf	Gravettian	AMH	–	–	12.9	–	–	–	–	KIA-17744	27780	150	31890 – 31200	Conard and Bolus (2003)	Y	Y
charcoal	charcoal	–	III	Aurignacian	AMH	ZR	36.5	31.5	-24.7	–	51.4	–	OxA-4979	27600	800	33690 – 30460	Housley et al. (1997)	Y	Y
charcoal	charcoal	–	IIIa	Aurignacian	AMH	–	–	–	–	–	–	–	KIA-18876	31010	+600/-560	36180 – 33980	Conard (2003)	Y	Y
charcoal	charcoal	–	IIIa	Aurignacian	AMH	–	–	–	–	–	–	–	KIA-18877	30170	+250/-240	34670 – 33800	Conard (2003)	Y	Y
charcoal	charcoal	–	IIIb	Aurignacian	AMH	–	–	–	–	–	–	–	KIA-18878	29780	+330/-310	34550 – 33370	Conard (2003)	Y	Y
charcoal	charcoal	–	IV	Aurignacian	AMH	ZR	37.0	29.4	-25.6	–	51.4	–	OxA-4980	28750	750	34250 – 31270	Housley et al. (1997)	Y	Y
charcoal	charcoal	–	Va	Aurignacian	AMH	–	–	–	–	–	–	–	KIA-18880	34190	+340/-330	39590 – 37900	Conard (2003)	Y	Y

Table C.10: Reference Sites: published radiocarbon dates from Geißenklösterle (Germany) used for modelling. Dates calibrated in OxCal 4.3 (Bronk Ramsey, 2009a) using IntCal13 (Reimer et al., 2013). Date part of model: 'S' = stratigraphic, 'K' = KDE.

Material	Type	Sample	Context	Culture	Author	Treat.	Yield (mg)	Yield (%)	$\delta^{13}C$	$\delta^{15}N$	%C	C:N	Lab-no.	^{14}C (BP)	σ	Date (calBP)	Ref.	S	K
bone	cutmarks	GK 26 Ia 18	Ia	Gravettian	AMH	AF	43.3	7.8	-20.6	8.5	49.6	3.4	OxA-21739	28600	290	33460 – 31700	Higham et al. (2012)	Y	Y
bone	cutmarks	GK 48 VII 456	VII	MP	Neand.	AF	38.9	8.1	-18.7	7.0	48.3	3.3	OxA-21741	48600	3200	>49850	Higham et al. (2012)	Y	N
bone	cutmarks	GK 57 IIb 706	Iib	Aurignacian	AMH	AF	37.9	8.6	-20.7	9.3	47.2	3.3	OxA-21727	34100	550	39920 – 36960	Higham et al. (2012)	Y	Y
bone	cutmarks	GK 67 IIIa 1453	IIIa	Aurignacian	AMH	AF	51.8	7.5	-18.7	3.5	45.4	3.4	OxA-21746	36850	800	42650 – 39930	Higham et al. (2012)	Y	Y
bone	cutmarks	GK 99 Ir 185	Ir	Gravettian	AMH	AF	18.3	4.6	-21.7	8.3	44.3	3.3	OxA-21740	26420	230	31090 – 30170	Higham et al. (2012)	Y	Y
bone	impact	GK 130 It 328	It	Gravettian	AMH	AF	22.5	2.2	-20.4	9.4	41.5	3.2	OxA-21660	27960	290	32680 – 31220	Higham et al. (2012)	Y	Y
bone	impact	GK 58 IIb 246	Iib	Aurignacian	AMH	AF	16.4	2.6	-21.0	7.7	45.4	3.3	OxA-21724	33950	550	39740 – 36790	Higham et al. (2012)	Y	Y
bone	impact	GK 66 IIIa 1073	IIIa	Aurignacian	AMH	AF	42.3	5.5	-19.0	3.6	45.2	3.4	OxA-21745	36650	750	42440 – 39820	Higham et al. (2012)	Y	Y
bone	impact	GK 77 III 627	III	Aurignacian	AMH	AF	12.1	2.5	-18.9	5.1	44.1	3.2	OxA-21659	35050	600	41030 – 38470	Higham et al. (2012)	Y	Y
bone	impact	GK 78 IV 1495	IV	MP	Neand.	AF	14.0	2.2	-20.7	4.6	46.9	3.3	OxA-21720	35500	650	41460 – 38780	Higham et al. (2012)	Y	N
bone	impact	GK 86 Ic 122	Ic	Gravettian	AMH	AF	12.2	4.1	-18.3	4.8	44.2	3.1	OxA-21661	32900	450	38380 – 36040	Higham et al. (2012)	Y	Y
bone	impact, cutmarks	GK 67 IIIb 1655	IIIb	Aurignacian	AMH	AF	72.0	6.8	-18.6	3.7	46.6	3.4	OxA-21743	36100	700	42010 – 39330	Higham et al. (2012)	Y	Y
bone	no mod	GK 33 Iia 80	Iia	Aurignacian	AMH	AF	30.3	4.8	-21.0	4.5	46.0	3.3	OxA-21737	35700	650	41630 – 38970	Higham et al. (2012)	Y	N
bone	no mod	GK 57 IIIc 2389	IIIc	none	none	AF	12.6	3.0	-18.3	3.4	44.2	3.1	OxA-21658	38300	900	44160 – 41220	Higham et al. (2012)	Y	N
bone	no mod	GK 57 IIIc 2430	IIIc	none	none	AF	20.4	4.2	-19.4	5.7	43.9	3.1	OxA-21657	39400	1100	45420 – 41840	Higham et al. (2012)	Y	N
bone	no mod	GK 66 III 1144	III	Aurignacian	AMH	AF	27.8	5.2	-19.6	4.2	46.8	3.3	OxA-21722	38900	1000	44820 – 41590	Higham et al. (2012)	Y	N
bone	no mod	GK 67 IIb 931	Iib	Aurignacian	AMH	AF	23.5	4.5	-20.3	9.0	44.9	3.3	OxA-21742	34800	600	40890 – 38210	Higham et al. (2012)	Y	N
bone	no mod	GK 69 IIIb 958	IIIb	Aurignacian	AMH	AF	28.1	4.8	-19.1	6.2	47.4	3.4	OxA-21723	37800	900	43670 – 40630	Higham et al. (2012)	Y	N
bone	no mod	GK 77 III 641	III	Aurignacian	AMH	AF	17.0	1.6	-19.4	6.0	45.4	3.3	OxA-21744	36850	750	42580 – 40020	Higham et al. (2012)	Y	N
bone	no mod	GK 86 III 294	III	Aurignacian	AMH	AF	24.4	4.4	-20.4	7.8	46.4	3.3	OxA-21725	37400	800	43050 – 40440	Higham et al. (2012)	Y	N
bone	no mod	GK Iia 131	Iia	Aurignacian	AMH	AF	27.4	5.3	-20.2	9.5	43.4	3.2	OxA-21656	33000	500	38510 – 36050	Higham et al. (2012)	Y	N
bone	retouch	GK 55 Iid 319	Iid	Aurignacian	AMH	AF	13.2	2.1	-18.5	8.2	46.3	3.3	OxA-21726	34200	550	40060 – 37120	Higham et al. (2012)	Y	Y
bone	retouch	GK Iib 143	Iib	Aurignacian	AMH	AF	20.4	3.4	-20.7	6.4	46.0	3.3	OxA-21738	34900	600	40940 – 38340	Higham et al. (2012)	Y	Y
bone	scrape marks	GK 57 IIIb 1238	IIIb	Aurignacian	AMH	AF	8.1	1.4	-19.6	6.8	43.6	3.3	OxA-21721	37300	800	42970 – 40350	Higham et al. (2012)	Y	Y

Table C.11: Reference Sites: published radiocarbon dates used for modelling: top – from Vogelherd (Germany); bottom – from Hohlenstein-Stadel (Germany). Dates calibrated in OxCal 4.3 (Bronk Ramsey, 2009a) using IntCal13 (Reimer et al., 2013). Date part of model: 'S' = stratigraphic, 'K' = KDE.

Material	Type	Sample	Context	Culture	Author	Treat.	Yield (mg)	Yield (%)	$\delta^{13}C$	$\delta^{15}N$	%C	C:N	Lab-no.	^{14}C (BP)	σ	Date (calBP)	Ref.	S	K
bone	charred	–	IV/V	Aurignacian	AMH	–	–	–	–	–	–	–	GrN-6662	27630	830	33760 – 30430	Hahn (1977)	N	Y
bone	charred	–	V	Aurignacian	AMH	–	–	–	–	–	–	–	GrN-6661	30650	560	35810 – 33750	Hahn (1977)	N	Y
bone	cutmarks	–	IV	Aurignacian	AMH	–	–	–	–	–	–	–	KIA-8957	26160	150	30850 – 29950	Conard and Bolus (2003)	N	Y
bone	cutmarks	–	IV/V	Aurignacian	AMH	–	–	–	–	–	–	–	PL0001342A	34100	1100	41210 – 36160	Conard and Bolus (2003)	N	Y
bone	cutmarks	–	V	Aurignacian	AMH	–	–	–	–	–	–	–	PL0001337A	35810	710	41800 – 38990	Conard and Bolus (2003)	N	Y
bone	cutmarks	–	V	Aurignacian	AMH	–	–	–	–	–	–	–	PL0001338A	32400	1700	41340 – 33790	Conard and Bolus (2003)	N	Y
bone	impact	–	V	Aurignacian	AMH	–	–	–	–	–	–	–	KIA-8968	31790	240	36220 – 35120	Conard and Bolus (2003)	N	Y
bone	impact	–	V	Aurignacian	AMH	–	–	–	–	–	–	–	KIA-8969	32500	+260/-250	37280 – 35790	Conard and Bolus (2003)	N	Y
bone	impact	–	V	Aurignacian	AMH	–	–	–	–	–	–	–	KIA-8970	33080	+260/-250	38170 – 36450	Conard and Bolus (2003)	N	Y
bone	impact, cutmarks	–	IV/V	Aurignacian	AMH	–	–	–	–	–	–	–	PL0001339A	32180	960	38810 – 34440	Conard and Bolus (2003)	N	Y
Material	**Type**	**Sample**	**Context**	**Culture**	**Author**	**Treat.**	**Yield (mg)**	**Yield (%)**	**$\delta^{13}C$**	**$\delta^{15}N$**	**%C**	**C:N**	**Lab-no.**	**^{14}C (BP)**	**σ**	**Date (calBP)**	**Ref.**	**S**	**K**
bone	fresh break	–	19 m, spit 10	Aurignacian	AMH	–	–	–	–	–	–	–	KIA-8946	39970	+490/-460	44530 – 42860	Conard and Bolus (2003)	N	Y
bone	fresh break	–	19 m, spit 11	Aurignacian	AMH	–	–	–	–	–	–	–	KIA-8945	40220	+550/-510	44840 – 42960	Conard and Bolus (2003)	N	Y
bone	fresh break	–	19 m, spit 7	Aurignacian	AMH	–	–	–	–	–	–	–	KIA-8949	33920	+310/-300	39150 – 37400	Conard and Bolus (2003)	N	Y
bone	fresh break	–	19 m, spit 7	Aurignacian	AMH	–	–	–	–	–	–	–	KIA-8950	36910	+490/-460	42230 – 40570	Conard and Bolus (2003)	N	Y
bone	fresh break	–	19 m, spit9	Aurignacian?	AMH	–	–	–	–	–	–	–	KIA-8947	42410	+670/-620	47120 – 44600	Conard and Bolus (2003)	N	N
bone	fresh break	–	20 m, spit 6	Aurignacian?	AMH	–	–	–	–	–	–	–	KIA-13077	32270	+270/-260	36820 – 35550	Conard and Bolus (2003)	N	N
bone	impact	–	19 m, spit 6	Aurignacian?	AMH	–	–	–	–	–	–	–	KIA-8951	31440	250	35920 – 34790	Conard and Bolus (2003)	N	N
bone	impact	–	19 m, spit 8	Aurignacian?	AMH	–	–	–	–	–	–	–	KIA-8948	41710	+570/-530	46160 – 44170	Conard and Bolus (2003)	N	N

Table C.12: Reference Sites: published radiocarbon dates used for modelling: top – from Castelcivita (Italy); bottom – from Fumane (Italy). Dates calibrated in OxCal 4.3 (Bronk Ramsey, 2009a) using IntCal13 (Reimer et al., 2013). Date part of model: 'S' = stratigraphic, 'K' = KDE.

Material	Type	Sample	Context	Culture	Author	Treat.	Yield (mg)	Yield (%)	$\delta^{13}C$	$\delta^{15}N$	%C	C:N	Lab-no.	^{14}C (BP)	σ	Date (calBP)	Ref.	S	K
bone	charred	–	gic	Aurignacian	AMH	–	–	–	–	–	–	–	F-105	31950	650	37850 – 34650	Stage 3 db	Y	Y
bone	charred	–	pie	Uluzzian	AMH	–	–	–	–	–	–	–	F-107	33220	780	39460 – 35710	Gambassini (1997)	Y	Y
bone	charred	–	rsa (lower)	Uluzzian	AMH	–	–	–	–	–	–	–	F-71	32470	650	38380 – 35170	Gambassini (1997)	Y	Y
bone	charred	–	rsa (upper)	Aurignacian	AMH	–	–	–	–	–	–	–	F-72	32930	720	38930 – 35500	Stage 3 db	Y	Y
bone	n/a	–	rsa (upper)	Aurignacian	AMH	–	–	–	–	–	–	–	Beta-58184/ CAMS-4622	32930	490	38460 – 36000	Stage 3 db	Y	Y
bone	n/a	–	tg.29-30	Mousterian	Neanderthal	ABA	–	–	–	–	–	–	GrN-13982	39100	1300	45800 – 41330	Stage 3 db	Y	N
bone	n/a	–	tg.29-29	Mousterian	Neanderthal	ABA	–	–	–	–	–	–	GrN-13984	42700	900	48240 – 44500	Stage 3 db	Y	N
charcoal	charcoal	–	rpi	Uluzzian	AMH	ABA	–	–	–	–	–	–	GrN-13985	33330	430	38620 – 36430	Gambassini (1997)	Y	Y
charcoal	charcoal	–	rsa", spit 11	Uluzzian	AMH	XR	6.0	7.4	-24.0	-	76.7	–	OxA-22622	36120	360	41520 – 39990	Douka et al. (2014)	Y	Y
Material	**Type**	**Sample**	**Context**	**Culture**	**Author**	**Treat.**	**Yield (mg)**	**Yield (%)**	$\delta^{13}C$	$\delta^{15}N$	%C	C:N	**Lab-no.**	^{14}C (BP)	σ	**Date (calBP)**	**Ref.**	**S**	**K**
bone	cutmark	RF28	A4II	Uluzzian	AMH	AF	17.5	2.9	-18.8	4.7	46.3	3.3	OxA-21733	41000	1300	47600 – 42610	Douka et al. (2014)	Y	Y
bone	cutmark	RF29	A4II	Uluzzian	AMH	AF	20.0	3.3	-20.5	3.8	48.2	3.4	OxA-21734	42000	1400	48860 – 43230	Douka et al. (2014)	Y	Y
bone	cutmark	RF30	A4	Uluzzian	AMH	AF	3.9	0.6	-19.7	5.8	43.7	3.2	OxA-21735	42000	1700	49350 – 43100	Douka et al. (2014)	Y	Y
bone	cutmark	RF44	A3	Uluzzian	AMH	AF	17.4	2.9	-19.6	6.3	46.9	3.4	OxA-21736	39100	1000	44960 – 41750	Douka et al. (2014)	Y	Y
bone	cutmark	RF49	A3	Uluzzian	AMH	AF	38.6	6.2	-18.8	7.6	45.5	3.3	OxA-X-2295-52	41300	1300	47910 – 42800	Douka et al. (2014)	Y	Y
charcoal	charcoal	–	A1	Proto-Aurig.	AMH	–	–	–	–	–	–	–	UtC-2049	31900	500	37130 – 34730	Bartolomei et al. (1992)	Y	Y
charcoal	charcoal	–	A2	Proto-Aurig.	AMH	–	–	–	–	–	–	–	UtC-2048	36500	600	42120 – 39950	Bartolomei et al. (1992)	Y	Y
charcoal	charcoal	–	A2, hearth S14	Proto-Aurig.	AMH	–	–	–	–	–	–	–	UtC-2688	36800	1200	43420 – 39020	Bartolomei et al. (1992)	Y	Y
charcoal	charcoal	–	A2, hearth S14	Proto-Aurig.	AMH	–	–	–	–	–	–	–	UtC-2689	35400	1100	42290 – 37800	Bartolomei et al. (1992)	Y	Y
charcoal	charcoal	–	A2, hearth S14	Proto-Aurig.	AMH	–	–	–	–	–	–	–	UtC-2690	34200	900	40830 – 36460	Bartolomei et al. (1992)	Y	Y
charcoal	charcoal	–	A2	Proto-Aurig.	AMH	–	–	–	–	–	–	–	UtC-2047	32100	500	37550 – 34930	Bartolomei et al. (1992)	Y	Y
charcoal	charcoal	–	A2, hearth S10	Proto-Aurig.	AMH	–	–	–	–	–	–	–	UtC-1774	40000	4000	>40030	Bartolomei et al. (1992)	Y	Y
charcoal	charcoal	–	A2, hearth S10	Proto-Aurig.	AMH	–	–	–	–	–	–	–	UtC-2051	32800	400	38230 – 36000	Bartolomei et al. (1992)	Y	Y
charcoal	charcoal	–	A2, hearth S9	Proto-Aurig.	AMH	–	–	–	–	–	–	–	UtC-2044	31600	400	36310 – 34730	Bartolomei et al. (1992)	Y	Y
charcoal	charcoal	–	D3b	Early Aurig.	AMH	–	–	–	–	–	–	–	UtC-1775	31700	1200	39090 – 33740	Bartolomei et al. (1992)	Y	Y
charcoal	charcoal	–	D3b	Early Aurig.	AMH	–	–	–	–	–	–	–	UtC-2045	32300	400	37540 – 35310	Bartolomei et al. (1992)	Y	Y
charcoal	charcoal	–	D6	Early Aurig.	AMH	–	–	–	–	–	–	–	UtC-2046	32300	500	37870 – 35140	Bartolomei et al. (1992)	Y	Y

Table C.13: Reference Sites: published radiocarbon dates from Willendorf II (Austria) used for modelling. Dates calibrated in OxCal 4.3 (Bronk Ramsey, 2009a) using IntCal13 (Reimer et al., 2013). Date part of model: 'S' = stratigraphic, 'K' = KDE.

Material	Sample	Context	Culture	Author	Treat.	Yield (mg)	Yield (%)	$\delta^{13}C$	%C	Lab-no.	^{14}C (BP)	σ	Date (calBP)	Ref.	S	K
charcoal	A-166a	C8-2 stretched, N129	Aurignacian	AMH	ABA	–	–	–	–	GrA-896	37930	750	43391 – 41093	Nigst et al. (2014, SI)	Y	Y
charcoal	A-1905	C4-1, N125-126	Aurignacian	AMH	ABA	–	–	–	–	GrA-35403	31250	'+230/-210	35643 – 34687	Nigst et al. (2014, SI)	Y	Y
charcoal	A-1906	C4-1, N125-126	Aurignacian	AMH	ABA	–	–	–	–	GrA-35404	31770	'+250/-230	36201 – 35110	Nigst et al. (2014, SI)	Y	Y
charcoal	A-1907	D1 middle, N127	Micoquian	Neanderthal	ZR	24.6	63.7	-24.8	61.9	OxA-17398	39980	350	44336 – 42998	Nigst et al. (2014, SI)	Y	N
charcoal	A-1908	D1 lower, N127	Micoquian	Neanderthal	ZR	29.7	66.4	-23.6	60.5	OxA-17400	41800	400	45934 – 44476	Nigst et al. (2014, SI)	Y	N
charcoal	A-1911	D1 upper, N127	Micoquian	Neanderthal	ZR	26.1	72.7	-24.3	61.7	OxA-17399	41280	380	45505 – 44057	Nigst et al. (2014, SI)	Y	N
charcoal	A-1912a	C4-1, N125-126	Aurignacian	AMH	ABA	–	–	–	–	GrA-35406	31170	'+230/-210	35570 – 34633	Nigst et al. (2014, SI)	Y	Y
charcoal	A-1912b	C4-1, N125-126	Aurignacian	AMH	ZR	50.4	75.0	-24.3	62.5	OxA-17396	32230	190	36535 – 35665	Nigst et al. (2014, SI)	Y	Y
charcoal	A-1915c1	C8-2 in situ, N124-124.5	Aurignacian	AMH	ABA	–	–	–	–	GrA-45012	38790	'+400/-350	43284 – 42210	Nigst et al. (2014, SI)	Y	Y
charcoal	A-1915c3	C8-2 in situ, N124-124.5	Aurignacian	AMH	XR	5.7	4.6	-25.4	83.6	OxA-23520	39000	500	43764 – 42190	Nigst et al. (2014, SI)	Y	Y
charcoal	A-1933	C8-2 stretched, N127	Aurignacian	AMH	ZR	21.6	55.7	-24.2	62.8	OxA-17397	37980	300	42663 – 41799	Nigst et al. (2014, SI)	Y	Y
charcoal	A-1935a	C8-2 in situ, N124-124.5	Aurignacian	AMH	ABA	–	–	–	–	GrA-44894	37420	'+300/-270	42297 – 41414	Nigst et al. (2014, SI)	Y	Y
charcoal	A-1935b	C8-2 in situ, N124-124.5	Aurignacian	AMH	ABA	–	–	–	–	GrA-35409	37910	'+440/-380	42756 – 41622	Nigst et al. (2014, SI)	Y	Y
charcoal	A-1935c2	C8-2 in situ, N124-124.5	Aurignacian	AMH	ZR	8.5	61.8	-25.8	63.2	OxA-22295	36500	450	41912 – 40224	Nigst et al. (2014, SI)	Y	Y
charcoal	A-2017	D3	Micoquian	Neanderthal	ZR	42.1	85.7	-23.3	61.8	OxA-17401	48500	800	50301 – 47030	Nigst et al. (2014, SI)	Y	N
charcoal	A-2039	C8-2 stretched, N127	Aurignacian	AMH	ABA	–	–	–	–	GrA-35411	37320	'+390/-350	42346 – 41220	Nigst et al. (2014, SI)	Y	Y
charcoal	A-2131	C7-1 (AH3ab), N121	Aurignacian	AMH	ABA	–	–	–	–	GraA-38250	34570	'+410/-330	39957 – 38400	Nigst et al. (2014, SI)	Y	Y
charcoal	A-2421a	C4-2, N126	Aurignacian	AMH	ABA	–	–	–	–	GrA-45804	32360	'+210/-190	36745 – 35765	Nigst et al. (2014, SI)	Y	Y
charcoal	A-2421a (hom)	C4-2, N126	Aurignacian	AMH	ABA	–	–	–	–	GrA-45011	32790	'+210/-200	37593 – 36228	Nigst et al. (2014, SI)	Y	Y
charcoal	A-2421b (hom)	C4-2, N126	Aurignacian	AMH	ZR	8.2	65.1	-24.1	65.5	OxA-22294	31750	260	36213 – 35059	Nigst et al. (2014, SI)	Y	Y
charcoal	A-2421c (hom)	C4-2, N126	Aurignacian	AMH	XR	8.5	4.4	-23.2	78.3	OxA-23562	33850	800	40180 – 36296	Nigst et al. (2014, SI)	Y	Y
charcoal	A-2537	D1/D2, N121	Micoquian	Neanderthal	XR	8.5	8.5	-23.8	79.8	OxA-25837	45100	1100	>46622	Nigst et al. (2014, SI)	Y	N
charcoal	A-2541a	D1 top, N121	Micoquian	Neanderthal	ABA	–	–	–	–	GrA-52417	40870	'+480/-400	45241 – 43536	Nigst et al. (2014, SI)	Y	N
charcoal	A-2541b	D1 top, N121	Micoquian	Neanderthal	XR	6.8	5.8	-24.0	79.6	OxA-25836	43200	900	48755 – 44952	Nigst et al. (2014, SI)	Y	N
charcoal	A-2542	D1 upper, N121	Micoquian	Neanderthal	XR	8.0	9.0	-23.9	82.6	OxA-25838	43400	900	48950 – 45130	Nigst et al. (2014, SI)	Y	N

Table C.14: Reference Sites: published radiocarbon dates from the Bohunician in Moravia (Czech Republic) used for modelling (after Škrdla, 2017). Dates calibrated in OxCal 4.3 (Bronk Ramsey, 2009a) using IntCal13 (Reimer et al., 2013). Date part of model: 'S' = stratigraphic, 'K' = KDE.

Site	Material	Sample	Context	Culture	Author	Treat.	Yield (mg)	Yield (%)	$\delta^{13}C$	%C	Lab-no.	^{14}C (BP)	σ	Date (calBP)	Ref.	S	K
Bohunice 2002	charcoal	BOH-11	4a	Bohunician	AMH	ZR	6.3	63.0	-22.7	61.6	OxA-18300	38770	330	43200 – 42240	Richter et al. (2009)	N	Y
Bohunice 2003	charcoal	BOH-12	4a	Bohunician	AMH	ZR	6.3	51.2	-22.7	62.3	OxA-18301	40050	360	44410 – 43030	Richter et al. (2009)	N	Y
Bohunice 2004	charcoal	BOH-13	4a	Bohunician	AMH	ZR	6.6	44.9	-22.5	61.8	OxA-18302	34770	240	39890 – 38700	Richter et al. (2009)	N	Y
Bohunice 2005	charcoal	BOH-14	4a	Bohunician	AMH	ZR	3.1	44.9	-23.3	61.0	OxA-18303	38200	330	42830 – 41900	Richter et al. (2009)	N	Y
Bohunice 2006	charcoal	BOH-7	4a	Bohunician	AMH	ZR	5.9	26.3	-23.3	62.0	OxA-18298	36050	260	41320 – 40090	Richter et al. (2009)	N	Y
Bohunice 2007	charcoal	BOH-8	4a	Bohunician	AMH	ZR	5.5	42.6	-24.0	58.8	OxA-18299	38690	320	43140 – 42210	Richter et al. (2009)	N	Y
Bohunice 2008	charcoal	BOH-9	4a	Bohunician	AMH	ZR	3.9	32.5	-23.4	55.3	OxA-18343	36540	310	41770 – 40490	Richter et al. (2009)	N	Y
Bohunice 2009	charcoal	–	4a	Bohunician	AMH	–	–	–	-23.2	–	WK-17757	40000	2000	48920 – 41410	Richter et al. (2008)	N	Y
Bohunice 2010	charcoal	–	4a	Bohunician	AMH	–	–	–	–	–	ANU-12024	32740	530	38380 – 35700	Škrdla and Tostevin (2005)	N	Y
Bohunice 2011	charcoal	–	4a	Bohunician	AMH	–	–	–	–	–	ANU-27214	35025	730	41370 – 38250	Škrdla and Tostevin (2005)	N	Y
Bohunice-brickyard	charcoal	–	–	Bohunician	AMH	–	–	–	-25.2	–	GrN-6165	42900	1700	49890 – 44120	Mook (1976)	N	Y
Bohunice-brickyard	charcoal	BOH-1/1.2	–	Bohunician	AMH	ZR	48.1	66.8	-21.4	61.6	OxA-14843	42100	450	46300 – 44640	Valoch (2008)	N	Y
Bohunice-brickyard	charcoal	BOH-2/1.4	–	Bohunician	AMH	ZR	44.3	69.7	-23.2	60.1	OxA-14844	43250	550	47820 – 45430	Valoch (2008)	N	Y
Bohunice-brickyard	charcoal	BOH-3/1.6	–	Bohunician	AMH	ZR	21.7	64.6	-23.5	57.2	OxA-14845	41250	450	45600 – 43890	Valoch (2008)	N	Y
Bohunice-brickyard	charcoal	BOH-4/2.1	–	Bohunician	AMH	ZR	46.6	70.7	-25.1	63.9	OxA-14846	43600	550	48210 – 45710	Valoch (2008)	N	Y
Bohunice-brickyard	charcoal	–	4a	Bohunician	AMH	ABA	–	–	–	–	GrN-16920	36000	1100	42550 – 38570	Svoboda (1993)	N	Y
Bohunice-Kejbaly	charcoal	BOH-5/2.4	–	Bohunician	AMH	ZR	23.4	68.4	-24.8	61.3	OxA-14847	42750	550	47240 – 45010	Valoch (2008)	N	Y
Bohunice-Kejbaly	charcoal	BOH-6/2.7	–	Bohunician	AMH	ZR	25.6	67.5	-23.0	63.5	OxA-14848	41350	450	45680 – 44000	Valoch (2008)	N	Y
Bohunice-Kejbaly	charcoal	–	–	Bohunician	AMH	–	–	–	–	–	Q-1044	40173	1200	46340 – 42190	Switsur (1976)	N	Y
Bohunice-Kejbaly I	charcoal	BOH-10	3	Bohunician	AMH	ZR	1.3	22.8	-23.9	72.5	OxA-18320	29490	240	34110 – 33150	Valoch (2008)	N	Y
Bohunice-Kejbaly II	charcoal	–	–	Bohunician	AMH	–	–	–	-24.4	–	GrN-6802	41400	1400	48320 – 42790	Mook (1976)	N	Y
Stránská skála III	charcoal	–	5	Bohunician	AMH	ABA	–	–	–	–	GrN-12297	38200	1100	44570 – 40750	Svoboda and Simán (1989)	N	Y
Stránská skála III	charcoal	–	5	Bohunician	AMH	ABA	–	–	–	–	GrN-12298	38500	1400	45640 – 40500	Svoboda and Simán (1989)	N	Y
Stránská skála IIIa	charcoal	–	4	Bohunician	AMH	ABA	–	–	–	–	GrN-12606	41300	3100	>42150	Svoboda and Simán (1989)	N	Y
Stránská skála IIIc	charcoal	–	5	Bohunician	AMH	–	–	–	–	–	AA-32058	38300	1100	44660 – 40870	Svoboda (2001)	N	Y
Stránská skála IIIc	charcoal	–	5	Bohunician	AMH	–	–	–	–	–	AA-41475	34440	720	40740 – 37050	Svoboda (2003)	N	Y
Stránská skála IIIc	charcoal	–	5	Bohunician	AMH	–	–	–	–	–	AA-41476	36570	940	42700 – 39370	Svoboda (2003)	N	Y
Stránská skála IIIc	charcoal	–	5	Bohunician	AMH	–	–	–	–	–	AA-41477	34530	770	40970 – 37090	Svoboda (2003)	N	Y
Stránská skála IIIc	charcoal	–	5	Bohunician	AMH	–	–	–	–	–	AA-41478	36350	990	42600 – 39030	Svoboda (2003)	N	Y
Stránská skála IIIc	charcoal	–	5	Bohunician	AMH	–	–	–	–	–	AA-41480	34680	820	41250 – 37270	Svoboda (2003)	N	Y
Stránská skála IIIc	charcoal	–	5	Bohunician	AMH	–	–	–	–	–	AA-32058	38300	1100	44660 – 40870	Svoboda (2001)	N	Y
Stránská skála IIIc	charcoal	–	5	Bohunician	AMH	–	–	–	–	–	AA-41475	34440	720	40740 – 37050	Svoboda (2003)	N	Y
Stránská skála IIIc	charcoal	–	5	Bohunician	AMH	–	–	–	–	–	AA-41476	36570	940	42700 – 39370	Svoboda (2003)	N	Y
Stránská skála IIIc	charcoal	–	5	Bohunician	AMH	–	–	–	–	–	AA-41477	34530	770	40970 – 37090	Svoboda (2003)	N	Y
Stránská skála IIIc	charcoal	–	5	Bohunician	AMH	–	–	–	–	–	AA-41478	36350	990	42600 – 39030	Svoboda (2003)	N	Y
Stránská skála IIIc	charcoal	–	5	Bohunician	AMH	–	–	–	–	–	AA-41480	34680	820	41250 – 37270	Svoboda (2003)	N	Y
Stránská skála IIId	charcoal	–	5	Bohunician	AMH	–	–	–	–	–	AA-32059	37900	1100	44300 – 40410	Svoboda (2001)	N	Y
Stránská skála IIId	charcoal	–	5	Bohunician	AMH	–	–	–	–	–	AA-32060	37270	990	43360 – 39930	Svoboda (2001)	N	Y
Stránská skála IIId	charcoal	–	5	Bohunician	AMH	–	–	–	–	–	AA-32061	35080	830	41610 – 38060	Svoboda (2001)	N	Y
Stránská skála IIId	charcoal	–	5	Bohunician	AMH	ABA	–	–	–	–	GrN-11504	34530	830	41070 – 36970	Svoboda (2001)	N	Y
Stránská skála IIId	charcoal	–	5	Bohunician	AMH	ABA	–	–	–	–	GrN-11808	35320	320	40710 – 39100	Svoboda (2001)	N	Y

Table C.15: Reference Sites: published radiocarbon dates from the Aurignacian and Szeletian in Moravia (Czech Republic) used for modelling (after Škrdla, 2017). Dates calibrated in OxCal 4.3 (Bronk Ramsey, 2009a) using IntCal13 (Reimer et al., 2013). Date part of model: 'S' = stratigraphic, 'K' = KDE.

Site	Material	Sample	Culture	Author	Treat.	Yield (mg)	Yield (%)	$\delta^{13}C$	%C	Lab-no.	^{14}C (BP)	σ	Date (calBP)	Ref.	S	K
Milovice I, D	–	–	Aurignacian	AMH	ABA	–	–	–	–	GrN-14826	29200	450	34220 – 32080	Oliva (2009)	N	Y
Milovice I, L	–	–	Aurignacian	AMH	ABA	–	–	–	–	GrN-22107	28780	230	33590 – 32100	Oliva (2009)	N	Y
Milovice I, L	–	–	Aurignacian	AMH	ABA	–	–	–	–	GrN-22108	32030	370	36790 – 35060	Oliva (2009)	N	Y
Napajedla III	charred bone	Npjdla 1	Aurignacian	AMH	ZR	54.4	68.0	-25.9	68.8	OxA-18304	32230	190	36540 – 35660	Škrdla (2010)	N	Y
Napajedla III	charred bone	–	Aurignacian	AMH	–	–	–	–	–	GrA-32568	30620	190	34940 – 34160	Škrdla (2010)	N	Y
Napajedla III	charcoal	Npjdla 2	Aurignacian	AMH	ZR	6.8	46.3	-25.2	60.1	OxA-18305	32540	200	37070 – 35930	Škrdla (2010)	N	Y
Napajedla III	charcoal	–	Aurignacian	AMH	ABA	–	–	–	–	GrA-32566	29820	180	34270 – 33620	Škrdla (2010)	N	Y
Napajedla III	tooth	–	Aurignacian	AMH	–	–	–	–	–	GrA-28280	32330	900	38770 – 34660	Škrdla (2010)	N	Y
Stránská skála Iia	charcoal	–	Aurignacian	AMH	ABA	–	–	–	–	GrN-14829	32350	900	38790 – 34670	Svoboda (2003)	N	Y
Stránská skála IIIa	charcoal	–	Aurignacian	AMH	ABA	–	–	–	–	GrN-12605	30980	360	35680 – 34210	Svoboda (2003)	N	Y
stránská skála IIIb	charcoal	–	Aurignacian	AMH	ABA	–	–	–	–	GrN-16918	32600	1700	41430 – 33940	Svoboda (2003)	N	Y
Stránská skála IIIc	charcoal	–	Aurignacian	AMH	–	–	–	–	–	AA-41479	33030	620	38770 – 35810	Svoboda (2003)	N	Y
Stránská skála IIIf	charcoal	–	Aurignacian	AMH	–	–	–	–	–	AA-41472	29020	440	34010 – 31870	Svoboda (2003)	N	Y
Moravský Krumlov IV	charcoal	Mor-KrumIV 1	Szeletian	Neanderthal	ZR	10.6	48.0	-23.4	64.2	OxA-18295	37980	290	42660 – 41810	Davies and Nerudová (2009)	N	Y
Moravský Krumlov IV	charcoal	Mor-KrumIV 2	Szeletian	Neanderthal	ZR	32.0	57.1	-23.7	60.2	OxA-18294	37550	280	42380 – 41510	Davies and Nerudová (2009)	N	Y
Moravský Krumlov IV	charcoal	Mor-KrumIV 2	Szeletian	Neanderthal	ZR	5.1	63.8	-22.9	64.0	OxA-18296	38350	310	42900 – 42010	Davies and Nerudová (2009)	N	Y
Moravský Krumlov IV	charcoal	Mor-KrumIV 3	Szeletian	Neanderthal	ZR	10.7	56.2	-23.5	62.6	OxA-18297	36820	250	41900 – 40930	Davies and Nerudová (2009)	N	Y
Vedrovice V	charcoal	A-2006	Szeletian	Neanderthal	ABA	–	–	–	–	GrA-35395	40670	550	45250 – 43240	Haesaerts et al. (2013)	N	Y
Vedrovice V	charcoal	A-2006	Szeletian	Neanderthal	ABA	–	–	–	–	GrA-44892	40190	390	44565 – 43094	Haesaerts et al. (2013)	N	Y
Vedrovice V	charcoal	A-2006	Szeletian	Neanderthal	ABA	–	–	–	–	GrA-44961	39810	550	44550 – 42680	Haesaerts et al. (2013)	N	Y
Vedrovice V	charcoal	A-2006	Szeletian	Neanderthal	ZR	24.2	78.3	-22.4	60.0	OxA-17735	37640	300	42460 – 41560	Haesaerts et al. (2013)	N	Y
Vedrovice V	charcoal	A-2006	Szeletian	Neanderthal	ZR	–	–	–	–	OxA-17753	37540	300	42400 – 41480	Haesaerts et al. (2013)	N	Y
Vedrovice V	charcoal	MP09-1 (A-2006)	Szeletian	Neanderthal	XR	3.9	2.4	-22.6	82.0	OxA-23518	41500	700	46280 – 43670	Haesaerts et al. (2013)	N	Y
Vedrovice V	charcoal	MP09-6 (A-2006)	Szeletian	Neanderthal	ZR	9.6	57.5	-23.4	65.5	OxA-22292	38600	550	43490 – 41880	Haesaerts et al. (2013)	N	Y
Vedrovice V	charcoal	MP09-6 (A-2006)	Szeletian	Neanderthal	ZR	11.3	68.9	-23.4	63.5	OxA-22293	39100	650	44200 – 42110	Haesaerts et al. (2013)	N	Y
Vedrovice V	charcoal	–	Szeletian	Neanderthal	ABA	–	–	-24.2	–	GrN-15513	35150	650	41210 – 38490	Valoch (1993)	N	Y
Vedrovice V	charcoal	–	Szeletian	Neanderthal	ABA	–	–	-24.0	–	GrN-12374	37650	550	42810 – 41220	Valoch (1993)	N	Y
Vedrovice V	charcoal	–	Szeletian	Neanderthal	ABA	–	–	-23.1	–	GrN-15514	37600	800	43220 – 40640	Valoch (1993)	N	Y
Vedrovice V	charcoal	–	Szeletian	Neanderthal	ABA	–	–	-22.8	–	GrN-12375	39500	1100	45490 – 41910	Valoch (1993)	N	Y
Želešice III	charcoal	Selesice03	Szeletian	Neanderthal	ZR	17.3	56.0	-25.4	67.5	OxA-27342	41300	700	46070 – 43500	Škrdla et al. (2014)	N	Y

Table C.16: Reference Sites: published radiocarbon dates used for modelling. Top – from Cavallo (Italy); bottom – from Riparo Mochi (Italy). Dates calibrated in OxCal 4.3 Bronk Ramsey (2009a) using IntCal13 (Reimer et al., 2013) for terrestrial, and using Marine13 (Reimer et al., 2013) with a local ΔR of 40 ± 15 (Reimer and McCormac, 2002). Date part of model: 'S' = stratigraphic, 'K' = KDE.

Material	Type	Sample	Context	Culture	Author	Treat.	Yield (mg)	Yield (%)	δ^{13}C	%C	A/C%	Lab-no.	^{14}C (BP)	σ	Date (calBP)	Ref.	S	K
marine shell	beads	Cvl 11	D II	Uluzzian	AMH	OX	2.5	9.9	2.3	94.0	99.8-0.2	OxA-20631	36780	310	41610 – 40290	Douka et al. (2014)	Y	Y
marine shell	beads	Cvl 2	DI = DIb	Uluzzian	AMH	OX	6.8	9.8	0.8	100.0	100-0	OxA-19254	35080	230	39730 – 38610	Douka et al. (2014)	Y	Y
marine shell	beads	Cvl 3	E4 = E II-I	Uluzzian	AMH	OX	0.7	8.5	3.3	92.3	50-50	OxA-19242	39990	340	43950 – 42700	Douka et al. (2014)	Y	Y
marine shell	beads	Cvl 4	D2 = DIb	Uluzzian	AMH	OX	6.8	8.5	2.1	94.4	100-0	OxA-19255	36260	250	41100 – 39840	Douka et al. (2014)	Y	Y
marine shell	beads	Cvl 5	E1 = E-D	Uluzzian	AMH	NRC	1.0	6.0	3.3	100.0	100-0	OxA-X-2280-16	38300	400	42720 – 41590	Douka et al. (2014)	Y	Y
marine shell	beads	Cvl 5	E1 = E-D	Uluzzian	AMH	OX	6.0	10.1	3.1	97.0	99.7-0.3	OxA-19256	39060	310	43070 – 42170	Douka et al. (2014)	Y	Y
marine shell	beads	Cvl 6	D3 = D II	Uluzzian	AMH	OX	6.2	10.2	1.7	94.7	100-0	OxA-19257	42360	400	46040 – 44560	Douka et al. (2014)	Y	Y
marine shell	beads	Cvl 8	D8 = D II?	Uluzzian	AMH	OX	6.0	9.7	2.5	100.0	100-0	OxA-19258	36000	400	41140 – 39250	Douka et al. (2014)	Y	Y
Material	**Type**	**Sample**	**Context**	**Culture**	**Author**	**Treat.**	**Yield (mg)**	**Yield (%)**	**δ^{13}C**	**%C**	**A/C%**	**Lab-no.**	**^{14}C (BP)**	**σ**	**Date (calBP)**	**Ref.**	**S**	**K**
charcoal	charcoal	–	F-top (hearth)	Early Aurig.	AMH	ABA	–	–	–	–	–	Rome-1	27230	570	32810 – 30340	Bietti et al. (2004)	Y	Y
charcoal	charcoal	–	G 50	Proto-Aurig.	AMH	ZR	14.6	15.0	-22.3	51.9	–	OxA-3588	32280	580	38070 – 35040	Hedges et al. (1994)	Y	Y
charcoal	charcoal	–	G 51	Proto-Aurig.	AMH	ZR	20.0	13.1	-23.6	52.2	–	OxA-3589	33400	750	39590 – 35980	Hedges et al. (1994)	Y	Y
charcoal	charcoal	–	G 56/67	Proto-Aurig.	AMH	ZR	33.0	15.6	-22.9	48.3	–	OxA-3590	34680	760	41170 – 37460	Hedges et al. (1994)	Y	Y
charcoal	charcoal	–	G 59	Proto-Aurig.	AMH	ZR	12.9	11.5	-24.3	53.6	–	OxA-3591	35700	850	41910 – 38690	Hedges et al. (1994)	Y	Y
charcoal	charcoal	–	G 60	Proto-Aurig.	AMH	ZR	29.8	19.6	-24.6	59.1	–	OxA-3592	34870	800	41400 – 37730	Hedges et al. (1994)	Y	Y
charcoal	charcoal	–	G-base (hearth)	Proto-Aurig.	AMH	ABA	–	–	–	–	–	Rome-2	37400	1300	44410 – 39550	Bietti et al. (2004)	Y	Y
charcoal	charcoal	RM-1	G 60	Proto-Aurig.	AMH	XR	10.5	10.0	-25.4	45.7	–	OxA-19569	36350	260	41550 – 40380	Douka et al. (2012)	Y	N
marine shell	beads	Mochi 15	D 29	Gravettian	AMH	OX	1.2	8.1	1.6	87.4	99.7-0.3	OxA-19800	24600	100	28510 – 27880	Douka et al. (2012)	Y	Y
marine shell	beads	Mochi 18	E 32	none	none	OX	1.3	5.0	1.6	82.5	99.7-0.3	OxA-19801	25490	110	29430 – 28770	Douka et al. (2012)	Y	N
marine shell	beads	Mochi 25	F 34	Early Aurig.	AMH	OX	2.2	9.4	1.3	96.7	100-0	OxA-19857	26030	110	30190 – 29360	Douka et al. (2012)	Y	Y
marine shell	beads	Mochi 31	F 40	Early Aurig.	AMH	OX	2.4	7.8	1.7	91.2	99.8-0.2	OxA-19728	26410	110	30660 – 29770	Douka et al. (2012)	Y	Y
marine shell	beads	Mochi 32	F 44	Early Aurig.	AMH	OX	2.7	9.3	1.8	94.3	100-0	OxA-20629	32910	220	37000 – 35810	Douka et al. (2012)	Y	Y
marine shell	beads	Mochi 35	F 49	Early Aurig.	AMH	OX	2.5	8.9	2.7	86.8	99.8-0.2	OxA-19614	32370	160	36230 – 35430	Douka et al. (2012)	Y	Y
marine shell	beads	Mochi 39	G 51	Proto-Aurig.	AMH	OX	2.0	8.6	2.3	92.2	100-0	OxA-20360	31960	150	35810 – 34970	Douka et al. (2012)	Y	Y
marine shell	beads	Mochi 40	G 51	Proto-Aurig.	AMH	OX	1.2	9.3	2.4	75.6	99.9-0.1	OxA-19802	30770	150	34670 – 34000	Douka et al. (2012)	Y	Y
marine shell	beads	Mochi 42	G 54	Proto-Aurig.	AMH	OX	1.5	9.3	2.2	92.3	n/a	OxA-20630	33180	230	37610 – 36140	Douka et al. (2012)	Y	Y
marine shell	beads	Mochi 43	G 57	Proto-Aurig.	AMH	OX	2.3	8.9	-0.9	95.8	99.9-0.1	OxA-19290	36750	260	41520 – 40340	Douka et al. (2012)	Y	Y

Table C.17: Reference Sites: published radiocarbon dates used for modelling: top – Šalitrena Pećina (Serbia); bottom – Bacho Kiro (Bulgaria). Dates calibrated in OxCal 4.3 (Bronk Ramsey, 2009a) using IntCal13 (Reimer et al., 2013) for terrestrial, and Marine13 (Reimer et al., 2013) and a local ΔR of 58 ± 15 (Reimer and McCormac, 2002) for marine samples. Date part of model: 'S' = stratigraphic, 'K' = KDE.

Material	Type	Sample	Context	Culture	Author	Treat.	Yield (mg)	Yield (%)	δ^{13}C	δ^{15}N	%C	C:N	Lab-no.	^{14}C (BP)	σ	Date (calBP)	Ref.	S	K
bone	artefact	–	5a, out	Aurignacian	AMH	AF	12.3	2.1	-19.7	8.0	42.7	3.3	OxA-27975	29700	340	34520 – 33190	Marín-Arroyo and Mihailović (2017)	Y	Y
bone	n/a	–	2, in	Aurignacian	AMH	–	–	–	-19.5	–	–	–	Beta-237684	29980	280	34590 – 33630	Marín-Arroyo and Mihailović (2017)	Y	Y
bone	n/a	–	5a, out	Aurignacian	AMH	–	–	–	-20.8	–	–	–	Beta-224720	30190	400	34950 – 33620	Marín-Arroyo and Mihailović (2017)	Y	Y
bone	n/a	–	5a, out	Aurignacian	AMH	–	–	–	-19.1	–	–	–	Beta-237688	31980	360	36680 – 35050	Marín-Arroyo and Mihailović (2017)	Y	Y
bone	n/a	–	5b, out	Mousterian	Neanderthal	–	–	–	-19.8	–	–	–	Beta-237690	37760	520	42830 – 41350	Marín-Arroyo and Mihailović (2017)	Y	N
bone	n/a	–	5c, out	Mousterian	Neanderthal	AF	16.3	2.7	-21.1	4.5	43.8	3.3	OxA-27682	50200	0	>50200	Marín-Arroyo and Mihailović (2017)	Y	N
bone	n/a	–	6a, out	Mousterian	Neanderthal	AF	18.9	3.1	-19.9	2.6	40.4	3.2	OxA-27829	45700	0	>45700	Marín-Arroyo and Mihailović (2017)	Y	N
shell	beads	–	5a, out	Aurignacian	AMH	OX	2.5	9.6	0.9	–	100.0	–	OxA-27683	30150	150	34120 – 33570	Marín-Arroyo and Mihailović (2017)	Y	Y
tooth	n/a	–	3, in	Mousterian	Neanderthal	AF	26.3	4.2	-19.8	7.6	42.3	3.4	OxA-27948	36150	750	42110 – 39280	Marín-Arroyo and Mihailović (2017)	Y	N
Material	**Type**	**Sample**	**Context**	**Culture**	**Author**	**Treat.**	**Yield (mg)**	**Yield (%)**	**δ^{13}C**	**δ^{15}N**	**%C**	**C:N**	**Lab-no.**	**^{14}C (BP)**	**σ**	**Date (calBP)**	**Ref.**	**S**	**K**
bone	no mod	no.2	6a/7	Aurignacian	AMH	–	–	–	–	–	–	–	Ly-1102	29150	950	35110 – 31270	Evin et al. (1978)	Y	Y
bone	no mod	BK-2	11	Bachokirian	AMH	AI	6.5	–	-20.5	–	32.1	–	OxA-3213	38500	1700	46790 – 39950	Hedges et al. (1994)	Y	Y
charcoal	charcoal	BK-3	11	Bachokirian	AMH	ZR	16.8	19.0	-23.8	–	27.0	–	OxA-3183	37650	1450	45080 – 39540	Hedges et al. (1994)	Y	Y
charcoal	charcoal	BK-4	6b	Aurignacian	AMH	ZR	93.0	52.2	-22.9	–	46.9	–	OxA-3182	33300	820	39660 – 35730	Hedges et al. (1994)	Y	Y
charcoal	charcoal	BK-5	7	Aurignacian	AMH	ZR	34.0	31.5	-25.1	–	36.1	–	OxA-3181	32200	780	38400 – 34750	Hedges et al. (1994)	Y	Y
charcoal	charcoal	–	11 [level I]	Bachokirian	AMH	–	–	–	–	–	–	–	GrN-7545	43000	0	>43000	Mook (1982)	Y	N
charcoal	charcoal	–	6b	Aurignacian	AMH	–	–	–	–	–	–	–	GrN-7569	32700	300	37820 – 35990	Mook (1982)	Y	Y
n/a	n/a	–	13	Mousterian	Neanderthal	–	–	–	–	–	–	–	GrN-7570	47500	0	>47500	Mook (1982)	Y	N
n/a	n/a	–	7/6b	Aurignacian	AMH	–	–	–	–	–	–	–	GrN-7560	32700	300	37820 – 35990	http://carbon14.univ-lyon1.fr/banadora/ (Aug 2016)	Y	Y
tooth	no mod	BK-3	11	Bachokirian	AMH	AI	2.6	–	-26.0	–	–	–	OxA-3212	34800	1150	41830 – 36740	Hedges et al. (1994)	Y	Y
tooth	no mod	BK1255	13	Mousterian	Neanderthal	AF	39.2	4.9	-17.2	12	43.8	3.3	OxA-11421	51500	2400	60060 – 47450	J.-L. Guadelli (pers. comm. 17 July 2015) db	Y	N

Table C.18: Reference Sites: published radiocarbon dates from Mitoc-Malul Galben (Romania) used for modelling. Dates calibrated in OxCal 4.3 (Bronk Ramsey, 2009a) using IntCal13 (Reimer et al., 2013). Date part of model: 'S' = stratigraphic, 'K' = KDE.

Material	Sample	Context	Culture	Author	Treat.	Yield (mg)	Yield (%)	$\delta^{13}C$	$\delta^{15}N$	%C	C:N	Lab-no.	^{14}C (BP)	σ	Date (calBP)	Ref.	S	K
charcoal	61	10b inf.	Aurignacian	AMH	ZR	532	–	-26	–	–	–	OxA-1646	31100	900	37650 – 33620	Anghelinu and Niţă (2014); Chirica and Vornicu (2015)	N	Y
charcoal	62	10b inf.	Aurignacian	AMH	–	–	–	–	–	–	–	GrA-1648	31000	330	35650 – 34280	Anghelinu and Niţă (2014); Chirica and Vornicu (2015)	N	Y
charcoal	64	11 sup	Aurignacian	AMH	–	–	–	–	–	–	–	GrN-20443	30240	470/-440	35130 – 33570	Anghelinu and Niţă (2014); Chirica and Vornicu (2015)	N	Y
charcoal	65	11 sup	Aurignacian	AMH	–	–	–	–	–	–	–	GrN-20770	31160	570/-530	36240 – 34120	Anghelinu and Niţă (2014); Chirica and Vornicu (2015)	N	Y
charcoal	66	11 inf	Aurignacian	AMH	–	–	–	–	–	–	–	GrN-20442	30920	390	35680 – 34120	Anghelinu and Niţă (2014); Chirica and Vornicu (2015)	N	Y
charcoal	67	12a	Aurignacian	AMH	–	–	–	–	–	–	–	GrN-20444	31160	550/-510	36200 – 34150	Anghelinu and Niţă (2014); Chirica and Vornicu (2015)	N	Y
charcoal	68	12b	Aurignacian	AMH	–	–	–	–	–	–	–	GrA-1357	32730	220	37560 – 36150	Anghelinu and Niţă (2014); Chirica and Vornicu (2015)	N	Y
charcoal	"comb. 8B"	8b?	Aurignacian	AMH	–	–	–	–	–	–	–	GrA-27261	27700	180	31860 – 31130	Anghelinu and Niţă (2014); Chirica and Vornicu (2015)	N	Y
charcoal	"comb. 8B"	8b?	Aurignacian	AMH	–	–	–	–	–	–	–	GrA-27268	27750	160	31870 – 31170	Anghelinu and Niţă (2014); Chirica and Vornicu (2015)	N	Y
charcoal	–	11 sup	Aurignacian	AMH	–	–	–	–	–	–	–	GrN-15456	25930	450	30990 – 29170	Anghelinu and Niţă (2014); Chirica and Vornicu (2015)	N	Y
charcoal	–	8b	Aurignacian	AMH	–	–	–	–	–	–	–	GrN-11190	27410	430	32500 – 30770	Anghelinu and Niţă (2014); Chirica and Vornicu (2015)	N	Y
charcoal	–	8b	Aurignacian	AMH	–	–	–	–	–	–	–	GrN-12637	31850	800	38190 – 34410	Anghelinu and Niţă (2014); Chirica and Vornicu (2015)	N	Y
charcoal	–	9b	Aurignacian	AMH	–	–	–	–	–	–	–	GrN-15454	29410	310	34140 – 32890	Anghelinu and Niţă (2014); Chirica and Vornicu (2015)	N	Y
charcoal	–	–	Aurignacian	AMH	–	–	–	–	–	–	–	GrA-1355	25380	120	29820 – 29070	Anghelinu and Niţă (2014)	N	Y
charcoal	–	–	Aurignacian	AMH	–	–	–	–	–	–	–	GrN-15451	26530	400	31270 – 29810	Anghelinu and Niţă (2014)	N	Y

Table C.19: Reference Sites: published radiocarbon dates from Buran-Kaya III (Crimea) used for modelling. Dates calibrated in OxCal 4.3 (Bronk Ramsey, 2009a) using IntCal13 (Reimer et al., 2013). Date part of model: 'S' = stratigraphic, 'K' = KDE.

Material	Type	Sample	Culture	Author	Treat.	Yield (mg)	Yield (%)	$\delta^{13}C$	$\delta^{15}N$	%C	C:N	Lab-no.	^{14}C (BP)	σ	Date (calBP)	Ref.	S	K
bone	cutmark	–	Micoquian	Neand.	AF	17	2.7	-18.2	10.9	44.4	3.2	OxA-25879	37700	900	43550 – 40520	Péan et al. (2013)	Y	N
bone	human	–	Gravettian	AMH	–	–	–	–	–	–	3.1	GrA-50457	32450	+250/-230	37060 – 35740	Péan et al. (2013)	Y	Y
bone	human	–	Gravettian	AMH	–	–	–	–	–	–	3.3	GrA-37938	31900	+240/-220	36300 – 35260	Prat et al. (2011), Péan et al. (2013)	Y	Y
bone	human	–	Gravettian	AMH	AF	19.9	2.8	-18.9	16.6	45.1	3.3	OxA-13302	32790	280	37870 – 36120	Higham et al. (2007)	N	Y
bone	no mod	Combine "Horse"	Aurignacian	AMH	ABA	–	–	–	–	–	3.3	GrA-40485	34050	+260/-240	39170 – 37890	Péan et al. (2013)	Y	Y
bone	no mod	Combine "Horse"	Aurignacian	AMH	ninhydrin	–	–	–	–	–	3.3	GifA-80181/SacA-12260	34910	950	41670 – 37340	Péan et al. (2013)	Y	Y
bone	no mod	Combine 4	Swiderian	AMH	ABA	–	–	–	–	–	–	GrA-50461	10010	60	11760 – 11260	Péan et al. (2013)	Y	Y
bone	no mod	Combine 4	Swiderian	AMH	ninhydrin	–	–	–	–	–	–	GifA-11219/SacA-25139	10050	70	11950 – 11270	Péan et al. (2013)	Y	Y
bone	no mod	Combine 5-2	Gravettian	AMH	ABA	–	–	–	–	–	3.6	GrA-47316	30100	+180/-170	34530 – 33820	Péan et al. (2013)	Y	Y
bone	no mod	Combine 5-2	Gravettian	AMH	ninhydrin	–	–	–	–	–	3.6	GifA-11222/SacA-25139	33790	880	40350 – 36130	Péan et al. (2013)	Y	Y
bone	no mod	Combine 6-1	Gravettian	AMH	ABA	–	–	–	–	–	3.3	GrA-53942	29640	+170/-160	34110 – 33520	Péan et al. (2013)	Y	Y
bone	no mod	Combine 6-1	Gravettian	AMH	AF	10.3	1.7	-15.2	10.2	45.7	3.3	OxA-25669	32200	450	37540 – 35100	Péan et al. (2013)	Y	Y
bone	no mod	Combine 6-4	Aurignacian	AMH	ABA	–	–	–	–	–	–	GrA-48399	31250	+2450/-1880	41810 – 31490	Péan et al. (2013)	Y	Y
bone	no mod	Combine 6-4	Aurignacian	AMH	ninhydrin	–	–	–	–	–	–	GifA-11220/SacA-25134	35900	1100	42510 – 38490	Péan et al. (2013)	Y	Y
bone	no mod	Combine 6-5	Aurignacian	AMH	ABA	–	–	–	–	–	3.3	GrA-47318	32800	+230/-210	37670 – 36210	Péan et al. (2013)	Y	Y
bone	no mod	Combine 6-5	Aurignacian	AMH	ninhydrin	–	–	–	–	–	3.3	GifA-11217/SacA-25134	35900	1100	42510 – 38490	Péan et al. (2013)	Y	Y
bone	no mod	Combine B	Micoquian	Neand.	ABA	–	–	–	–	–	3.3	GrA-47319	35590	+290/-270	40930 – 39540	Péan et al. (2013)	Y	N
bone	no mod	Combine B	Micoquian	Neand.	ninhydrin	–	–	–	–	–	3.3	GifA-11218/SacA-25135	36500	1200	43120 – 38770	Péan et al. (2013)	Y	N
bone	no mod	–	Aurignacian	AMH	ninhydrin	–	–	–	–	–	–	GifA-11221/SaxA-25138	32740	780	38860 – 35160	Péan et al. (2013)	Y	Y
bone	no mod	–	Gravettian	AMH	ABA	–	–	–	–	–	3.3	GrA-50460	29440	+190/-180	34010 – 33240	Péan et al. (2013)	Y	Y
bone	no mod	–	Gravettian	AMH	ninhydrin	–	–	–	–	–	3.3	GifA-10021/SacA-19018	31320	820	37560 – 33870	Péan et al. (2013)	Y	Y
bone	no mod	–	Gravettian	AMH	ninhydrin	–	–	–	–	–	3.4	GifA-11216/SacA-25133	31530	670	37250 – 34160	Péan et al. (2013)	Y	Y
bone	no mod	–	Swiderian	AMH	AF	14.9	2.4	-15.5	11.1	48.7	3.4	OxA-25670	10040	45	11770 – 11320	Péan et al. (2013)	Y	Y

Table C.20: Reference Sites: published dates from Ksar Akil (Lebanon) used for modelling. U-series dates (grey) given in calendar years BP. Radiocarbon dates calibrated in OxCal 4.3 (Bronk Ramsey, 2009a) using IntCal13 for terrestrial, and Marine13 (Reimer et al., 2013) with a local ΔR of 53 ± 43 (Reimer and McCormac, 2002) for marine samples. Date part of model: 'S' = stratigraphic, 'K' = KDE.

Material	Type	Sample	Culture	Author	Treat.	Yield (mg)	Yield (%)	δ^{13}C	δ^{15}N	%C	C:N	Arag./Cal.%	Lab-no.	^{14}C (BP)	σ	Date (calBP)	Ref.	S	K
charcoal	charcoal	–	Early Ahmarian	AMH	XR	4.0	2.6	-25.3	–	85.1	–	n/a	OxA-19194	30250	170	34630 – 33930	Douka et al. (2013)	Y	Y
charcoal	charcoal	–	Early Ahmarian	AMH	ZR	10.6	8.8	-26.0	–	28.3	–	–	OxA-1804	31200	1300	39060 – 32950	Douka et al. (2013)	Y	Y
charcoal	charcoal	–	Early Ahmarian	AMH	ZR	22.4	16.0	-26.0	–	13.4	–	–	OxA-1803	30250	850	36310 – 32620	Douka et al. (2013)	Y	Y
charcoal	charcoal	–	Early Ahmarian	AMH	ZR	57.0	25.9	-26.0	–	11.7	–	–	OxA-1805	32400	1100	39500 – 34460	Douka et al. (2013)	Y	Y
charcoal	charcoal	–	Early Ahmarian	AMH	ZR	80.0	26.7	-26.0	–	11.7	–	–	OxA-1798	29300	800	34900 – 31510	Douka et al. (2013)	Y	Y
charcoal	charcoal	–	Early Ahmarian	AMH	ZR	90.0	40.9	-26.0	–	16.7	–	–	OxA-1797	26900	600	32420 – 29700	Douka et al. (2013)	Y	Y
charcoal	charcoal	–	Early Ahmarian	AMH	–	–	–	–	–	–	–	–	MC-1191	26500	900	32780 – 28800	Douka et al. (2013)	Y	Y
charcoal	charcoal	–	Early Ahmarian	AMH	–	–	–	–	–	–	–	–	MC-1192	32000	1500	40430 – 33650	Douka et al. (2013)	Y	Y
Clay	burnt	–	Mousterian	Neand.	–	–	–	–	–	–	–	–	GrN-2579	43750	1500	49980 – 45150	Douka et al. (2013)	Y	N
marine shell	beads	KA 11	Early Ahmarian	AMH	OX	1.6	7.3	-0.5	–	93.2	–	99.9-0.1	OxA-20023	30360	140	34290 – 33710	Douka et al. (2013)	Y	Y
marine shell	beads	KA 15	Early Ahmarian	AMH	OX	3.4	11.9	1.0	–	95	–	n/a	OxA-25585	34550	250	39240 – 37970	Douka et al. (2013)	Y	Y
marine shell	beads	KA 16	Early Ahmarian	AMH	OX	2.3	8.5	-1.6	–	-1.57	–	99.9-0.1	OxA-20024	35520	200	40150 – 39030	Douka et al. (2013)	Y	Y
marine shell	beads	KA 17	Early Ahmarian	AMH	OX	2.0	9.4	-0.2	–	95.7	–	100-0	OxA-20876	35020	240	39680 – 38540	Douka et al. (2013)	Y	Y
marine shell	beads	KA 18	Early Ahmarian	AMH	OX	2.1	8.3	0.2	–	121.2	–	100-0	OxA-22665	36040	240	40850 – 39590	Douka et al. (2013)	Y	Y
marine shell	beads	KA 22	Early Ahmarian	AMH	OX	2.5	9.5	0.2	–	104.9	–	100-0	OxA-20486	35780	240	40540 – 39260	Douka et al. (2013)	Y	Y
marine shell	beads	KA 25	Early Ahmarian	AMH	OX	2.2	9.7	-0.3	–	98.8	–	99.5-0.5	OxA-20487	33930	220	38480 – 36970	Douka et al. (2013)	Y	Y
marine shell	beads	KA 27	Early Ahmarian	AMH	OX	2.4	8.7	2.1	–	99.9	–	99.8-0.1	OxA-22269	35390	250	40090 – 38820	Douka et al. (2013)	Y	Y
marine shell	beads	KA 29	Early Ahmarian	AMH	OX	3.3	12.0	1.9	–	91.2	–	100-0	OxA-25652	33300	230	37780 – 36230	Douka et al. (2013)	Y	Y
marine shell	beads	KA 30	Early Ahmarian	AMH	OX	1.8	8.3	-5.1	–	102.2	–	99.9-0.1	OxA-X-2342-57	28130	110	31660 – 31170	Douka et al. (2013)	Y	Y
marine shell	beads	KA 31	Early Ahmarian	AMH	OX	2.0	9.0	3.4	–	90.8	–	99.7-0.3	OxA-20877	36270	240	41080 – 39850	Douka et al. (2013)	Y	Y
marine shell	beads	KA 34	Early Ahmarian	AMH	OX	2.8	11.0	0.8	–	107.4	–	99.8-0.2	OxA-25653	34830	240	39500 – 38390	Douka et al. (2013)	Y	Y
marine shell	beads	KA 35	Early Ahmarian	AMH	OX	2.6	9.7	0.2	–	92.8	–	100-0	OxA-20488	34230	210	38770 – 37500	Douka et al. (2013)	Y	Y
marine shell	beads	KA 37	Early Ahmarian	AMH	OX	2.4	10.3	2.0	–	103.6	–	99.8-0.2	OxA-X-2338-8	33760	210	38340 – 36780	Douka et al. (2013)	Y	Y
marine shell	beads	KA 38	Early Ahmarian	AMH	OX	2.6	9.5	0.4	–	99	–	100-0	OxA-22664	35510	240	40210 – 38950	Douka et al. (2013)	Y	Y
marine shell	beads	KA 39	Early Ahmarian	AMH	OX	2.2	10.4	1.2	–	116.3	–	99.7-0.3	OxA-X-2361-14	32960	160	36870 – 35990	Douka et al. (2013)	Y	Y
marine shell	beads	KA 4	Early Ahmarian	AMH	OX	2.0	9.7	-0.4	–	100	–	100-0	OxA-20875	30640	160	34580 – 33880	Douka et al. (2013)	Y	Y
marine shell	beads	KA 41	Early Ahmarian	AMH	OX	1.6	7.4	0.4	–	93.5	–	100-0	OxA-20879	35010	240	39670 – 38530	Douka et al. (2013)	Y	Y
marine shell	beads	KA 45	IUP	AMH	OX	3.6	10.3	0.3	–	91.8	–	100-0	OxA-20025	36390	210	41150 – 40030	Douka et al. (2013)	Y	Y
marine shell	beads	KA 47	IUP	AMH	OX	3.0	10.0	0.0	–	99.6	–	100-0	OxA-20880	34940	200	39530 – 38520	Douka et al. (2013)	Y	Y
marine shell	beads	KA 48	IUP	AMH	OX	1.8	8.5	0.1	–	121.1	–	99.9-0.1	OxA-22667	34320	190	38820 – 37760	Douka et al. (2013)	Y	Y
marine shell	beads	KA 49	IUP	AMH	OX	2.8	10.5	2.4	–	116.8	–	99.5-0.5	OxA-25655	30890	160	34760 – 34060	Douka et al. (2013)	Y	Y
marine shell	beads	KA 51	IUP	AMH	NRC	2.4	10.7	1.0	–	96.1	–	93-7	OxA-20490	37430	320	42080 – 40950	Douka et al. (2013)	Y	Y
marine shell	beads	KA 52	IUP	AMH	OX	2.9	9.6	0.6	–	104.3	–	20-80	OxA-20489	36790	270	41560 – 40350	Douka et al. (2013)	Y	Y
marine shell	beads	KA 54	Mousterian	Neand.	OX	3.1	10.7	1.6	–	102.6	–	0-100	OxA-20491	39310	330	43270 – 42290	Douka et al. (2013)	Y	N
marine shell	beads	KA 55	Mousterian	Neand.	OX	3.0	10.3	1.0	–	129.4	–	n/a	OxA-25656	39530	330	43450 – 42410	Douka et al. (2013)	Y	N
marine shell	beads	–	Early Ahmarian	AMH	–	–	–	–	–	–	–	–	GrN-2195	28840	380	33380 – 31420	Douka et al. (2013)	Y	Y
bone surface	no mod	–	Mousterian	Neand.	–	–	–	–	–	–	–	–	G-88174	47000	9000	56000 – 38000	Douka et al. (2013)	Y	N
bone surface	no mod	–	Mousterian	Neand.	–	–	–	–	–	–	–	–	G-88177	51000	4000	55000 – 470000	Douka et al. (2013)	Y	N

D: Reference sites - model outputs

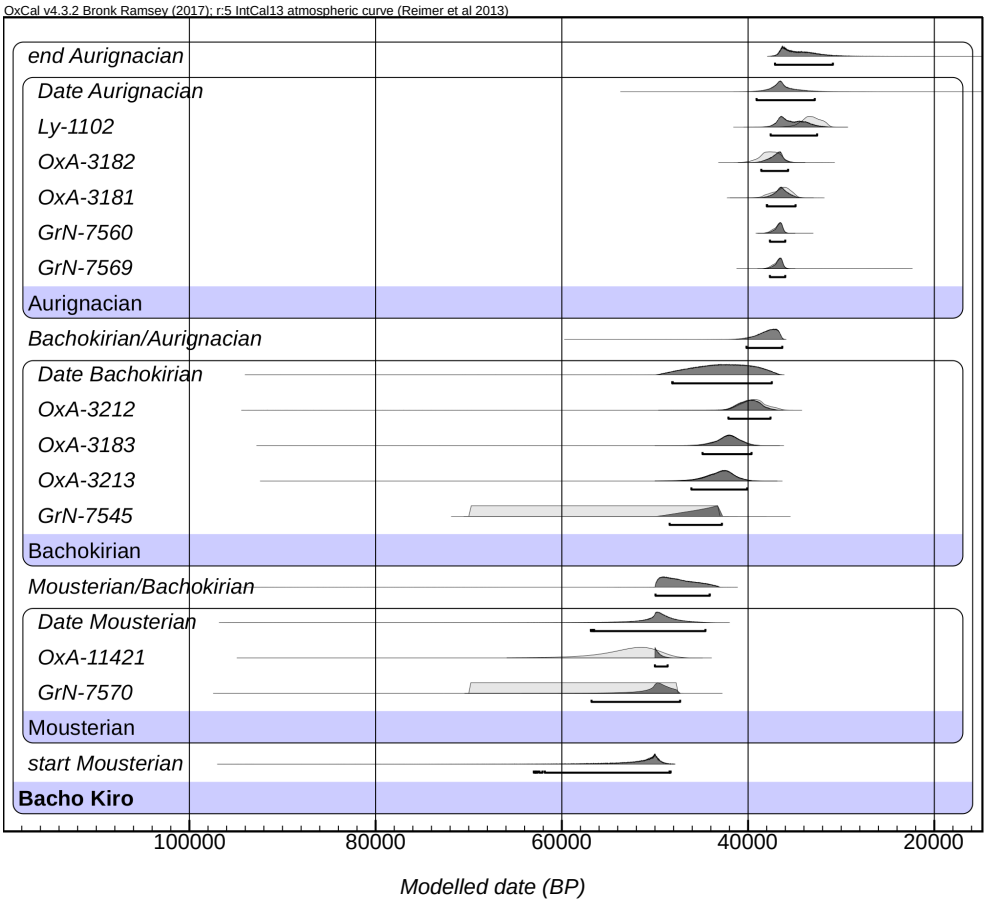


Figure D.33: Stratigraphic model for Bacho Kiro (code: p. 765).

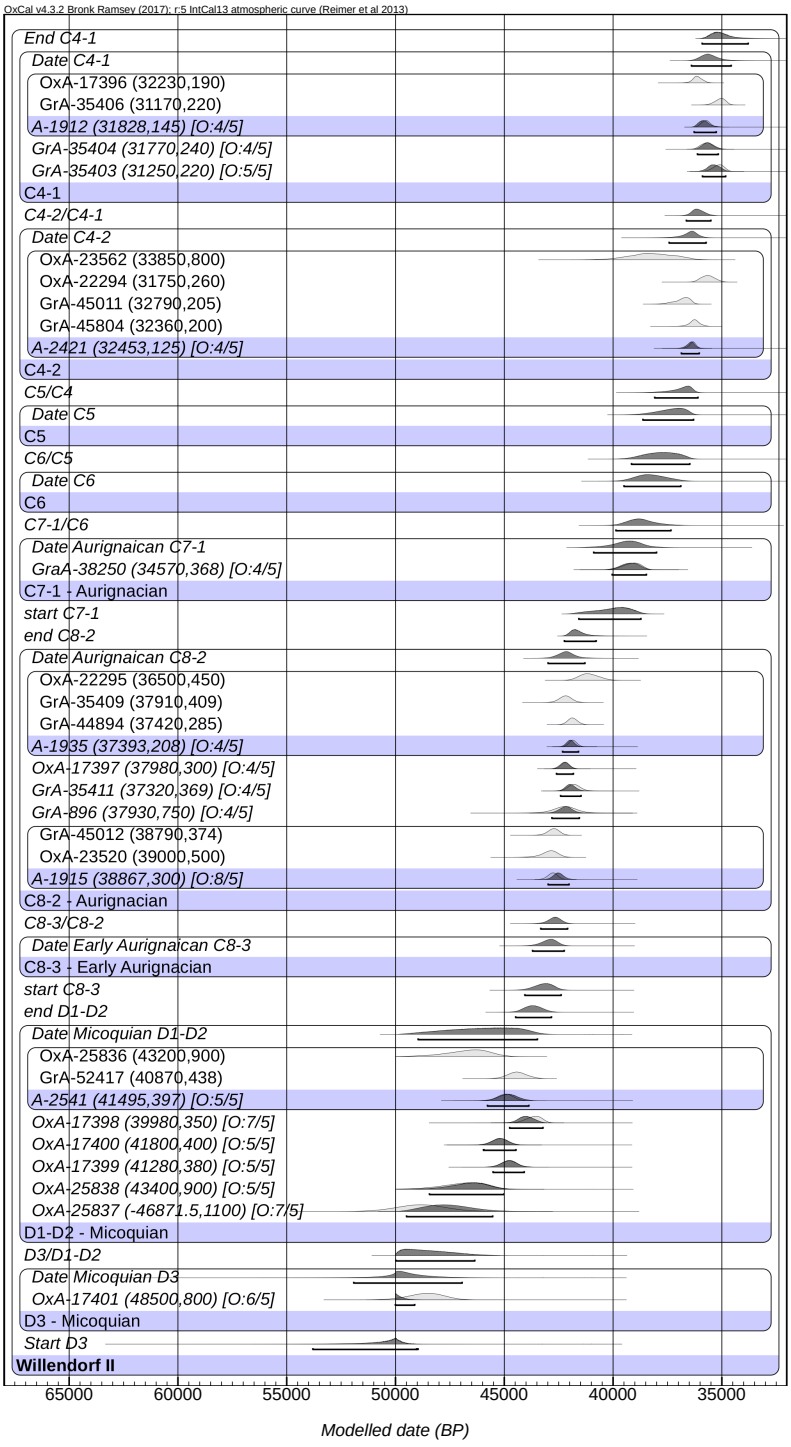


Figure D.34: Stratigraphic model for Willendorf II (code: p. 762).

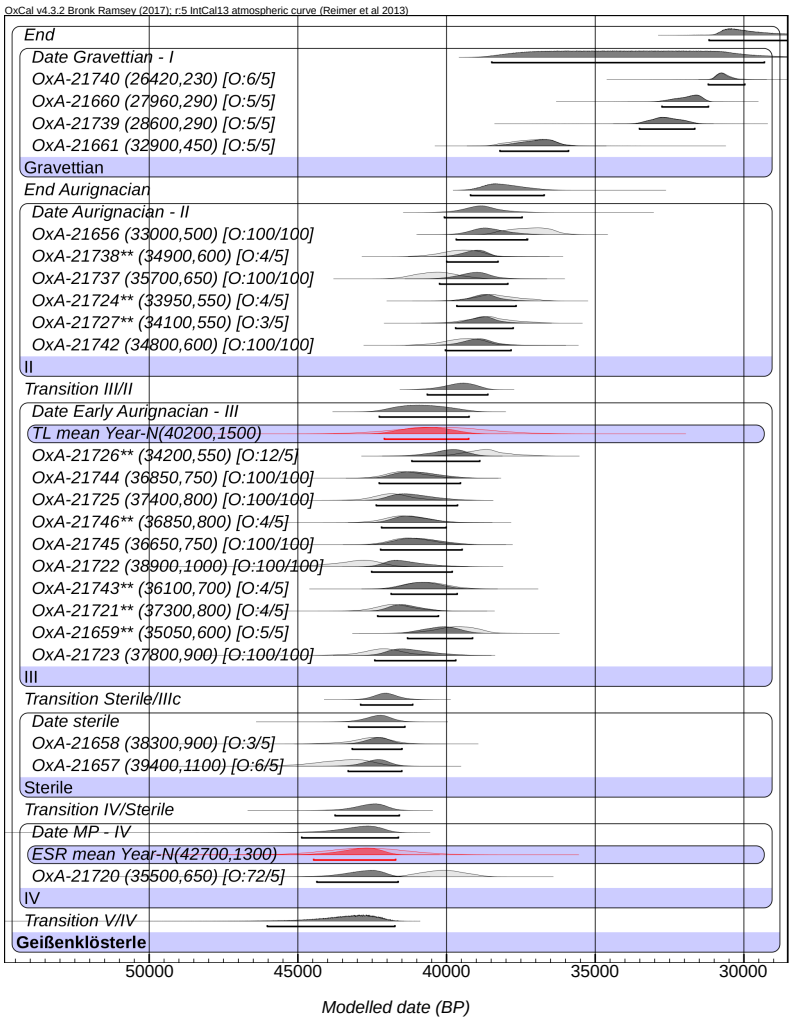


Figure D.35: Stratigraphic model for Geißenklösterle (code: p. 759).

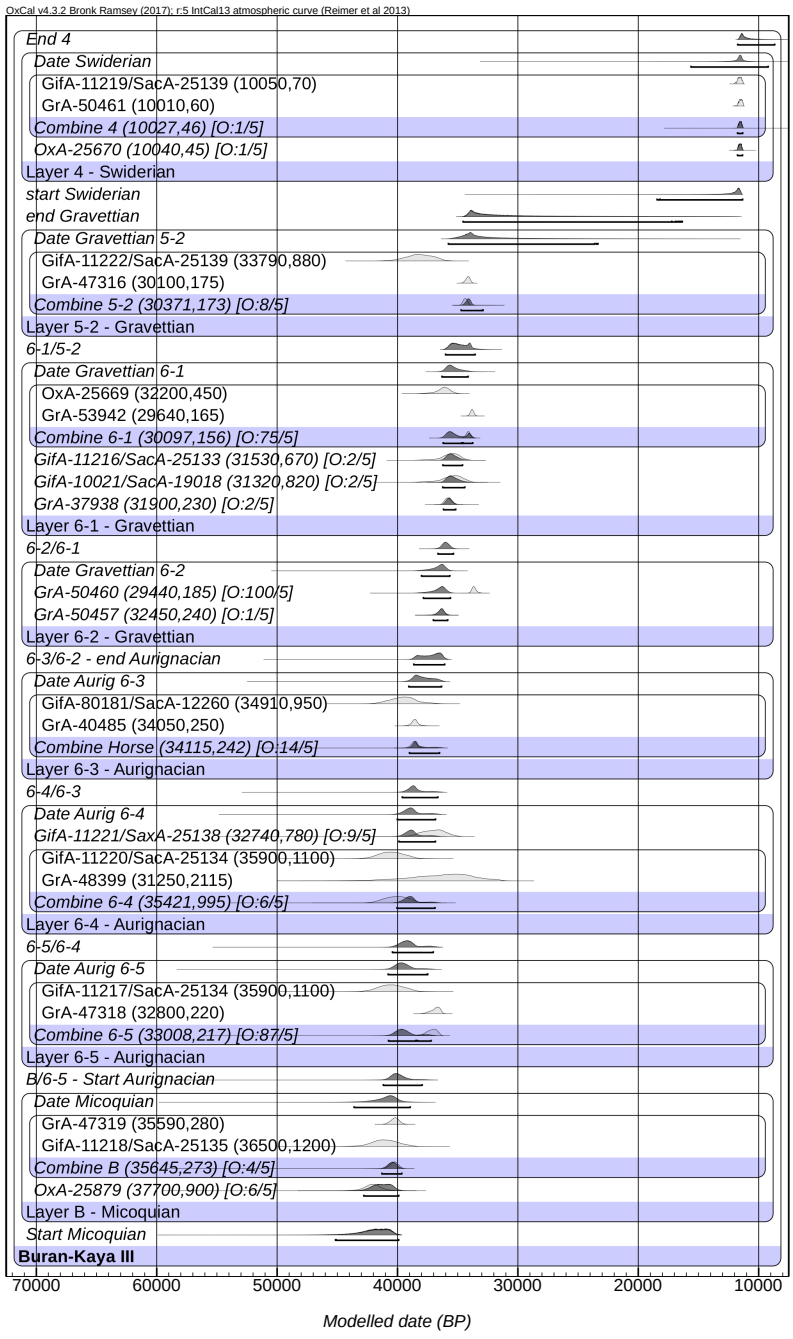


Figure D.36: Stratigraphic model for Buran-Kaya III (code: p. 766).

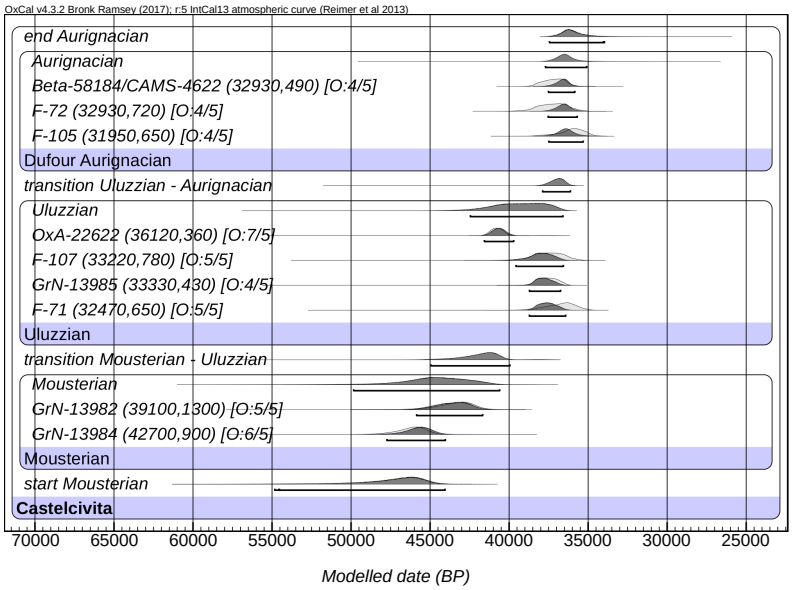


Figure D.37: Stratigraphic model for Castelcivita (code: p. 761).

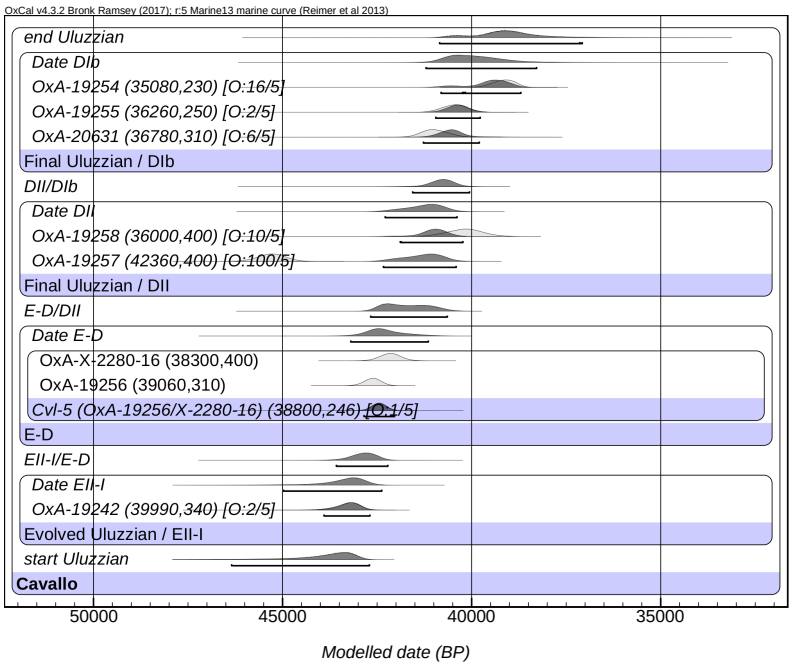


Figure D.38: Stratigraphic model for Cavallo (code: p. 764).



Figure D.39: Stratigraphic model for El Castillo (code: p. 752).

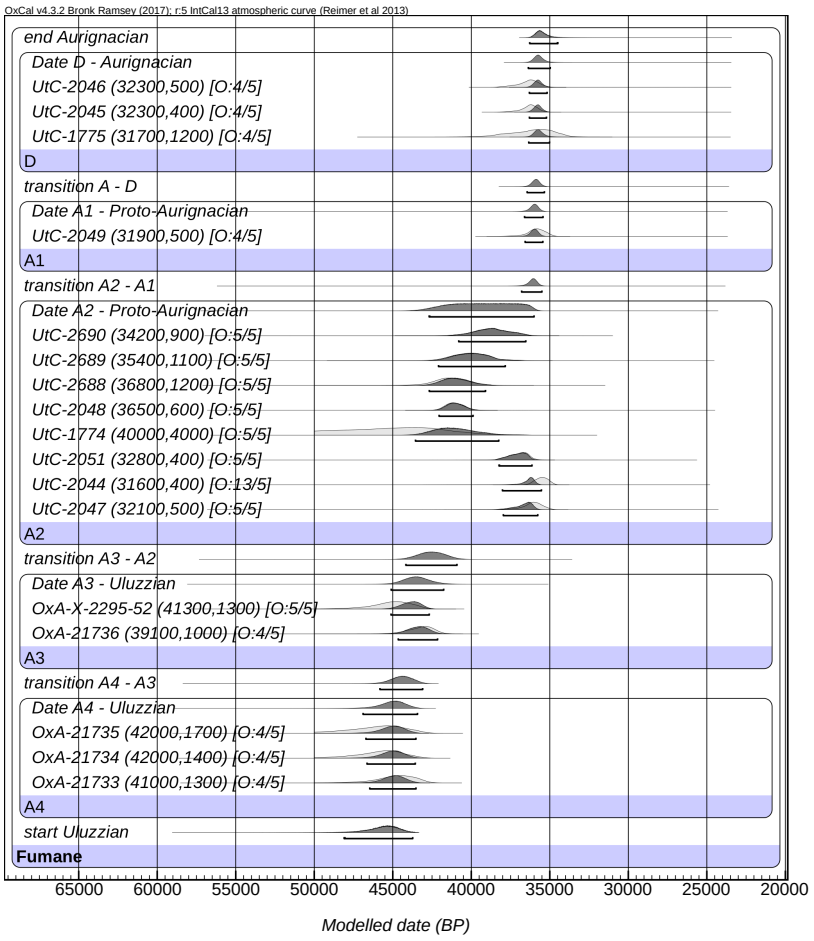


Figure D.40: Stratigraphic model for Fumane (code: p. 760).

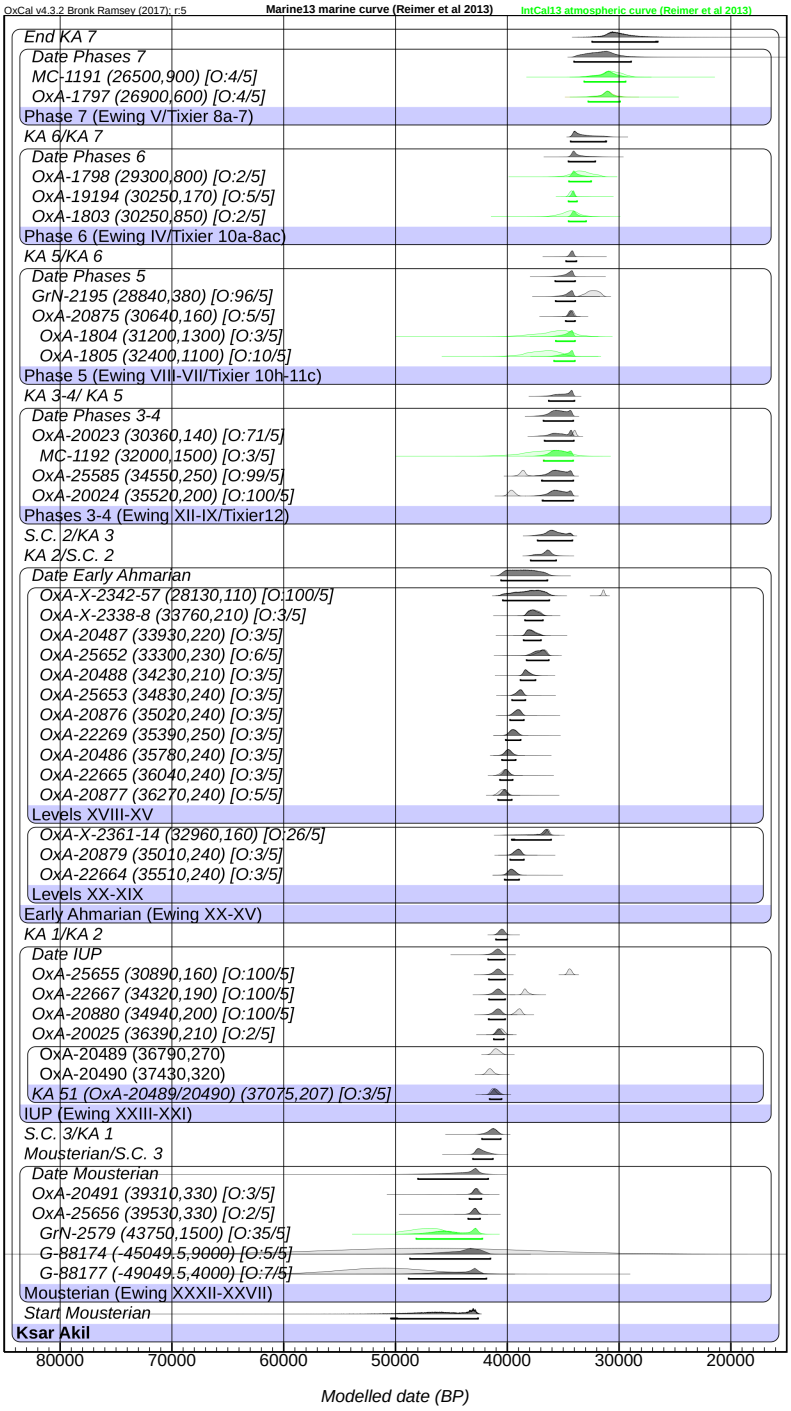


Figure D.41: Stratigraphic model for Ksar Akil (code: p. 768).

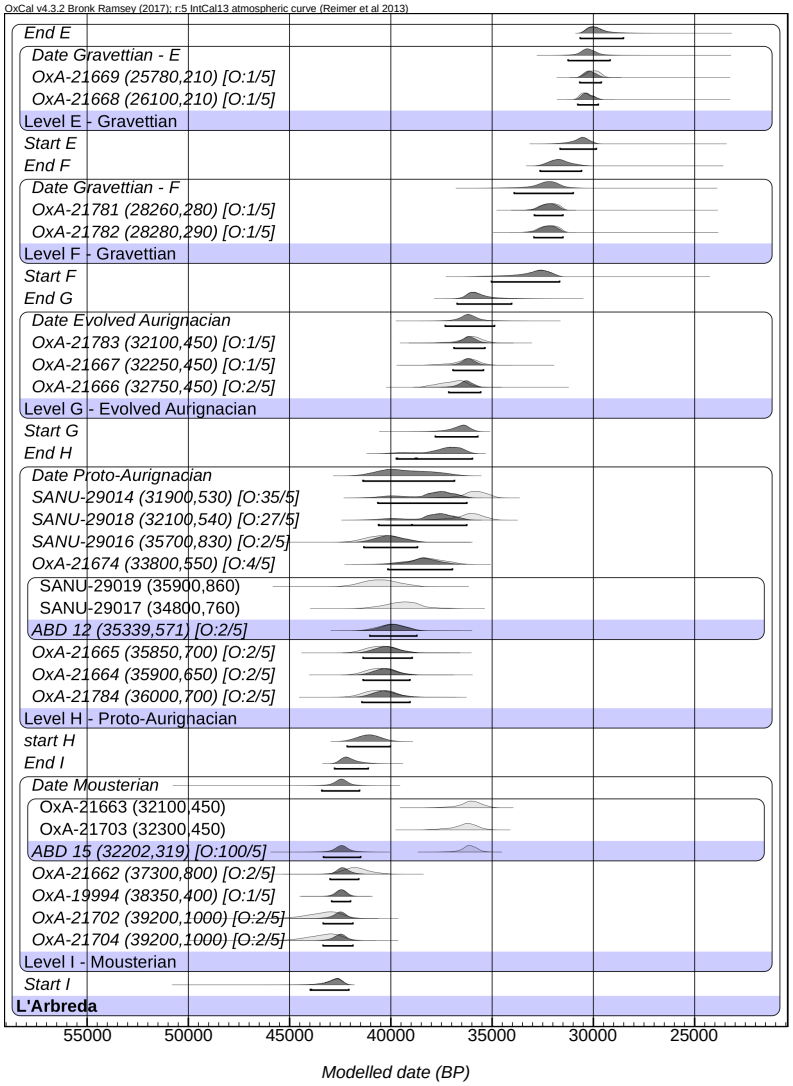


Figure D.42: Stratigraphic model for L'Arbreda (code: p. 755).

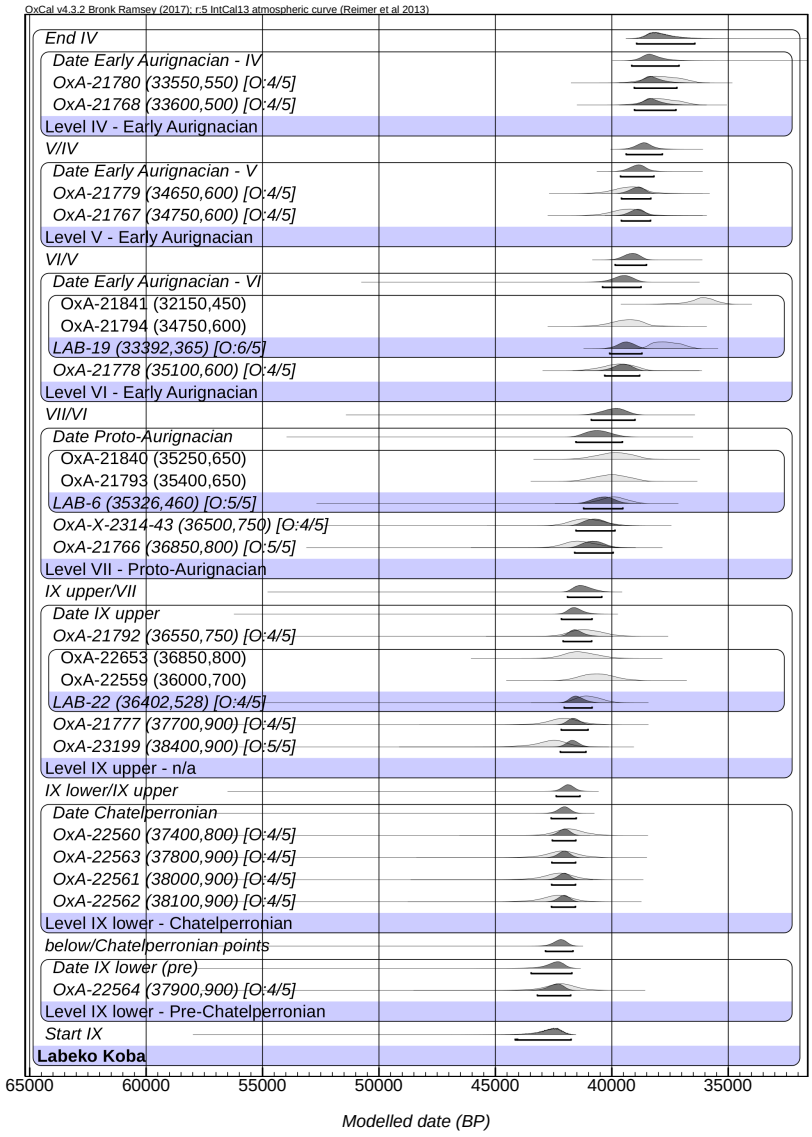


Figure D.43: Stratigraphic model for Labeko Koba (code: p. 753).

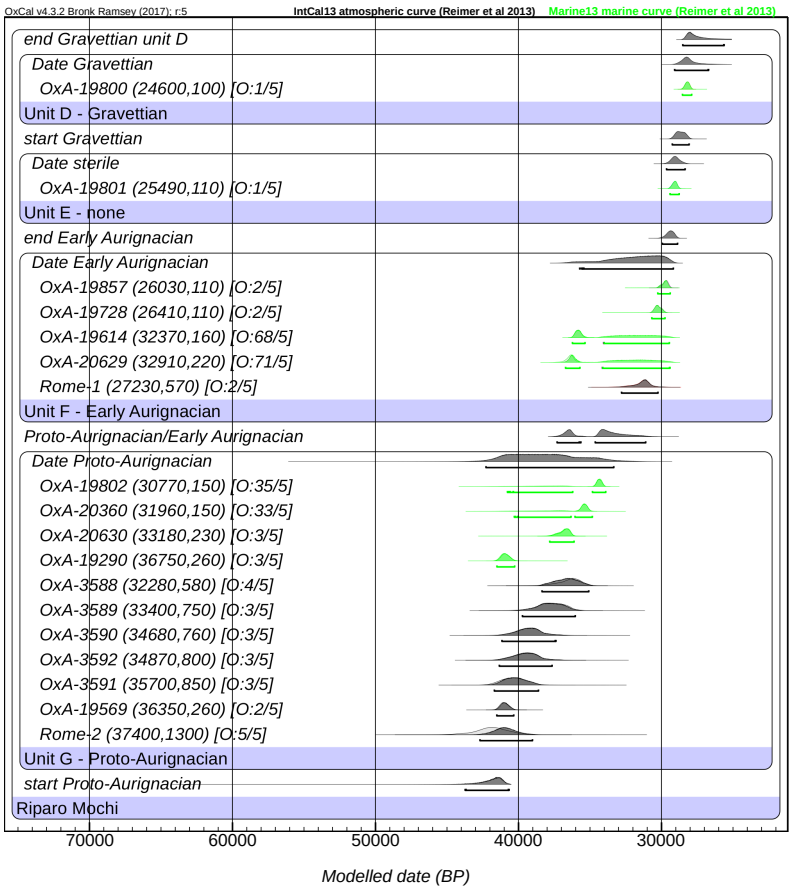


Figure D.44: Stratigraphic model for Riparo Mochi (code: p. 756).

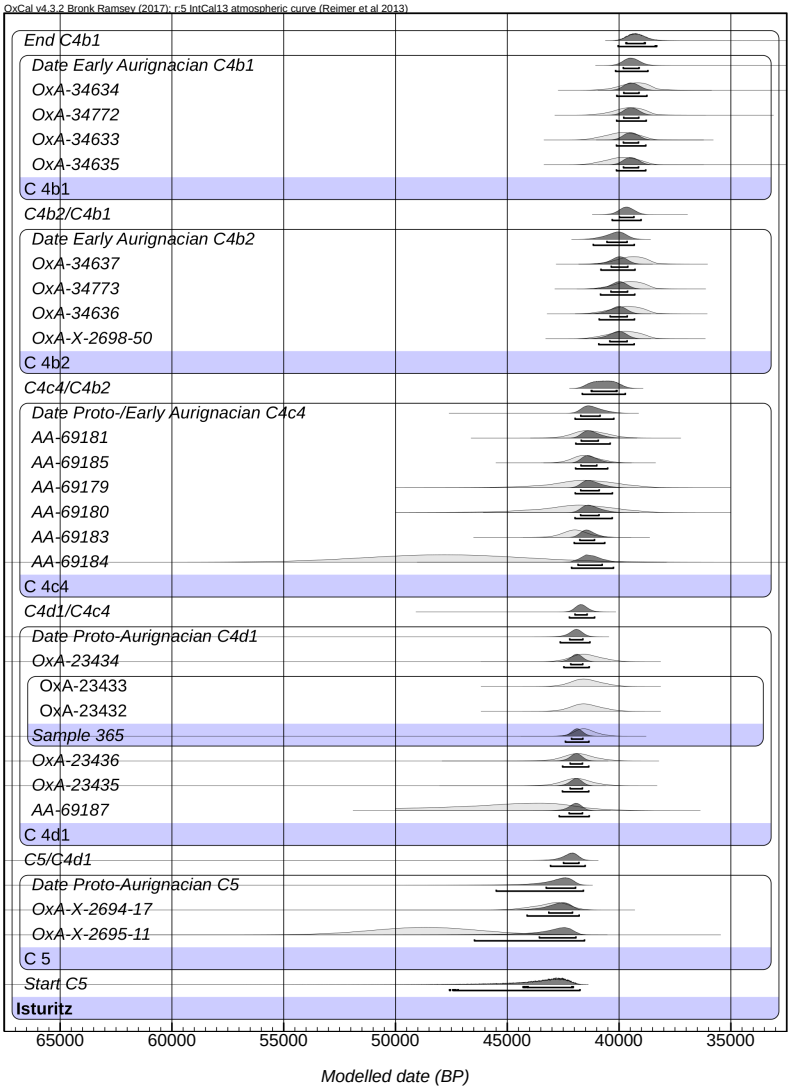


Figure D.45: Stratigraphic model for Isturitz (code: p. 754).

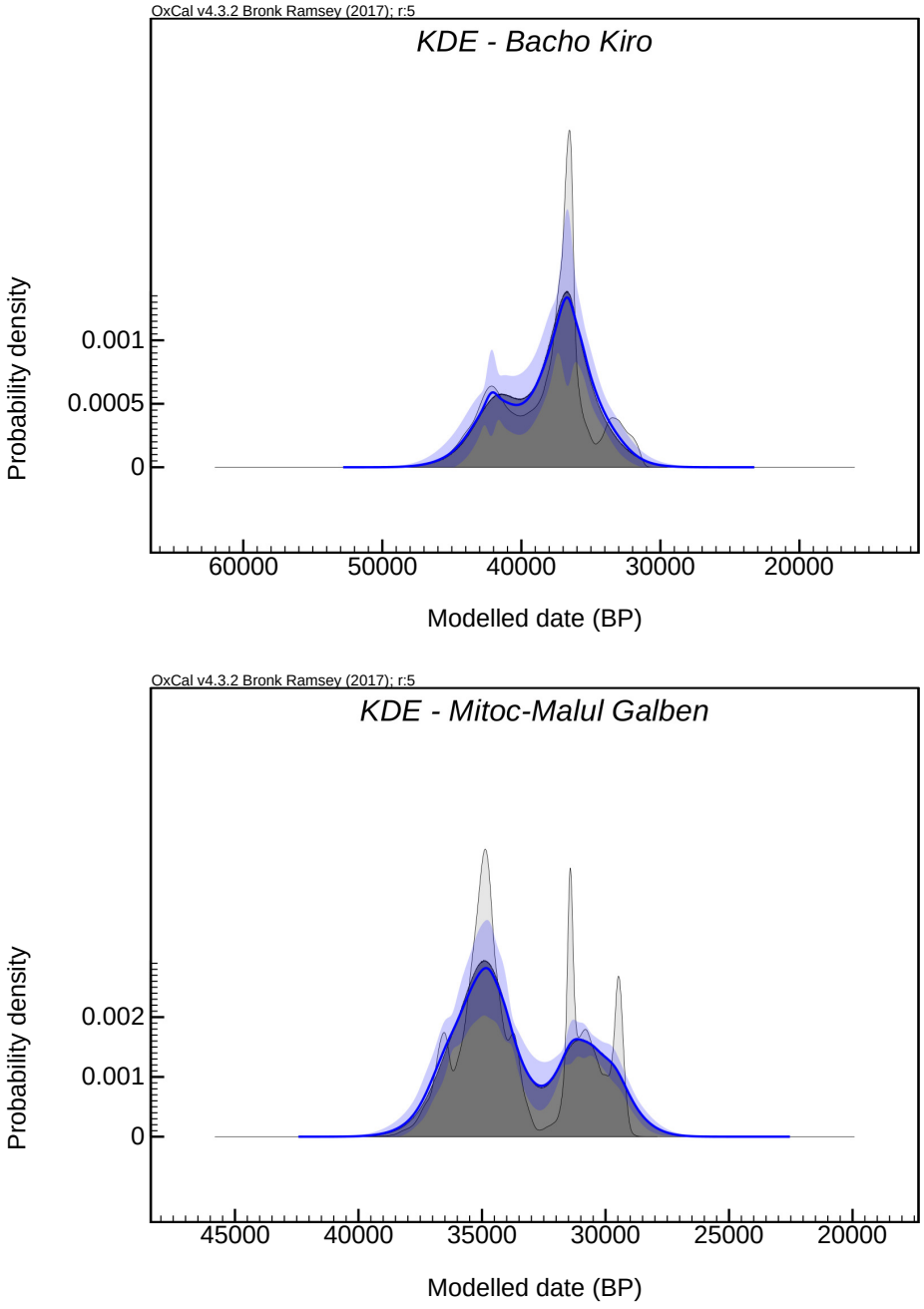


Figure D.46: KDE models for Bacho Kiro (code: p. 767) and Mitoc-Malul Galben (code: p. 766).

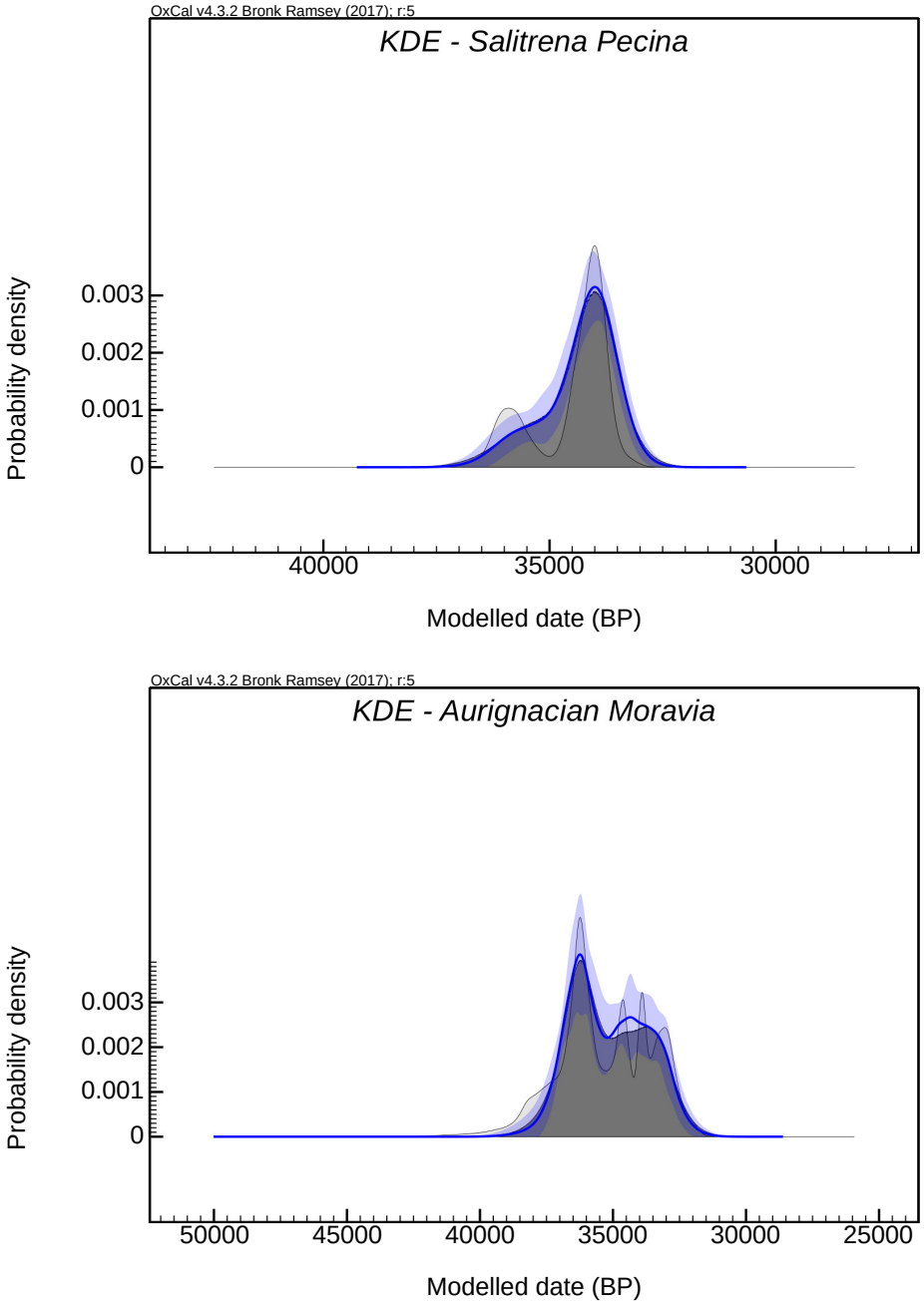


Figure D.47: KDE models for Šalitrena Pećina (code: p. 765) and the Moravian Aurignacian (code: p. 764).

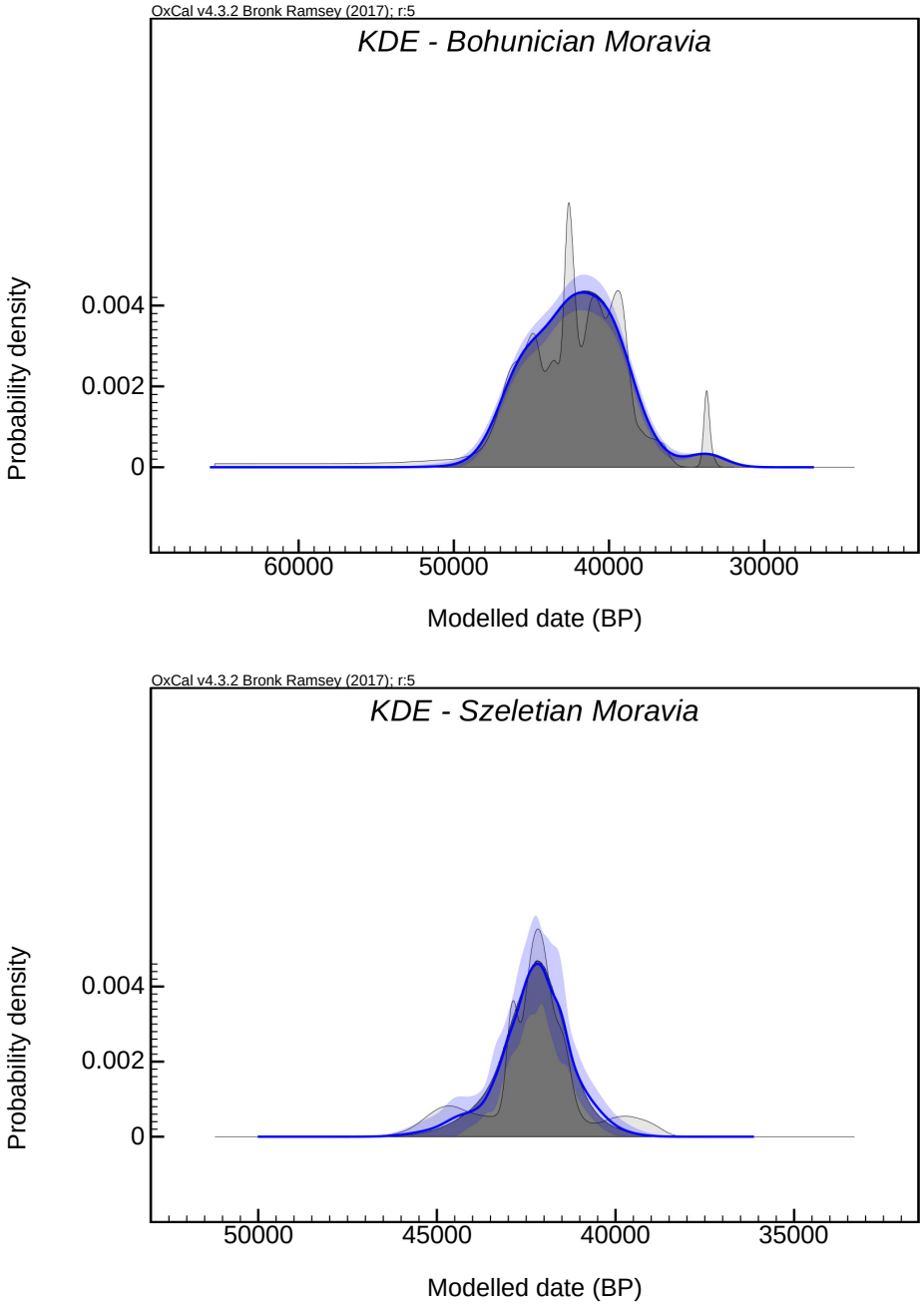


Figure D.48: KDE models for the Moravian Bohunician (code: p. 763) and Szeletian (code: p. 763).

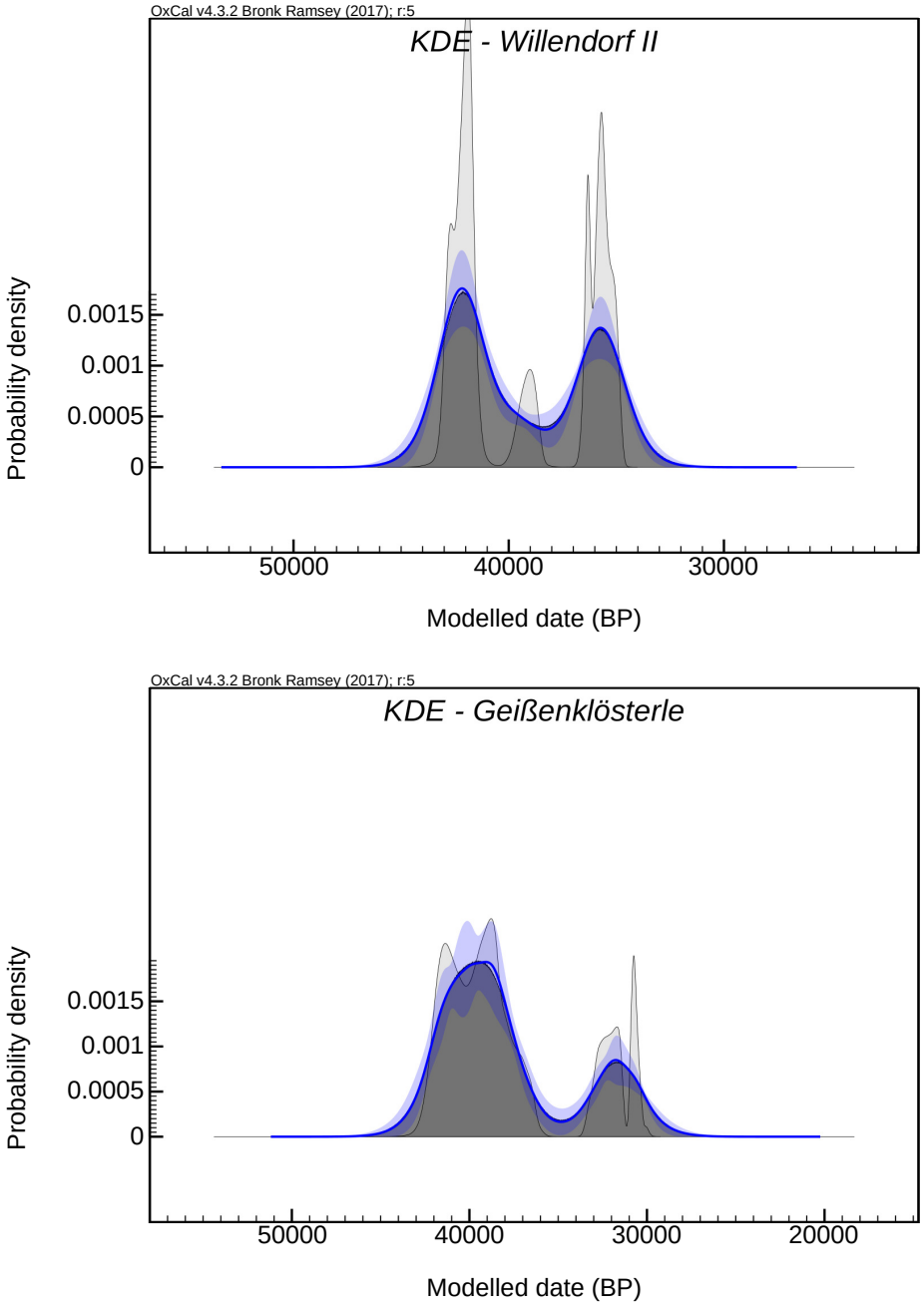


Figure D.49: KDE models for Willendorf II (code: p. 763) and Geißenklösterle (code: p. 760).

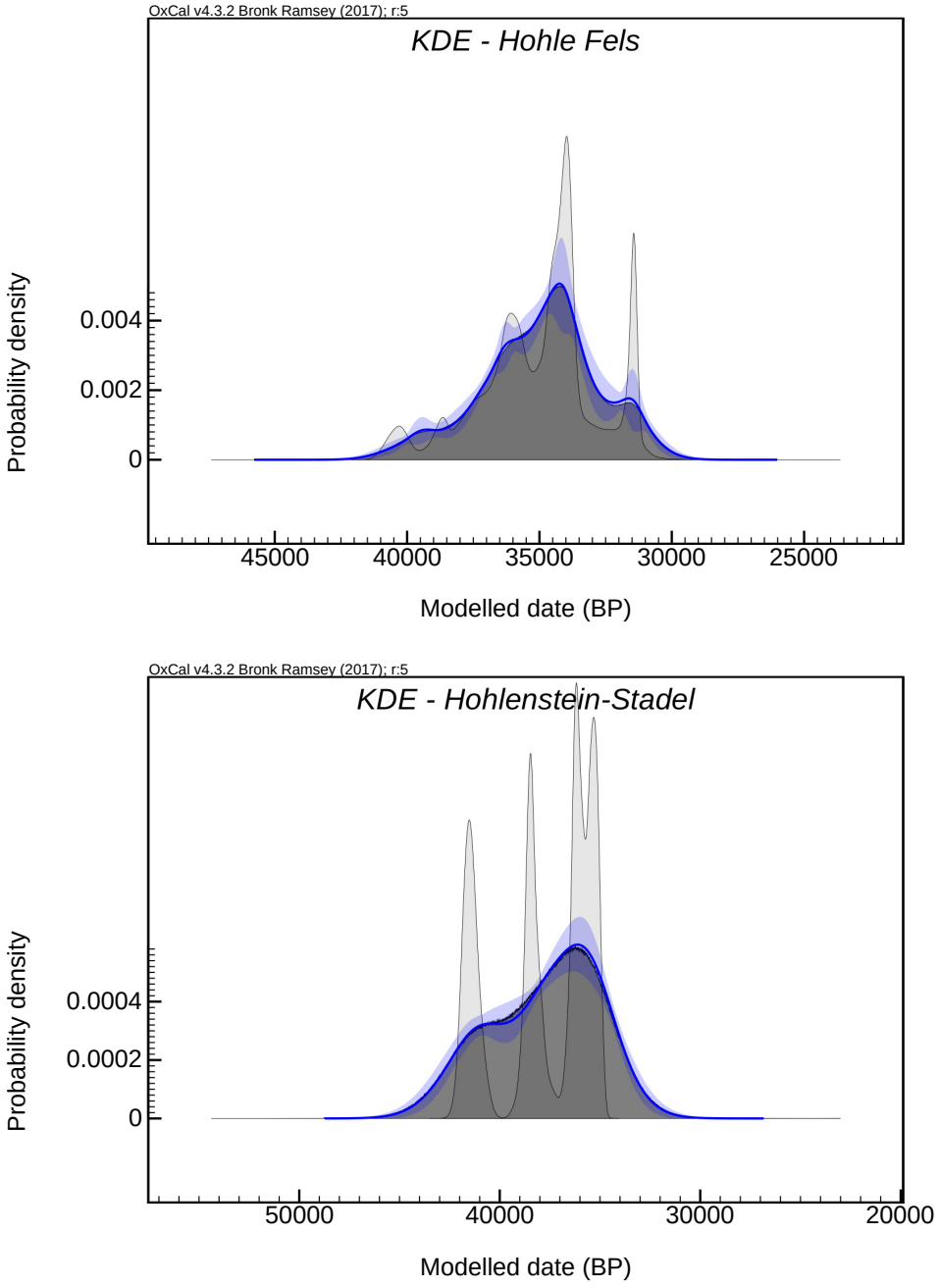


Figure D.50: KDE models for Hohle Fels (code: p. 758) and Hohlenstein-Stadel (code: p. 760).

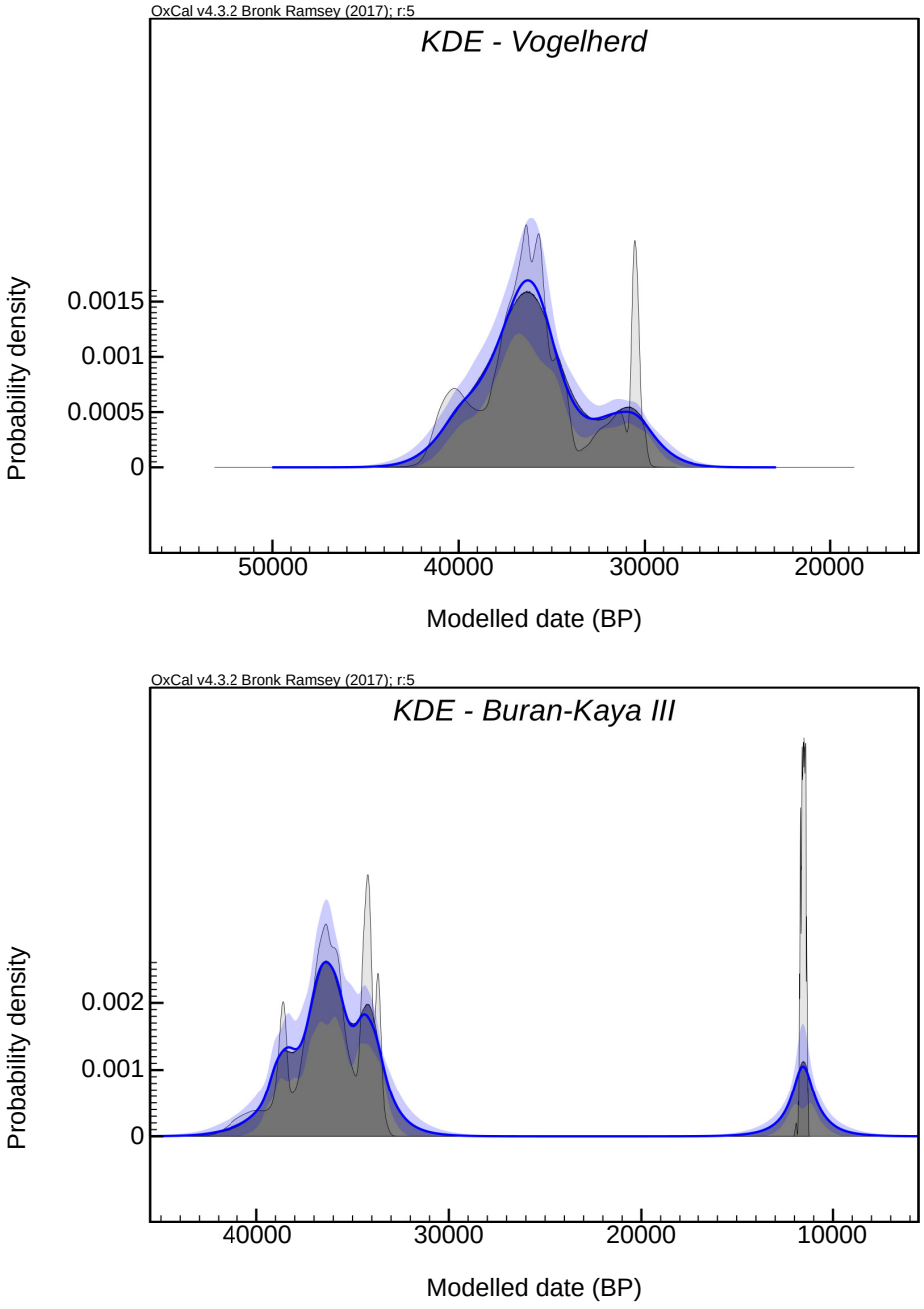


Figure D.51: KDE models for Vogelherd (code: p. 760) and Buran-Kaya III (code: p. 767).

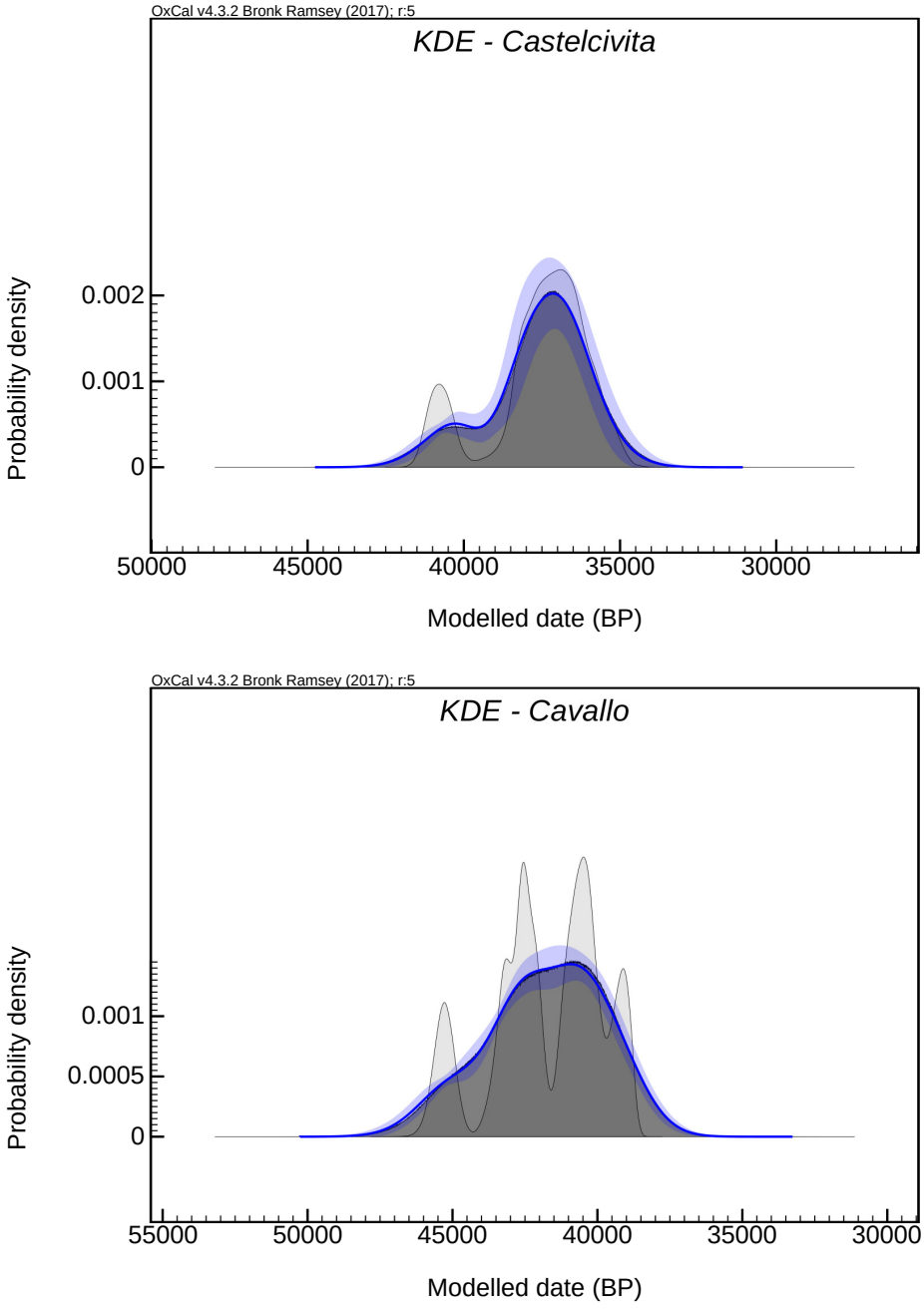


Figure D.52: KDE models for Castelcivita (code: p. 761) and Cavallo (code: p. 764).

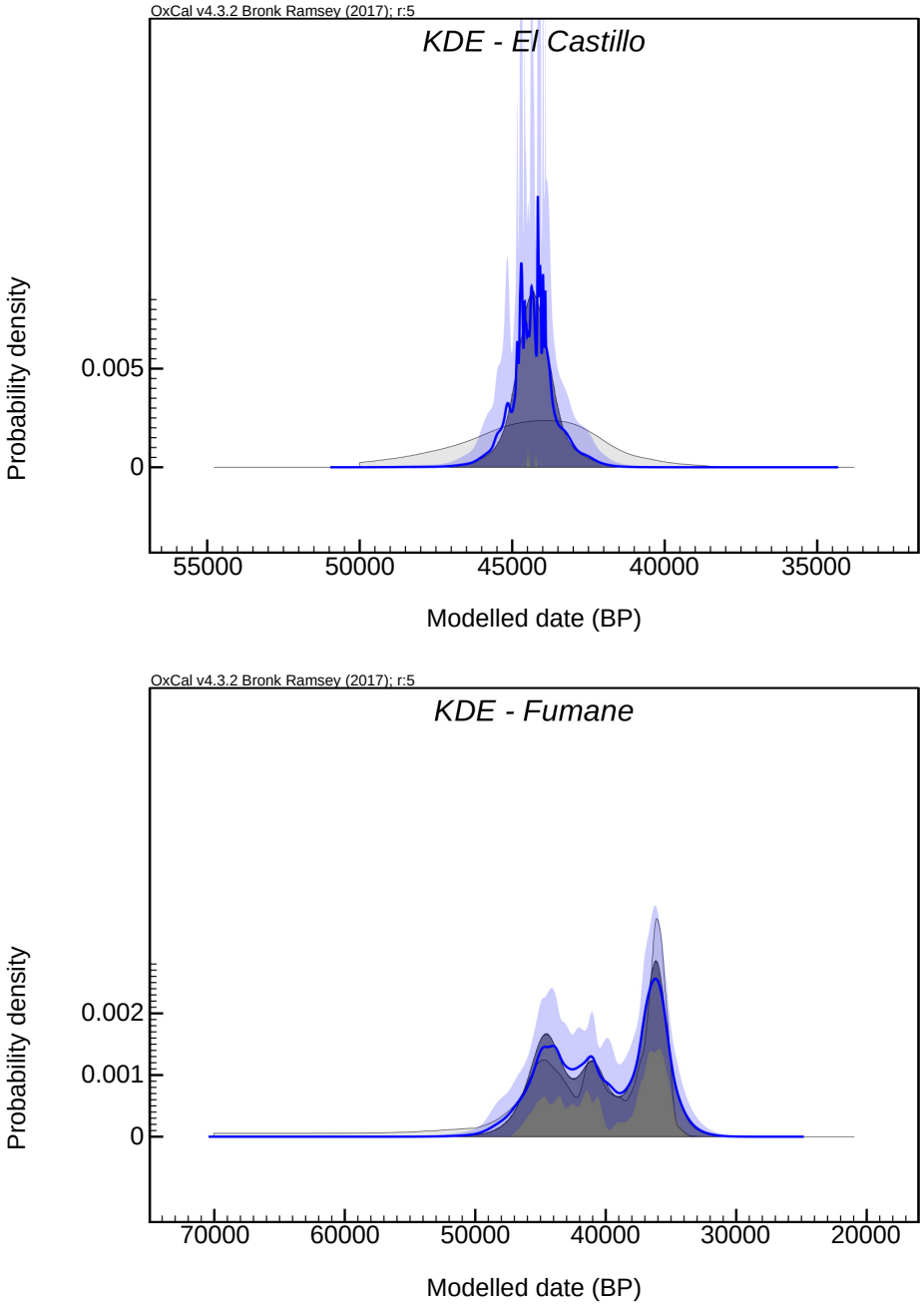


Figure D.53: KDE models for El Castillo (code: p. 753) and Fumane (code: p. 761).

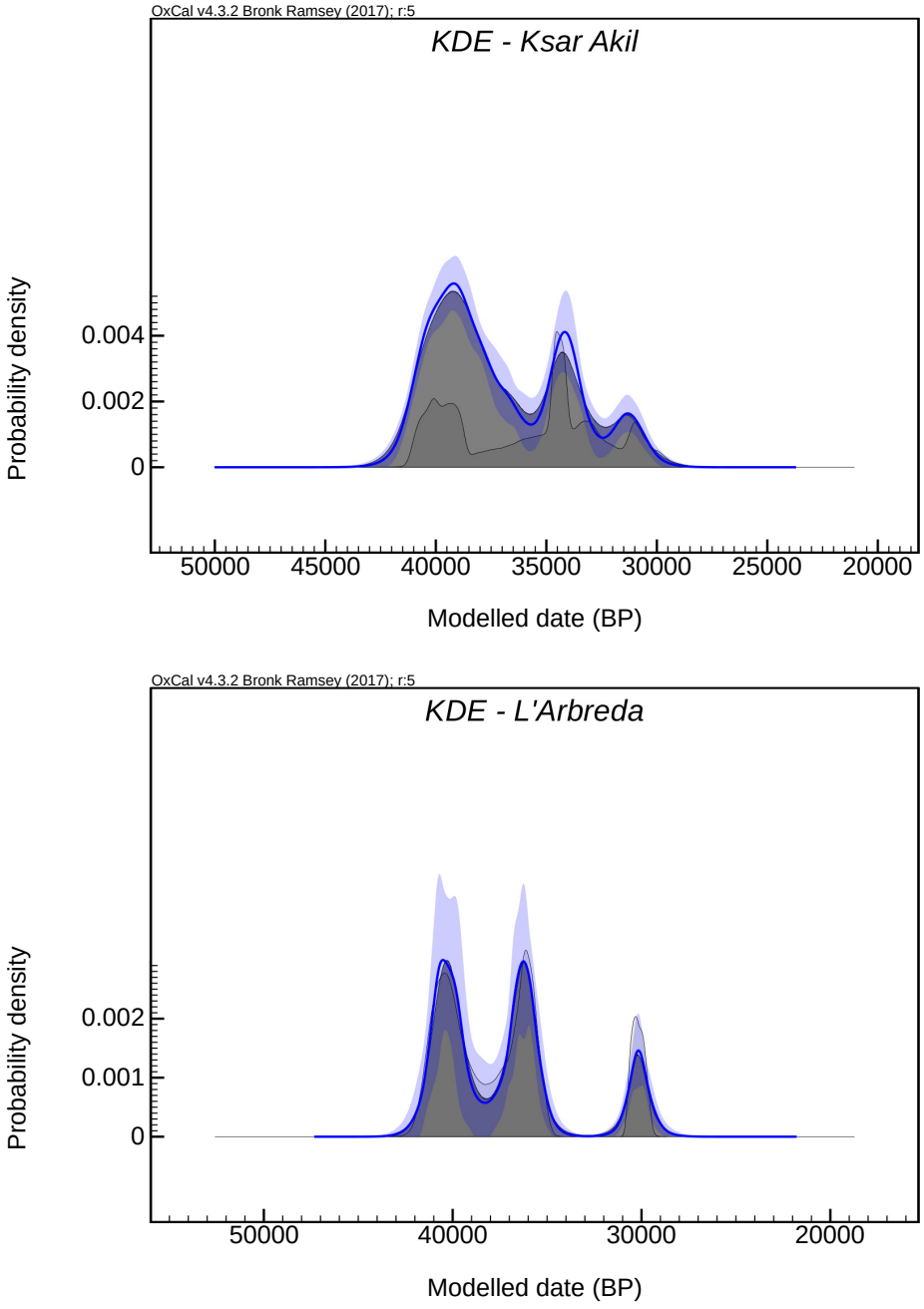


Figure D.54: KDE models for Ksar Akil (code: p. 769) and L'Arbreda (code: p. 756).

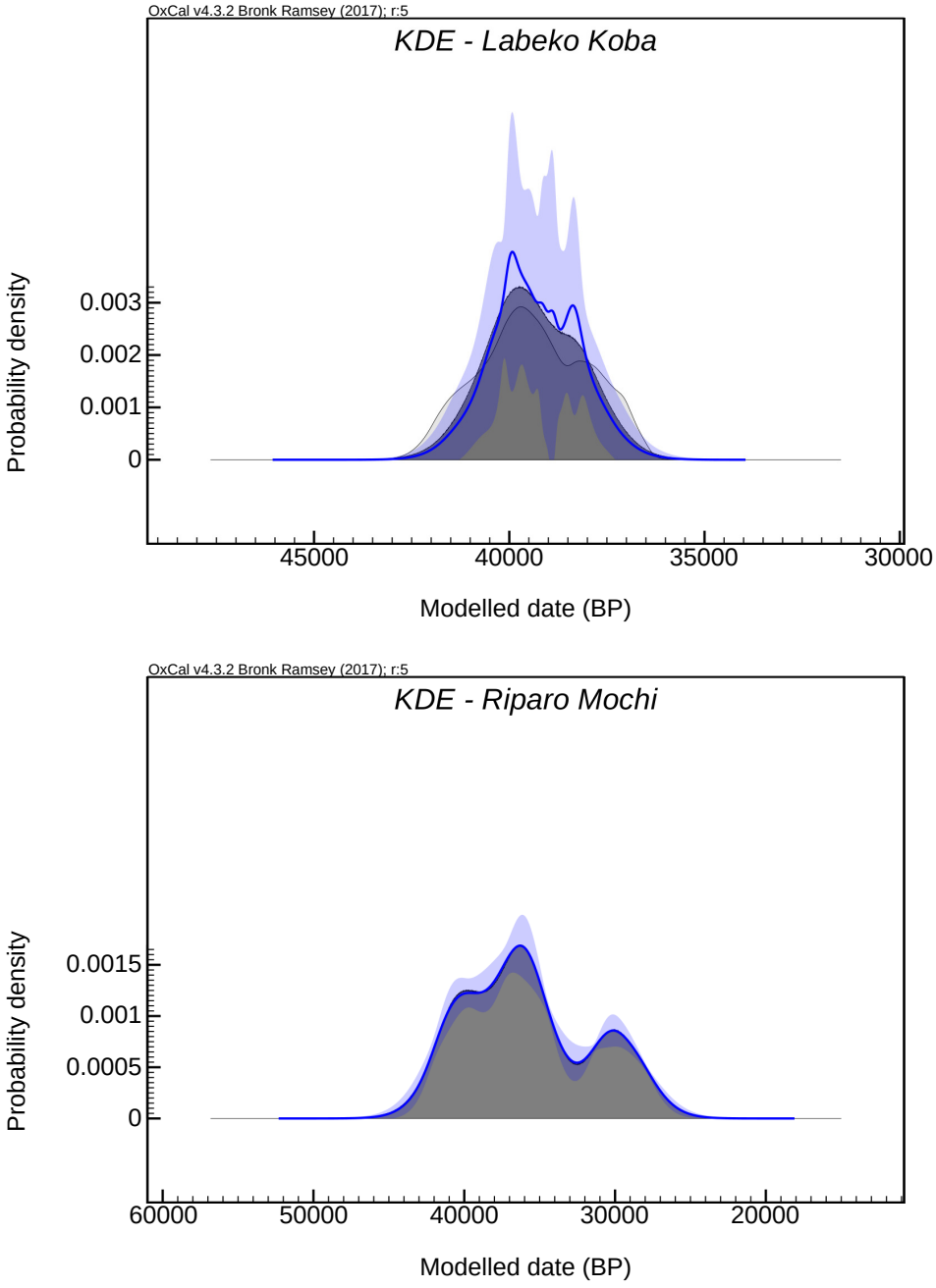


Figure D.55: KDE models for Labeko Koba (code: p. 754) and Riparo Mochi (code: p. 757).

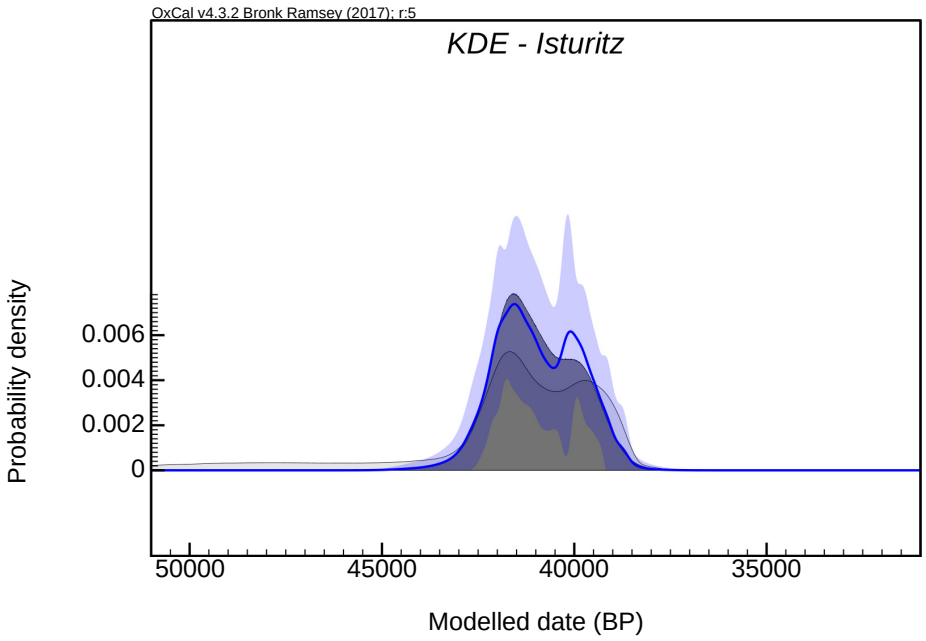


Figure D.56: KDE model for Isturitz (code: p. 755).